

2018 IM & EM TECHNOLOGY SYMPOSIUM

INNOVATIVE INSENSITIVE MUNITION SOLUTIONS FOR ENHANCED WARFIGHTER EFFECTIVENESS



April 23 – 26, 2018

Doubletree by Hilton Portland

Portland, OR

NDIA.org/IMEM2018

WELCOME TO THE IM & EM TECHNOLOGY SYMPOSIUM

On behalf of the Insensitive Munitions and Energetic Materials Committee and our MSIAC partner, I would like to welcome you to the 2018 Insensitive Munitions and Energetic Materials Technology Symposium. This international gathering of the top chemists, system designers and engineers from government laboratories, private industry and academia will provide a venue for exchange and dissemination of the latest research in synthesis, formulation, system design, testing, characterization and safety – all aimed at advancing munitions effectiveness

WHILE improving safety for the warfighter. In recent decades great advances have been made and our munitions are less vulnerable to attack than ever before; however, challenges remain. It is through the continuing work of the authors, presenters, sponsors and attendees at this conference and across our worldwide defense industry that these challenges will be overcome resulting in safer munitions being produced in our factories and fielded to our warfighters.

Melissa Hobbs-Hendrickson
Director Business Development
Orbital ATK

SCHEDULE AT A GLANCE

MONDAY, APRIL 23

Registration and Welcome Reception

First Level Foyer and
Broadway | Weidler | Halsey Ballroom
4:00 pm - 5:30 pm

TUESDAY, APRIL 24

Registration and Breakfast

First Level Foyer and
Broadway | Weidler | Halsey Ballroom
7:00 am

General Session

Lloyd Center Ballroom
8:00 am

Concurrent Presentations

Multnomah & Holladay Ballrooms
10:55 am

Lunch

Cascade Ballroom
12:15 pm

Concurrent Presentations

Multnomah and Holladay Ballrooms
1:45 pm

Symposium Reception

Cascades Ballroom
5:30 pm - 7:00 pm

WEDNESDAY, APRIL 25

Registration and Breakfast

First Level Foyer and
Broadway | Weidler | Halsey Ballroom
7:00 am

Concurrent Presentations

Multnomah & Holladay Ballrooms
8:00 am

Symposium Adjourns for the Day

11:20 am

THURSDAY, APRIL 26

Registration and Breakfast

First Level Foyer and
Broadway | Weidler | Halsey Ballroom
7:00 am

Concurrent Presentations

Multnomah & Holladay Ballrooms
8:00 am

Lunch

Cascades Ballroom
11:40 am

Concurrent Presentations

Multnomah & Holladay Ballrooms
1:00 pm

Spanish Wine Celebration and Awards

Broadway | Weidler | Halsey Ballroom
4:20 pm

TABLE OF CONTENTS

WELCOME	2
SCHEDULE AT A GLANCE	2
WHO WE ARE	3
EVENT INFORMATION	4
AGENDA	5
ABSTRACT PRESENTATIONS	16
BIOGRAPHY	19
TABLE TOP DISPLAYS	20
SPONSOR DESCRIPTIONS	22
VENUE MAP	24
THANK YOU TO OUR SPONSORS	25
SAVE THE DATE	26



NDIA

WHO WE ARE

The National Defense Industrial Association is the trusted leader in defense and national security associations. As a 501(c)(3) corporate and individual membership association, NDIA engages thoughtful and innovative leaders to exchange ideas, information, and capabilities that lead to the development of the best policies, practices, products, and technologies to ensure the safety and security of our nation. NDIA's membership embodies the full spectrum of corporate, government, academic, and individual stakeholders who form a vigorous, responsive, and collaborative community in support of defense and national security. For more information, visit NDIA.org



MUNITIONS TECHNOLOGY

MISSION

Works to maintain an open exchange of technical information among government and industry programs and technical managers, and to identify changes and trends in policy, guidance and organizational functions that affect the development, production, maintenance and demilitarization of munitions.

LEADERSHIP AND COMMITTEES

Tim Bagniefski

Division Chair
tbagniefski@gd-ots.com

Roy Streetz

Chair
Fuze

Melissa Hobbs-Hendrikson

Chair
Insensitive Munitions and Energetic Materials

EVENT INFORMATION

EVENT WEBSITE

NDIA.org/IMEM2018

EVENT CONTACT

Carol Dwyer
Meeting Planner
(703) 247-2582
cdwyer@ndia.org

Loey Bleich
Program Manager
(703) 247-2575
lbleich@ndia.org

PLANNING COMMITTEE

Melissa Hobbs-Hendrickson
Event Chair

Paul Braithwaite
Mike Ervin

Steve Nicolich
Michael Sharp

Wade Babcock

Ken Graham

Stephen Struck

Matthew Beyard

Kathryn Hunt

Tom Swierk

David Hunter

Andrew Wilson

WI-FI

Network: DOUBLETREE
Password: There is no password

ATTENDEE ROSTER, PROCEEDINGS & SYMPOSIUM SURVEY

NDIA will be emailing all participants the symposium attendee roster, the link for symposium proceedings (those which have been approved) and the symposium survey information within three week of the conclusion of the symposium.

SPEAKER GIFTS

In lieu of speaker gifts, a donation is being made to the Fisher House Foundation.

HARASSMENT STATEMENT

NDIA is committed to providing a professional environment free from physical, psychological and verbal harassment. NDIA will not tolerate harassment of any kind, including but not limited to harassment based on ethnicity, religion, disability, physical appearance, gender, or sexual orientation. This policy applies to all participants and attendees at NDIA conferences, meetings and events. Harassment includes offensive gestures and verbal comments, deliberate intimidation, stalking, following, inappropriate photography and recording, sustained disruption of talks or other events, inappropriate physical contact, and unwelcome attention. Participants requested to cease harassing behavior are expected to comply immediately, and failure will serve as grounds for revoking access to the NDIA event.

AGENDA

MONDAY, APRIL 23

4:00 pm **CONFERENCE REGISTRATION AND WELCOME RECEPTION**
FIRST LEVEL FOYER AND BROADWAY | WEIDLER | HALSEY BALLROOM

5:30 pm **ADJOURNMENT**

TUESDAY, APRIL 24

7:00 am **CONFERENCE REGISTRATION AND BREAKFAST**
FIRST LEVEL FOYER AND Broadway | Weidler | Halsey Ballroom

SESSION 1 PLENARY

Melissa Hobbs-Hendrickson
Orbital ATK
Session Chair

8:00 am **WELCOME**
LLOYD CENTER BALLROOM
CAPT Frank Michael, USN (Ret)
National Defense Industrial Association

Melissa Hobbs-Hendrickson
Orbital ATK

8:10 am **KEYNOTE ADDRESS**
Dr. Christine Michienzi
OUSD (AT&L) Manufacturing and Industrial Base Policy

8:40 am **20188 IM PLANS AND JIMTP FUTURE IN THE UNITED STATES**
Anthony Di Stasio
OUSD (AT&L)/TWS/LWM

9:00 am **20156 NATO WORKING GROUP ON INSENSITIVE MUNITIONS AND HAZARD CLASSIFICATION REQUIREMENTS, ASSESSMENT AND HAZARD FREQUENCY**
Philip Cheese
Defence Equipment and Support

9:20 am **20249 U.S. NAVY INSENSITIVE MUNITIONS HANDBOOK**

Dr. Jerry Ward
Booz Allen Hamilton

9:40 am **20149 MSIAC – HIGHLIGHTS AND FUTURE PRIORITIES**

Dr. Michael Sharp
NATO Munitions Safety Information Analysis Center

10:00 am **MUNITIONS SAFETY AWARDS**

Dr. Michael Sharp
NATO Munitions Safety Information Analysis Center

10:10 am **NETWORKING BREAK**

BROADWAY | WEIDLER | HALSEY BALLROOM

CONCURRENT BREAKOUT SESSIONS

SESSION 2A IM REQUIREMENTS & ASSESSMENTS

MULTNOMAH

Wade Babcock
NATO Munitions Safety Information Analysis Center
Session Chair

SESSION 2B ENERGETIC MATERIALS

HOLLADAY

Mike Ervin
BAE Systems
Session Chair

10:55 am **20265 Historical Review of Fragment Impact Standardization**

Kathryn Hunt
MARCORSYSCOM

**20119 GrIMEx (Green IM Explosive):
Development of Novel IM Comp B
Replacements Based on Green TNT
and RDX Replacements**

Dr. David Price, Jr
BAE Systems.

11:15 am **20112 Review and Update of STANAG 4496
Fragment Impact, Munitions Test Procedure**

Christophe Jacq
DGA Missiles Testing

**20059 A New IMI Systems Less Sensitive
Brisant Explosive Composition**

Dr. Gila Strul-Yudkiewicz
IMI Systems

11:35 am **20063 US Navy Insensitive Munitions (IM) Munitions Reaction Evaluation Board (MREB)**

Ken Tomasello
Naval Ordnance Safety and Security Activity

20127 CRASH-P and X-ray Laboratory Scale Slow Cook-off Tests to Quantify the Reaction Violence of High Performance Rocket Propellants

Dr. Jonathan Essel
NAWCWD China Lake

11:55 am **20137 MSIAC Workshop 2018: Improved Explosives and Munitions Risk Management**

Dr. Michael Sharp
NATO Munitions Safety Information Analysis Center

20164 New Polycarbonate-Based Thermoplastic Polyurethane Binder for HMX Based Explosives

Emily Robertson
Lawrence Livermore National Laboratory

12:15 pm **LUNCH**
CASCADE BALLROOM

SESSION 3A LARGE SCALE TESTING 1

MULTNOMAH

Michael Sharp
NATO Munitions Safety Information Analysis Center
Session Chair

SESSION 3B FORMULATIONS

HOLLADAY

Paul Braithwaite
Orbital ATK
Session Chair

1:45 pm **20082 Gun Launch and Setback Actuators**

Dr. Ernest Baker
NATO MSIAC

20077 Evaluation of Composition B Using Nano-Energetics

Philip Samuels
ARDEC

2:05 pm **20183 Fragment Impact Testing of the XM25**

Nausheen Al-Shehab
US Army

20261 The DOTC Enterprise – Helping You Accelerate Technologies to the Field

James Wilson
DOTC Program Office - Picatinny NJ

2:25 pm **20057 Novel Slow Cook-off Test Method to Replicate Worst Case for Munitions Containing Internal Fuel**

Ben Blazek
NAVAIR

20111 Effect of Microstructure Control on the Reaction Characteristics In Al/Ni Reactive Powder

Dr. Sang-Hyun Jung
Agency for Defense Development (South Korea)

2:45 pm **20118 Advancing the Propane Fast Cookoff Burner and Testing**

Dr. Ephraim Washburn
Naval Air Warfare Center Weapons Division

20074 Characterization of MTNP (1-Methyl-3,4,5-Trinitro-1,2-Pyrazole)

Philip Samuels
ARDEC

3:05 pm **20260 Comparative Fire Response of Simulated Rocket Motors in Steel and Carbon Fiber Composite Missile Launching Canisters**

Dr. Jon Yagla
Bowhead Technical Services

20069 Influence of Concentration, Type and Particle Size of Fillers on the Dynamic Mechanical Behaviour of Elastomeric HTPB Binder

Manfred Bohn
Fraunhofer ICT

3:25 pm **NETWORKING BREAK**

BROADWAY | WEIDLER | HALSEY BALLROOM

SESSION 4A THERMAL HAZARD TESTING

MULTNOMAH

Tom Swierk
Hart Technologies, Inc.
Session Chair

SESSION 4B EM PROCESSING I

HOLLADAY

Ron Hollands
BAE Systems
Session Chair

3:45 pm **20080 Slow Heating Testing Survey and Historical Events Review**

Dr. Ernest Baker
NATO MSIAC

20145 Property-Processing Implications in Additive Manufactured Materials for Munitions

Wade Babcock
NATO Munitions Safety Information Analysis Center

4:05 pm **20126 An Investigation into a Proper Heating Rate for Slow Cook-Off Testing**

Dr. David Hubble
NSWC Dahlgren Division

20174 Robust Enhanced Blast Explosive Manufacturing at Holston Army Ammunition Plant

Virgil Fung
BAE Systems

4:25 pm **20267 Insensitive Munitions Industry Contribution for New Stanag - AOP Edition of the Slow Heating Test**

Yves Guengant
ARIANEGROUP SAS

20155 New NTO Workshop and Associated Product Characterizations

Arthur Delage
EURENCO

4:45 pm **20279 Scaling of Fast Cook Off Fires**

Dr. Jon Yagla
Bowhead Technical Services

20179 Characterization of LX-14 FEM / PBXN-9 FEM High Energy Explosives

Brian Alexander
BAE Systems Inc, Ordnance Systems

5:05 pm **20258 Cost of Propane Fast Cook-Off Testing**

Dr. Ephraim Washburn
Naval Air Warfare Center Weapons Division

20157 Development of a CONUS Manufacturing Capability for FOX-7

Dr. Bradley Sleadd
NSWC IHEODTD

5:30 pm **GRAND RECEPTION**

CASCADE BALLROOM

7:00 pm **ADJOURNMENT**

WEDNESDAY, APRIL 25

7:00 am **CONFERENCE REGISTRATION AND BREAKFAST**

FIRST LEVEL FOYER AND BROADWAY | WEIDLER | HALSEY BALLROOM

CONCURRENT BREAKOUT SESSIONS

SESSION 5A LARGE SCALE TESTING II

MULTNOMAH
Ken Graham
Aerojet Rocketdyne
Session Chair

SESSION 5B ENERGETIC MATERIALS II

HOLLADAY
Steve Nicolich
U.S. Army
Session Chair

8:00 am **20275 Passing Sympathetic Reaction Responses in 500 and 1,000-lb General Purpose Bombs with AFX-770**

Dr. Christopher Crouse
Air Force Research Laboratory

20172 MDNT: IM Melt-Phase Energetic Binder

Omar Abbassi
US ARMY ARDEC

8:20 am **20268 An Explosive Fragment Projector for IM Testing**

Tal Eliash
Rafael

20171 Melt-Pour Explosive Formulation Development Featuring TNBA

Virgil Fung
BAE Systems

8:40 am **20122 Outgassing Pad for Cook-Off Mitigation in Warheads**

Josiah Garfield
NAWCWD-China Lake

20166 Particle Size and Surface Area Effects on the Initiation of Diaminoazoxyfurazan (DAAF)

Elizabeth Francois
Los Alamos National Laboratory

9:00 am **20083 Insensitive Munitions Explosive Ordnance Disposal Challenges**

Dr. Ernest Baker
NATO MSIAC

20289 Manufacturing of PAX-3 High Explosive

Sean Swaszek
ARDEC

9:20 am **20273 Explosive Ordnance Disposal (EOD) of Insensitive Munitions: Challenges and Solutions**

Patrick Brousseau
DRDC - Valcartier RC

20153 Qualification Of Malleable Plastic Explosive Hexomax and its Application in a Flexible Linear Shaped Charge System

Christelle Songy
EURENCO

9:40 am **NETWORKING BREAK**

BROADWAY | WEIDLER | HALSEY BALLROOM

SESSION 6A MITIGATION & TESTING

MULTNOMAH

Patrick Brousseau
DRDC - Valcartier RC
Session Chair

SESSION 6B SYNTHESIS

HOLLADAY

Matthew Andrews
NATO Munitions Safety Information Analysis Center
Session Chair

10:00 am **20141 Mitigation Technologies for Propulsion Applications**

Christelle Collet
MSIAC

20123 Modernization and Capabilities of the Lawrence Livermore National Laboratory Pilot Facility for Remotely Controlled Energetic Materials Synthesis

Dr. Nathaniel Zuckerman
Lawrence Livermore National Laboratory

10:20 am **20154 Sheet-metal Ammunition Packing Tray for Mitigation of Secondary Cook-off of Medium-caliber Ammunition**

Greg Little
Naval Surface Warfare Center, Dahlgren Division

20180 Synthesis, Formulation, and Testing of 3,4-DNP

Dr. Jacob Morris
BAE Systems

10:40 am **20159 Development and Successful Demonstration of a Lightweight, Particle Impact Mitigation Sleeve (PIMS) With Specified Hardness and Perforation Features**

Daniel Pudlak
ARDEC

20271 Microfluidic Synthesis of Energetic Materials

Dr. Joe Scavuzzo
Orbital ATK

11:00 am **20147 Stopping KM/S Blunt Fragments and Limiting Shock Lensing with a New Advanced Energy Absorbing Composite**

Dr. Gareth Tear
Synbiosys Ltd

20228 Synthesis Development of Novel Energetic Ingredients

Dr. Sarah Headrick
BAE Systems

11:20 am **ADJOURNMENT**

THURSDAY, APRIL 26

7:00 am **CONFERENCE REGISTRATION AND BREAKFAST**

FIRST LEVEL FOYER AND BROADWAY | WEIDLER | HALSEY BALLROOM

CONCURRENT BREAKOUT SESSIONS

SESSION 7A SYSTEMS I

MULTNOMAH

Steve Struck

Energetic Materials Branch, Munitions Directorate
Session Chair

SESSION 7B HE CHARACTERISTICS

HOLLADAY

Melissa Mileham

Orbital ATK
Session Chair

8:00 am **20182 Additive Manufacturing for Net Shape Munitions**

Dr. Bhanu Chelluri
BAE Systems- Dayton

20081 Gap Test Calculations and Correlations

Dr. Ernest Baker
NATO MSIAC

8:20 am **20140 Reaction Mechanisms for Rocket Motors**

Christelle Collet
MSIAC

20276 PBXN-5 Mechanical Characterization and Proposed Constitutive Model

Dr. Daniel Peairs
L-3 Fuzing and Ordnance Systems

Dr. Ericka Amborn
ARA

8:40 am **20132 Loading Density and Vent Area Ratio Effects on the Structural Response of Reinforced Concrete Structures Storing HD 1.3 Gun Propellant**

Cynthia Romo
Naval Air Warfare Center Weapons Division

20113 Investigation of the Hugh James Criteria using Estimated Parameters

Dr. Justin Sweitzer
Practical Energetics Research, Inc

9:00 am **20114 Life Cycle Demilitarization Considerations for IM Development**

Gary Mescavage
PD Demil

20290 Electronic Properties and Hirshfeld Surface Analysis of Insensitive High Energy Density Material Dihydroxylammonium 5,5'-bistetrazole-1,1'-diolate under Compression

Bokinala Abraham
Advances Centre of Research in High Energy Materials

9:20 am **20274 New Generation Influence Mine Classified as 1.6N**

Björn Granqvist
OY FORCIT AB

OPEN

9:40 am **NETWORKING BREAK**

BROADWAY | WEIDLER | HALSEY BALLROOM

SESSION 8A SUB-SCALE TESTING I

MULTNOMAH

Brian Fuchs
Company
Session Chair

SESSION 8B PROPELLANTS

HOLLADAY

Jessica Vaughn
Company
Session Chair

10:00 am **20139 Correlation of Response for Munitions Containing RDX/TNT: Bullet Impact and EMTAP Tube Testing Results**

Phil Cheese
UK Ministry of Defence

20135 The Unknown Detonation Transition (XDT) Mechanisms Associated with Damaged Rocket Propellant Impacting a Surface: Understanding and Applications to IM

Dr. Mark Pfeil
US Army AMRDEC

10:20 am **20262 Radiant Chamber for Fast Cook of Testing and Simulation**

Dr. Jon Yagla
Bowhead Technical Services

20115 Innovative Nitrogen-doped Boron Propellants

Dr. Thelma Manning
US ARMY RDECOM ARDEC

10:40 am **20117 Analysis of Temperature Profiles of Chemical Reaction upon Impact of Reactive Materials**

Ki-bong Lee
Agency for Defense Development(South Korea)

20264 Insensitive Minimum Smoke Propellants

Dr. Thomas Deschner
Nammo Raufoss AS

11:00 am **20121 Validating Experiments for Vulnerability Calculations of Munitions and Lessons Learned**

Gert Scholtes
TNO Defence, Safety & Security

20152 Increased Impulse of Solventless Extruded Double Base Rocket Propellant by Addition of High Explosives RDX And FOX-7.

Erik Tunestål
Eurenco Bofors

11:20 am **20241 Effect of Insensitive HE on Shaped Charge Jets**

Werner Arnold
MBDA - TDW

20134 Initial Steps Towards Large Scale Production of UK Lova Thermoplastic Elastomer (TPE) Propellants

Mr. Owain Sowden
BAE SYSTEMS Land (UK)

11:40 am **LUNCH**
CASCADE BALLROOM

SESSION 9A MODELING & ANALYSIS

MULTNOMAH

Gert Scholtes
TNO Defence, Safety & Security
Session Chair

SESSION 9B SUB-SCALE TESTING II

HOLLADAY

Genevieve Eck
EURENCO
Session Chair

1:00 pm **20259 Fast Cook-Off Modeling and Simulation**

Dr. Jon Yagla
Bowhead Technical Services

20282 Insensitive Munitions (IM) Gun Propellant Optimization Efforts for Medium Caliber Application

Dr. Melissa Liberatore-Moretti
Picatinny Arsenal

1:20 pm **20269 Thermal Modeling of Fast Cook-Offs**

Dr. Markus Graswald
TDW GmbH

20131 Critical Diameter and Gap Tests for Hazard Classification of Solid Propellants and Motors

Cynthia Romo
Naval Air Warfare Center Weapons Division

1:40 pm **20266 An Approach to Predict the Cook-off Response of Confined and Vented Full Scale Munitions Based on Small Scale Tests**

Dr. N. Albert Moussa
BlazeTech Corp

20133 Small Scale Assessment of LOVA Thermoplastic Elastomer (TPE) Propellants for Large Calibre Gun Systems

Mr. Owain Sowden
BAE SYSTEMS Land (UK)

2:00 pm **30000 International Sympathetic Reaction Testing Survey**

Dr. Ernest Baker
NATO MSIAC

20146 Age-Related Mechanical Damage and Ageing of Munition Materials

Wade Babcock
NATO Munitions Safety Information Analysis Center

2:20 pm **20161 Filling the Gap between the Initiation Behavior of Shaped Charge Jets and Fragments**

Werner Arnold
MBDA - TDW

20136 Subscale Testing to Predict Full-Scale Response to Fragment Impact in Solid Propellants

Dr. Jamie Neidert
AMRDEC

2:40 pm **NETWORKING BREAK**
BROADWAY | WEIDLER | HALSEY BALLROOM

SESSION 10A SYSTEMS II

MULTNOMAH
Jamie Neidert
AMRDEC
Session Chair

SESSION 10B EM QUALIFICATION & SUSTAINABILITY

HOLLADAY
Andrew Wilson
Exploinsights
Session Chair

3:00 pm **20150 Heavyweight Torpedo Warhead – IM Assessment**

Luc Chaffois
EURENCO

20138 Qualification and Energetic Materials Challenges

Dr. Matthew Andrews
NATO MSIAC

3:20 pm **20181 Improving Knowledge of Tactical Rocket Motor Response under Insensitive Munition Threats: BI, FI and FH Tests Results of the Research Program**

Laurent Bonhomme
ROXEL

20163 Impacts of REACh, ITAR and Other Regulations on Energetic Materials Sustainability

Geneviève Eck
EURENCO

3:40 pm **20245 IM Characteristics of Large Diameter Extruded Double Base Rocket Motors with Composite Cases**

Joseph Bellotte
BAE Systems Inc. OSI

20233 Qualification of Explosives Formulations Manufacturers and Ingredient Manufacturers for US Navy Use

Michael Kenyon
NSWC IHEODTD

4:00 pm **20263 IM Technology for Stryker Tank Munitions**

Adriana Eng
US Army ARDEC

20151 Influence of Ageing on the Properties of IHE

Hendrik Radies
Rheinmetall Weapon & Munition

4:20 pm **SPANISH WINE CELEBRATION AND AWARDS**
BROADWAY | WEIDLER | HALSEY BALLROOM

4:45 pm **SYMPOSIUM CONCLUDES**

The NDIA has a policy of strict compliance with federal and state antitrust laws. The antitrust laws prohibit competitors from engaging in actions that could result in an unreasonable restraint of trade. Consequently, NDIA members must avoid discussing certain topics when they are together at formal association membership, board, committee, and other meetings and in informal contacts with other industry members: prices, fees, rates, profit margins, or other terms or conditions of sale (including allowances, credit terms, and warranties); allocation of markets or customers or division of territories; or refusals to deal with or boycotts of suppliers, customers or other third parties, or topics that may lead participants not to deal with a particular supplier, customer or third party.



VOTE NOW

PEOPLE'S CHOICE AWARD

Vote for your favorite presentation by going to surveymonkey.com/r/9553S8P or by using the QR Code.

The People's Choice Award will be presented at the Spanish Wine Celebration and Awards at the end of the Symposium on Thursday, April 26th!

ABSTRACT PRESENTATIONS

ABSTRACT #	TITLE	AUTHOR	SESSION
20057	Novel Slow Cook-off Test Method to Replicate Worst Case for Munitions Containing Internal Fuel	Blazek	3A
20059	A New IMI Systems Less Sensitive Brisant Explosive Composition	Strul-Yudkiewicz	2B
20063	US Navy Insensitive Munitions (IM) Munitions Reaction Evaluation Board (MREB)	Tomasello	2A
20069	Influence of concentration, type and particle size of fillers on the dynamic mechanical behaviour of elastomeric HTPB binder	Bohn	3B
20074	Characterization of MTNP (1-methyl-3,4,5-trinitro-1,2-pyrazole)	Samuels	3B
20077	Evaluation of Composition B using Nano-Energetics	Samuels	3B
20080	Slow Heating Testing Survey and Historical Events Review	Baker	4A
20081	Gap Test Calculations and Correlations	Baker	7B
20082	Gun Launch and Setback Actuators	Baker	3A
20083	Insensitive Munitions Explosive Ordnance Disposal Challenges	Baker	5A
20111	Effect of microstructure control on the reaction characteristics in Al/Ni reactive powder	Jung	3B
20112	Review and Update of STANAG 4496 Fragment Impact, Munitions Test Procedure	Jacq	2A
20113	Investigation of the Hugh James Criteria using Estimated Parameters	Sweitzer	7B
20114	Life Cycle Demilitarization Considerations for IM Development	Mescavage	7A
20115	Innovative Nitrogen-doped Boron Propellants	Manning	8B
20117	Analysis of Temperature Profiles of Chemical Reaction upon Impact of Reactive Materials	Lee	8A
20118	Advancing the Propane Fast Cookoff Burner and Testing	Washburn	3A
20119	GrIMEx (Green IM Explosive): Development of Novel IM Comp B Replacements Based on Green TNT and RDX Replacements	Price	2B
20121	Validating experiments for vulnerability calculations of munitions and lessons learned	Scholtes	8A
20122	Outgassing Pad for Cook-Off Mitigation in Warheads	Garfield	5A
20123	Modernization and Capabilities of the Lawrence Livermore National Laboratory Pilot Facility for Remotely Controlled Energetic Materials Synthesis	Zuckerman	6B
20126	An Investigation into a Proper Heating Rate for Slow Cook-off Testing	Hubble	4A
20127	CRASH-P and X-ray Laboratory Scale Slow Cook-off Tests to Quantify the Reaction Violence of High Performance Rocket Propellants	Essel	2B
20131	Critical Diameter and Gap Tests for Hazard Classification of Solid Propellants and Motors	Romo	9B
20132	Loading Density and Vent Area Ratio Effects on the Structural Response of Reinforced Concrete Structures Storing HD 1.3 Gun Propellant	Romo	7A
20133	Small scale assessment of LOVA Thermoplastic elastomer (TPE) propellants for Large Calibre Gun Systems	Sowden	9B

ABSTRACT #	TITLE	AUTHOR	SESSION
20134	Initial steps towards large scale production of UK LOVA Thermoplastic Elastomer (TPE) propellants	Sowden	8B
20135	The Unknown Detonation Transition (XDT) Mechanisms Associated with Damaged Rocket Propellant Impacting a Surface: Understanding and Applications to IM	Pfeil	8B
20136	Subscale Testing to Predict Full-Scale Response to Fragment Impact in Solid Propellants	Neidert	9B
20137	MSIAC workshop 2018: Improved Explosives and Munitions Risk Management	Sharp	2A
20138	Qualification and Energetic Materials Challenges	Andrews	10B
20139	Correlation of Response for Munitions Containing RDX/TNT: Bullet Impact and EMTAP Tube Testing Results	Cheese	8A
20140	Reaction Mechanisms for Rocket Motors	Collet	7A
20141	Mitigation Technologies for Propulsion Applications	Collet	6A
20145	Property-processing implications in additive manufactured materials for munitions	Babcock	4B
20146	Age-related mechanical damage and ageing of munition materials	Babcock	9B
20147	Stopping km/s blunt fragments and limiting shock lensing with a new advanced energy absorbing composite	Tear	6A
20149	MSIAC – Highlights and Future Priorities	Sharp	1
20150	Heavyweight Torpedo warhead – IM assessment	Chaffois	10A
20151	Influence of ageing on the properties of IHE	Radies	10B
20152	Increased impulse of solventless extruded double base rocket propellant by addition of high explosives RDX and FOX-7.	Tunestål	8B
20153	Qualification of malleable plastic explosive hexomax and its application in a flexible linear shaped charge system	Songy	5B
20154	Sheet-metal Ammunition Packing Tray for Mitigation of Secondary Cook-off of Medium-caliber Ammunition	Little	6A
20155	New NTO workshop and associated product characterizations	Delage	4B
20156	NATO Working Group on Insensitive Munitions and Hazard Classification Requirements, Assessment and Hazard Frequency.	Cheese	1
20157	Development of a CONUS Manufacturing Capability for FOX-7	Sleadd	4B
20159	Development and successful demonstration of a lightweight, particle impact mitigation sleeve (pims) with specified hardness and perforation features	Pudlak	6A
20161	Filling the Gap between the Initiation Behavior of Shaped Charge Jets and Fragments	Arnold	9A
20163	Impacts of REACh, ITAR and other regulations on Energetic Materials Sustainability	Eck	10B
20164	New Polycarbonate-Based Thermoplastic Polyurethane Binder for HMX Based Explosives	Robertson	2B
20166	Particle size and surface area effects on the initiation of Diaminoazoxyfurazan (DAAF)	Francois	5B

ABSTRACT #	TITLE	AUTHOR	SESSION
20171	Melt-pour explosive formulation development featuring TNBA	Fung	5B
20172	MDNT: IM Melt-Phase Energetic Binder	Abbassi	5B
20174	Robust enhanced blast explosive manufacturing at holston army ammunition plant	Fung	4B
20179	Characterization of LX-14 FEM / PBXN-9 FEM High Energy Explosives	Alexander	4B
20180	Synthesis, Formulation, and Testing of 3,4-DNP	Morris	6B
20181	Improving knowledge of tactical rocket motor response under Insensitive Munition threats: BI, FI and FH Tests results of the research program	Bonhomme	10A
20182	Additive Manufacturing for Net Shape Munitions	Chelluri	7A
20183	Fragment Impact Testing of the XM25	Al-Shehab	3A
20188	IM Plans and JIMTP Future in the United States	Di Stasio	1
20228	Synthesis Development of Novel Energetic Ingredients	Headrick	6B
20233	Qualification of Explosives Formulations Manufacturers and Ingredient Manufacturers for US Navy Use	Kenyon	10B
20241	Effect of Insensitive HE on Shaped Charge Jets	Arnold	8A
20245	IM Characteristics of Large Diameter Extruded Double Base Rocket Motors with Composite Cases	Bellotte	10A
20249	U.S. Navy Insensitive Munitions Handbook	Ward	1
20258	Cost of Propane Fast Cook-Off Testing	Washburn	4A
20259	Fast Cook Off Modeling and Simulation	Yagla	9A
20260	Comparative Fire Response of Simulated Rocket Motors in Steel and Carbon Fiber Composite Missile Launching Canisters	Yagla	3A
20261	The DOTC Enterprise - Helping You Accelerate Technologies to the Field	Wilson	3B
20262	Radiant Chamber for Fast Cook of Testing and Simulation	Yagla	8A
20263	IM Technology for Stryker Tank Munitions	Eng	10A
20264	Insensitive Minimum Smoke Propellants	Deschner	8B
20265	Historical Review of Fragment Impact Standardization	Hunt	2A
20266	An Approach to Predict the Cook-off Response of Confined and Vented Full Scale Munitions Based on Small Scale Tests	Moussa	9A
20267	Insensitive Munitions Industry Contribution for New Stanag - AOP Edition of the Slow Heating Test	Guengant	4A
20268	An Explosive Fragment Projector for IM testing	Eliash	5A
20269	Thermal modeling of fast cook-offs	Graswald	9A
20271	Microfluidic synthesis of energetic materials	Scavuzzo	6B
20273	Explosive Ordnance Disposal (EOD) of Insensitive Munitions: Challenges and Solutions	Brousseau	5A
20274	New generation Influence Mine classified as 1.6N	Granqvist	7A

ABSTRACT #	TITLE	AUTHOR	SESSION
20275	Passing Sympathetic Reaction Responses in 500 and 1,000-lb General Purpose Bombs with AFX-770	Struck	5A
20276	PBXN-5 Mechanical Characterization and Proposed Constitutive Model	Peairs / Amborn	7B
20279	Scaling of Fast Cook Off Fires	Yagla	4A
20282	Insensitive munitions (im) gun propellant optimization efforts for medium caliber application	Liberatore-Moretti	9B
20289	Manufacturing of PAX-3 High Explosive	Swaszek	5B
20290	Electronic properties and Hirshfeld surface analysis of insensitive high energy density material Dihydroxylammonium 5,5'-bistetrazole-1,1'-diolate under compression	Abraham	7B
30000	International Sympathetic Reaction Testing Survey	Baker	9A

BIOGRAPHY



DR. CHRISTINE MICHIEZI

Senior Industrial Analyst, Missiles and Munitions
 OUSD(AT&L), Manufacturing and Industrial Base Policy

Dr. Michienzi began her career with the Department of Defense (DoD) at the Naval Surface Warfare Center, Indian Head Division, where she initially worked as a formulation chemist, developing new explosive and propellant formulations for DoD weapons systems, for which she holds five patents. She transitioned to program manager, establishing and leading the Navy's gun propellant development program, and eventually became the acting Research, Development, Test and Evaluation Department Head. She has also served

as the munitions technical expert for the Technical Director, Program Executive Office, Integrated Warfare Systems (PEO IWS) for Surface Ship Weapons.

She is currently in the Office of the Under Secretary of Defense for Acquisition Technology and Logistics (OUSD(AT&L)), where she has held several positions. She served as a munitions expert and the Insensitive Munitions (IM) lead for the DoD for the Deputy Assistant Secretary of Defense, Tactical Warfare Systems (DASD TWS) and is currently the Senior Industrial Analyst for Missiles and Munitions for DASD Manufacturing

and Industrial Base Policy (MIBP). Dr. Michienzi is responsible for assessing the health of the industrial base for all components of all DoD munitions, identifying issues and potential mitigation plans for senior OSD leadership. She also reviews acquisition strategies for new munitions and yearly DoD budget submissions to identify and work to solve any industrial base issues.

Dr. Michienzi received her Bachelor of Science degree in Chemistry from the University of Maryland, College Park (UMCP) and her Doctorate in Analytical Chemistry, also from UMCP.

TABLE TOP DISPLAYS



DEFENSE OPTIMIZATION INC.

Defense Optimization Inc. is a National Defense corporation - a Think Tank and a next-generation weapon-system group. Our mission is to serve as a catalyst for victory and world-wide peace, by fielding the best weapon systems known to man. We assess the performance of various classes of weapon systems and sub-systems, providing assistance to the Department of Defense and to weapon-system contractors.

Defense Optimization Inc's capabilities eliminate major root causes that prevent thoughtful weapon system conception, development, production, fielding and application. We mentor top weapon-system professionals and DoD agency leaders.

All current weapon systems are susceptible to a host of system instabilities (noises) which wreak havoc with weapon system performance in the field - whether that field includes

underwater, on the ground, in space, or across global and spatial electromagnetic spectrums.

Our team members have over 50 years combined experience in weapon-system conception and performance optimization.

The results of our efforts lead to:

- Lower system costs,
- Higher performance,
- Higher System reliability,
- Extended weapon-system lifetimes, and
- Capable systems for all environments.

Our Secret Sauce includes leading-edge conceptual, optimization and data tools, which we pass along to our partners.



DSIAC

The Defense Systems Information Analysis Center (DSIAC) is a component of the U.S. Department of Defense's Information Analysis Center (IAC) enterprise. Our organization's purpose is to provide information research and analysis for DoD and Federal government users to stimulate innovation, foster collaboration, and eliminate redundancy. DSIAC's mission is to generate, collect, analyze, synthesize, and disseminate Scientific and Technical Information (STI) to DoD and Federal government users and industry contractors. The scope of DSIAC includes nine subject areas, six of which were part of the legacy DoD IAC operations: Advanced Materials; Energetics; Military Sensing;

Reliability, Maintainability, Quality, Supportability, Interoperability (RMQSI); Survivability and Vulnerability; and Weapon Systems; plus three more focus areas of Autonomous Systems; Directed Energy; and Non-lethal Weapons.

DSIAC is chartered to become the premier information research partner and curator of technology advancements and trends for the defense systems community. Our website is www.DSIAC.org where you can find the DSIAC Digest, published twice-monthly, for the latest news and technical articles, and the quarterly DSIAC Journal of technical publications. Requests for STI and literatures searches can be submitted through our website



NTS

For more than a half-century, NTS has been a trusted partner to the Department of Defense, U.S. military, defense industry, aerospace, and other industries; providing comprehensive services and testing. Our network of national and international labs offer:

- Engineering services
- Extreme & combined environmental & dynamics testing
- Single location insensitive munitions & hazard classification testing
- Transportation & packaging safety testing
- Mechanical stress, strain & function testing
- Performance, safety & functional testing
- Static & dynamic firings of weapons & ordnance
- Body armor & firearm safety
- Function & reliability testing

- Integrated program management, planning & procedures

Within our facilities or on a customer’s site, we integrate into each client’s internal team. From technical expertise and exclusive accreditations, to an extensive physical infrastructure and engineering excellence, NTS is adept at maximizing quality and efficiency across our extensive customer base.

Our defense laboratories maintain multiple contract levels with the government, strictly adhere to National Industrial Security Operating Manual (NISPOM) regulations, and are accredited to a wide range of regulatory standards, including MIL-STD-810, MIL-STD-461, MIL-STD-2105, MIL-DTL-901E, MIL-STD-167, MIL-STD-120, MIL-STD-248, MIL-STD-516 and MIL-STD-767.

NTS also provides many related services, supporting all phases of customer-defined engineering projects that require a range of specialized services.



ORBITAL ATK

Orbital ATK is a global leader in aerospace and defense technologies. The company designs, builds and delivers space, defense and aviation systems for customers around the world, both as a prime contractor and merchant supplier. Its main products include launch vehicles and related propulsion systems; missile products, subsystems and

defense electronics; precision weapons, armament systems and ammunition; satellites and associated space components and services; and advanced aerospace structures. For more information, visit www.orbitalatk.com.

SPONSOR DESCRIPTIONS



BAE SYSTEMS OSI

Headquartered in Radford, Virginia, BAE Systems Ordnance Systems Inc. (OSI) operates the Holston and Radford Army ammunition plants in support of U.S. Department of Defense (DoD) and commercial requirements. In addition to production, OSI provides a host of ammunition related services including modernization program management, inventory management, and energetics research and development.

Holston Army Ammunition Plant is the single source for U.S. DoD high explosives. Portfolio product mix includes RDXs, HMXs, IMXs, and PBXs. Radford Army Ammunition Plant is the single source for high-volume U.S. DoD Nitrocellulose /

Propellants. Portfolio product mix includes Nitrocellulose, single-base propellants, multi-base propellants and rocket propellants.

OSI is an innovation leader in next generation explosives and propellants development thru its robust IR&D program. OSI is an active supporter of U.S. DoD and commercial product development through a wide variety of CRAD programs. In addition, OSI has provided total Program Management for all modernization projects conducted at its two ammunition plants. This extensive program includes modernization planning, project management, design, construction, and prove-out of a wide variety of projects.



ORBITAL ATK

As battlefield threats evolve, our warfighters need the best tools and technologies to successfully execute their missions safely. The U.S. Army Aviation and Missile Research Development and Engineering Center (AMRDEC) has leaned forward in maturing insensitive munitions (IM) technology and delivering it to the front line where the threats are high. With the recent introduction of IM technology to Orbital ATK's rocket motors for the Guided Multiple Launch Rocket System (GMLRS) and HELLFIRE® missiles – among the first rocket motors ever to fully integrate IM technology – our nation is taking a major step in meeting new standards of weapon safety.

A common misconception is that new technology requires a complete overhaul. To the contrary, Orbital ATK's IM rocket motor technology can be tailored to fit both new and existing tactical systems affordably. In fact, Orbital ATK has successfully

introduced all the safety benefits of IM technology to the rocket motors without significantly changing the current design of legacy systems without sacrificing effectiveness or performance.

Orbital ATK is proud to serve the warfighter. That responsibility drives our team to invest, improve and innovate. This summer, the company will expand its capabilities at the Allegany Ballistics Laboratory (ABL) in Rocket Center, West Virginia when it opens its new Large Tactical Motor Manufacturing Facility specializing in high efficiency manufacturing of IM-compliant motors. Looking ahead, Orbital ATK will continue to develop and qualify similar rocket motor technology for other military applications, fielded systems and next generation upgrades to improve the strength of our armed forces.

Learn more about our IM technology at www.OrbitalATK.com



AEROJET ROCKETDYNE

Making munitions that are safer for our warfighters to handle is a shared goal of the military and industry. Aerojet Rocketdyne has an extensive history in developing insensitive munition solutions for both warheads and rocket motors. Our insensitive munitions and energetic materials solutions provide an increased margin of safety for our men and women who are deployed across the globe to protect the interests of America and its allies.

- Capabilities include:
- Tailored insensitive energetic formulations for warheads and rocket motors
- Innovative solutions to make systems meet IM criteria
- Composite case manufacturing
- Insensitive munitions mitigation methods
- Modeling and simulation
- Small-scale development testing
- Insensitive munitions tests per NATO STANAGS
- Production of components and systems for government and industry customers worldwide

Aerojet Rocketdyne is an innovative company delivering solutions that create value for its customers in the aerospace and defense markets. The company is a world-recognized aerospace and defense leader that provides propulsion and energetics to the space, missile defense and strategic systems, tactical systems and armaments areas, in support of domestic and international markets. Additional information about Aerojet Rocketdyne can be obtained by visiting our websites at www.Rocket.com and www.AerojetRocketdyne.com.

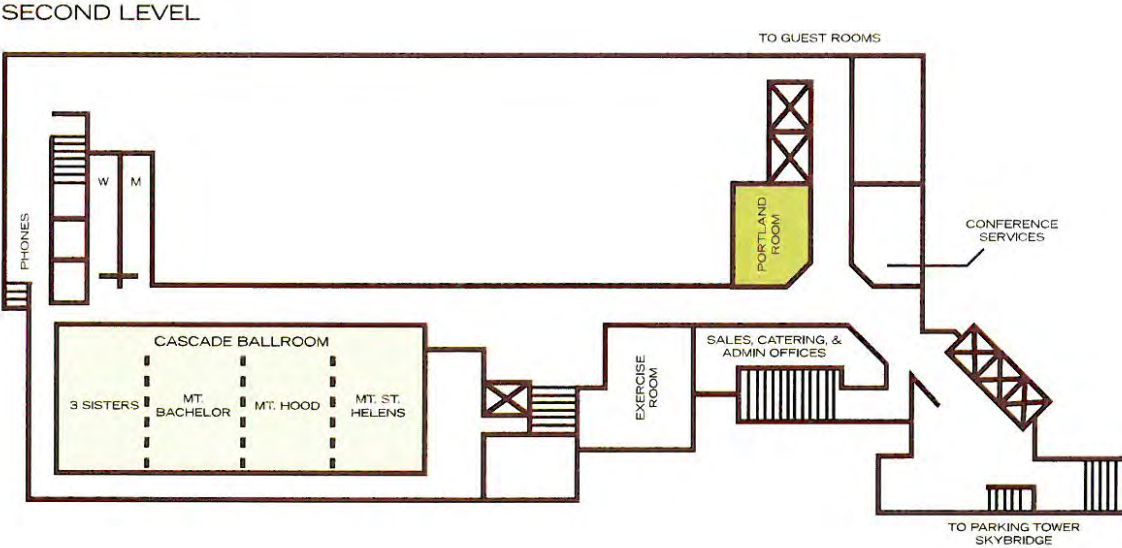
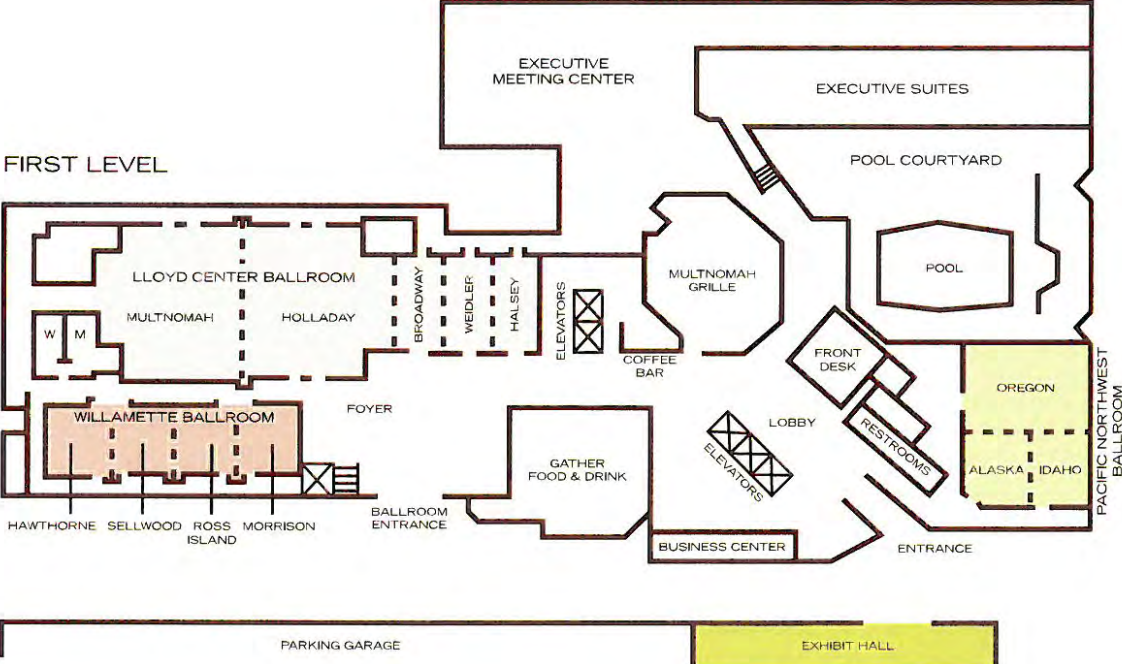
Corporate Contact:

Jared Holt, Director, Contract Administration
E-mail: Jared.Holt@Rocket.com
Telephone: (256) 922-2575

Technical Contact:

Kenneth J. Graham, Engineering Fellow
Insensitive Munitions and Explosives
E-Mail: Ken.Graham@Rocket.com
Telephone: (540) 854-2182

VENUE MAP



THANK YOU TO OUR SPONSORS

BAE SYSTEMS

I N S P I R E D W O R K



NOTES

A series of horizontal lines for writing notes, consisting of 20 evenly spaced lines.

SAVE THE DATE

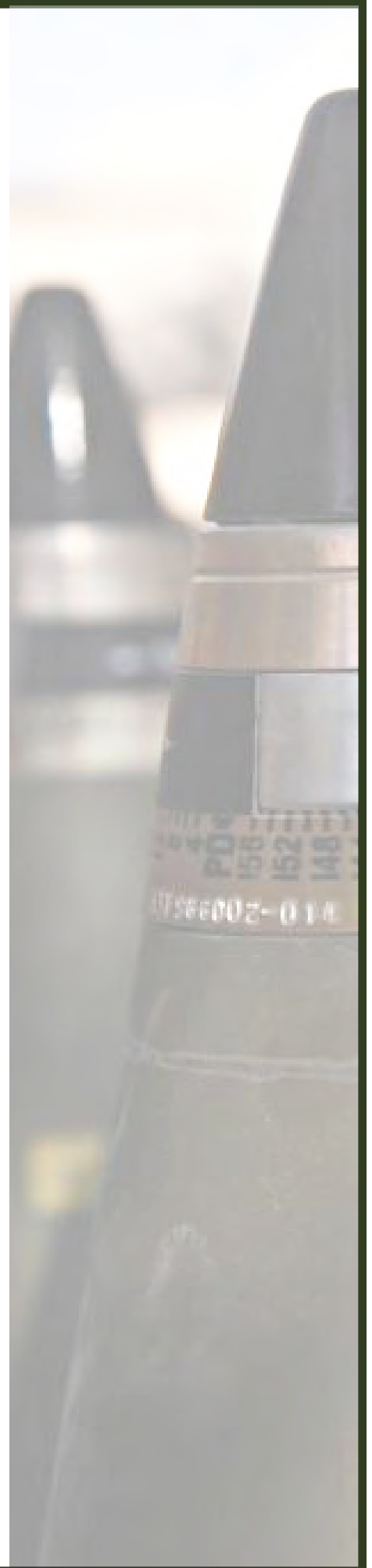


2019 IMEMTS

Fall 2019

Spain

NDIA.org/Events





A New IMI Systems Less Sensitive Brisant Explosive Composition

G. Strul, A. Maish, I. Mandel

04 2018 IMEMTS, Portland, OR



MEETING YOUR TARGETS

Outline of the presentation:

- IMI Systems Introduction.
- Objectives.
- Approach.
- Qualification Protocol.
- Test results of the qualification process.
- Summary.



IMI Systems



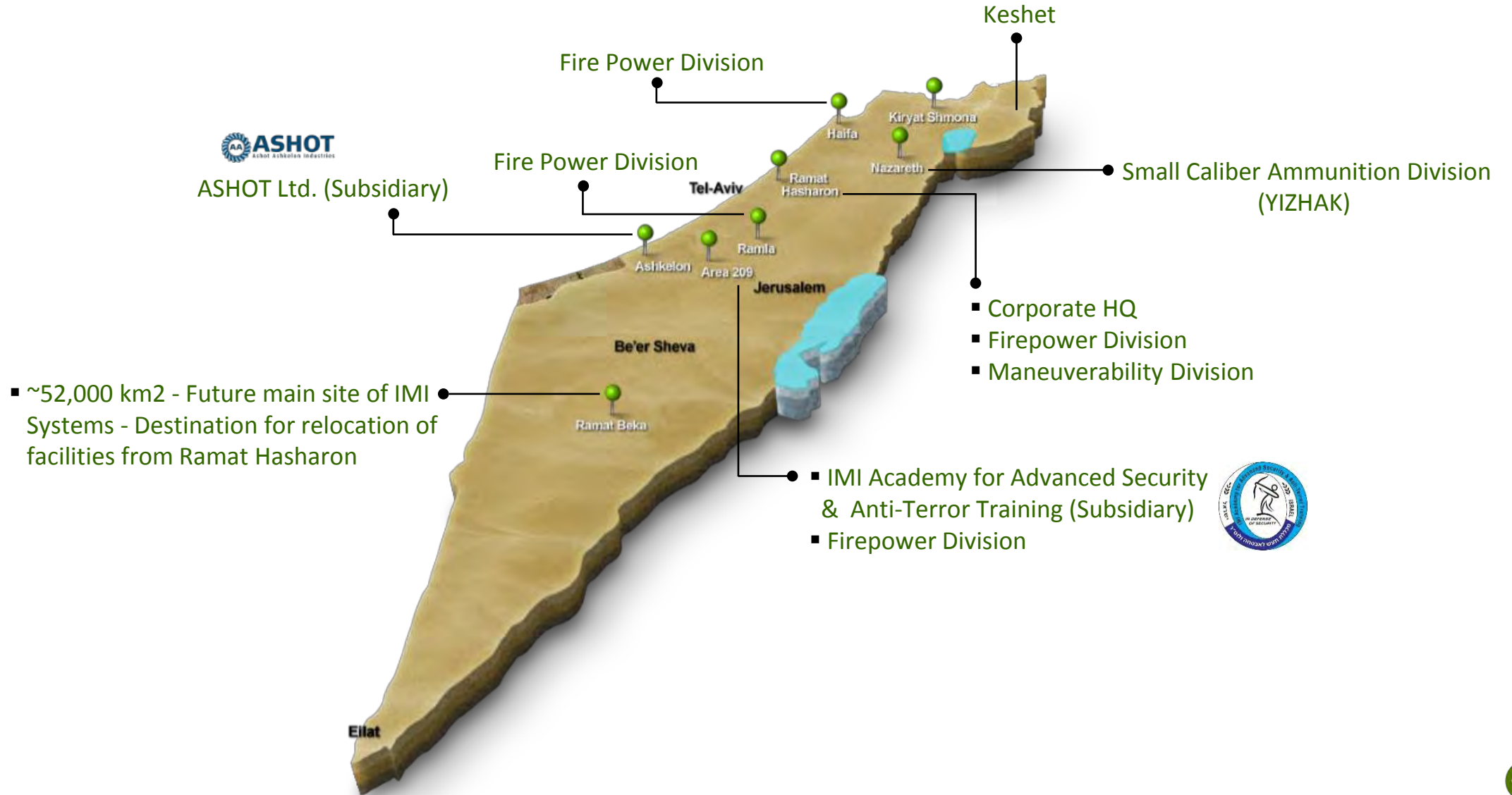
Vision

To be a world class leading defence company, providing cutting edge systems and solutions for Land, Air and Naval forces

In 1 Jan 2016, IMI transferred its core business activities, assets, obligations, rights and its employees, to IMI Systems Ltd.

- an Israeli company wholly owned by the State of Israel

IMI Systems Locations



Objectives

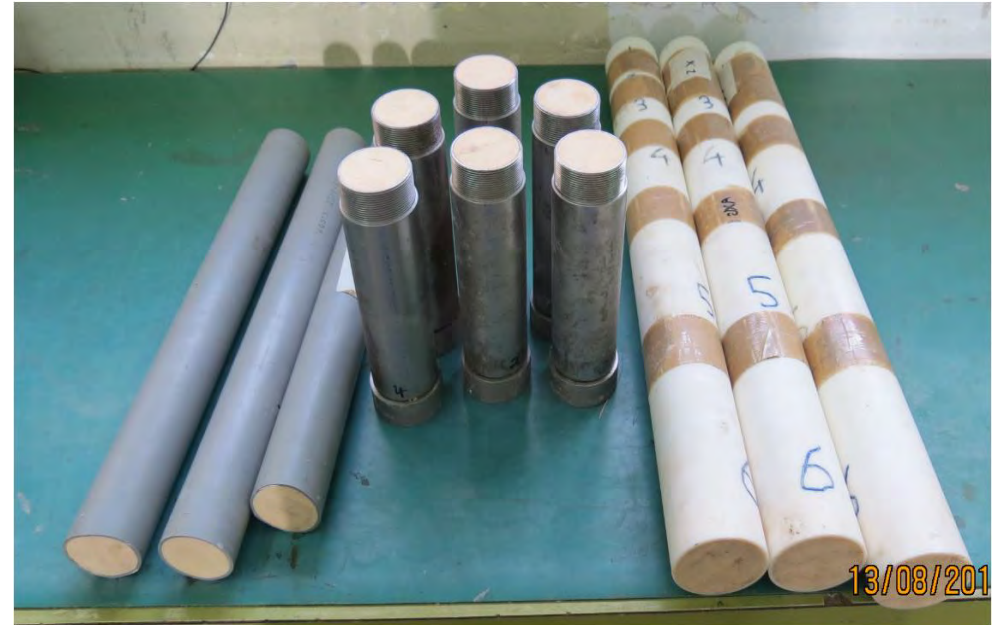
- *The objective of this task was to introduce a new brisant HE composition with high fragmentation features and an output greater than that of PBXN-109.*
- *Qualify the new composition for the IDF using CLX-663s* as a reference.*



* CLX-663S – IMI Systems analog to PBXN-109

Approach

- ❑ *Identify PBXN-110 as the target composition.*
- ❑ *Develop an HMX based IMI systems' composition analogous to PBXN-110.*
- ❑ *Configuration of the production process for this composition.*
- ❑ *Characterization and Qualification of the composition according to IDF standard and protocol, based upon STANAG 4170.*



Qualification Protocol (Partial)

- *Hazard analysis – Friction, Impact, ESD*
- *Vacuum stability*
- *Thermal analysis*
- *Mechanical properties*
- *Accelerated aging*
- *Detonation velocity and critical diameter*
- *Additional tests : Bullet Impact*

LSGT

Cap test

Small external burning test

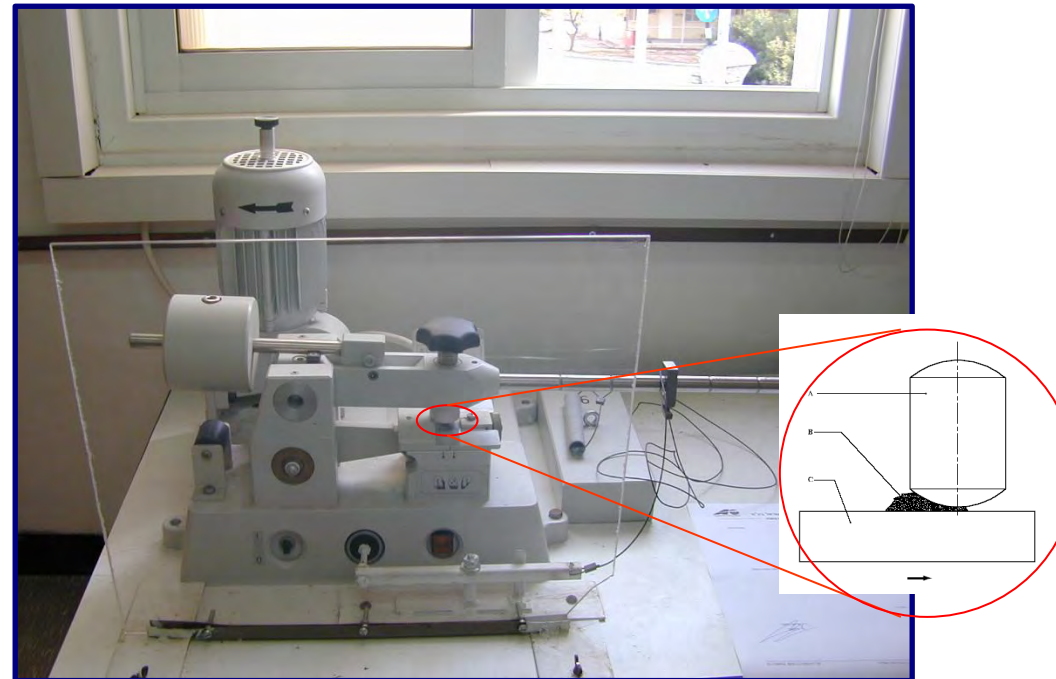
CLX-881 qualification protocol was dictated by IDF - based upon STANAG 4170

Hazard Characterization - Friction Sensitiveness

IDF Requirement: 6/6 consecutive negative tests.

Method: BAM Friction Machine, Stanag 4487 Annex A, MIL-STD-1751 Method 1024

Results : 6/6 consecutive negative tests - no reaction at 36 Kg F for both CLX 881 and CLX 663s



* CLX-663S – IMI Systems analog to PBXN-109

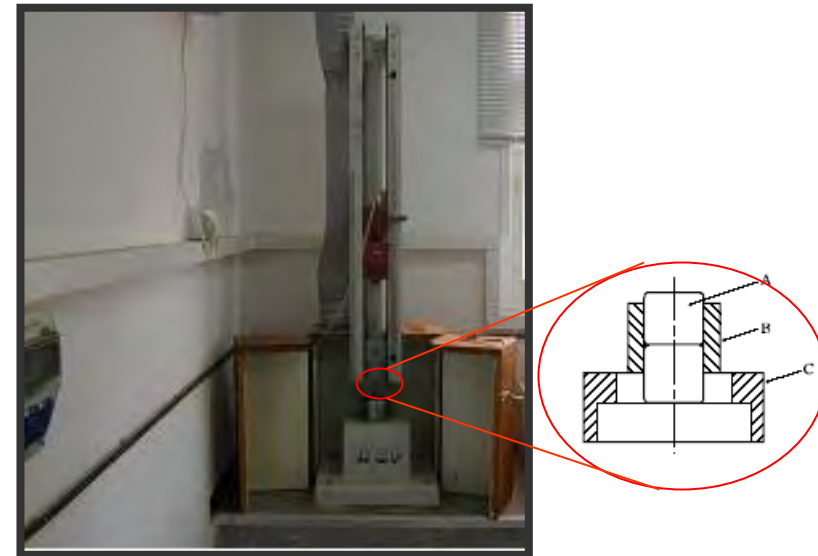
Hazard Characterization - Impact Sensitiveness

IDF Requirement: $E_{50\%} \geq 5$ joule for secondary explosive .

Method: Bam Impact Machine, Stanag 4489, Annex C

Results : $E_{50\%} \geq 5$ joule, less sensitive than CLX 663s

Explosive	Energy [Kg m]	H _{50%} [cm]
CLX-663s	2.92	58.4 (5 kg)
CLX-881	4.00	80.0 (5 kg)



* CLX-663S – IMI Systems analog to PBXN-109

Hazard Characterization - ESD Sensitiveness

IDF Requirement: 20/20 No Fires at 0.25 J

Method: MIL-STD-1751 Method 1032

Results : 20/20 consecutive negative tests - no fires at 0.25 J for both CLX 881 and CLX 663s



Vacuum Stability

IDF Requirement: Less than 1 ml/gr.

Method: Stanag 4556, MIL-STD-1751 Method 1061

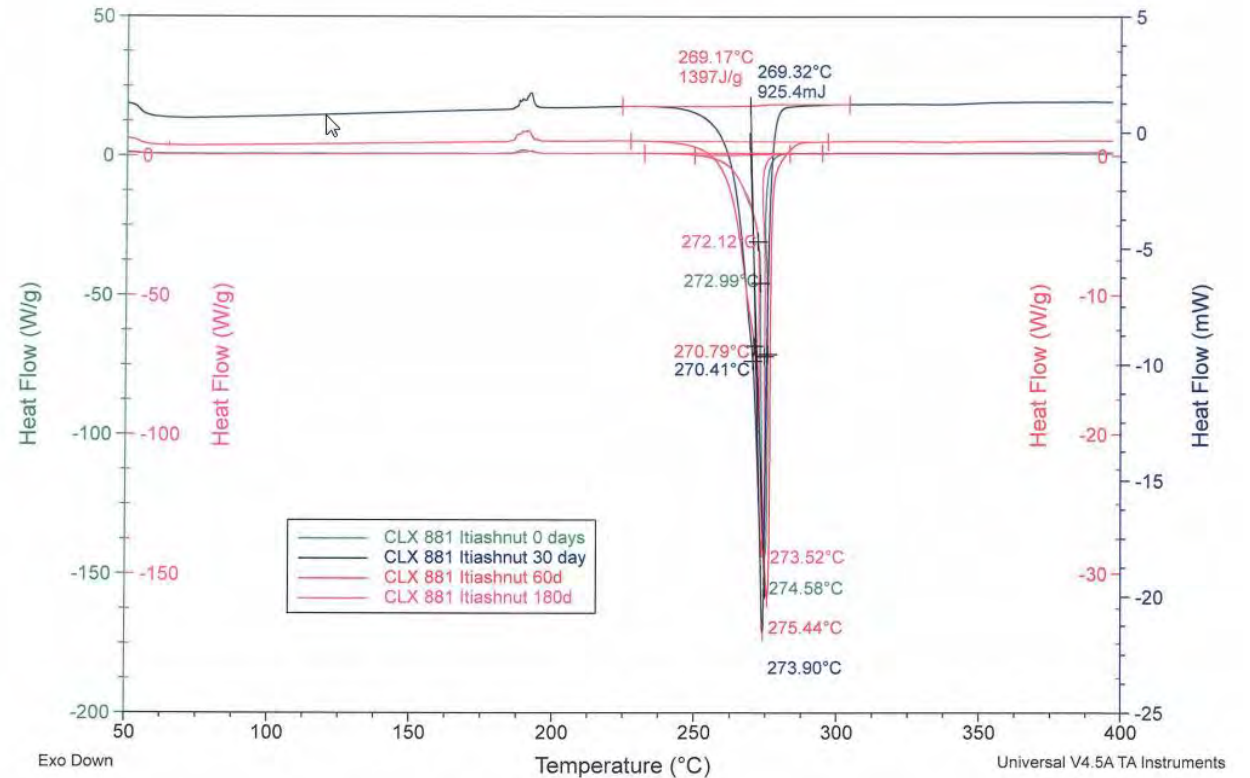
Results:

Explosive	Volume/gr (ml)	IDF Req.
CLX-663s	0.05	Less than 1 ml/gr
CLX-881	0.21	

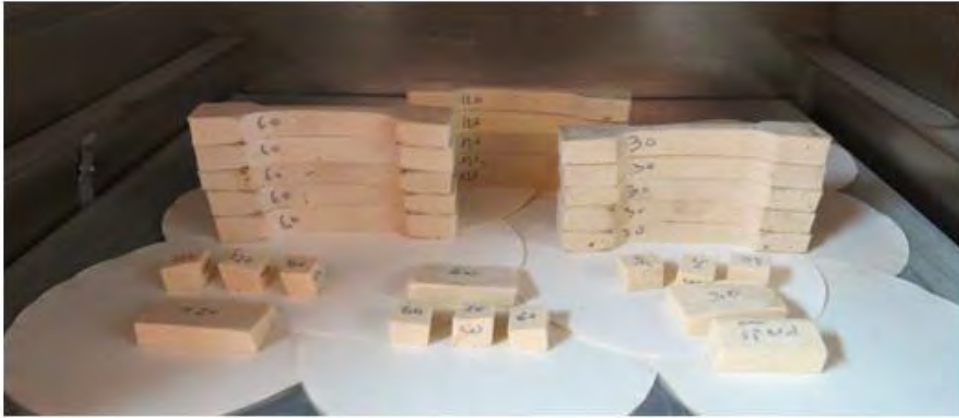
Thermal Analysis : Self Ignition Temp. and Thermal Stability

Method: Stanag 4515

Explosive	Self ignition temp. [°C]
CLX-663s	220.2
CLX-881	273.0



Accelerated Aging - Mechanical properties



Aging (d)*	Hardness [Shore A]	Stress at Max. Load [kg/cm ²]
0	21	1.548
30	34	2.105
60	46	3.223
180	71	6.599

* According to IDF protocol

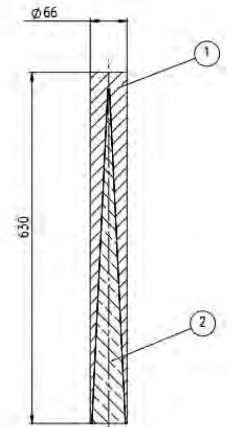


Detonation Velocity & Critical Diameter

Method: MIL-STD-1751 Method 1101



Method: MIL-STD-1751 Method 1091



Explosive	Detonation Velocity [m/sec]	Critical Diameter [mm]
CLX-881	8427	9.7
CLX-663s*	7600	10.3

* CLX-663S – IMI Systems analog to PBXN-109

Bullet Impact

Requirement: Up to moderate reaction – type V.

Method: TB 700-2 Chapter 5-8 (UN Test 7 (d))

Results : 2/6 Explosive scattered.

4/6 Explosive burned moderately inside the tube.



Test setup



Test Results

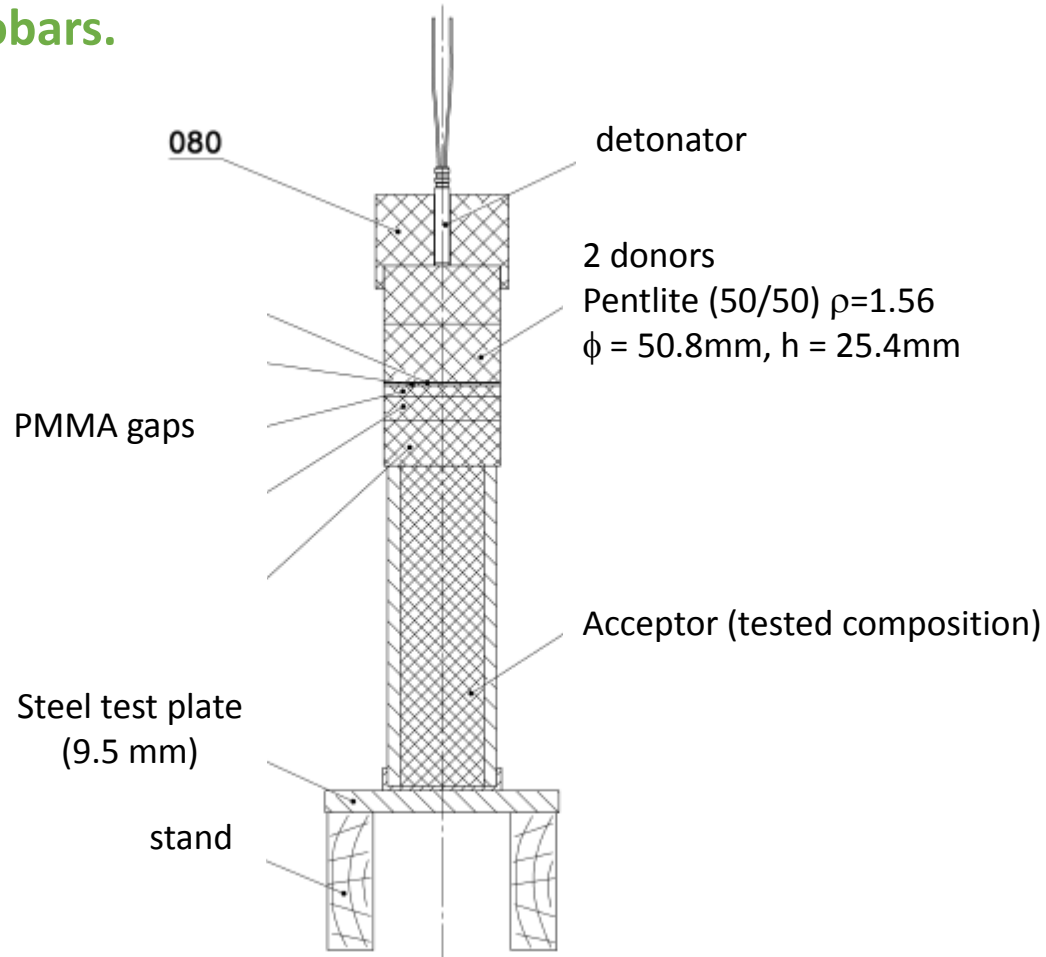


Type V reaction

NOL LSGT - Large Scale Gap Test

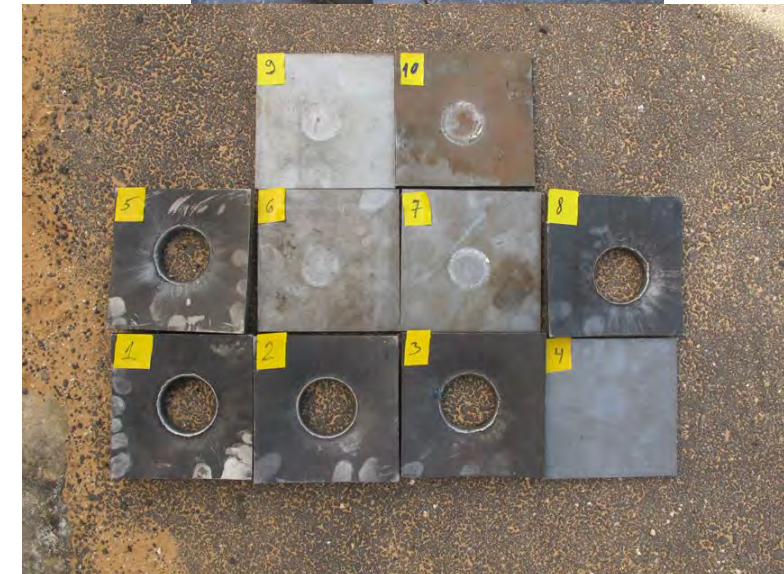
Method: MIL-STD-1751A Method 1041

Results : **34 Kilobars.**



Test results of the qualification process

Test setup



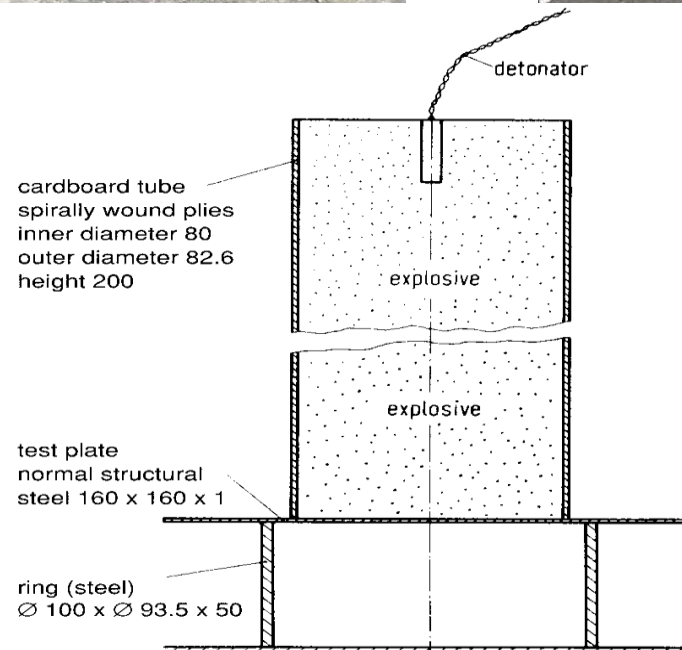
NOL LSGT Results – MIL-STD-1751A

Explosive	Cards	Kilobars
CH-6 (pressed)	267	11
Comp A3 (cast)	242	13.8
Comp B (cast)	201-220	16.9-20.5
Comp C-4	192	22.8
H-6 (cast)	197	21.5
LX-14	199	21
OCTOL 85/15	236	14.5
PBXN-7	217	17.4
PBXN-9	166-201	20.5-31.4
RDX	323	7.4
TATB	78	66.1
PBXN-110 (Cast)**	154-178	27.0-36.8
CLX-663S (cast) ***	178	27
CLX-881(cast) ***	160	34

*** Current study

** High Performance Polymer-Bonded Explosive Containing PolyNIMMO for Metal Accelerating Applications / R. Hollands, V. Fung and K. Burrows, IMEMTS 2014

Cap Sensitivity – CLX-533



Presented at IMEMTS 2009

CLX-881 'Cap Test'

Test results of the qualification process



Test setup

detonator

Test Results



CLX-881 cannot be classified as EIDS

CLX-881 - Tests results Summary

HMX based PBX explosive with an HTPB inert binder

Test	CLX-881	CLX-663s*
Vacuum Stability (ml)	0.21	0.05
Autoignition Temp. (°C)	273.0	220.2
ESD (5 KV up to 0.25 j)	No reaction	No reaction
Impact Sensitivity (L ₅₀ %, Bruetone Method)	4.00 Kg•m	2.92 Kg•m
Friction Sensitivity	No reaction (max 36 kgf)	No reaction (max 36 kgf)
Detonation Velocity	8427 m/sec ($\rho=1.66$)	7600 m/sec ($\rho=1.64$)
Critical Diameter (mm)	9.7	10.3

CLX-881 qualification protocol was dictated by IDF - based upon STANAG 4170

* CLX-663S – IMI Systems analog to PBXN-109

CLX-881 Tests results

Test	CLX-881	CLX-663s*
Small external burning test [UN Test Series 3(d)(i)]	Type V reaction (moderate burning)	Type V reaction (moderate burning)
Bullet impact (Stanag 4241)	Type V reaction	Type V reaction
NOL LSGT (MIL-STD-1751A Method 1041)	34 Kilobars	27 Kilobars
Cap Test	reaction	reaction

* CLX-663S – IMI Systems analog to PBXN-109

Thank you for listening !



US Navy Insensitive Munitions (IM) Munitions Reaction Evaluation Board (MREB)

Ken Tomasello
Insensitive Munitions Office
Naval Ordnance Safety and Security Activity
Indian Head, MD

Heather Hayden, PhD
Naval Surface Warfare Center Indian Head Explosive Ordnance Disposal
Technology Division
Indian Head, MD

ABSTRACT

In August 2017, the Naval Ordnance Safety and Security Activity (NOSSA) issued NOSSA Instruction (NOSSAINST 8010.1A, Munitions Reaction Evaluation Board (MREB). This instruction is an update to the original NOSSAINST 8010.1 of July 2009 which created the US Navy unified board for scoring Insensitive Munitions (IM), Hazard Classification (HC) and basic safety tests. The guidance provided by this instruction ensures consistent evaluation of ordnance hazard assessment test plans and scoring technical performance (i.e., test/no-test and reaction level) of hazard testing in support of IM compliance, HC and Weapon System Explosive Safety Review Board (WSESRB) review processes for munitions. NOSSAINST 8010.1A clarifies and updates the operating philosophy of the MREB including: Leadership, Membership, Meetings, Authority and Responsibility, and Documentation for the Board. This paper describes the background of formation of the unified US Navy board, reviews the applicability of the instruction and provides highlights from the instruction.

INTRODUCTION

OBJECTIVE

The objective of this paper is to inform the international Insensitive Munitions (IM) and Munitions Safety communities on the US Navy Munitions Reaction Evaluation Board's (MREB) mission, authority, responsibility, and membership. The MREB's mission is:

- (1) provide guidance and recommendations for the proper design and conduct of ordnance hazard assessment testing
- (2) provide evaluation of ordnance hazard assessment test plans
- (3) provide scoring of technical performance (i.e., test/no-test and reaction level) of hazard testing in support of Insensitive Munitions (IM) compliance, Hazard Classification (HC), and Weapon Systems Explosives Safety Review Board (WSESRB) review processes for munitions.

BACKGROUND

Since the implementation of the IM policy by the Chief of Naval Operations (CNO) in 1984, IM issues have received increasing attention within the Department of Defense (DoD). As an example, in 2006, the Joint Requirements Oversight Council (JROC) established Standardized IM tests and then in 2010 The Office of the Secretary of Defense (OSD) established the Joint US IM test standards and passing criteria. The Joint US IM test standards are based on the NATO AOP-39, Ed.2 policy document which provides the guidance on IM and HC assessment and testing. In its execution of IM policy and procedures, OSD continues to strive to harmonize IM and HC test requirements. Weapons system programs are frequently Joint Service programs or the weapons are operating in a Joint Warfighter Environment. Therefore, Joint safety requirements are becoming more important to implement and evaluate. With the increased levels of Joint oversight, it is imperative that the DON has one single authority for the review of weapons systems test plans and results for compliance with safety, IM, and HC requirements. Standardized criteria must be applied to munitions reactions during internal reviews prior to presentations to external review boards. In 2008 a decision was made by NOSSA that the three Navy scoring boards would be consolidated into one board. A new Navy Instruction NOSSAINST 8010.1 established policy that brought together the Ordnance Hazards Explosive Board (OHEB- NAWCWD China Lake), the Insensitive Munitions Board (IMB – NSWC Dahlgren) and the Insensitive Munitions Board (IMB – NSWC Crane) to form the MREB. The instruction was finalized in late 2009 and the MREB officially began operating in January 2010. The board has operated effectively since its inception. The MREB board members are

comprised of Subject Matter Experts (SME) from IM, HC and basic safety testing. The MREB has provided the board members an environment to learn from the strengths of the members from each of the three sites. A recent update to the instruction was made in 2017 which clearly reflects how the board currently operates. This paper reflects the most current revision of the instruction.

MREB PHILOSOPHY

The MREB convenes either in person or by video/web/teleconference at a DON Warfare Center. The Lead Chairperson will coordinate the meeting time and location with the MREB Site Chairperson's and voting members. Attendance by the full membership at every meeting is encouraged, either in person (if required) or by video/web/teleconference, so that judgments are consistently rendered independent of the meeting location, program, sponsor, or test activity.

Leadership

The Leadership of the MREB consists of a Lead Chairperson, Site chairperson and Vice chairperson described as follows:

Lead Chairperson: A Lead Chairperson shall be nominated from the current Site Chairpersons by the DON Warfare Center appropriate Department/Director Head and concurred with by the Naval Ordnance Safety and Security Activity (NOSSA). The Lead Chairperson will provide overall direction for the MREB. This position will rotate among the sites every two years.

Site Chairperson: Each DON Warfare Center location will have a Site Chairperson nominated by their appropriate Department/Director Head and concurred with by NOSSA.

Vice Chairperson: A Vice Chairperson will be selected by each Site Chairperson and will act as an Alternate Chairperson if the Lead Chairperson cannot attend.

Membership

The MREB membership is defined as follows:

Voting Members: Membership of the MREB shall include individuals with expertise related to munitions development, IM requirements, HC requirements, ordnance technology, and test and evaluation technologies and methods. Potential members will be nominated in writing by their parent organization to NOSSA for approval.

Executive Secretary: Executive Secretaries will be appointed by the Lead Chairperson to coordinate MREB meetings at their respective location. The Executive

Secretary will also be responsible for meeting minutes, summarizing the Board's findings, summarizing and distributing MREB comments on test plans to NOSSA, and distributing the minutes and findings for review and approval.

Ad Hoc Members can be voting or non-voting as follows:

Voting Members: The MREB can appoint technical specialists, special appointees, as ad hoc voting members to advise the board with unique cases.

Non-voting Members:

(a) The Site Chairperson can appoint technical specialists as ad hoc members for the consideration of unique cases.

(b) NOSSA and/or PEOs/PMs may be ad hoc non-voting members as necessary.

Meetings

The MREB meetings are conducted as required and typically once per month. The MREB maintains records of all of the meetings. Meetings are only called when a quorum is present. Although consensus is preferred, rulings can be made on a two-thirds majority. If a two-thirds majority does not exist for a ruling, then the Site Chairperson will assign representatives to write majority and minority opinions. The Site Chairpersons will review the test data and opinions and provide a recommendation to the Lead Chairperson, who will issue a final ruling.

The following conditions must be met for a quorum to exist:

- (a) At least six members are present
- (b) The goal is to have representation from each site; however this requirement may be waived upon agreement of the Site Chairpersons.
- (c) A site Chairperson or Vice Chairperson is present.

Program Offices will arrange meetings with the appropriate Chairperson and Executive Secretary. Each Site Chairperson will schedule meetings as required. The Executive Secretary will notify all members preferably at least four weeks before a meeting is held on a particular topic, and will instruct the Program Offices where to send test data. Test data for review must be received by the membership preferably at least ten working days before the meeting is held.

Authority and Responsibility

Weapons Program Offices submit their Point of Contact (POC) and detailed test plans, to include a full detailed description of the test item configuration(s) and test method(s), on the NOSSA Web Site via the NOSSA Test Plan Submission Tool. The

detailed test plan will be in concert with the NOSSA Weapons Assessment Directorate (NOSSA N8) approved Threat Hazard Assessments (THA), if applicable, and the System Safety Program Plan. If the test is for an official score and not for developmental purposes, it is important that the program receive concurrence on the detailed test plan from NOSSA N8 before testing may proceed. It is also recommended that even the plans for developmental tests be reviewed prior to each test or test series. If the test plan includes harmonized IM and HC tests, a DoD Explosives Safety Board (DDESB) concurrence may be necessary for those tests being used for HC. DDESB concurrence would be required if the test plan deviates from TB 700-2. In these cases, the tests for HC shall not proceed until the DDESB concurrence is received.

Weapons Program Offices must submit test results to MREB for review in order to obtain an assessment of official score. For engineering assessments, it is not necessary for Weapons Program Offices to submit test results to MREB for review. However, where appropriate, Weapons Program Offices may submit test assessments with IM scores based on engineering analysis of engineering level tests, modeling, comparison to like items, etc., to obtain official assessments.

MREB Responsibilities as follows:

- (1) Will provide a response to the Program Office within 30 days of receiving the detailed test plan, test results and test assessments.
- (2) Will provide recommendation for approval of test plans to be sent to NOSSA, which will coordinate as necessary within NOSSA for final approval.
- (3) Will evaluate the results of ordnance hazards assessment tests including both IM and Basic Safety Tests in accordance with MIL-STD-2105D and provide an official assessment of record of the reactions.
- (4) Will report its findings/recommendations and corroborating information, within 15 working days, to NOSSA N8, who will obtain official NOSSA concurrence before sending to requesting Program Office. Gross safety anomalies will be reported immediately.

NOSSA Responsibilities as follows:

- (1) Will provide concurrence on the appointments of Lead Chairpersons and Site Chairpersons.
- (2) Will render a decision on final approval with MREB recommendation for approval of test plans and findings/ recommendations within 10 business days of receipt. If NOSSA does not approve the test plan or findings/recommendations, the reason(s) will be provided to the MREB.
- (3) Will provide the detailed procedures for obtaining approval of test plans and for presenting test results to the Board.

- (4) Will publish an MREB Process Guide and Reporting Format.
- (5) Will provide test plan submittal guidelines.

Documentation:

NOSSA (N8) will agree on and promulgate a common format for test plans, presentations to the Board, and Board findings. The Chairpersons and NOSSA will ensure that all records are accounted for and accessible by current and future programs.

CONCLUDING REMARKS

NOSSA has created an updated NOSSA Instruction which clearly defines the duties and responsibilities of the US Navy MREB. The MREB scores IM, HC and basic safety tests that ensures consistent evaluation of ordnance hazard assessment test plans and scoring technical performance (i.e., test/no-test and reaction level) of hazard testing. The MREB supports IM compliance, HC and Weapon System Explosive Safety Review Board (WSESRB) review processes for munitions in accordance with the current NATO and US standardized tests.

As the US/NATO IM/HC/basic safety tests, procedures and requirements evolve, NOSSA will continue to maintain/update the MREB instruction.

The US Navy's MREB instruction is a proven model of cooperation and consistency for a unified board for scoring IM, Hazard Classification (HC) and basic safety tests.

ACKNOWLEDGEMENTS

The Naval Ordnance Safety & Security Activity sponsored the development of the NOSSA INSTRUCTION 8010.1A "Munitions Reaction Evaluation Board" and the preparation and presentation of this paper.

REFERENCES

1. MIL-STD-2105D, **Military Standard, Hazard Assessment Tests for Non-Nuclear Munitions**, 30 October 2013.
2. NAVSEAINST 8010.5C, **Insensitive Munitions Program Planning and Execution**, 15 September 2015.
3. TB 700-2/NAVSEAINST 8020.8B/TO 11A-1-47/DLAR 8220.1, Joint Technical Bulletin, **Department of Defense Ammunition and Explosives Hazard Classification Procedures**, 5 January 1998.
4. JROCM 235-06 **Insensitive Munitions Standards and Passing Criteria**, 6 November 2006
5. NATO AOP-39, Ed 2, **Guidance on the Assessment and Development of Insensitive Munitions (IM)**, March 2010.
6. OUSD Memorandum, Subject: **Joint Insensitive Munitions Test Standards and Compliance Assessment**, 1 February 2010.
7. JROCM 102-05, **Safe Weapons in Joint Warfighting Environments**, 20 May 2005

APPENDIX

APPLICABLE SPECIFICATIONS AND STANDARDS

MIL-STD-2105D	Hazard Assessment Tests for Non-Nuclear Munitions, 19 April 2011.
TB700-2	Joint Technical Bulletin, Department of Defense Ammunition and Explosives Hazard Classification Procedures, 5 January 1998.
NATO STANAG 4439	Policy for Introduction, Assessment and Testing for Insensitive Munitions (MURAT), Edition 3. 17 March 2010.
NATO STANAG 4240	Liquid Fuel/External Fire, Munition Test Procedures, Edition 2. 15 April 2003.
NATO STANAG 4382	Slow Heating Munitions Test Procedures, Edition 2. 15 April 2003.
NATO STANAG 4241	Bullet Impact, Munition Test Procedures, Edition 2. 15 April 2003.
NATO STANAG 4496	Fragment Impact Munitions Test Procedure, Edition 1, 13 December 2006.
NATO STANAG 4396	Sympathetic Reaction Munition Test Procedures, Edition 2. 15 April 2003.
NATO STANAG 4526	Shaped Charge Jet, Munitions Test Procedure, Edition 2, 10 December 2004
NATO STANAG 4375	Safety Drop Munition Test Procedure, Edition 3. 15 June 2010.
NAVSEAINST8020.8C	Department of Defense Ammunition and Explosives Hazard Classification Procedures, 30 July 2012.

NAVSEAINST 8010.5C

Insensitive Munitions Program Planning and
Execution, 15 September 2015.

US Navy Insensitive Munitions (IM) Munition Reaction Evaluation Board (MREB)



Presented by Ken Tomasello

NOSSA

Indian Head, MD

Distribution Statement A: Approved for public release; distribution is unlimited



Acknowledgements

Co-author
Heather Hayden, PhD

Distribution Statement A: Approved for public release; distribution is unlimited



Outline

- **BLUF**
- **Background**
- **MREB Philosophy**
- **MREB Leadership**
- **MREB Membership**
- **MREB Meetings**
- **MREB Authority and Responsibility**
- **MREB Responsibilities**
- **NOSSA Responsibilities**
- **Concluding Remarks**

Distribution Statement A: Approved for public release; distribution is unlimited



BLUF

Paper

To inform the Insensitive Munitions (IM) and Munitions Safety communities on the US Navy Munitions Reaction Evaluation Board's (MREB) mission, authority, responsibility and membership.

Mission

- To provide guidance and recommendations for the proper design and conduct of ordnance hazard assessment testing;
- Provide evaluation of ordnance hazard assessment test plans
- Provide scoring of technical performance (i.e. test/no test and reaction level) of hazard testing in support of IM compliance, Hazard Classification (HC) and Weapons Systems Explosive Safety Review Board (WSESRB) review processes for munitions

Distribution Statement A: Approved for public release; distribution is unlimited



Background

- Joint Requirements Oversight Council (JROC) established joint US Standardized IM tests 2006
- Office of Secretary of Defense (OSD) established the joint US IM test standards and passing criteria 2010
 - Joint standards are based on NATO AOP-39 policy document which provides guidance on IM and HC assessment and testing
 - Strive to harmonize IM and HC test requirements
 - It became imperative that the US Navy have one single authority for the review of weapons systems test plans and results for compliance with safety, IM and HC requirements
- NOSSA decision to consolidate 3 Navy Boards into one board in 2008
 - NOSSAINST 8010.1 established that forms MREB 2009
 - MREB began officially in January 2010
 - MREB board members comprised of Subject matter experts from IM, HC and basic safety testing.
 - NOSSAINST 8010.1 updated in 2017

Distribution Statement A: Approved for public release; distribution is unlimited



MREB Philosophy

- Convenes in person and/or by video/web/teleconference at a US Navy installation
- Lead Chairperson coordinates meeting time and location with the MREB Site Chairperson's and voting members
- Attendance by full membership is encouraged so that judgements are consistent and independent of meeting location, program, sponsor or test activity

Distribution Statement A: Approved for public release; distribution is unlimited



MREB Leadership

- Leadership of the MREB consists of:
 - Lead Chairperson
 - Nominated by the appropriate US Navy Warfare Center Dept/Director Head and concurred with by NOSSA.
 - Provides overall direction for the MREB
 - Rotates among site every two years
 - Site Chairperson
 - Each US Navy Warfare Center will have a Site Chairperson nominated by the appropriate Dept/Director Head and concurred with by NOSSA
 - Vice Chairperson
 - Each US Navy Warfare Center will have a site Vice Chairperson nominated by the appropriate Dept/Director Head and concurred with by NOSSA



MREB Membership

- MREB membership is as follows:
 - Voting Members
 - Individuals with expertise related to munitions development, IM requirements, HC requirements, ordnance technology, and test and evaluation technologies and methods
 - Executive Secretary
 - Appointed by Lead Chairperson to coordinate MREB meetings
 - Responsible for meeting minutes, summarizing Board's findings. Summarizing and distributing comments on test plans to NOSSA and distribution of the minutes and findings for review and approval
 - Ad Hoc Members
 - The MREB can appoint technical specialists, special appointees as ad hoc voting members to advise board
 - The MREB can appoint technical specialists as ad hoc non-voting members for consideration of unique cases
 - NOSSA and/or PEOs/PMs may also be ad hoc non voting members

Distribution Statement A: Approved for public release; distribution is unlimited



MREB Meetings

- MREB meetings are conducted as required and typically once per month
- Meetings are called only when a quorum is present
 - At least six members are present
 - Goal is to have representation from each site- can be waived
 - A Site Chairperson or Vice Chairperson is present
- Consensus is preferred but rulings can be made with a two-thirds majority
 - If a two-thirds majority doesn't exist then the Site Chairperson will assign representatives to write majority and minority opinions
 - The Site Chairpersons will provide a recommendation to the Lead Chairperson who will issue the final ruling
- Program offices will arrange meeting with the appropriate Chairperson and Executive Secretary

Distribution Statement A: Approved for public release; distribution is unlimited



MREB Authority and Responsibility

- Weapons Program Offices submit their POC and detailed test plans on the NOSSA Website via the NOSSA Test Plan Submission tool
 - Including approved THA
 - System Safety Program Plan - if applicable
 - If test is for official score it is important that the program receives concurrence on the test plan prior to testing
 - Recommended to submit developmental tests for review
 - If test plan includes harmonized IM/HC tests the DoD Explosives Safety Board (DDESB) concurrence may be necessary
- Weapons Program Offices must submit test results to MREB for review to obtain an assessment for official score
 - It is not necessary to submit test results for engineering assessments, however, submission of test assessment based on engineering analysis of engineering level tests, modeling, etc. to obtain official assessments



MREB Responsibilities

- Provide a response to the Program Office within 30 days of receiving the test plan, results and assessments
- Provide recommendation for approval of test plans sent to NOSSA
- Evaluate the results of ordnance hazard assessment tests including IM/HC and Basic safety tests in accordance with MIL-STD-2105D and NATO STANAGs/APs and provide an official assessment of record of the reactions
- Report it's findings/recommendations and corroborating information to NOSSA for official NOSSA concurrence



NOSSA Responsibilities

- Provide concurrence on the appointments of Lead and Site Chairpersons
- Render a decision with MREB concurrence on final approval of test plans and findings/recommendations
- Provide detailed procedures for approval of test plans and presenting test results to the MREB
- Provide MREB Process Guide and Reporting Format
- Provide test submittal guidelines
- Ensure all records are accounted for and are accessible by current and future program



Concluding Remarks

- NOSSA has created an updated NOSSA Instruction which clearly defines the duties and responsibilities of the US Navy MREB. The MREB ensures consistent evaluation of ordnance hazard assessment test plans and scoring reaction levels of hazard testing
- As U.S./NATO IM/HC tests, procedures, and requirements evolve, NOSSA will continue to maintain/update the MREB instruction
- The US Navy's MREB instruction is a proven model of cooperation and consistency for a unified board for scoring IM, HC and basic safety tests

QUESTIONS?

BACKUP SLIDE



APPLICABLE SPECS & STDs

ASTM Standard E1742/E1742M-12
MIL-STD-2105D

“Standard Practice for Radiographic Examination,” ASTM International,
Hazard Assessment Tests for Non-Nuclear Munitions, 19 April 2011.
West Conshohocken, PA, 1 November 2012

NATO STANAG 4439

Policy for Introduction, Assessment and Testing for IM (MURAT), Edition 3,
17 March 2010.

NATO STANAG 4240

Liquid Fuel/External Fire, Munition Test Procedures, Edition 2, 15 April 2003.

NATO STANAG 4382

Slow Heating Munitions Test Procedures, Edition 2, 15 April 2003.

NATO STANAG 4241

Bullet Impact, Munition Test Procedures, Edition 2, 15 April 2003.

NATO STANAG 4496

Fragment Impact Munitions Test Procedure. Edition 1, 13 December 2006.

NATO STANAG 4396

Sympathetic Reaction Munition Test Procedures. Edition 2, 15 April 2003.

NATO STANAG 4526

Shaped Charge Jet, Munitions Test Procedure. Edition 2, 10 December 2004.

NATO STANAG 4375

Safety Drop Munition Test Procedure, Edition 3, 15 June 2010.

NAVSEAINST8020.8C

Department of Defense Ammunition and Explosives HC Procedures, 30 July 2012.

NAVSEAINST 8010.5C

Insensitive Munitions Program Planning and Execution, 15 September 2015.

Distribution Statement A: Approved for public release; distribution is unlimited

Influence of concentration, type and particle size of fillers on the dynamic mechanical behaviour of elastomeric HTPB binder

Manfred A. Bohn¹, Mauricio Ferrapontoff Lemos^{2, 1}, Günter Mussbach^{3, 1}

¹ Fraunhofer Institut für Chemische Technologie (ICT), Pfinztal, Germany

² Brazilian Navy Research Institute, Rio de Janeiro, RJ, 21931-090, Brazil

³ Bayern-Chemie GmbH, D-84544 Aschau am Inn, Germany

Abstract

Recently, it was found that the second peak of the loss factor curve determined by DMA of HTPB bonded composite propellants and high explosives can change significantly in intensity and shape with composition. Composite propellants with AP, whereby the AP particles are connected via bonding agents to the binder matrix, can show a pronounced second peak, whereas HMX and RDX produce a weaker peak and with high contents of them, it can show only as shoulder attached to the first peak. The second peak is much more sensitive to ageing and to de-wetting. This means interactions between filler and matrix influence the appearance of the peak. Therefore, a more detailed investigation was started to elucidate the influences of fillers on the loss factor curve. Polyurethane binders made from polyol HTPB and isocyanate IPDI were filled with 20, 40 and 60 mass-% of ammonium perchlorate (AP), aluminum (Al) or RDX, using fine and coarse particles. For obtaining the cured composite, a special turning device constructed and manufactured at Fraunhofer ICT was installed inside the curing oven in order to avoid sedimentation of the fillers during curing. The composites were characterized by DMA in torsion mode from -100°C to +70°C, and the quality of distribution of fillers was evaluated by X-ray micro-tomography, which showed homogenous distribution of the filler particles in the samples. The part of loss factor $\tan\delta$ at lower temperatures originates from the glass-rubber transition of the binder parts, which are unrestricted in mobility. This is defined in this way in comparison of the second broader peak at the high temperature side of the first peak, which is caused by binder parts restricted in mobility. The temperatures at each maximum are called Tg^{unr} and Tg^{res} , respectively. The results are: AP and RDX cause more changes in intensity of the first main peak in $\tan\delta$ than Al particles. The maximum temperature Tg^{unr} is nearly not changed by any of the fillers. The changes in $\tan\delta$ intensity determined from baseline corrected loss factor curves and modelled by EMG (exponentially modified Gauss) distributions indicate that Al has a stronger interaction with HTPB binder than AP and RDX particles. The particle sizes of AP and RDX and probably their shapes effect the viscoelastic properties. Increasing content of AP and RDX increase the storage shear modulus G' and somewhat the loss shear modulus G'' , but as a whole $\tan\delta$ intensity is lowered in the main peak.

Keywords: AP; aluminum; RDX; HTPB; filler effects on loss factor; DMA loss factor modelling

1. Introduction

In a series of investigations [1 to 14] it was found that the second peak in the DMA loss factor curve of HTPB (hydroxyl terminated polybutadiene) bonded composite rocket propellants (CRP) can change significantly with composition. AP (ammonium perchlorate) bonded with bonding agents to the binder matrix causes a pronounced peak see Fig. 1, curve CRP1, whereas HMX and RDX show only a small peak, see Fig.1 curve HX1, which changes to a shoulder with high degree of filling, see Fig. 1, curve HX2. Up to now for HMX and RDX no such bonding agents exist as for AP. Total intensity and position of the maxima is also deter-

mined by the used plasticizer and its amount and somewhat by the curing agent [2, 5, 15 to 18]. The second peak is also very ageing dependent [1,4,7,12 to 14], especially with HTPB-based binders. In spite of the presence of antioxidants, ageing happens, when oxygen access is possible. Surely, the ageing rate is reduced by antioxidants, but it is not brought to zero. The ageing causes additional cross-links between binder chains and reduces the strain capacity of the formulation. This second peak is also indicative for de-wetting between binder and filler particles. From all observations it becomes evident that intermolecular interactions between filler and binder matrix are important [20, 21].

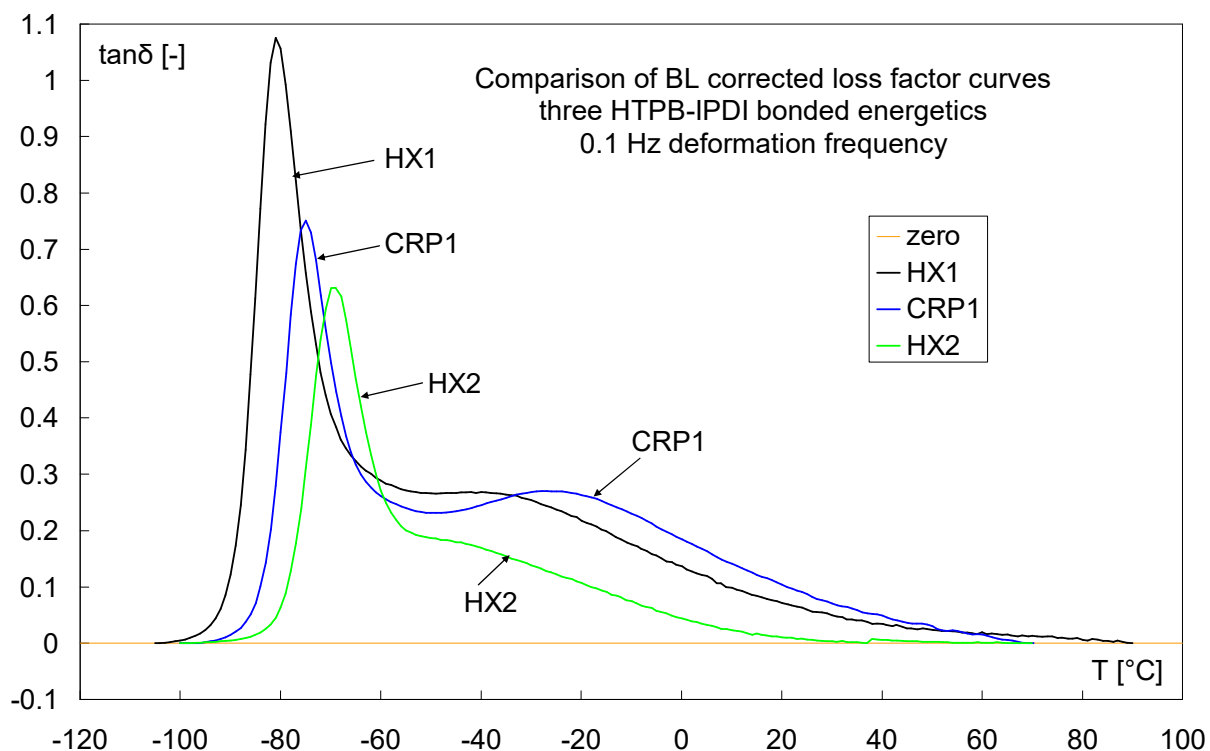


Figure 1: Three examples of loss factor, all obtained by torsion DMA and with substances based on HTPB-IPDI binder. The principle structure is equal with all three formulations. The main components in mass-% are, besides antioxidant (AO) and bonding agent (BO):

CRP1	HTPB-IPDI (12), AP (78), Al (6),	DOA (4, 25% of binder), AO, BO
HX1	HTPB-IPDI (12), RDX (80),	DOA (8, 40% of binder), AO
HX2	HTPB-IPDI (14), HMX (85),	DOA (1, 6,7% of binder), AO

The aim is therefore to perform detailed experimental investigations on the influences of the typical fillers AP, Al (aluminium) and RDX on the loss factor intensity and loss factor shape and on its shift in temperature with deformation frequency. It is intended to find out, in which way the different filler types interact with the binder. In a first step of investigation, three filler types are selected and formulations with three different contents, 20, 40 and 60 mass-% are manufactured, including coarse and fine particles.

2. Experimental

2.1 Substances

The binder comprises of HTPB R45 HTLO (from Sartomer, Polybd, Oakland, USA), IPDI (isophorone diisocyanate, from Evonik, Marl, Germany), DOA (dioctyl adipate, better named

di(ethyl-hexyl) adipate, from BASF, Ludwigshafen, Germany), antioxidant Vulkanox™ BKF (from Bayer AG, Leverkusen, Germany).

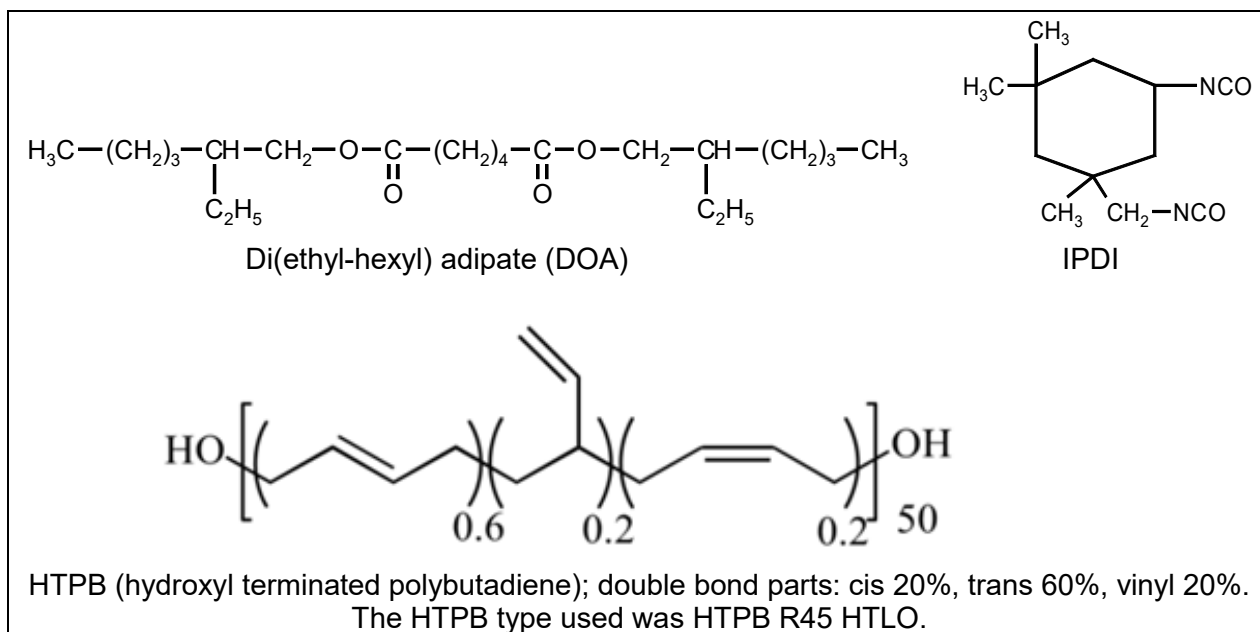


Figure 2: Ingredients of the used binder.

The three solid fillers were characterized by particle size distributions. The mean diameters are the so-called Dx50 median values, which separate the total sample in the lower and upper part, with x naming the type of particle distribution function, v = volume, m = mass, s = surface, n = number. Here the distributions with x = v are considered (normally gained from laser scattering), this means the Dv50 is the particle size in micrometer that splits the distribution with half of the total particle volume above and half of the total particle volume below this diameter. The Dv50 parameter is named the median of the volume distribution. It is with equal density for all particles equal to the mass median of a mass distribution.

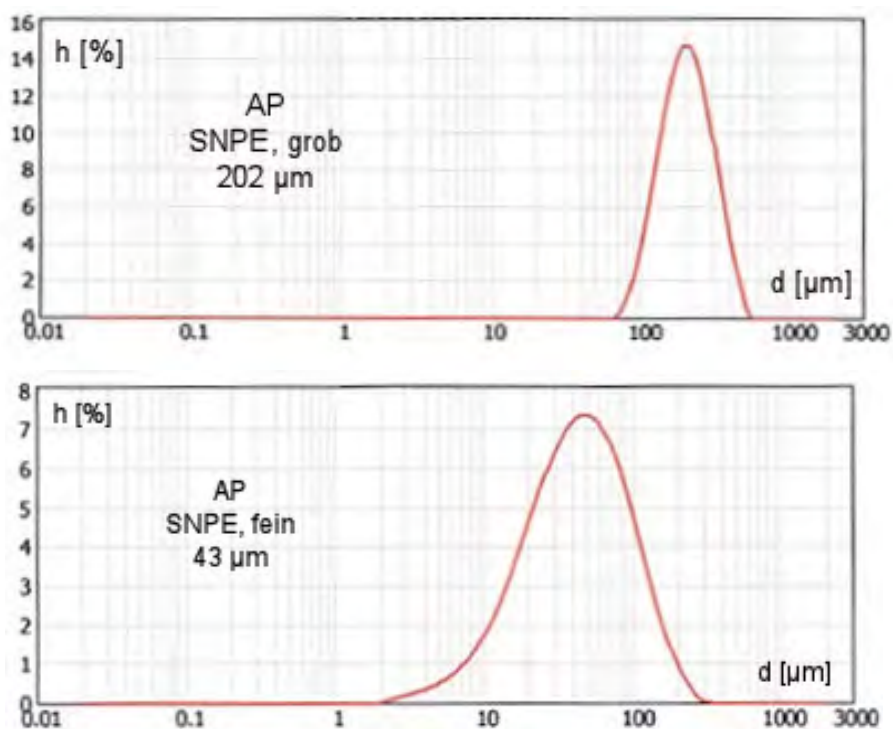


Figure 3: Particle size distributions of AP, above coarse and below fine. Material obtained from former SNPE, now EURENCO, France.

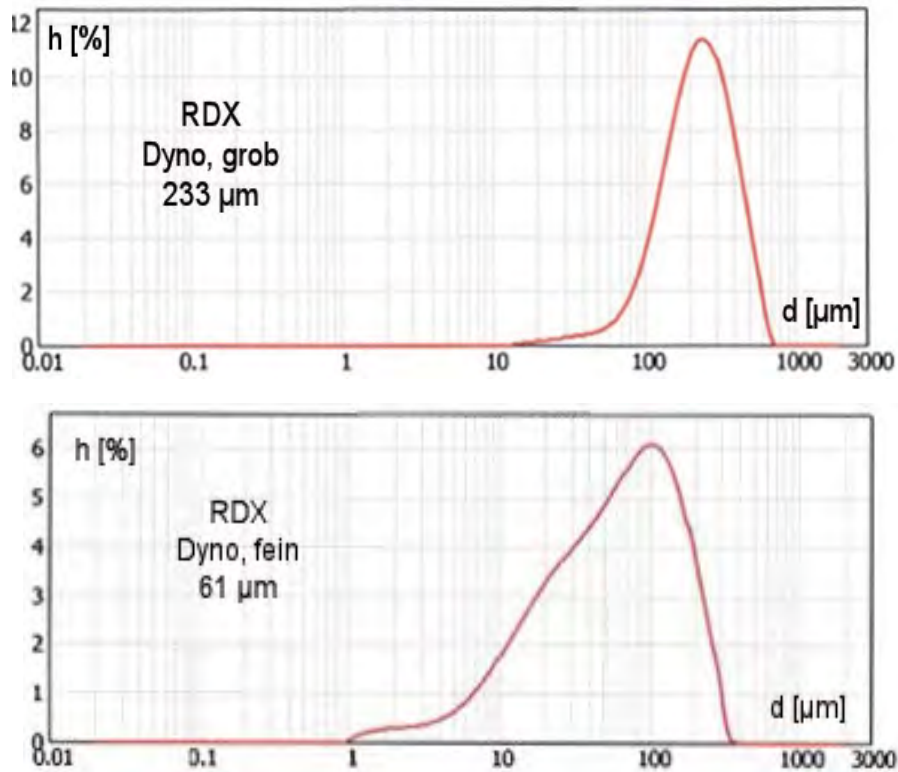


Figure 4: Particle size distributions of RDX, above coarse and below fine. Material obtained from former Dyno, Norway, now Chemring.

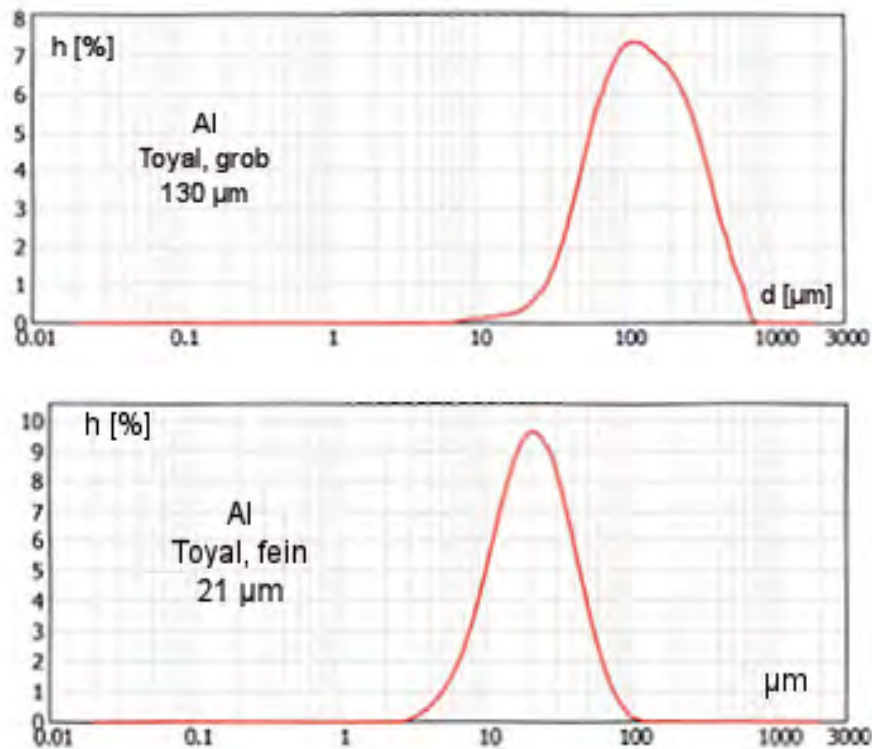


Figure 5: Particle size distributions of AL powder, above coarse and below fine. Material obtained from company Toyal, USA.

2.2 Sample manufacturing

The composite samples were manufactured at Fraunhofer ICT in a planetary-rotary centrifugal vacuum mixer (from Thinky Corporation, Tokyo, Japan). The scheme of the manufacturing is shown in Fig. 6. No curing catalyst was used, and no bonding agents have been used with the fillers. All formulations were made with an equivalent ratio R_{eq} (NCO / OH) = 0.85. The plasticizer content was always 5 mass-% in binder.

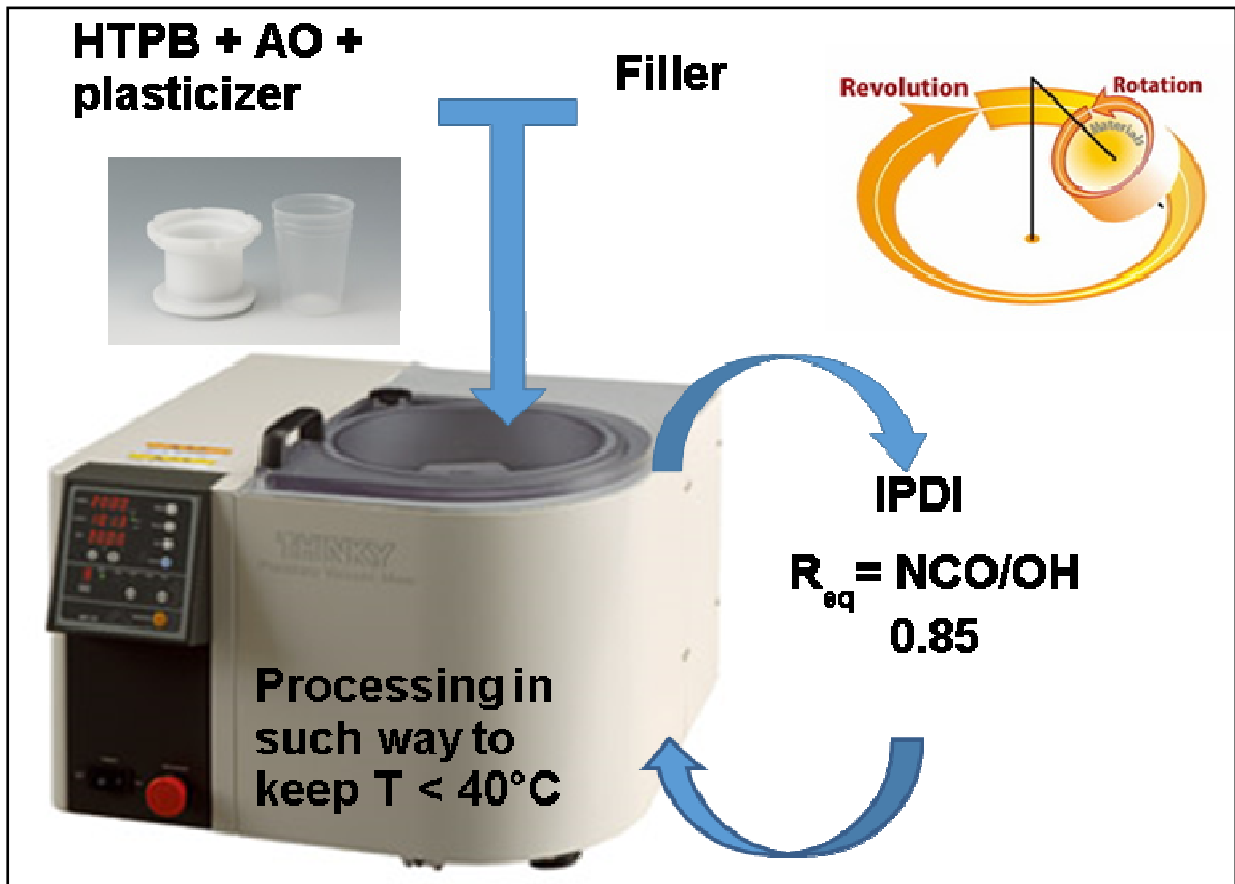


Figure 6: Scheme of the manufacturing process using a planetary-rotary mixer, of type Thinky® mixer, produced by Thinky Corporation, Tokyo, Japan.

Operational conditions were 1600 rpm rotation speed and 30 mbar = 3 kPa vacuum during the few minutes of mixing time. The temperature in the mix was kept below 40°C. Every formulation was produced in small batches and poured into a cylindrical glass recipient, sealed and cured in air at 60°C for 130 hours. The binder was protected by the addition of an antioxidant.

Shortly after the mixing the particles are homogeneously distributed all over the sample volume. However, the particles tend to sediment in the liquid binder mix in early stages of the curing process, when the viscosity is not yet high. This problem is even more critical with samples with lower amounts of solid loading, as with 20 and 40 mass-%. Thus, in order to keep the fillers homogeneously distributed during the curing process a special turning device was manufactured at Fraunhofer ICT and installed inside the curing oven, see Fig. 7, 8, 9. The turning machine provides a rectangular frame for mounting the samples within a standard laboratory circulation oven of type UFE500 from company Memmert (Germany). The frame is rotated not permanently to avoid concentration gradients of filler particles due to inertia forces. It is rotated

stepwise by 180 degrees, controlled by encapsulated, low-voltage magnetic switches. A belt drive in combination with a screw wheel transmission is powered by a brushless AC-motor. An additional transmission is necessary for suppressing so-called rattle-effects. The switches and the motor are connected to a programmable electronic circuit, which allows controlling the rotation speed and the holding time. The circuit is equipped with a mechanical counter to monitor the number of rotation cycles, useful for instance in case of failures in power network.

After curing, the glass bottles were broken and the DMA samples cut from the middle of the cured composite. In this way surface effects induced from the interface glass –binder or binder with residual air were circumvented.

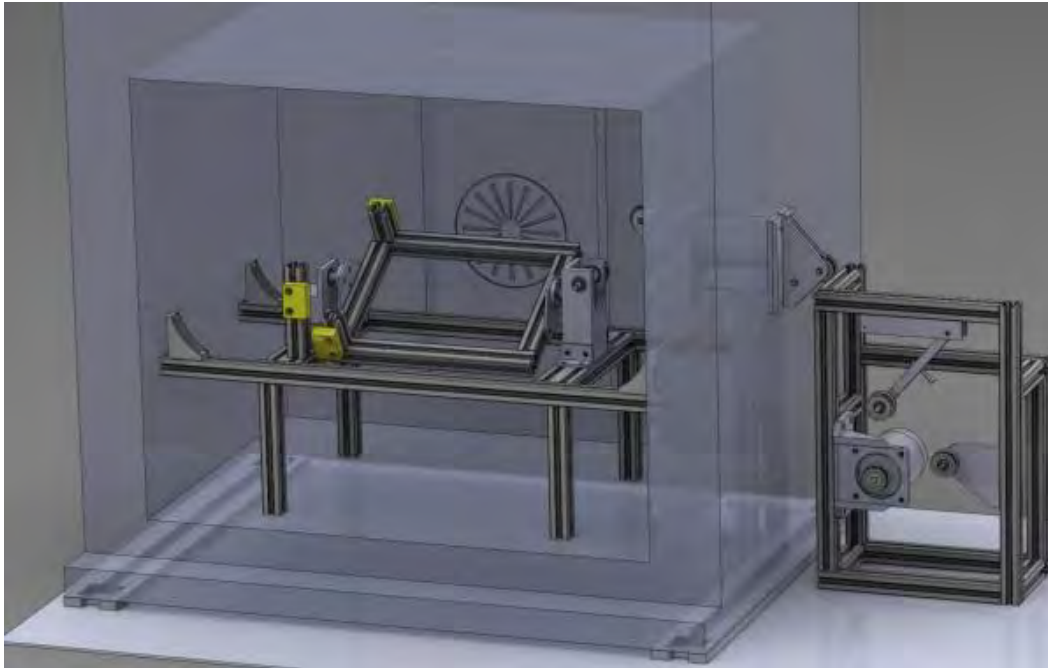


Figure 7: Construction photograph of the turning device mounted inside an air circulation oven and driven by an electromotor with stepping gear system.



Figure 8: Real photograph of the turning device inside the oven with mounted samples in small glass bottles.

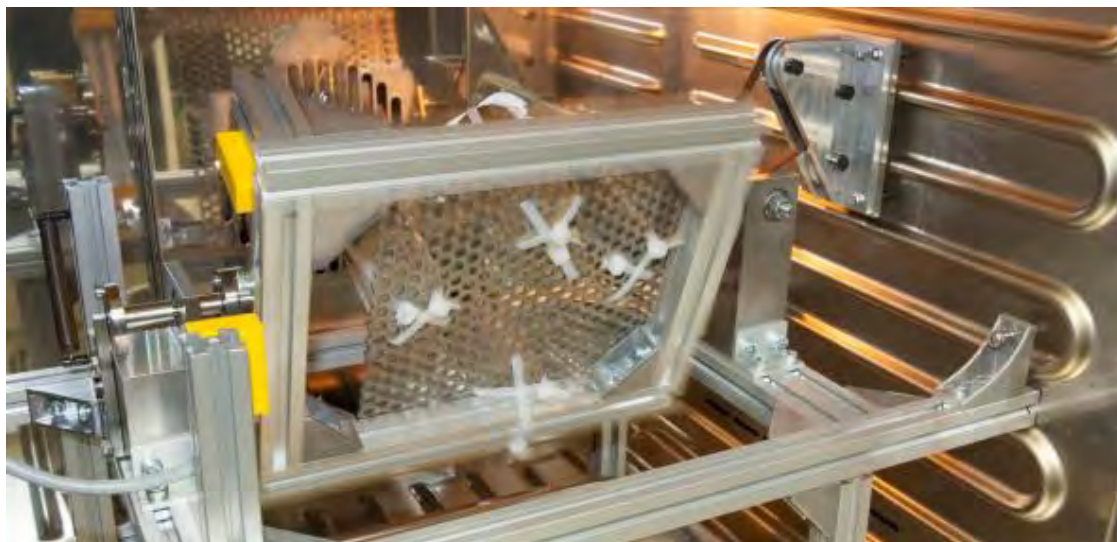


Figure 9: Real photograph of the turning device inside the oven with mounted samples in small glass bottles, indicating step-wise turning by 180°.

2.3 Characterization methods

2.3.1 X-ray (Röntgen)-Computer Tomography (X-CT)

Using a computer tomography instrumentation of type Micro-CT in-vivo Skyscan 1076 of company Bruker, Germany, the cured samples were tested, whether the distribution of the solid fillers was homogeneous. The maximum peak voltage of the X-ray is 100 kV with a maximum power of 10 W. It has a Tungsten reflection target and a focal spot of 5 μm . The detection system consists of a 8000 x 8000 large megapixel X-ray camera. A micro-focus X-ray source illuminates the object and the planar X-ray detector collects magnified projection images. Based on hundreds of angular views acquired while the object rotates, a computer synthesizes a stack of virtual cross section slices through the object. After the acquisition of the projection images, the reconstruction was done using a modified Feldkamp cone beam algorithm. Finally, the 2D cross-sectional images of the sample were obtained in consecutive slices throughout the object. Also 3D images can be constructed.

2.3.2 Scanning Electron Microscopy (SEM)

Scanning electron microscopy of type Supra 55VP, manufactured by company ZEISS, Germany was used to characterize the surfaces of the particles with regard to their roughness or smoothness.

2.3.3 Dynamic Mechanical Analysis (DMA)

Dynamic mechanical analysis measurements in torsion mode were carried out with a DMA of type ARES™ (Advanced Rheometric Expansion System) manufactured by the former Rheometric Business Unit of Rheometric Scientific, Inc. (this BU now belongs to TA Instruments, New Castle, DE, USA). The following parameters were determined: storage shear modulus G' , loss shear modulus G'' , loss factor $\tan\delta = G''/G'$ as well as the phase angle δ and the torque. Measurements were performed in torsion mode from -100°C to +70°C, with heating steps of 1°C/min and soak time of 28s. At -100°C a pre-strain sweep test was performed to determine the value of the strain control, in order to stay in the linear viscoelastic region during the measurements. At each temperature step, the samples were measured at four sinusoidal

deformation frequencies, here 0.1; 1.0; 10 and 30 Hz. The geometrical dimensions of the rectangular samples were about 40 mm in length, 10 mm in width and 5 mm in thickness. In the cases where the material was too soft, as with pure binder and binder with 20 and 40 mass-% of filler, the signal scattered at higher temperatures and a second strain sweep was necessary at -40°C to determine a higher second strain control to be used up to +70°C.

The temperatures of the two evident maxima in the loss factor curve $\tan\delta(T) = G''(T)/G'(T)$ of the HTPB-IPDI binder were determined by using fits of polynomials of degree 3 around the maxima and calculating the temperatures connected with the maxima. These temperatures are named $T_{g,DMA}$ and represent glass-rubber transitions (GRT) in the corresponding binder parts. The temperatures at maxima of the loss factor curve are seen as the representative transition temperatures, because around these temperatures the necessary molecular reorientations (= transitions in molecular arrangements) to come from glassy to rubbery state (and vice versa) have the highest 'intensity' or activity. The assignments to these both evident peaks is $T_{g,unr}$ (unrestricted binder mobility) and $T_{g,res}$ (restricted binder mobility). Unrestricted binder regions are parts of the inter-cross-link chain segments, which are not restricted in mobility by the fillers, as sterically-geometrically and by energetic interaction, and also not by other mobility hindrances, as they occur in the cross-link ranges of the binder. These binder parts in cross-link volume elements with restricted mobility are one origin for the second apparent maximum in the loss factor curve, situated at higher temperatures than the first peak maximum, what is caused by the transition of the unrestricted binder parts.

2.3.4 Exponentially Modified Gauss distribution (EMG distribution)

The peaks of the loss factor curves correspond with the different mobility of the polymer chains of the elastomer network. An objective is to identify and quantify the corresponding binder parts. For this, a suitable description has to be applied. The so-called EMG functions have shown to provide with the looked for parameters [5,6,7,8,9]. The EMG function is a convolution between a Gauss distribution function, Eq.(1) and an exponential decay function, Eq.(2), resulting in Eq.(3).

$$f_G(T) = \frac{A}{w \cdot \sqrt{2\pi}} \cdot \exp\left[-0.5 \cdot \left(\frac{T - T_c}{w}\right)^2\right] \quad (1)$$

$$f_E(T) = \exp\left(-\frac{T}{\tau}\right) \quad (2)$$

$$\tan \delta_{BLC} = td_0 + \frac{A}{\tau} \cdot \frac{1}{2} \cdot \exp\left[0.5 \cdot \left(\frac{w}{\tau}\right)^2 - \frac{T - T_c}{\tau}\right] \cdot \left\{1 - \operatorname{erf}\left[-\frac{1}{\sqrt{2}} \left(\frac{T - T_c}{w} - \frac{w}{\tau}\right)\right]\right\} \quad (3)$$

- T measurement temperature, in [°C];
- $\tan\delta_{BLC}$ value of loss factor as function of T after BLC (baseline correction), in [-];
- A peak area of the EMG peak, also equivalent to the area of the corresponding Gauss peak alone, in [°C];
- w half peak width at half height of only the Gauss part, in [°C];
- Tc temperature at peak maxima in the Gauss part of EMG (not the peak maxima of EMG), in [°C];
- τ relaxation parameter in exponential part of EMG, also named To, in [°C];
- td₀ to consider an eventually residual offset in $\tan\delta$ data, in [-];
- erf error function.

Meanwhile it was several times found and confirmed that the total loss factor curve of an HTPB-IPDI binder needs three EMG functions for full description [2,3,4,5,6], see Eq.(4).

$$\tan \delta_{\text{BLC}} = t_{d_0} + \sum_{i=1}^N \frac{A_i}{\tau_i} \cdot \frac{1}{2} \cdot \exp \left[0.5 \cdot \left(\frac{w_i}{\tau_i} \right)^2 - \frac{T - T_{c_i}}{\tau_i} \right] \cdot \left\{ 1 - \operatorname{erf} \left[-\frac{1}{\sqrt{2}} \left(\frac{T - T_{c_i}}{w_i} - \frac{w_i}{\tau_i} \right) \right] \right\} \quad (4)$$

Each EMG function comprises four parameters. In spite of the high number of parameters, the fit is mostly easy to perform and is unique, because the structures of the peaks and the equations limit the possibilities for the fit [2]. To apply the EMG description the loss factor curves must be baseline corrected, see [6]. Figure 10 presents an example of modelling the loss factor curve; the three single EMG (peak 1, 2, 3) and the total EMG are shown.

There are some rules for the change of the parameters A, T_c and τ (T₀)

> **Peak areas A_i:**

Reduction of A is caused by:

- (1) – Hindrance of mobility
- (2) – increase in storage shear modulus G' or increase in stiffness or in rigidity
- (3) – increase in cross-linking
- (4) – loss of plasticizer

> **Peak temperature T_c of the Gauss curve**

This temperature can be considered as glass-rubber-transition temperature of the relaxation free transition, means the transition without an exponential decay part. It changes by interactions, which restrict the mobility.

> **Relaxation parameter τ_i**

The more influence the exponential part the larger is τ_i or T₀ and the more scewed is the EMG curve.

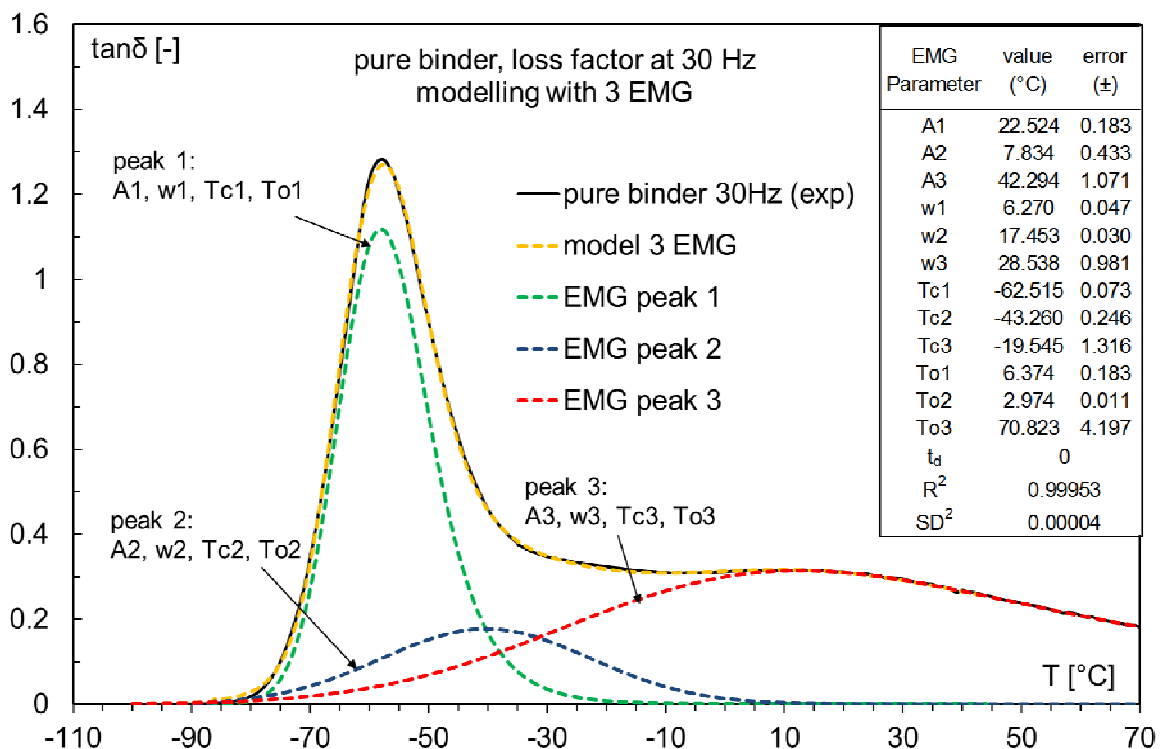


Figure 10: Example of description with three EMG function of baseline corrected loss factor curve of the HTPB-IPDI binder (with plasticizer) used here. Deformation frequency was 30 Hz.

Peak 1 describes the mobility unrestricted binder part, peak3 the mobility restricted binder part (in cross-link volume elements) and peak 2 is caused by intermediate restricted binder parts.

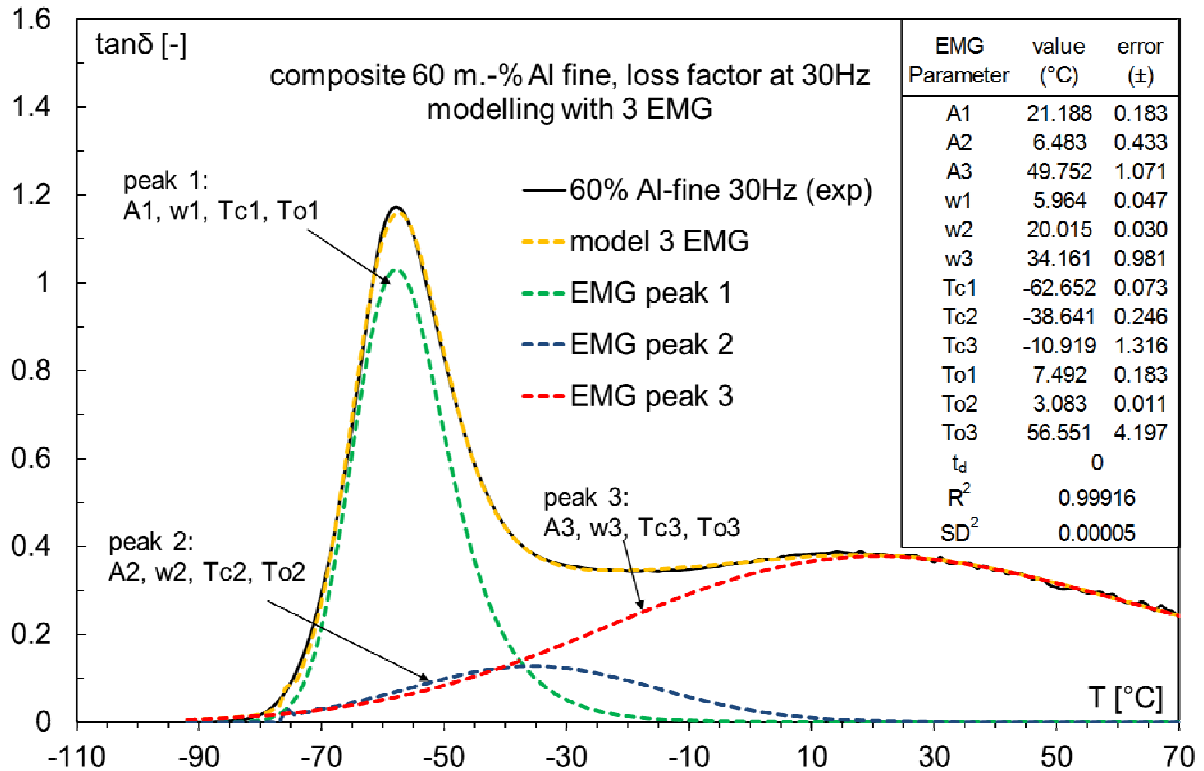


Figure 11: Description with three EMG function of the baseline corrected loss factor curve of HTPB-IPDI binder (with plasticizer) filled with 60 mass-% fine Al. Deformation frequency was 30 Hz.

Figure 11 shows the description with three EMG functions of the baseline corrected loss factor curve of HTPB-IPDI binder filled with 60 mass-% fine Al. By comparison with Figure 10, the binder alone, the following effects can be stated: The main peak 1 is a bit lowered in intensity, but the shape is not much influenced by relaxation, the T_o values are similar and the maximum is not shifted. This means the changes are caused just by geometrical hindrance from the Al particles. The peak 3 has increased in intensity and is more clearly established. Further on the maximum of the apparent peak has shifted from about +11°C to +15°C (binder + Al). The corresponding Gauss peaks have the maxima at -19.5°C and -10.9°C. Because of the large T_o values, the actual EMG peak shifts massively to higher temperatures. This means Al particles interfere strongly with the binder parts restricted already in mobility. There in this binder part they cause more mobility restrictions indicated by the shift of the maximum temperature of Al filled binder to higher values. This is not contradicting the increase in intensity of this peak, because now more parts of the binder are involved, which increases intensity of this peak. In addition, as already said, the first peak is not shifted or only very minor, means here the hindrance is only sterically and not much interaction energy caused.

3. Results and Discussion

3.1 Uniformness of filler distribution in the cured binder

In Fig 12a and 12b, the sample with 20 mass-% of coarse AP is shown as an example of how the particles stayed homogeneously distributed in the elastomers after curing when applying the turning machine. The 3D image obtained with Bruker Micro-CT X-ray Skyscan is shown in

Figure 12b, and it demonstrates the uniformness of the distribution of the AP particles, given in grey colour. The binder itself is not visible because of contrast adjustment.

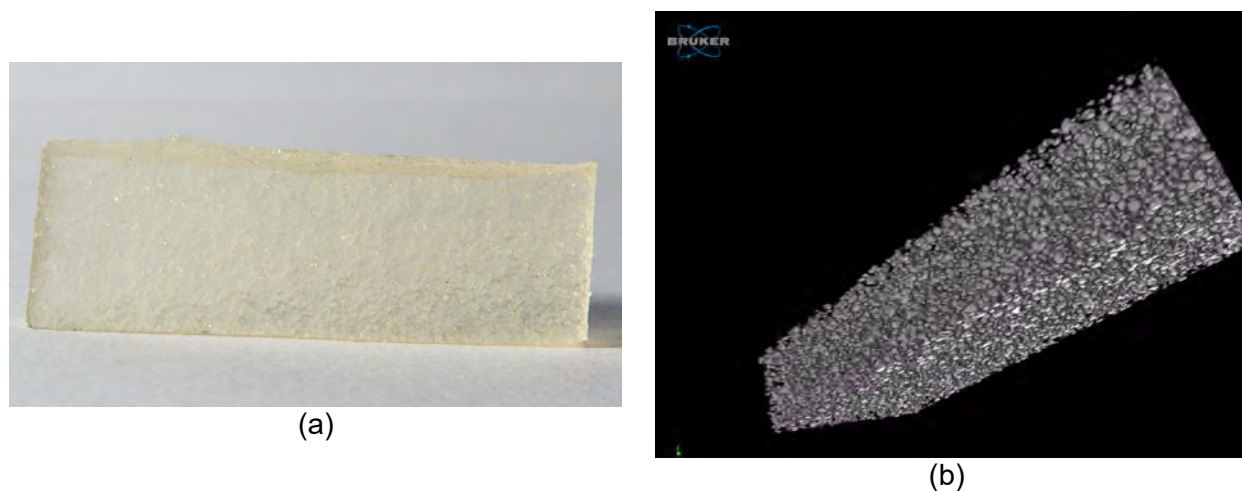


Figure 12: Images from a DMA sample with 20 mass-% AP. (a) a normal optical photograph and (b) a 3D image evaluated with the Bruker Micro-CT X-ray Skyscan, showing the AP particles in grey (binder cannot be seen).

3.2 DMA measurements

The Figures 13a to 13c show an overview of the loss factor curves of the samples with 60 mass-% of coarse AP, 60 mass-% of coarse RDX and 60 mass-% of fine Al at the deformation frequencies of 0.1 to 30 Hz. In Figures 14a to 14c, the elastic (storage) shear modulus G' and the (viscous) loss shear modulus G'' are presented for all the samples, tested at the deformation frequency of 10 Hz.

The molecular rearrangements during glass-rubber transition enhance the thermo-mechanical energy loss inside the polymer. Therefore, the loss shear modulus increases. During glass-rubber transition, when the molecules are stimulated to pass the threshold of energy, long range chain mobility takes place along the segments and the loss factor is at its maximum. By increasing the deformation frequency in DMA, the chains have less time to move and rearrange in order to accommodate the mechanical energy. When heating up the samples from very low temperatures, the energy elastic state is retained longer, up to higher temperatures. This effect is also named strain rate hardening of the material.

Despite having less effect on the first peak, the Al addition imparts more intensity to $\tan\delta$ of the second peak; and it is shifted to higher temperatures (see T_g^{res} values of 60 m.-% filled samples in Table 2). However, a distinguishable change in the first peak with the addition of AP and RDX in comparison to Al could be related with volumetric effects. The densities of AP and RDX are 1.95 g/cm^3 and 1.82 g/cm^3 , respectively, whereas Al has 2.7 g/cm^3 . The use of an equal mass results in a higher occupied volume by the particles in composites with AP and RDX, imparting more geometrical hindrance to chain mobility than by the Al particles which are less in number. Table 1 shows the data.

Table 1: Connection between mass-% and vol-%

	density in g/cm^3	mass-%	volume in 100g $[\text{cm}^3]$	total vol- ume of 100g $[\text{cm}^3]$	vol.-%	degree of volume filling rela- tive to AP

AP	1.95	60	30.77	73.78	41.71	1
RDX	1.816	60	33.04	76.05	43.45	1.04
Al	2.7	60	22.22	65.23	34.06	0.82
HTPB-IPDI-DOA	0.93	40	43.01	-	-	-

On the other hand, Al filled samples present a higher intensity on the second peak, which might originate from higher filler-binder interactions. By increasing the amount of AP and RDX particles, the T_g^{unr} is shifted slightly to higher temperatures. And it decreased considerably the $\tan\delta$ intensity of the first peak especially at higher deformation frequencies.

Before the transition, G' and G'' are very similar for the composites. Only G' of samples with 60 mass-% is significantly higher. Increasing the amount of AP and RDX particles enhances G' and G'' , although with AP this happens mainly after T_g^{unr} . Al produces this effect more pronounced at lower temperatures. After transition the differences increase, and it is notable that the increase in solid filler content in the composites increases both G' and G'' . Storage modulus increase is related with a reinforcement of the material, whereas loss modulus increase with increasing solid fillers in composites is known to be caused by an enhanced internal friction in dynamic mechanical loading experiments [8,22]. Regarding particle sizes, the use of fine AP and fine RDX incremented G' more than G'' .

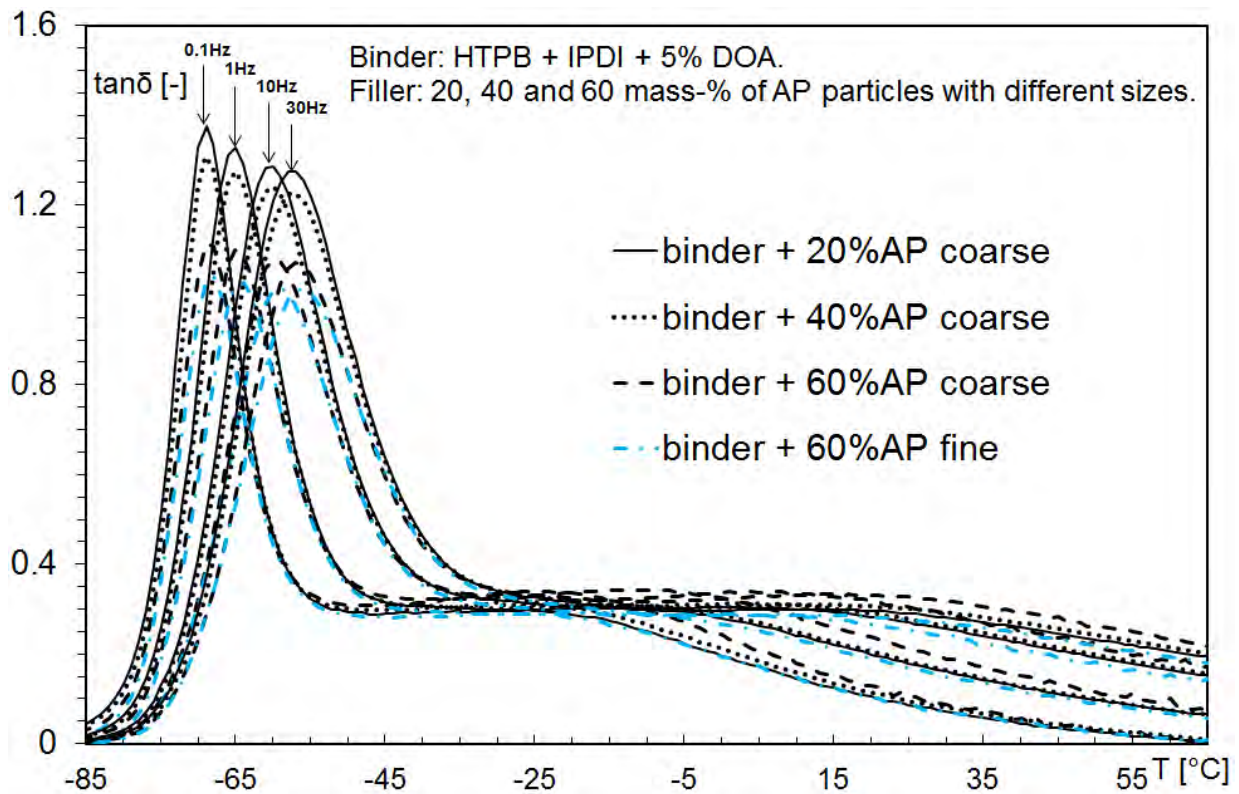


Figure 13a: Deformation frequency dependence of the loss factor curve of composites samples with 20, 40 and 60 mass-% of AP coarse and 60 mass-% of AP fine particles.

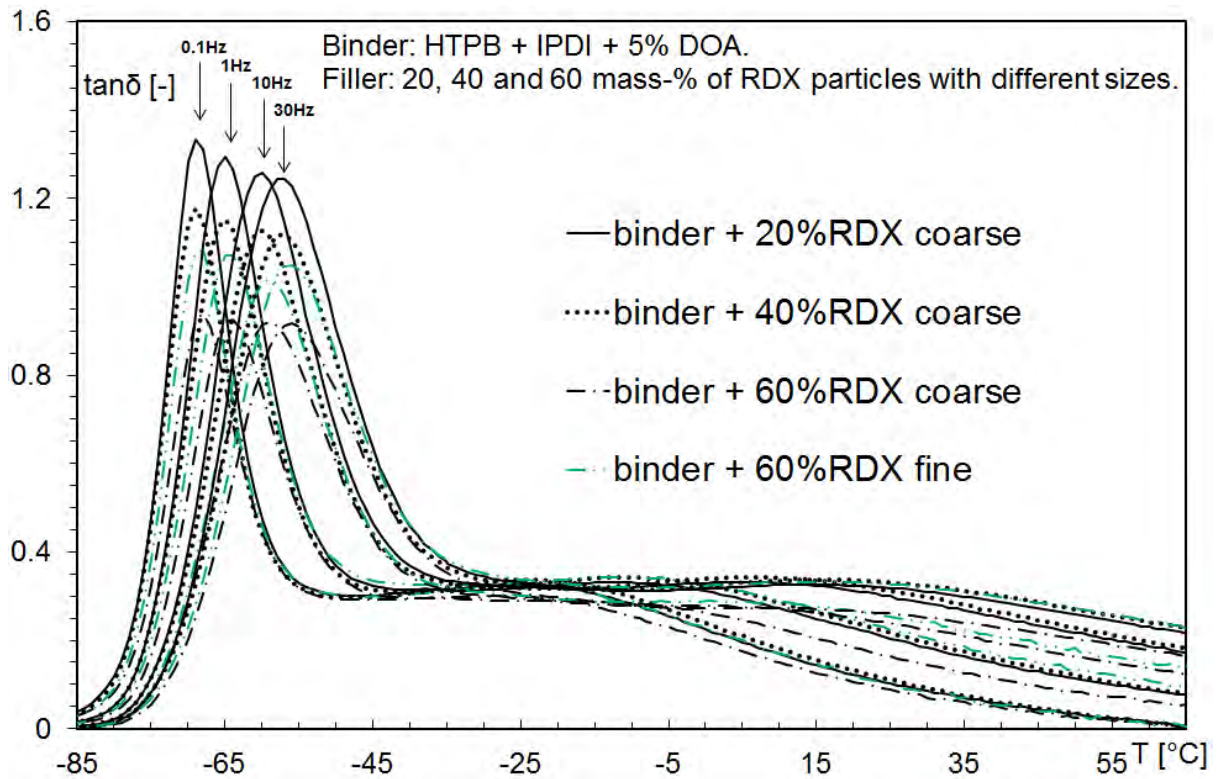


Figure 13b: Deformation frequency dependence of the loss factor curve of composites samples with 20, 40 and 60 mass-% of RDX coarse and 60 mass-% of RDX fine particles.

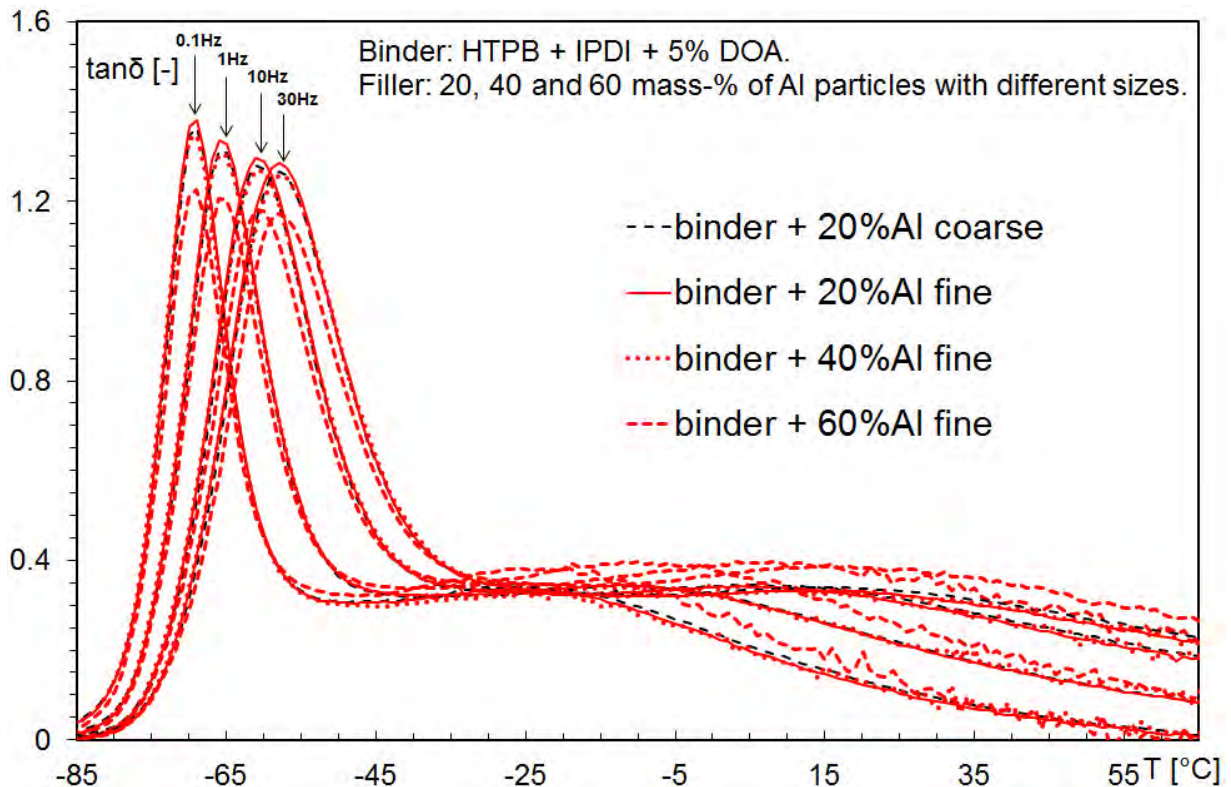


Figure 13c: Deformation frequency dependence of the loss factor curve of composites samples with 20, 40 and 60 mass-% Al fine and 60 mass-% Al coarse particles.

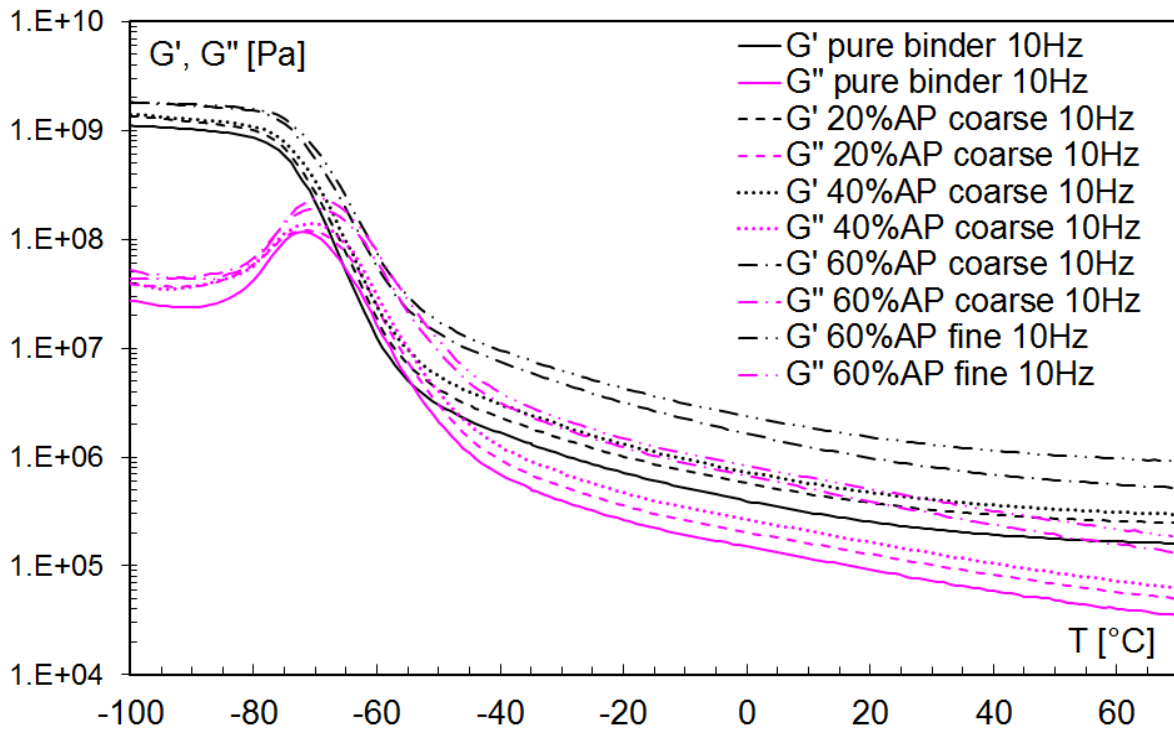


Figure 14a: G' and G'' curves of samples tested at 10 Hz deformation frequency of applied strain in torsion mode DMA. Samples consisting of pure binder and binder with increasing amount (20, 40 and 60 mass-%) of coarse AP particles and 60 mass-% of fine AP.

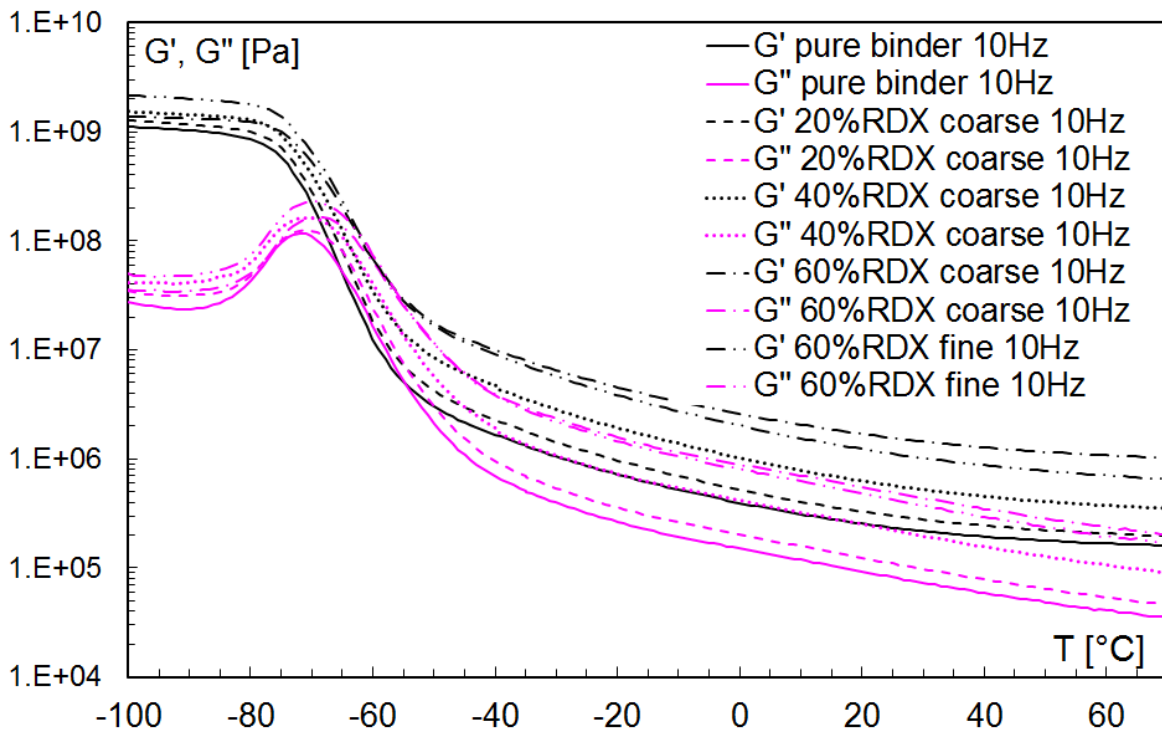


Figure 14b: G' and G'' curves of samples tested at 10 Hz deformation frequency of applied strain in torsion mode DMA. Samples consisting of pure binder and binder with increasing amount (20, 40 and 60 mass-%) of coarse RDX particles and 60 mass-% of fine RDX.

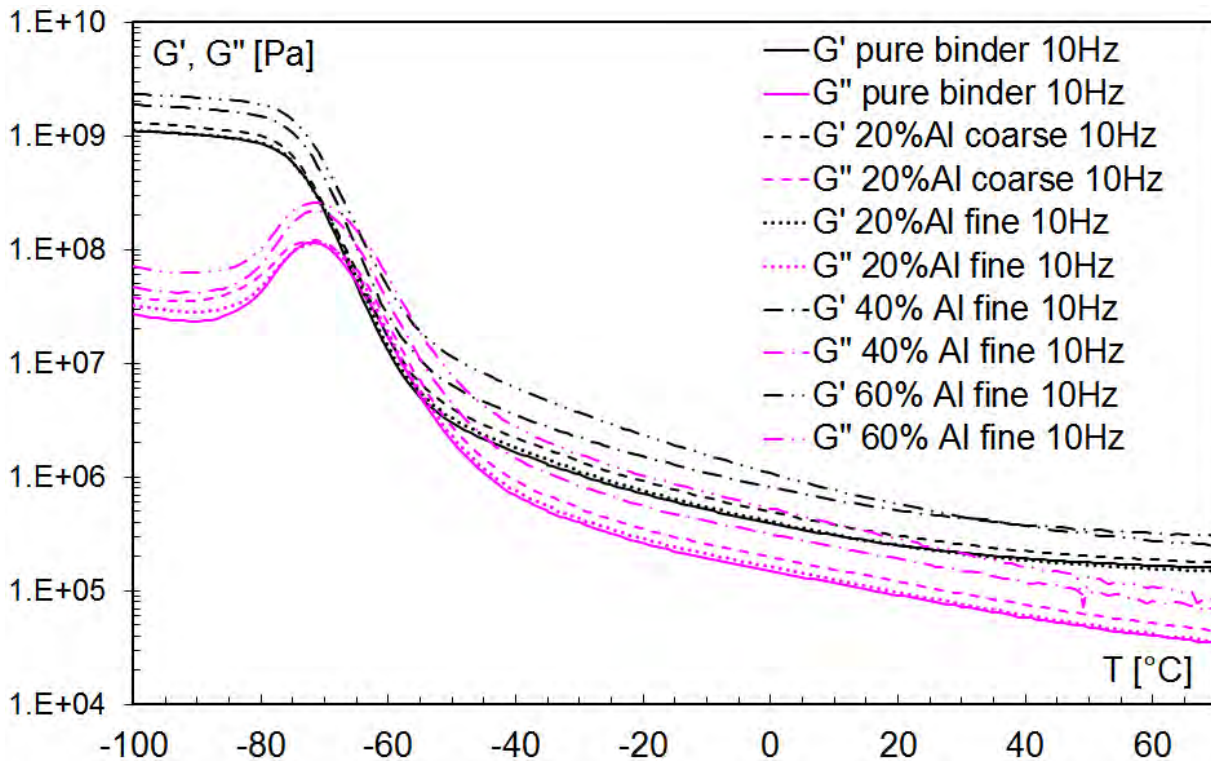


Figure 14c: G' and G'' curves of samples tested at 10 Hz deformation frequency of applied strain in torsion mode DMA. Samples consisting of binder and binder with increasing amount (20, 40 and 60 mass-%) of fine aluminum particles and of 20 mass-% coarse Al.

3.3 EMG modelling of loss factor data

The quantification of the effects caused by energetic interaction and by the amount of each filler on the loss factor curve is possible with the use of exponentially modified Gauss (EMG) distribution functions. In Fig. 10 and Fig. 11, each three EMG functions are used to describe the total $\tan\delta$ data of the pure binder and of the composite filled with 60 mass-% of fine Al particles. This was done for all samples at all deformation frequencies. The parameters obtained for the samples filled with 60 mass-% fine and coarse particles are presented in Table 2.

Figure 15 shows the loss factor curves and the EMG functions of the samples filled with 60 m.-% of fine RDX at different frequencies of applied strain and their EMG modelling. It shows the systematic development with deformation frequency of the total loss factor curve and of the three EMG functions used at each frequency. In Fig 16a to Fig. 16d the changes with deformation frequency of the four parameters A_i , T_{ci} , w_i and T_{oi} of the three EMG peak are presented graphically. There is always an increase with frequency. To note: the changes for peak 3. This peak is always more sensitive to deformation rate than the other two.

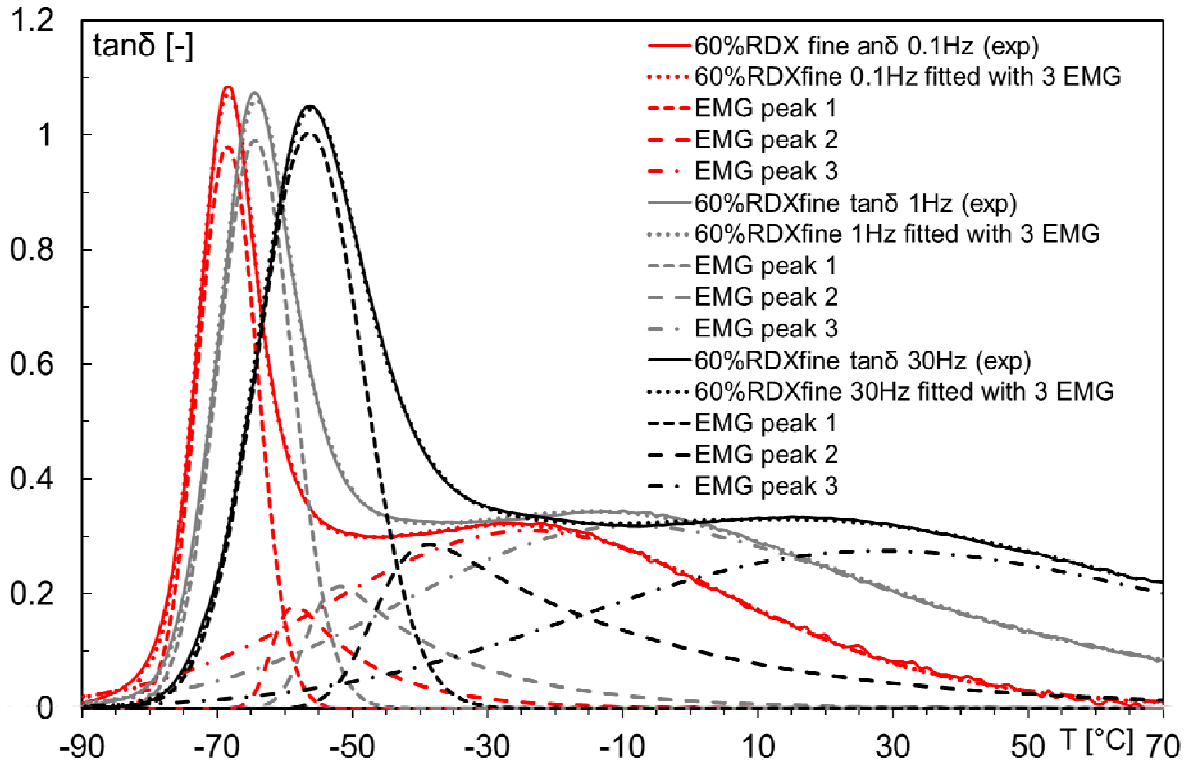


Figure 15: Description of loss factor curves with 3 EMG functions, of the sample with 60 m.-% of fine RDX. Torsion DMA in 0.1, 1 and 30Hz. The indication (exp) means experimental data.

Table 2: Values of EMG parameters of samples with 60 mass-% coarse and fine particles, in comparison with the pure binder.
Data given at all four applied deformation frequencies f [Hz]. The unit of all quantities is °C, also the one of the areas.

f [Hz]	pure binder				60 m.% AP coarse				60 m.% AP fine				60 m.% RDX coarse				60 m.% RDX fine				60 m.% Al fine			
	0.1	1	10	30	0.1	1	10	30	0.1	1	10	30	0.1	1	10	30	0.1	1	10	30	0.1	1	10	30
A₁	13.3	16.7	20.3	22.5	10.8	13.5	16.2	18.0	11.0	13.9	17.0	22.5	9.7	12.1	16.2	19.2	10.8	13.7	17.4	19.4	13.4	14.9	17.7	21.2
A₂	2.6	5.6	7.2	7.8	2.8	4.8	8.2	8.3	3.7	7.9	7.6	6.7	3.3	6.3	7.3	6.1	3.0	5.4	10.1	13.4	2.6	5.2	7.5	6.5
A₃	24.8	29.0	39.0	42.3	25.2	30.9	38.7	45.8	19.9	21.3	31.3	34.1	21.3	22.9	28.6	33.5	23.9	32.5	35.6	37.4	25.4	35.6	48.2	49.8
∑A_i	40.8	51.3	66.5	72.7	38.8	49.3	63.2	72.2	34.5	43.1	56.0	63.3	34.3	41.2	52.2	58.8	37.7	51.6	63.1	70.2	41.4	55.7	73.4	77.4
w₁	4.2	5.2	5.6	6.3	4.3	5.2	5.6	6.3	4.5	5.5	6.1	6.7	4.5	5.5	6.0	6.7	4.3	5.4	6.8	7.6	4.2	5.2	5.1	6.0
w₂	2.0	2.7	16.4	17.5	2.1	2.8	17.0	17.5	2.3	3.1	16.5	6.6	2.2	3.1	17.4	17.3	2.2	3.1	4.1	4.8	1.7	2.9	21.1	20.0
w₃	25.3	26.3	26.7	28.5	26.8	27.7	25.5	28.1	24.7	25.6	23.9	30.6	25.9	27.0	23.8	27.4	26.2	26.7	31.6	34.6	25.8	27.0	30.1	34.2
Tc₁	-70	-66	-65	-63	-69	-66	-64	-61	-69	-65	-63	-65	-69	-65	-64	-62	-69	-65	-61	-58	-70	-66	-65	-63
Tc₂	-63	-58	-46	-43	-62	-57	-46	-42	-61	-56	-43	-57	-61	-57	-41	-34	-62	-57	-50	-47	-63	-58	-49	-39
Tc₃	-43	-33	-23	-20	-38	-32	-20	-17	-39	-28	-19	-12	-40	-31	-18	-14	-39	-33	-16	-5	-41	-30	-20	-11
To₁	0.9	1.0	5.6	6.4	0.8	1.0	5.5	6.1	0.9	1.0	5.8	23.8	0.8	1.0	6.8	8.2	0.8	1.0	1.4	1.5	0.8	1.0	6.6	7.5
To₂	9.6	17.1	2.7	3.0	11.4	16.6	3.2	3.0	15.4	26.8	3.3	1.0	15.5	22.4	3.3	3.2	11.6	17.9	29.3	35.5	9.9	16.0	3.0	3.1
To₃	22.3	37.6	60.1	70.8	17.6	35.1	59.3	75.1	20.9	34.5	57.9	66.6	19.7	32.8	54.4	65.3	19.3	43.3	54.6	60.1	21.0	35.8	59.3	56.6

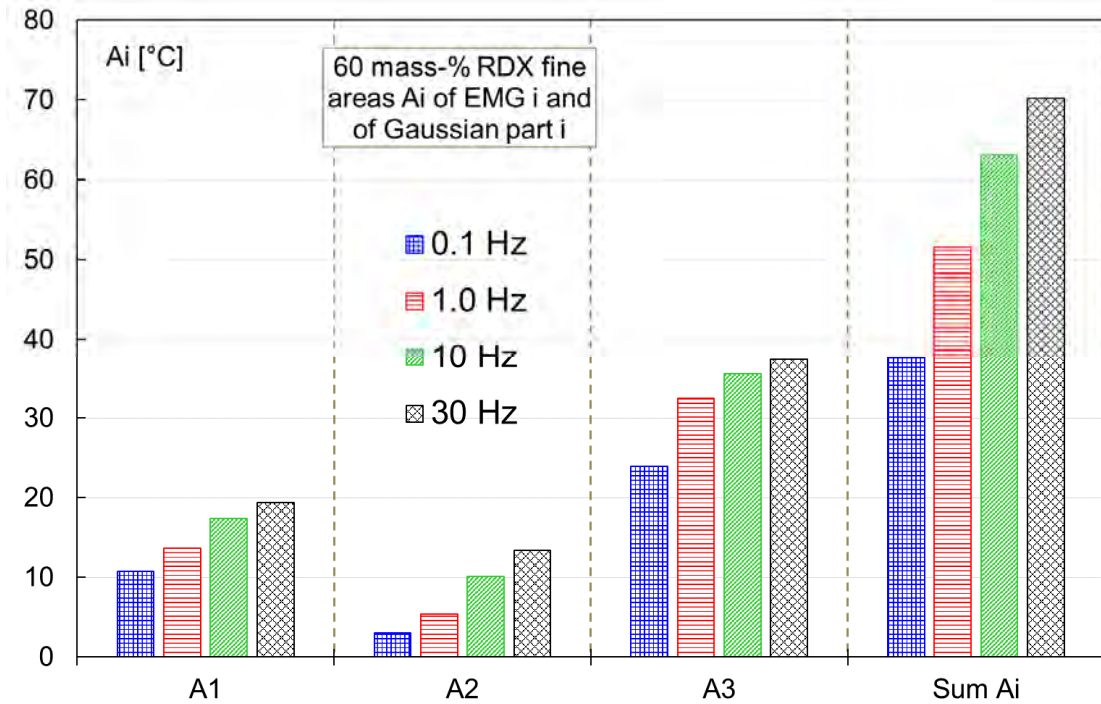


Figure 16a: Change in areas A_i of the three EMG peaks in composite HTPB-60 m.-%-RDX fine with applied deformation frequency. All three areas increase with frequency. Area A_i is the same for total EMG curve and the corresponding Gauss curve.

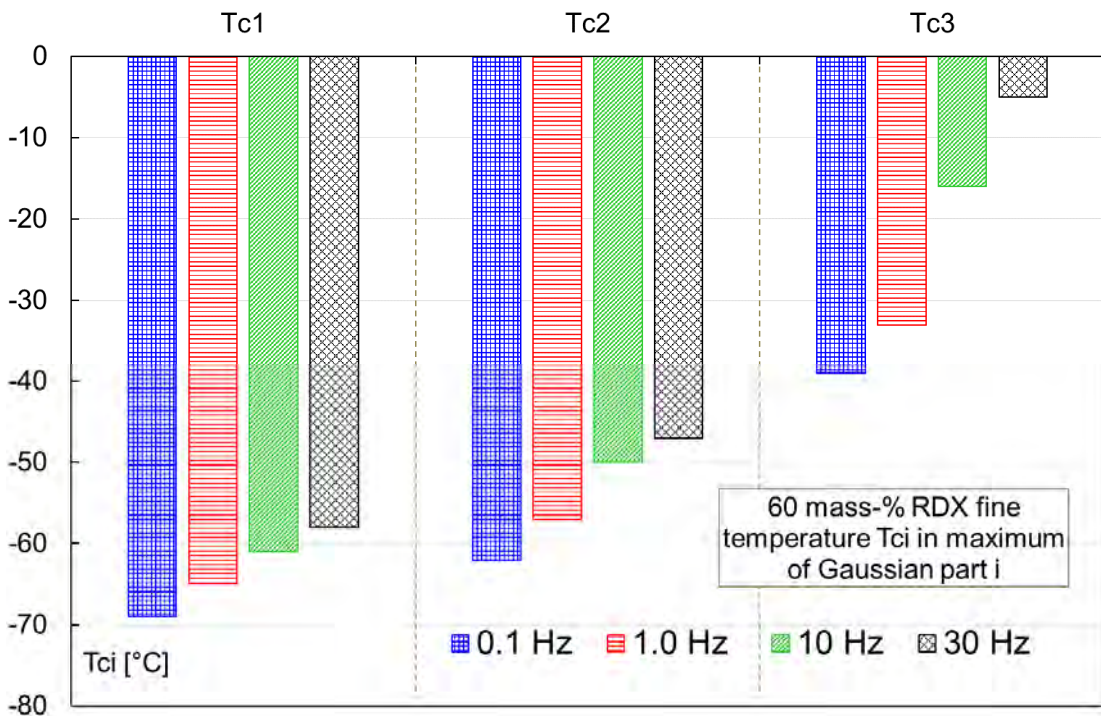


Figure 16b: Change in Gauss peak temperatures T_{ci} of the three EMG peaks in composite HTPB-60 m.-%-RDX fine with applied deformation frequency. All three temperatures are shifted to less negative values with frequency. Relatively seen is the change in T_{c3} greatest.

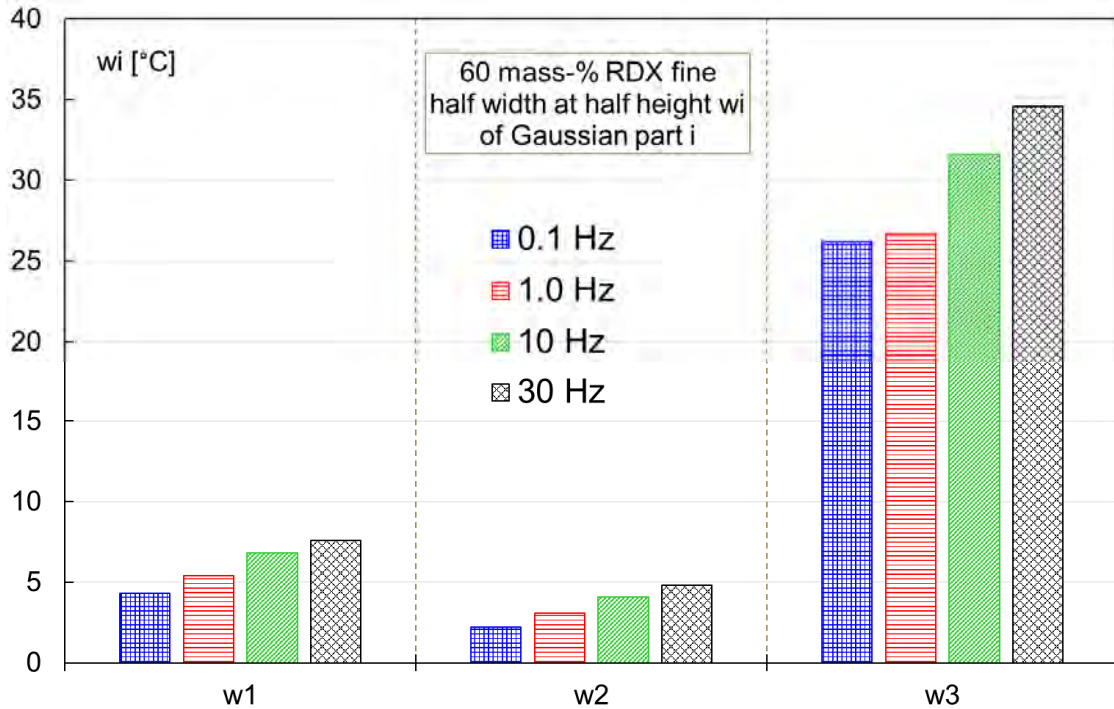


Figure 16c: Change in Gauss peak half width w_i of the three EMG peaks in composite HTPB-60 m.-%-RDX fine with applied deformation frequency. The half width always increases in one group with frequency. The half width of peak 3 is largest and the relative increase is pronounced.

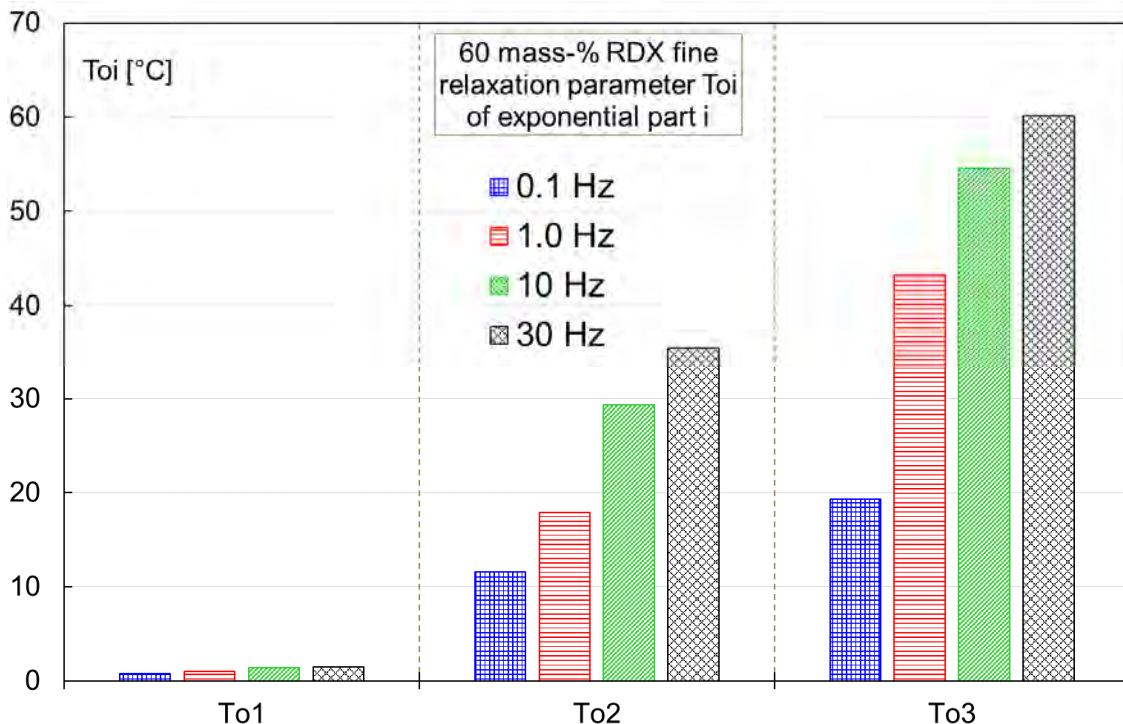


Figure 16d: Change in relaxation parameter To_i of the three EMG peaks in composite HTPB-60 m.-%-RDX fine with applied deformation frequency. All three parameters increase with frequency. The parameter of peak 3 is largest and the relative increase is pronounced.

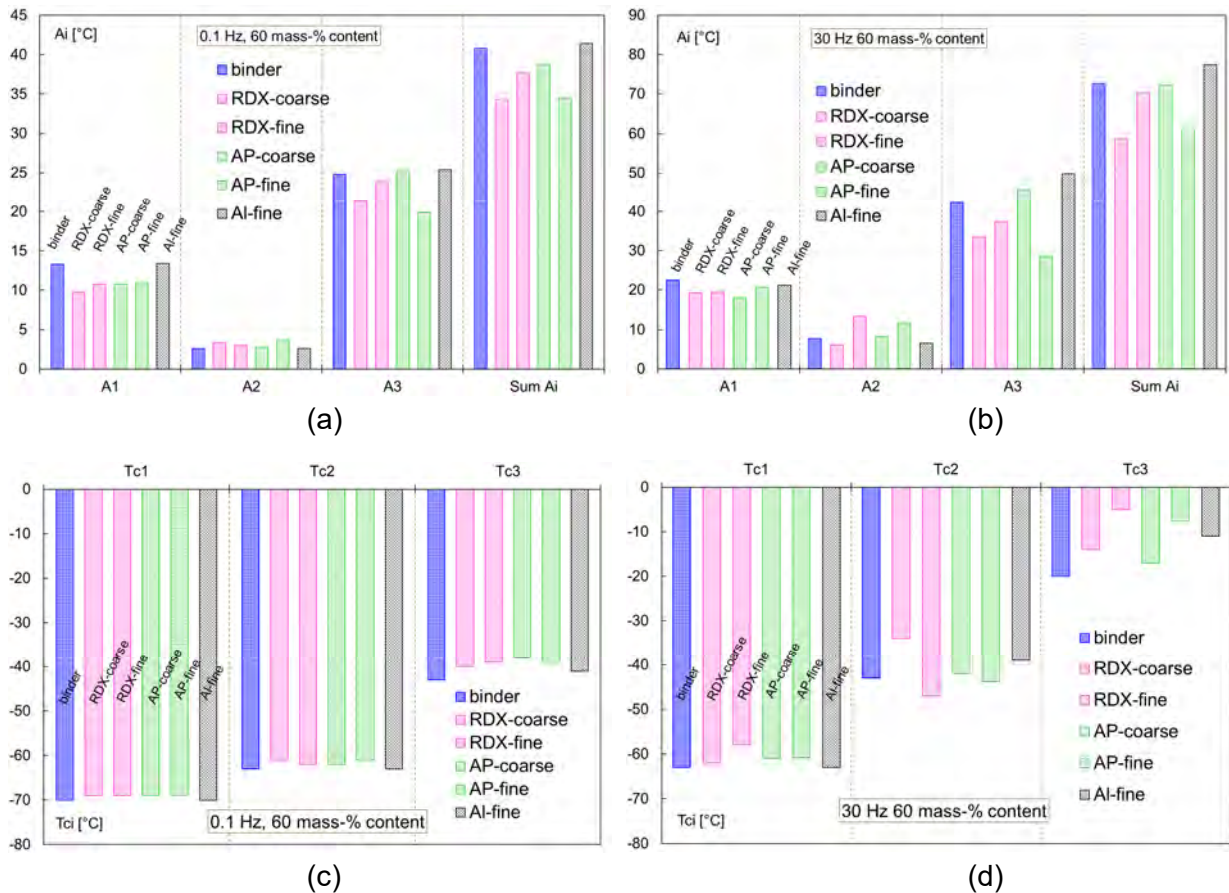


Figure 17: Comparison of the modelling parameters area A_i (a and b) and Gauss peak temperature T_{ci} (c and d) at 0.1 Hz (left) and 30 Hz (right) deformation frequency, composites with 60 mass-% filler. In each figure one series of the columns is named, the naming is always equal for the other series.

Two parameters are important for composites and are discussed now in more detail. One parameter is the intensity or area parameter A_i . The other parameter is the peak temperature T_{ci} . When the intensity of the glass-rubber transition expressed by A is small, the reasons can be: (1) more hindrance in mobility for the pre-polymer or (2) a more elastic behavior of the polymer, means a more dominant elastic (storage) shear modulus. The temperature of the glass-rubber transition approximated by T_{ci} is decisive for the use or application. Composites with elastomeric binders have the operational in-service above the glass-rubber transition temperature, this means it must be low enough to afford low temperature use.

The following refers to Fig 17a till Fig. 17d. Regarding the sum of the peak areas ($\sum A_i$), filling the binder with AP coarse particles had nearly no effect on the area. Fine AP however causes an overall depreciation of A_i parameters. This means that the polymer gained more in the elastic shear modulus than in the loss shear modulus – one can say the sample is more elastic and less viscous compared to AP coarse. But the higher the $\tan\delta$ or the area of it the greater the binder part which can perform the transition from glassy to rubbery transition. RDX has a reversed effect: the filling with coarse particle size decreases the sum of A_i parameters. SEM analysis of AP fine and RDX coarse particles (Fig. 18b and 18c) show that both are less round, means they have more irregular geometry and edges, whereas coarse AP and fine RDX (Fig. 18a and Fig. 18d) have a shape closer to a sphere or are at least rounded. This is an indication that the sum of A_i parameters is more affected by the AP and RDX particle shape than by their size. The round particles exert less mobility restrictions but create a higher amount of amorphous binder structures instead of rigid ones. The rigid binder parts cannot transform from glassy to rubbery state. The both AI powders have more or less rounded particles (Fig. 18e and 18f). See also Fig. 19 and Fig. 20.

Area A_3 is the one of the loss factor peak attributed to the transition of binder parts with more mobility restriction, i.e hindrance of chain mobility by filler-particle interactions and by the cross-link ranges. But these types of hindrances are not rigidity promoting as this is caused by increasing cross-link density during ageing. It is evident from the results that the addition of Al particles has a stronger effect on increasing the value of parameter A_3 than the other particles have, and this effect is more pronounced when deformation frequency is increased.

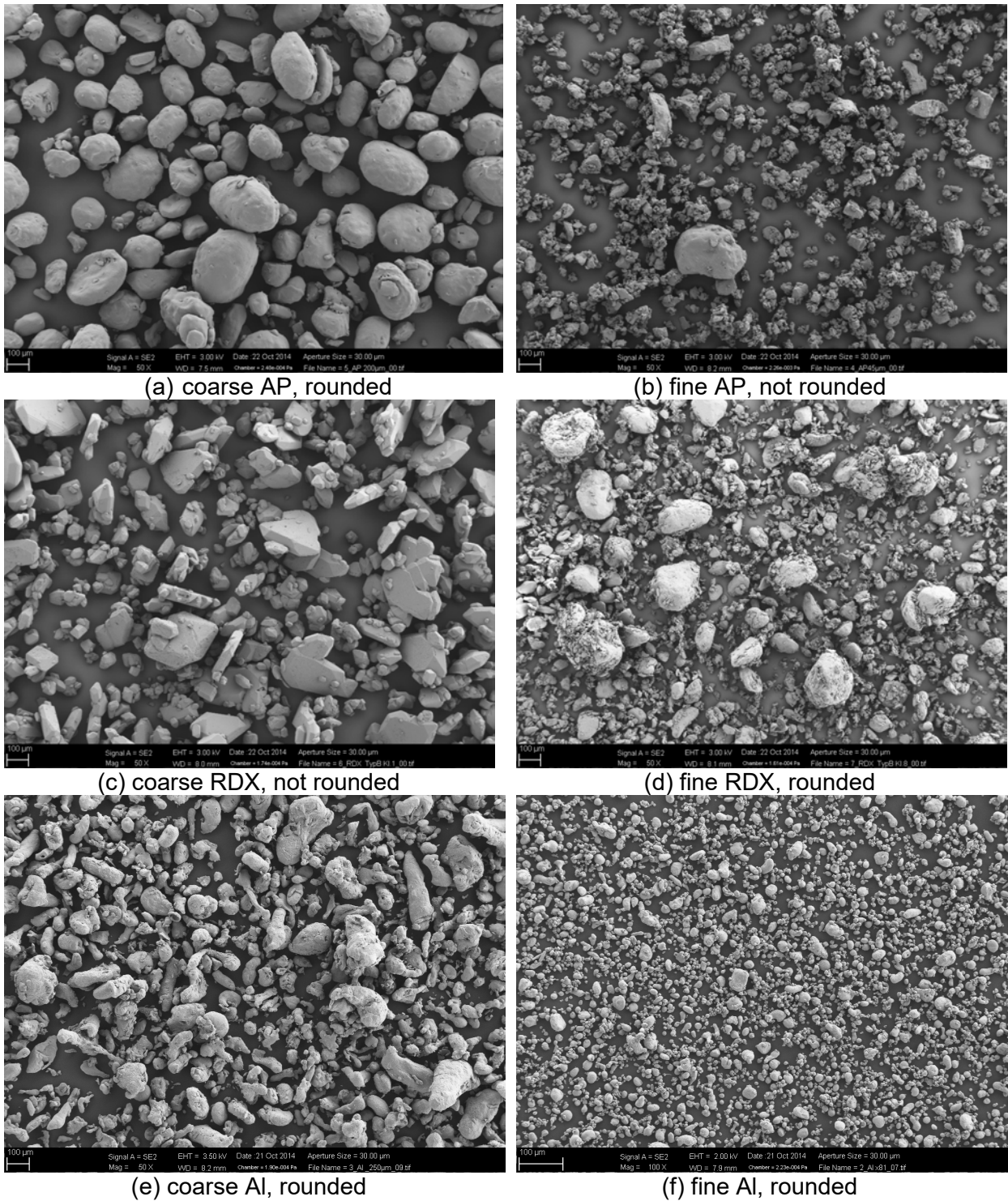


Figure 18: SEM images (magnification of 50X) of the particles used here; (a) coarse AP (b) fine AP; (c) coarse RDX; (d) fine RDX; (e) coarse Al; (f) fine Al. Scale of 100µm.

On the surface of aluminum particles species as Al hydroxide can be formed due to contact of the metallic Al with air (oxygen) and humidity. It was already discussed in the literature that the OH on Al may capture one end of isocyanate molecules [3], leaving less isocyanate groups to react with pre-polymer and more not bonded polyol chain ends are available. This may change the R_{eq} in the binder near the Al particles. According to literature, the second apparent loss factor peak in HTPB-based solid propellants, represented mainly by the EMG-3 (peak 3), can be caused by two effects:

(1) from the flow of free polymer chains in the polymer network with a reptation mechanism (snake like movement). If more polymer or polyol chains are available to move near the particle due to isocyanate "capture" near the aluminum surface, one could expect an increase in A_3 value [19];

(2) from a more intense intermolecular interaction between Al and HTPB than between the polyol and AP.

(2-1) From molecular dynamics one knows that metallic Al has higher intermolecular interaction energies with HTPB than AP. Therefore, the hindrance of HTPB chains is larger, which extends the range of the polymer shell around Al and this effect increases the intensity of the loss factor [20, 21]. Due to stronger interactions, the Al exert more hindrance on the mobility of the HTPB chains in the polymer shell around the particles [7,8,9]. As a consequence the glass-rubber transition temperature of such binder fractions is shifted to higher temperature values compared to not mobility restricted HTPB chains (see T_{c3} parameters).

(2-2) Secondly, because of the increased binder part in this fraction, it creates a relative intense glass-rubber transition in the polymer chains, since the mobility restriction imparted by Al is not high enough to hinder the transition to take place.

(2-3) Another effect is the stronger chemical bonding of Al particles to the network, when isocyanate attaches to the Al surface via its OH groups and bonds it to the binder via the second NCO group. This enlarges the polymer shell around Al particles and the intensity of A_3 is increased.

This effect of reducing mobility can be also the case, if one has increasing cross-linking between the polymer chains in the neighborhood of particles, which form then a more rigid amorphous region and the transition intensity is reduced, but the storage modulus increases. This was found with ageing of composite RP [7].

Regarding the T_{ci} parameters, T_{c1} is nearly not affected, independent of particle size or type. T_{c2} and T_{c3} are increased (become less negative), and the increase is more pronounced at higher deformation frequencies, especially with fine particle sizes. This is an indication that an increase in solid filler tend to enhance chain mobility restrictions, affecting the T_g^{res} , and corroborating the results shown in Table 2 and in Figure 17.

In Fig. 19 and Fig. 20 some features are expressed and will be discussed. The base is the loss factor curve of the unfilled binder. The Al-coarse composite curve coincides nearly completely along the first peak with the curve of the unfilled binder. In the range of the second evident peak, the Al-coarse causes higher intensity than the binder, not much, but significantly. This is indicative for the build-up of a polymer shell around the Al particles. Another feature is shown by the RDX-coarse composite. From Fig. 18c is clear that RDX coarse has not rounded particles. Plates can be identified. Such particle shapes hinder effectively chain mobility and therefore the first loss factor peak is reduced more than with rounded particles. This is expressed also in the second evident peak with an intensity lower than the one of the unfilled binder. In Fig. 20 the situation is reverse with AP-fine and RDX-fine. Now AP-fine is not rounded but RDX-fine is. AP-fine reduces the intensity of first peak a bit more than RDX fine, but the second peak is now reduced by AP-fine whereas RDX-fine opens (reduces) the interactions between the HTPB chains and the intensity increases. Pronounced said: RDX fine acts as a plasticizer in this binder part.

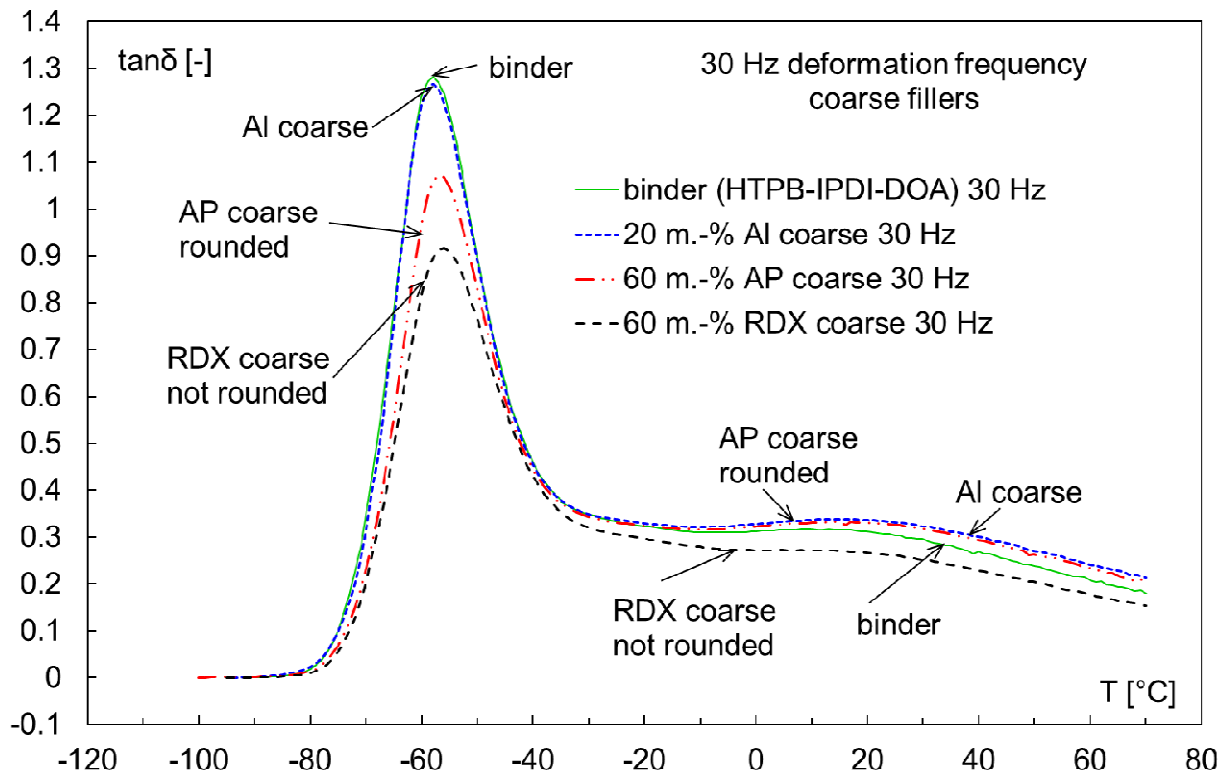


Figure 19: Four loss factor curves obtained at 30 Hz deformation frequency, comparison of three composites with **coarse** Al, AP and RDX with the unfilled binder.

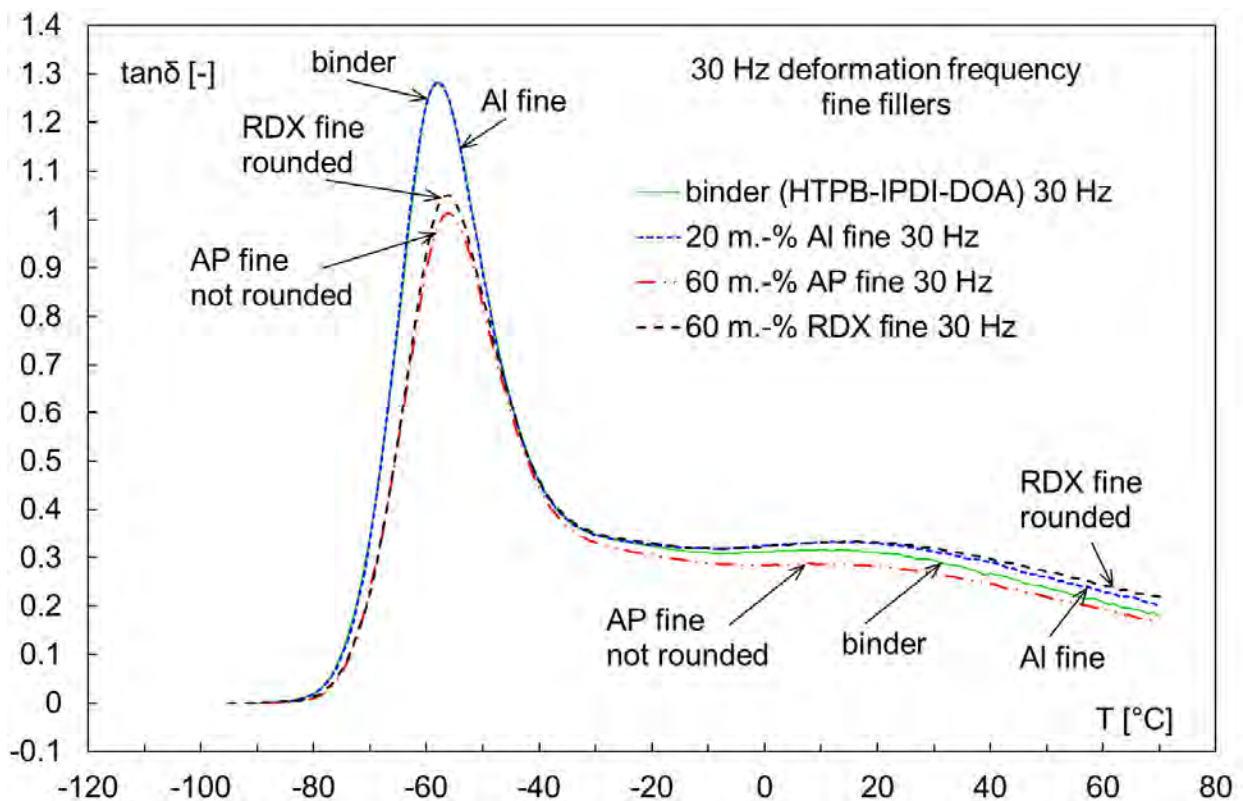


Figure 20: Four loss factor curves obtained at 30 Hz deformation frequency, comparison of three composites with **fine** Al, AP and RDX with the unfilled binder.

3.4 Parameterization of loss factor shift with deformation frequency

The deformation frequency dependence of the thermo-mechanically activated glass-rubber transition can be expressed by Arrhenius parameterization. With the use of an Arrhenius type equation, Eq.(5), an apparent activation energy E_{a_f} of the binder chain separation process can be estimated. This is possible when the process under consideration is activatable by thermal energy and the change in free volume and molecular volume effects are not involved. Then the determined activation energy is representing molecular interaction energy.

$$f = f_0 \cdot \exp\left(-\frac{E_{a_f}}{R \cdot T_g(f)}\right) \quad (5)$$

f	applied deformation frequency [Hz];
f_0	pre-exponential factor [Hz], deformation frequency at T infinitely high;
E_{a_f}	activation energy for the shift of T_g (glass-rubber transition) by deformation rate hardening (strain rate hardening) of the material [$\text{kJ} \cdot \text{mol}^{-1}$];
R	general gas constant [$8.31441 \text{ J} \cdot \text{K}^{-1} \text{ mol}^{-1}$];
T_g	glass-rubber transition temperature [K] as function of deformation frequency, T_g is taken here in the maximum of the loss factor.

For the purpose of this parameterizations, it is necessary to determine the maximum temperatures T_g quite well. Therefore, the temperatures of the two evident maxima in the loss factor curve $\tan\delta(T) = G''(T)/G'(T)$ of the samples were determined by using fits of polynomials of degree 3 just around the maxima and calculating the temperatures connected to the maxima. In Table 3 the data are compiled together with the Arrhenius parameters according to Eq.(5). Some fields of the E_{a_f} column are highlighted by boxes in Table 3. These data will be discussed in the following. First, a look on the E_{a_f} values of the pure binder. The first maximum at lower temperatures provides with 180.7 kJ/mol, which coincides well with data of HTPB-IPDI binder determined earlier with 196 kJ/mol [7,9]. The parameterization of the second maximum gives much smaller activation energies, for the binder it is 84.7 kJ/mol. This expresses the differences in interaction energies between the molecular regions of the binder. At lower temperatures the distances between the binder chain elements are smaller than at the temperature of the second maximum (-70°C to -58°C versus -28°C to +11°C) and therefore the energetic interaction is greater at lower temperatures.

From Table 3 the following can be concluded, see the highlighted parts in E_{a_f} column.

- AP coarse reduces E_{a_f} values in first peak with increasing content. AP coarse increases E_{a_f} values in second peak with increasing content. In second peak, AP coarse acts as intermolecular bond breaker, because the E_{a_f} value first decreases with small contents. The differences in peak temperature with regard to the pure binder are small in first peak. They increase with deformation frequency. In second peak, the differences to the reference are larger. AP fine causes a shift to lower temperatures in second peak
- RDX coarse reduces quite strongly E_{a_f} values in first peak with increasing content. In second peak no clear direction, more or less the E_{a_f} values stay constant. Also RDX fine reduces strongly the E_{a_f} value in first peak. The differences in peak temperature with regard to the pure binder are small in first peak. They increase with deformation frequency. In second peak the differences to the reference are larger.
- Al fine causes increase of E_{a_f} values in first peak with increasing content, same direction probably also in second peak. The interactions of Al via the polar surface groups (OH) may cause this. Al coarse shows also the effect of intermolecular bond breaking. The differences in peak temperature with regard to the pure binder are even

smaller in first peak compared to AP and RDX. They have the tendency to decrease with deformation frequency. But in second peak the differences to the reference are as large as with AP coarse and RDX coarse.

Table 3: Values of T_g^{unr} and T_g^{res} of the first and second peak of $\tan\delta$ curve, given for all investigated samples, at deformation frequencies 0.1, 1.0, 10 and 30 Hz. The reference is the unfilled binder. The arrows in the column of activation energy show the change in values with changing filler content.

Sample	T_g^{unr} (first apparent peak)				Difference to reference				E_a [kJ.mol ⁻¹]	$\ln(f_0)$ [Hz]
	0.1Hz	1.0Hz	10Hz	30Hz	0.1Hz	1.0Hz	10Hz	30Hz		
binder alone	-69.42	-65.58	-60.72	-57.95	(reference)				180.7	45.43
20% AP coarse	-68.86	-65.24	-60.28	-57.51	0.56	0.34	0.44	0.44	182.6	45.79
40% AP coarse	-68.78	-65.04	-60.11	-57.27	0.64	0.54	0.61	0.68	180.9	45.34
60% AP coarse	-68.63	-64.76	-59.62	-56.74	0.79	0.82	1.10	1.21	175.4	43.91
60% AP fine	-68.29	-64.38	-59.06	-56.16	1.13	1.20	1.66	1.79	172.3	43.04
20% RDX coarse	-68.95	-65.02	-60.09	-57.37	0.47	0.56	0.63	0.58	179.8	45.07
40% RDX coarse	-68.97	-65.01	-59.91	-57.22	0.45	0.57	0.81	0.73	176.7	44.30
60% RDX coarse	-69.58	-64.28	-59.02	-55.94	-0.16	1.30	1.70	2.01	154.9	38.78
60% RDX fine	-69.44	-64.56	-59.19	-56.19	-0.02	1.02	1.53	1.76	158.6	39.71
20% Al coarse	-68.90	-65.65	-60.76	-57.91	0.52	-0.07	-0.04	0.04	187.3	47.05
20% Al fine	-69.54	-65.71	-60.81	-57.95	-0.12	-0.13	-0.09	0	179.1	45.00
40% Al fine	-69.23	-65.69	-60.71	-57.77	0.19	-0.11	0.01	0.18	180.6	45.34
60% Al fine	-69.01	-65.56	-60.60	-57.80	0.41	0.02	0.12	0.15	184.0	46.18
	T_g^{res} (second apparent peak)				Difference to reference					
binder alone	-28.04	-13.65	2.52	10.87	(reference)				84.7	17.06
20% AP coarse	-29.42	-15.63	2.00	11.03	-1.38	-1.98	-0.52	0.16	80.7	16.33
40% AP coarse	-28.33	-14.14	2.94	12.46	-0.29	-0.49	0.42	1.59	81.3	16.37
60% AP coarse	-24.92	-11.96	4.22	14.98	3.12	1.69	1.70	4.11	85.4	17.03
60% AP fine	-29.25	-16.82	0.23	8.49	-1.21	-3.17	-2.29	-2.38	85.2	17.31
20% RDX coarse	-25.36	-12.23	4.57	14.24	2.68	1.42	2.05	3.37	85.1	17.00
40% RDX coarse	-24.34	-10.94	6.36	15.75	3.70	2.71	3.84	4.88	84.6	16.82
60% RDX coarse	-25.38	Not well defined			2.66	Not well defined				
60% RDX fine	-24.05	-11.76	4.96	15.47	3.99	1.89	2.44	4.60	86.1	17.14
20% Al coarse	-26.01	-11.7	6.13	15.09	2.03	1.95	3.61	4.22	81.7	16.29
20% Al fine	-25.88	-12.44	3.76	13.54	2.16	1.21	1.24	2.67	85.5	17.10
40% Al fine	-25.91	-11.74	4.35	11.32	2.13	1.91	1.83	0.45	88.7	17.74
60% Al fine	-23.25	-10.33	7.38	15.8	4.79	3.32	4.86	4.93	86.5	17.14

In short it is mentioned that some authors prefer the Williams-Landel-Ferry (WLF) equation for the temperature parameterization of quantities connected with polymers. Often it gives a better description than the standard Arrhenius equation, shown above. Especially to describe the so-

called horizontal shift factor obtained during construction of master curves is better described with WLF. But the WLF equation, Eq.(6), is completely congruent with the modified Arrhenius equation, Eq.(7), what was shown in a recent paper, see [23]. There also applications are shown and the difference in Ea_{0M} and Ea_f is discussed. An important outcome is that the second WLF invariant $C_1 \cdot C_2$ is proportional to activation energy Ea_{0M} , Eq.(8), and the first WLF invariant T_∞ is the same as T_{0M} , Eq.(9)

$$\lg(a_T(T, Tr) [-]) = \lg\left(\frac{f(Tr)}{f(T)}\right) = -\frac{C_1 \cdot (T - Tr)}{C_2 + (T - Tr)} \quad (6)$$

$$f = f_{0M} \cdot \exp\left(-\frac{Ea_{0M}}{R \cdot (T_g(f) - T_{0M})}\right) \quad (7)$$

f	applied deformation frequency [Hz];
f_{0M}	pre-exponential factor [Hz];
Ea_{0M}	activation energy for the shift of T_g by strain rate hardening [$\text{kJ} \cdot \text{mol}^{-1}$];
R	general gas constant [$8.31441 \text{ J} \cdot \text{K}^{-1} \text{ mol}^{-1}$];
T_g	glass-rubber transition temperature [K] as function of deformation frequency
T_{0M}	mobility freezing reference temperature, identical to T_∞ of WLF equation (spoken T zero mobility)

$$Ea_{0M} = R \cdot C_1 \cdot C_2 / \lg(e) \quad (8)$$

$$T_{0M} = Tr - C_2 = T_\infty \quad (9)$$

4. Summary and conclusions

The formulations with low to medium to high filler content could be manufactured successfully by using a turning machine during curing, in order to get a homogenous distribution of the filler particles all over the binder matrix volume. For the mixing, a planetary-rotary mixer was used to produce smaller amounts of composites. The binder is based on HTPB-IPDI polyurethane with 5 mass-% DOA added. The equivalent ratio R_{eq} (NCO / OH) = 0.85, as typical for CRP type formulations. Fillers have been AP coarse and fine (202 and 43 μm), RDX coarse and fine (233 and 61 μm) and Al coarse and fine (130 and 21 μm). No bonding agents have been used. Content steps were 20, 40 and 60 mass-% in binder.

The possible effects of filler concentration on the visco-elastic properties of the composites have been investigated with DMA (dynamic mechanical analysis) in torsion mode. Two properties of the loss factor curves have been used, determined at four deformation frequencies: The deformation rate caused shift of the temperatures at the two apparent maxima and the shape of the curves. The temperature shift was parameterized by a standard Arrhenius expression. The shape analysis was performed by applying three EMG distributions to each loss factor curve, providing with intensities for binder parts with different glass-rubber transition temperatures, caused by different molecular mobilities in the binder parts.

Main results are:

AP and RDX cause more changes in intensity of first peak of loss factor than Al fine particles. The temperature in first maximum is not much changed by the fillers at all concentrations. Al particles change least in comparison to unfilled binder. The changes in temperature of second peak are greater. The intensity changes in loss factor were determined via EMG modelling. AP fine decreases intensity compared to AP coarse. The effect is vice versa with RDX. It seems

that particle shape has a distinct influence. The rounder particles have a less hindrance effect on molecular mobility and finally increase the intensity in the transition glass to rubber. Increasing content of AP and RDX increase the elastic (storage) modulus G' and a bit increase in the loss modulus G'' also. But in total the main peak in loss factor curve is reduced in intensity. From the change in loss factor intensity and temperature shifts, it is concluded that Al particles have a stronger molecular interaction with the binder than AP and RDX, if no bonding agents are used.

5. Abbreviations

Al	aluminium, powder, fuel
AO	antioxidant
AP	ammonium perchlorate, powder, oxidizer
BLC	baseline correction of loss factor
BO	bonding agent
CRP	composite rocket propellant
CT	computer tomography
DMA	dynamic mechanical analysis
DOA	dioctyl adipate or better di-(ethyl-hexyl) adipate, plasticizer
EMG	exponentially modified Gauss distribution
HMX	Octogen, octahydro-1,3,5,7-tetranitro-1,3,5,7-tetrazin, high explosive compound
HTPB	hydroxyl terminated polybutadiene, binder pre-polymer
HX	abbreviation for high explosive formulation
IPDI	isophorone diisocyanate, cross-linker or curing agent
RDX	hexahydro-1,3,5-trinitro-1,3,5-triazin, high explosive compound (known also as cyclo-trimethylene-trinitramine, royal demolition explosive, research department explosive, Hexogen, Cyclonite, T4)
SEM	scanning electron microscopy
G'	Storage or elastic shear modulus
G''	Loss or viscous shear modulus
$\tan\delta$	Loss factor, $\tan\delta = G''/G'$

6. References

- [1] Sara Cerri, Manfred A. Bohn, Klaus Menke, Luciano Galfetti. Ageing Behavior of HTPB Based Rocket Propellant Formulations. *Central European Journal of Energetic Materials*, 6(2), 149-165, **2009**.
- [2] Manfred A. Bohn
Impacts on the loss factor curve and quantification of molecular rearrangement regions from it in elastomer bonded energetic formulations.
in 'Energetics Science & Technology in Central Europe' edited by R. Armstrong, J. Short, and D.K. Anand. CALCE EPSC Press, University of Maryland, College Park, MD 20742, USA. **2012**.
- [3] Sara Cerri, Manfred A. Bohn.
Separation of molecular mobility ranges in loss factor curves by modeling with exponentially

modified gauss distributions.

Paper 87, pages 87-1 to 87-16 in Proceed. of 41th International Annual Conference of ICT on 'Energetic Materials – High Performance, Insensitive Munitions, Zero Pollution', June 29 to July 2, 2010, Karlsruhe, Germany. ISSN 0722-4087. Fraunhofer-Institut für Chemische Technologie (ICT), D-76318 Pfinztal-Berghausen. Germany. **2010.**

[4] Manfred A. Bohn, Sara Cerri.

Aging Behavior of ADN Solid Rocket Propellants and Their Glass-Rubber Transition Characteristics. pages 771 to 800 in

De Luca L.T., Shimada T., Sinditskii V.P., Calabro M. (eds) (2016) Chemical rocket propulsion: A comprehensive survey of energetic materials. ISBN 978-3-319-27746-2. DOI 10.1007/978-3-319-27748-6. Springer International Publishing AG, CH-6330 Cham, Switzerland. **2016.**

[5] Manfred A. Bohn and Sara Cerri.

Molecular mobility in binder systems.

Proc. 42nd International Annual Conference of ICT on 'Energetic Materials', June 28 to July 1, 2011, Karlsruhe, Germany. ISSN 0722-4087. Version CD-Proceedings. Paper 96, pages 96-1 to 96-33, **2011.**

[6] Manfred A. Bohn, Günter Mußbach, Sara Cerri.

Influences on the Loss Factor of Elastomer Binders and its Modeling.

Paper 60, pages 60-1 to 60-43 in Proceedings of the 43rd International Annual Conference of ICT on 'Energetic Materials – Synthesis, Characterisation, Processing', June 26 to 29, 2012, Karlsruhe, Germany. ISSN 0722-4087. Fraunhofer-Institut fuer Chemische Technologie (ICT), D-76318 Pfinztal. Germany. **2012.**

[7] Sara Cerri, Manfred A. Bohn, Klaus Menke, Luciano Galfetti,

Ageing of HTPB/AL/AP rocket propellant formulations investigated by DMA measurements. Propellants, Explosives, Pyrotechnics, vol. 38, pp. 190-198. **2013.**

[8] Manfred A. Bohn, Günter Mußbach, Sara Cerri.

Modeling of loss factors of elastomer binders of high explosive charges and composite rocket propellants to separate binder fractions with different molecular mobility used to follow aging.

Proc. of 10th Int. Symposium on Special Topics in Chemical Propulsion & Energetic Materials, Poitiers, **2014.**

[9] Sara Cerri, Manfred A. Bohn, Klaus Menke, Luciano Galfetti,

Aging of ADN Rocket Propellant Formulations with Desmophen-Based Elastomer Binder. Propellants, Explosives, Pyrotechnics, vol. 39, pp. 526-537. **2014.**

[10] Mauricio F. Lemos, Guenter Mussbach, Manfred A. Bohn.

Evaluation of filler effects on the dynamic mechanical analysis of elastomer applied as binder in composite propellants.

J. Aerospace Tech. Management. Paper in production.

[11] Manfred A. Bohn, Günter Mußbach, Gunnar Kronis

Data interpretation and comparison of DMA results from HTPB-IPDI bonded composite elastomer samples used in an international Round Robin Test.

Paper 131, pages 131-1 to 131-19. CD-Proc. of the 47th International Annual Conference of ICT on 'Energetic Materials – Synthesis, Characterization, Processing', June 28 to July 1, 2016, Karlsruhe, Germany. ISSN 0722-4087. Fraunhofer-Institut fuer Chemische Technologie (ICT), D-76318 Pfinztal, Germany. **2016.**

- [12] Tijen Seyidoglu, Manfred A. Bohn.
Effect of Butacene® on ageing of composite propellants.
Proc. of the 19th NTREM (New Trends in Research of Energetic Materials), Pardubice, pages 904-925. Pardubice, Czech Republic, April 20-22, **2016**.
- [13] Tijen Seyidoglu, Manfred A. Bohn, Guenter Mussbach.
Accelerated Aging and Cure Kinetics of Butacene® Containing Composite Propellants
Paper 78, pp 78-1 to 78-22, on CD Proceedings of the 47th International Annual Conference of ICT on 'Energetic Materials – Synthesis, Characterization, Processing', June 28 to July 1, 2016, Karlsruhe, Germany. ISSN 0722-4087. Fraunhofer-Institut fuer Chemische Technologie (ICT), D-76318 Pfinztal. Germany. **2016**.
- [14] Tijen Seyidoglu, Manfred A. Bohn.
Characterization of Aging Behavior of Butacene® Based Composite Propellants by Loss Factor Curves.
Propellants, Explosives, Pyrotechnics, in production, **2017**.
- [15] Tijen Seyidoglu, Manfred A. Bohn.
Modelling of Loss Factor Curves Obtained by Torsion-DMA of HTPB and GAP Based Binders manufactured with Different Curing Agents and Plasticizers.
Proc. 46th International Annual Conference of ICT, June 23 to 26, 2015, Karlsruhe, Germany. ISSN 0722-4087. Paper 118, pp 118-1 to 118-26, **2015**.
- [16] Mauricio F. Lemos, Manfred A. Bohn.
The effect of plasticizers on the glass-to-rubber behavior of Desmophen® 2200 based elastomers used for composite propellants.
Paper 22, pages 22-1 to 22-26 in Proc. of the 46th International Annual Conference of ICT on 'Energetic Materials – Performance, Safety and System Applications', June 23 to 26, 2015, Karlsruhe, Germany. ISSN 0722-4087. Fraunhofer-Institut fuer Chemische Technologie (ICT), D-76318 Pfinztal. Germany. **2015**.
- [17] Mauricio F. Lemos, Manfred A. Bohn.
Evaluation of the effect of plasticizers on the DMA loss factor, the thermal and mechanical properties of Desmophen® 2200- based elastomers used for composite propellants.
Proc. of the 18th NTREM (New Trends in Research of Energetic Materials), Pardubice, p. 670-694, **2015**.
- [18] Mauricio F. Lemos, Manfred A. Bohn.
DMA of polyester-based polyurethane elastomers for composite rocket propellants containing different energetic plasticizers.
J. Therm. Anal. Calorim., DOI 10.1007/s10973-016-5945-1, 2016, **2017**.
- [19] A. Azoug, R. Nevière, A. Constantinescu,
Molecular Origin of the influence of the temperature on the loss factor of solid propellant. Propellants, Explosives, Pyrotechnics, 40, pp.469-478, **2015**.
- [20] Michael M. Nardai, Manfred A. Bohn.
Cohesion properties in PBX and composite propellants – computational results and experimental aspects.
Paper 19, pages 19-1 to 19-17 in Proc. of the 46th International Annual Conference of ICT on 'Energetic Materials – Performance, Safety and System Applications', June 23 to 26, 2015, Karlsruhe, Germany. ISSN 0722-4087. Fraunhofer-Institut fuer Chemische Technologie (ICT), D-76318Pfinztal. Germany. **2015**.

- [21] Michael M. Nardai, Manfred A. Bohn.
Wetting of oxidizer particles by binder and plasticizer molecules – microcalorimetry experiments and computer simulations.
Proc. of the 18th NTREM (New Trends in Research of Energetic Materials), Pardubice, pages 212-228. Pardubice, Czech Republic, April 15–17, **2015**.
- [22] H.L. Ornaghi, Jr., A.S. Bolner, R. Fiorio, A.J. Zattera, S.C. Amico.
Mechanical and dynamic mechanical analysis of hybrid composites molded by resin transfer molding.
Journal of Applied Polymer Science, 118, pp. 887–896, **2010**.
- [23] Manfred A. Bohn,
The connection between WLF equation and Arrhenius equation.
Proceed 21th International Seminar NTREM (New Trends in Research of Energetic Materials), April 18-20, **2018**. Pages 64 to 81. University of Pardubice, Pardubice, Czech Republic.
Editors: Jiří Pachman, Jakub Šelešovský. Conference and proceedings number: 21. Published by University of Pardubice, Czech Republic, April **2018**. Pages 1227 + 16. ISBN 978-80-7560-136-0 (Print), ISBN 978-80-7560-137-7 (CD).

Influence of concentration, type and particle size of fillers on the dynamic mechanical behaviour of elastomeric HTPB binder

Dr. Manfred A. Bohn^{*}, Mauricio Ferrapontoff Lemos^{**,*}, Günter Mussbach^{***,*}

Manfred.Bohn@ict.fraunhofer.de

^{*} Fraunhofer Institut für Chemische Technologie (ICT), D-76318 Pfinztal, Germany

^{**} Brazilian Navy Research Institute, Rio de Janeiro, RJ, 21931-090, Brazil

^{***} Bayern-Chemie GmbH, 84544 Aschau am Inn, Germany

Presentation on the NDIA IMEMTS, event # 8550

Presentation reference number 20069

(Insensitive Munitions & Energetic Materials Technology Symposium)

April 23-26, 2018

Portland, Oregon, USA

Overview

Introduction

Objective

Substances

Manufacture of samples

- Mixing of ingredients

- Achieving homogenous distribution of filler in binder

Characterisation methods – Röntgen (X-ray)-CT, SEM, DMA, $T_{g,DMA}(f)$, EMG modelling

Results

- Parameterisation of the shift of glass-rubber transition (GRT) temperature $T_{g,DMA}$ with the DMA deformation frequency f

- Quantification of loss factor $\tan\delta$ with EMG (exponentially modified Gauss distribution)

Discussion

Conclusions

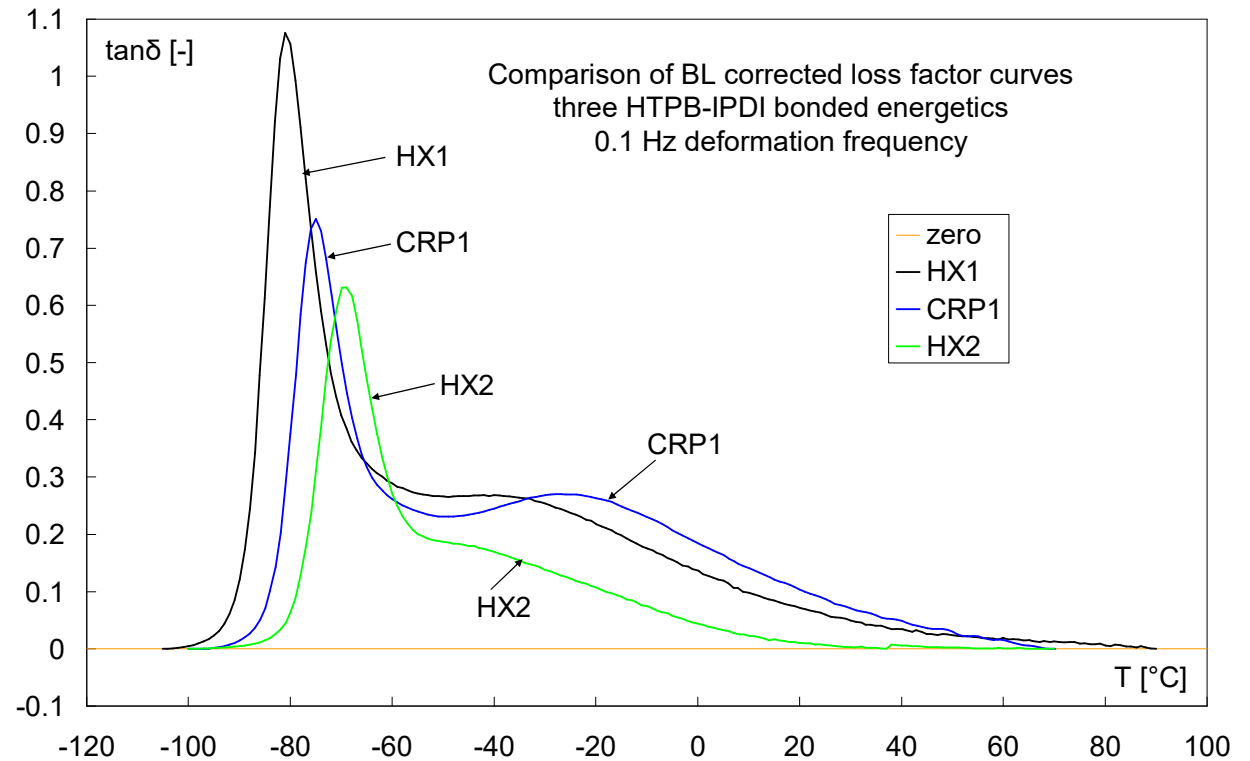
Introduction

What is known

In a series of investigations it was found that the second evident peak in the DMA loss factor curve of HTPB bonded composite RPs and PBXs changes in shape with composition. Bonded AP gives a clear established peak, HMX and RDX develop a smaller one; and with high degree of filling it is present as a shoulder only, see HX2.

This second peak is very ageing sensitive. It can be indicative for (1) de-wetting between filler and binder; (2) formation of a polymeric shell around the particle.

This means intermolecular interactions (pure sterical, energetic) show influence on second peak and on the shape of loss factor as a whole.



The principle structure / shape of loss factor is the same with all three compounds. Always two evident maxima.

Composition in mass-%

CRP: HTPB-IPDI (12), AP (78), Al (6), DOA (4, 25% of binder)
HX1: HTPB-IPDI (12), RDX (80), DOA (8, 40% of binder)
HX2: HTPB-IPDI (14), HMX (85), DOA (1, 6.7% of binder)

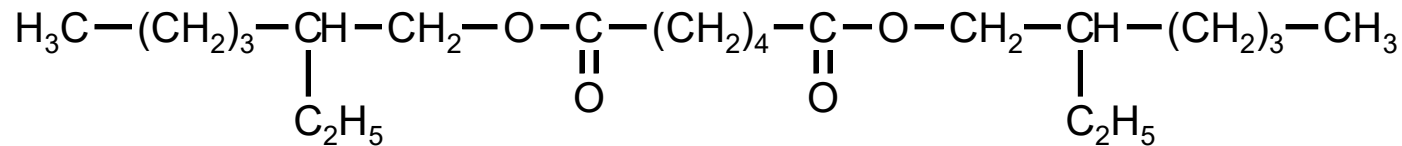
The plasticizer content determines mainly the position and the height of first peak.

Objective

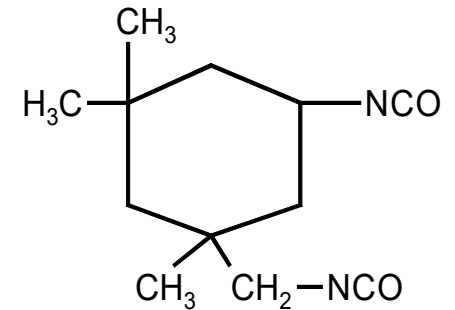
Experimental investigation on the **influence of concentration and type of fillers on the shape and intensity** of loss factor and on its shift with deformation frequency.

Three types of fillers with two particle sizes each are used in formulations with standardized binder matrix.

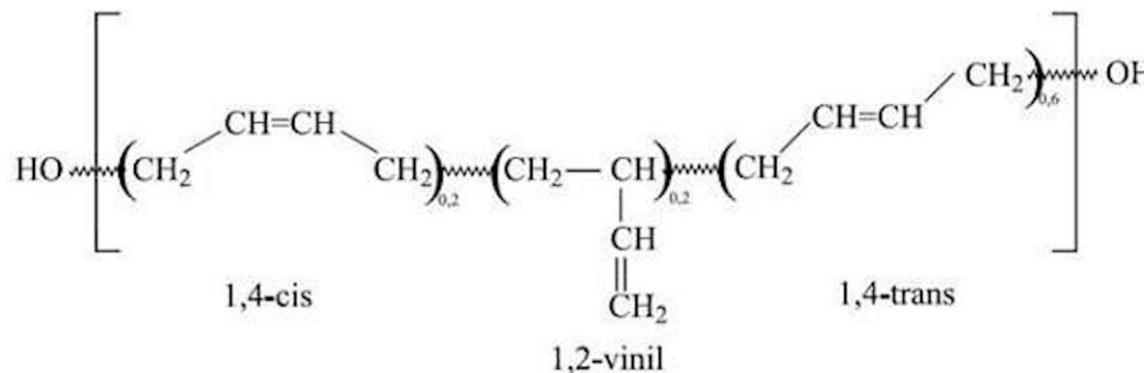
Substances – binder ingredients for the investigated formulations



Di-iso-octyl adipate
DOA (plasticizer)



Isophorone diisocyanate
IPDI (cross-linker)



Hydroxyl-terminated polybutadiene
HTPB (pre-polymer)

HTPB + IPDI form the elastomer binder as polyurethane

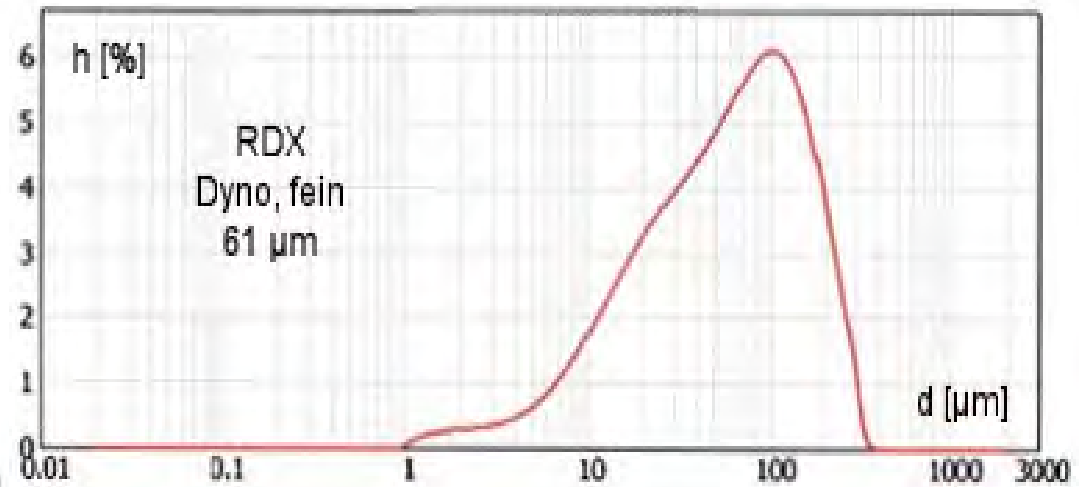
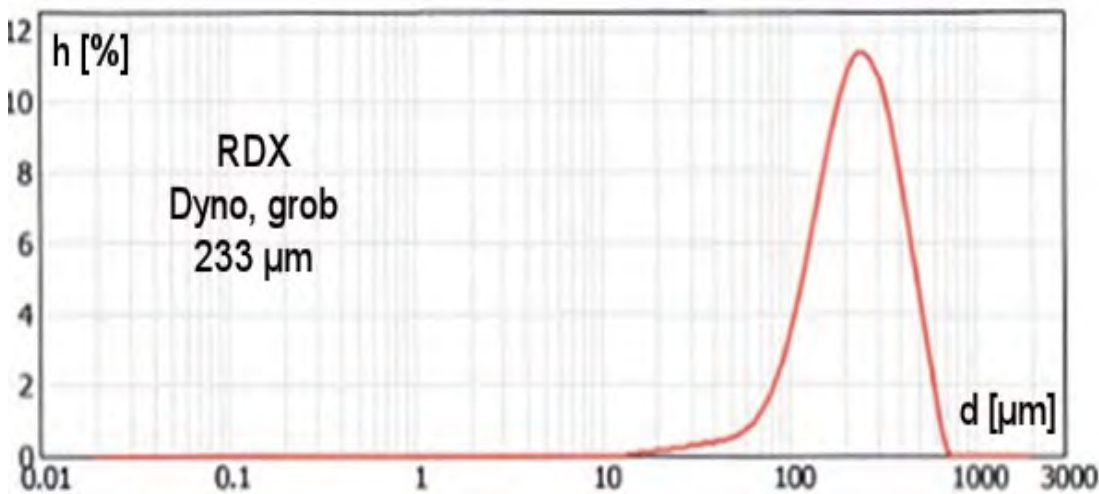
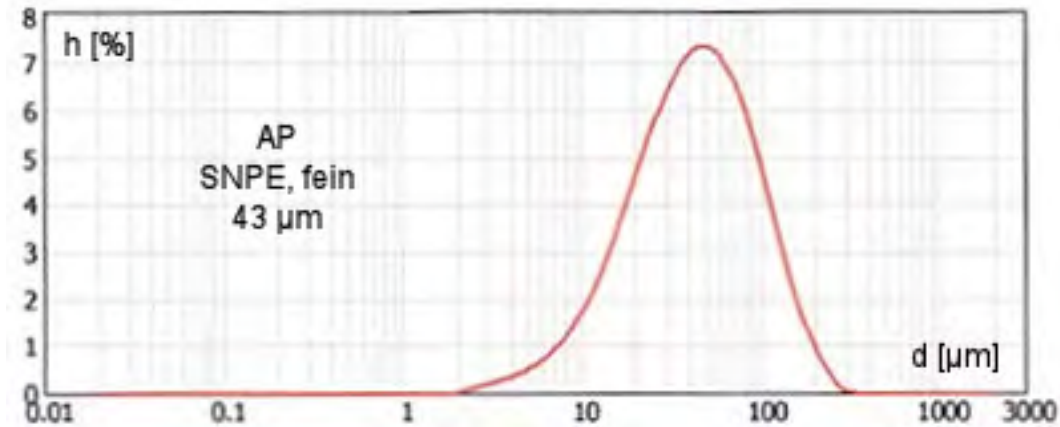
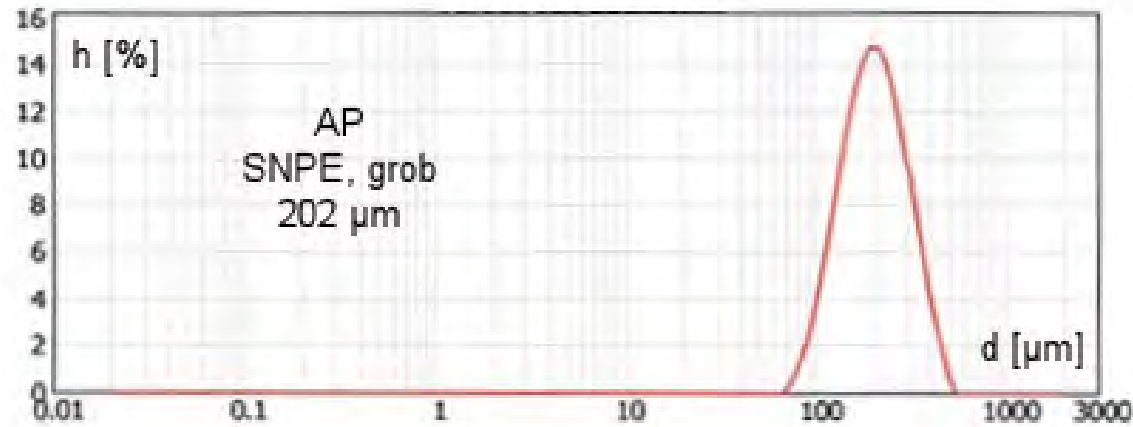
All formulations made with equivalent ratio $\text{Req} (\text{NCO} / \text{OH}) = 0.85$ (RP type curing)

Antioxidant added to protect the HTPB

No curing catalyst added. Equal curing at 60°C , 130 h (5d, 10h)

Always with 5 mass-% plasticizer (DOA) in binder

Substances – fillers AP (ammonium perchlorate) and RDX, two particle sizes

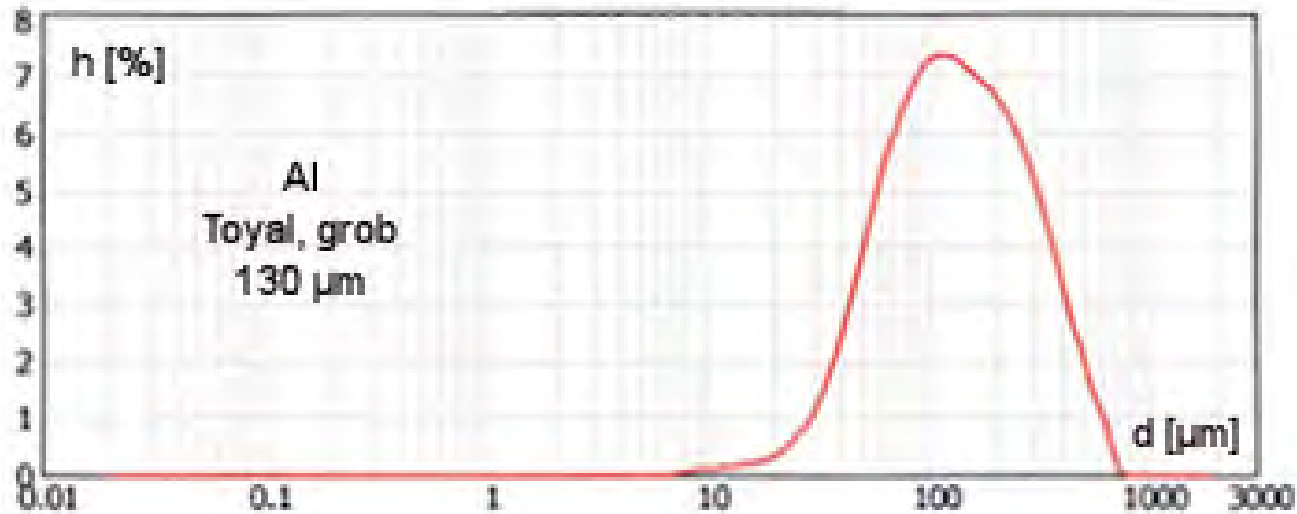


grob = coarse

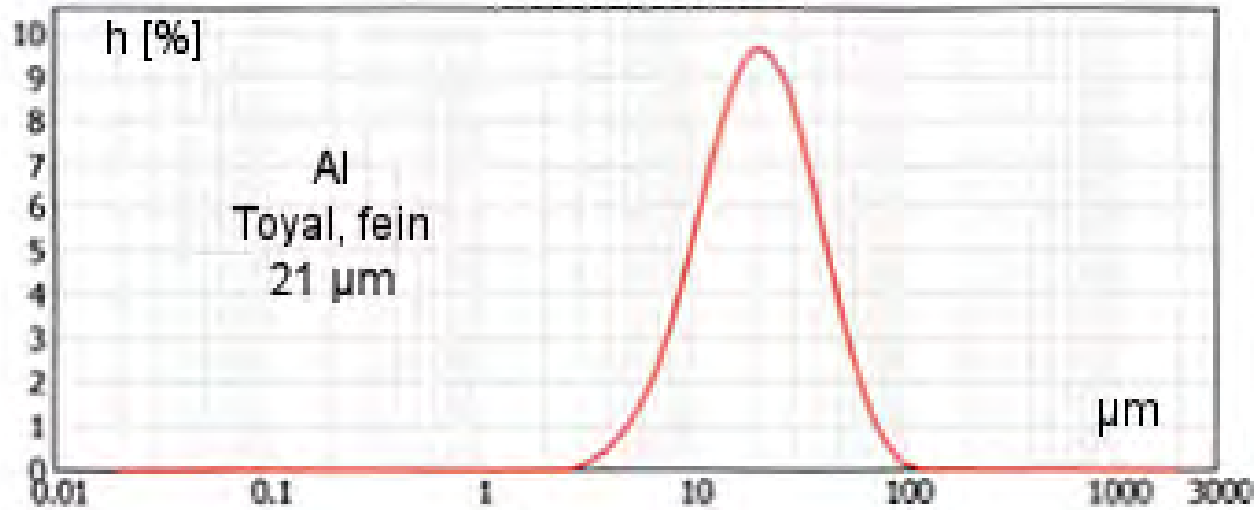
fein = fine (small)

Substances – filler Al (aluminium), two particle sizes

Aluminium - Al



grob = coarse



fein = fine

Manufacturing of the samples

With each of the six filler substances formulations were manufactured
Different filler contents: 20 mass-%, 40 mass-%, 60 mass-%

The formulations were mixed with a planetary-rotary mixer (PRM) of type 'Thinky mixer'.
Conditions: 1600 rpm, $p = 30 \text{ mbar} = 3 \text{ kPa}$, mixing in the way to keep $T < 40^\circ\text{C}$.

Pouring the final mix in small glass bottles with lid.

It is known:

Even with highly filled binders a certain sedimentation of fillers is observed.
Sedimentation will happen with such low content of fillers for sure.

To get useful results with DMA, the samples must be homogenous.

Therefore, a special curing method was developed.

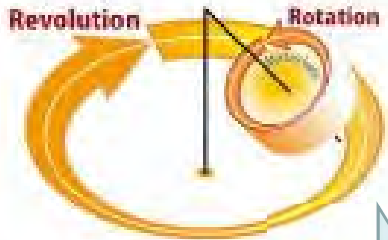
The curing was done with a turning device mounted in the curing oven.

Samples - Manufacturing - curing - characterisation

HTPB
+
plasticizer



Filler



$$R_{eq} = \text{NCO/OH} = 0.85$$



Mix procedure
in the way to
keep $T < 40^{\circ}\text{C}$

Using planetary –
rotary mixer called
'Thinky mixer'

Addition of IPDI at
end of main mixing.
One minute further
mixing.

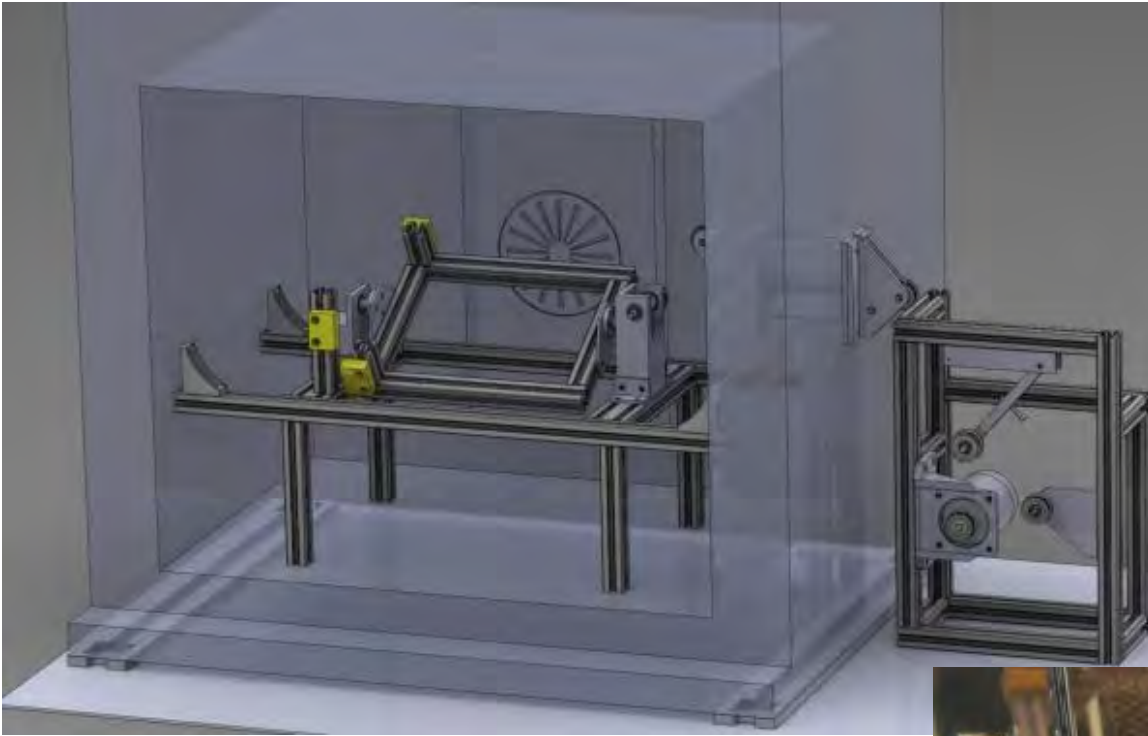


Curing in oven at 60°C with turning device

After curing analysis with

DMA

Turning device to achieve homogenous filler distribution during curing

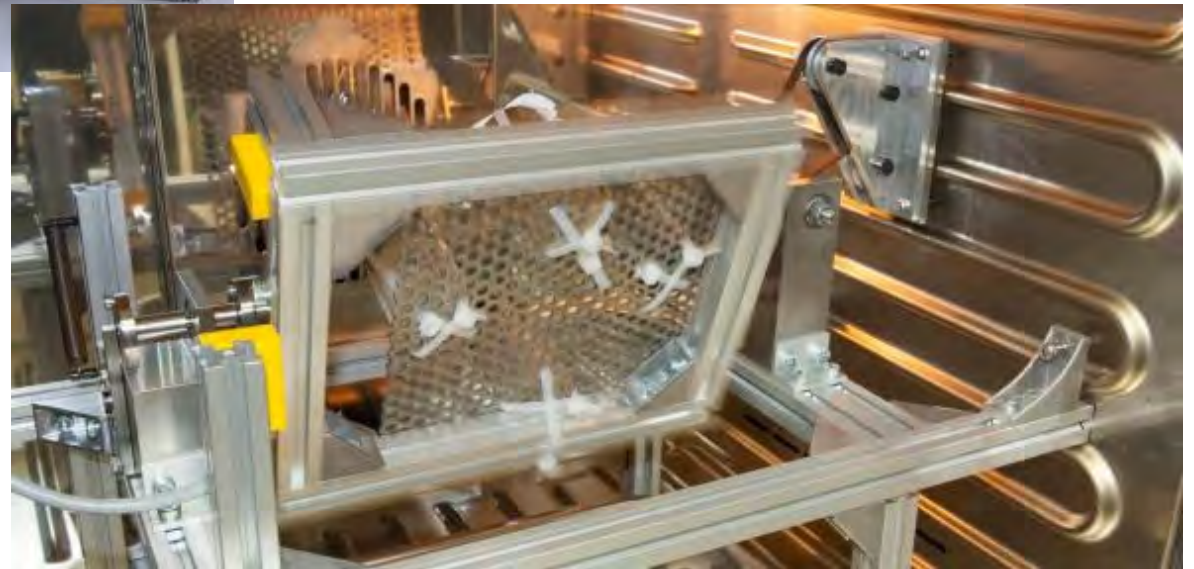


'Construction' (artificial) photo

Turning device manufactured at Fraunhofer ICT, mounted in circulating air oven. Motor drive (brushless) outside of oven.

Turning time for 180°: 3 seconds
Hold time: 1 minutes (adjustable).
Important: it may not be a continuous turning.

Real photograph



Characterisation methods

Röntgen (X-ray)-micro-CT

(Wilhelm Conrad Röntgen discovered the effect, he got the first Nobel price in Physics 1901)
With computer tomography of type Micro-CT in-vivo Skyscan 1076 of company Bruker, Germany, the cured samples were tested on the quality of filler distribution.

SEM

Scanning electron microscopy, type Supra 55VP, ZEISS, Germany was used to analyse the surface and shape of the particles: rough, smooth, irregular, spherical.

DMA (dynamic mechanical analysis) - complex shear modulus and loss factor

DMA performed in torsion mode which provides the complex shear modulus. Used deformation frequencies: 0.1Hz, 1Hz, 10Hz and 30Hz. T-range -100°C to +70°C

The glass-rubber transition (GRT) temperatures $T_{g,DMA}$ were determined from both evident maxima in the loss factor curve $\tan\delta(T) = G''(T)/G'(T)$ by fitting a polynomial of degree 3 carefully at each of the two maxima ranges, selecting the data range for optimal fitting.

EMG – Quantification of baseline corrected (BLC) loss factor curve

The peaks of loss factor curve correspond the binder parts with different mobility of the polymer chains. For quantification of these curve parts so-called EMG functions have been applied to baseline corrected loss factor. **The total loss factor curve of HTPB needs three EMG functions.**

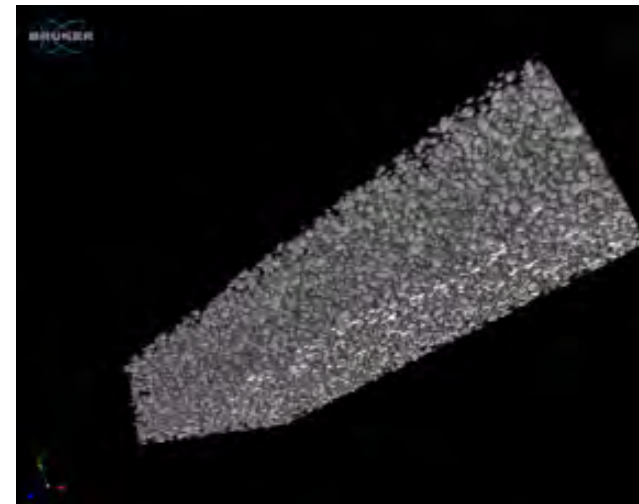
(EMG: exponentially modified Gauss distribution)

Testing on homogenous distribution of fillers

Verification of the homogenous distribution of the fillers during the curing of HTPB-IPDI binder with 20 mass-% AP, achieved by the turning device.

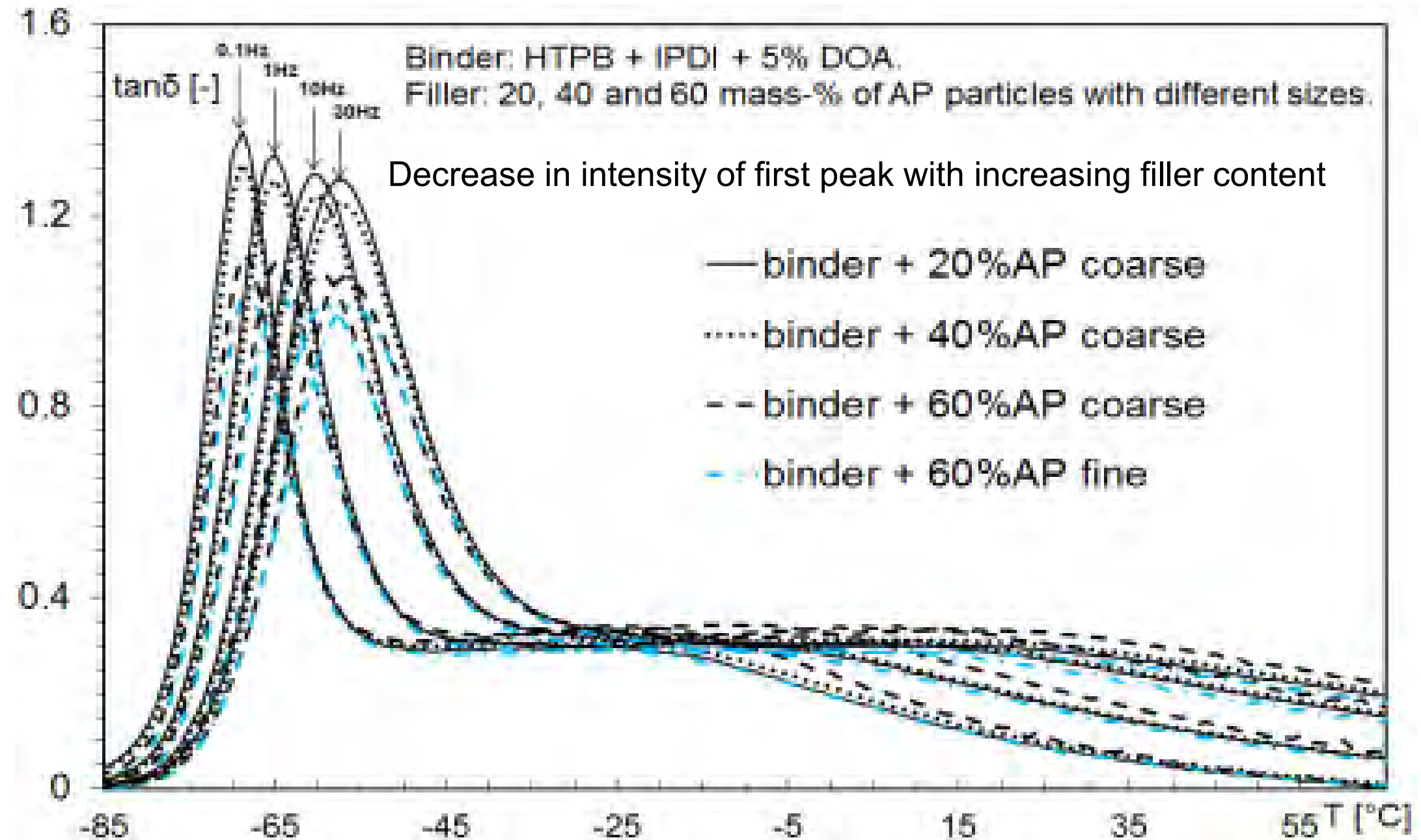


Normal photograph of sample
20 mass-% AP



Röntgen (X-ray)-Micro-CT
20 mass-% AP

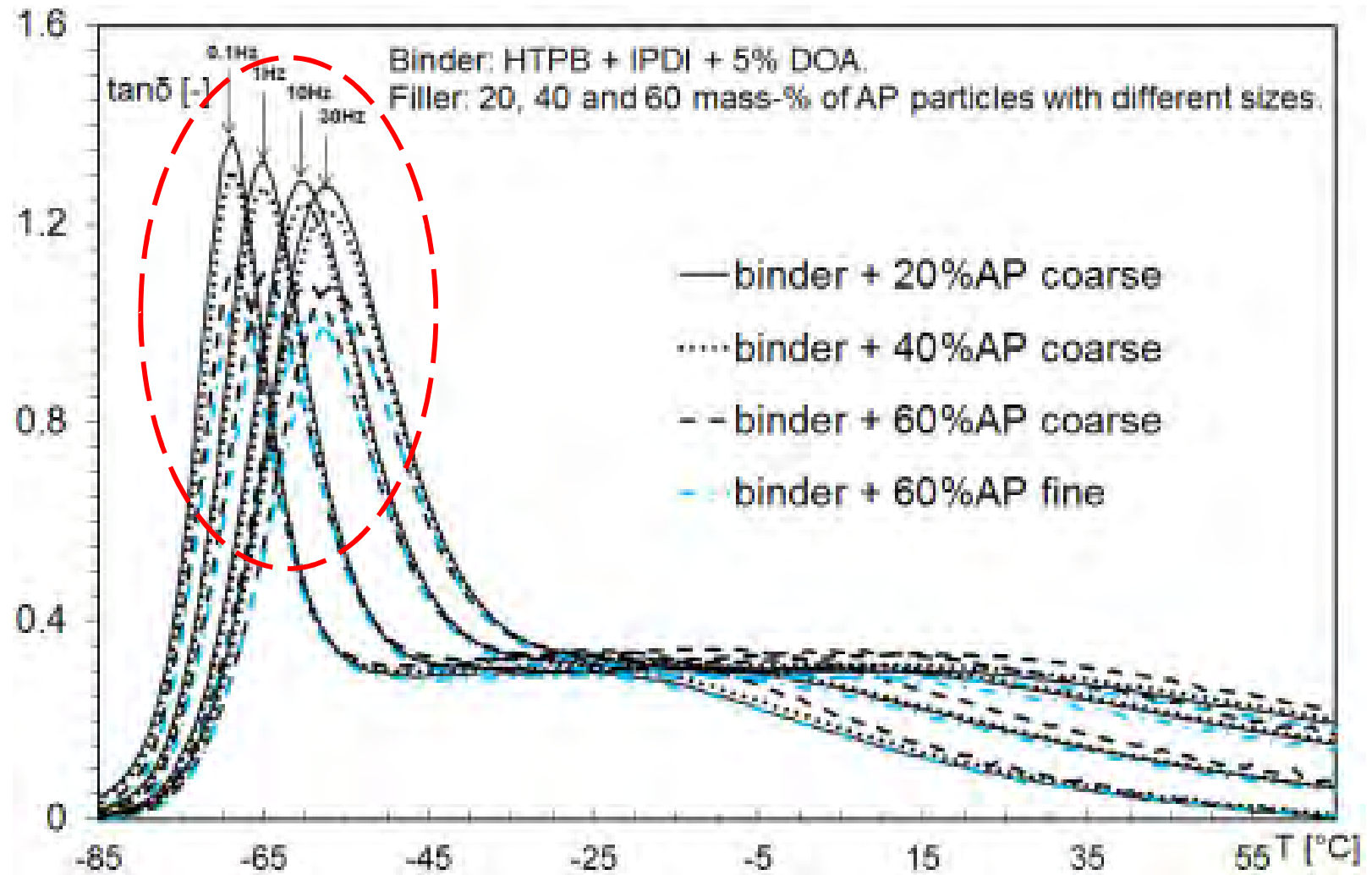
Typical DMA measurement result on loss factor – filler is AP



Assignment of peaks to binder parts – first main peak

The first evident peak gives the GRT temperature T_g^{unr}

The first peak is created by the binder part with **non**-hindered chain mobility. It is the 'un-restricted' glass-rubber transition.



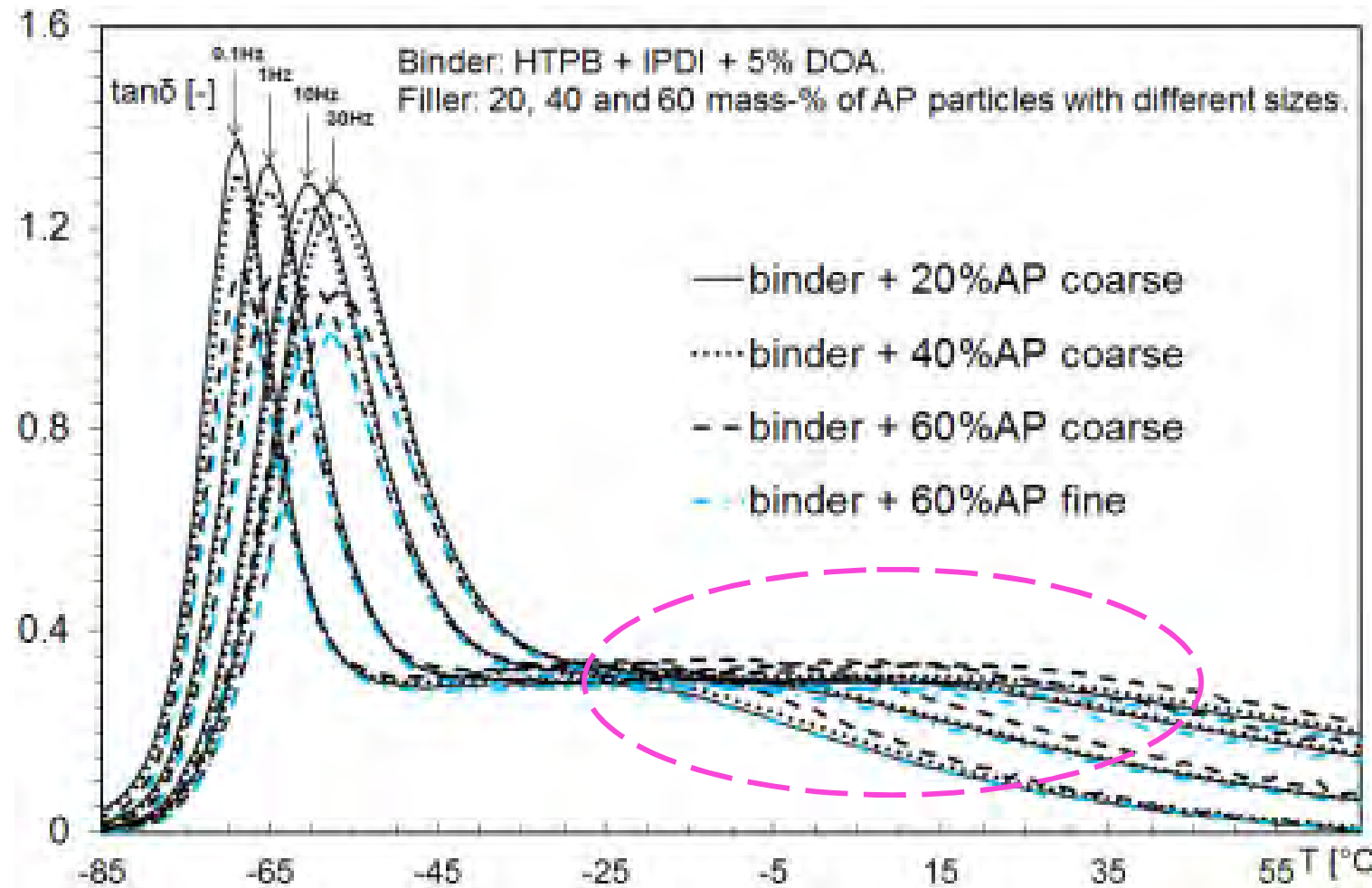
The non-hindered binder part is formed by the polymer chains of HTPB not restricted in their mobility.

Assignment of peaks to binder parts – second main peak

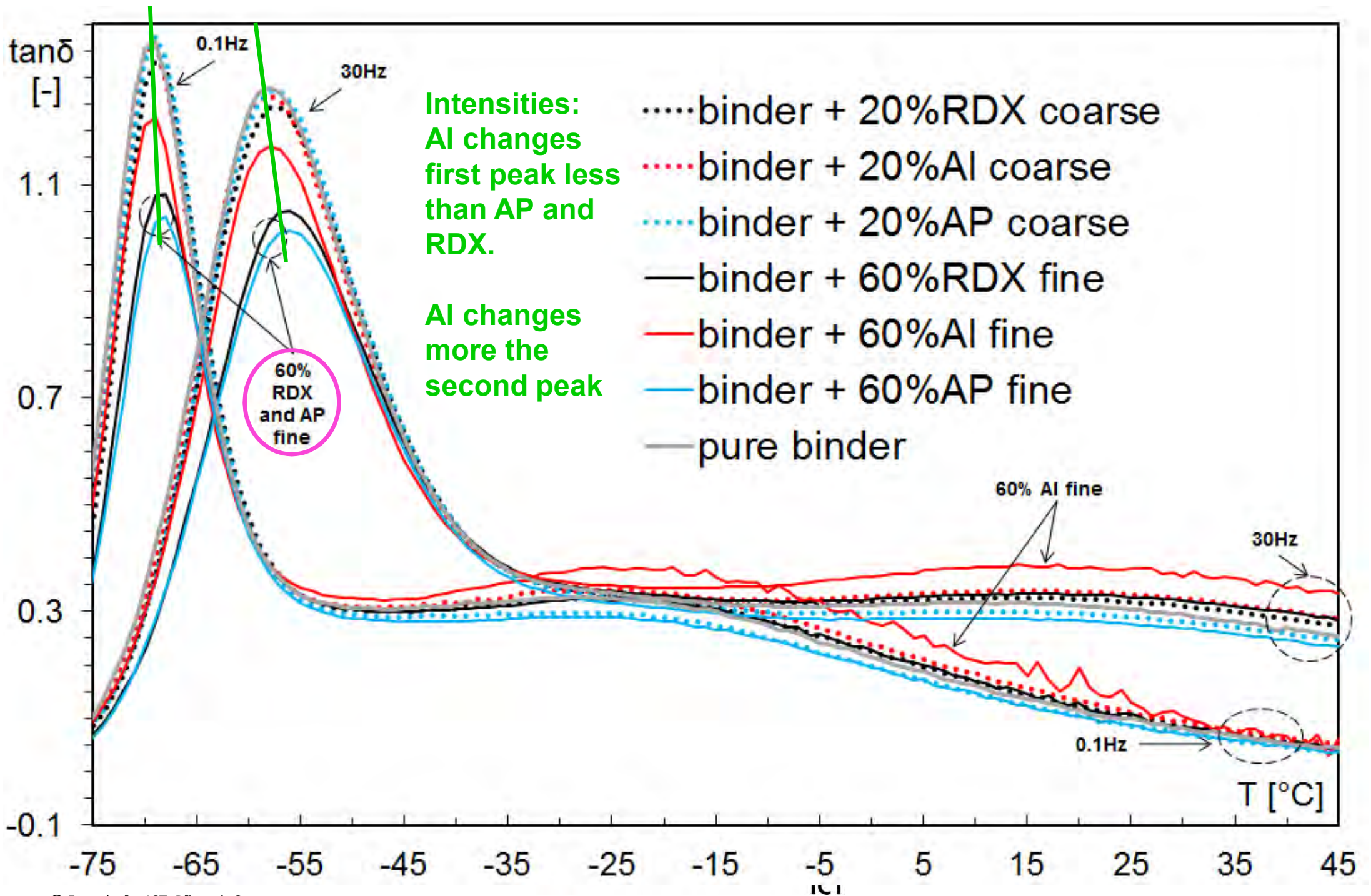
The second evident peak gives the GRT temperature T_g^{res}

The second peak is created by the binder part with hindered chain mobility. It is the 'restricted' glass-rubber transition.

These mobility hindered binder parts are found
(1) around the IPDI cross-linking ranges
(2) with binder chains, which are mobility-restricted by the interaction with the filler, in part geometrically-sterically in part by energetic interactions..



Changes in loss factor – caused by AP and RDX



Parameterisation of shift of $T_{g,DMA}$ with deformation frequency f

Both the glass-rubber transition temperatures T_g^{unr} and T_g^{res} are determined from the loss factor curves.

For this a polynomial of degree 3 was fitted in the maxima ranges to determine the maxima data. To take the values just from measured temperature interval data is not precise enough.

Parameterisation of shift according to Arrhenius with following equation

$$f = f_0 \cdot \exp\left(-\frac{Ea_f}{R \cdot T_g(f)}\right)$$

This shift with temperature is not based on free volume effect, it is an inertia effect and interaction energy determined

f	applied deformation frequency [Hz];
f_0	pre-exponential factor [Hz];
Ea_f	activation energy for the shift of T_g by strain rate hardening [$\text{kJ}\cdot\text{mol}^{-1}$];
R	general gas constant [$8.31441 \text{ J}\cdot\text{K}^{-1} \text{ mol}^{-1}$];
T_g	glass-rubber transition temperature [K] as function of deformation frequency

The obtained activation energy is a measure for the internal interaction energy in the binder.

Parameterisation of shift of $T_{g,DMA}$ with deformation frequency f

Parameterisation of shift according to **modified Arrhenius** with following equation

$$f = f_{0M} \cdot \exp\left(-\frac{Ea_{0M}}{R \cdot (T_g(f) - T_{0M})}\right)$$

The modified Arrhenius equation is **completely congruent** to the WLF equation !

$$\lg(a_T(T, Tr) [-]) = \lg\left(\frac{f(Tr)}{f(T)}\right) = -\frac{C_1 \cdot (T - Tr)}{C_2 + (T - Tr)}$$

f	applied deformation frequency [Hz];
f_{0M}	pre-exponential factor [Hz];
Ea_{0M}	activation energy for the shift of T_g by strain rate hardening [$\text{kJ} \cdot \text{mol}^{-1}$];
R	general gas constant [$8.31441 \text{ J} \cdot \text{K}^{-1} \text{ mol}^{-1}$];
T_g	glass-rubber transition temperature [K] as function of deformation frequency
T_{0M}	mobility freezing reference temperature, identical to T_∞ of WLF equation (T zero mobility)

$$Ea_{0M} = R \cdot C_1 \cdot C_2 / \lg(e) \quad T_{0M} = Tr - C_2 = T_\infty$$

The Arrhenius activation energy is proportional to the second WLF invariant $C_1 \cdot C_2$

See: Manfred A. Bohn, *The connection between WLF equation and Arrhenius equation.*

Proceedings 21th International Seminar NTREM (New Trends in Research of Energetic Materials), April 18-20, **2018**. Pages 64 to 81. University of Pardubice, Pardubice, Czech Republic.

For a copy send me an e-mail: bo@ict.fhg.de

Activation energies from strainrate shift of first peak (un-restricted GRT with T_g^{unr})

sample	T_g^{unr}				difference to reference				Ea_f^* [kJ.mol ⁻¹]	$\ln(f_0)$ [Hz]
	0.1Hz	1Hz	10Hz	30Hz	0.1Hz	1Hz	10Hz	30Hz		
only binder	-69.42	-65.58	-60.72	-57.95	+ means to higher temp.				180.7	45.43
20 % AP coarse	-68.86	-65.24	-60.28	-57.51	0.56	0.34	0.44	0.44	182.6	45.79
40 % AP coarse	-68.78	-65.04	-60.11	-57.27	0.64	0.54	0.61	0.68	180.9	45.34
60 % AP coarse	-68.63	-64.76	-59.62	-56.74	0.79	0.82	1.10	1.21	175.4	43.91
60 % AP fine	-68.29	-64.38	-59.06	-56.16	1.13	1.20	1.66	1.79	172.3	43.04
20 % RDX coarse	-68.95	-65.02	-60.09	-57.37	0.47	0.56	0.63	0.58	179.8	45.07
40 % RDX coarse	-68.97	-65.01	-59.91	-57.22	0.45	0.57	0.81	0.73	176.7	44.30
60 % RDX coarse	-69.58	-64.28	-59.02	-55.94	-0.16	1.30	1.70	2.01	154.9	38.78
60 % RDX fine	-69.44	-64.56	-59.19	-56.19	-0.02	1.02	1.53	1.76	158.6	39.71
20 % Al coarse	-68.90	-65.65	-60.76	-57.91	0.52	-0.07	-0.04	0.04	187.3	47.05
20 % Al fine	-69.54	-65.71	-60.81	-57.95	-0.12	-0.13	-0.09	0	179.1	45.00
40 % Al fine	-69.23	-65.69	-60.71	-57.77	0.19	-0.11	0.01	0.18	180.6	45.34
60 % Al fine	-69.01	-65.56	-60.60	-57.80	0.41	0.02	0.12	0.15	184.0	46.18

AP-coarse: decrease in Ea with content increase

RDX-coarse: decrease in Ea with content in increase

Al -fine: increase in Ea with content increase; at change from coarse to fine a change in Ea

Activation energies from strainrate shift of second peak (restricted GRT with T_g^{res})

sample	T_g^{res}				difference to reference				Ea_f [kJ.mol ⁻¹]	$\ln(f_0)$ [Hz]
	0.1Hz	1Hz	10Hz	30Hz	0.1Hz	1Hz	10Hz	30Hz		
Only binder	-28.04	-13.65	2.52	10.87	+ means to higher temp.				84.71	17.06
20 % AP coarse	-29.42	-15.63	2.00	11.03	-1.38	-1.98	-0.52	0.16	80.66	16.33
40 % AP coarse	-28.33	-14.14	2.94	12.46	-0.29	-0.49	0.42	1.59	81.25	16.37
60 % AP coarse	-24.92	-11.96	4.22	14.98	3.12	1.69	1.70	4.11	85.41	17.03
60 % AP fine	-29.25	-16.82	0.23	8.49	-1.21	-3.17	-2.29	-2.38	85.24	17.31
20 % RDX coarse	-25.36	-12.23	4.57	14.24	2.68	1.42	2.05	3.37	85.12	17.00
40 % RDX coarse	-24.34	-10.94	6.36	15.75	3.70	2.71	3.84	4.88	84.64	16.82
60 % RDX coarse	-25.38	<i>Not good defined</i>			2.66	<i>Not good defined</i>				
60 % RDX fine	-24.05	-11.76	4.96	15.47	3.99	1.89	2.44	4.60	86.13	17.14
20 % Al coarse	-26.01	-11.7	6.13	15.09	2.03	1.95	3.61	4.22	81.66	16.29
20 % Al fine	-25.88	-12.44	3.76	13.54	2.16	1.21	1.24	2.67	85.51	17.10
40 % Al fine	-25.91	-11.74	4.35	11.32	2.13	1.91	1.83	0.45	88.67	17.74
60 % Al fine	-23.25	-10.33	7.38	15.8	4.79	3.32	4.86	4.93	86.54	17.14

AP-coarse: increase in Ea with content increase

RDX-coarse: no defined result, probably Ea stays rather constant with content increase

Al –fine: more constant Ea with content increase; at change from coarse to fine a change in Ea

Modelling of loss factor curve of HTPB-IPDI with three EMGs

Quantification of the effects of fillers via exponentially modified Gauss distribution function

$$\tan \delta_{\text{BLC}} = \text{td}_0 + \sum_{i=1}^N \frac{A_i}{\tau_i} \cdot \frac{1}{2} \cdot \exp \left[0.5 \cdot \left(\frac{w_i}{\tau_i} \right)^2 - \frac{T - T_{c_i}}{\tau_i} \right] \cdot \left\{ 1 - \operatorname{erf} \left[-\frac{1}{\sqrt{2}} \left(\frac{T - T_{c_i}}{w_i} - \frac{w_i}{\tau_i} \right) \right] \right\}$$

Gauss distribution

$$f_G(T) = \frac{A}{w \cdot \sqrt{2\pi}} \cdot \exp \left[-0.5 \cdot \left(\frac{T - T_c}{w} \right)^2 \right]$$

EMG is mathematically a convolution between Gauss and exponential

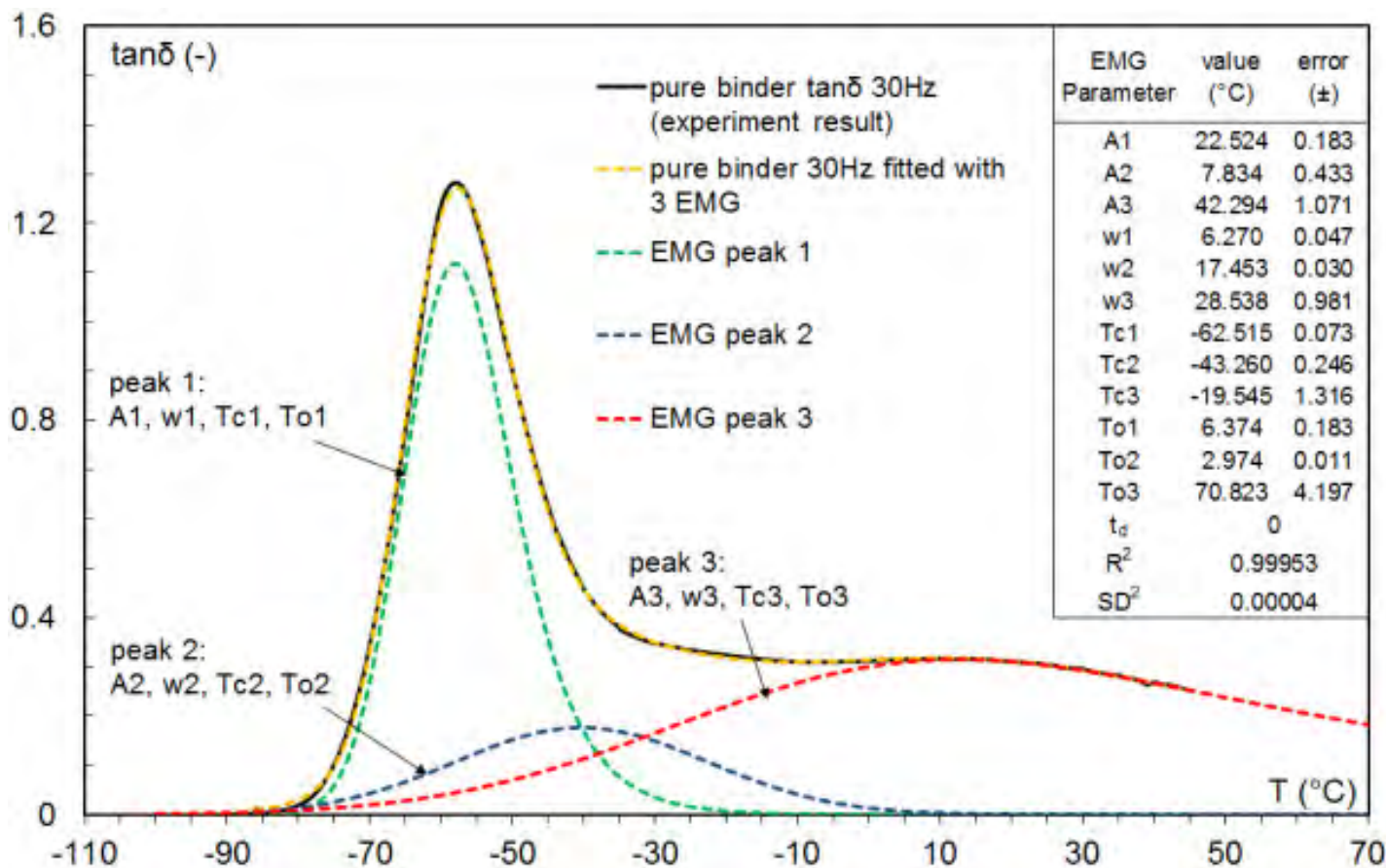
exponential relaxation

$$f_E(T) = \exp \left(-\frac{T}{\tau} \right)$$

One EMG has 4 parameters:

- Peak area, A_i ;
- Half width at half height of Gauss function, w_i ;
- Temperature in maximum of Gauss function, T_{c_i} ;
- Relaxation parameter τ_i of exponential part, here also named as T_0 .

Modelling of loss factor curve of HTPB-IPDI with three EMGs



Information from EMG parameters

Peak areas A_i

small A is caused by:

- (1) – hindrance in mobility
- (2) – increase of stiffness (G')
- (3) – increase of cross-linking gives rigidity, means a smaller binder part can transform to rubber

Peak temperature Tc_i of Gauss part

It can be interpreted as “ T_g ” of the relaxation free transition (transition without exponential part) one has a pure Gauss distribution.

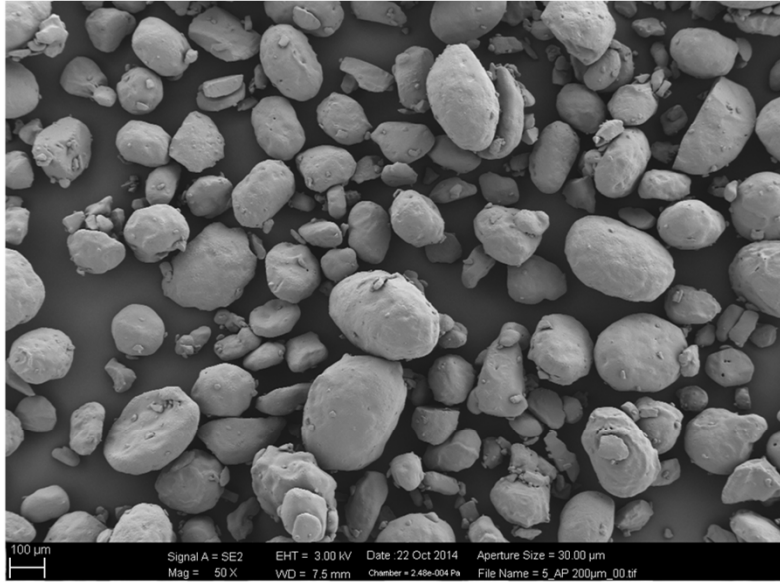
Exponential relaxation τ_i

The more exponential part the greater τ_i (To_i) or the more residual internal friction.

Influence of particle shape – AP and RDX

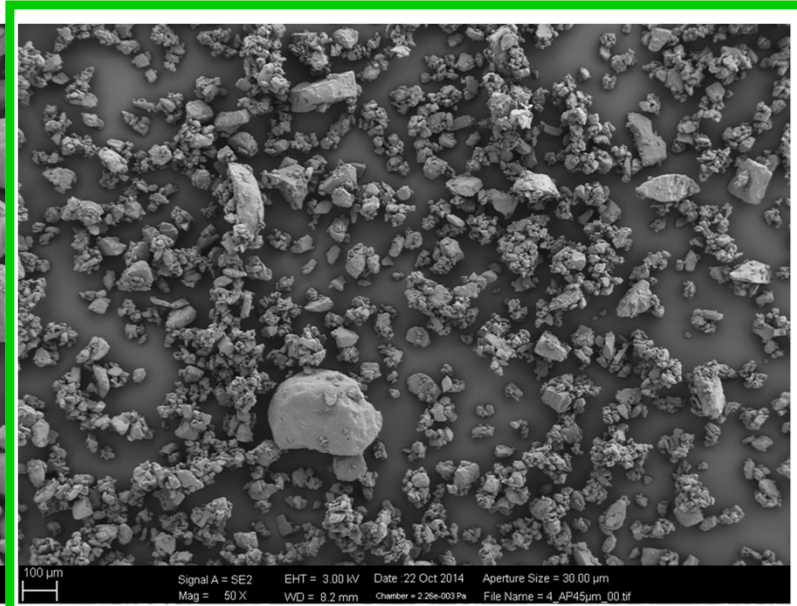
SEM analysis reveals that AP-fine and RDX-coarse are not round or less rounded in contrast to AP-coarse and RDX-fine.

AP coarse,
rounded



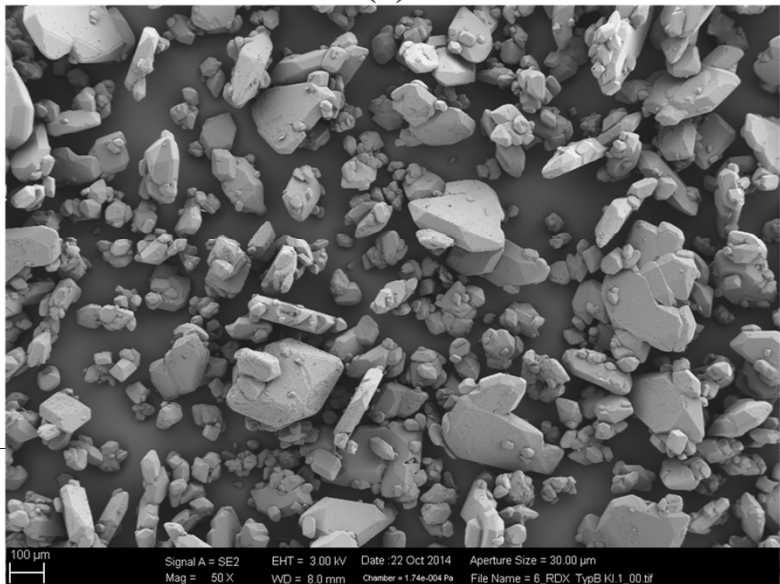
(a)

AP fine,
not rounded



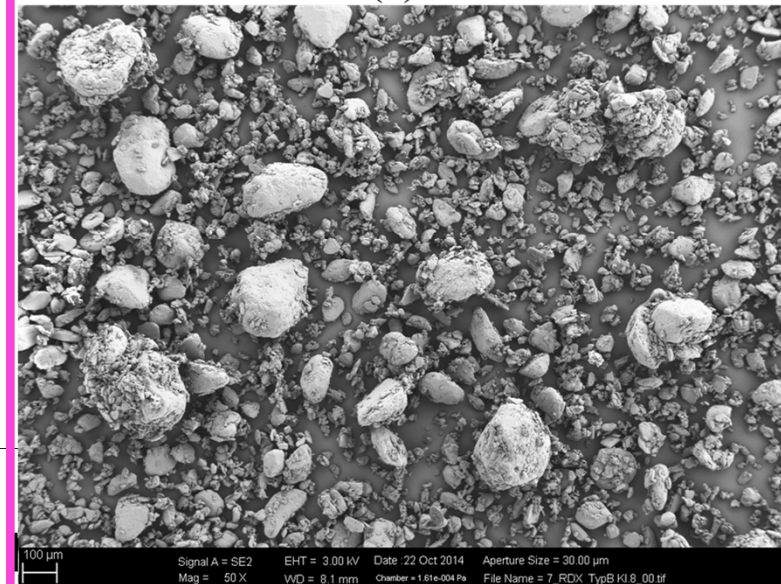
(b)

RDX
coarse,
not rounded



(c)

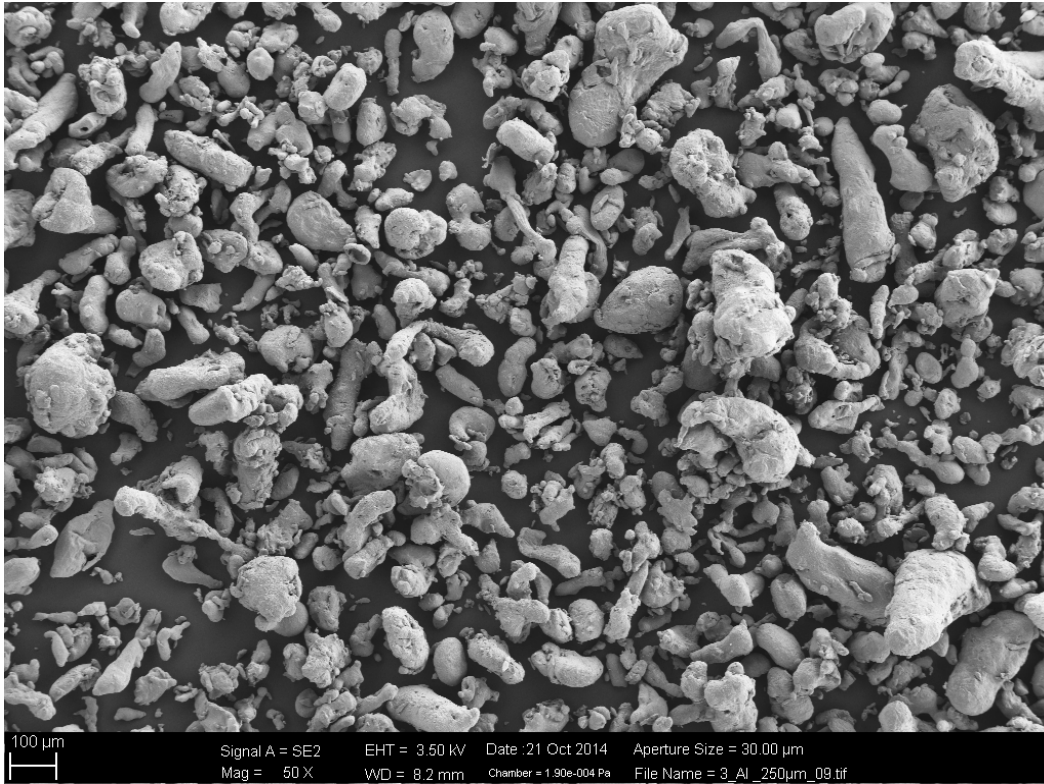
RDX fine,
rounded



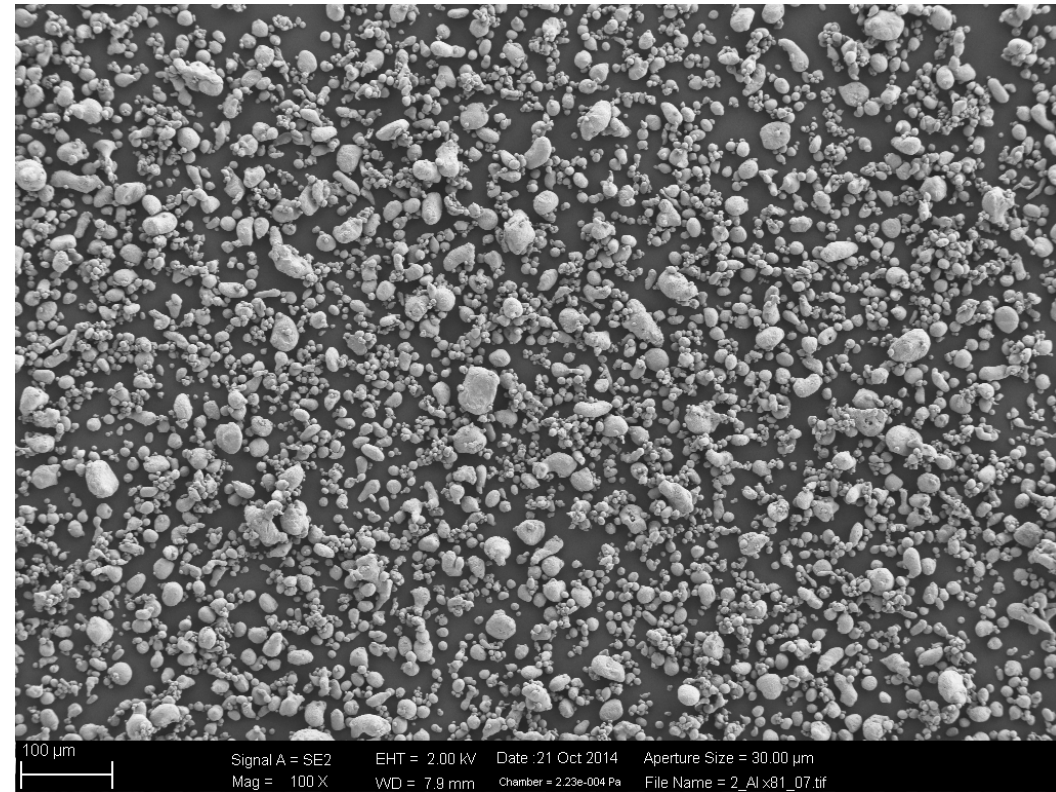
(d)

Influence of particle shape – Al

SEM analysis reveal that Al coarse and Al-fine are rounded



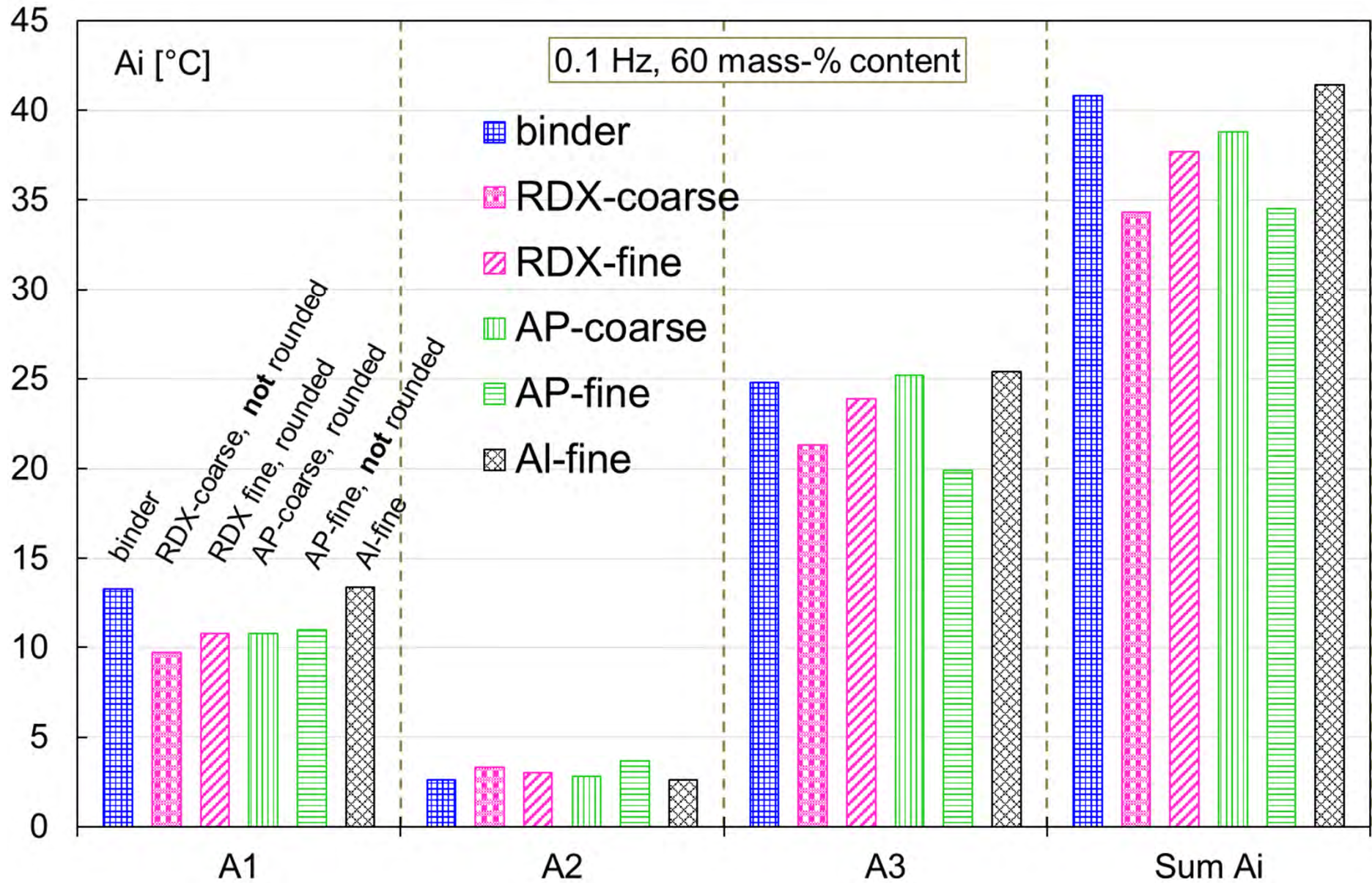
**Al coarse,
rounded**



**Al fine,
rounded**

Generally, rounded particles disturb less the binder structure.
Means, they decrease less the intensity of the loss factor.

Changes in areas A_i of EMG curves at 0.1 Hz, filling is 60 mass-%



Effect of AP on total intensity (sum of areas) of loss factor in glass-rubber transition

f (Hz)	only Binder				60 m.-% AP coarse				60 m.-% AP fine			
	0.1	1	10	30	0.1	1	10	30	0.1	1	10	30
A ₁	13.3	16.7	20.3	22.5	10.8	13.5	16.2	18.0	11.0	13.9	17.0	22.5
A ₂	2.6	5.6	7.2	7.8	2.8	4.8	8.2	8.3	3.7	7.9	7.6	6.7
A ₃	24.8	29.0	39.0	42.3	25.2	30.9	38.7	45.8	19.9	21.3	31.3	34.1
∑A _i	40.8	51.3	66.5	72.7	38.8	49.3	63.2	72.2	34.5	43.1	56.0	63.3
w ₁	4.2	5.2	5.6	6.3	4.3	5.2	5.6	6.3	4.5	5.5	6.1	6.7
w ₂	2.0	2.7	16.4	17.5	2.1	2.8	17.0	17.5	2.3	3.1	16.5	6.6
w ₃	25.3	26.3	26.7	28.5	26.8	27.7	25.5	28.1	24.7	25.6	23.9	30.6
Tc ₁	-70	-66	-65	-63	-69	-66	-64	-61	-69	-65	-63	-65
Tc ₂	-63	-58	-46	-43	-62	-57	-46	-42	-61	-56	-43	-57
Tc ₃	-43	-33	-23	-20	-38	-32	-20	-17	-39	-28	-19	-12
To ₁	0.9	1.0	5.6	6.4	0.8	1.0	5.5	6.1	0.9	1.0	5.8	23.8
To ₂	9.6	17.1	2.7	3.0	11.4	16.6	3.2	3.0	15.4	26.8	3.3	1.0
To ₃	22.3	37.6	60.1	70.8	17.6	35.1	59.3	75.1	20.9	34.5	57.9	66.6

Small to nearly no effect from coarse AP on sum A_i compared to binder

Decrease of sum A_i with fine AP compared to binder

Effect of RDX on EMG-parameters of loss factor in glass-rubber transition (GRT)

f (Hz)	only binder				60 m.-% RDX coarse				60 m.-% RDX fine			
	0.1	1	10	30	0.1	1	10	30	0.1	1	10	30
A ₁	13.3	16.7	20.3	22.5	9.7	12.1	16.2	19.2	10.8	13.7	17.4	19.4
A ₂	2.6	5.6	7.2	7.8	3.3	6.3	7.3	6.1	3.0	5.4	10.1	13.4
A ₃	24.8	29.0	39.0	42.3	21.3	22.9	28.6	33.5	23.9	32.5	35.6	37.4
ΣA _i	40.8	51.3	66.5	72.7	34.3	41.2	52.2	58.8	37.7	51.6	63.1	70.2
w ₁	4.2	5.2	5.6	6.3	4.5	5.5	6.0	6.7	4.3	5.4	6.8	7.6
w ₂	2.0	2.7	16.4	17.5	2.2	3.1	17.4	17.3	2.2	3.1	4.1	4.8
w ₃	25.3	26.3	26.7	28.5	25.9	27.0	23.8	27.4	26.2	26.7	31.6	34.6
Tc ₁	-70	-66	-65	-63	-69	-65	-64	-62	-69	-65	-61	-58
Tc ₂	-63	-58	-46	-43	-61	-57	-41	-34	-62	-57	-50	-47
Tc ₃	-43	-33	-23	-20	-40	-31	-18	-14	-39	-33	-16	-5
To ₁	0.9	1.0	5.6	6.4	0.8	1.0	6.8	8.2	0.8	1.0	1.4	1.5
To ₂	9.6	17.1	2.7	3.0	15.5	22.4	3.3	3.2	11.6	17.9	29.3	35.5
To ₃	22.3	37.6	60.1	70.8	19.7	32.8	54.4	65.3	19.3	43.3	54.6	60.1

RDX-coarse reduces the intensity of GRT at strainrate hardening compared to binder

RDX- fine changes less in intensity of GRT at strainrate hardening compared to binder

Tc₁ but especially Tc₃ are shifted to higher temp. The shift is larger at high strainrate, especially with RDX-fine compared to binder

Effect of Al-fine on EMG-parameters of loss factor in glass-rubber transition

f (Hz)	only binder				60 mass-% Al fine			
	0.1	1	10	30	0.1	1	10	30
A ₁	13.3	16.7	20.3	22.5	13.4	14.9	17.7	21.2
A ₂	2.6	5.6	7.2	7.8	2.6	5.2	7.5	6.5
A ₃	24.8	29.0	39.0	42.3	25.4	35.6	48.2	49.8
∑A _i	40.8	51.3	66.5	72.7	41.4	55.7	73.4	77.4
w ₁	4.2	5.2	5.6	6.3	4.2	5.2	5.1	6.0
w ₂	2.0	2.7	16.4	17.5	1.7	2.9	21.1	20.0
w ₃	25.3	26.3	26.7	28.5	25.8	27.0	30.1	34.2
Tc ₁	-70	-66	-65	-63	-70	-66	-65	-63
Tc ₂	-63	-58	-46	-43	-63	-58	-49	-39
Tc ₃	-43	-33	-23	-20	-41	-30	-20	-11
To ₁	0.9	1.0	5.6	6.4	0.8	1.0	6.6	7.5
To ₂	9.6	17.1	2.7	3.0	9.9	16.0	3.0	3.1
To ₃	22.3	37.6	60.1	70.8	21.0	35.8	59.3	56.6

Area A₃ of second evident peak:

Al particles have a larger effect on increase of area A₃ than the AP and RDX have.

Increase of deformation frequency amplifies this effect.

From molecular dynamics studies it is known, that Al has a stronger **intermolecular interaction with HTPB than AP**. Therefore **more mobility hindrance** of HTPB chains, this increases the range of the polymer shell around Al particles, therefore a higher intensity in loss factor.

Al has always OH-groups on its surface, therefore:

- (1) Reaction with NCO, which can promote more free polymer chains around Al – reptation possible
- (2) chemical bonding of the Al particle with the binder network via NCO enlarges the polymer shell around the Al particle, whereby the area A₃ increase.
- (3) Significant increase of maximum temperature Tc₃ (Gauss peak of second evident peak or the third peak in EMG)

Conclusions on interactions filler - binder

AP and RDX cause more changes in intensity of first evident peak of loss factor than AL.

The peak temperature in first maximum is changed not much (only a bit lowered) by any of the fillers at all concentrations.

AL changes it least of all fillers (always in comparison to unfilled binder).

The changes in peak temperature of second peaks are clearly larger, especially with increasing deformation frequency.

AP-fine stronger decrease of $\tan\delta$ intensity compared to AP-coarse.

RDX-fine less decreases of $\tan\delta$ intensity compared to RDX-coarse.

There is indication that particle shape has an influence.

The more rounded particles have a less hindrance effect on molecular mobility, and reduce the $\tan\delta$ intensity less than not rounded particles.

Change in loss factor intensity and temperature shifts indicate that AL particles have a stronger molecular interaction with the binder than AP and RDX.

It seems AL is bonded to the binder network via isocyanate coupling, because on AL surfaces always OH groups are present.

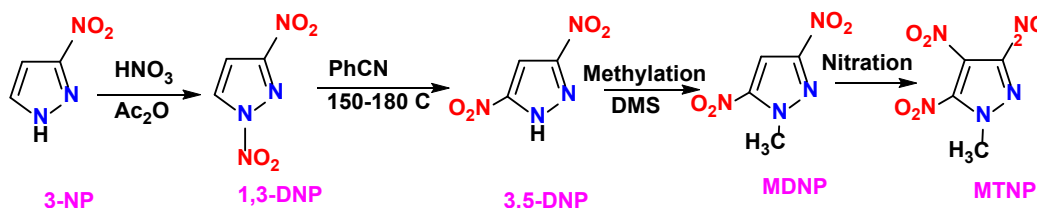
Characterization of MTNP (1-methyl-3,4,5-trinitro-1,2-pyrazole)

Philip Samuels*, Dr. Reddy Damavarapu, Henry Grau, Dr. Kimberly Spangler, Dr. Kelley Caflin, Erik Wrobel
 U.S. Army ARDEC
 Energetics, Warheads, and Manufacturing Technology Directorate
 Picatinny Arsenal, New Jersey 07806
 Email: philip.j.samuels2.civ@mail.mil; Phone: 973-724-4064

ABSTRACT

The Ordnance Environmental Program (OEP) from RDECOM has recently funded synthesis efforts evaluating new green synthesis routes to produce both RDX and TNT replacements. MTNP (1-methyl-3,4,5-trinitro-1,2-pyrazole) is a low melting energetic compound. Recently, MTNP has shown promise in terms of a relatively simple synthesis route. ARDEC has characterized this compound from lab scale batches for safety testing.

Thermo-chemical codes such as Cheetah and Jaguar were used to predict the Gurney energy for this high energy material. MTNP was reported in literature using pyrazole, chloro pyrazole and Methyl Pyrazole as starting materials. Our approach involves commercially available 3-Nitropyrazole as starting compound and its synthetic transformation to MTNP as outlined in the following scheme.



Small scale safety testing was completed, including impact, friction and electrostatic discharge testing. The crystal density was determined by pycnometry and the thermal stability was accessed via DSC, isothermal weight loss, and vacuum thermal stability (<2 cc gas/48hrs at 100°C). MTNP has proven to be compatible with most energetics and metals. This paper will discuss the synthesis, thermal, sensitivity and analytical results of pure MTNP.

Introduction

In modern ordnance there is a strong requirement for explosives having good thermal stability, impact insensitivity and explosive performance. However, these requirements are somewhat mutually exclusive. Those explosives having good thermal stability and impact insensitivity exhibit poorer explosive performance and vice versa. TNT has been the mainstay of melt-castable formulations. Among the TNT-based compositions known for making melt-cast explosives, Composition B (TNT/RDX/Wax) is one of the more widely known and practiced. As widely acknowledged in the art, however, melt-cast explosives compositions such as Composition B have several drawbacks. In order to overcome the above-mentioned problems with the existing melt-cast explosive formulations and to meet the U. S. DoD requirements for future high performance munitions systems, it is critical to develop other promising candidates, which possess properties superior to TNT, in an environmentally benign manner. A number of

polynitroazoles have been reported in the literature that are thermally stable, have higher densities and, in some cases, outstanding insensitivity characteristics. Use of a higher density polynitroazole such as 1-Methyl 3,4,5-trinitropyrazole (MTNP) as the melt-cast matrix replacement for TNT would not only result in a formulation with higher performance but also, by virtue of its higher power contribution, allow for a lower added energetic solids fill resulting in lower sensitivity to unplanned stimuli. MTNP was selected for evaluation as a promising new low melting energetic ingredient under the RDECOM Ordnance Environmental Program. It has a crystal density of 1.82 g/cc @ 25 C (measured, Xray).

Synthesis of MTNP has been reported in literature in different approaches: Direct and sequential nitration of Methyl pyrazole, Synthesis of 3,4,5-trinitropyrazole followed by N-methylation, Nitrolysis of 1-Methyl triiodopyrazole, and Nitration of 1-Methyl 3,5-dinitropyrazol. This effort focused on the N nitration of 3-NP as was used in the literature.

Experimental

Scanning Electron Microscopy (SEM)

SEM images were obtained using a JEOL JCM 5700 tungsten filament scanning electron microscope using palladium/gold-coated samples in high vacuum mode as shown in Figure 1.

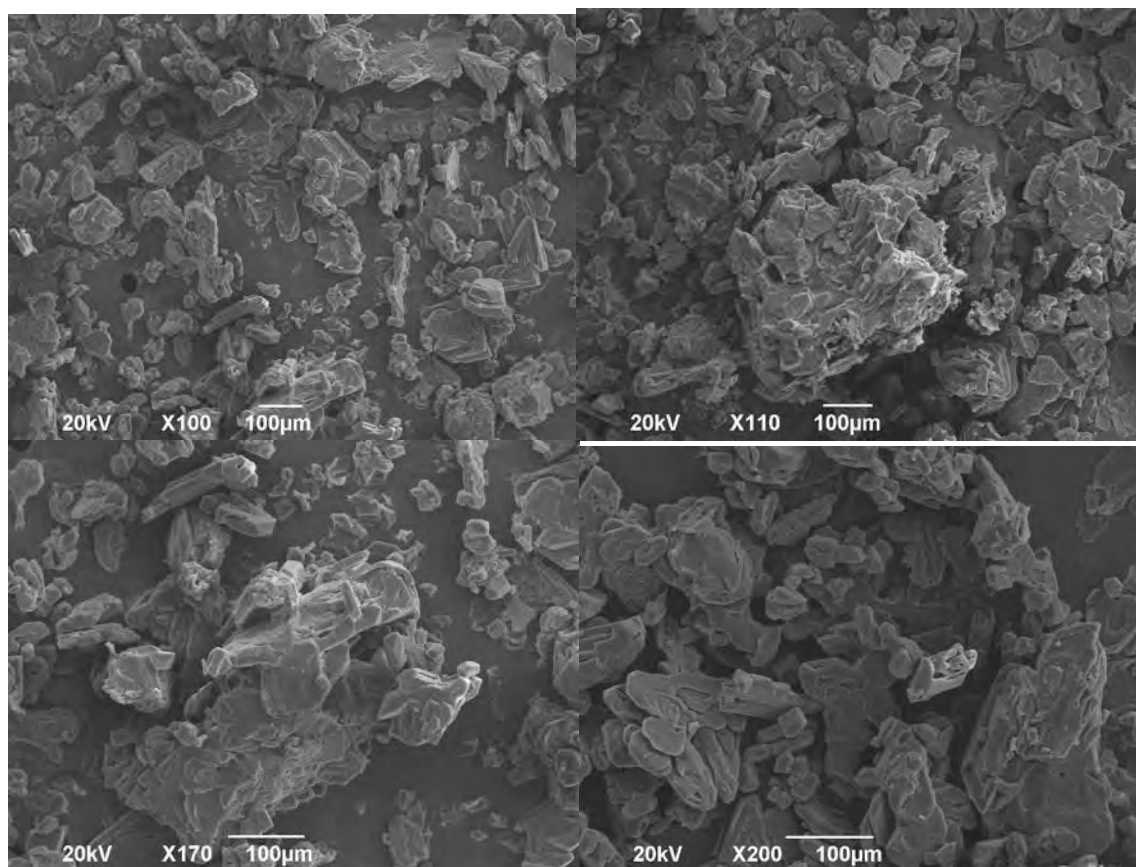


Figure 1. SEM images of MTNP

Differential Scanning Calorimetry (DSC)

The DSC was performed according to AOP-7, US 202.01.020 or STANAG 4515 where 20 mg MTNP was subjected to a heating rate of 10 °C/min until decomposition of the sample occurred. The sample endotherm(s), exotherm(s), onset temperature(s), and peak temperature(s) are recorded. MTNP exhibited a melting point of 91.25 °C, exotherm onset at 225.06 °C, and an exotherm peak temperature at 252.16 °C as shown in Figure 2. By comparison, RDX exhibited an exotherm onset at 210 °C, and an exotherm peak temperature at 241 °C.¹

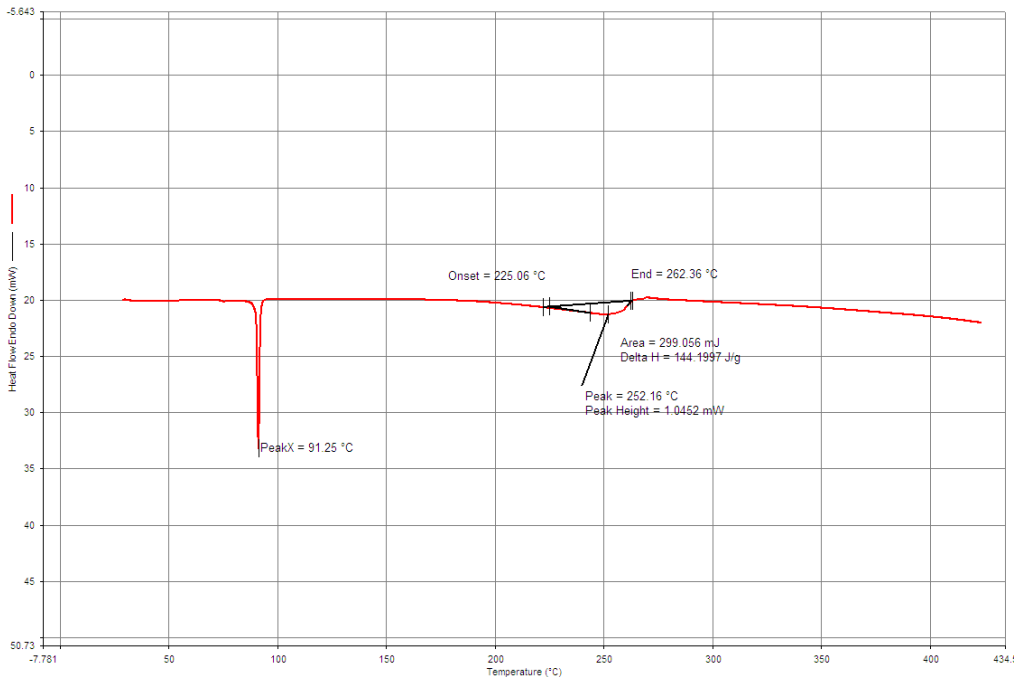


Figure 2. DSC Scan of MTNP

Critical Temperature Determination

Critical temperature determination is a type of thermal stability testing and is defined as the lowest constant surface temperature at which a given material of a specific shape and size will catastrophically self-heat. Experimental data obtained from a Differential Scanning Calorimeter (DSC) is used to determine various kinetic parameters associated with a given chemical reaction or decomposition. Table 1 shows the summary of the thermal properties attained for MTNP.

Critical Temperature Calculations using Frank-Kamenetski (F-K) equation

$$T_C = \frac{E_a / R}{\ln \left[\frac{a^2 \rho Q A E_a}{T_C^2 \lambda \delta R} \right]}$$

Self-heating requirements defined in AOP-7 provide the acceptance criteria for this test are as follows: An explosive should have a critical temperature greater than 82C for a given geometry and size. According to military specifications the average calculated critical temperatures for MTNP (238.7C) as shown in Table 2 exceed the minimum value of 82C for explosive material.¹

Table 1. Thermal Properties of MTNP

Variable	Description	Unit	Value	Comment
E _a	Activation Energy	cal/mol	21426.94	Variable heating rate data from DSC
R	Gas constant	cal/mol.K	1.707	
a	geometry dimension	Cm	6.123	For 1-LCO
ρ	Density	g/cm ³	1.7057	Gas pycnometer
Q	heat of self-heating rx	cal/g	500	(%wt)
A (Z)	pre-exponential factor	1/sec	4.08E+05	From variable heating rate data from DSC
λ	thermal conductivity	cal/cm.sec.C	0.007	30 deg C
δ	shape factor	geometry dependent	2	for cylinder

Based on test results, which were conducted in accordance with the defining criteria of STANAG 4147 ED.2, MTNP is incompatible with NTO, FOX-7, HMX and O-ring (Vacuum Thermal Stability testing required). MTNP is compatible with Al. MTNP requires VTS testing with brass and 304/316 stainless steel to determine compatibility due to the appearance of a new exotherm. VTS testing is also needed with copper (Figure 3) and A2 Steel due to earlier onset of the decomposition (around 250°C). VTS testing was completed with copper as shown in Table 3 in which MTNP/Copper combination passed this test.

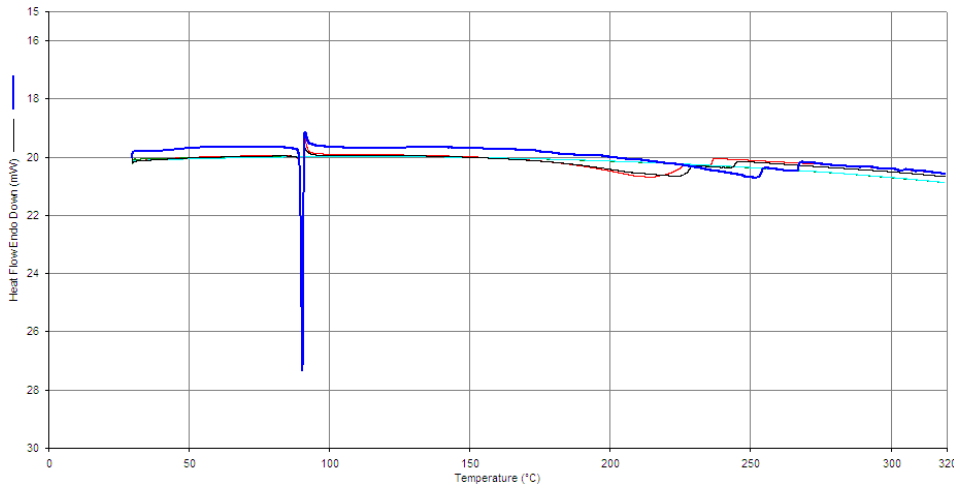


Figure 3. DSC of MTNP and Copper

Table 3. Vacuum Thermal Stability Results for MTNP & Copper

1:1 ratio	Reactivity of mix (ml)	Result
MTNP & copper	negligible	Pass

SENSITIVITY TESTS

Electrostatic Sensitivity (ESD)

The Electrostatic Discharge Sensitivity Test (AOP-7, 201.03.001) determines the energy threshold required to ignite explosives by electrostatic stimuli of varying intensities. The MTNP did not react in 20 trials at 0.051 Joule as shown in Table 4.¹

Impact Sensitivity Test

The ERL, Type 12 impact tester, utilizing a 2 ½ kg drop weight, was used to determine the impact sensitivity of the sample. The drop height corresponding to the 50% probability of initiation is used to measure impact sensitivity. The ERL, Type 12 Impact Test Method is described in STANAG 4489 Ed.1 “Explosives, Impact Sensitivity Tests”. All impact tests were conducted using 180A garnet sandpaper and the test procedures given in AOP-7, 201.01.001. Bruceton method of statistical analysis was used to determine the 50% point of 54.1 cm for MTNP.¹

Friction Sensitivity Test

The Large BAM Friction Test Method is described in AOP-7, 201.02.006, "BAM Friction Test". A sample of MTNP was placed on the porcelain plate. The porcelain pin was lowered onto the sample and a weight was placed on the arm to produce the desired load. The tester was activated and the porcelain plate was reciprocated once to and fro. The results are observed as either a reaction (i.e. flash, smoke, and/or audible report) or no reaction. Testing is begun at the maximum load of the apparatus (360 N) or lower if experience warrants it. If a reaction occurs in ten trials, the load is reduced until no reactions are observed in ten trials. MTNP did not react in 10 trials at 360 N.¹

Table 4. MTNP Safety Test Results Compared to RDX, DNP, and TNT

Molecule	Impact (cm)	BAM Friction (N)	ABL ESD (J)
MTNP	54.1	No Reaction in 10 trials @ 360N	Reacted @ 0.063J, did not react in 20 trails @ 0.051J
RDX Class I Type II	18	Reacted @ 216N, did not react in 10 trials at 192N	Reacted @ 0.063J, did not react in 20 trails @ 0.051J
RDX Class V Type II	>100	Reacted @ 324N, did not react in 10 trials at 288N	Reacted @ 0.051J, did not react in 20 trails @ 0.040J
DNP	>100	No Reaction in 10 trials @ 360N	Reacted @ 0.063J, did not react in 20 trails @ 0.051J
TNT	88.3	Reacted @ 240N, did not react in 10 trials at 216N	Did not react in 20 trials @ 0.25J (Old Test Method)

Theoretical Calculations

Jaguar thermo-chemical code was utilized for determining the performance of MTNP and comparing it to other low melting energetic and crystalline compounds as shown in Table 5. MTNP is an attractive compound due to its high density and metal pushing capability for a low melting energetic compound.

Table 5.

Explosive	Formula	Density g/cm ³	DH _f kJ/mol	Det Vel km/s	C-J P GPa	Gurn Vel(3) km/s	Gurn Vel(7) km/s	OB %
DNAN	C7H6N2O5	1.546	-186.5	6.14	14.8	1.88	2.10	-96.9
3,4 DNP	C3H2N4O4	1.791	120.5	8.31	30.9	2.63	2.86	-30.4
MTNP	C4H3N5O6	1.82	4.53	8.36	31.1	2.59	2.82	-25.8
PrNQ	C4H10N4O2	1.335	-217.3	6.45	14.4	1.95	2.10	-120
TNT	C7H5N3O6	1.654	-63	6.89	19.8	2.20	2.43	-74.0
RDX	C3H6N6O6	1.816	70	8.76	34.8	2.73	3.01	-21.6
HMX	C4H8N8O8	1.905	75	9.09	38.7	2.76	3.04	-21.6

UNCLASSIFIED

Conclusions

The synthesis team performed a literature search and analyzed the reported methods for isolating MTNP. The team identified suitable methods and made attempts to synthesize MTNP in one pot process from pyrazole. MTNP was prepared using sequential nitration processes. Safety and Handling as well as thermal testing has been completed on MTNP to date. The next step is to develop a scale up process to produce sufficient material for shock sensitivity and performance testing. Future work consists of continuing to investigate alternative nitrating agents, process improvements, and incorporation of multiple nitro groups in one process.

References

1. AOP-7: Manual of Data Requirements and Tests for the Qualification of Explosive Materials for Military Use. Edition 2 Version 2
2. STANAG 4147 ED.2 Chemical Compatibility of Ammunition Components with Explosives (Non-Nuclear Applications)



**Characterization of MTNP
(1-methyl-3,4,5-trinitro-1,2-
pyrazole)**

Philip Samuels*, Dr. Reddy Damavarapu,
Henry Grau, Dr. Kimberly Spangler, Dr.
Kelley Caflin, Erik Wrobel

IMEM April 2018, Portland, OR

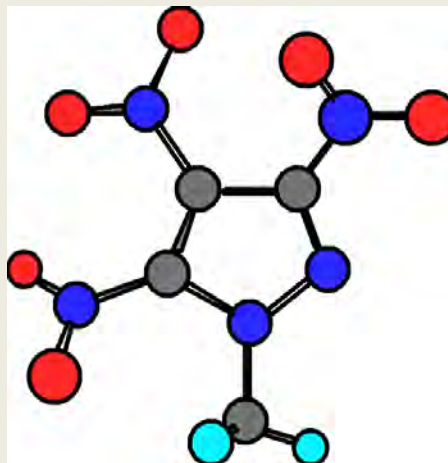
UNPARALLELED
**COMMITMENT
& SOLUTIONS**

Act like someone's life depends on what we do.



U.S. ARMY ARMAMENT
RESEARCH, DEVELOPMENT
& ENGINEERING CENTER

Distribution A: Approved for Public Release

**MTNP OVERVIEW**

Molecular Formula	C₄ H₃ N₅ O₆
Molecular Weight	217
Melting Point	91 C
Exotherm	256 C
Density	1.839 g/cc
Heat of Formation	50.7 kJ/mol

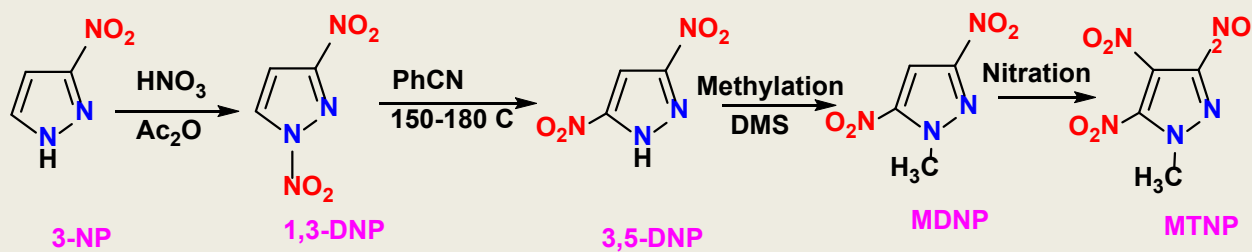


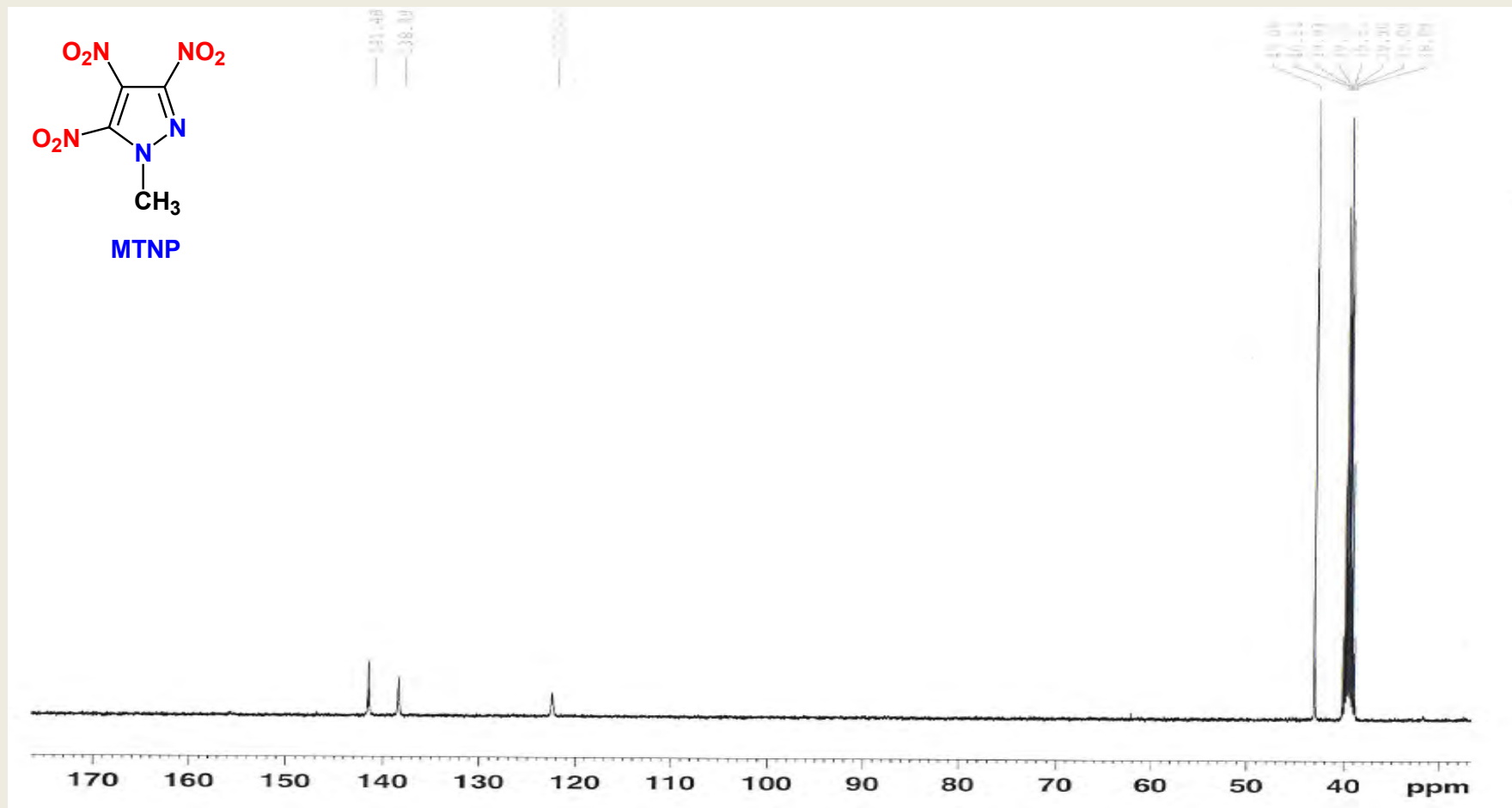
SYNTHESIZE AND PROVIDE MTNP FOR INITIAL EVALUATION EFFORTS

- UP TO DATE LITERATURE SEARCH AND ANALYSIS OF LITERATURE
- IDENTIFICATION OF SUITABLE ROUTES
- CONDUCT EXPERIMENTS TO DETERMINE THE SUITABILITY OF IDENTIFIED METHODS FOR LAB SCALE PREPARATION – DOWN SELECT THE RIGHT METHOD
- ANALYSIS, CHARACTERIZATION AND PROPERTIES DETERMINATION
- DEVELOP PROCESSES AND METHODS FOR LAB SCALE SCALE-UP PROCESS
 - ENVIRONMENTALLY FRIENDLY
 - LEAST NUMBER OF STEPS
 - BETTER YIELDS
 - REPRODUCEABLE METHODS
 - LESS HAZARDOUS WASTE
- DEMONSTRATE THE VIABILITY OF THE DEVELOPED PROCESS BY PRODUCING SIGNIFICANT QUANTITY OF MTNP
- PROVIDE MTNP FOR PERFORMANCE EVALUATION

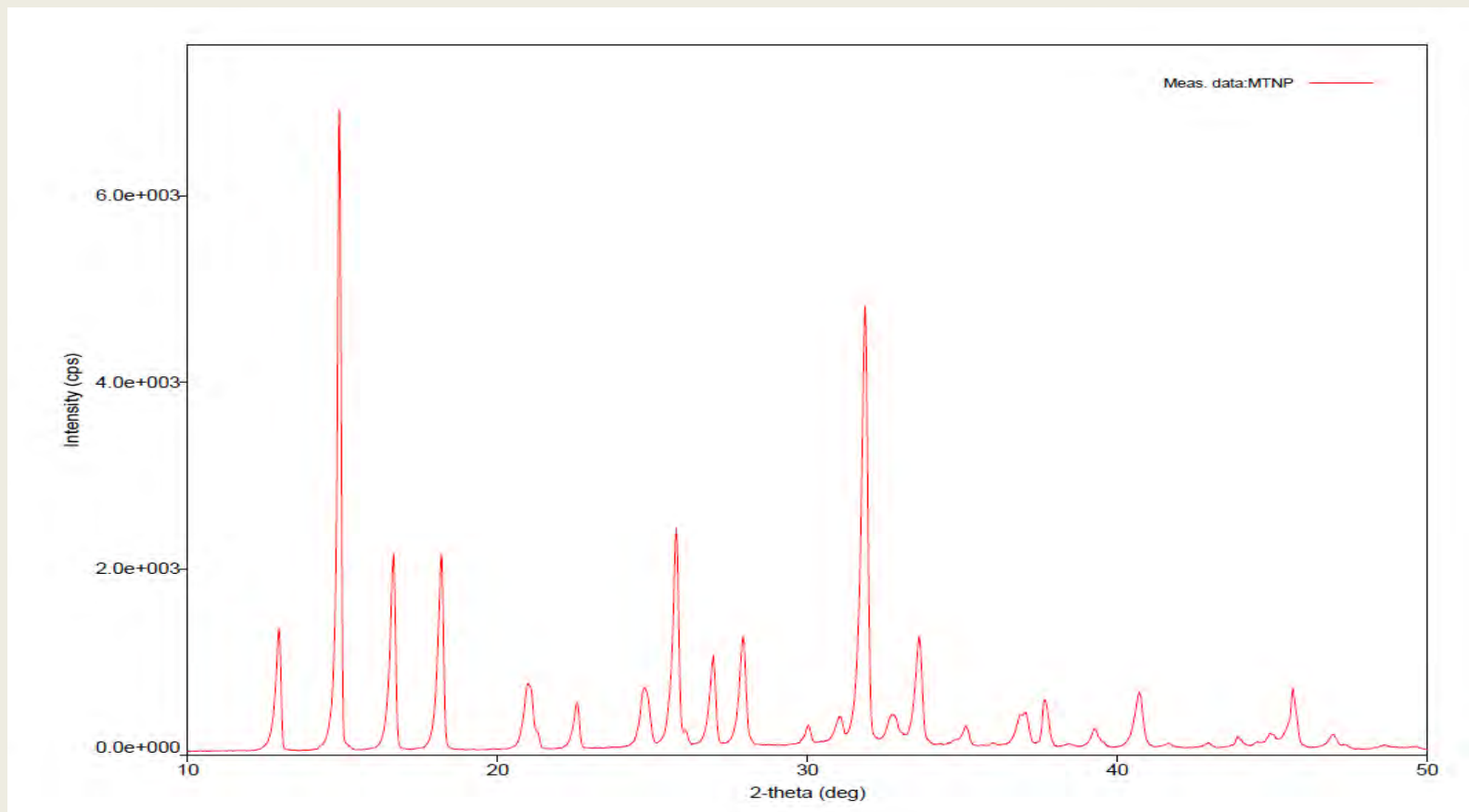
**JAGUAR CALCULATIONS**

Explosive	Formula	Density	DH_f	Det Vel	C-J P	Gurn Vel(3)	Gurn Vel(7)	OB
		g/cm³	kJ/mol	km/s	GPa	km/s	km/s	%
DNAN	C7H6N2O5	1.546	-186.5	6.14	14.8	1.88	2.10	-96.9
3,4 DNP	C3H2N4O4	1.791	120.5	8.31	30.9	2.63	2.86	-30.4
MTNP	C4H3N5O6	1.82	4.53	8.36	31.1	2.59	2.82	-25.8
PrNQ	C4H10N4O2	1.335	-217.3	6.45	14.4	1.95	2.10	-120
TNT	C7H5N3O6	1.654	-63	6.89	19.8	2.20	2.43	-74.0
RDX	C3H6N6O6	1.816	70	8.76	34.8	2.73	3.01	-21.6
HMX	C4H8N8O8	1.905	75	9.09	38.7	2.76	3.04	-21.6





^{13}C -NMR of 1-methyl-3,4,5-trinitropyrazole in DMSO-d_6



XRD of MTNP



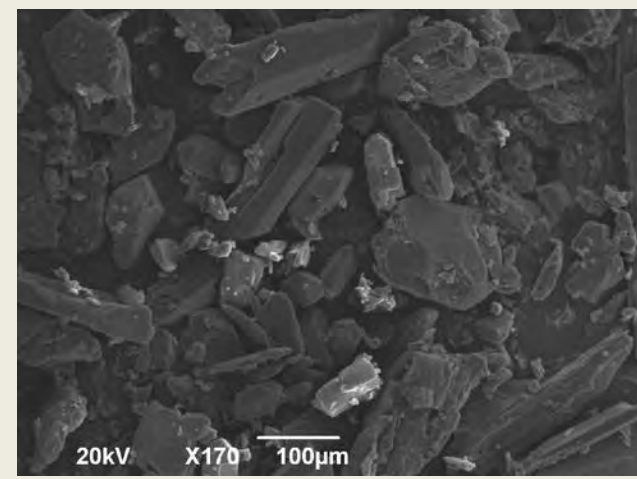
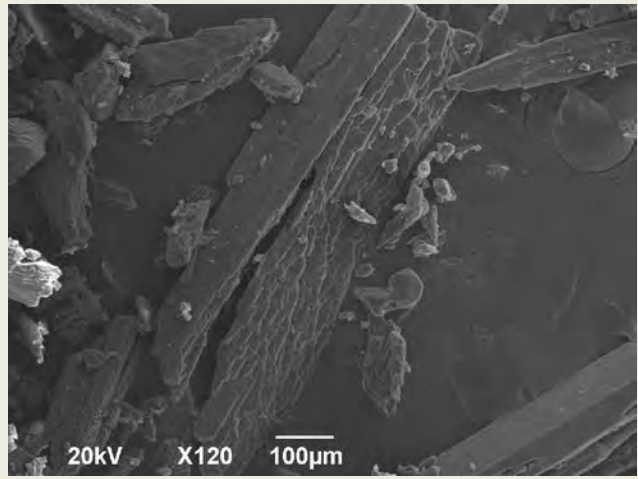
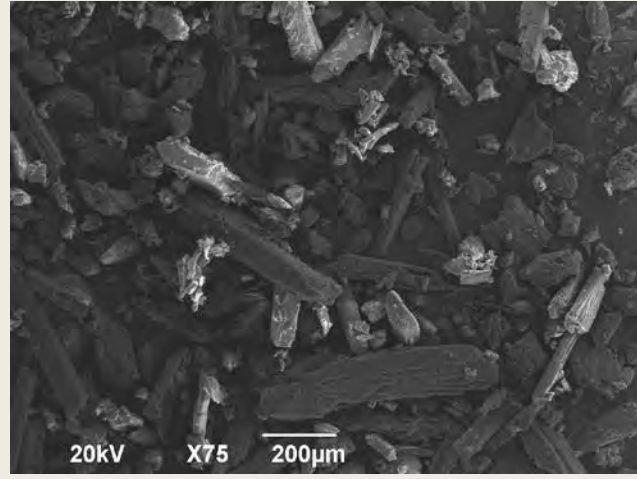
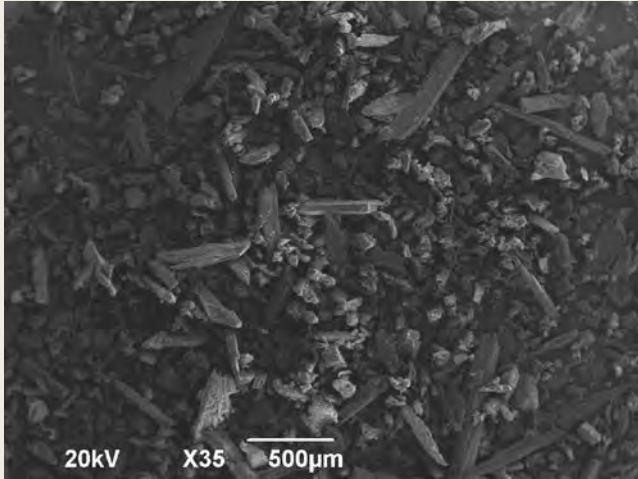
Properties of 1-methyl-3,4,5-trinitropyrazole (MTNP)



Molecule	Impact (cm)	BAM Friction (N)	ABL ESD (J)
MTNP	54.1	No Reaction in 10 trials @ 360N	Reacted @ 0.063J, did not react in 20 trails @ 0.051J
RDX Class I Type II	18	Reacted @ 216N, did not react in 10 trials at 192N	Reacted @ 0.063J, did not react in 20 trails @ 0.051J
RDX Class V Type II	>100	Reacted @ 324N, did not react in 10 trials at 288N	Reacted @ 0.051J, did not react in 20 trails @ 0.040J
DNP	>100	No Reaction in 10 trials @ 360N	Reacted @ 0.063J, did not react in 20 trails @ 0.051J
TNT	88.3	Reacted @ 240N, did not react in 10 trials at 216N	Did not react in 20 trials @ 0.25J (Old Test Method)

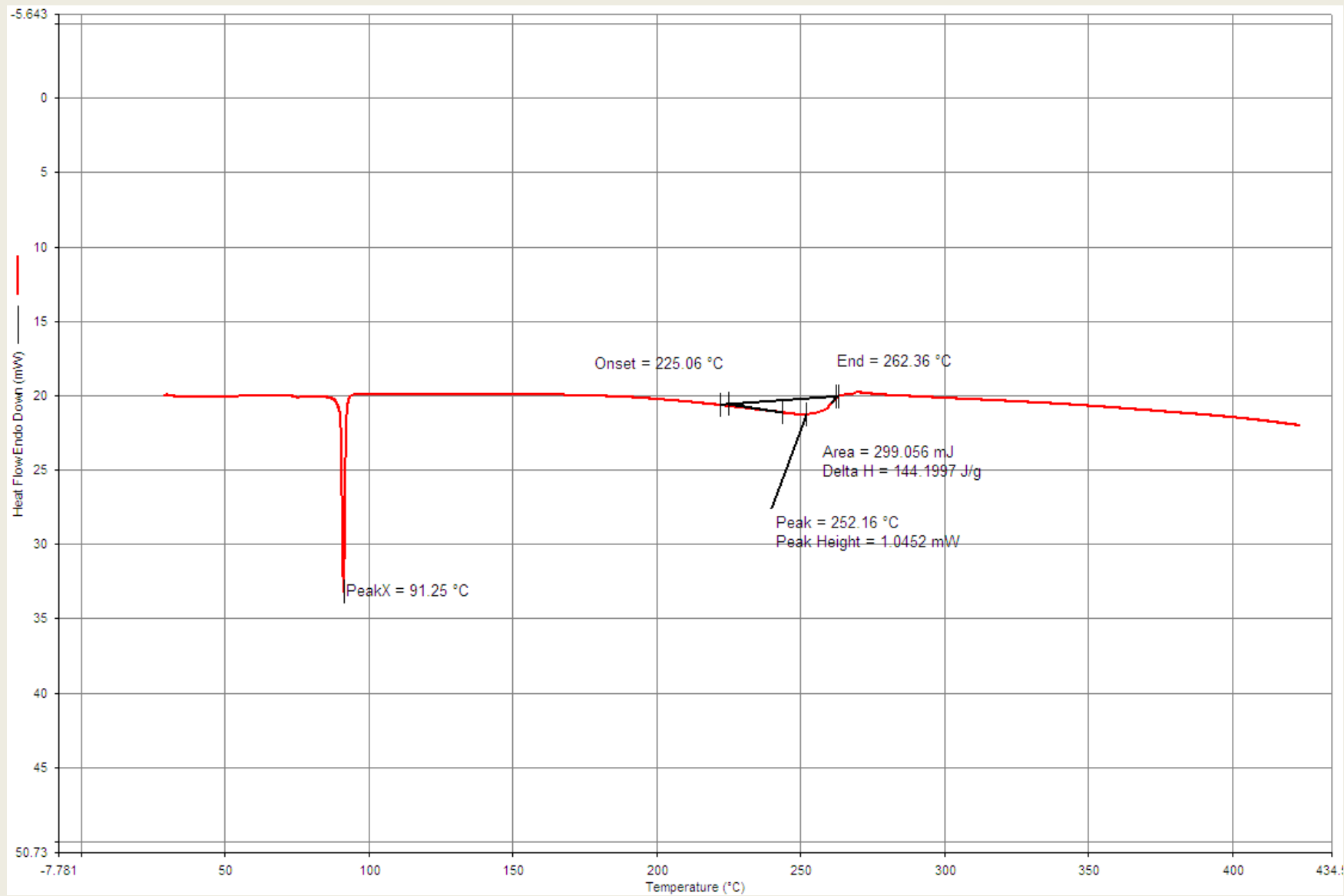


SEM Images of MTNP



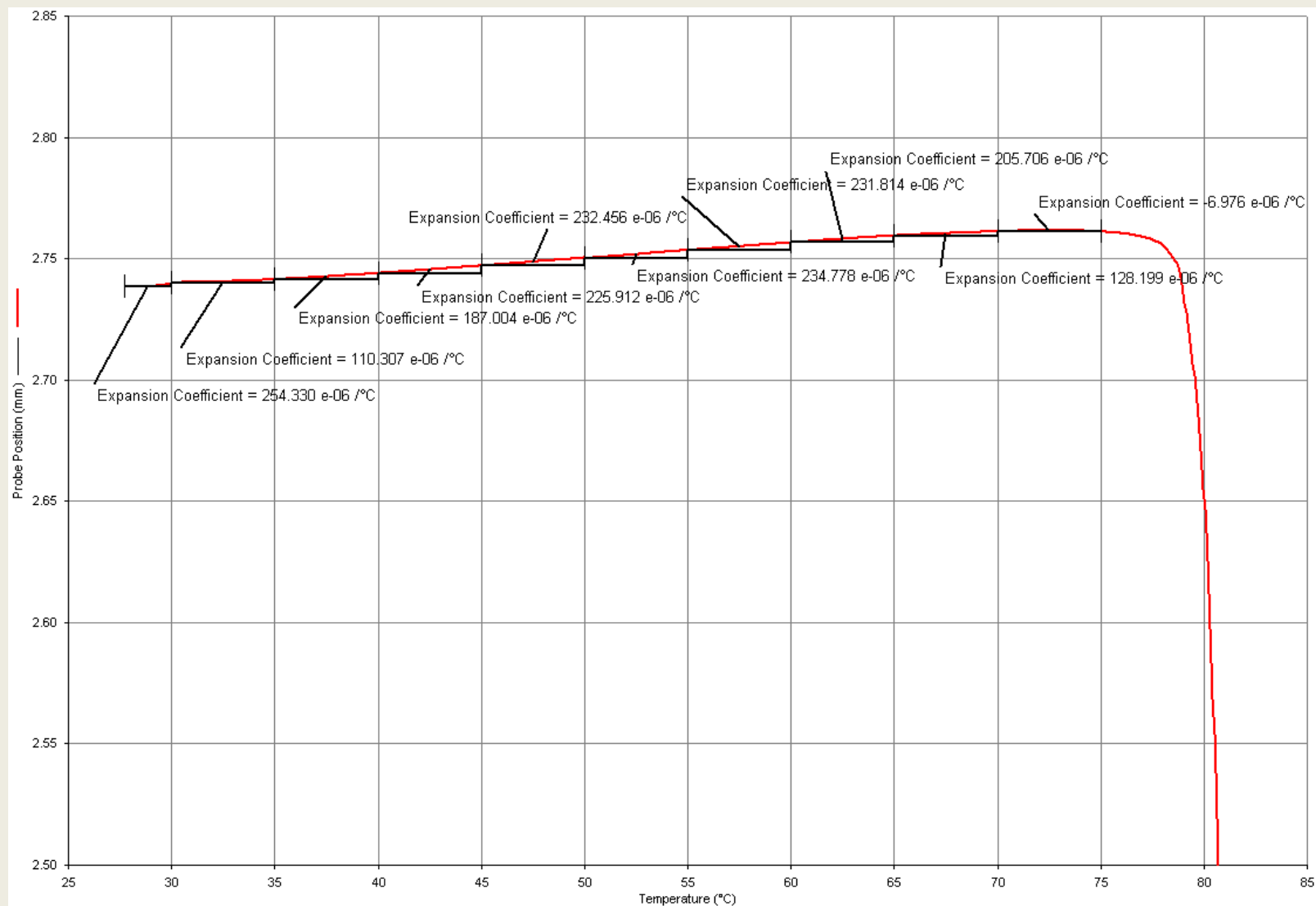


DSC of MTNP





TMA analysis of MTNP





- Performed compatibility testing in accordance to STANAG 4147 ED.2
- A DSC for each individual explosive, test material and mixture shall be run in duplicate
- Explosives and test materials are mixed in a 1:1 (w/w) ratio
- Samples are heated at a rate of 5°C/min from room temperature to 300°C or more for each sample
- The reactivity (compatibility) is then determined by comparing the decomposition profiles of the individual components to the mixture



- MTNP is compatible with Al.
- MTNP requires VTS testing with NTO, FOX-7, HMX and O-ring since DSC compatibility showed more than 10C exotherm shift
- MTNP requires VTS testing with brass and 304/316 stainless steel to determine compatibility due to the appearance of a new exotherm
- VTS testing is also needed with copper and A2 Steel due to earlier onset of the decomposition (around 250°C)
- VTS testing with Copper: Pass



Conclusions



- **Performed Literature Search and Analyzed Reported Methods**
- **Made attempts to synthesize MTNP in one pot process from Pyrazole**
- **Will Investigate Preparing MTNP Using Sequential Nitration Process**
- **Looking to Reduce the Amount of Required Reagents**
- **Characterized and Determined Small Scale Safety and Handling and Thermal Properties of MTNP**
- **Developed Scale up process**
- **FUTURE WORK:**
 - **Continue Investigating Alternate Nitrating Agents/Reagents**

UNCLASSIFIED

Evaluation of Nanoenergetics Based Composition B

Philip Samuels,^{*[a]} Erik Wrobel,^[a] Victor Stepanov,^[a] Rajen B. Patel,^[a] Katherine H. Guarini,^[a] Aleksander Gandzelko,^[a] and Hongwei Qiu^{*[b]}

^[a] Philip Samuels,* E. Wrobel, V. Stepanov, R. B. Patel, K. H. Guarini, A. Gandzelko
U.S. Army, RDECOM-ARDEC,
Picatinny Arsenal, NJ 07806 (USA)
Email: Philip.j.samuels2.civ@mail.mil

^[b] H. Qiu*
Mission Operations & Infrastructure Protection Division
Leidos, Inc.
Picatinny Arsenal, NJ 07806 (USA)
Email: Hongwei.qiu@leidos.com

Abstract:

This paper discusses the preparation and evaluation of nanoenergetics-based Composition B (N-Comp B) consisting of nanocrystalline RDX and TNT. The formulation was prepared by compacting Comp B molding powder that was produced by spray drying an acetone solution of RDX and TNT. The N-Comp B molding powder was characterized using scanning electron microscopy (SEM), X-ray diffraction (XRD), differential scanning calorimetry (DSC), and high performance liquid chromatography (HPLC). Its non-shock sensitivities were evaluated in the safety tests (impact, friction, and electrostatic discharge). The nanostructure of compacted N-Comp B was characterized by focused ion beam-scanning electron microscopy (FIB-SEM) and the shock sensitivity was evaluated using small scale gap test (SSGT), which shows that the majority of the voids in the formulation are in the nanoscale range, leading to a reduction in shock sensitivity. However, when there is a large number density of voids, the reduction seems to be limited. The addition of a polymeric binder during the spray drying process mediated the compaction and is demonstrated as an effective method to reduce the size and the number density of voids, leading to a 50% sensitivity reduction compared to melt-cast Comp B. This work continues to demonstrate that the spray drying based materials processing method is a facile and versatile method for producing high performance and low sensitivity nanoenergetics-based explosives.

UNCLASSIFIED

Distribution Statement A: Approved for public release; distribution is unlimited

I. Introduction

Composition B (Comp B) is a widely used heterogeneous explosive consisting of 59.5 weight percent (wt. %) cyclotrimethylenetrinitramine (RDX), 39.5 wt.% trinitrotoluene (TNT), and 1 wt.% wax [1]. Most Comp B is produced by a melt-cast process in which a slurry of RDX crystals dispersed in molten TNT is cast and allowed to solidify into a charge [1]. During the solidification process of molten TNT, numerous voids and other defects are formed [2-4], which contribute to the relatively high sensitivity of Comp B.

To reduce the voids size and therefore the sensitivity of Comp B, nanoscale high explosives (i. e., nanoenergetics) based Comp B, N-Comp B, was prepared by spray drying an acetone solution of dissolved RDX and TNT in a recent work [2]. N-Comp B pellets were produced by compacting the N-Comp B powder. Detailed characterization shows that N-Comp B powder consists of nanoscale RDX and TNT. The nanostructure of N-Comp B was characterized by focused ion beam-scanning electron microscopy (FIB-SEM) and the shock sensitivity was evaluated using small scale gap test (SSGT). The characterization of the nanostructure shows that the majority of the voids inside the N-Comp B formulation are in the nanoscale range but have a large number density. Reduction in shock sensitivity was observed in SSGT test and is attributed to the elimination of large voids, and yet the large number density of smaller voids seems to have limited the sensitivity decrease.

In this work, we aim to further reduce the shock sensitivity of N-Comp B by introducing a polymeric binder during the spray drying preparation of N-Comp B powder. The polymer is expected to coat the nanoscale crystals of HEs in spray drying. We also hypothesized that the polymer coating can flow and significantly reduce the population of the voids in N-Comp B, leading to a reduced sensitivity. N-Comp B powder with polymer was prepared. The material was characterized in details. The compacted pellets were characterized using FIB-SEM and the shock sensitivity was evaluated using SSGT test. The results were compared to those of Comp B and N-Comp B with no polymeric binder, and were further discussed. The samples that were evaluated in this work were listed in Table 1.

Table 1. Summary of the evaluated samples.

Materials		Form	Description
Comp B		Powder/Flakes	Melt-cast Comp B
N-Comp B	N-Comp B1	Powder/pellets	As spray dried and compacted Comp B with no polymer binder
	N-Comp B2	Powder/pellets	As spray dried and compacted Comp B with a polymer binder

UNCLASSIFIED

II. Experimental

2.1 Material characterization

The N-Comp B molding powder was characterized using scanning electron microscopy (SEM, Auriga CrossBeam Workstation, Carl Zeiss), powder X-ray diffraction (XRD, Rigaku Ultima IV XRD system with Cu K α radiation at $\lambda = 1.5418 \text{ \AA}$), differential scanning calorimetry (DSC, PerkinElmer DSC 6000, at a scan rate of 5 °C/min).

The structure of N-Comp B was studied using SEM after exposing the cross-sections of the pellets by sectioning using a focused ion beam (FIB). The FIB cross-sectioning and SEM imaging (FIB-SEM) was performed at a cryogenic temperature (-135°C) to reduce the radiation damage from both the electron beam and the ion beam. The surface of the specimen was coated with a ~1-2 μm thick platinum layer before FIB cross-sectioning to further protect the specimens from the ion beam damage. Structure of Comp B was also imaged after fracturing a melt-cast flake.

2.2 Safety tests

Basic safety sensitivity tests (impact, friction, and electrostatic discharge) were conducted according to AOP-7 and STANG 4489 ED1. As spray dried N-Comp B samples were used. Comp B sample was prepared by grinding raw material in a Wiley Mill until it passed through a 25 mesh screen and dried at ~ 50 °C to a constant weight.

The impact test (Explosives Research Laboratory (ERL) impact test) was completed using an ARDEC ERL type 12 impact tester with a 2 ½-kg drop weight. The drop height corresponding to the 50% probability of initiation measures impact sensitivity. The test method is described in STANAG 4489 Ed.1 "Explosives, Impact Sensitivity Tests."

The friction test method (BAM friction test) is described in AOP-7, 201.02.006, "BAM Friction Test." In a typical test, a sample was placed on a porcelain plate and a porcelain pin was lowered onto the sample. Then a weight was placed on the arm to produce the desired load. Once the tester was activated, the porcelain plate was reciprocated once to and fro. The results are observed as either a reaction (i.e., flash, smoke, and/or audible report) or no reaction. Testing begins at the maximum load of the apparatus (360 N) or lower if experience warrants it. If a reaction occurs in ten trials, the load is reduced until there are no reactions observed in ten trials.

The ESD test was run per a modified variant of AOP-7, 201.03.001 with the SMS ABL ESD machine. This test determines the energy threshold required to ignite explosives by electrostatic stimuli of varying intensities. In a typical test, if there is a reaction in twenty trials, the ESD energy load is decreased until there are no reactions in twenty trials.

UNCLASSIFIED

Distribution Statement A: Approved for public release; distribution is unlimited

2.3 SSGT shock sensitivity tests

The shock sensitivity of samples was evaluated using the SSGT test according to AOP-7, 201.04.003. This is a standard test used to determine the shock wave pressure required to achieve a 50% probability of detonation. The specimens had a dimension of 5.08 mm × 38.1 mm (diameter × length) as compacted in Section 2.1. Pressed Comp B production flake was also evaluated in SSGT as a reference material.

III. Results and Discussion

3.1 Characterization of N-Comp B molding powder

SEM images of N-Comp B molding powder are shown in Figure 1. N-Comp B1 particles (Fig. 1A and 1B) and N-Comp B2 particles (Fig. 1A and 1B) have very similar morphology. Particles are larger than 10 μm and have irregular shapes. At high magnification (Fig. 1B and 1D), sub-micron sized crystals can be observed from both samples. Figure 2 shows the XRD pattern of N-Comp B samples along with the pattern from melt-cast Comp B. Major peaks of RDX and TNT crystals are labeled. The XRD pattern of the molding powder is consistent with the pattern from melt-cast Comp B. However, significant peak broadening from RDX and TNT is observed in both N-Comp B1 and N-Comp B2 samples. The peak broadening in XRD analysis happens when the crystal size is small [3]. Therefore, the SEM and XRD analysis suggest that N-Comp B molding powder prepared by spray drying consists of nanoscale RDX and TNT crystals. This is consistent with previous reports of nanoenergetic materials by spray drying [4-6]. The formation of nanoscale crystals is attributed to the rapid solvent evaporation and subsequent crystal nucleation in spray drying [4-6]. Compared to other spray-dried energetic materials which are typically spherical, the irregular morphology of N-Comp B molding powder is likely due to the fusion of particles because TNT has a relatively low melting point [7].

UNCLASSIFIED

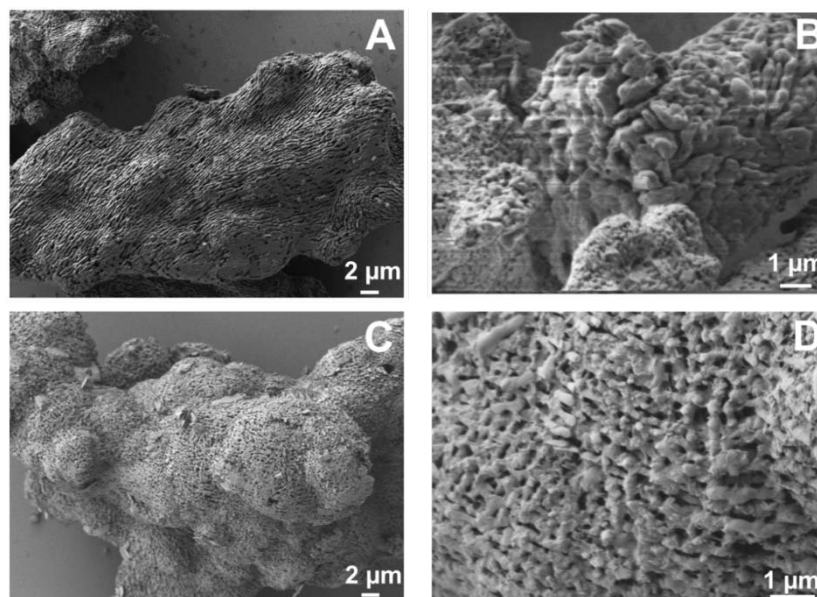


Figure 1. The SEM images of N-Comp B samples. (A) and (B): N-Comp B1 molding powder at low and high magnifications. (C) and (D): N-Comp B2 molding powder at low and high magnifications.

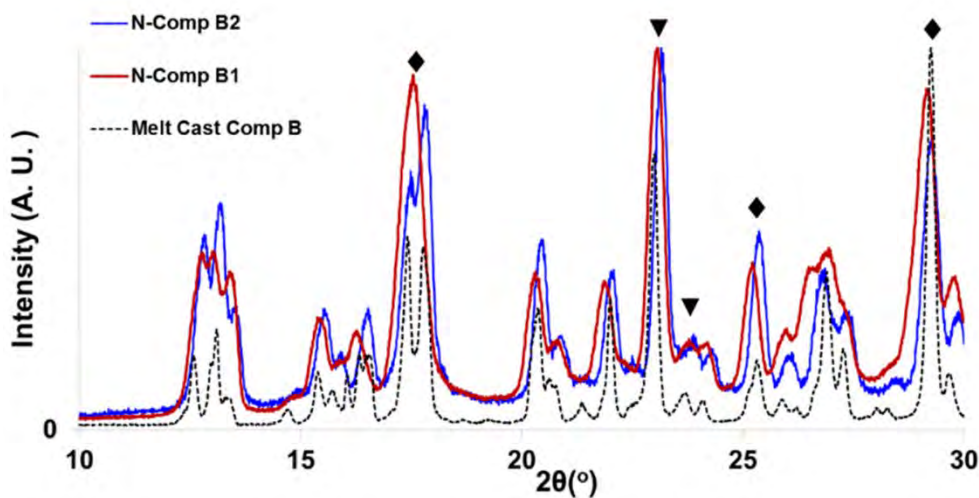


Figure 2. The X-ray diffraction (XRD) patterns, of N-Comp B molding powder and melt-cast Comp B (♦, RDX and ▼, TNT).

The DSC analysis of N-Comp B molding powder and melt-cast Comp B is shown in Figure 3. The peaks at ~ 80 °C and 230 °C corresponds to the melting temperature of TNT phase and the decomposition temperature of the material, respectively. Fig. 3 shows that there is a left-shift of the melting temperature from N-Comp B compared to melt-cast Comp B. This is probably due to the nanoscale size of TNT crystals. The decomposition temperature of N-Comp B1 is almost identical to that of melt-cast Comp B.

UNCLASSIFIED

Distribution Statement A: Approved for public release; distribution is unlimited

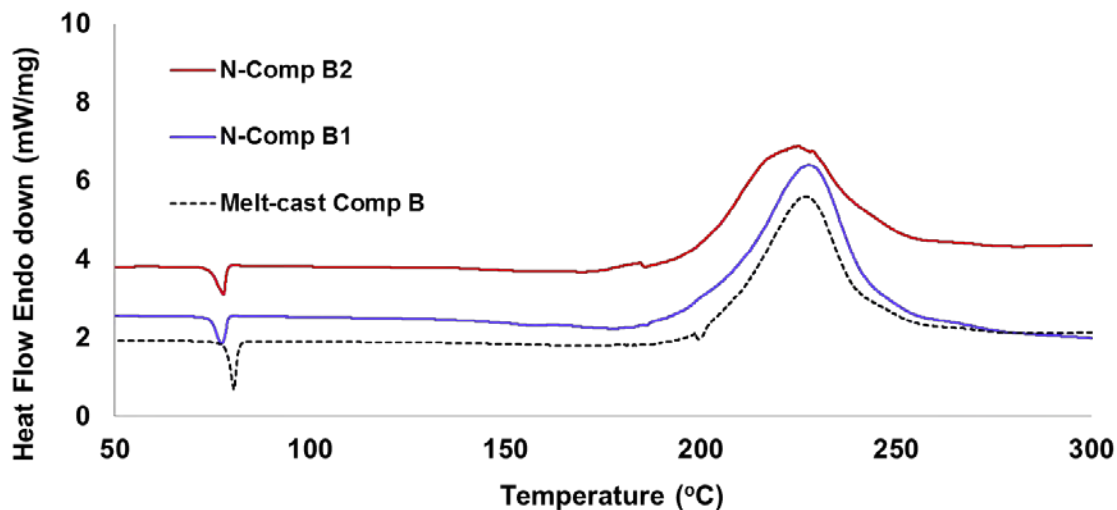


Figure 3. DSC analysis of N-Comp B1, N-Comp B2, and melt-cast Comp B obtained at a scan rate of 5 °C/min.

3.2 Structure of Comp B

SEM images of cross-sections that were prepared by FIB are shown in Figure 4A and 4B for N-Comp B1 and N-Comp B2, respectively. Although individual crystals cannot be differentiated from each other, all the features are on the nanoscale level. Surprisingly, at a relatively high TMD of about 94.5%, the N-Comp B1 formulation has a large number density of voids, which are estimated to be approximately $5/\mu\text{m}^2$, although majority of the voids have dimensions in the nanoscale range. Many of the voids are also observed to be interconnected.

Interestingly, the nanostructure of N-Comp B2 seems to be very different from N-Comp B1: (1) the voids seem to have evens smaller average size; (2) the number density of voids is dramatically reduced, to an estimated lever of $1.8/\mu\text{m}^2$; and (3) there is no interconnection between voids due to the smaller number density of voids. Therefore, the introduction of a polymeric binder during spray drying seems to be a very effective measure regarding to decrease the number density of voids and further reduce the size of voids in N-Comp B. This is attributed to the formation of a polymer coating on the surface of nanoscale crystals during spray drying, which could flow and fill the voids during compaction as evidenced from the higher achieved %TMD compared to N-Comp B1 under similar compaction conditions.

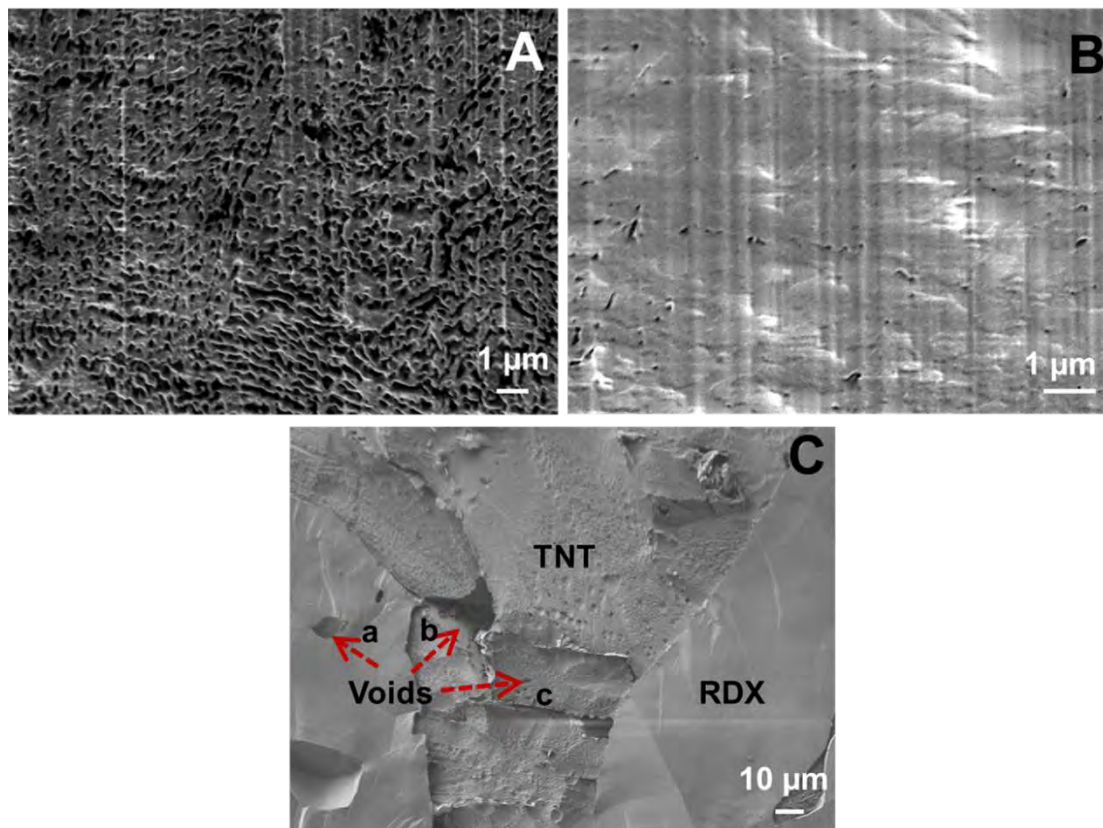


Figure 4. Structures of Comp B. (A) and (B), the SEM images of cross-sections prepared by FIB from N-Comp B1 and N-Comp B2, respectively; (C) the SEM image from a fractured surface of melt-cast Comp B.

In comparison, Figure 4C shows an SEM image from fractured melt-cast Comp B. The RDX crystals, with a smooth surface and crystalline facets, are embedded in the continuous TNT matrix, as labeled in the figure. The TNT crystals are in the commonly observed needle-like/columnar shape [8-10]. Both RDX and TNT crystals are large, on the order of hundreds of microns. Both intra- and inter-crystal voids can be observed. The voids are relatively large (tens of microns), especially the inter-crystalline voids which are generally located adjacent to the tip of TNT crystals.

3.3 Safety tests

The results of safety tests, including impact, friction and ESD, of N-Comp B molding powder and Comp B are summarized in Table 2. The results from the impact test show that N-Comp B molding powder has much lower impact sensitivity than Comp B and the addition of polymer further reduces the sensitivity of N-Comp B. Nanoscale RDX and TNT in N-Comp B powder may contribute less to the friction and hot spots formation in impact test, leading to reduced impact sensitivity.

UNCLASSIFIED

Results from friction test indicate that N-Comp B and Comp B are not friction sensitive. Particularly, N-Comp B2 has no reaction under the instrument maximum load in the friction test. The N-Comp B has moderate ESD sensitivity. The results from the safety tests suggest that N-Comp B, especially N-Comp B2, has reduced non-shock sensitivities and is safer to handle compared to Comp B.

Table 2. The results of safety tests (impact, friction, and ESD).

Materials		Impact (cm)	Friction (N, go/no-go)	ESD (J, go/no-go)
Comp B		33.9	318/282	---
N-Comp B	N-Comp B1	51.6	252/240	0.051/0.040
	N-Comp B2	69.5	360	0.040/0.031

3.4 SSGT sensitivity test

The shock sensitivities from SSGT test are reported in Table. 3. Melt-cast Comp B is used as the reference material and its SSGT shock sensitivity as described in shock wave pressure is treated as the reference point (100%). A value larger than 100 (%) means that the material is less sensitive than the melt-cast Comp B. At a relatively lower %TMD, N-Comp B1 illustrates a value of 116 (%), a 16% shock sensitivity reduction over melt-cast Comp B. The shock sensitivity of N-Comp B2 is impressive with a normalized value of 150 (%), or a 50% sensitivity decrease compared to melt-cast Comp B.

The reduced shock sensitivity from N-Comp B is attributed to the nanoscale size of voids, as they require stronger shock wave pressure to reach the critical temperature so that they can survive the conduction and continue to burn [11-13]. The sensitivity test and the nanostructure characterization also suggest that the number density of voids has a significant effect on the shock sensitivity. With a large number density of voids of $\sim 5/\mu\text{m}^2$, N-Comp B1 has only a slight sensitivity reduction compared to melt-cast Comp B. The large number density of voids and the interconnection between voids are believed to cause hot-spot merging, leading to the formation of critical hot-spots despite of the small void size [13]. Dramatic sensitivity decrease from N-Comp B2 is attributed to the small void number density of $\sim 1.8/\mu\text{m}^2$.

Table 3. Results from SSGT sensitivity test.

Materials		% TMD	SSGT Sensitivity (%)
Comp B		95.2	100
N-Comp B	N-Comp B1	94.8	116
	N-Comp B2	98.4	150

IV. Conclusion

Nanoenergetics-based Comp B (N-Comp B) consisting of nanoscale RDX and TNT crystals was prepared by spray drying and mechanical compaction. Structural characterization shows that the majority of the voids inside the formulation are in the nanoscale range, leading to a reduction in shock sensitivity. However, when there is a large number density of voids, the

UNCLASSIFIED

Distribution Statement A: Approved for public release; distribution is unlimited

UNCLASSIFIED

reduction seems to be limited. The addition of a polymeric binder during the spray drying process mediated the compaction process and was demonstrated as an effective method to reduce the size and the number density of voids, leading to a 50% sensitivity reduction compared to melt-cast Comp B. This work continues to demonstrate that the spray drying based materials processing method is a facile and versatile method for producing high performance and low sensitivity nanoenergetics-based explosives.

References

- [1] Smith DL, Thorpe BW. Fracture in the high explosive RDX/TNT. *Journal of Materials Science*. 1973;8:757-9.
- [2] Qiu H, Stepanov V, Patel RB, Samuels P, Maier KH. Preparation and Characterization of Nanoenergetics Based Composition B. *Propellants, Explosives, Pyrotechnics*. 2017;42:1309-14.
- [3] Langford JI, Wilson AJC. Scherrer after sixty years: A survey and some new results in the determination of crystallite size. *Journal of Applied Crystallography*. 1978;11:102-13.
- [4] Qiu H, Stepanov V, Di Stasio AR, Chou T, Lee WY. RDX-based nanocomposite microparticles for significantly reduced shock sensitivity. *Journal of Hazardous Materials*. 2011;185:489-93.
- [5] Qiu H, Stepanov V, Chou T, Surapaneni A, Di Stasio AR, Lee WY. Single-step production and formulation of HMX nanocrystals. *Powder Technology*. 2012;226:235-8.
- [6] Qiu H, Stepanov V, Di Stasio AR, Surapaneni A, Lee WY. Investigation of the crystallization of RDX during spray drying. *Powder Technology*. 2015;274:333-7.
- [7] Ravi P, Badgujar DM, Gore GM, Tewari SP, Sikder AK. Review on melt cast explosives. *Propellants, Explosives, Pyrotechnics*. 2011;36:393-403.
- [8] Tian Y, Liu S, Zhang WB, Dai B, Zhou HP, Luo G. Experimental study on crystallization of casting tnt explosive during solidification by high-resolution X-ray CT. *Hanneng Cailiao/Chinese Journal of Energetic Materials*. 2009;17:173-7.
- [9] Lanzerotti YD, Sharma J, Armstrong RW, McKenney RL, Krawietz TR. Nanofractography of composition B fracture surfaces with AFM. *Materials Research Society Symposium – Proceedings*. 2003; p. 233-41.
- [10] Philip DK, Thorpe BW. Nucleation of 2,4,6-trinitrotoluene by 2,2', 4,4',6,6'-hexanitrostilbene. *Journal of Crystal Growth*. 1976;35:133-8.
- [11] Akiki M, Menon S. A model for hot spot formation in shocked energetic materials. *Combustion and Flame*. 2015;162:1759-71.
- [12] Levesque G, Vitello P, Howard WM. Hot-spot contributions in shocked high explosives from mesoscale ignition models. *Journal of Applied Physics*. 2013;113.
- [13] Levesque G, Vitello P, Nichols III AL, Tarver C, Willey T, Friedman G, et al. Analyses on the effect of hot spot density on material consumption rate. *Journal of Physics: Conference Series*. 2014;500.

UNCLASSIFIED

Distribution Statement A: Approved for public release; distribution is unlimited



Evaluation of Nano Comp B

Philip Samuels*, Erik Wrobel, Alex Gandzelko, Dr. Victor Stepanov, Dr. Rajen Patel, Katherine Guarini

Dr. Hongwei Qiu (Leidos)
IMEM April 2018, Portland, OR

UNPARALLELED
**COMMITMENT
& SOLUTIONS**

Act like someone's life depends on what we do.



U.S. ARMY ARMAMENT
RESEARCH, DEVELOPMENT
& ENGINEERING CENTER

Distribution A: Approved for Public Release



BACKGROUND



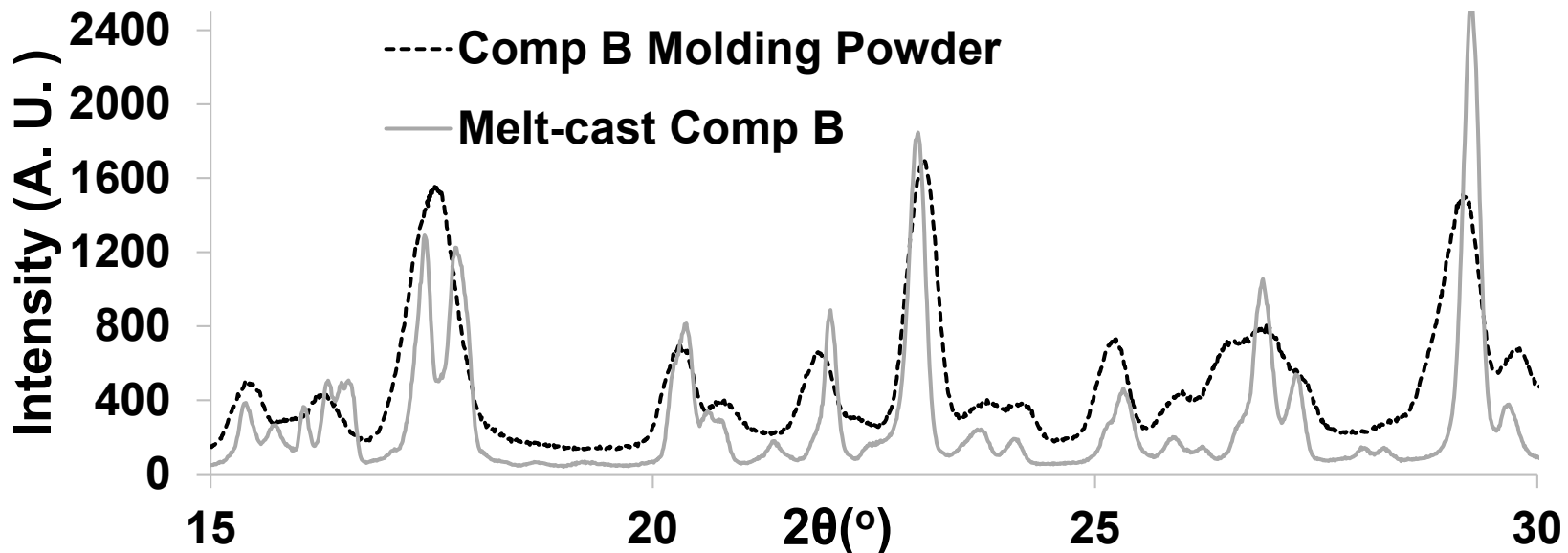
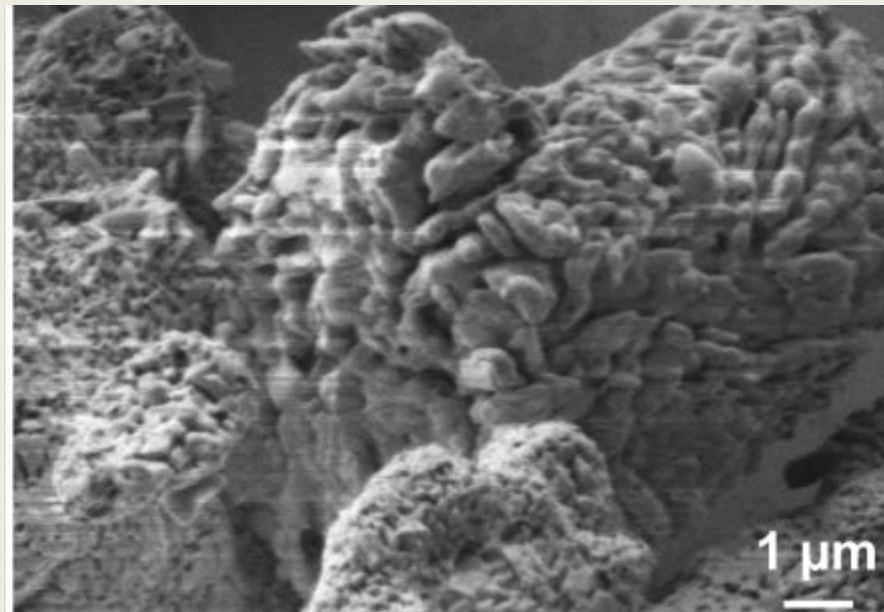
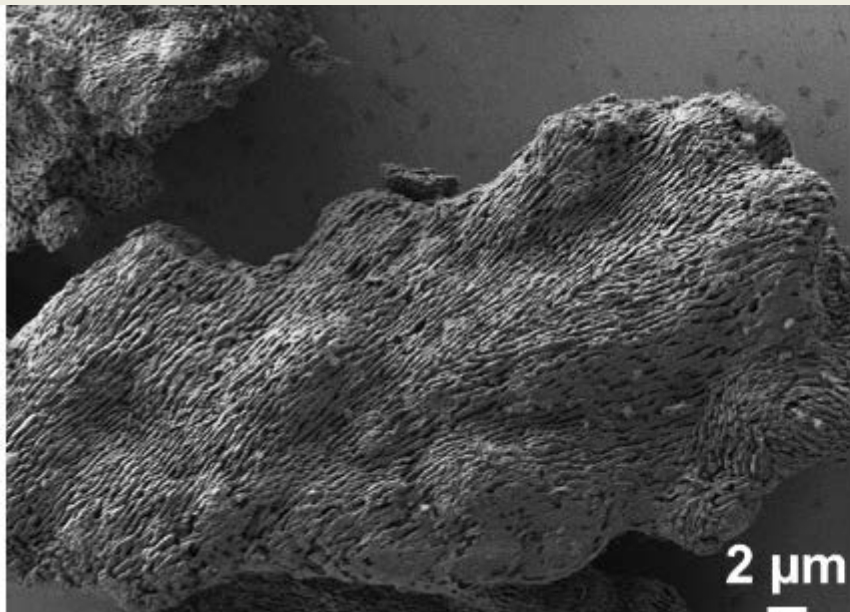
- To reduce the void size and therefore the sensitivity of Comp B, nanoscale high explosives were prepared by spray drying
- N-Comp B pellets were produced by compacting the N-Comp B powder.
- Detailed characterization shows that N-Comp B powder consists of nanoscale RDX and TNT
- The nanostructure of N-Comp B was characterized by focused ion beam-scanning electron microscopy (FIB-SEM)
- Shock sensitivity was evaluated using small scale gap test (SSGT)
- The characterization of the nanostructure shows that the majority of the voids inside the N-Comp B formulation are in the nanoscale range but have a large number density
- Reduction in shock sensitivity was observed in SSGT test and is attributed to the elimination of large voids, and yet the large number density of smaller voids seems to have limited the sensitivity decrease



U.S. ARMY
RDECOM

UNCLASSIFIED

SEM AND XRD ANALYSIS OF N-COMP B1 MOLDING POWDER





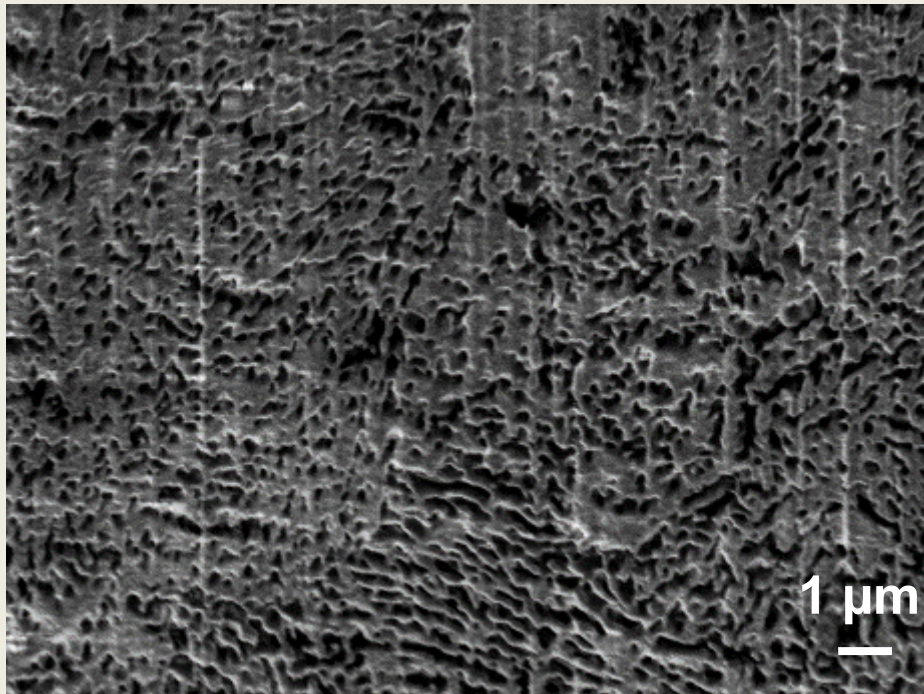
U.S. ARMY
RDECOM

UNCLASSIFIED

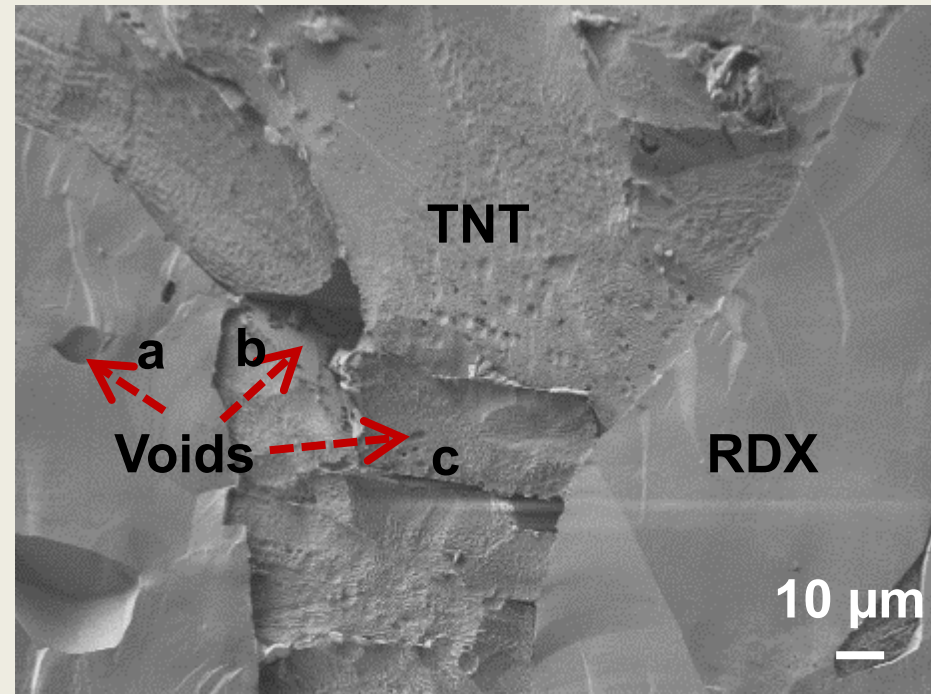
Structure of Compacted N-Comp B1 and Melt-cast Comp B



Compacted Pellets of N-Comp B1



Melt-cast Comp B





Safety and SSGT Tests Results

	Impact (cm)	BAM Friction (N)	ESD (J)	SSGT (%)
Comp B	33.9	192-168	-	100
N-Comp B1	51.6	252-240	0.051/0.040	116



SUMMARY OF SAMPLES



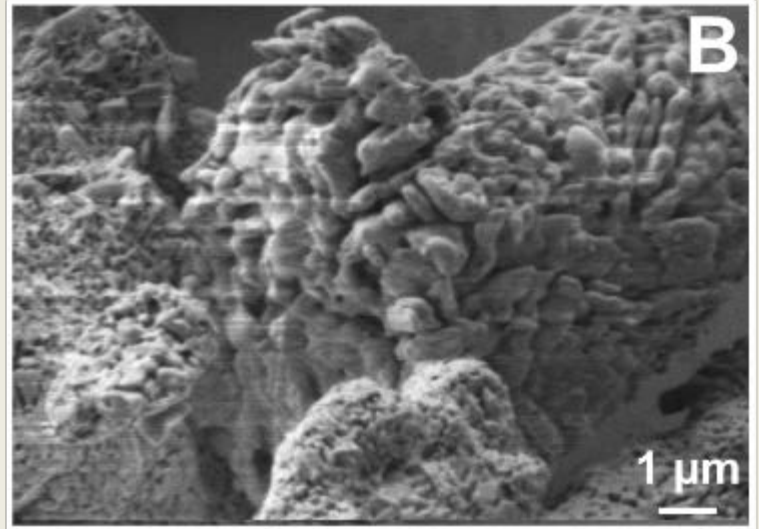
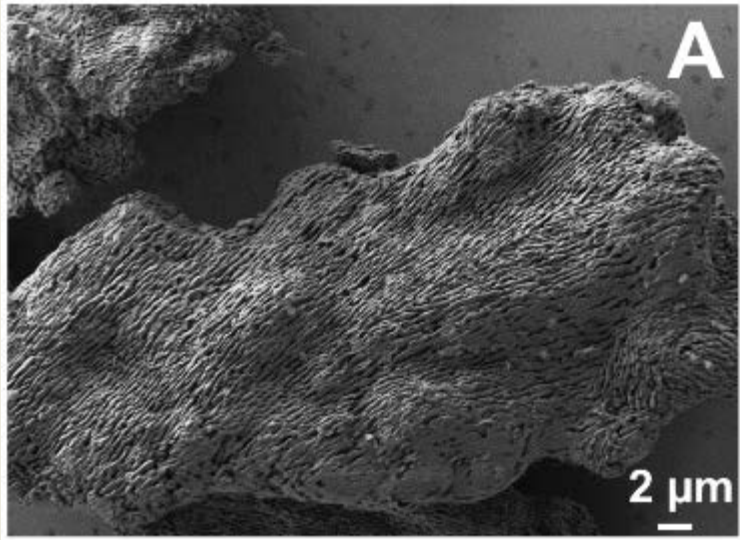
Samples	Form	Description
Comp B	Powder/Flakes	Melt-cast Comp B; Powder was prepared by grounding the flakes
N-Comp B1	Powder/pellets	As spray dried and compacted Comp B with no polymer binder
N-Comp B2	Powder/pellets	As spray dried and compacted Comp B with a polymer binder



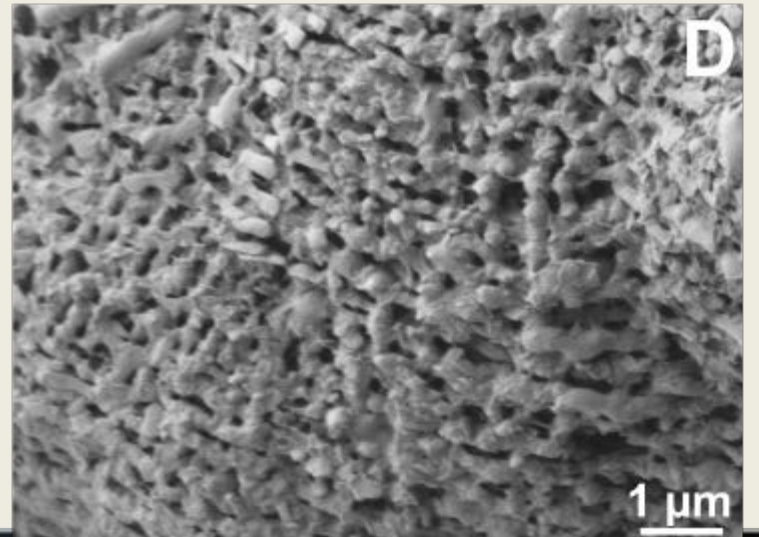
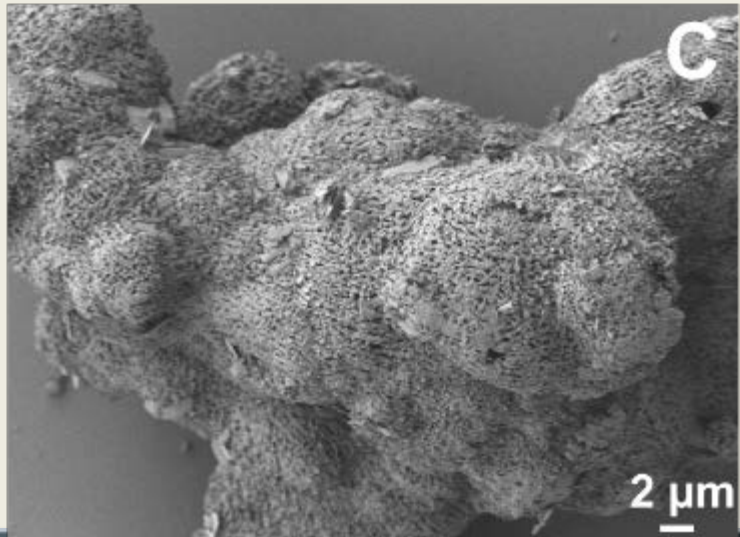
SEM ANALYSIS OF N-COMP B MOLDING POWDER



N-Comp B1



N-Comp B2

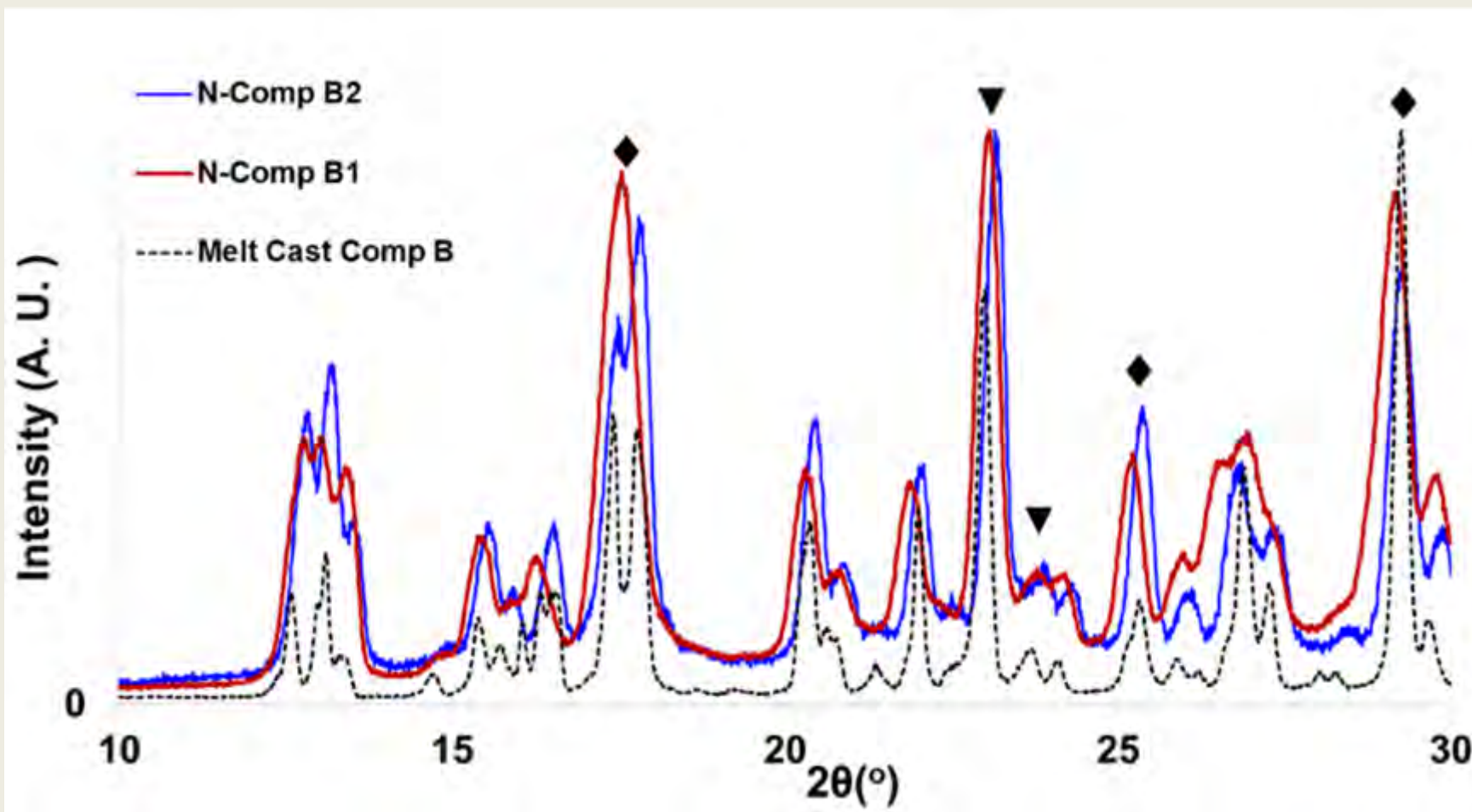




U.S. ARMY
RDECOM

UNCLASSIFIED

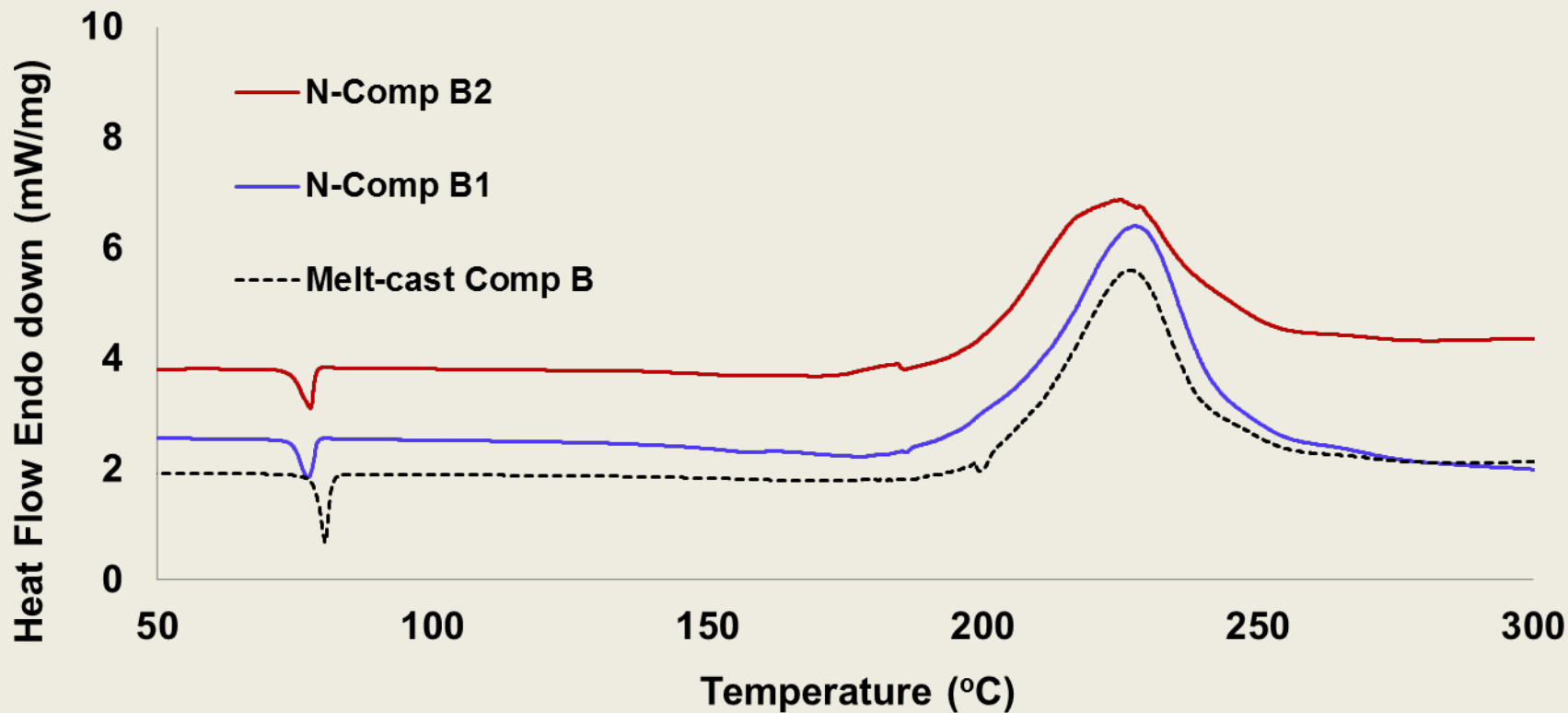
XRD ANALYSIS OF N-COMP B MOLDING POWDER



◆, RDX and ▼, TNT



DSC SCAN OF N-COMP B MOLDING POWDER





SAFETY TESTS

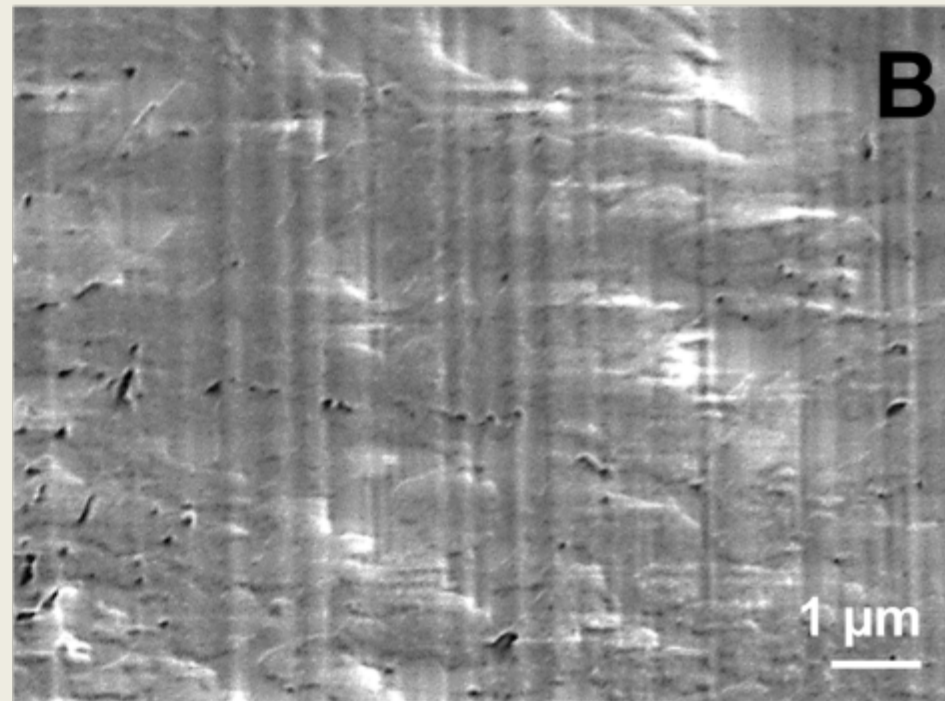
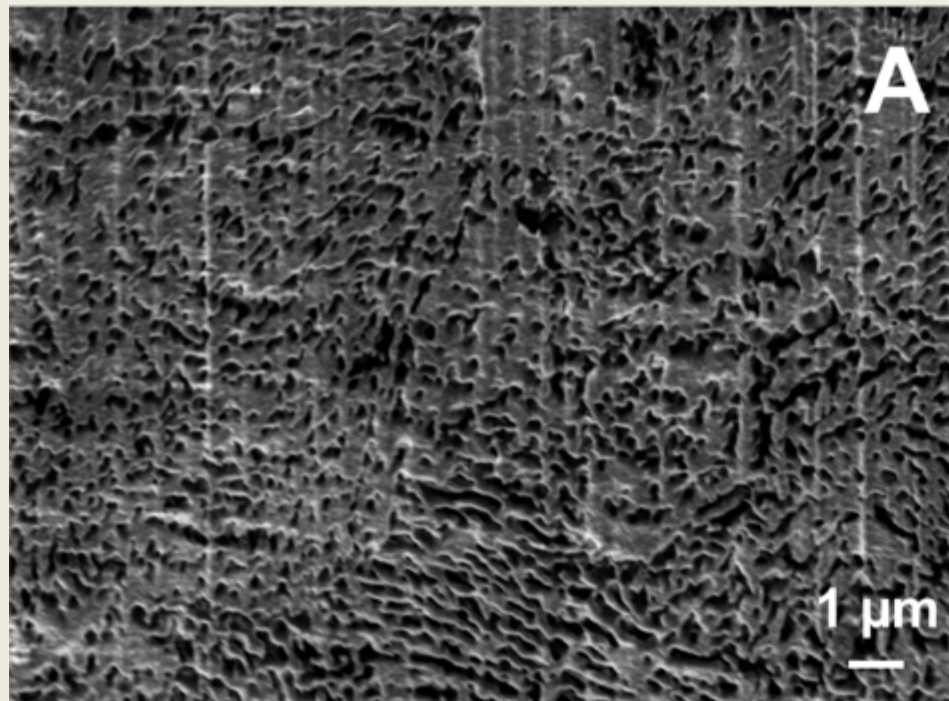


Samples	Impact (cm)	Friction (N, go/no-go)	ESD (J, go/no-go)
Comp B	33.9	318/282	-
N-Comp B1	51.6	252/240N	0.051/0.040
N-Comp B2	69.5	360N	0.040/0.031



Compacted Pellets of N-Comp B1

Compacted Pellets of N-Comp B2

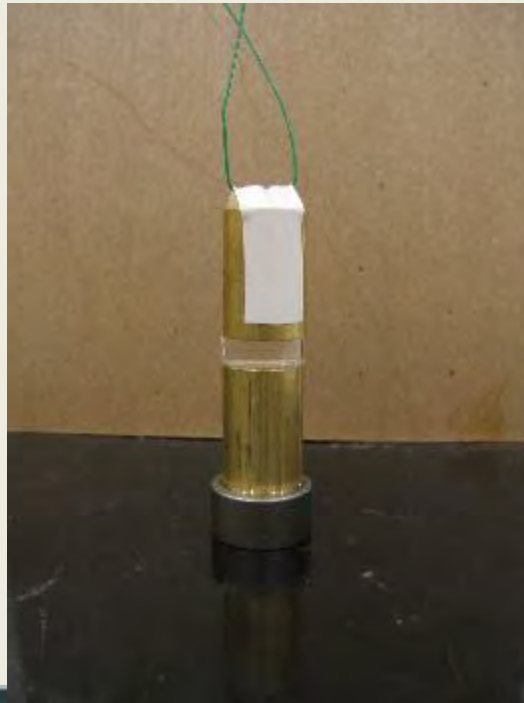




SSGT TEST RESULTS



Samples	%TMD	SSGT Shock Sensitivity (%)
Comp B	95.2	100
N-Comp B1	94.8	116
N-Comp B2	98.4	150





CONCLUSIONS



- **Nanoenergetics-based Comp B (N-Comp B) consisting of nanoscale RDX and TNT crystals was prepared by spray drying and mechanical compaction.**
- **The addition of a polymeric binder during the spray drying process mediated the compaction and is demonstrated as an effective method to reduce the size and the number density of voids, leading to a sensitivity reduction.**
- **This work continues to demonstrate that the spray drying based materials processing method is a facile and versatile method for producing high performance and low sensitivity nanoenergetics-based explosives.**



U.S. Army, ARDEC:

Anthony R. Di Stasio

Dr. Kelley C. Caflin

Henry Grau

Sanjeev K. Singh

Steven M. Nicolich

Slow Heating Testing Survey and Historical Events Review

Ernest L. Baker

Munitions Safety Information Analysis Center (NATO), Brussels, Belgium

This report describes the results of an international review of the STANAG 4382 Slow Heating, Munitions Test Procedures, as well a review of heating rates and durations associated with actual fire events. The purpose of the slow heating test is to assess the reaction, if any, of munitions and weapon systems to a gradually increasing thermal environment. To perform the review, MSIAC created a questionnaire in conjunction with the custodian of this STANAG, the United States, and sent it to subject matter experts including test centers in most of the AC/326 nations. The questionnaire questions deal with the test purpose, test procedure, heating rate, actual events, oven design, oven standardization, temperature preconditioning, energetics melting, reaction temperature, test item restraints, test item orientation, instrumentation, and number of tests. This report provides an analysis of the answers received, summarizes best practice and provides some recommendations to potentially support an amendment of STANAG 4382. These recommendations are being discussed within the NATO AC/326 SG/B Slow Heating Custodial Working Group (SH CWG). The working group has already reviewed the review results and is currently drafting updates to STANAG 4382 NATO documentation, which includes the technical content of the STANAG that is being migrated into a new AOP 4382.

INTRODUCTION

This report describes the results of an international review of the STANAG 4382 Slow Heating, Munitions Test Procedures, as well a review of heating rates and durations associated with actual fire events. The purpose of the slow heating test is to assess the reaction, if any, of munitions and weapon systems to a gradually increasing thermal environment. To perform the review, MSIAC created a questionnaire in conjunction with the custodian of this STANAG, the United States, and sent it to subject matter experts including test centers in most of the AC/326 nations. Moreover, an analysis of similar standards has been done in order to achieve more consistency in the recommendations. From a NATO point of view, the requirements for the slow heating test are defined within three documents: STANAG 4439, STANAG 4382 and AOP-39. The test 7 (h) from the "UN – Manual of Tests and Criteria" specifies a slow cook-off test for the classification into hazard division 1.6. The questionnaire questions deal with the test purpose, test procedure, heating rate, actual events, oven design, oven standardization, temperature preconditioning, energetics melting, reaction temperature, test item restraints, test item orientation, instrumentation, and number of tests. This report provides an analysis of the answers received, summarizes best practice and provides some recommendations to potentially support an amendment of STANAG 4382.

BACKGROUND

In 2015, MSIAC carried out a review of STANAG 4496 related to the fragment impact test. This review was managed the same way as this current one, and resulted in a list of recommendations that are currently being discussed in a custodian working group to update STANAG 4496. Following the review of the bullet and fragment impact tests, MSIAC proposed

to perform a similar review for the slow heating test, on behalf of the United States who is the custodian for this STANAG.

REQUIREMENTS

From a NATO point of view, the requirements for the slow heating test are defined within three documents: STANAG 4439 [1], STANAG 4382 [2] and AOP-39 [3]. The test 7 (h) from the “UN – Manual of Tests and Criteria” [4] specifies a slow cook-off test for the classification into hazard division 1.6.

Analysis of the requirements

The table hereafter compares the STANAG 4382, AOP-39, and the UN Manual of Tests and Criteria test 7(h) regarding the slow heating test:

Table 1: Differences between the STANAG 4382, AOP-39 and UN orange book test 7(h)

	STANAG 4382 ed.2	AOP 39 Ed. 3	UN 7 (h)
Alternative procedure	Yes		No
Number of tests	2		2
Item configuration	Bare or logistical, as agreed by the national authority	Bare or logistical	Logistical
Test Procedure	Yes		Yes
Heating rate	3.3°C/hr		3.3°C/hr
Preconditioning Temperature	50°C for 8 hours or until equilibrium at 50°C		°C below the predicted reaction temperature
Maximum Temperature			365°C
Reaction level acceptable	Burning or no reaction		Burning or no reaction

The main difference between the documents is related to the item configuration:

- In logistical configuration for the UN document. This seems logical, as this document relates to the transport classification of the article;
- Bare or packed, as agreed by national authority, in the STANAG, which seems logical as the national authority is able to define when a fire is more likely to impact the munitions during the life cycle.

An alternative procedure is provided in the STANAG: if no analysis has been done, a rate of 25°C per hour should be used as a default rate. With respect to temperatures specified, there are 2 main differences: the preconditioning temperature is different (higher for the UN) and the UN defines a maximum temperature. The STANAG provides more details on the test procedure and includes a basic test set-up description. Neither the STANAG nor the UN document provides a detailed example of test set-up. In addition, there are redundancies between the STANAG 4382 and the AOP-39, especially in the observations and reports part. They should be avoided to allow these 2 documents to remain independent. Indeed, the AOP-39 is linked to the STANAG 4439, and it is not automatically updated when there is a change in one of the STANAGs that defines the test procedure, like the STANAG 4382. The 3rd edition of AOP-39 includes Appendices which provided intermediate updates of all the IM full scale tests not referenced from STANAG 4382 and the contents of the Slow Heating appendix needs to be included in the review of STANAG 4382.

MSIAC was requested to support AC/326 SG/B, which was agreed by the MSIAC SC, to review all these documents to remove redundancies or contradictions and to clarify where the

information should reside. As a result, most of the redundancies will no longer exist in the updated documents. The review includes drafting of a Standards Related Document to provide guidance on common aspects of IM testing, reporting and documenting. Other IM full scale tests STANAGs have recently been reviewed in conjunction with this MSIAC review and changes to STANAG 4382 need to reflect a common structure and content with these other STANAGs

QUESTIONNAIRE

The questionnaire was conducted through the MSIAC web site. A notice was sent to the MSIAC nation representatives for distribution, as well as a large group of identified laboratories and test sites from previous survey responses. The questions deal with the test purpose, test procedure, heating rate, actual events, oven design, oven standardization, temperature preconditioning, energetics melting, reaction temperature, test item restraints, test item orientation, instrumentation, and number of tests. For each question, a breakdown of the responses is provided with additional comments.

Origin of the Answers

MSIAC has received answers from 11 nations. Within these answers, one nation acknowledged the fact that they were not performing this test. Therefore, only the 34 responses from 10 nations were taken into account for the analysis. Answers were analyzed from 7 NATO nations (Canada, France, Germany, The Netherlands, UK, Norway and the USA) and 3 partner nations (South Africa, Sweden and Finland). 62% of the answers come from governmental test centers and 38% from private test centers. It should be noted that the majority of responses represented group responses, rather than individuals.

The following chart shows the origin of the answers by nations:

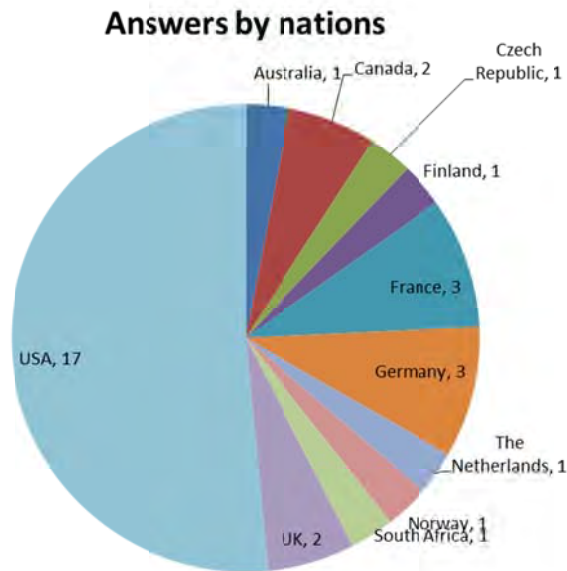


Figure 1: Number of answers received by nations

The following table presents the complete list of test centers and national authorities who replied (duplicates indicate multiple individuals from the same organization):

Table 2: List of facilities and nations who replied to the survey

Organization	Country	Status
DOS	Australia	Government
DRDC Valcartier	Canada	Government
GD-OTS Canada	Canada	Private
AC/326	Czech Republic	Government
Test Firing Center	Finland	Government
AC/326 – DGA	France	Government
NEXTER Munitions	France	Private
Airbus Safran Launchers	France	Private
WTD91	Germany	Government
MBDA Systems	Germany	Private
MBDA Systems	Germany	Private
Centre of Excellence Weapons and Ammunition	Netherlands	Government
AC/326	Norway	Government
AC/326	South Africa	Government
Bofors Test Center	Sweden	Private
QinetiQ	United Kingdom	Private
BAE Systems	United Kingdom	Private
US Army IM Board	United States of America	Government
NSWC Dahlgren D	United States of America	Government
Redstone (Army)	United States of America	Government
Eglin Air Force	United States of America	Government
Eglin Air Force	United States of America	Government
AFLCMC/EBDP	United States of America	Government
NAWC China Lake	United States of America	Government
NSWC Dahlgren D	United States of America	Government
NSWC Dahlgren D	United States of America	Government
NAWC China Lake	United States of America	Government
NAWC China Lake	United States of America	Government
DDESB	United States of America	Government
YPG ATC	United States of America	Government
NAWC China Lake	United States of America	Government
NSWC Crane	United States of America	Government
NSWC Crane	United States of America	Government
NSWC Crane	United States of America	Government

TEST PURPOSE

The survey participants were asked about the purpose of the test. They were asked if the test purpose was to provide an extreme heat rate different from the fast cook-off test, if the test purpose is to characterize the munition being tested, and/or if the test purpose is to simulate a real life accident scenario. Additionally, they were asked to comment as to the reason that the slow heating test was developed. The majority agreed with all three statements, but a larger number agreed that the test purpose was to characterize the munition being tested. Figure 2 presents circle graphs of the responses.

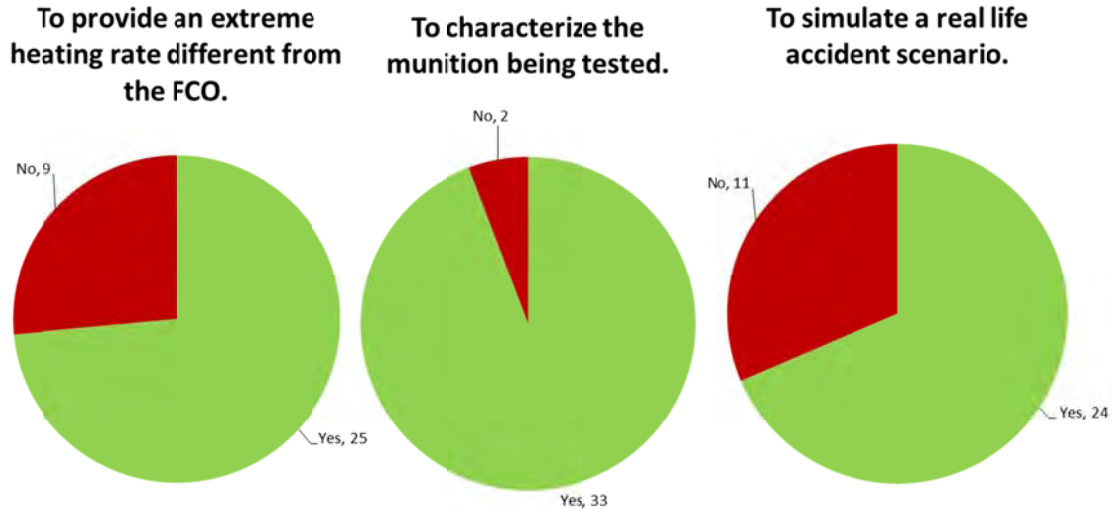


Figure 2: Test purpose responses

For What Reason Was the Slow Heating Test Developed?

A large number of comments were received. These comments were:

- The primary reason for doing any IM test is to characterize the munition – to find out what it might do in the real world and then figure out a way to minimize the impact of the reaction.
- Simulate the slow heating of a test item due to heating from an adjacent building
- It should be performed to simulate a real life accident scenario but with the heating rate now in use (3.3°C/h). I doubt that it actually does so.
- The test forms a hypothetical scenario which is worst case. Other additional more specific testing is required to relate to specific scenarios that fall between FCO and SCO. Over time, we have been able to improve the reaction of munitions to this “severe” environment. We would have never gotten to where we are today without testing to the extremes. SCO aids in down selection of design concepts or materials early on in the design process
- It may not necessarily be reality but it will be a standard comparator that can be referenced for all customers and munitions requiring testing.
- Tests performed to fulfill the customer requirements.
- To simulate a fire in a storage hold that slowly heats a nearby or adjacent storage hold, presumably on a ship, or in a depot or railcar.
- Anecdotally, it was to serve as a worse case test to simulate a series of fires occurring aboard a ship with multiple below deck magazines. I’ve seen anecdotal statements that “one US Navy ship burned for three days”, but no other rationale on how this SCO cook-off environment can exist (in its current extreme form) anywhere else.
- Originally several rates were tested providing thermal characteristics for a munition. Due to financial constraints, this slowly evolved into using only the most extreme slow rate achievable as a “bookend” to the Fuel-fire test.
- The 6°F or C/hr heating rate was intended to achieve heating in a near-isothermal condition to reduce the influence of item size, mass, and other physical features; and was based on the limitation of test equipment available in that era.
- The test already existed – it was just adapted to SCO. Prior to that it was used to test to ensure a munition didn’t auto ignite under very extreme conditions prior to a certain temperature or within a certain period of time. At that time, the reaction wasn’t

important, just the time to reaction. And, the heating rate was the slowest that could be tested at the time.

- Developed to provide a scenario in which the test item is heated at a much slower rate than in a fast cook-off test
- It has been established that in the case of fire on the ship deck, neighboring magazines can be slow heated as low as 6°F/hr.
- Historically SCO was imposed by the US in UN Manual of Tests and Criteria 2nd Edition (HD 1.6) and then introduced in the IM policy (MIL-STD 2105 and STANAG 4382).

TEST PROCEDURE

The survey participants were asked about the test procedure. They were asked if they conduct the SCO test as required by the STANAG 4382 primary test procedure, and if they have a separate nationally approved procedure. Additionally, for what reason was a specific nationally approved procedure developed. The vast majority of responders conduct SCO tests as required by the STANAG 4382 primary test procedure. Germany and France provided the designation of their nationally agreed test procedures. Additionally, the US Navy NAWCWD and the US Navy NSWC Crane divisions provided the designations of their locally agreed test procedures and reasoning for developing these locally agreed procedures. Figure 3 presents circle graphs of the responses.

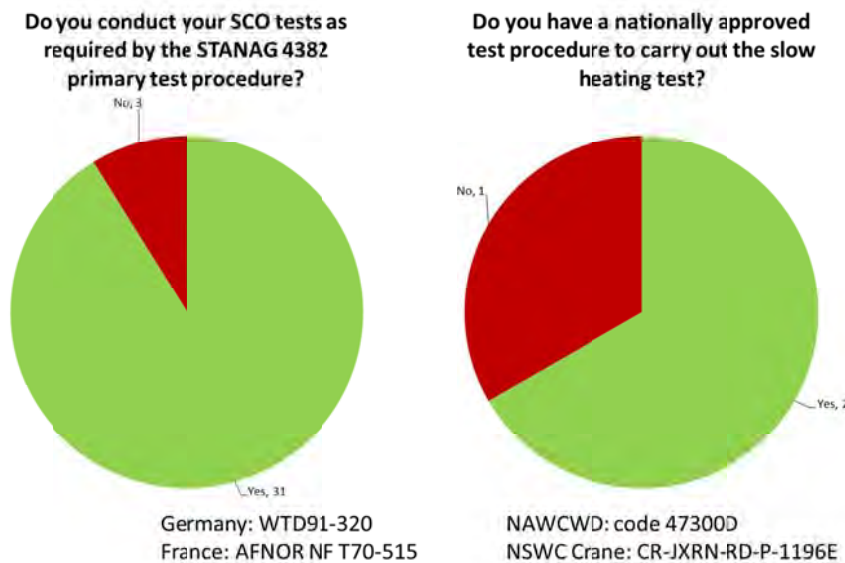


Figure 3: Test procedure responses.

Nationally Approved Specific Procedure

When asked for what reason was this nationally approved specific procedure developed, the comments received were:

- Confirm that our trials plan meet the requirement and has objective review and acceptance from all parties concerned.
- This is a procedure created to give clear concise steps to conduct a slow cook off test per latest requirements as well as other Hazard Classification Tests

Locally Approved Specific Procedure

The comments associated with local specific procedures were:

- Procedures developed to meet STANAG requirements, safety requirements (local and national), environmental requirements, and gather quality test data at a reasonable cost
- Simpler design and it is easier to control the temperature if the outside temperature is cold

Another interesting related comment was that some test areas use the test set-up defined in the former MIL-STD 2105B (12 January 1994). It is described as a very convenient and efficient definition. Figure 4 presents a diagram of the slow heating test configuration from MIL-STD 2105B.

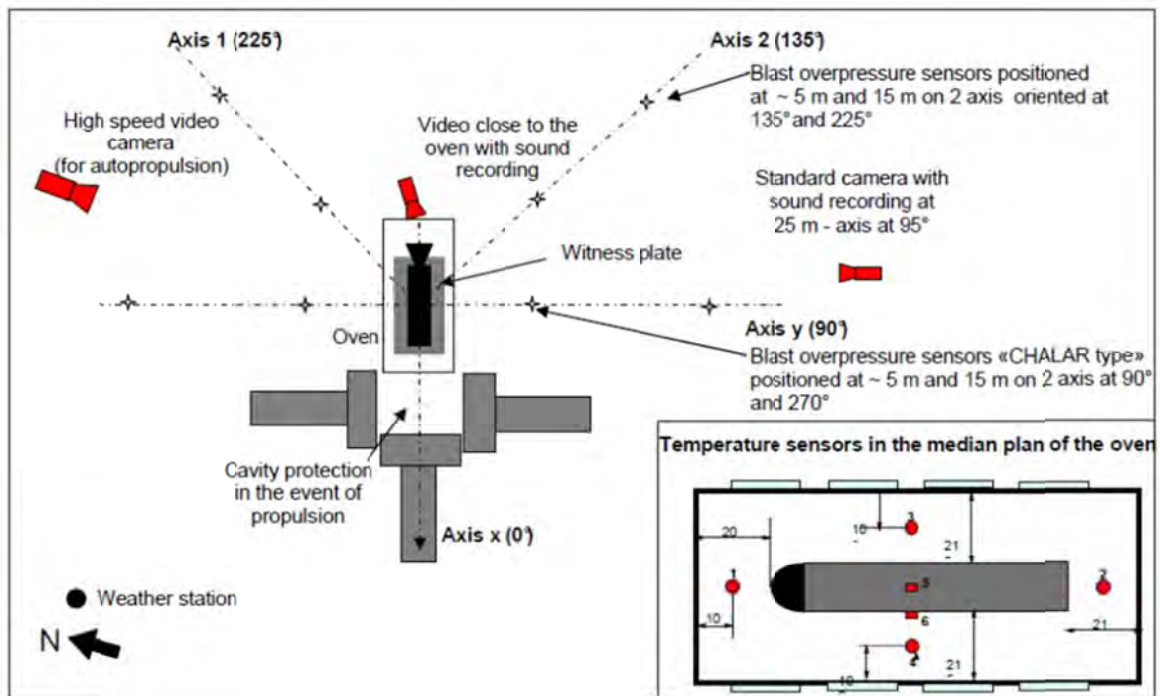


Figure 4: MIL-STD 2105B configuration of the slow heating test.

HEATING RATE

The survey participants were asked about the test heating rate. They were asked if the heating rate should be changed and if item size should be a consideration in defining a slow heating rate. Specifically, they were asked to comment on what heating rate they use, what heating rate should be used in procedure 1, why should this rate be used, should size be a consideration, and whether they had any information on duration or rates of actual real world slow heating events. About half of the responders agreed that the heating rate should be changed. However, several responders were unsure or stated that it depends on the test intent. The majority of the responders thought that item size should not be a consideration in defining the rate. Figure 5 presents circle graphs of the responses.

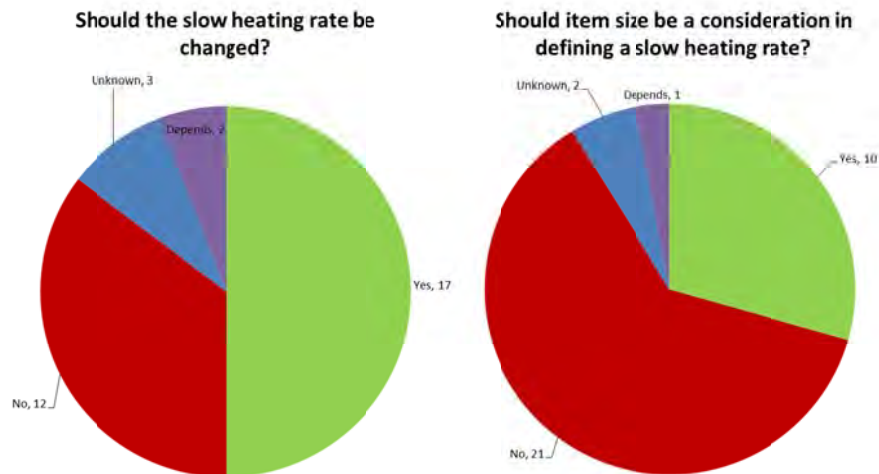


Figure 5: Heating rate responses

What Rates Are Currently Used?

The comments received were:

- Majority response: 3.3°C/hr
- Sometimes faster rates – up to 100 °F/hr – are used for evaluation of mitigation systems to ensure they will work for more than the standard rate which may or may not be real world.
- Whatever the customer wants ...but almost always 3.3°C/hr
- As requested by customers...typically 6°F/hr or 50°F/hr.
- Either 3.3°C/hr or 25°C/hr
- We use 3.3°C/hr for standard tests for qualification. For routine, we often use an intermediate rate, to allow us to run one test per day.

What Range of Rates is Accessible with your Heating Equipment?

The comments received were:

- Less than 3.3°C/hr and greater than 25°C/hr
- This is very dependent on the size of the item under test. We can test at almost any rate if the item is not extremely large.
- Nearly any rate can be programmed. Low rates are easily accommodated, but high rates are limited by the number of heating elements. At this time, an upper limit of 150 amps to the elements.

What Should be the Heating Rate be in Procedure 1?

The comments received can be divided into three responses: keep the original rate, the rate should be based on “real world data” and that the rates should be worst and the most likely.

Should keep the original rate:

- It should remain at 3.3°C/hr.

Should be based on “real world data”:

- It should be realistic to the scenario that a slow cook-off test is simulating. This should be based on real world data, past occurrences, and SME evaluations of what is and

what is not a realistic heating rate in real world incidents. A suggested heating rate with some supporting data is 45-50 degrees F per hour.

- The heating rate should be changed to a rate that is consistent with reaching cook-off temperature within a reasonable time for a fire to be extinguished. If the worst case is 24 hours, then the heating rate should be determined based on the item reaching cook-off temperature in 24 hours.

Should be worst case and most likely:

- The problem with the current rate is that we don't know if it will produce the worst reaction. No, it's not "real world". But, the real world rate for any munition will be highly dependent on the life cycle of that item. There should probably be at least two rates – a worst case rate and a most likely rate (one set by the specific program depending on the life cycle assessment).

Why This Rate?

The received comments are:

- Maintain compatibility and comparability with previous test data.
- We should be assessing for IM compliance over a range of slow rates, rather than just at a single point. Having a single point may enable developers to focus on passing just that single requirement, whereas passing over a range of rates might make them more focused on a better IM solution.
- A suggested heating rate with some supporting data is 45-50 degrees F per hour.
- With modern day fire fighting equipment aboard ships, fires should be completely extinguished in less than xx-hours. I do not know what that reasonable timeframe is but we should be able to determine it from the experts. The example I cited above was for a 24-hour fire. Using a cook-off temperature of 180-Deg C, starting at 50-Deg C, $130 \div 24$ hours equals 5.5-Deg C per hour.
- Various energetic materials will have their worst case reaction at different rates. There will not be one rate value that will invoke the worst case reaction in all or most articles or even components. Retaining rates of 3, 4, 5° C etc. will only be valuable for scientific research. A real fire will be extinguished well before any reaction occurs (and won't last for two days).

Should Size be a Consideration?

The received comments are:

- The size of the item to be tested is not foreseeable. It is as big as it is.
- The rate should be based on what can be expected in a real world application.
- It might be necessary/prudent to tailor the heating rate(s) to item size in order to assess the effectiveness of reaction mitigation features across a range of credible stressing conditions (see previous comment).
- We already have an artificial rate...don't make it worse by adjusting the rate based on size. How does that relate to anything real?
- We should remain standardized for all, rather than variable.
- Worst case should be used, whatever that rate is.

OVEN DESIGN

The survey participants were asked about test oven design information, including oven construction material and thickness, the oven heating system, the oven airflow and oven photographs. They were also asked about oven design issues that affect the testing and potential test outcome, including the item spacing to the oven wall, the observed temperature homogeneity while testing and about protection for energetic material exuded out of the item.

General Oven Design Information

Figures 6-17 present provided photographs and diagrams of various testing facility oven designs. The oven designs vary significantly and it is clear that test areas use different designs depending on the scale and type of test item. Below are the comments received on general oven design:

- Our oven designs are tailored for individual items.
- Design for oven: Square oven or cylinder oven dependent on dimension of asset being tested.
- It's an expandable design constituted of a metallic pipe surrounding the munition, this pipe being covered with an electric blanket. This set is enclosed itself in a thermal insulated box.
- We have various ovens.



Figure 6: NSWC China Lake, US Navy.



Figure 7: Qinetiq, UK.



Figure 8: Bundeswehr Technical Center for Weapons and Ammunitions, Germany.



Figure 9: Yuma Proving Grounds, US Army.



Figure 10: Explosives Centre, Finnish Defence Forces, Finland

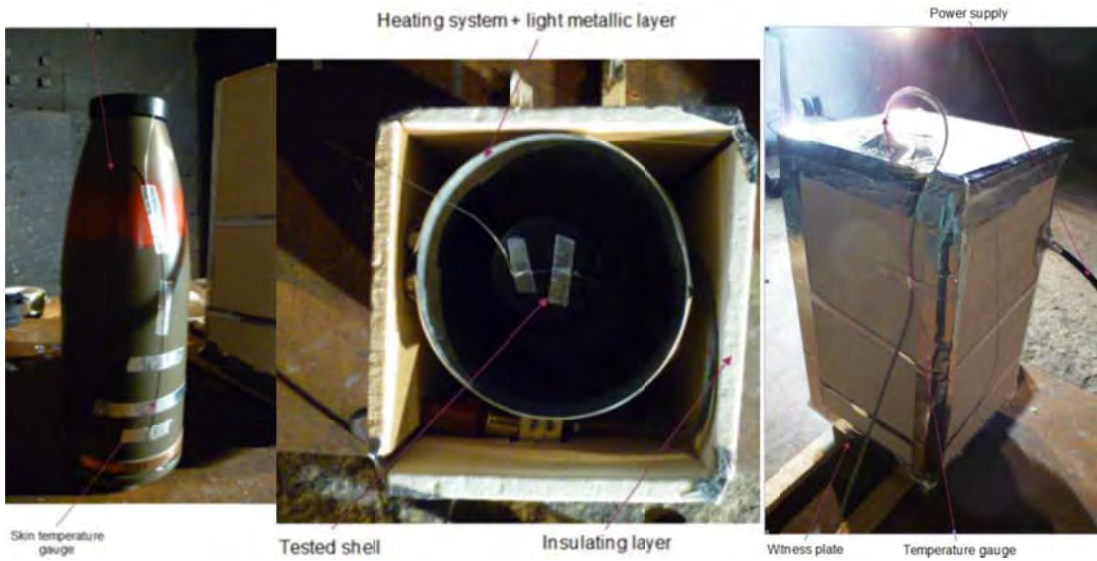
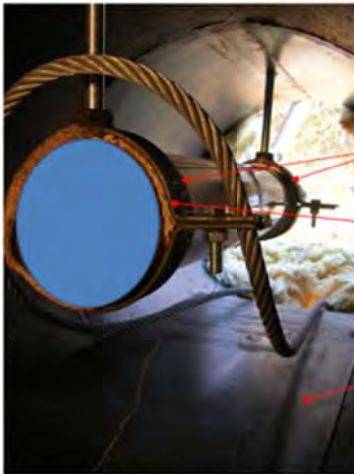


Figure 11: NEXTER Munitions, France.



Figure 12: GD-OTS, Canada.



Photograph No. 1: Motor in the oven before the test

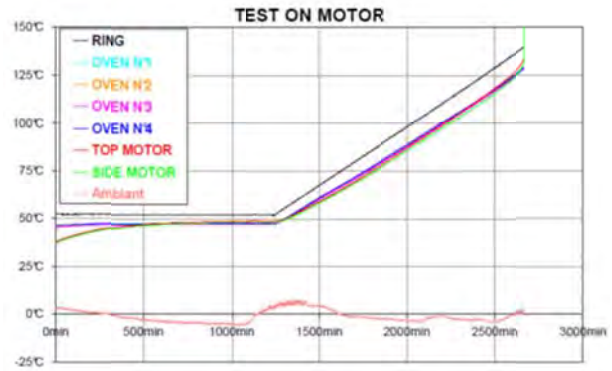


Figure 13: Airbus Safran Launchers, France.



Figure 14: BAE, UK.



Figure 15: BAE, UK.



Figure 16: MOD NLD / KCW&M, Netherlands.



Figure 17: Redstone Test Center ATEC, USA.

Oven Material and Thickness

A very large variety of materials and thicknesses are used for the oven construction. Below is a listing of the different responses:

- 16 and 18 gage steel depending on the size of the oven for structural integrity.
- 4 inch thick insulation material.
- Usually we use large air conditioning pipe/tube or “chicken wire” and frame. For insulation we use mineral wool (thickness 10-20cm), aluminium foil and tape.
- Made from 4 ft x 8 ft x 3” Home Insulation sheeting polyisocyanurate R3 assembled with aluminum tape. The oven is mounted on a steel frame/table.
- Regular steel, around 1mm thick.
- The ovens used are thin double walled aluminium designed with fibreglass or other form of insulation. These ovens are custom built for size and are all deemed as sacrificial.
- Double wall design: 1” thick, foil-faced, fiberglass duct board lined with single layer of 1” Ceramic Thermal blanket rated to 2400F. (“Soft” oven design with no hard surfaces present to interfere with potential fragment flight) for the inner box, which is covered

with an outer box made from the same duct board allowing 3 inches airspace between the inner and outer to allow for circulation.

- Standard Stone Wool inside steel grid.
- 1/16" aluminium walls with a 1" aluminium angle skeleton to produce a box which is then covered with high temperature insulation as needed and then covered by a clear tarp to protect the insulation from dew or rain.
- Double-wall construction with inner wall of 1-in thick fiberglass duct-board and outer wall of 2-in thick rigid polystyrene foam.
- Usually steel sheet, appx 1/16" (China Lake) or appr 1/8" (Eglin)
- Bespoke oven created for each individual test scenario.
- Mild steel with insulating material sandwich between inner and outer layer.
- Double-wall design (i.e. inner chamber/outer chamber). Inner chamber constructed from 1-inch thick duct board. Outer chamber constructed from 1 ½ inch thick foam insulation.
- We use reinforcement mats for the framework of the oven and 200 mm thick mineral wool for insulation. The oven is protected from wind and rain with polyethylene foil.
- Heat resistant wool. Thickness is very much dependent on the outer conditions, i.e. thicker insulation in the winter time than in the summer time.
- Oven material and thickness 1mm steel plate on light frames, rockwool insulation
- Thin steel sheet metal, see NAWCWD 473000D for detail info
- Ceramic, approx. 3 inches.

Heating Systems and Airflow

There appears to be much less variation in the heating systems, with two main approaches: internal heat source convection oven, or external heat source convection oven both using electric heating elements. Almost all responses indicated that they used forced airflow in order to try and achieve temperature homogeneity. So the primary difference between the two heating systems approaches is the location of the heat source: internal for convection ovens and external for heat source convection ovens which employ a pipe to transfer the heat...are that for the internal heat source convection ovens, the electric heating elements are within the oven, and for the external heat source convection oven, the electric heating elements are in a separate unit from the oven and heated air is piped into the oven.

Below are some associated comments from the survey:

- Heating system is like large "fan-oven".
- Convection oven heated by four 120 Volt, 500W strip heaters protected by thin aluminium witness plates. The heaters may be reusable from test to test.
- Electrical resistances.
- One or more heating elements off the ground and away from the item under test within the oven system and fan assisted for air circulation.
- (4) 500 Watt heating elements.
- Hielkema Air Heaters.
- Typically 3 each tubular heaters controlled by a Watlow control device that regulates the time that the heaters receive voltage, thereby, providing heat to the box.

Wall Distance

All survey responders indicated that they maintained the distance between the test item and the oven wall to be >200mm per the STANAG requirement.

Temperature homogeneity

The STANAG lists a requirement for temperature homogeneity to be within 5°C. Most respondents indicated that this requirement was not difficult to meet, except for large test items.

Associated comments are:

- When testing new items, dry run with inert dummy is always performed to ensure a valid test.
- Temperature homogeneity has almost always been kept below 5°C. On very rare occasions, this tolerance has been exceeded.
- Typically we can meet the required homogeneity. However, we have had problems with relatively large, elongated items (e.g., large surface-launched rocket motors).
- Usually 4-7°C. If insulation is not done well, it can be 10°C or more.
- Usually less than 5°C but with strip heaters the oven wall, especially on the bottom can be at least 30°C hotter.
- Why should there be uniform temperature? Based on what real world rationale?

Protection for Exuded Energetic Materials

The survey asked if any protection was used to prevent exuded energetic material being prematurely ignited on contacting the oven wall. . About 40% of the respondents indicated that they did use some protection, as seen in Figure 18.

Associated comments were:

- A “drip tray” is located below the test item to avoid energetic material dropping onto the heating element.
- We have a tray added to the inside of the oven so fill that exudes out of the case can be insulated from the hotter oven wall.
- Depends on the test item, in some occasions, “trays” are added to prevent melted EM to have contact with oven walls
- We put thermally insulated receptacle below tested munition. In the aim to avoid a prompt ignition when energetic material fall on the oven wall.
- Our ovens are built of heat resistant wool which is insulating and do not act like a hot surface. We try also to insulate the fixtures in the ovens which hold the test item
- I understand why the concern exists about exuded material: it makes the test look bad. As we don't have a valid rationale for the test, how do you make the assumption that you won't have hot spots on the floor? What if the fire is in the portion of the ship right under the weapon? Then the floor will be the hottest part.
- We consider the pyrolysis gases as having more influence on premature ignitions.

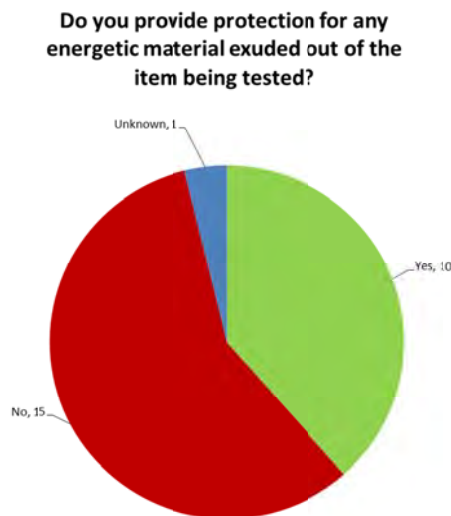


Figure 18: Protection from exuded energetic material.

OVEN DESIGN ISSUES

The survey asked that any issues with the oven designs be raised. The primary topics discussed by the respondents were that the oven should be: 1) very well Thermally insulated and 2) designed so as not to significantly confine the reaction, fragmentation or blast.

Thermal issues

Comments associated with thermal insulation are:

- Forced air flow ovens have resulted in varying responses from the same munition. It is believed the air inlet is creating localized hotspots.
- The convective oven wall is much hotter than the oven air so when fill contacts it ignites. This not only causes a slightly earlier reaction but ignites the remaining fill in the case in a location that may not be realistic.
- We use heat resistant wool as construction material and place most metal parts (heating elements, fans etc.) beneath the test item.
- The ultimate SCO oven material would be a heat resistant, light colored (better "in oven camera" coverage) affordable, light weight / density and environmental friendly plate.
- Air flow in our test set up does not have high velocity. On my opinion that does not have significant influence to test item and test result.
- Several different cameras that look through a window in the oven and the most difficult problem is determining how to keep the camera cool to keep the internal view camera alive. I have had successes and failures, but I haven't found the perfect answer for that yet.

Confinement and Fragment Flight Issues

Comments associated with confinement and fragment flight are:

- Heavy wall construction can influence the flight of fragments.
- I feel that the greatest issue is ensuring that the design of the oven truly provides the minimum confinement that can be achieved practically, in order to minimize suppressive effects on the ejection of debris and attenuation/focusing of blast
- Oven walls should be constructed of foam/fiber panels with minimal structural integrity to lessen their effect of slowing fragment projections
- Even if the confinement exacerbates oven throw distance we do not believe it throws test item parts farther.
- Confinement will always be an issue, but items can be compared using the same test setup and a "calibration" shot can be used to measure/determine the full detonation properties of the test item.
- Oven design should have minimal effect on the projection of fragments from the oven.

OVEN STANDARDIZATION

The survey asked whether the oven design should be standardized. The results split fairly evenly as seen in Figure 19. The problem with standardizing the design is that different munition types require different considerations. Differing sizes of munitions required different sized ovens. Rocket motors will need to be restrained to prevent flight in case of a strong propulsive reaction. Also, munitions tested inside a shipping container or canister can affect the oven design. One thing to consider is the use of the oven itself as a surrogate shipping container or canister. This could avoid duplicate confinement. Another point to discuss will be the consideration of the effect of heating bands on the reaction if material is extruded out of the test item. Heating bands create localised hot surfaces which are eliminated if forced air is used. So, guidance could be provided to use forced air if energetic extrusion is anticipated. External conditions affect the design as well: if it's very cold outside additional insulation will be needed. Recommendations could be

developed for oven design to limit masking of primary blast and fragment effects whilst limiting the potential of secondary fragmentation.

TEMPERATURE PRECONDITIONING

The survey participants were asked about temperature preconditioning. The STANAG states that prior to commencement of the heating condition (rate), the test item should be preconditioned at 50°C for 8 hours or until the test item reaches thermal equilibrium at 50°C, whichever occurs first. The survey asked if they did precondition per the STANAG, whether a melt cast energetic should be pre-soaked differently and should the preconditioning requirement be changed.

Preconditioning Responses

As seen in Figure 19, almost all responded that they precondition per the STANAG. About half of the respondents thought that melt cast energetic should be pre-soaked identically to non-melt materials, whereas about 1/4 of respondents thought that they should be pre-soaked differently. About 1/3 of respondents thought that the requirement should be changed and about 1/3 of respondents thought that it should remain the same.

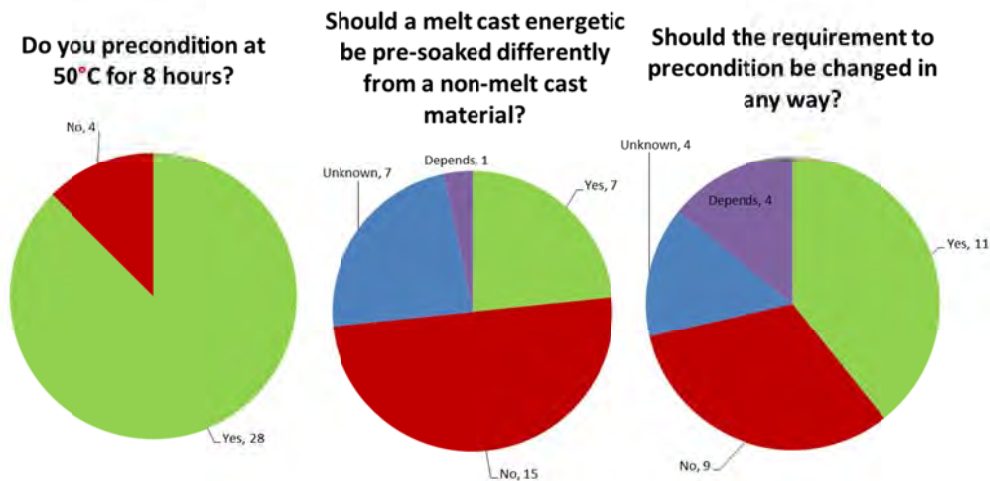


Figure 19: Temperature preconditioning.

Should a Melt Cast Energetic be Pre-soaked Differently?

Comments associated with pre-soaking melt cast energetic are:

- It is useful to have the same starting temperature for all f munition types. Especially as we are performing the tests in autumn and winter times and the munition cools down before the test starts.
- I don't see any reason to. During firing tests we would also condition these energetics to 120°F (~50° C) before firing.
- If the soaking temperature is much lower than the typical melt temperature (i.e. around 80°C for the TNT which is the lowest of the melting explosive used) as it is the case now, the soaking should be the same.
- If the test is to be used as characterization test, the material should be soaked just above the melting point until all material has melted.
- If it is intended to be used a real-life surrogate, then all pre-soaks are no longer needed.

Should the Requirement to Precondition be Changed?

Comments associated with potentially changing preconditioning are:

- Some guidance should be provided on the minimum time to precondition. Smaller items may reach thermal equilibrium in 8 hours but larger items definitely will not. I think the STANAG should provide a guide for pre-conditioning time based on item size (diameter, weight, amount of container/item insulation).
- The only reason I can see for it is if it affects the onset of self-heating and if self-heating is a driver of the reaction severity.
- Consider making it even higher if that can be shown to not change results.
- We do not see the need to change this. Preconditioning should be performed to ensure that initial temperatures are identical from test to test, regardless of the ambient air and oven walls temperature. The preconditioning temperature should however be much lower than the temperature at which degradation begins in the energetic materials or other materials.
- I'm not aware of the history of why 50°C was chosen as the soak temperature.
- I would consider establishing and documenting the need for preconditioning at 50 deg. What is gained by doing this? Why 50 degrees? What does it represent in the munitions life cycle or threat profile? How does a potential thermal threat scenario map to this requirement?
- I think that one should take a look at the entire heating rate profile so that it would better fit one of the most common accident scenarios.

MELTING

The survey participants were asked whether melting of energetics during a test should affect the testing requirement. As seen in Figure 20, about 75% of respondents think that melting of energetics during a test should not affect the requirement.

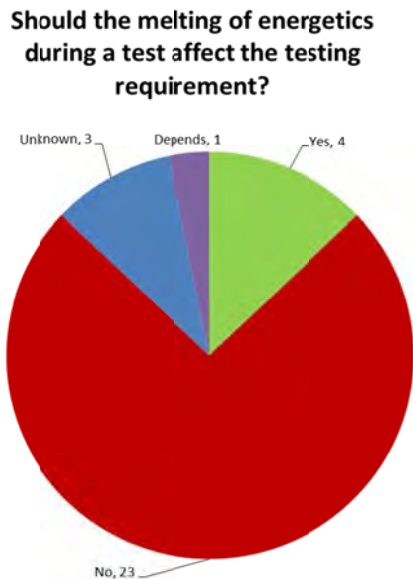


Figure 20: Melting energetics.

PROPULSION

As seen Figure 21, almost half of the respondents stated that they do not restrain items to prevent propulsion. More than half said that they do restrain potentially propulsive items if they believe that they pose some safety risk. Many of the described restraint methods allow some

item movement, providing the testing facility has some information on propulsive potential of the item.

Some of the received comments are:

- Test item is normally strapped to the test stand with steel banding.
- The motor is placed in relatively open but strong steel cage to prevent the motor from flying away during reaction due to the onset of thrust – this is a general requirement of the test site.
- Mostly by using vertical orientation when testing rocket motor or propulsive items.
- System dependent, range safety dependent. Tethering, catch boxes, barrier walls, thrust cells, are used as needed
- We only restrain items in instances where propulsion of the case might present a range-safety hazard. Typically this is uniquely associated with items that have live rocket motors.
- In spite of a nearest neighbor at 20 miles, we must be prepared for a propulsive event that takes ordnance off the station boundaries.
- We normally always allow propulsion in IM tests. We handle that with our risk areas.

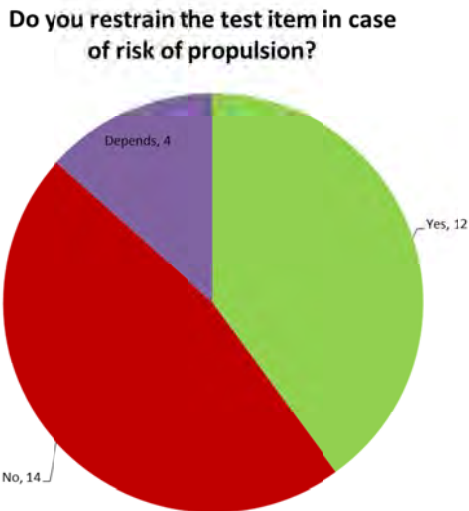


Figure 21: Item restraint from propulsion.

ITEM ORIENTATION

When asked about item orientation during testing, the majority stated that the test orientation is usually representative of the orientation during most or all of the item logistics life-cycle. Often, this is the horizontal orientation, which can facilitate the assessment of the debris hazard posed by end caps, plugs, etc. that might be ejected from the test item. Vertical orientation can impede the ejection of these pieces of debris by directing downward into the oven floor or directing them straight up, which can result in a misleadingly short apparent ejection range. The latter can pose problems evaluating the results if video coverage is poor; or the reaction occurs at night-time.

INSTRUMENTATION

The survey requested information on instrumentation used for the slow heating testing. The responses were very similar from all of the respondents in terms of the instrumentation that was normally used: digital data acquisition recorders, video coverage, microphones, witness plates, pressure gauges and thermocouples. Typically type K thermocouples are used for temperature measurement and piezoelectric pressure gauges for blast overpressure measurement. One test facility listed bikini pressure gauges for blast measurement.

Number of Thermocouples

The STANAG is somewhat inconsistent in that it states “A minimum of four thermocouples should be used to be sure that the oven is uniformly heated and to monitor the surface temperature of the test item.”, but goes on to state “In general, there should be at least two thermocouples mounted on opposite surfaces of the test item, one each in the air space near the air inlet and exit, and one each in the air space on opposite sides of the round (see Figure 1).”, implying at least 6 thermocouples should be used. The number of thermocouples used by test facilities appears to vary greatly from 4 to 100.

Below are some of the responses:

- 4 as per the STANAG.
- 6 (minimum) installed in accordance with the STANAG to assess compliance with the heating conditions and provide an indication of reaction of the test item.
- Between 8 – 16: near the oven wall, near the item, and when possible inside the item (charging tubes).
- Typically fifteen. This includes the typical air temp at various points near the item, oven wall temp, skin temp in several locations including just outside the oven wall, and one or two internal to the item to detect self heating.
- Ten to thirty thermocouples are typical. Some dictating factors include, size of the oven (ensure temperature homogeneity), specific test information about a location, efficiency of heat transfer, STANAG requirement, engineering considerations, etc. We are equipped to use as many as 100 thermocouples.

VISUALIZATION ISSUES

A number of respondents described visualization issues:

- Occasionally an internal camera will fail or be obscured by fill exudate prior to initiation. This will compromise diagnostics.
- A minimum of four cameras are used. Two are fielded to view the test store inside the oven and two are deployed to view the outside of the oven.
- We use two cameras outside and one camera inside the oven to record the reaction of the munition.
- Cameras are used external to the event. Disposable internal cameras are often used, as many as four in a single test.
- We have a camera outside oven, shooting through window to inside oven, to the test item. It has been very useful and has given information during test and just before reaction.
- The window allows the ability to confirm reaction of the item but our current set-up does not allow for visualization of the test item reaction, since we prefer using a general surveillance camera. A system using bigger window, mirrors, and high speed camera is possible. Trigger is an issue with some instruments, although we used bridge-wire to acquire data (ex.: pressure) at a higher speed rate during reaction.

SUMMARY OF RECOMMENDATIONS

This is a summary of the recommendations, the explanations have been provided in the core of this document:

- Develop a group consensus as to the intent of the test and document it.
- Query all of the MSIAC nations to provide information on actual event durations and rates.
- Based on consensus test intent and supporting data, develop a consensus as to changing rate or leaving the rate unchanged.
- Clarify the minimum number of required thermocouples and thermocouple positioning.

- Observations of events inside the oven.
- Develop and provide a best practice oven design examples for different types and scales of test items.
- Characterize the heating equipment and perform calibration testing.
- Provide a best practices example test configuration.
- Remove redundancies or contradictions and clarify where the information should sit between the STANAG 4382 and the AOP-39 (AC/326 SG/B has already begun this process).

ACTUAL EVENTS HEATING RATES

There were 32 responses that the individuals had no information on the duration or rates of actual slow heating incidents. As a result, during the NATO AC/326 SG10-11 April 2017 /B Slow Heating Custodial Working Group (SH CWG) meeting, MSIAC was requested to conduct a review of actual event heating rates and durations and share any available historical information from the MSIAC safety database regarding real-life slow heating events and potential thermal threats. A search of the MSIAC MAD-X accident database provided no applicable information. A report search resulted in a large number of references [5-32], including the previous 2003 MSIAC report “Assessing Thermal Threats” [33] that was published in 2003. The review results provided many examples of fire durations and very few actual temperature rate measurements. As a result, fire modelling results of actual events are required in order to estimate credible actual or minimum heating rates. The vast majority of fire events are complete within a day. Some events have occurred over multiple days, but it needs to be recognized that these events are all multiple day fires that have occurred sequentially. The individual fire events associated with these multiple day fires appear to be complete in much shorter times. The summary inferred actual fire events temperature rise rates remains the same as that assessed in the 2003 MSIAC report [33]. A summary of this assessment is presented in figure 22. This review, and the previous assessment conclude that actual credible adjacent compartment fires could produce rates as low as 25°C/hr. Lower rates appear very difficult to justify based on actual fire events and associated thermal modelling. Dr. David Hubble from NSWCCD, USA recently completed a similar study, which included supporting fire modelling [34]. The results and conclusions appear to be very similar.

Heating Source	<ul style="list-style-type: none"> • Torching • EM Burning • Exhausts • Pyrotechnics 	<ul style="list-style-type: none"> • Fuel Fire • Wood fire • Propane burner • Building Fire 	<ul style="list-style-type: none"> • Hot Breach • Gun Battlecarry • Launcher • Nuclear plant • Aircraft debris • Remote fire • Aerodynamic Heating • Adjacent compartment fire 	<ul style="list-style-type: none"> • Solar Heating • Steam leak
Regime	Fast Cookoff (FCO)		Intermediate Cookoff (ICO)	Slow Cookoff (SCO)
Temperatures (Order of magnitude)	1000 to 2000 °C	~1000 °C	100 to 300 °C	~ 100 °C
Heating rates (Order of magnitude)	50 to 100 °C/sec	1 to 20 °C/sec	25°C/hr to 50 °C/min	< 20 °C/hr

Figure 22: Thermal threat categorization.

CONCLUSIONS

This study and the associated historical events assessment was an efficient way to identify recommendations to further improve the STANAG 4382. These recommendations are being

discussed with AC/326 SG/B who has already chartered a working group to review and update the STANAG. The working group has already reviewed the survey results. According to the new requirements in the NATO documentation, the technical content of the STANAG will be migrated into an AOP.

ACKNOWLEDGEMENT

MSIAC would like to acknowledge the custodian of the STANAG, USA, and particularly Dr. Stephen Struck for his review and amendment of the survey. MSIAC also acknowledge the individuals from all the nations who have contributed to the survey by providing an answer to the questionnaire or information related to this test.

REFERENCES

1. STANAG 4439, edition 3: Policy for introduction and assessment of Insensitive Munitions.
2. STANAG 4382, edition 2: Slow heating, munitions test procedures.
3. AOP 39, edition 3: Guidance on the assessment and development of Insensitive Munitions.
4. UN, Recommendations on the transport of dangerous goods, Manual of tests and criteria, sixth revised edition, 2015.
5. Back, G., R. Darwin, J. Scheffey, "Propellant fires in a simulated shipboard compartment: Project HULVUL Phase III, Naval Research Laboratory NRL/MIU6180 --99-8394, 1999.
6. Boggs, T., K.P. Ford, J. Covino; "Realistic Safe-Separation Distance Determination for Mass Fire Hazards", NAWCWD TM 8668, March 2013.
7. Booz-Allen & Hamilton, Inc.; Threat Hazard Analysis prepared for Program Executive Office for Theater Air Defense, 26 November, 1996.
8. Budnick, E., D. Evans, H. Nelson, "Simplified fire growth calculations", SFPE Handbook of Fire Protection Engineering, Section 11, Chapter 10, 1997.
9. Bukowski, R., "Fire Hazard Assessment", SFPE Handbook of Fire Protection Engineering, Section 11, Chapter 7, 1997.
10. Doolan, C.; "Ordnance Heating Rates in Shipboard Magazines", DSTO-TR-1188, July 2001.
11. Fontenot, J. and M. Jacobson; "Analysis of Heating Rates for the Insensitive Munitions Slow Cookoff Test", NWC TM 6278 (1988).
12. Fournier, A., C. Lallemand, "Phénomènes thermiques induits par un accident de munition à bord d'un navire", AGARD-CP-511, paper 22, 1992.
13. Frey, R.; "Appropriate Slow Cookoff Heating Rates" Army Research Laboratory, 18 April 2000.
14. Guinn, W.R., "A study of heat transfer in liquid pool fires from steady burning through boilover", Paper for Fire Protection Engineering -520.
15. Kennett, S., G. Gamble, J. De Li, "Modelling of the HMAS Westralia fire", DSTO -TR-0698, 1998.
16. Heimdahl, O., L. Bowman, "Standoff distance effect on cookoff of ordnance stowed in MDCS ship cargo holds", Twenty-ninth DoD Explosives Safety Seminar, 2000.
17. Leblanc, D., "Fire environments typical of Navy ships", Thesis, submitted to the Faculty of the Worcester Polytechnic Institute in partial fulfillment of the requirements for the Degree of Master of Science in Fire Protection Engineering, 1998.
18. King, B., "Unplanned Explosions at Munitions Sites", Small Arms Survey Organization (<http://www.smallarmssurvey.org>), 2016.
19. Lundstrom, E., "Slow cookoff analysis", Proceedings of the NIMIC 1993 Workshop on Cookoff, paper TP-7, 1993.
20. Mansfield, J., "Preliminary Analysis of the Heating of Ordnance in Ship Magazines Due to a Fire in an Adjacent Compartment", NAWCWPNS TP 8186 (1996).
21. Madrzykowski, D., R. Vettori, "Simulation of the dynamics of the fire at 3146 Cherry Road NE, Washington D.C., May 30, 1999", Buildings and Fire Research Laboratory, National Institute of Standards and Technology, NISTIR 6510 (2000).

22. Null, G., "Computer simulation of the thermal effects on a concentric canister missile launcher with a fire in an adjacent compartment", Naval Postgraduate School Thesis, ADA337018, 1997.
23. Pitts, W., "Improved real-scale fire measurements having meaningful uncertainty limits", W. Pitts, Workshop on Fire: Testing measurement needs: Proceedings, W. Grosshandler, Building and Fire Research Laboratory, 2001.
24. Stokes B.B., Fitzgerald-Smith J. DeFourneaux M., Kernen P., "Summary of NIMIC 1993 Workshop on Cookoff", NIMIC-BS-307-94, 1994.
25. Taylor, T.N., "Ammunition Accident at the Evangelos Florakis Naval Base, Zygi, Cyprus 11 July 2011", MSIAC Report O-150 Rev. 1, September 2014.
26. Victor, A., "Threat Hazard Assessment for Insensitive Munitions", Presented at NIMIC Hazards Analysis Workshop, 1996.
27. Victor, A., "Exploring cookoff mysteries", JANNAF Propulsion Systems Hazards Subcommittee meeting, 1994.
28. Wallace, I., "Cookoff – a UK naval perspective", Proceedings of the NIMIC 1993 Workshop on Cookoff, paper TP-5, 1993.
29. Wharton, R., J. Harding, A. Barratt, R. Merrifield, "Measurement of the size, duration and thermal output of fireballs produced by a range of pyrotechnics", 21st international pyrotechnics seminar, pp.916-931, 1995.
30. Wilkinson, A., "Ammunition Depot Explosions", SAS Conventional Ammunition in Surplus Book 15 Chapter 13.
31. "Recent Explosive Events in Ammunition Storage Areas," South Eastern and Eastern Europe Clearinghouse for the Control of Small Arms and Light Weapons (<http://www.seesac.org>), 2007.
32. "Dangerous Depots: The Growing Humanitarian Problem Posed by Aging and Poorly Maintained Munitions Storage Sites Factsheets", Fact Sheet produced by the U.S. Department of State's Bureau of Political-Military Affairs, 2010.
33. Peugeot, F., "Assessing Thermal Threats" MSIAC Technical Report L-097 published in 2003.
34. Hubble, D., "An Investigation into a Proper Heating Rate for Slow Cook-off Testing", Insensitive Munitions & Energetic Materials Technology Symposium, Portland, OR, 2018.

- Background
- Process / Questionnaire
- Analysis
- Test Setup Photos
- Historical Events Review

- In 2015, MSIAC initiated a survey of STANAG 4240 (Fast Cook-off Test) that led to a list of recommendations to update the document.
- NATO AC/326 SG/B has tasked MSIAC to initiate the same type of survey for STANAG 4382 (Slow Heating Test).
- MSIAC was subsequently tasked to review actual events heating rates and durations.

Baker, E.L., "An International Review of the Slow Heating Test",
MSIAC Report O-177, June 2017

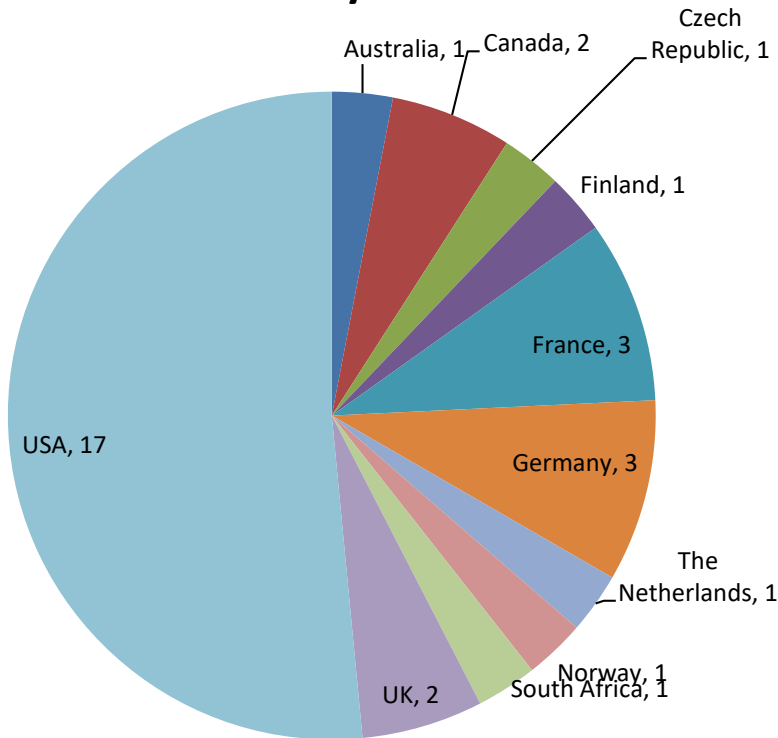
Determine the reaction of munitions to the slow application of heat which is in contrast to that occurring during fast cookoff tests. Although not necessarily intended as such, this slow heating may result from indirect exposure to fire.



- MSIAC has written a survey related to the Slow Cook-off Test
- The survey was reviewed by the custodian of STANAG 4382 (USA)
- The survey was sent to the nations
- After reception & analysis of the answers and other related documents, MSIAC is summarizing the results in a report.

- 34 responses from 11 nations.
- 62/38 government / private

Answers by nations

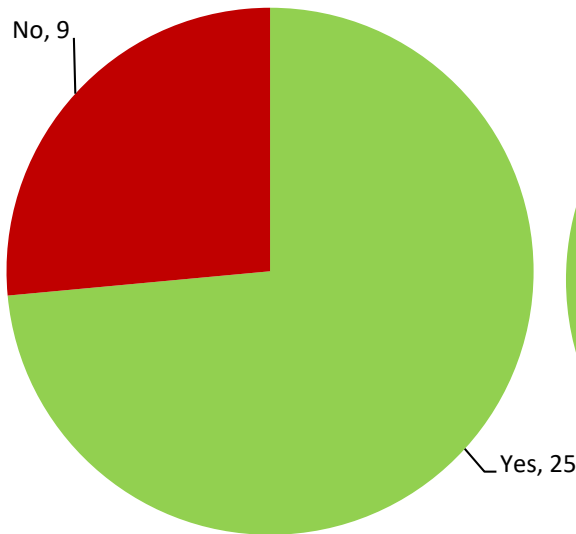


THANK YOU

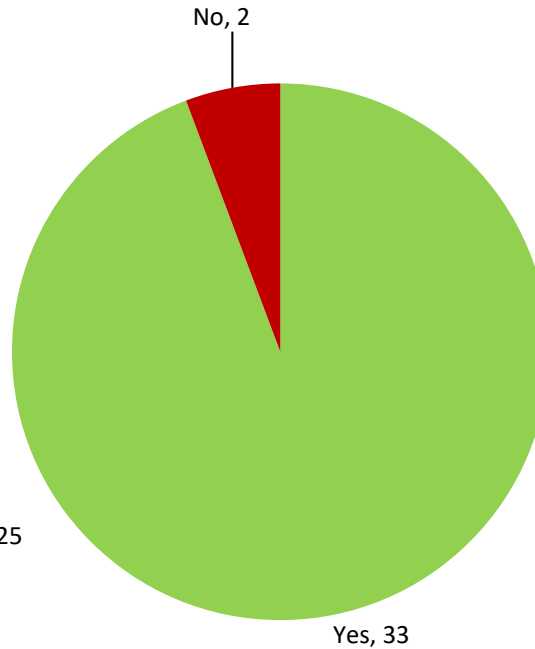
for the number and the quality of your answers

Country	Organisation	Status
DOS	Australia	gov
DRDC Valcartier	Canada	gov
GD-OTS Canada	Canada	private
AC/326	Czech Republic	gov
Test Firing Center	Finland	gov
AC/326 - DGA	France	gov
NEXTER Munitions	France	private
Airbus Safran Launchers	France	private
WTD91	Germany	gov
MBDA Systems	Germany	private
MBDA Systems	Germany	private
Centre of Excellence Weapons and Ammunition	Netherlands	gov
AC/326	Norway	gov
AC/326	South Africa	gov
Bofors Test Center	Sweden	private
QinetiQ	United Kingdom	private
BAE Systems	United Kingdom	private
US Army AIMB	United States of America	gov
NSWC Dahlgren D	United States of America	gov
Redstone (Army)	United States of America	gov
Eglin Air Force	United States of America	gov
Eglin Air Force	United States of America	gov
AFLCMC/EBDP	United States of America	gov
NAWC China Lake	United States of America	gov
NSWC Dahlgren D	United States of America	gov
NSWC Dahlgren D	United States of America	gov
NSWC Dahlgren D	United States of America	gov
NAWC China Lake	United States of America	gov
NAWC China Lake	United States of America	gov
DDESB	United States of America	gov
YPG ATC	United States of America	gov
NAWC China Lake	United States of America	gov
NSWC Crane	United States of America	gov
NSWC Crane	United States of America	gov
NSWC Crane	United States of America	gov

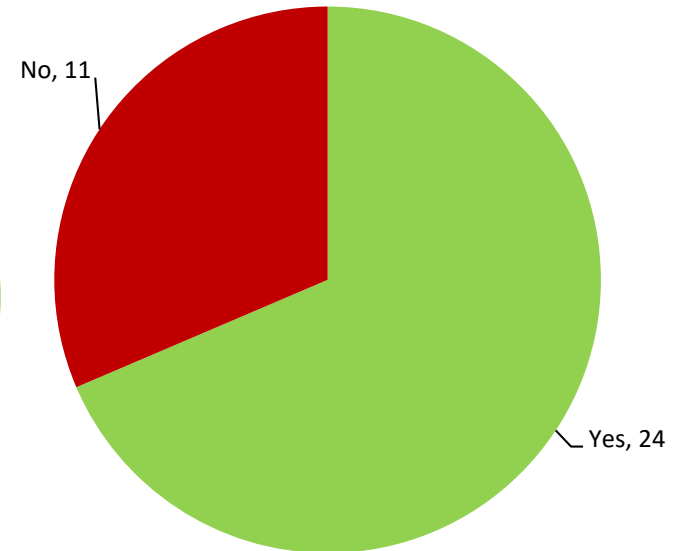
To provide an extreme heating rate different from the FCO.



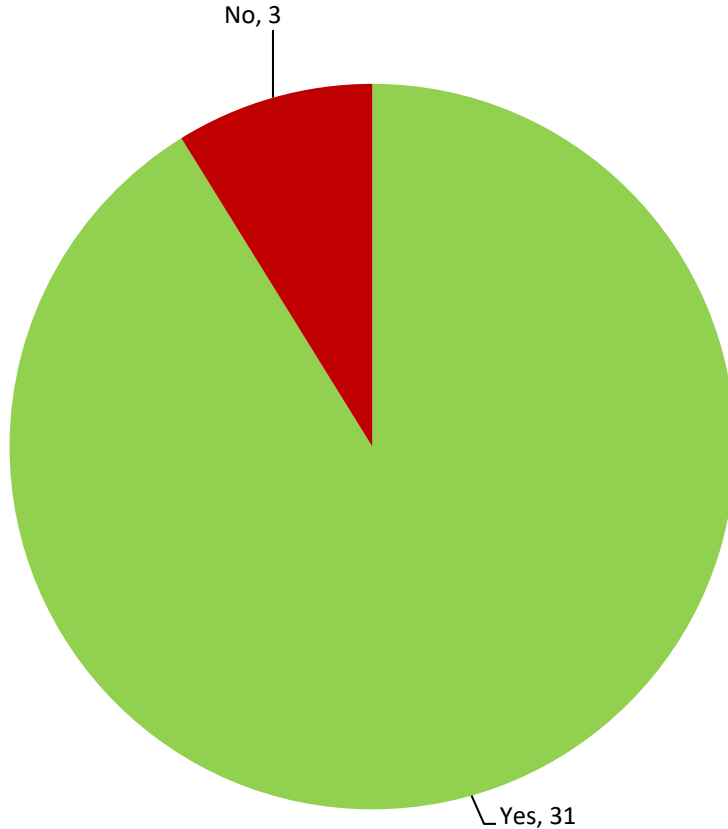
To characterize the munition being tested.



To simulate a real life accident scenario.

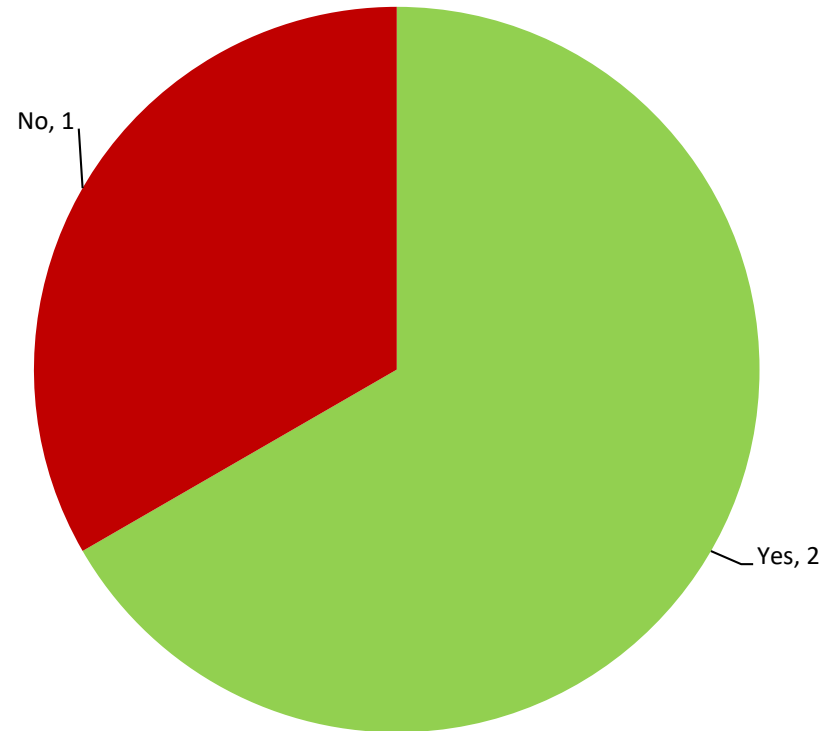


Do you conduct your SCO tests as required by the STANAG 4382 primary test procedure?



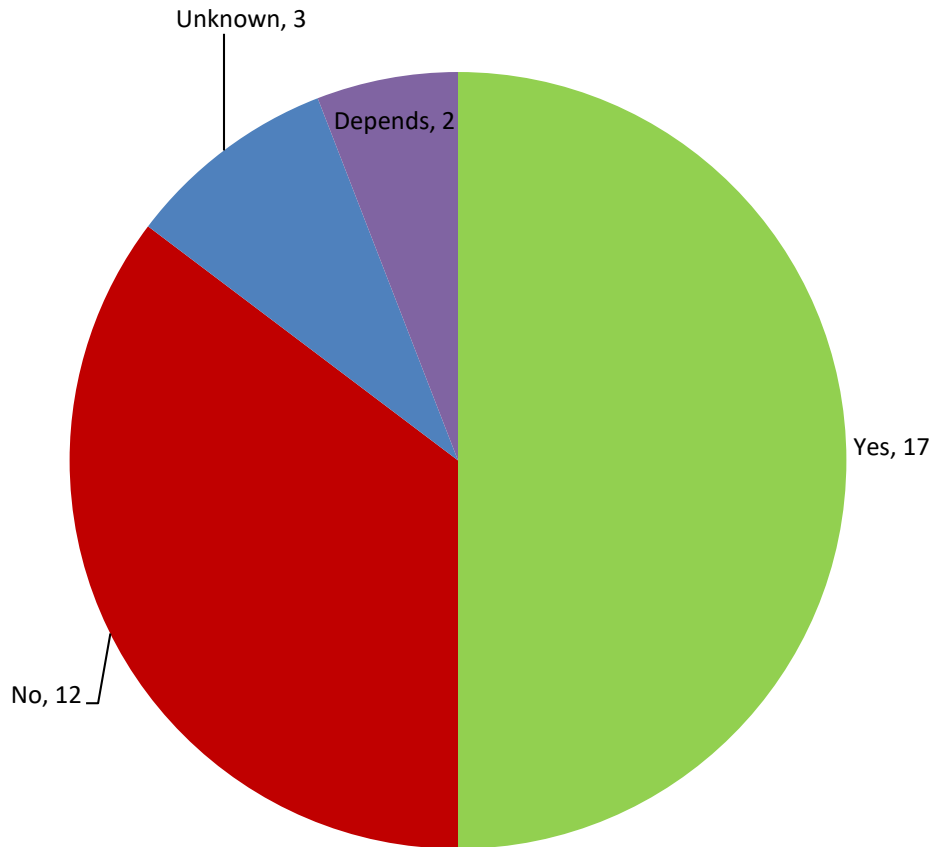
Germany: WTD91-320
France: AFNOR NF T70-515

Do you have a nationally approved test procedure to carry out the slow heating test?

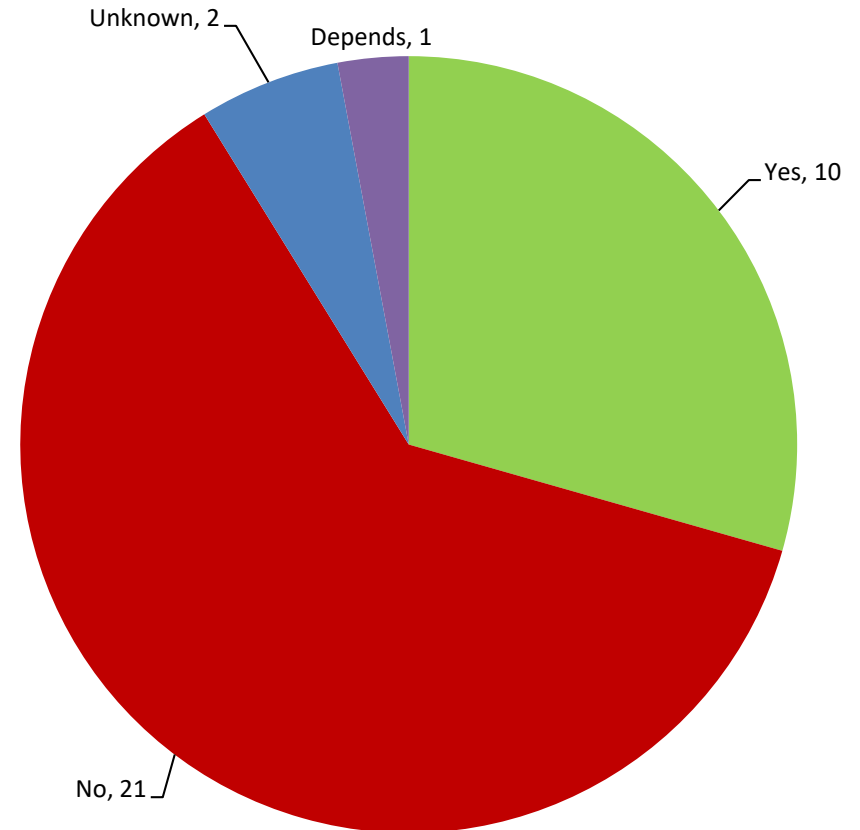


NAWCWD: code 47300D
NSWC Crane: CR-JXRN-RD-P-1196E

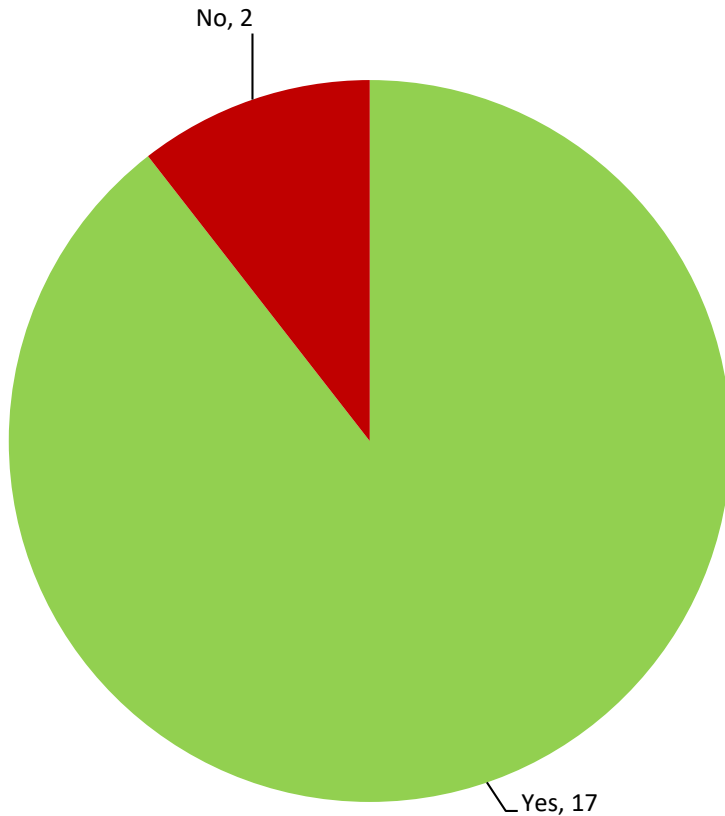
Should the slow heating rate be changed?



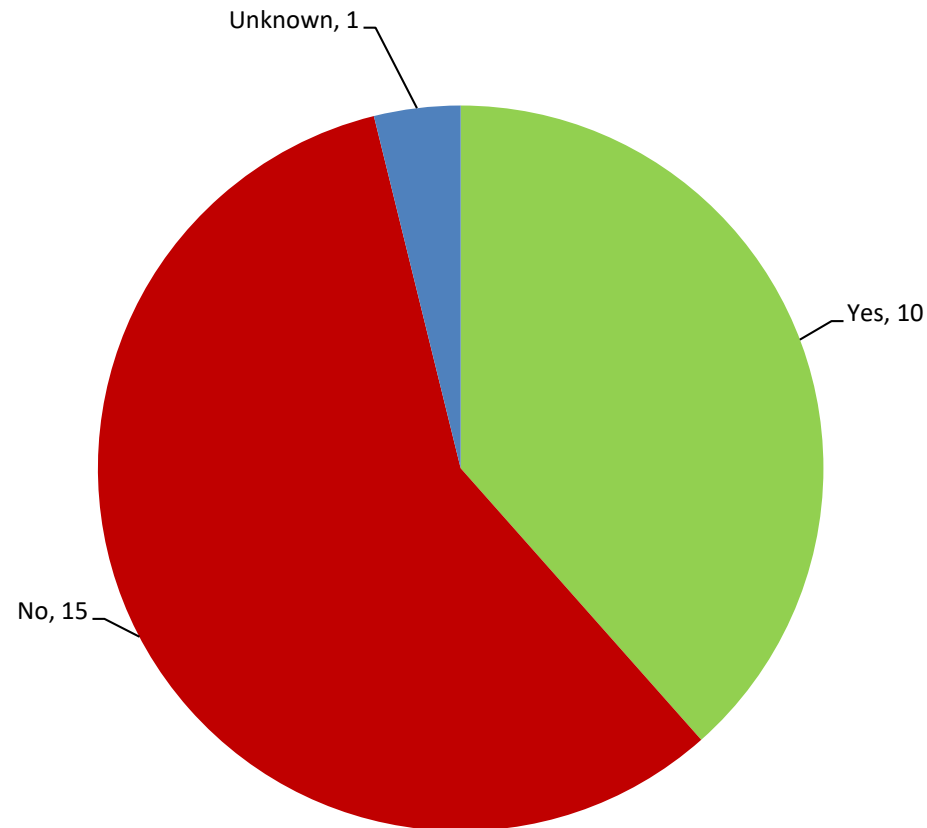
Should item size be a consideration in defining a slow heating rate?



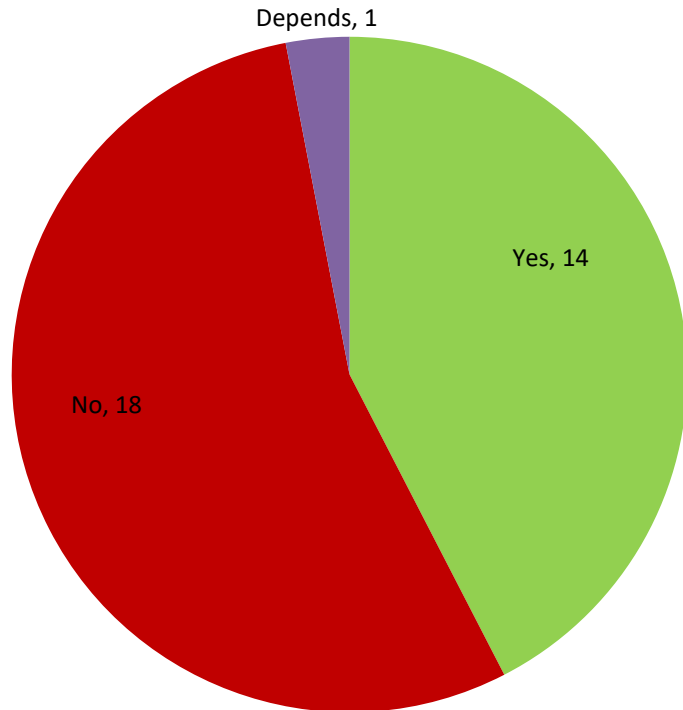
Do you have equipment to force the airflow?



Do you provide protection for any energetic material exuded out of the item being tested?

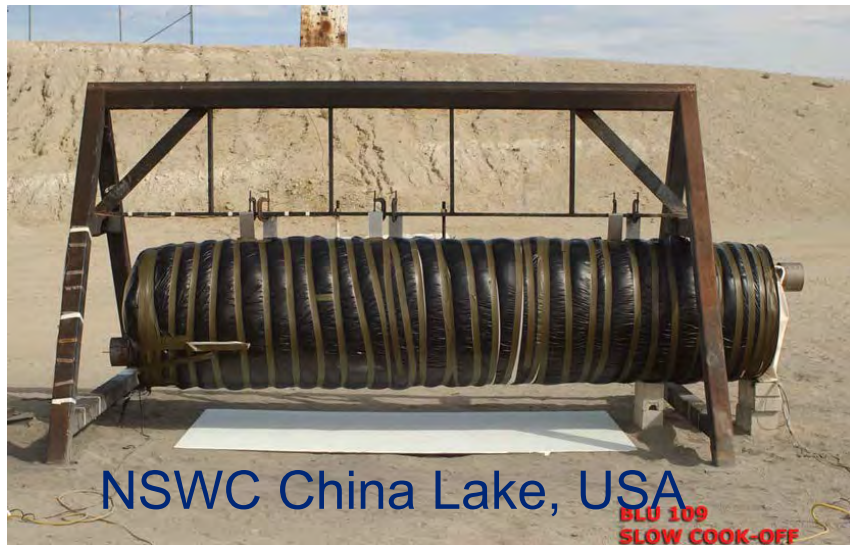


Should we standardize the oven design?



- Different munition types require different considerations.
- Differing sizes of munitions required different sized ovens.
- Some items need to be restrained to prevent flight in case of a strong propulsive reaction.

At least recommendations and guide to a well designed oven to avoid blast wave absorption, fragment location into the oven and secondary fragments.



KCW&M, Netherlands



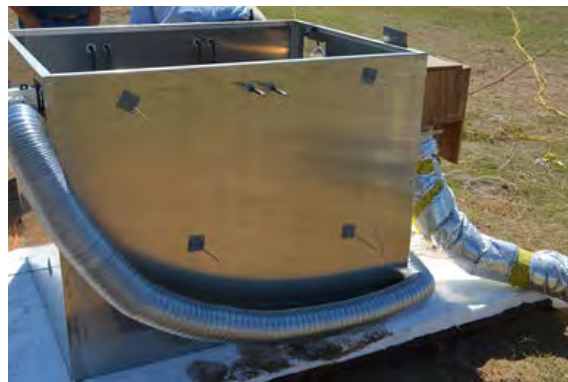
Finnish Defence Forces, Finland



Bundeswehr
Germany



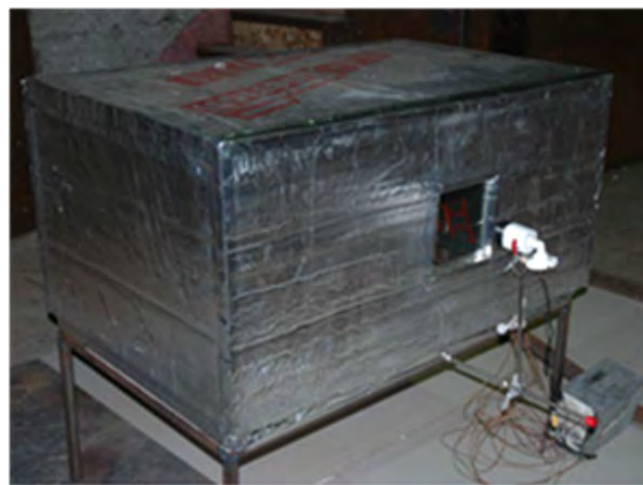
YPG, US Army



Redstone Test
Center, USA



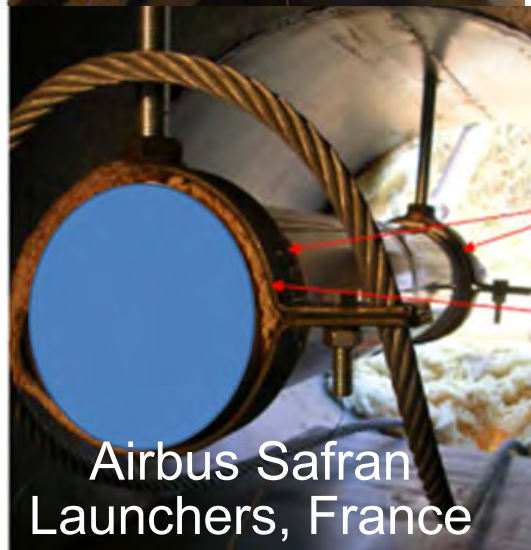
NEXTER France



GD-OTS, Canada



Redstone Test Center, USA



Airbus Safran Launchers, France



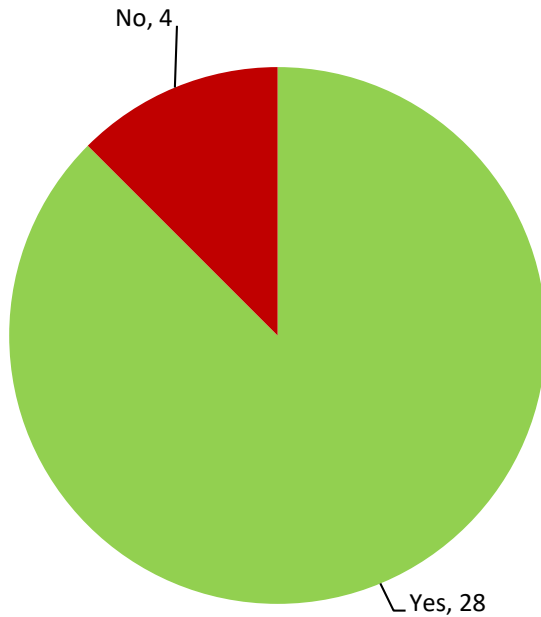
Qinetiq UK



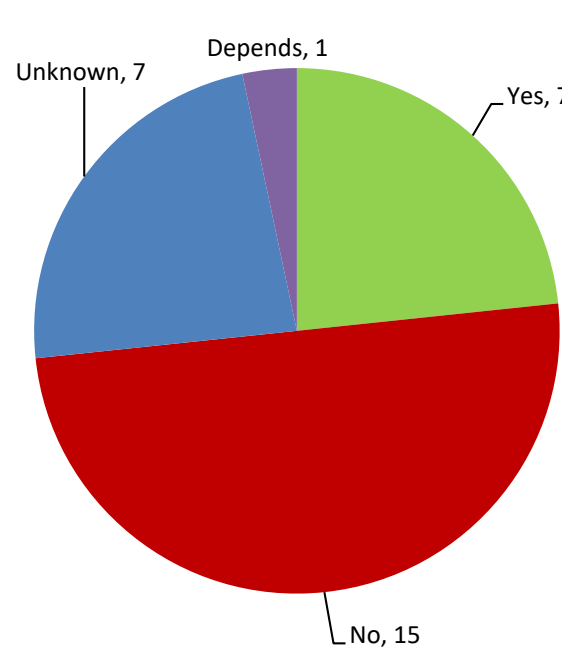
BAE UK

Many different designs!

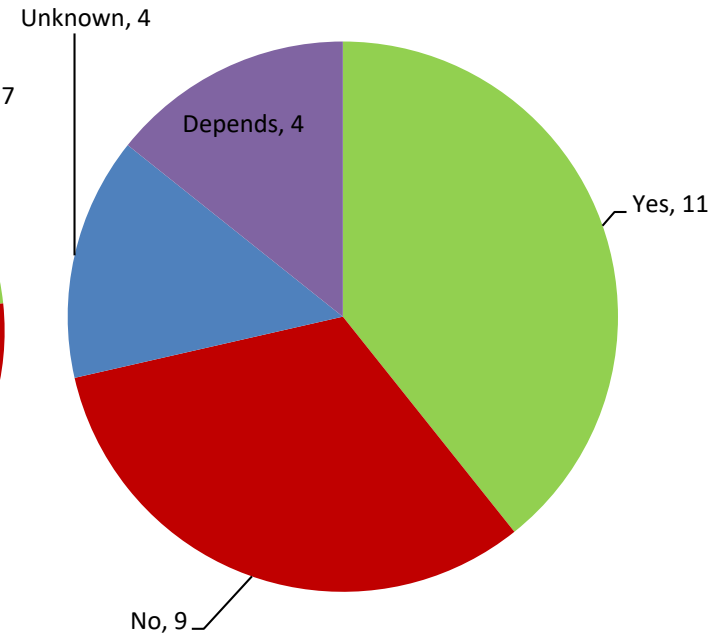
Do you precondition at 50°C for 8 hours?



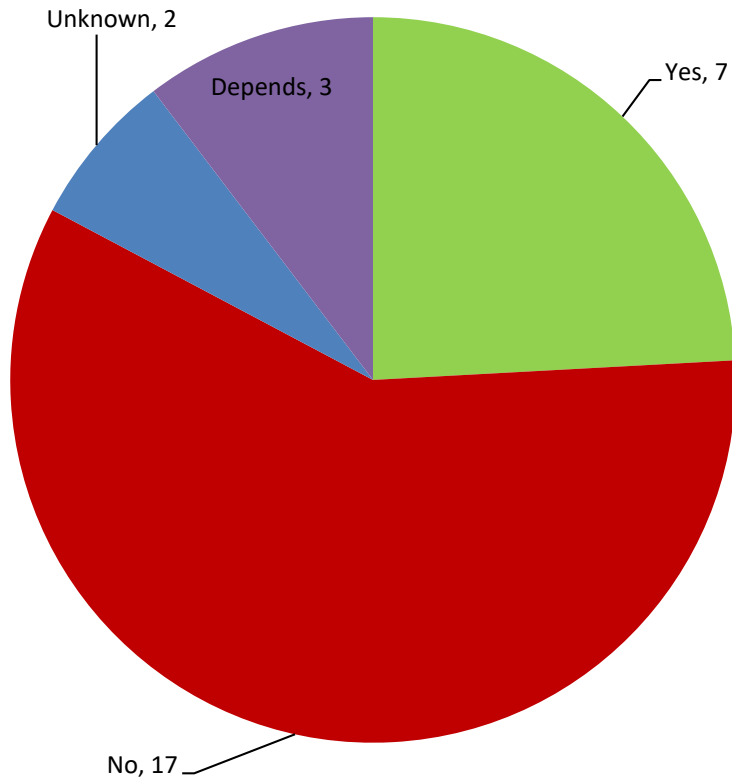
Should a melt cast energetic be pre-soaked differently from a non-melt cast material?



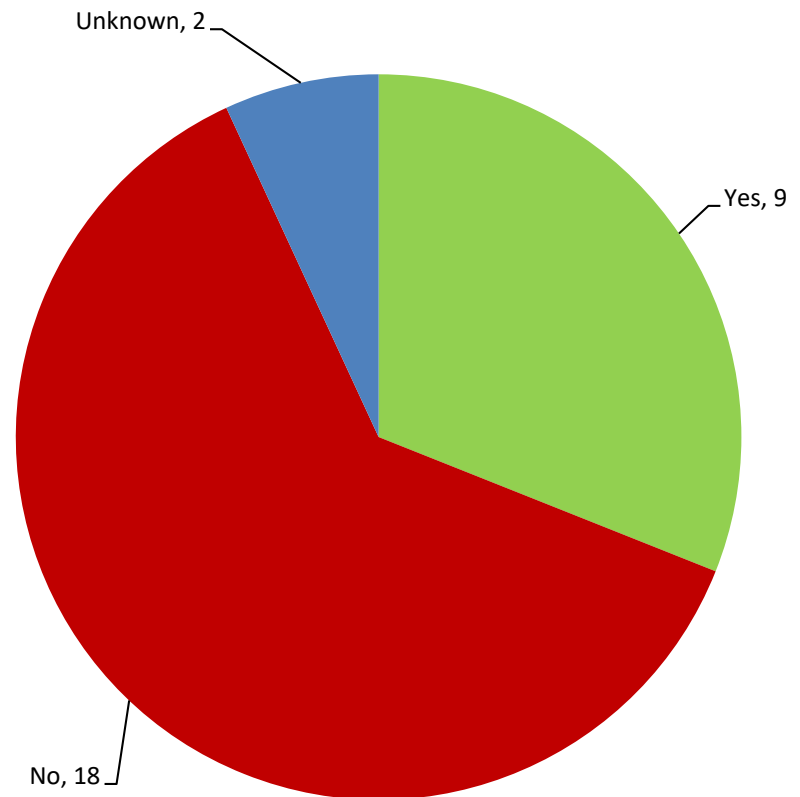
Should the requirement to precondition be changed in any way?



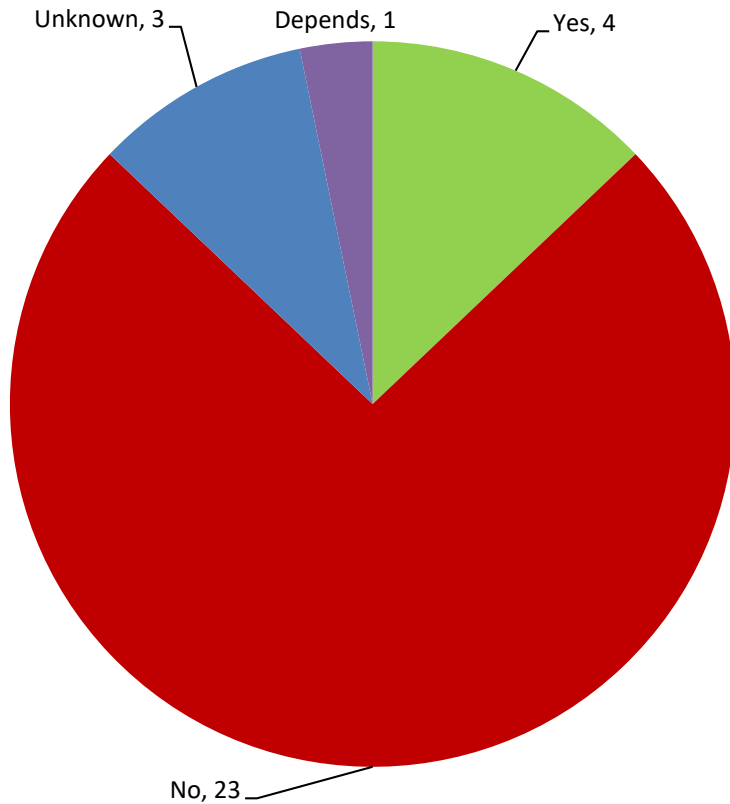
Should we recognize the benefit of having a higher reaction temperature?



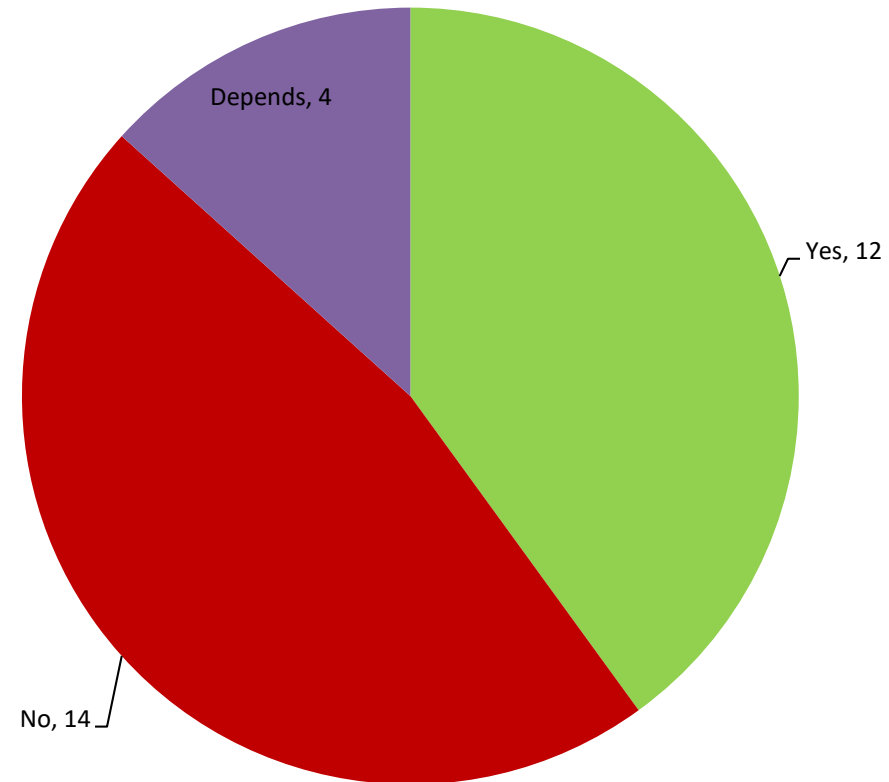
Should a maximum temperature be defined as defined by Hazard Classification Tests?



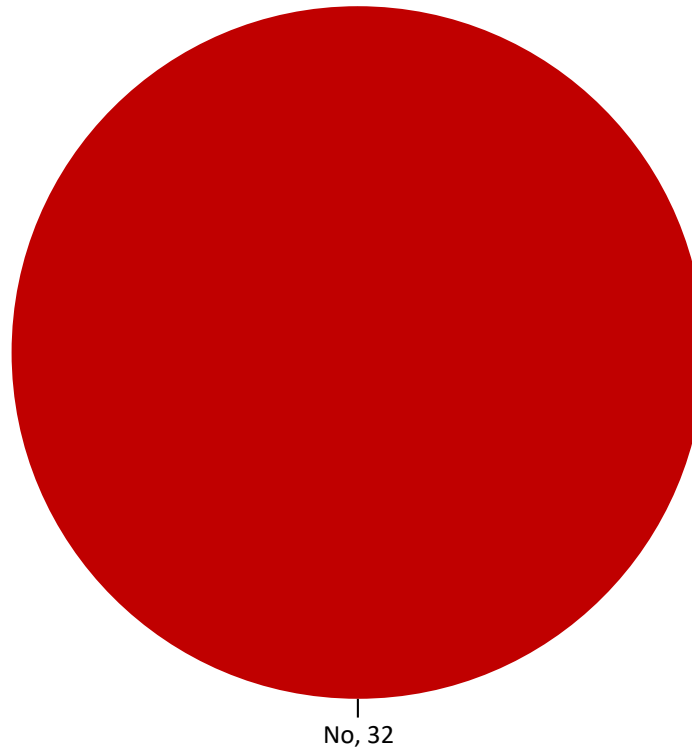
Should the melting of energetics during a test affect the testing requirement?



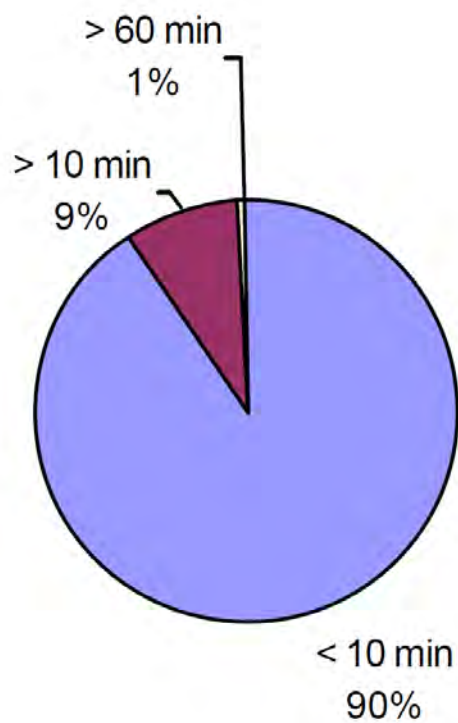
Do you restrain the test item in case of risk of propulsion?



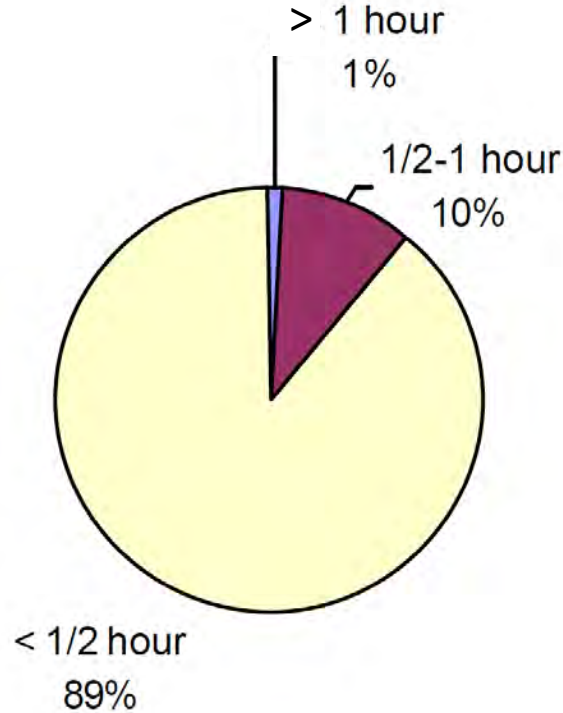
Do you have any information on duration or rates of actual slow heating incidents?



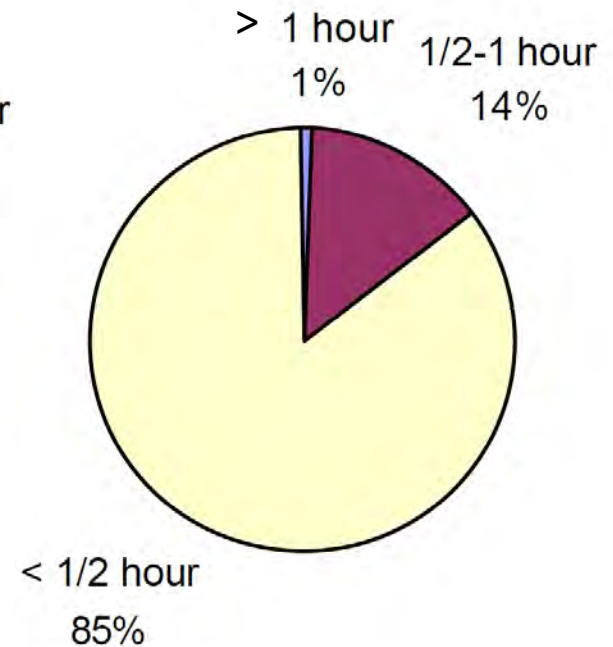
- During the AC/326 SG/B SH CWG meeting, 10-11 April 2017, MSIAC was asked to obtain and share any available historical information from the MSIAC safety database regarding real-life slow heating events and potential thermal threats.
- F. Peugeot, “Assessing Thermal Threats” MSIAC Technical Report L-097 published in 2003.
- A search of MAD-X provided no applicable information
- A report search resulted in a large number of references
- K. Hunt from OSD provided further references
- Dr. David Hubble from NSWCCD, USA did a similar study, along with supporting fire modeling. He had very similar results and conclusions



UK Navy statistics related to ship fire duration (1989)



US truck transport statistics related to fire duration (1969)



US rail transport statistics related to fire duration (1969)

*Real world durations have relatively short durations
-5 events identified to be longer than 1 day*

“Cookoff – a UK naval perspective”, I. Wallace, Proceedings of the NIMIC 1993 Workshop on Cookoff, paper TP-5 (1993)

“Probability of transportation accidents”, W. Brobst, Transportation Branch, US Atomic Energy Commission, F 192092 (1972)

- there exist a wide variety of heating rates
- these rates depend on many factors
 - direct exposure: fire size
 - indirect exposure: adjacent compartment size

Order of magnitude of the maximum temperature and the heating rate

Heating Source	<ul style="list-style-type: none"> • Torching • EM Burning • Exhausts • Pyrotechnics 	<ul style="list-style-type: none"> • Fuel Fire • Wood fire • Propane burner • Building Fire 	<ul style="list-style-type: none"> • Hot Breach • Gun Battlecarry • Launcher • Nuclear plant • Aircraft debris • Remote fire • Aerodynamic Heating • Adjacent compartment fire 	<ul style="list-style-type: none"> • Solar Heating • Steam leak
Regime	Fast Cookoff (FCO)		Intermediate Cookoff (ICO)	Slow Cookoff (SCO)
Temperatures (Order of magnitude)	1000 to 2000 °C	~1000 °C	100 to 300 °C	~ 100 °C
Heating rates (Order of magnitude)	50 to 100 °C/sec	1 to 20 °C/sec	25°C/hr to 50 °C/min	< 20 °C/hr

NATO AC/326 SG/B Slow Heating Custodial Working Group is using this information as part of the process to update STANAG 4382

- Backup

- “Analysis of Heating Rates for the Insensitive Munitions Slow Cookoff Test”, Fontenot J.S., Jacobson M., NWC TM 6278, Naval Air Warfare Center China Lake, California (1988)
- “Navy Insensitive Munitions and Shipboard Fire Protection Workshop”, NAWC China Lake, California (1995)
- “Summary of NIMIC 1993 Workshop on Cookoff”, Stokes B.B., Fitzgerald-Smith J. DeFourneaux M., Kernan P., NIMIC-BS-307-94, (1994)
- “Threat Hazard Assessment for Insensitive Munitions”, Victor, A., Presented at NIMIC Hazards Analysis Workshop (1996)
- “Exploring cookoff mysteries”, A. Victor, JANNAF Propulsion Systems Hazards Subcommittee meeting (1994)
- “Insensitive Munitions Threat Hazard Assessment of the PAC-3 Missile System”, Victor Technology, Final Report, US Restricted (1994)
- “AMRAAM rocket motor slow cookoff mitigation”, J. Gross, NAVY IM/Shipboard fire protection workshop (1995)
- “2.75-Inch rocket system slow cookoff heating rate”, H. Gokee, NAVY IM/Shipboard fire protection workshop (1995)
- “In-Bore Measurement of 120-mm Ammunition Temperatures”, Kolasa, Gregory M.; Flyash, Boris, Technical report ARCCD-TR-01001 (2001)
- “Characteristics of liquid fuel fire and gas burner heating”, E. Lundstrom, Proceedings of the NIMIC 1993 Workshop on Cookoff, paper TP-8 (1993)
- “Slow cookoff analysis”, E. Lundstrom, Proceedings of the NIMIC 1993 Workshop on Cookoff, paper TP-7 (1993)
- “Measured temperatures of solid rocket motors dump stored in the tropics and desert-Part 4. Tropics”, Naval Air Systems Command, NWC TP 5039, Part 4 (1989)
- “Preliminary analysis of the heating of ordnance in ship magazines due to a fire in an adjacent compartment”, J. Mansfield, NAWCWPNS TP 8186 (1996)
- “Ordnance heating rates in shipboard magazines”, C. Doolan, DSTO-TR-1188 (2002)
- “Computer simulation of the thermal effects on a concentric canister missile launcher with a fire in an adjacent compartment”, G. Null, Naval Postgraduate School Thesis, ADA337018 (1997)
- “Modelling of the HMAS Westralia fire”, S. Kennett, G. Gamble, J. De Li, DSTO -TR-0698 (1998)
- “Propellant fires in a simulated shipboard compartment: Project HULVUL Phase III, G. Back, R. Darwin, J. Scheffey, Naval Research Laboratory NRL/MIU6180 --99-8394 (1999)
- “Phénomènes thermiques induits par un accident de munition à bord d’un navire”, A. Fournier, C. Lallemand, AGARD-CP-511, paper 22 (1992)
- « A preliminary model for heat transfer from an uncontained solid rocket propellant burn », W. Gill, L. Kent, N. Keltner, W. Schimmel, JANNAF Propulsion Systems Hazards Subcommittee, pp.297 - 302 (1994)

- “Cookoff – a UK naval perspective”, I. Wallace, Proceedings of the NIMIC 1993 Workshop on Cookoff, paper TP-5 (1993)
- “Standoff distance effect on cookoff of ordnance stowed in MDCS ship cargo holds”, O. Heimdahl, L. Bowman, Twenty-ninth DoD Explosives Safety Seminar (2000)
- “Measurement of the size, duration and thermal output of fireballs produced by a range of pyrotechnics”, R. Wharton, J. Harding, A. Barratt, R. Merrifield, 21st international pyrotechnics seminar, pp.916-931 (1995)
- “Probability of transportation accidents”, W. Brobst, Transportation Branch, US Atomic Energy Commission, F 192092 (1972)
- “Heat feedback to the fuel surface in pool fires”, A. Hamins, S. Fischer, T. Kashiwagi, M. Klassen, J. Gore, Combustion science and Technology, vol.97, n°1-3, 37 -62 (1994)
- “Temperatures in flames and fire”, Dr. Vytenis Babrauskas, Fire Science and Technology Inc. (1997)
- “Improved real-scale fire measurements having meaningful uncertainty limits”, W. Pitts, in “Workshop on Fire: Testing measurement needs: Proceedings”, W. Grosshandler, Building and Fire Research Laboratory (2001)
- “An international survey of computer models for fire and smoke”, R. Friedman, Journal of Fire Prot. Engr, 4 (3), pp.81-92 (1992)
- “State of the art in zone modeling of fires”, W. Jones, International Fire Protection Seminar, 9th. Engineering Methods for Fire Safety, pp. 126 pp (2001)
- “Zone computer fire models for enclosures”, W. Dalton in DiNunno, SFPE Handbook of Fire Protection Engineering 2nd Edition, Chapter 7, Section 3, 3, pp.148 -151 (1997)
- “CFAST, the consolidated model of fire growth and smoke transport”, Richard D. Peacock, Glenn P. Forney, Paul A. Reneke, Rebecca M. Portier, Walter W. Jones, National Institute of Standards and Technology Technical note 1299
- “Fire environments typical of Navy ships”, D. Leblanc, Thesis, submitted to the Faculty of the Worcester Polytechnic Institute in partial fulfillment of the requirements for the Degree of Master of Science in Fire Protection Engineering (1998)
- “United Nations Recommendations on the transport of dangerous goods, Manual of tests and criteria”, Third revised edition (1999)
- “Center for the simulation of accidental fires and explosions, Annual Report, October 2000 to September 2001, submitted to the DoE LLNL under subcontract B341493, D. Pershing (2001)
- “Modeling of Buildings, houses... fires”, <http://UoC-Fire Engineering.htm>
- “Fire Hazard Assessment”, R. Bukowski, in SFPE Handbook of Fire Protection Engineering, Section 11, Chapter 7 (1997)

- “Simplified fire growth calculations”, E. Budnick, D. Evans, H. Nelson in SFPE Handbook of Fire Protection Engineering, Section 11, Chapter 10 (1997)
- “Simulation of the dynamics of the fire at 3146 Cherry Road NE, Washington D.C., May 30, 1999”, D. Madrzykowski, R. Vettori, Buildings and Fire Research Laboratory, National Institute of Standards and Technology, NISTIR 6510 (2000)
- “A study of heat transfer in liquid pool fires from steady burning through boilover”, W.R. Guinn, Paper for Fire Protection Engineering -520
- “Appropriate Slow Cookoff Heating Rates”, R. Frey, Army Research Laboratory, 18 April 2000.
- Threat Hazard Analysis prepared for Program Executive Office for Theater Air Defense, Booz-Allen & Hamilton, Inc.; 26 November, 1996.
- “Realistic Safe-Separation Distance Determination for Mass Fire Hazards”, T. Boggs, K.P. Ford, J. Covino, NAWCWD TM 8668, March 2013.
- “Ammunition Accident at the Evangelos Florakis Naval Base, Zygi, Cyprus 11 July 2011”, T.N. Taylor, MSIAC Report O-150 Rev. 1, September 2014.
- “Ammunition Depot Explosions”, A. Wilkinson, SAS Conventional Ammunition in Surplus Book 15 Chapter 13.
- “Dangerous Depots: The Growing Humanitarian Problem Posed by Aging and Poorly Maintained Munitions Storage Sites Factsheets”, Fact Sheet produced by the U.S. Department of State’s Bureau of Political-Military Affairs, Summer 2010
- “Major Ammunition Accidents—1917 to 2009” compiled by Colonel George Zahaczewsky, U.S. Army (Retired). Colonel Zahaczewsky Former Director of the U.S. Department of Defense’s Humanitarian Demining Research & Development Program
- “Recent Explosive Events in Ammunition Storage Areas,” a report of 137 incidents released in June 2007 by the South Eastern and Eastern Europe Clearinghouse for the Control of Small Arms and Light Weapons (<http://www.seesac.org>).
- “Environmental Monitoring of Stored Ammunition in South Korea (1995-1997)”, U.S. Army Defense Ammunition Center, Report No. 94-28-1, July 1997.

Acknowledgment: Thanks to Kathryn Hunt, US OSD for further information and references on fire events.

Gap Test Calculations and Correlations

Ernest L. Baker, V. Pouliquen, M. Voisin and M. Andrews

Munitions Safety Information Analysis Center (NATO), Brussels, Belgium

NEWGATES (New Excel Worksheets on GAP TESTs) is a large data base and computational tool for gap test data. NEWGATES includes pressure calibration curves for the various gap tests based on test results, numerical simulations and analytical calculations. NEWGATES can also calculate the shock pressure transmitted in the tested energetic using the attenuator material Hugoniot and tested energetic unreacted Hugoniot. We have conducted studies investigating laboratory test characteristics correlations. Correlations found included: NOL-SSGT to NOL-LSGT, NOL-LSGT to critical diameter, critical diameter to Held criteria and NOL-LSGT to density for a given explosive. The Gurney energy, the Figure of Insensitiveness of the Rotter Impact test, the detonation velocity and the detonation pressure characteristics do not provide any correlation relationship with the gap test results or critical diameter. Most recently, NEWGATES has been modified to include an improved NOL small scale to large scale gap test correlation and a critical diameter estimation calculation.

INTRODUCTION

The Munitions Safety Information and Analysis Center (MSIAC) has developed a number of safety related computational tools, including NEWGATES (New Excel Worksheets on GAP TESTs) [1] which is a large data base and computational tool for gap test data. NEWGATES currently contains information about 10 gap tests (dimensions, scope, principles); pressure calibration curves; time calibration curves; shock curvature calibration curves; 1455 gap test results; and over 250 Hugoniots. In order to reduce the cost, time and risks involved in the conception of an explosive researchers have often tried to determine ways to predict the sensitivity properties of an explosive. We have conducted studies investigating laboratory test characteristics correlations [2], including the NEWGATES gap test data. The explosive characteristics investigated included the Held criterion, the weight percentage of RDX, the composition density, the composition, the Gurney energy, the Rotter impact test and the detonation state properties.

ATTENUATOR AND ACCEPTOR GAP TEST PRESSURES

Reported gap test "incident pressures" represent the shock pressure in the attenuator material just before it shocks the energetic material being tested. As the shock pressure is reduced as it passes through the attenuator, a pressure calibration curve is required [3,4]. Figure 1 presents a general diagram of a gap test and calibration curves for the Naval Ordnance Laboratory – Large Scale Gap Test (NOL-LSGT). Donor-produced shock pressures are sustained at higher levels for longer distances as either the test diameter or confinement is increased. This makes the calibration curve highly test dependent. NEWGATES includes pressure calibration curves for the various gap tests based on test results, numerical simulations and analytical calculations.

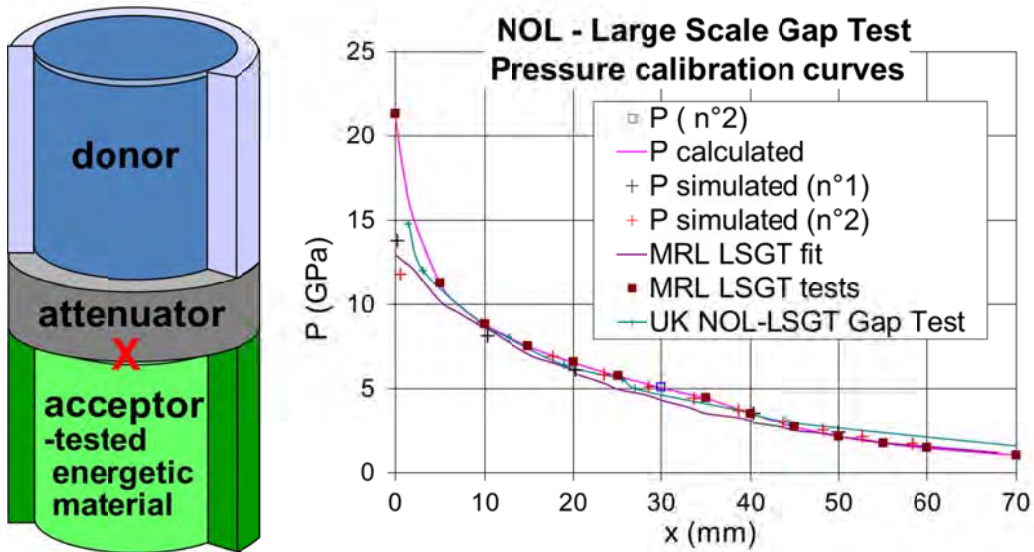


Figure 1. Gap test diagram (left) and calibration curves for the NOL-LSGT.

NEWGATES can also calculate the shock pressure transmitted in the tested acceptor energetic using the attenuator material Hugoniot and tested energetic unreacted Hugoniot. The acceptor shock pressure can be either higher or lower than the attenuator shock pressure, depending on the unreacted Hugoniot of the acceptor energetic. Figure 2 presents a diagram of the acceptor shock pressure calculation.

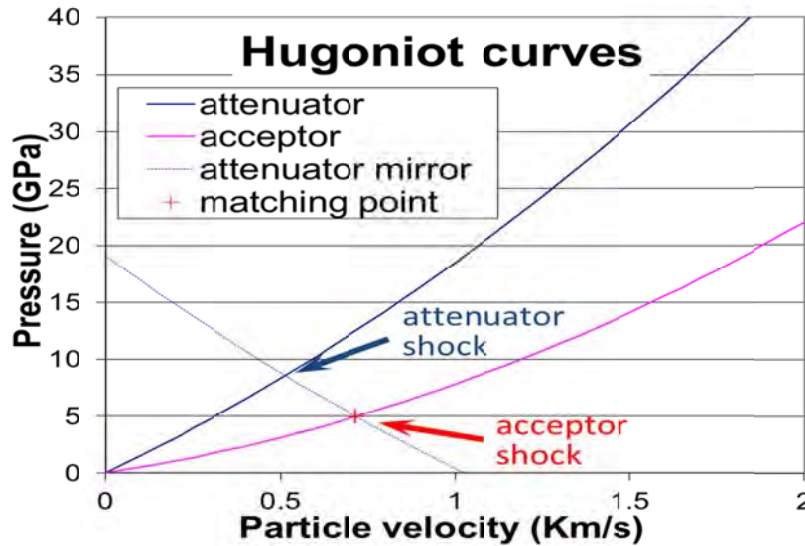


Figure 2. Calculation of acceptor shock pressure from Hugoniot characteristics.

As the unreacted Hugoniot of most tested energetics is not available, NEWGATES includes an analytical module that estimates the unreacted Hugoniot of a material using a rule of mixtures approximation [5,6]. The unreacted Hugoniot approximation requires the material density, the composition and the Hugoniot of its ingredients. The unreacted Hugoniot calculation includes porosity effects of a mixture at less than the theoretical maximum density [7]. The required input data are the mass percentages of the different ingredients, the density of the composition and the pressure range for the Hugoniot calculation. Up to 5 ingredients can be used to calculate the Hugoniot mixture. Figure 3 presents a comparison between the calculated mixed Hugoniot, a standard Hugoniot fit using experimental data and the associated experimental data for Rowanex 1400 [8].

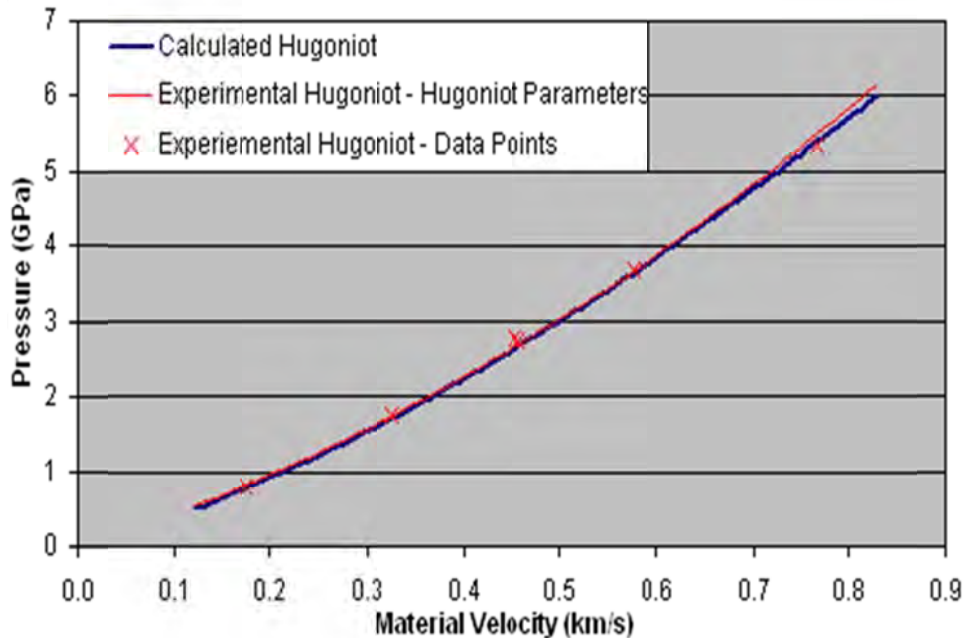


Figure 3. Comparison between the calculated mixed Hugoniot, a standard Hugoniot fit using experimental data and the associated experimental data for Rowanex 1400.

NOL LARGE VERSUS SMALL SCALE GAP TESTS

Gap tests of different sizes and geometries give different results in term of gap length for the same material. Additionally, the use energetic materials with large critical diameters compared to the diameter of a given gap tests can yield misleading results. It is therefore suggested that correlations for different gap tests are only appropriate for materials with critical diameters on the order or smaller than the diameters of the gap tests being correlated. The main point of this interrogation was therefore to add more data to an existing correlation of interest made by Donna Price [9] in 1966. The two tests of interest are the NOL-LSGT and the NOL small scale gap test (NOL-SSGT). As the two tests came from the same laboratory, the methods and protocols used are similar for these two tests. The incident initiation pressures were compared for nine different explosives at several densities. She made the correlation with twenty-nine values. In this investigation, eight values (for six new explosives) were added at this comparison and several larger critical diameter explosives were removed. Figure 4 shows the comparison between the two gap tests. The resulting correlation does not change significantly the comparison. This new correlation was implemented into NEWGATES. It is interesting to note that although a correlation exists, it is not particularly strong.

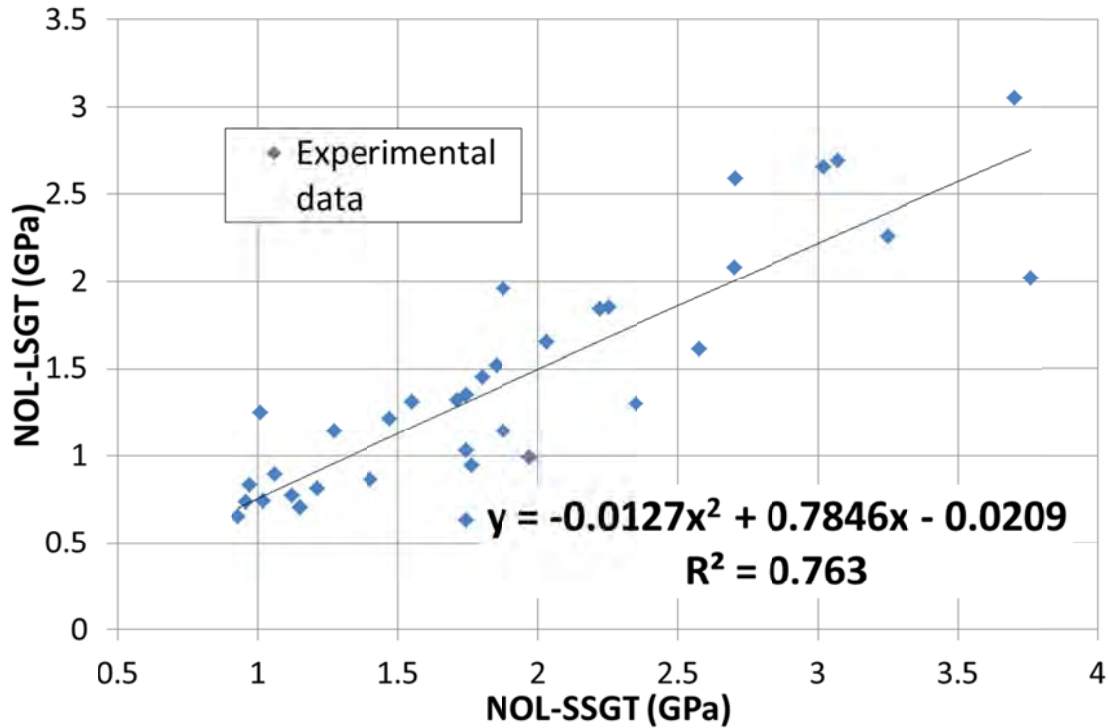


Figure 4. Comparison and correlation between NOL small scale and large scale gap test results.

CRITICAL DIAMETER VERSUS GAP LENGTH

Patel [10] previously looked for critical diameter correlations. In particular, he noted a correlation between critical diameter and Held's criteria for shaped charge jet initiation. He did not investigate gap test correlations. To expand upon Patel's work, this work used the critical diameter data held within EMC [11] and compared this to the gap data held in NEWGATES for the same formulations. The first gap test chosen was the NOL-LSGT gap test. The comparison has been made for forty-three different energetic materials. The results of critical diameter tests are dependent upon the exact composition, the density, the particle size, the ingredients properties and the composition processing. It is common to see a range of values for the same explosive in the same conditions. In this case, and if the values are similar, an average has been made. If the database indicated a range of value like "between 30 and 40 mm", the average of the two values has been made. And finally if the critical diameter was indicated below a certain value such as "< 3 mm", this value was selected if it was below 10 mm. Above 10 mm (e.g. "<70 mm"), the explosive has been removed. The results of this correlation are shown in Figure 5. A graph of the gap length and the gap pressure versus the critical diameter under logarithmic regression was interesting, providing a correlation coefficient R-squared of 0.7982. Although this would mean that it has been found empirically that there is a correlation, the correlation is not particularly strong and should not be construed to be a fundamental physically based relationship. There is significant experimental evidence showing that small critical diameters can be realized for less shock sensitive energetic materials. The identification of such materials is both an ongoing research area for ultra-fine grain scale explosives [12] and has also been observed for some higher performance reduced sensitivity rocket propellants [13].

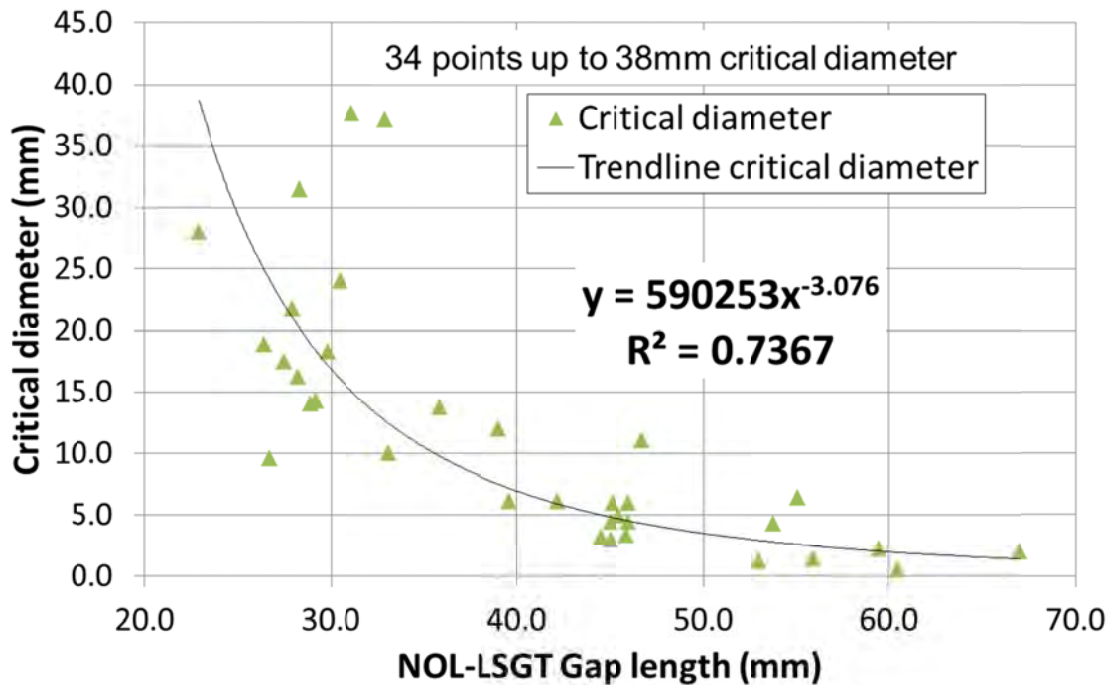


Figure 5. Critical diameter correlation to LSGT gap length.

HELD CRITERION VERSUS CRITICAL DIAMETER

The Held criterion [14] is a measure of an energetic material's susceptibility to initiation from a copper shaped charge jet. Some studies indicated that when dealing with initiation due to shaped charges, the square of the velocity of the minimum jet needed to cause initiation multiplied by its diameter is nearly constant for an energetic material. This constant is called the Held criterion, and is treated as a constant unless the jet material is changed [15, 16]. Patel [10] previously noted a correlation between critical diameter and Held's criteria for shaped charge jet initiation. The relation found by Patel has the attribute that if the critical diameter is less than 4.05 mm, the Held criterion becomes negative. This was due to using only data for explosives with critical diameters down to 4mm. Additionally, the largest critical diameter used was 9mm. Therefore, a new correlation was investigated using a broader data set down to a 2.5mm critical diameter and up to a 13mm critical diameter [16, 17, 18]. After comparing various correlation mathematical forms, a power correlation was chosen. Figure 6 presents the correlation and a comparison to data.

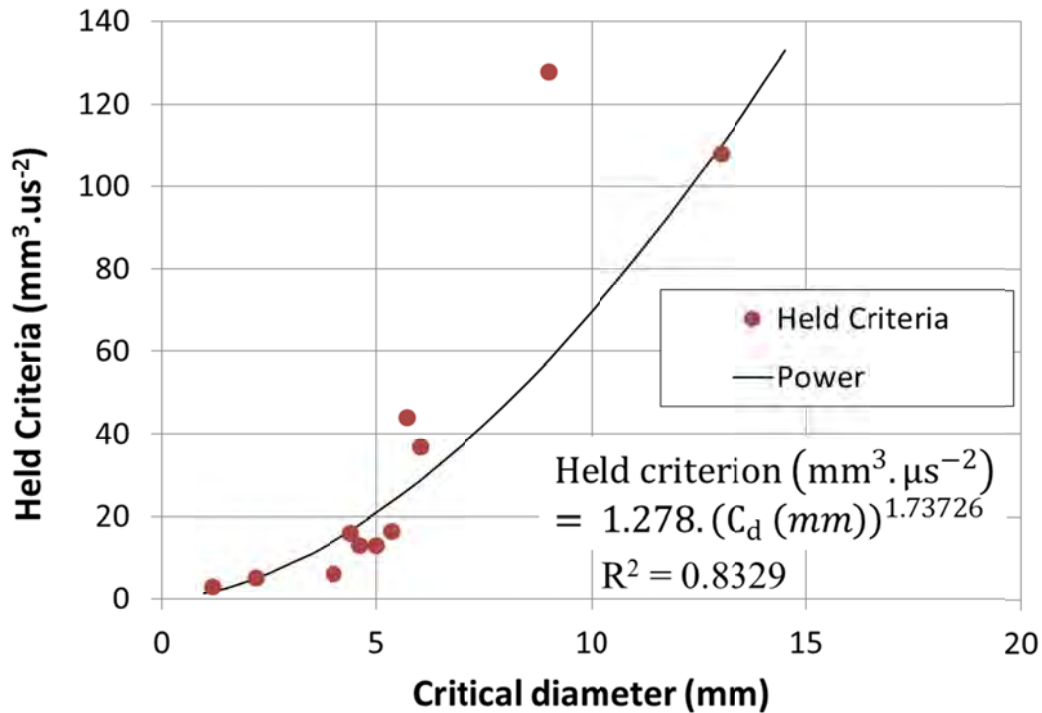


Figure 6. Held criteria vs. critical diameter correlation.

GAP TEST VERSUS DENSITY

Gap length versus density was investigated for five different explosives: TNT, CH-6, AP/Wax, PBX-9404 and Comp A-3. Very good correlations were obtained for all of the explosives when a single data source was used for a given explosive. Figure 7 gives an example of this, which is actually the same data used in a similar study [Price 1974]. However, when multiple data sources are used, the correlation is much weaker as seen for CompA-3 in figure 8 [Price 1974, Peterson 1981, Newman 1997]. Several conclusions can be inferred from this study. Firstly, ingredients and processing can vastly change the shock sensitivity. Secondly, for a given explosive material and processing, a denser explosive will be less shock sensitive. This can be explained traditionally by the fact that a more porous explosive will have more or larger voids, so when a shock wave runs into the explosive, more or stronger hot spots will be set up in these voids. Thirdly, as it has been previously seen, the critical diameter typically increases when the gap length decreases so it should be logical that the critical diameter increases with the density for a given energetic material.

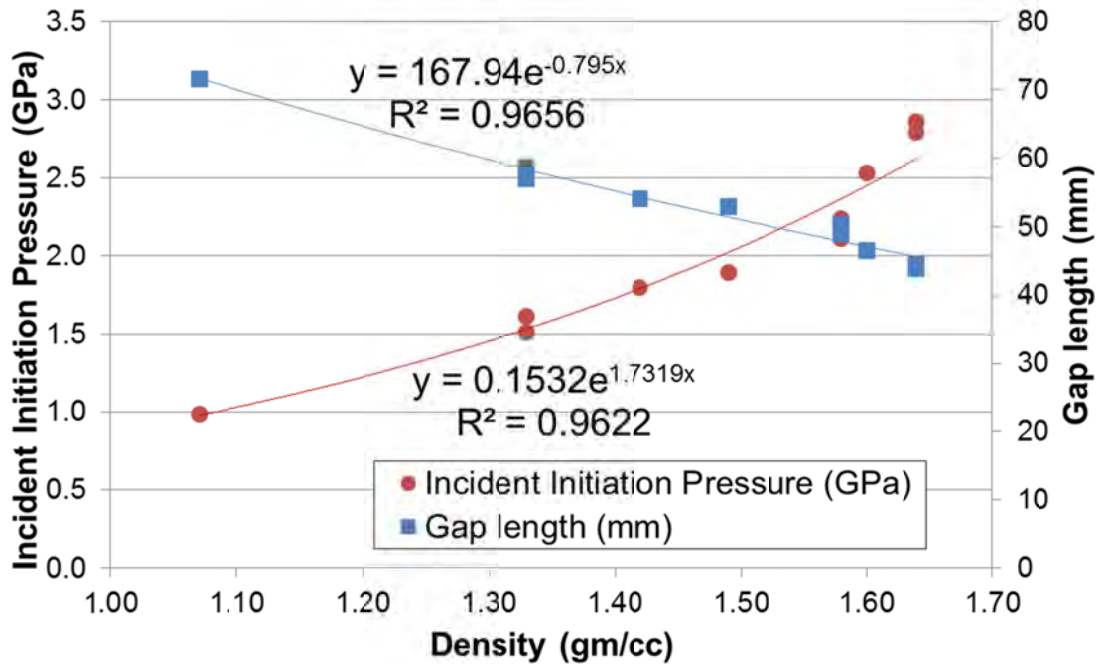


Figure 7. TNT NOL-LSGT density correlation for a single data source.

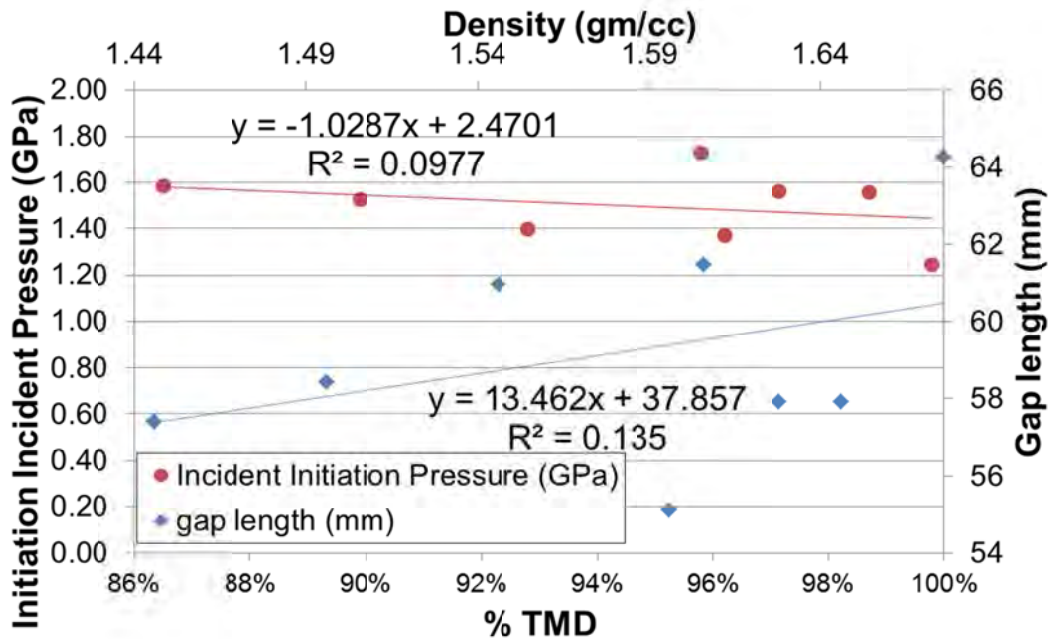


Figure 8. TNT NOL-LSGT density correlation using multiple data sources.

GURNEY ENERGY VERSUS GAP LENGTH AND CRITICAL DIAMETER

Gurney energy [22] has long been used as an explosive characteristic for the quantification of early work output of high explosives. The Gurney energy represents the kinetic energy per explosive mass resulting from the work performed by the expansion of the detonation products. Often, explosive work output is thought to correlate to sensitivity or the ability to detonate. For this reason, correlations of the Gurney energy with NOL-LSGT gap length and critical diameter were

investigated. Figure 9 presents resulting plots from this investigation. From the plot, it appears clear that strong gap test and critical diameter correlations do not exist with the Gurney energy. A small trend of increased gap length with increased Gurney energy is potentially visible, but poorly correlated. No trend is observed for critical diameter versus Gurney energy. Patel [10] had already found a similar result with just eight explosives. This study, with twenty-four materials, supports the same conclusions. The study also investigated the the Figure of Insensitiveness of the Rotter Impact test, the detonation velocity and the detonation pressure. The Rotter figure of Insensitiveness, the detonation velocity and the detonation pressure characteristics did not provide any correlation relationship with the gap test results or critical diameter.

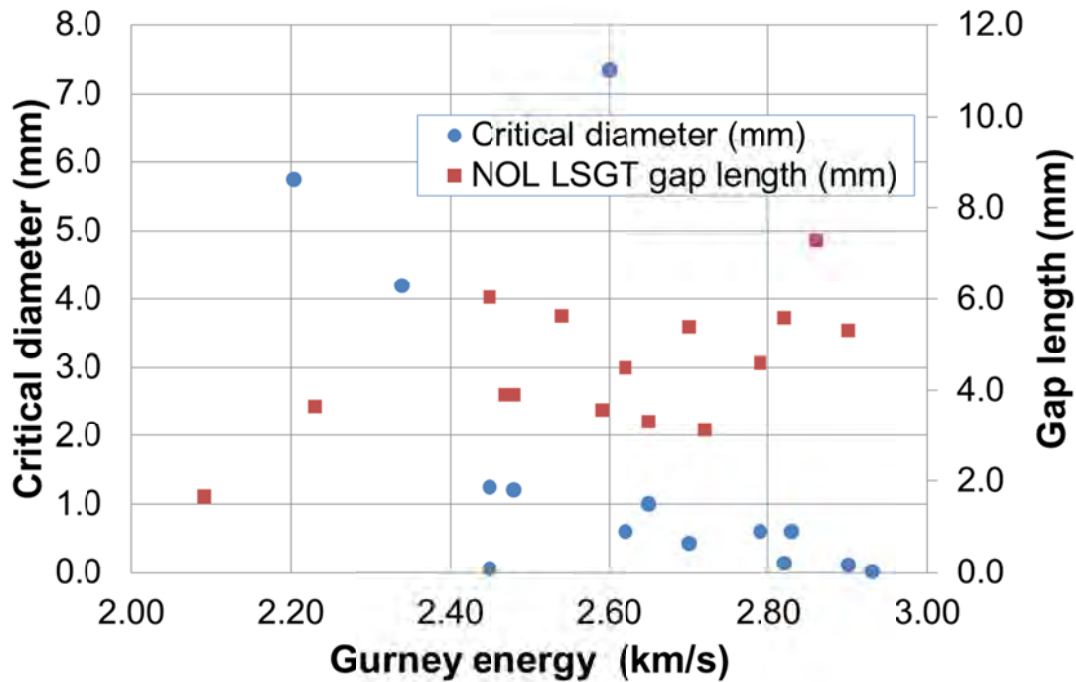


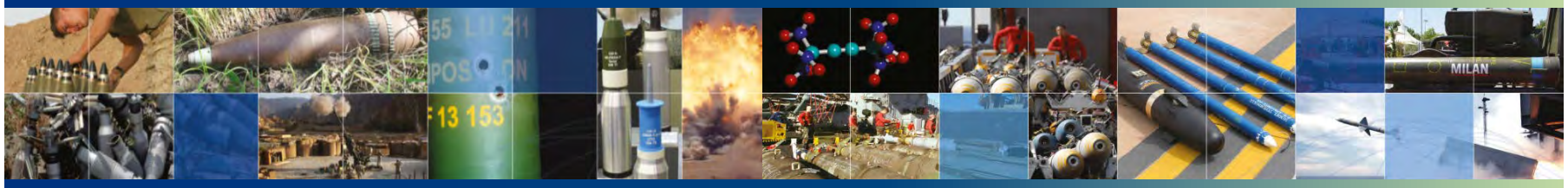
Figure 9. Critical diameter and NOL-LSGT gap length vs. Gurney energy.

CONCLUSIONS

We have conducted studies investigating laboratory test characteristics correlations. Correlations found included: NOL-SSGT to NOL-LSGT, NOL-LSGT to critical diameter, critical diameter to Held criteria and NOL-LSGT to density for a given explosive. Most of the correlations were not particularly strong. This seems reasonable, as none of the characteristics are definitively linked through fundamental physical processes. For example, extremely fine grained high explosives have been found to produce low shock sensitivity, yet have small critical diameters, counter to the overall trend. However, the NOL-LSGT to density correlations were very strong for data from a single explosive data source, presumably using similar ingredients and processing for all of the explosives. It is therefore clear, that ingredients and processing are important factors in resulting shock sensitivity and that porosity is normally fundamentally linked to shock sensitivity through hot spot initiation theory. The Rotter figure of Insensitiveness, the detonation velocity and the detonation pressure characteristics do not provide any correlation relationship with the gap test results or critical diameter. Most recently, NEWGATES has been modified to include an improved NOL small scale to large scale gap test correlation and critical diameter estimation calculations. It is important to realize that they only provide rough estimates, and should not be construed as accurate results.

REFERENCES

1. Peron, P.F., "NEWGATES Version 1.10 User Guide", NATO MSIAC Report L-148 Edition 3, November 2011.
2. Voisin, M., "Critical Diameter Correlations", MSIAC Report L-202, September 2006.
3. Bowman, A.L., S.C.Sommer and J.H.Fu, "Calibration curves for four standard gap tests", Report LA-11763-MS, 1990.
4. Price, D., "Gap tests and how they grow", 22nd DDESB Seminar, pp.365-380 (1986)
5. R.R. Bernecker, "The Calculation of Unreacted Hugoniot. I. TNT, RDX, and their Mixtures," JANNAP Propulsion Systems Hazards Subcommittee Meeting, CPIA Publication 582, Vol. I, April 1992, p. 285.
6. R.R. Boade, "Compression of Porous Copper by Shock Waves", J. App. Phys.. 39,5693-5702, 1968.
7. Erkman, J.O. and D.J. Edwards, "Computed and Experimental Hugoniot for Unreacted Porous High Explosives", 6th Symposium on Detonation, 1976.
8. Milne, A. Longbottom and J. Millet, "On the Unreacted Hugoniot of Three Plastic Bonded Explosives", Propellants, Explosives, Pyrotechnics, Vol. 32, n° 1, pp 68-72, 2007.
9. Price, D. and T.P. Liddiard, Jr., "The small scale gap test: calibration and comparison with the large scale gap test", Naval Ordnance Laboratory, White Oak, Maryland, United States, NOLTR 66-07, Jul. 1966.
10. Patel, R.J., "Investigation of Possible Correlations Between Burney Constant, Held Criteria, and Critical Diameter", Technical Report ARAET-TR-06022, US Army ARDEC, January 2007.
11. Andrews, M. and E. Schultz, "The Development and Future of EMC", MSIAC Report O-157, September 2014.
12. Stepanov, V., "Production of Nanocrystalline RDX by RESS: Process Development and Material Characterization", Ph.D dissertation, New Jersey Institute of Technology, NJ, USA, 2008.
13. Graham, K.J. and P.J. Cahill, "Super Large-Scale Gap Tests on Energetic Formulations", 2006 Insensitive Munitions and Energetic Materials Technology Symposium, Bristol, UK, 2006.
14. Held, M. "Initiation Phenomenon with Shaped Charged Jets," presented at the Ninth International Symposium on Detonation, Portland, Oregon, United States, 1989.
15. James, H.R. and I.B. Macintyre, "The jet Initiation of Solid Explosives," Eighth International Symposium on Detonation, Albuquerque, New Mexico, United States, 1985.
16. James, H.R. "Predicting the response of explosives to attack by high-density shaped-charge jets," Journal of Energetic Materials, vol. 7, no. 4-5, pp. 243-264, Nov. 1989.
17. Frédéric Peugeot, Peugeot Critical Energy Modified. Brussels, Belgium: MSIAC, 2006.
18. Energetic Materials Compendium. Brussels, Belgium: MSIAC, 2016.
19. Price, D., A. R. Clairmont, Jr., and J. O. Erkman, "The NOL Large Scale Gap Test III. Compilation of Unclassified Data and Supplementary Information for Interpretation of Results," Naval Ordnance Laboratory, White Oak, Maryland, United States, AD-780 429, Mar. 1974.
20. Peterson, R. "Susceptibility Index of Explosives to Accidental Initiation," Naval Weapons Station, Yorktown, Virginia, United States, NWSY TR 81-6, Oct. 1981.
21. Newman, K. and S. Brown, "Development of PBXW-17: An RDX Filled Polyacrylic Elastomer," presented at the Insensitive Munitions & Energetic Materials Technology Symposium, Tampa, Florida, United States, 1997.
22. Gurney, R.W., "The Initial Velocities of Fragments from Bombs, Shells, and Grenades," Ballistic Research Laboratory, Aberdeen, Maryland, United States, BRL-R-405, Sep. 1943.

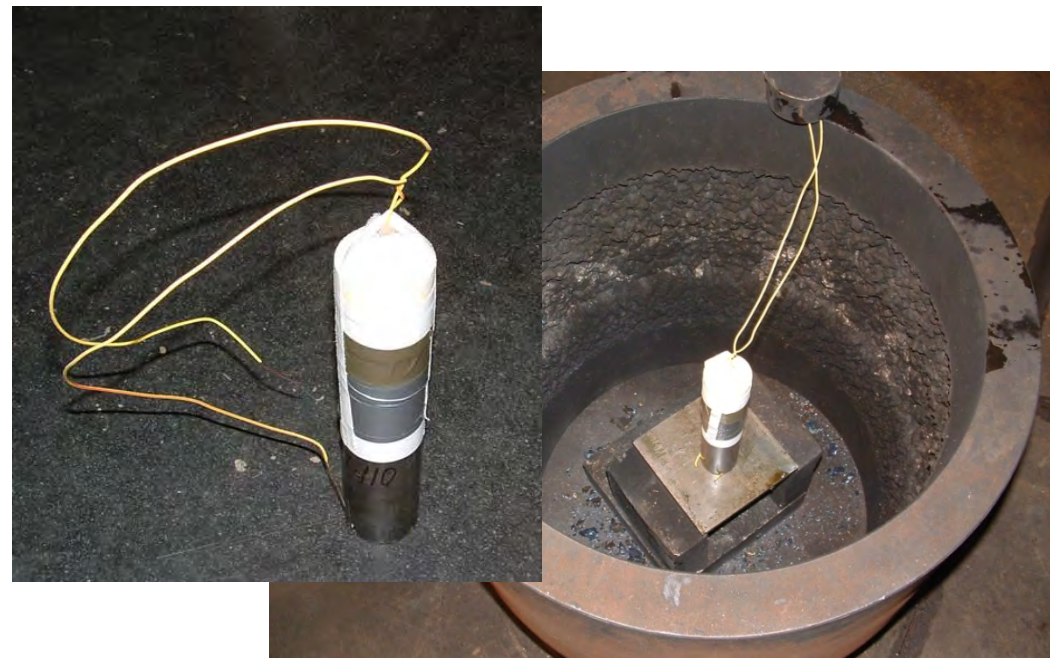


GAP TEST CALCULATIONS AND CORRELATIONS

Dr. Ernest L. Baker

Warheads Technology TSO
+32 (0)2 707 3844
e.baker@msiac.nato.int

IMEMTS 2018
Portland, OR, USA



- Introduction
- Gap test shock pressures
- Correlations
 - SSGT vs. LSGT
 - LSGT vs. density
 - Critical diameter vs. LSGT
 - Held criteria vs. critical diameter
 - Gurney energy
- Conclusions

M. Voisin, “Critical Diameter Correlations”, MSIAC Report L-202, SEP 2016.

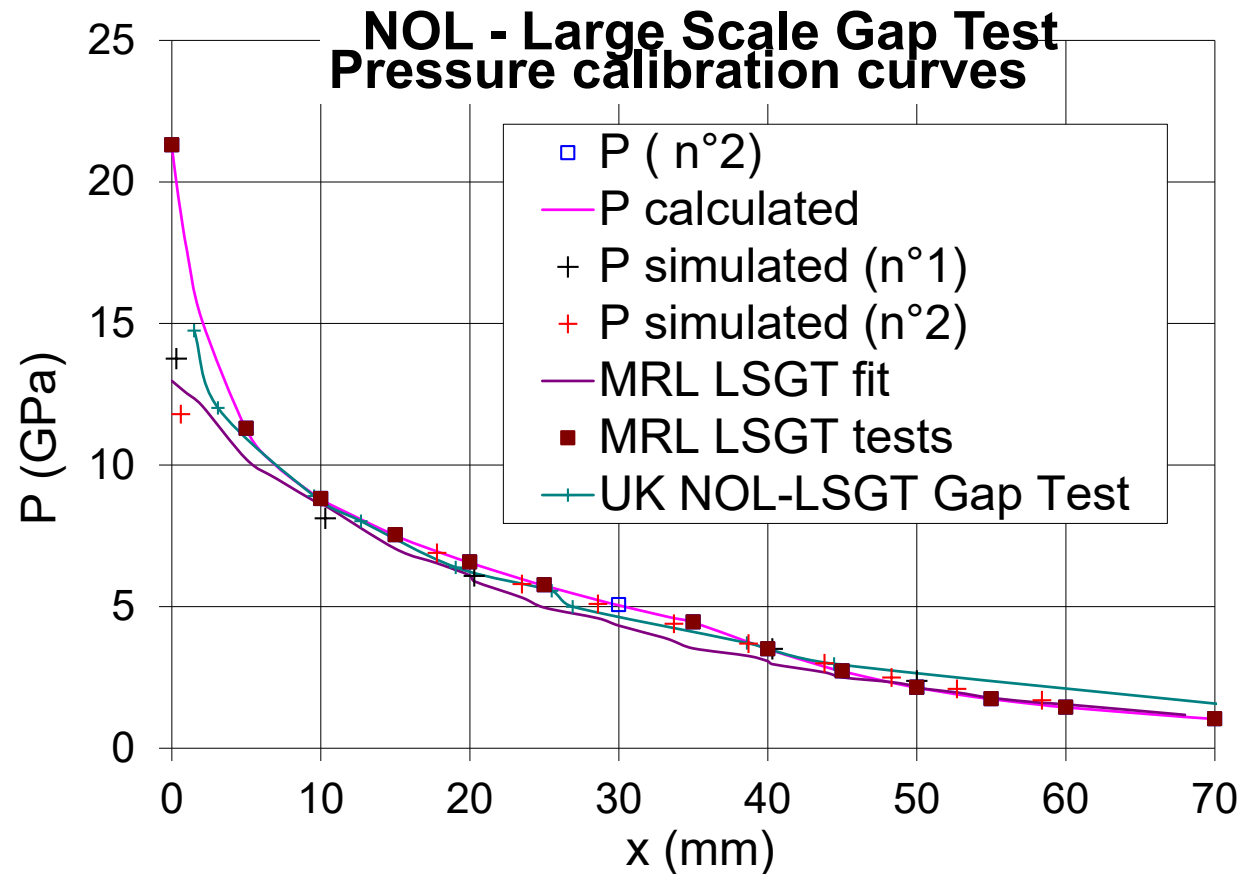
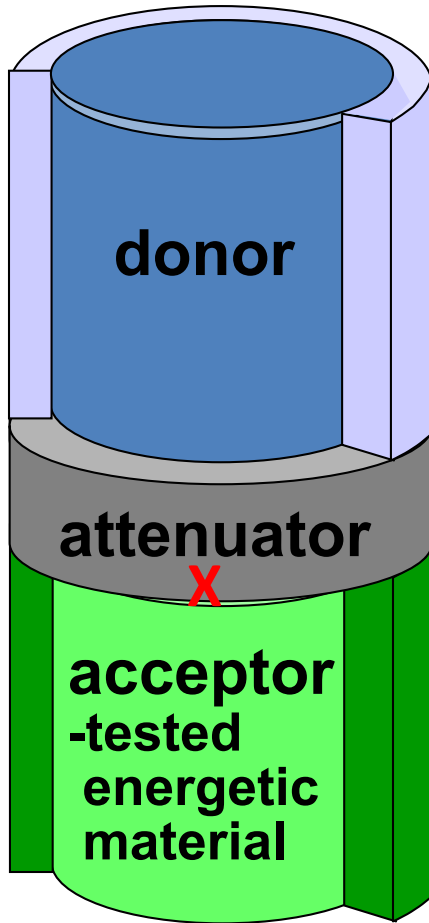
P. Peron, E. Baker, and V. Pouliquen, “NEWGATES 1.11 User’s Guide”, MSIAC Report L-148, Ed. 4, SEP 2017.

- NEWGATES: NIMIC Excel Worksheets on Gap TESTs
 - developed in Excel, Version 1.11 released in 2017
 - gap test references, data and calculations
 - 10 gap tests (dimensions, scope, principles)
 - pressure calibration curves
 - time calibration curves
 - shock curvature calibration curves
 - 1455 gap test results
 - Unreacted Hugoniot
- Laboratory test characteristics correlation study: “Critical Diameter Correlation”, Voisin M. , MSIAC Report O-171 (2016).
- New correlations in NEWGATES: SCGT, LSGT, d_{crit}

GAP TEST SHOCK PRESSURES

Reported gap test “incident pressures” represent the shock pressure in the attenuator material just before arriving to the acceptor

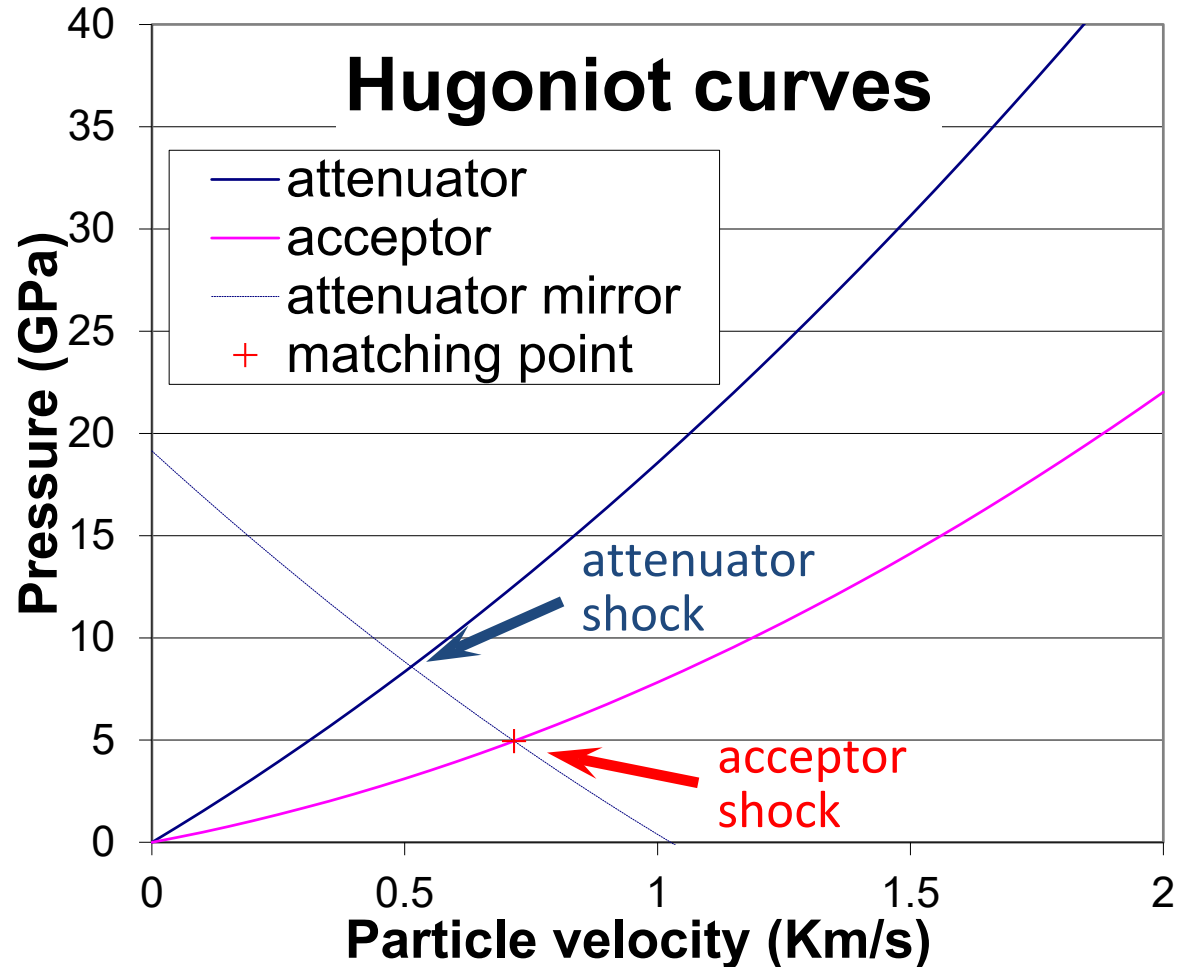
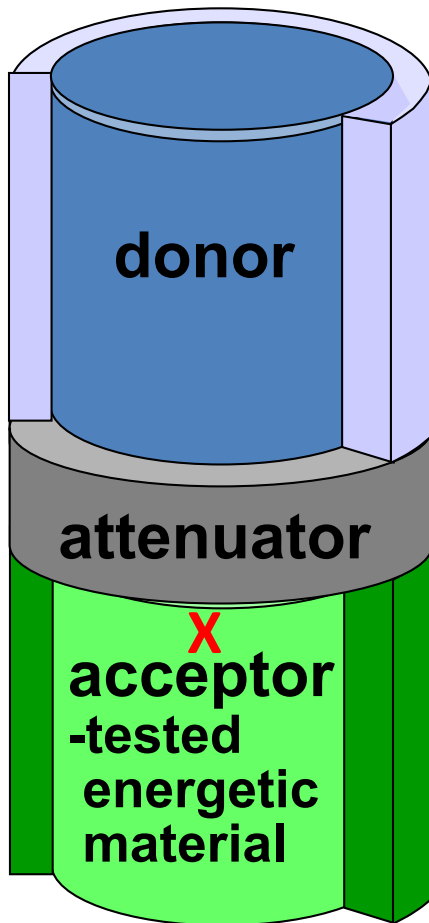
– requires a pressure calibration curve



MSIAC ATTENUATOR VS. ACCEPTOR SHOCKS

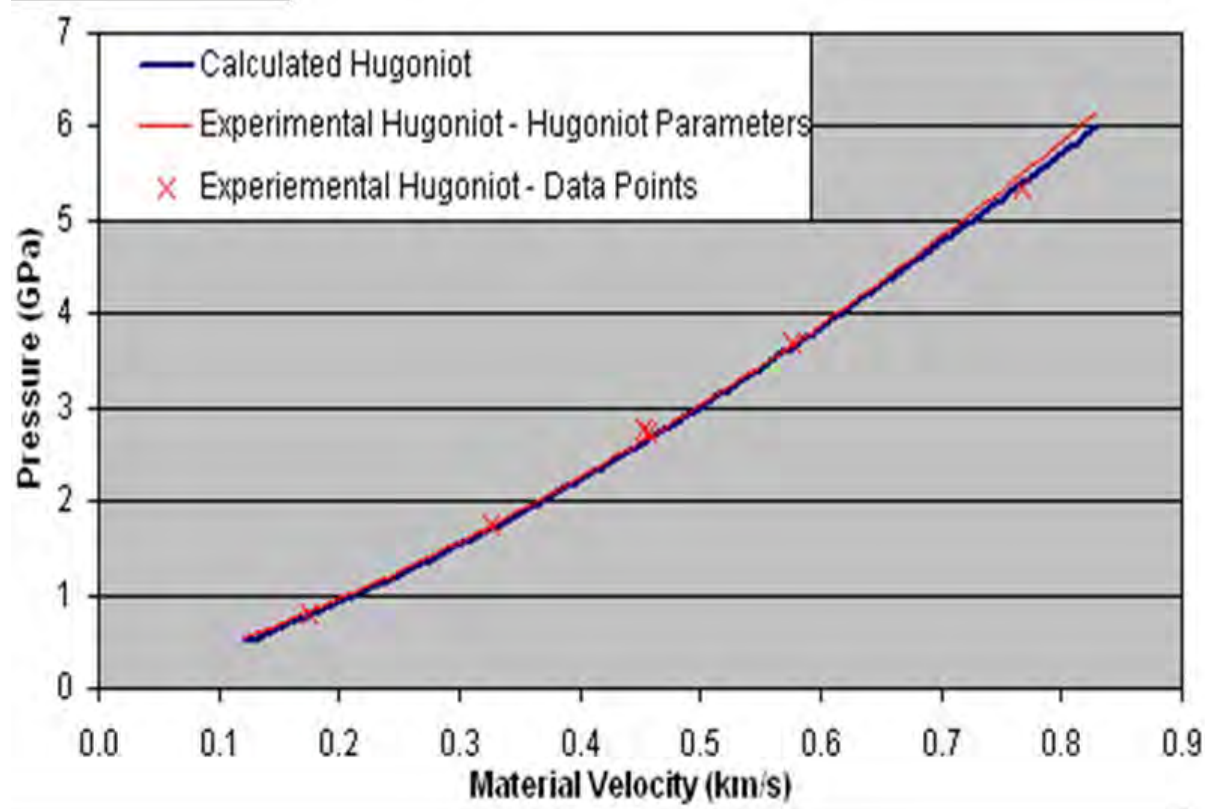
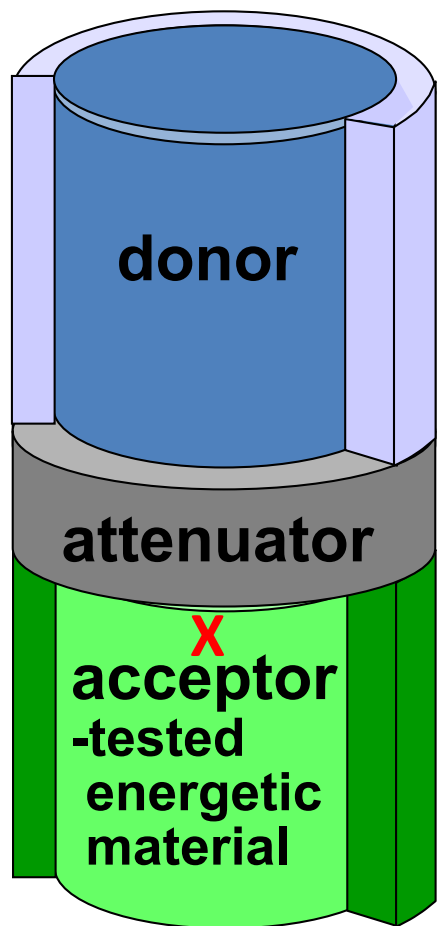
Supporting Munitions Safety

The shock pressure in the acceptor material just after the shock arrives can be calculated using Hugoniot matching

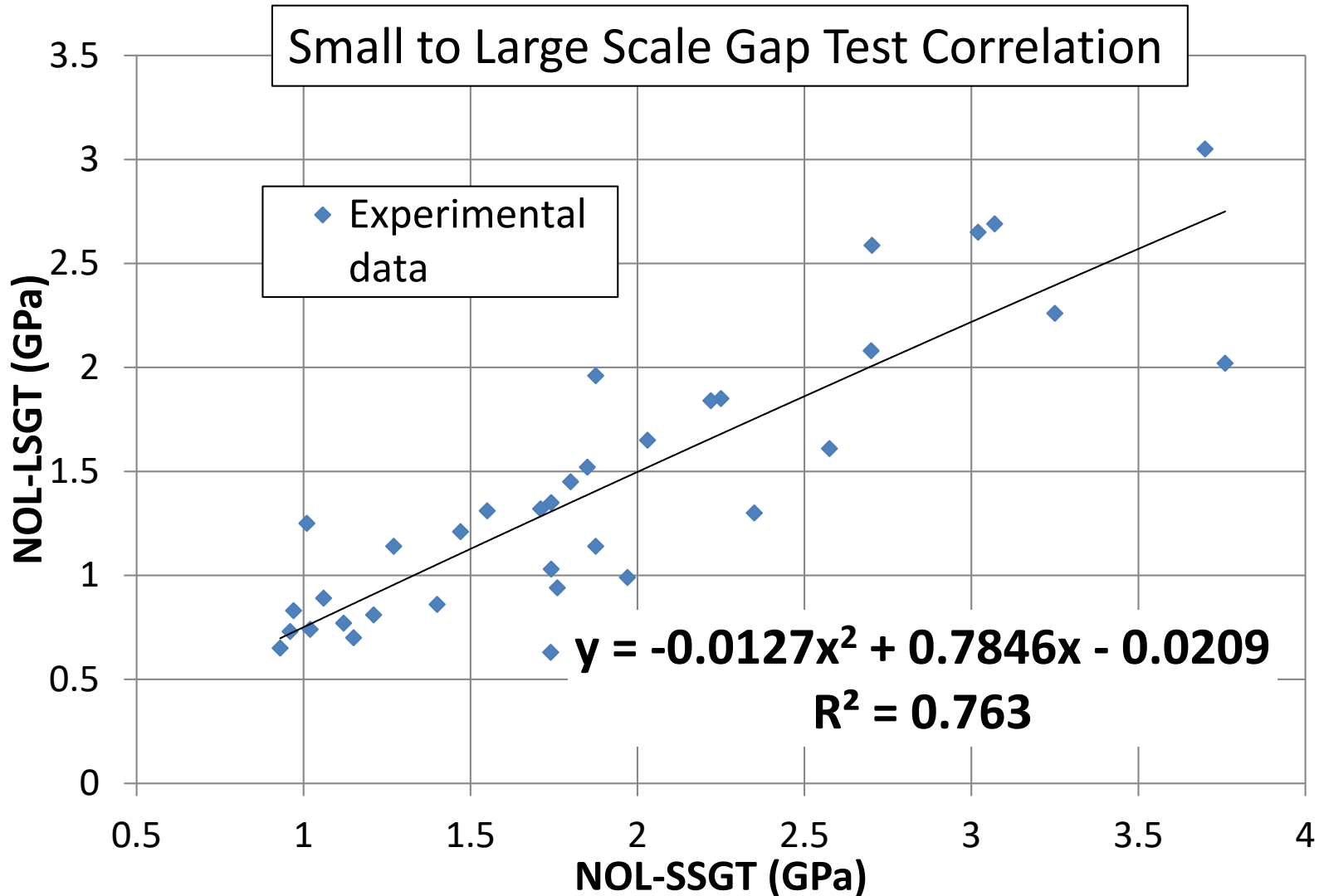


*NEWGATES can calculate the initial acceptor shock pressure
–requires the acceptor material unreacted Hugoniot*

NEWGATES includes a model to calculate the acceptor unreacted Hugoniot based on Hugoniot of the acceptor ingredients

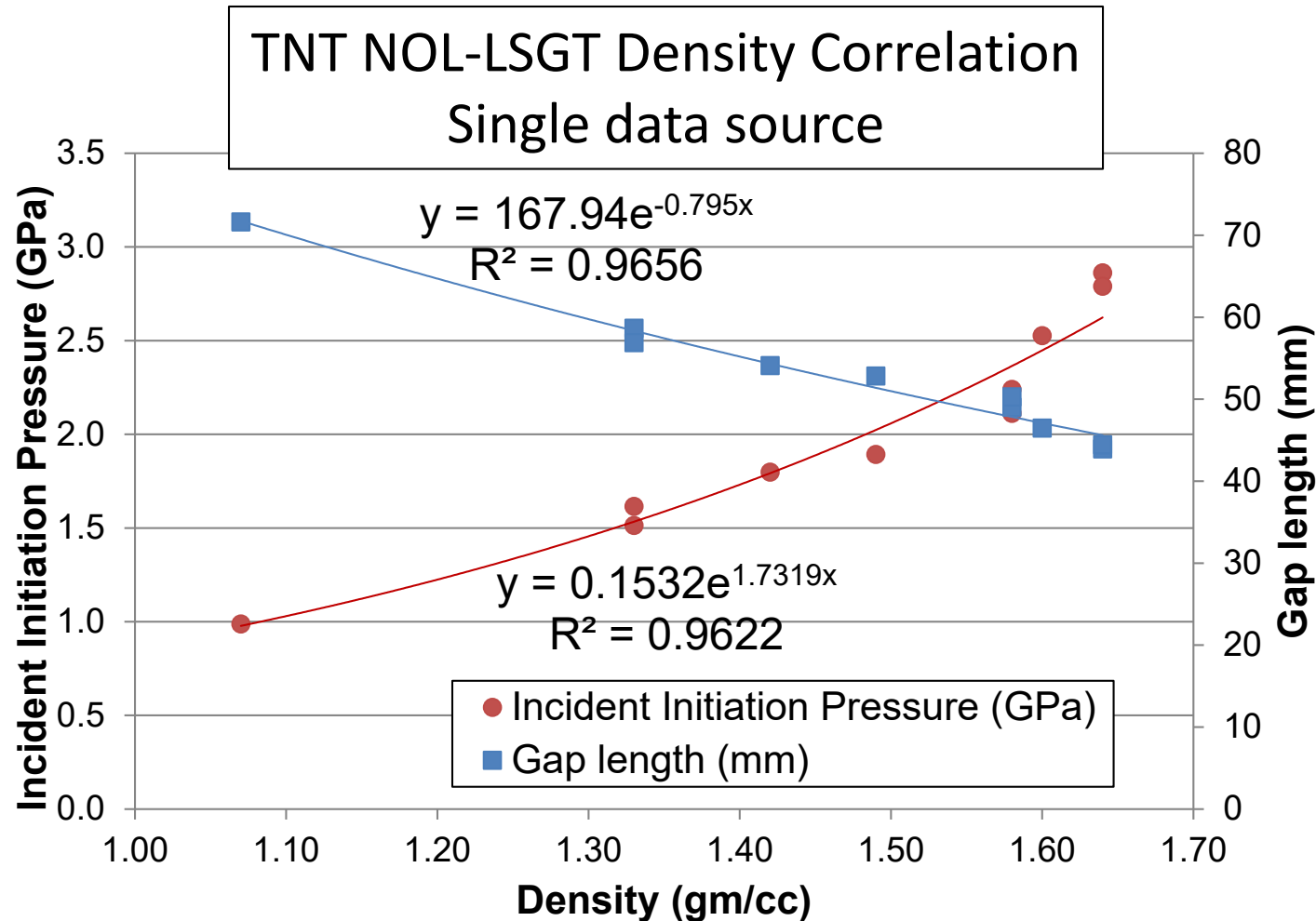


Calculated mixed Hugoniot: Rowanex 1400



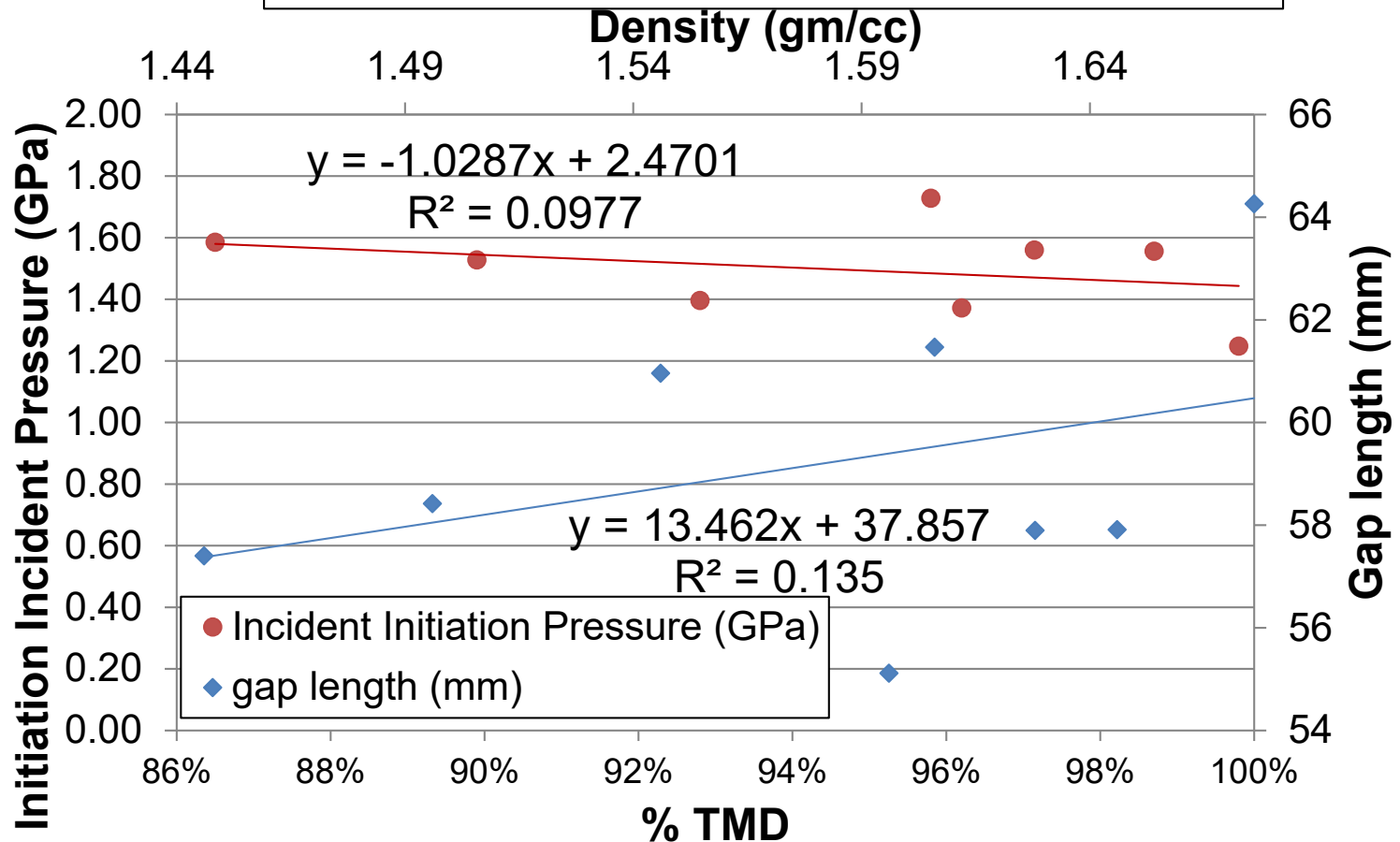
-Extended original correlation by D. Price (1966)

-Removed larger critical diameters and added more data



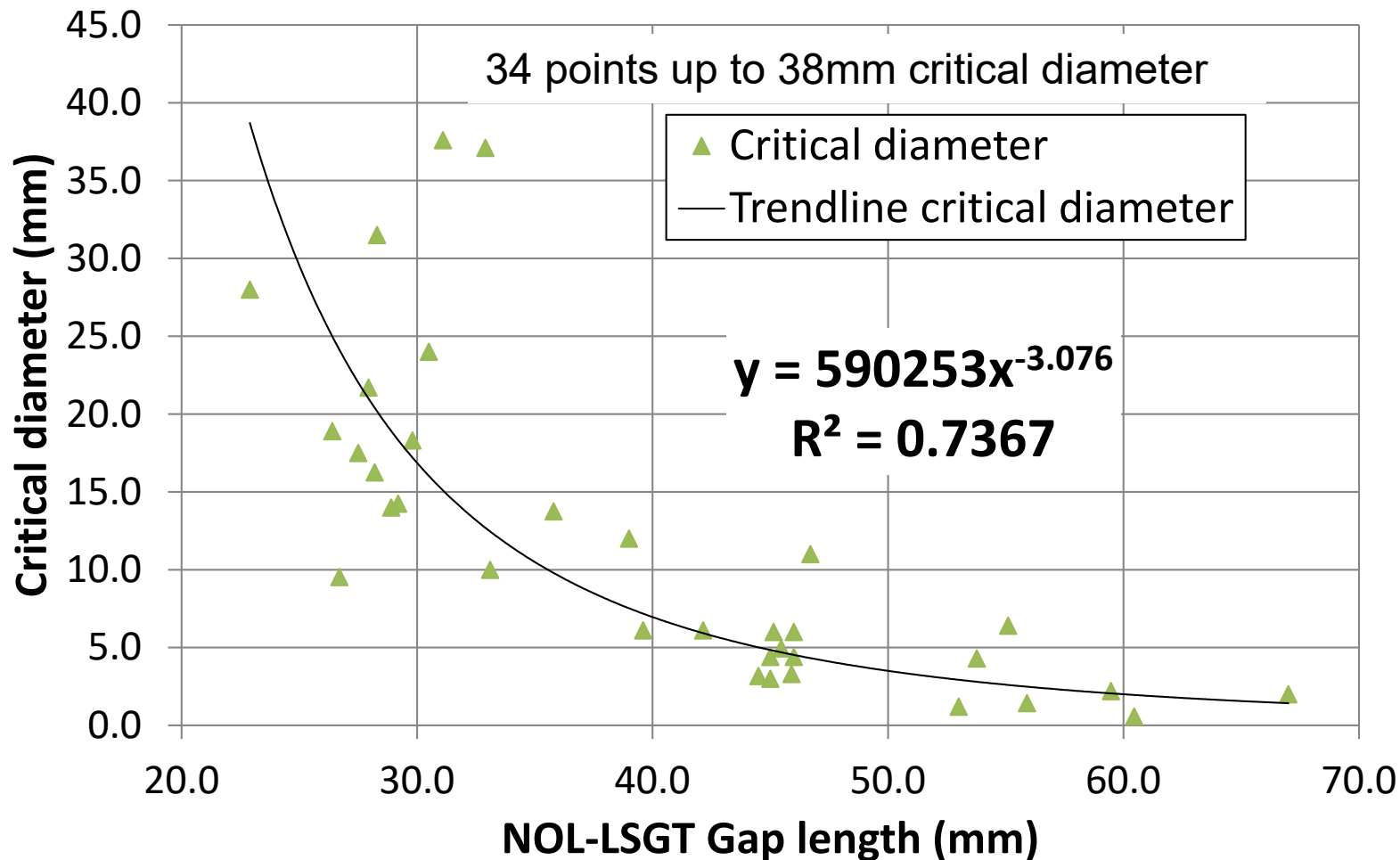
Donna Price, A. R. Clairmont, Jr., and J. O. Erkman, "The NOL Large Scale Gap Test III. Compilation of Unclassified Data and Supplementary Information for Interpretation of Results," Naval Ordnance Laboratory, White Oak, Maryland, United States, AD-780 429, Mar. 1974.

COMP-A3 NOL-LSGT Density Correlation Multiple Source



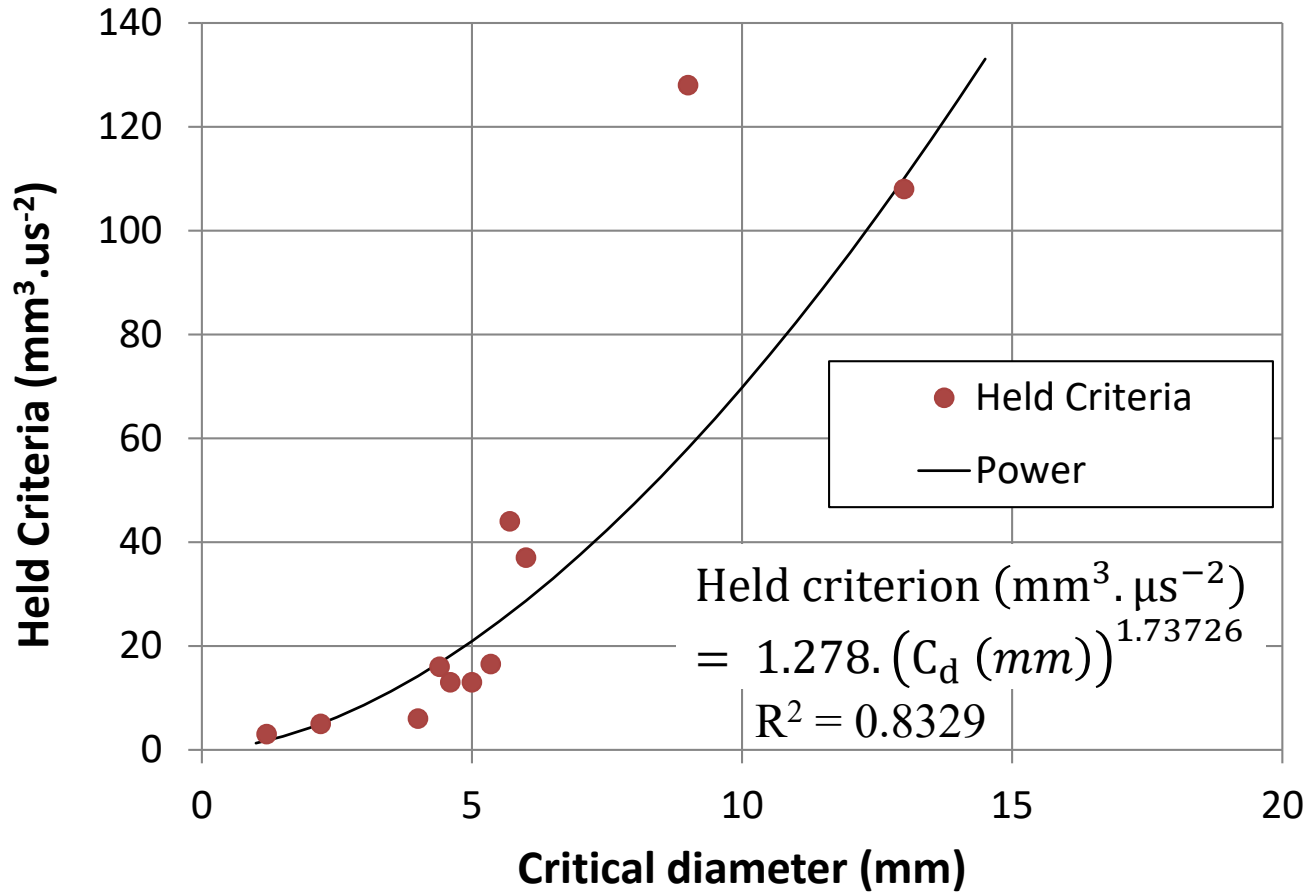
Ingredients and processing are very important!

- Study included CH-6, TNT, AP/Wax, PBX9404 and CompA-3
- More dense, less shock sensitive

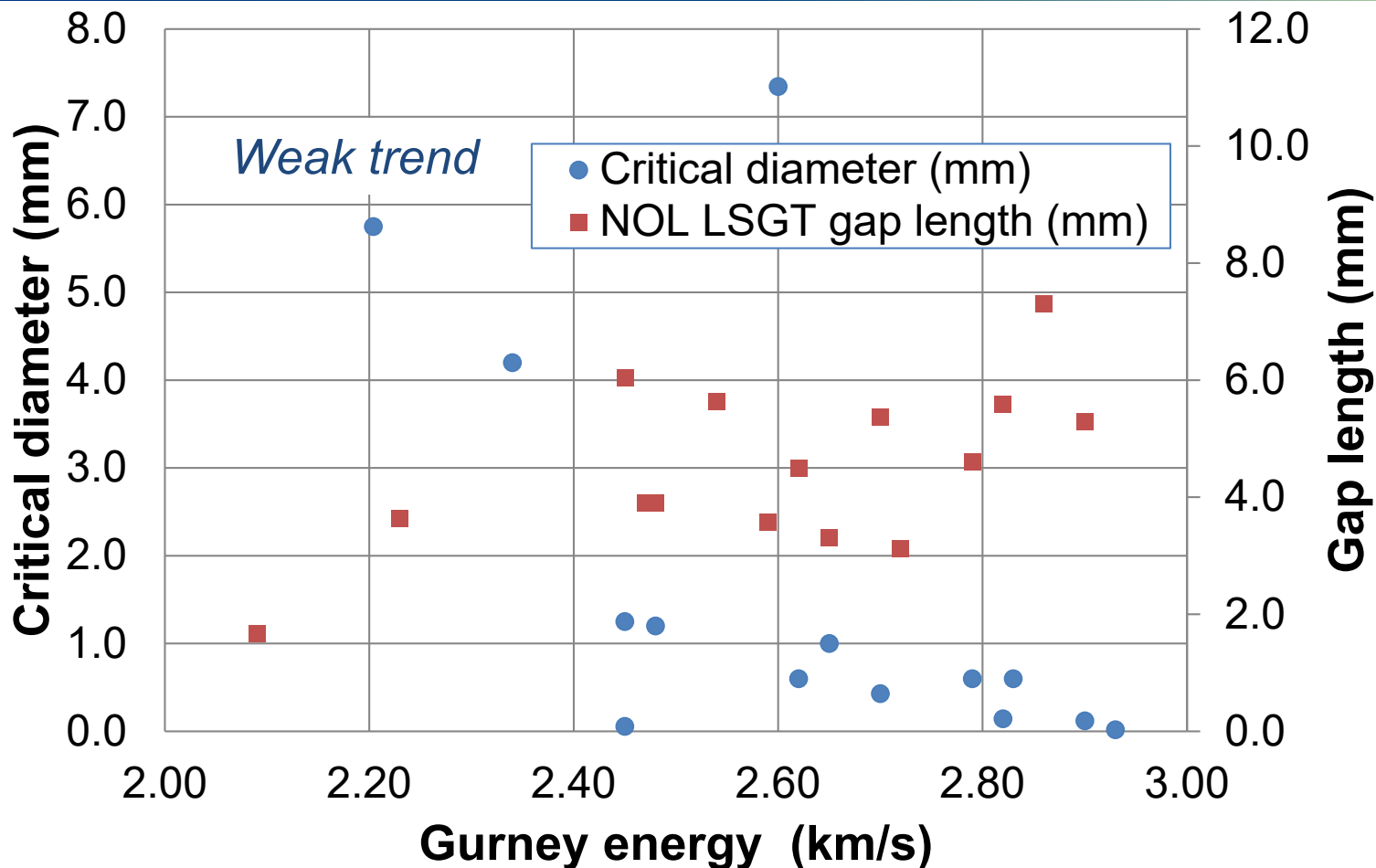


Not a fundamental physically based relationship!

- Low shock sensitivity and critical diameters have been observed
- Fine grained RDX explosives
- Higher performance reduced sensitivity rocket propellants



Data from 1.2mm to 13mm critical diameters



Also investigated LSGT to:
Rotter figure of Insensitiveness
Detonation velocity
Detonation pressure *No correlations!*

- Investigated laboratory test characteristics correlations
- Correlations:
 - NOL-SSGT to NOL-LSGT
 - NOL-LSGT to critical diameter
 - critical diameter to Held criteria
 - NOL-LSGT to density for a given explosive
- Weak correlation
 - NOL-LSGT to Gurney energy
- No Correlations:
 - NOL-LSGT to Rotter figure of Insensitiveness
 - NOL-LSGT to detonation velocity
 - NOL-LSGT to detonation pressure
- NEWGATES now includes correlations
 - NOL-SSGT to NOL-LSGT
 - NOL-LSGT to critical diameter

It is important to realize that these correlations only provide rough estimates, and should not be construed as accurate results!



Gun Launch and Setback Actuators

Ernest L. Baker and Michael W. Sharp

Munitions Safety Information Analysis Center (NATO), Brussels, Belgium

There is currently no agreed standard methodology for assessing the suitability of explosives for gun launch or for the determination of acceptance criteria for explosive fill defects. Laboratory setback activator testing has been used as an assessment tool for investigating the suitability of explosives for gun launch. Unfortunately, laboratory setback activator testing is not standardized and large variations exist in activator design, function and results between different laboratories. However, it is the only currently available tool for assessing an explosives safety and suitability to launch-induced setback forces. In laboratory setback activator tests, ignitions are observed at setback loadings that are much higher than produced in actual gun launched projectiles. This may be related to the defects in actual projectiles, which appear to be very different than the laboratory tests.

INTRODUCTION

A major safety concern for energetic materials present in gun launched munitions is the exposure to severe set-back forces which develop as the shell is accelerated. Table I presents a listing of typical projectile accelerations associated with different gun launches [1,2]. Under these conditions, energetic materials have been observed to occasionally react prematurely. The term in-bore premature is used for the explosion of a munition whilst it is still travelling down the barrel.

This is not a new phenomenon and a number of nations have developed laboratory setback actuator testing that can be used to understand ignition mechanisms for energetic material when exposed to an acceleration environment. However, these capabilities appear to be used mainly for research purposes and there is little evidence that they are mandated as part of a nation's formal qualification assessment process. None are included in NATO Standards on qualification of energetic materials.

TABLE I. PROJECTILE MAXIMUM ACCELERATIONS AND PRESSURES

Gun System	Max Projectile Acceleration Range (kGs)	Max Chamber Pressure Range (MPa)
Artillery	4-30	70-500
Mortars	1-13	20-140
Tank Guns	25-120	200-830
Medium Caliber	50-200	140-1400

MUNITION SAFETY ASSESSMENT PROCESS

The development of explosives requires a rigorous regimen of tests, both small-scale, and large-scale, before explosives can be judged safe and suitable for service use. NATO nations have agreed that all energetic materials be qualified in accordance with NATO STANAG 4170, with guidance provided in the associated AOP-7. Final or Type qualification is the process by which the safety and suitability of energetic material for its intended application and role are assessed. A

number of STANAGs have been developed to cover the specific requirements for artillery as part of the type qualification process, which includes STANAGs, 4667, 4493, 4224 and 4517.

However, the NATO Standards provide no guidance on how to set rejection criteria for defects. This is stated to be a role for the developing nation and the design authority. Projectile Safety criteria (STANAG 4224 Annex C) are that there should be no premature explosion or detonation in-bore or flight and further that there shall be no significant voids, crack etc. There is no guidance on the types of defect that may be present in the shell prior to firing. As a result, individual nations have made their own decisions on worst case allowable defects. For example, MIL-DTL-60377C, sets the allowable defect criteria for the M107 155mm projectiles using radiographic examination based on four segments as defined in figure 1. The basis for these maximum allowable defects sizes are largely unknown, and are believed to be based primarily on historical precedence. Whatever methodology was used for their definitions appears to be lost in antiquity.

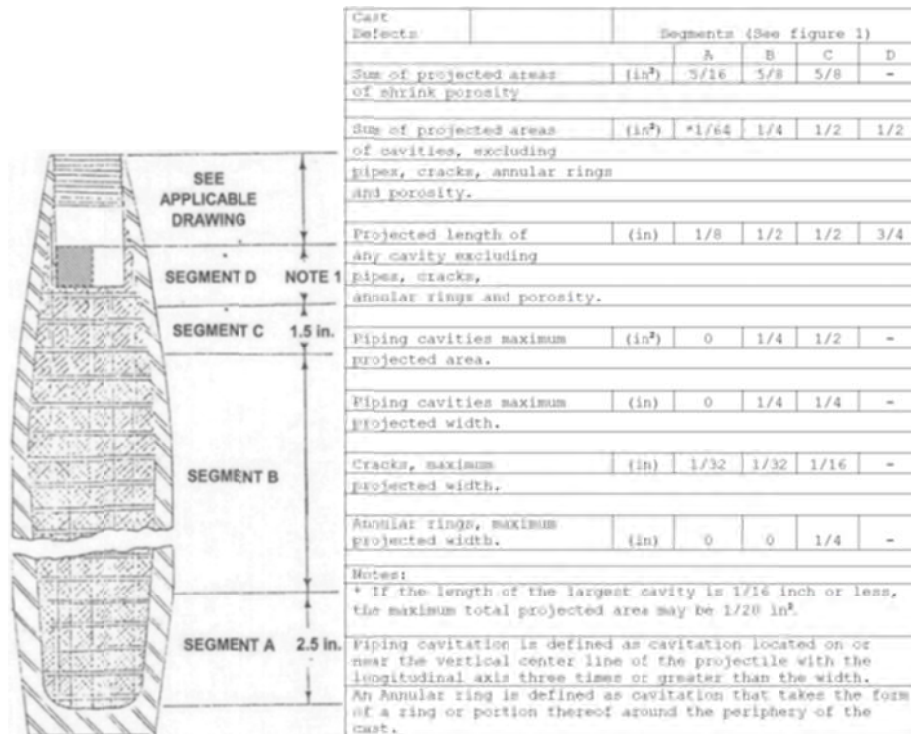


Figure 1. M107 inspection zones and maximum acceptable defect dimensions as defined by MIL-DTL-60377C.

GUN LAUNCH CONDITIONS

When a projectile is accelerated by a gun launch, the actual pressure history in the high explosive filling is considerably less than the pressure history delivered by the propellant gases to the projectile. This is because the explosive is loaded by the acceleration of the projectile, and not the by the propellant gases. During the acceleration of the projectile, the produced internal force is commonly called setback, as the acceleration produces a force in the negative direction of the projectile motion on the internal projectile components during the forward acceleration. As a result, the explosive will see an increased pressure from the forward explosive surface to the explosive supported base surface, which theoretically sees the highest pressure. The pressure at the supported base surface of the explosive is called the explosive base pressure. Often literature will simply state "explosive pressure", when referring to the explosive base pressure. It is relatively difficult to measure the explosive base pressure and almost no measurements of the

explosive base pressure during gun launch have actually been done. As a result, almost all studies of gun launch setback ignition rely on calculated explosive base pressures, which are commonly also called “theoretical” explosive base pressures. Rotational acceleration and associated body forces are also generated for rifled gun launch configurations.

Theoretical Explosive Base Pressures

The theoretical explosive pressure is generated by the acceleration of the projectile, and is calculated in the same manner as the pressure at any depth of a fluid. The theoretical pressure is simply, $P = \rho Gh$ where ρ is the explosive density, G is the acceleration, and h is the explosive column height. For the explosive base pressure, h is the full length of the explosive. So, the explosive pressure is zero at the forward explosive surface and increases proportionally with depth to a maximum at the explosive supported base surface. For 155mm artillery projectiles, typical theoretical maximum explosive base pressure is ~100 MPa, pressurization rate is 5 to 50 MPa/ms and durations on the order of 10 ms. Figure 2 presents calculated theoretical explosive base pressure histories for a 127mm and 155mm projectiles based on projectile base pressure histories.

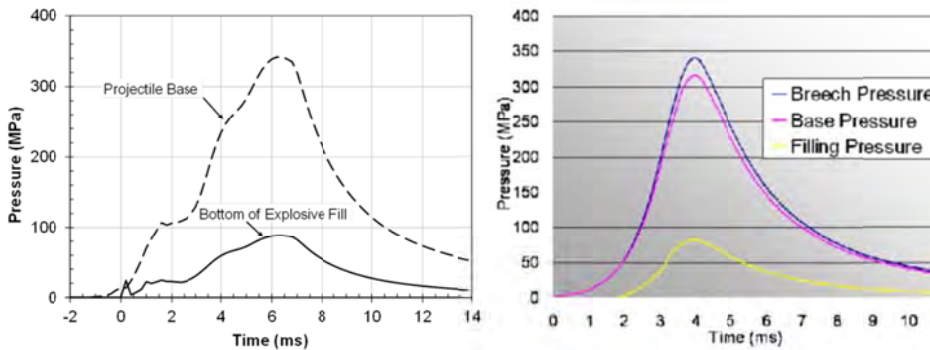


Figure 2. Calculated maximum explosive base pressure histories for 127mm projectile [3] (left) and 155mm projectile [4] (right).

For 120mm mortars, the typical theoretical maximum explosive base pressure is ~50 MPa, pressurization rate is ~18 MPa/ms and durations on the order of 10 ms. In general, the maximum explosive base pressures and rates of explosive pressurization of mortars are well below those of artillery projectiles. This provides some basis for much lower likelihood of ignitions for mortars as compared to 155mm projectiles, as it is believed that these parameters are strongly associated with explosive setback ignitions. Figure 3 presents calculated theoretical explosive base pressure history for a 120mm M62P3 mortar [5] based on projectile base pressure history [6].

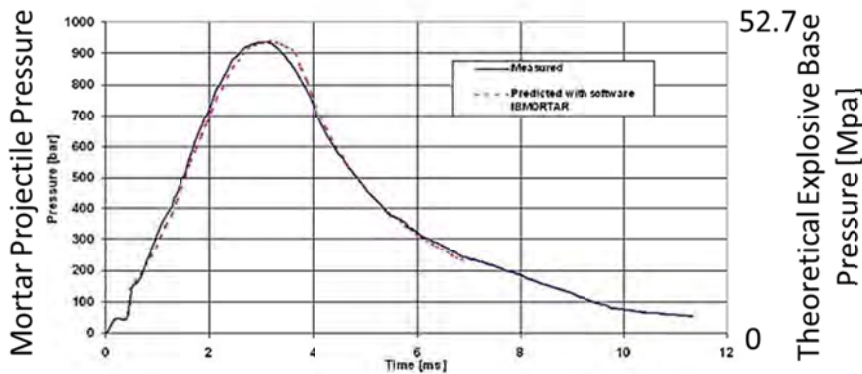


Figure 3: Calculated maximum explosive base pressure history for 120mm mortar.

Actual Explosive Base Pressures

Actual explosive base pressure history measurements were made by ARDEC personnel of the explosive pressure inside projectiles during launch [7]. Good fill castings had between 7% and 16% of the theoretical base pressure, whereas lubricated case good castings had between 10% and 20% of the theoretical base pressure. A conclusion from these tests was that large variations in stress distribution occur from shot to shot without any obvious cause. This ranges over a factor of three. No parameter external to the projectile would indicate this variation. Nominal setback explosive base pressure appears to be only a fraction of the theoretical explosive base pressure.

Projectile Acceleration Perturbations

Projectile acceleration perturbations can be caused by projectile balloting, erratic propellant burning and associated pressure waves during projectile launch. The yawing or wobbling motion of a projectile within a gun tube is an important consideration in internal ballistics and is known as balloting. This motion is a function of a number of small, difficult-to-measure parameters such as manufacturing tolerances, lack of concentricity of the engraving of the obturator, projectile and tube deformation, obturation of the propellant gases and obturator wear [8]. Unstable or erratic burning of the propelling charge may be an inherent characteristic of the charge caused by exceeding or failing to meet some critical value of a design parameter, or due to the failure of some component in the ignition train giving rise to an undesirable ignition mode [9,10]. The resulting projectile acceleration perturbations can potentially cause malfunctions to occur which include poor projectile launch, damage to the fuze mechanism, and perhaps even explosive fill ignition. There is some published information on projectile balloting, indicating that the resulting acceleration perturbations in the radial direction are commonly up to 5% of the maximum axial accelerations [11]. Actual axial acceleration perturbation levels produced by erratic burning or other pressure wave sources are commonly up to 10% of the maximum axial accelerations [11]. Figure 4 presents a 155mm projectile acceleration measurement [11].

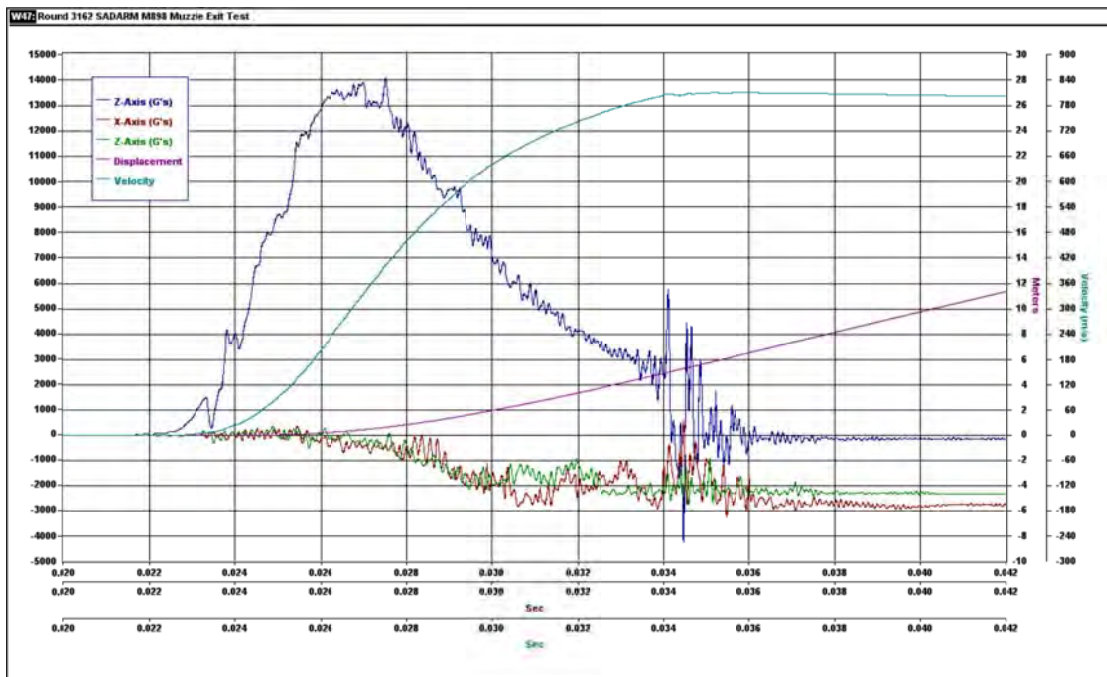


Figure 4. Acceleration, velocity and distance measurements during launch of a 155mm projectile [11].

There is little information on the occurrence of larger perturbations and how often this occurs. The investigation and effect of these larger potential acceleration perturbations on projectile explosive fills has received surprising little investigation.

DEFECTS

Defects are important because they act as sites for stress strain concentrations which can lead to localised heating, hot spot formation, and ignition. A review of literature, accident results and attributed potential causes in the MSIAC database indicates that gun launch candidate high explosives are unlikely to react without voids or interface defects to allow shear or adiabatic heating to drive the formation of hot spots [12,13,14,15]. To give an idea of the sort of defects that can be observed in artillery shell, a listing is given. It should be noted that where multiple defects occur, they may potentially act together.

Voids

Voids of 0.1-10 mm in diameter are common in cast cure and melt pour explosive fillings. Void collapse can cause a critical hot-spot to occur by viscoplastic work as the material around the void is rapidly deformed and adiabatic heating occurs as the gas inside the void is compressed. Evidence from set-back simulation work indicates that a combination of both processes may be required to develop a critical hot-spot. Analysis of voids requires a statistical treatment, with defined limits and rejection criteria, because of their role in determining probability of an ignition on gun launch. It is known that the more defects present the greater the probability of critical defect. A critical defect is defined as one which forms a hot spot and causes ignition.

Cracks

These are often observed in explosive fillings and can be caused by a number of factors. Shrinkage during processing, ageing or environmental stresses, rough handling etc. Cracks can lead to ignition through frictional processes or by generating site for adiabatic gas heating during cavity collapse. Figure 3 presents a photograph of a cross sectioned 155mm Comp-B cast projectile with observable cracks in the explosive fill.

Porosity

Any explosive charges can exhibit regions of porosity due to poor mixing or via chemical reaction or incompatibility. Formulations which do not meet the specification may also have increased porosities due to insufficient binder to filler ration. If present these porosities can act as sites of localised failure giving rise to viscoplastic deformation or adiabatic heating. Figure 5 presents a photograph of a cross sectioned 155mm Comp-B cast projectile with observable porosity in the explosive fill.

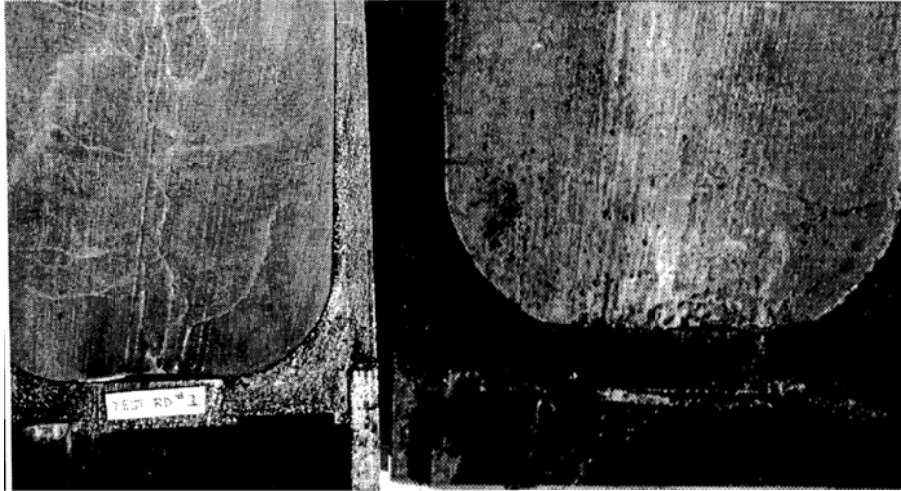


Figure 5. Photographs cross sectioned 155mm Comp-B cast projectiles with observable cracks (left) and porosity (right) in the explosive fill [16].

Cavities

Larger than voids, these are a consequence of poor fill quality. Deformation with viscoplastic work and frictional heating as the cavity breaks up are possible to form a critical hot-spot. These voids can take the form of long axially oriented voids known as piping that form in melt cast filled shells as a consequence of air entrainment during explosive pouring. Another form of observed cavity is a gap at the explosive and projectile body interface. This type of cavity often forms at the projectile base, and is commonly referred to as an explosive base gap.

Geometric Discontinuities and Foreign Material

Stepped cases or other complex geometries can produce high local stresses during gun launch. The presence of foreign material i.e. paint flecks, grit, screws, tools etc. These can act as sites for viscoplastic deformation, frictional heating, and shear.

EXISTING LABORATORY SETBACK TESTS

A variety of different laboratory setback activators have been developed with the objective of subjecting explosive samples to setback forces intended to replicate gun launch conditions. There have been two main approaches: 1) the use of gun propellant to drive a piston into the sample, or 2) developing loading conditions by modifying a pressure pulse derived from an alternative mechanical means such as a drop weight or gas gun. The key launch parameters that are attempted to be replicated are the peak pressure (P), pressurization rate (dP/dt), and pressure duration (t_p). To varying degrees, these parameters are tailored to match and over stress specific launch conditions for different gun systems and propellants. None of the laboratory setback activators include rotational acceleration. An extensive review of laboratory setback activators has been completed [17]. Figure 6 presents diagrams of some of the laboratory setback activators that were investigated. Two of the actuators are highlighted in this report, as they appear to produce loadings more similar to actual gun launch the others examined.

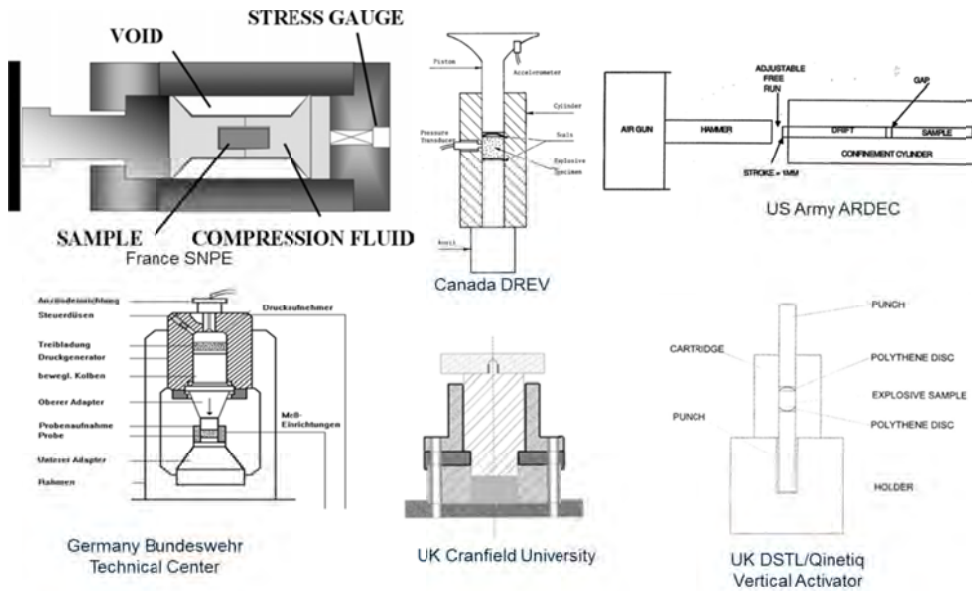


Figure 6. Setback laboratory activators.

US – NSWC-IHD

The US Navy Naval Surface Warfare Center Indian Head Division (NSWC-IHD) setback tester [18] consists of a small propellant bed that drives a hardened steel piston into an explosive sample that is strongly supported. The apparatus has a 25.4 mm diameter by 21.2 mm long sample in a thick-wall steel tube with a stationary anvil on one end and a piston on the other. Figure 7 presents a diagram of the NSWC-IHD setback testing and a plot of driver pressure histories that can be produced. The lowest pressure-time (p-t) loading rate is about 16 MPa/ms to a peak of 83 MPa. The highest loading rate has been 5.6 GPa/ms to a peak of 370 MPa. Driving pressure on the piston and sample pressure on the anvil are both measured by piezoelectric transducers. The 1X curve attempts to replicate the 127mm gun theoretical explosive base pressure history and does so very well. Typically 12.7 mm diameter cavities are introduced to the sample with depths being varied from about 3.2 to 6.3 mm. These cavities are much larger than any acceptable by production standards. Normally, loading rates of 2X or greater are required to observe any ignitions, which is considerably higher than theoretical and perhaps an order of magnitude larger than actual gun loadings.

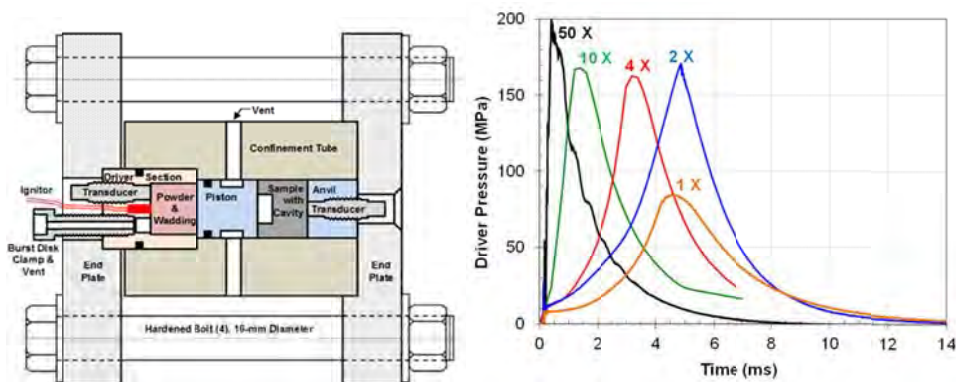


Figure 7. Diagram of the NSWC-IHD setback tester (left) and typical driver pressure histories that can be applied to the explosive sample (right).

UK – BAe Global Combat Systems

The BAe Global Combat Systems (BAE-GCS) Gun Launch Simulator (GLS) [4] is a laboratory setback activator that consists of a breech section, bursting disk and six identical symmetrically mounted test rigs. Each test rig consists of piston assembly that loads an explosive test sample (HE Pellet). The piston is driven by a central propellant charge which is ignited in the breech section. The burst disk is designed to allow pressure relief at a preselected peak pressure. The breech pressure history is recorded, but no pressure measurements are made at the explosive test sample. The GLS is designed to provide the explosive test samples with pressure loading similar to the axial pressure loading, a pressure time profile matched to gun launch and conditions representative of specific position in filling. Figure 8 presents a schematic of the BAE-GCS GLS and pressure time history plots from actual 155mm gun system firings and the GLS. The presented GLS peak pressure, pressurization rate and durations are very different. The GLS pressure history with the closest peak pressure to the presented 105mm result has about 1/4 of its rate and about 3 times its duration. The GLS pressure history with the closest peak pressure to the presented 155mm result has about twice its rate and about 1.5 times its duration. To our knowledge, the GLS results are the only laboratory setback actuator test results that have been reduced using statistical analysis [19]. The results have been presented for a single defect type (a small spherical air filled defect) as a probability of ignition for a given peak pressure, as well as probability of ignition versus spherical void size and peak pressure.

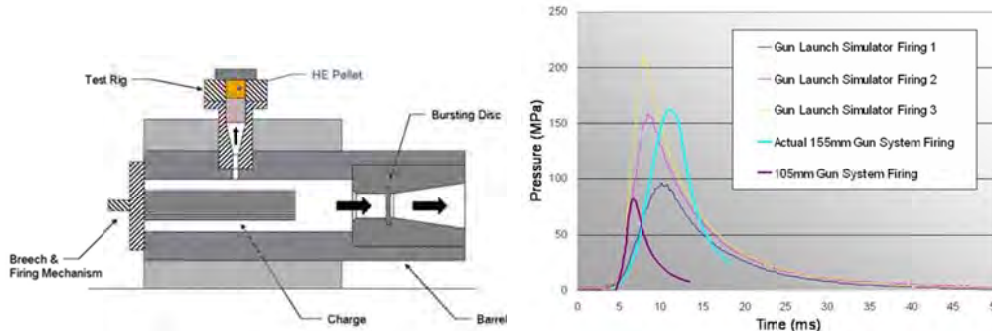


Figure 8. Schematic of the BAE-GCS GLS (left) and pressure loading plots (right).

LABORATORY SETBACK ACTUATOR IGNITIONS

There are two experimental facts that are firmly established. First, Bridgman [20] showed that explosive could be isothermally compressed to 5 GPa without ignition. Thus, slow compression to extremely high pressure and small pressurization rate (dP/dt) will not cause ignition of explosive. Second, Liddiard [21] showed that shock compression (<0.1 ms rise time) of pressed Comp-B would cause ignition at the 0.40 GPa pressure level ($dP/dt >4$ GPa/m). This establishes that the pressures and pressurization rates associated with setback accelerations are not capable of igniting pristine explosive fills. Other mechanisms associated with explosive fill defects are required.

The experimental evidence to date indicates that the ignitability and reaction violence of explosive samples in laboratory setback tests is governed by a number of factors. The processes may be the same as the processes leading to actual projectile premature ignitions, but there is little evidence linking the two. Specifically the observed factors that effect laboratory setback actuator test ignitions are: introduced defect, sample total run, peak pressure, pressurization rate, initial air gap thickness, air leakage, initial air pressure, piston thermal conductivity, and state of the explosive surface. Generally speaking, increased total run, peak pressure, pressurization rate, initial air gap thickness, and initial air pressure increase ignitability and reaction violence, whereas air leakage and high piston thermal conductivity tend to reduce ignitability and reaction violence [22,3]. For actual laboratory setback actuator testing, either air filled gaps or air filled

cavities are almost the only configurations used. For these configurations, three ignition sources appear to dominate: explosive extrusion and pinching, adiabatic air heating, and shear.

Explosive Extrusion and Pinching

This type of ignition is very common in earlier setback actuator tests and is sometimes observed in later testing as well. It consists of the unintentional ignition associated with sample holding geometry and materials. Due to fit configuration tolerance typically between a loading piston and cylinder, explosive can be extruded into the associated small gaps during loading and then subsequently pinched to cause ignition [23,24]. For pristine samples without introduced defects or gaps, it is believed that this is the dominant observed ignition phenomena. Various approaches have been used in order to eliminate or minimize the occurrences. The approaches include higher precision hardware with tighter tolerances [23, 6] or sealing the cylindrical surface by using plastic materials on the piston surface [25, 26]

Adiabatic Air Heating

This ignition mechanism is due to the air compression in introduced gaps or cavities. For smaller gaps and voids, it requires small (less than 50 μ m) energetic particles to be present [27]. This appears dominant for cast cure explosives, where energetic particles are ejected into the sample cavity as a result of the initial impact. Whether or not a collapsing defect ignites the sample depends on its size and rate at which it is collapsed, the ease of deformation, the condition of the cavity surface, and the filler particle size. The ability of a cavity surface to entrap or bind energetic crystals during its collapse, small crystal size, and a non-cracking binder all contribute to insensitiveness. The reaction of coarse energetic crystals ejected from the surface during the collapse of an air-filled cavity along with adiabatic heating from entrapped air appears to be the mechanism for deformable explosives [3]. This has been in part verified through vacuum experiments. The ignition threshold increases with evacuation of air from the cavity, which reduces heating but also back pressure which is required to achieve high burning rates. Additionally, coating of the cavity surfaces with binder materials has been shown to inhibit ignition. Internal cavities have been shown to ignite easier and produce much more violent responses than surface cavities of the same volume [28]. Possible reasons for this observation are reduced air leakage, increased pressurization durations and lack of heat transfer mechanisms.

Shear

This mechanism is associated with the mechanical deformation work causing heating, as well as the associated material damage and creation of fine debris. Strong hard explosives, such as most melt pour formulations, are heated by shear deformation. Fracture and mechanical failure of the sample creates debris, as well as additional surface area for increasing the reaction violence. For melt pour explosives, this mechanism appears to be coupled with adiabatic heating to cause ignition [3].

Friction

There is little information in the literature and it appears that only limited frictional laboratory setback actuator testing has been conducted. Taylor [12] demonstrated frictional ignitions in laboratory setback activator testing when sufficient large grit was present. However, no ignition were observed using the grit in standard primer paints. Frictional ignitions were produced only when high-melting-point grit was present at the sliding surface [12]. Bélanger [28] noted that the friction reaction depends upon (1) the explosive type and (2) the amount of friction which varies with surface roughness and the presence of hard inclusions. Such friction is found negligible on smooth surfaces for all explosives tested, except when hard inclusions are present. With hard inclusions, Composition A-3, CX-84A and Comp-B are highly sensitized, but TNT is not.

Accelerating Affects

Adiabatic compression model calculations predict the highest possible values of the explosive-air interface temperature. However, such calculations indicate that sufficiently high temperatures can only be produced at compression ratios higher than many at which ignition is observed [22]. In addition, at finite pressurization rates even lower temperatures are predicted and in no case can the experimentally observed ignitions be accounted for. The situation is further aggravated by the fact that air leakage in laboratory setback activators can render the environment even less hostile. Among the real world effects that may come into play are: enhanced energy transport due to turbulent air flow, rapid pressurization due increased air mass as a result of convergent flow, convergent air flow near the end of defect closures, dieseling, alternate gas, large exposed surface crystals, multiple defects and precompression [27,12].

IGNITION SENSITIVENESS VS. EXPLOSIVENESS

The susceptibility of explosives to premature ignition is often assessed by comparing their ignition thresholds in laboratory setback actuator tests to those of Comp-B and TNT. However, the issue is complicated by the fact that the explosiveness of the burning response is also a factor. Explosiveness has been defined as the reaction violence that is normally characterized by the degree of damage that occurs to the test fixture. It has been speculated that the infrequency of reported prematures with TNT may be due to its relatively slow burning response rather than a lower ignitability. This would lead to the premature explosion occurring down range rather than in the gun tube for which there is anecdotal evidence. If this is the case, the sensitiveness assessment is more difficult as both ignitability and explosiveness must be considered. There is a noted trend in results to exhibit some tendency toward an increase in reaction violence with decreasing ignition sensitiveness [28].

There are significant discrepancies in the literature related to the ignitability and explosiveness of TNT compared to Composition-B. Taylor [12] conducted planar gap tests that show TNT is somewhat more ignitable than comp-B. Sandusky [3] noted that unlike TNT, the initial sealing of cavities made Comp-B much more ignitable. Sandusky [3] also noted that Comp-B exhibits one of the highest sensitiveness levels and responds violently. Starkenberg [27] states that the data for TNT provide no reason to believe that it is less sensitive to ignition than Comp-B. For friction ignition studies, Bélanger [28] found that Comp-B was highly sensitized by the addition of hard inclusion, whereas TNT was not. Meyers [29] had less consistency, but the explosive responses showed extensive burning for TNT, and explosions for Comp-B.

Comp A3 Type II was the least sensitive explosive tested by Starkenberg [27]. It exhibited a moderately high level of response violence. LX-14 exhibited a sensitiveness intermediate between those of Comp-B and Comp A-3 Type 11 and reacts very violently. PBXW-113, was by far the most sensitive. Late ignitions were observed in LX-14 that occurred on the second strike of the driving. Sandusky [3] noted that ignition of cast-cure samples was always delayed with respect to cavity collapse, often several milliseconds after maximum pressure. He observed delays as long as 24 ms when the driver pressure was fully vented. He noted extensive burning for TNT, explosions for Comp-B, mild reactions for cast-cure PBXs, and little decomposition for TATB-based explosives.

FORMULATION FOR REDUCED PREMATURES

The path toward more premature-resistant explosives is not clear. Velicky has suggested that an explosive's mechanical strength should be increased to reduce the probability of collapse of casting flaws [30]. However, it seems likely that this will have little effect on cavities large enough

to present a problem since the launch acceleration environment appears to produce stresses well above those required to collapse larger cavities. Because of the importance of the gas pressurization rate, increasing mechanical strength might even have a negative effect. Delaying cavity collapse until higher stress levels have been reached could increase the pressurization rate. Cavities in a softened material, meanwhile, might collapse slowly during the very early portion of launch, thus resisting ignition. On the other hand, they might better trap hot air, thus promoting ignition. In the latter case, the low ignited surface area can be expected to yield low initial reaction rates which may sufficiently delay any violent response. Approaches which reduce the incidence of flaws in explosive fills, reduce the ignitability of the explosive or retard the burning response of the explosive are, of course, desirable. Because of the complexity of the issues involved, characterization of explosives through testing is the only available approach to discovering premature resistant formulations [29].

CONCLUSIONS AND DISCUSSION

Observations indicate that actual gun launch setback ignitions cannot be clearly correlated with the results of ignition sensitiveness results from laboratory setback activator tests. The laboratory setback activator tests normally indicate ignitions at much higher setback than are believed to be produced in actual gun launched projectiles. Additionally, the defects in actual projectiles appear to be very different than the laboratory tests. Both ignitability and explosiveness should be considered in assessing an explosive's resistance to launch-induced explosion. For this reason, some explosives are not rejected on the basis of exhibiting high ignition sensitiveness in the activators unless the reaction violence levels are also high. In the controversy between brittle and soft explosives, ignition sensitiveness results are biased towards the strong brittle materials, often observed for melt pour explosives. In spite of all this, the activator, remains the currently only available tool for assessing an explosives resistance to launch-induced premature explosions and it is recommended that the munitions community should work toward developing an understanding of the ignition phenomena and laboratory setback activator technology as part of a process development for defining physically based acceptable defect criteria.

REFERENCES

1. Stiefel, L., Gun Propulsion Technology, Chapter 3, Progress in Astronautics and Aeronautics Book 109, Amer Inst of Aeronautics, ISBN-10: 0930403207, April 1988.
2. Carlucci, D., Personal Communication, U.S. Army ARDEC, Picatinny Arsenal, NJ, 7 JUL 2016.
3. Sandusky, H.W., Granholm, R.H. and Felts, J.E., "Survivability of Explosives with Dynamically Collapsing Cavities", 15th Detonation Symposium (International), San Francisco, CA, 13-18 July 2014.
4. Hollands, R., "Minimising Risk Throughout The Life Cycle of Tube Launched Munitions", Land Munitions Solutions 2009, Prague, Czech Republic, 3-5 November 2009.
5. Röpcke, J., <https://twitter.com/hashtag/m62p3>, 20 Apr 2015.
6. Odjeljenje za odbrambene tehnologije, <http://www.dtd.ba/index.php/istrazivanje/software/interior-ballistics>, 2016.
7. Collett, R.W., "Measurement of In-Bore Set-Back Pressure on Projectile Warheads Using Hard-Wire Telemetry", 19th International Telemetry Conference, San Diego, CA, 24-27 October 1983.
8. Ansari, K.A. and Baugh, J.W., "Dynamics of a Balloting Projectile in a Moving Gun Tube", Contract Report BRL-CR-605, US Army Ballistic Research Laboratory, AD-A205540, 1985.
9. Gerri, N.J., "A Parametric Study of Gas Flow and Flame Spreading in Packed Beds of Ball Propellant Part I.", Report BRL-R-1988, US Army Ballistic Research Laboratory, AD-A041417, 1988.

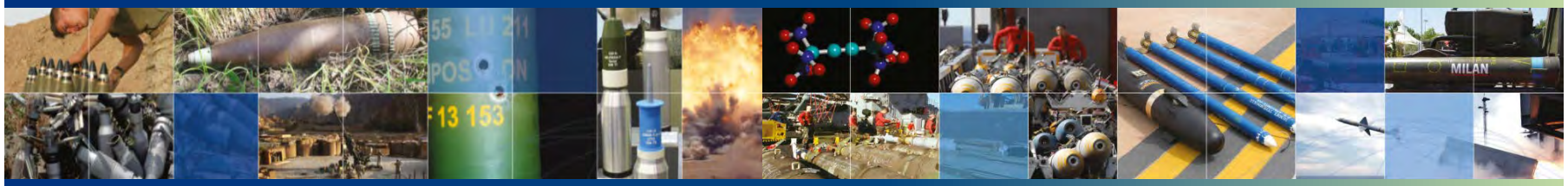
10. Kuo, K.K. and Coates, G.R., "Review of Dynamic Burning of Solid Propellants in Gun and Rocket Propulsion Systems", Symposium (International) on Combustion, Volume 16, Issue 1, 1977.
11. Cordes, J.A. et al., "Dynamics of a Simplified 155-mm Projectile", Proceedings of the 21st International Symposium on Ballistics, vol. 2, pp. 1164–1170, Adelaide, Australia, 2004.
12. Taylor, B.C, Starkenberg, J. and Ervin, L.H., "An Experimental Investigation of Composition-B Ignition under Artillery Setback Conditions", Technical Report ARBRL-TR-02276, AD A095348, US Army Ballistic Research Laboratory, December 1980.
13. Bélanger, C. "Study of Explosive Shell Fillings with Defects in Simulated Gun Launch Conditions," The Ninth Symposium (International) on Detonation, Portland, Oregon, August 28-September 1, 1989.
14. Cartwright, M. and Delany, P., "An Investigation into Set back Force simulation in Composition B fillings subjected to Hot Gun Scenarios", 8th Australian Ordnance Symposium (PARARI 2007), Melbourne, NSW, Australia, 13-15 November 2007.
15. Lécume, S., Lefrancois, A. and Chabin, P., "Structural and Chemical Changes in PBX induced by Rapid Shear followed by Compression", 12th Detonation Symposium (International), San Diego, CA, August 2002.
16. Fishburn, B., "Setback Safety Testing at ARDEC", JANNAF Propulsion Systems Hazards Subcommittee Meeting (1997), Volume 1, West Palm Beach, FL, 27-30 October 1997.
17. Baker, E., "Use of Laboratory Setback Activator Tests to Assess Suitability for Gun Launch", NATO MSIAC Report L-212, 18 January 2017.
18. Sandusky, H.W. and Granholm, R.H., "Violent Reaction from Non-Shock Stimuli", Shock Compression of Condensed Matter, CP955, 2007.
19. Boyd, M., "Realisation of the UK IM Strategy for Tube Launched Applications ", European IM Day, Bussels, Belgium, 29 May 2009.
20. Bridgman, P.W., "The Effect of High Mechanical Stress on Certain Solid Explosives", J. Chem. Phys. 15, 311 (1947).
21. Liddiard, T.P., "The Initiation of Burning in High Explosive by Shock Waves", Fourth Symposium on Detonation, October 1965, pp.487-498.
22. Starkenberg, J., "Analytical Models for the Compressive Heating Ignition of High Explosives", Ballistics Research Laboratory Technical Report ARBRL-TR-02225, March 1980.
23. Taylor, B.C, and Ervin, L.H., "Mode of Ignition in the Picatinny Arsenal Activator (Artillery Setback Simulator)", Proceedings of the Conference on the Standardization of Safety and Performance Tests for Energetic Materials, Vol 1, 1977, pp. 481-494.
24. DeVost, V.F. and Coffey, C.S., "The Premature Susceptibility of Defective Main Charge Loads," NSWC TR 81249, Nov. 1981.
25. Bélanger, C., "A Testing Method to Evaluate Explosiveness," Proceedings of Tenth Int'l. Detonation Symposium, ONR 33395-12, Office of Naval Research, 1993, pp. 305-319.
26. Featherstone, L.W. and Gower, R.A., "Vertical Activator: Modifications & Summary of Results to Date", DRA/DWS/WX4/WP96730/1.0, Defense Evaluation and Research Agency, Farborough, Hampshire, November 1996.
27. Starkenberg, J. et al., "Sensitivity of Several Explosives to Ignition in the Launch Environment," Proceedings of Ninth Symposium (Int'l.) on Detonation, OCNR 113291-7, Office of the Chief of Naval Research, 1989, pp. 1460-1472.
28. Bélanger, C., Demers, C. and Beaupré, "Study of Explosive Shell Filling Defects as causes of Prematures in Setback Environment", Defence Research Establishment, Valcartier, DREV Report 4778/94, September 1994.
29. Meyers, T. F. and Hershkowitz, J., "The Effect of Base Gaps on Setback-Shock Sensitivities of Cast Composition B and TNT as Determined by the NSWC Setback-Shock Simulator," Proceedings of Seventh Symposium (Int'l.) on Detonation, NSWC MP 82-334, Naval Surface Warfare Center, 1982, pp. 914-923.
30. Velicky, R.W., Voigt, H.W. and Voreck, W.E., "The effect of some additives on the closed bomb burning and ignitability of RDX/TNT (60/40)", Journal of Energetic Materials, Volume 3, Issue 2, pg. 129-148, 1985.



MSIAC

Munitions Safety Information Analysis Center

Supporting Member Nations in the Enhancement of their Munitions Life Cycle Safety



GUN LAUNCH SETBACK AND LABORATORY ACTIVATOR TESTS

Dr. Ernest L. Baker

Warheads Technology TSO

+32 (0)2 707 3844

e.baker@msiac.nato.int

IMEMTS 2018
Portland, OR, USA



- Background
- Energetic Material Qualification
- Projectile Gun Firing Qualification
- Laboratory Setback Actuators
- Actuator Ignition Physics
- Conclusions and Recommendations

- **Objective:**
 - Assess setback activator technology (2016) and gun launch ignition (2017). Inform on the need to develop a NATO standardized approach to proving the suitability of energetic materials for gun launch.
- **Issue:**
 - Need to assess new energetic materials for which there is little knowledge base and experience
 - Provide supplementary data for complex artillery
 - Allowing reduced the reliance on costly all-up-round level tests while maintaining confidence



- EM Qualification: STANAG 4170 – Principles and Methodology for the Qualification of Explosive Materials for Military Use
 - Chemical, Physical and Mechanical Properties
 - Sensitivity/Sensitiveness/Explosiveness
 - Performance Assessment

- Intrinsic hazard properties with respect to impact and friction
 - Some use for ranking
- Shock
 - Time scale is much shorter than gun launch
- Confined Burning
 - Not representative of dynamic confinement of gun launch
 - (note: under 15,000G the fuze has 15,000 times equivalent mass)
- Mechanical properties not measured at appropriate strain rates (10^3 - 10^4 s⁻¹) or pressures (up to 160 Mpa)

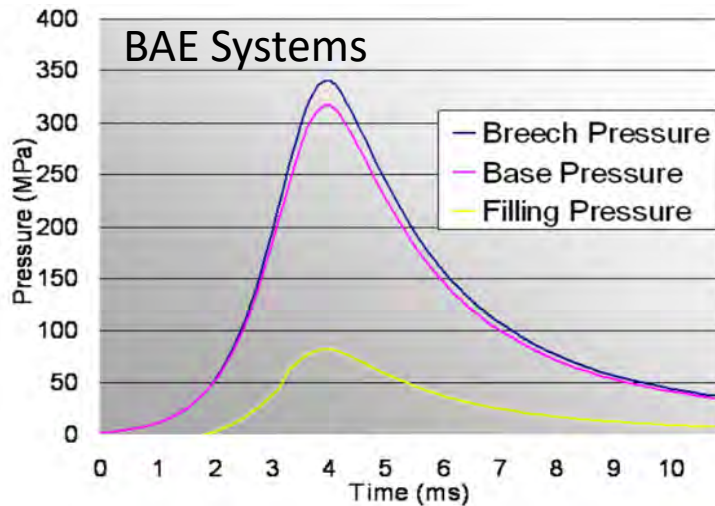
- Testing of mechanical properties at appropriate strain rates.
- Methodology needed to develop an understanding of behaviour of energetic material under gun launch conditions, which would facilitate answering the following questions:
 - How the energetic material respond to gun launch set-back and centripetal forces (for rifled ammunition)?
 - Does apparently pristine energetic material (with defects less than approximately 100 μ m) react under gun launch conditions (what is the probability and is it acceptable)?
 - What are the characteristics of critical defects and what is the probability of one being formed under gun launch conditions?
 - What is the probability of a critical defect being present in the energetic material destined for artillery?
 - How do we set rejection criteria?

- STANAG 4224 Large Calibre Artillery and Naval Gun Ammunition Greater than 40mm
- With respect to Energetic Material exposure to setback:
- Projectile Safety (Annex C)
 - Preliminary evidence to assess whether a projectile is prone to premature detonation; 120 or 60 split between firing at UFT or LFT
- Sequential Environmental Test: To determine the safety and suitability for service of ammunition subjected to environmental conditions representative of service use
 - 120 rounds fired after sequential environmental exposure
- In reality rounds fired in qualification may be as little as around 240 compared to 100,000s during artillery program lifecycle. It is statistically insignificant.

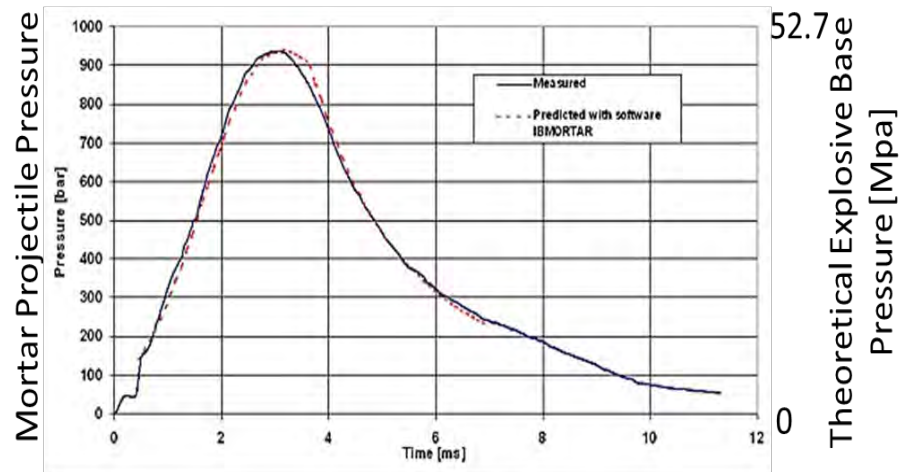
- Obviously, if there is an in-bore premature!
- “There shall be no significant voids, cracks, HE dust, bonding failures or other unacceptable features in the condition of the projectile, and, where appropriate, the sub-munition filling. Where there is evidence of voids, cracks, bonding failure, or other unacceptable features, the significance of these shall be explained by the developing nation.”
- No guidance on how to set rejection criteria for defects
 - Role for the developing nation and the design authority

- The pressure that an explosive fill or component is exposed to is determined by the acceleration of the shell and increases linearly in an energetic component from the top of the charge (nose of the projectile) towards the base.
- The theoretical pressure in the explosive charge can be calculated at any point from the shell acceleration:

$$\text{Pressure} = \text{Density} \times \text{Depth in fill} \times \text{Acceleration}$$

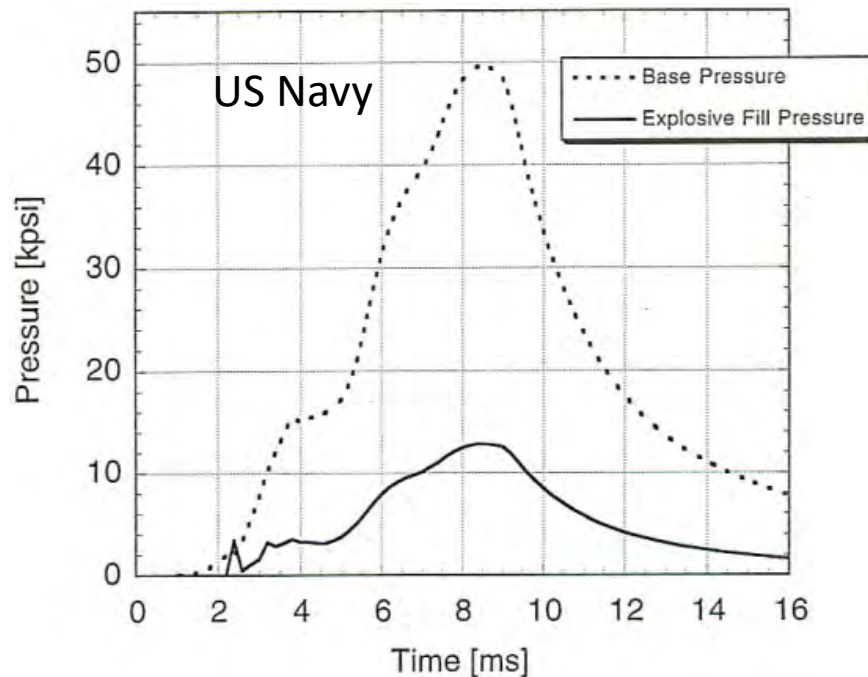


105mm artillery
calculated filling pressure



120mm mortar
calculated filling pressure

- From available data, actual explosive filling compressive loads are significantly less than theoretical explosive filling compressive loads
- Limited gun launch filling pressure measurements by ARDEC
 - Good fill castings between **7% and 16%** of the theoretical pressure
 - Lubricated case good castings between **10% and 20%**
 - Bad fill castings between **24% and 66%**



123mm Artillery
calculated filling pressure

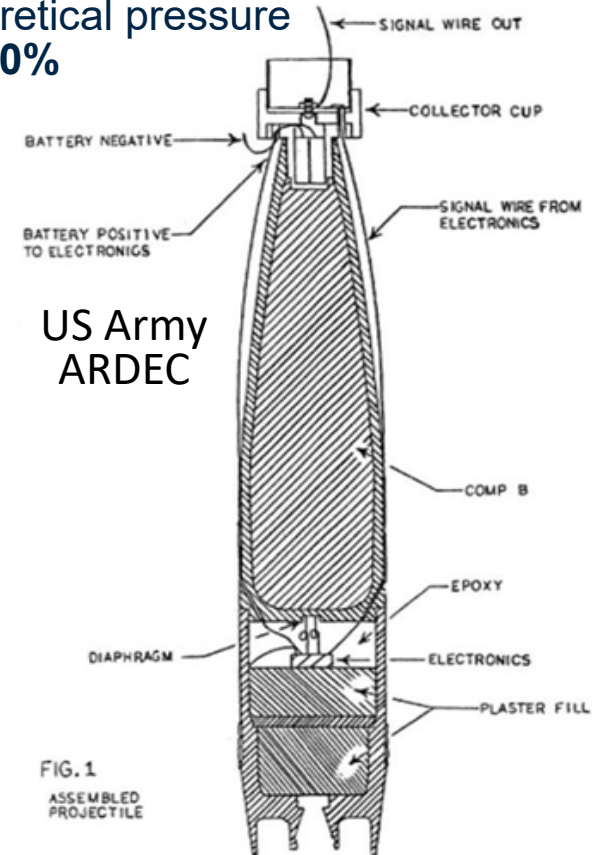
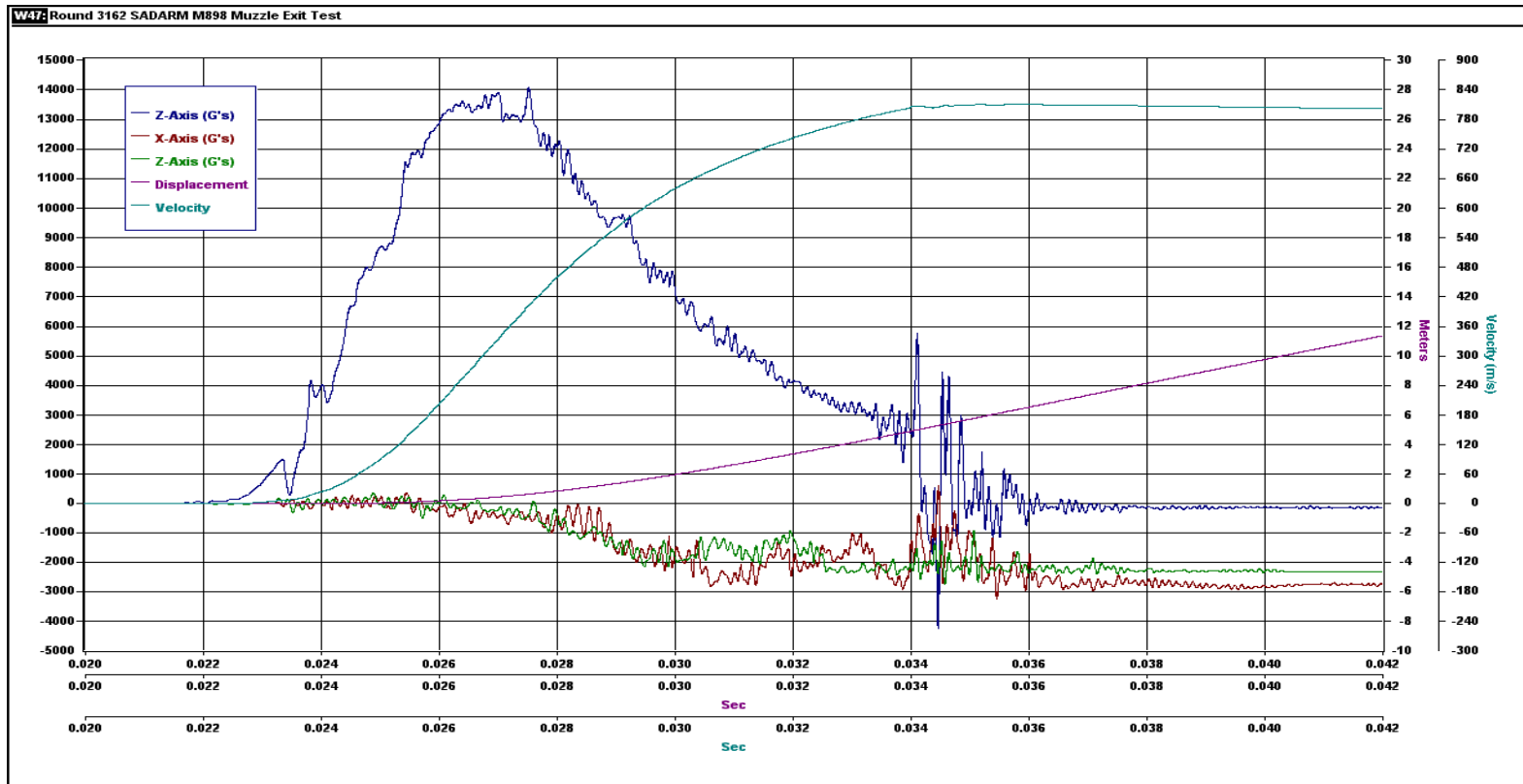


FIG. 1
ASSEMBLED PROJECTILE

155mm explosive filling
pressure measurement

- Projectile balloting: commonly radial accelerations up to 5% of axial
- Axial acceleration perturbations: commonly up to 10%
- How much larger and how often do these perturbations occur?



155mm projectile acceleration, velocity and distance measurements during launch

Cordes, J.A. et al., "Dynamics of a Simplified 155-mm Projectile", Proceedings of the 21st International Symposium on Ballistics, vol. 2, pp. 1164–1170, Adelaide, Australia, 2004.

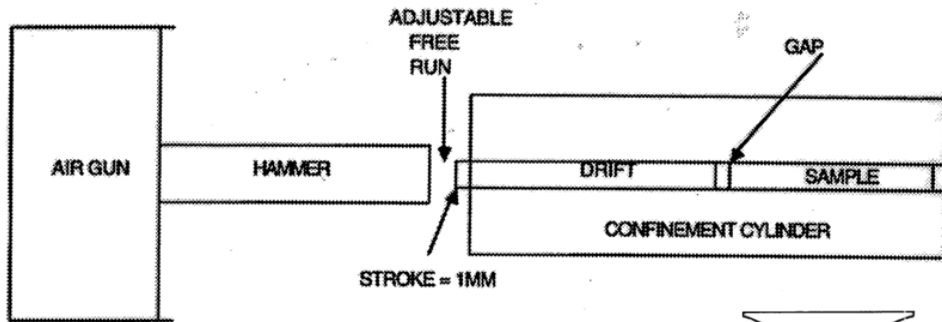
- Defects are important because they act as sites for stress strain concentrations which can lead to localised heating, hot spot formation, and ignition.
 - friction; adiabatic shear; viscoplastic work and if voids are present, adiabatic gas heating during cavity collapse and jetting.
- Defects can be EM Bulk or Interfacial, examples include:
 - Voids, Cavities, Cracks, Porosity, Foreign Material
 - Base Gaps, Shell Body roughness



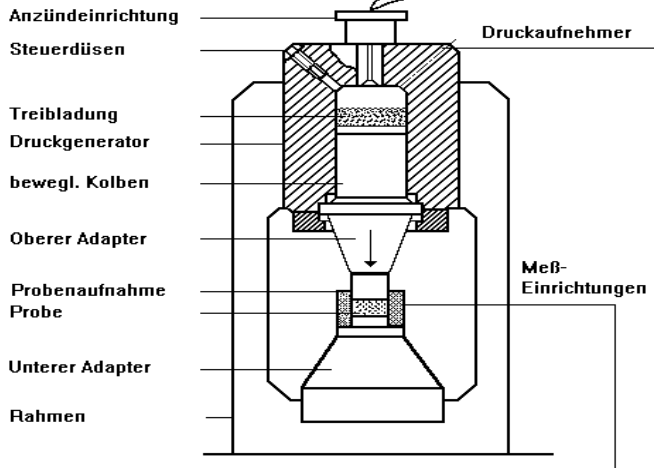
155mm Comp-B cast projectiles with porosity (left) and cracks (right)

- A setback actuator test is a small scale test that involves exposing energetic material to setback forces similar to those experienced in an artillery round on gun launch.
- Techniques described in the 2016 paper generally apply a compressive load to a pellet of explosive via a piston and the response is observed as a go or no go reaction.
- The compressive load can be varied to try and mimic different gun systems and artillery types and calibres.
 - P_{max}
 - dP/dt
 - Duration

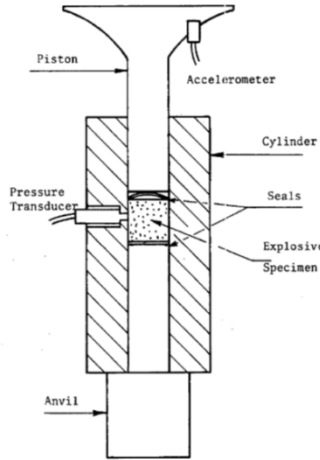
- 3 methods described for developing the initial pressure:
 - drop weight
 - gas gun
 - via gun propellant combustion
- Some advantages and disadvantages of each technique
 - Explosive extrusion and pinching is a common issue
 - Control and vary dP/dt , P_{max} and duration
- This can be complex.
 - For drop weight and gas gun driven pistons, the pressure pulse is tailored using intermediate conditioning materials.
 - For propellant driven systems, pressure release is required to tailor the pressure pulse
 - Requirement to measure driving pressure and sample pressures
 - An area for collaboration?



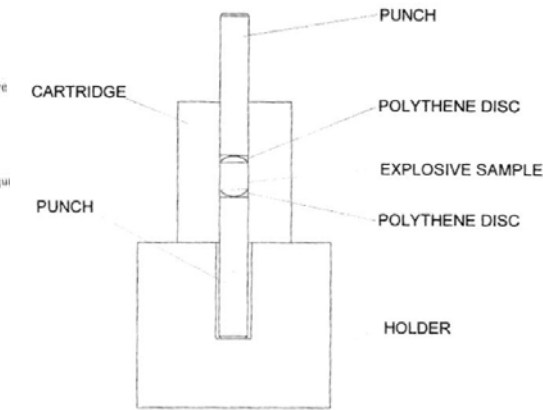
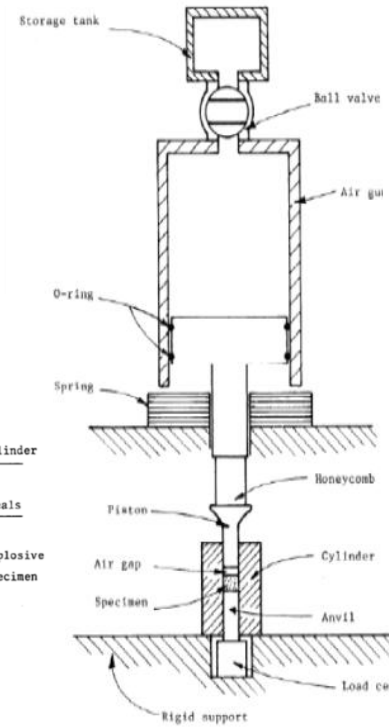
**ARDEC
Setback Tester**



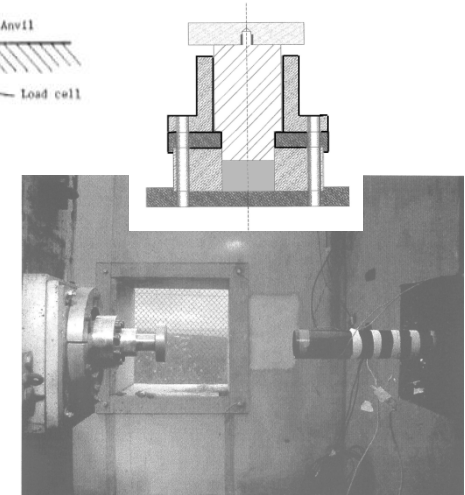
WTD 91



DREV Setback Simulator

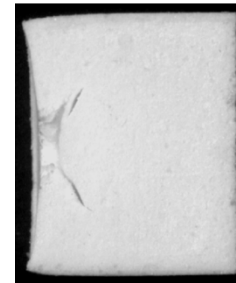
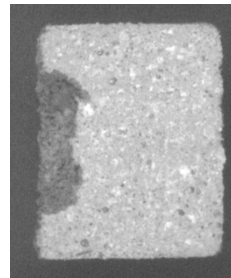


**DSTL/QinetiQ
Vertical Activator**

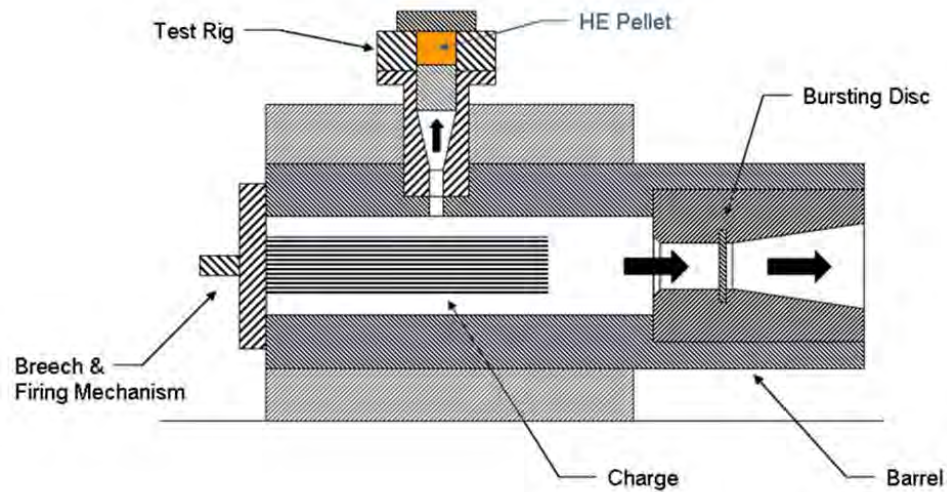


**Cranfield University
COTEC Setback Simulator**

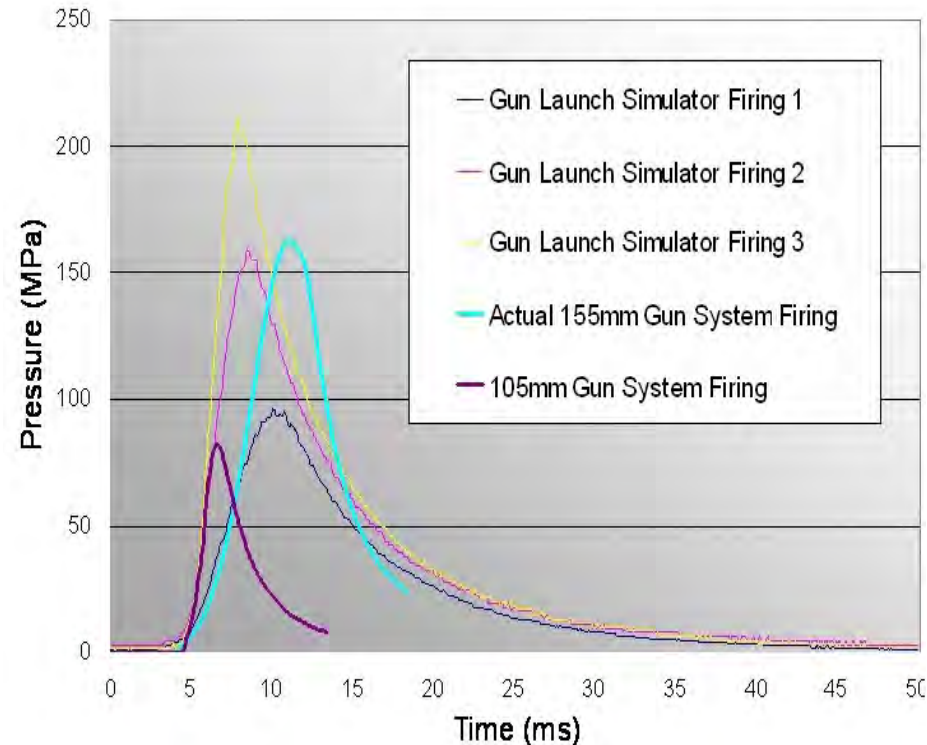
- Manufacture and characterize pellets (2-4cm diameter) that include cavities
- Match the pressure history to in-service condition and then vary peak pressure.
- Increase pressure to achieve go reactions
 - Optimize the generation of data based on the results obtained (e.g. Bruceton Test, Langlie Test, Neyer D-Optimal)
 - Characterize variability.
 - mean and standard deviation and probability distribution.



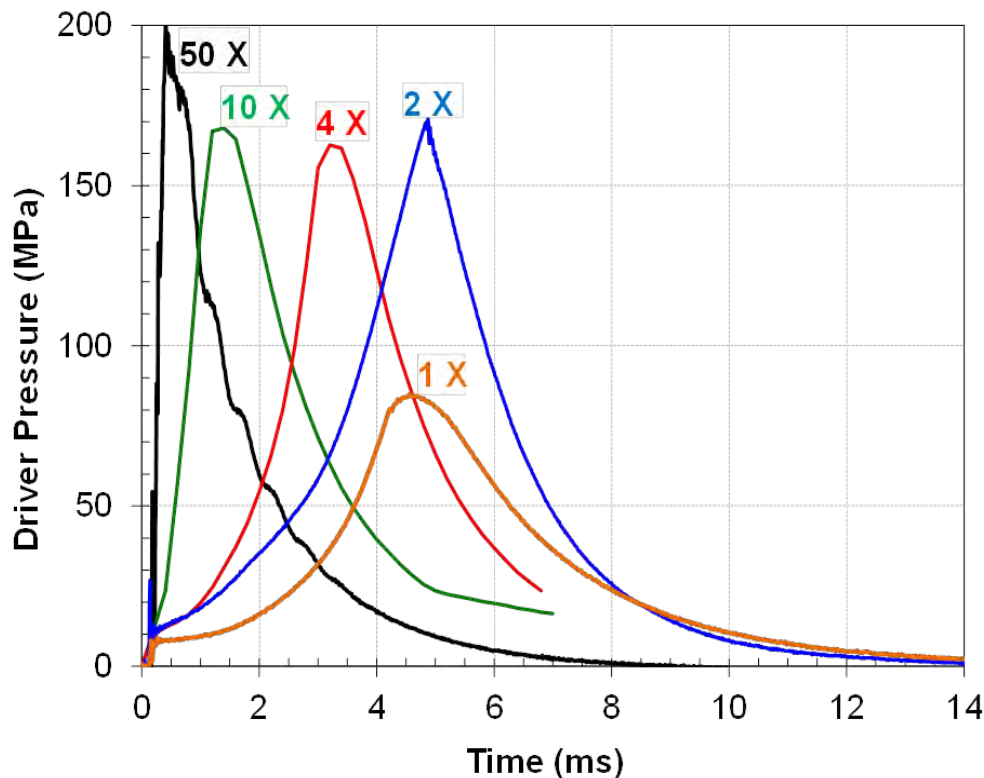
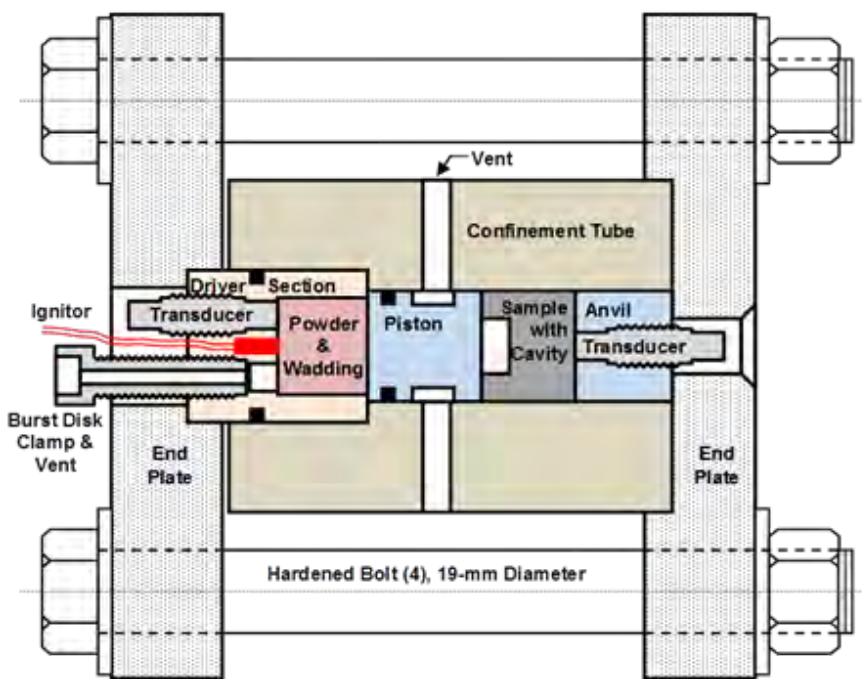
- The pressure history with the closest peak pressure to the 105mm has about 1/4 of it's rate and about 3 times it's duration.
- The pressure history with the closest peak pressure to the 155mm has about twice it's rate and about 1.5 times it's duration.



BAE-GCS
Gun Launch Simulator



- Of the reviewed laboratory activator data produced pressure histories, only the NSWC-IH test appeared to match the theoretical in-service condition.
- Typical “go” reactions occur at 2X or 4X conditions



- For Setback Activator testing three ignition sources appear to dominate
 - Explosive extrusion and pinching: common unintentional ignition associated with sample holding geometry and materials (various approaches to eliminate or minimize the occurrence)
 - Adiabatic air heating: requires small (less than 50um) energetic particles to be present. Appears dominant for cast cure explosives, where small energetic particles are ejected into the sample cavity as a result of the initial impact.
 - Shear: mechanical deformation and the associated material damage. For melt pour (strong) explosives, this mechanism appears to be coupled with adiabatic heating to cause ignition.
- How do these mechanisms compare to real gun launch ignition?
 - Inspection to eliminate gaps, voids and cracks in the lower zones
 - Projectile acceleration perturbations
 - balloting, erratic burning and associated pressure waves
 - how large and how often?
- There is little data providing evidence that setback activator ignitions correlate to real gun launch ignitions

Reviewing the tests indicates some common issues or areas for potential collaboration or standardization:

- Means to develop compressive load which can be varied and simulates the gun launch environment.
- Sampling; relationship to production and sample population size (linked to analysis)
- Defect analysis; energetic material and interface defect analysis.
- Many past activators have had issues with ignition due to explosive flow and pinching rather than the g-loading

Results analysis

- Statistical analysis and treatment of results
- Inference of reaction violence.
- Techniques appear to be used Ad Hoc Nationally.
- Can we agree an assessment methodology!

MSIAC report on setback actuators: L-212 “Use of Laboratory Setback Activator Tests to Assess Suitability for Gun Launch”, Dec 2016



BACKUP

- 50,000 rounds are fired a year in training and limited operations over a 20 year munition life the probability of an event per firing must be:

<i>Per firing</i>	<i>Events per Year</i>	<i>Events per Programme (20 years)</i>
1.00E-06	0.05	1
1.00E-07	0.005	0.1
1.00E-08	0.0005	0.01
1.00E-09	0.00005	0.001
1.00E-10	0.000005	0.0001

- Safety target of 1 event every 50 years equates to probability of 4×10^{-7} per firing.

Effect of microstructure control on the reaction characteristics in Al/Ni reactive powder

Sang-Hyun Jung^{1*}, Kibong Lee¹

¹The 4th Research and Development Institute-2nd Directorate, Agency for Defense Development, Daejeon, 34060, Korea

Abstract

A microstructure and reaction characteristics that appear in Al/Ni reactive materials and the correlation between those were investigated. 3 types of Al/Ni reactive material powders, that are clearly distinguishable in terms of microstructure, were prepared by using 3 kinds of mixing processes (i.e. turbula mixing, attrition milling, and planetary milling). The Al/Ni powder prepared by using turbula mixer shows that the shape was maintained from initial state of raw Al and Ni powder. In contrast, the Al/Ni powder prepared by using attrition mill shows that the shape was distorted and grain size largely decreased from the raw materials. And the powder prepared by using planetary mill was completely deformed from the initial state of raw materials and represents a new type of microstructure (i.e. nano-lamella structure). To compare the reaction initiation temperatures of these powders, differential scanning calorimetric analysis was performed. As a result, the initiation temperature varied more than 200 °C according to the changes in microstructure. In order to compare reaction rate, 3 types of compacts which is consolidated from the different powders were also observed for their reaction characteristics by high speed camera at a condition of 10,000 fps (frame per seconds). And it was found that the reaction rates also varies greatly depending on the microstructure of the powders. These results suggest that reaction characteristics of reactive materials can be controlled by tailoring their microstructure.

Keywords: reactive materials, mechanical alloying, nano-lamella, Al-Ni reactive powder, self-propagating reaction

*Corresponding author: Sang-Hyun Jung (sanghyun@add.re.kr); Tel: +82-42-821-4282; Fax: +82-42-823-3400-16265

1. Introduction

Recently, the studies have been attracting attention to use Reactive Materials (RM) and Reactive Material Structures (RMS) for military purposes [1]. RM are usually classified into two categories. One is an intermetallic system in which an intermetallic reaction occurs between a metal and a metal such as Al-Ni [2], Al-Zr [3], and Al-Ti [4] and the other is a thermite system in which a thermite reaction occurs between a metal and a metal oxide such as Al-CuO [5], Al-MoO₃ [6], and Al-Fe₂O₃ [7]. The RMS are usually prepared by structuralizing RM of a powder state. For structuralizing, cold isostatic pressing and cold spray techniques are generally used.

RMS are also called as HDEM (High Density Energetic Materials) in a sense that

they are structurally very stable energetic materials, unlike conventional energetic materials such as explosives and propellants [8]. Since RMS are not only energetic materials but also structural materials, they are very attractive materials in that they can be utilized as energy-releasing structural materials [8]. For example, when RMS is used as a case of warhead, the energy per unit mass of the warhead can be increased up to two times compared to when conventional structural materials are used such as steel [1]. This is because the RMS is not a simple structural materials such as steel but an energetic structural material that can react in the explosion environment and thus release additional energy.

RMS could be utilized in a variety of military use as structural materials, but there are still many technical obstacles to overcome. In particular, the reaction rate of ordinary RMS is in a cm/s level [1], which is very slow compared to the reaction rate of common explosives (km/s), so it may not be suitable for military use as energetic materials that require a lot of energy release in a short time. However, if the microstructure of RMS is reduced to a nanometer level, the reaction rate could be increased more than 100 times [1], and the reaction initiating point could also be lowered. However, if we use just nano-sized raw materials to prepare the nanostructured RMS, first, it is dangerous to handle, second, it becomes very difficult to mix (due to agglomeration of nano-powder), and third, the manufacturing cost may also be increased.

It has been attempted to produce nanostructured RM without nano-powder. As a representative example, a high-energy ball mill such as Attrition Mill (AM) or Planetary Mill (PM) have been used to induce mechanical alloying of micro-sized raw powders [9]. The preparation of nanostructured RM using a high-energy ball mill is very useful in terms of that it is safer than using a nano-powder and the manufacturing cost could be lowered. In this study, RM powder were prepared with different mixing method (i.e. TM, AM and PM) in Al-Ni system, and microstructural changes were analyzed by Scanning Electron Microscopy (SEM) and Transmission Electron Microscopy (TEM). And the reaction initiation temperatures and the reaction rates of the prepared RMS were also compared according to the microstructural changes of the RM powders.

2. Experimental procedures

2.1. Materials preparation. RM powder samples were prepared using Al powder (10SF, ChangSung, South Korea) with a 99.0% purity and 10 μm average particle size and Ni powder (T123, Vale, Canada) with a 99.8% purity and 4 μm average particle size. The Al powder and Ni powder were mixed with 31.5 wt.% Al - 68.5 wt.% Ni composition, using TM, AM, and PM. The method of each mixing process are shown in Table 1. It is note that a cooling step of 10 minutes was added between each mixing step to reduce the heat generated by the mixing process. When preparing RM powder using TM (TM-powder), 100 g of Al/Ni powder, 500 g of stainless steel ball (10 mm) and inert gas (3 bar of Ar) were added in a cylindrical jar of 2L, and the mixture was mixed twice at 60 rpm for 15 minutes. When preparing RM powder using AM (AM-powder), 100 g of Al/Ni powder, 500 g stainless steel ball (10mm), inert gas (3 bar of Ar), and 360cc hexane were added in a 2L size cylindrical jar, and the mixture was milled twice at 400 rpm for 10 minutes. When preparing RM powder using PM (PM-powder), 70 g of Al/Ni powder, 350 g of stainless steel ball (10 mm), and inert gas (3 bar of Ar) were added to a 500 ml cylindrical jar, and the

mixture was milled twice at 600 rpm for 5 minutes. And then 40 cc of hexane was added to the milling jar, and the mixture was further milled twice at 600 rpm for 5 minutes. The prepared three types of RM powders were uniaxially compacted at 300 MPa to form pellets having a diameter of 5 mm and a height of 2 mm.

Table 1. Processing conditions according to mixing methods (TM: Turbula Mixing, AM: Attrition Milling, PM: Planetary Mill, RPM: Rotation per Minute, BPR: Ball to Powder Ratio)

Method	Conditions	1st step	2nd step	3rd step	4th step
TM	PCA	-	-	No action	
	Atmosphere	Ar (3 bar)	Ar (3 bar)		
	RPM	60	60		
	BPR	5:1	5:1		
	Duration (min)	15	15		
AM	PCA	Hexane (360 cc)	Hexane (360cc)	No action	
	Atmosphere	Ar (3 bar)	Ar (3 bar)		
	RPM	400	400		
	BPR	5:1	5:1		
	Duration (min)	10	10		
PM	PCA	-	-	Hexane (40 cc)	Hexane (40 cc)
	Atmosphere	Ar (3 bar)	Ar (3 bar)	Ar (3 bar)	Ar (3 bar)
	RPM	650	650	650	650
	BPR	5:1	5:1	5:1	5:1
	Duration (min)	5	5	5	5

2.2. Material characterization. Internal microstructure of the RM powder was analyzed by SEM (S-4800, Hitachi, Japan) and TEM (Tecnai G² F30 S-twin, FEI, Netherlands). TEM samples were prepared using a FIB (Focus Ion Beam; Nova 200, FEI, Netherlands). Phase analysis of the prepared RM powders was performed using HR-XRD (High Resolution X-ray Diffraction, X'Pert-Pro MRD, PANalytical, Netherlands) equipped with Ni-filtered Cu K α radiation.

2.3. Reaction characterization. DSC (STA 449 F5, Netzsch, Germany) analysis was also performed for the thermal characterization of the RM powder and the RMS. The thermal analysis was carried out under the conditions of a heating rate of 10 ° C/min and an atmosphere of pure Ar (5N) with a flow rate of 20 cc/min. The obtained DSC data were analyzed using Netzsch proteus thermal analysis software. In order to compare the reaction rate of RMS pellets, the samples were heated for 100 seconds on a torch set at 1000 ° C, and the occurred reaction phenomenon was observed by high speed camera (dimax HS4, PCO co., Germany) set at 10,000 frames/sec.

3. Results and discussion

3.1. Material characterization. Figure 1 shows the microstructure of the Al and Ni raw powder used in this study. The Al particles show a smooth spherical shape (Fig. 1 (a)), and one particle is consisted of one crystal (Fig. 1 (b)). In contrast, the surfaces of the Ni particles show spiky shapes (Fig. 1 (d), (e)), and one particle is consisted of several grains with different orientations, and then several grain boundaries were observed in the particle as shown in fig. 1 (f). In addition, a passivation layer of about 5 nm, which is regarded as Al₂O₃, was uniformly observed on the surface of the Al particle (Fig. 1 (c)), but additional

layer such as an oxide film was not observed on the Ni particle surface. (Fig. 1 (f)).

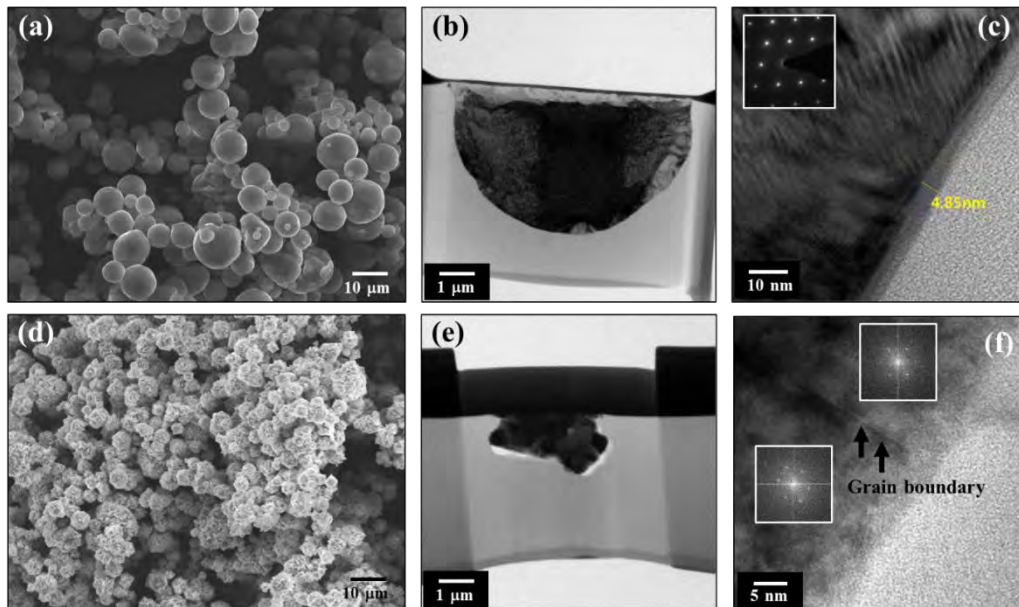


Fig 1. (a) SEM, (b) BF-(bright field-) TEM, and (c) HR-(high resolution-) TEM image of Al powder and (d) SEM, (e) BF-TEM, and (f) HR (high resolution) TEM image of Ni powder

The XRD peaks of the prepared RM powders were examined in order to confirm whether a secondary phase such as Al_mNi_n intermetallic formed during the mixing process. As a result, no visible peaks were observed except for Al and Ni peaks as shown in Fig. 2, and it was also difficult to recognize the differences in XRD patterns acquired from the different RM powders.

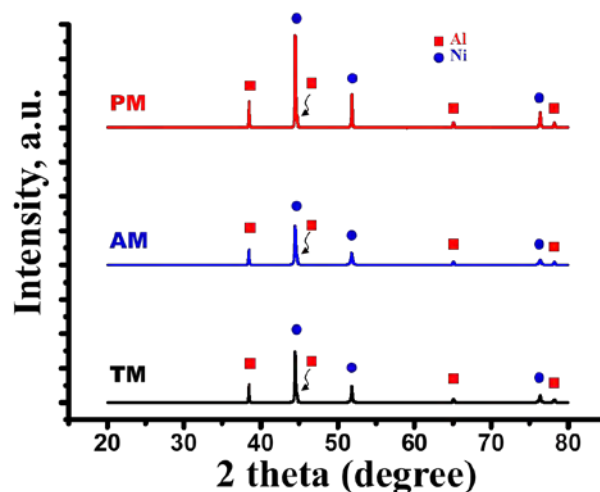


Fig. 2. XRD patterns for RM powders prepared by TM, AM, and PM.

In order to investigate the changes in microstructure according to the mixing methods, the RMS pellets were cut, the cut surfaces were polished, and the cut surfaces were observed by SEM. As a result, the microstructure of each powder are clearly distinguishable. The microstructure of TM-powder shows the original shape of Al and Ni raw powder. However, the microstructure of AM-powder is significantly

different from the shape of raw powder. In particular, the needle shape of the Ni raw powder disappear, and the overall shape is also elongated. In the case of PM-powder, the original shape of the raw material is completely collapsed and mixed at the nano-level.

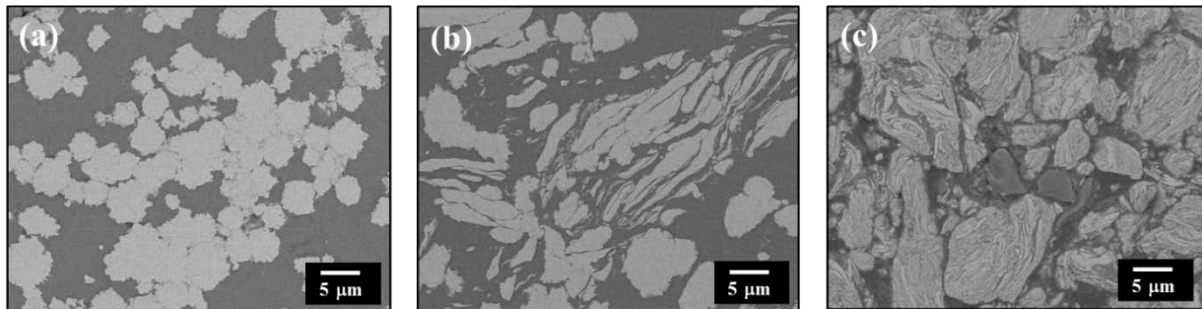


Fig 3. Back scattered SEM images for (a) TM- (b) AM- (c) PM- powders (in the figures, grey areas represent Al and white areas represent Ni)

The crystallographic microstructure of each RM powder was observed by TEM, and the results are shown in fig. 4. In the case of TM-powder, the needle shape which was observable in the Ni raw powder is maintained even after the mixing. However, Al particles which were confirmed as one grain, are broken into several grains of ca. 1 μm after the mixing. In the case of AM-powder, Al grain refinements are more pronounced, and most of the grains are found as ca. sub-micron size, and the needle shapes of Ni surface almost disappear. In addition, a number of lamella - type microstructures is observed in which several tens of nanometers of Al layer and Ni layer are alternately stacked. In the case of PM-powder, a typical mechanical alloying microstructure, in which Al layers and Ni layers are alternately stacked, that is, nano-lamella microstructure, is observed throughout the specimen.

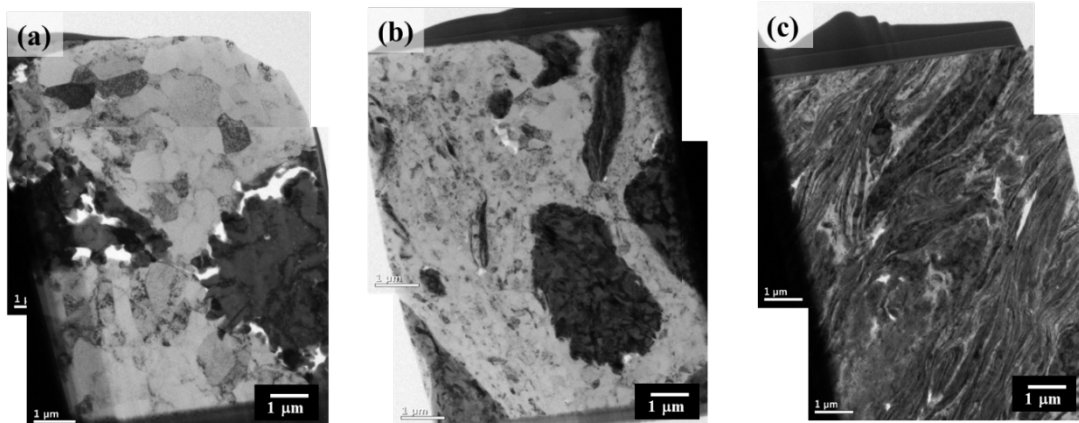


Fig 4. BF-TEM images for (a) TM- (b) AM- (c) PM- powders (bright areas represent Al and dark area represent Ni in these figures)

3.2. Reaction characterization. DSC analysis was carried out to analyze the thermal characteristics of RM powders and RMS pellets with the change of microstructure. The results are shown in Fig 5. The exothermic curve of PM-powder is much broader than that of TM-powder and AM-powder, and the reaction initiation temperature of PM-powder is found to be at least 200 degrees lower than that of other powders as shown fig. 5 (a). The decrease in reaction initiation temperature

is thought to be due to the decrease in grain size of RM powders. The total heat formation is gradually decreased in the order of TM-powder (720 J/g), AM-powder (630 J/g), and PM-powder (540 J/g). The reduction of heat formation is thought to be due to the partial reaction that capable to occur during milling (although any intermetallic phase could not be observed in XRD analysis).

The decrease of the reaction initiation temperature and the reduction of heat formation of the PM-powder were similarly observed in the DSC curves of the RMS pellets as shown fig. 5 (b). In the analysis of the RMS pellets, the reaction initiation temperature of the TM-pellet or the AM-pellet tends to decrease by more than 100 degrees from the reaction initiation temperature in the analysis of the RM powder. These results suggest that the changes of reaction initiation temperature is not only related to grain size reduction but also related to whether the reactant materials are contacted each other. In order for the intermetallic reaction, inter-diffusion between Al and Ni materials should occur smoothly. However, in a powder state, there is no direct contact interface between Al and Ni, and the paths of inter-diffusion are surely limited. In order words, in a powder state, the reaction proceeds only through the evaporation diffusion path, whereas in a consolidated pellet state, the reaction can proceed through the grain boundary diffusion path and the surface diffusion path, and hence, the reaction initiation temperature could be greatly reduced below the Al melting temperature.

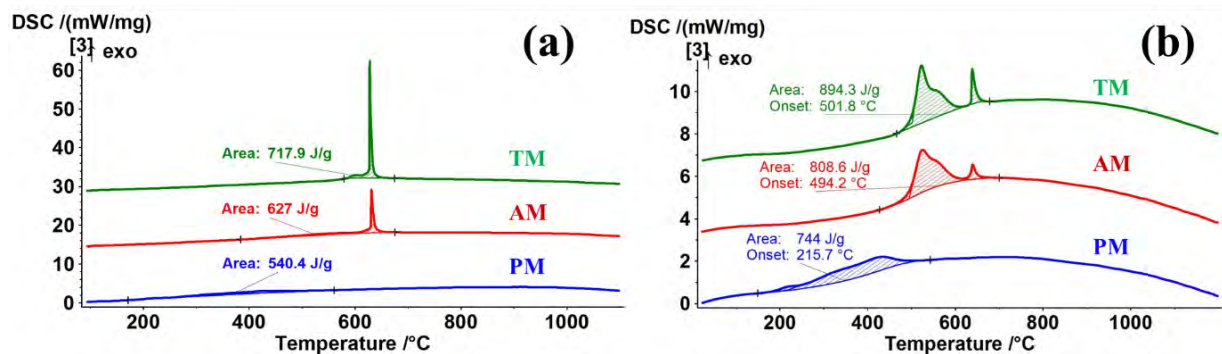


Fig 5. DSC curves obtained using (a) RM powders and (b) RMS pellets

In order to observe the self-propagation reaction [10] of three kinds of RMS pellets, the reaction phenomena occurred by heating one side of the pellet was photographed with high speed camera at 10,000 fps condition. In the case of the TM-RMS pellet, the reaction did not occur even after 100 seconds of heating. In the case of the AM-RMS pellet, a reaction started at the heated surface of the pellet after about 12 seconds of heating, and the reaction propagation was completed within 100 ms as shown fig. 6 (a)-(c). On the other hand, in the case of the PM-RMS pellet, the reaction started after about 2 seconds of heating, and the reaction propagation was completed before 10 ms as shown fig. 6 (d)-(f). That is, the reaction propagation rate of the PM-RMS pellet was about 10 times faster than that of AM-RMS pellet. In addition, the AM-RMS pellet showed a mild reaction propagation with maintaining the original shape, but the PM-RMS pellet showed a very rapid reaction propagation by splashing the fragments in all directions as shown fig. 6. These differences in the propagation phenomena were thought to be due to the microstructural differences of RMS.

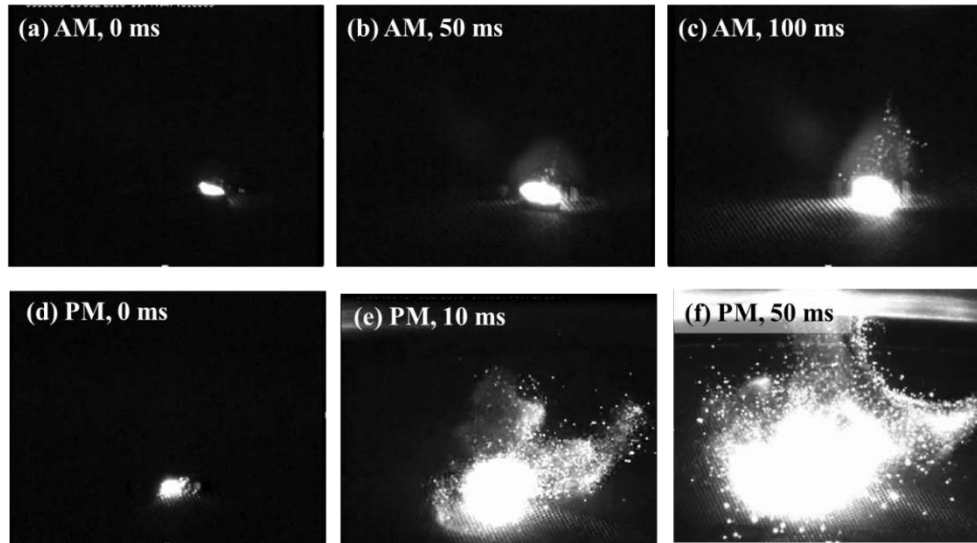


Fig 6. Self-propagation reaction images observed at (a) 0 ms, (b) 50 ms, and (c) 100 ms for AM-RMS pellet and (d) 0 ms, (e) 10 ms, and (f) 50 ms for PM-RMS pellet.

4. Conclusions

Three types of Al/Ni RM powders were prepared by varying mixing methods, and their reaction characteristics were compared. The TM powder showed just mixed microstructure with maintaining the shape of the Al and Ni raw powder. In contrast, the AM powder showed a distorted microstructure deviating from the original shape of raw powder. And PM powder showed a completely new microstructure (i.e. nano lamella structure) deviating from the shape and average size of the raw powder. Three kinds of Al/Ni RM powders are clearly distinguishable in terms of microstructure. DSC analysis was performed to compare the reaction initiation temperature of these RM powders. As a result, the reaction initiation temperatures of RM powders and RMS pellets varied more than 200 °C with changing the microstructure. In order to compare the self-propagation reaction phenomena of the three kinds of RMS pellets, the generated reactions resulting from heating one side of the pellet were recorded with high speed camera at 10,000 fps condition. As a result, it is confirmed that the reaction propagation rate varies greatly depending on the microstructure of RMS. These results suggest that the reaction characteristics of the RMS could be controlled by tailoring the microstructure of RM and RMS.

Acknowledgements

This work was supported by the Agency for Defense Development (ADD).

References

- [1] D. L. Daniel, E. L. Dreizin, Reactive Structural Materials: Preparation and Characterization, *Adv. Eng. Mater.* (2017) 1700631.
- [2] E.M. Hunt, K. B. Plantier, M. L. Pantoya, Nano-scale reactants in the self-propagating high-temperature synthesis of nickel aluminide, *ACTA Mater.* 52 (2004) 3183-3191.
- [3] M. S. Song, M. X. Zhang, B. Huang, S. G. Zhang, J. G. Li, Reaction Synthesis of ZrAl₃ Intermetallic Compound and Its Nucleation Behavior, *Rare*

- Metal Mater. & Eng. 39 (2008) 1570-1574.
- [4] Y. Liu, B. Y. Huang, Y. H. He, Mechanism of non-isothermal reaction between elemental powders Ti and Al, *Trans. of Nonferrous Metals Soc. of China* 10 (2000) 29-33.
- [5] K. J. Blobaum, M. E. Reiss, J. Lawrence, T. P. Weihs, Deposition and characterization of a self-propagating CuOx/Al thermite reaction in a multilayer foil geometry, *J. Appl. Phys.* 94 (2003) 2915-2922.
- [6] V. E. Sanders, B. W. Asay, T. J. Foley, B. C. Tappan, A. N. Pacheco, S. F. Son, Reaction propagation of four nanoscale energetic composites (Al/MoO₃, Al/WO₃, Al/CuO, and Bi₂O₃), *J. Prop. & Power Mater.* 23 (2007) 707-714.
- [7] C. Cuadrado, L. C. Damonte, L. Mendoza-Zelis, Theoretical treatment of a self-sustained, ball milling induced, mechanochemical reaction in the Fe₂O₃-Al system, *Mater. Sci. & Eng.* 355 (2003) 106-113.
- [8] R. Zaharieva, S. Hanagud, Preliminary Design of Multifunctional Structural-Energetic Materials for High Density, High Strength and Release of High Enthalpic Energy, *Int. J. Sci. Eng. & Techno.* 3 (2014) 1189-1192.
- [9] E. B. Herbold, J. L. Jordan, N. N. Thadhani, Effects of processing and powder size on microstructure and reactivity in arrested reactive milled Al plus Ni, *Acta Mater.* 59 (2011) 6717-6728.
- [10] A. I. Kirdyashkin, Y. M. Maksimov, V. D. Kitler, V. V. Burkin, V. S. Seodoi, Electroimpulsive activation of self-propagating high-temperature synthesis in powder mixtures, *Comb. Expl. & Shock Waves.* 36 (2000) 540-542.



Effect of Microstructure Control on Reaction Characteristics in Al/Ni Reactive Powder

2018. 04. 24 | Agency for Defense Development

Sang-Hyun Jung, Kibong Lee

Outline

- Background and Objectives

(what is reactive materials (RM) and reactive material structures (RMS))

- Experimental Procedure

(how to make RM and RMS)

- Microstructure Characteristics

- Reaction Characteristics

- Summary

Reactive Material (RM)

- **Reactive materials (RM)** are mixtures such as metal-metal, metal-oxide, and metal-polymer that cannot be detonated, but are **capable of releasing large amounts of thermodynamic energy** very rapidly.
- Examples of RM

※ TNT : 1,900 cal/cc

Category	System	Heat of Reaction (cal/cc)
Metal-metal (Intermetallic)	$\text{Al} + \text{Ni} = \text{AlNi}$	1,710
	$\text{Al} + \text{Ni} = \text{AlNi} + \text{O}_2 = \text{NiAlO}_2$	8,000
	$2\text{Al} + \text{Zr} = \text{Al}_2\text{Zr}$	1,130
	$2\text{Al} + \text{Ti} = \text{Al}_2\text{Ti}$	1,100
Metal-oxide (Thermite)	$2\text{Al} + 3\text{CuO} = 3\text{Cu} + \text{Al}_2\text{O}_3$	4,976
	$2\text{Al} + \text{Fe}_2\text{O}_3 = 2\text{Fe} + \text{Al}_2\text{O}_3$	3,947
Metal-polymer	Al-PTFE	6,000
Metal-non metal	$3\text{Ti} - 5\text{Si} = \text{Ti}_3\text{Si}_5$	428

■ **RMS**, which are made of RM powder, are **energetic structures** designed to have structural strength and store energy to be released at a desired time.

Reactive Case

- Inert structural materials based on steel are normally used as missile's cases
- If we **replace the inert steel case** currently used **with reactive material structures**?

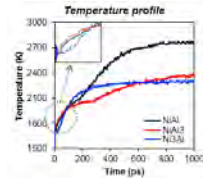
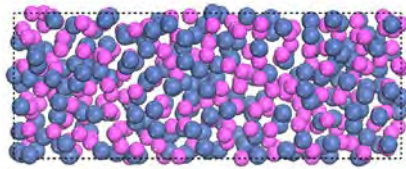


- The delivered energy to target would be increased, because **the RMS case is capable to react in the exploding environment of explosives**, unlike steel case
- ADD has been working on a project to develop reactive cases since 2014

Objectives

- Secure the core technologies to develop reactive cases

Design technology



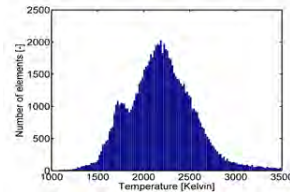
- Design technology to design RMS that release a large amount of energy

Fabrication technology



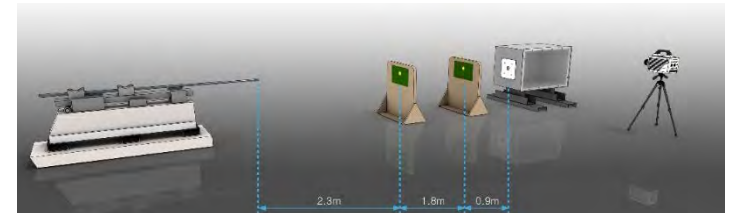
- Fabrication technology to fabricate RM powder and RMS as designed states

Analysis technology



- Analysis technology to analyze acquired data from RMS tests

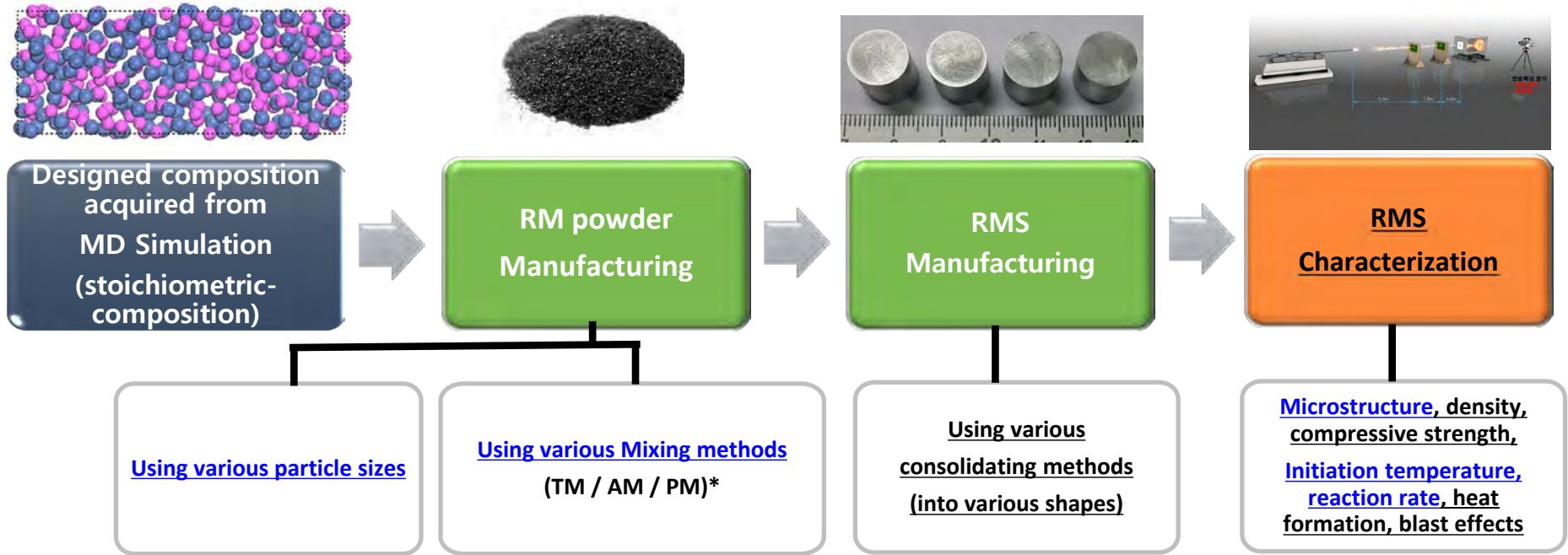
Test technology



- Test technology to simulate the RMS operating environment

Schematic Procedure for developing RMS

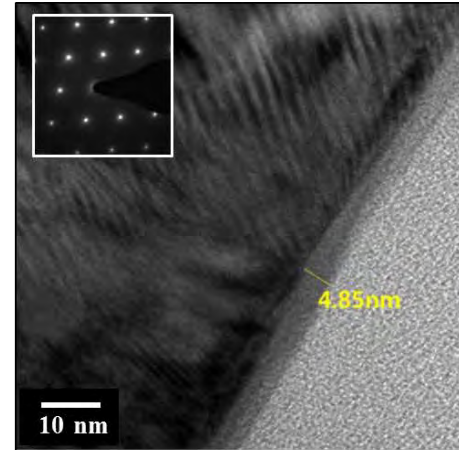
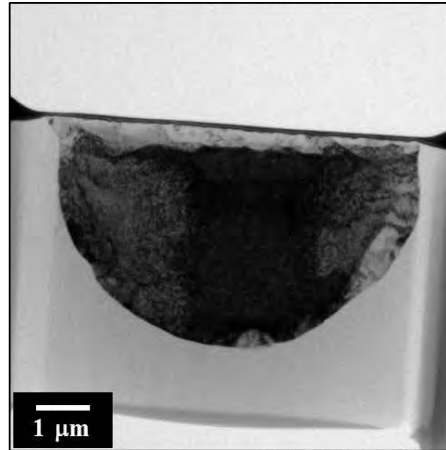
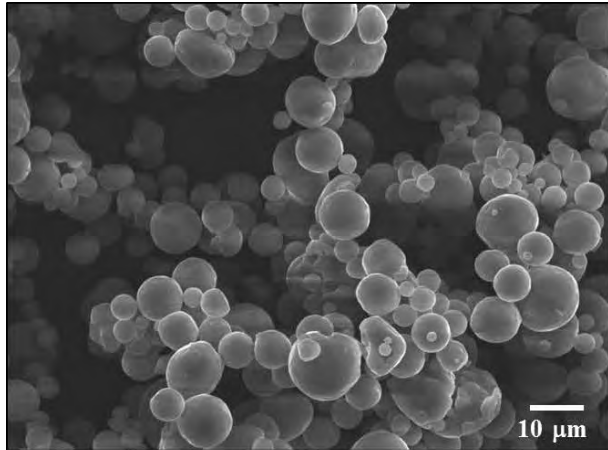
*TM: Turbula Mixing // AM: Attrition Milling // PM: Planetary Milling



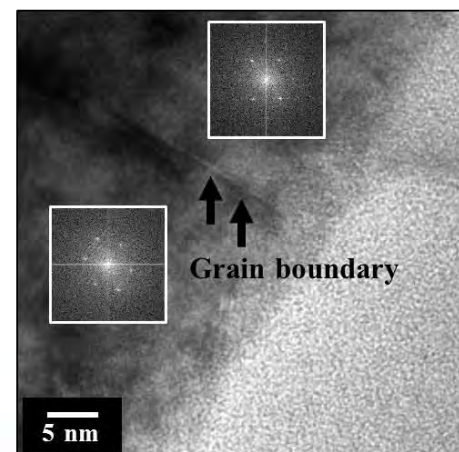
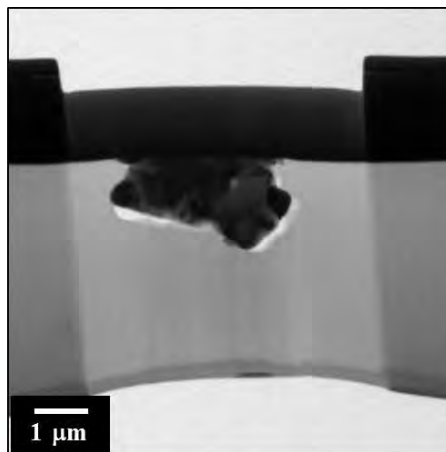
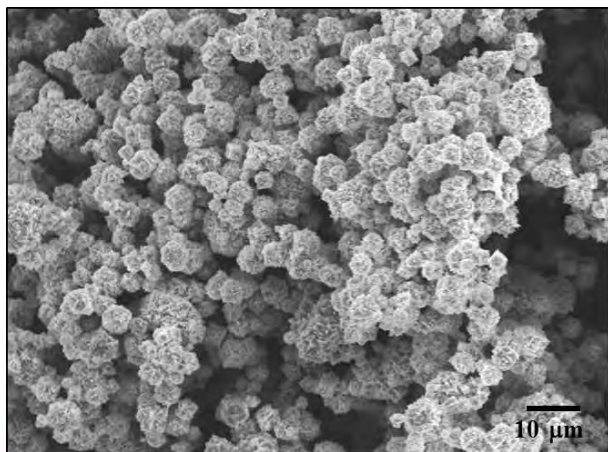
- How to make RM powder
- Microstructural development according to mixing methods
- A Correlation between the microstructure and their reaction characteristics

Microstructure of raw powder (Al, Ni)

■ Spherical shape of Al (AVG = 10 μm)



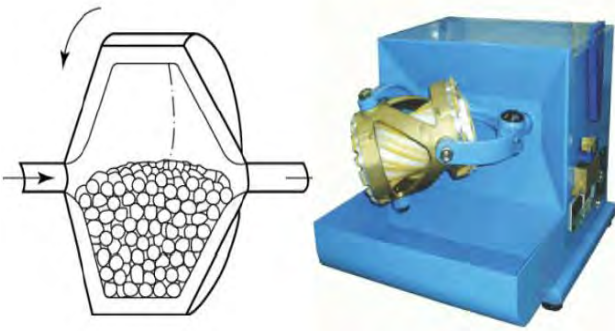
■ Needle (spiky) shape of Ni (AVG = 4 μm)



Manufacturing of Al/Ni reactive powder

- Use 3 types of mixing methods to modulate microstructure of Al/Ni reactive powder

■ Turbula Mixing (TM)



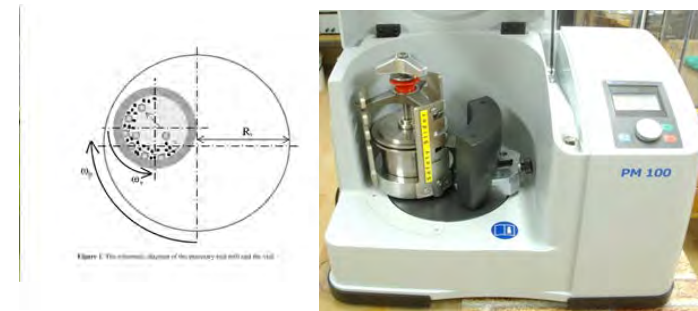
- ➔ 3D movement of container

■ Attrition Milling (AM)



- ➔ Rotation of impeller in container

■ Planetary Milling (PM)

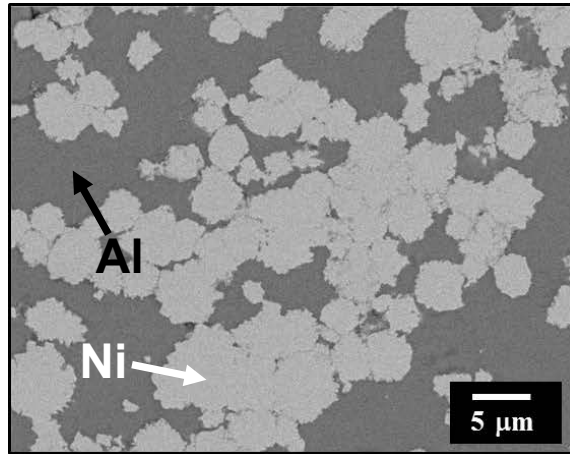


- ➔ Planetary (rotation and revolution) movement of container

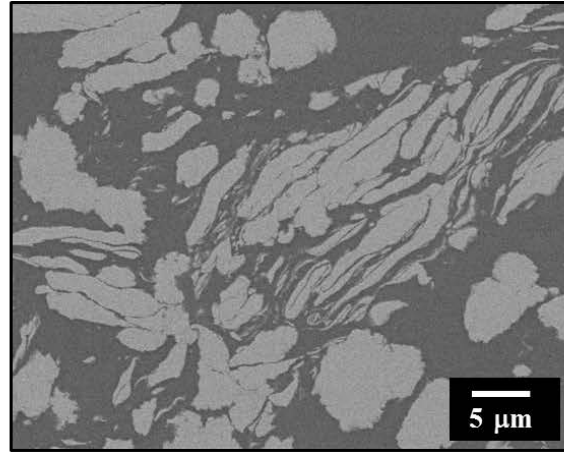
- The amount of energy applied to the powder gradually increases in order of TM, AM, and PM.

Microstructure of the Al/Ni reactive powder

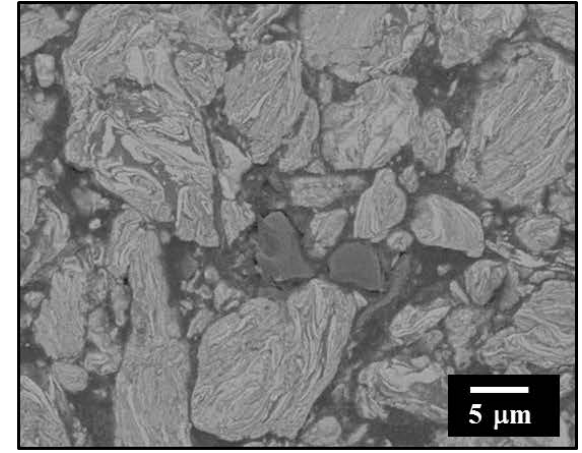
■ Turbula Mixing (TM)



■ Attrition Milling (AM)



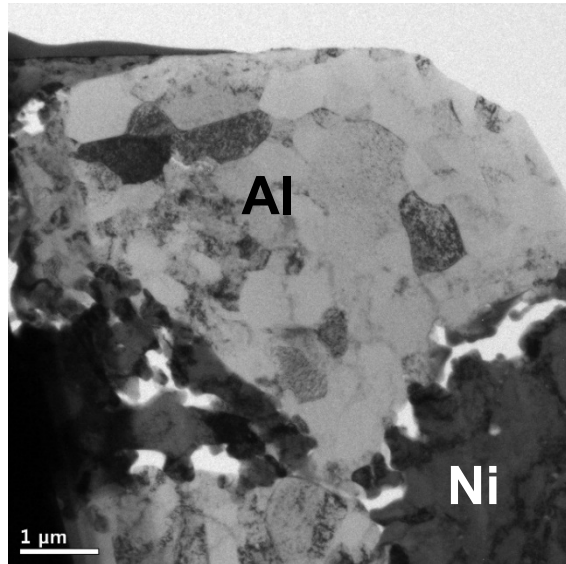
■ Planetary Milling (PM)



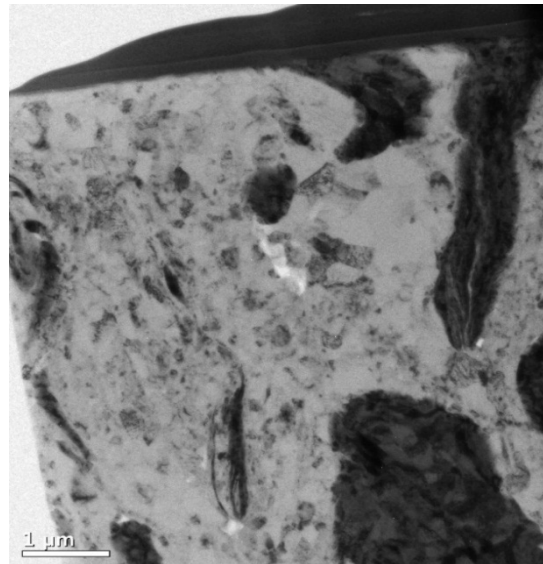
- In TM-powder, the original shape of Al and Ni raw powder is maintained
- In AM-powder, the needle shape of Ni gradually disappear and shows elongated microstructure
- In PM-powder, the original shape of raw powder is completely collapsed and mixed at nano-level

Microstructure of the Al/Ni reactive powder

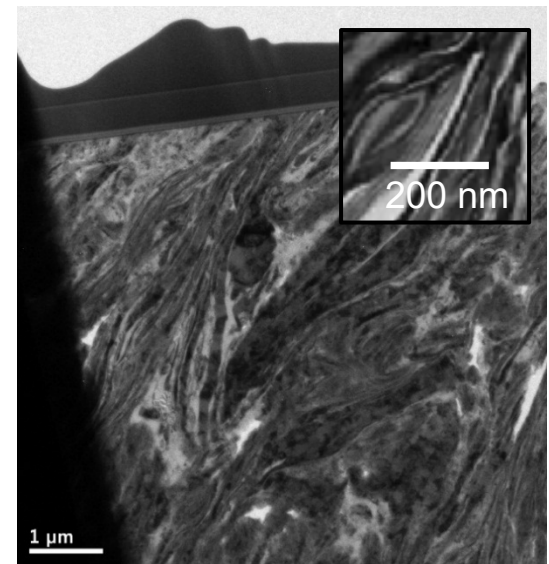
■ Turbula Mixing (TM)



■ Attrition Milling (AM)



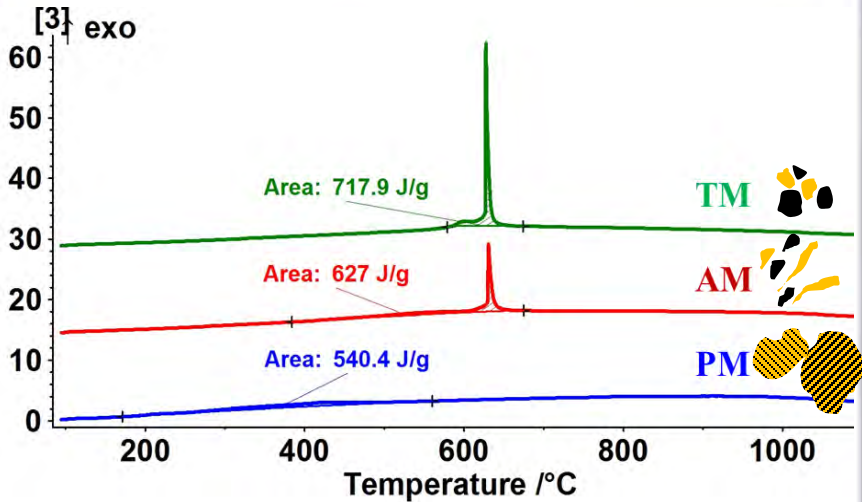
■ Planetary Milling (PM)



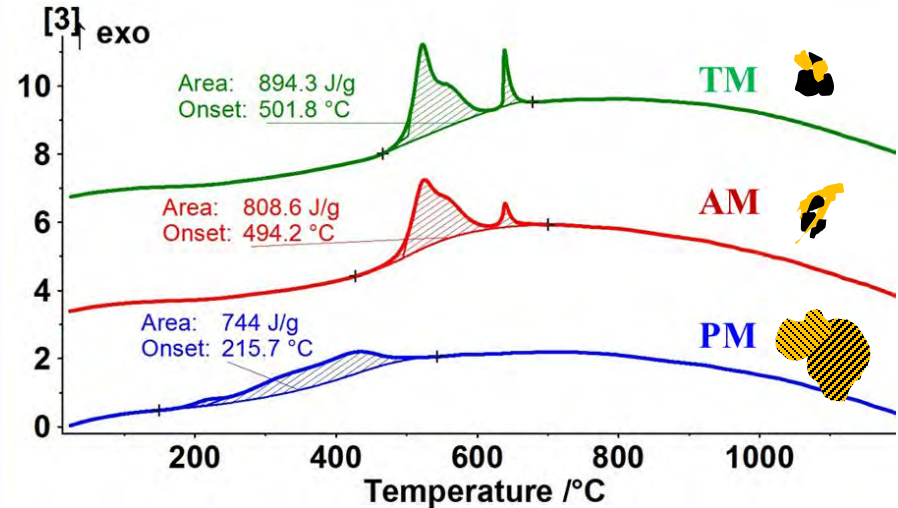
- In TM-powder, the needle shape of Ni is maintained, but Al particle is broken into several grains of 1 μm (grain refinement of Al particle)
- In AM-powder, the grain refinements are more pronounced, and most of Al grains represent sub-micron size
- In PM-powder, the original shape of raw powder is completely collapsed and shows nano-lamella structure in which Al layer and Ni layer stacked alternatively and mixed at nano-level

DSC analysis

Powder DSC Curve



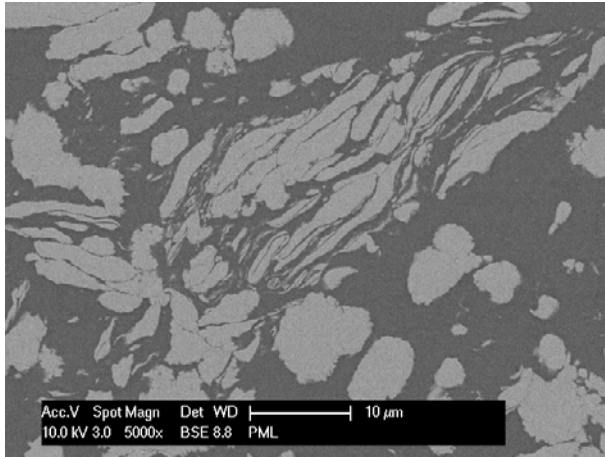
Compact DSC Curve



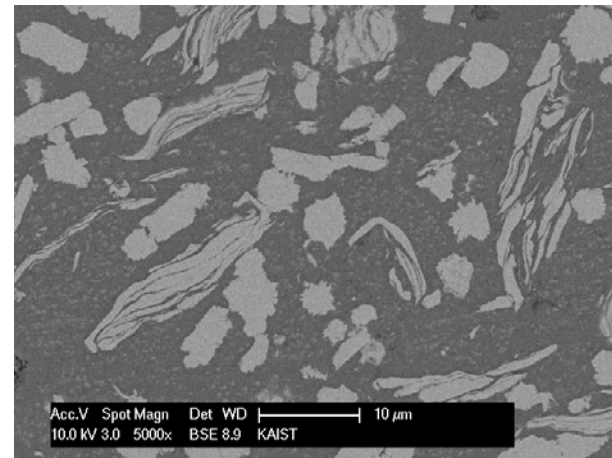
- ➔ TM- and AM- powder are reacted around Al melting point which is about 660 °C (hetero. Rx)
- ➔ PM-powder is reacted below Al melting point => PM-powder can react in solid state (homo. Rx)
- ➔ TM- and AM- compact are reacted at about 500 °C (the reaction initiation temperature changes)
=> In order for the reaction to initiate, it is important whether the interface between components is bonded or not
- ➔ The quantity of heat of reaction is gradually decreased with microstructure development
=> A small amount of components are already reacted in the mixing process.

Microstructure of the Al/Ni reactive powder

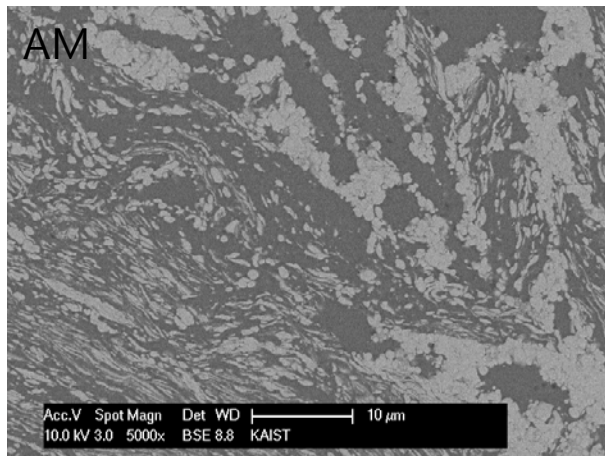
■ Al (10 μm) + Ni (4 μm) -



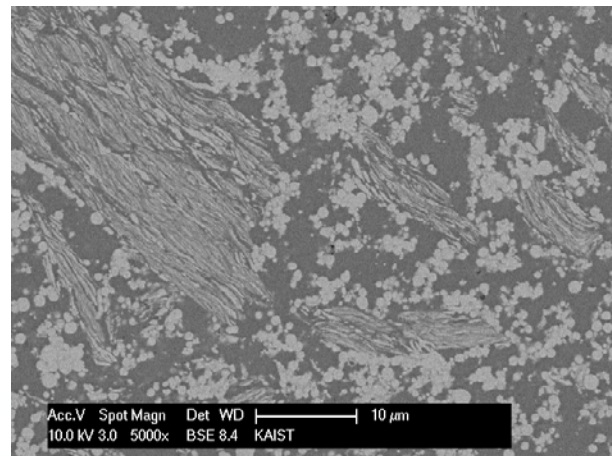
■ Al (1 μm) + Ni (4 μm) - AM



■ Al (10 μm) + Ni (1 μm) -

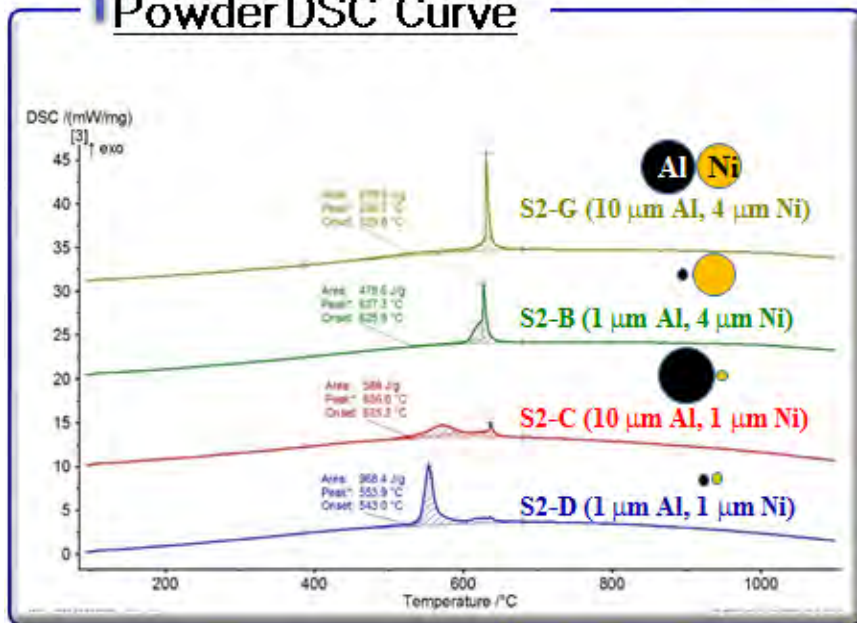


■ Al (1 μm) + Ni (1 μm) - AM

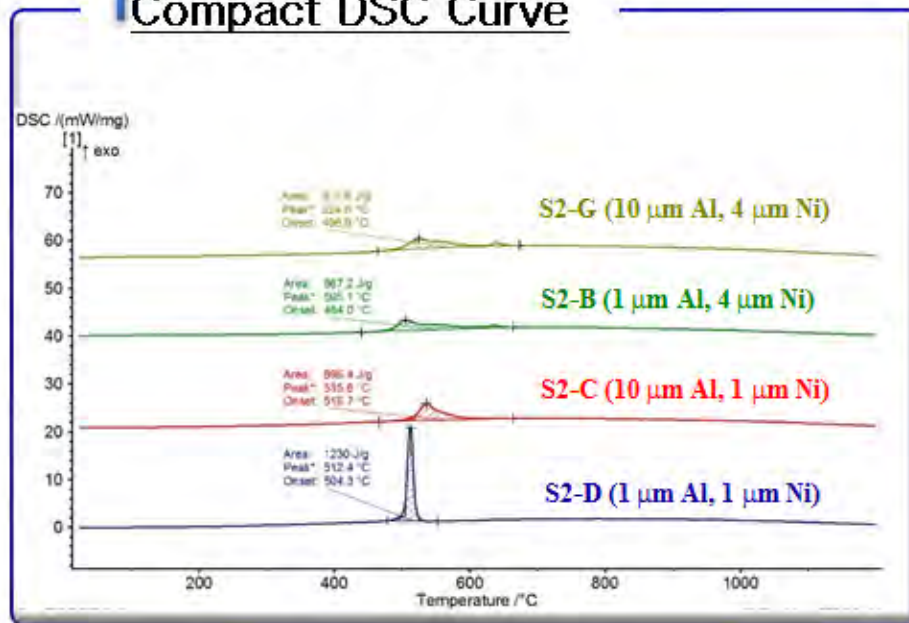


DSC analysis

Powder DSC Curve



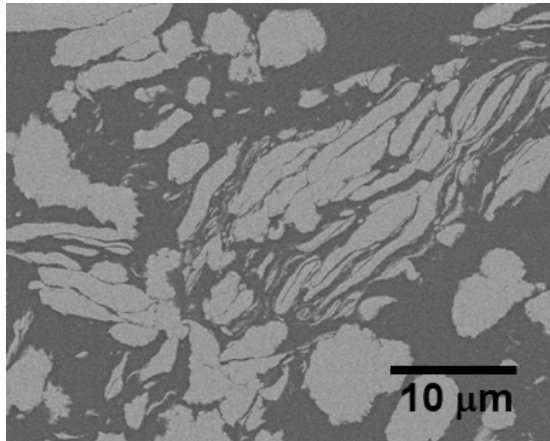
Compact DSC Curve



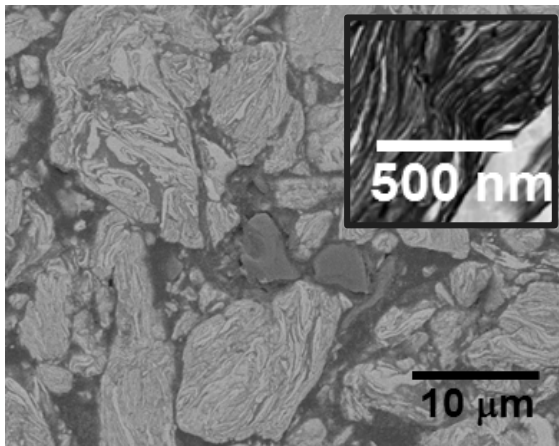
- ➔ The reaction initiation temperature is dropt only when using 1 μm Ni powder
=> In order for a RM to react, the mass transport of the component exhibiting a slow diffusion rate becomes important
- ➔ In the case of compact analysis, there are no big differences in terms of reaction initiation temperature
=> In order for the reaction to initiate, it is important whether the interface between components is bonded or not

Reaction rate (of RM compacts with changing microstructure)

- Attrition Milling (AM): The reaction is completed within about 100 ms to propagate 5 mm (0.05 m/s)



- Planetary Milling (PM): The reaction is completed within about 10 ms to propagate 5 mm (0.5 m/s)



Summary

- Various types of Al/Ni RM powders were prepared by varying mixing methods, and they are clearly distinguishable in terms of microstructure
- In DSC analysis, the reaction initiation temperatures of RM powder and RM compacts varied more than 200 °C with the changes of microstructure
- In order for the reaction to initiate, it is important whether the interface between components is bonded or not
- The reaction propagation rate varies greatly depending on the microstructure
- ➔ The reaction characteristics of the RM (or RMS) could be controlled by tailoring the microstructure of RM (or RMS)



Thank You

Q & A



Review and Update of STANAG 4496 Fragment Impact, Munitions Test Procedure

Christophe **JACQ***, Florian **PECHOUX**

DGA Missiles Testing

BP 80070 – 33166 Saint-Médard-en-Jalles Cedex, France

*Presenter e-mail address: christophe.jacq@intradef.gouv.fr



BACKGROUND



- MSIAC survey: O159 - Review of the Fragment Impact test - edition 2, January 2017



- 2 Custodial Working Group meetings

- DGA Missiles Testing, Bordeaux, France (January 2017)
- Kromhout Kazerne, Utrecht, Netherlands (April 2017)



- **STANAG 4496 ed.1** will be replaced by Allied Ordnance Publication (**AOP-4496 ed.A version 1**) to allow for more efficient updates



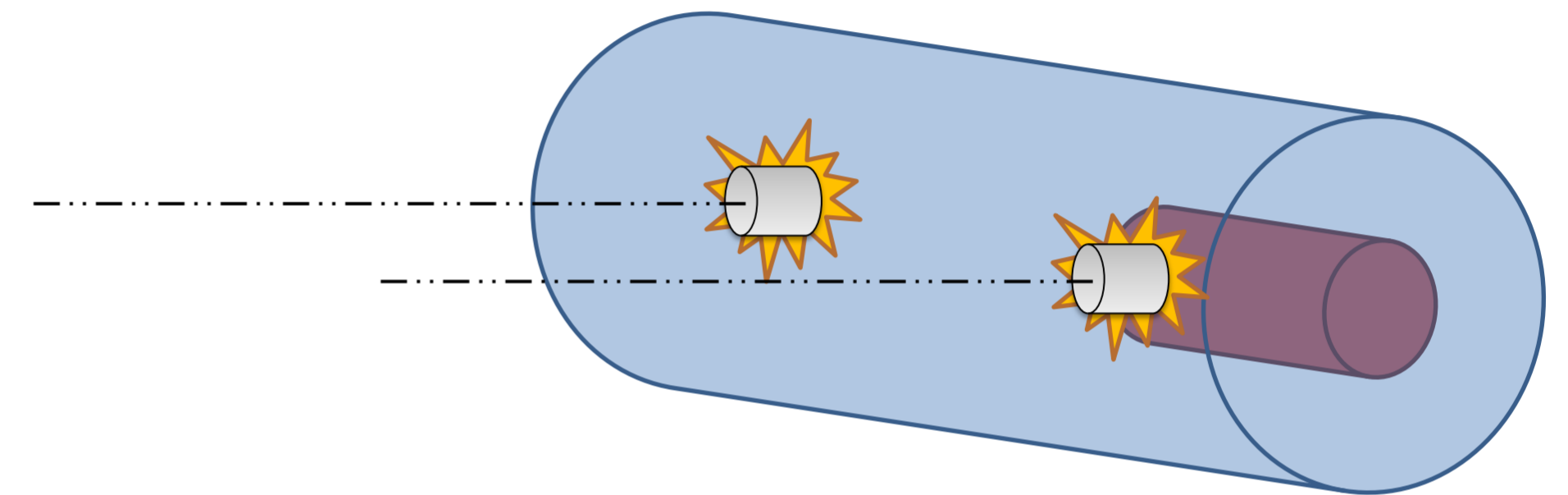
PROCEDURES AND NUMBER OF TESTS

■ Procedures

- Procedure 1: 2530 +/- 90 m/s
- Procedure 2: 1830 +/- 60 m/s

■ Number of tests

- Shall be carried out twice by sub-component of the munition;
- Once against the **main charge filling**
- Once against the **most sensitive component/energetic material** (e.g. motor igniter, warhead booster)



UNCHANGED

MODIFIED

AIM POINT SELECTION

MODIFIED

- Shall be selected to create the most stressing condition on the target energetic
- Shall represent a credible exposure condition, based on the THA
 - First test **at the centre of the energetic component**
 - Second test **on the most vulnerable area**
 - Nota Bene:
 - Aim point and shotline for each test should be approved by national authorities prior to testing
 - Guidance for choosing aim point and shotline can be found in SRD AOP-39.1



ACCURACY REQUIREMENT

NEW

- Shall be defined prior to testing and recorded after the test

Current STANAG 4496 ed.1



New AOP-4496 ed.1



- Should be agreed by the National Authority



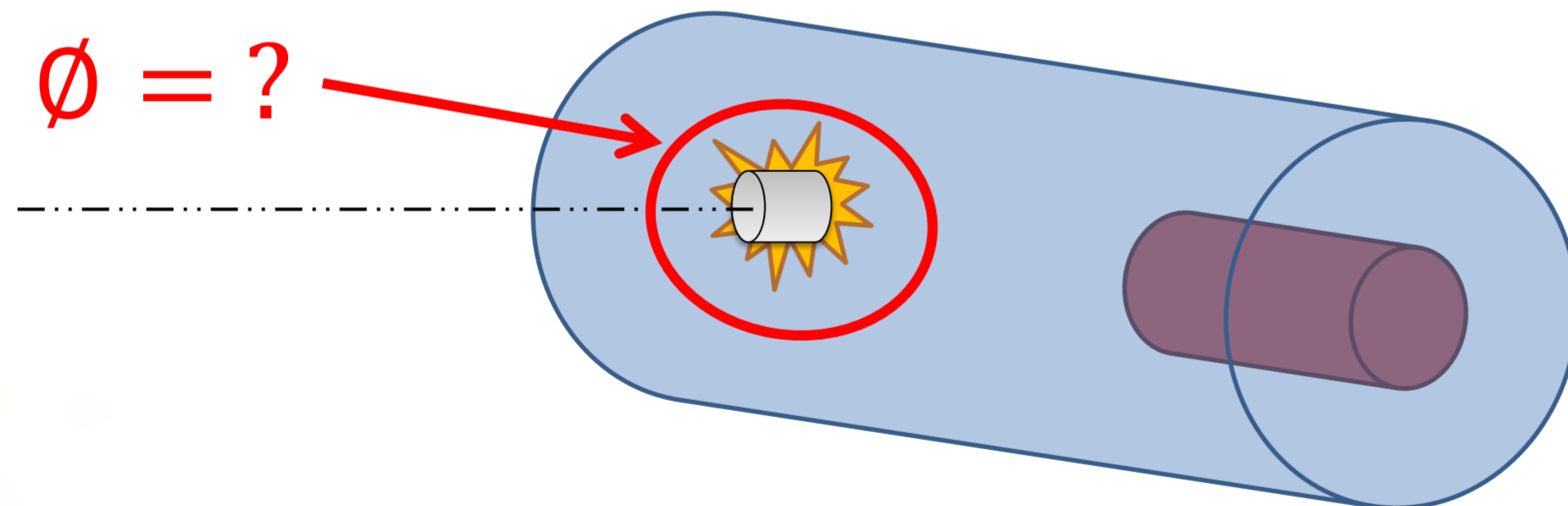
ACCURACY REQUIREMENT

NEW

- Shall be dependent on the geometry of the item under test

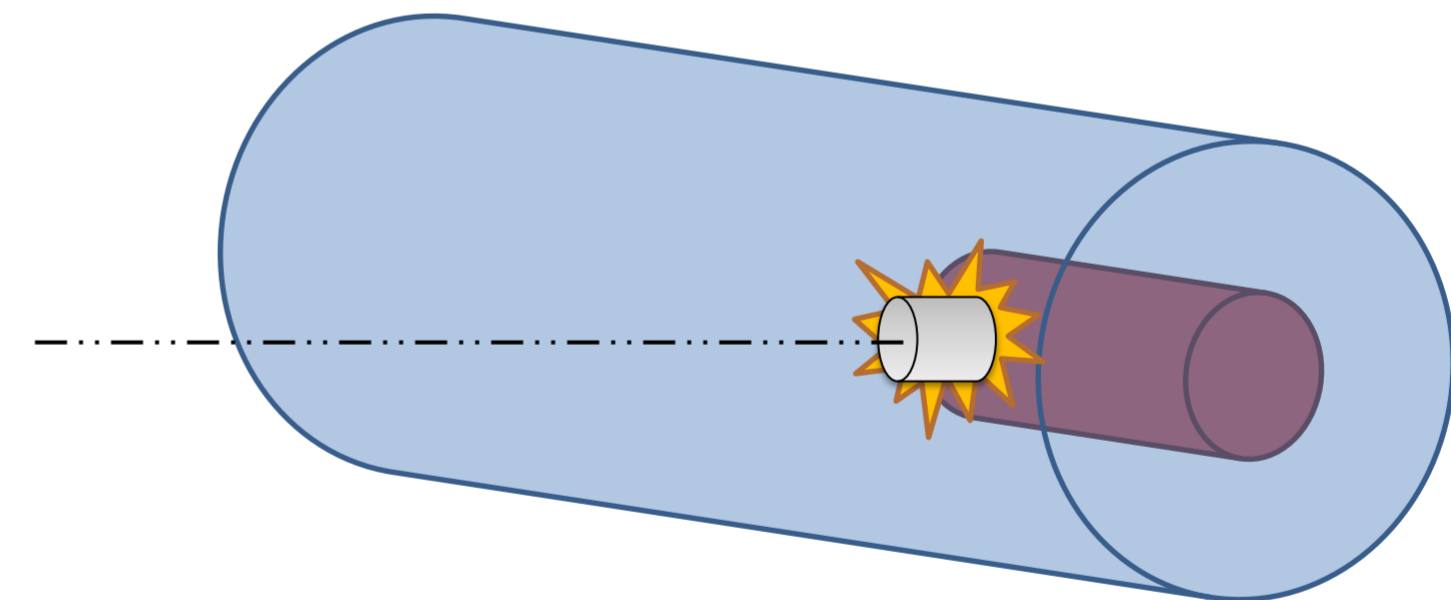
Large area:

Hit the centre of the EM with an accuracy to define prior to testing



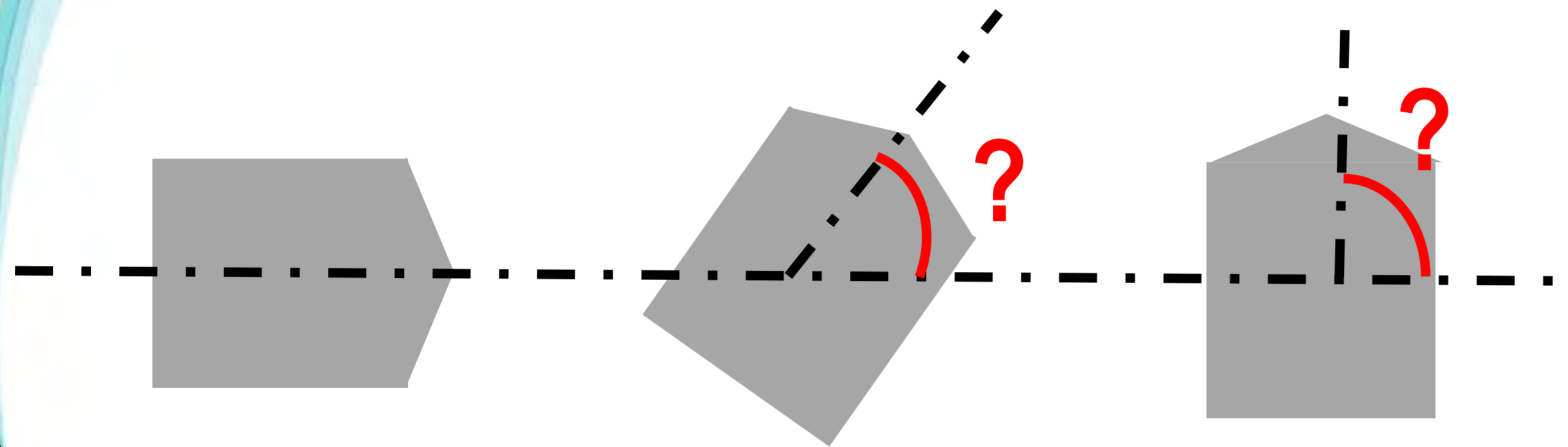
Small area (booster, small munition, ...):

Hit the energetic component

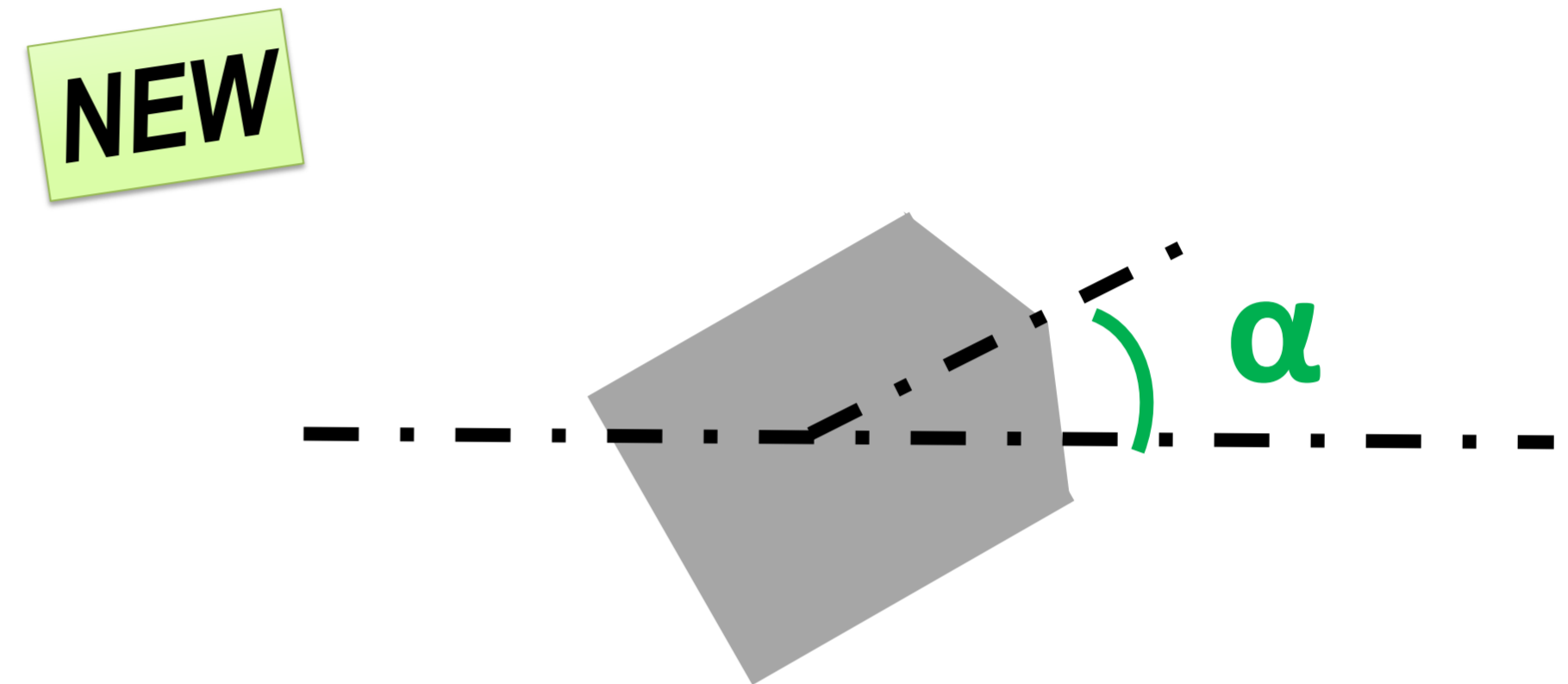


ORIENTATION OF THE FRAGMENT AT IMPACT

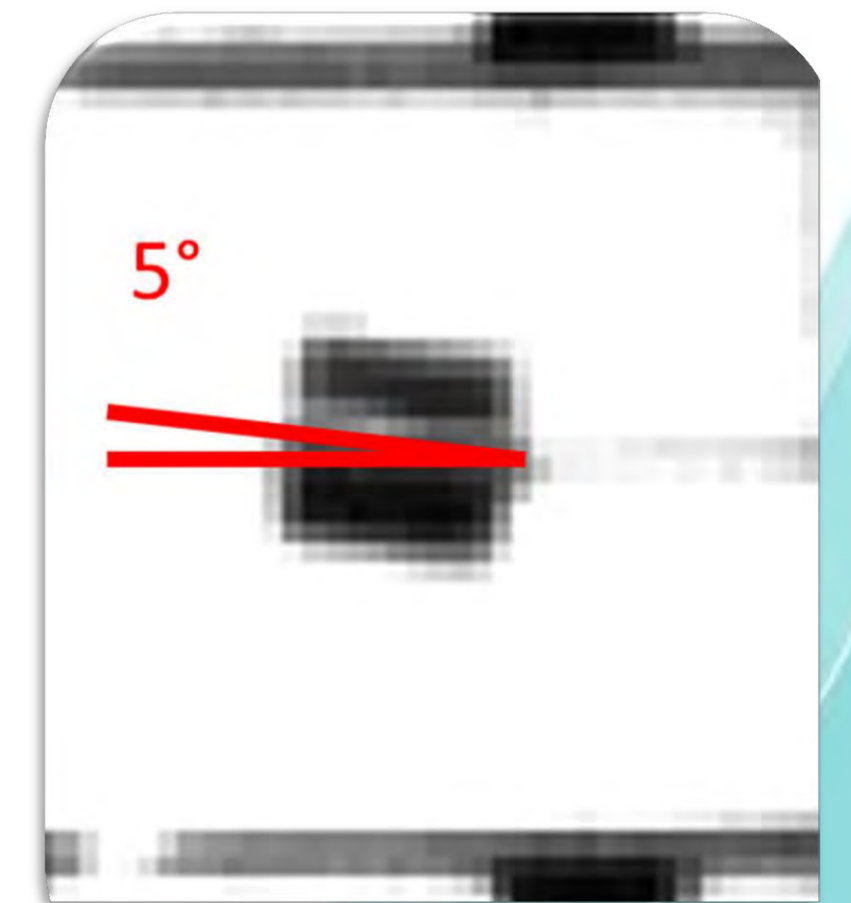
Current STANAG 4496 ed.1



New AOP-4496 ed.1



- Angular deviation (e.g. vector sum of yaw and pitch) for the threat fragment at impact shall be measured and recorded
- Should be limited to $\pm 10^\circ$
- Collect data before imposing an acceptable limit value (next edition of the AOP)



LOWER VALUE FOR THE BRINELL HARDNESS

- Addition of a lower value for the Brinell Hardness
- Measurement and record of the value

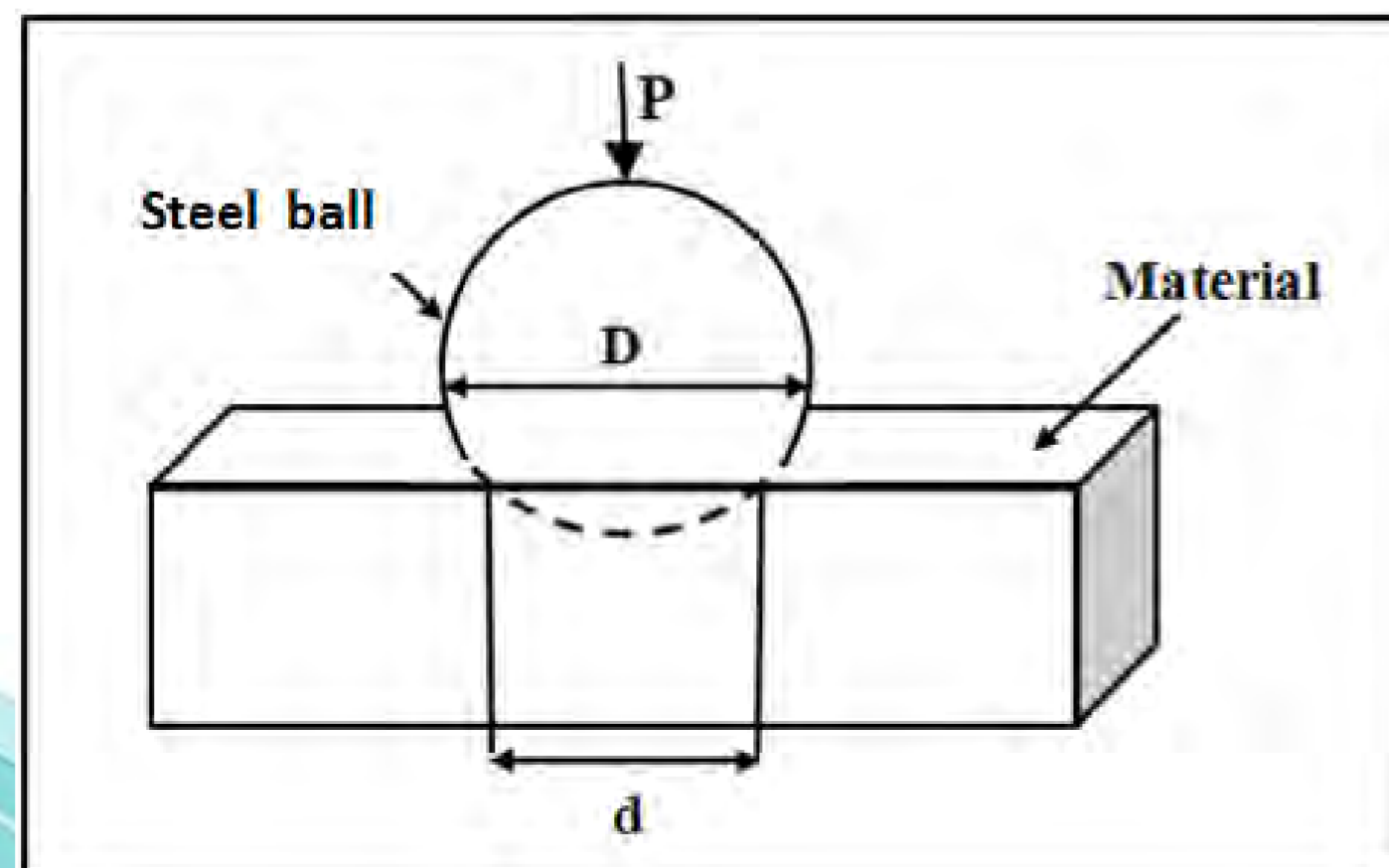
NEW

Current STANAG 4496 ed.1

$HB < 270$

New AOP-4496 ed.1

$190 < HB < 270$



OTHER ISSUES DISCUSSED (1/2)

- No **sabot** design guidance

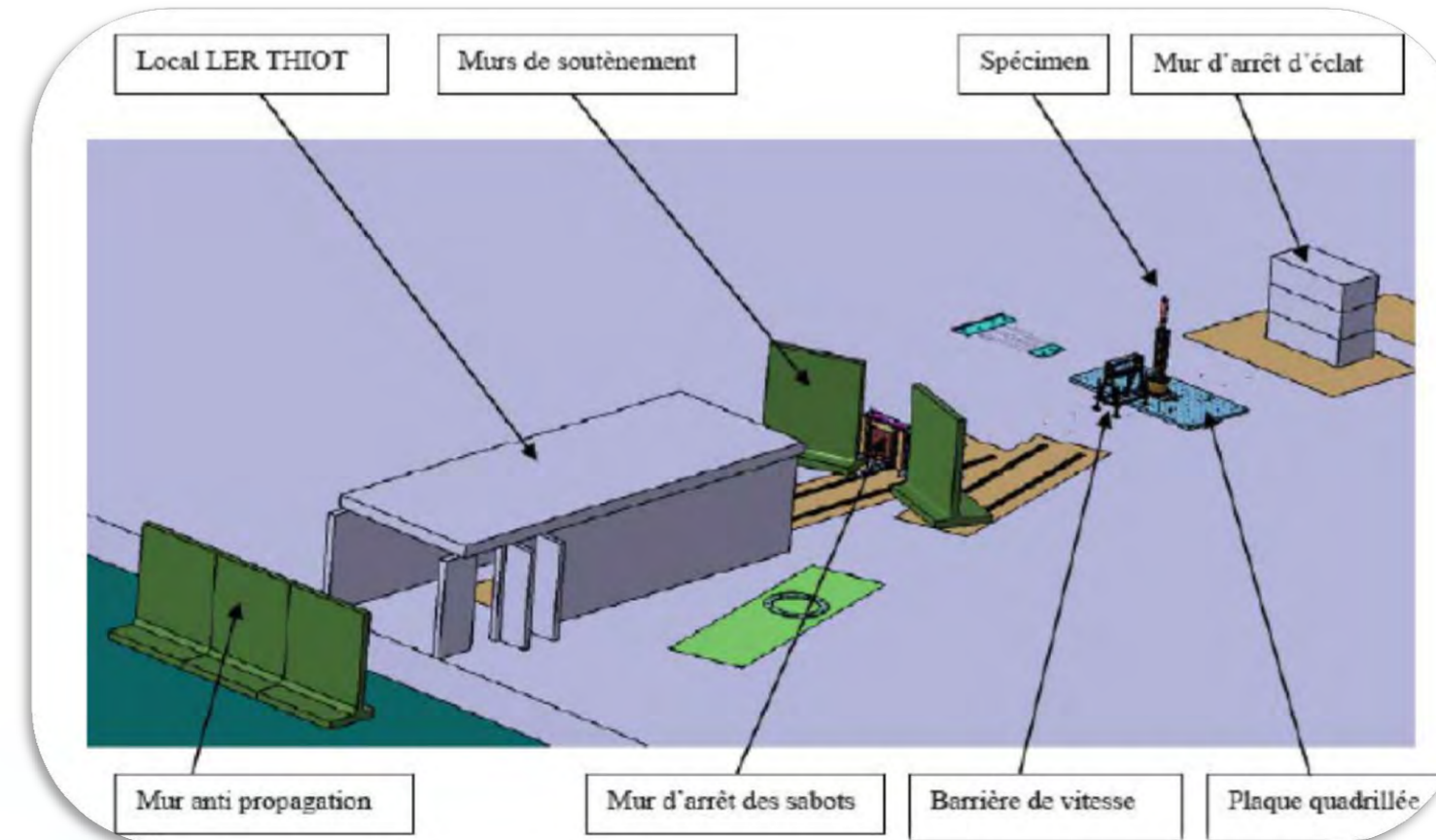
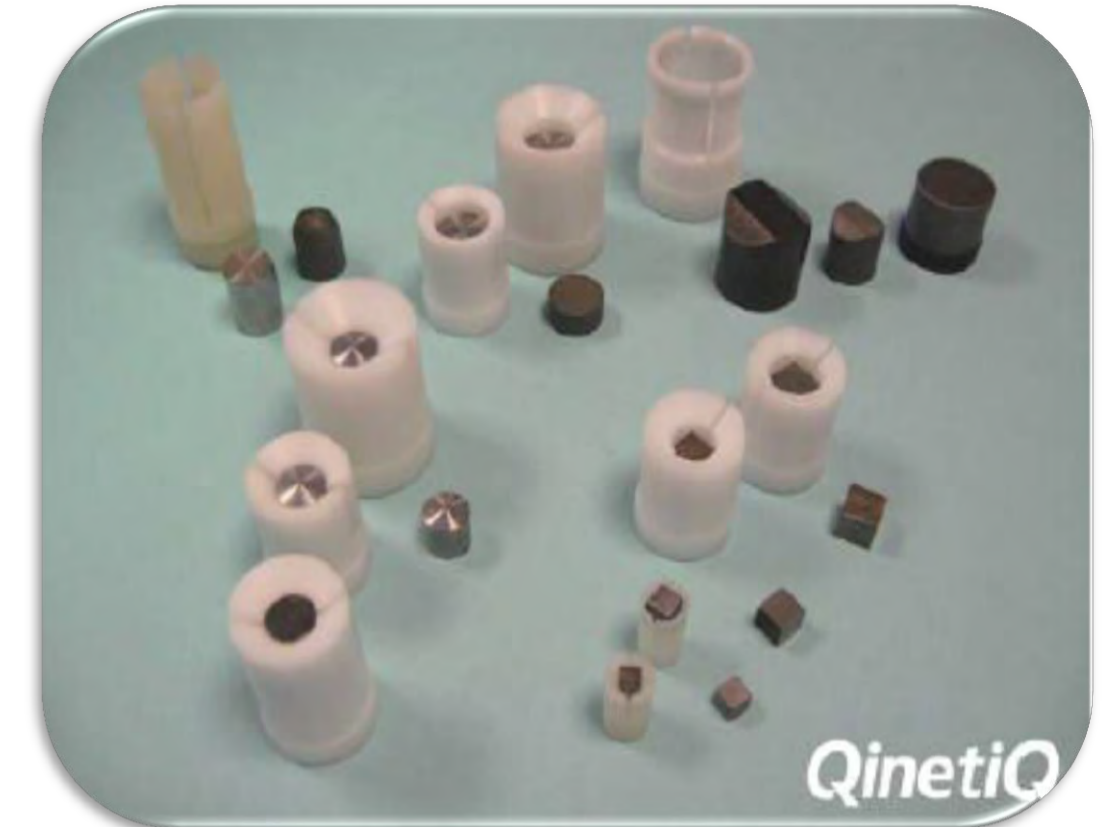
UNCHANGED

- No **launcher system** design guidance

UNCHANGED

- No example of the **test set-up** design

UNCHANGED



OTHER ISSUES DISCUSSED (2/2)

- **No requirement for a standoff distance** between the launching system and the test item
- **No new requirement** on the measurement of the fragment velocity
 - Assess the measurement **uncertainties** of the impact velocity, the impact location, and the total angular deviation

UNCHANGED

UNCHANGED

NEW

NEW OBSERVATIONS AND RECORDS



NEW

- Aim point(s) selected, hit point(s) (if possible) and whether the fragment exited from the test item or remained within it (if possible)
- Impact velocity of the fragment and **method of determination**
- Suitable blast or pressure gauges **shall** be positioned around the test item. The location and height of the gauges have to be recorded
- Accuracy at impact
- Brinell hardness of the threat fragment
- Total angular deviation of the fragment at impact (e.g. vector sum of yaw and pitch)
- Estimated measurement uncertainties for: (a) the impact velocity, (b) impact location, and (c) total angular deviation

OBSERVATIONS AND RECORDS

Unchanged / Rewording (1/2)

- Test item identification and configuration; Type and weight of energetic material; Listing of environmental preconditioning test performed; Spatial orientation of the test item;
- Test setup/configuration: Type of procedure, details of weapon(s) and munition used; Distance between weapon(s) and test item; Method of mounting and/or restraint; Distances from the test item to any protective wall or enclosure; Identification and location of any other instrumentation if used;
- Record of events versus time from the order to fire to the end of the trial; The nature of any reactions by the test item

MODIFIED

MODIFIED

UNCHANGED

UNCHANGED

OBSERVATIONS AND RECORDS

Unchanged / Rewording (2/2)

- Imagery of the item under test and the test setup shall be done before and after performing the test
- The nature and distribution of residue and debris (included recovery and mapping)
- Meteorological data (wind speed, direction) during the trial
- Indication of propulsion (video or other suitable means)
- Microphone or other suitable listening device to record audible events and enable correlation with visible events and indicated time
- Witness screens as a measure of projection severity

MODIFIED

MODIFIED

MODIFIED

UNCHANGED

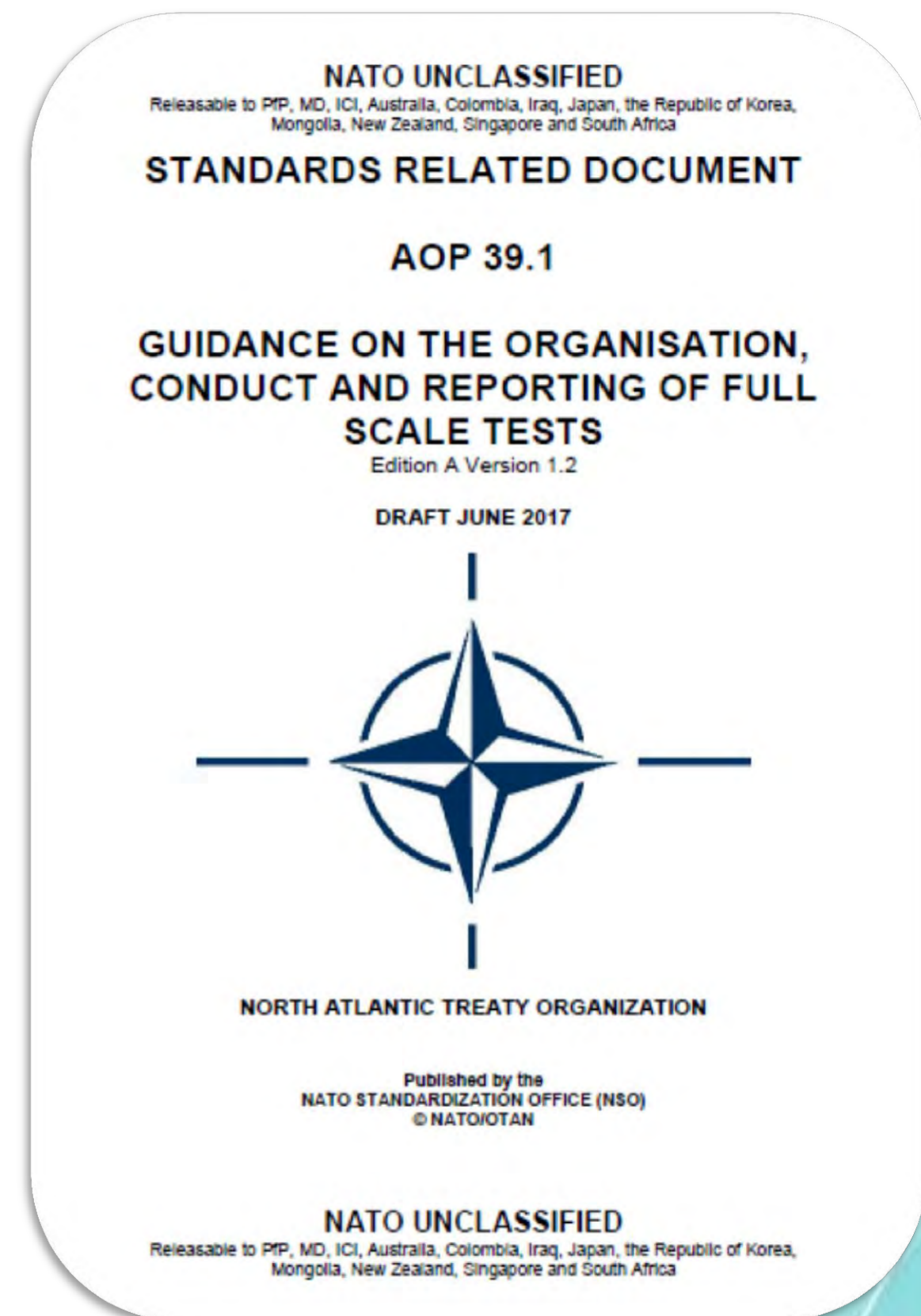
MODIFIED

MODIFIED

SOME MOVING SENTENCES TO SRD AOP-39.1

■ Sentences which are not specific to Fragment Impact test

- Tested Sample selection
- Layout of the munition
- Preliminary Shot
- Safety
- Orientation of impact normal to the surface of the munition
- Calibration of blast gauges

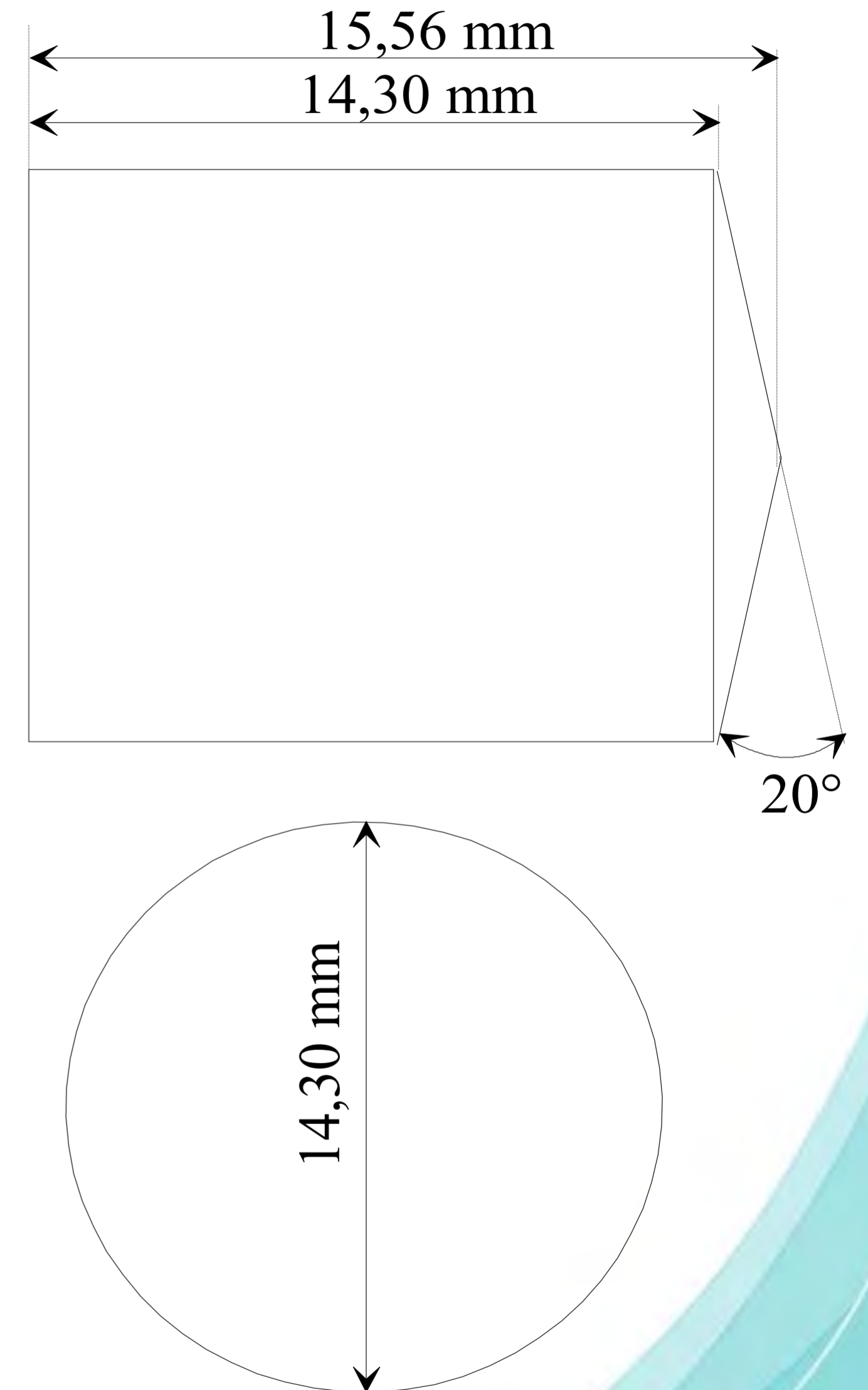


ANNEXES

■ Annex A: Standard fragment

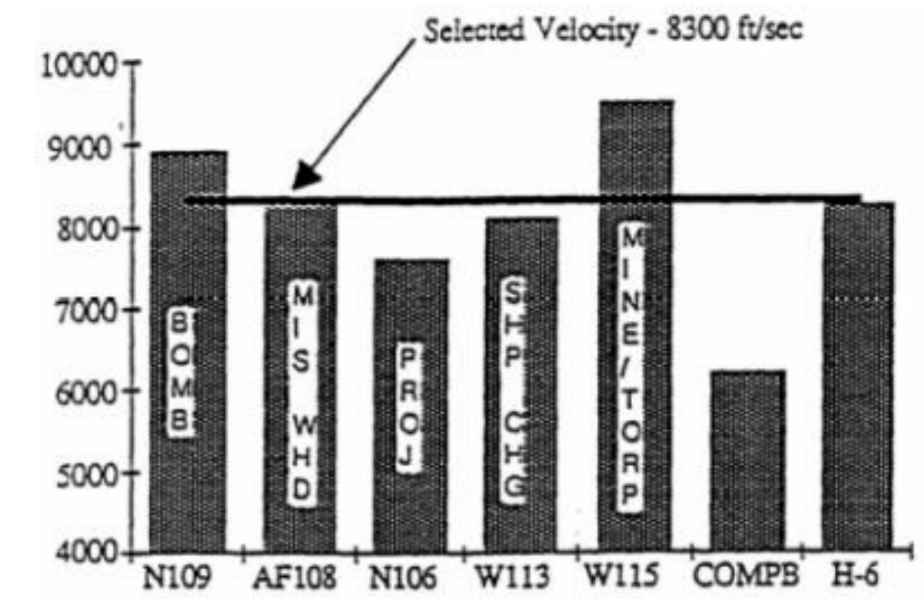
- Conical ended cylinder
- Tolerances: ± 0.05 mm and $\pm 0^{\circ}30'$
- Fragment Mass: 18.6 g
- Fragment material: mild, carbon steel with Brinell Hardness (HB) between **190** and 270

MODIFIED



ANNEXES

NEW



■ Annex B: Historical overview

- Changes between STANAG 4496 ED 1 and AOP 4496 ed.A version 1
- Historical information on the shape, the material and velocities of the fragment from the first version to now

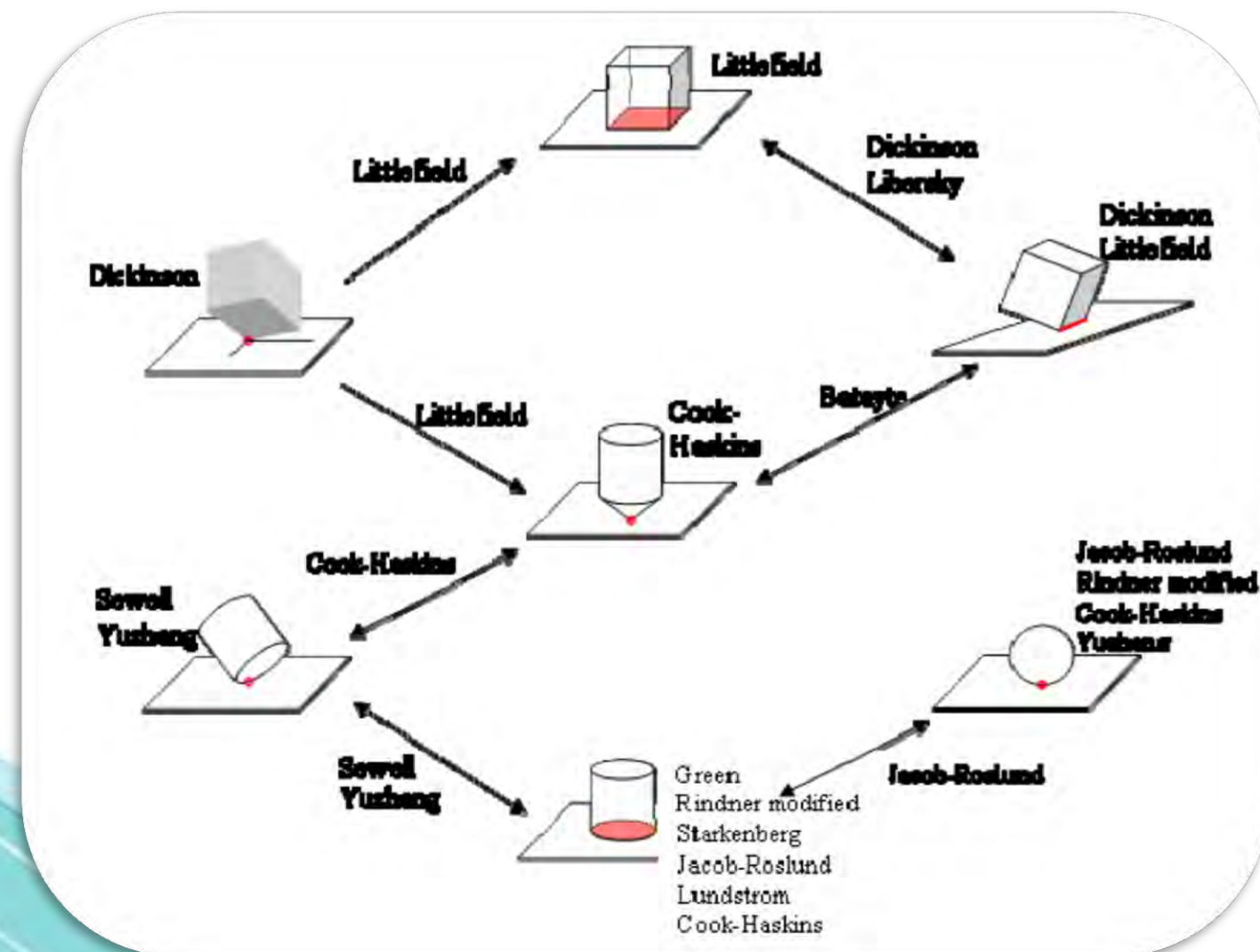


Table XXVIII: MSIAC Preferred Fragment Mass and Velocity

Munition	Worst Most Credible Mass Fragment (95±2% Confidence Level)	Largest Initial Fragment Velocity
	(g)	(m/s)
Anti-Aircraft missile (current)	4 (tungsten, tantalum)	2000
Anti-Aircraft missile (next generation)	4 -16	2600*
Ø 80mm mortar	16	1400
Ø 80mm to 105 mm shell	16	-
250lb bomb (Mk-81)	16	-
500lb bomb (Mk-82)	16	2000
Mk-48 torpedo	16 (aluminium)	2800
750lb bomb (M-117)	32	-
Ø 120 mm to 155 mm shell	64	1400
1000lb bomb (Mk-83)	64	2100
2000lb bomb (Mk-84)	64	2200
Exocet (natural fragmentation)	64	2000
Anti-ship missile (preformed fragments)	256	1800

* Using aimable/focused fragment warhead technology, fragment velocities are expected to increase by 20-35% within the next 5-10 years.

STATUS



- **Sent to AC/326 SG/B members for approval (March 2018)**
 - **silence procedure**



- **Next steps**

- Approbation by AC/326 Main Group (June 2018)
- Ratification process
- Formal application of STANAG 4496 ed.2 and AOP-4496 ed.A version 1

PARTICIPANTS

Thanks to all!



Florian Péchoux (FRA - Lead)

Fabien Chassagne (FRA)

Christophe Jacq (FRA)

Nicolas Kmiec (FRA)

Pauline Tabozzi (FRA)

Albert Bouma (NLD)

Gunnar Ove Nevstad (NOR)

Jon Toreheim (SWE)

Hakan Sahin (TUR)

Tahir Turgut (TUR)

Ben Keefe (UK)

Thomas Reeves (UK)

Nathan White (UK)

Jacek Foltynski (US)

Brian Fuchs (US)

Heather Hayden (US)

Dave Houchins (US)

Dave Hubble (US)

Kathryn Hunt (US)

Lori Nock (US)

Dan Pudlak (US)

Brian Roos (US)

Daniel Ross (US)

Stephen Struck (US)

Tom Swierk (US)

Ken Tomasello (US)

Ernie Baker (MSIAC)

Emmanuel Schultz (MSIAC)



Thank you for your attention!



Any Questions?



Investigation of the Hugh James Criteria Using Estimated Parameters

Justin C. Sweitzer^{1*}, Nicholas R. Peterson², and Nausheen Al-Shehab³

ABSTRACT:

The ability to predict the response of an energetic device to IM stimulus is one of the major focus areas within the IM community. Several methodologies have been proposed and used for this purpose, including direct calculation via reactive burn models, analytic criteria such as Held's V^2D criteria, and semi-empirical techniques such as the Hugh James criteria. A method was recently presented that leverages the James criteria with estimated parameters combined with the ALE3D hydrocode and statistical models to predict reaction threshold. In this paper, this methodology is examined in detail by applying it to a well-characterized explosive.

The basis for the methodology is in threshold statistics, as detailed by Hrousis, et al. Energetic materials are often characterized in terms of '50% go/no-go' thresholds, underscoring the inherent variability in material response. These concepts were initially applied to an explosive for which James parameters were not readily available (LX-14), but a large body of Fragment Impact (FI) test data was. Values for the missing parameters were 'guessed' by substituting parameters from a similar explosive. The initiation threshold was developed by applying the 'guess' parameters to the existing data, and extrapolated forward through a Binary Logistic Regression (BLR) model.

To test this methodology, the UF-TATB parameters from Hrousis, et al, were used in place of test data. The mean and variance of the ignition threshold were calculated using the QMU method and applied to a BLR model. Model variations were then simulated to test the predictive capability of the method.

¹ Practical Energetics Research, Inc.

² U.S. Army Aviation and Missile Research, Development, and Engineering Center

³ U.S. Army Armaments Research, Development, and Engineering Center

* Corresponding Author, (1) 256-867-1222, justin.sweitzer@per-hq.com

Introduction

Computational prediction of munition response to impact stimulus is routinely performed via hydrocode analysis. The material models used to simulate energetic materials are usually either a reactive flow model, such as Tarver-Cochran Ignition & Growth Reactive Burn (IGRB) or History Variable Reactive Burn (HVRB) or an inert material. Reactive models are capable of directly predicting the material response, but carry some disadvantages, such as increased computational load and binary response. Simulations using this type of model are capable of predicting detonation or non-detonation, but do not provide an estimate of distance from initiation threshold.

When instead an inert material model is used, prediction of initiation behavior relies on an external analysis. Multiple initiation criteria are used for this purpose, such as the Held's¹⁻³ V^2D for shaped charge jets, Walker & Wasley's⁴ $P^2\tau$, or the James criteria⁵ combined specific kinetic energy and energy fluence. These approaches are capable of producing excellent agreement with experiment, provided a suitable threshold value has been provided for the explosive under investigation. Previously, a method for predicting energetic response to impact stimulus has been presented⁶ that relies on the James method, but uses the outcome of previous tests⁷ instead of compiled critical values.

In the previous study, the critical values of James' parameters were not located for LX-14, but several Fragment Impact (FI) tests had already been conducted. These values were substituted arbitrarily for those of another explosive, and a BLR model was used for threshold to reaction. The justification for doing so was that within the geometry and impact conditions investigated, the calculated result should at least trend in a physically meaningful way. At that time, no further justification was offered for the approach. This paper investigates the idea further, and provides a validation study for the previous effort.

James Criteria and QMU Threshold

The James criteria has roots⁸ in the critical energy criteria of Walker & Wasley⁴. James extended⁵ the critical energy concept to include both the energy fluence across a unit area, E_c , and a specific kinetic energy, Σ_c . The resulting initiation threshold is hyperbolic in E - Σ space, in accordance with the relationship

$$1 = \frac{E_c}{E} + \frac{\Sigma_c}{\Sigma} \quad (1)$$

The concept was further extended by Hrousis, et al⁹ to develop a single parameter, J , as a combination of the two critical parameters. Additionally, a functional form of energy fluence was suggested that is well-suited to hydrocode calculation. Their relationships are

$$J = \frac{E_c}{E} + \frac{\Sigma_c}{\Sigma}, \quad E = \int P u dt, \quad \Sigma = \frac{u^2}{2} \quad (2)$$

In the above equation, P represents pressure and u is particle velocity. In this form, the value of $J_{\max} = 1$ corresponds to marginal initiation, while numbers less than 1 or greater than 1 imply non-initiation or initiation with margin, respectively. By carrying forward the measured uncertainty in experimental results

and assuming that J_{critical} is normally distributed with a mean of 1.0, they developed an engineering sense of margin from initiation.

The p-values associated with the computed value of J_{max} can then be viewed as a probability of initiation occurring. They demonstrated the developments with parameters for $\mu\text{F TATB}$ as the explosive, providing a set of critical parameters and standard deviation of J as

$$E_c = 0.26 \frac{MJ}{m^2}, \quad \Sigma_c = 0.67 \frac{MJ}{kg}, \quad \sigma_J = 0.15 \quad (3)$$

These parameters were used in this study as the basis for computational predictions.

Binary Logistic Regression Model

Binary Logistic Regression¹⁰ is a regression technique by which categorical data can be used as a response variable. The model approach allows overlap in predictor variables versus observed category to build a probabilistic function describing the likelihood of a predictor to fit into a given category. In the previous study⁶ the predictor variable was J_{max} and the categorical response variable was detonation or non-detonation. Some attempt was made to delineate IM reaction type (I,II,III, etc) as the response variable, but the experimental uncertainty caused this analysis to be ineffective.

Mathematically, the approach takes the exponential of a linear function to represent the probability of category fit, as shown in Eq. 4 below, where x represents a predictor variable and p is the probability that the response will fit in a base (null) category.

$$p(x) = \frac{1}{1 + e^{-ax-b}} \quad (4)$$

In a least-squares regression model the parameters are fit by minimizing the squared error, which is analytically tractable in the case of continuous predictor and response variables. In the logistic regression models, a likelihood function optimization is used to fit the slope and intercept of the linear function to experimental data. The likelihood function is a measure of model error, and is defined

$$LL = \sum_{i=1}^n y_i \ln(p_i) + (1 - y_i) \ln(1 - p_i) \quad (5)$$

The y in Eq. 5 is the observed fraction of observations fitting into the null category, and the subscript i refers to the predictor variable level. This equation is maximized numerically to fit the slope and intercept (a and b from Eq. 4).

Simulation Approach

In order to validate the described approach, a simulation strategy was devised to represent the process. Using the parameters in Eq. (3) 2D, axisymmetric hydrocode simulations were performed in ALE3D¹¹ with a null-constitutive model and Mie-Gruneisen Equation of State for μ F TATB. The explosive was modeled as a 100 mm diameter by 50 mm length cylinder, with a 3mm case and the impact occurring on one of the two flats. The standard IM fragment geometry (STANAG 4496) was used, and impact velocity varied from 300 – 3,000 m/s. The simulation geometry is shown in Fig. 1.

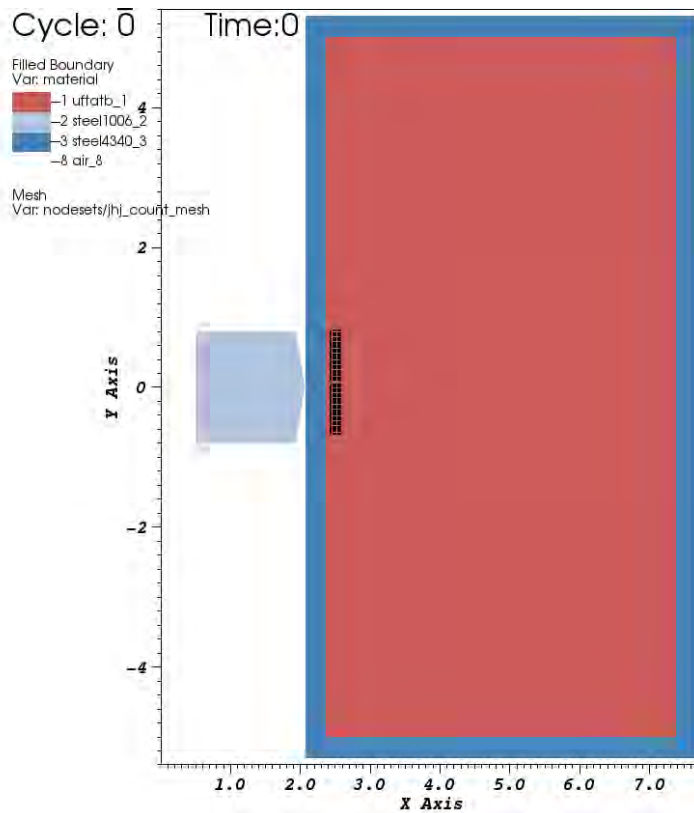


Figure 1. Hydrocode model geometry. This geometry was used throughout the simulation series.

The value of J was calculated by defining a derived variable in the hydrocode analysis. The derived variable is calculated across the mesh domain. It is extracted as the mean value from a nodeset of the same radius as the tracer particle and 0.2 mm thick located 0.05 mm inside the explosive. Nodes on the case boundary and symmetry plane were excluded intentionally to avoid numeric noise. Calculated values of J_{\max} are plotted versus velocity in Fig. 2.

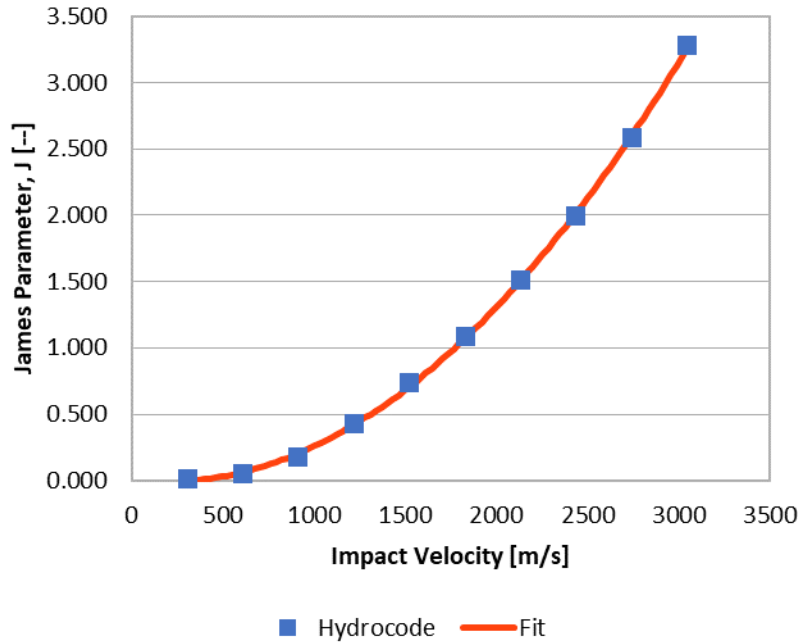


Figure 2. Calculated J_{max} at various impact velocities. Relationship is approx. quadratic.

The mean (1.0) and standard deviation (0.15) of J were used to calculate the Z-statistic, leading to the probability of detonation represented in Fig. 3.

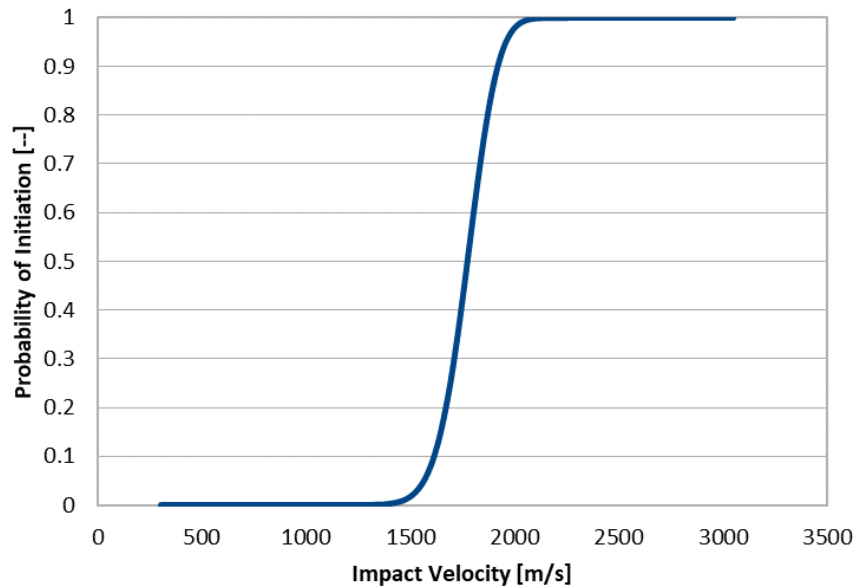


Figure 3. Probability curve plotted with impact velocity for known James parameters.

This probability function was used to generate a set of 25 ‘observations’. Using random numbers, impact velocities between 1675 and 1980 m/s were generated to represent test data. Another random number was compared against the p-value at the given velocity. If the random number exceeded the p-value, non-detonation (0) versus detonation (1) was recorded. This process represents experimental uncertainty such as impact location variations while providing the actual p-value (devoid of external influence) to compare with the predictions made with arbitrary critical values. The generated data appears in Table 1.

Table 1. Randomly generated observations from known parameter probability curve.

Impact Velocity m/s	J (KNOWN) --	Z --	P --	Random Number --	Result
1798	1.167	1.111	0.867	0.629	1
1719	1.075	0.501	0.692	0.836	0
1924	1.137	0.912	0.819	0.023	1
1873	1.019	0.128	0.551	0.313	1
1870	1.108	0.717	0.763	0.939	0
1768	1.095	0.632	0.736	0.584	1
1867	1.001	0.007	0.503	0.637	0
1798	0.947	-0.356	0.361	0.679	0
1693	0.996	-0.027	0.489	0.022	1
1829	1.035	0.233	0.592	0.184	1
1725	1.025	0.164	0.565	0.840	0
1837	1.200	1.332	0.909	0.119	1
1737	1.096	0.641	0.739	0.475	1
1816	0.966	-0.226	0.410	0.753	0
1683	1.057	0.381	0.648	0.251	1
1772	1.031	0.204	0.581	0.889	0
1901	1.144	0.961	0.832	0.442	1
1829	1.166	1.107	0.866	0.110	1
1848	1.124	0.828	0.796	0.122	1
1854	1.094	0.625	0.734	0.455	1
1803	1.030	0.201	0.580	0.964	0
1790	1.025	0.168	0.567	0.502	1
1843	1.153	1.018	0.846	0.923	0
1811	0.978	-0.144	0.443	0.296	1
1770	1.096	0.643	0.740	0.267	1

Further simulations were performed using arbitrary values of the critical parameters, which appear in Table 2.

Table 2. Simulation matrix showing the ‘guess’ values of E_c and Σ_c .

	E_c	Σ_c
	MJ/m ²	MJ/kg
Known	0.26	0.67
Variation 1	0.1	0.1
Variation 2	0.1	0.9
Variation 3	0.9	0.9
Variation 4	0.9	0.1

Results & Discussion

When the arbitrary values of E_c and Σ_c are substituted for the known values, the response curve changes shape significantly, though a quadratic regression still fits extremely well. The J_{max} versus velocity plots for several iterations appear in Fig. 4.

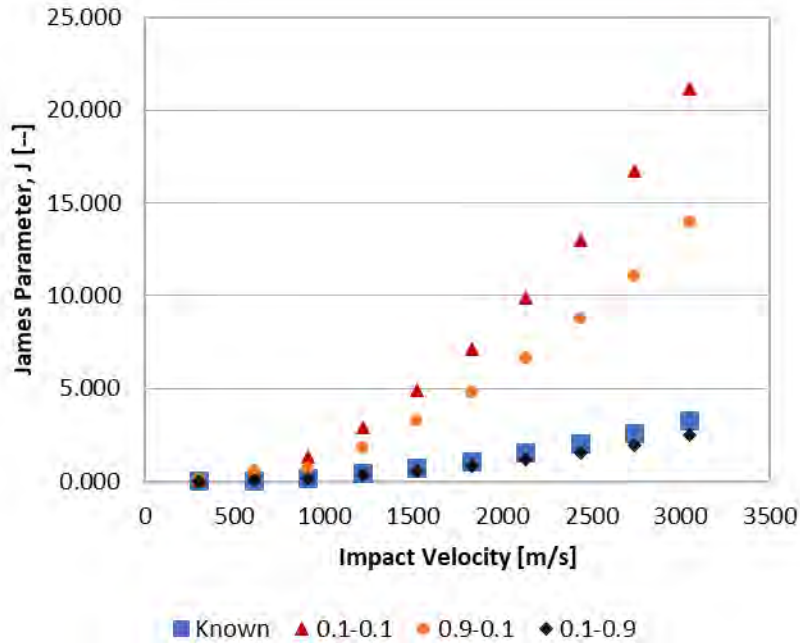


Figure 4. Predicted J_{max} values for arbitrary values at various velocities

For each set of parameters, the J_{max} parameter was computed from the regression fit for each velocity in the observation data. A BLR model was fit to the J_{max} predictor with the randomized result as response variable for the first 5, 10, 15, and 20 observations. The remainder of observations were then used to test predictive capability of the resulting model fit. Probability of detonation versus impact velocity is shown in Fig. 5 for the known case compared to the two most different sets of E_c and Σ_c in terms of J (0.1-0.1 and 0.1-0.9). The prediction is only marginally improved by increasing the size of the sampled dataset from 10 to 20. In each case, it was found that the BLR model detonation probability remained unchanged for

any value of E_c and Σ_c , which does tend to validate the previous approach. No attempt has been made to verify this finding mathematically at this point. The function optimization aspect of the BLR method is handled numerically, making it difficult to analytically prove the finding.

In terms of model accuracy, 76% of observations were correctly categorized according to recorded reaction (1 or 0) and approximately the same proportion according to known probability. The number of observations correctly categorized remains consistent across the range of sample size. This is a similar accuracy to the previous study, though in that case the true underlying distribution parameters were unknown.

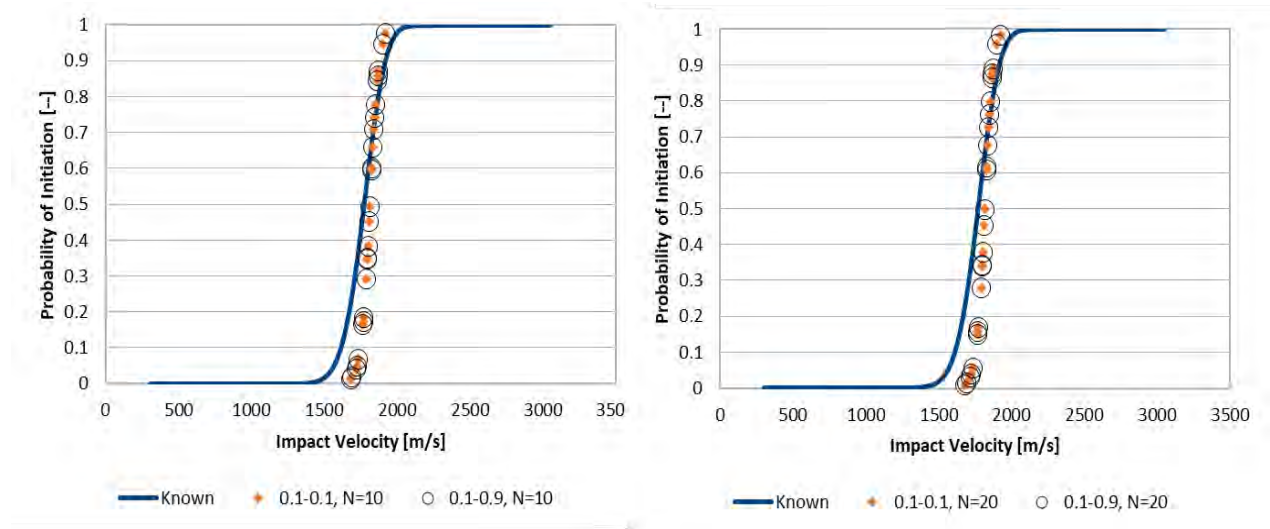


Figure 5. Estimated probability curves from BLR compared to known probability curve.

In light of the findings that show BLR results remaining across different values of E_c and Σ_c another question is raised. How can the predictive capability of this approach be improved? From Fig. 5, it can be seen that the slope of the BLR probability is steeper than the known probability curve. It was speculated that this stems from all of the observation data being close to the threshold, without bounding values on the extremes. The first two observations were altered to 2,430 m/s (1.0 Reaction = Detonation) and 610 m/s (0.0 Reaction = Non-detonation) and the analysis was repeated for the $E_c, \Sigma_c = 0.1, 0.1$ case.

The BLR predictive capability improved to 96% using 20 observations, and dropped to 72% using 5 observations. This is likely due to the first two observations being changed, leaving only 3 threshold observations in the 5 sample dataset versus 18 in the 20 sample dataset. The effect is to skew the probability estimate, as there are fewer anchor points toward the center of the curve. When 20 observations, including the bounding samples, are included the curve is well enough characterized to nearly replicate the known probability curve. The improved probability estimates appear in Fig. 6.

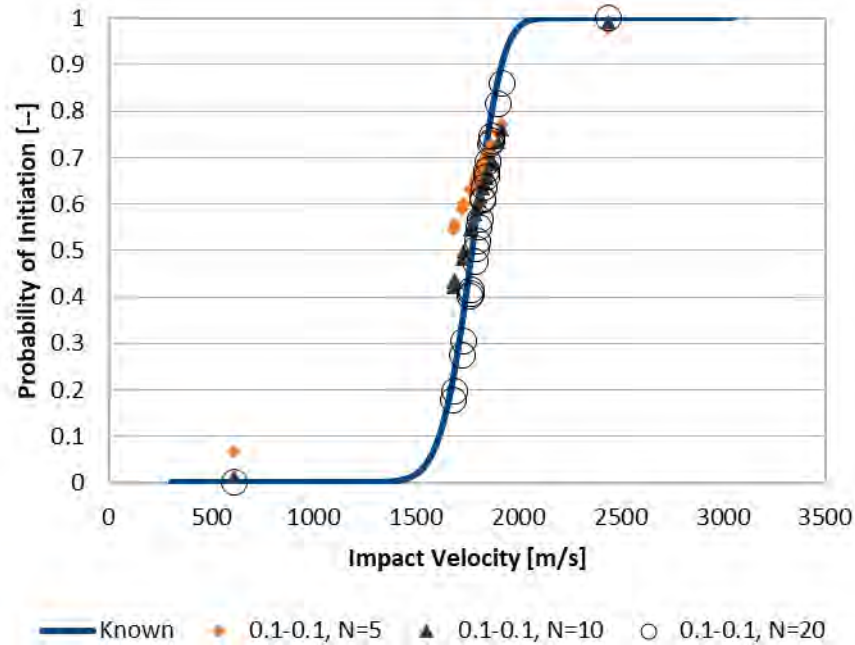


Figure 6. Improved estimate probability curves from BLR compared to known probability curve.

Conclusion

The simulation approach utilized in a previous study⁶ has been validated through a series of hydrocode simulations designed to investigate the variance of predictions made with a combined James model / binary logistic regression model. Through these simulations, it was shown that the BLR predictions remain unchanged when parameters are selected arbitrarily. It was further shown that the addition of bounding cases to the data set drastically improves the predictive capability of the model.

The importance of this study lies in the ability to pivot from a relatively small number of impact tests into a predictive capability for further tests. As in the prior work, the intent is to provide a means to iteratively improve a munition's response to impact stimulus. As more design variations are tested within a geometry envelope, the model prediction will become increasingly accurate.

References

1. Held, M. Experiments of Initiation of Covered, but Unconfined High Explosive Charges by means of shaped charge jets. *Propellants, Explos. Pyrotech.* **12**, 35–40 (1987).
2. Held, M. Shaped Charge Jet Initiation on Explosive Charges equipped with barriers made up of various materials. *Propellants, Explos. Pyrotech.* **19**, 290–294 (1994).
3. Held, M. Initiation Criteria of High Explosives at different projectile or jet densities. *Propellants, Explos. Pyrotech.* **21**, 235–237 (1996).
4. Walker, F. E. & Wasley, R. J. A General Model for the Shock Initiation of Explosives. *Propellants, Explos. Pyrotech.* **1**, 73–80 (1976).
5. James, H. R. An extension to the critical energy criterion used to predict shock initiation thresholds. *Propellants Explos. Pyrotech.* **21**, 8–13 (1996).
6. Sweitzer, J. C. & Peterson, N. R. Method for Prediction of Fragment Impact Response Using Physics Based Modeling and Statistical Analysis. *Procedia Eng.* **103**, 601–609 (2015).
7. Peterson, N. R. & Sweitzer, J. C. Composite Material Particle Impact Mitigation Sleeve Testing. *Procedia Eng.* **103**, 475–481 (2015).
8. James, H. R. Critical energy criterion for the shock initiation of explosives by projectile impact. *Propellants, Explos. Pyrotech.* **13**, 35–41 (1988).
9. Hrousis, C. a, Gresshoff, M. & Overturf, G. E. *Probabilistic Shock Initiation Thresholds and QMU Applications.* (2009).
10. Dodson, B., Hammett, P. C. & Klerx, R. Binary Logistic Regression. in *Probabilistic Design for Optimization and Robustness for Engineers* 202–224 (John Wiley & Sons, Ltd, 2014). doi:10.1002/9781118796245.ch11
11. Nichols (ed), A. *User's Manual for ALE3D: An Arbitrary Lagrange/Eulerian 3D Code System.* (2007).

Investigation of the Hugh James Criteria Using Estimated Parameters

Justin Sweitzer, Practical Energetics Research, Inc.

Nicholas Peterson, US Army AMRDEC

Nausheen Al-Shehab, US Army ARDEC





Background – Hugh James Criteria

- The James criteria is a phenomenological model of shock initiation
 - “James Space” – energy fluence and specific kinetic energy
 - If critical values of energy fluence, E , and specific kinetic energy, Σ , are surpassed, then initiation is predicted.
- Concept extended by Hrousis, et al, to a generalized parameter, J
 - $J < 1 \rightarrow$ non-initiation with margin
 - $J = 1 \rightarrow$ marginal initiation
 - $J > 1 \rightarrow$ initiation with margin

$$J = \frac{E_c}{E} + \frac{\Sigma_c}{\Sigma}, \quad E = \int P u dt, \quad \Sigma = \frac{u^2}{2}$$

James, H. R. An extension to the critical energy criterion used to predict shock initiation thresholds. *Propellants Explos. Pyrotech.* **21**, 8–13 (1996).

Hrousis, C. a, Gresshoff, M. & Overturf, G. E. *Probabilistic Shock Initiation Thresholds and QMU Applications.* (2009).



Background – QMU Thresholds

- Hrousis' extensions result in a probability density function for initiation.
 - Mean value of 1.0 for initiation
 - Estimate of uncertainty in critical values leads to standard deviation
 - Assume normally distributed



Background – BLR Model

- Linear regression between categorical observations
- Probability density function yields likelihood that observation fits into a category

$$p(x) = \frac{1}{1 + e^{-ax-b}}$$

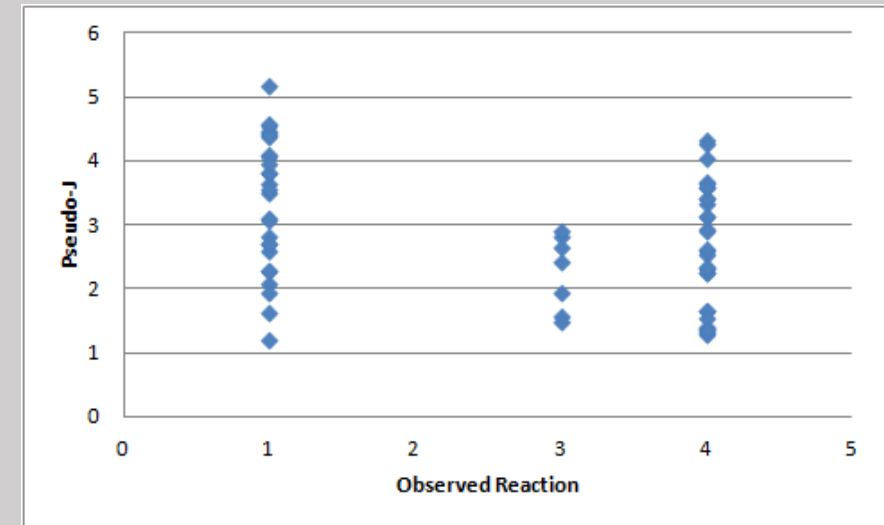
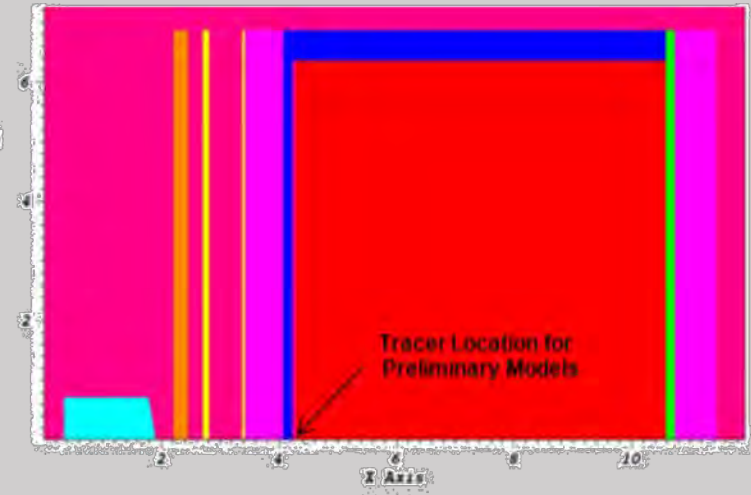
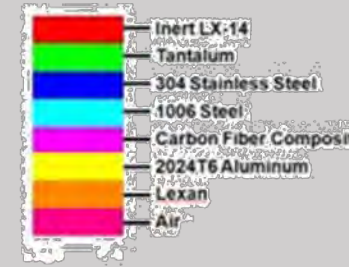
- Log-Likelihood function must be numerically optimized to maxima to fit slope and intercept of linear function $f(x) = ax + b$

$$LL = \sum_{i=1}^n y_i \ln(p_i) + (1 - y_i) \ln(1 - p_i)$$



Background – Prior Effort

- Previous effort substituted arbitrary values for critical values
 - Suitable critical values not located for main fill HE (LX-14)
 - Multiple Fragment Impact (FI) test data points were available
 - Hydrocode simulations of test data used to estimate J-parameter
 - Binary Logistic Regression (BLR) model tied to FI test observations





Problem Statement

- The previous effort substituted arbitrary parameters for the critical values under the assumption that the BLR would correctly categorize results from FI tests.
- The validity of this assumption was not investigated in detail

Hypothesis:

A BLR model fit to experimental data is a good estimator of the true probability density.

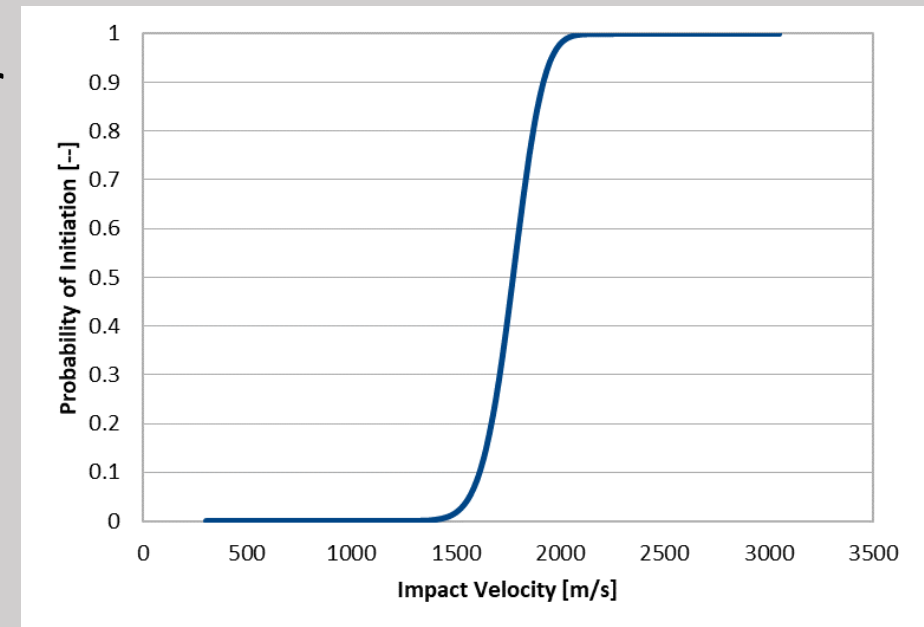


Methodology

- Validity of hypothesis tested by using the parameters of Hrousis, et al for uF-TATB to generate a matrix of simulated ‘observations’
 - Hydrocode calculations performed with the known E_c, Σ_c
 - Yields ‘True’ probability density
 - Iterations with arbitrary E_c, Σ_c , random number compared to p-value from ‘True’ probability function.
 - Yields ‘Observations’ to fit BLR model

Hypothesis is tested by comparing pdf of BLR model to ‘True’ pdf.

	E_c MJ/m ²	Σ_c MJ/kg
Known	0.26	0.67
Variation 1	0.1	0.1
Variation 2	0.1	0.9
Variation 3	0.9	0.9
Variation 4	0.9	0.1

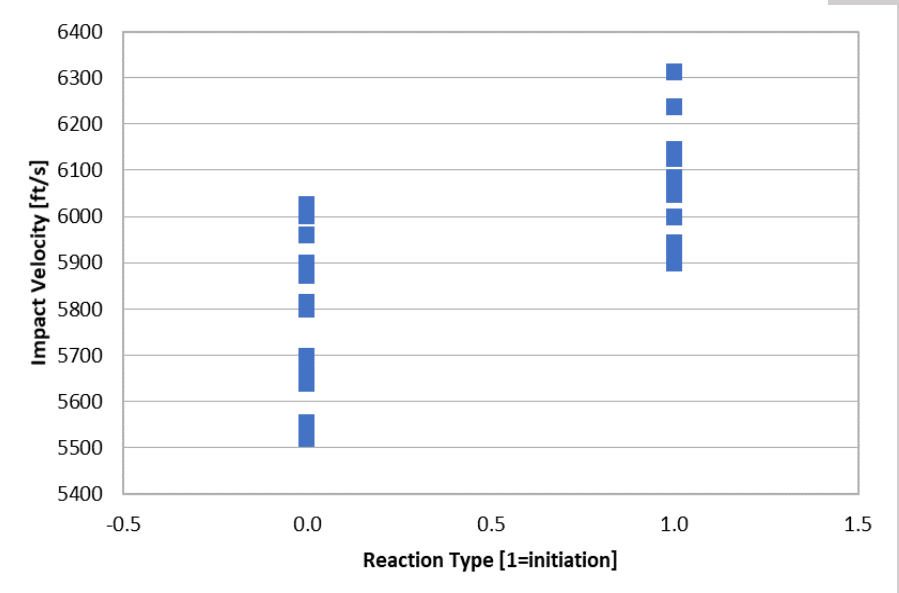
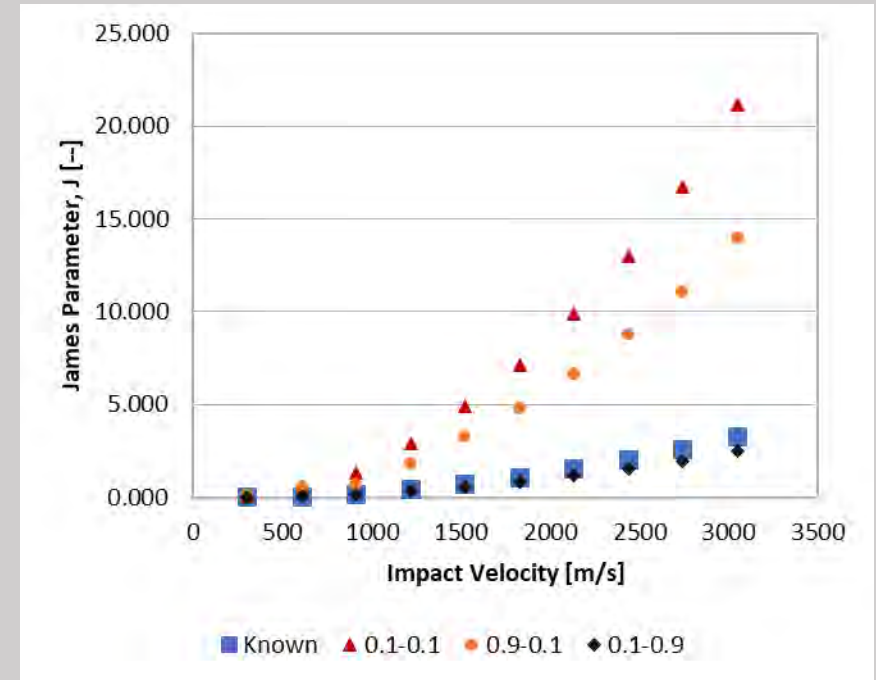


Probability of initiation at various impact velocities



Calculation Results

- Quadratic relationship between impact velocity and calculated J_{max} in all cases.
- P-value vs random number results in overlap of observations
 - Some impacts with $J < 1$ initiate
 - Some impacts with $J > 1$ do not
- Consistent with observations in FI & Gap Tests





Generated Observation Matrix

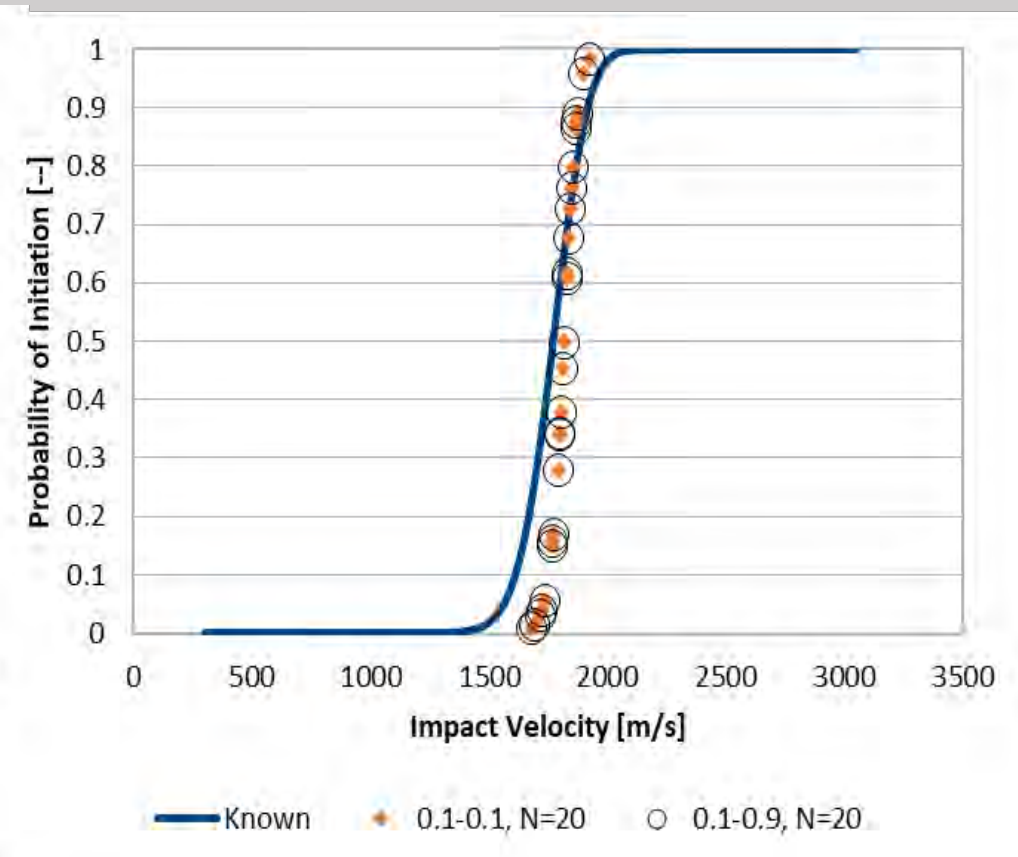
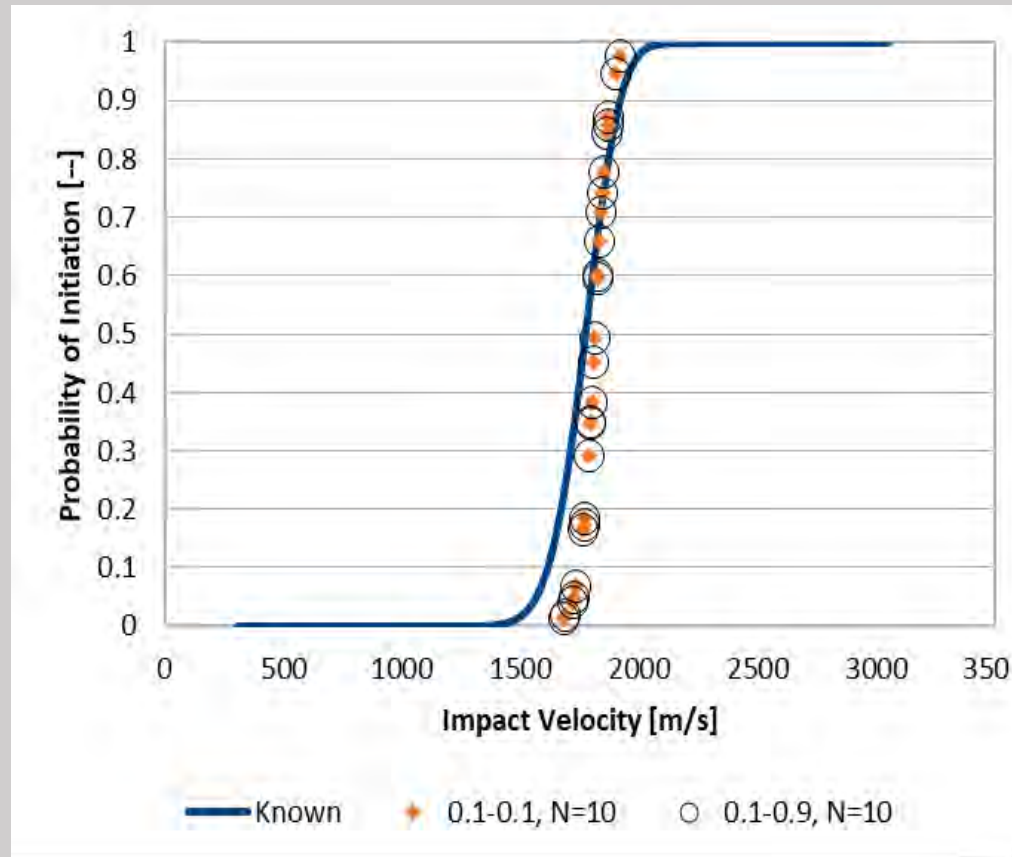
- Set of 25 'observations' generated
 - Randomized impact velocity
 - J-values from known critical parameters used for probability density
 - BLR models fit to increments of 5 data points for each set of arbitrary parameters
 - N = 5, 10, 15, 20, 25

Impact Velocity m/s	J (KNOWN) --	Z --	P --	Random Number --	Result
1798	1.167	1.111	0.867	0.629	1
1719	1.075	0.501	0.692	0.836	0
1924	1.137	0.912	0.819	0.023	1
1873	1.019	0.128	0.551	0.313	1
1870	1.108	0.717	0.763	0.939	0
1768	1.095	0.632	0.736	0.584	1
1867	1.001	0.007	0.503	0.637	0
1798	0.947	-0.356	0.361	0.679	0
1693	0.996	-0.027	0.489	0.022	1
1829	1.035	0.233	0.592	0.184	1
1725	1.025	0.164	0.565	0.840	0
1837	1.200	1.332	0.909	0.119	1
1737	1.096	0.641	0.739	0.475	1
1816	0.966	-0.226	0.410	0.753	0
1683	1.057	0.381	0.648	0.251	1
1772	1.031	0.204	0.581	0.889	0
1901	1.144	0.961	0.832	0.442	1
1829	1.166	1.107	0.866	0.110	1
1848	1.124	0.828	0.796	0.122	1
1854	1.094	0.625	0.734	0.455	1
1803	1.030	0.201	0.580	0.964	0
1790	1.025	0.168	0.567	0.502	1
1843	1.153	1.018	0.846	0.923	0
1811	0.978	-0.144	0.443	0.296	1
1770	1.096	0.643	0.740	0.267	1



BLR Model Fit

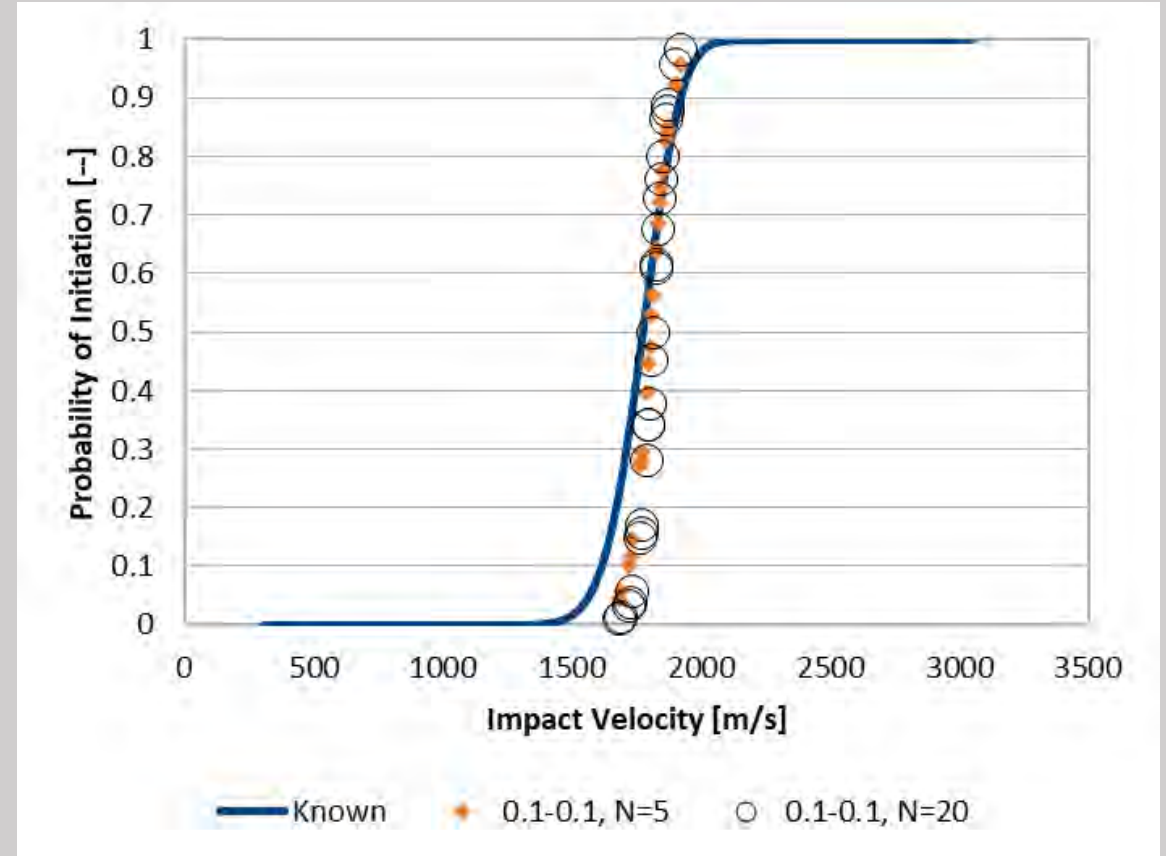
- The BLR model predictions remain consistent regardless of critical parameter values used.





Sample Size Dependence

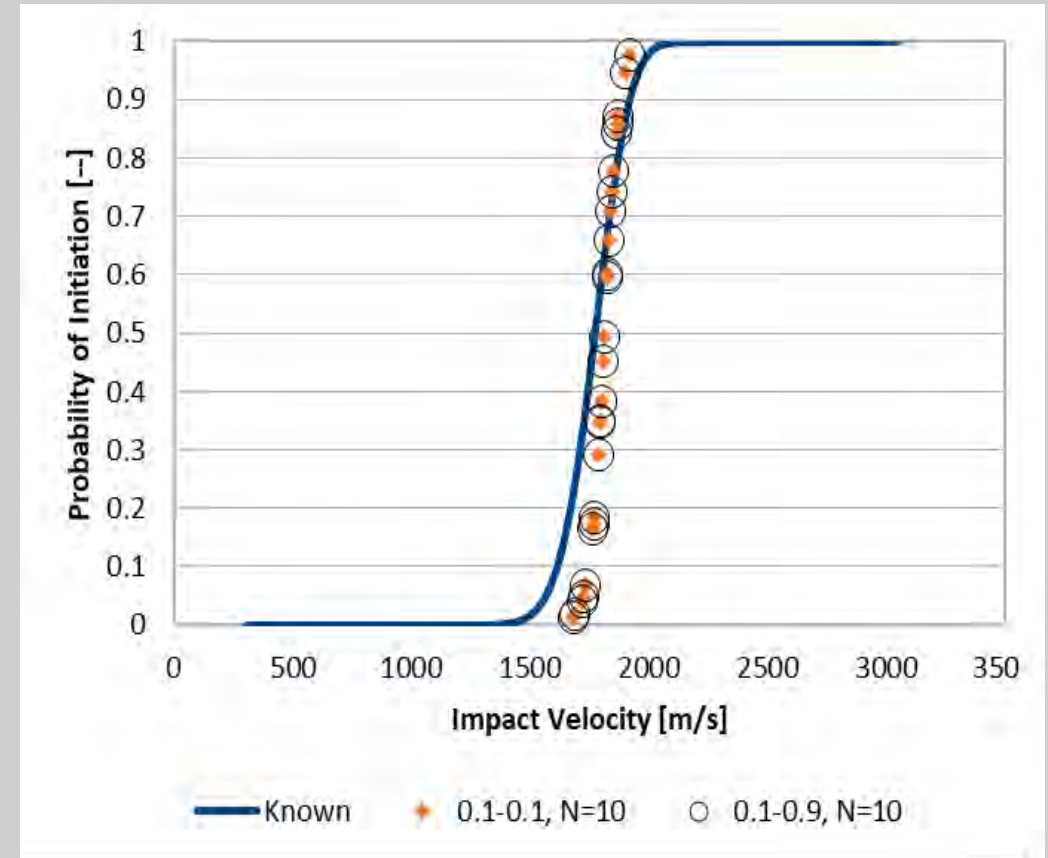
- Some sensitivity to sample size, but generally consistent with $N=5$ through $N=20$
 - Provided that all observations are in the vicinity of initiation threshold
- Caveat: The BLR model fit requires overlap in the observations, ie sub-threshold initiation and supra-threshold non-initiation.





Improved BLR Model Fit – Anchor Points

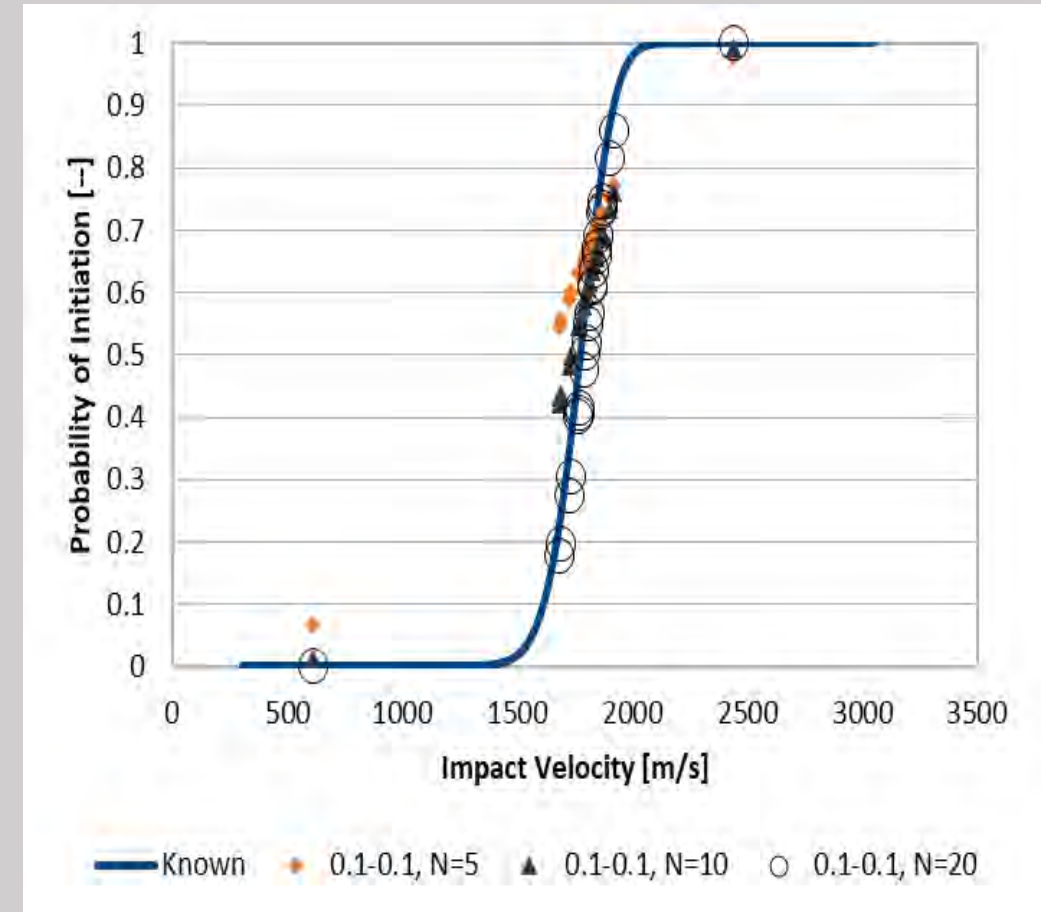
- The BLR model correctly categorized ~76% of observations.
 - Deviation mostly limited to the high and low impact velocities.
- Observations were purposely generated to be near the initiation threshold.
- Predictive capability could be improved by adding ‘Anchor Points’ at velocity extremes.





Improved BLR Model Fit – Anchor Points

- First two observations replaced with anchor points
 - 500 m/s – Non-initiation
 - 2500 m/s – Initiation
- Ordered observations skew the sample size for smaller sets (N=5,10 diverge more)
 - N=5, 72% categorized correctly
 - N=10, 88% categorized correctly
 - N=20, 96% categorized correctly
- Approaches the 'True' probability curve





Conclusions

- This technique is effective as an estimator of initiation threshold in the absence of well-characterized Hugh James parameters, given that some test data is available.
 - Generally small sample sizes produce very reasonable estimates of initiation threshold, provided that they are all near-margin (76%, N=5)
 - Much improved accuracy is possible by providing anchor points, but larger sample sizes are necessary (72%, N=5 -> 96%, N=20)
- Critical parameters and associated standard deviation in J could potentially be backed-out of this analysis.
 - Complicated by numeric optimization of LL function in regression analysis.



Questions?

Insensitive Munitions and Energetic Materials Technology Symposium
 April 23 – 26, 2018, Portland, OR

Life Cycle Demilitarization Considerations for IM Development

Gary Mescavage,
 Chief Engineer (Acting),
 Product Manager for Demilitarization

Abstract Number 20114

Demilitarization in the Life Cycle

Demilitarization is the end stage of the life cycle of military materiel. Acquisition policy states that “at the end of its useful life, a system will be demilitarized and disposed of” (DoD Instruction 5000.02 5.d.(14)(b)2, 7 Jan 2015) This requirement includes “conventional ammunition.” “Conventional ammunition” is defined in DoDD 5160.65 as: “An end item, complete round, or materiel component charged with explosives, propellants, pyrotechnics, or initiating composition for use in connection with defense or offense (including demolitions) as well as ammunition used for training, ceremonial, or non-operational purposes. This includes inert devices that replicate live ammunition, commonly referred to as dummy ammunition, which contain no explosive materials.” Examples of conventional ammunition are identified in DoDD 5160.65 and shown in Table 1 below. Tactical missiles (not strategic missiles) are included and sometimes classified separately from other conventional ammunition. Conventional ammunition does not include nuclear, chemical, or biological munitions.

<ul style="list-style-type: none"> • Small arms, mortar, automatic cannon, artillery, and ship gun ammunition. • Bombs (cluster, fuel air explosive, general purpose, and incendiary) • Unguided rockets, projectiles, and submunitions • Chemical ammunition filled incendiary, riot control, smoke, burster igniters, peptizers and thickeners for flame fuel (but not chemical agent) • Land mines (ground-to-ground and air-to-ground delivered) 	<ul style="list-style-type: none"> • Demolition materiel • Grenades • Flares and pyrotechnics • Guided projectiles, rockets, missiles, and submunitions • Naval mines, torpedoes, and depth charges • Cartridge and propellant-actuated devices • Chaff and chaff Dispensers • Guidance kits for bombs and other ammunition • Swimmer weapons
---	--

Table 1. Examples of Conventional Ammunition

Both “demilitarization” and “disposal” are accomplished as part of the final stage of the life cycle as required in DoD Instruction 5000.02. These terms are defined in the Defense Materiel Disposition Manual (DoD 4160.21-M, Aug 1997) as follows.

- Demilitarization – The act of destroying the military offensive or defensive advantages ... to prevent the further use of this equipment and material for its originally intended military or lethal purpose ...”
- Disposal – The process of reutilizing, transferring, donating, selling, destroying, or other ultimate disposition of personal property.

Conventional ammunition is designated for demilitarization by each Service when it is determined to be obsolete, unserviceable, or excess or is unsafe for continued storage.

Aside from being a requirement, demilitarization is significant from a number of life cycle perspectives. Demilitarization, or “demil” for short, is recognized as a notable portion of overall life cycle cost, generically estimated at 10%, though this value differs with munition type. In addition, there are significant safety and environmental liabilities associated with demil and disposal since Government employees interact with live munitions during demil operations and waste streams are generated that potentially have negative environmental impacts. Finally, demil is important from a readiness perspective. Since demil stocks are co-mingled with war stocks, the elimination of the no longer needed ammunition frees storage space for current ammunition storage and streamlines outload of ammunition to the warfighter.

Demil Stockpile, Mission, and Methods

The “demil stockpile” of ammunition identified as obsolete, unserviceable or excess is significant, comprising about one third of covered storage space at depots. It is large and varied, totaling approximately 414,000 short tons (as of Feb 2018) and consisting of over 7,000 unique Department of Defense Identification Codes (DODICs). This ammunition represents a liability of approximately \$1.15B using current average demil costs. And new munitions are continually being added as Services identify additional ammunition that is no longer needed.

The mission for performing demilitarization of conventional ammunition and managing the demil stockpile falls to the Product Director for Demilitarization, located at Picatinny Arsenal, NJ. Under the Single Manager for Conventional Ammunition (SMCA), certain logistics responsibilities have been consolidated within the Army and under the Program Executive Officer for Ammunition as the SMCA Executor. PEO Ammo has delegated the responsibility for demilitarization in particular down through the Project Director for Joint Services to PD Demil. PD Demil is supported by a variety of organizations, principally those identified below, that perform different aspects of the demil mission.

- Joint Munitions Command, Rock Island Arsenal, IL (conventional ammunition stockpile management and execution)
- Armaments Research, Development and Engineering Center, Picatinny Arsenal, NJ (conventional ammunition research and development)
- Aviation and Missile Command, Redstone Arsenal, AL (missile execution)
- Aviation and Missile Research, Development and Engineering Center, Picatinny Arsenal, NJ (missile research and development)

Approximately half of demil (by cost) is accomplished at a number of Army depots, identified below.

- McAlester Army Depot, McAlester (MCAAP), OK
- Crane Army Ammunition Activity (CAAA), Crane, IN

- Hawthorne Army Depot (HWAD), Hawthorne, NV
- Tooele Army Depot (TEAD), Tooele, UT
- Blue Grass Army Depot (BGAD), Richmond, KY
- Letterkenny Munitions Center (LEMC), Chambersburg, PA
- Anniston Munitions Center (ANMC), Anniston, AL

The other half of demil is accomplished by a variety of commercial firms under Government contract.

Historically, munitions were demilitarized by being open burned or open detonated (OB/OD). This involved detonating munitions using “donor charges” or burning munitions on burn pans in open air. This method is still used today for a considerable number of munitions and is an environmentally permitted process. However, its use is not allowed for some munitions that present specific environmental concerns and in general its use has declined in favor of “closed disposal” process that contain and treat all by-products of the process before release. Due to the variety of different types of conventional ammunition, a suite of different closed disposal demil capabilities are required to perform demilitarization on the stockpile. These can generically be divided into disassembly, explosives removal, and thermal treatment process. Some examples of existing closed disposal demil processes located at Government depots are shown in Table 2 below. These capabilities are augmented through contracts with commercial entities, who also use a suite of different processes. Approximately one fourth of the demil stockpile (by weight) is demilitarized through commercial contracts. Demil capabilities are tailored to a munitions type and fill and can be complex and costly involving multiple thermal, chemical, and/or mechanical process steps including manual and automated operations.

	ANMC	BGAD	CAAA	HWAD	LEMC	MCAAP	TEAD
Incineration APE 1236 Rotary Kiln Incinerator or Equivalent			X	X		X	X
Autoclave (APE 1401) or Equivalent				X		X	
High Pressure Water Washout		X		X			
Steam Out				X			
Base Hydrolysis CADS/PADS							X
Hot Water Wash Out		X					
White Phosphorous Recovery			X				
Navy Gun Explosive D Conversion to Picric Acid			X				
MLRS Demil	X						
D563 155mm DPICM Demil			X	X		X	
Hot Gas Decon				X			

Table 2. Closed Disposal Demil Capabilities

Insensitive Munitions Challenges

Munitions with larger energetic fills such as mortars, 105/155MM projectiles, and bombs are typically demilitarized by removing the explosive fill. This removal can be accomplished in a number of ways including autoclave (applying steam heat to the outside of a projectile), water wash out (high pressure or hot water), and sectioning. Autoclave is preferred where possible as it does not contaminate the explosive with water and allows it to be reconstituted and reused.

UNCLASSIFIED

Distribution A. Approved for Public Release. Distribution is Unlimited.

Removal and reuse of explosives is performed when possible as it provides valuable economic return to the Government. In some cases, significant quantities of explosives have been recovered and reused in new production, resulting in significant cost avoidance to the production program. In other cases, recovered material is used as donor charges in OD operations again resulting in cost avoidance by providing "free" donor material precluding the need to procure donor explosives.

The traditional method of explosives removal relies on the melt properties of the energetic material to allow re-melting and removal. Steam is applied to the outer shell of projectiles with the explosive melting into a system that captures, cools, flakes and boxes the material. However, cast-cured insensitive munitions (IM) fills in particular cannot be remelted. Since the existing demil infrastructure for larger munitions is based on remelting energetic material, it cannot be used in the demil of cast-cured IM munitions with larger energetic fills. This presents a number of cost impacts. First, the cost avoidance value of the recovered explosive is lost and is replaced with an additional cost burden of needing to process the energetic material for its destruction. This represents an ongoing issue associated with demil operations. In addition, new infrastructure will be needed to establish facilities to perform the demilitarization of the cast-cured fills. These facilities involve industrial type processes and the cost to construct and commission them is significant. This represents a one-time capital investment requirement for each new facility. As another consideration, in cases where munitions could historically have been demilitarized by OD, they will now need more expensive closed disposal processes. OD is typically a lower cost demil method. In general, IM filled munitions cannot be OD due to their insensitive nature and large amount of donor required to initiate the munition. Where munitions can be detonated an incomplete destruction of the munitions typically occurs leaving residual large pieces of explosive. All of these factors will increase the life cycle cost for cast-cured IM filled munitions.

In addition to cost issues, environmental and occupational health impacts are also a consideration due to some of the materials that comprise the IM fills. One example is ammonium perchlorate (AP), which is widely used in IM fills. Early investigations of methods to demil cast-cured IM fills indicate that high pressure water wash out is one method to remove the material. However, the AP enters the waste water and is sent to the depot's water treatment system, which are not currently equipped to handle AP contamination. This will require upgrades to water treatment facilities. As another example, 2,4-Dinitroanisole (DNAN) presents toxicology concerns for humans and will require special handling during the demil process to protect workers.

One specific example of IM challenges is in the demil of the M795 155MM projectile. This round is filled with IMX-101, which actually is melt cast and can be remelted during demil. However, the melt dynamics are different than traditional explosives and required some adjustments to the autoclave process to achieve an acceptable melt out rate. This improvement was made on a pilot scale autoclave and the same modification will be required across the existing production systems. Another example is the XM1112 projectile, also filled with IMX-101. Demil of this round was also tested in a pilot autoclave facility. A tar layer in the projectile melted along with the energetic material causing significant contamination and clogging of the process lines. This contamination is a safety hazard and the equipment had to be disassembled and thorough cleaned. Consequentially, these rounds cannot be processed using existing autoclaves.

Another specific example of IM challenges is the BLU-109C/B round filled with AFX-757. These bombs are in production and while demil of stockpiled ammunition has not been attempted, there has been a need to remove explosives from production rejects, which provides good

UNCLASSIFIED

Distribution A. Approved for Public Release. Distribution is Unlimited.

indication of future demil operations. After applying heat to the shell body, a slug of explosive is removed that is then sectioned and open burned. This procedure might inform an eventual demil method, though in the future OB is not expected to be acceptable. Currently, no closed disposal demil facility exists for this munition.

Design Considerations

Systems engineering is the DoD's approach to munitions development and involves incorporation of all life cycle considerations into the up-front design process. Demil is clearly a life cycle consideration that warrants inclusion. While not necessarily a design driver, proper inclusion in the systems engineering process will ensure low cost options for mitigating risk and cost during demil are not overlooked.

As a general principal, energetics present the greatest challenge during demil operations. And facilitating the removal of energetics through design features should significantly improve demil operations. This involves the ability to readily disassemble and access energetics or otherwise enabling their removal and segregation. Factoring this need into the design process can result in munitions that can be more easily and economically demilitarized. In addition to removal, reuse is an important consideration. To the degree explosive fills can be formulated to allow reuse, value will be added to the life cycle rather than increasing the life cycle cost burden. Environmental and occupational exposure impacts should also be considered to minimize risk and streamline the demil process. Finally, innovative approaches can be used to facilitate end of life cycle demil operations. One example is early research currently being considered in the area of "depolymerizable thermosets." This involves a cast-curable polymer that can be "liquitized" on demand for removal. While in the early research phase, it represents the type of innovative thinking that could ensure compliance with IM requirements while at the same time significantly facilitating demil operations and minimizing overall life cycle cost and risk.

Inclusion of demil during up front design, or "Design for Demil," is an initiative that is supported by the Office of the Undersecretary of Defense. A Design for Demil handbook has been developed and is available from the Office of the Product Manager for Demilitarization at Picatinny Arsenal, NJ.

Conclusion

Demilitarization is a life cycle function that is an acquisition requirement and is important to sustaining warfighter readiness by improving stockpile management. The demil stockpile is significant and represents a very large cost, safety, and environmental liability to the DoD that is largely created and defined during the up-front munitions design process. In particular, cast-cured IM fills present unique challenges in that they cannot be demilitarized using existing infrastructure and result in lost value due to the inability to reuse the energetic material. Efforts at incorporating demil considerations into the systems engineering of conventional ammunition, and IM munitions in particular, early in the life cycle will yield real life cycle benefits. These benefits can be accomplished with design features that facilitate explosives removal and reuse. In addition, innovative thinking at the early research level has the potential to ensure IM requirements are met while greatly simplifying demilitarization operations resulting in significant life cycle benefit.



Inensitive Munitions and Energetic Materials Technology Symposium

April 23-26, 2018 | Portland, OR

Life Cycle Demilitarization Considerations for IM Development



Agenda



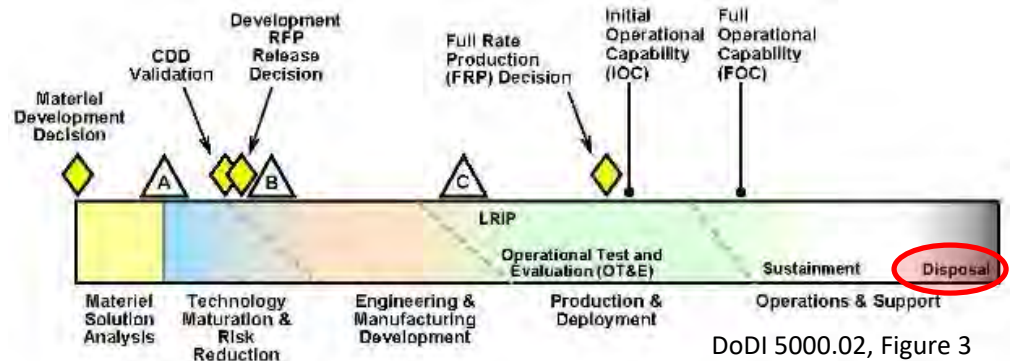
- Demil in the Life Cycle
- Demil Stockpile
- Demil Mission
- Demil Capabilities
- IM Challenges in Demil
- IM Examples in Demil
- Design Recommendations
- Design for Demil



Demil in the Life Cycle

- **Requirement:** “At the end of its useful life, a system will be demilitarized and disposed of ...”

– DoDI 5000.02 5.d.(14)(b)2, 7 Jan 2015



Definitions

Demilitarization: “The act of destroying the military offensive or defensive advantages ... to prevent the further use of this equipment and material for its originally intended military or lethal purpose ...”

Disposal: The process of reutilizing, transferring, donating, selling, destroying, or other ultimate disposition of personal property.

- DoD 4160.21-M, Aug 1997 (Defense Materiel Disposition Manual)

- Ammunition is designated for demil by each Service when it becomes obsolete, unserviceable, or excess or is unsafe for storage.

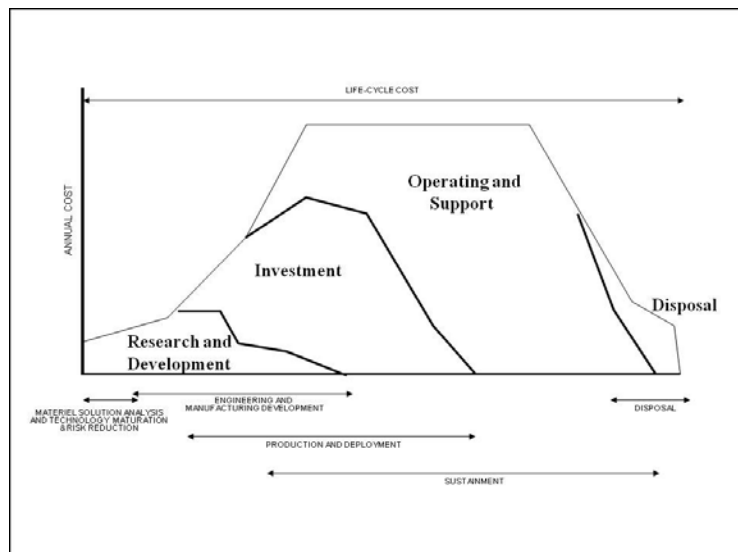


UNCLASSIFIED



Demil Significance

➤ Life cycle cost.



Operating and Support Cost-Estimating Guide, March 2014



➤ Facilitates storage & outload efficiencies (demil stocks co-mingled with go-to-war).

➤ Safety and environmental liability/implications.



Need to ensure sustainability over the life cycle.

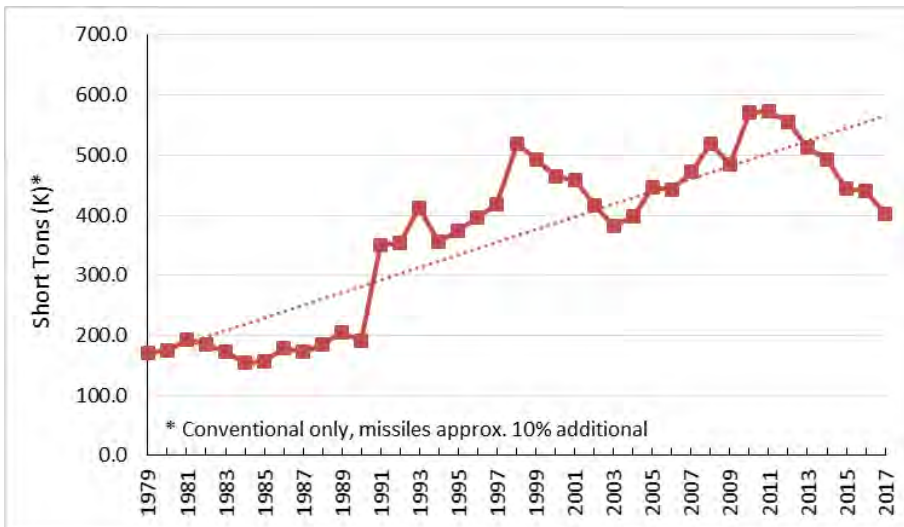
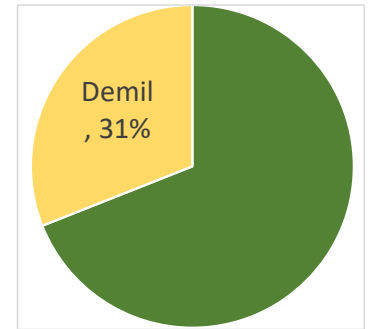


Demil Stockpile

- Large, diverse stockpile
 - ~414K short tons*
 - >7,000 DODICs
 - Continual generations into
 - >\$1.15B liability

* as of EOM Feb 2018

- Demil stockpile occupies over 31% of covered storage space at depots.



- Future ammo more complex.





Demil Mission

- Single Manager for Conventional Ammunition (SMCA)
 - *Established to gain efficiencies in the procurement, production, and demilitarization of conventional ammunition for all Military Services (DODD 5160.65)*
- *PEO Ammo delegated as SMCA Executor in 2002; PD Demil established to execute the demil mission.*



Mission:

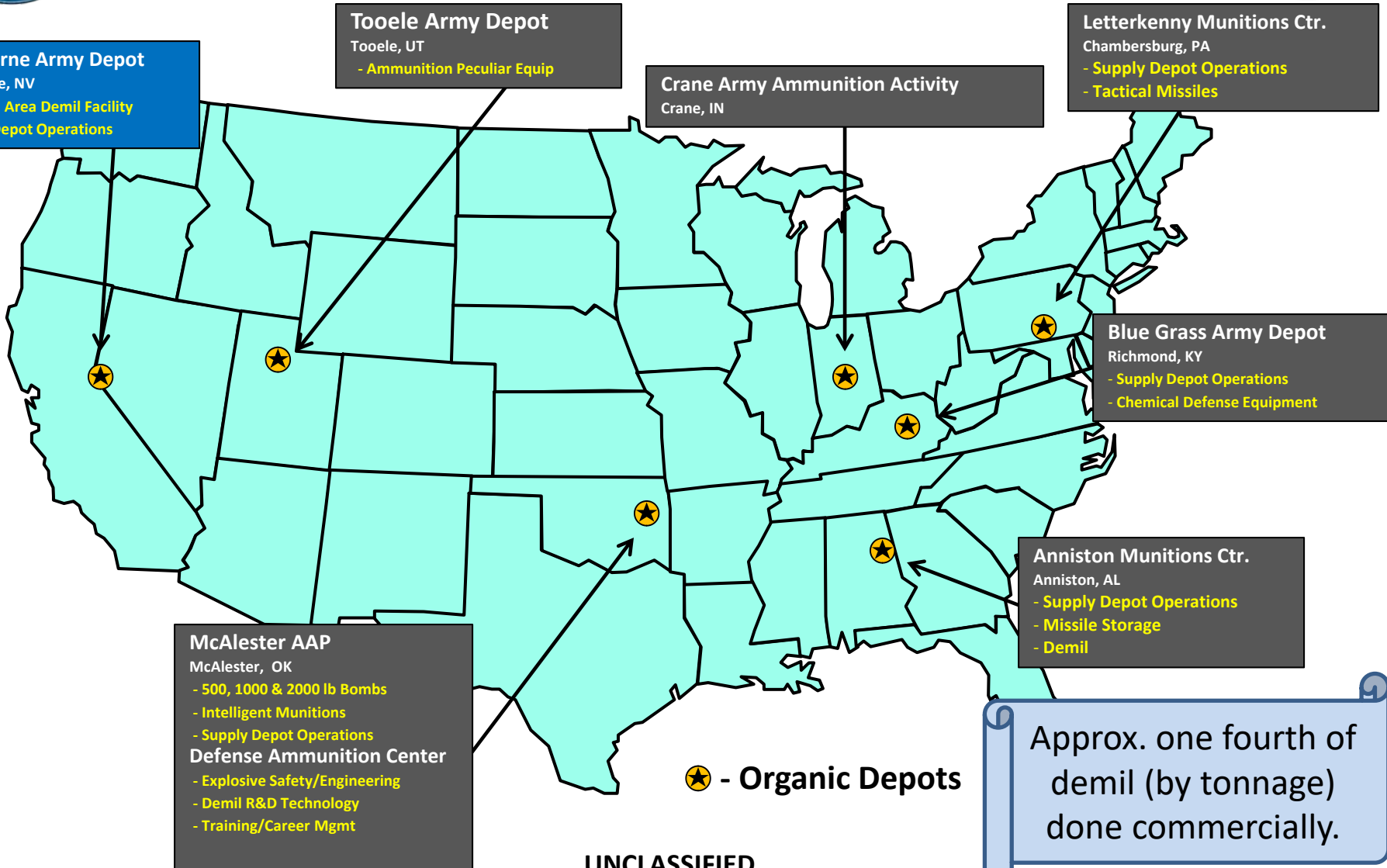
Perform Life-Cycle Management for Demilitarization of Conventional Ammunition for the Department of Defense

**All Services – All Conventional Ammo
Currently Over 7,000 DODICs**

- Supported by the Demilitarization Enterprise.
 - Joint Munitions Command
 - Armament RDT&E Center
 - Aviation and Missile Command
 - Aviation and Missile RDT&E Center

UNCLASSIFIED

Organic Demil Sites



Approx. one fourth of demil (by tonnage) done commercially.

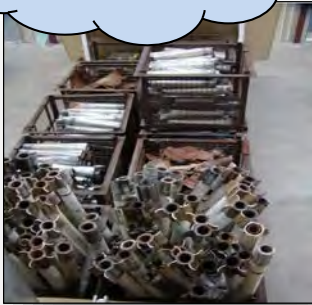


Demil Capabilities



Closed Disposal

FY13 R3 value
\$8.16M



Disassembly



Explosives Removal



Thermal Treatment

New Capabilities
Under Development



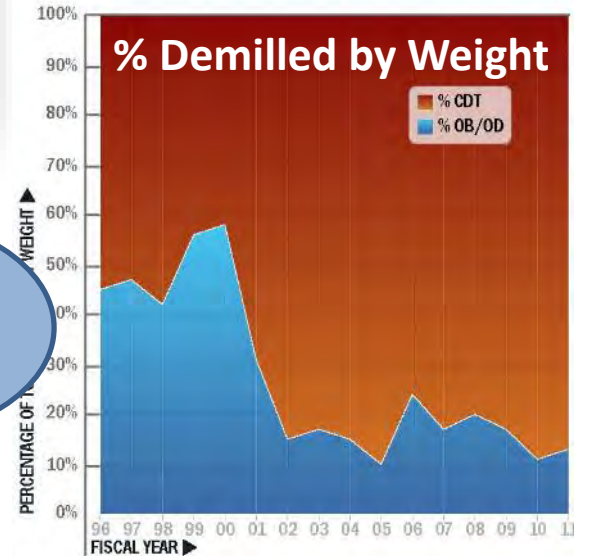
Open Burn /
Open Detonate



100% Done
at Organic
Sites



60-100K
stons per
year





Demil Capabilities

- Demil capabilities tailored to munition type and fill, can be complex and costly.



UNCLASSIFIED



Demil of Larger Energetic Fills

- Energetics are the biggest challenge to demil.
- For larger items (mortars, 105/155MM, bombs), energetics typically removed.
 - Autoclave (melt out by application of heat)
 - Water wash out (high pressure, hot water, etc.)
 - Sectioning
- Energetics reused where possible (new production, donor material for open detonation).



IM Challenges

- Traditional method of demil (melt out and recovery) not possible with cast-cured energetics.
- Technologies are available for cast-cure, but ...
 - Energetics can't be reused, resulting in lost value & increased demil cost.
 - OD not possible, more costly demil.
 - Will require extensive facility modifications (i.e. \$\$\$) to implement removal and destruction capabilities.
 - Environmental, health and safety challenges (e.g. AP, DNAN) requires modifications to water treatment facilities, personnel protection.



105MM/155MM Example

Existing Demil Process Autoclave Melt-Out



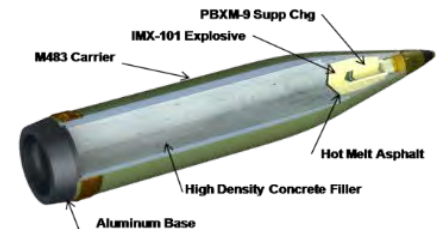
- Melt pour explosives remelted and removed through steam heating
- Explosives recovered for reuse in new production or as a donor for open detonation

IM Issues

- M795 IMX 101 is melt pour but different melt dynamics. Requires modification to autoclaves, capital investment at depots.



- XM1122 tar lining difficult to process.
- New facilities needed for explosives destruction.





BLU-109C/B (AFX-757) Example



- Air Force 2,000 lb penetrator warhead.
- Production rejects demilitarized to recover metal body for reuse.
 - Explosive slug removed through applied heat.
 - Open burning of the removed explosive.
- No demil facilities exist.



Design Considerations

- General design considerations.
 - Ease of disassembly.
 - Facilitate removal/segregation of energetic fills.
 - Potential for reuse of energetics, separation from binders.
 - Minimize environmentally impacting ingredients.
- Innovative approaches.
 - Example: Early research being considered in “depolymerizable thermosets.” Cast-curable polymer that can be “liquitized” on demand for removal.



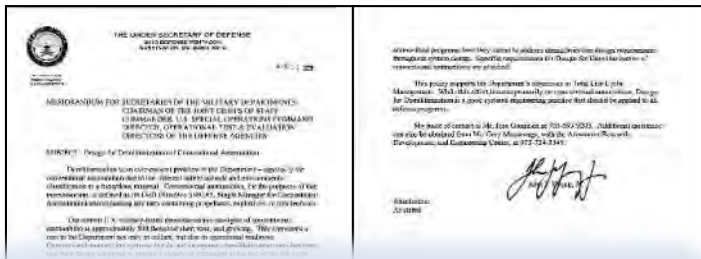
Design for Demil (DFD)

- Early consideration of demil as a life cycle requirement, i.e. good systems engineering.

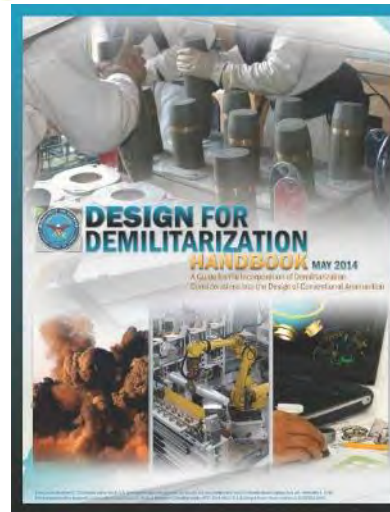
DFD policy by USD(AT&L)



DFD Handbook



“... include in ... acquisition documentation ... how (you) intend to address demilitarization design requirements throughout system design.”



- Endorsed by OSD and the Joint Ordnance Commander's Group.
 - Roles & Responsibilities
 - DFD in the Acquisition Process
 - Design Considerations & Best Practices
 - Policy & Regulation
 - Demil Process Info
 - Lessons Learned

Not a design driver, but opportunities exist if properly considered.



Summary

- Demil is a life cycle function important to sustaining warfighter readiness and impacts safety, environmental, and cost.
- A proper systems engineering approach will ensure demil is properly considered during early development, resulting in positive life cycle impacts.

UNCLASSIFIED

Innovative Boron Nitride-doped Propellants

Thelma Manning*, Richard Field*, Kenneth Klingaman*, Michael Fair*, John Bolognini*, Robin Crownover*, Carlton P. Adam*, Viral Panchal*, Eugene Rozumov*, Henry Grau*, Paul Matter**, Samuel Sopok***

US Army RDECOM ARDEC*
Picatinny Arsenal, NJ
pH Matter, LLC**
Columbus, Ohio
Benet Laboratory***
Watervillet, NY

Abstract

The U.S. military has a need for more powerful propellants with balanced/stoichiometric amounts of fuel and oxidants. However, balanced and more powerful propellants lead to accelerated gun barrel erosion and markedly shortened useful barrel life. Boron nitride (BN) is an interesting potential additive for propellants that could reduce gun wear effects in advanced propellants (US Patent Pending 2015-026P). Hexagonal boron nitride is a good lubricant that can provide wear resistance and lower flame temperatures for gun barrels. Further, boron can dope steel, which drastically improves its strength and wear resistance, and can block the formation of softer carbides. A scalable synthesis method for producing boron nitride nano-particles that can be readily dispersed into propellants has been developed. Even dispersion of the nano-particles in a double-base propellant has been demonstrated using a solvent-based processing approach. Stability of a composite propellant with the BN additive was verified. In this paper, results from propellant testing of boron nitride nano-composite propellants is presented, including closed bomb and wear and erosion testing. Detailed characterization of the erosion tester substrates before and after firing was obtained by electron microscopy, inductively coupled plasma and x-ray photoelectron spectroscopy. This promising boron nitride additive shows the ability to improve gun wear and erosion resistance, without any destabilizing affects to the propellant. Potential applications could include less erosive propellants in propellant ammunition for large, medium and small diameter fire arms.

Keywords: nano-Boron Nitride; additive; lubricant; gun barrel; wear and erosion; gun propellant

1. Introduction

The U.S. military has a need for more powerful propellants with balanced/stoichiometric amounts of fuel and oxidants to provide an advantage to its warfighters. The useful life of each gun is limited either by the effects of barrel erosion on its performance or metal fatigue. The enlargement of the origin of rifling or the down bore area can affect ammunition performance resulting in range and accuracy loss, fuze malfunctions, excessive torsional impulse and excessive muzzle flash and blast overpressure. With increased demands for guns that fire faster, farther, and more accurately, barrel erosion has worsened and become a major limitation in developing better guns [1,2,3]. For example, with advanced propellants 155 mm artillery barrels may only survive a couple hundred rounds before they must be replaced at a cost of over \$70,000 [4].

Many Low Vulnerability (LOVA) propellant formulations contain RDX, and it has been convincingly shown by several investigators that RDX is highly chemically erosive. New, experimental low-erosivity LOVA propellants have been produced by reducing RDX content and introducing nitrogen-rich energetic binder or filler compounds. The resulting propellant combustion gases, rich in nitrogen, act to re-nitride bore surfaces during firing and inhibit erosive surface reactions. The result is increased bore hardness, increased resistance to melting, and reduced chemical erosion. The lowered hydrogen

DISTRIBUTION STATEMENT A: Approved for public release; distribution is unlimited.

UNCLASSIFIED

UNCLASSIFIED

concentration in the combustion gas of some of these propellants may also reduce hydrogen-assisted cracking of the bore surface. Of the high-nitrogen propellants under development, the majority possess impetus and flame temperatures lower than RDX: a compromise between performance, sensitiveness and erosivity must be reached in these cases.

Significant effort has recently been directed at understanding the erosion mechanisms for barrels coated with protective refractory metals. The most plausible mechanism is that micro-cracks in the coatings, present from the time of manufacture, propagate due to pressure and thermal stress cycling and eventually reach the gun steel substrate. Through numerical modelling and analysis of eroded barrels, a number of investigators have shown that once cracks reach the substrate, chemical erosion, gas wash, and high interfacial temperatures cause pitting of the substrate and eventually undermine the coating. Segments of coating are subsequently removed by the flow or engagement with the projectile, and at this point the erosion rate of coated barrels may exceed that of steel barrels. A number of ways to mitigate this erosion pathway have been suggested, including: development of better coating techniques to avoid the initial micro-cracks, pre-nitriding the gun steel before coating to slow substrate erosion, introducing a protective interlayer, and controlled barrel storage and post-firing treatment to prevent oxidation of exposed substrate. Modelling and experiments have additionally shown that, with the notable exception of chromium, the erosion resistance of refractory metal coatings varies amongst different propellant gas chemistry environments. Ceramic additives to the propellant can theoretically reduce barrel deterioration by coating the inside of barrels, but implementation of composite propellants with conventional ceramics (i.e. alumina) has not resulted in improved wear resistance to date. Due to challenges with dispersing the particles in the propellant, and due to abrasion from incomplete sublimation, propellant and ceramic composites that produce regenerative wear-resistant coatings have not been demonstrated. Due to very good wear characteristics and thermal resistance, ceramic barrel liners have been identified as a promising technology for some time. However, the susceptibility of ceramics to fracture, driven by stress induced by the different thermal expansion properties of steel and ceramics, have prevented their widespread use.

The currently fielded 155mm artillery propelling charge, M232/M232A1, has exhibited spiral wear and erosion problems. This was due to either the wear reducing liner, containing titanium dioxide, talc and wax, and other contributing factors. This resulted from the propellant chemistry and interaction of the combustion products within the gun tube wall. Modeling & Simulation studies performed by Dr Samuel Sopok from Benet Labs has determined that the reaction of titanium dioxide with the talc and wax produced a residue that was hard to remove[5]. This product was an abrasive residue (number 80 ceramic grit) that built up in the gun barrel. This caused a spiral rifling imbalance and accelerated gun barrel erosion which markedly shortened gun barrel life. Boron nitride is an interesting potential additive to propellants that could reduce gun wear effects in advanced propellants. It has the properties of providing metal coating/lubricating, and steel hardening properties and nitrogen cooling effects.

On the other hand, Boron Nitride (in the form of crystalline hexagonal BN or amorphous BN) has interesting properties for a propellant additive (US Patent Pending). BN can form a lubricating coating on barrel walls. BN coated ammunition is currently used commercially for small arms to lubricate barrels and ammunition [2]. Further, boron can be used to dope steel, which drastically improves its strength and wear resistance. Boron-doped steel is used to reduce wear in numerous industrial applications, and is typically produced by annealing steel that has been packed in boron oxide [6-12]. In this paper, we explore a new concept where BN is used as a propellant additive that can regeneratively coat and harden steel barrels. The BN is in the form of a nano-particle that can be evenly dispersed in the propellant without negative impact on its performance. Dispersion studies were performed to determine how easily the amorphous BN nano-particles could be dispersed in propellants. Scanning Electron Microscope (SEM) image of the BN in a commercial off-the-shelf double base propellant (1:1 by weight) dispersed with acetone/alcohol is shown in figure 1 below. The BN nano-particles were evenly dispersed, and measured 38 nm on average.

DISTRIBUTION STATEMENT A: Approved for public release; distribution is unlimited.

UNCLASSIFIED

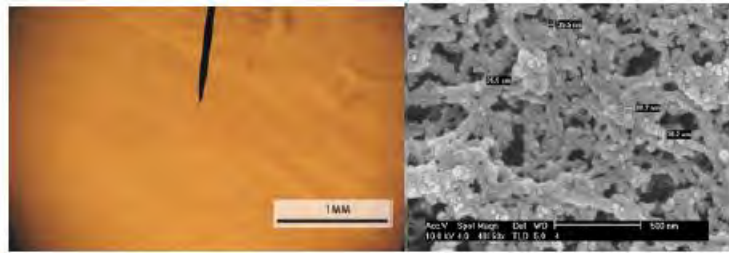


Figure 1. SEM image of double base powder and amorphous BN (1:1 by weight) dispersed with acetone/ethanol using a sonic horn, and deposited onto a glass slide (48,000X magnification); the BN nano-particles were evenly dispersed, and measured 38 nm on average.

Further, the production of the nano-scale boron nitride is economical. An economic model was constructed to project the cost of producing BN nano-particles from raw materials at the anticipated commercial scale (50,000 kg/yr). Based on this analysis, the projected cost of BN at the 50,000 kg/yr scale was found to be \$91.15 per kg. This cost is reasonable because we use such a small percentage in the propellant formulation.

2. Experimental Section

2.1 X-ray Photoelectron Spectroscopy (XPS)

For XPS analysis, powder samples were pelletized by hand and loaded into a steel pellet sample holder. The samples were loaded into a Kratos Axis Ultra XPS, and pumped down overnight to achieve ultra-high vacuum levels. All samples were first analyzed in a survey scan from 1200 to 0 eV to determine the elements present on the surface. All samples analyzed contained B, N, and lower levels of C, and O. The carbon and oxygen is typical from atmospheric contamination (dust and oils). Detailed scans were run for B 1s and N 1s regions to determine the oxidation state and ratio of species, with a charge neutralizer applied to the samples to prevent spectra shifting.

2.2. Differential Scanning Calorimetry (DSC) and Vacuum Thermal Stability (VTS) Tests

Testing was conducted per NATO PIP US/202.01.020 “*Differential Scanning Calorimetry (DSC)*” which is also described in ASTM E537 - 07 “*Standard Test Method for the Thermal Stability of Chemicals by Differential Scanning Calorimetry*” and MIL-STD 1751A Method 1072 “*Differential Scanning Calorimetry (DSC)*.” A Differential Scanning Calorimeter (TA Instruments Model 2910) was utilized to determine the ignition temperature (exothermic peak) and melting temperature (endothermic peak) of the material. The test was carried out in nitrogen gas. The temperature ranged from room temperature to 400°C. The sample container (aluminum pan and cover) containing the material was placed into the measuring cell and heated at a rate of 10°C and 20°C per minute. The peak temperatures (corresponding to exothermic decomposition and endothermic melting) along with onset temperature were determined and recorded.

Vacuum stability testing is performed in accordance to STANAG 4556 ED.1 (*Explosives: Vacuum Stability Test*). This standard testing procedure measures the stability of an explosive at an elevated temperature under vacuum. The stability of a candidate explosive is determined by the amount of gas evolved. To qualify as a chemically stable material, no explosive may produce more than 2ml of gas per gram. The material is tested for 48 hours at 90 degrees Celsius.

DISTRIBUTION STATEMENT A: Approved for public release; distribution is unlimited.

UNCLASSIFIED

UNCLASSIFIED

2.3. Closed Bomb Testing

One of the ways to assess propellant performance is through combustion testing. The closed bomb test is a standard device used to measure gasification rates for energetic materials. Knowledge of propellant chemical formulation and geometry allows for calculation of a linear burn rate from the measured pressure versus time data. Performance is given in terms of relative quickness (RQ) and relative force (RF). Relative quickness applies to the speed with which the material burns and is a comparison of the pressurization rates (dP/dt). Relative force is a comparison of the peak pressure levels observed in the bomb (P_{max}). There were two closed bomb tests conducted using the procedure P1-BPP MIL-STD-286C, Section 801.1.2 and guided by STANAG 4115. For the first test, two shell-shaped inserts of heat-treated and polished 4340 steel were placed inside the chamber to determine if any reactivity occurs between the BN and the steel, and to determine if a boron-based coating forms. The second test was performed to determine the burn rates of the RPD-380 composite propellant with and without BN in preparation for the wear and erosion test.

2.4 Composite Propellant Preparation for Wear and Erosion Test

It is hypothesized that boron nitride (BN) in nano-particle size range incorporated into a propellant during mixing may reduce the erosion that propellant combustion gases cause to a gun bore. In order to provide an initial test of this proposal, two batches of nominal double base propellant composition RPD-380 were fabricated using a solvent mixing process. The two batches consisted of the baseline RPD-380 formulation and the same formulation with nano-scale boron nitride sample provided. The propellants were extruded in single perforation strand form and cut to grain length, as shown in figures 2 and 3, respectively. Closed bomb testing was conducted on each of the materials and then analyzed for acceptable burning properties and burning rate. Both propellants are high energy propellants with high flame temperatures. Using the MCVEC[13] thermochemical equilibrium program, baseline RPD-380 calculated heat of explosion is 1156 cal/gram, with a flame temperature 3573 K at loading density 0.13 gram/cc; the baseline RPD-380 with BN composition has a calculated heat of explosion of 1100 cal/gram and flame temperature of 3451 K at the same loading density.



Figure 2: RPD380 without BN - Single Perf grain used in erosion testing

DISTRIBUTION STATEMENT A: Approved for public release; distribution is unlimited.

UNCLASSIFIED



Figure 3: BN-RPD380 (US Patent Pending) Single Perf grains used in erosion testing

2.5. Propellant Wear and Erosion Testing

The goal of this testing is to determine whether the addition of the nano-scale BN to a propellant does reduce the erosion on typical gun steel, and to provide gun steel samples exposed to erosive gas flows for further analysis. The ARDEC erosion tester used, produces the erosive environment by burning a known amount of propellant in a high pressure vented 200 cc bomb, and recording the weight of a metal insert sleeve before and after firing. The loss in weight of the insert sleeve is the erosive loss. The erosion tester is a modified closed bomb that has a burst disk which breaks at a certain pressure (determined by the thickness and material of the disk) and then vents the bomb gases outward through the bore of the cylindrical steel test insert sleeve.

The two propellants were each fired using two steel sleeves of different hardness. Prior to firing the baseline or propellant with BN, all sleeves had a shot of JA2 fired through them with the intent to smooth out machining defects in the sleeves and have them be at a more uniform initial state prior to testing. The hardened steel sleeves had three shots each fired in them; these were sleeves labeled 1 and 2, with the baseline propellant fired in sleeve 1 and the propellant with BN in sleeve 2, shown in figures 4 and 5 respectively. The unhardened sleeves had four (baseline) or five (with BN) shots each fired in them, with the baseline propellant in sleeve 3 and the propellant with BN in sleeve 4. The final shots in sleeves 3 and 4 were not cleaned and the sleeves were not weighed after those shots so that the residue could be retained for analysis.

The propellant with added BN burned at a lower rate than the baseline, so based on a closed bomb calculation an extra gram of that propellant was fired in each of its shots to account for the pressure difference and thus provide a better pressure match with the shots generated by the baseline propellant. In order to get the best and most accurate results it is important to keep conditions in the erosion tester as similar as possible. In the present tests the maximum pressure range of 20,000-22,000 psi typically used for routine erosion tests was targeted. The thermo-chemistry, burning rate and form function of the propellant grains to be tested resulted in required propellant sample loading densities (grams of propellant per unit bomb volume) nearly 50% lower than is typically employed. Consideration of the propellant weight burned obviously affects the flow time of the combustion gases through the insert sleeve. In addition, in comparing individual tests, there are always some minor variations in the burning process and the peak pressure developed at burst disk rupture.

The 26.4 grams of baseline propellant and 27.3 grams of propellant with BN were fired. The propellants did not have the exact same weight due to variation in weights of individual grains. An extra shot was fired in sleeve 4 due to having enough remaining material. All shots were ignited by using an electric match initiated 1-gram sample of M38 ball powder. Using ball powder rather than black powder as an igniter reduces the sulfur and potassium compound content of the combustion products to a very low level.

DISTRIBUTION STATEMENT A: Approved for public release; distribution is unlimited.

UNCLASSIFIED

UNCLASSIFIED

The sleeves are marked with a number of small indentations equal to their sleeve number to identify them and to ensure that the sleeve was facing the same way on every shot. Each sleeve was cleaned and weighed before and after every shot (excluding the last shots on sleeves 3 and 4, as mentioned above) in order to measure the weight loss that each shot caused. Sleeves were cleaned with soap and water until no visible residue remained and then thoroughly dried prior to weighing.

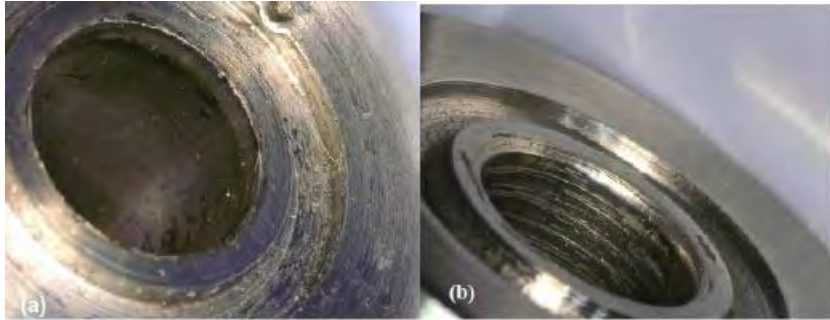


Figure 4: Hardened Steel Sleeves (a) RPD380 P2 flow entrance end, sleeve 1. (b) BN-RPD380 P5 Flow Exit end, sleeve 2 – cleaned after 3 shots.

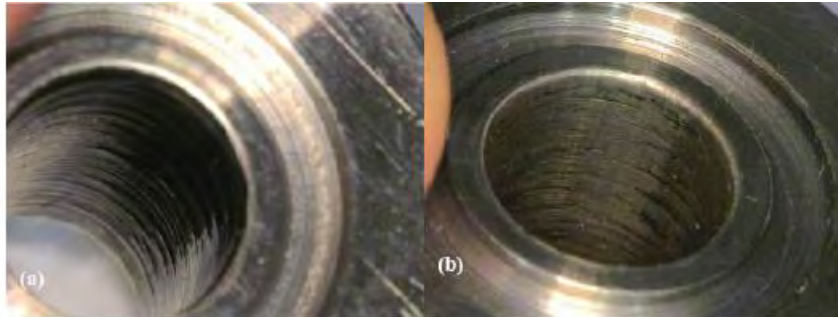


Figure 5: Insert Sleeve 2 – (a) hardened Steel, after firing 3 shots RPD380 Propellant (Cleaned) RPD380 P - Flow Entrance End –cleaned after 3 shots (b) RPD380 P - Flow Exit End –cleaned after 3 shots

3. Results and Discussion

3.1 Boron Nitride Characteristics

Under this project, a proprietary process for production of dispersible boron nitride nano-particles to use as a propellant additive was developed. The process does not use a catalyst, and the boron nitride precursor is free (<1 ppm detection limit) of metal contamination. The process involves nucleation of a boron and nitrogen based precursor, so the product particle size can be controlled based on the reactant concentration. Typical bulk BET surface areas range from 20 m²/g to 80 m²/g, depending on process conditions, consistent with spherical particle diameters from 143 nm down to 37 nm.

Electron microscopy of the BN product shows that the morphology of the BN is indeed nano-particle spheres. Figure 6 shows SEM images of typical particles. Although the particles agglomerate upon drying, it is clear from the images that the individual particles are spheres with diameters in the nanometer range.

DISTRIBUTION STATEMENT A: Approved for public release; distribution is unlimited.

UNCLASSIFIED

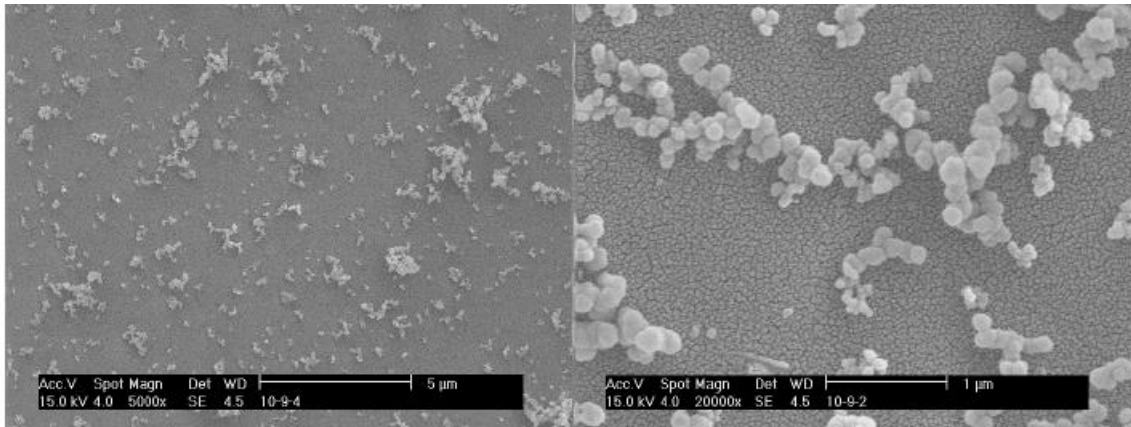


Figure 6: Scanning electron micrographs of BN nano-particles (US Patent Pending) used for propellant additive testing.

The surface of the BN nano-particles was characterized to verify the material composition and how it may interact with propellant. X-ray photo-electron spectroscopy (XPS) was used for this characterization. XPS analysis is sensitive to the first few atomic layers of a material, so it can be considered a surface analysis tool.

Figures 7a and 7b show the N 1s and B 1s regions for the samples respectively. The BN nano-particles prepared are compared to conventional commercial hexagonal boron nitride obtained from Alfa Aesar. As can be seen from these figures, the ratio of B:N is the same for both materials. Further the oxidation states of the boron and the nitrogen are the same in each sample. The binding energy (oxidation state) for boron is consistent with literature values for boron nitride. It should be noted that XPS analysis has been repeated on materials that were aged in air for 6 months, and no change in oxidation states were observed.

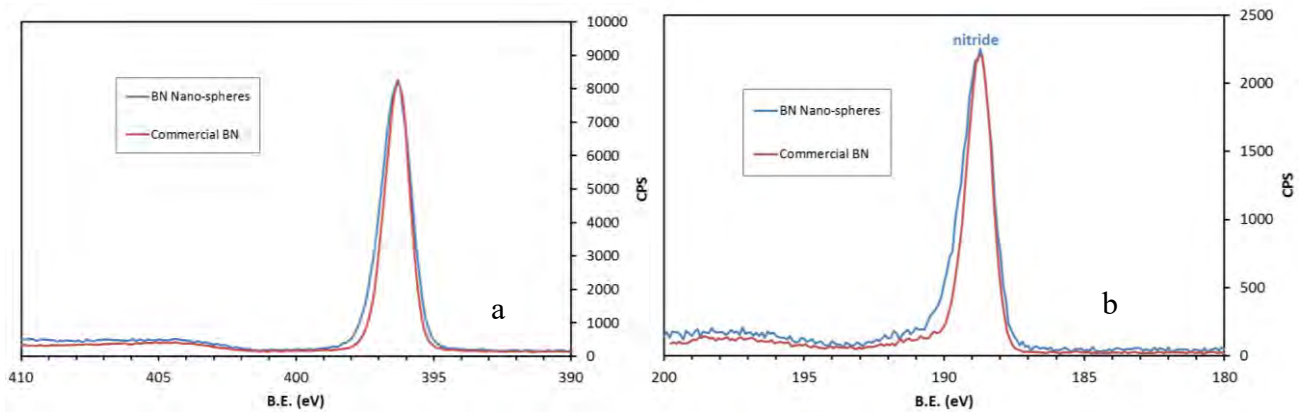


Figure 7: XPS analysis showing (a) the N 1s region, and (b) the B 1s region for the BN nano-particle propellant additive compared to a commercial hexagonal boron nitride sample.

Transmission electron microscopy (TEM) imaging in conjunction with electron energy loss spectroscopy (EELS) was also run on the material to characterize the BN particles. Figure 8a shows the TEM images of the particles, which appear to be amorphous spheres. Figure 8b shows the EELS analysis, within the accuracy of the measurement, verified that the material has a 1:1 B:N ratio, consistent with boron nitride.

DISTRIBUTION STATEMENT A: Approved for public release; distribution is unlimited.

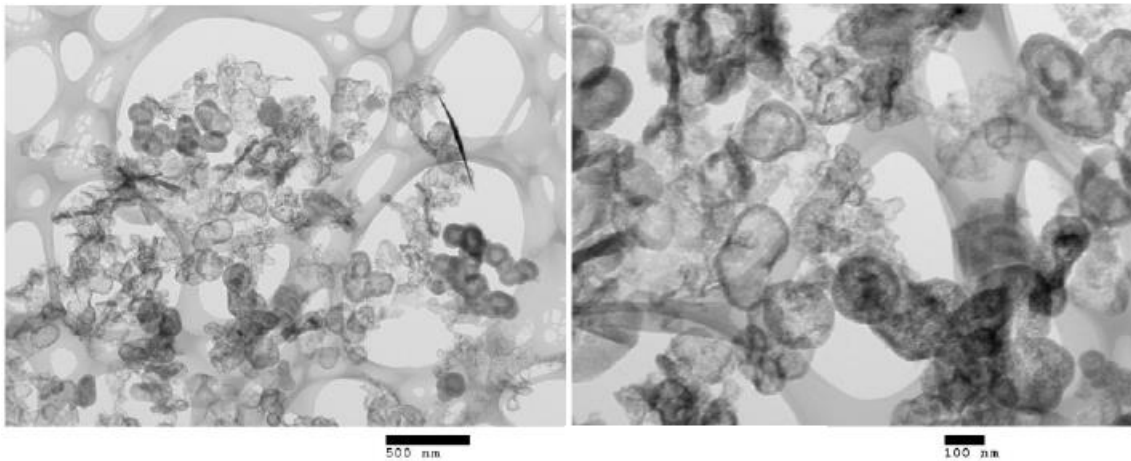


Figure 8a: TEM images showing nano-spheres of boron nitride used for propellant additive testing(US Patent Pending).

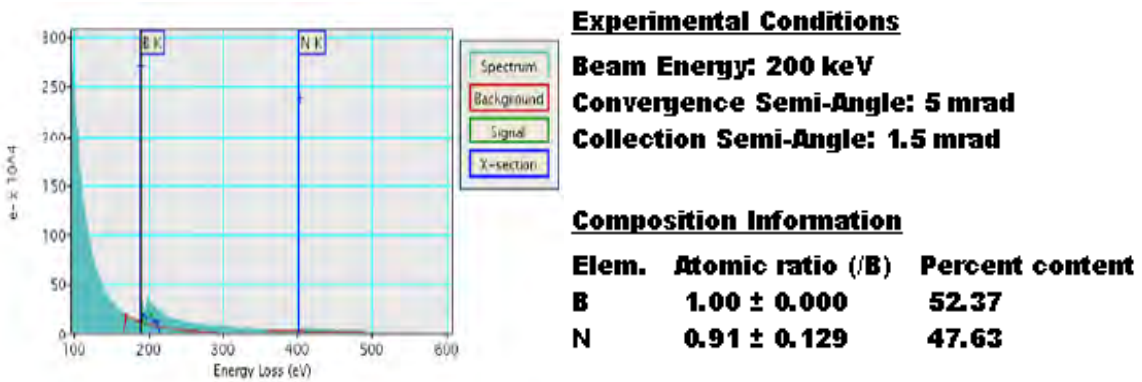


Figure 8b: EELS analysis, showing the material has a 1:1 B:N ratio (US Patent Pending).

3.2 Composite Propellant Testing

In the first round of testing, a composite propellant was prepared using a commercially-available nitrocellulose double-base propellant, IMR-4198 (Hodgdon). Preparation of composite propellant was conducted under solvent (acetone:ethanol 1:1) in a small rotating mixing chamber, with sufficient solvent added to soften the propellant to a dough-like consistency. Two batches were prepared, one with additional B-wt% BN nano-particles, the other without addition of BN. Both propellants were subjected to the same mixing conditions (~2 days in the mixing chamber) to provide a control comparison in testing.

RPD-380 nitrocellulose based propellant with and without BN were prepared using the conventional solvent process in a horizontal sigma blade mixer. The propellants were extruded into single perforated geometry.

3.2.1. Differential Scanning Calorimetry and Vacuum Thermal Stability Tests

DISTRIBUTION STATEMENT A: Approved for public release; distribution is unlimited.

UNCLASSIFIED

DSC measures the temperatures and heat flows associated with transitions in materials as a function of time and temperature in a controlled atmosphere. These measurements provide quantitative and qualitative information about physical and chemical changes that involve endothermic or exothermic processes, or changes in heat capacity. This test method is recommended as an early screening test for detecting the thermal hazards of an uncharacterized substance. For explosives and energetic materials study or development, a DSC may be used to measure safely, the energy released by a small amount of a sample without any catastrophic consequences.

DSC tests were performed in triplicate on the materials (both IMR 4198 and IMR 4198 with B-wt% BN) to determine the combustion initiation temperatures. The onset temperature is indicated by examining any deviation in the reaction mass temperature from the heating rate. The peak height or area under the curve indicates the magnitude of the energetic activity. The DSC test results showed the average onset exothermic reaction at heating rate of 10°C/min was 161°C and the average peak exothermic was 207°C for both samples tested. It appears the addition of BN (B wt %) did not have any significant effect on DSC thermal test results, indicating the BN does not destabilize the propellant under the DSC conditions. The heat of reactions also remained unchanged within the measurement capabilities of the technique.

VTS is performed in accordance to STANAG 4556 ED.1 (Explosives: Vacuum Stability Test). This standard testing procedure measures the stability of an explosive at an elevated temperature under vacuum. The stability of a candidate explosive is determined by the amount of gas evolved. To qualify as a chemically stable material, no explosive may produce more than 2ml of gas per gram. The material was tested for 48 hours at 90 degrees Celsius. Based on test results, which were conducted in accordance with the defining criteria of STANAG 4556 ED., the RDD24F-001T5 propellant lot with B% BN produced less than 2ml of gas per gram for a five gram sample and therefore passes vacuum stability criteria according to military specifications.

3.2.2. Bomb Testing with Steel Inserts

The first closed bomb test was used to determine the Relative Quickness(RQ)/ Relative Force (RF) to characterize propellant samples and the resulting coating formed on steel inserts. An overview of the results of the tests is given below in Table 1A. Pure IMR-4198 and the B% composite propellant were tested at different loadings. Additionally, a physical mixture of 1:1 IMR-4198 and the composite were tested to obtain B% BN composite. The maximum pressure was measured with a high speed DAQ system for the pure IMR-4198 and the B% BN composite.

Propellant	Amount (g)	Pressure (psig)	Insert in Figure 9	Observation
IMR-4198	5.0	9,170	(a)	Rust color
IMR-4198	7.5	15,470	(b)	Rust color
A% BN	5.0	10,250	(c)	Black
B% BN	5.0	~10,000	(d)	Black
B% BN	7.5	~15,000	(e)	Black/green

Table 1A: Overview of Bomb Tests with Steel Inserts (A<B).

A photograph of the steel inserts that resulted from this testing is shown in Figure 9. Stark differences in surface oxidation of the steel inserts were observed. Visually, there were some dramatic differences between steel inserts that were fired without an additive, versus inserts with BN additive.

DISTRIBUTION STATEMENT A: Approved for public release; distribution is unlimited.

UNCLASSIFIED

UNCLASSIFIED

Samples (a) and (b) did not have any additive, and both samples looked oxidized with a distinctive orange rust color. The oxidation was worse for the higher propellant loading (higher chamber pressure). Samples (c) and (d) with B% BN respectively at 5 grams loading each were darker after firing, but did not have an orange color indicative of steel oxidation. Sample (e) was fired with 7.5 grams of IMR-4198 with B% BN and had a green color. These initial results are promising, as it seems BN may be preventing steel oxidation; however, more work remains to understand the nature of this coating and verify any effect on wear and erosion resistance.

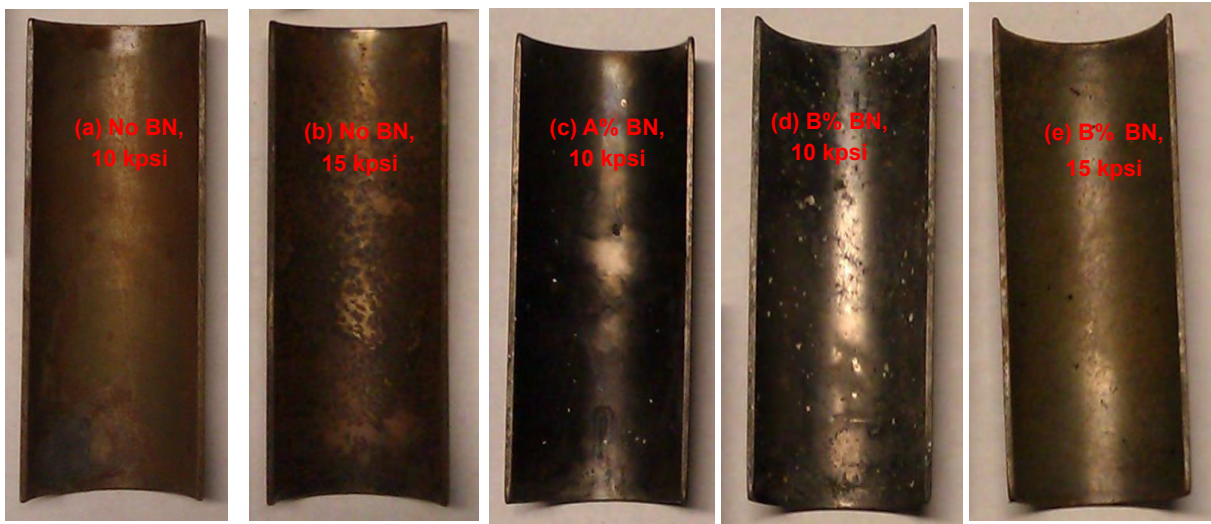


Figure 9: Photographs of steel inserts after closed bomb testing at ~10,000 psi and ~15,000 psi; listed in Table 1; Steel inserts after bomb testing samples fired with a composite propellant containing BN (A<B) had less oxidation than sample fired with pure propellant.

A 200cc high pressure closed bomb testing of the RPD-380 baseline propellant was also performed to determine the burn rates with and without BN added in the propellant, shown in Table 1B. The RQ, RF and Relative Vivacity (RV) values less than 100% value can be explained as due to the high percentage of BN added in the propellant formulation to simulate the worst case scenario of adding an inert additive. The propellants burned much better than their appearance might have indicated and followed the form function geometry of a single perforated grain geometry, shown previously from figures 2 and 3. The graphite was not incorporated. Using the data obtained from this test, the burn rate can be predicted using the Vieille's burn rate law shown in equation 1, wherein P is the pressure in the chamber, α is the burn rate coefficient, and β is the burn rate pressure exponent [2,4].

$$\text{Burn Rate} = \alpha P^\beta \quad (1)$$

Propellant Lot Number	α , Pressure Coefficient	β , Pressure Exponent
-0192 (no BN)	0.6515E-03	0.9309
-0193 (with BN)	0.7736E-03	0.9089
RQ = 90.79%		
RF = 96.68%		
RV = 94.28%		

Table 1B: Closed Bomb Test Results for RPD-380 baseline propellant with and without BN.

DISTRIBUTION STATEMENT A: Approved for public release; distribution is unlimited.

UNCLASSIFIED

3.2.3. Steel Insert Characterization

In order to better understand the first closed bomb test results, the steel inserts were characterized by XPS and SEM. Insert samples were first characterized by XPS to determine surface composition and element oxidation states after firing. All fired samples contained B, C, N, O, F, K, and Fe on the surface. The fresh sample had only C, N, O, and Fe on the surface, indicating some of the C, N, and O was in the steel or originated from atmospheric contamination. The first sample fired contained boron, so apparently boron in the chamber re-deposited on samples that were fired in a non-boron propellant; however, the amount of boron in non-BN inserts was significantly less, as will be discussed. The K and F likely originated from the propellant, and remained on the inserts after firing and rinsing. Figure 10 shows the relative abundance of B, Fe, K, and F in the samples. It should be noted that all samples had a similar amount of C (33-44%), and O (33-41%). Clearly the samples fired with the BN composite propellant had more boron, with the 5 gram sample, which was the least oxidized, having the most boron coverage. The amount of iron on the surface increased steadily with the extent of apparent surface oxidation. Based on binding energies of these species, it was apparent that the BN additive is at least partially oxidized on the surface during propellant firing, and that the presence of boron does not seem to affect the iron oxidation state. However, ppm levels of boron doping in the steel would improve hardness, and would not be detectable from XPS analysis of the iron. Samples fired with a composite propellant containing BN exhibited less oxidation than samples fired with pure propellant. Clearly, the less oxidized samples had less iron on the surface, which was generally displaced by boron.

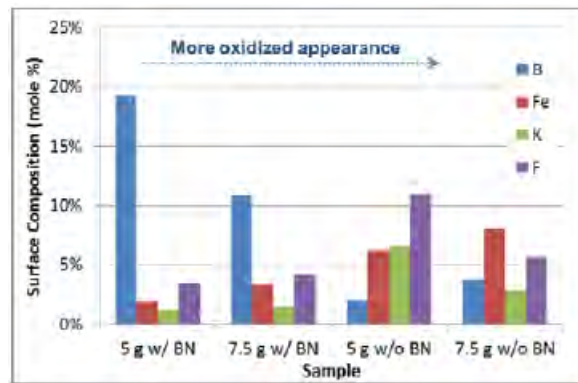


Figure 10: Surface elemental compositions for steel inserts after firing in bomb tests.

SEM with energy dispersive x-ray (EDX) spectroscopy analysis of sample surfaces was performed to characterize the morphology of any coatings formed during propellant firing tests. For reference, an unfired steel insert was imaged, as seen in Figure 11a. The steel insert showed few features at 2500x magnification, as only straight grooves were visible. Figures 11b and 11c compare steel inserts fired without and with BN additive respectively. Both samples seemed to have rougher surfaces compared to unfired steel. At 2500x major differences were visible in the surface morphology. The surface of the sample fired with BN had what appeared to be micron sized platelets covering the surface. These platelets are consistent with the shape of hexagonal BN. The sample fired without BN had spheres and pits, and what appears to be octahedral crystals consistent with Fe_3O_4 . EDX elemental analysis confirmed that the samples fired with BN additive were mostly boron, oxygen, and carbon on the

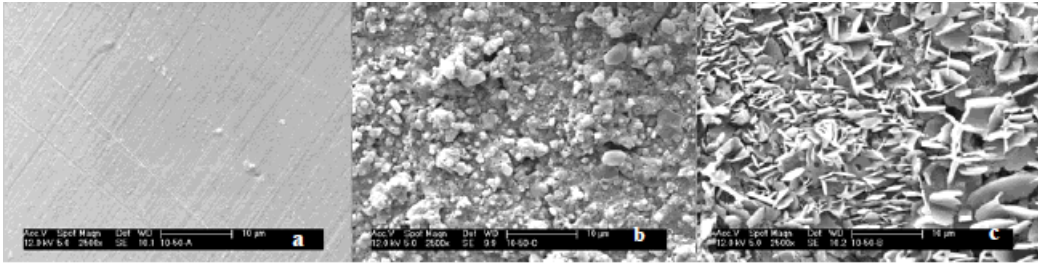


Figure 11: SEM images of (a) unfired steel insert (b) steel insert fired with 5 grams of IMR-4198, and (c) steel insert fired with 5 grams of B% BN composite propellant.

surface. The samples fired without BN did not have any B detectable by EDX, and were mostly Fe, K, and F. This analysis supports that hypothesis that the inserts fired with BN-containing propellant formed a boron-based coating, that apparently covers the iron and reduces the extent of oxidation. It is not clear if the crystals are partially oxidized hexagonal BN or mostly oxidized boron.

3.1.4 Wear and Erosion Test Results

The two types of insert sleeves used for these tests were prepared much earlier for another test. The initial bore surface roughness in both sets of inserts used were of a lower quality than ideal. Based on prior experience with high flame temperature propellants, imperfections in the bore surfaces are usually rapidly removed due to much higher mass loss rates than were observed in tests with highly energetic propellants. From the photos shown in figures 4 and 5, it can be seen that the hardened inserts had rough surfaces with extensive machining features, even after firing. With these features, and the corresponding higher surface area, the mass loss for the hardened inserts is higher than the annealed inserts despite the higher hardness. In both cases with the hardened inserts the shot to shot variation in mass loss is reasonable. The unhardened inserts apparently had less severe initial machining roughness, which apparently accounts for the lower mass loss values despite the lower hardness. From the data shown in figure 12, it appears that the first shot in each group of unhardened inserts experienced a much larger weight loss than the following shots. The small number of shots limits the ability to demonstrate statistically supportive conclusions.

The effect of the BN propellant additive (US Patent Pending) suggests an apparently significant reduction in the mass loss for both hardened and unhardened insert sleeves. The results look compelling at 2.8 and 1.8 times life increase for hard and unhardened insert sleeves shown in figures 13 and 14, respectively. These results must be considered in light of the less than ideal test insert bore surface conditions mentioned above. However, since the propellant formulation with B% BN has a theoretical flame temperature only approximately 100 K less than the baseline composition, mechanisms other than thermal (bore heat transfer) leading to the reduced mass loss must be considered. The presence of particles in the wall boundary layer during flow typically relates to heat transfer alteration to the substrate. The un-cleaned insert sleeves shown in figure 15 following BN-propellant firing show deposits collected as a result of the entire blow-down process of the bomb gas emptying process. Due to the limited number of exposures of the inserts to the combustion products containing BN derived materials, alteration of the steel would seem to be minimal. The very limited number of shots with the BN propellant does not show a progressive reduction in mass loss on subsequent shots after the initial shot. Probing of the steel surface layers and the coating residue may provide added information.

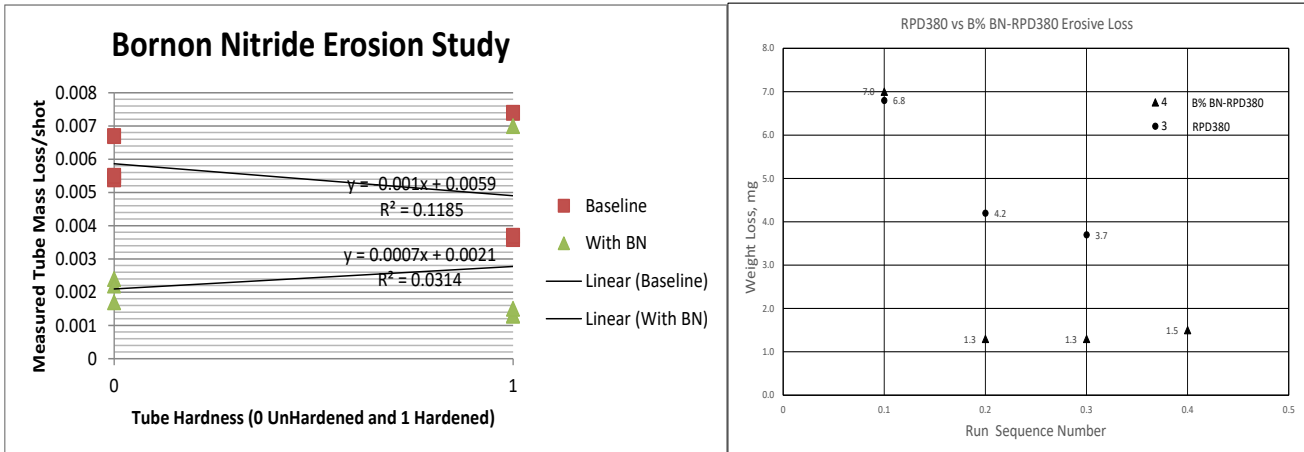


Figure 12: Wear and Erosion Test Results for hard and unhardened sleeves (US Patent Pending). Note: Sleeves 1 and 2 were hardened to approximately Rockwell Hc 41. Sleeves 3 and 4 were approximately Rockwell Hc 12.

4. Characterization of Steel Inserts after Wear and Erosion Testing

4.1. Composition Analysis.

After firing, the samples were analyzed by XPS to determine surface composition, and Inductively Coupled Plasma (ICP) analysis to determine the bulk composition. A number of elements were detected on the surface, including Pb, Fe, Cu, Zn, Sn, Si, Al, S, F, O, N, and B. Since many of the elements may only be surface contamination from the test, and not significant to erosion effects, we focused the analysis on Fe, N, C, and B. A breakdown of the surface composition is given in Table 2 below. After cleaning, very little boron remained on the surface. Only the unhardened sample fired with B% boron contained a detectable amount of boron (0.4%); the detectable limit is about 0.1%. Boron was detected in the coating that was scraped from the surface, but it was lower than the amount present during closed bomb testing, and less than the amount of iron removed with the coating. The bulk ICP analysis showed less than 0.01% B in all samples, and the remaining composition is consistent with the respective steel specification. This low boron content in the 1 mm thick sample indicates that the weight loss differences are real and not due to build-up of boron on the steel.

A large amount of carbon was found on the surface of all samples, but less was present in samples fired with boron. It is not clear if this surface carbon is related to erosion, but iron carbides are softer and melt at a lower temperature than iron. It is possible the boron, apparently in small amounts, could dope (or coat) the steel and block carbide formation. It is also possible, as will be discussed below, that boron dopes the steel in small amounts, resulting in hardened steel. Again, similar to closed bomb tests, based on the oxidation state of boron in the XPS analysis (data not shown) the boron nitride is at least partially oxidized. The iron oxidation state (data not shown) indicates that the iron is mostly 3+ on the surface with a small amount of reduced iron as well.

UNCLASSIFIED

Element	Relative Composition				
	Hardened (0% BN)	Hardened (B% BN)	Unhardened B% BN)	(Unhardened (B% BN)	Coating from Unhardened B% BN
C	0.652	0.199	0.299	0.131	0.646
B	0	0	0	0.004	0.023
N	0.028	0.014	0	0.009	0.052
Fe	0.32	0.787	0.701	0.856	0.279

Table 2: Relative surface composition for samples fired in wear and erosion testing.

4.2. SEM Imaging.

SEM images of the cleaned and uncleaned samples fired in the erosion test stand are shown below. The steel had a number of surface cracks, but the crack density appeared to be less, or cracks were filled in, for the samples fired in boron nitride shown in figures 13, 14 and 15. The surface also appeared to be smoother and less pitted for the samples fired with boron.

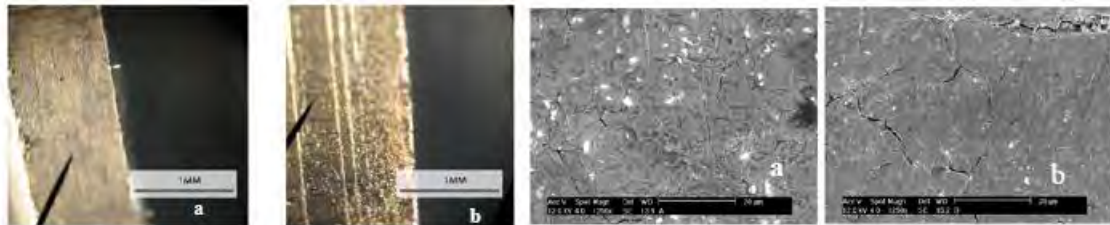


Figure 13: Hardened Steel Fired (a) no BN (b) with BN

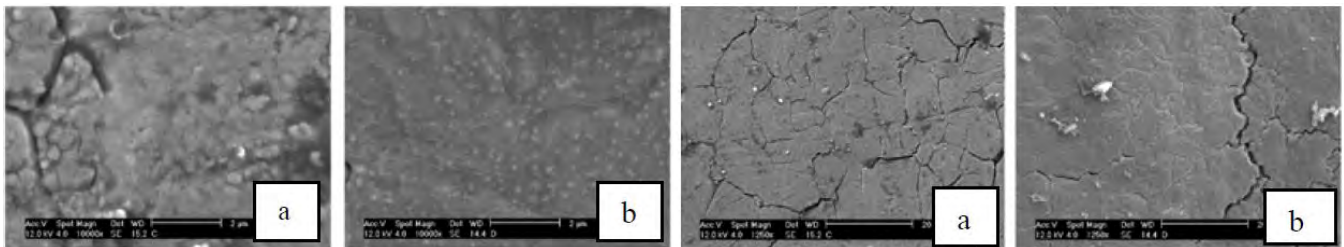


Figure 14: Un-Hardened Steel Fired (a) no BN (b) with BN

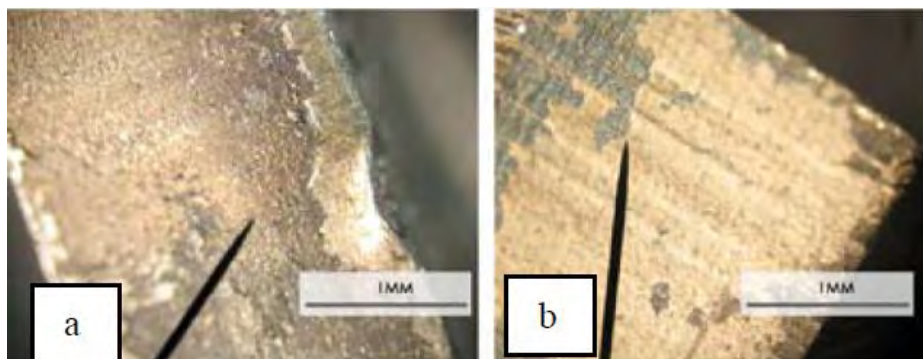


Figure 15: Un-Hardened Un-cleaned Steel (a) no BN (b) with BN

DISTRIBUTION STATEMENT A: Approved for public release; distribution is unlimited.

UNCLASSIFIED

UNCLASSIFIED

4.1. Hardness Testing

A simple Moh's hardness test was performed on the samples after erosion testing to determine if the boron is playing a role in hardening the steel. Table 3 shows the results of this analysis. A reference unhardened steel sample was measured to have a hardness of 5.5, typical for steel. Surprisingly, the unhardened steel samples showed an increase in hardness up to 7.5 after being fired with boron in the propellant. The sample fired without any boron remained at 5.5. The hardened sample fired with boron was also 7.5, and the hardened sample fired without boron was approximately 7.0. Based on these results, it is possible that boron doping could regeneratively harden the steel, thus reducing erosion. However, more quantitative testing, such as Rockwell Hardness testing, after extended firing tests would be beneficial to verify this possible mechanism. Further, improved characterization of how the boron may or may not be infiltrating the steel in small amounts would be beneficial to determine if the reduced erosion results from a chemical mechanism (i.e. increased hardness from B doping) and/or a more physical mechanism (i.e. protection of the steel surface or cracks through a coating).

Sample	Hardness
Unhardened steel reference	5.5
Hardened, 0% BN	7.0
Hardened, B% BN	7.5
Unhardened, 0% BN	5.5
Unhardened, B% BN	7.5

Table 3: Hardness Testing Results for insert sleeves fired in wear and erosion test apparatus.

5. Conclusion

A scalable and economical proprietary process for production of BN nano-particles has been developed. An economic model was constructed to project the cost of producing BN nano-particles from raw materials at the anticipated commercial scale (50,000 kg/yr). Based on this analysis, the projected cost of BN at the 50,000 kg/yr scale was found to be \$91.15 per kg. This cost is reasonable because we use such a small percentage in the propellant formulation.

DISTRIBUTION STATEMENT A: Approved for public release; distribution is unlimited.

UNCLASSIFIED

UNCLASSIFIED

These particles were confirmed to be spherical, with an average size less than 100 nm, and can be dispersed in propellants using the conventional solvent approaches. The particles were confirmed to not destabilize the nitro-cellulose based propellants such as the RPD-380 and IMR 4198. To simulate the interaction of BN nano-particles with gun barrels under combustion environments, steel inserts were fired in a closed bomb test chamber in the presence of propellant compositions with and without the BN additive. Samples fired with BN additive in the propellant showed signs of less oxidation in this testing. XPS showed that boron oxide coated the surface of samples fired with BN additive, and less iron was present on the surface in samples that were less oxidized. SEM and EDX analysis showed stark differences in surface morphology and composition for samples fired with or without BN additive. Samples fired with BN had a boron oxide surface coating of flat platelets, and seemed to lack significant iron oxide (less than 10%). Samples fired without BN were covered with pits, bumps, and octahedral crystals indicative of Fe_3O_4 . Hardness testing of the insert surfaces was performed to quantify any differences between samples, but the results for these samples were inconclusive.

While at first glance, the results do show that the propellant with the added BN propellant shows less erosion than the baseline propellant, the sample size is clearly too small for the results to be considered proof that the BN does reduce erosion. Further testing of the propellants is recommended. Other differences in the two propellants or side effects from the addition of the BN could also be the cause of the lower erosion seen, for example, the lower flame temperature that the propellant with BN generates. Better control of the insert bore surface roughness is needed in future tests. Only a small amount of boron remained on the surface after firing and cleaning, but ppm levels of boron doping can harden steel, and an increased hardness was observed in unhardened steel fired with boron nitride additive. SEM imaging showed less surface crack density in the samples fired with boron nitride. Important considerations for any further tests are an alternate grain form to allow larger bomb loading density, and the corresponding larger amount of propellant necessary for that condition, as well as to support a sufficient number of firings to generate supportable statistical conclusions. More quantitative hardness testing after extended firing would be useful to verify a hardening mechanism, and better characterization of the boron possibly in or on the steel surface would also be beneficial.

Further wear and erosion testing of the propellant additive is planned in a projectile test stand that will simulate the conditions of 155 mm artillery.

Acknowledgements

This work was supported by the US ARMY RDECOM Tech Base Program and Small Business Innovative Research (SBIR) Army Contract Number W15QKN-12-C-0041.

References

- 1) Lawton, B. (1984) Thermal and Chemical Effects of Gun Barrel Wear, in 8th International Symposium on Ballistics, Orlando, United States.
- 2) Bracuti, A. J. Wear-Reducing Additives-Role of the Propellant, in L. Stiefel, ed., Gun Propulsion Technology, Vol. 109 of Progress in Astronautics and Aeronautics, AIAA, Washington DC, United States, 1988, Chapter 12, , pp. 377-411,.
- 3) Sopok, S., O'Hara, P., Pegl, G., Dunn, S., Coats, D. & Nickerson, G., Unified Computer Model for Predicting Thermochemical Erosion in Gun Barrels, Journal of Propulsion and Power, 1999, 15(4), 601–612.
- 4) Johnston, I.A., Understanding and Predicting Gun Barrel Erosions, DSTO-TR-1757, August 2005, Edinburg, South Australia, Australia 5111.

DISTRIBUTION STATEMENT A: Approved for public release; distribution is unlimited.

UNCLASSIFIED

UNCLASSIFIED

- 5) Spiral Wear Discussion with Dr Samuel Sopok and Duncan Park, Bennet Labs and ARDEC-Picatinny Arsenal, May 11, 2015, respectively.
- 6) Hasenbein, R.G., Wear and Erosion in Large Caliber Gun Barrels, Unclassified Army Report, last accessed June 2011 at: <http://www.dtic.mil/cgi-bin/GetTRDoc?Location=U2&doc=GetTRDoc.pdf&AD=ADA440980>
- 7) Tubb Precision Blended Boron Nitride Bullet Coating Kit, website accessed August 2013 at: <http://www.davidtubb.com/boron-nitride-coating-bullets>
- 8) Calik, A., Duzgun, A., Ekinci, A.E., Karakas, S., Ucar, N., Comparison of hardness and wear behavior of boronized and carburized AISI 8620 steels, Acta Physica Polonica A 116 (2009) p. 1029-1032.
- 9) Marucci, M., Lawley, A., Causton, R. and Saritas, S. Effect of small additions of boron on the mechanical properties and hardenability of sintered P/M steels last accessed on 6/17/2011 at: <http://www.hoeganaes.com/TechPapersv2/113.pdf>
- 10) Suwattananont N, Petrova, R., Zunino, J., Schmidt, D., Surface treatment with boron for corrosion protection, Tri-Service Corrosion Conference (2005). Last accessed 6/17/2011 at: <https://www.corrdefense.org/Academia%20Government%20and%20Industry/06T041.pdf>
- 11) Qian, L. and Stone, G.A. A Study of the behavior of boron diffusion in plain carbon steels, Journal of Materials Engineering and Performance 4 (1995) p. 59-62.
- 12) Fichtl, W. Boronizing and Its Practical Applications, Materials and Design (1981), p. 276-286.
- 13) Vladimiroff, T, Carignan, YP, Chiu, DS, Macpherson, AK. Flame Temperature Calculations at High Temperature and Pressure. Propellants, Explosives, Pyrotechnics, 1994:19(6): 281-285.

DISTRIBUTION STATEMENT A: Approved for public release; distribution is unlimited.

UNCLASSIFIED

UNCLASSIFIED



Innovative Nitrogen-Doped Boron Propellants

Presented by:

Thelma G. Manning, Ph. D, P.E.

Insensitive Munitions & Energetic Materials

Technology (IM/EM) Symposium,

23-26 Apr 2018

Portland, OR

UNPARALLELED
**COMMITMENT
& SOLUTIONS**

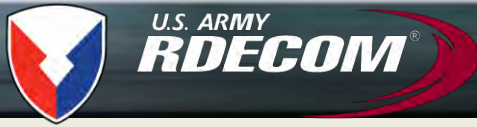
Act like someone's life depends on what we do.



**U.S. ARMY ARMAMENT
RESEARCH, DEVELOPMENT
& ENGINEERING CENTER**

DISTRIBUTION STATEMENT A: Approved for public release; distribution is unlimited.

UNCLASSIFIED



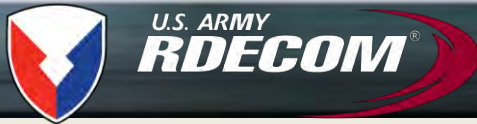
Thelma Manning*, Michael Fair*, Richard Field*, Robin
Crownover*, John Bolognini*, Viral Panchal*, Eugene
Rozumov*,

US Army RDECOM ARDEC*

Picatinny Arsenal, NJ

P H Matter**

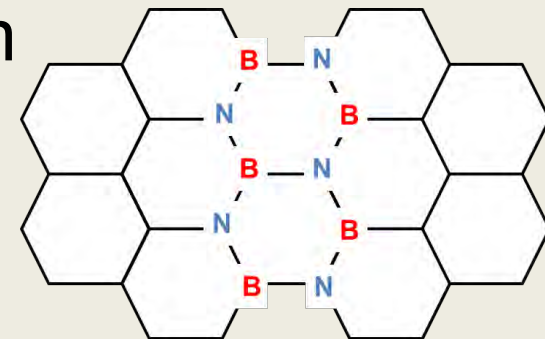
Paul H. Matter, LLC**



- **The Problem**
- **Status/Testing**
 - Experimental Section
 - Propellant Processing
 - Closed Bomb Test
 - Propellant Wear and Erosion Test
- **Prior Art and Advantages Over Prior Art Status/Testing**
 - Results and Discussion
 - Nano-Boron Nitride
 - Burn Rates
 - XPS/SEM/TEM
- **Conclusions / Future Work**



- Army needs more powerful and balanced propellants
- Barrel wear and erosion is a problem
- BN is interesting because:
 - Hexagonal BN is lubricating
 - Boron doping of steel improves its hardness
 - Boron has low molecular weight
 - Resistant to chemical attack





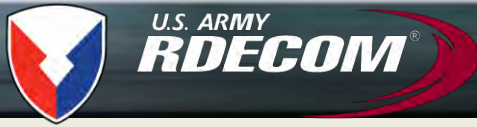
THE PROBLEM



- Currently fielded 155mm artillery propelling charge, M232/M232A1, has exhibited spiral wear and erosion problems.
 - Wear reducing liner



- Many Low Vulnerability (LOVA) Propellant Formulations contain RDX.
 - RDX is highly chemically erosive
- New, experimental low-erosivity LOVA propellants have been produced by
 - Reducing RDX content
 - Introducing nitrogen-rich energetic binder or filler compounds.
 - Compromises between performance, sensitive and erosivity must be reached in these cases



PRIOR ART AND ADVANTAGES OVER PRIOR ART

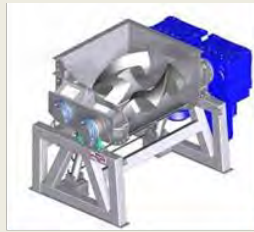


- Ceramic additives to the propellant can theoretically reduce barrel deterioration by coating the inside of the barrels[3]
 - Challenges with dispersing the particles in the propellant, and due to abrasion from incomplete sublimation, propellant and ceramic composites that produce regenerative wear-resistant coatings have not been demonstrated
- Ceramic Barrel Liners have been identified as a promising technology for some time.
 - Very good wear characteristics and thermal resistance
 - Susceptibility of ceramics to fracture, driven by stress, induced by the different thermal expansion properties of steel and ceramics



Approach:

**Additive +
Propellant**



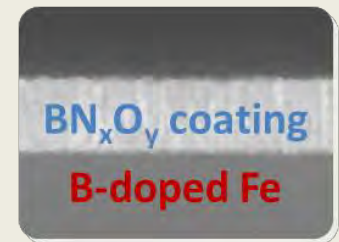
Mix and extrude



**Propellant
Composite**



Propellant Fired



(dramatized image)

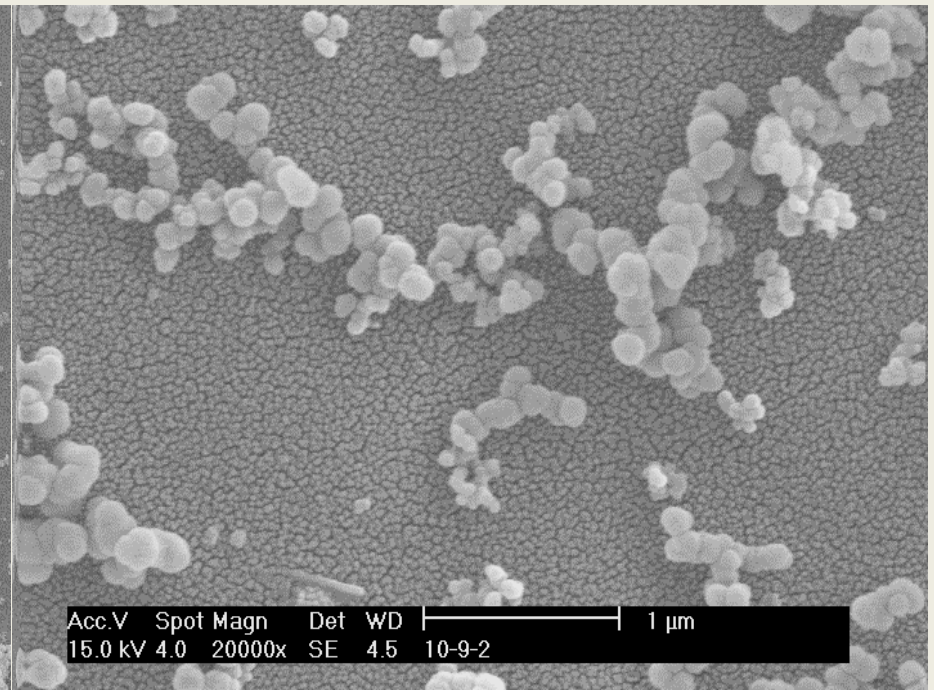
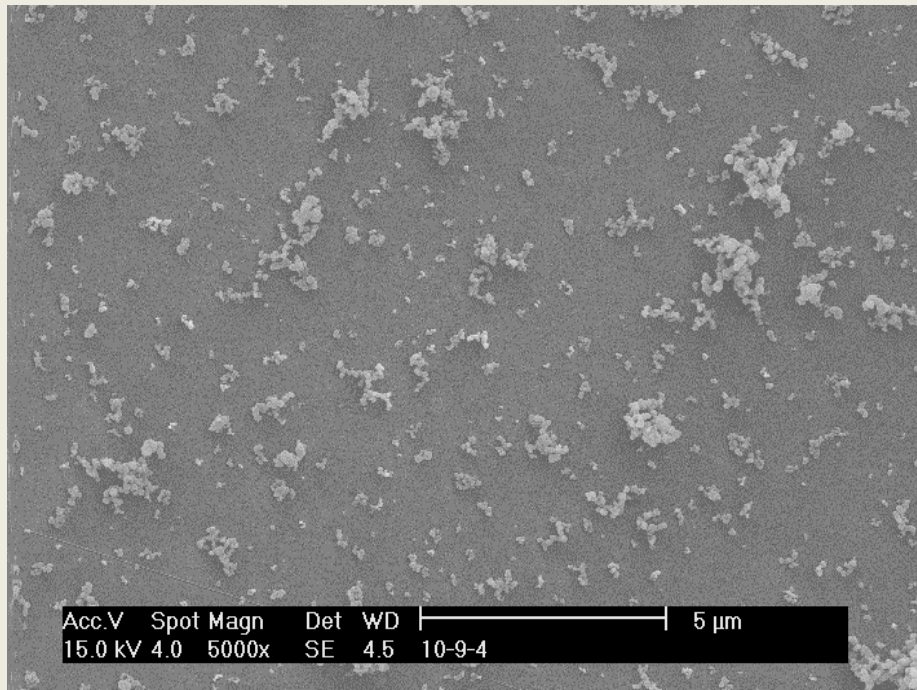
**Coated and
Hardened Barrel**



Particles Size / Surface Area Control

Synthesis Condition	Surface Area (m ² /g)	Calculated Particle Diameter (nm)
High Conc. A	20.0	143
High Conc. B	23.0	124
Intermediate Conc. A	37.8	76
Intermediate Conc. B	51.2	56
Low Conc.	77.4	37

SEM Imaging

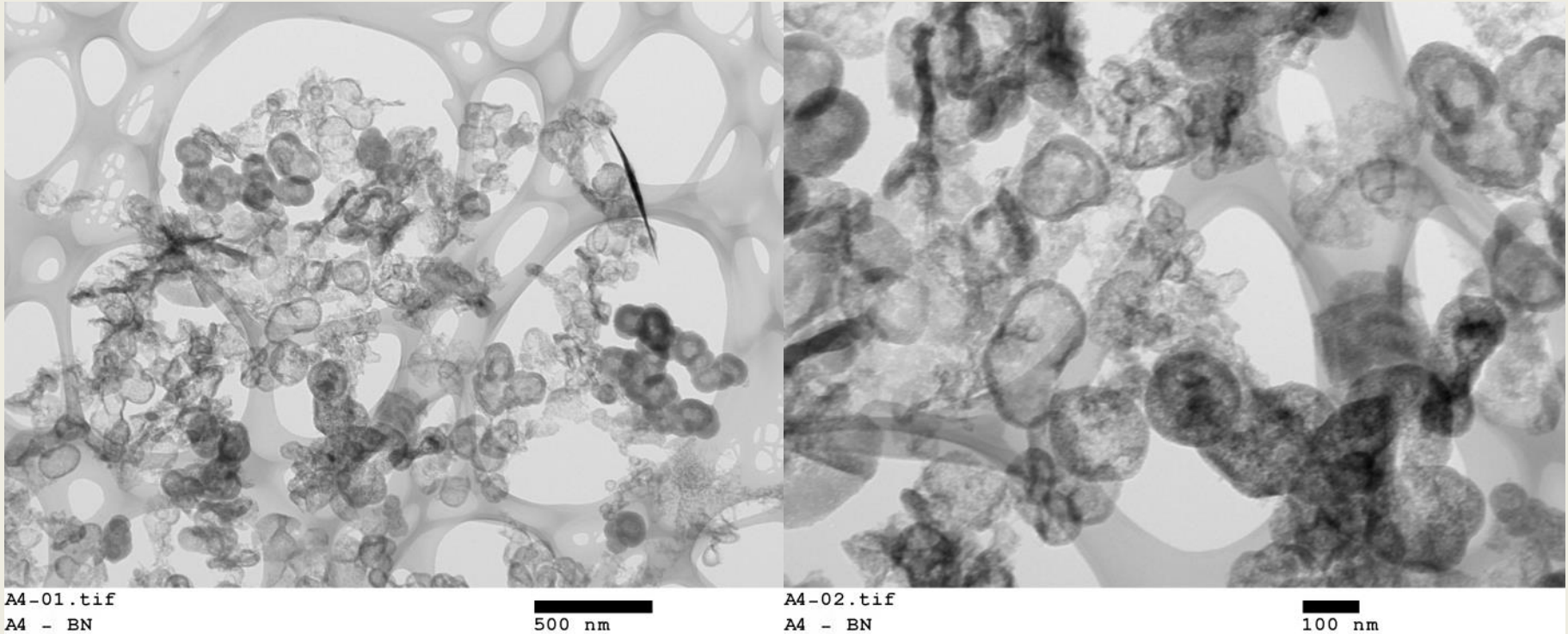


BN NANO-PARTICLE SPHERES

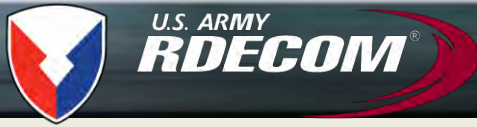
- Particle agglomerate upon drying
- Individual particles are spheres
- Spheres with diameters in the nanometer range.



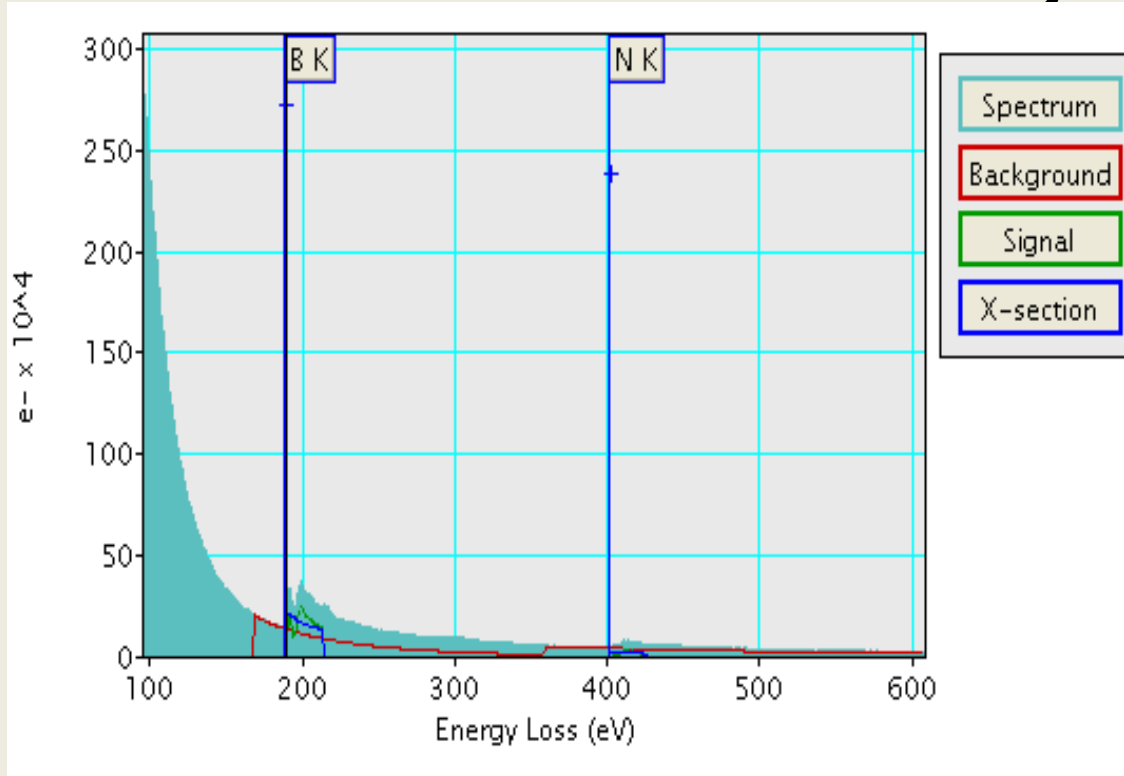
TEM Imaging



TEM images showing nano-spheres of boron nitride used for propellant additive testing (US Patent Pending).



EELS Analysis



Experimental Conditions

Beam Energy: 200 keV

Convergence Semi-Angle: 5 mrad

Collection Semi-Angle: 1.5 mrad

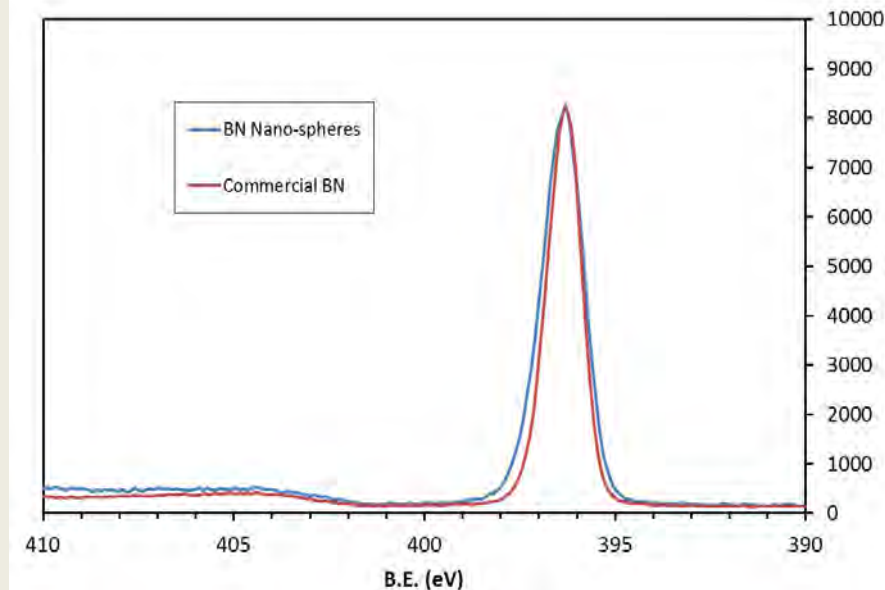
Composition Information

Elem.	Atomic ratio (/B)	Percent content
B	1.00 ± 0.000	52.37
N	0.91 ± 0.129	47.63

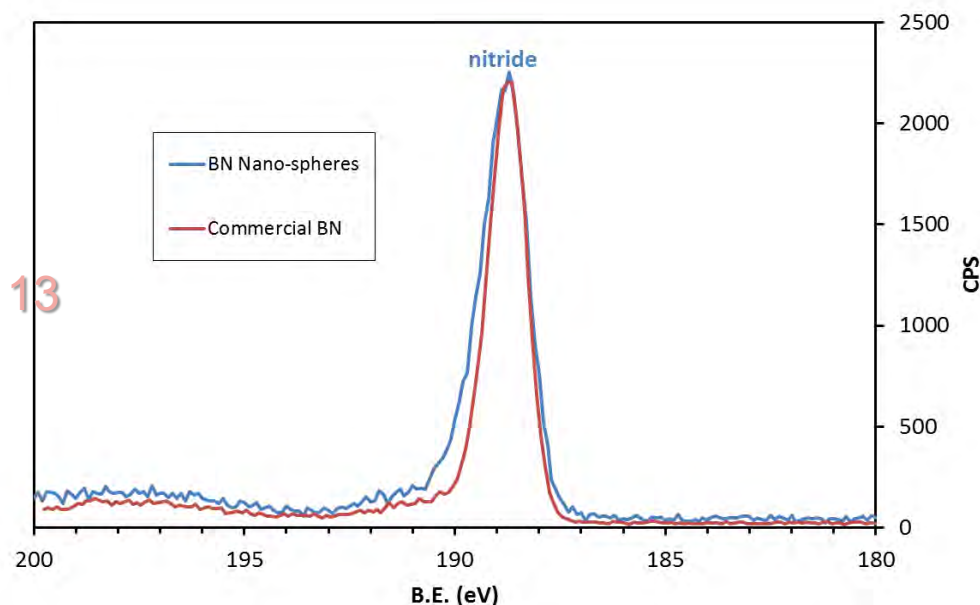
EELS Analysis, showing the material has a 1:1 B:N ratio (US Patent Pending).



XPS Analysis – N 1s Region



XPS Analysis – B 1s



XPS Analysis showing (a) the N 1s region, and (b) the B 1s region for the BN nano-particle propellant additive compared to a commercial hexagonal boron nitride sample.



IMR-4198 Composition

Propellant Name	Nitrocellulose Composition (wt%)	Dinitrotolulene Composition (wt%)	Other Components (wt%)
M1	86%	9.9%	3% Dibutylphtalate 1% Diphenylamine
M14	90%	8%	2% Dibutylphtalate 1% Diphenylamine 0.7% Residual solvent 0.6% Moisture 0.2% Graphite
IMR 4198 (Hodgdon)	>85%	<10%	<10% Non-hazardous additives



Propellant Testing



DSC Testing

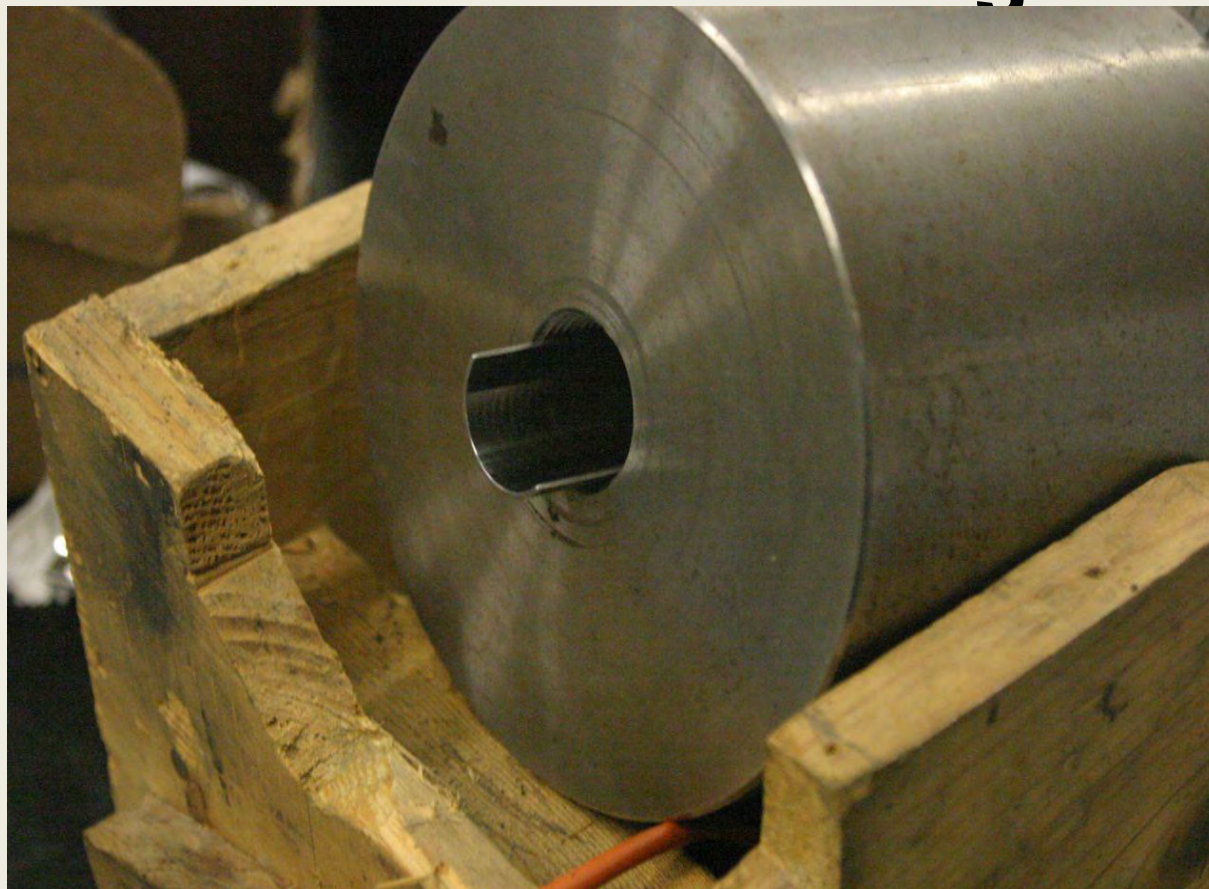
Propellant Material Tested	Heating Rate (°C/min)	Sample Amount (mg)	Exotherm		
			Onset (°C)	Peak (°C)	End (°C)
IMR4198 w/o BN	10	0.36	162	206	265
	10	0.15	162	207	265
	10	0.58	159	207	265
Average			161	207	265
IMR4198 w/ BN	10	0.22	163	207	265
	10	0.40	158	207	265
	10	0.45	161	207	265
Average			161	207	265



Heat of Combustion

Material Tested	Heat of Combustion; ASTM D240 (J/g)
IMR-4198 w/o BN	10038
IMR-4198 w/ BN	10036

Closed Bomb Testing



200 CC CLOSED BOMB

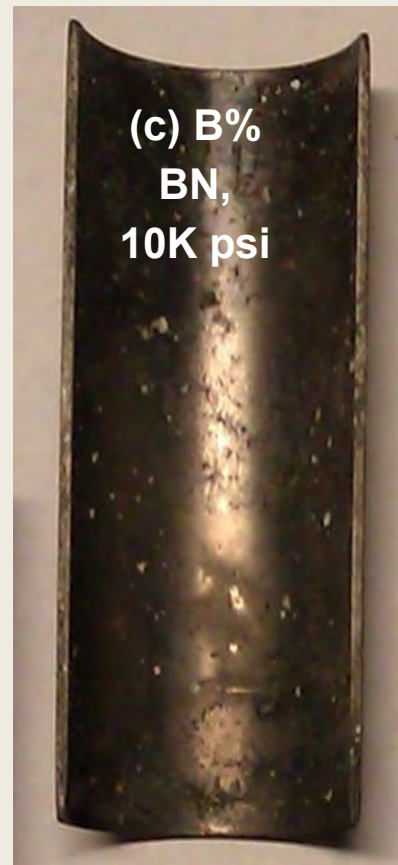


Closed Bomb Testing

Material Tested	Amount (gram)	Closed Bomb Chamber pressure (psig)	Observations
IMR-4198 w/o BN	5.0	10k	Oxidation (rust color)
	7.5	15k	Deep oxidation (rust)
Mix 50/50 of pure and composite (WITH A% BN)	5.0	10,250	Black residue on the surface, no visible oxidation
IMR-4198 w/ BN	5.0	10k	Black residue on the surface, no visible oxidation
	7.5	15k	Possible slight oxidation (green color)
IMR 4198 as received	5.0	9,170	Reference sample, used high speed DAQ system.
	7.5	15,470	Reference sample, used high speed DAQ system.



Closed Bomb Inserts



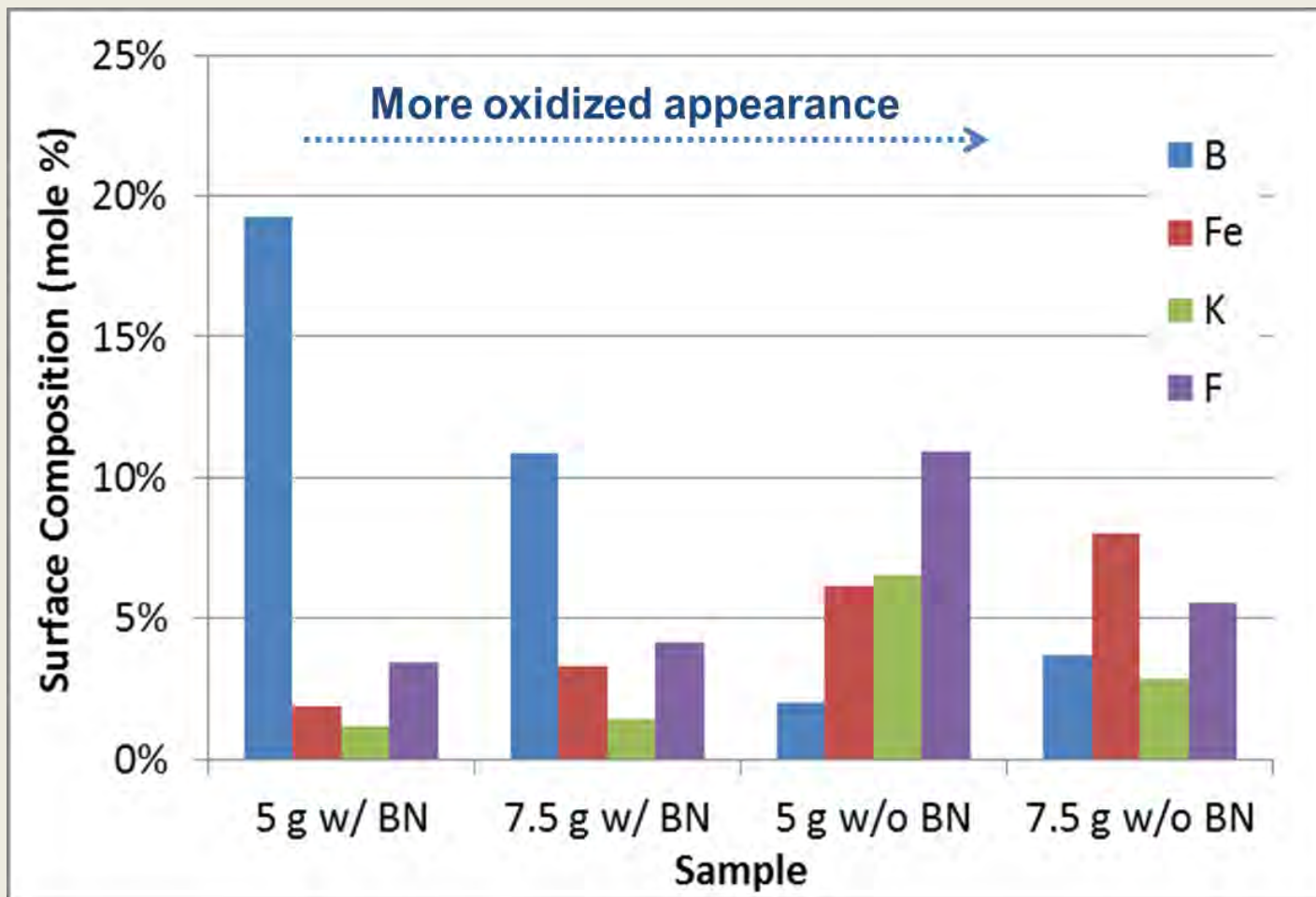


Closed Bomb Inserts



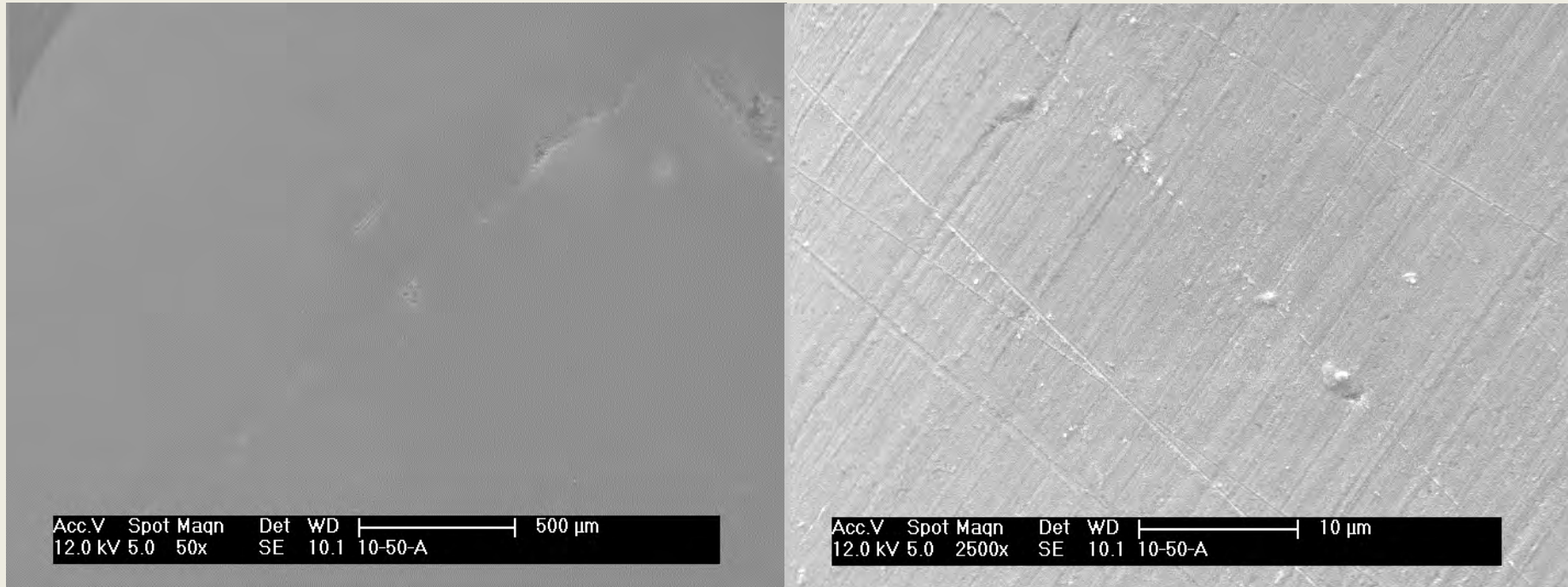


XPS Analysis



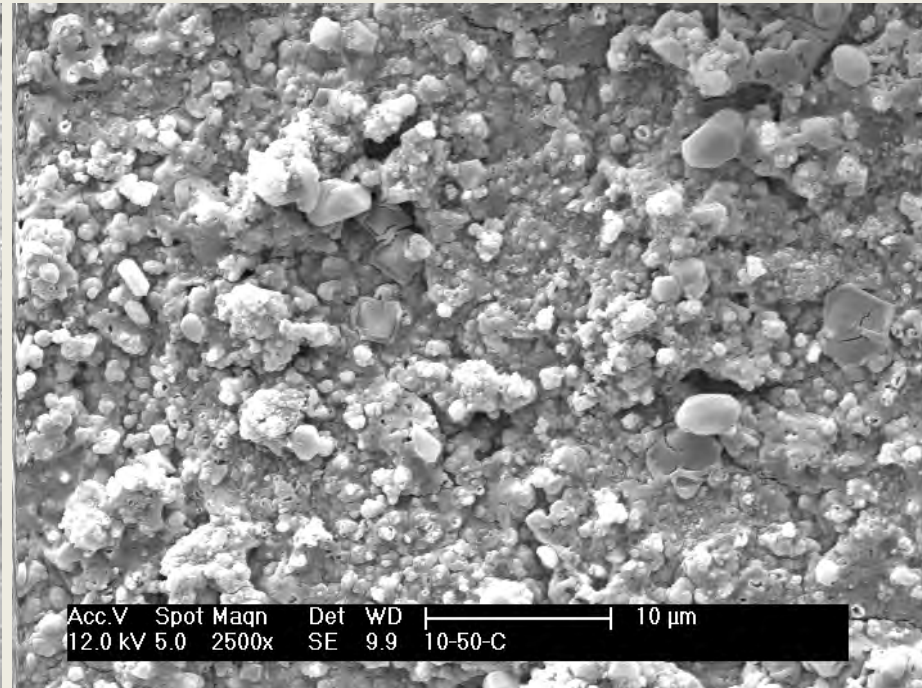
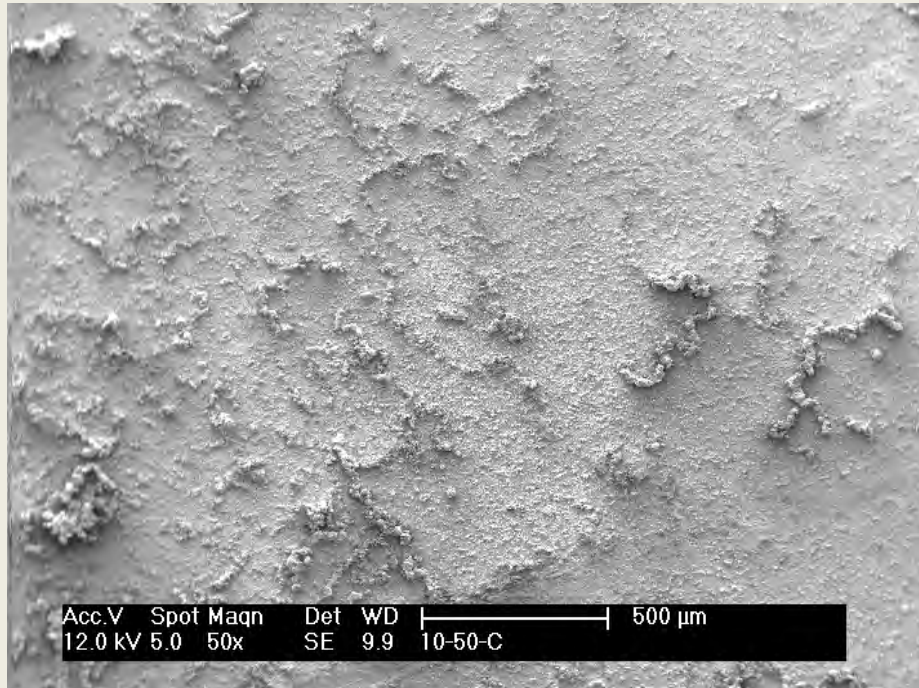


SEM – Fresh Insert



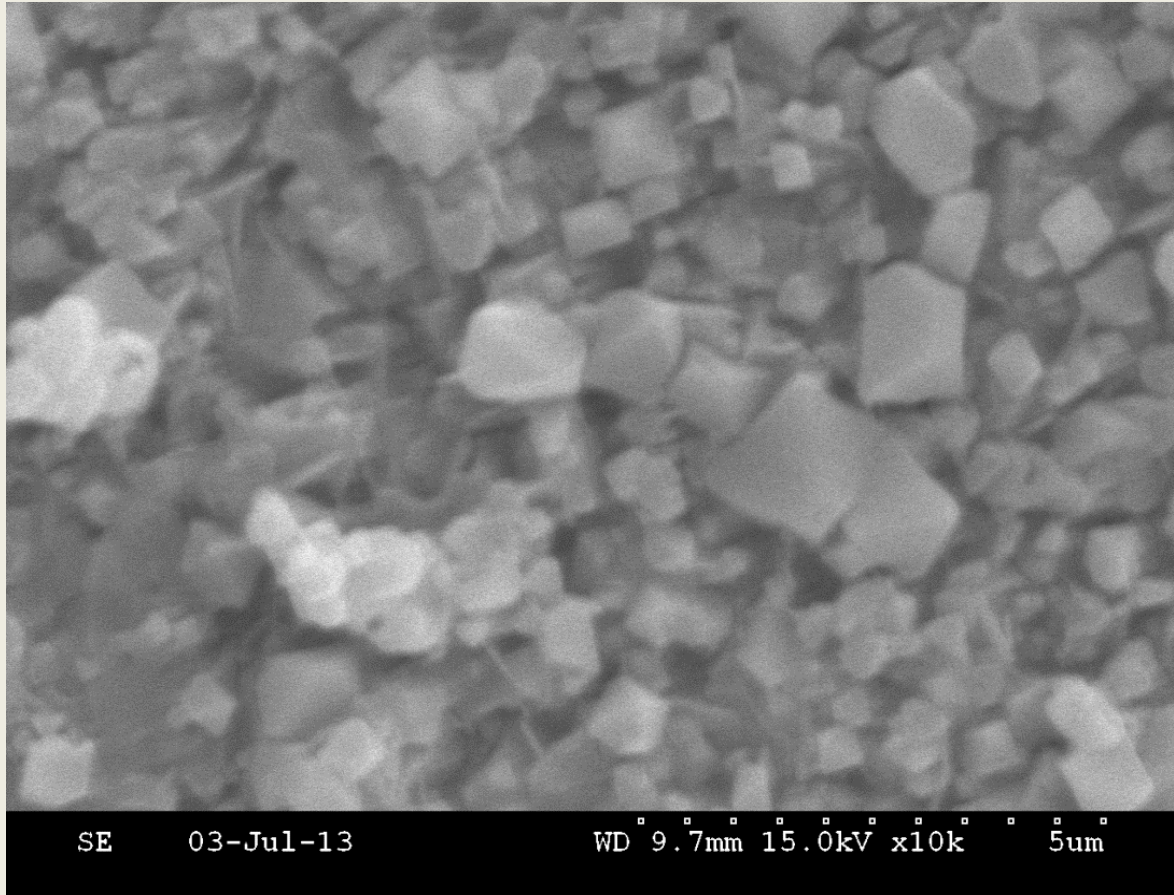


SEM – Insert Fired w/o BN





SEM – Insert Fired w/o BN





SEM – Insert Fired with BN

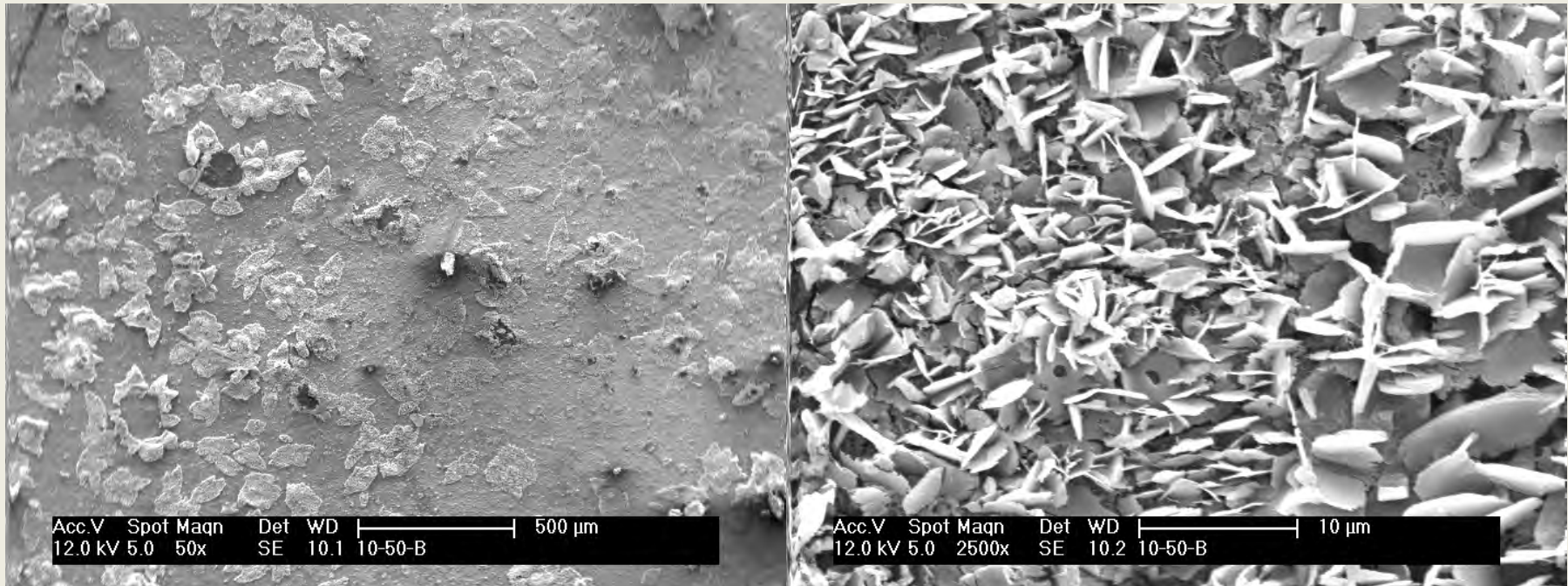




**Figure 1: RPD380 w/o BN -
Single Perf grain used in
erosion testing**

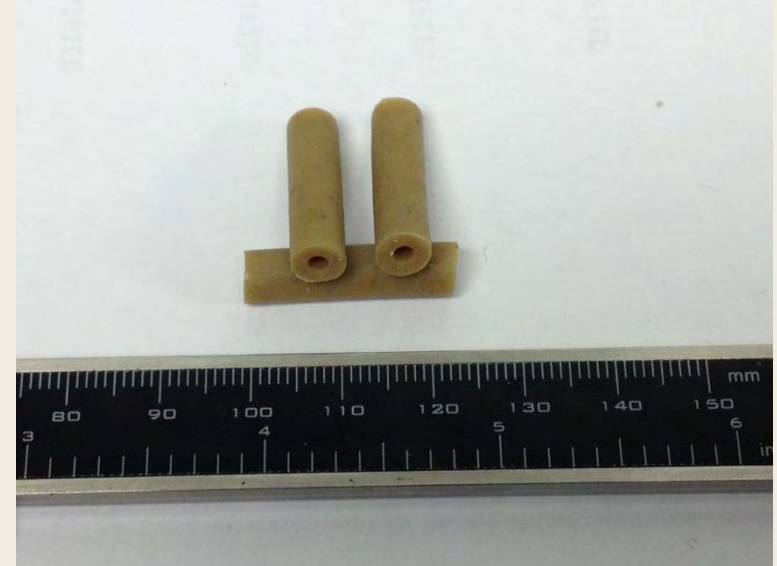
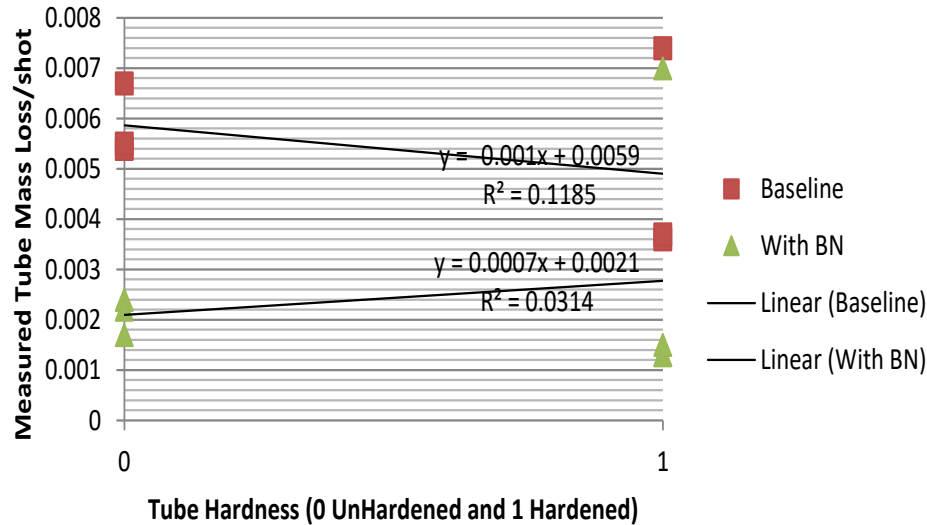


**Figure 2: RPD-380 w/BN
Single Perf grains used in
erosion testing**



Boron Nitride Erosion Study



RPD380 vs B% BN-RPD380 Erosive Loss

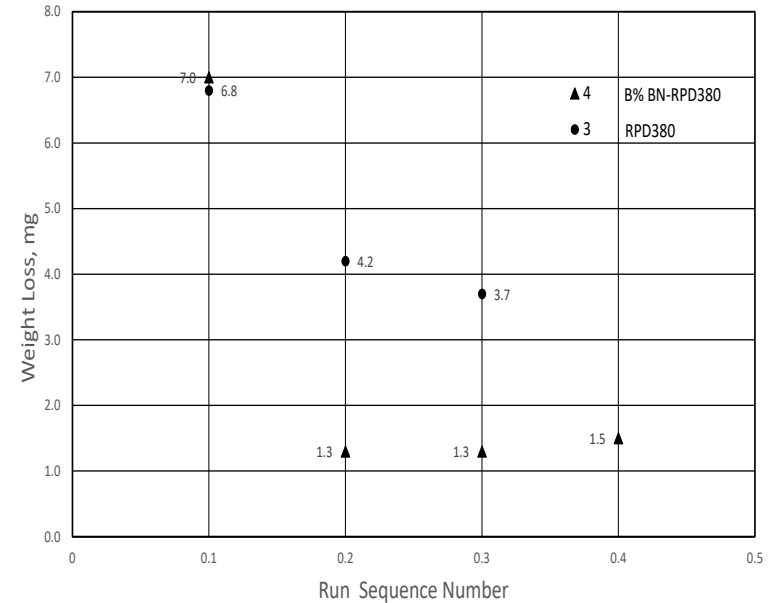


Figure 10: Wear and Erosion Test Results for hard and unhardened sleeves (US Patent Pending).

Note: Sleeves 1 and 2 were hardened to approximately Rockwell Hc 41. Sleeves 3 and 4 were approximately Rockwell Hc 12. See ICP

The effect of the BN propellant additive (US Patent Pending) suggests an apparently significant reduction in the mass loss for both hardened and unhardened insert sleeves relative to baseline RPD-380 propellant. The results look compelling at 2.8 and 1.8 times life increase for hard and unhardened insert sleeves, respectively



- **SEM:**

- Hardened and cleaned – both with and without BN
- Unhardened and un-cleaned – imaged cleaned areas of both with and without BN (un-cleaned areas were too resistive).

- **ICP:**

- Hardened and cleaned – both with and without BN

- **XPS:**

- Hardened and cleaned – both with and without BN
- Unhardened and cleaned –
- Unhardened and un-cleaned coating
- Saw material –

- ❖ **Moh's Hardness Testing:**

- Hardened and cleaned – both with and without BN
- Unhardened and cleaned – both with and without BN

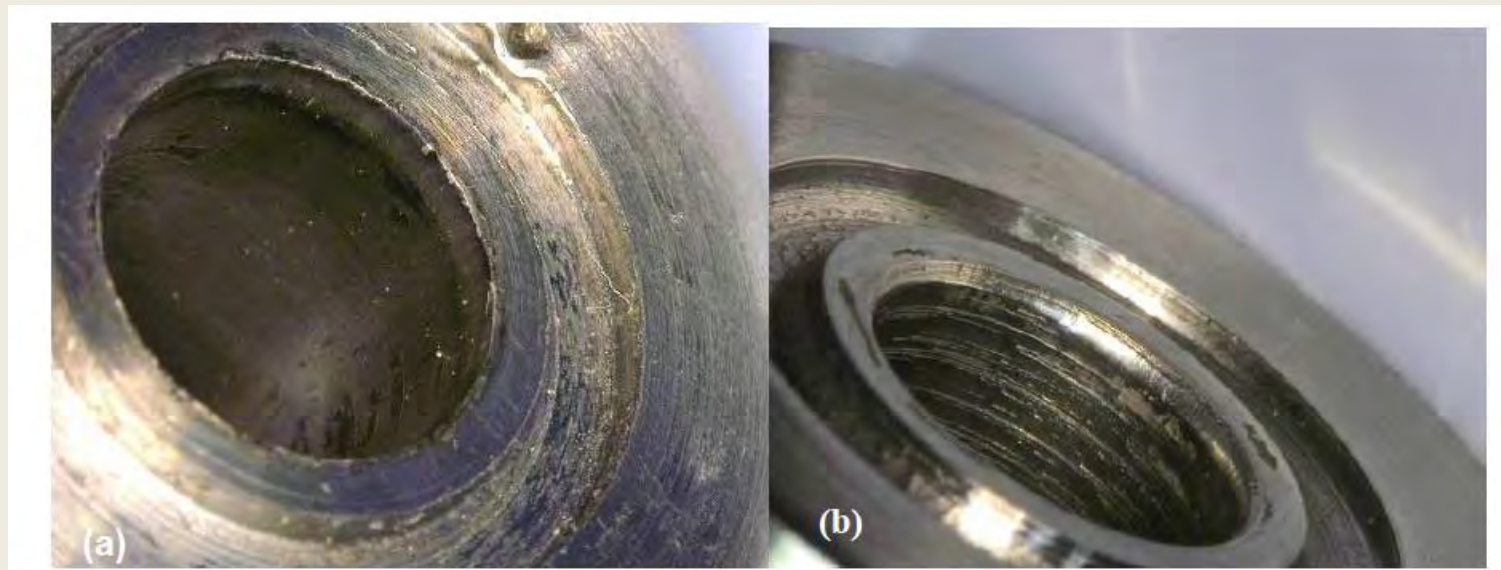


Figure 3: Hardened Steel Sleeves (a) RPD380 P2 flow entrance end, sleeve 1. (b) BN-RPD380 P5 Flow Exit end, sleeve 2 – cleaned after 3 shots

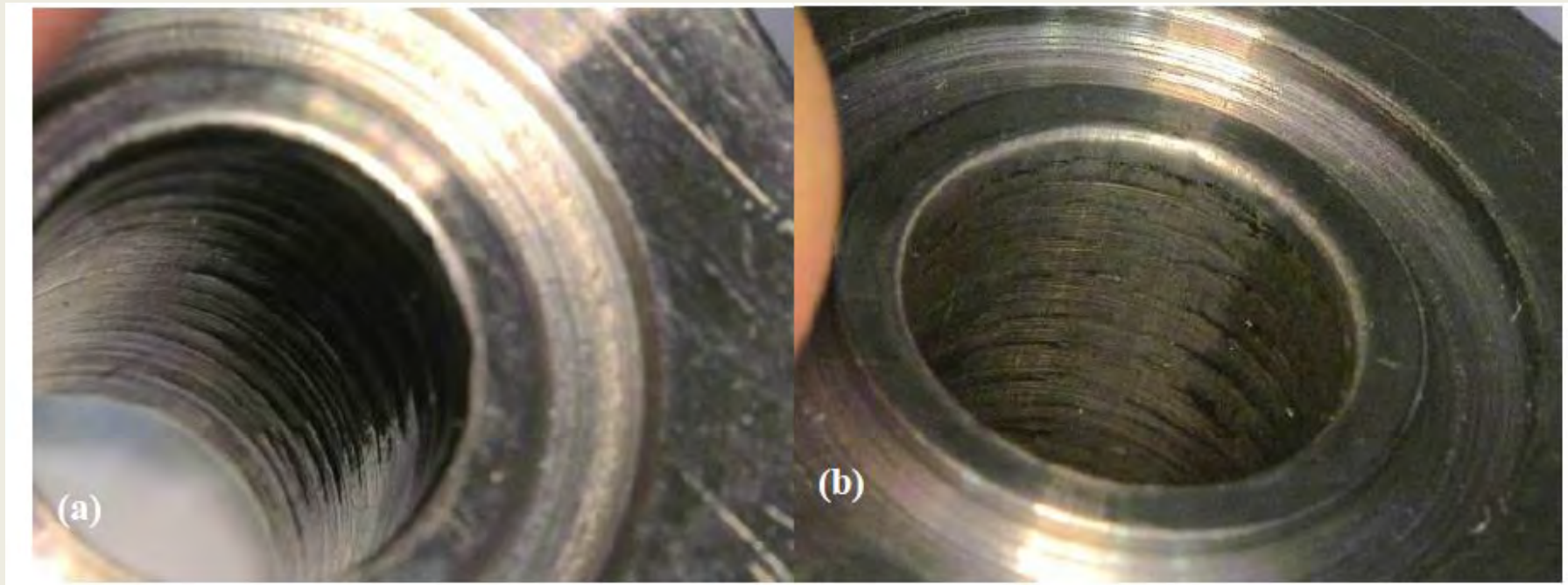
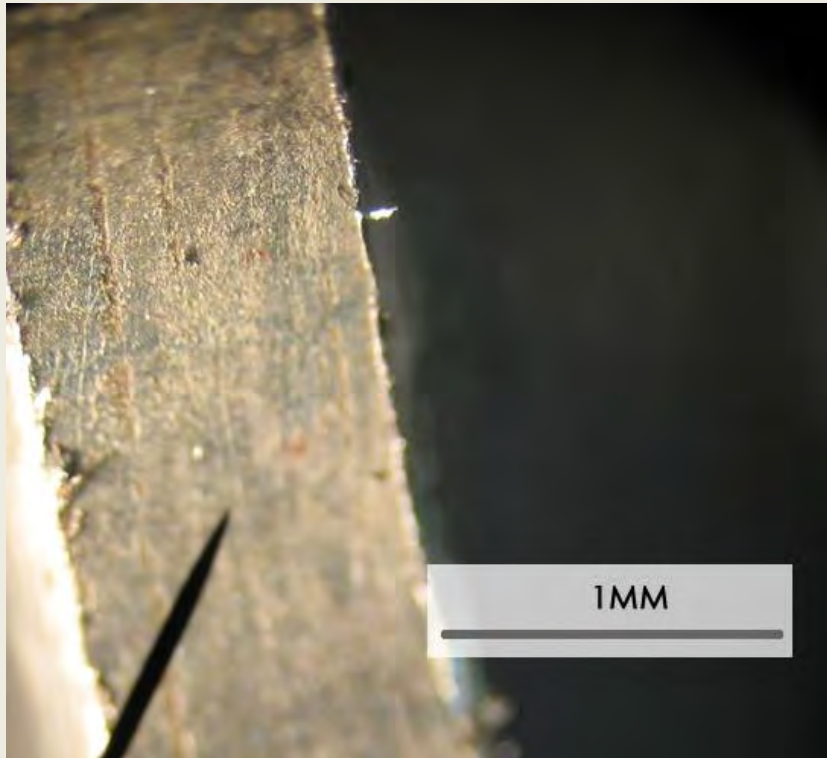


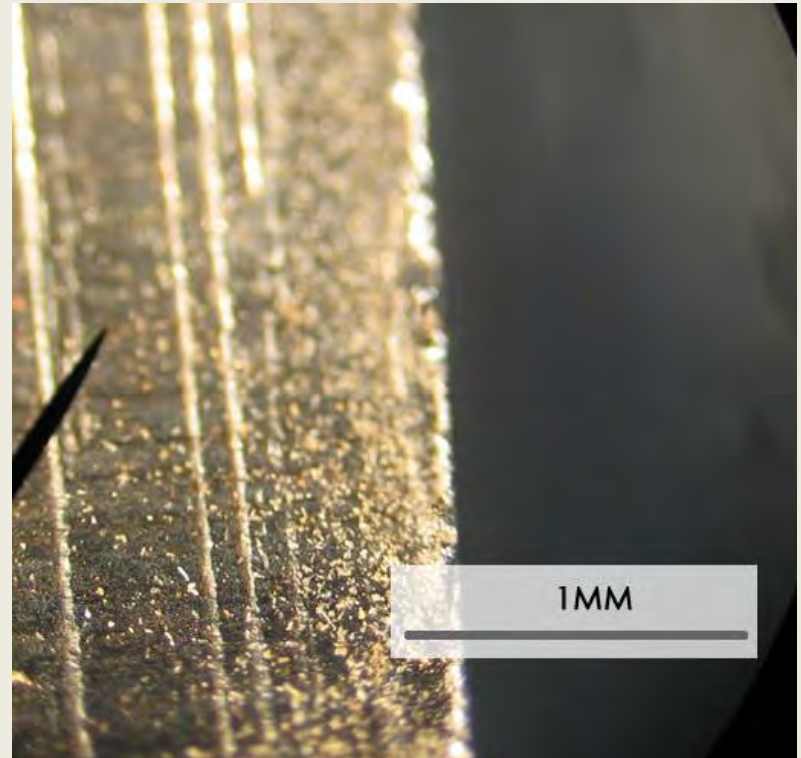
Figure 4: Insert Sleeve 2 – (a) hardened Steel, after firing 3 shots RPD380 Propellant (Cleaned) , RPD380 P - Flow Entrance End – cleaned after 3 shots (b) RPD380 P - Flow Exit End – cleaned after 3 shots



Light Micrographs

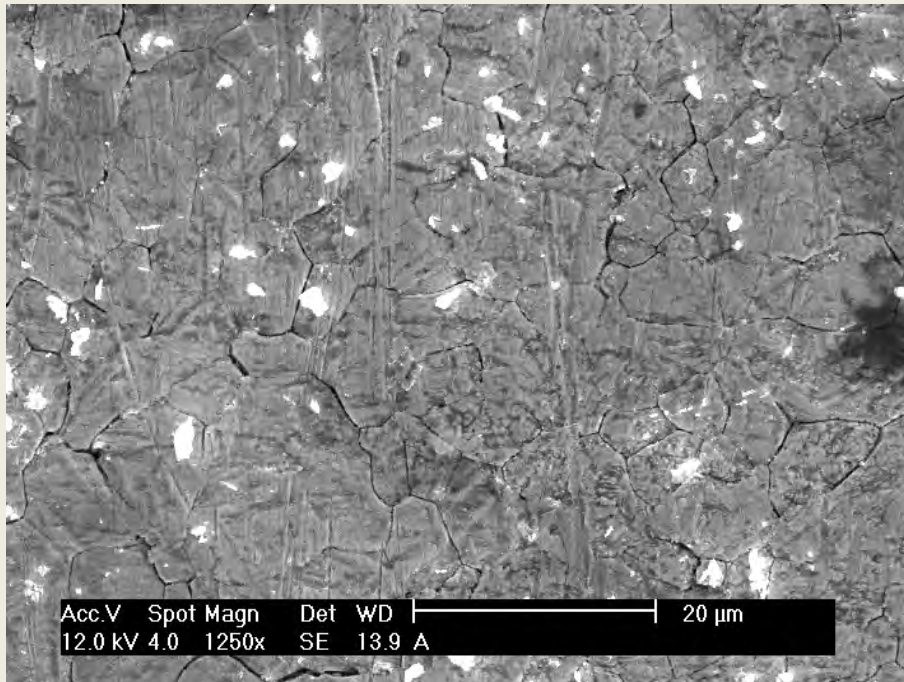
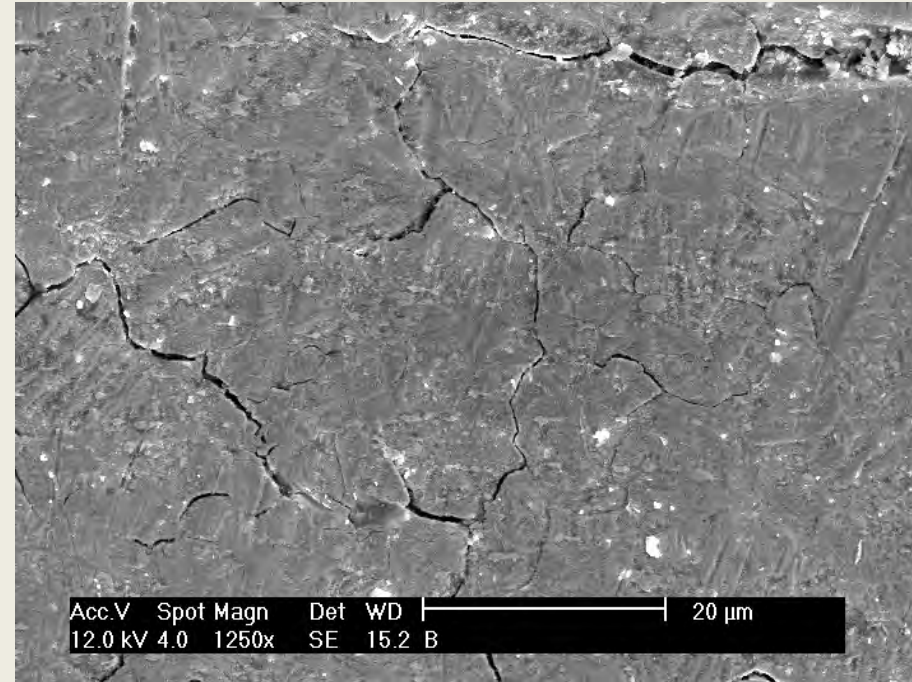


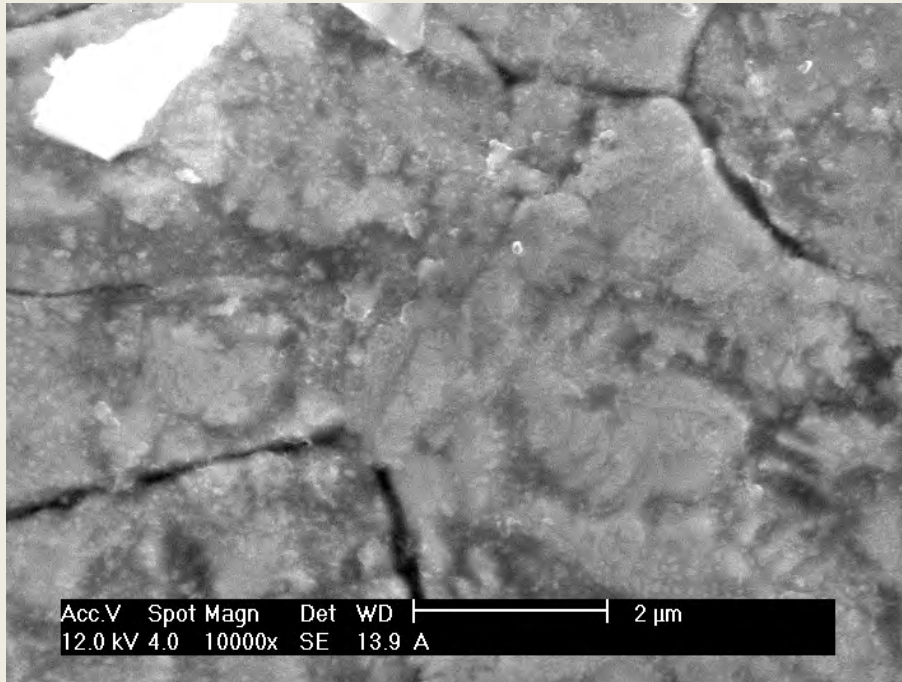
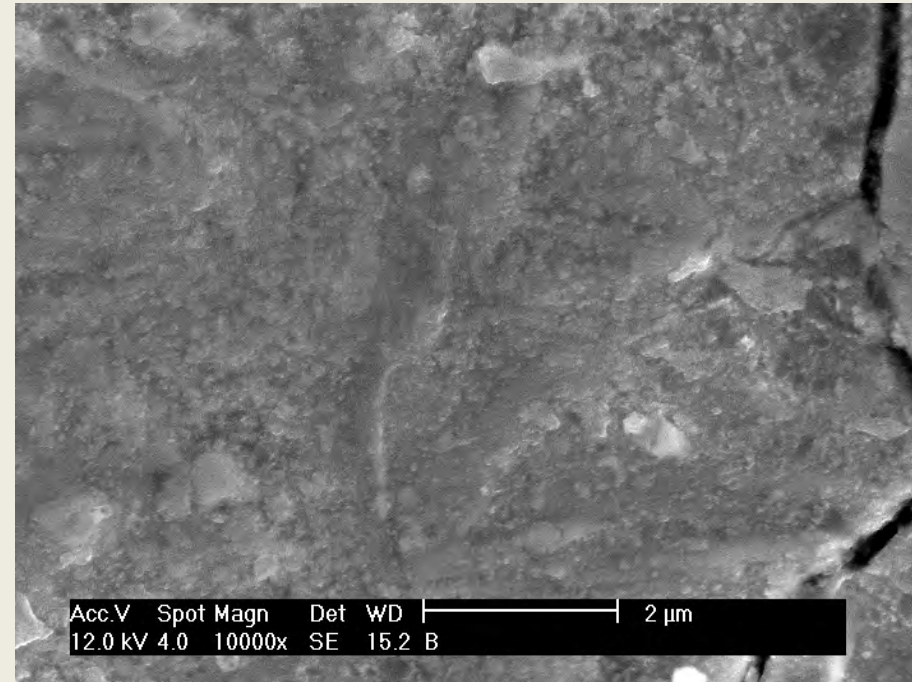
Without BN

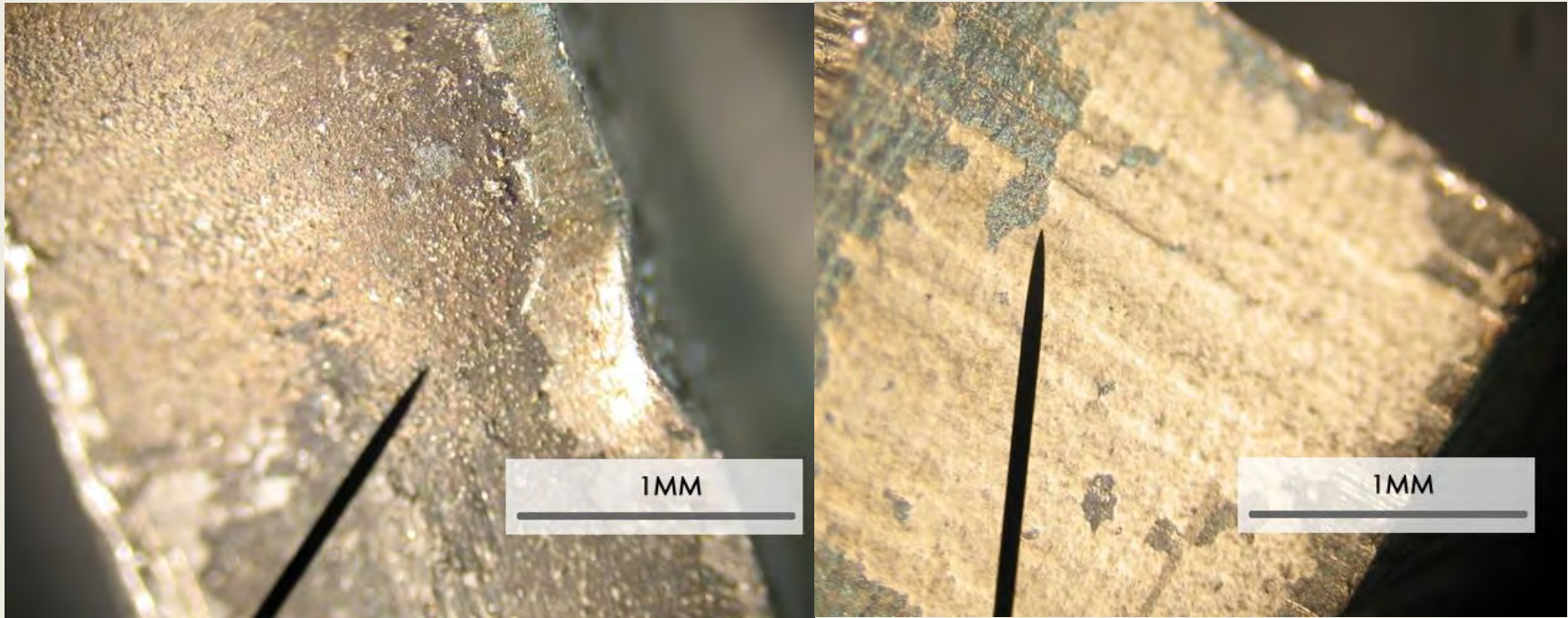


With BN

Hardened, Cleaned

**Without BN****With BN****Hardened, cleaned**

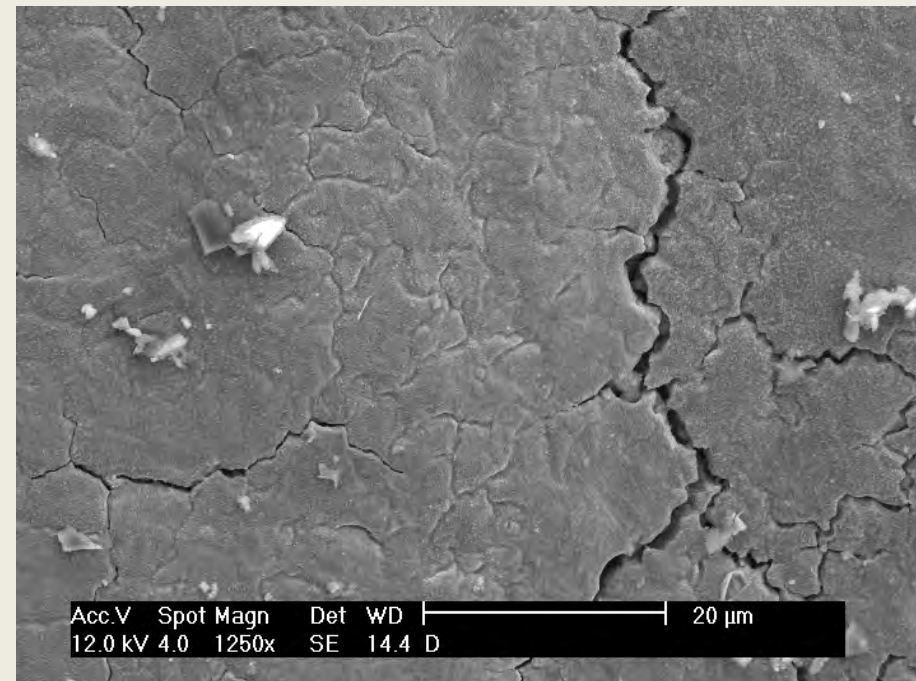
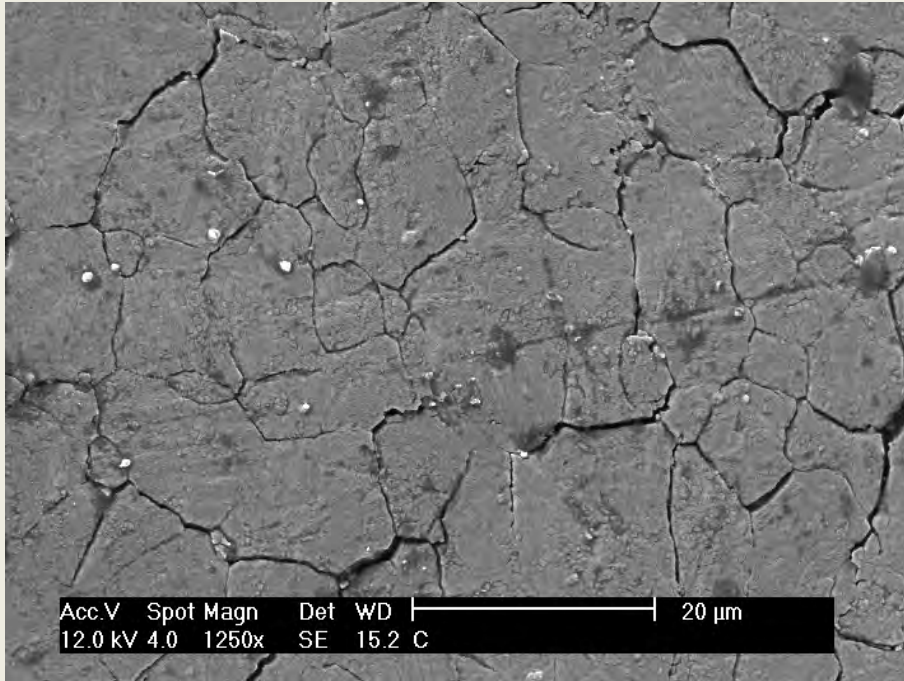
**Without BN****With BN****Hardened, Cleaned**



Unhardened, un-cleaned surface

Without BN

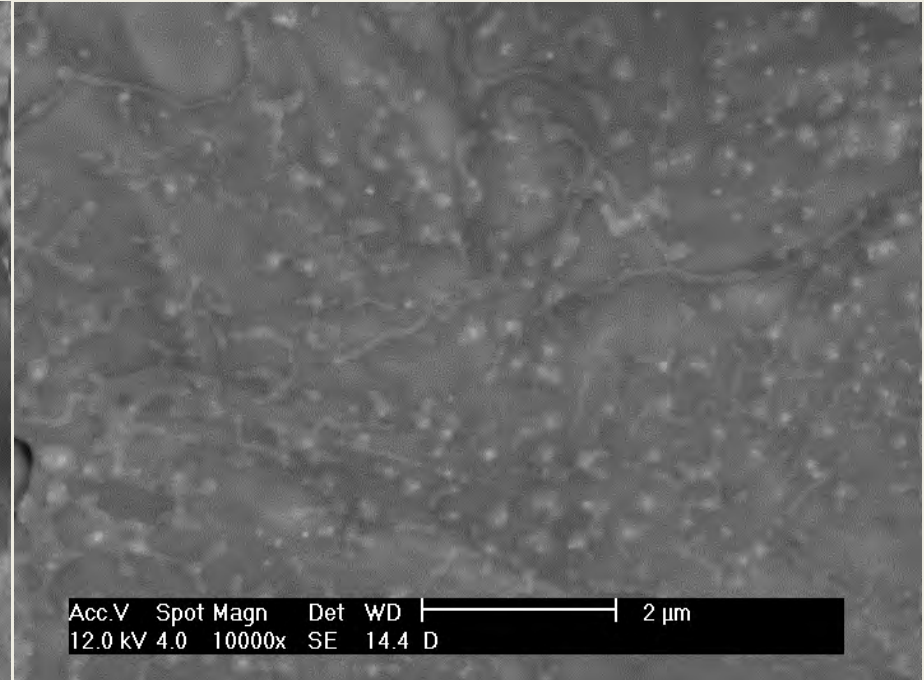
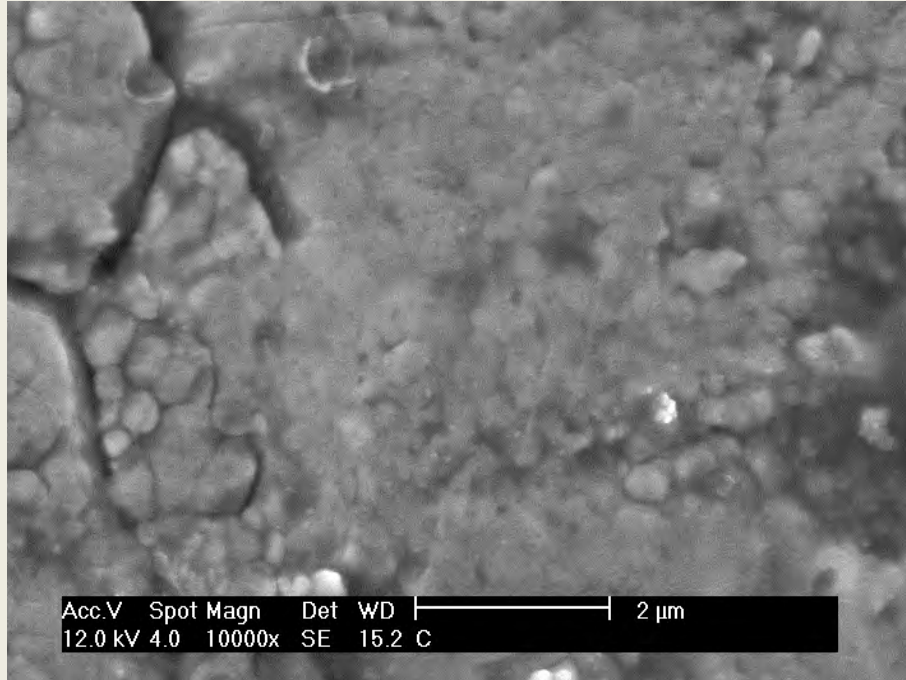
With BN



Unhardened (clear area)

Without BN

With BN



Unhardened (clear area)

Non BN

With BN



Relative Composition

Element	Hardened (0% BN)	Hardened (B% BN)	Unhardened (B% BN)	Unhardened (B% BN)	Coating from Unhardened B% BN
C	65.2%	19.9%	29.9%	13.1%	64.6%
B	0.0%	0.0%	0.0%	0.4%	2.3%
N	2.8%	1.4%	0.0%	0.9%	5.2%
Fe	32.0%	78.7%	70.1%	85.6%	27.9%

Hardened and cleaned surface composition

After firing, the samples were analyzed by XPS to determine surface composition, and ICP analysis to determine the bulk composition.

- Relative surface composition for samples fired in wear and erosion testing.
- ICP analysis showed less than 0.01% B in all samples, and the remaining composition is consistent with the respective steel specification.



Sample	Hardness
Unhardened steel reference	5.5
Hardened, without BN	7.0
Hardened, with BN	7.5
Unhardened, without BN	5.5
Unhardened, with BN	7.5



Sample	Hardness
Unhardened steel reference	5.5
Hardened, without BN	7.0
Hardened, with BN	7.5
Unhardened, without BN	5.5
Unhardened, with BN	7.5



- Evidence for reduced erosion observed.
 - The results look compelling at 2.8 and 1.8 times life increase for hard and unhardened insert sleeves, respectively.
- Propellant with BN generates a lower flame temperature.
- Increased hardness was observed in unhardened steel fired with BN additive.
- SEM imaging showed less surface crack density in the samples fired with boron nitride.
- No destabilizing effects on propellant.
- Boron-based coating was observed.



FUTURE WORK



- More quantitative hardness testing after extended firing would be useful to verify a hardening mechanism
- Characterization of the boron, possibly in or on the steel surface, would also be beneficial.
- Further wear and erosion testing of the propellant additive is in progress in a 25mm gun test fixture/projectile test stand that will simulate the conditions of 155 mm artillery.
 - Larger amount of propellant necessary to support a sufficient number of firings to generate supportable statistical conclusions
 - Alternate grain form to allow larger bomb loading density



U.S. ARMY
RDECOM

Acknowledgements



**US Army Small Business Innovative Research (SBIR)
Contract No. W15QKN-12-C-0041**

Thanks to:

**US ARMY RDECOM ARDEC Propulsion Pilot
Processes Branch**

Dr. Sheldon Shore, Ohio State University

Analysis on Pressure and Temperature Profiles upon Impact of Reactive Material Structures

Kibong Lee¹, Yong-Soo Cho¹, Sang-Hyun Jung^{1*},

¹The 4th Research and Development Institute-2nd Directorate, Agency for Defense Development, Daejeon, 34060, Korea

Abstract

The pressure and temperature profiles upon high speed impact of Reactive Material Structures (RMS) were compared with the pressure and temperature profiles upon high speed impact of inert material structures. The shape of the pressure profile generated by the high speed impact of RMS is clearly different from the pressure profile generated by the high speed impact of inert material structure. In particular, the maximum pressure formed by the high speed impact of RMS was about two times higher than the maximum pressure formed by the high speed impact of inert material structure. The temperature profile resulting from the high speed impact of RMS also showed a large difference from the temperature profile resulting from the high speed impact of inert material structure. In particular, the difference in the duration and the size of high temperature regions over 3000 K was remarkable. It is also found that the pressure and the temperature profiles generated in the RMS test were also changeable by the development of microstructure even though they are same compositions.

Keywords: reactive materials, reactive material structures, Al-Ni, high-speed impact test, two-wavelength pyrometer

*Corresponding author: Sang-Hyun Jung (sanghyun@add.re.kr); Tel: +82-42-821-4282; Fax: +82-42-823-3400-16265

1. Introduction

Reactive cases are interesting areas to weapon system researchers as an advanced missile body, because it is able to sympathize with explosives when it explodes [1, 2]. In order to develop a reactive case, it is necessary to develop an energetic structural material that can release a large amount of energy by sympathizing with explosives when it explodes, although it normally works as an inert structure that can protect the internal explosives safely. These materials are called as reactive material structures (RMS) and many advanced defense research institutes are making efforts to develop them [3]. Although reactive cases have been reviewed theoretically many times, there are still many technical limitations to make it practical. Recently, however, a variety of basic studies have been carried out for the practical application with a development of RMS manufacturing and testing techniques. In particular, the studies for the reaction characteristics of the RMS resulting from a propagation of shock waves (which could be caused by the high speed impact of RMS) has been attempted in various research groups, since it can simulate the reaction characteristic of the RMS according to the propagation of the shock waves caused by the exploding of explosives [4-8].

In this study, Al-Ni mixed powder which is known as typical reactive materials were consolidated in the form of bullets, and they were impacted on steel target at a velocity of 1600 m/s. Then, the instantaneous pressure and temperature changes resulting from the impacts were measured. The obtained pressure and temperature profiles were compared with the pressure and temperature profile of inert structure (Ni) bullets.

2. Experimental procedures

2.1. High speed impact test. The setup of high speed impact test system used in this study is shown in Fig. 1. The high speed impact test system includes a ballistic gun that propels the metal bullets at a high speed, a sabot that improves the flight straightness of the metal bullets, a speedometer that measures the velocity of the bullets, an observation chamber in which a reaction phenomenon occurs caused by the impact, two piezoelectric sensors for measuring the pressure generated in the observation chamber, and a two-wavelength pyrometer for measuring the temperature generated in observation chamber.

A 5 mm thick steel plate was placed in front of the observation chamber in order that shock waves propagate into the metal bullet when the metal bullets enter into the observation chamber, and a Rolled Homogeneous Armour (RHA) steel was placed at the end of the chamber to induce full propagation of the shock wave to the metal bullets and to protect the observation chamber. Two piezoelectric sensors were mounted at front and back side of the observation chamber to measure the pressure caused by the impact of the bullets. In addition, the right side of the chamber (the right side of the bullet flight direction) was protected with a transparent polycarbonate plate (thickness: 25 mm) to fully acquire the emitted spectrum (resulting from high speed impact of metal bullets) which is required for the two-wavelength pyrometer analysis. Using the high speed impact test system, the prepared RMS bullets and the inert metal bullets were propelled at a velocity of 1600 m/s (and were impacted on the back side of the observation chamber), and the pressure and temperature generated in the chamber were obtained and compared with each other.

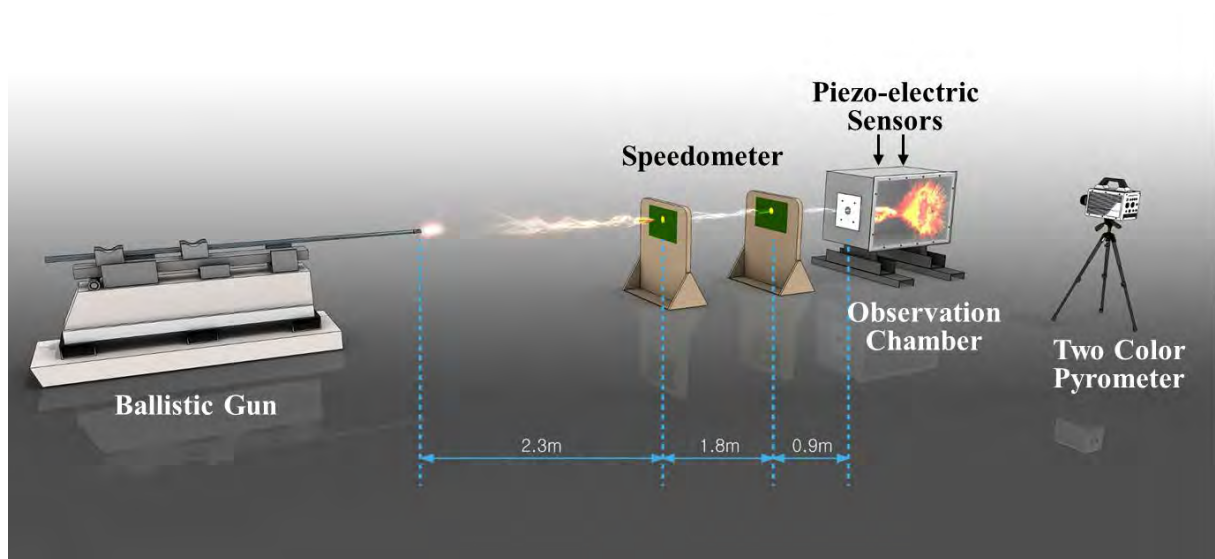


Fig. 1. Experimental setup of a high speed Impact test for reactive material structures

2.2. Metal bullets manufacturing. The metal bullets used in this test were five types, all of which were manufactured in the form of a cylindrical shape with a diameter of 14.3 mm and a height of 14.3 mm. Table 1 summarizes the manufacturing method (i.e. compositions, raw materials, mixing methods, and forming methods) of the metal bullets used in this experiment. Ni bullet and Al bullet were prepared by cold isostatic pressing of 4 μm Ni powder (T-123, Vale Co.) and 10 μm Al powder (10sf, Changsung Co.) at a pressure of 400 MPa without any pretreatments. The other bullets were all prepared of 68.5 wt.% Ni - 31.5 wt.% Al composition. However, they were prepared by different mixing methods (Turbula mixing or Attrition milling) or different sizes of Ni raw powder (4 μm or 1 μm).

Table 1. The sample names and manufacturing methods of the metal bullets used in this experiment (TM refers Turbula mixer, AM refers Attrition Mill, and CIP refers Cold Isostatic Pressing)

Sample Name	Composition		Raw Material		Mixing Method	Forming
	(wt. % of Ni)	(wt. % of Al)	Ni powder	Al powder		
Ni	100	0	4 μm	-	-	CIP (400 Mpa)
Al	0	100	-	10 μm	-	CIP (400 Mpa)
NA-T	68.5	31.5	4 μm	10 μm	TM	CIP (400 Mpa)
NA-A	68.5	31.5	4 μm	10 μm	AM	CIP (400 Mpa)
nA-A	68.5	31.5	1 μm	10 μm	AM	CIP (400 Mpa)

Figure 2 shows the internal microstructure of the NA-T, NA-A, and nA-A RMS bullets used in this experiment. The NA-T specimen shows a microstructure in which Ni powder (4 μm) and Al powder (10 μm) are just mixed, and the Ni particles are slightly agglomerated. The NA-A specimen shows an elongated microstructure of Ni particles (by attrition milling), and the aggregation of Ni particles are relaxed compared to NA-T specimen. The nA-A specimen shows a much better dispersion than the other RMS specimens in terms of microstructure, although the aggregation of small Ni particles is locally observed. The prepared bullets of five types were compared for their reaction characteristics through the high speed impact test introduced in Section 2.1.

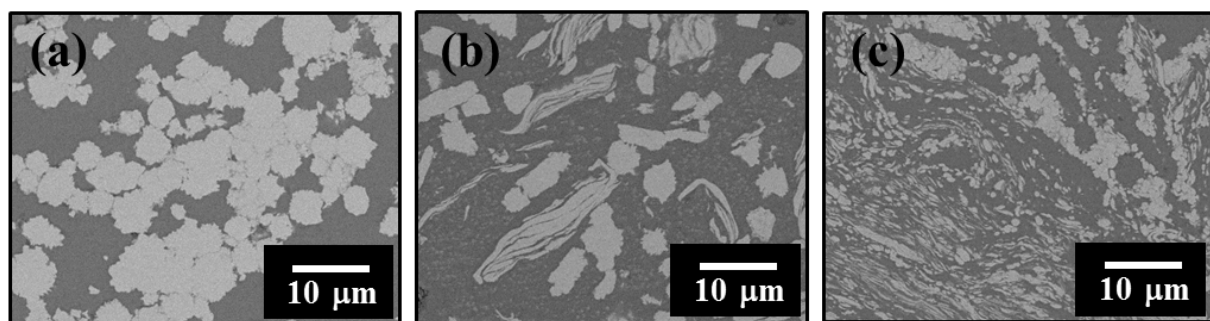


Fig. 2. BS- (Back Scattered-) SEM images for (a) NA-T, (b) NA-A, and (c) nA-A RMS bullet used in this study.

2.3. Two-wavelength pyrometer analysis. In this study, the changes of temperature distribution occurred in observation chamber which is caused by high speed impact of RMS were analyzed using two-wavelength pyrometer. To analyze the changes of

temperature distribution at the level of ms, the spectral splitter which is equipped with filters of 700 and 900 nm wavelength was mounted on a high speed camera operating under the condition of ms. And the phenomena occurring in the observation chamber was separated and acquired into two-wavelength band images. Using the two-wavelength band images, the intensity ratios of radiation were calculated for each location (=for each pixel) in observation chamber, and the temperature distribution in observation chamber was obtained from the positional intensity ratios. The resolution of the temperature distribution obtained in this study is 765 x 490 pixels, which is equivalent to 100 pixels (10 x 10 pixels) in 1 x 1 cm area. Under the resolution quality, the temperature distribution in the chamber (of 84 X 54 cm size) was analyzed. In addition, the changes of temperature frequency distribution were analyzed which could be obtained from the temperature distribution data for each location. For details of the above two-wavelength pyrometer analysis, refer to the previous studies [4].

3. Results and discussion

3.1. Pressure profile in observation chamber. Figure 3 shows typical high speed impact images of a RMS (NA-A) bullet (Fig. 3 (a)-(d)) taken with a high speed camera and the pressure profile (Fig. 3. (e), (f)) caused by the RMS impact in observation chamber. The RMS bullet was impacted on the back side of the observation chamber within 0.7 ms after passing through the target skin in front of observation chamber (Fig. 3 (b)), which generated a shock wave (Fig. 3 (a)). The shock wave formed due to the incident of the RMS was measured at the piezoelectric sensor 1 at about 0.5 ms (Fig. 3 (a), (e)) and at the piezoelectric sensor 2 at about 0.7 ms (Fig. 3 (b), (f)). A negative pressure was observed at the back of the RMS debris (Fig. 3 (c), (f)), but it was abruptly changed to positive by mixing with the positive pressure formed by the main impact of RMS (Fig. 3 (d), (f)). The Maximum pressure was observed on sensor 2 at 1.35 ms after RMS entered the observation chamber (= about 0.65 ms after the main impact), and then the pressure profile was fluctuated complicatedly by mixing various reflected waves resulting from main impact (Fig. 3 (d), (f)).

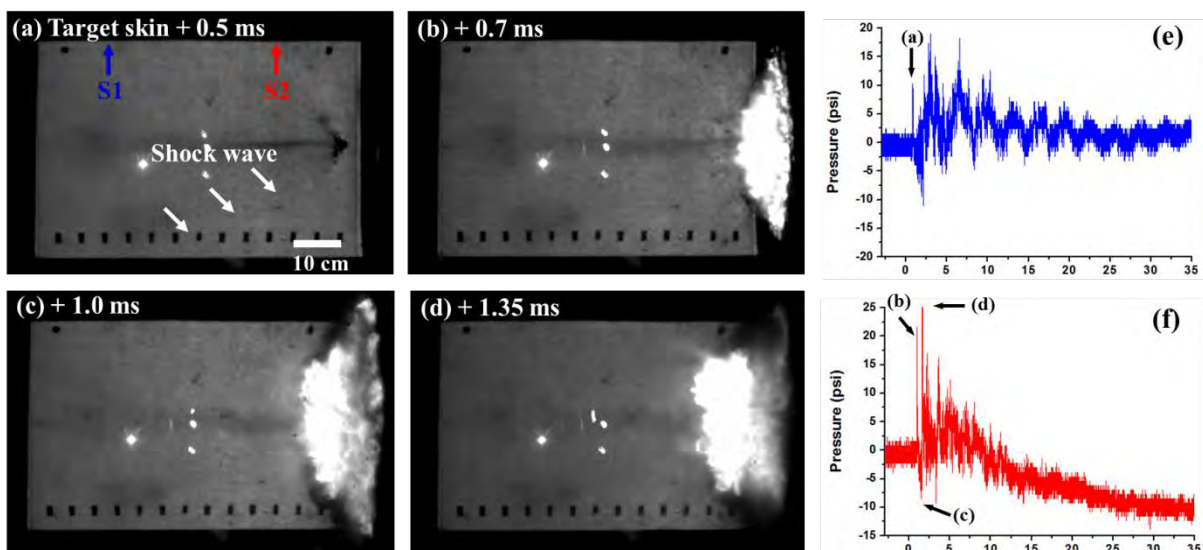


Fig. 3. Typical high speed impact images of a RMS (NA-A) bullet at (a) 0.5 ms, (b) 0.7 ms, (c) 1.0 ms,

and (d) 1.35 ms, and pressure profiles acquired in observation chamber at (e) Sensor 1 and (f) Sensor 2. (The S1 (or S2) arrow in fig. 3 (a) represents the installed locations of sensor 1 (or sensor 2))

Figure 4 shows the pressure profiles (at S2) resulting from the impact of (a) Ni, (b) Al, (c) NA-T, (d) NA-A, and (e) nA-A bullet. The maximum pressure of the Ni specimen was measured about 17 psi and the pressure fluctuation was gradually decreased around 0 point as shown in fig. 4 (a). The maximum pressure of the Al specimen was about 16 psi, which was not significantly different from the maximum pressure of the Ni specimen (Fig. 4 (b)). However, the pressure profile of Al specimen mostly varied above 0 point unlike Ni specimen. This difference of the profiles between Ni and Al is considered to be related to the oxidation of Al.

The maximum pressure of the NA-T specimen was about 20 psi, which was slightly higher than the maximum pressure of Ni specimen or Al specimen. In addition, the pressure profile up to 10 ms showed a tendency to fluctuate above 0 point similar to the Al specimen, but the negative pressures were mainly measured after 10 ms. The change of pressure profile from positive values to negative values suggests that the pressure is mostly increased due to the reaction of RMS in the initial state, but the pressure is gradually decreased due to deficiency of oxygen in the late state, which is need to react with Ni-Al intermetallics. The maximum pressure of NA-A and nA-A specimen was gradually increased to 25 psi and 30 psi. It is note that their microstructure is clearly different although they have a same composition. This result represents that the NA-A and nA-A specimen react more in a shorter duration than NA-T. It is also found that the similar phenomena in pressure profiles (in which the pressure varies mostly above 0 point in the initial state and varies mostly under 0 point in the late state) were also observed in the NA-A and nA-A specimen like in NA-T specimen.

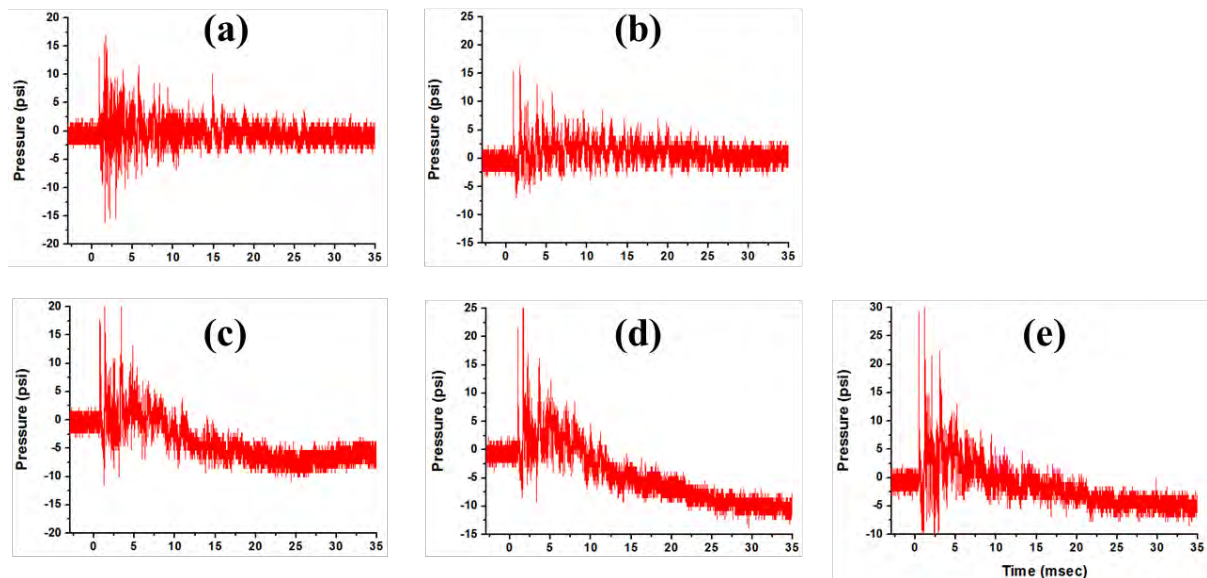


Fig. 4. Pressure profiles acquired from the impact test of (a) Ni, (b) Al, (c) NA-T, (d) NA-A, and (e) nA-A bullet at sensor 2.

3.2. Temperature profile in observation chamber.

Figure 5 shows the temperature distribution and the temperature frequency distribution generated in observation chamber, which was conducted to analyze temperature development resulting from RMS (NA-A) bullet impact. While the NA-A specimen entered into observation chamber, it showed a maximum temperature of 3500 K in a small area. And the temperature areas above 2000 K were gradually widened due to the following debris. After the main impact, the temperature area more than 1000 K tend to widen gradually up to 8 ms, but thereafter, the temperature area more than 1000 K tend to become narrow again. This result suggests that the total reaction time of the RMS is about 10 ms.

Although the temperature frequency distributions shows a normal distribution form (median value is about 1700 K) at the initial time of impact, new normal distributions appear as time passes, and they separated from the previous normal distribution. The median value of the new normal distribution peak increased gradually up to 8 ms. The appearance of the new normal distribution peak implies that a new source of heat is generated in observation chamber, which is thought to be due to the reaction of RMS.

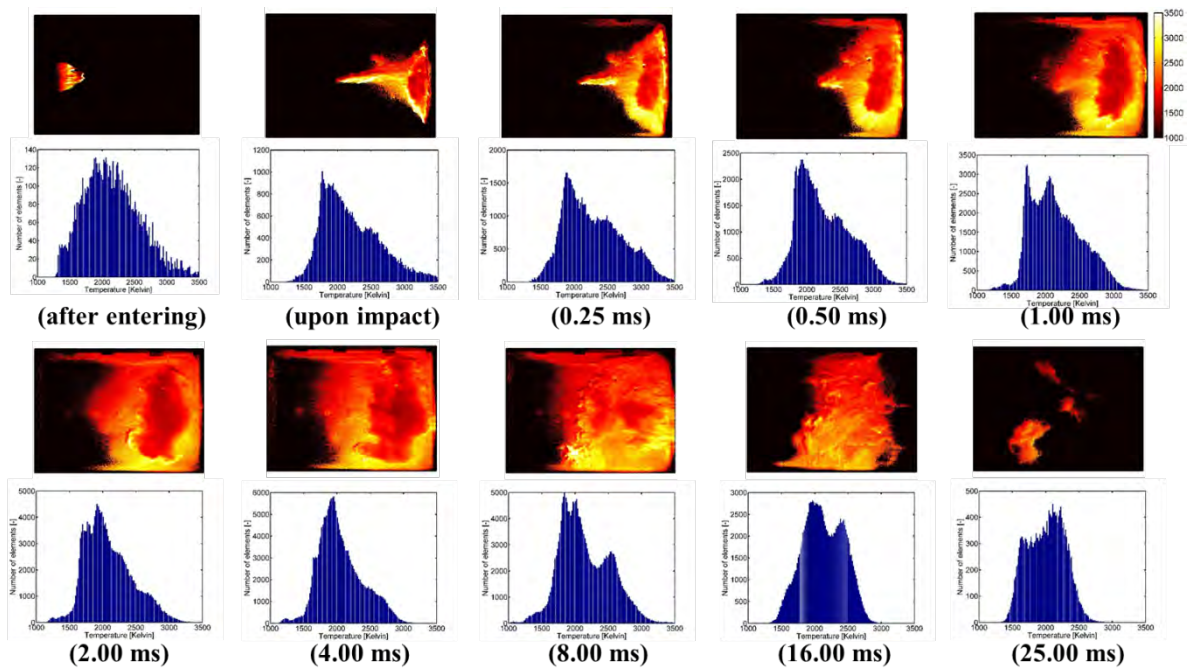


Fig. 5. Spatial distributions (top) and histograms (bottom) of measured temperatures at different time upon impact of NA-A samples.

Figure 6 shows the temperature distributions and temperature frequency distributions in observation chamber, which were obtained from the high speed impact test at the time of 0.5 ms after the specimens impacted on a target. In the case of Ni specimen, the temperature area more than 1000 K appear in a very narrow region as shown fig. 6 (a). On the other hand, in the case of the Al specimen, the temperature area more than 1000 K appear in a wider region than that of the Ni specimen, and the maximum temperature is higher than that of the Ni specimen as shown fig. 6 (a) and (b). In the case of the NA-T specimen, the temperature area more than 1000 K appear in a wider region than that of Al specimen (Fig. 6 (c)). In the case of NA-A and nA-A specimen, the temperature area over 1000 K is not

significantly increased when comparing to the NA-T specimen (Fig. (c) – (e)), but peak separation phenomena already appear at this time unlike the other specimens. These results indicate that the heat source caused by the RMS reaction is generated in the NA-A and nA-A specimen more quickly than in NA-T specimen.

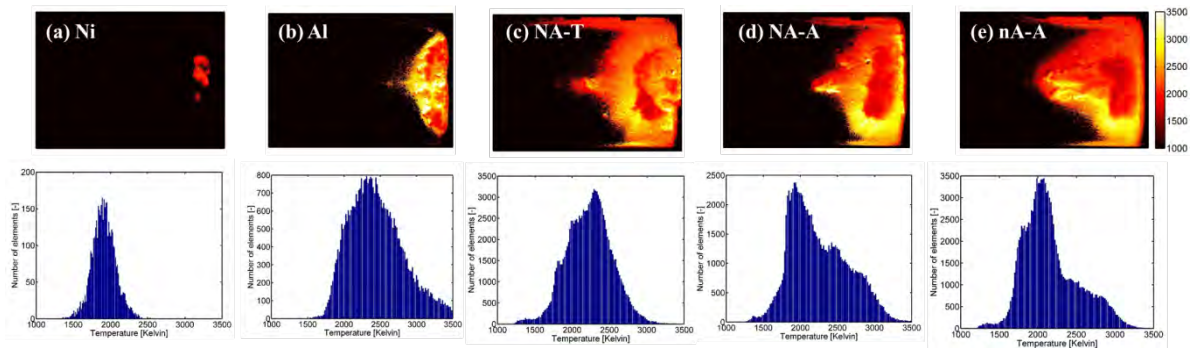


Fig. 6. Spatial distributions (top) and histograms (bottom) of measured temperatures after 0.5 ms upon impact of (a) Ni, (b) Al, (c) NA-T, (d) NA-A, and (e) nA-A sample.

The pressure and the temperature profiles which were obtained from high speed impact test of RMS and inert bullet were compared with each other. The pressure profiles and the temperature frequency distributions of RMS bullets show a marked difference from that of inert bullets. These results suggest that the RMS can react by shock compression which is caused by propagation of shock waves resulting from high speed impact of RMS. In addition, it was found that the pressure and the temperature profiles upon high speed impact of RMS can be also changed according to the microstructural developments of the RMS. These results represent that the tailoring reaction characteristics of the RMS is achievable through microstructural developments of RMS.

4. Conclusions

In this study, to investigate the reaction characteristics upon high speed impact of RMS, various RMS bullets were impacted on the target with a high speed of 1600 m/s, and pressure and temperature profiles generated by the impact were analyzed. As a result, the pressure and the temperature profiles caused by high speed impact of RMS showed a marked difference from the pressure and the temperature profile caused by high speed impact of inert structure. These results indicate that the RMS can react by high speed impact (more precisely, by shock compression applied to the RMS). It was found that the reaction characteristics of RMS were greatly changed according to the microstructural development of RMS, which indicates that the reaction characteristics of RMS could be tailored by the microstructural control of RMS.

Acknowledgements

This work was supported by the Agency for Defense Development (ADD).

References

- [1] F. Zhang, W.H. Wilson, The effect of charge reactive metal cases on air blast, AIP Conf. Proceedings 1195 (2010) 149-152.

- [2] F. Zhang, R. Ripley, and W.H. Wilson, Air Blast Characteristics of Laminated al and NI_AL Casings, AIP Conf. Proceedings, 1426 (2012) 275.
- [3] D.L. Hastings, E.L. Dreizin, Reactive Structural Materials: Preparation and Characterization, Adv. Eng. Mater. 1700631 (2017) 1-20.
- [4] J.J. Ritter, A.L. Brant, J.W. Colburn, B.E. Homan, K.L. McNesby, Characterization Techniques Employed to Determine the Energy Release of Reactive Materials," ARL-TR-5125, Army Research Laboratory (2009).
- [5] R.V. Reeves, A.S. Mukasyan, and S.F. Son, Thermal and Impact Reaction Initiation in Ni/Al Heterogeneous Reactive Systems, J. Phys. Chem. C, 114 (2010) 14772-14780,
- [6] H.F. Wang, Y.F. Zheng, Q.B. Yu, Z.W. Liu, and W. M. Yu, Impact-induced Initiation and Energy Release Behavior of Reactive Materials, J. Appl. Phys., 110 (2011) 074904-1-074904-6.
- [7] J.M. Densmore, M.M. Biss, B.E. Homan, and K. L. McNesby, Thermal Imaging of Nickel-aluminum and Aluminum-polytetrafluoroethylene Impact Initiated Combustion, J. Appl. Phys., 112 (2012) 084911-1-084911-5.
- [8] X.R. Zhang, A.S. Shi, L. Qiao, J. Zhang, Y.G. Zhang, and Z.W. Guan, Experimental Study on Impact-initiated Characters of Multifunctional Energetic Structural Materials, J. Appl. Phys., 113 (2013) 083508-1-083508-10



Pressure and Temperature Profiles upon Impact of Reactive Material Structures (RMS)

2018. 4. 26 | Agency for Defense Development

Kibong Lee, Yong-Soo Cho, Sang-Hyun Jung

Outline

- Background and Objectives
- Fabrication procedures of RMS
- High speed impact test of RMS
- Blast effect test of RMS
(in detonation environment)
- Summary and Future works

Reactive Material Structures (RMS)

■ **Reactive Material Structures (RMS)**, which are made of Reactive Materials (RM), are **energetic structures** designed to have structural strength and store energy to be released at a desired time.

■ Examples of RMS

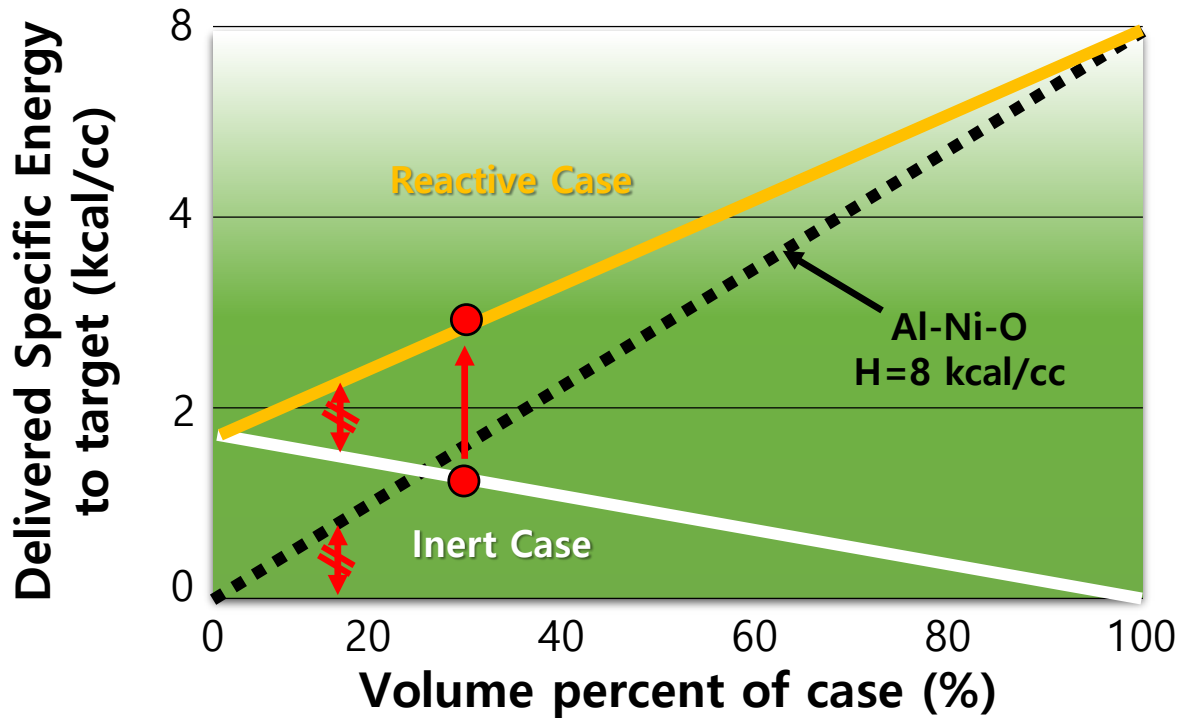
※ TNT : 1,900 cal/cc

Category	System	Heat of Reaction (cal/cc)
Metal-metal (Intermetallic)	$\text{Al} + \text{Ni} = \text{AlNi}$	1,710
	$\text{Al} + \text{Ni} = \text{AlNi} + \text{O}_2 = \text{NiAlO}_2$	8,000
	$2\text{Al} + \text{Zr} = \text{Al}_2\text{Zr}$	1,130
	$2\text{Al} + \text{Ti} = \text{Al}_2\text{Ti}$	1,100
Metal-oxide (Thermite)	$2\text{Al} + 3\text{CuO} = 3\text{Cu} + \text{Al}_2\text{O}_3$	4,976
	$2\text{Al} + \text{Fe}_2\text{O}_3 = 2\text{Fe} + \text{Al}_2\text{O}_3$	3,947
Metal-polymer	Al-PTFE	6,000

■ Since **RMS** are not only energetic materials but also structural materials, they are very attractive structural materials in terms of that they can be utilized as **energy-releasing structural materials**.

Reactive Case

- Inert structural materials based on steel are normally used as missile's cases
- If we **replace the inert steel case** currently used **with reactive material structures** that provide both structural integrity and energy within the same system?

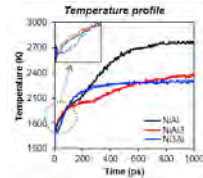
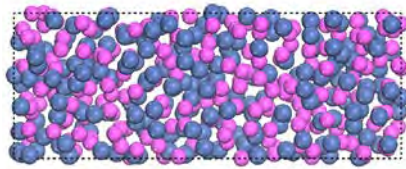


- ADD have studied for developing RMS as reactive cases since 2014

Objectives

- Secure the core technologies to develop reactive cases

Design technology



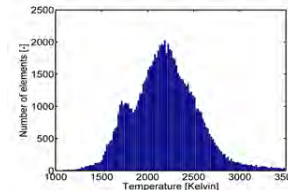
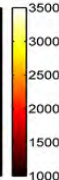
- Design technology to design RMS that release a large amount of energy

Fabrication technology



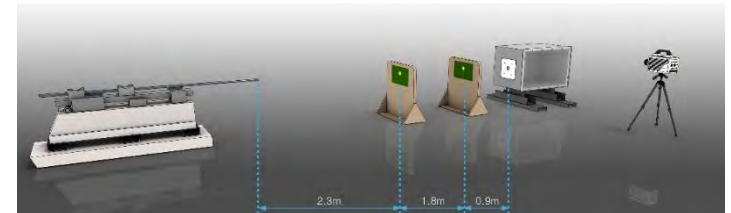
- Fabrication technology to fabricate RM powder and RMS as designed states

Analysis technology



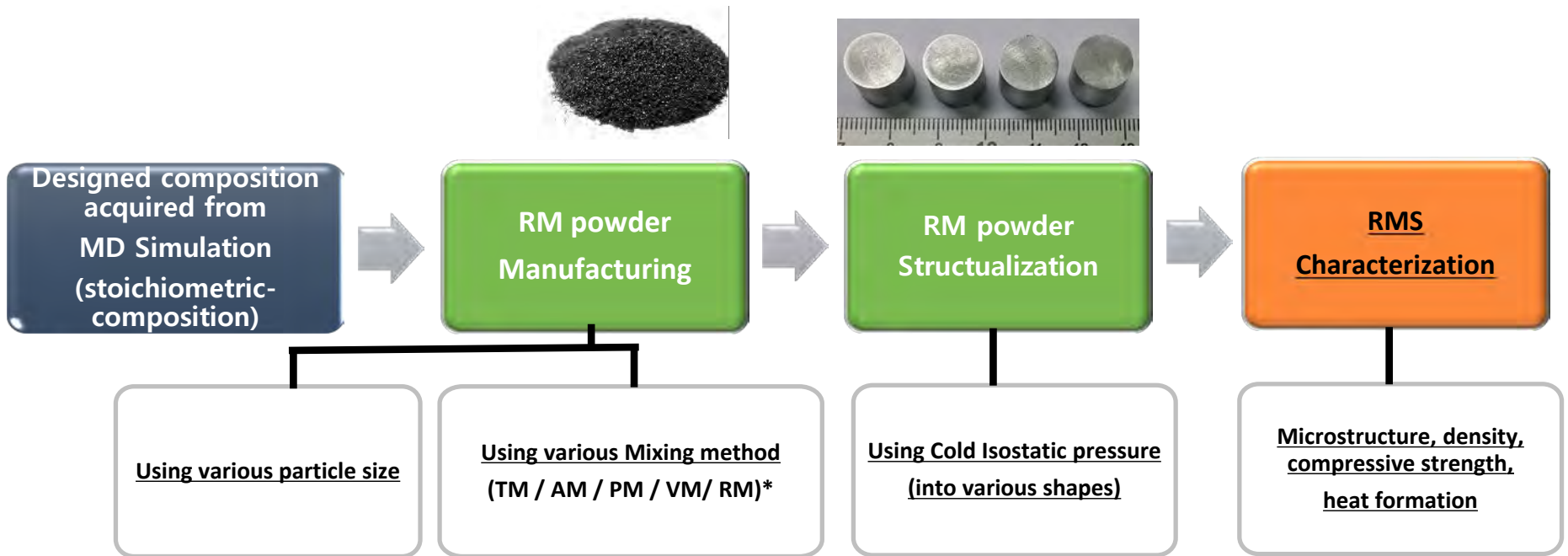
- Analysis technology to analyze acquired data from RMS tests

Test technology



- Test technology to simulate the RMS operating environment

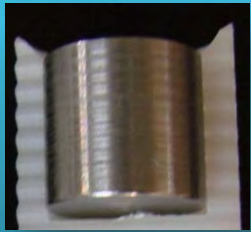
Fabrication procedure of RMS



*TM: Turbula Mixing // AM: Attrition Milling // PM: Planetary Milling // VM: V-type Mixing // RM // Rotary Mixing

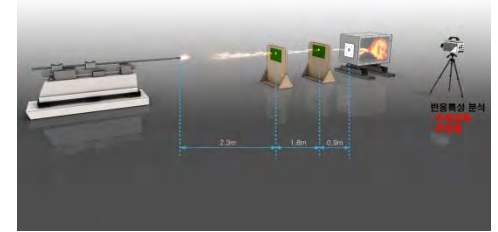
Structuralization of mixed powder

- Structuralized into 3 types of specification using cold isostatic pressure technique



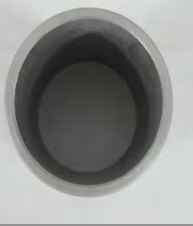
For High-speed impact test

- Shape: Cylinder type
- Specification: diameter-00.0, length-00.0 (mm)



For Energy density test

- Shape: Cylinder type
- Specification: diameter-00, length-00 (mm)



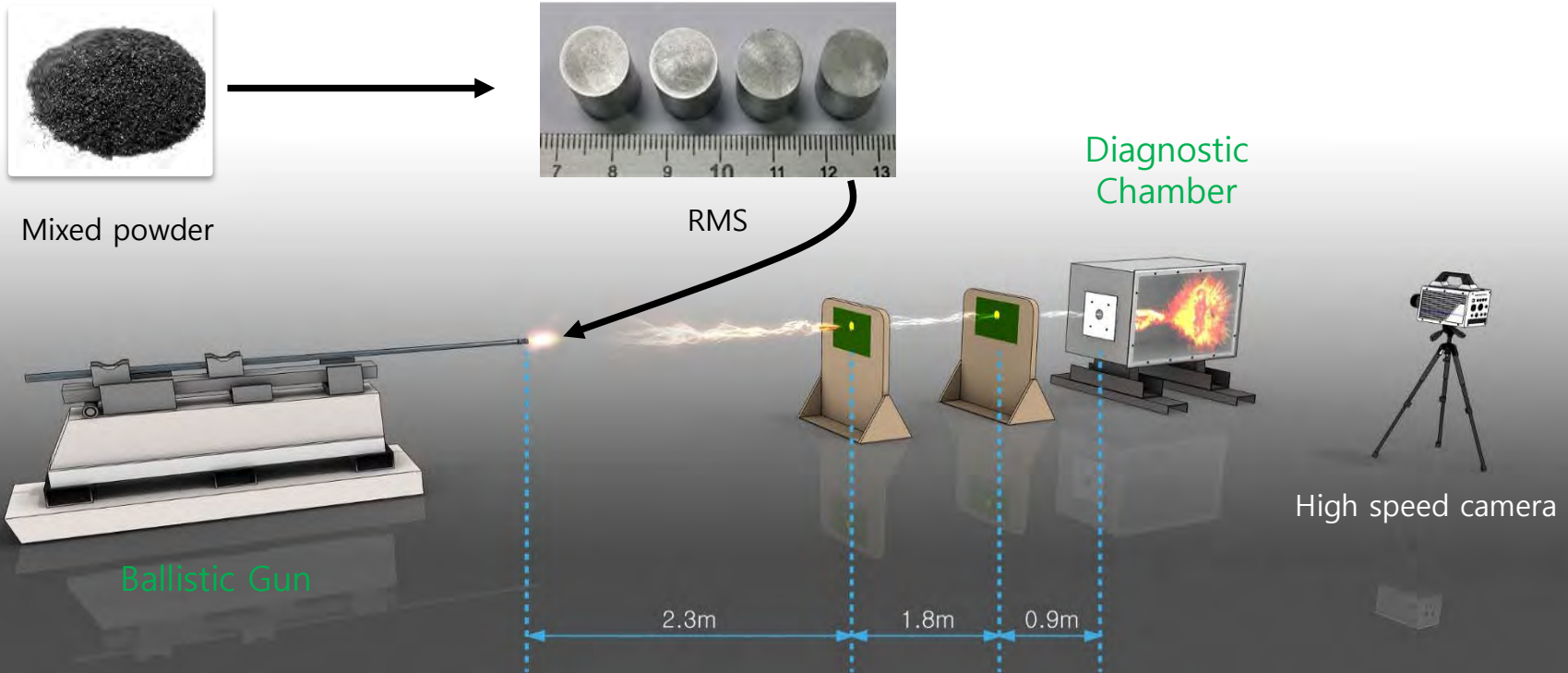
For Blast effect test

- Shape: tube type
- Specification: diameter-00(O), 00(I), length-00 (mm)



High speed impact test

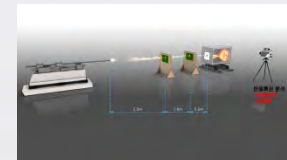
Experimental setup



Analyze reaction characteristics of RMS by observing diagnostic chamber with high speed camera when RMS impacted to target in diagnostic chamber

- Purpose: Analyze ballotechnic reaction characteristics when RMS are subjected by shock waves propagation which could be produced from high speed impact
- Advantage: can be conducted without explosive (capable to classify the performance grade of various RMS very easily)

High speed impact test



Inert structures

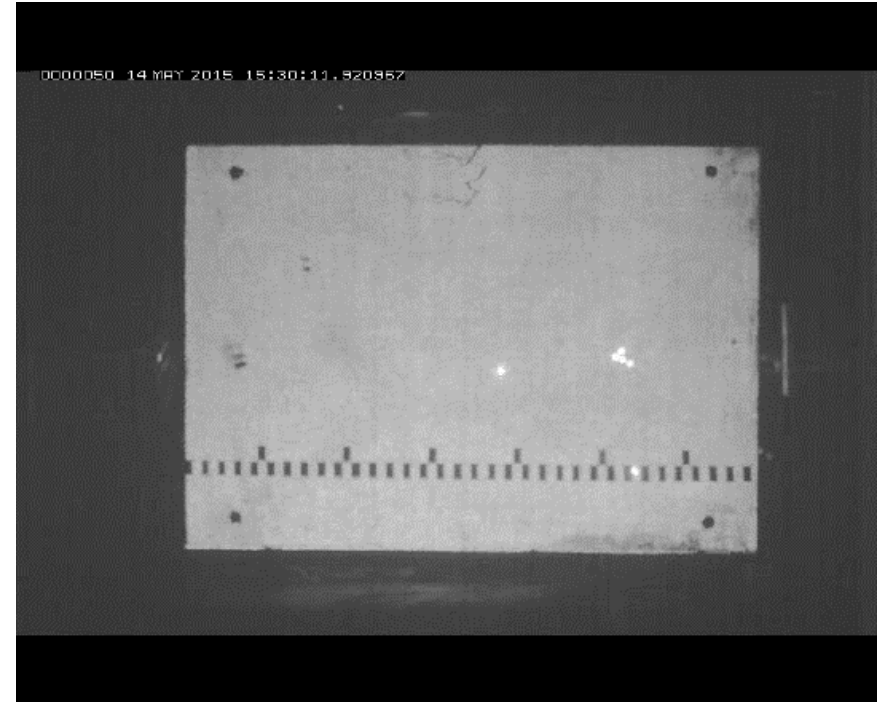
Ni; 15g, CIP 400 Mpa



➔ Small area and short duration of flame (1 ms)

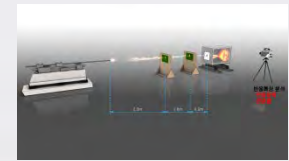
RMS

Al-Ni (AM); 10g, CIP 400 Mpa



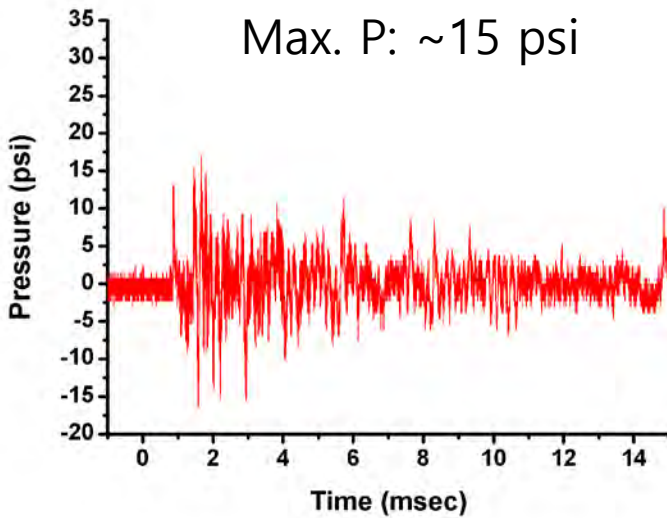
➔ Large area and long duration of flame (20 ms)

Pressure Profile



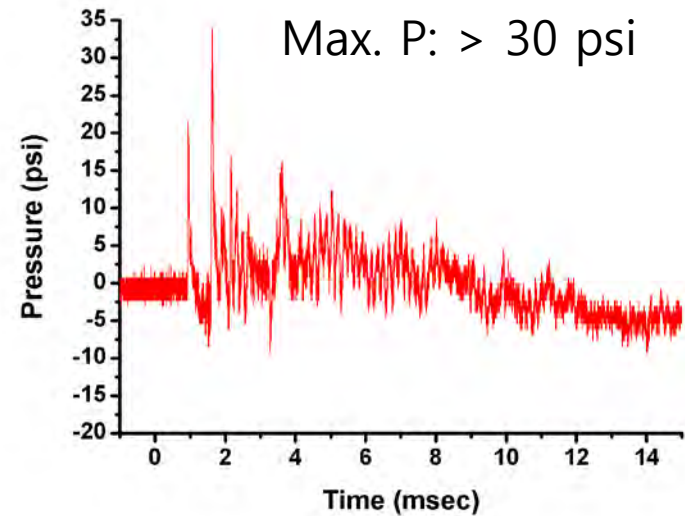
Inert structures

Ni; 15g, CIP 400 Mpa



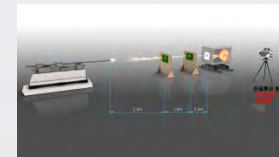
RMS

Al-Ni (AM); 10g, CIP 400 Mpa

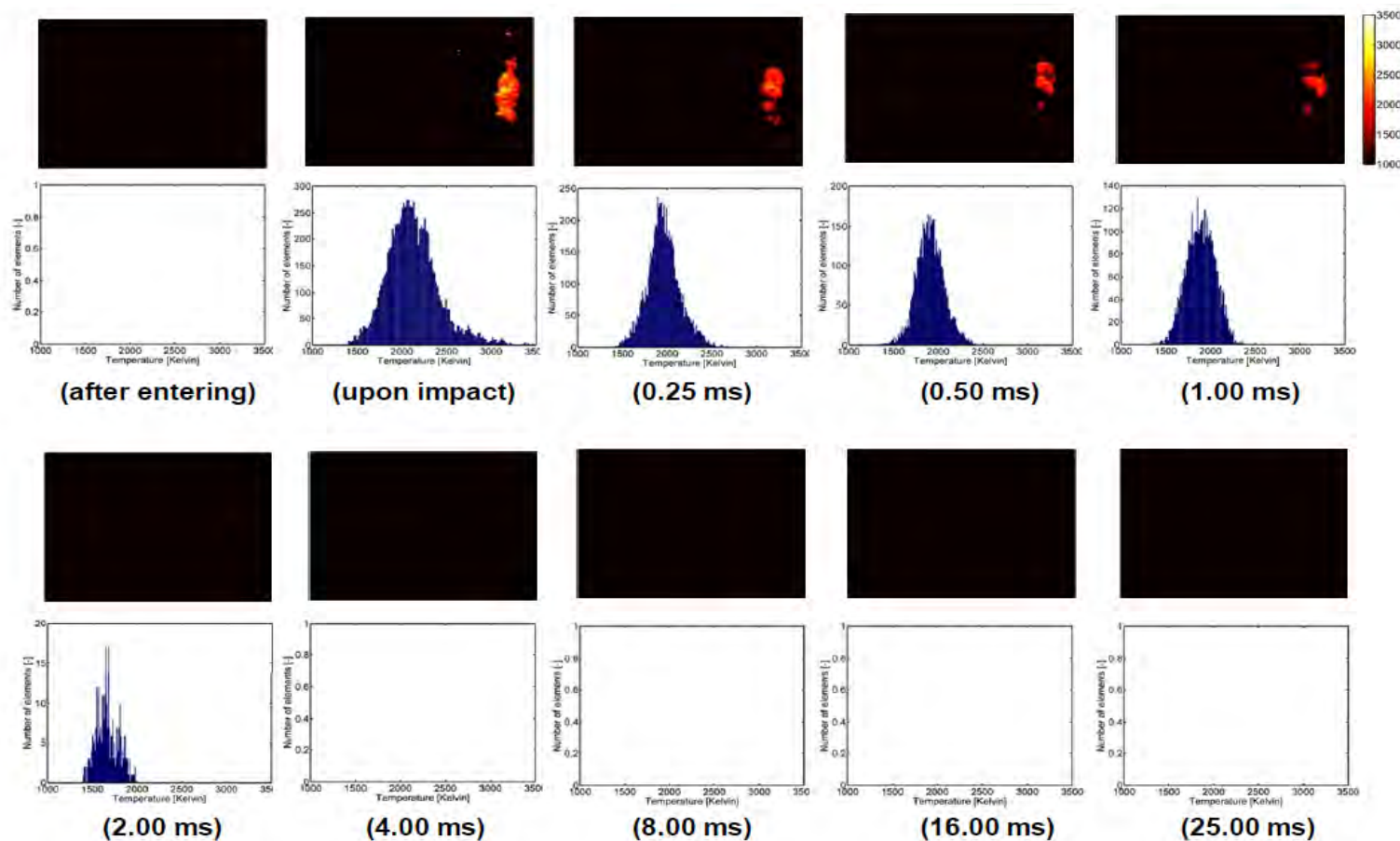


- ➔ Pressure profile of Inert structures is fluctuated around the zero points
- ➔ Pressure profile of RMS is mostly fluctuated beyond the zero points
- ➔ **RMS can create positive blast effects** when subjected shock waves

Temperature profile (Inert structures)

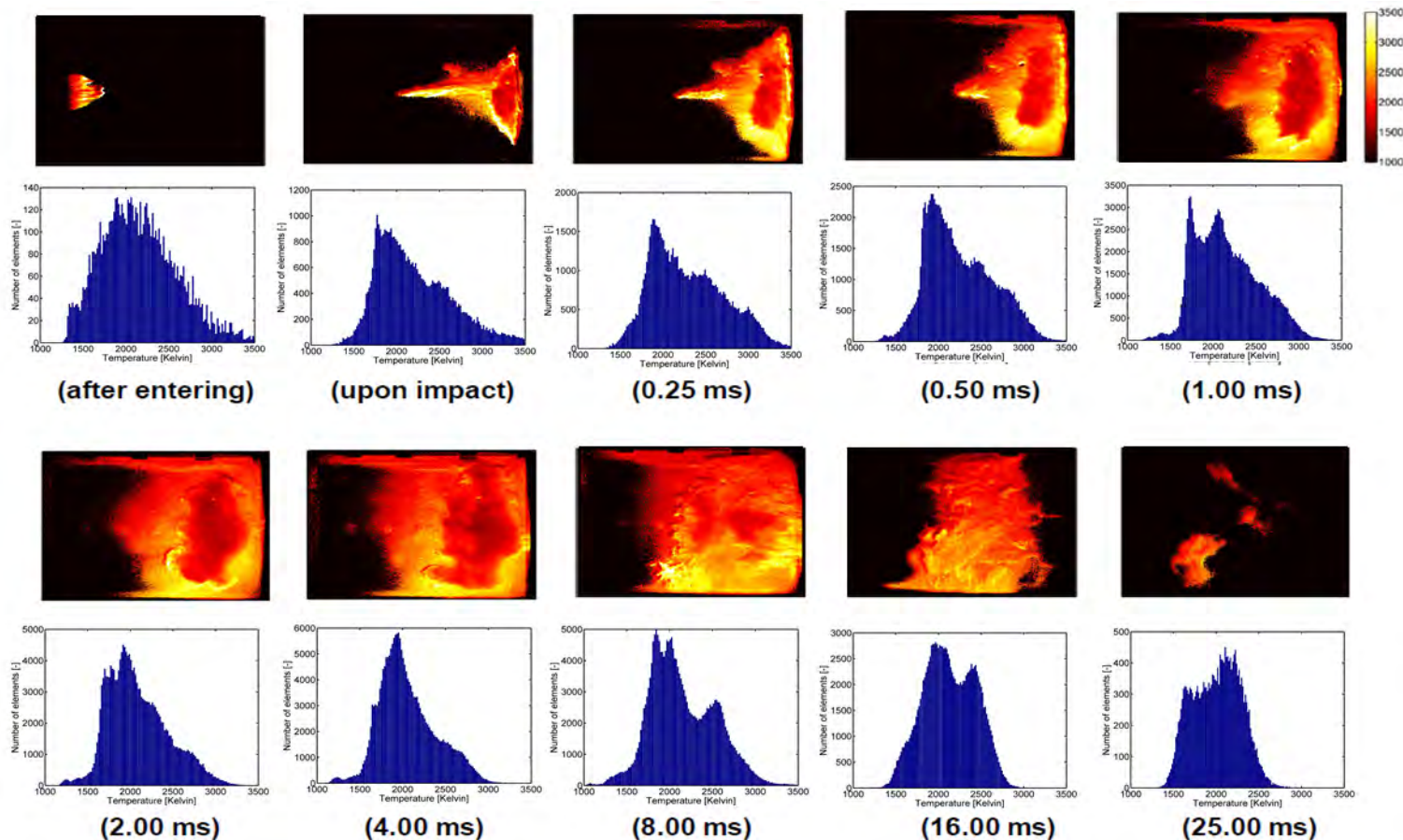
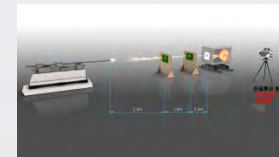


Spatial distributions (top) and histograms of measured temperature at different time upon impact of inert sample (Ni)



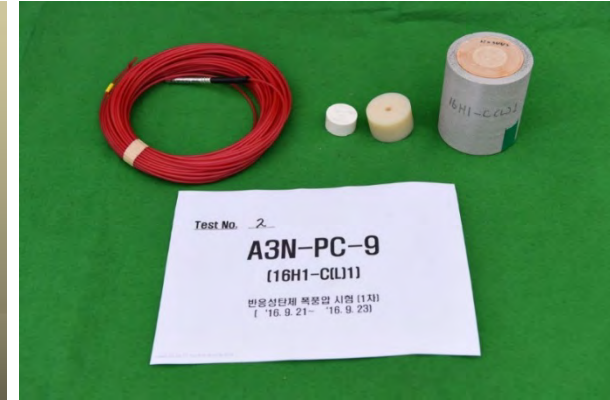
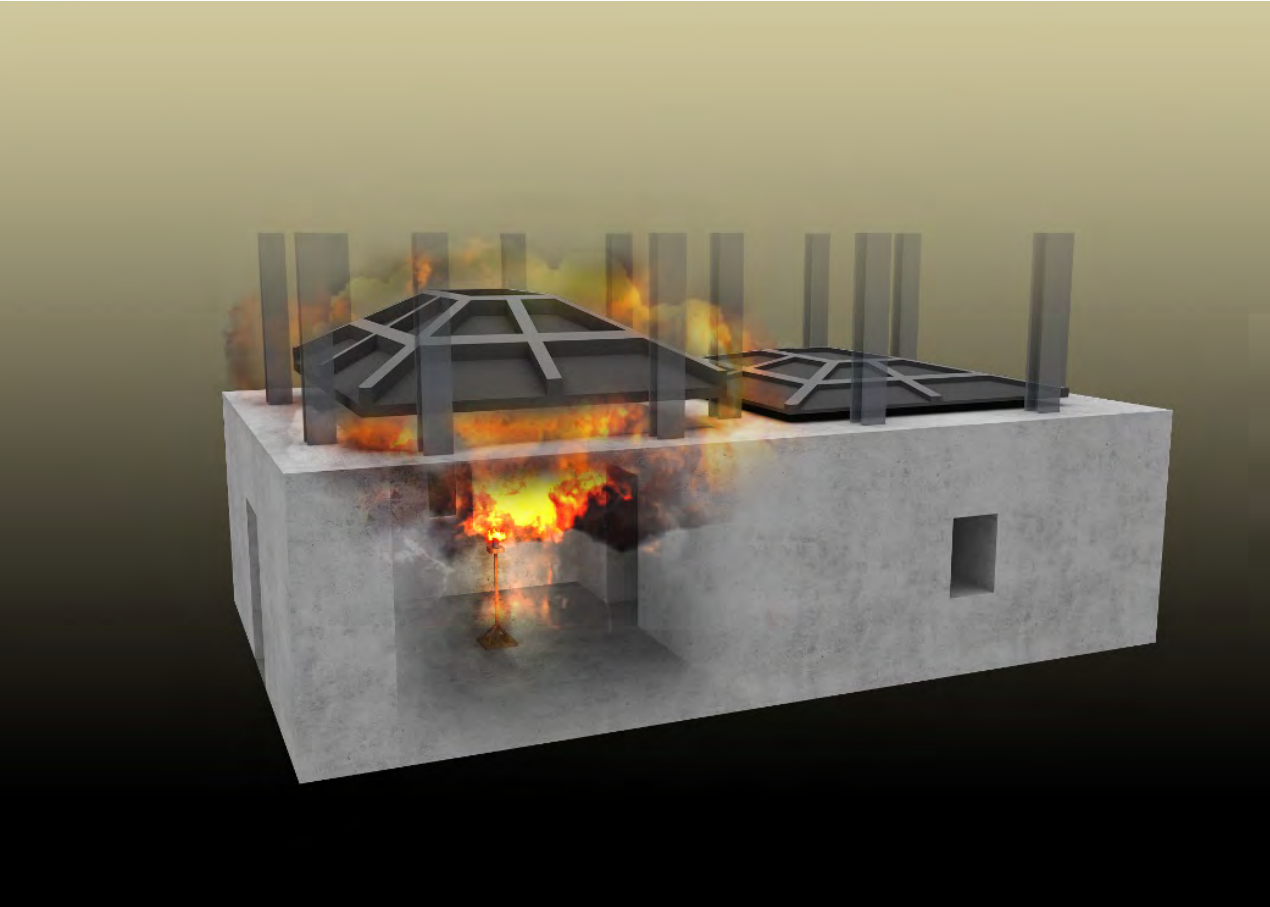
➡ After 1 ms of impact, the temperature drops rapidly to below 1000 K

Temperature profile (RMS)



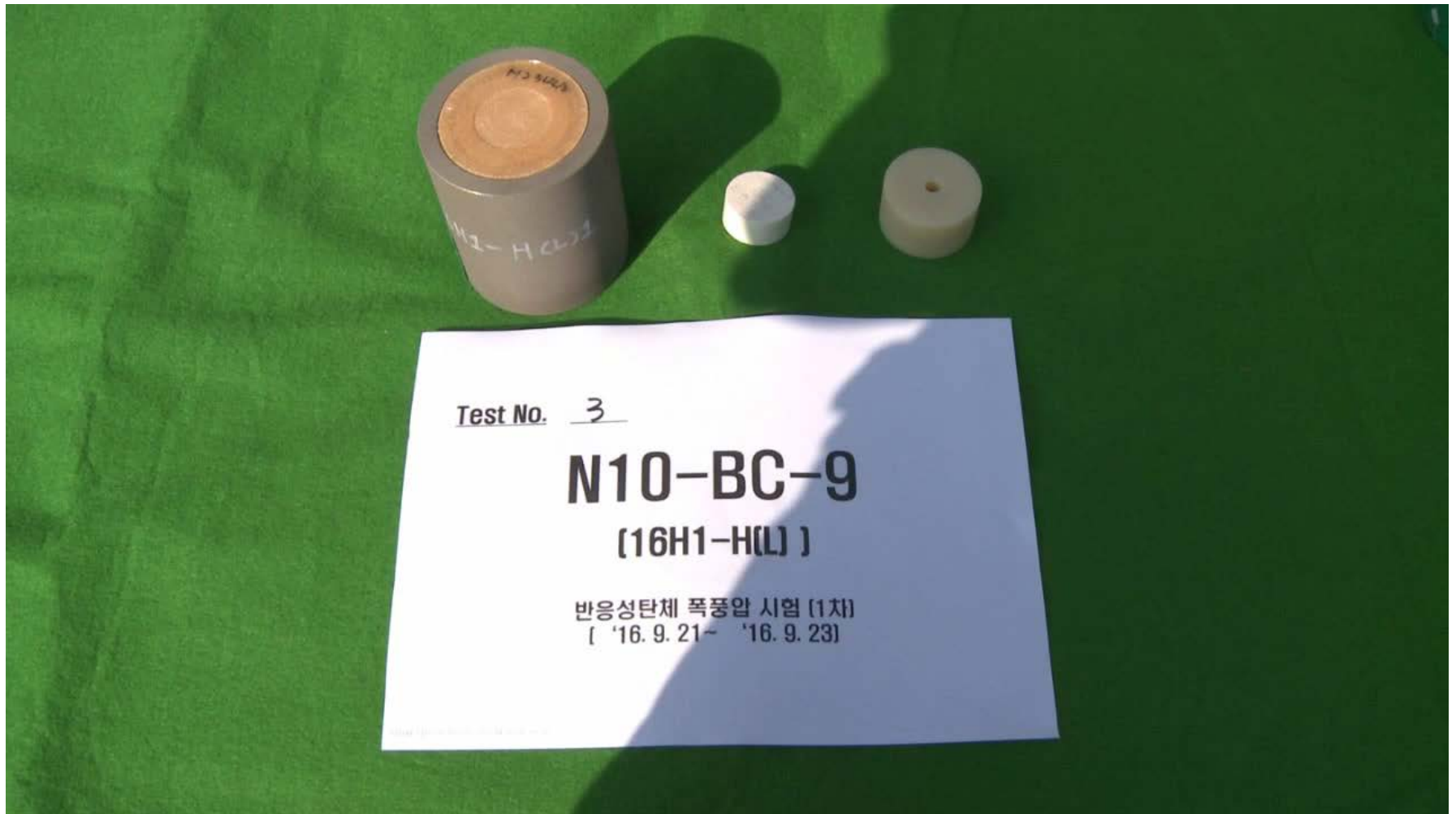
- ➡ Up to 8 ms of impact, the Maximum temperature doesn't drop to below 3500 K
- ➡ Larger area and longer duration of flame in RMS sample than inert sample

Blast effect test of RMS (in detonation environment)



- Make composite sample which is consisted of explosive (TNT) and tube shape RMS
- Locate the composite sample at the center of room with a 4.5 ton roof
- Ignite the composite sample by igniting TNT inserted in tube shape RMS
- Measure the height of roof moved and acquire pressure profile from installed sensors

Movie for results of blast effect test

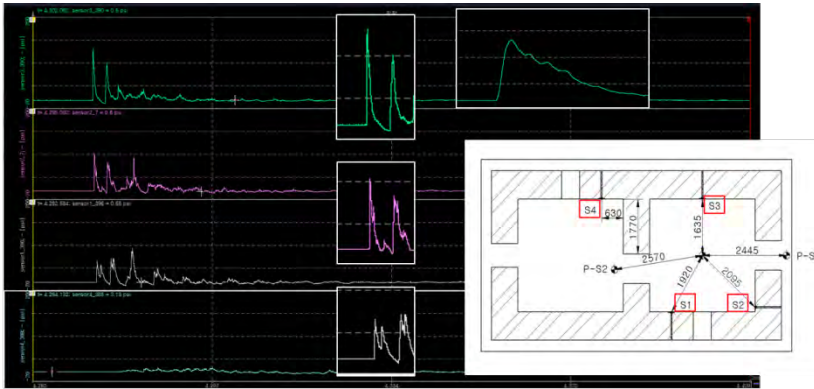


➔ RMS can create positive blast effects when subjected in detonation environment

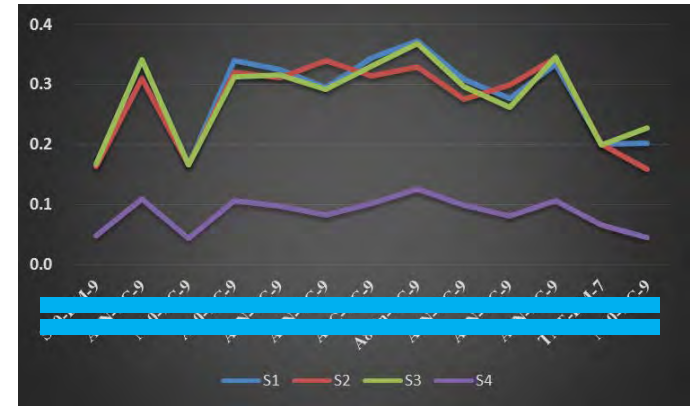
Comparison on blast effects of various RMS

① acquire pressure profiles from sensors

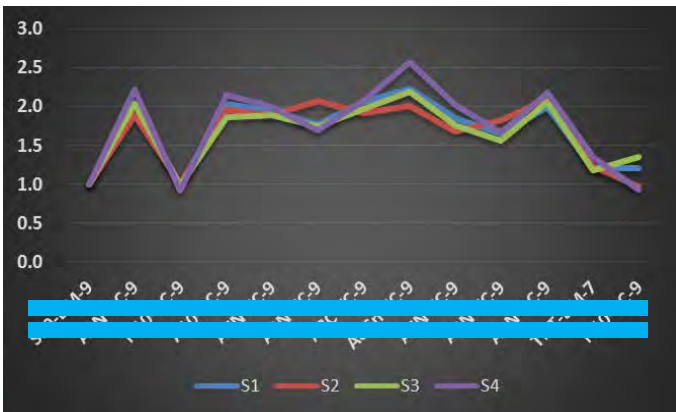
S3
S1
S2
S4



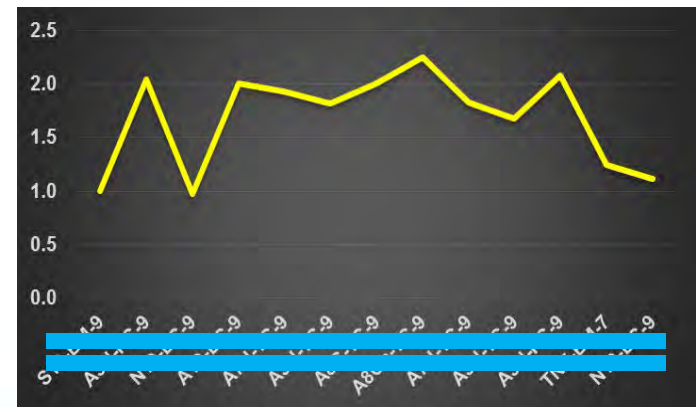
② integrate the pressure profile until the convergence position to zero



③ perform numerical processing



④ compare the blast effect



Summary and Future works

■ Summary

- Various RMS are fabricated into various shapes and various microstructures
- The reaction characteristics of RMS are analyzed through high speed impact test and blast effect test
- RMS can create positive blast effects when subjected shock waves and when subjected in detonation environment

■ Future works

- The RMS samples made by Cold Isostatic Pressing represent very weak mechanical strength (~ 200 Mpa)
- It is need to improve mechanical strength of RMS to use as munition cases



Thank You

Q & A

Advancing the Propane Fast Cookoff Burner and Testing

Ephraim Washburn, Ross Falen, and Jeffrey Prevost
Naval Air Warfare Center Weapons Division, China Lake, California

David Hubble and Jon Yagla
Naval Surface Warfare Center Dahlgren Division, Dahlgren, Virginia

Abstract

Propane burners have already been shown to produce the temperature and heat flux requirements to replicate the thermal environment of a liquid-pool-fire fast cookoff test. Ordnance items tested for fast cookoff in both propane burners and liquid pool fires have shown to have comparable reactions in the test. Further design work was done on the propane burner to allow it to be used to test larger ordnance items. The fuel delivery system to the larger burner was optimized and calibration showed that it produced a uniform flame that met the thermal requirements. It was then used to test a 500 lb bomb which was also tested in a liquid pool fire. The results of the testing are compared and demonstrate the ability to test large ordnance items in the propane burners. Additional testing was performed on an ammunition can containing a large number of energetic items. This test demonstrated that the multiple reactions that occur in such a test do not damage the burner or cause the test to change. Within the variation expected from fast cookoff testing the results from this test were very similar to the results from an identical test that was performed in a liquid pool fire. These test results continue to show that propane burners are safer, less expensive, and more environmentally friendly compared to the liquid pool fire for conducting fast cookoff tests.

Expansion of Large Burner

The propane burner located at China Lake, CA was increased from 3.1 m by 6.1 m (10 ft by 20 ft) to 4.6 m by 6.1 m (15 ft by 20ft). The smaller burner had met the temperature and heat flux requirements for a 4.3 m by 1.2 m by 1.8 m (14 ft by 4 ft by 6 ft) volume in the flame hearth [1]. However, the burner was increased in size to have greater flame coverage and the burner design was changed to have evenly spaced burner pipes throughout the entire length of the burner. The burner was then calibrated using a thermocouple grid and heat flux gauges. The burner with the thermocouple grid is shown in Figure 1.



Figure 1. 4.6 m by 6.1 m Propane Burner Built at China Lake

During the testing with the thermocouple grid, there was higher than desired wind and no consistent temperature volume was measured. Also, in operation, the burner did not qualitatively produce as high a flame as the 3.1 m by 6.1 m burner. The surface area of the

burner was increased by 50% going from 3.1 m by 6.1 m to 4.6 m by 6.1 m. It was hypothesized that the current fuel delivery system was inadequate and not enough fuel was reaching the burner. The burner was reduced to a 4.6 m by 4.6 m burner, which only increased surface area by 12.5% compared to the 3.1 m by 6.1 m burner. Heat flux measurements were taken within the 4.6 m by 4.6 m burner. Two test stands were inserted and used to measure the heat flux. The measurement locations on the stand were 45.7 cm, 91.4 cm, 137 cm, 183 cm (18 in, 36 in, 54 in, and 72 in) above the ground. One of the test stands was placed at the center of the burner and the other test stand was placed 1.22 m from the center of the burner. Two tests were performed with this configuration. The first test had high winds and the heat fluxes were below the required value of 80 kW/m². The second test had little wind and the heat fluxes measured were above the required value. The quantitative results of these two tests are shown in Table 1.

Table 1. Heat Flux Results from 4.6 m by 4.6 m Burner

Height Above Ground	Heat Flux Center of Burner (kW/m ²)		Heat Flux 4' from Center of Burner (kW/m ²)	
	Test #1	Test #2	Test #1	Test #2
182 cm	63	96	30	89
137 cm	106	115	38	109
91.4 cm	118	135	54	135
45.7 cm	115	147	97	154

The heat fluxes from test #2 were sufficient to meet the STANAG requirements. However, the flames were not always consistent and a full 4.6 m by 6.1 m burner was desired. A new burner setup was designed. The size of the burner was returned to 4.6 m by 6.1 m. As shown in Figure 1, the previous burners at China Lake had the entrance of propane into the burner on the same side for all of the pipes. This is different than the Dahlgren design, which had entrance of the propane into the burner alternating sides up the length of the burner. The new China Lake design adopted the alternating entrance of the propane into the burner. Also the modified 4.6 m by 6.1 m burner was made of 3.1 m pipes. This meant that the center 1.5 m is where the alternating pipes overlapped. The inner-pipe spacing is 15 cm in this region. The 1.5 m on both sides of the center region had 30.5 cm spacing for the pipes. The change was done to inject the majority of the propane in the center of the burner and provide for a more stable flame. There were convenience benefits from this design change as well. The 3.1 m pipes were the largest that could fit in the water drilling facility. The propane-injecting orifices for the 4.6 m pipes had to be drilled by hand, which was tedious and time consuming. Also the 30.5 cm spacing at the ends of the propane burner will allow for A-frame placement during testing. The modified 4.6 m by 6.1 m burner is shown in Figure 2.

For both the Dahlgren and China Lake burner setups, the vapor pressure of the liquid propane in the tank provides the pressure difference to flow the propane through the burner. The testing with inconsistent measured temperatures in the flame was completed in the winter. Although the winters in the China Lake desert are relatively mild, early morning temperatures in November are often around -1 °C (30 F) compared to early morning temperatures in July at 27 °C (80 F). This difference in temperature equates to about double the vapor pressure at the

higher temperature. To remove the temperature dependence and variance of the propane vapor pressure, a heating blanket was placed on the propane tank. A commercially available Powerblanket ©, model GCW1KS Rev C was placed around the propane tank. The temperature of the propane tank was set to be maintained at 32 °C (90 F). After the burner design and setup changes were completed the flame consistency and volume were improved as shown in Figure 3.



Figure 2. Modified 4.6 m by 6.1 m Burner



Figure 3. Qualitative Flame Structure for Modified 4.6 m by 6.1 m Propane Burner

Quantitative measurements of the flame structure were also performed on the modified 4.6 m by 6.1 m propane burner. The temperature grid was composed of 17 temperature measurement locations in a horizontal plane. There were 4 vertical locations of the horizontal

planes for a total of 68 temperature measurements. The heat flux measurements consisted of 2 test stands that had 4 heat flux gauges at different vertical locations for 8 heat flux measurements per test. The heat flux test stands were placed at nine different locations. The temperature and heat flux measurement setup is shown in Figure 4 and Figure 5.

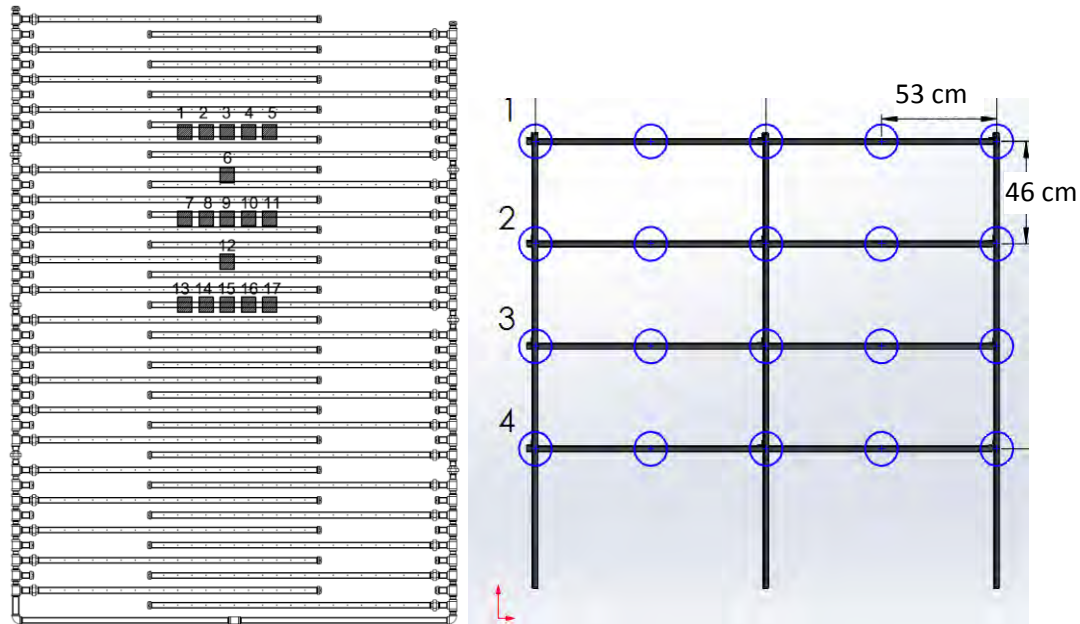


Figure 4. Temperature Grid Setup for Modified 4.6 m by 6.1 m Propane Burner

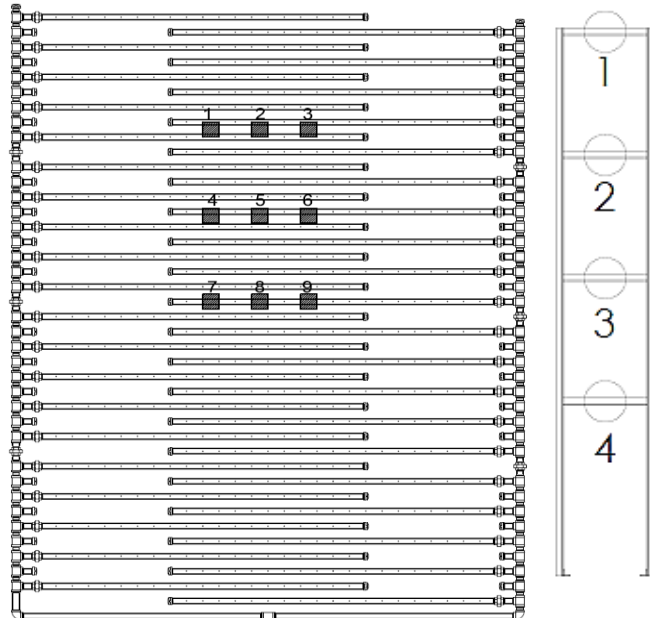


Figure 5. Heat Flux Measurement Setup for Modified 4.6 m by 6.1 m Propane Burner

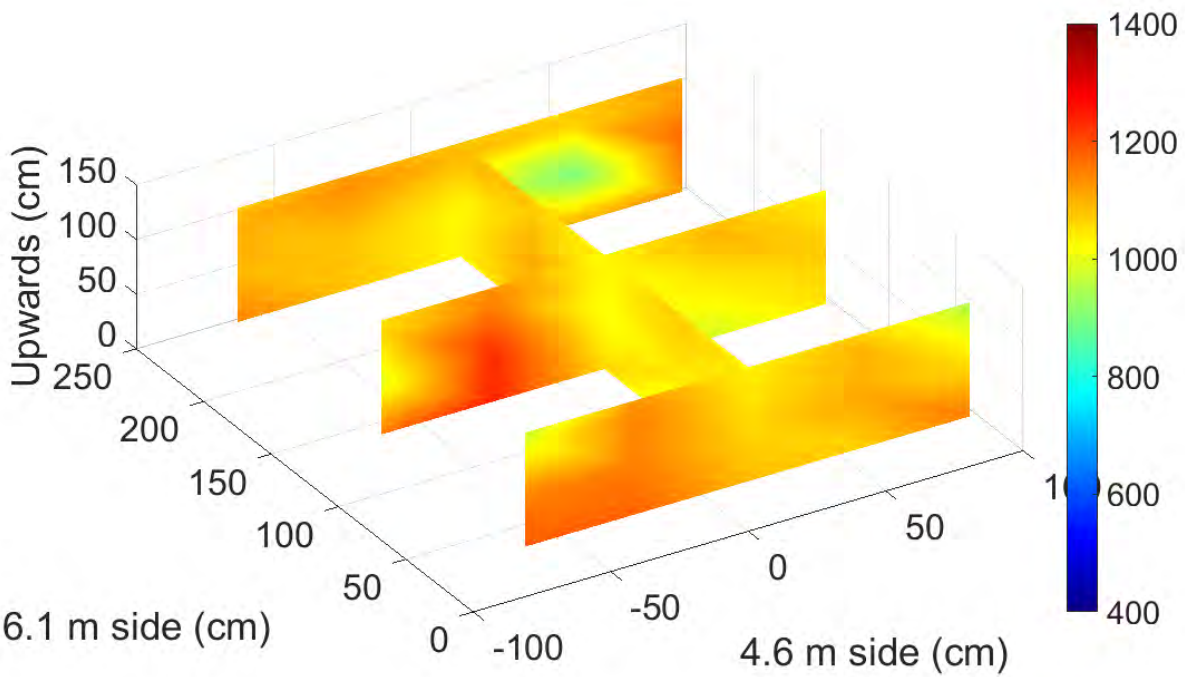


Figure 6. Temperature Contours ($^{\circ}\text{C}$) from Temperature Measurements of Modified 4.6 m by 6.1 m Propane Burner

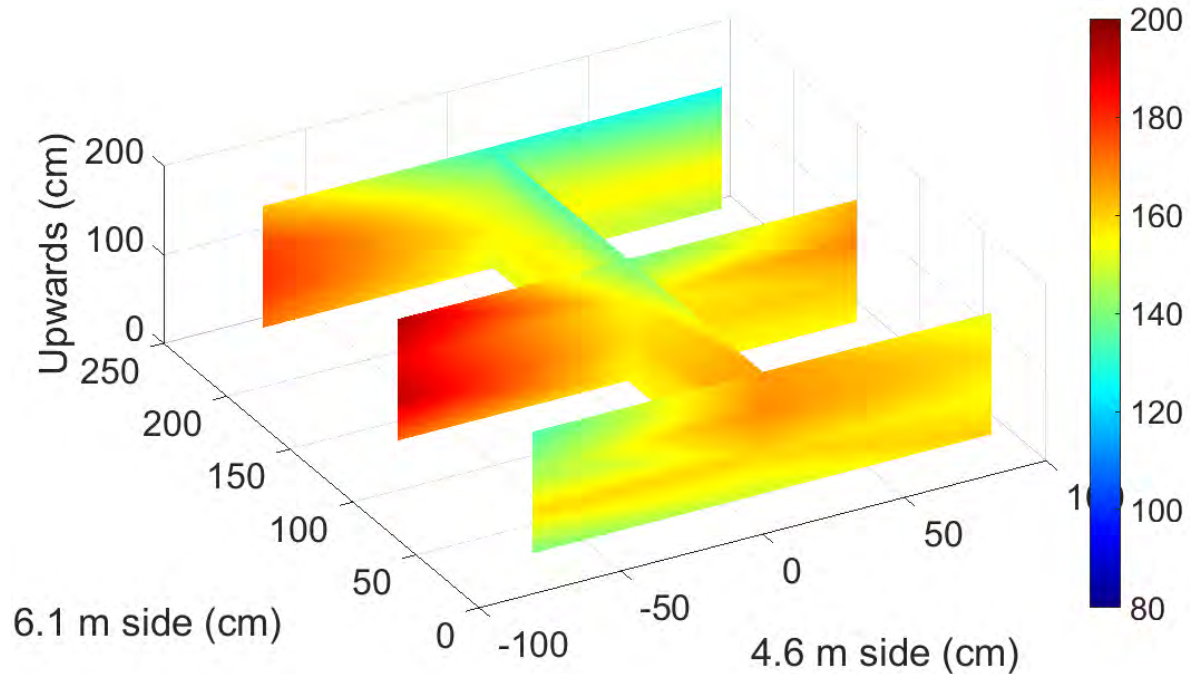


Figure 7. Heat Flux Contours (kW/m^2) from Heat Flux Measurements of Modified 4.6 m by 6.1 m Propane Burner

Figure 6 and Figure 7 show contours that were generated from the temperature and heat flux measurements. The STANAG requirement is that the temperatures are greater than 800°C

and the heat fluxes are greater than 80 kW/m². Both of these conditions were met. Another requirement of the STANAG is that the standard deviation of the average temperatures at each location be less than 10% of the overall average temperature. The measured standard deviation was 7% of the overall average temperature, which fulfilled the requirement and indicated a uniform flame. The results show that the China Lake burner produced a volume 4.3 m by 1.5 m by 1.8 m that meets the STANAG requirements and can be used for fast cookoff (FCO) testing.

Continued Ordnance Testing

At Dahlgren, Virginia, a FCO test with the 3.7 m by 3.7 m (12 ft by 12 ft) propane burner was performed on an ammunition can containing 110 medium ammunition cartridges. This test was performed for two reasons. First, data exist from an identical test performed in the liquid pool fire and this test will help show whether energetic items perform similarly between the two types of FCO tests. Second, there has been concern within the community that items that contain multiple energetics would not perform well in the propane burner. The concern is that after the initial reaction scatters energetic items within the burner, that subsequent reactions of items in contact with the burner tubes will cause extensive damage and alter the fire created by the burner.

The ammunition can is shown in Figure 8. In this test, the rounds tested were training and practice (TP) rounds and therefore contained live propellant but inert (no HE) projectiles. It was decided that testing of multiple high explosive items should be avoided until it had been demonstrated that the burner could handle multiple lower order explosions. Each cartridge contained 50 grams of propellant for a total NEW of 12.25 lbs.



Figure 8. Ammo Can Containing 110 Medium Ammunition Rounds. Shown at Right, Ammo Can on Test Stand Prior to Propane FCO Test in 3.7 m by 3.7 m Burner.

The test was performed on a day with nearly perfect weather conditions and no wind. The item was fully engulfed in the flame for 14m 40s at which point the firing director decided that no further reactions were likely and the burner was shut off. The first reaction occurred at 2m 30s and the final reaction was heard at 9m 10s. Throughout the interim period, a large number of explosions could be heard and debris could be seen leaving the burner area. At no point did the flame appearance change or give any indication that damage had occurred to any of the burner tubes. Posttest inspection did show some minor damage to a few burner tubes

indicating where rounds had exploded while in contact with the tubes, but none of these created new holes or impacted the gas flow in any way.

As an additional test of the propane burner, the FCO test of the medium ammunition cartridges was performed as if it were to be presented to the munitions reactions evaluations board (MREB) of the US Navy. Therefore, all fragments from the test were collected and all those that travelled further than 50 feet were catalogued, weighed, and their final location (distance and angle) were documented. A photograph of the fragments recovered is shown in Figure 9 as they are sorted into three categories; those that remained within the burner, those that left the burner but traveled less than 50 feet, and those that traveled further than 50 feet.

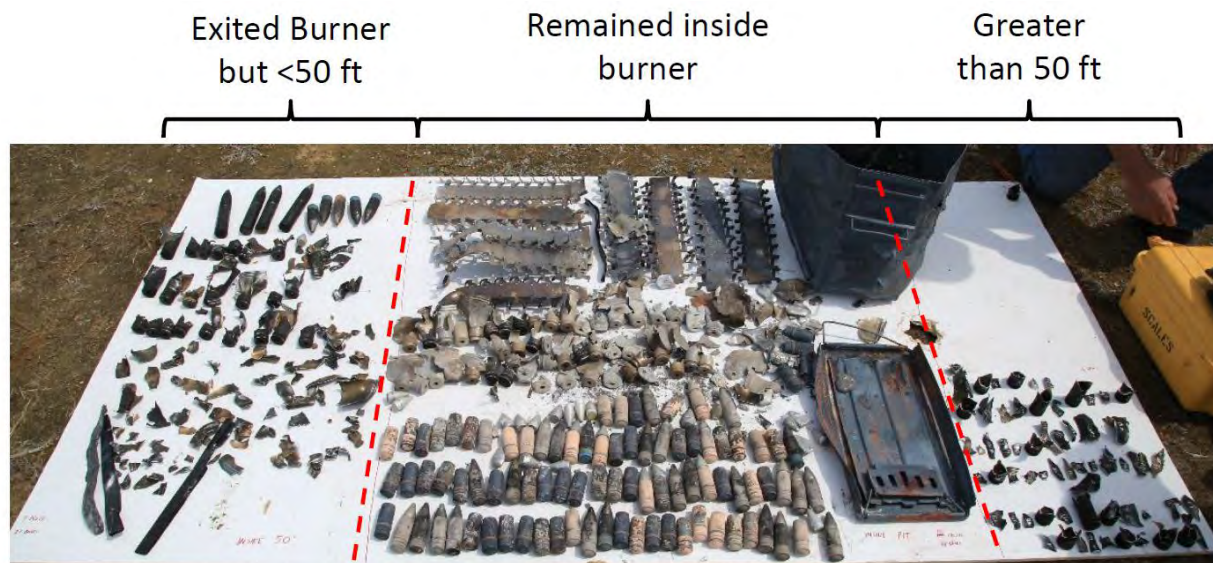


Figure 9. Fragments Recovered from Multiple Medium Ammunition in FCO test in 3.7 m by 3.7 m Propane Burner.

64 fragments were thrown a distance greater than 50 feet. The debris map and resulting energy plot for these 64 fragments is shown in Figure 10. Note that in the plot at right the distribution of fragment weights is bimodal. The lighter fragments (at left) are all pieces of the cartridge case closer to the neck where the material is thin. The heavier fragments are all pieces of the cartridge case at the base. The base is heavier material and remains largely intact and therefore all these fragments have approximately the same weight. Also note that none of the fragments had an energy that exceeded the 20 Joule criteria, although one was very close. If this item had gone to the MREB, it would almost certainly have been scored a type V based on this energy plot.

When the same medium ammunition container was tested in the liquid pool fire, it received a type IV reaction evaluation. While this differs from the type V that it received in the propane burner, the reactions were actually very similar. This is apparent when the fragment energy plots from the two tests are viewed side by side as shown in Figure 11. Note that in the liquid pool fire test plot shown at right that the fragment weight dispersion is very similar and that the only real difference is that one of the fragments barely exceeded the 20 J criteria. Under the new criteria, this could have been scored a Type V reaction. So while the two tests received different scores, the reaction of the item was nearly identical. This is another indication that

within the typical variation of a FCO the propane burner accurately simulates the liquid pool fire FCO test.

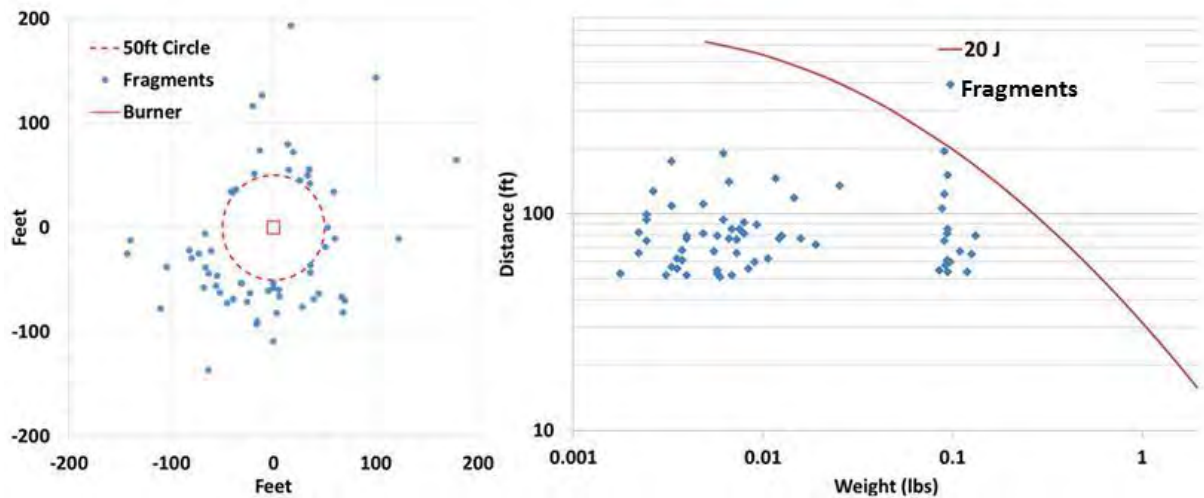


Figure 10. Debris map and energy of the 64 fragments that traveled greater than 50 feet. None exceed the 20 J criteria but one is very close.

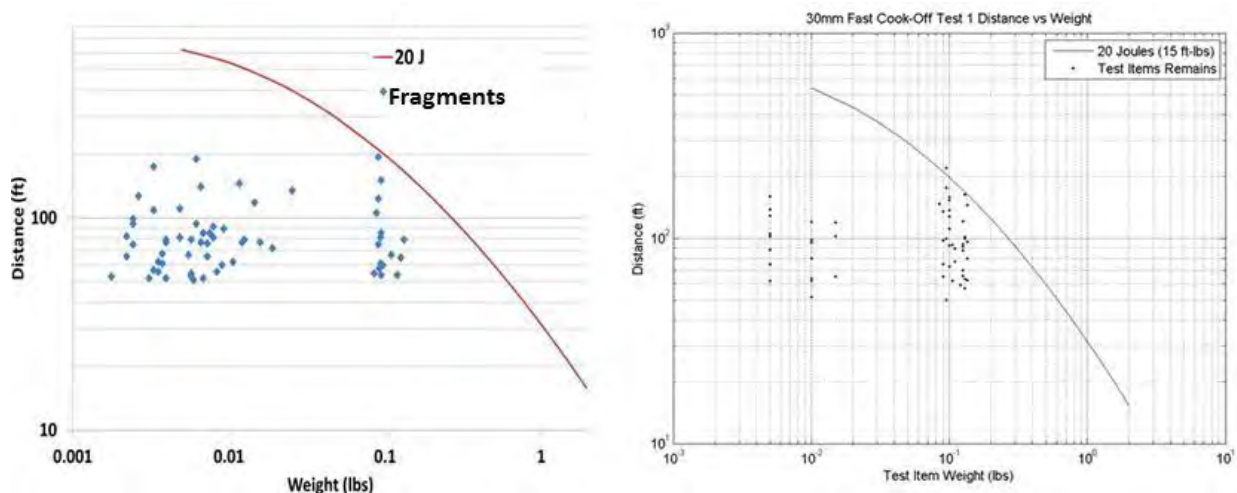


Figure 11. Fragment energy plots from propane FCO test (left) and liquid pool FCO test (right)

An additional task undertaken during this fiscal year was the development of a technical data package (TDP) including detailed drawings of the 3.7 m by 3.7 m square burner used at Dahlgren. As the burner transitions from a developmental project to an established test platform, the TDP will help other test centers who want to build their own propane burner. As shown in Figure 12, the drawings created contain not only the assembly and machine drawings needed to build the burner itself, but also the details related to the plumbing and controls of the burner. The complete TDP is available upon request.

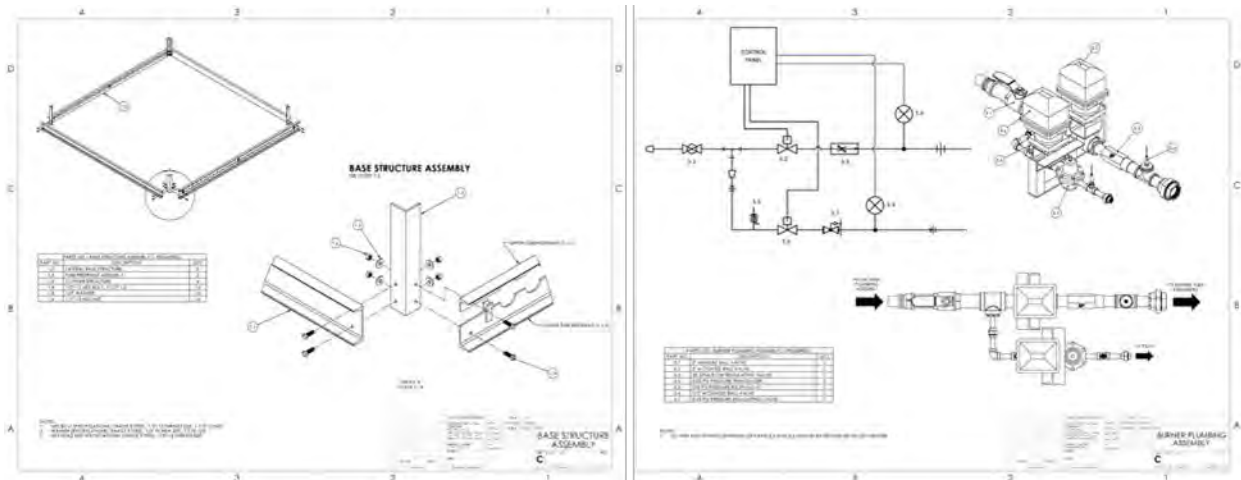


Figure 12. Sample of TDP Drawings Showing Assembly Type Drawings (left) and Valve Schematic and Assembly (right)

A 227 kg (500 lb) class bomb was tested at China Lake in the traditional FCO liquid fuel fire and in the modified 4.6 m by 6.1 m propane burner. The bomb had an installed fuze, nose plug, and tail kit. For one test, the bomb was suspended on an A-frame in the middle of a pool of 11360 liters of F-24 fuel. The other test suspended the bomb on an A-frame centered over the modified 4.6 m by 6.1 m propane burner. The objective of these tests were to test a large ordnance item in the propane burner and have a direct comparison of reaction with a liquid fuel fire. The bomb had 87 kg of energetic material. The expected result of the test was a Type V reaction.



Figure 13. FCO Test Setup and Post Test for Liquid Fuel Fire

In the pool fire, the asset was tested in the tactical configuration. The asset had a reaction occur in the aft end 11 minutes and 26 minutes into the test. The asset began venting from about 12 minutes and 42 seconds to 18 minutes into the test. A piece of the tail kit that was mapped was found beyond the 50 foot distance arc, but no items were beyond the 20 J level. Data was captured on all channels by the ground mounted piezoelectric blast pressure gages but no significant blast pressure was observed. Temperature data was recorded for the duration of the test and the temperatures met the STANAG requirements.

The same class and configuration of bomb was later tested in the modified 4.6 m by 6.1 m propane burner. The burner was ignited with the bomb suspended on the A-frame. A large engulfing flame was produced. At approximately 1:20 into the test the propane flow was cut and the flames disappeared. After determining that the fuze was not armed in the bomb, an

investigation was conducted. A relay had corroded and shorted the electricity to the propane valve, which failed shut. The relay was replaced and the test was retried the next day. The burner ignited again without issues and burned the entire test without difficulty. The flames were large and luminous and completely engulfed the item and test stand for the entirety of the test. There was a loud noise and short vent that occurred at 6 minutes and 39 seconds. The item began to vent from the aft and top of the item at 7 minutes and 50 seconds. The item stopped venting about 11 minutes and 45 seconds after the start of the test. The propane was shut-off after about 17:45 minutes after the test started. The test used 3600 liters of liquid propane. At the time of the writing of this paper, the photography and video of the test are still being processed along with the mapping of the fragments.

Some important lessons were learned from this first large ordnance FCO test with the propane burner. First, having the propane shut off mid-test is one of the worst things that can happen. This is not an issue with the pool fuel fire test as once it starts it will burn to completion of the pool of fuel. This occurrence left a partially thermally damaged item on the test stand. Fortunately, the time at temperature was short and the fuze was not armed and the test was completed the next day. Contingency plans need to be in place for the occurrence of a stoppage of propane during the FCO test. Also, care needs to take place to prevent this occurrence. Future FCO tests with the modified 4.6 m by 6.1 m propane burner will have a checkout procedure for all electrical relays before the test occurs. Second, the propane burner could provide an adequate thermal environment for the FCO test even with the large A-frame and ordnance item. Third, it was very convenient to not have to plan for fuel delivery. As the test was postponed one day there was no need to worry about fuel that had been delivered to the fuel pit. Also, there was some concern for excessive wind conditions those two days. There was no need to worry about whether to pump the fuel into the pit. The operators just waited in the control room until the wind was at a sufficiently low level and then started the test. Finally, within the normal variability of FCO, the initial comparison of the liquid fuel fire FCO test and the propane burner FCO test showed same reaction violence.

Conclusions

Propane FCO burners are being developed and demonstrated at Dahlgren, VA and China Lake, CA. These two sites represent vastly different climates and their successfully demonstration at these locations is an indication that the technology would be applicable almost anywhere. As additional testing is completed, the applicability of the technology is further demonstrated and now virtually all of the subject matter experts are in agreement that the propane burner is a suitable test platform for performing FCO testing.

References

[1] E. Washburn, R. Falen, J. Prevost, D. Hubble, and J. Yagla. "Calibration of a Propane Fast Heating Burner Used to Test Large Ordnance Items," Proceedings of the Insensitive Munitions and Energetic Materials Technology Symposium, Nashville, Tennessee, August 2016.

Advancing the Propane Fast Cookoff Burner and Testing



Ephraim Washburn, Ross Falen, and Jeff Prevost
NAWCWD, China Lake, CA

David Hubble and Jon Yagla
NSWCDD, Dahlgren, VA

2018 Insensitive Munitions and Energetic
Materials Technology Symposium
Portland, Oregon





Background



- Fast cookoff is an international standard safety test required for all explosive ordnance
- Environmental concerns
 - Tests use large pools of hydrocarbon fuel such as JP5, JP8, kerosene, etc.
 - Emissions from one test: 200 kg CO, 35 kg NO_x, 30 kg SO_x, 225 kg soot, 125 kg unburned HC, and 20,000 kg CO₂
 - Ground water concerns
 - Public relations
- Propane viable substitute fuel
 - Gas at atmospheric conditions
 - Cleaner burning
 - Readily available
 - Sufficient heat content





Outline



- Calibration of burner at China Lake, CA
- Testing of ordnance items in burner at Dahlgren, VA and China Lake, CA
- Technical drawing package of 3.7 m by 3.7 m propane burner



6.1 m by 4.6 m Propane Burner



- Constructed a 6.1 m by 4.6 m burner: Hoped for better engulfment on sides compared to previous 6.1m by 3.0 m burner
- Tested burner November 2016
 - Flame not as high as previous testing
 - Not enough fuel to burner
 - Reduced burner to 4.6 m by 4.6 m
- Heat fluxes sufficient but not consistent
 - Lower than desired
 - Flame not as high as before
- Reduced pressure drop from propane tank increased propane flow, but still not sufficient
- Added heating blanket to propane tank
 - Temperature in tank determines pressure
 - Winter testing creates low pressures and variable flows
 - Installed Model GCW1KS Rev C from Powerblanket®
 - Maintained temperature in propane tank at 32 °C

Modified 6.1 m by 4.6 m Burner

- Burner changes
 - 6.1 m by 4.6 m burner with 3.0 m pipes
 - Alternating side of entrance
 - Overlap in center 1.5 m
 - 3.0 m pipes provide for ease of hole drilling with water drilling facility
 - Fuel directed to center





Modified 6.1 m by 4.6 m Burner

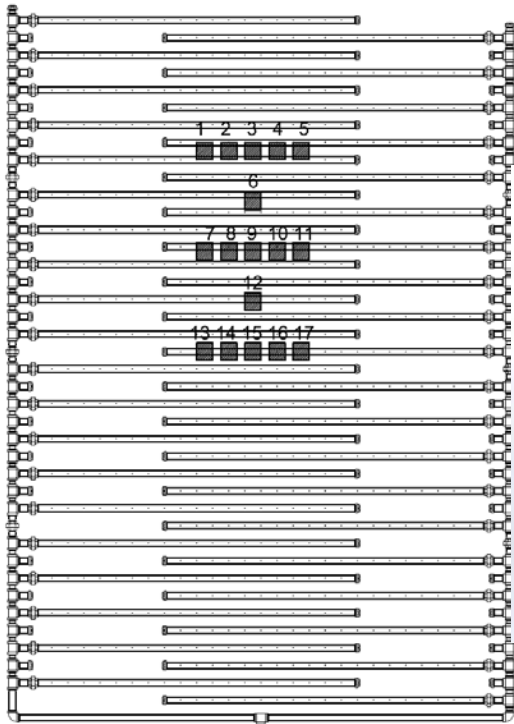




Qualitative Results

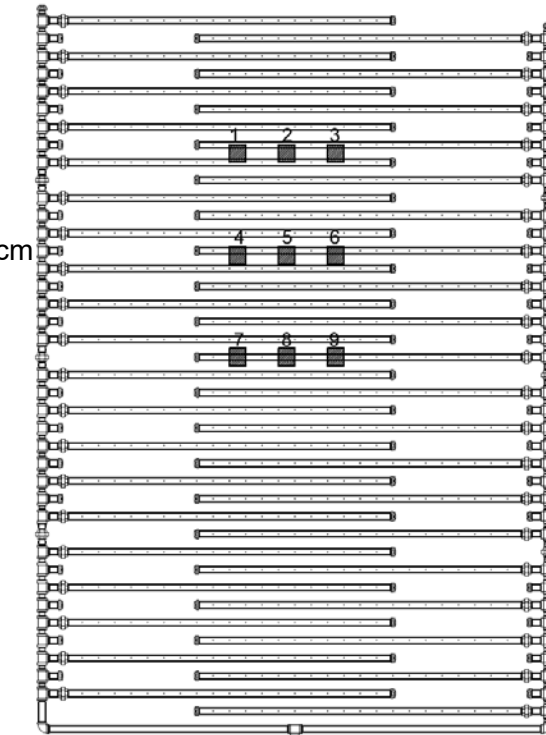
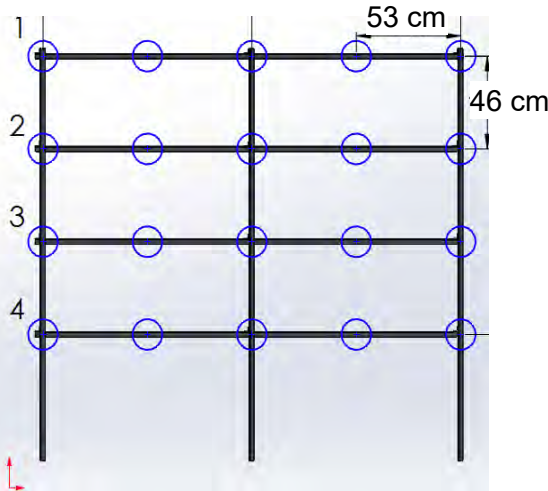


Quantitative Results



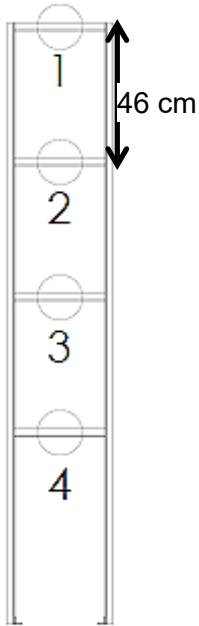
Wall

Temperature Measurement Set Up

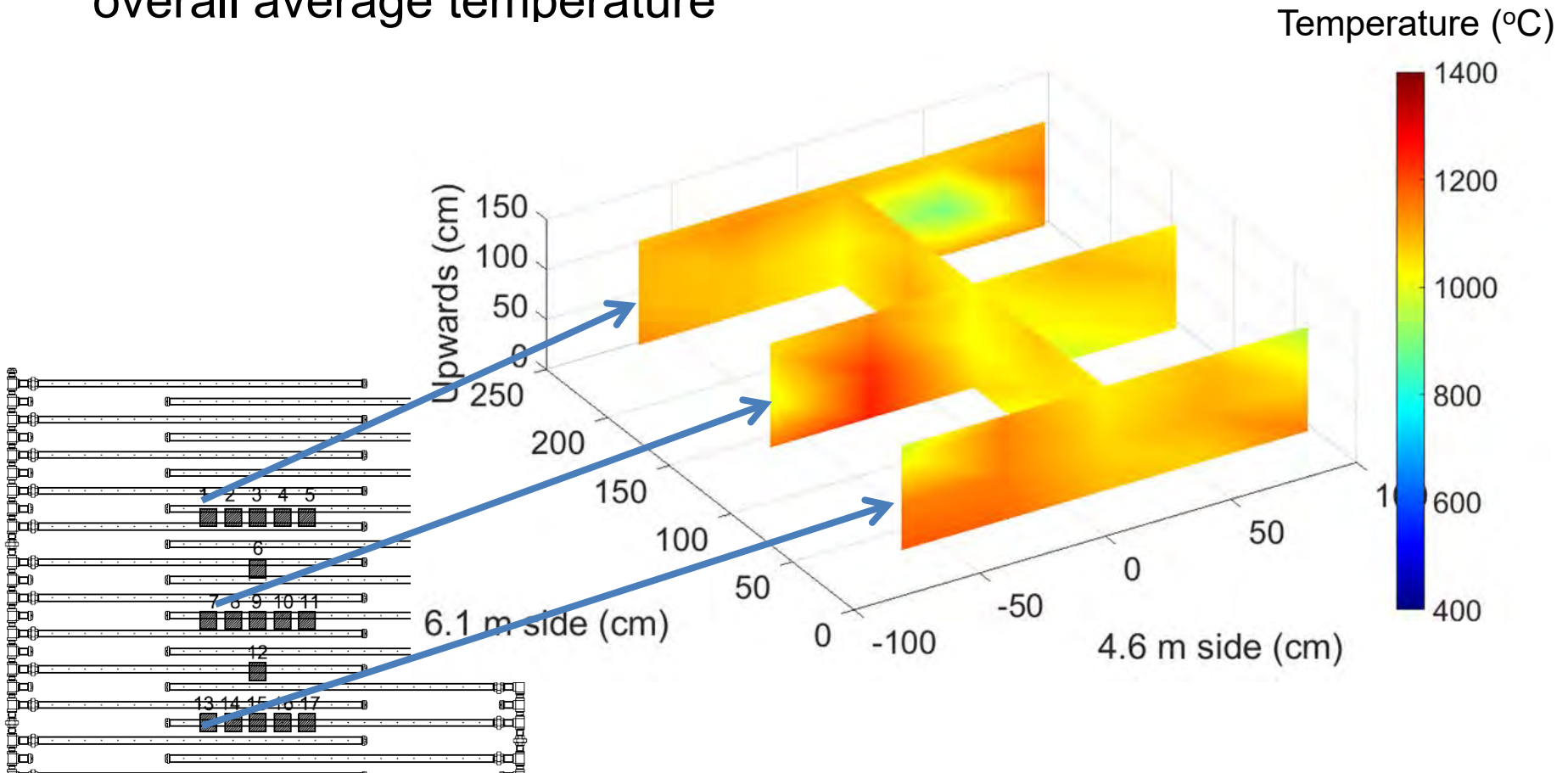


Wall

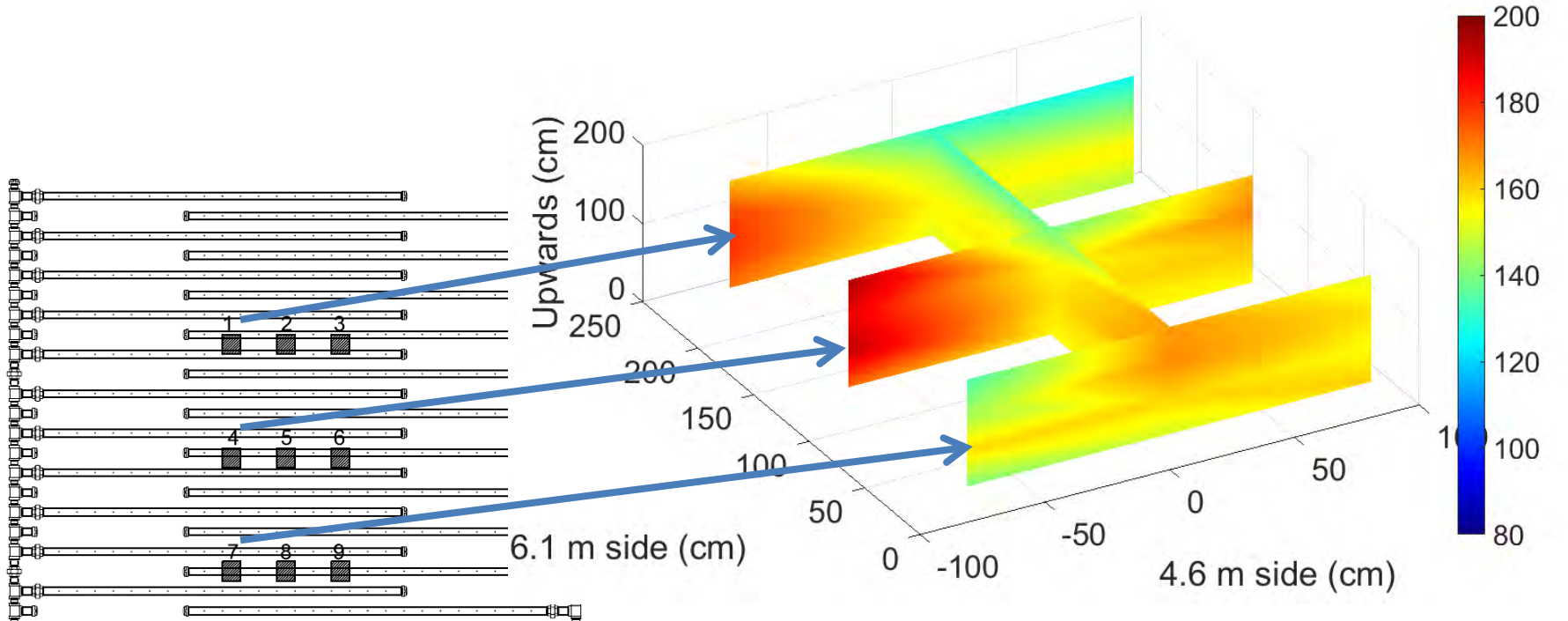
Heat Flux Measurement Set Up



- All temperatures above 800 °C
- Standard deviation of average local temperatures less than 10% of overall average temperature



- All heat fluxes above 80 kW/m²
- Higher heat fluxes representative of large jet fuel pool fire
- Repeatable: two tests at location 8
 - 1st test: 167, 168, 160, 150 kW/m²
 - 2nd test: 163, 162, 155, 147 kW/m²





Modified 6.1 m by 4.6 m Burner



- Large test volume where thermal requirements are met: 4.3 m by 1.8 m by 1.5 m
- Replaced 3790 liter tank with 14760 liter tank
 - US regulations on propane tank greater than 15140 liters
 - Increased burn time from ~13 minutes to ~ 50 minutes
- Performed FCO test with 227 kg (500 lb) class bomb

Modified 6.1 m by 4.6 m Burner

- FCO tested 227 kg (500 lb) class bomb in both pool fuel fire and propane burner

Pool Fuel Fire FCO Pretest



Post-test



Propane FCO Pretest



Post-test





Modified 6.1 m by 4.6 m Burner



- FCO tested 227 kg (500 lb) class bomb in both pool fuel fire and propane burner
- Largest item tested in propane burner to date
- Propane burner was able to produce a flame that was large enough to engulf both A-frame and ordnance item
- Learned the importance of propane valve electrical system
 - A corroded relay led to a test stoppage and retest of item
 - Contingency plan needed for stoppage of burner during test before reaction
- No need to plan for same day fuel delivery
 - Provided flexibility in testing
 - Aided dealing with wind variability
- Initial results show similar reaction of bomb in pool fuel fire and propane burner

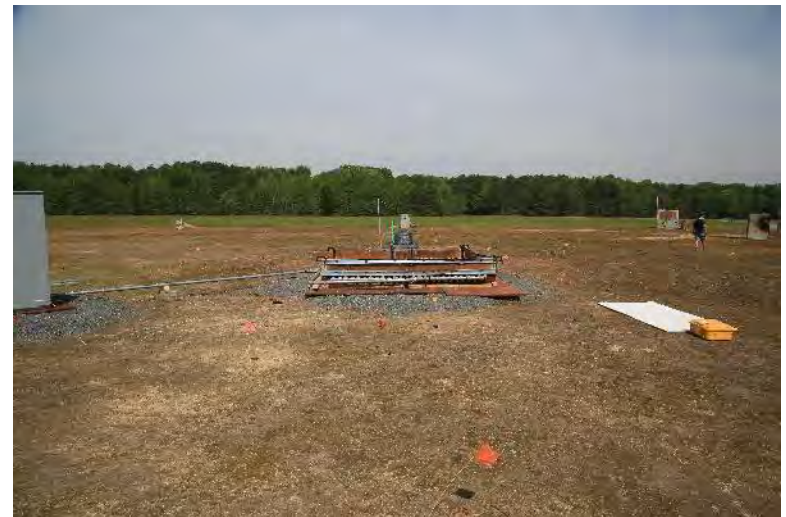
- Propane FCO test was performed on an ammo can of medium ammunition cartridges
- Ammo can contained 110 training and practice (TP) cartridges (live propellant, inert projectile)
- This was the first test in the propane FCO burner that contained multiple energetic items
- Concern that items cooking off while in contact with the burner tubes would cause damage





12:44:45.550

- Item was engulfed in flame for 14:40
- First reaction occurred 2:30 into test and the last audible reaction occurred 9:10 after ignition
- Burner remained on for 5 minutes after last audible reaction
- Test produced a large number of fragments, 64 of which traveled beyond 15 m (50 ft)
 - Only fragments beyond 15 m were catalogued and weighed



- Fragments were collected and catalogued as if going to MREB
- Majority of fragments remained within the burner and the workers were happy with how easy collection was compared to JP5 test

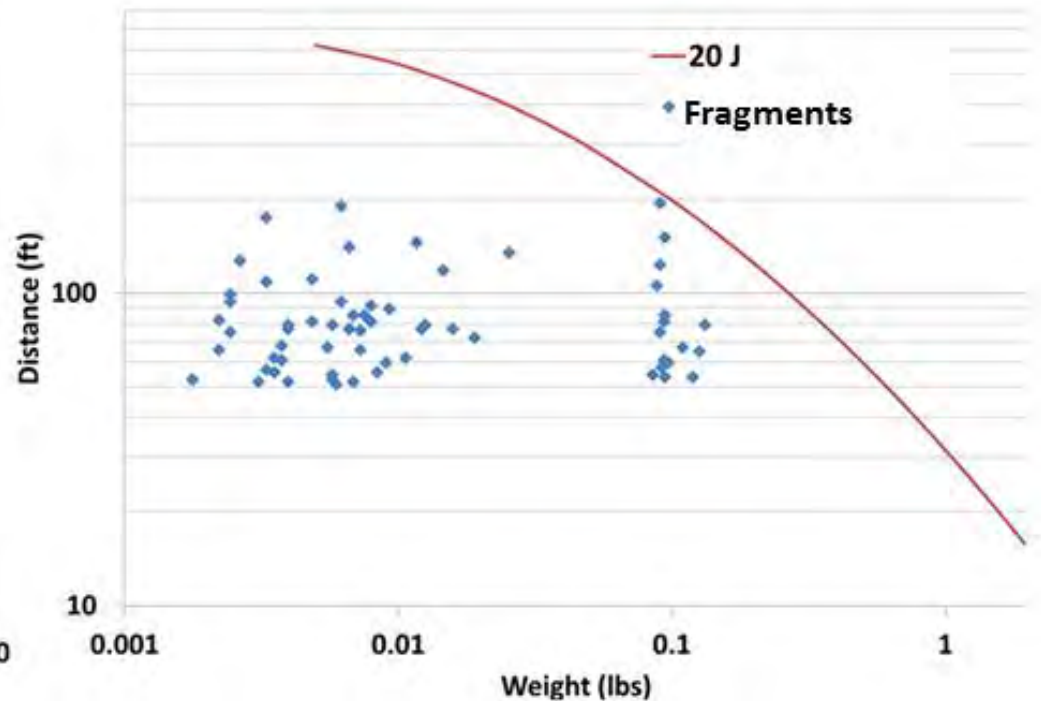
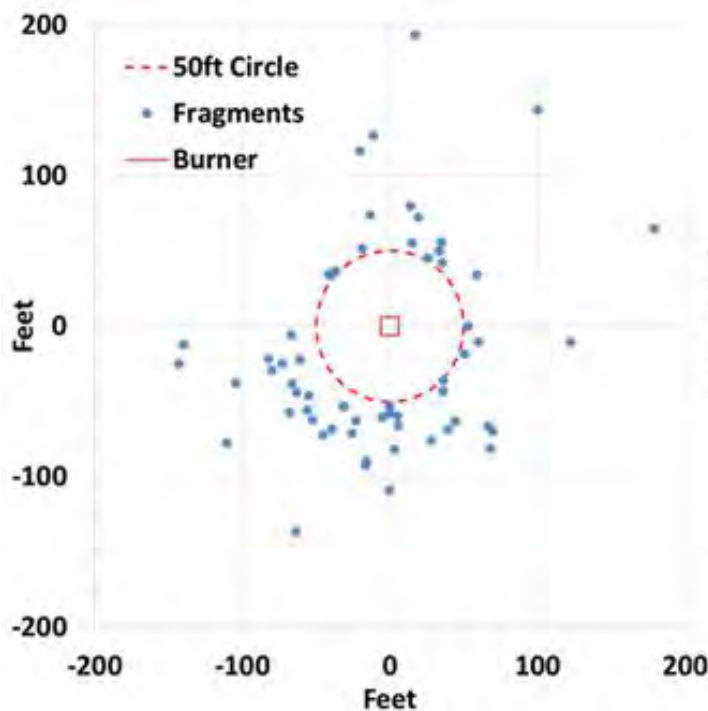
Exited Burner
but <15 m

Remained inside
burner

Greater
than 15 m



- Test produced 64 fragments that traveled further than 15 m
- None exceeded the 20 Joule threshold resulting in a type [V] assessment



Comparison to Liquid FCO Test



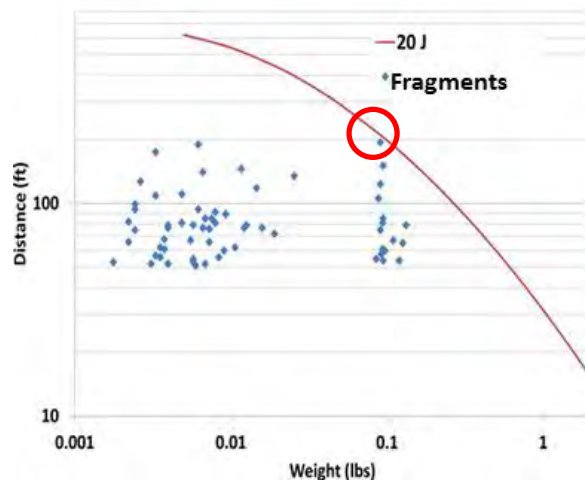
- Test was scored a type IV in the liquid fuel test and a type [V] in the propane test
- Debris map was very similar, barely exceeded 20J in the liquid test, just under 20J in propane test
- No quenching of ordnance items in propane test (shorter duration of reactions)

Propane

Average Temp: 1702°F

Time to 1st reaction: 2:30

Duration of reactions: 6min, 40s

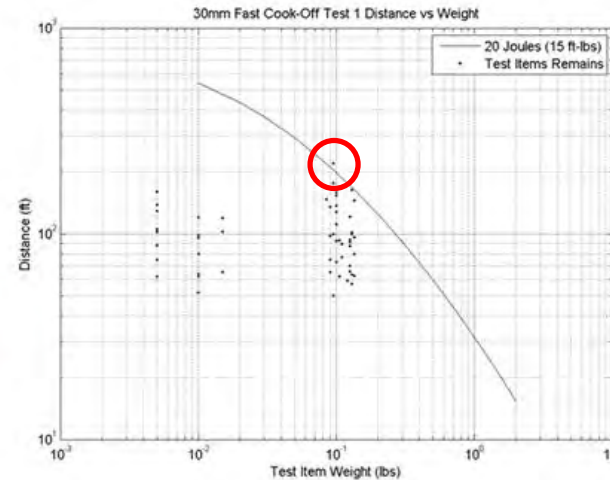


Jet Fuel

Average Temp: 1727°F

Time to 1st reaction: 1:40

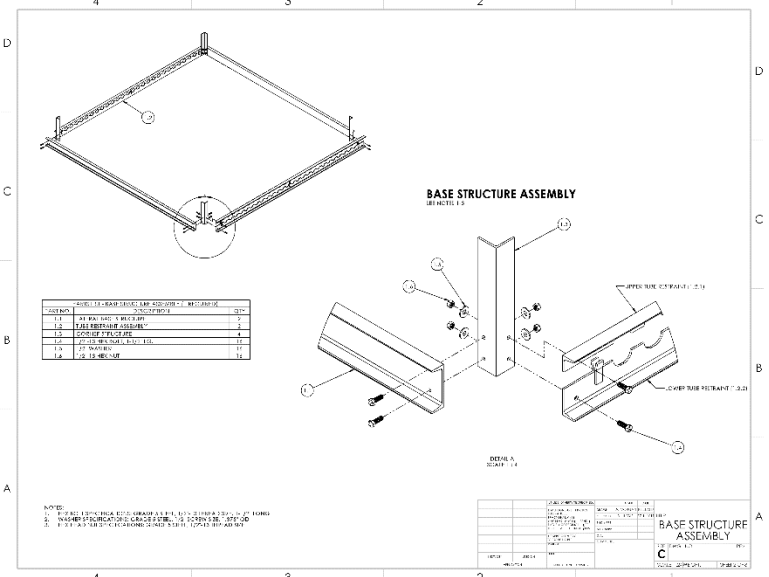
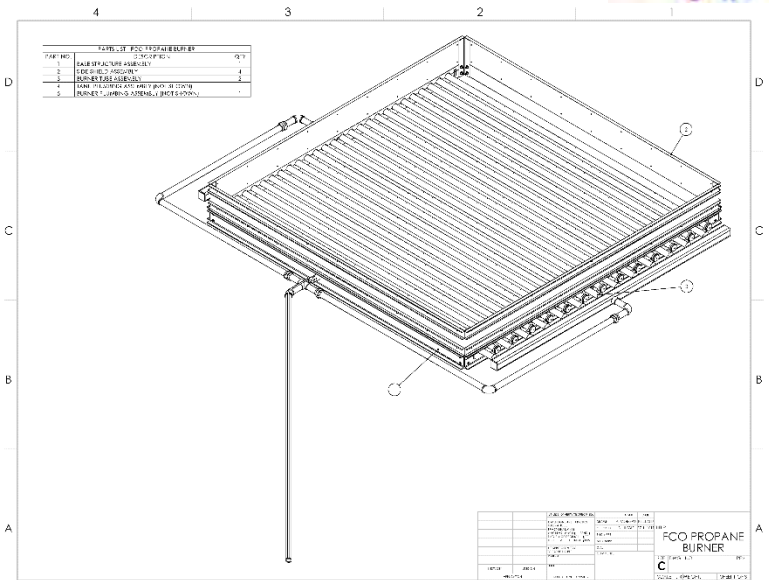
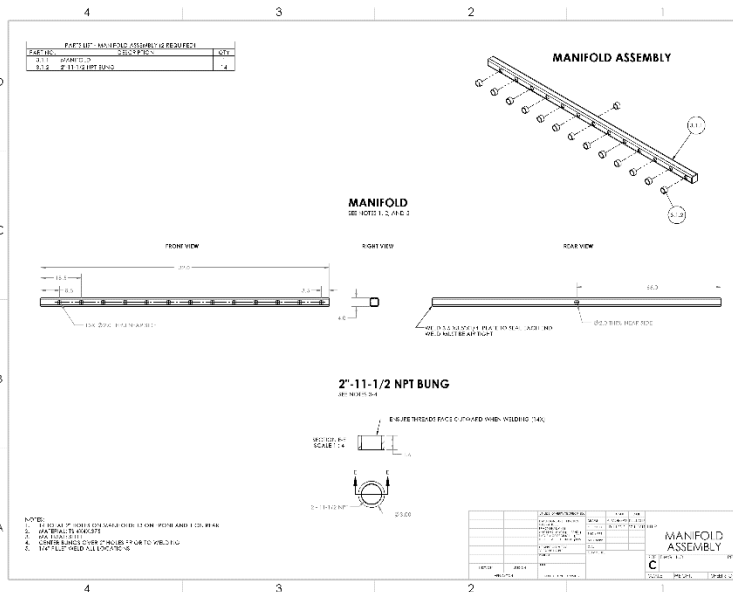
Duration of reactions: 13min, 30s



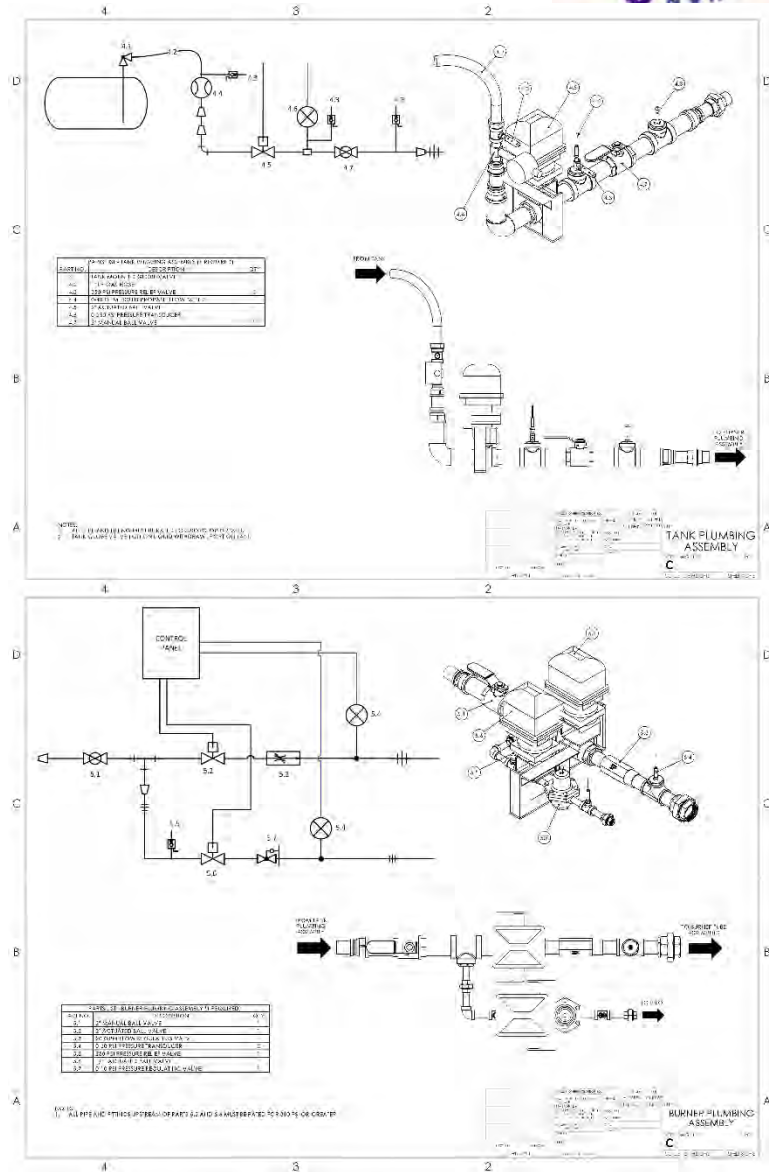
- Fragments produced during the test easily punctured the ammunition can and the side shields
- Reactions of items in contact with the burner tubes did cause some slight denting but no punctures occurred



- A technical drawing package was developed to aid in the dissemination of the burner
- Since the propane burner was developed as a series of prototypes with refinements, no official drawings existed



- The drawing package also includes detailed plumbing schematics
- These incorporate all the lessons that were learned through trial and error
- The drawing package provides all the information needed to fabricate the 3.7 m by 3.7 m propane burner in use at Dahlgren



- A modified 6.1 m by 4.6 m propane burner was designed, built, and calibrated
 - Large engulfing flame
 - Meets temperature and heat flux requirements
- 227 kg class bomb tested in modified 6.1 m by 4.6 m propane burner
- Ammo can of medium caliber ammunition tested in 3.7 m by 3.7 m propane burner
 - Similar result to liquid fuel fire test
 - Easy clean up
 - Multiple reactions did not damage burner
- Technical drawing package for 3.7 m by 3.7 m propane burner developed and available upon request



Acknowledgments



Funded by:

The Environmental Security Technology
Certification Program (ESTCP)



The Insensitive Munitions Advanced
Development (IMAD) Program





MUNITION VULNERABILITY IN PLATFORMS

Gert Scholtes

TNO innovation
for life

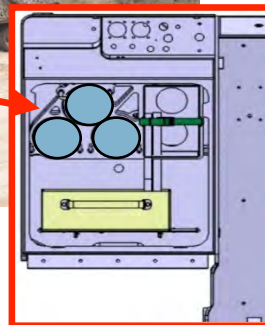


OVERVIEW

- Introduction
- Fragment impact and sympathetic reaction model; stat. toolbox
- Validation
- Test series with shells
- Test series with missile warheads
- Lessons learned
- Conclusions



LIFE-CYCLE MUNITIONS - THREATS



- Fragments
- SCJ
- Bullets
- Cook-off
- Sympathetic reaction

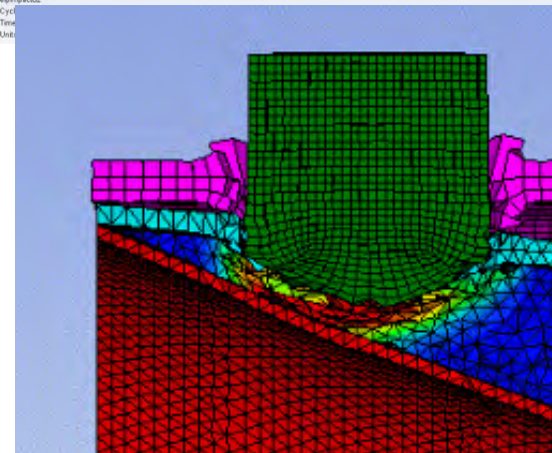
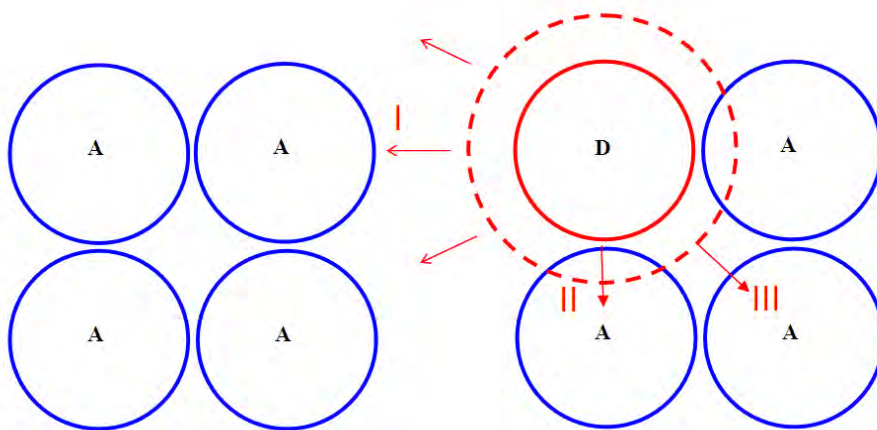
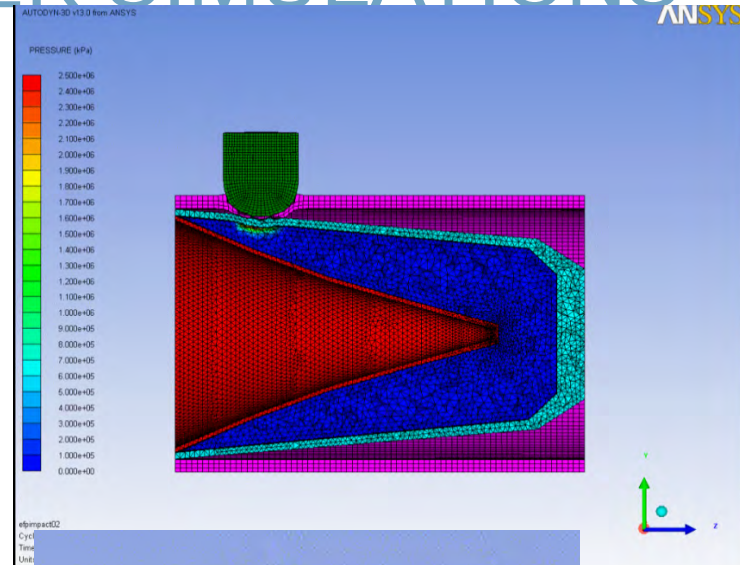
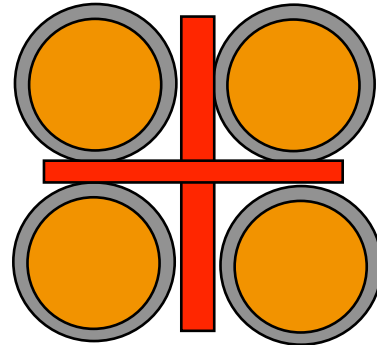
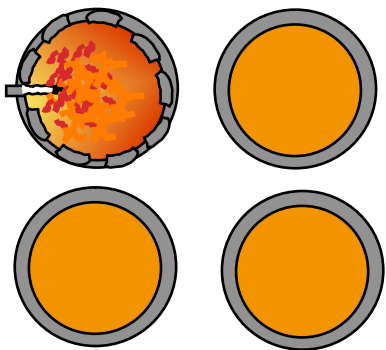


WHAT DOES THE NL MOD WANT/NEED

- › The MOD wants to know the danger of certain threats to our stored munitions and the expected reaction and the danger for personnel and materiel/platforms.
- › With validated munition vulnerability calculations coupled to the platform vulnerability code RESIST the MOD/TNO to be able to estimate the effects of their stored munitions when hit by a certain threat and investigate the effect of protection measures.
- › Projects/Investigation: Combination of test series with munitities, munition vulnerability calculations and Ship/platform vulnerability calculations

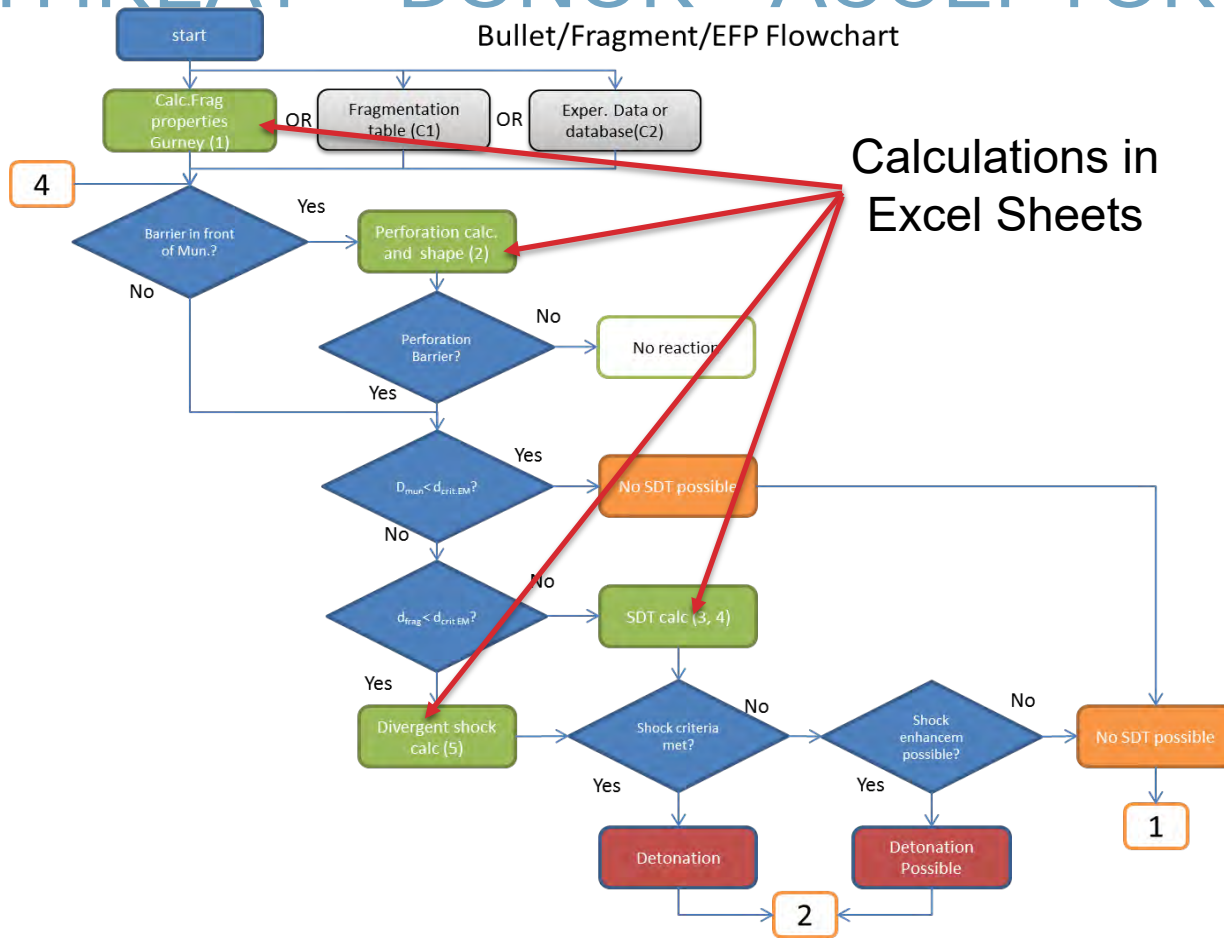
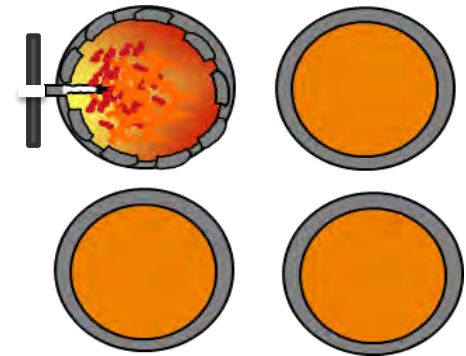


PROBLEM AND COMPUTER SIMULATIONS





TNO APPROACH MUNITION VULNERABILITY TOOLBOX THREAT - DONOR - ACCEPTOR



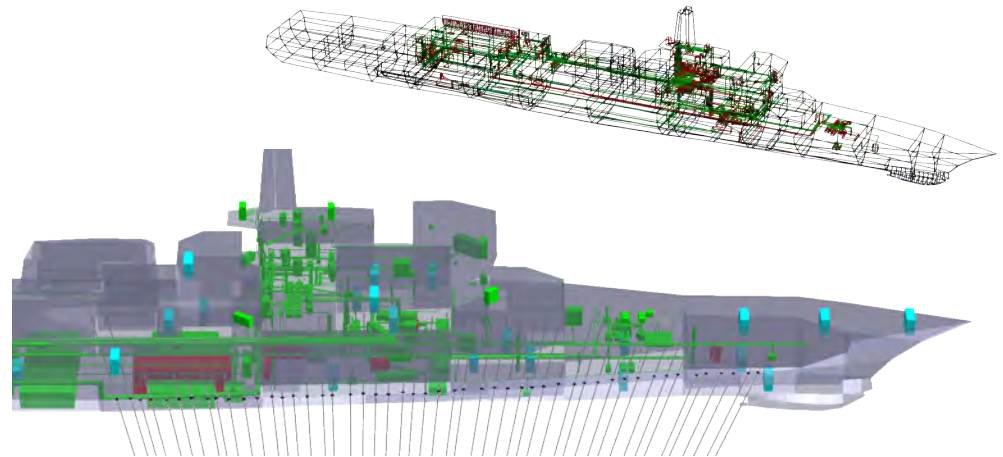
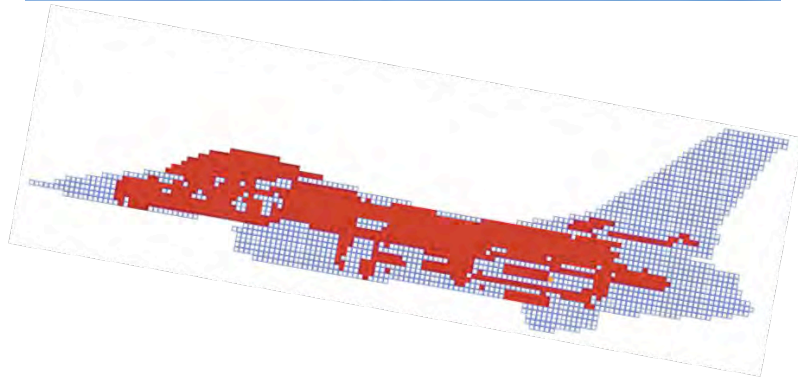
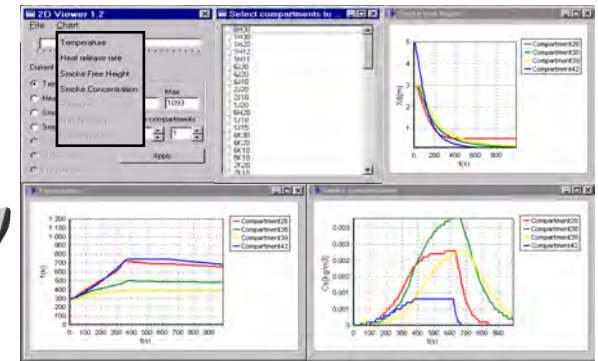
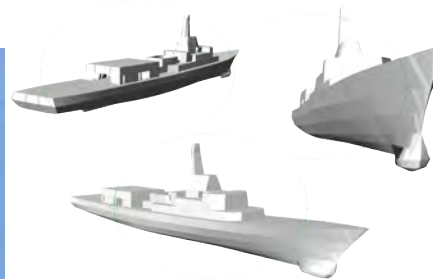
Spreadsheets/comments:

- (1) Fragment velocity calculation with Gurney
- (2) Perforation calculation using Thor equations
- (3) SDT calculation Ec theory Haskins and Cook
- (4) SDT calculation Green or Lundstrom
- (5) Divergent shock calculation Green/Lundstrom
- (6) EM heating due to penetration
- (7) EM cook-off reaction calculation after penetration of bullet
- (8) Pressurisation calculation after ignition and burning of EM
- (9) Sympathetic reaction calculation confined stack and ono-on-one
- (10) TNT equivalent blast/shock calculation
- (C1) Fragmentation table of munitions (table #.#)
- (C2) Fragmentation data from experiments or databases
- (C3) Bullet and fragment test result database (e.g. BIRD or FRAID)
- (C4) SG table ref [#] tabel #.#
- (C5) Cook-off database test results
- Excel spreadsheet calculation
- Excel spreadsheet not implemented
- Excel spreadsheet (needs data)
- Data from database or Experiments
- Detonation reaction (possible)
- No Prompt shock detonation (SDT)
- Decision
- Reference Number



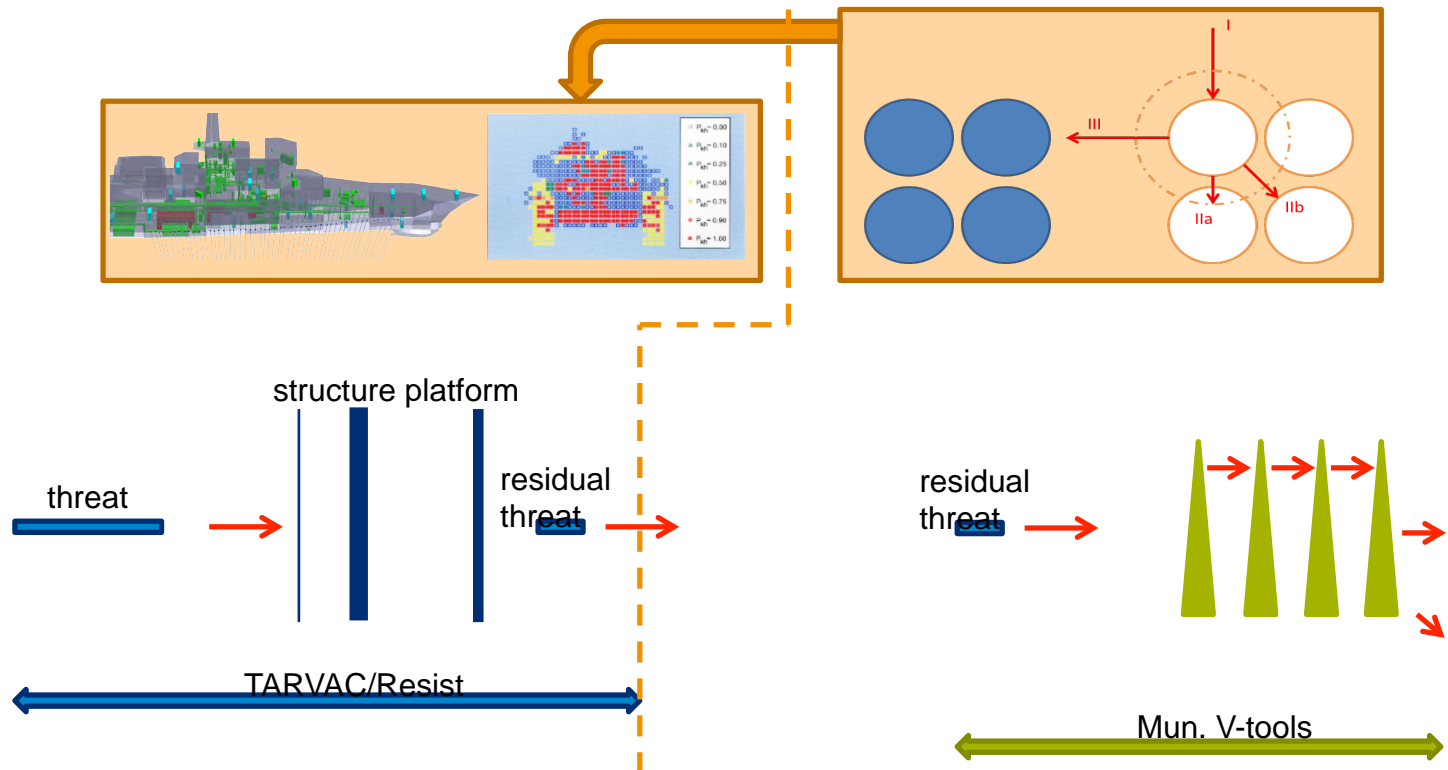
PLATFORM VULNERABILITY CODES

- › 'RESIST' ship vulnerability assessment
- › TARVAC (TARget Vulnerability Assessment Code)





ENVISIONED SITUATION



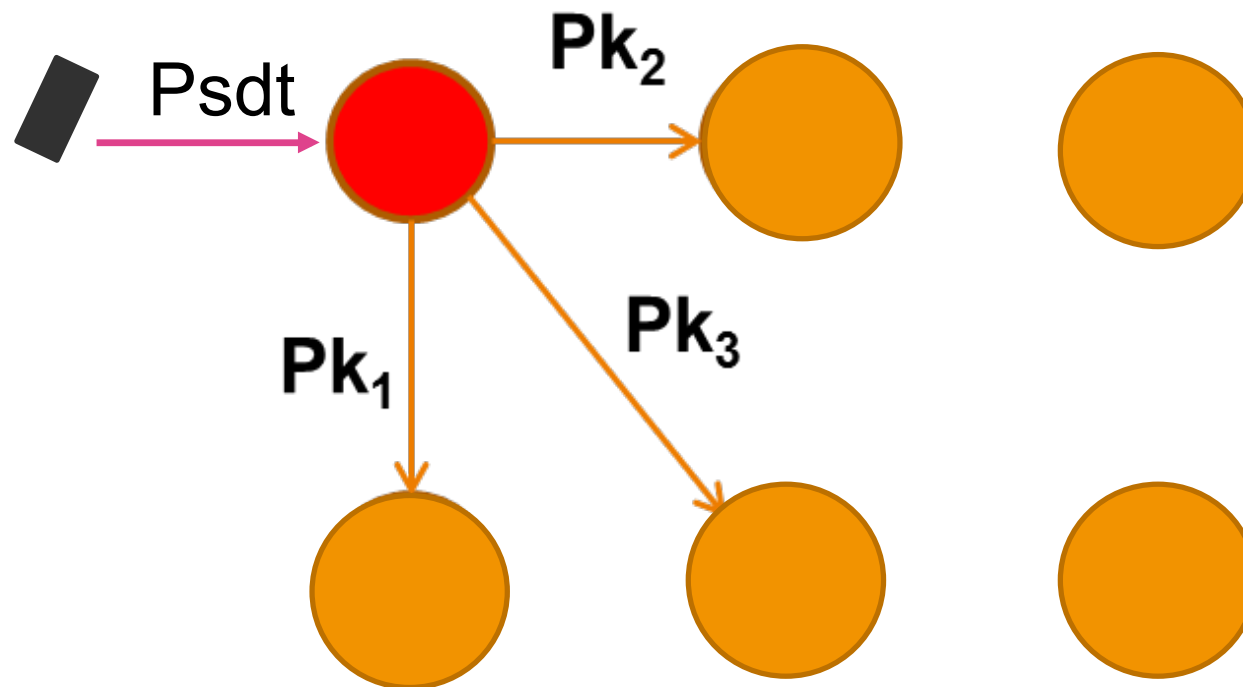


FRAGMENT IMPACT AND SYMPATHETIC REACTION MODELS; STATISTICAL TOOLBOX



SCENARIO - PROBABILITY

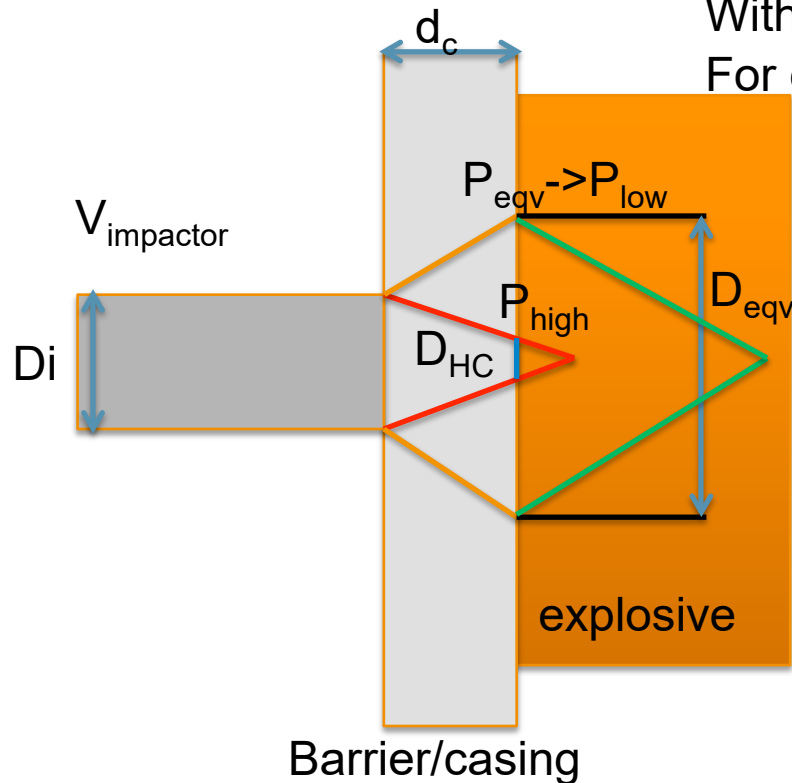
- › Missile hit: fragments travelling towards munition storage



NEW SHOCK MODEL: COMBINATION OF HASKINS&COOK AND P_{EQV} IDEA OF GREEN → E_{FLUX}

Energy Fluence: $E = \int P \cdot u_{p,x} \cdot dt$

With: P= pressure, u_p Part. Velocity and t the time
For explosive $E_{impactor} > E_{crit,exp} \rightarrow$ Detonation

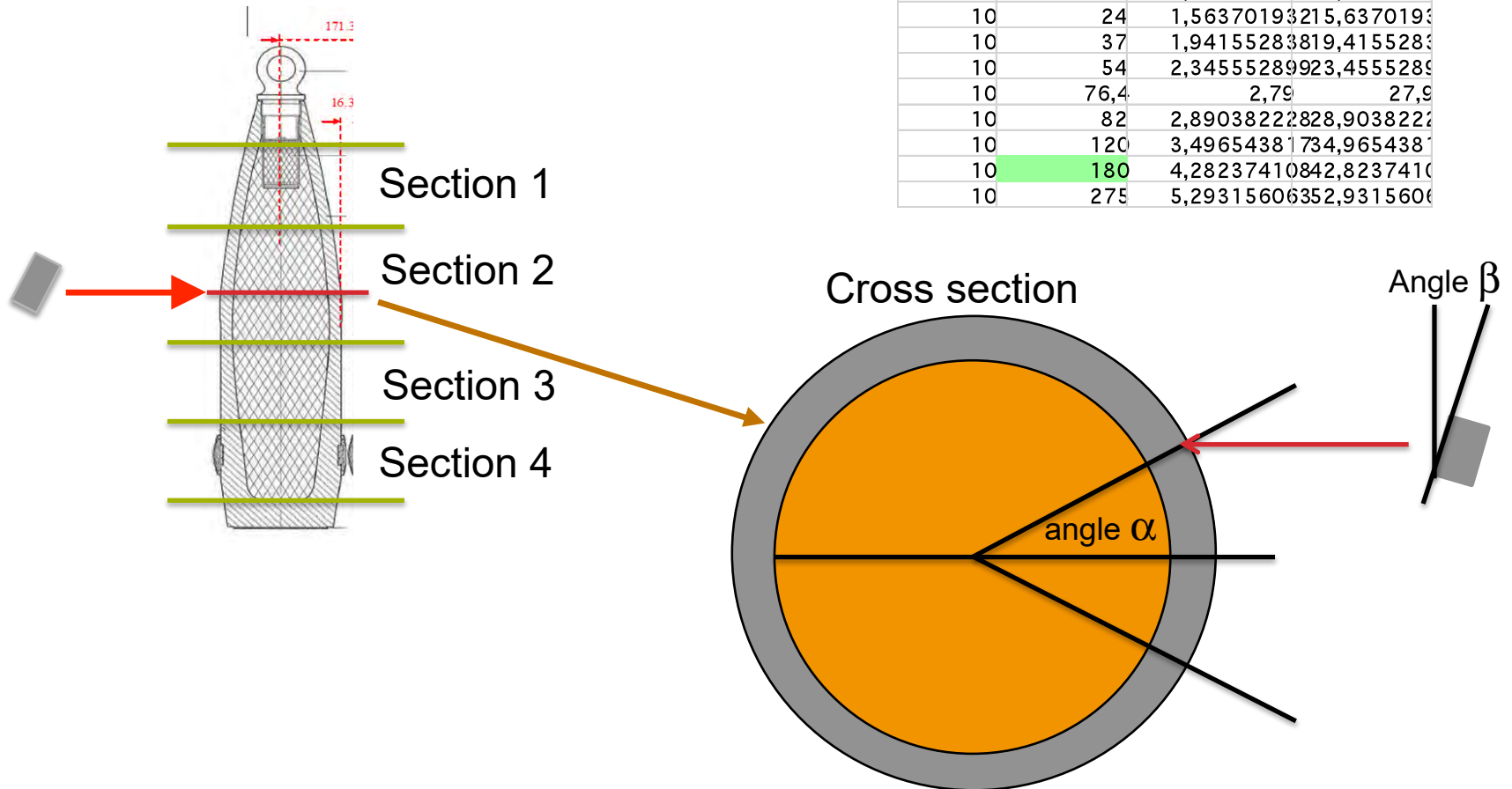


- › Barrier old model: High pressure component reduced by rarefaction wave from the edge
- › New model expansion of pressure wave:
- › E_{green} and E_{HC} component for E. flux
- › $E_c - \{E_{green} (R_{gr}^2 - R_{HC}^2) + E_{HC} R_{HC}^2\} / R_{green} = 0$
- › With $R_{gr} = D_{eqv}/2$ and $R_{hc} = D_{HC}/2$
- › Advantage : standard E_{crit} can be used
- › $D_{eqv} = Di + 2 d_c$
- › P_{low} from P_{eqv} and shock impedance match
- › P_{high} from P in barrier and shock impedance match



STATISTICS → PROBABILITY OF A KILL: $P_{KILL} (SDT)$

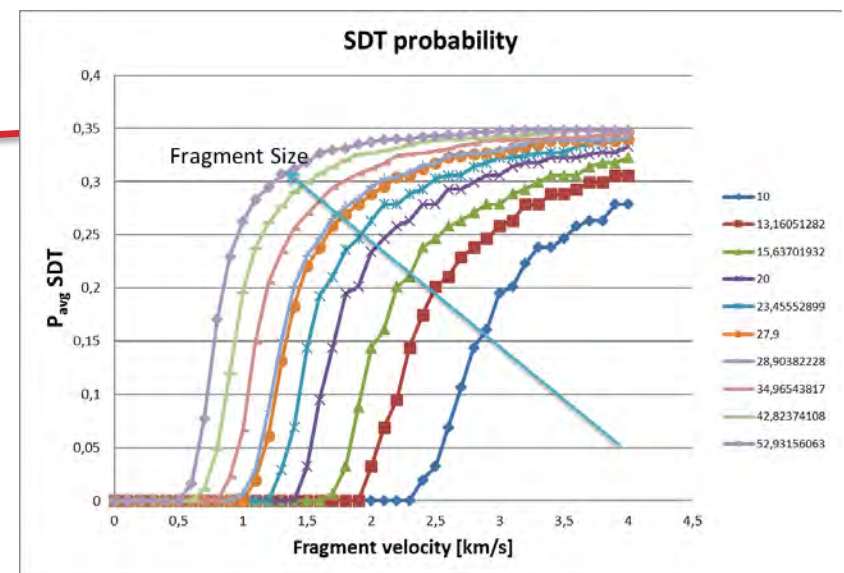
thickness	weight (gr)	diameter [cm]	diameter [mm]
10	17	1,31605128	13,1605128
10	24	1,56370193	15,6370193
10	37	1,94155283	19,4155283
10	54	2,34552899	23,4552899
10	76,4	2,79	27,9
10	82	2,89038222	28,9038222
10	120	3,49654381	34,9654381
10	180	4,28237410	42,8237410
10	275	5,29315606	52,9315606



SPREADSHEET CALCULATIONS

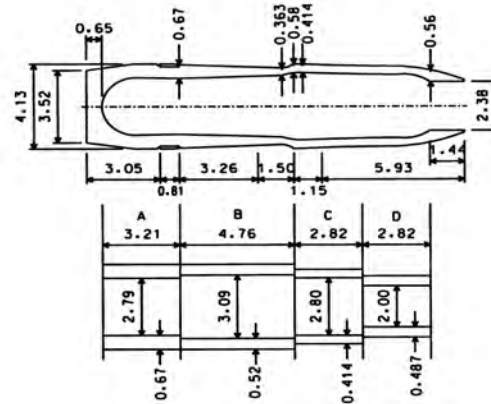
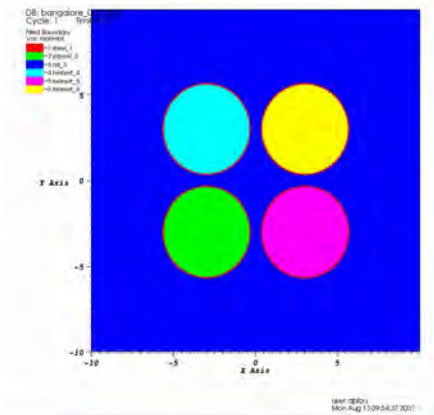
- Results of 10 different fragment diameters
- With 40 different velocities
- 625 different angles (location and fragment impact angle)
- Maximum of 4 different section of warhead
- Graphs display 10 x 625 x 40 X 4 solver calculations
- = 1,000,000 solver calculations (in a few seconds)

Statistical input for
Platform vulnerability
codes

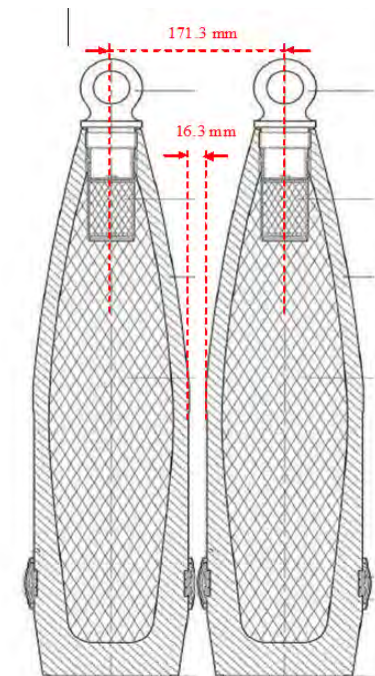
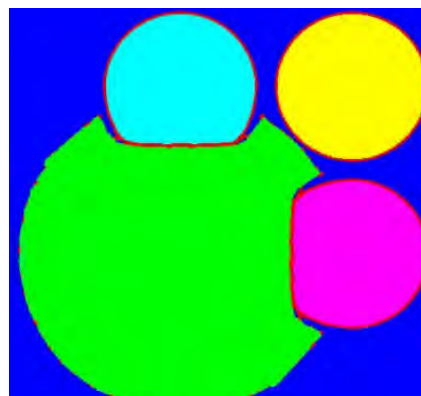
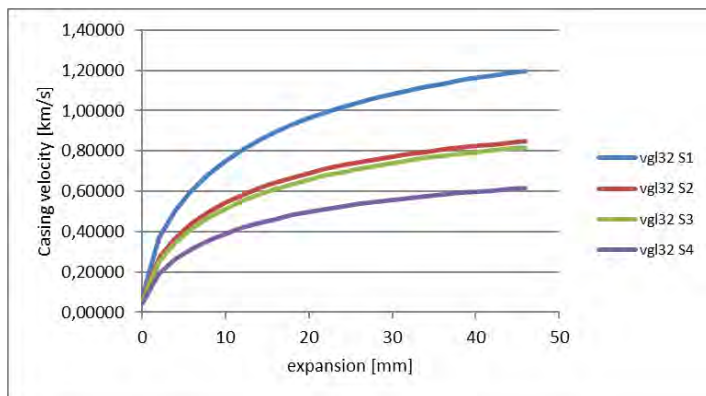




SYMPATHETIC REACTION CALCULATION (GURNFY)

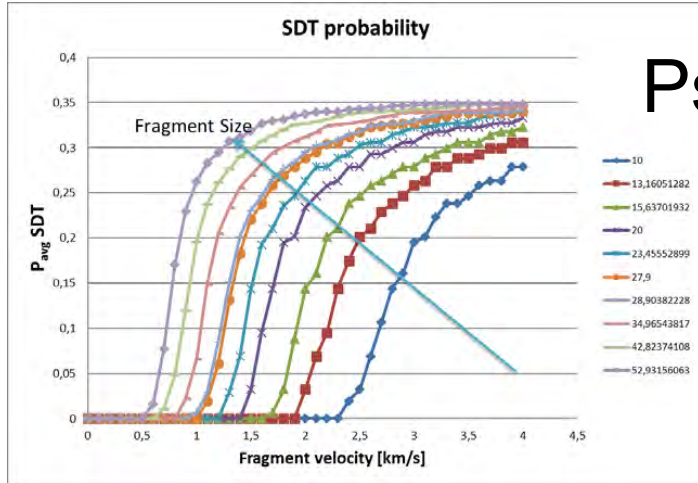


Input parameters:						
Us=Co+sl	Co	S	r	dcrit	Ecrit	
1,2	4,58	1,49	7,89	0	0	
Steel	4,58	1,49	7,89	0	0	
TNT/RDX	3,03	1,73	1,715	0	1,381	
Number of Sections	4		max velocity calc		4	
Casing thickness			length section			
16 mm			121 mm			
22 mm			150 mm			
25 mm			66 mm			
30 mm			97 mm			
total length munition			434 mm			

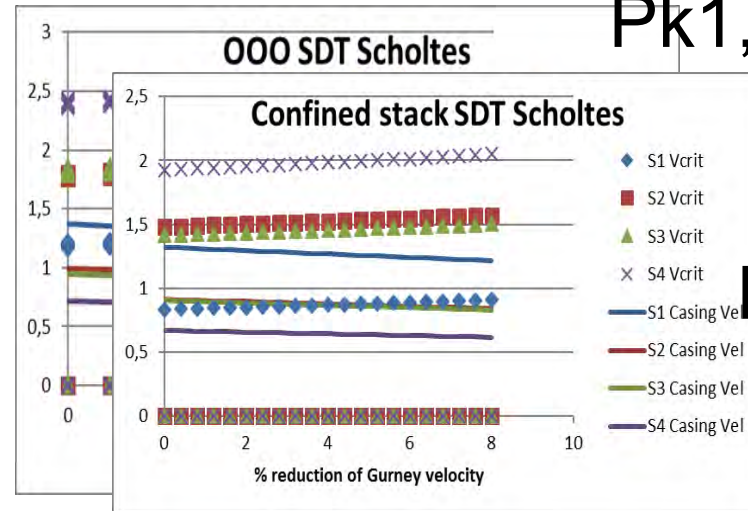




TYPE OF RESULTS

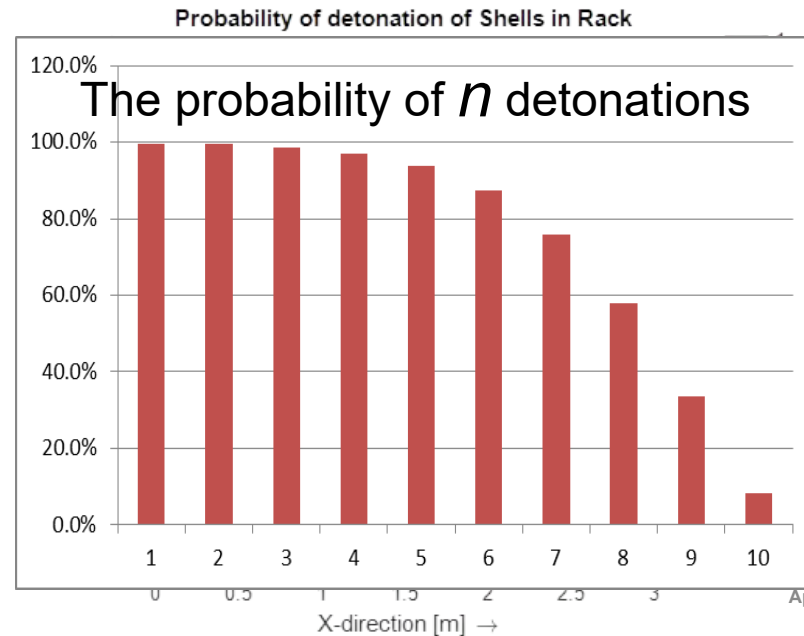
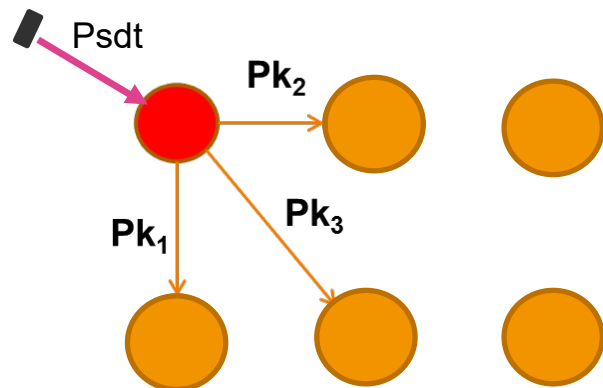


P_{sdt}



P_{k1}, P_{k2}

P_{k3}





Defensie Materieel Organisatie
Ministerie van Defensie

TNO innovation
for life

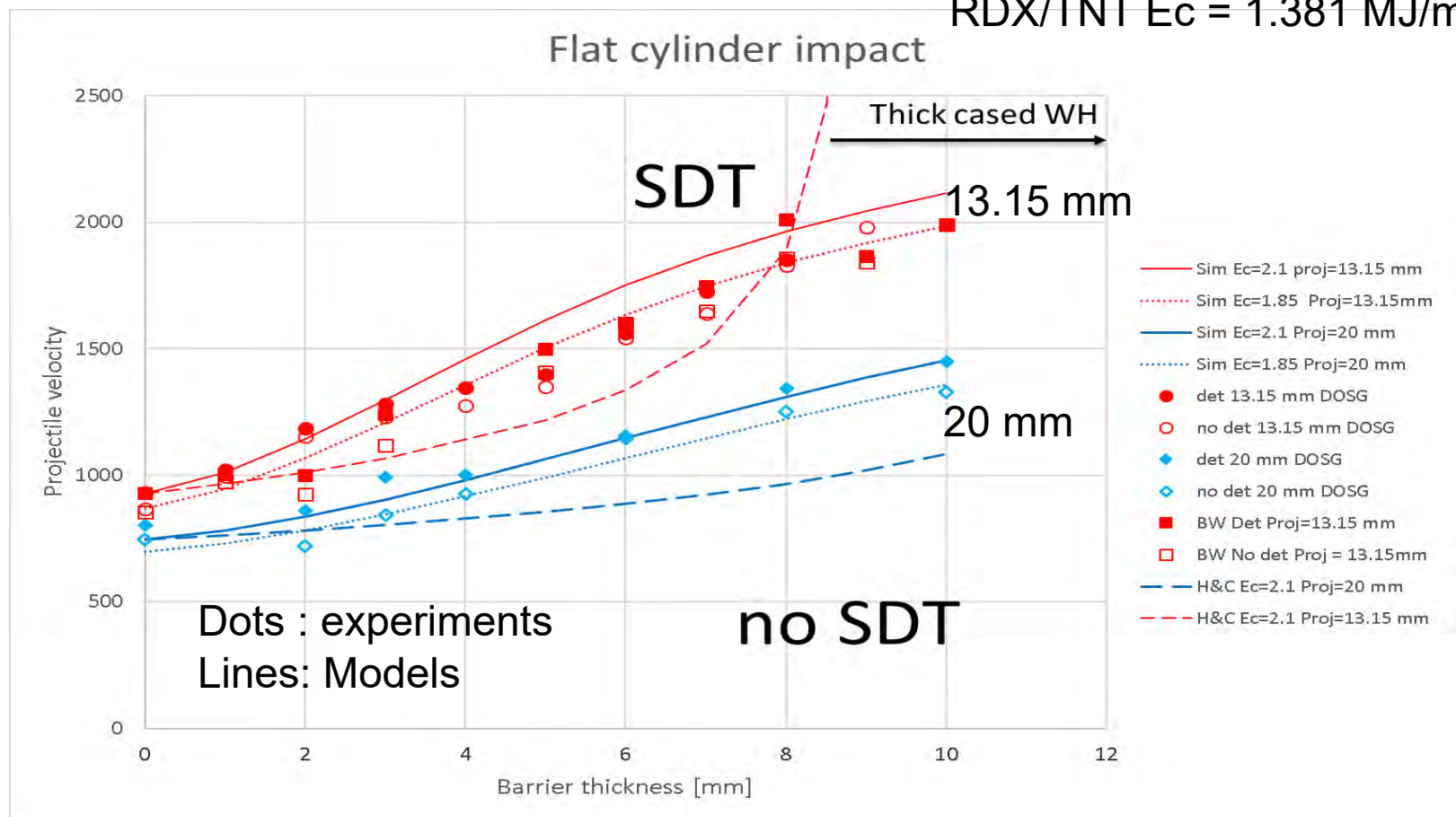
VALIDATION: LITERATURE VALUES



VALIDATION WITH DATA FROM LITERATURE

Comp B $E_c = 1.85/2.1 \text{ MJ/m}^2$

RDX/TNT $E_c = 1.381 \text{ MJ/m}^2$





Defensie Materieel Organisatie
Ministerie van Defensie

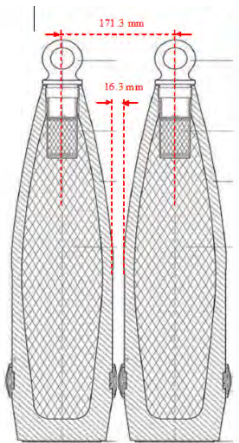
TNO innovation
for life

MUNITIONS TEST SERIES

TEST PROGRAM WITH SHELLS

3 types of experiments:

- › Reaction of a certain threat?
- › Sympathetic reaction?
- › Effect of the detonation to the surrounding of the ship and personnel.



Facts and Figures

Several Shells

3 weeks of testing

40 experiments

All test in duplo

6 DMO employees

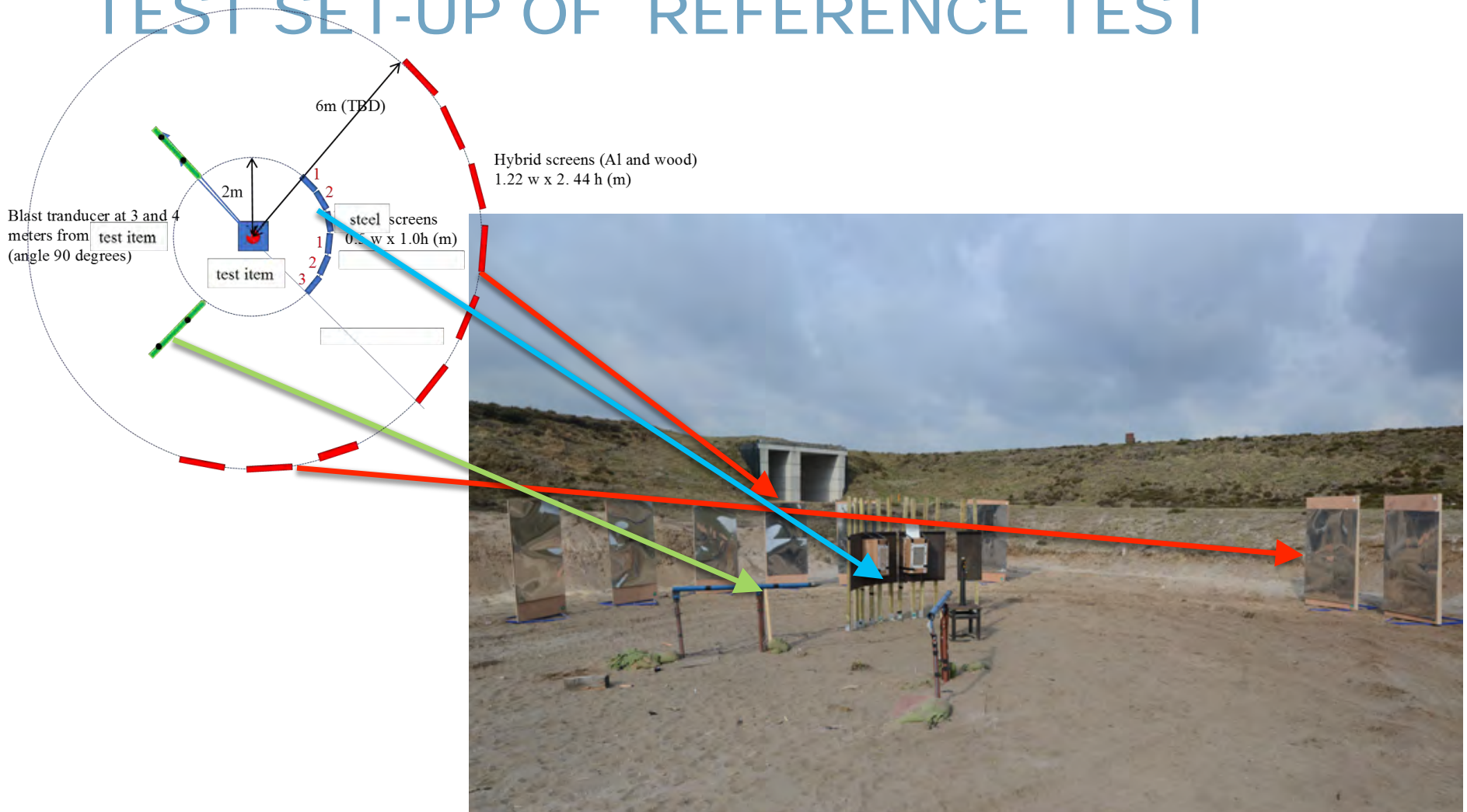
4 TNO employees

2 international visitors

Terabytes of data



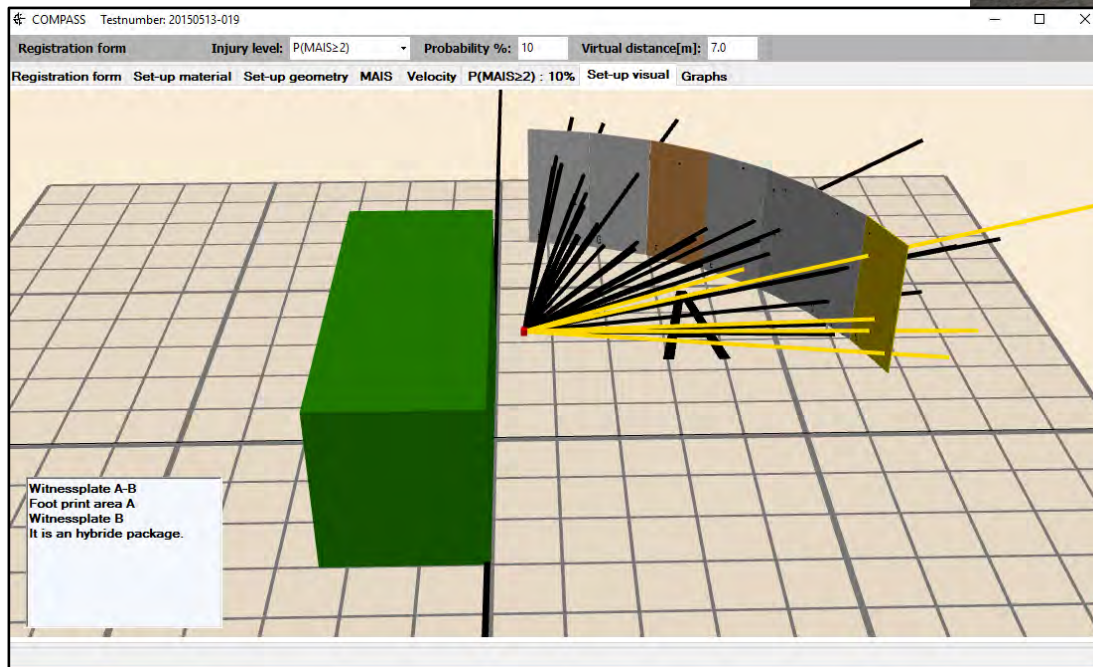
TEST SET-UP OF REFERENCE TEST



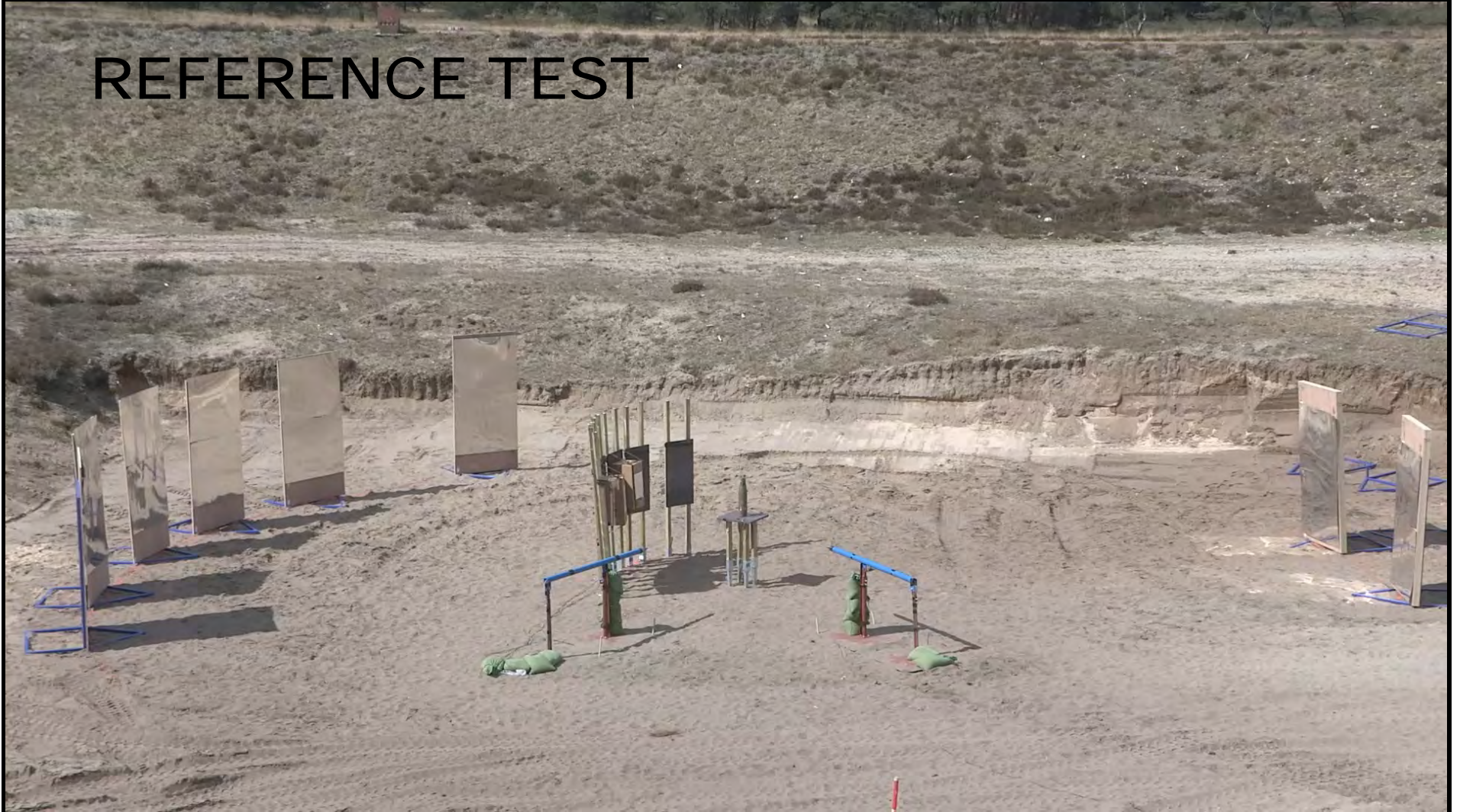


HYBRIDE SCREEN METHOD AND COMPASS ANALYSES

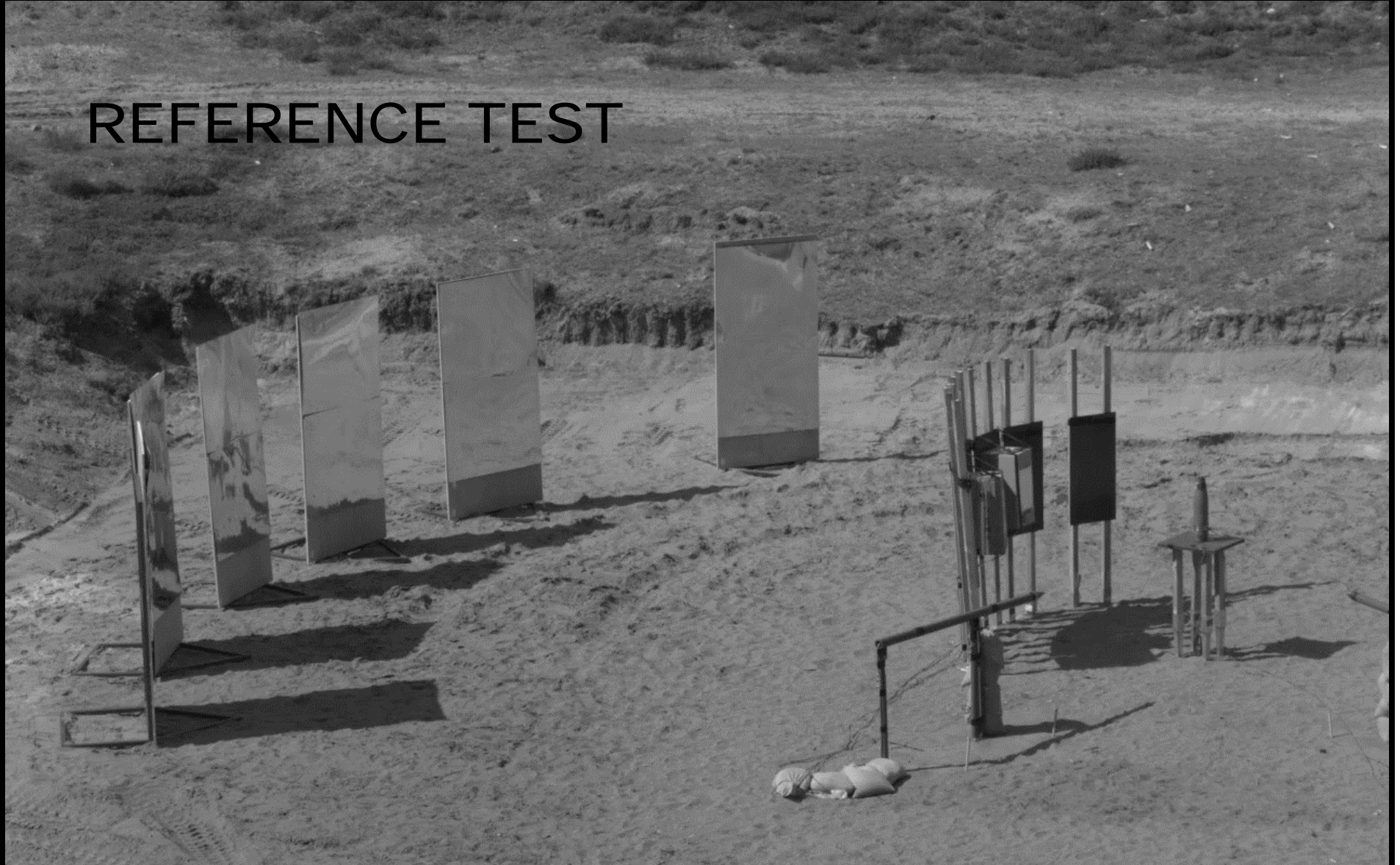
Method from STANAG
4686, under development



REFERENCE TEST



REFERENCE TEST



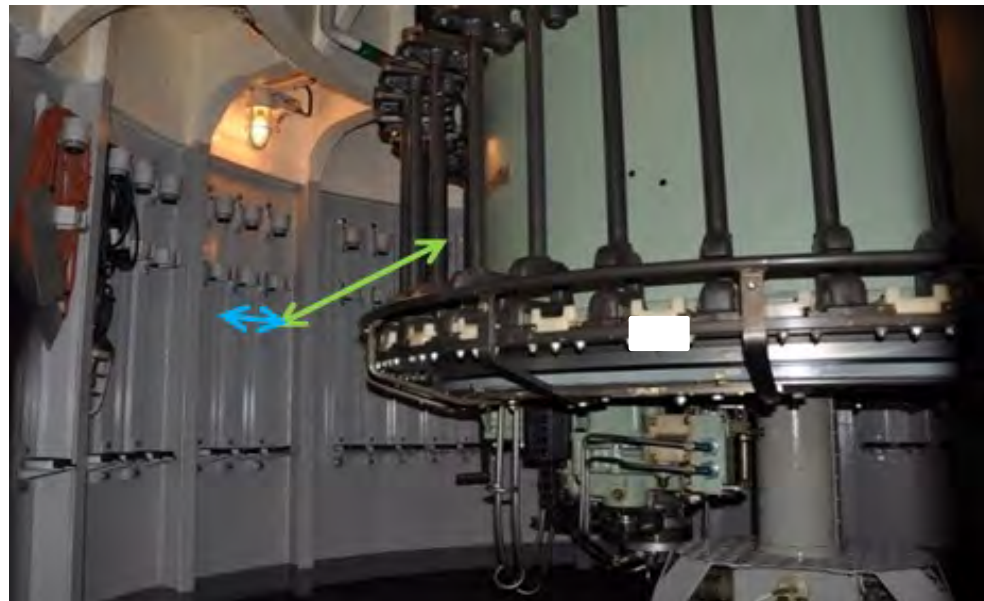
REFERENCE TEST





MUNITION TEST SET-UP

- › Testing of all kind of storage situation of munitions
 - › Distances
 - › Adjacent munitions
 - › Munition in near area
 - › Barriers
 - › Metal plates
 - › Foams etc





SYMP REACTION TEST





NORWAY, WEEK 34-36, 2018

RENA TEST SITE





TESTPROGRAM SHELLS

3 types of experiments:

- › Reaction of a certain threat?
- › Sympathetic reaction?
- › Effect of the detonation for the surrounding of the ship and personnel.

Facts and Figures

Several warheads/32 WH tot.

~3 weeks of testing

18 experiments

8 MOD NL employees

4 TNO employees

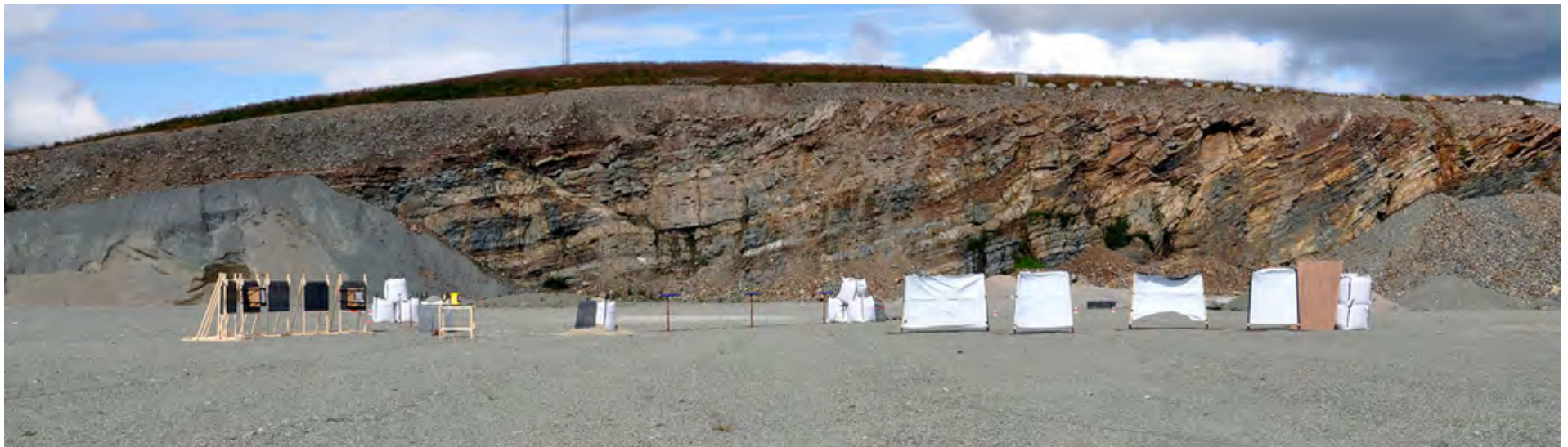
4 Norwegian MOD employees

Terabytes of data



CHARACTERISATION OF A SINGLE WARHEAD

- › Assessment of effect by means of steel plates
- › Fragment velocity measurement with triggering foils
- › HS video of fragments at distance of 15-30 meters
- › HS video overview and close-up of warhead
- › Normal speed video
- › Pressure measurement in 2 lines at 3 positions





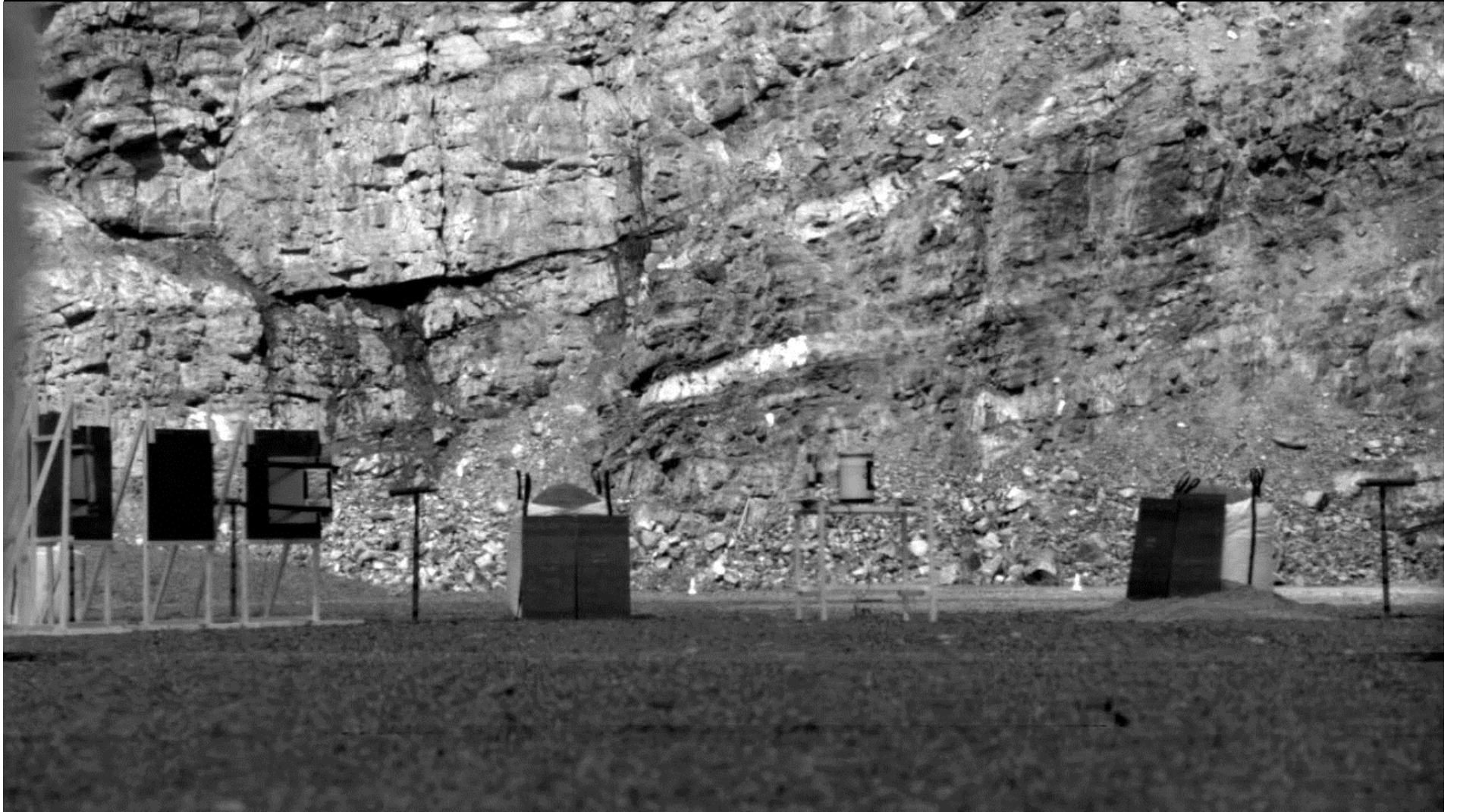
IMPRESSIONS





IMPRESSIONS







SYMPATHETIC REACTION

- › Warheads set-up simulating storage situation
- › HS video overview and close-up of warheads
- › Normal video
- › Pressure measurement







LESSONS LEARNED

- › Not all instrumentation needs to be expensive
- › Protect your expensive camera's and data acquisition well
- › Some unexpected results in current storage situations → need for mitigation
- › Also a type III reaction can result in a sympathetic reaction giving a type III reaction or more severe !
- › Smaller caliber bullets sometimes give a more violent reaction!
- › A large SCJ does not always give a detonation! (non IM WH)
- › These type of tests can give more than just vulnerability results:
 - Performance of warhead (fragment speed, perforation performance, fragmentation patterns, actual size of fragments)
 - Effects of the detonation to the surrounding of the ship and personnel

SCJ impact on warhead





CONCLUSIONS

- › Shock model works quite good and will be implemented in platform vuln. codes
- › Experiments:
 - › Obtained several types of reaction
 - › Results led to preliminary advise for safe storage of munitions on board a ship
 - › Analyses still in progress but Terabyte of data available for validation of data for:
 - › Munition vulnerability toolbox
 - › Fragmentation codes (SPLIT-X, TARVAC of RESIST)
 - › RESIST: effect of certain reactions on board of ship
- › Very good co-operation between DMO (Naval vulnerability), DMO Centre of Excellence, Norwegian MOD and TNO.

Results will contribute to reduction of risks in general and of munitions storage and more balanced ship design.

Modernization and Capabilities of the Lawrence Livermore National Laboratory Pilot Facility for Remotely Controlled Energetic Materials Synthesis

Nathaniel B. Zuckerman*, Philip F. Pagoria*, Alan J. DeHope*, Edwin F. Virgin III*, Fred E. Wade**, William L. Collins**, and Brock K. Parsons**

Materials Science Division* and
Defense Technologies Engineering Division**
Lawrence Livermore National Laboratory, Livermore, CA USA 94550

zuckerman2@llnl.gov

Abstract:

Lawrence Livermore National Laboratory has invested in the modernization of their synthesis pilot facility for the kilo-scale preparation of energetic materials and precursors. This capability will serve to accelerate the research and development progression toward new energetic materials as well as for the optimization of processes for existing conventional materials. The first two planned campaigns for the facility will include the nitration of 2,6-diaminopyrazine-N-oxide (DAPO) to 2,6-diamino-3,5-dinitropyrazine-N-oxide (LLM-105), and the amination of 1,3,5-trichloro-2,4,6-trinitrobenzene to TATB. The presentation will focus on the design and agile capabilities of the pilot facility, the transition from all glass vessels to the new two-story integrated skid with glass-lined carbon steel reactors, and the efforts to provide optimal operator safety by utilizing a custom Wonderware® platform for reagent additions and the majority of process manipulations.

Keywords: LLM-105, TATB, Pilot Scale Synthesis, SCADA

Disclaimer

This document was prepared as an account of work sponsored by an agency of the United States government. Neither the United States government nor Lawrence Livermore National Security, LLC, nor any of their employees makes any warranty, expressed or implied, or assumes any legal liability or responsibility for the accuracy, completeness, or usefulness of any information, apparatus, product, or process disclosed, or represents that its use would not infringe privately owned rights. Reference herein to any specific commercial product, process, or service by trade name, trademark, manufacturer, or otherwise does not necessarily constitute or imply its endorsement, recommendation, or favoring by the United States government or Lawrence Livermore National Security, LLC. The views and opinions of authors expressed herein do not necessarily state or reflect those of the United States government or Lawrence Livermore National Security, LLC, and shall not be used for advertising or product endorsement purposes.

Introduction

The energetic materials synthesis group of Lawrence Livermore National Laboratory delivers research capabilities for the development of new and conventional high explosives, with a primary focus on insensitive high explosives.¹⁻⁴ Our synthetic chemists work primarily within Livermore's High Explosives Applications Facility (HEAF), which provides

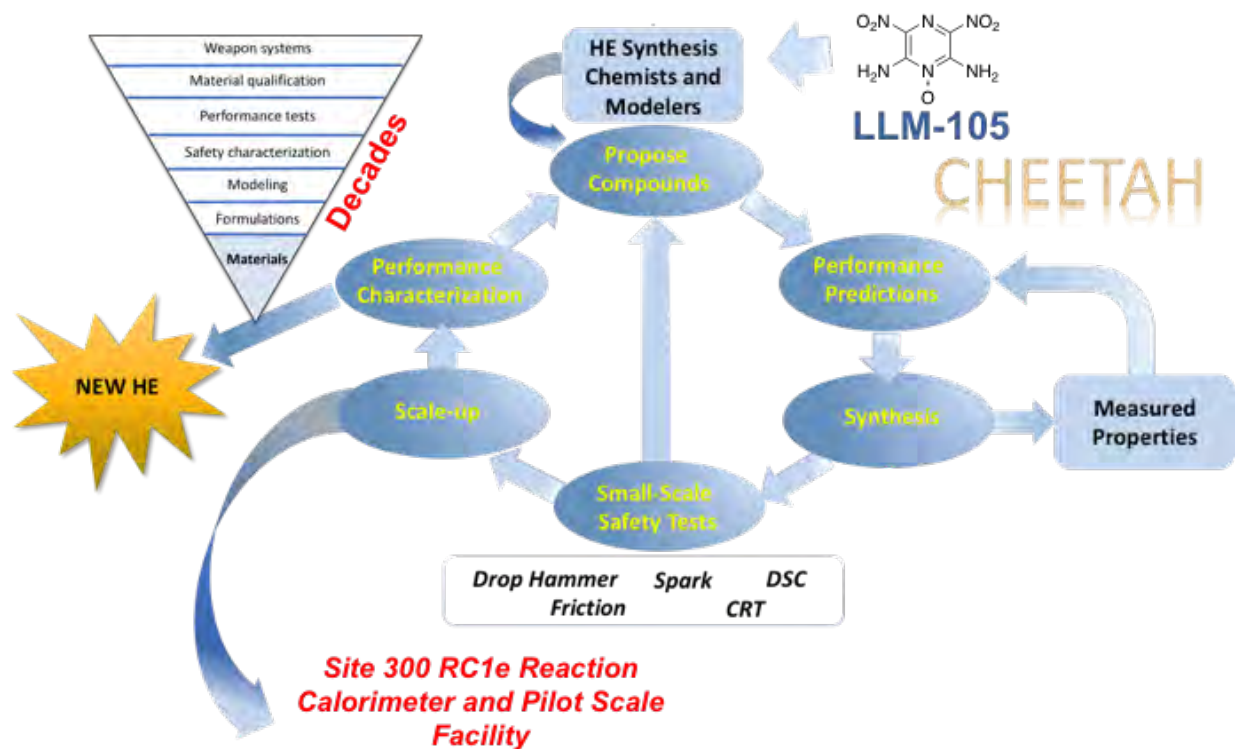


Figure 1 LLNL HE synthesis developmental process.

interdisciplinary collaboration in all facets of energetic materials science. The HEAF is a unique facility that allows for the conception and testing of new energetic materials, all under one roof (Figure 1). Within the HEAF, HE synthesis chemists can produce several gram quantities of new materials to determine its safe handling conditions (small-scale safety testing), density, heat of formation, and small-scale performance testing (Disc Accelerating eXperiment, DAX^{5,6}). As the inverse pyramid depicts in Figure 1, in order to progress from the bottom (materials) to the ultimate goal of weapons systems, candidate materials must be scaled to multi-kilogram quantities to allow for the refinement of formulations, scaled performance, and large-scale safety testing. For multi-kilogram scale syntheses of energetic materials and their precursors, the Livermore Experimental Test Site (Site 300) contains a newly renovated and modernized pilot facility scheduled to be complete in 2018. With the newly renovated facility and future plans to add new capabilities such as continuous process equipment, LLNL hopes to accelerate and streamline the transition of new HE materials to our production partners.

Discussion

With the intent to be a fully sufficient HE R&D institution, LLNL began the modernization and renovation of the Site 300 pilot facility in 2015, with design and demolition completed by mid-2016 in partnership with the Hart Design Group.⁷ The re-establishment of LLNL's pilot scale HE synthesis capabilities was a safety driven effort to transition from fully contact synthesis operations with large glass reactors, to a modernized and industrial class design with remote and automated features (Figure 2). The incorporation of remote capabilities and automation while still maintaining flexibility for a wide variety of synthetic processes (current and future) required a careful balance and compromise for the ultimate design and materials of construction. Eight comprehensive processes were evaluated to develop the final agile facility design. As will be discussed, the control of such a system requires a specialized, integrated software package.

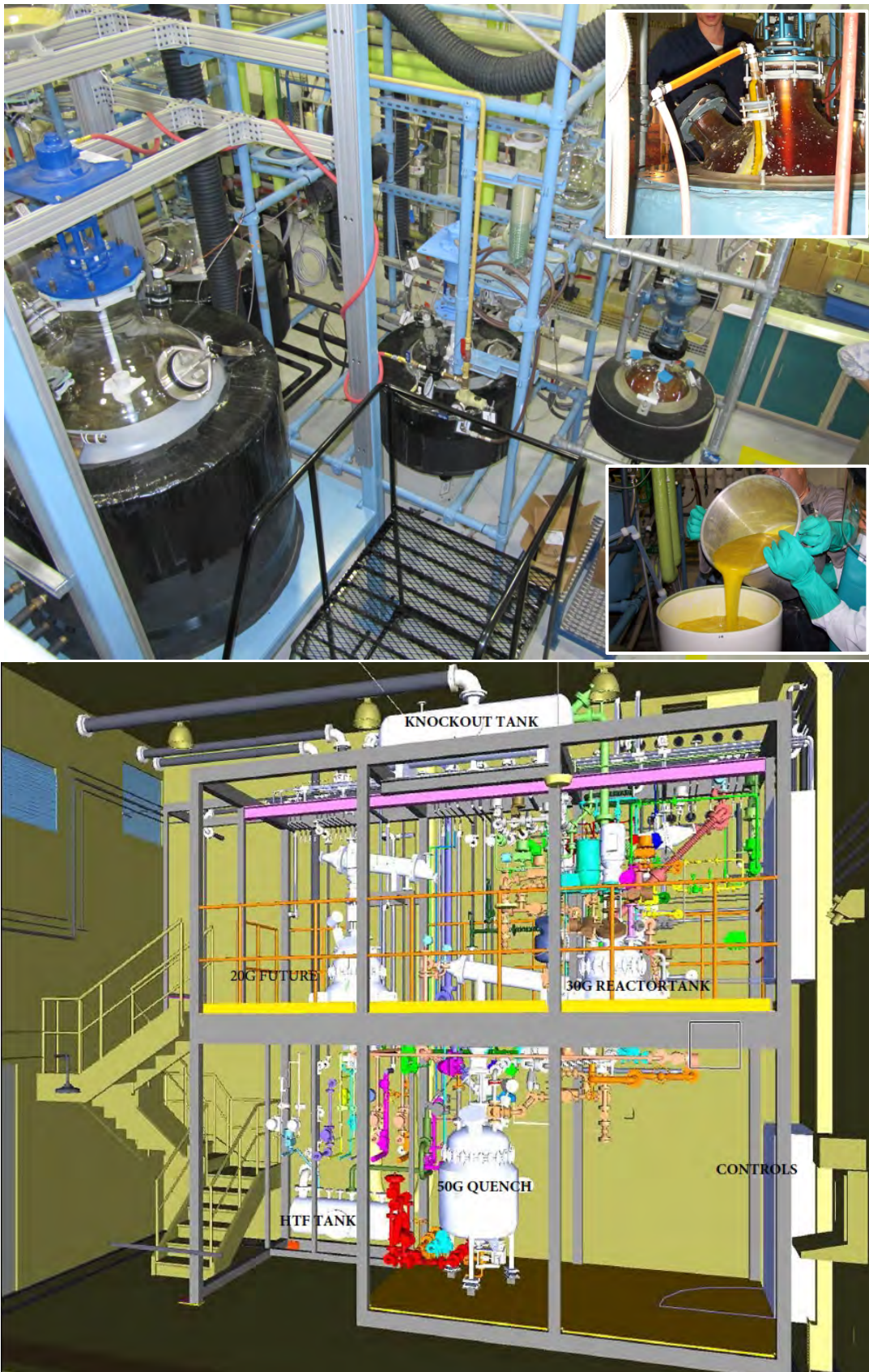


Figure 2 *Top:* Past LLNL pilot scale setup and contact manipulations. *Bottom:* 3D rendering of the modernized LLNL pilot facility with remote handling.

Facility and Pilot Skid Design

The safe scale-up of energetic materials syntheses reactions requires thorough planning, proper facilities, and an understanding of calculated risk. The last factor of calculated risk relates to the typical reaction processes for the preparation of high explosives, including nitration and oxidation conditions that generate high heats of reaction, unwanted, yet unavoidable decomposition pathways, and relatively unstable reaction products. In many instances, high explosive synthetic processes cannot be modified to a level of severity practiced in the majority of industrial production facilities.⁸ One example is in the preparation of the TATB precursor 1,3,5-trichloro-2,4,6-trinitrobenzene (TCTNB), which requires a one-pot trinitration of 1,3,5-trichlorobenzene in mixed acid at temperatures up to 150-155 °C. Reports studying the ideal synthesis conditions indicate that temperatures exceeding this range by only 5 °C leads to significant product loss through decomposition⁹, and 5-10 °C more leads to a runaway reaction and loss of containment.¹⁰ This example and the nature of high explosives chemistry dictates the attention that must be factored into facility design and process safety.

The layout of the LLNL pilot facility is shown in Figure 3. The building was originally constructed and designed to contain explosive materials with earthen berms surrounding three sides of the structure. All electrical and mechanical utilities were removed and replaced, and the two-story pilot skid components are in compliance with Class I/Division I electrical ratings for explosive proof electrical equipment. Where available, dual rated equipment was also used for both explosive vapor and dust.

In order to minimize hazards of contact transferring of reagents to the pilot reactors, the former storage room was converted to a remote reagent delivery room. Contained within a fume hood are air operated diaphragm pumps, a metering pump, and vacuum/nitrogen pressure delivery options from two weigh stations. Each weigh station is connected to the control software for either remote operation from the control room (separate building), or from two other human machine interfaces (HMI) located within the pilot facility. Depending on the nature of the liquid addition, full flow, temperature, and rate-controlled additions can be locally or remotely controlled with minimal worry of operator exposure. Remote chemical transfers are a simple way to minimize risk as many of the reagents would pose significant hazards to operators during a standard contact transfer operation.

With the eight processes evaluated, the ideal design for the pilot skid would have contained three reactors of 50 (future), 100, and 200 L. At a minimum, two reactors (100 and 200 L) were needed to perform the majority of processes including the first two campaign materials of LLM-105 and TATB. Attention then turned to material of construction and configuration design.

Material of construction for high explosives chemistry is a challenge as the three major reaction categories of nitration, oxidation, and amination require rather different materials of construction under ideal conditions. Glass is more than acceptable for these processes in a wide range of temperatures, and a certain degree of glass lining loss over time is expected. However, metal components are not unavoidable and further compromises must be made. All attempts were made to use hastelloy C (276 and 22), PTFE, ETFE, tantalum, stainless steel, and glass as wetted parts. Additional constraints for construction came into play due to the limited space above and below the reactors. Limited space is exemplified by the use of a single port and common header for all reagents into the reactor, including sparge nitrogen, liquids, and reactive gases. Multi-purposing was a key component used by Hart Design Group to fit all the required needs for reagent addition by utilizing a tube within a tube approach.

In a typical nitration reaction, for example the nitration of 2,6-diaminopyrazine-1-*N*-oxide (DAPO) to LLM-105, the 100 L vessel serves as the nitration pot and the 200 L reactor serves two purposes: 1) emergency or off-normal quench, and 2) normal quench/product precipitation. Under normal controlled quench conditions, the precipitated product would be filtered, rinsed, and collected. The pilot skid utilizes a Nutsche-type filter for additional processing of the final product by allowing temperature controlled re-slurrying of the product for a purer material, ultimately limiting additional handling and reprocessing of the explosive material.

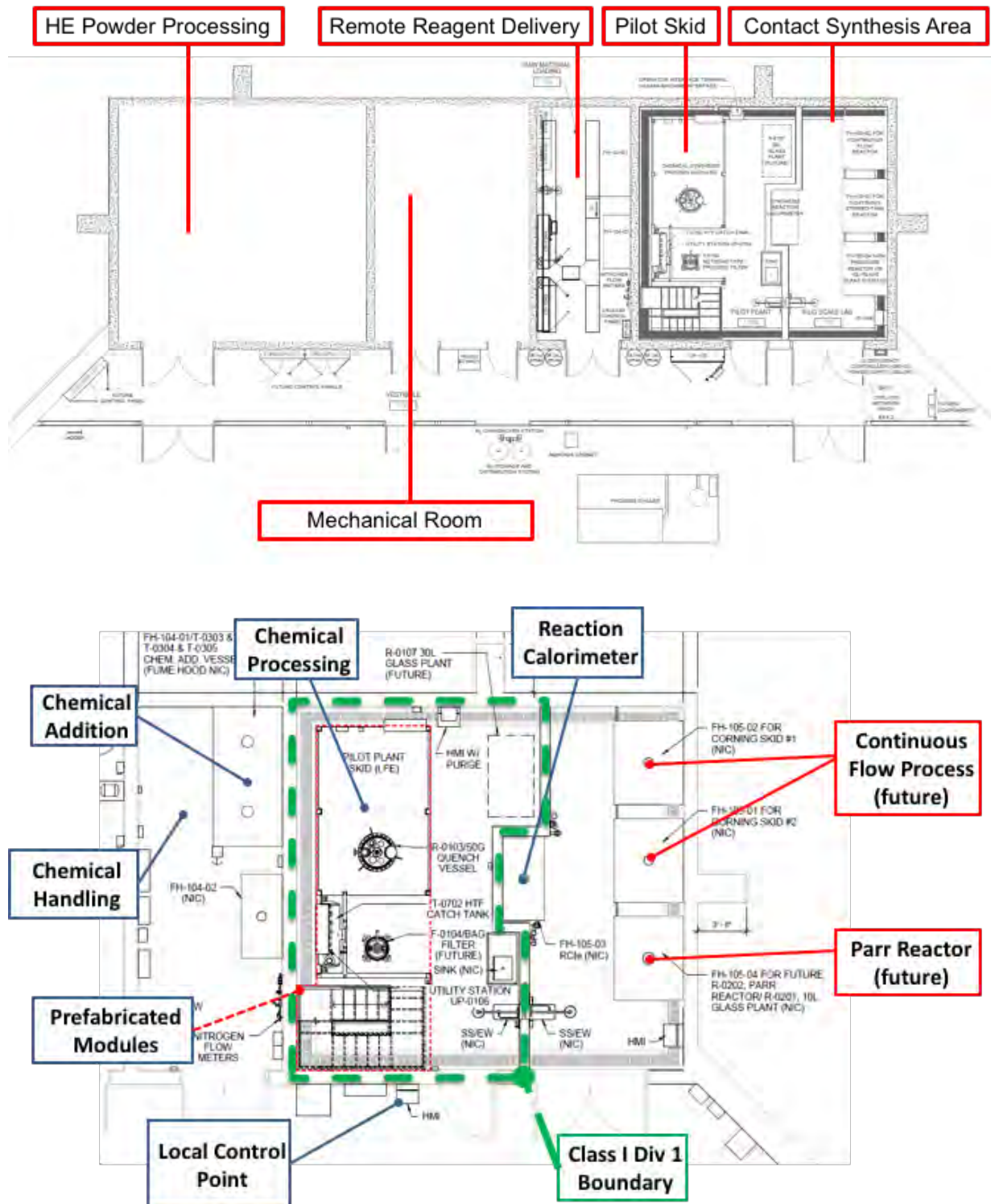


Figure 3 *Top*: Pilot facility basic floor plan. The two-story pilot skid is pushed to one side of the room and the room was then divided in half to allow for fume hood contained equipment for contact HE synthesis research. *Bottom*: Expansion of pilot skid/reagent delivery rooms and HE contact operations room. The pilot skid area is outfitted with explosives rated electronic equipment and enclosures. Directly next to the pilot skid is the reagent delivery fume hoods to allow remote transfers of liquid reagents. The general purpose contact synthesis area will contain a RC1e calorimeter and room for future expansion equipment.



Figure 4 Pilot skid installed at LLNL Site 300.

Pilot Reactors

- 50L Pfaudler w/sample loop (future)
- 100L Pfaudler w/sample loop
- 200L Pfaudler

Process Analytical Technology (PAT)

- Raman spectrometer
- pH Meter
- Cauty particle sizer
- Reaction monitoring camera

Ancillary Equipment

- Solids addition conveyor
- Molten addition funnel
- Remote liquid reagent addition
 - Air operated diaphragm pumps
 - Piston metering pump
- Ammonia gas cabinet
- Nutsche filter
- Bag filter
- Tantalum condensers
- RC1e reaction calorimeter

Industrial Control SCADA Software

From reagent addition, process monitoring, to material collection, the new pilot skids provide significant reductions in operator contact operations and the likely risk of chemical and related exposure to employees is greatly reduced. This is all made possible by the careful design of the Supervisory Control and Data Acquisition (SCADA) control software (CS) developed by LLNL and Avanceon.¹¹

The complexity of the required control software is portrayed in the P&ID below (Figure 5, top), which is only one subset of many components in the pilot skid (excluding weigh stations

for reagent delivery, quench reactor, and all other connected components). In summary, the control software contains over 1,180 alarms, 800+ I/O points, 100+ automated control valves, 160 phase operations (temperature control, transfer segments, agitation speed, etc.), and 111+ interlocks, which are all detailed in the control system functional specification of greater than 415 pages. The complexity of the control software leads to a simplified and safer process for the operator, as can be seen in the depiction of the same P&ID of the 100L reactor in the top of Figure 5 (bottom).

One may notice that although the control screen in Figure 5 is simplified, there is an absence of vibrant colors. This is done intentionally to follow the practice of HMI "situational awareness" whereby color is used in a consistent manner to draw attention to items of need. For example, alarms have different levels of severity, and yellow, light blue, pink, and red will all have different meanings for an alarm event. Essentially, in a generally bland background of light and dark grey, the operator is more likely to have their attention drawn to an event with a flashing color that is consistently utilized.

The software platform chosen by LLNL as the basis for the Avanceon prepared CS is Wonderware[®]. This software platform provides a completely customizable and expandable product that allows for commercial off-the-shelf (COTS) instrument/part integration and is used by many industrial facilities worldwide. This aspect is important to LLNL as transitioning our processes to our industry partners is the overall goal of our pilot facility. Additionally, the pilot skids will utilize Wonderware's[®] InBatch software product, which is consistent with the ISA-88¹² standard for batch management processes, providing assurance that all necessary information from batch to batch is appropriately captured and documented. The use of InBatch will provide batch parameter control, but it will also provide operational safety by utilizing a set recipe for each run, which can limit the automation of each step as well as the level of approval at each step (dual sign-off requirements and custom security settings). As the pilot batch runs will still be R&D processes, flexibility to adjust the recipe or to have some leeway during a process is desired. Accounting for flexibility with upper and lower bounds and logic loops can be integrated into the recipe. However, the CS is also designed to allow overriding for manual operation of individual valves, if necessary.

Other key functions of the CS that are built in, are the integration of low-low, low, high, and high-high alarms for individual instrument responses depending on the process. For example, for exothermic reagent additions, the reaction temperature alarms can be adjusted to initiate different system responses based on the severity of the upper and lower bounds from stopping reagent addition, to initiating an immediate system cooldown. In addition to the CS safety functions are hardware interlocks that are tripped in events such as power outage and seismic activity. These interlocks can also be tripped via operator initiated emergency stops, and facility door interlocks.

Over time, it is anticipated that changes/additions to equipment, modifications to control screens, and tweaking of automated valve sequence events will be necessary for improved performance and to enhance safety features despite our best efforts to put forth the best CS possible. The chosen software platform allows for this necessary flexibility and a refined system focused on operator safety, process safety, and process efficiency will evolve over time.

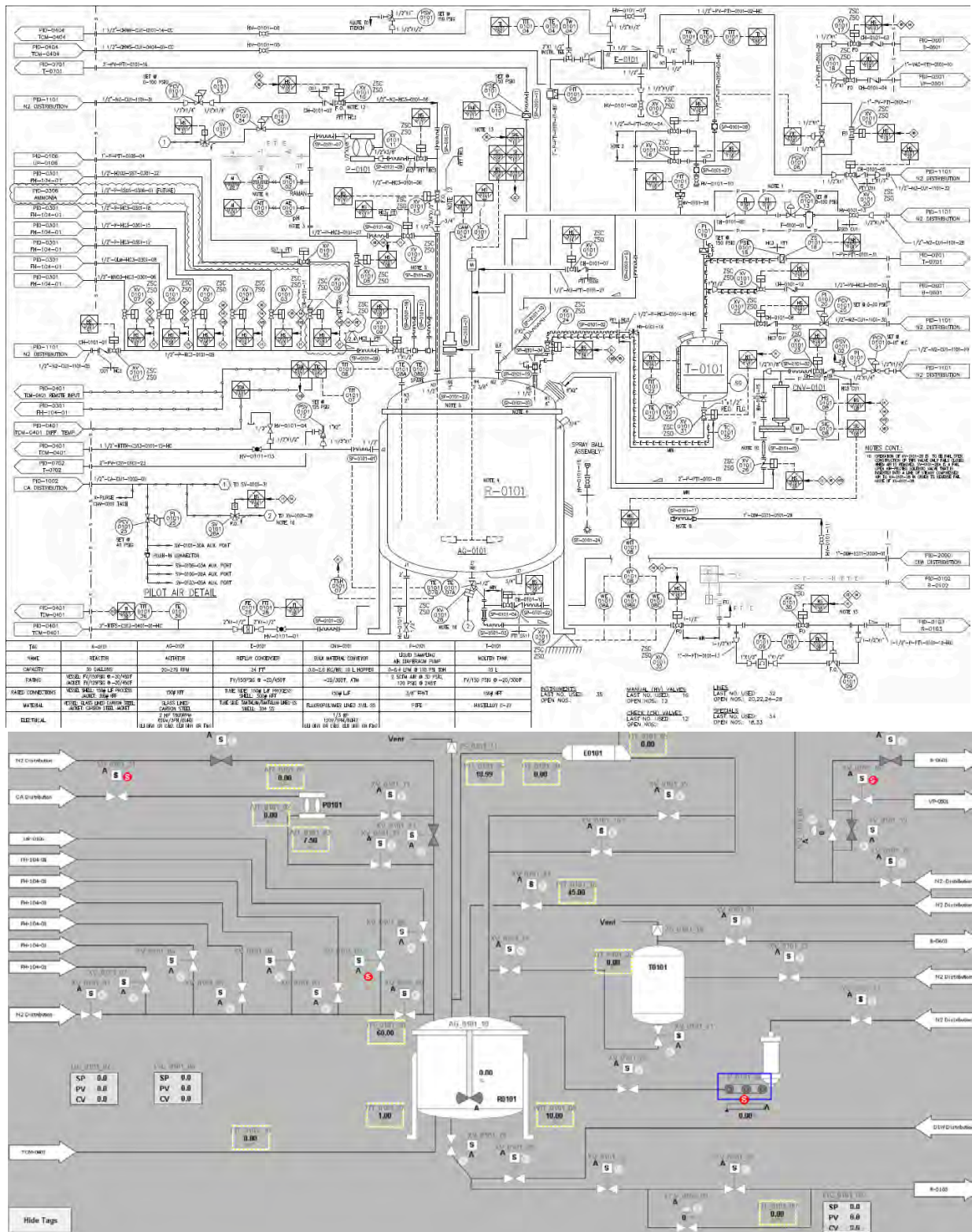


Figure 5 Top: P&ID of 100 L glass-lined carbon steel reactor with associated inputs, outputs, valves, and utilities. Key components include reagent header with ammonia and hydrogen peroxide capabilities, and a molten addition tank. Bottom: Rendering of the industrial control software graphical user interface for the same reactor depicted above. Colouring is in line with “situational awareness” scheme where shades of grey indicate on/off and red, yellow, blue are meant to draw attention to immediate needs.

Conclusion

LLNL's new energetic materials synthesis facility provides a safe, remotely controlled skid for a variety of synthetic processes. The following is a summary of the skid capabilities. The reactors are rated for operating pressures of up to 135 psi and all wetted parts include glass-lined carbon steel vessels, hastelloy, tantalum, and PTFE. Reaction temperatures of -10 to 170 °C are possible with the current combination of heat transfer fluid and thermal control units. The ability to add ammonia (vaporizer) to both 100L and 200L vessels will allow for the synthesis of energetic compounds such as TATB. Hydrogen peroxide dosing can be used with the incorporation of a special PTFE coated line. Solids can be metered via conveyor, which is also rate controlled capable through the CS. All liquid reagent additions are remotely controlled via metering pump, diaphragm pump, vacuum, or pressure. Flexibility for various synthetic methods is available through the ability to phase separate, distill, and recirculate between vessels. A sample loop on the 100L vessel contains three inputs for the in-situ monitoring of reaction conditions with Raman and pH currently installed. Clean in place (CIP) is available with InBatch® automated recipe development. Final product isolation and impurity removal is accomplished with a Nutsche and bag filter respectively.

Acknowledgements

The authors would like to thank funding sources from DOE and NNSA Headquarters as well as contributions from LLNL's Mark Coons, Jeff Packard, Steve Chan, Kenn Knittel, Veronica Harwood, Lou Bertolini, Lou Ferranti, Mao Xi Zhang, Spencer Vartanian, Levi Merrell, Yong Han, Lara Leininger, Jon Maienschein, Sabrina DePiero, Mark Zagar, Kevin Vandersall, Kevin Merrell, Barbara Jesus, Hiroshi Saito, Dawn Kramer, Shari Brigdon, Alex Gash, George Overturf, Ken Newman, Wes Davis, Dave Hill, John Scott, Deanna Kahmke, Kim Elam, Donovan Day, Annette Warner, Cameron Cornell, and Trini Gonzalez, as well as subcontractors Hart Design Group, Hart Engineering (facility design and fabrication), RORE Inc. (construction installation), Total Facility Solutions (mechanical systems), Wilhite (electrical), Avanceon (control software), Nalas Engineering (process hazard analysis). This work performed under the auspices of the U.S. Department of Energy by Lawrence Livermore National Laboratory under Contract DE-AC52-07NA27344. LLNL-PROC- 749068.

References

- 1 Pagoria, P. "A Comparison of the Structure, Synthesis, and Properties of Insensitive Energetic Compounds" *Propellants Explos. Pyrotech.* **2016**, *41*, 452–469.
- 2 Pagoria, P.; Zhang, M. X.; Zuckerman, N. B.; Lee, G.; Mitchell, A.; DeHope, A.; Gash, A.; Coon, C.; Gallagher, P. "Synthetic Studies of 2,6-Diamino-3,5-Dinitropyrazine-1-Oxide (LLM-105) from Discovery to Multi-Kilogram Scale" *Propellants Explos. Pyrotech.* **2017**, *43*, 15–27.
- 3 Zuckerman, N. B.; Shusteff, M.; Pagoria, P. F.; Gash, A. E. "Microreactor Flow Synthesis of the Secondary High Explosive 2,6-Diamino-3,5-Dinitropyrazine-1-Oxide (LLM-105)" *J. Flow. Chem.* **2015**, *5*, 178–182.
- 4 Pagoria, P. F.; Zhang, M. X.; Zuckerman, N. B.; DeHope, A. J.; Parrish, D. A. "Synthesis and Characterization of Multicyclic Oxadiazoles and 1-Hydroxytetrazoles as Energetic Materials" *Chem. Heterocycl. Compd.* **2017**, *53*, 760–778.
- 5 Lorenz, K. T.; Lee, E. L.; Chambers, R. "A Simple and Rapid Evaluation of Explosive Performance- The Disc Acceleration Experiment" *Propellants Explos. Pyrotech.* **2015**, *40*, 95–108.
- 6 DeHope, A.; Zhang, M.; Lorenz, K. T.; Lee, E.; Parrish, D.; Pagoria, P. F. "Synthesis and Small-scale Performance Characterization of New Insensitive Energetic Compounds" *IMEMTS*, Rome, Italy, **2015**.
- 7 Design and construction subcontracted to Hart Design Group and Hart Engineering, Cumberland, Rhode Island, 02684.

- ⁸ Stoessel, F. "Thermal Safety of Chemical Processes, Risk Assessment and Process Design" **2008**, Weinheim: Wiley-VCH.
- ⁹ Benziger, T. M. "Manufacture of Triaminotrinitrobenzene" presented at *Internationale Jahrestagung - Fraunhofer-Institut fuer Treib- und Explosivstoffe*, **1981** (LA-UR-81-992).
- ¹⁰ Quinlin, W. T.; Estes, Z. L.; Evans, V. H.; Schaffer, C. L. "Pilot Scale Synthesis of TATB" **1976**, Report MHSMP-76-20.
- ¹¹ Avanceon of Exton, PA prepared the control software in accordance with LLNL specifications.
- ¹² ANSI/ISA-88 or S88 standard: ANSI/ISA-88.01-2010, ANSI/ISA-88.00.02-2001, ANSI/ISA-88.00.03-2003, ANSI/ISA-88.00.04-2006, ISA-TR88.00.02-2008.

Modernization and Capabilities of the Lawrence Livermore National Laboratory Pilot Facility for Remotely Controlled Energetic Materials Synthesis

Insensitive Munitions and Energetic Materials Technology Symposium,
Portland, Oregon

April 22-26, 2018

Nathaniel B. Zuckerman

P. F. Pagoria, A. J. DeHope, E. F. Virgin III, F. E. Wade, W. L. Collins, B. K. Parsons



LLNL-PRES-748549

This work was performed under the auspices of the U.S. Department of Energy by Lawrence Livermore National Laboratory under Contract DE-AC52-07NA27344. Lawrence Livermore National Security, LLC

LLNL Energetic Materials Synthesis Group

- Six PhD synthesis chemists with primary residence in the LLNL High Explosives Applications Facility (HEAF, Site 200)

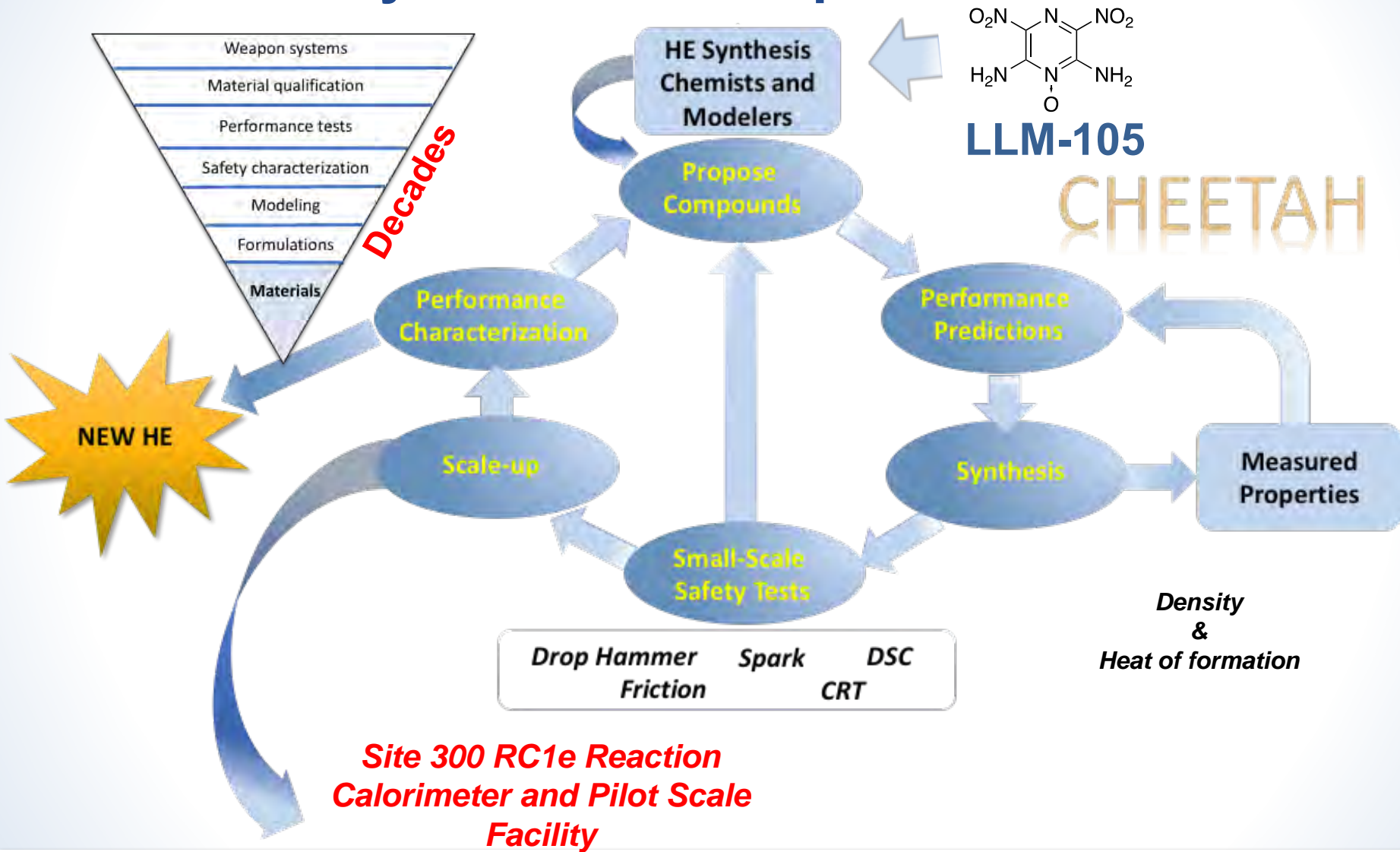


LLNL Energetic Materials Synthesis Group

- Six PhD synthesis chemists with primary residence in the LLNL High Explosives Applications Facility (HEAF, Site 200)
- **Focus:** Synthesis of new insensitive high explosives (IHE) and conventional high explosives (CHE)
- Synthesis group supports :
 - Basic explosives R&D
 - Stockpile stewardship
 - Counterterrorism
 - Development of HE for military and commercial use



LLNL HE Synthesis Developmental Process



LLNL HE Synthesis Developmental Process

- **Small-scale R&D:** Aim to provide enough information on new HE to “put it on the shelf” and make it available as needs arise from customers.
 - Safety testing: Friction, spark, impact, thermal stability.
 - Heat of formation, density and small scale performance
- **Down-select and scale-up:** Perform small scale reaction calorimetry and synthesize multi-gram quantities.
 - Formulation and pressing studies, ODTX, detonation calorimetry
- **Pilot Scale Process:** Full safety analysis of a synthetic process before pilot scale synthesis conducted. Aim to make 1-2 kg scale before transitioning process outside LLNL.

LLNL working toward enhancing efficiency of new material qualification.

LLNL and Site 300 HE Synthesis Capability

- **HEAF synthesis capabilities:** 1 kg, typically < 95 g.
 - Small-scale safety testing, calorimetry, and performance testing.
- **Livermore's Experimental Test Site, Site 300 (S300):** Provides pilot scale synthesis and formulation capabilities for several kilogram quantities of HE (827D).
- **S300 synthesis capabilities have not been utilized since 2013.**

HEAF Bench Scale

(A) Round bottom flask,
(B) Automated
synthesis work station,
(C) Modular continuous
flow reactor



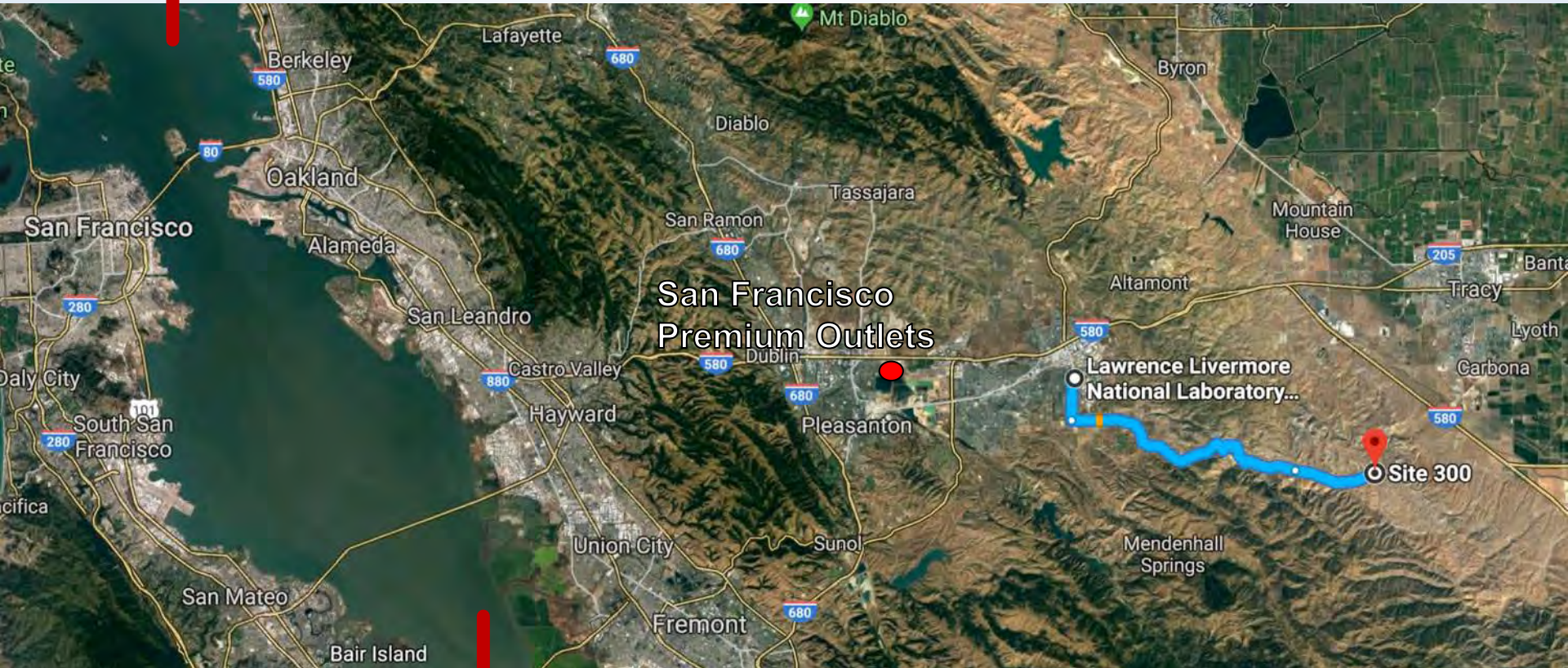
Need for Pilot Scale HE Synthesis at LLNL

- Viable new HE materials must have a scalable and cost effective synthetic and purification process.
- Determination of viability requires significant material for testing.
 - *Sub-100 g quantities*: initial handling safety, chemical and physical properties, and small-scale performance testing.
 - *Multi-kilo quantities*: required for formulation, pressing, and large scale performance and safety studies.
- Design and planning for the modernization and renovation of 827D began in early 2016 with subcontractor Hart Design Group (Cumberland, Rhode Island).
- **LLNL HE chemists strive to transition a fully scalable synthesis and purification process for new materials.**

LLNL is dedicated to R&D and is not a production facility.

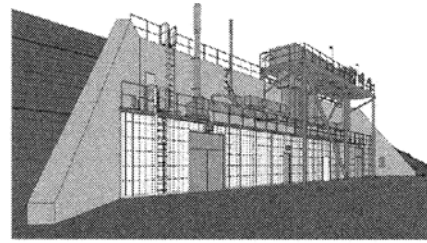
San Francisco Bay area and Site 300

Napa
↑

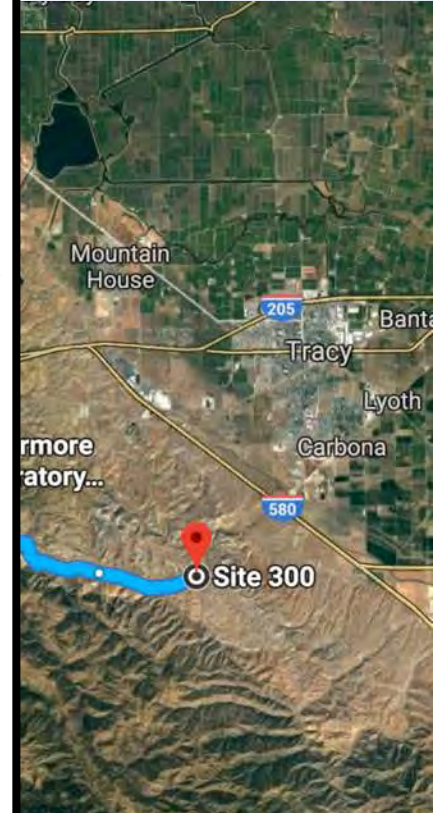
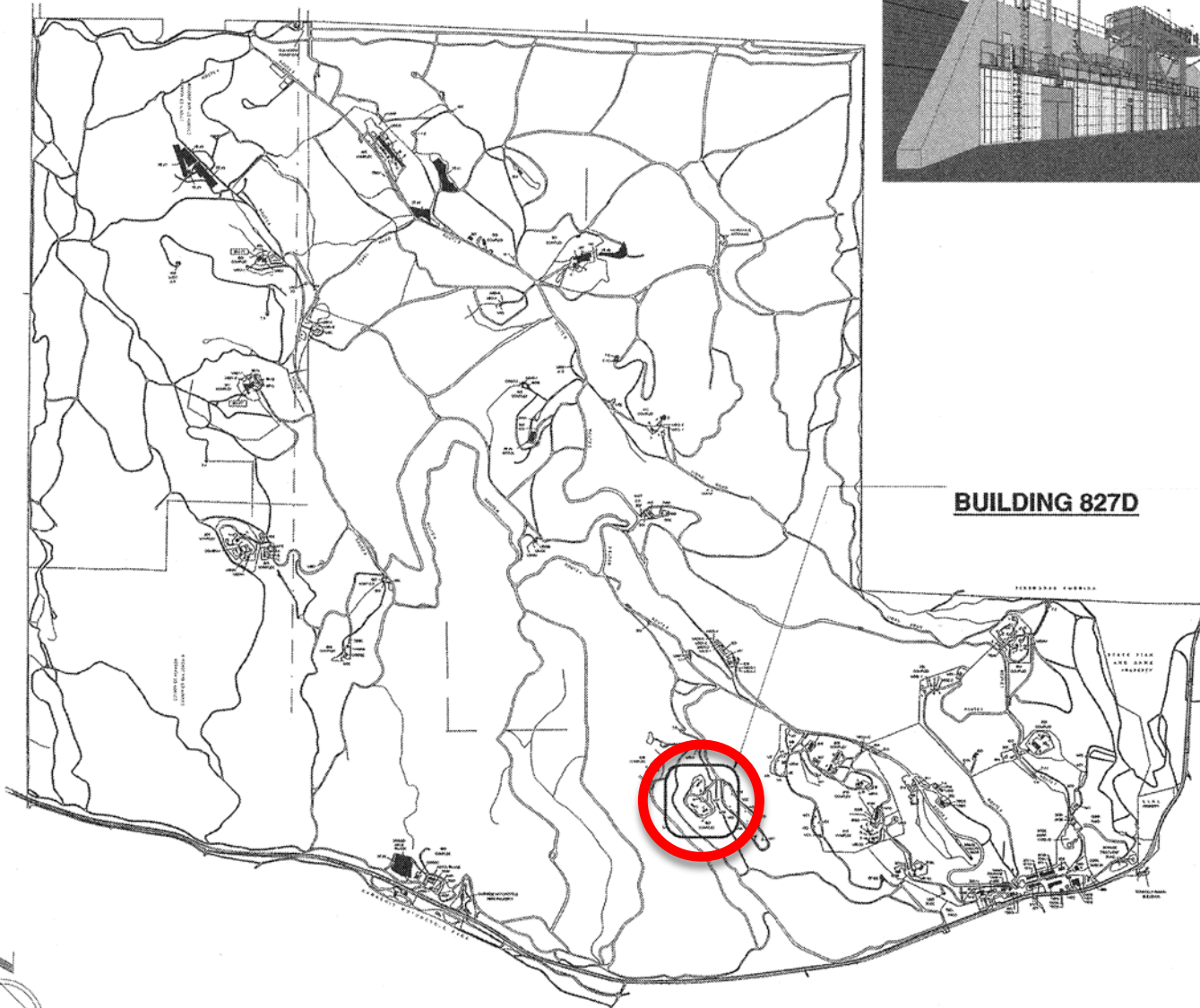


↓
San José

Google Maps



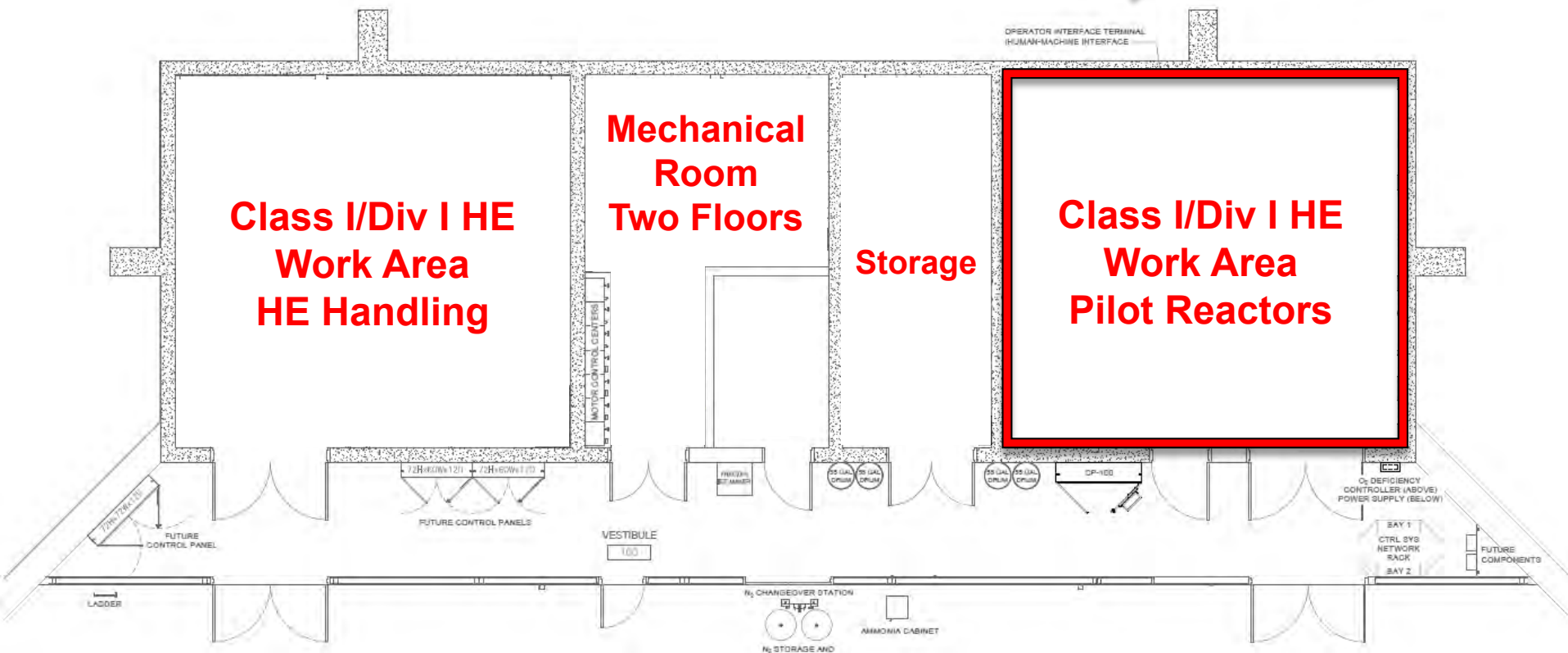
BUILDING 827D



Site 300: 7,000 acres rural foothills

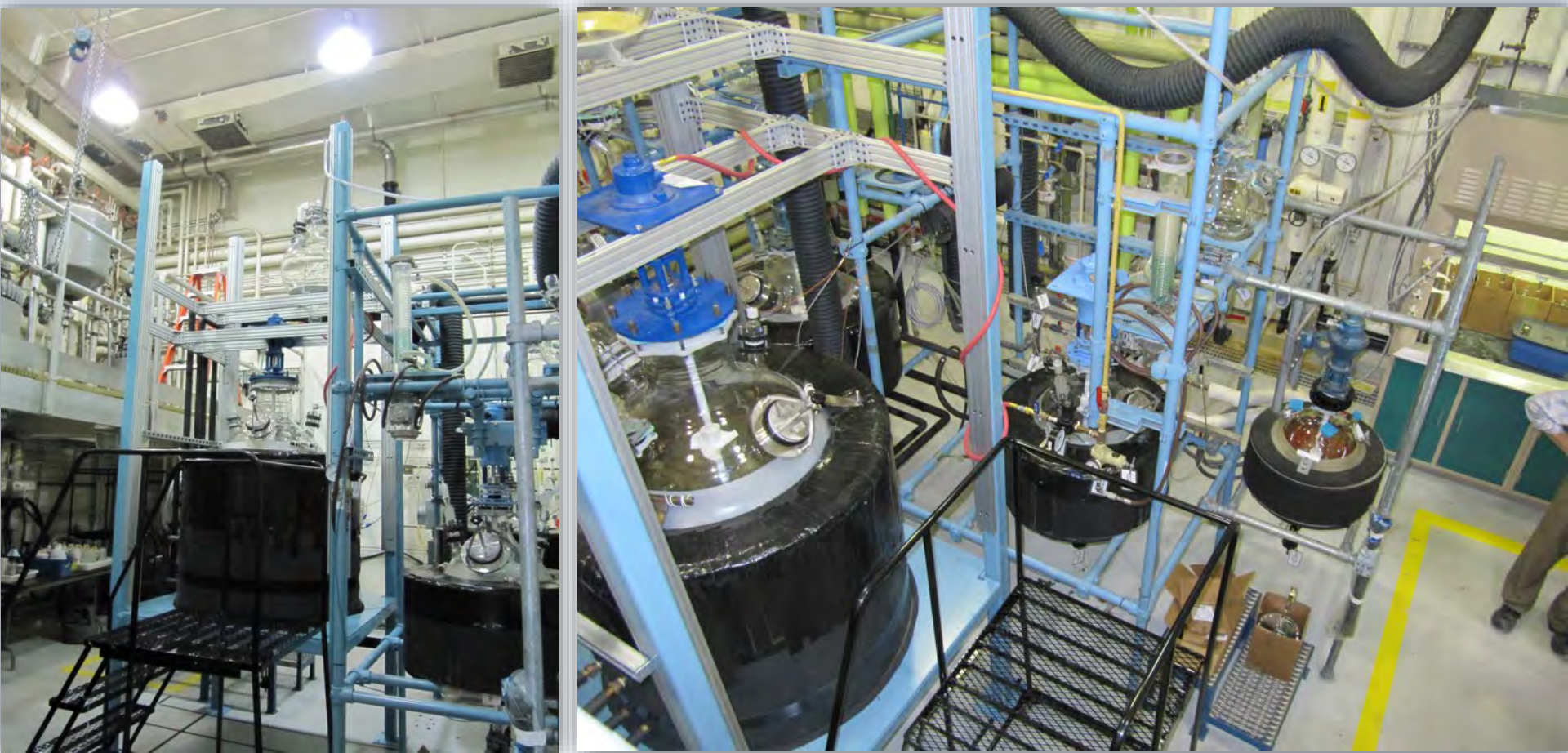
HE Synthesis: 827D First Floor Layout and Former Utilization of Space

827A Control Room



827A Control room about 150 yards away

Former Glass Pilot Scale Reactors



Out of commission since 2013 and demoed in 2015.

Pilot Facility Operations in Recent Past

- Pilot operations were hands on, contact operations: “bucket” chemistry.
- Heavily reliant on operator monitoring of processes and manual transfers of hazardous chemicals.
- Capability for remote operations were very limited.



Safety driven renovation and modernization began in 2015.

Modernization Project Focused on Remote Capabilities and an Agile Facility

- As an R&D facility, flexibility in synthesis is required.
 - Very difficult (and expensive) to meet the demands of all chemistry in one system.
- Desire to convert hands-on processes to majority remote processes adds difficulty and cost.
 - Specialized custom software required.
 - In-situ reaction and process monitoring required.
- A completely remote system is extremely cost-prohibitive and not necessary for all steps in a process.
- Agility can be added by having modular reactors and separate scalable capabilities: continuous flow processes, high pressure reactors, and pilot vessels of varied materials of construction.

Recipe for an Agile Pilot Facility

- 8 chemical processes were considered that encompass the entire range of anticipated synthesis schemes to develop the list below:

Pilot Reactors

- 50L Pfaudler w/sample loop (future)
- 100L Pfaudler w/sample loop
- 200L Pfaudler

Process Analytical Technology (PAT)

- Raman spectrometer
- pH Meter
- Canty particle sizer
- Reaction monitoring camera

Ancillary Equipment

- Solids addition conveyor
- Molten addition funnel
- Remote liquid reagent addition
 - Air operated diaphragm pumps
 - Piston metering pump
- Ammonia gas cabinet
- Nutsche filter
- Bag filter
- Tantalum condensers
- RC1e reaction calorimeter

Fully integrated industrial control software.

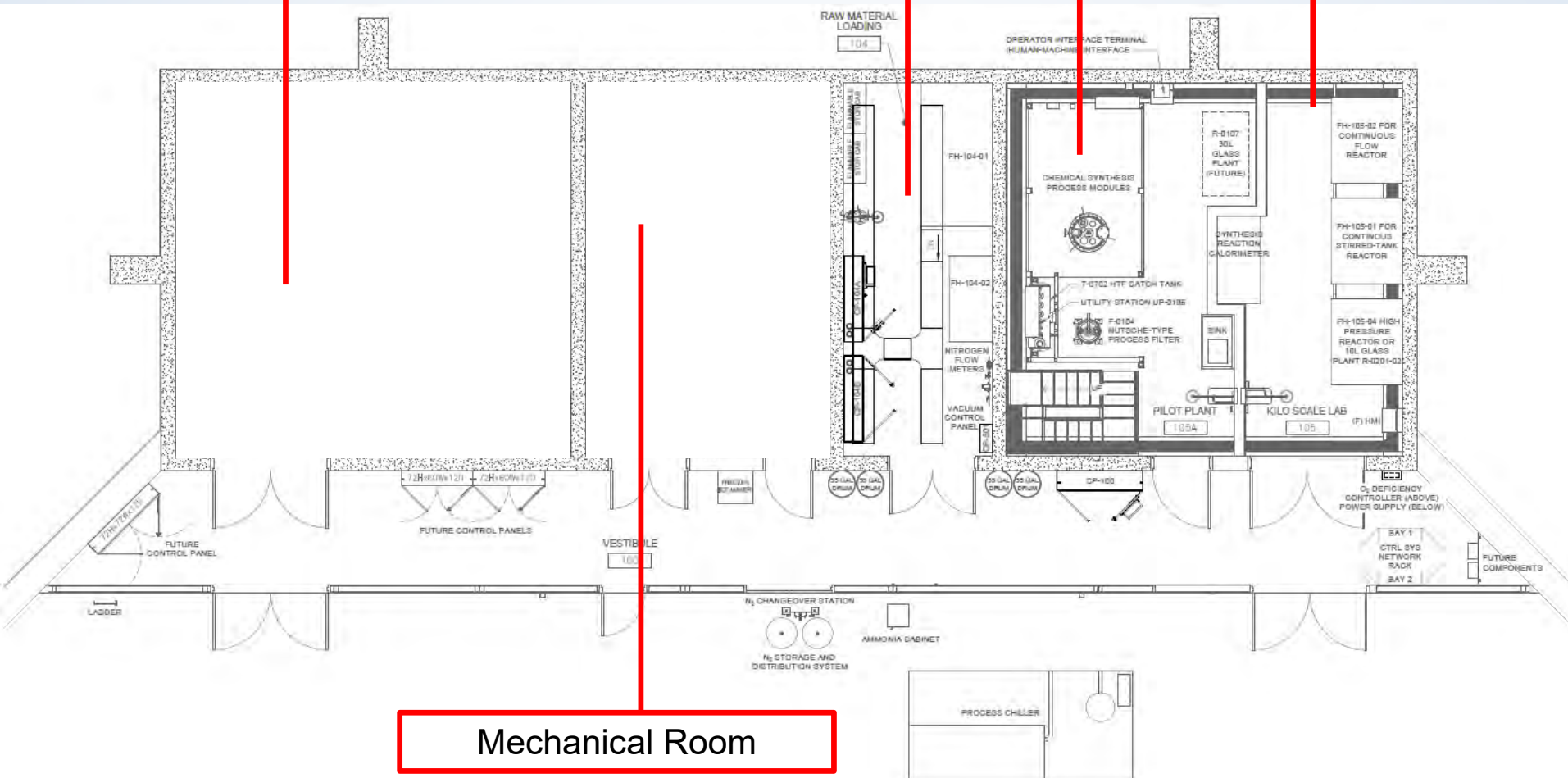
Renovated 827D First Floor Layout

HE Powder Processing

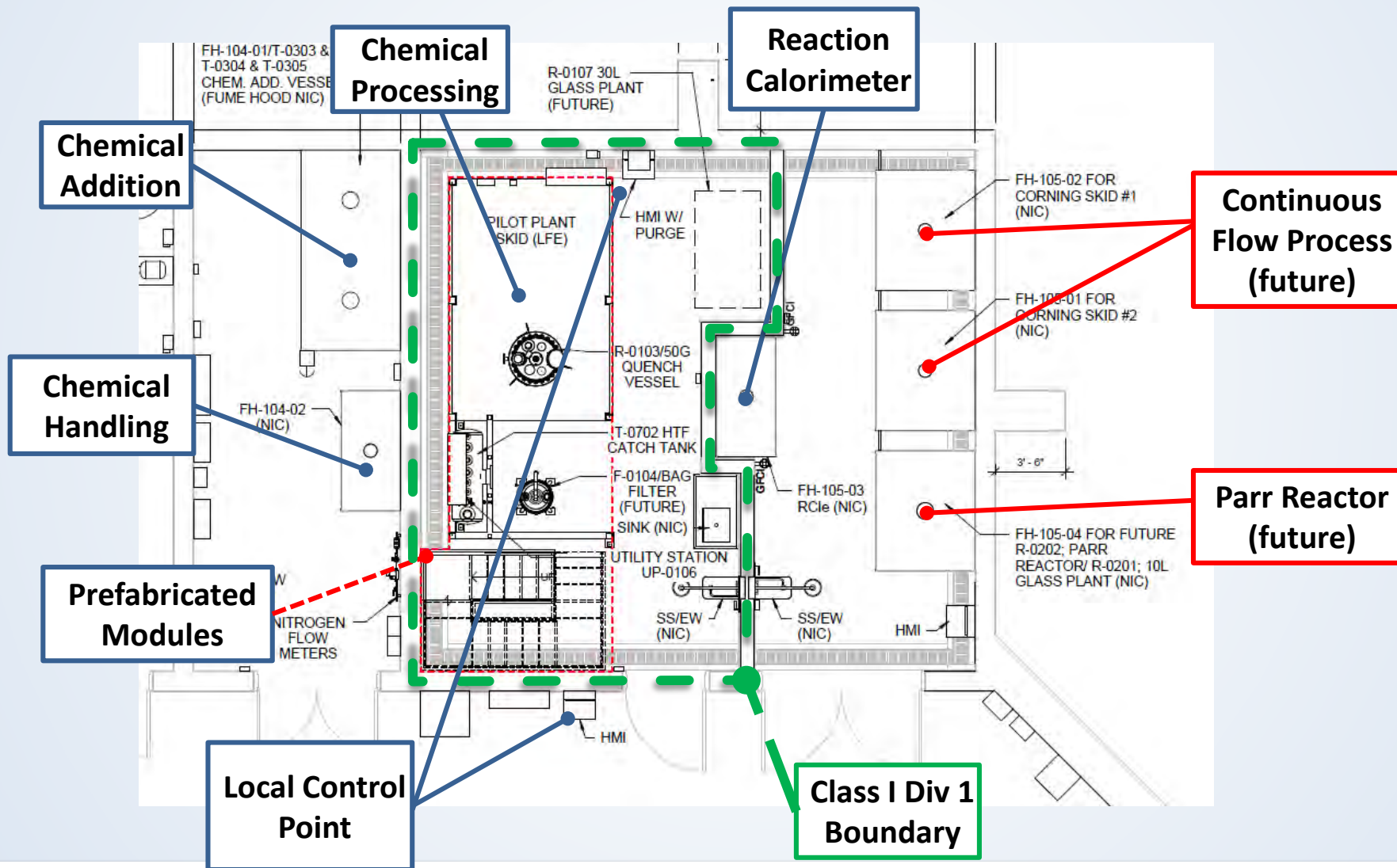
Remote Reagent Delivery

Pilot Skid

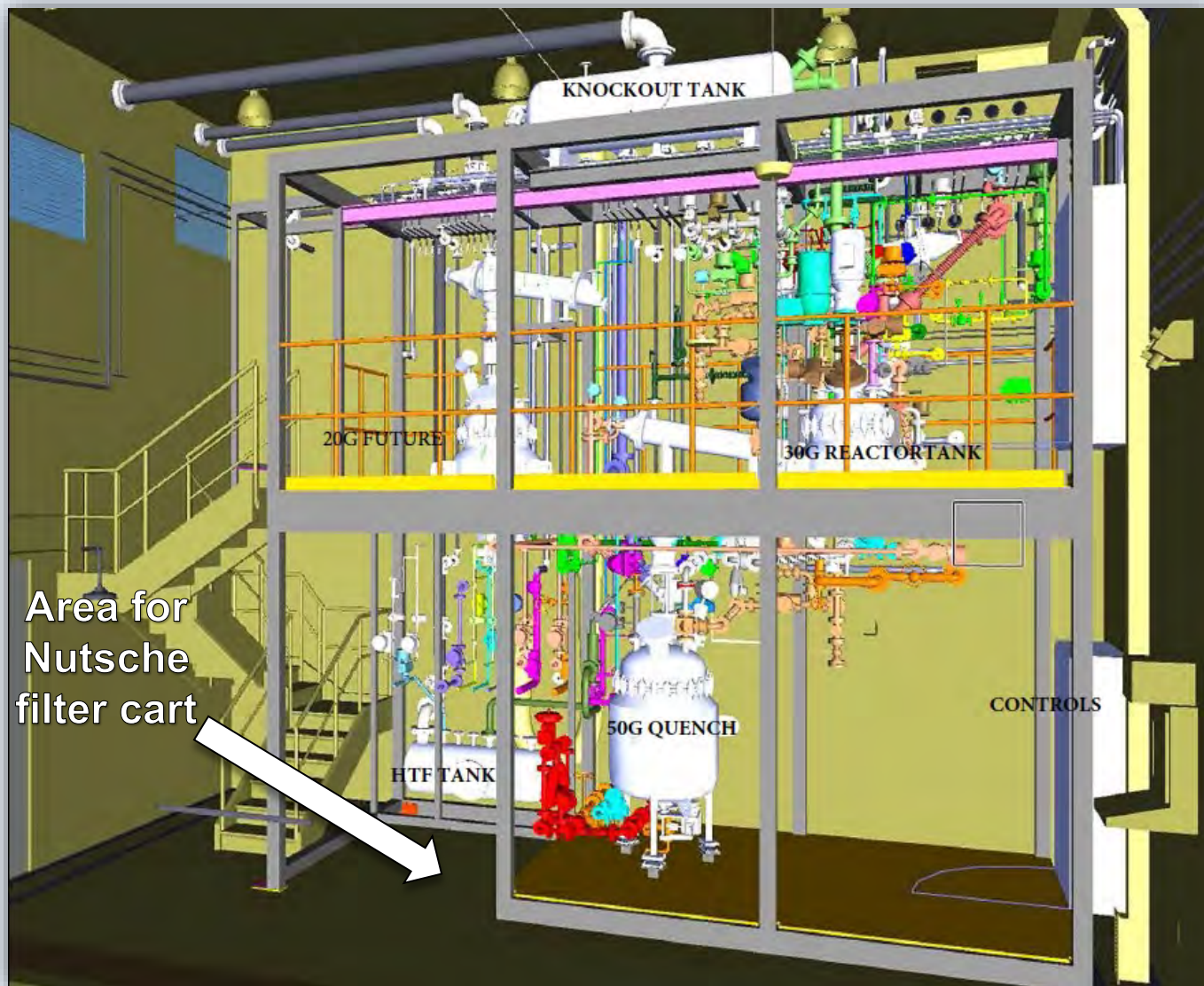
Contact Synthesis Area



Pilot Skids, Reagent Delivery, and General Purpose Scale-up area



3D Model of Pilot Reactor Skid



Constructed Pilot Skid



Pilot Skids at
Fabrication:
Hart,
Cumberland, RI

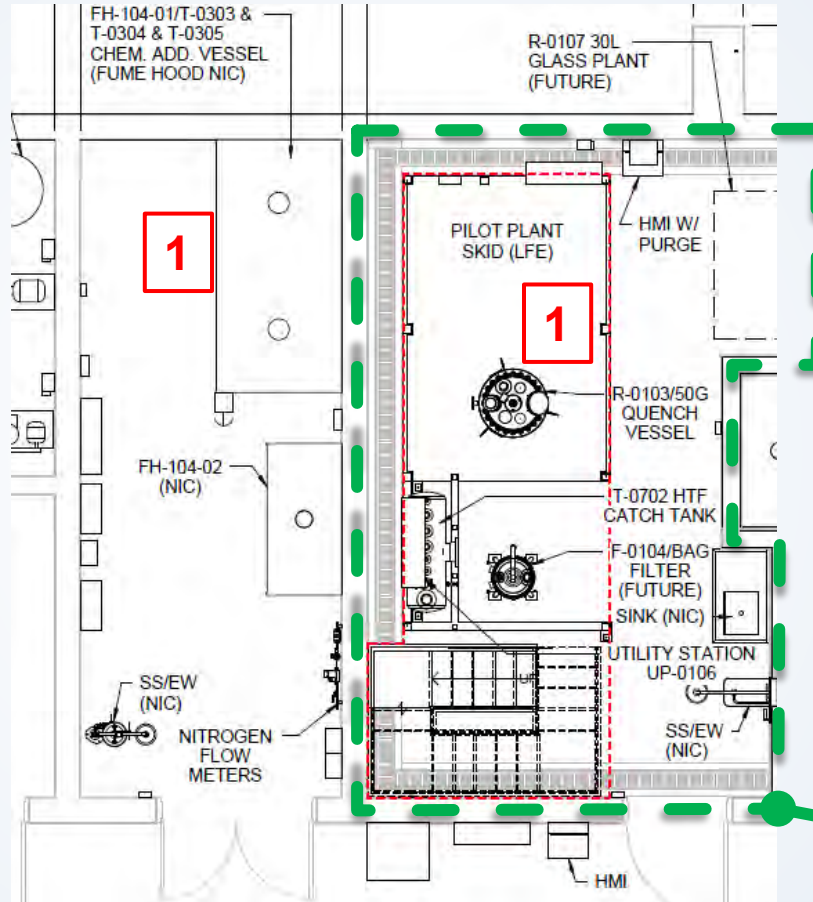
Pilot Skid Critical
Lift and Installation:
B827D, Site 300



Typical Synthetic Process in Pilot Skid: Nitration

1. Load liquid and solid reagents

Contact operation conducted in a fume hood.

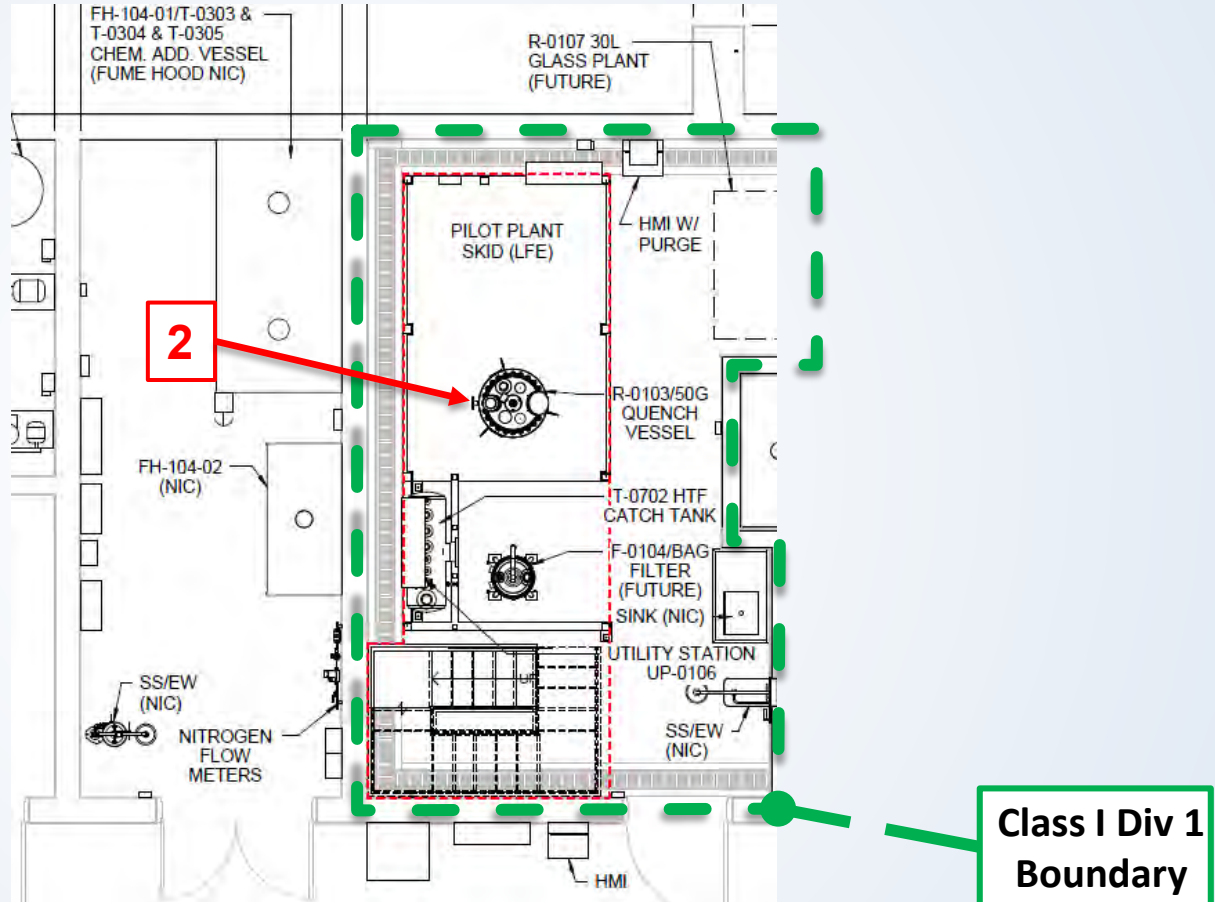


**Class I Div 1
Boundary**

Typical Synthetic Process in Pilot Skid: Nitration

1. Load liquid and solid reagents
2. Charge solvent (sulfuric acid)

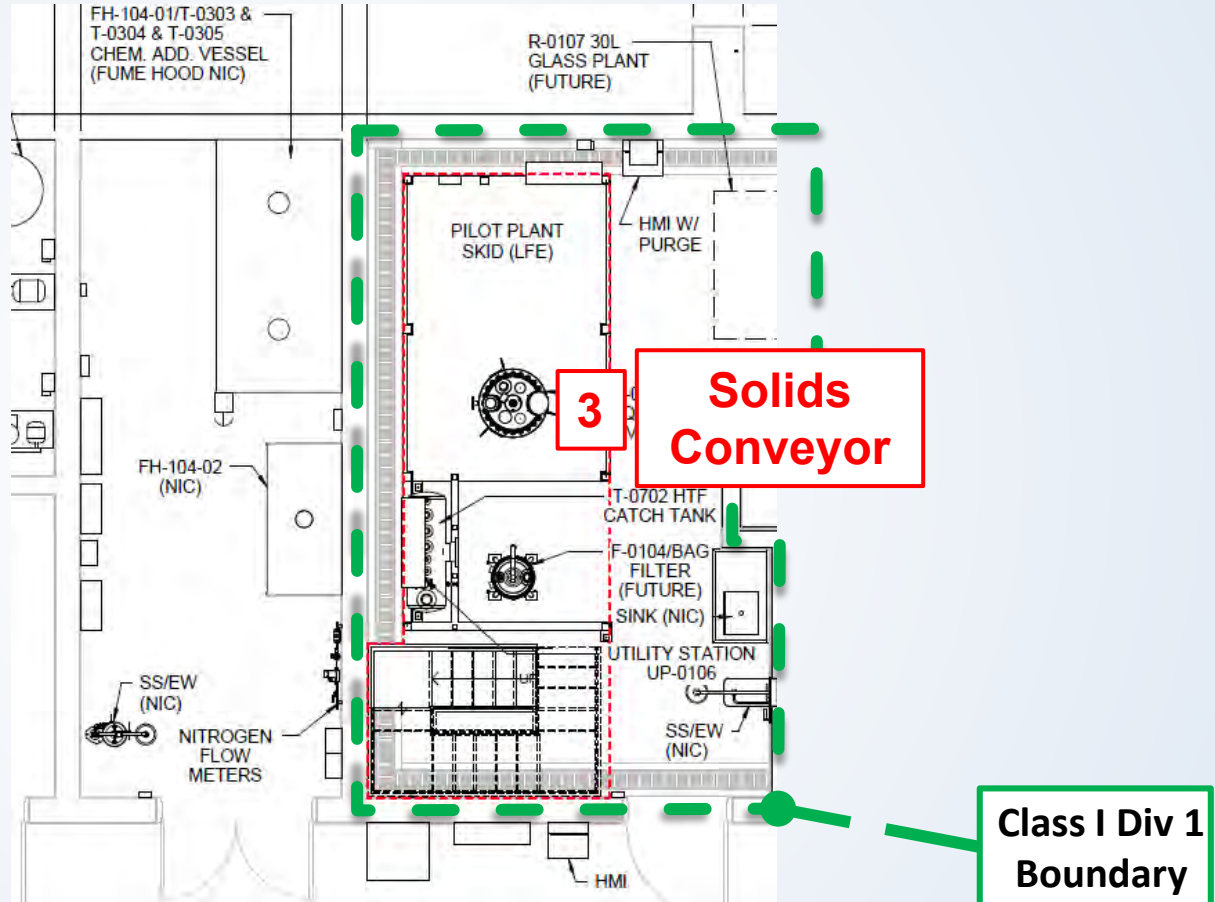
Remote operation conducted from any of the HMI stations.



Typical Synthetic Process in Pilot Skid: Nitration

1. Load liquid and solid reagents
2. Charge solvent (sulfuric acid)
3. Dose/dissolve starting material.

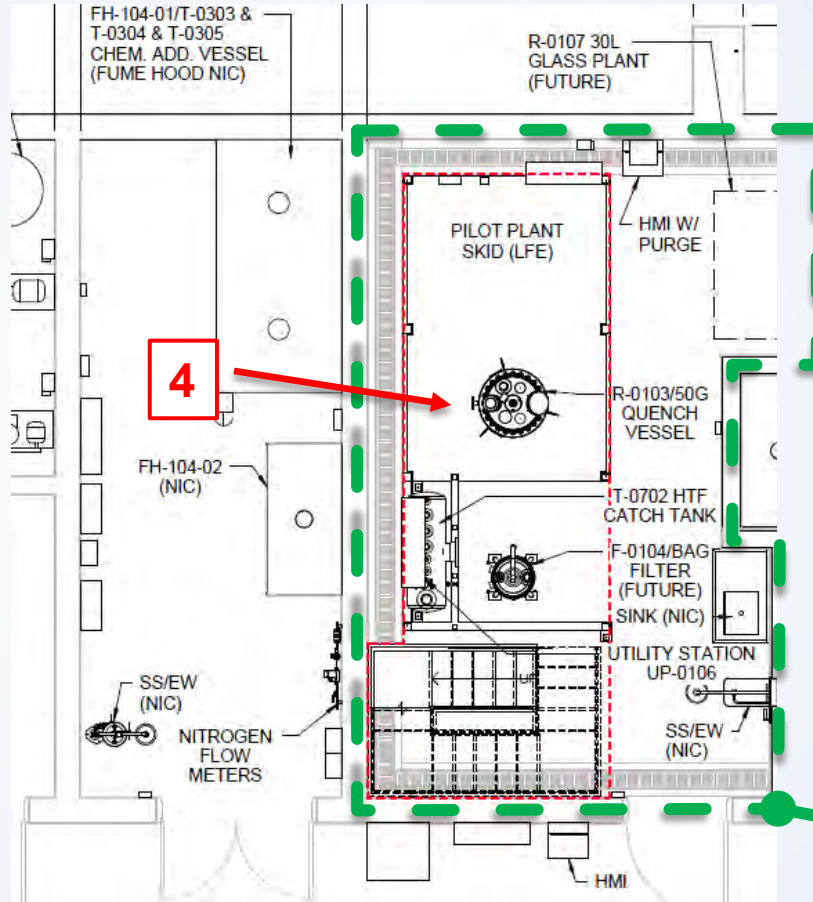
**Remote operation
from HMI.**



Typical Synthetic Process in Pilot Skid: Nitration

1. Load liquid and solid reagents
2. Charge solvent (sulfuric acid)
3. Dose/dissolve starting material.
4. Dose nitric acid.

**Remote operation
from Control
Room.**

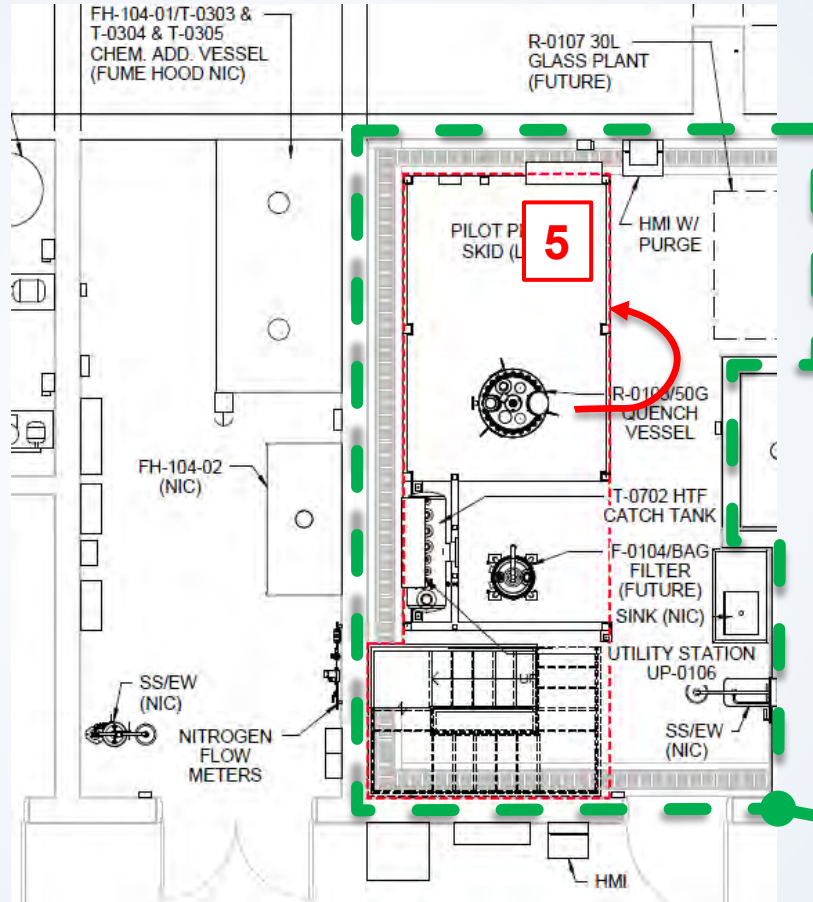


**Class I Div 1
Boundary**

Typical Synthetic Process in Pilot Skid: Nitration

1. Load liquid and solid reagents
2. Charge solvent (sulfuric acid)
3. Dose/dissolve starting material.
4. Dose nitric acid.
5. Quench Reaction

Remote operation from control room.

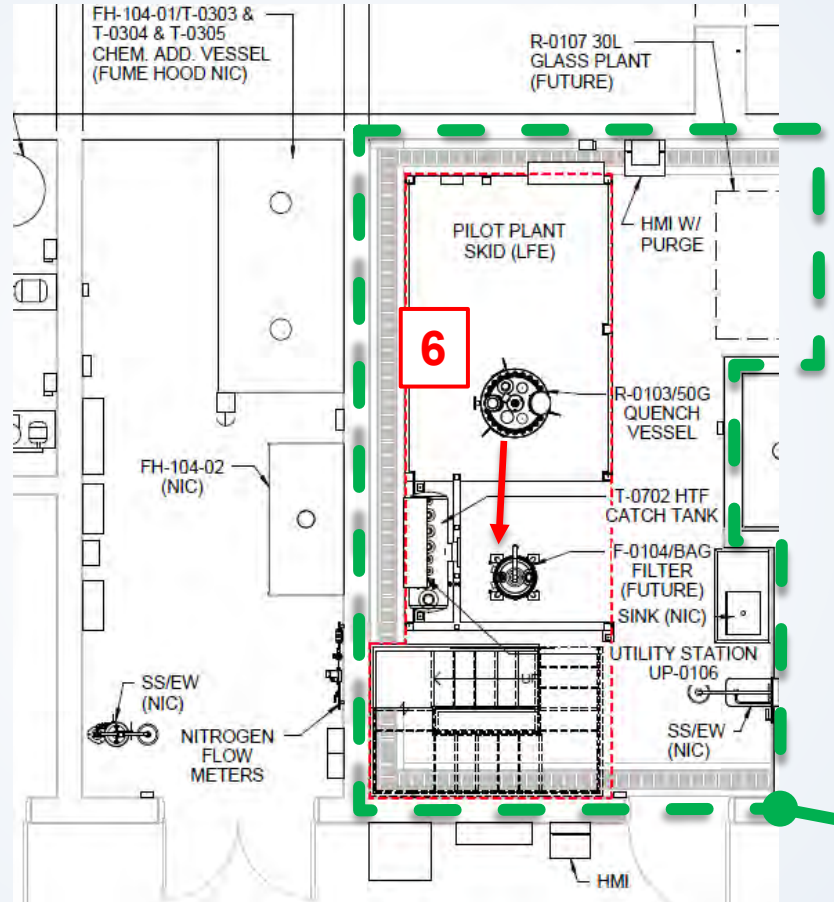


Class I Div 1 Boundary

Typical Synthetic Process in Pilot Skid: Nitration

1. Load liquid and solid reagents
2. Charge solvent (sulfuric acid)
3. Dose/dissolve starting material.
4. Dose nitric acid.
5. Quench Reaction
6. Filter Reaction

Remote and potentially contact from HMI.

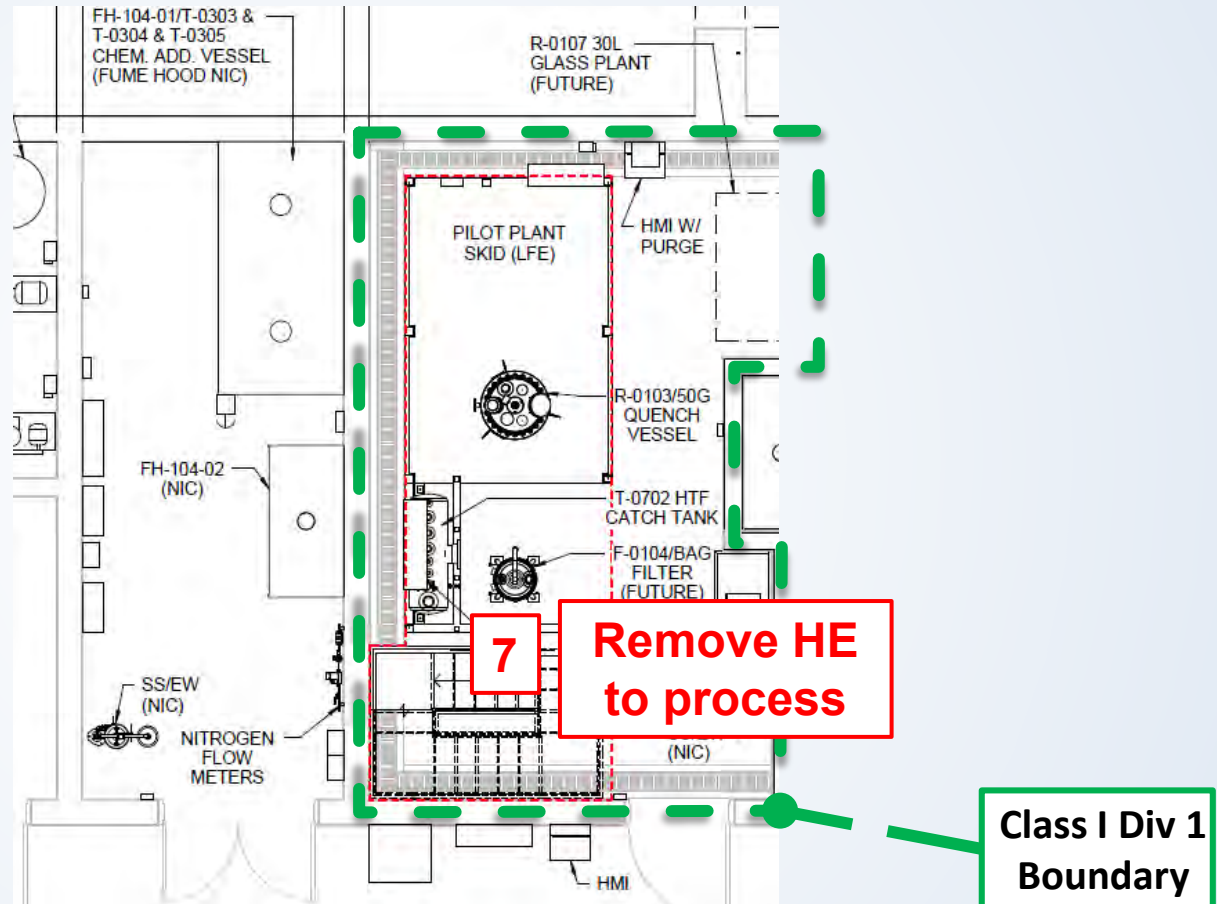


**Class I Div 1
Boundary**

Typical Synthetic Process in Pilot Skid: Nitration

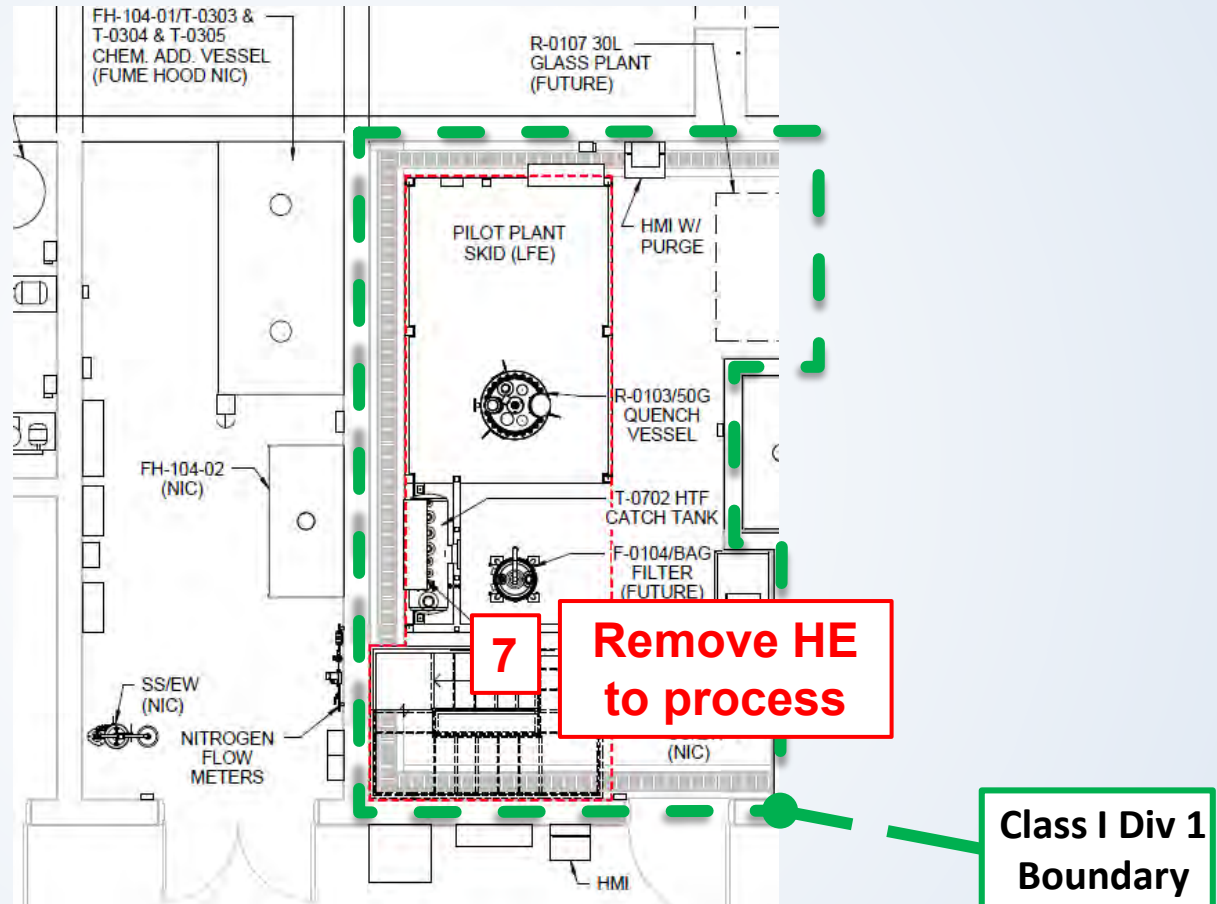
1. Load liquid and solid reagents
2. Charge solvent (sulfuric acid)
3. Dose/dissolve starting material.
4. Dose nitric acid.
5. Quench Reaction
6. Filter Reaction
7. Collect Product.

Contact operation



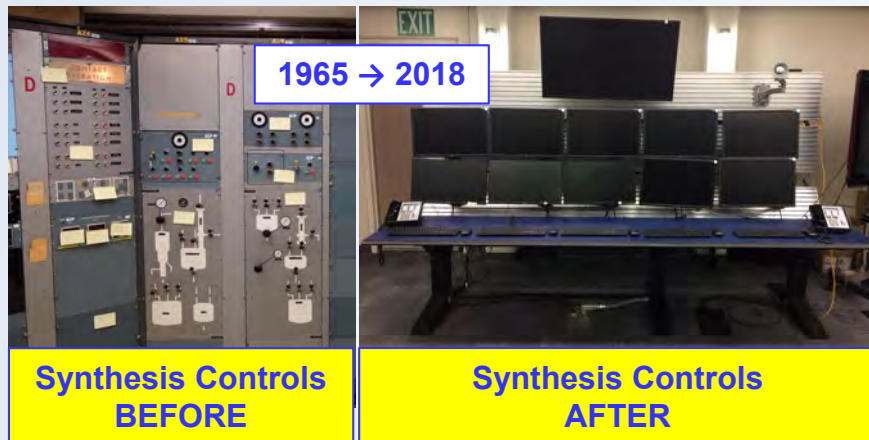
Typical Synthetic Process in Pilot Skid: Nitration

1. Load liquid and solid reagents
2. Charge solvent (sulfuric acid)
3. Dose/dissolve starting material.
4. Dose nitric acid.
5. Quench Reaction
6. Filter Reaction
7. Collect Product.



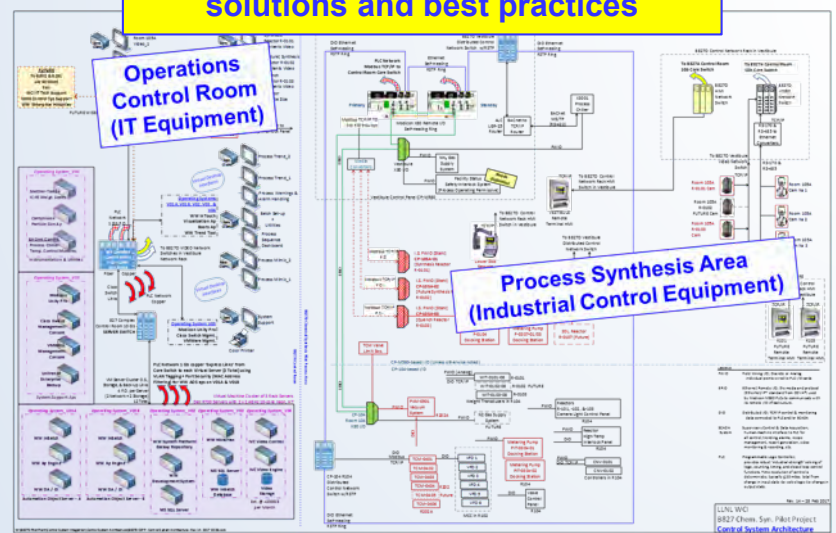
Timing of valve sequence actuation, alarm parameters, emergency stops, and PID control managed through integrated control system (ICS)

Industrial Control System (CS)



- State of the art Modicon system for remote operation
 - CS infrastructure will be expandable to future projects.
- Controls System Integration (CSI) Subcontract (Avanceon, Exton, PA)
 - Offers engineering controls while delivering batch process flexibility and data collection capability using Schneider Electric's **Wonderware software platform**.
 - COTS hardware & software with industry standards-based configurable batch control software (**Wonderware InBatch**)

CS Architecture uses contemporary industrial process control systems solutions and best practices



Modern, safe, capable, remotely operable controls

Control System Summary

- The CS has been developed by LLNL and Avanceon (Exton, PA)

1. 1180+ Alarms

4. 160 Phases

2. 800+ I/O Points

5. 111+ Interlocks

3. 100+ Control Valves

6. 415+ Page Functional Specification

- There are three operator interface terminals (OIT) for the pilot plant:

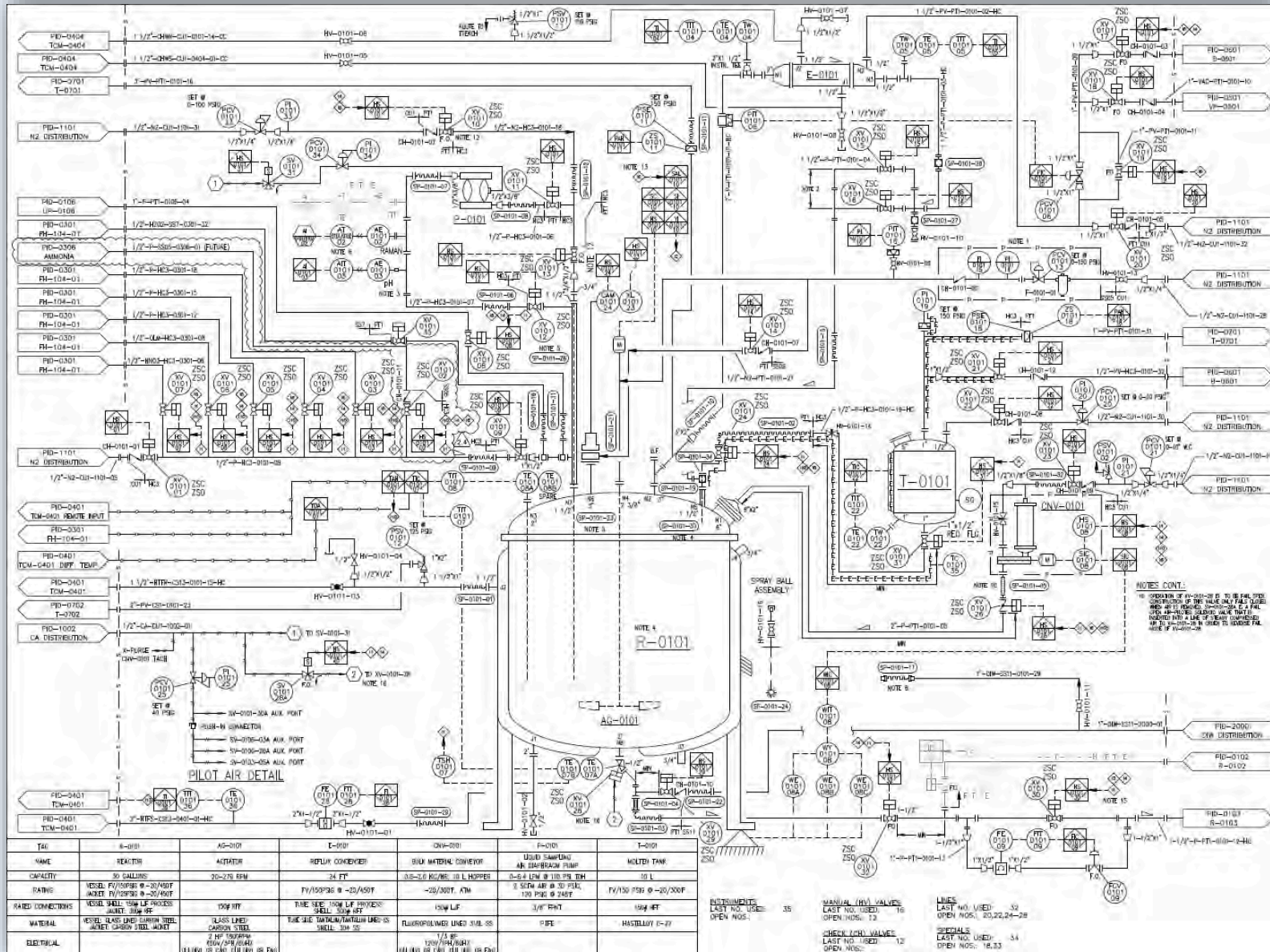
827A – Control Room, 827D Chemical Addition Room, and 827D Pilot Skid

Special system designed to prevent control room operation while operator is in the pilot facility.

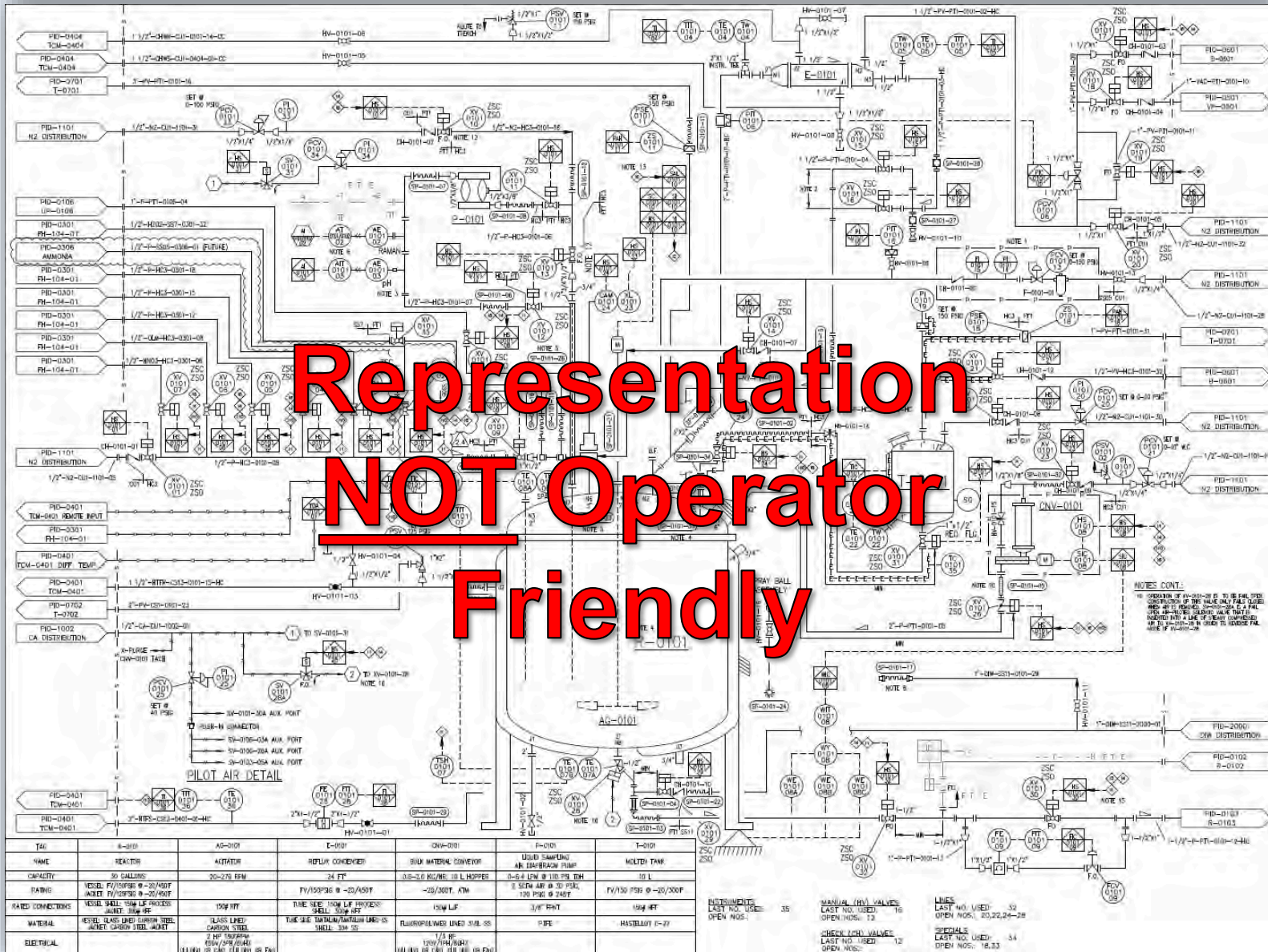
Capabilities of Integrated Control Software

- **Pre-coded operational functions built into custom Wonderware InBatch software (phases).**
 - *For example:* Purging the vessels with inert gas will not require the operator to manually open all valves in sequence. The system will open all appropriate valves on a command to “purge” a vessel.
 - InBatch provides a traceable, reliable, and structured “recipe” based process for running a synthetic process from start to finish. The capability to exit the recipe and proceed manually is still available.
- **In situ vessel cameras and Raman spectrometer allow for real time visualization of the physical and chemical reaction processes.**
 - Ability to tie a spectral result to a control system response is possible. For example, add more reagent until a spectral peak disappears.
- **Custom alarms set on instruments (pressure, temperature, etc.) that elicit varied levels of response.**
 - Exceed desired process temperature can stop a dose, or initiate maximum cooling of the TCM depending on a High or High-High alarm.

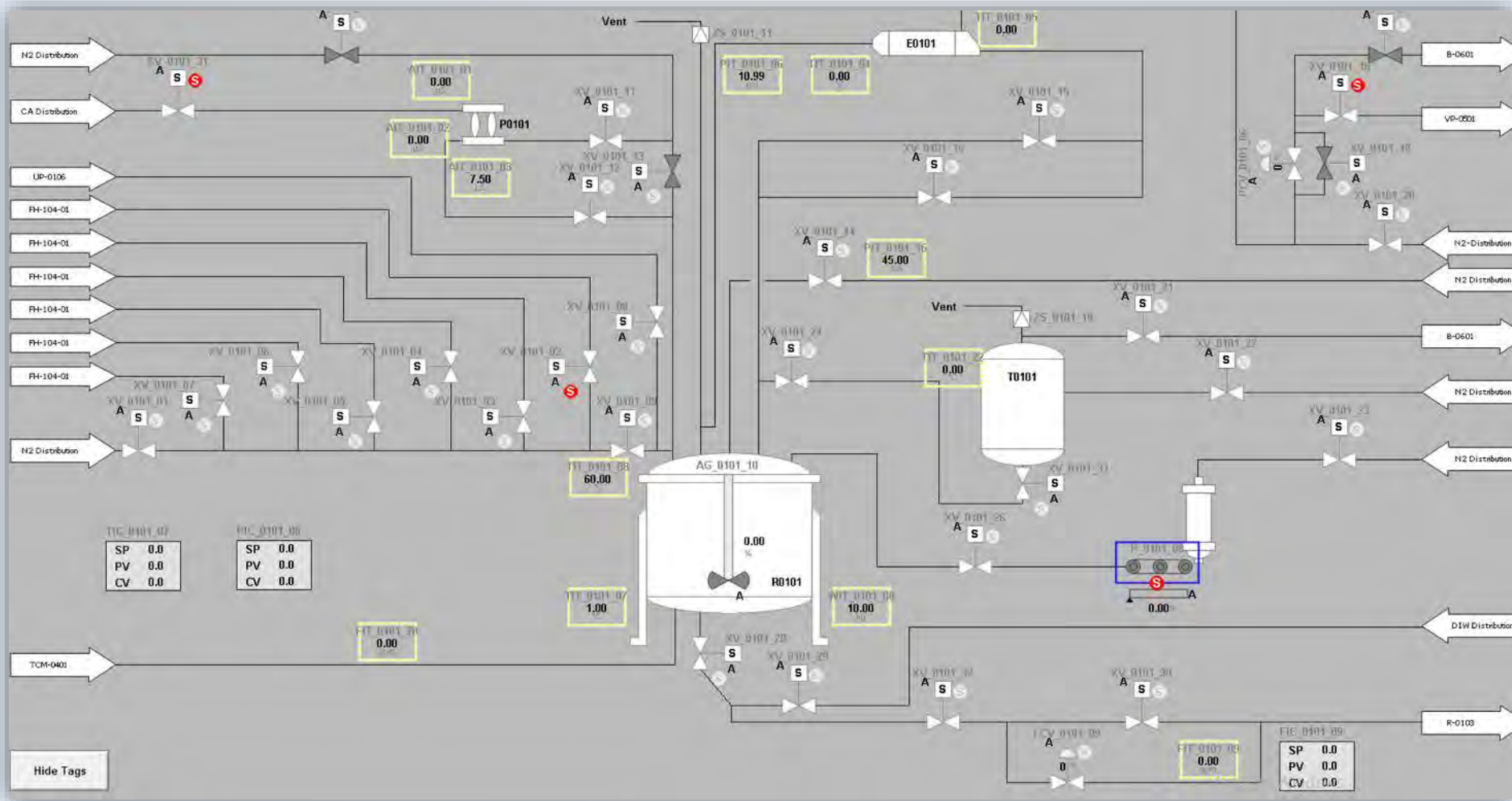
P&ID for 100 L Glass Lined Reactor



P&ID for 100 L Glass Lined Reactor



Control Screen for 100 L Glass Lined Reactor



Operator friendly and fully interactive screens developed by Avanceon.

Summary of Pilot Skid Capabilities

- **New facility provides a safe remotely controlled skid for a variety of synthetic processes:**
 - Rated for operating pressures of up to 135 psi.
 - MoC: glass-lined carbon steel vessels, hastelloy, tantalum, and PTFE for wetted materials.
 - Reaction temperatures of -10 to 150 °C.
 - Ammonia charging capability (vaporizer) for both 100L and 200L vessels.
 - Hydrogen peroxide dosing.
 - Metered solids addition via conveyor.
 - Remote reagent addition via metering pump, diaphragm pump, vacuum, or pressure.
 - Ability to phase separate, distill, and recirculate between vessels.
 - Sample loop on 100L vessel for three inputs: currently Raman and pH.
 - Ability to conduct CIP with InBatch automated recipe.
 - Nutsche and bag filtration.

Additional Pilot Facility Capabilities

- General purpose electrical area housing RC1e calorimeter.
- Space for future general purpose equipment: wish lists include continuous flow reactor, 5 gallon Parr reactor, and Buchi glass plants.
 - General purpose electrical room rating allows for HE synthesis and processing in fume hoods utilizing non-rated commercial equipment.
- Identically sized room on opposite side of building from pilot skid houses fume hood for powder handling and drying oven.

Acknowledgements

- Funding sources: DOE and NNSA Headquarters
- LLNL Project Managers: Bill Collins (retired), Brock Parsons, Mark Coons, Jeff Packard, Steve Chan, Fred Wade (control system integration), Kenn Knittel, Veronica Harwood, Lou Bertolini, Lou Ferranti
- Subcontractors: Hart Design Group and Hart Construction (facility design and fabrication), RORE Inc. (construction installation), TFS (construction installation), Wilhite (electrical), Avanceon (control software), Nalas Engineering (process hazard analysis)
- Scientists: Phil Pagoria, Alan DeHope, Mao Xi Zhang, Edwin Virgin, III, Spencer Vartanian, Levi Merrell, Yong Han, Lara Leininger, Jon Maienschein, Sabrina DePiero
- Reviewers, Work Control, and Support: Mark Zagar, Kevin Vandersall, Kevin Merrell, Barbara Jesus, Hiroshi Saito, Dawn Kramer, Shari Brigdon, Alex Gash, George Overturf, Ken Newman, Wes Davis, Dave Hill, John Scott, Deanna Kahmke, Kim Elam, Donovan Day, Annette Warner, Cameron Cornell, Trini Gonzalez



An Investigation into a Proper Heating Rate for Slow Cook-off Testing

David Hubble
Naval Surface Warfare Center Dahlgren Division, Dahlgren, Virginia

Abstract

Historically, slow cook-off (SCO) testing has been performed by heating the munition under test in an oven at a constant rate of 3.3°C/hr until a reaction occurs. Recently, however, the validity of this heating rate has been disputed and it has been argued that it is too slow to represent a realistic threat scenario. While many agree that the heating rate should be increased, there has been no real consensus on what the new rate should be. This investigation was performed to help determine what heating rates are possible for munitions and to help select a more appropriate heating rate for future SCO testing. This was done by examining historical accidents, reviewing existing analysis, and modelling possible threat scenarios. In the course of this analysis, no data was found or generated which supports a rate as slow as 3.3°C/hr and it is concluded that a heating rate faster than 10°C/hr is more appropriate and better represents real-world threats to munitions.

Background

SCO testing is performed to simulate accident scenarios in which a munition is slowly heated over an extended period of time. This can result when a fire occurs but is separated from the munition by some barrier such as the walls of a magazine. This is in contrast to a fast cook-off (FCO) where the munition is directly exposed to the fire. In a SCO scenario, the heat fluxes into the item are much smaller than in the FCO and the resulting temperature gradients are much lower. Therefore, if the munition cooks off, the reaction can be severe because much of the energetic material is at an elevated temperature when the cook-off occurs. This elevated temperature can cause normally stable energetics to detonate during slow heating. SCO testing is therefore necessary to help developers improve the response of munitions to this type of thermal threat and ensure that any reaction that occurs is as mild as possible.

The current SCO test procedure, as outlined in STANAG 4382, specifies that the munition be heated in an oven wherein the air temperature is increased at a constant rate of 3.3°C/hr (6°F/hr) until the item reacts. There is also a provision that allows a different heating rate to be selected (procedure 2) based on a threat hazard assessment (THA), but the test generally defaults to the 3.3°C/hr rate specified in procedure 1. In addition to the ramp rate, other parameters such as item preconditioning and temperature gradients within the oven are also specified in the test standard. A passing criteria is a reaction violence no more severe than burning (type V).

The origin of the 3.3°C/hr heating rate is not known for certain. Some point to ship fires during WWII that exploded up to 2 days after suffering below deck fires. By dividing the predicted cook-off temperature by the fire duration a heating rate of approximately 3°C/hr can be obtained. Others have speculated that the slowest possible heating was desired and 3.3°C/hr was simply as slow as oven controllers could reliably function at the time. Regardless of the origins, the SCO test has primarily been performed at a rate of 3.3°C/hr for more than 50 years. Recently, however, there has been increasing pressure to change the document so that the rate specified in procedure 1 better represents realistic heating scenarios. The concern is that an item that has been designed to pass the 3.3°C/hr heating rate of the SCO test could react more violently at the higher rates that the item is more likely to encounter while in service.

In the spring of 2016, AC326 approved the formation of the Slow Heating Custodial Working Group (SHCWG) to investigate the SCO heating rate and to revise STANAG 4382, creating a new Allied Ordnance Publication (AOP). At the first SHCWG meeting in Utrecht, Netherlands in April 2017, the topic of changing the heating rate was debated. Unfortunately, there was much disagreement among the participants as to what analysis had previously been done and what relevant accidents had occurred which made agreement on an appropriate heating rate impossible. This then led the AC326 subgroup B chairman to request that a study be performed which would summarize any SCO related accidents and previously performed SCO analysis to be presented at the subsequent SHCWG meeting. Additional modelling was also to be performed to specifically examine SCO heating rates. This material was meant to present facts to the group and help guide the discussion towards realistic threat scenarios. This paper presents the results of the requested study. These results were, in part, presented at the 2nd SHCWG meeting which was held in Brussels, Belgium in September 2017. This paper also includes work that was completed after the September meeting.

Investigation Overview

The investigation that was performed was done in three stages.

1. A review of historical incidents
2. A review of existing SCO related analysis
3. Additional modelling of SCO scenarios

The goal of this investigation was to determine the slowest possible heating rate that an ordnance item could experience in service that could result in a cook-off.

Incident Review

The goal of the incident review was to attempt to predict a lower bound for potential SCO heating rates from historical accounts of incidents involving explosives. By estimating cook-off temperatures and the total heating duration, the average heating rate could be calculated by dividing the temperature rise by the total heating time ($\Delta T/\Delta t$). Therefore, the primary goal of the incident review focuses on determining total heating duration prior to reaction.

In order for an item to experience a SCO while in service, it must be heated for an extended duration. In an attempt to determine realistic heating durations, a review was conducted to identify as many incidents as possible where explosives were subjected to heating. These were then sorted based on incident type and heating duration. A large number of the incidents examined were found in the paper by Boggs et al. (Thomas L. Boggs, 2013). Additional incidents were found using a variety of sources including the accident tool on MSIAC's web portal (MSIAC, 2017). In all, over 200 incidents were examined spanning from 1907 to 2015.

Since cook-off is the primary focus of this work, only incidents that involved some type of thermal threat were desired. Of the incidents that were identified there were 138 in which a fire was the initial reaction or a fire was created by the initial reaction or attack. In other words, 138 incidents were found where either a cook-off occurred or the potential for a cook-off existed for at least some period of time. Of these 138 incidents, 83 were documented in sufficient detail to determine the total heating duration. Typically, this means that both the time that the heating started and the time that the event concluded were both reported. Note that the event can conclude in a variety of ways. Examples include: the fire was extinguished, the factory

exploded, or the ship sunk. By defining the heating duration in this way, a very conservative (long) heating duration is obtained because it assumes that the munition is heated for the entirety of the heating event.

Of the 83 incidents identified, 10 involved bulk explosive material such as ammonium nitrate or ammonium perchlorate. Since the focus of the SHCWG is the testing of military explosives, it was decided to remove these from consideration. These refinements resulted in 73 incidents that involved military explosives where a cook-off was possible and where it was possible to at least put an upper bound on the heating duration. Finally, these 73 incidents were sorted by type:

1. Depot – incident occurred at a military facility where munitions are stored
2. Warship - incident occurred on a military ship other than a transport ship
3. Transportation - incident occurred while transporting energetics by truck, train, or ship
4. Plant - incident occurred at a production facility where energetics are manufactured

The bar chart in Figure 1 shows the total duration of the 73 incidents while the pie chart shows the distribution by type. Figure 1 demonstrates that the vast majority of the incidents occurred either at depots (34) or on warships (31) and only 5 transportation and 3 plant incidents were found. It is also apparent that incidents on warships are more likely to have a shorter duration as compared to depots. This is due to the way these fires are fought. When a fire occurs at a depot, firefighting efforts are typically abandoned very early on and the fire is left to burn out on its own which, in some cases, can take up to a week or more. On a ship, however, this is not an option and the fire is fought ferociously.

As can be seen, the incident durations span from 15 minutes all the way to 312 hours. In nearly all of these cases, the type of ordnance present is not identified and in many cases a variety of munitions are present. Therefore, to obtain a conservatively slow heating rate, a low cook-off temperature of 130°C is assumed for each case. A temperature of 130°C is based on the lowest cook-off temperatures seen in SCO testing for double base propellants. High explosives typically have higher cook-off temperatures and would result in faster calculated heating rates. If an initial temperature of 30°C is assumed (giving a $\Delta T=100^\circ\text{C}$) then the heating durations in Figure 1 result in heating rates ranging from 400°C/hr to 0.3°C/hr with an average value of 59°C/hr and a median value of 22°C/hr.

The preceding analysis assumes that the ordnance was heated for the entire incident duration. In actuality this is almost certainly not the case. In practice, it is impossible to determine how long any particular munition was heated prior to reacting. For example, consider the Roseville, California train accident in 1973. Here, a train that contained 21 boxcars loaded with 7,056 Mk81 250 lb bombs caught fire. The total incident duration, from fire ignition to last explosion, was 33 hours. If this heating duration is used to obtain an average heating rate a value of approximately 3°C/hr is obtained. But, was the last bomb that exploded actually heated for 33 hours? Of course not, the fire moved from one car to the next causing explosions along the way. In fact, the only information that can be known with certainty is that no munition was heated for *longer* than 33 hours. This example demonstrates the difficulty in determining a heating rate from accident data.

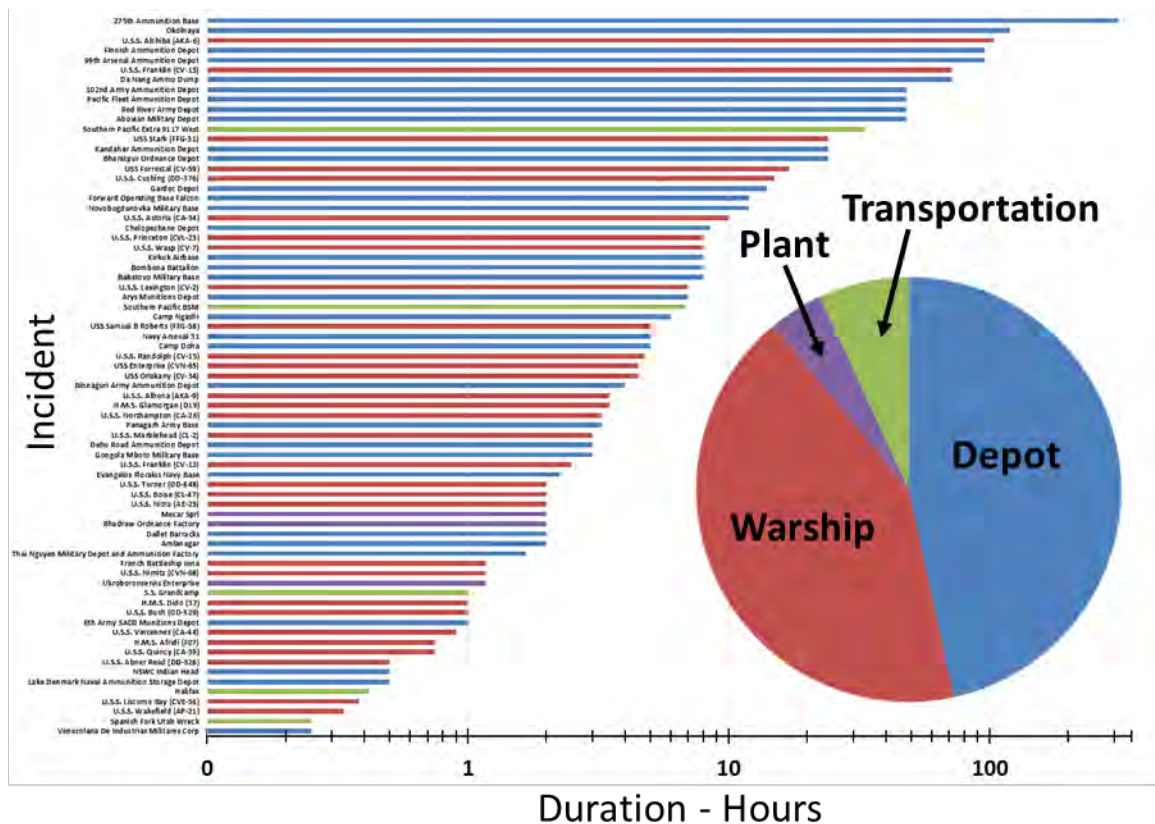


Figure 1: Plot showing the distribution of incident type and duration

In many of the incidents studied, there were multiple explosions throughout the total incident duration. These initial explosions make it difficult to draw any conclusions about the heating rate that led to later reactions because it is known that the initial reactions spread the fire from one area to another. One way to avoid this confusion is to look at the time from the fire ignition to the *initial* reaction. While it is still impossible to know if the first item that reacts was heated for this entire time, at least it is known that no earlier reactions contributed to it reacting. Unfortunately, the time from fire ignition to initial reaction is rarely known as shown in Figure 2. The information needed to determine the time to initial reaction was only available in 14 of the 73 incidents under review. However, it is worth noting that the longest duration found to initial reaction was just over 2 hours. If this value is used, along with the conservative cook-off temperature of 130°C used above along with the assumed initial temperature of 30°C, a heating rate of 44°C/hr is obtained which is a full order of magnitude faster than the currently specified rate. While this sample size is much too small to draw any real conclusions, it points to the possibility that the appropriate heating rate might be much faster than the 3.3°C/hr that is currently used for SCO testing.

Regrettably, most of the incidents that were examined were not documented in enough detail to accurately predict the heating rate that the munitions experienced prior to reacting. For this reason, the data available from actual incidents is sorely lacking. Instead, we must rely on models and analysis to determine what realistic SCO heating scenarios exist. These models can then be used to help determine the slowest possible heating rates that could result in a cook-off.

Review of Existing Analysis

One of the first attempts to analyze potential slow heating scenarios was done by Fontenot and Jacobson in 1988 (Jacobson, 1988). At this time the SCO test was an existing standard safety test and they were specifically trying to identify scenarios that could create the 3.3°C/hr heating rate that was already being used in the test. Through the course of their analysis, they identified and examined 5 scenarios that could result in the slow heating of munitions:

1. Transportation accident – truck or train fire
2. Dump storage accident – a fire moving past an ammunition storage area
3. Debris pile from a deck fire – aftermath of a FCO event
4. Below deck fire – fire heats the bulkhead of a storage magazine in a ship
5. Steam leak – steam leaks into a magazine on a ship and heats ordnance

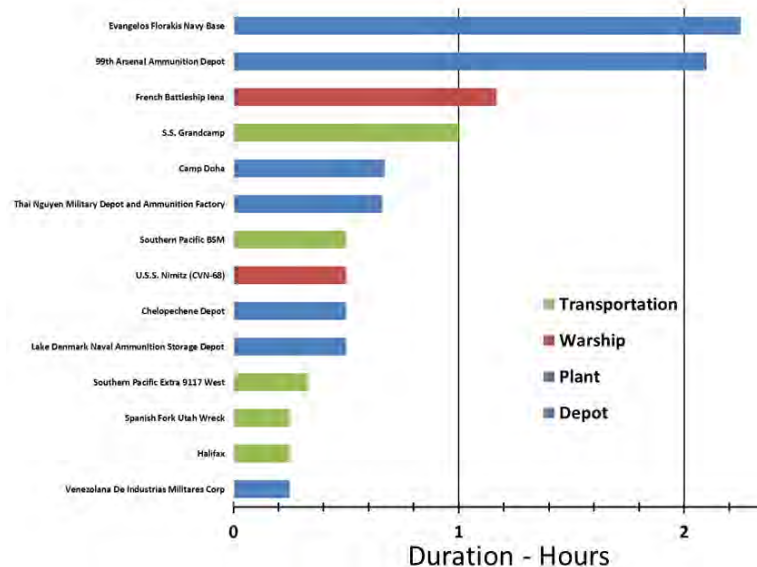


Figure 2: Time from fire ignition to initial reaction

For each of the five scenarios, mathematical models were constructed and the slowest possible heating rates that would result in ordnance temperatures of at least 150°C were identified. It was found that scenarios 1-3 all resulted in the slowest heating rates being on the order of 50-80°C/hr. For scenario 4, the below deck fire, the ordnance item was allowed to exchange radiation with a bulkhead which was being heated on the backside by a fire. The heating rate was calculated for four different sized munitions ranging from 250lb to 2,000lb. As one would expect, the larger munitions heated more slowly and the slowest heating rate obtained was 7°C/hr. It is worth noting that in this analysis the ordnance temperature was examined but not the temperature of the air surrounding the ordnance.

The final scenario examined an intermediate pressure (saturated at 3100kPa and 236°C) steam leak into a magazine. The steam would expand to superheated steam at 165°C which would condense within the magazine and heat everything within it to 100°C within the first 2 hours. The ordnance would then experience convective heating and asymptotically approach 165°C. After 45 hours a 1,000lb bomb would reach 164°C and by dividing the temperature change by this duration a heating rate of 3.3°C/hr was obtained. Here it is worth noting that the selection of 164°C as the final temperature was somewhat arbitrary and if 150°C had been selected, as was done for the previous scenarios, then a heating rate of 8°C/hr would have been obtained. Also, as in scenario 4, again the ordnance temperature was examined and not the temperature of the surroundings. Since a SCO test controls the surrounding air temperature perhaps that is a more important parameter to examine in real-world scenarios.

In a later report, Mansfield (Mansfield, 1996) identified the below deck fire as the most likely scenario that would result in a SCO and created a computer model that allowed it to be examined in detail. Specifically, the model allowed parameters such as fire size, bulkhead thickness, fire compartment size, magazine size, and soot concentration to be varied. For each set of parameters, the model was run and the temperatures of the fire compartment, the common bulkhead, and the magazine gas were calculated as a function of time. In this way, the effect of each parameter on the magazine gas temperature could be determined.

Mansfield's analysis allowed several interesting trends to be observed. First, in general, larger fires create higher heating rates and higher final temperatures compared to smaller fires. Another way of looking at this is all else being equal, a larger fire gets the magazine hotter quicker. Second, thicker bulkheads result in slower heating rates. Third, the size of the magazine did not significantly affect the response time of the magazine gas. Therefore, the slowest magazine gas heating rates will occur when a small fire exists and is separated from the magazine by thick walls. However, if the fire is too small, it will not create temperatures high enough within the magazine to create a cook-off. When a minimum final gas temperature of 150°C is considered, the longest time found to reach equilibrium was 8 hours. If an initial temperature of 30°C is assumed, this analysis results in an average heating rate of 15°C/hr ($[150^{\circ}\text{C}-30^{\circ}\text{C}]/8\text{hrs}$) which is significantly faster than the 3.3°C/hr currently being used.

Additional Modeling

Mansfield's analysis did a good job of studying the fire-magazine system but that analysis wasn't specifically trying to determine worst case heating rates. The current work expands upon this existing analysis in an attempt to help the SHCWG determine realistic worst case (slowest heating rate) scenarios that could result in a cook-off.

The Model

A simple thermal model was developed that is loosely based on Mansfield's work. Figure 3 shows an overview of the system that was modeled and the heat paths used. There are five temperatures histories calculated by the model: the fire compartment temperature T_F , the bulkhead temperature T_B , the ordnance temperature T_O , the magazine air temperature T_{MA} , and the magazine wall temperature T_{MW} . Each of these is modeled using the lumped capacitance assumption that each item is at a uniform (not constant) temperature. This was done to greatly simplify the approach instead of performing a full finite element model for each of the items modeled. This simplification also allowed each run of the model to be completed on the order of seconds. A number of simplifying assumptions were used in order to create a model that would be useful. First, it is assumed that all the walls of the fire compartment are at the same temperature as the bulkhead. That is, the energy from the fire is evenly distributed to the entire fire compartment area and all the walls have identical backside heat loss. Second, the magazine walls (with the exception of the common bulkhead) lose heat by convection and radiation to an infinite sink that is at the initial temperature. This implies that there isn't an additional compartment beyond the magazine. This may or may not be true depending on the ship layout. Third, the maximum ordnance loading density in the magazine is 700 kg/m². This was based on estimates for stack height and minimum clearances around stacks. In the model, the quantity of ordnance (loading ratio) was then varied from 0 to 100% of this loading density. Estimates had to also be made concerning the surface area of the ordnance. Here it was assumed that when fully loaded, for each m² of floor area, the ordnance surface area was 8 m².

Again, this was based on rough estimates after analyzing several different classes of munitions from bare rounds and bombs to munitions in boxes. The specific heat of the ordnance was also required in order to determine its thermal mass. For this analysis, a value of 300 J/kgK was used as it lies between the values for steel (434 J/kgK) and most explosives (~230J/kgK). Also, it was assumed that the fire size was constant with time and continued to output the same amount of heat. A real fire could grow or shrink over time in any number of different ways which would greatly increase the complexity of an already difficult problem. Finally, estimates had to be made to determine the view factor from the common bulkhead to the ordnance. Since the ordnance is likely to be stacked near the bulkhead, the view factor was assumed to be 0.75 times the loading ratio. That is, when fully loaded, 75% of the radiant energy leaving the bulkhead impacts the ordnance and the remaining 25% reaches the magazine walls. As the loading ratio decreases, the stacks become shorter and more of the radiant energy is allowed to reach the magazine walls.

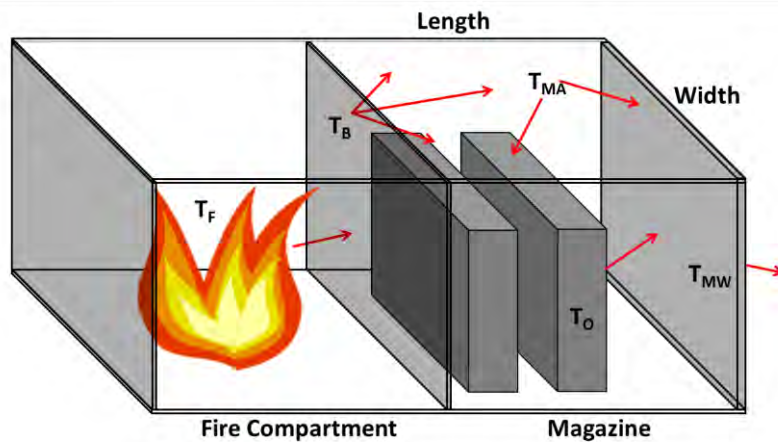


Figure 3: Overview of thermal model. Heat flows from the fire to the common bulkhead and then to the ordnance, magazine gas, and magazine walls.

Once this view factor was assumed, all of the remaining view factors could be calculated using standard procedures based on the defined geometry of the compartments.

For each of the five lumped masses that were analyzed, an energy balance was performed. The fire compartment temperature was modeled based on the correlations given by (Wickstrom, 2016). For any given fire size (q_{in} - Watts) the mass flow rate of air that is required to support combustion () can be calculated. This air must be supplied to the compartment, heated to the current fire compartment temperature, and then exhausted, carrying heat with it. Heat is also lost to the common bulkhead by convection and radiation from the compartment gas. For the radiation component, Wickstrom recommends assuming that the fire have an emissivity of 1 and the calculation is therefore straight forward. The convection heat transfer coefficient between the fire and the wall is also based on correlations found in Wikstrom's book and is calculated as:

$$\bar{h} = 76 \cdot [(T_F + T_B)/2]^{-0.66} \cdot |T_B - T_F|^{0.66}$$

Here, h is in W/m^2K and the temperatures are in Kelvin. The convection coefficient between the magazine gas and the bulkhead, ordnance, and magazine walls were all calculated using this same correlation. The convection between the fire compartment and the bulkhead as well as the convection on the outside of the magazine walls were also calculated using this correlation.

The mass of gas (m_{gas}) in each compartment was based on the volume of the compartment and the density of air calculated at the previous time step's temperature. The specific heat (C_p) of the gas was also allowed to vary based on the temperature, again based on the previous time

step temperature for that region. The lumped heat capacity equation for the fire compartment is then:

$$\dot{E}_{in} - \dot{E}_{out} = \dot{E}_{stored}$$

$$\dot{q}_{in} - \dot{m} \cdot C_p \cdot (T_F - T_\infty) - h \cdot A \cdot (T_F - T_B) - \sigma \cdot A \cdot (T_F^4 - T_B^4) = m_{gas} \cdot C_p \cdot \frac{dT}{dt}$$

Once an energy balance was created for each of the five lumped masses, a set of explicit finite difference equations were created. Care must be exercised when solving explicit finite difference equations that stability is maintained. In this work, it was found that a time step of 1 second was sufficiently small to ensure stability for all the cases analyzed.

Model Validation

As a qualitative validation of the model's performance, it was used to simulate an instrumented ship fire. In the work of Bailey and Tatum (Bailey, 1995), a fire that was set aboard the Ex-USS Shadwell was described in sufficient detail to be duplicated using the simple lumped mass model. Here, a 9MW diesel fire was allowed to burn in a compartment for 30 minutes while the temperatures of the fire compartment gas, common bulkhead, and adjacent compartment gas were measured. The results of the model and the data obtained during the test fire are shown in Figure 4. While the agreement is not perfect it is good considering the simplicity of the model.

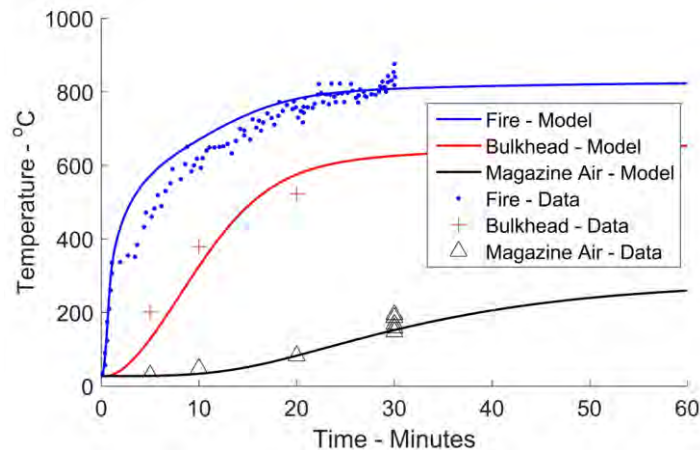


Figure 4: Comparison of model results to data obtained during a 9MW fire aboard the Ex-USS Shadwell

Model Results

The independent variables that were varied during the investigation were the fire size (q_{in}), the physical size of the fire compartment and magazine, the thickness of the walls, and the load ratio. For each combination of these parameters the model was run resulting in 5 temperature-time curves. Since the SCO test mimics the magazine gas temperature, the magazine gas temperature curve is of most interest and it will be used to calculate average heating rates. As shown in Figure 5, the magazine gas temperature curve is asymptotic and has a slope (dT/dt) that is continuously changing. Therefore, to determine the average rate of change, a threshold final temperature value must be selected. This is done as a percentage of the total temperature rise. In the right plot in Figure 5, five different selections from 50% to 95% temperature rise are shown. As can be seen, the selection has a significant effect on the value of the average heating rate as indicated by the different slopes of the red lines. For this particular case, selecting 50% temperature rise gives an average heating rate of nearly 24°C/hr while selecting

95% yields 12°C/hr. This is quite a large variation and demonstrates the difficulty in simulating a continuous curve with a straight line. For this work, a value of 90% was selected and all average heating results are calculated using the 90% temperature threshold. A value of 90% was selected for two reasons. First, the higher the value selected the more conservative (slower average heating rate) the results will be. Second, 90% was the value selected by Mansfield and this consistency allows the results to be directly compared.

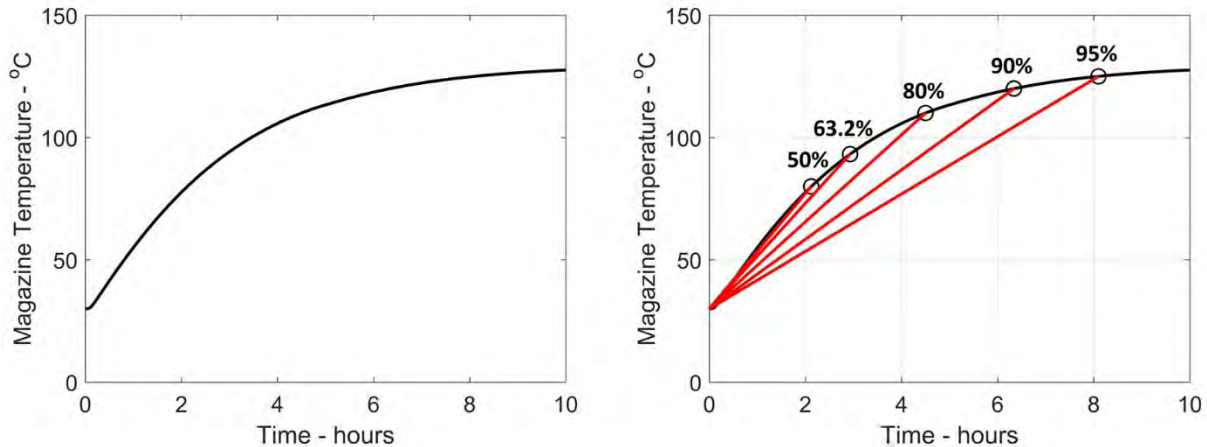


Figure 5: Example of magazine gas temperature curve (left) and effect of choice of equilibrium temperature (right) on calculation of average heating rate

The model allowed a number of parameters to be varied throughout the study. The first parameter that was investigated was the impact of the fire size as shown by the results in Figure 6. In the left plot, ten different magazine gas temperature curves are shown where the fire sized was varied from 0.25MW to 2.5MW. The circle on each curve represent the point where the magazine gas has reached 90% of its final temperature rise. As can be seen, as the fire size increases, the magazine gas reaches a higher final temperature and reaches its 90% equilibrium temperature in a shorter period of time. In the right hand plot in Figure 6, the final magazine temperature is plotted along with the time to 90% temperature rise and the average heating rate. The average heating rate is obtained by subtracting the initial temperature from the final temperature (to obtain the temperature rise or ΔT) and then dividing by the time to equilibrium (Δt). Note that as the fire size increases the calculated heating rate increases because ΔT is increasing *and* Δt is decreasing. Also, for the case shown here, the slowest rate of concern occurs for a fire size of 1MW because the final magazine temperature for that fire size is 130°C. The smaller fires result in a slower rate but would not achieve a cook-off (final temperature below 130°C) so they are not of concern. The larger fires would result in a cook-off but they would not result in the slowest heating rate. So, for every combination of bulkhead thickness, magazine size, and ordnance quantity, there is only one fire size that results in a final magazine temperature of exactly 130°C. Moving forward, as other parameters are varied, the first step is to determine the fire size that results in a final magazine temperature of 130°C. The heating rates that are then calculated are known to be the slowest possible that will still result in the possibility of a cook-off.

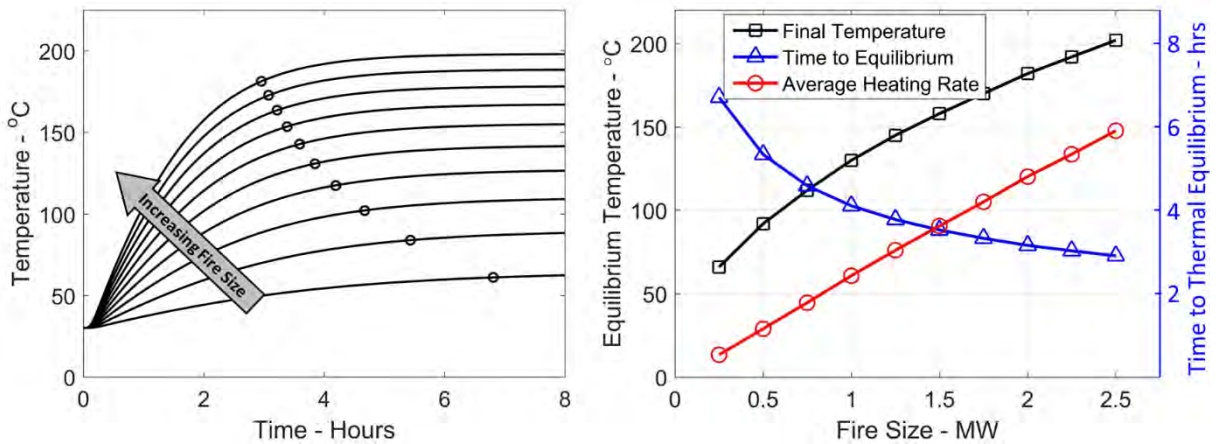


Figure 6: At left, increasing fire size causes the magazine gas to reach a higher temperature in a shorter time. End result is an increase in final temperature and average heating rate as shown at right.

The effect of the thickness of the bulkhead on magazine heating rate is shown in Figure 7. Here the bulkhead thickness was increased from ¼ inch to 1 inch (6 mm to 25 mm). Increasing the bulkhead thickness does not affect the size of the fire required to reach a final magazine temperature of 130°C because the area for the fire to lose heat to the surroundings is not affected. However, the time required for the magazine gas to reach equilibrium does increase as the bulkhead thickness increases. This is because increasing the wall thickness increases the thermal mass of the material that must be heated and more time is required for the magazine to reach the 90% threshold temperature. This increase in time has a direct influence on the average heating rate as shown at right.

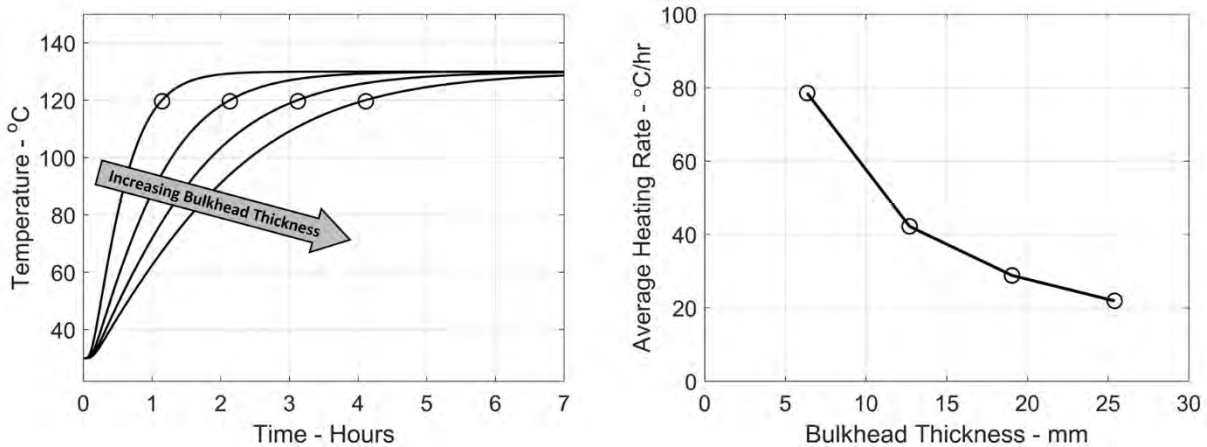


Figure 7: Effect of bulkhead thickness on magazine gas temperature (left), and average heating rate (right) for one particular magazine and fire size.

The effects of changing the size and aspect ratio (width/length) of the magazine was investigated. The results for empty magazines with 12.7 mm thick walls are shown in Figure 8. At left, the size of fire required to reach 130°C is shown as a function of magazine area. For each case, the time required to reach the 90% temperature rise was also calculated and was used to determine the average heating rate for each case as shown in the plot at right.

As would be expected, as the size of the magazine increases and its surface area increases, the size of the fire required to reach any given temperature (130°C in all cases here) also increases. Less obvious is the effect of the aspect ratio. The magazine has six surfaces, only one of which is heated by the fire. The area of the heated bulkhead is the product of the width and height. As the ratio of W/L decreases, the ratio of heated area to cooled area increases. Therefore, to reach any given final temperature, the common bulkhead must be hotter as W/L

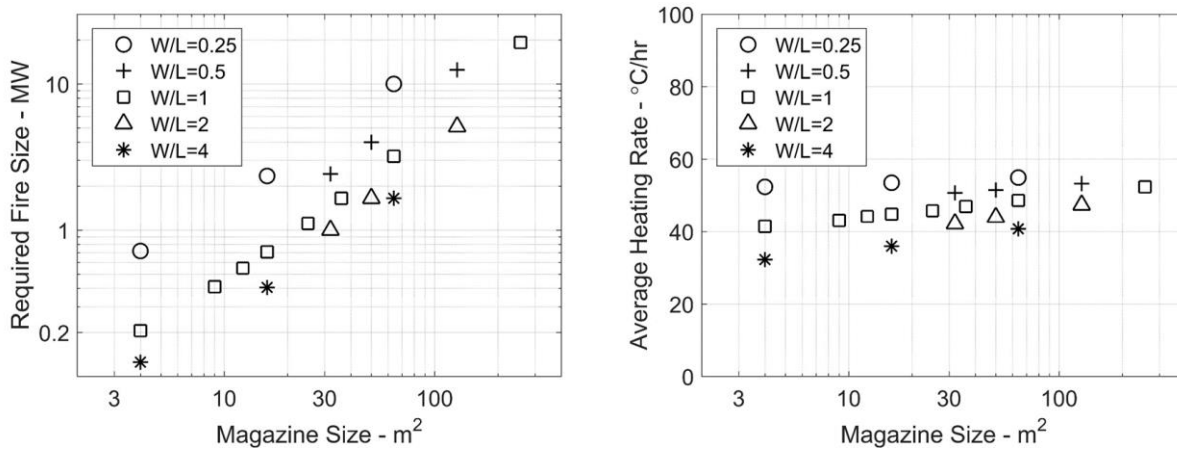


Figure 8: The size and aspect ratio of the magazine compartment has a large influence on the size of fire required to reach 130°C (left) but has a modest impact on the average magazine heating rate (right)

decreases. To obtain a higher bulkhead temperature, a larger fire is required.

More important is the effect on average heating rate. As the size of the magazine increases, its thermal mass increases but the size of fire required to reach 130°C also increases. The end result is that the two affects essentially cancel out and the effect of magazine size on the average heating rate is minimal. The aspect ratio actually has a larger influence on average heating rate than the size of the magazine. Results for magazines with thicker walls follow the same general trend and are therefore not shown. The slowest heating rate for empty magazines was 32°C/hr for 12.7 mm thick walls and 16°C/hr for 25 mm thick walls. These results compare well with the work of Mansfield.

The most important case to examine is magazines which are full of ordnance. The addition of ordnance to the magazine significantly affects the average heating rates as shown in Figure 9. Here, the average heating rates for full magazines are shown for two different wall thicknesses: 12.7 mm thick walls at left and 25 mm walls at right. As compared to empty magazines, the addition of ordnance significantly slows the average heating rates. There is also a stronger influence of magazine size on average heating rates. This is because as the magazines get larger, the mass of ordnance that they contain increases faster than the magazine's surface area increases which causes the average heating rate to decrease. Put a different way, the magazine's total thermal mass is increasing faster than its surface area. There is also an insulating effect that the ordnance has which reduces the radiation transfer from the hot bulkhead to the cold walls. This allows a smaller fire to reach the 130°C temperature threshold for a full magazine than would be require for an empty magazine. This also causes the average heating rate to decrease. The overall effect is that for full magazines the slowest average

heating rates that were calculated are 12°C/hr for magazines with 12.7 mm walls and 10.5°C/hr

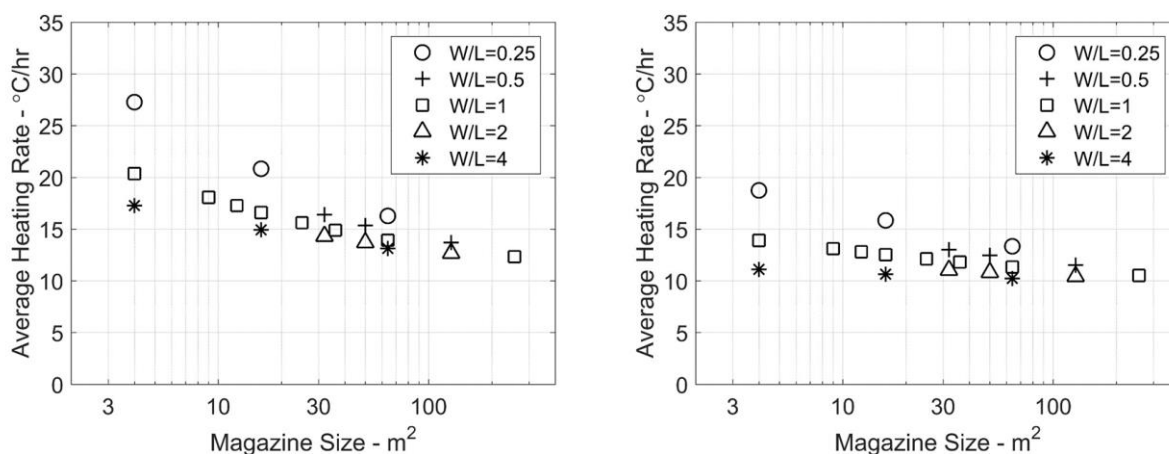


Figure 9: Average heating rates to 130°C for magazines full of ordnance with 12.7mm thick walls (left) and 25mm thick walls (right)

for magazines with 25 mm walls.

Discussion

The slowest heating rate that was identified was 10.5°C/hr for a large, fully loaded magazine with 25 mm thick walls. This means that a constant sized fire would heat the magazine air to 120°C (90% temperature rise to 130°C final temperature) in just over 9 hours. A smaller fire would result in a slower heating rate but would not result in a final temperature of 130°C. The only way to produce a slower average heating rate would be to allow the fire size to slowly grow with time over the course of many hours. In this way, it would be possible to achieve any heating rate and still eventually reach cook-off temperatures. This scenarios seems exceedingly unlikely and should not be the basis for a standard safety test.

The slow cook-off test is performed with a constant temperature ramp rate. As the results of the preceding analysis show, the magazine temperature does not increase at a constant rate but instead will follow a curve that asymptotically approaches its steady-state temperature. Simulating this behavior with a straight line is difficult but greatly simplifies the test. Specifically, if one wanted to perform a test with an asymptotic profile, a very difficult question would arise; what should the final temperature be? In this work 130°C was chosen because it was on the low end for a double base propellant and would result in the slowest possible heating rates. But, if a SCO test was designed where the temperature would only approach 130°C, most items would never react at all. By specifying a constant temperature ramp whose temperature continues to increase, an eventual reaction is assured.

The lumped thermal mass assumption greatly simplified the analysis but also ensured conservatism when calculating heating rates. The analysis performed assumed that both the magazine air and the ordnance were at two different uniform temperatures. In reality, the air and ordnance that are near the heated bulkhead will be heated more quickly than those near the cooled walls. Ordnance near the heated wall would therefore reach cook-off temperature and

react before any of the ordnance that was being heated more slowly would. This initial reaction is the only reaction of concern because once an item reacts within the magazine, even a type V reaction will lead to subsequent reactions or at the very least a rapid rise in magazine gas temperature.

Conclusions

The purpose of this work was to help identify possible slow cook-off heating rates and determine the most appropriate heating rate for SCO testing. Unfortunately, the review of historical accidents was of little help and only demonstrated the tragedy of these types of accidents and the importance of continued improvement through testing. The existing analysis review was helpful in identifying the most likely SCO scenarios but was incomplete insofar as calculating potential SCO heating rates. The analysis that was performed examined the effect of fire size, magazine size and arrangement, wall thickness, and ordnance quantity on magazine gas temperature histories. In each case, the fire size that resulted in a final magazine gas temperature of 130°C was first determined and then the time to 90% temperature rise was calculated. By dividing the change in temperature by this time ($\Delta T/\Delta t$) the average heating rate for each case was calculated. The slowest average heating rate that was found was 10.5°C/hr which is a little over 3 times faster than what is currently specified in STANAG 4382.

Acknowledgments

This work was funded by the Insensitive Munitions Advanced Development (IMAD) program.

References

- Bailey, J. T. (1995). *Validation of Fire/Smoke Spread Model Using Ex-USS Shadwell Internal Conflagration Control Fire Tests*. NRL/MR/6180-95-7781.
- Jacobson, J. S. (1988). *Analysis of Heating Rate for the Insensitive Munitions Slow Cookoff Test*.
- Mansfield, J. A. (1996). *Preliminary Analysis of the Heating of Ordnance in Ship Magazines Due to a Fire in an Adjacent Compartment* .
- MSIAC. (2017). *MSIAC Accident Database eXchange*. Retrieved from MSIAC Web Portal: <https://portal.msiac.nato.int/>
- Thomas L. Boggs, K. P. (2013). *Realistic Safe-Separation Distance Determination for Mass Fire Hazards*. TR.
- Wickstrom, U. (2016). *Temperature Calculation in Fire Safety Engineering*. Springer.



NAVAL SURFACE WARFARE CENTER · DAHLGREN DIVISION

An Investigation into a Proper Heating Rate for Slow Cook-off Testing

*GUN & ELECTRIC WEAPON
SYSTEMS DEPARTMENT (E)*

David Hubble, PhD

david.o.hubble@navy.mil

540-653-6450



NSWCDD-PN-18-00104; Distribution Statement A:
Approved for Public Release; distribution is unlimited

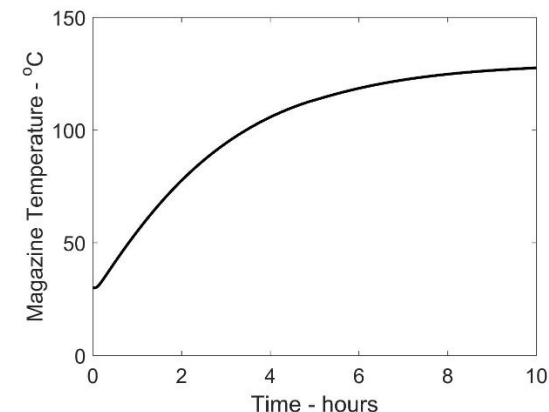
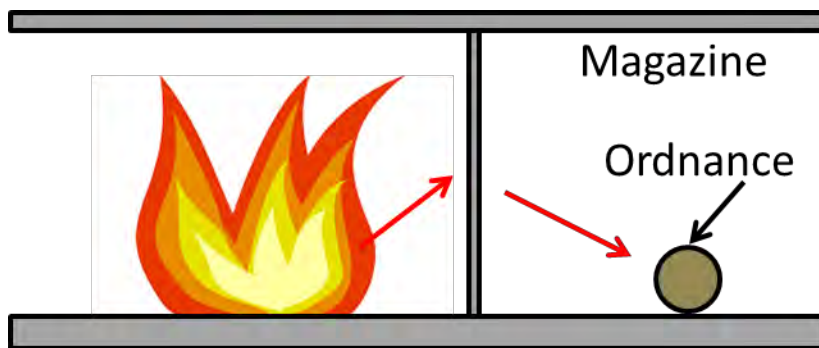
Overview

- The Slow Cook-off (SCO) test, as specified by STANAG 4382, specifies a constant heating rate of 3.3°C/hr
- The validity of this 3.3°C/hr heating rate has been questioned
 - Concern that it is too slow to represent accidents
 - Mitigations designed to work at 3.3°C/hr might not work at the higher rates that occur in accidents
- The Slow Heating Custodial Working Group (SHCWG) was formed to review the test standards and create a new Allied Ordnance Publication (AOP)
- A key topic for the SHCWG, what should the SCO heating rate be?

- The first SHCWG meeting was held in April 2017
 - There was disagreement within the group as to what accidents had occurred and what analysis had been performed
 - Agreement on an appropriate heating rate could not be reached
- The group chairman requested that an investigation be performed to be presented to the group at the second meeting
 - The investigation was meant to present facts and guide the discussion towards realistic threat scenarios
- A significant portion of this investigation was a modelling effort to identify realistic worst case SCO heating scenarios
- This paper presents the results of the modelling effort

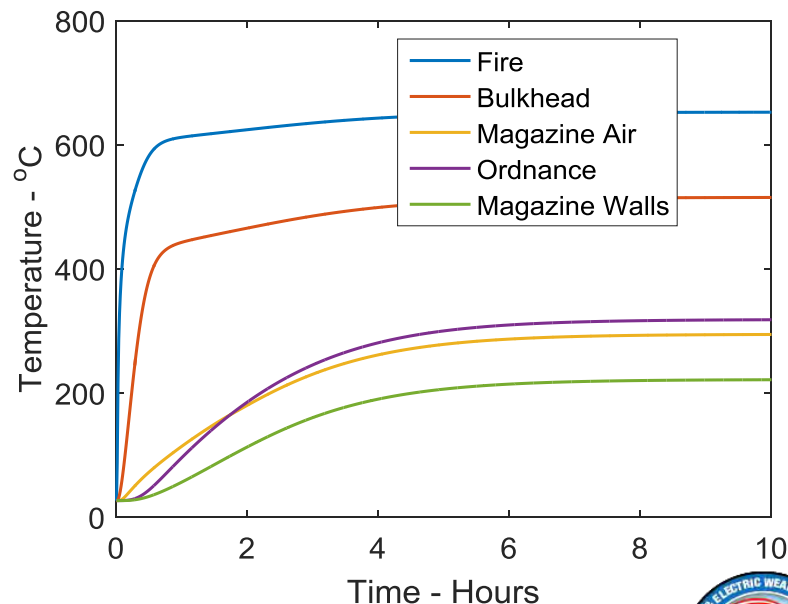
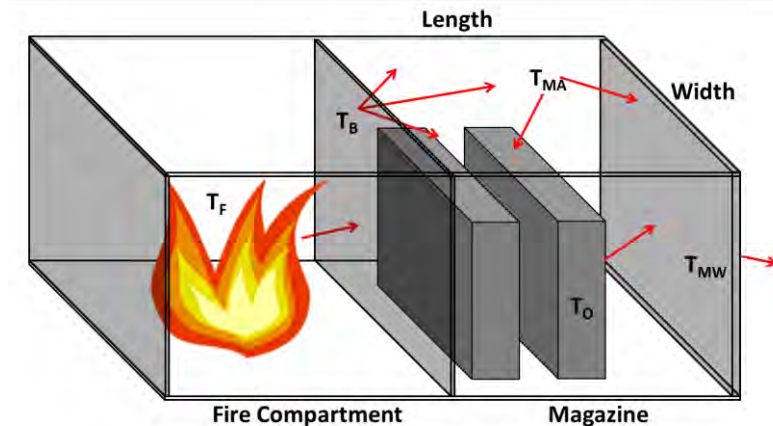
Modelling Overview

- The goal of the modelling effort was to attempt to determine the slowest heating rates that could result in a cook-off
- A review of existing analysis indicated that the slowest heating rates would result from a fire adjacent to a magazine
- A model was developed to study the fire/magazine system
- The magazine air temperature curves were then used to determine average heating rates



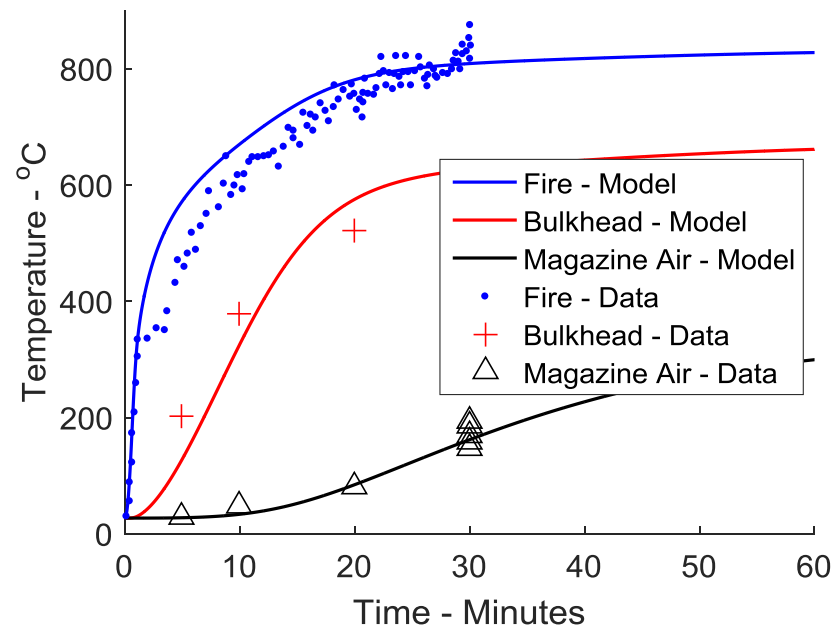
Model Overview

- A model was developed to calculate magazine temperatures during fires
 - Allows varying parameters that would influence the magazine temperature curve
 - Magazine dimensions, ordnance quantity, wall thickness, and fire size
 - Lumped mass model, includes convection and radiation but no conduction
 - Uses correlations given in Wikström 2016 – “Temperature Calculation in Fire Safety Engineering”
 - Solved using coupled, explicit finite difference equations



Model Validation

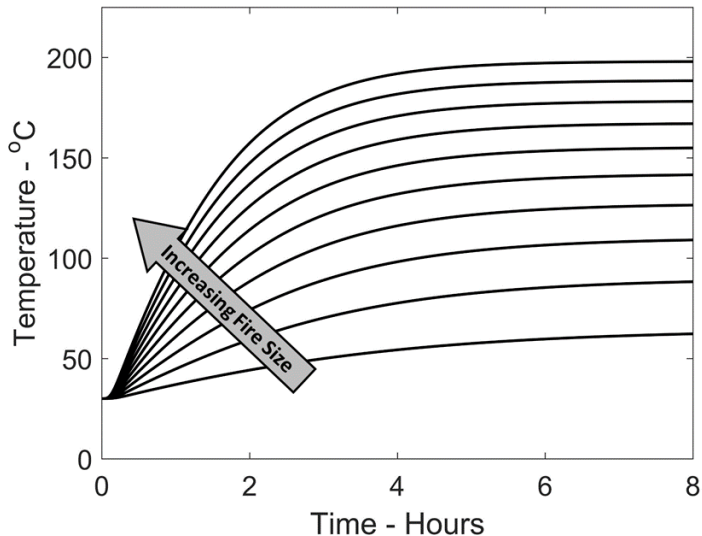
- Data from an instrumented fire aboard EX Shadwell was used to validate model
 - Compartments and fire size modeled based on data given in the report
 - The measured temperatures were compared to model results
- Model agreement with test data is sufficient to allow it to be used to simulate SCO scenarios



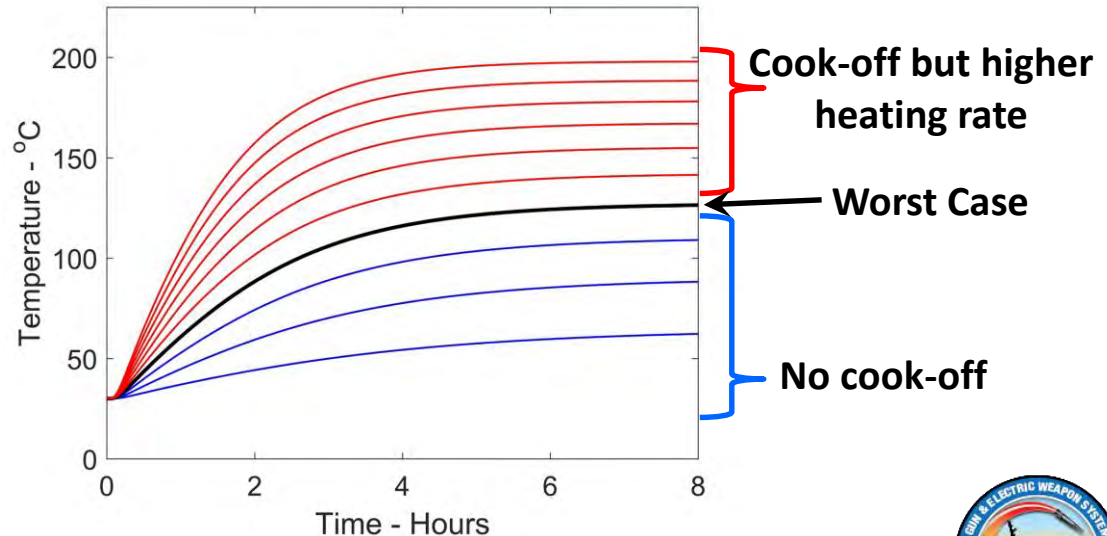
How Model is Used

- Determine the slowest heating rate that still produces cook-off temperatures within magazine
 - Increasing fire size increases final temperature
 - Assume that the lowest temperature that result in a cook-off is 130°C
 - Conservative assumption, higher value results in higher average heating rates
 - **For each set of model parameters, there is only 1 fire size that results in a final temperature of 130°C– Worst case fire size**

Magazine Gas Temperature History



Worst Case Fire Size



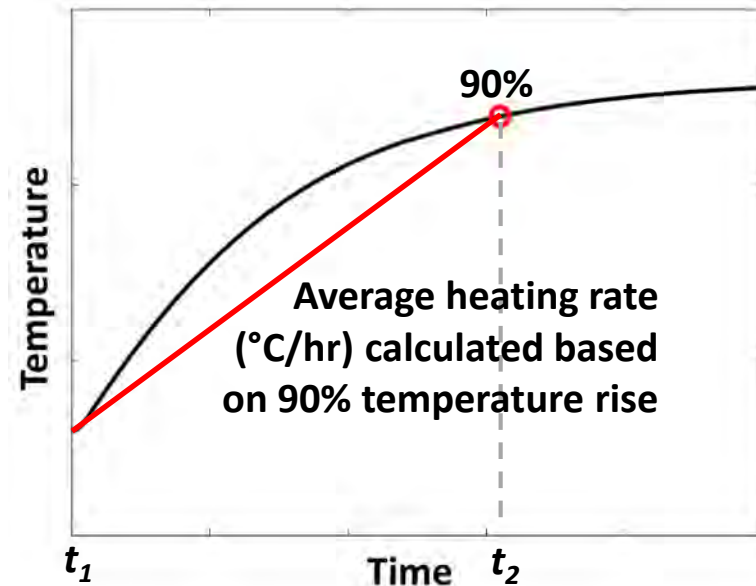
Average Heating Rate Calculation

- Want to calculate an average heating rate (average slope) from the worst case magazine temperature curve

$$\frac{\overline{dT}}{dt} = \frac{1}{t_2 - t_1} \int_{t_1}^{t_2} \frac{dT}{dt} \cdot dt = \frac{T(t_2) - T(t_1)}{t_2 - t_1} = \frac{\Delta T}{\Delta t}$$

- Must assume an equilibrium temperature, $T(t_2)$

- Equilibrium temperature selected as 90% of total temperature rise
 - Selection ensures conservatism, the higher the value the slower the calculated rate
 - Also, 90% has been used in prior analysis
- Time to 90%, t_2 , is then determined and average heating rate ($\Delta T/\Delta t$) is calculated
- **All results are based on a 130°C cook-off temperature and a 90% temperature rise**

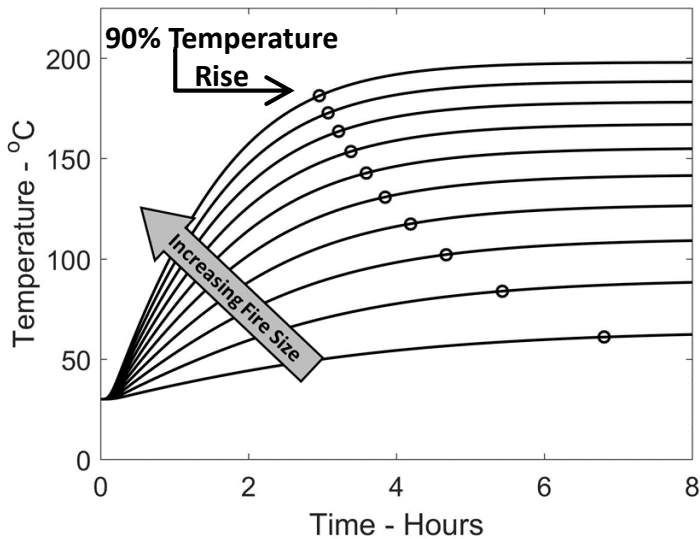


How Model is Used

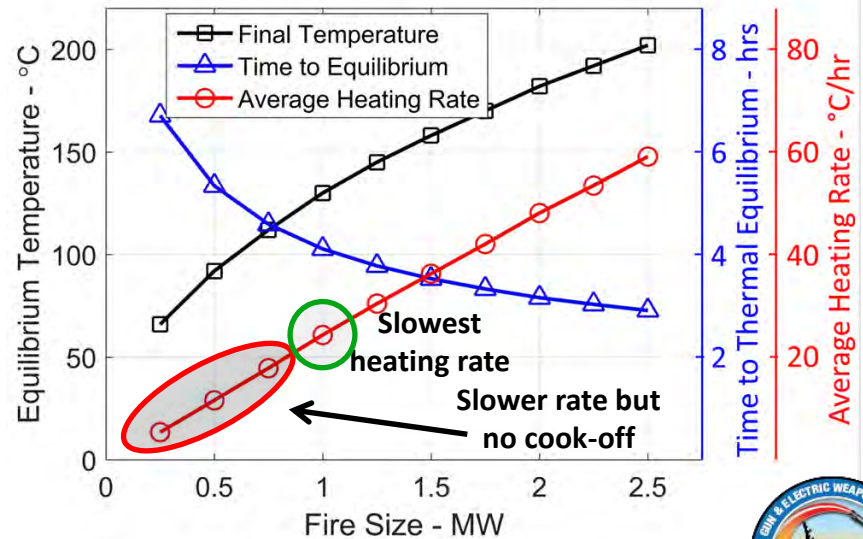
- Example for one particular set of model parameters
 1. Determine the fire size that results in 130°C final magazine temperature, 1 MW in this example
 2. Calculate time to equilibrium, $t_2 = 4.1$ hrs
 3. Use t_2 to calculate average heating rate, 24.3°C/hr

– Note that higher cook-off temperatures result in higher heating rates

Magazine Gas Temperature History

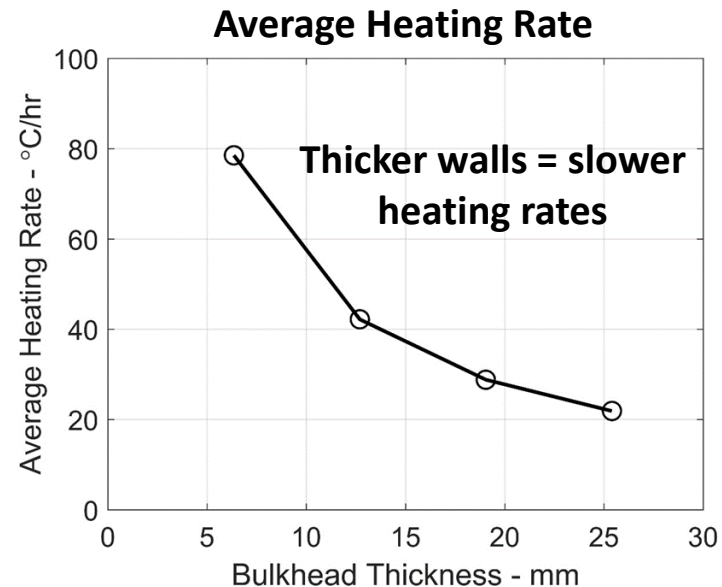
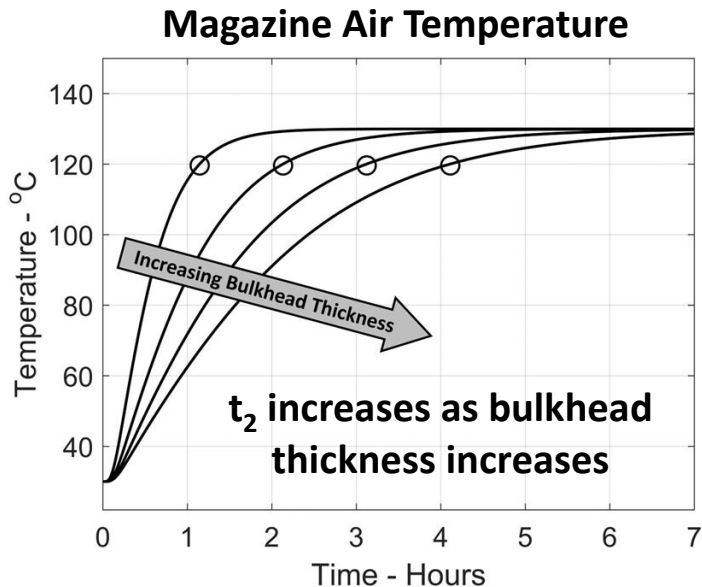


Average Heating Rate Calculation



Model Results – Bulkhead Thickness

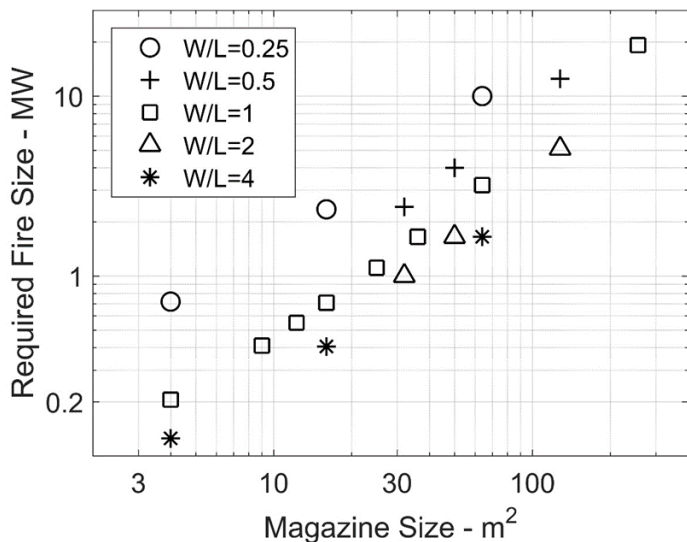
- Increasing the thickness of the bulkhead increases the total thermal mass and consequently increases the time to equilibrium
 - Does not effect equilibrium temperature within the magazine
 - Increasing bulkhead thickness decreases average heating rates**



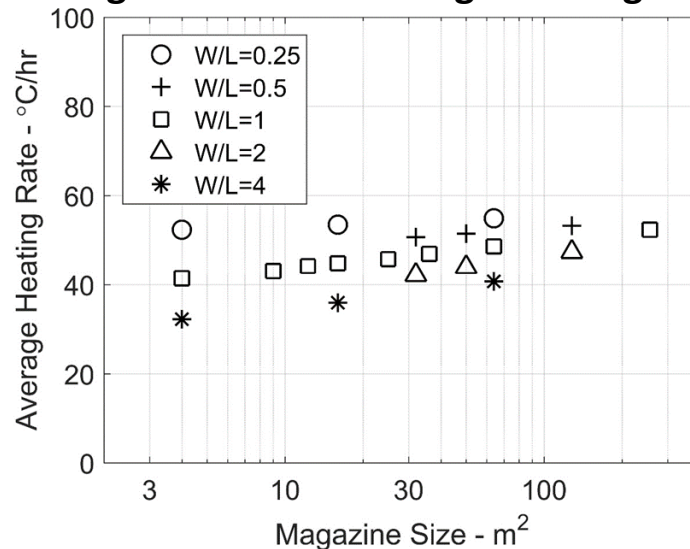
Model Results – Magazine Size

- Examined empty magazines of various sizes and aspect ratios
 - As magazines get larger, a larger fire is required to reach 130°C
 - More wall area to lose heat
 - Fire size and thermal mass both increase with increasing magazine size
 - Effects offset; magazine size has a minimal effect on average heating rate

Magazine Size vs Required Fire Size



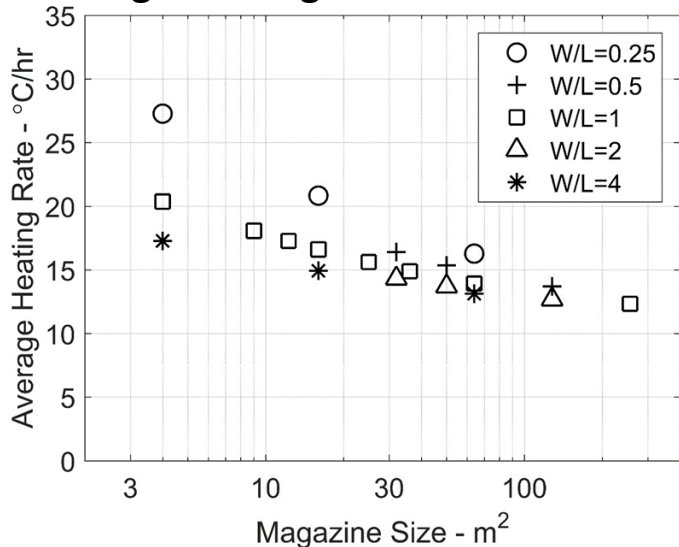
Magazine Size vs Average Heating Rate



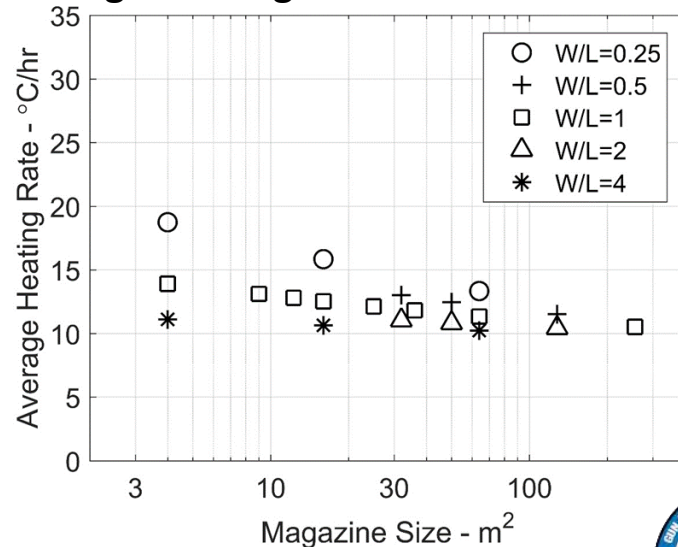
Model Results – Full Magazine

- Model was run with the magazines full of ordnance
 - Ordnance increases thermal mass which decreases the average heating rate
 - Ordnance partially blocks radiation exchange within the magazine which further decreases the average heating rate
 - Results shown are for magazines with 12mm and 25mm thick bulkheads
 - Slowest average heating rate found was **12°C/hr** for 12mm walls and **10°C/hr** for 25mm walls

Average Heating Rate – 12mm Bulkhead

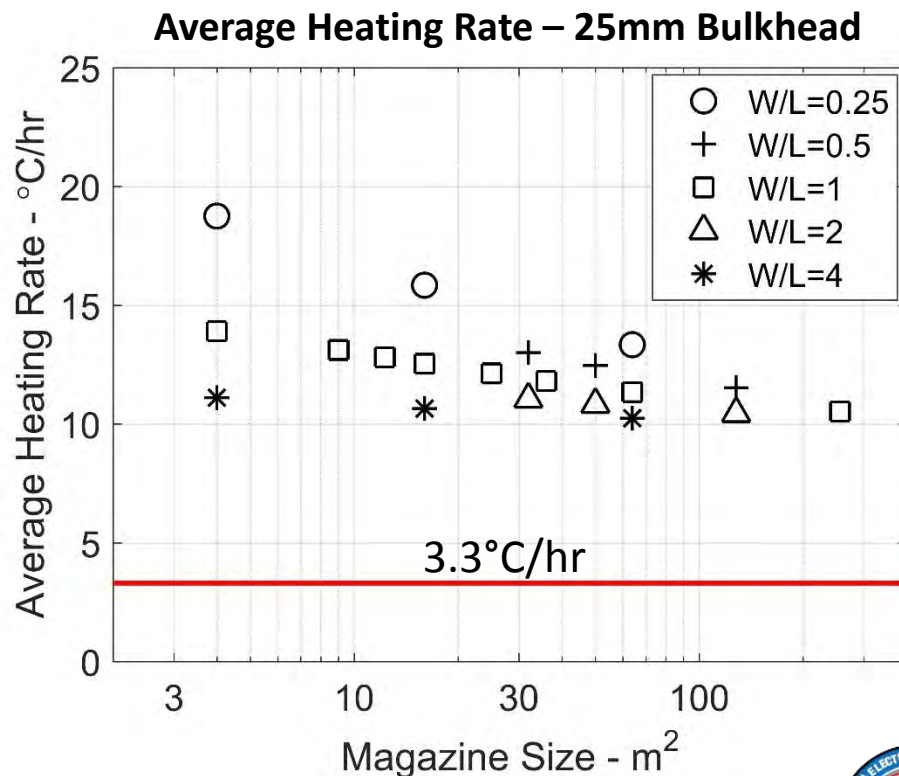


Average Heating Rate – 25mm Bulkhead



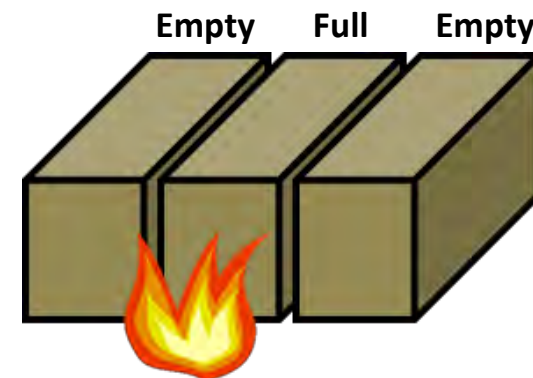
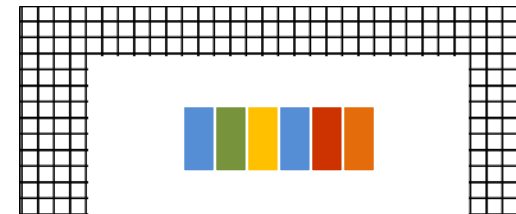
Model Results – Full Magazine

- Slowest heating rates will occur in full magazines with thick walls
- It is **not possible** for a constant sized fire to heat ordnance to cook off temperature any slower than 10°C/hr
 - Only way to get a slower rate would be a fire that gradually increased in size over many hours
 - Below deck fire size dependent on vent area, fire size usually remains essentially constant until it starts dying out
 - **Slowest rate calculated is 3 times faster than the currently specified heating rate**



Forward Operating Base

- MILVAN containers in the configuration in which they are used at forward operating bases (FOBs) were also analyzed
 - Size and maximum allowable ordnance quantity are specified
 - Assume a truck fire while loading/unloading ammunition
 - Worst case is one full container surrounded by empty containers and a fire that causes the final temperature to reach 130°C
 - Empty containers insulate magazine
 - Slowest average heating rate possible is **18°C/hr**



Summary

- Modelling was performed to determine the slowest heating rate that could be achieved within a magazine that could result in a cook-off
 - Assumed that heating was caused by an adjacent fire
 - Determined fire size that would result in a magazine temperature of 130°C
 - Calculated the average heating rate based on time to 90% temperature rise
 - Slowest heating rate found was **12°C/hr** for magazines with 12mm thick walls and **10°C/hr** for 25mm thick walls
 - A FOB MILVAN was analyzed and the slowest rate found was **18°C/hr**
- Based on these results, the current heating rate of 3.3°C/hr used in slow cook-off testing is too slow to represent a credible scenario and should be increased

Acknowledgements

Funding provided by:

- The Insensitive Munitions Advanced Development (IMAD) Program



Extra Material

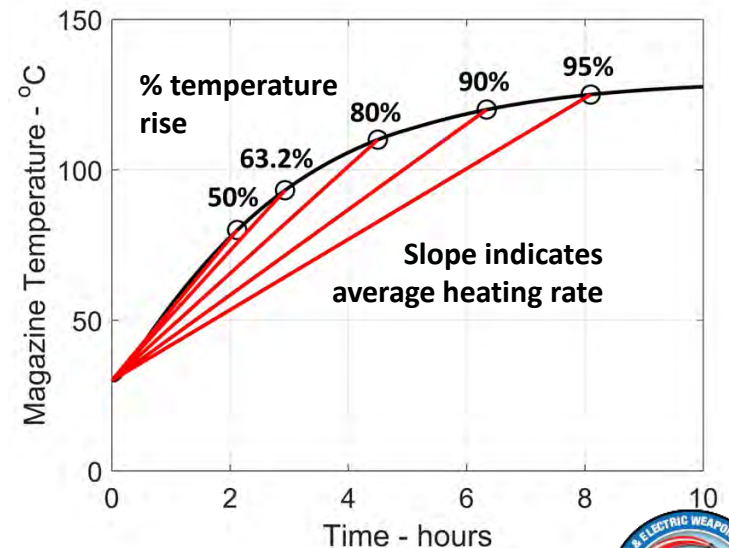


Determining the Average Heating Rate

- Temperature history , $T(t)$, is a curve with a changing heating rate, $dT(t)/dt$
- The average heating rate is the average of this changing rate:

$$\overline{\frac{dT}{dt}} = \frac{1}{t_2 - t_1} \int_{t_1}^{t_2} \frac{dT}{dt} \cdot dt = \frac{T(t_2) - T(t_1)}{t_2 - t_1}$$

- $T(t_1)$ is the initial temperature, t_1 is 0, and t_2 is the time to thermal equilibrium
- Curve is asymptotic, never reaches equilibrium
- Equilibrium temperature is therefore defined as point where the temperature reaches an arbitrary percentage of the total temperature rise
- Increasing percentage decreases average rate

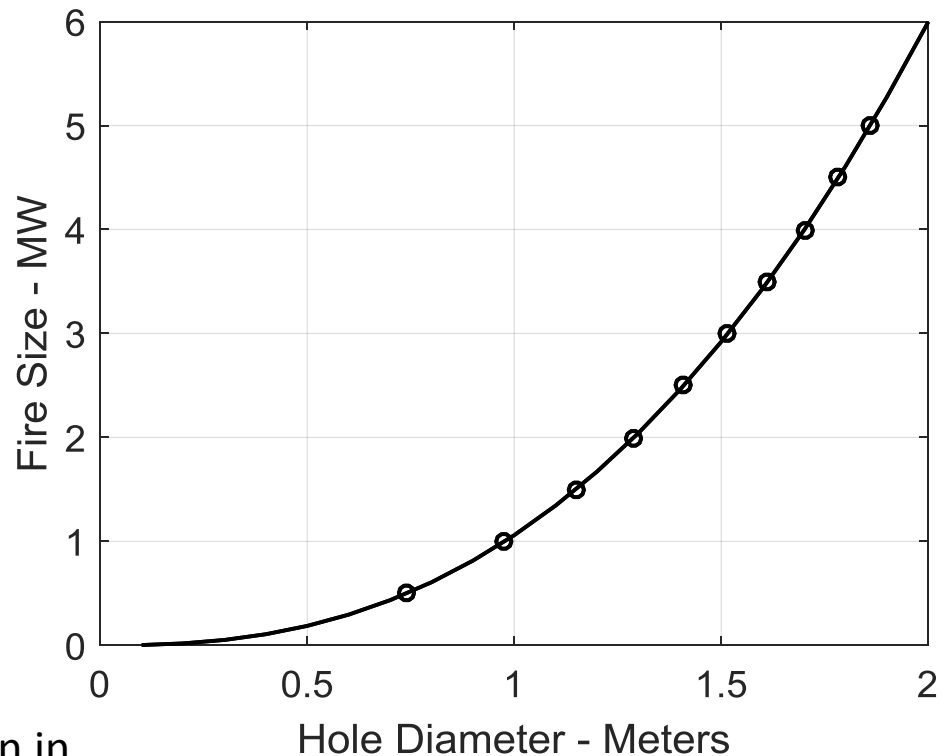


- 90% was chosen for this work



Fire Size vs Vent Size

- Heat released by fire is a function of the available air to support combustion
- For typical hydrocarbons:
- $q \sim 1.35E6 \cdot A\sqrt{h}$
- Assuming a circular hole:
- $q \sim 1.06E6 \cdot D^{2.5}$



Wikström 2016 – “Temperature Calculation in Fire Safety Engineering”

1. Transportation accident

- Railroad boxcar fires at Corning, Tobar, Benson, and Roseville
- Slow heating rates reported in the past have included long initial duration before ordnance is actually heated
- Analyzed test date where boxcars containing simulated bombs were burned
- Slowest rate recorded during testing was a Mk 81 bomb at **83°C/hr**

2. Dump storage accident

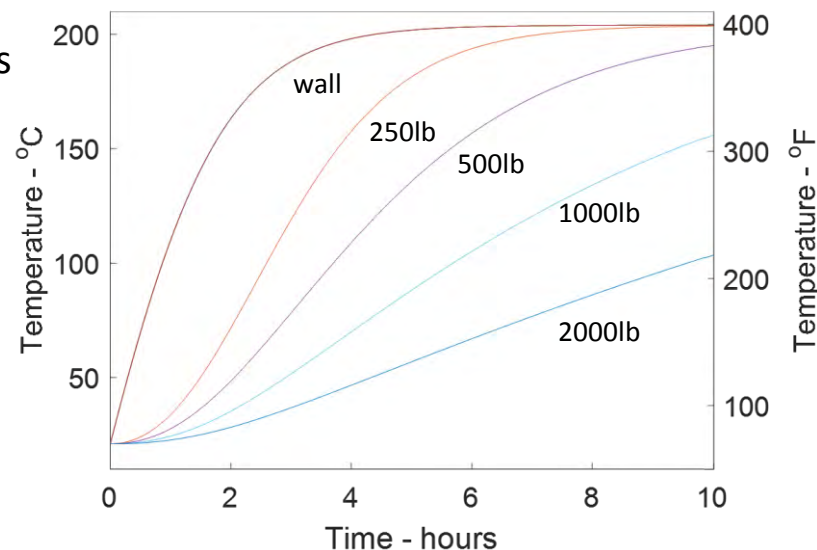
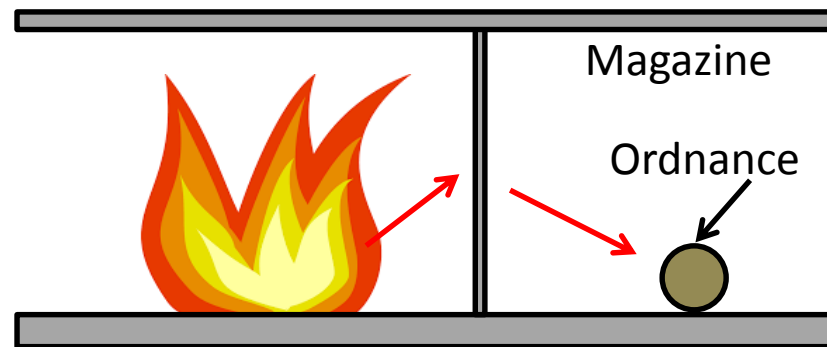
- Lowest heating rate results from a large, slow moving fire near the storage area
- Slowest heating rate from simulations, that still reaches cook-off temperatures, is **52°C/hr**

3. Debris pile from deck fire

- Ordnance is buried within debris pile during and after a fire/FCO event
- Slowest heating rate from simulations is **52°C/hr**

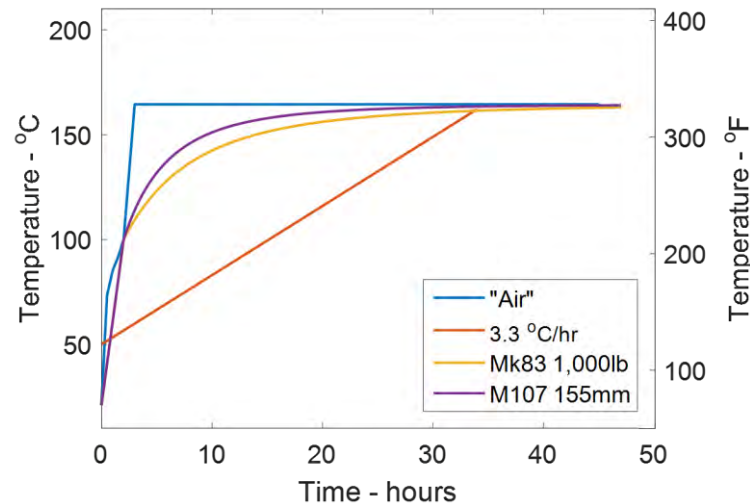
4. Below deck fire

- Fire in a compartment adjacent to a magazine which contains ordnance
- Fire heats common bulkhead which then heats ordnance by radiation
- Analysis **does not** calculate temperature of air within magazine, only the average ordnance temperature for four different sized munitions
- Average rate to 150°C for four sizes of munitions was calculated
 - 250 lb – **51°C/hr**
 - 500 lb – **29°C/hr**
 - 1,000 lb – **17°C/hr**
 - 2,000 lb – **7°C/hr**



5. Steam leak within magazine

- Intermediate pressure steam saturated at 3100 kPa and 236°C leaks into a magazine, expansion results in superheated steam at 165°C (328°F)
- Condensing steam heats magazine and everything in it to 100°C within 2 hours
- The ordnance (Mk83 1,000 lb bomb in Fontenot’s analysis) then asymptotically approaches 165°C (328°F) steam temperature
- By selecting ordnance temperature arbitrarily close to final temperature (e.g. 327°F), a heating rate of **3.3°C/hr** was obtained
- If time to 150°C is used for rate calculation (as in scenario 4) a rate of **8°C/hr** is obtained
- Rate is based on ordnance temperature, **not surrounding air temperature**
- Only 1 steam leak in the literature, no reaction occurred



Duration	Temp. (°F)	Rate (°F/hr)
10 hrs.	273	20
15 hrs.	297	15
25 hrs.	317	10
35 hrs.	325	7
45 hrs.	327	6

Temperature table copied from Fontenot report



STATUS - CRITICAL DIAMETER AND GAP TESTS FOR HAZARD CLASSIFICATION OF SOLID ROCKET MOTORS

Cynthia P. Romo & Dr. Josephine Covino

K.P. Ford, A.D. Farmer, R. Rose
Naval Air Warfare Center Weapons Division, China Lake, California
T.L. Boggs, A.I. Atwood
Naval Systems Incorporated, Ridgecrest, California

Insensitive Munitions and Energetic Materials Technology Symposium
23 – 26 April 2018
Portland, OR



OBJECTIVE

- Brief history of propellants
 - How formulations have changed with time
- Development of the gap test
 - Determine transportation and storage hazard classification
- Overview of current test procedures
- Options available to the system developer
 - Strengths and weaknesses of each option
- Facilitate dialogue on methods to improve gap testing



BACKGROUND

- World War II – Early 1950s: Double-base propellants
 - Small critical diameters
- 1950's – 1960's: Composite Propellants
 - AP/Al/binder replaced many NC/NG formulations
 - Critical diameter increased markedly
 - Proliferation of AP based systems
- 1970's: Improving propellant compositions
 - Adding nitramines to increase specific impulse
 - Range, velocity, and payload
 - Burning rate modifiers
 - Decrease time to target
 - Increased performance – decreased critical diameter



GAP TEST

- Shock initiation test (1950)
- Predict hazard from unintentional detonation
 - One explosive exposed to shock
 - Quantify the sensitivity of the material
- Los Alamos National Lab small-scale gap test
- Naval Ordnance Lab large-scale gap test (NOL LSGT)
- Super large-scale gap test (SLSGT)



CONCERN

- AP/Al/binder propellants
 - Critical diameter in multiple feet
 - Project SOPHY: d_{cr} greater than 62 inches
 - Industry stopped determining critical diameter
 - Hard to find large mechanical shock threat
- Reduce the hazard classification of a system propellant from HD 1.1 to HD1.3
 - Add nitramines until a “go” reaction, then decrease nitramine content until “no-go”
- Larger gap tests needed



1998: TB 700-2

- NOL LSGT and newer formulations
 - Could not help characterize large solid rocket motor hazard
- Modification of the Technical Bulletin 700-2
 - UN Test Series 6
 - Used for hazard classification HD1.1, 1.2, 1.3, and 1.4
 - Single package test – UN Test 6 (a)
 - Stack test – UN Test 6 (b)
 - Alternate tests
 - Performed on large solid propellant rocket motors – very expensive



1998 TB 700-2: ISSUES

- Shock input into propellant > 280 kbar
 - No attenuator between booster and donor
 - Storage and transportation hazards < 10 kbar
- 16-inch length sample
 - Did not allow shock to decrease to sonic velocity
- Test thick-wall steel-bomb-cased energetic materials
 - ½-inch-thick steel wall not representative of rocket motor cases
 - Greater pressures than shock wave from donor



1998 TB 700-2: ISSUES

- No velocity pins, no determination of shock wave velocity
 - Shock wave velocity could help determine “go or “no go”
- Maximum allowable sample diameter: 7 inches
 - Larger critical diameter propellants
 - Inadequate to determine sample’s hazard



1998 TB 700-2: SUGGESTED CHANGES

- Increase sample length
 - From 16-inch to 32-inch
 - Determine if detonation wave decayed
- Incorporate velocity pins
 - 14 pins, 1 inch away from donor
- Comp B conical booster
 - 8-inch by 8-inch cylindrical booster produced significant blast
- Adding an attenuator
 - Between donor and propellant
 - Provide a 70 kbar shock to sample



2012: TB 700-2



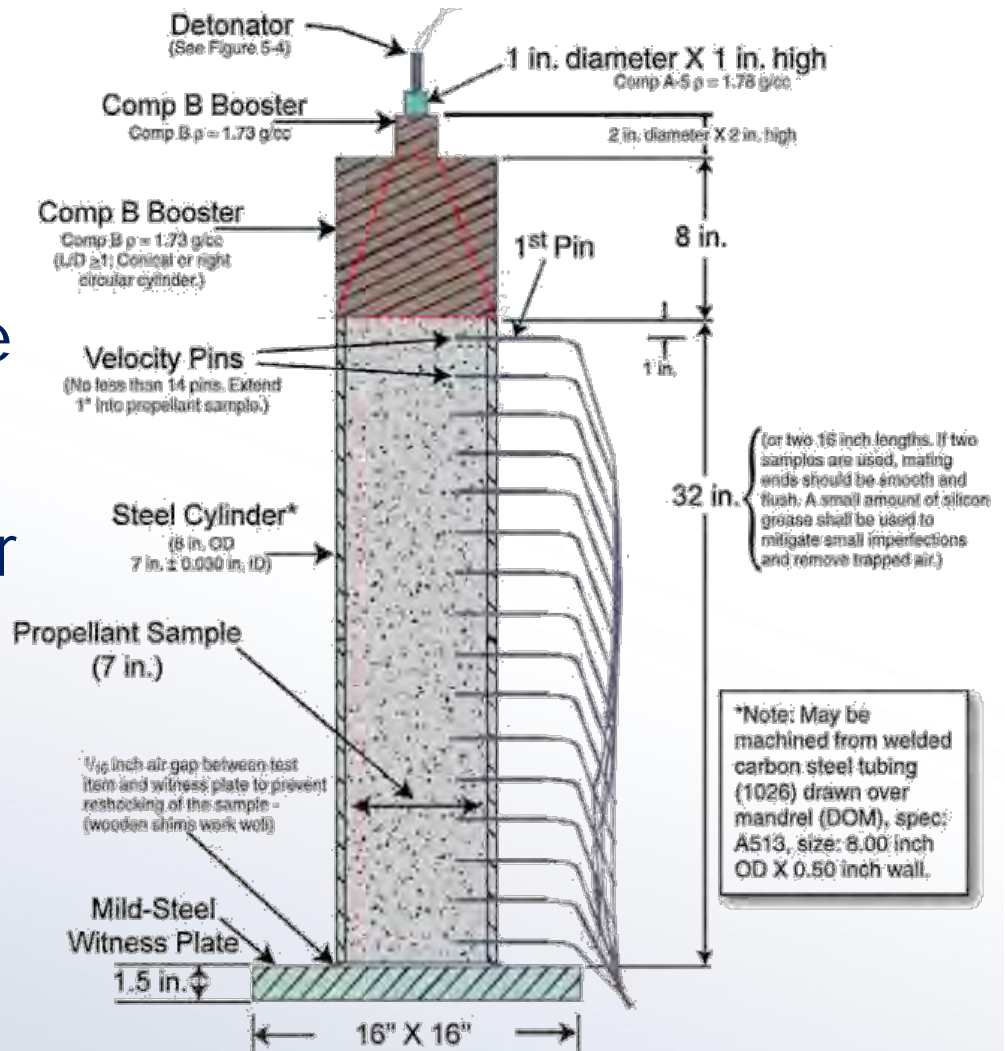
DDESB Memorandum

- SLSGT suggestions resulted in modifications
 - DDESB document signed by Capt. William Wright, Chairman
- Three options replace section 6-6(c) of 1998 TB 700-2
 - Option 1. Refined SLSGT
 - Option 2. Determine unconfined d_{crit}
 - Option 3. Missile motor diameter



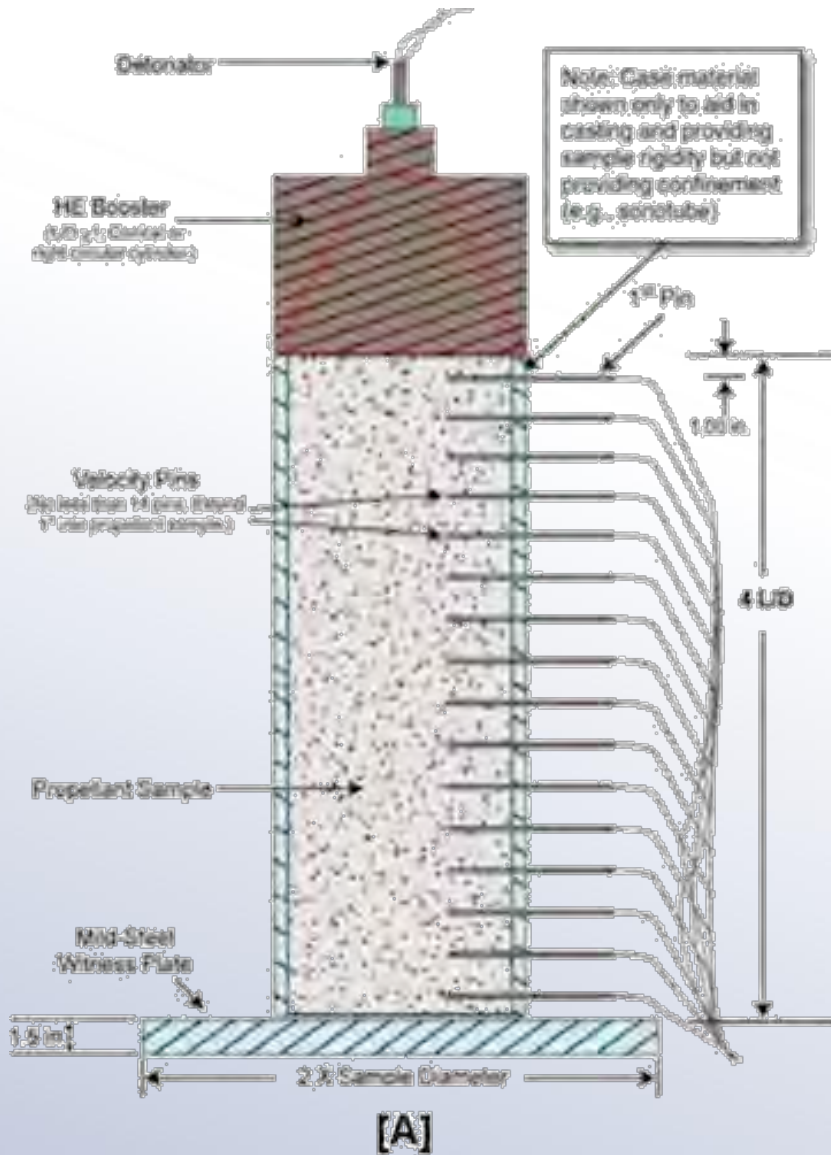
OPTION 1

- Refined version of SLSGT
- 32-inch-long sample
- 14 velocity pins
- Either a right circular cylinder or conical booster
- No PMMA attenuator





OPTION 2: D_{crit}

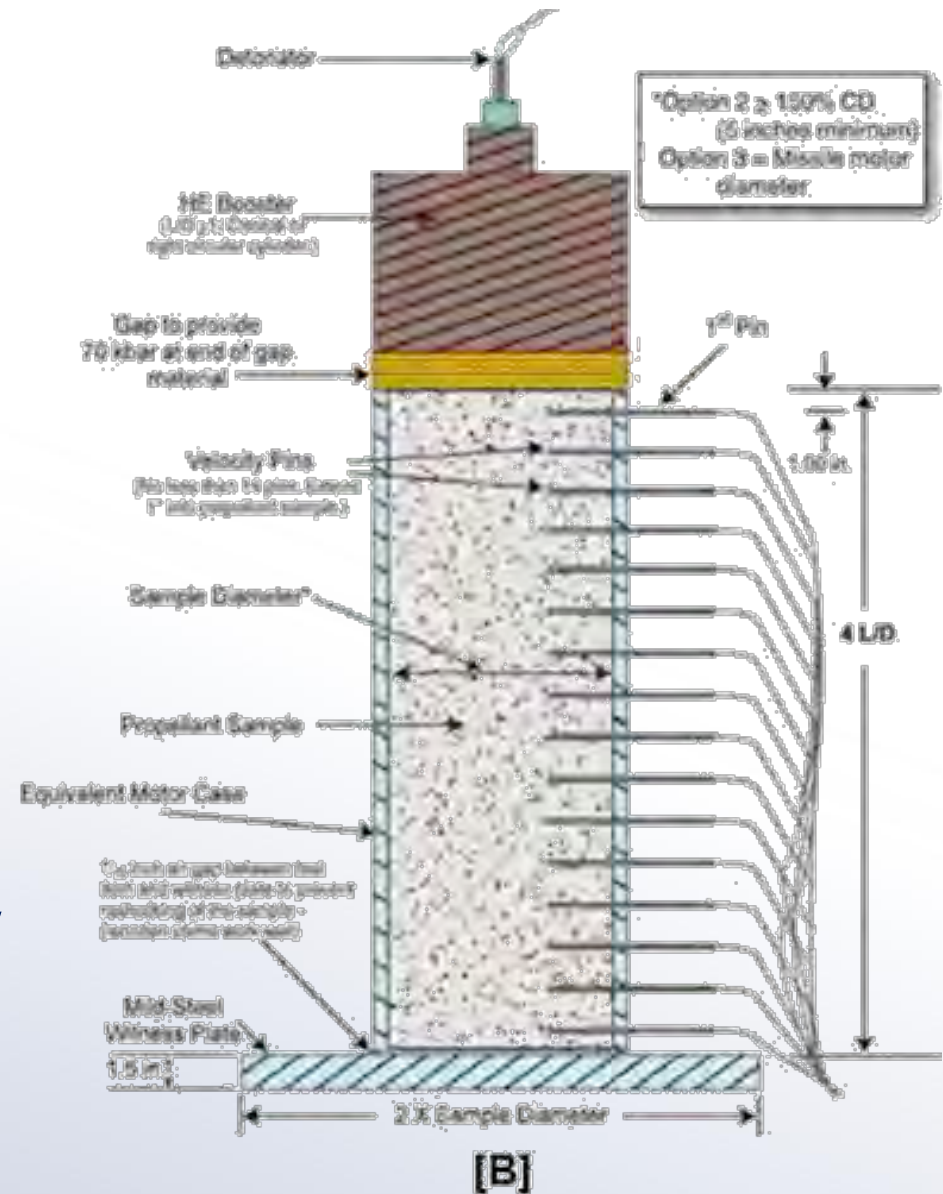


- Determine Critical Diameter [A]
- Address confinement thickness concern
 - Test in equivalent confinement to motor case



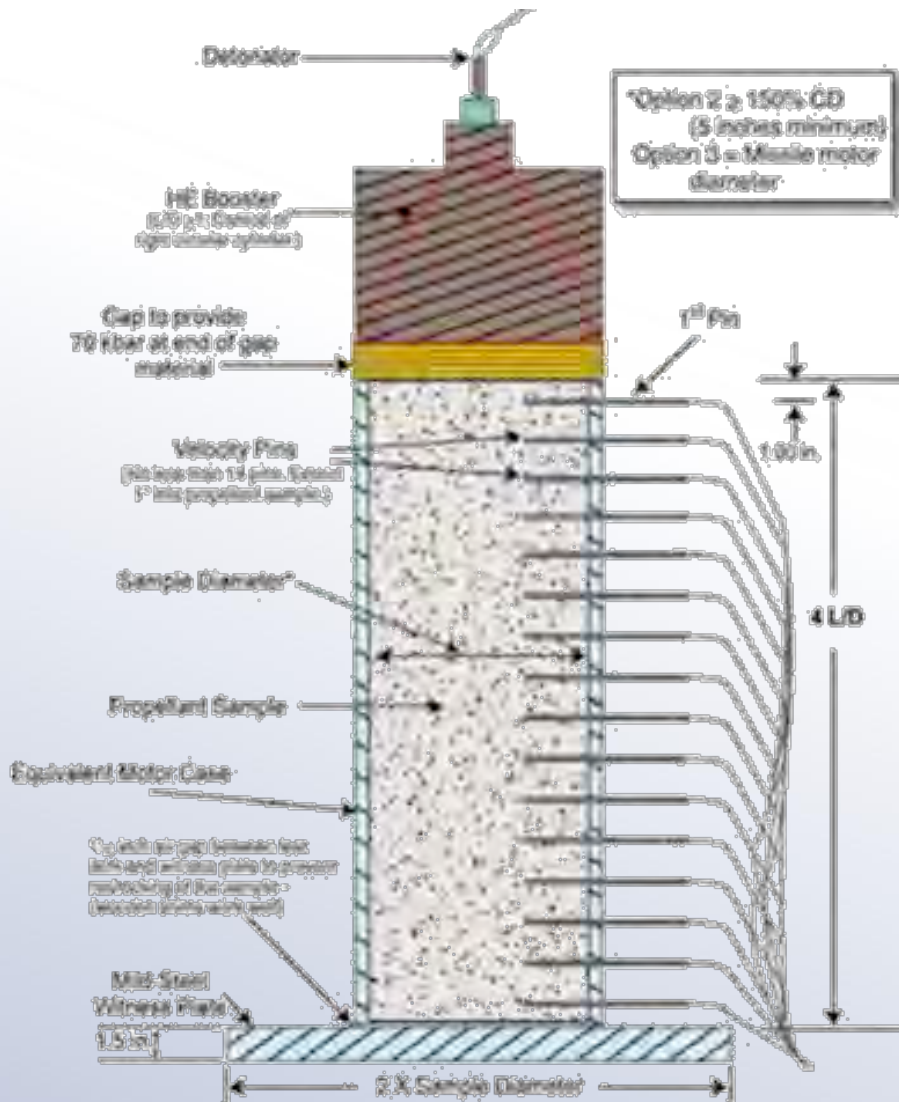
OPTION 2

- Minimum sample diameter [B]
 - 5-inches
 - 150 percent of unconfined critical diameter
- 14 velocity pins minimum
- Attenuation to allow 70-kbar shock





OPTION 3



- Similar to Option 2
- Confinement = motor case
- Sample diameter = missile diameter
- Closely recreate original environment an item would be used in
- More applicable to smaller tactical missiles
- Much less cost effective for larger diameter solid rocket motors



CONFINEMENT - LINDFORS et al.

- Gap research continued
- Role of confinement
 - Determine effects of different confinement
 - AP/Al/HTPB propellant 12-inch diameter sample
 - Different case materials
 - Different case wall thickness
 - No confinement
 - Schedule 40 PVC pipe
 - Schedule 80 PVC pipe
 - 0.37-inch aluminum wall thickness
 - 0.0687-inch aluminum wall thickness
 - 1/2-inch thick steel wall thickness



CONFINEMENT EFFECTS

Lindfors, et al. AP/AI/HTPB Propellant

Time/ Case (μ s)	Unconfined Propellant ($\rho = 1.850$)	12.75" x 0.5" Steel Case Rho = 7.90	Schedule 40 PVC Rho = 1.376	Schedule 80 PVC Rho = 1.376	12.75" x 0.375" Aluminum Rho = 2.703	12.75" x 0.687" Aluminum Rho = 2.703
100	103.2	103.4	98.5	99.4	99.3	100.1
125	111.2	139.4	109.2	109.32	110.3	119.0
150	118.1	186.8	115.0	115.4	124.6	141.3
175	137.4	312.2	133.4	132.4	162.9	194.5

- 1/2-inch steel case
 - Highest confinement
 - Highest pressure
 - Pressure at 175 μ sec = 312.2 kbar
 - Original shock wave pressure = 280 kbar



MODEL - MILLER et al.

- Studies of four different propellants
- Modified DYNA-2D predictions vs experimental data
 - Zero cards vs 50 cards
 - HD 1.1 vs HD 1.3
- Reduce size of donor – no apparent effect on walls
- Confinement change
 - From ½-inch steel walls to PVC
 - PVC impedance < steel impedance
 - Rocket motor case confinement
 - Reproduce observed gap test results
 - Model could be a viable tool in designing alternate gap test configurations



GENERAL FINDINGS

- Gap test continues to evolve
 - Solid rocket propellants < shock sensitive
- Option 1 may not be the most appropriate test
 - Confinement can vary reaction levels
 - Duration of the input pulse can affect reaction of material
 - Longer duration, lower pressure pulse – sufficient to initiate sample
- Understanding properties of the system is important
 - Critical diameter
 - Casing influence on shock sensitivity of material



GENERAL FINDINGS, cont'd.

- Which test to use?
 - Understand the system
- Some problems are known
 - Solutions have yet to be found
- Additional work is needed
 - Experimental and analytical

It is important to consult the Service Hazard Classifier early in the process when determining which test standard to implement during any program development effort



CURRENT WORK

- Extensive literature review
 - Use and evolution of critical diameter and gap tests through the years
- Papers are being reviewed and summarized
 - Hazard Classification
 - TB 700-2
 - Critical diameter
 - Gap tests
 - Alternate tests

The authors are soliciting papers in these areas to include in the study



WHY BOTHER?

- Important to understand the different types of gap tests used
 - Assess shock sensitivity
- More comprehensive understanding of each test configuration
 - Help identify methods to correlate data between tests
 - Identifying origins, test setup, applications, and limitations
 - Determine what the results of each test reveal about the material's shock sensitivity



ACKNOWLEDGEMENTS

The authors would like to thank:
B. E. Knoblett and G. E. Walseman



QUESTIONS



REFERENCES

- Paul W. Cooper. Explosives Engineering, 2nd Edition. John Wiley & Sons, 2008.
- E. A. Eyster, L. C. Smith, and S. R. Walton. "The Sensitivity of High Explosives to Pure Shocks," NOLM 10,336, 14 July 1949.
- Jonas A. Zukas and William P Walter. Explosive Effects and Applications, Springer, 1998.
- Donna Price. "Gap Tests and How They Grew," Minutes of the Explosives Safety Seminar (22nd), Anaheim, California, August 1986, pp. 365-380. (AD-A181 274.)
- D. Price, A. R. Clairmont, Jr., and J. O. Erkman. "The NOL Large Scale Gap Test III. Compilation of Unclassified Data and Supplementary Information for Interpretation of Results," Naval Surface Warfare Center, White Oak, Maryland, 8 March 1974. (NOLTR 74-40; publication UNCLASSIFIED.)
- R. B. Elwell, O. R. Irwin, and R. W. Vail, Jr. "Project SOPHY Solid Propellant Hazards Program," Aerojet-General Corporation, 88 pp, 31 December 1966. (AFRPL-TR-66-276; publication UNCLASSIFIED.)
- Department of Defense (DoD) Ammunition and Explosives Hazard Classification Procedures Joint Technical Bulletin TB 700-2/NAVSEAINST 8020.8B/TO 11A-1-47/DLAR 8220.1, 5 January 1998.
- Current Efforts to Develop Alternate Test Protocols for the Joint Technical Bulletin "Department of Defense Ammunition and Explosives Hazard Classification Procedures," TB 700-2, dated 5 January 1998.



REFERENCES

- A. J. Lindfors, O. E. R. Heimdahl, T. L. Boggs, and J. J. Davis. "Determination of Shock Sensitivity of Propellants in Gap Test Configuration," 38th JANNAF CS/APS/PSHS Meeting, Destin, Florida, April 2002.
- P. J. Miller and T. L. Boggs. "Recent Hazard Classification Test Data on SRM Propellants," 29th DoD Explosives Safety Seminar Proceedings, New Orleans, Louisiana, July 2000.
- J. C. Foster, Jr, K. R. Forbes, M. E. Gunger, and B. G. Craig. "An 8-Inch Diameter, Heavily Confined Card Gap Test," AFATL/DLJW, Eglin AFB, Florida, November 1985. (AFATL-TR-85-98; publication UNCLASSIFIED.)
- Current Efforts to Develop Alternate Test Protocols for the Joint Technical Bulletin "Department of Defense Ammunition and Explosives Hazard Classification Procedures" TB700-2, dated 5 January 1998. (Also see D. F. Schwartz, R. R. Bennett, K. J. Graham, and T. L. Boggs, 19th JANNAF Propulsion Systems Hazards Subcommittee Meeting, CPIA Publication 704, Vol. 1, pp. 117-131, Monterey, California, November 2000. (2001-0053KA.)
- P. J. Miller, T. L. Boggs, and K. J. Graham. "Reactive Flow Modeling of the SLSGT: Progress Towards Developing a New Shock Sensitivity Test for Hazards," 19th JANNAF Propulsion Systems Hazards Subcommittee Meeting, CPIA Publication 704, Vol. 1, pp 132-143, Monterey, California, November 2000.



REFERENCES

- Chemical Propulsion Information Agency. Joint JANNAF/DDESB Workshop on Hazards Classification of Large Rocket Motors Workshop Report, Alexandria, Virginia, June 2001.
- William Wright. "Changes to Alternate Test Procedures for Solid Propellant Rocket Motors," Department of Defense Explosives Safety Board Memorandum DDESB-KT, Alexandria, Virginia, January 2002.
- Department of Defense (DoD) Ammunition and Explosives Hazard Classification Procedures Joint Technical Bulletin TB 700-2. 2012.
- A. J. Lindfors, O. E. R. Heimdahl, T. L. Boggs, and T. AtienzaMoore. "Shock Sensitivity of Propellants Using the Super Large Scale Gap Test," 31st DoD Explosives Safety Seminar, San Antonio, Texas, August 2004.
- R. R. Bennett, D. F. Schwartz, K. J. Graham, and T. L. Boggs. "Comments and Position Regarding the Joint Technical Bulletin 'Department of Defense Ammunition and Explosives Hazard Classification Procedures' TB 700-2, dated 5 January 1998." 29th U.S. DoD Explosives Safety Seminar, New Orleans, Louisiana, July 2000.
- A. L. Bowman, C. A. Forest, J. D. Kershner, C. L. Mader, and G. H. Pimley. "Numerical Modeling of Shock Sensitivity Experiments," Proceedings of the Seventh Symposium (International) on Detonation, Annapolis, Maryland, June 1981.
- P. J. Miller and A. J. Lindfors. "Shock Loading and Reactive Flow Studies of Void Induced AP/AI/HTPB Propellants," in Shock Compression of Condensed Matter, AIP Publication CP429, 1997.



U.S. ARMY
RDECOM

Presented to:

INSENSITIVE MUNITIONS & ENERGETIC MATERIALS TECHNOLOGY SYMPOSIUM

*THE UNKNOWN DETONATION
TRANSITION (XDT) MECHANISMS
ASSOCIATED WITH DAMAGED
ROCKET PROPELLANT IMPACTING A
SURFACE: UNDERSTANDING AND
APPLICATIONS TO IM*

Distribution Statement A. Approved for public
release. Distribution is unlimited.



TECHNOLOGY DRIVEN. WARFIGHTER FOCUSED.

Presented by:

Dr. Mark Pfeil

**Dr. Jamie Neidert, Jessica Stanfield, and
David Huebner**

**U.S. Army Aviation and Missile Research,
Development, and Engineering Center**

April 26, 2018



Deliver collaborative and innovative aviation and missile capabilities for responsive and cost-effective research, development and life cycle engineering solutions.

~9,211
FY17 Strength



2,945
Civilian

16
Military

6,250
Contractor

907 / 5343
SETA Non-SETA

Core Competencies

- Life Cycle Engineering
- Research, Technology Development and Demonstration
- Design and Modification
- Software Engineering
- Systems Integration
- Test and Evaluation
- Qualification
- Aerodynamics/ Aeromechanics
- Structures
- Propulsion
- Guidance/Navigation
- Autonomy and Teaming
- Radio Frequency (RF) Technology
- Fire Control Radar Technology
- Image Processing
- Models and Simulation
- Cyber Security

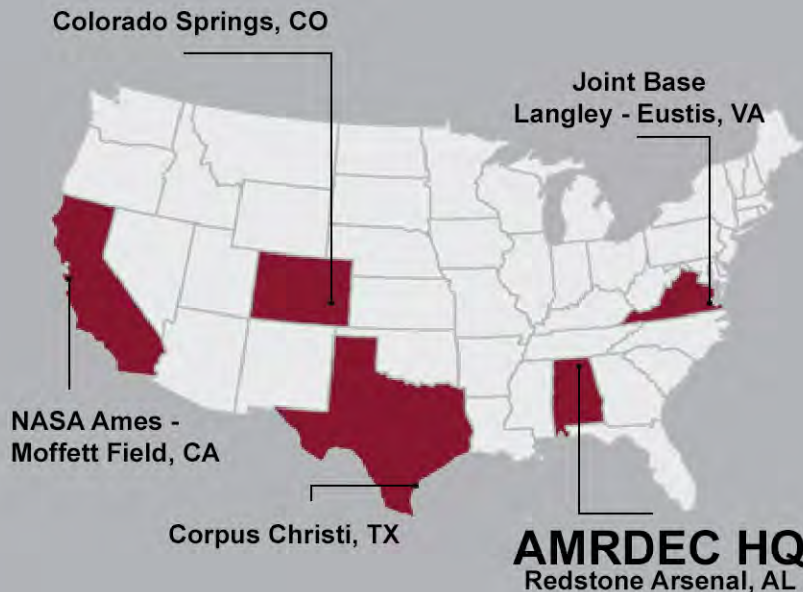
FY17
\$2,904M

6%
Aviation S&T

7%
Missile S&T

63%
Army

24%
Other



#1: Readiness

Provide aviation and missile systems solutions to ensure victory on the battlefield today.



#3: Soldiers and People

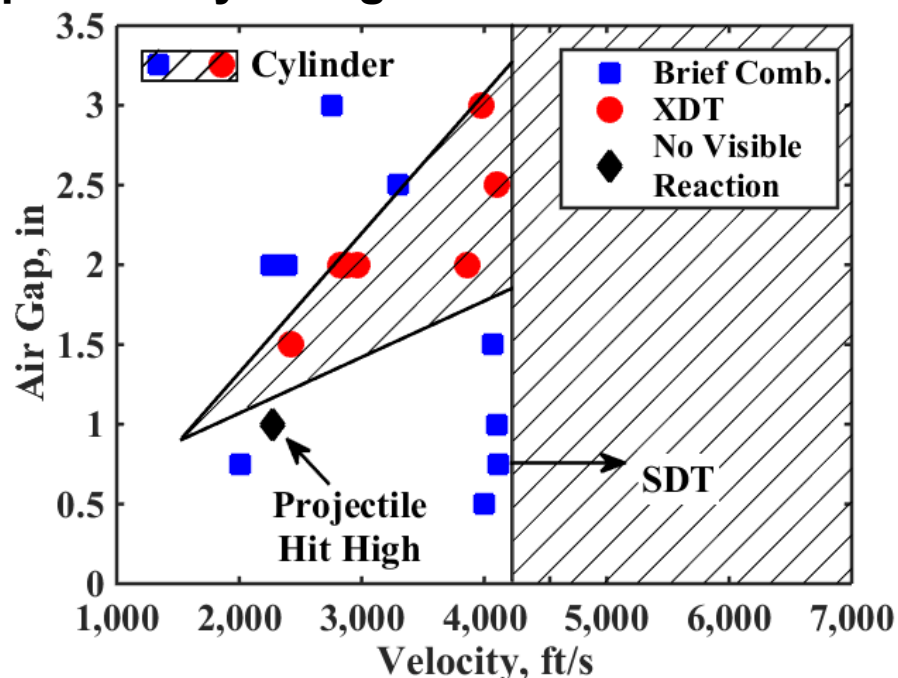
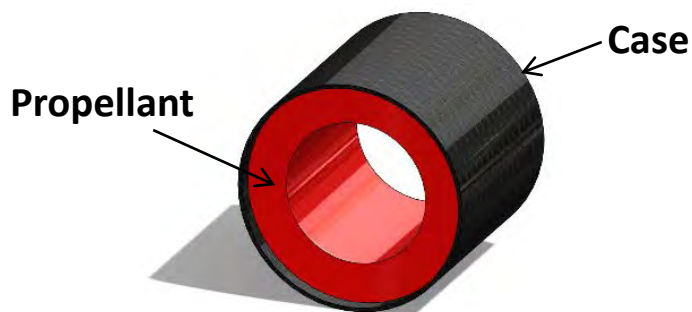
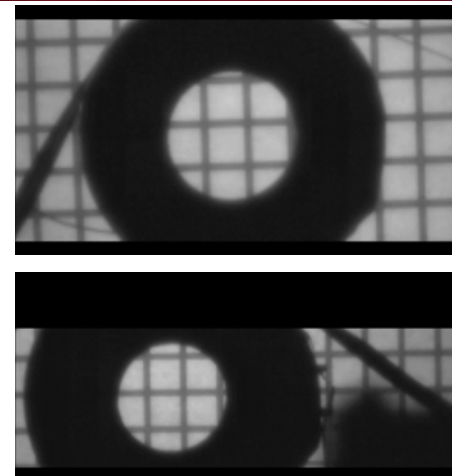
Develop the engineering talent to support both Science and Technology and the aviation and missile materiel enterprise

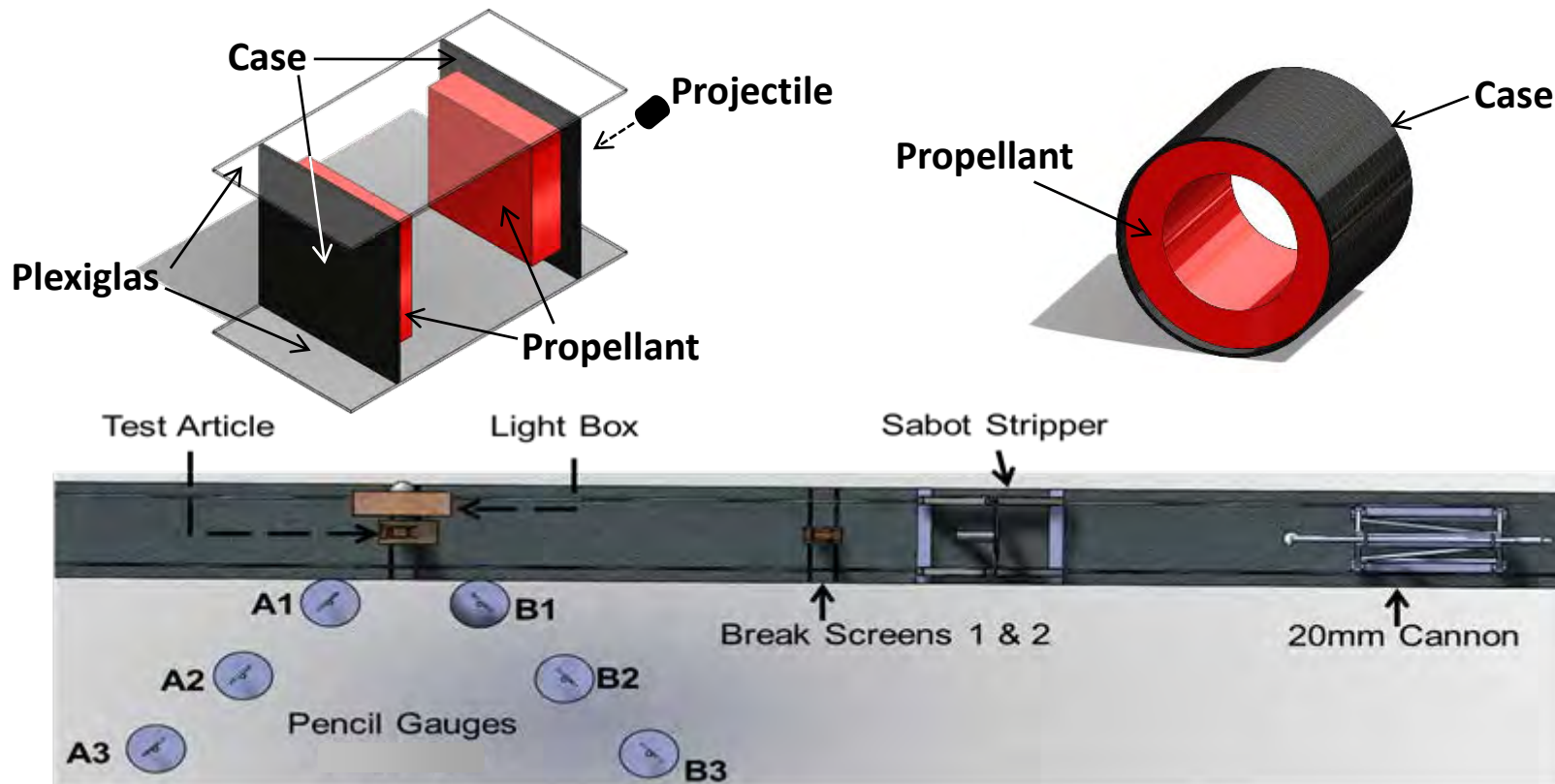
#2: Future Force

Develop and mature Science and Technology to provide technical capability to our Army's (and nation's) aviation and missile systems.



- Motors need to pass insensitive munition fragment impact requirements
 - Better understanding of motor reaction needed
- Motors containing 1.1 propellant can detonate via
 - Shock to Detonation Transition (SDT)
 - Unknown Detonation Transition (XDT)
 - More prevalent problem than previously thought



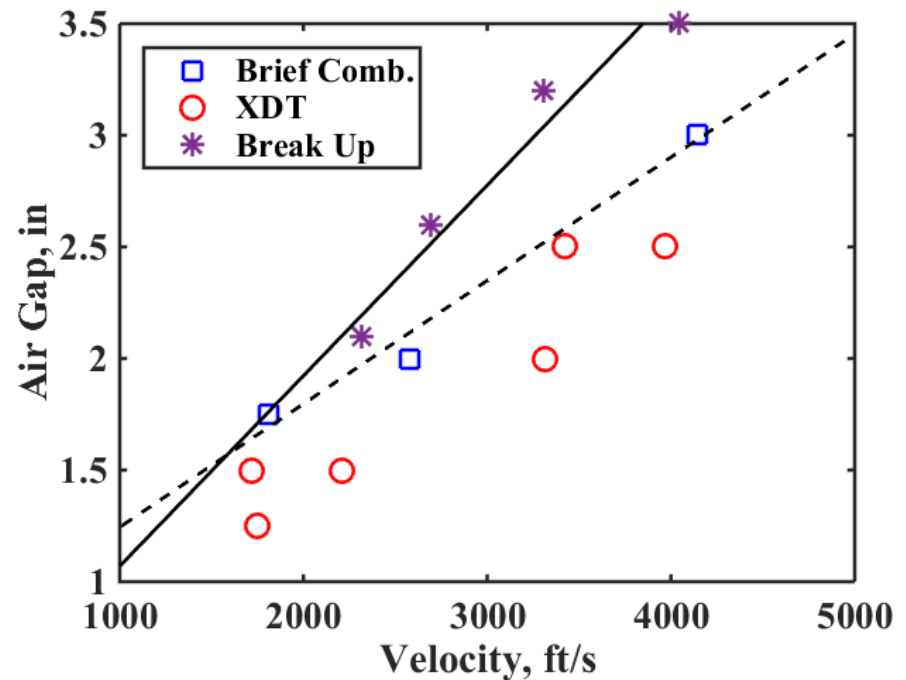
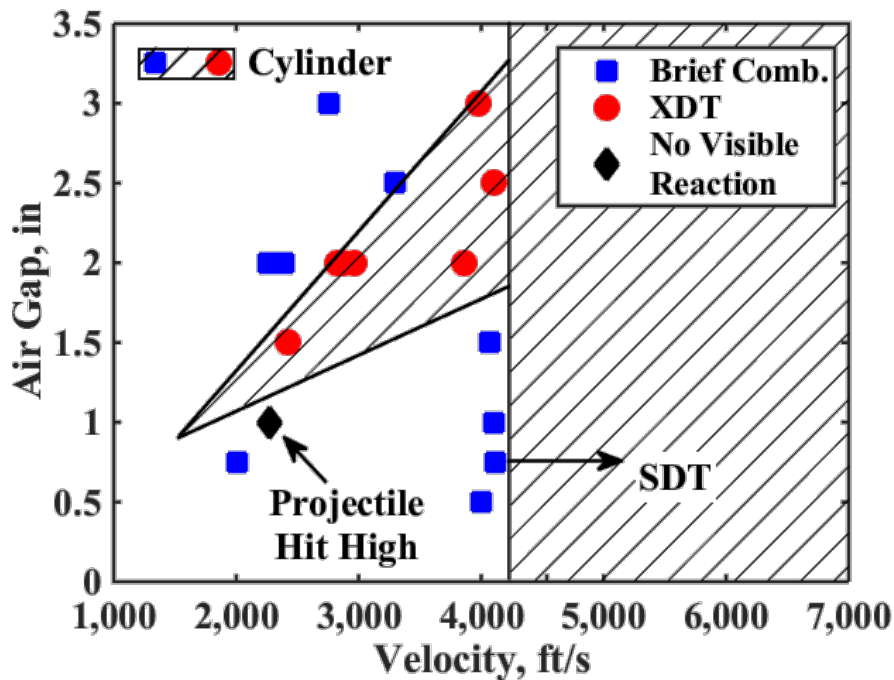


- **MSP-1 propellant**
 - ABVR web thickness – 1.25 or 2.50 in
 - Cylindrical web thickness – 1.09 or 2.34 in
- **Pressure gauges set at a 45° offset**
- **High speed cameras used to optically record event**



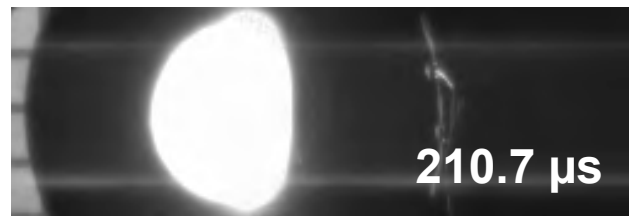
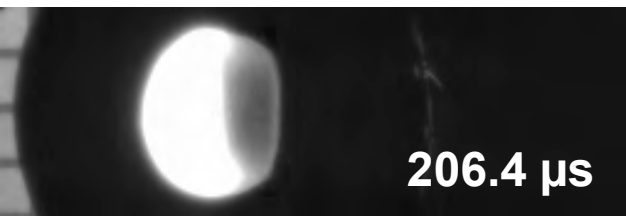
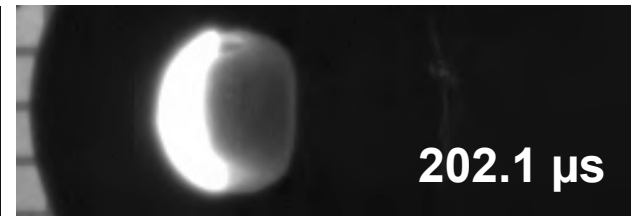
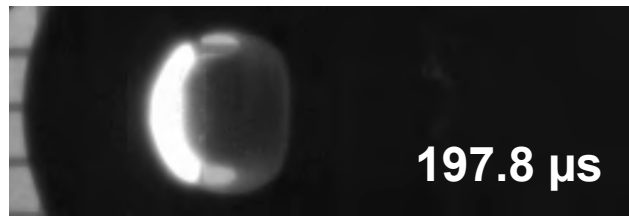
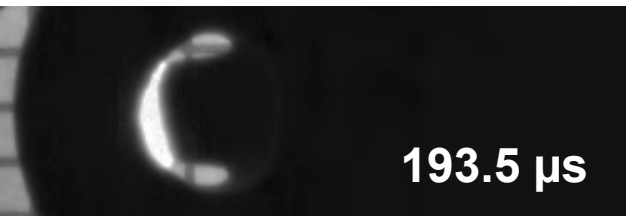
NATO STANAG Frag

- Change from XDT to brief combustion caused by debris cloud porosity
 - Visual break up of cloud correlates to XDT limit

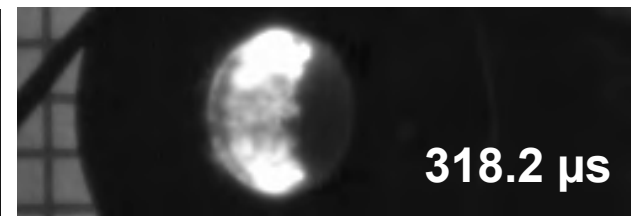
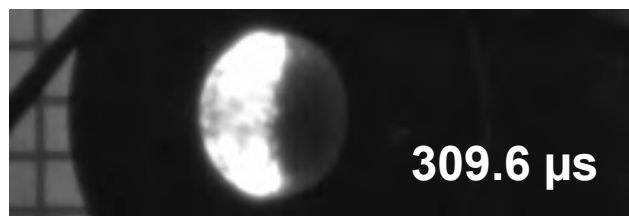
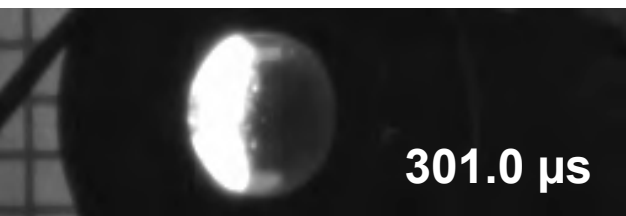
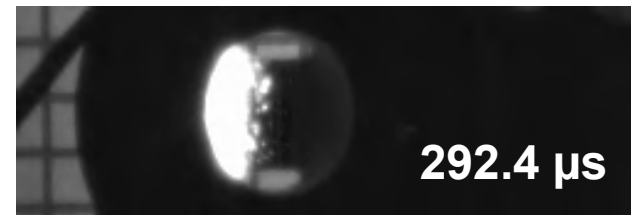
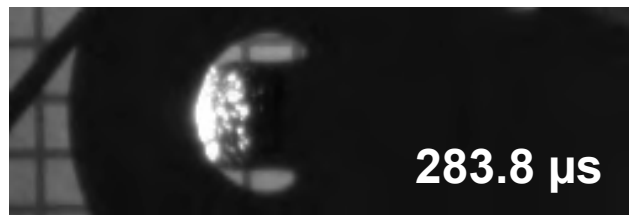
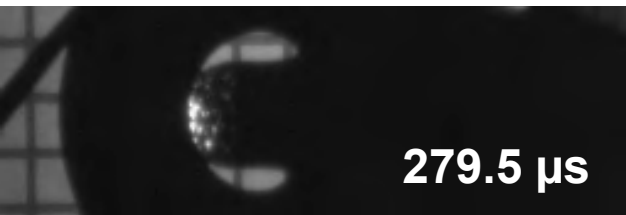


Data from Finnegan et al., Int. J. Impact Eng., 1993.

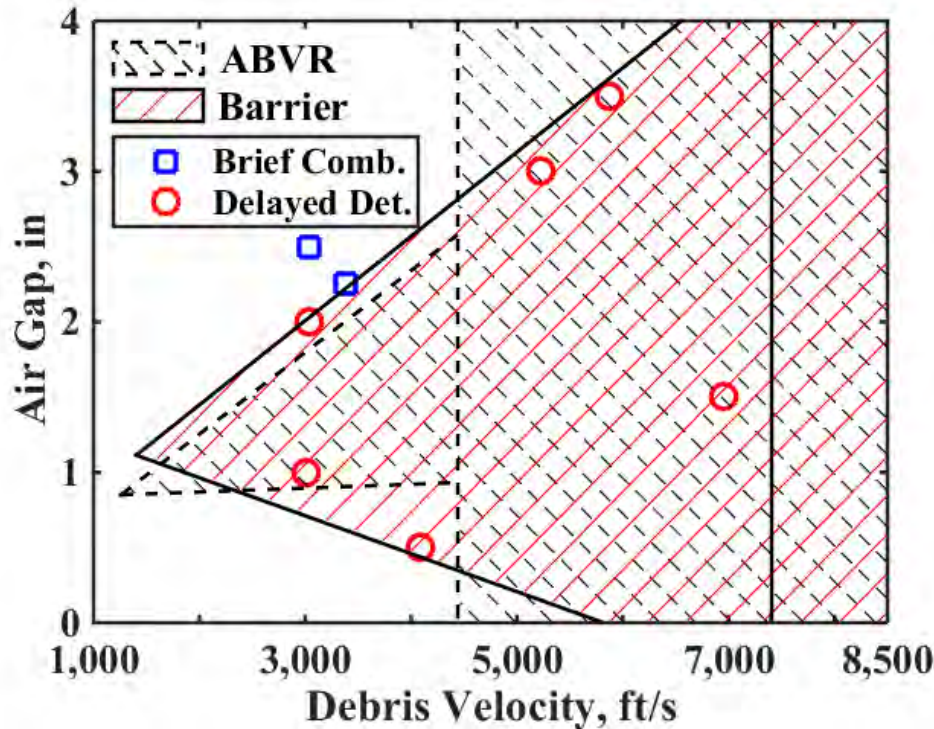
XDT – 3976 ft/s



Brief Combustion – 2756 ft/s

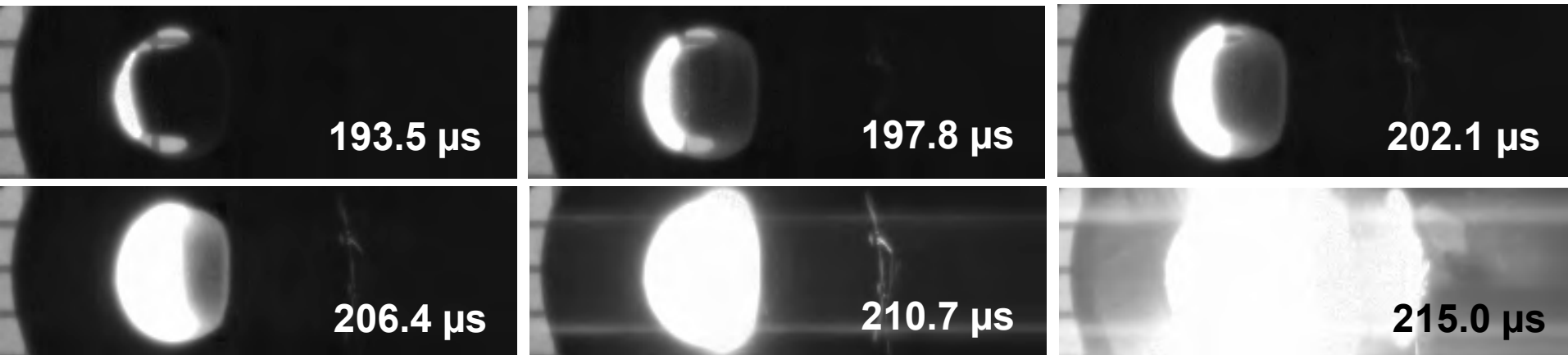


- The variation with fragment velocity appears to correlate with the amount of material in debris cloud
 - Material in debris cloud \propto kinetic energy of fragment, thickness of propellant, and presented area of fragment
 - More material means longer length required to obtain porosity necessary to mitigate XDT

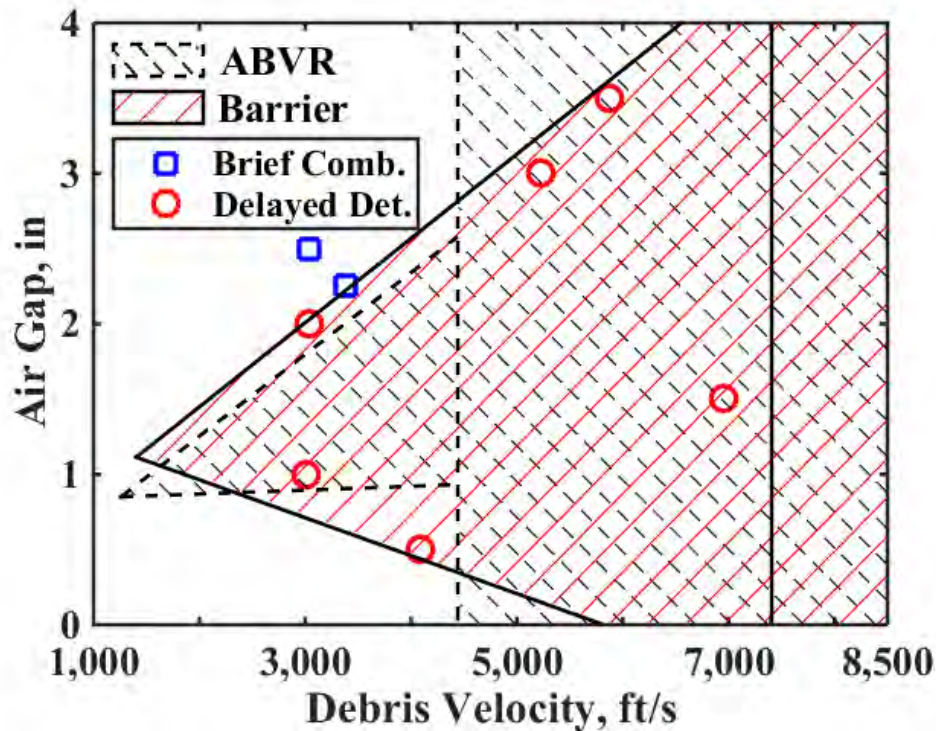


- Impact of debris cloud appears to cause localized SDT on leading edge of propellant debris cloud
 - Reaction propagates back through debris cloud at the velocity typical of a detonation through highly porous material
 - Velocity increases as porosity decreases

XDT – 3976 ft/s



- Decreasing cloud porosity decreases sensitivity to SDT
- Increasing cloud temperature increases sensitivity to SDT





- **XDT is likely a prominent detonation mechanism in real rocket motors and needs to be mitigated**
- **XDT can be controlled by influencing properties of the propellant debris cloud**
 - **Porosity**
 - **Temperature**
- **Mitigation strategies**
 - **Eliminate cavity**
 - **Completely solid fuel grain**
 - **Insert material**
 - **Design cavity to negate hazards associated with debris cloud**

- **Joint Insensitive Munitions Technology Program –Task 15-2-74**
- **Technical input**
 - **Dr. Bradley White and Dr. Keo Springer of Lawrence Livermore National Laboratory**
 - **Dr. Eric Harstad of Sandia National Laboratories**
 - **Dr. Malcolm Cook of Atomic Weapons Establishment**
 - **Kenneth Graham of Aerojet Rocketdyne**
 - **Benji Staggs/Scott Riley at OATK**
 - **Dr. Soonyoung Hong of Naval Surface Warfare Center**
- **AMRDEC support**
 - **Joey Reed, William Delaney, Ray Klaver, Patrick Parsons, Zachary Hoernschemeyer, and Jeremiah Davidson**

AMRDEC Web Site
www.amrdec.army.mil

Facebook
www.facebook.com/rdecom.amrdec

YouTube
www.youtube.com/user/AMRDEC

Twitter
[@usarmyamrdec](https://twitter.com/usarmyamrdec)

Public Affairs
AMRDEC-PAO@amrdec.army.mil

VALIDATION OF THE ARMY BURN TO VIOLENT REACTION (ABVR) TEST AS A TOOL TO PREDICT FULL-SCALE MOTOR RESPONSE TO FRAGMENT IMPACT

#20136

J. B. Neidert, M. A. Pfeil and J. A. Stanfield
Aviation and Missile Research, Development and Engineering Center
Redstone Arsenal, AL

ABSTRACT

While the ABVR experiment has been used rather extensively to investigate the reaction mechanisms of rocket motors subjected to fragment impact, no efforts have been made to validate that it truly represents how a full scale motor, with nitramine-based propellants, would behave under similar circumstances. Thus, efforts are made herein to validate the ABVR experiment by comparing the detonative response it produces to those obtained in cylindrical experiments and analog motors. Results indicate that the ABVR experiment is a valid sub-scale to predict the detonative response of full-scale motors. The insight gained from the ABVR experiments has resulted in a possible new screening tool during the development of new, insensitive compositions.

INTRODUCTION

Since 1989, the Burn to Violent Reaction (BVR) and Army Burn to Violent Reaction (ABVR) experiments have been implemented as a sub-scale experiment that could potentially represent the response of a full scale rocket motor subjected to fragment impact¹⁻⁵. Both nitramine and ammonium perchlorate (AP) based propellants have been investigated, and multiple parameters, including case material, propellant thickness, fragment type, fragment velocity, confinement, air gap (spacing between propellant slabs), and backing material, have been found to affect the outcome. In the case of nitramine based propellants, significant insight has been gained into the different detonation mechanisms that could occur inside a rocket motor and what critical parameters control those responses. For AP based propellants, the BVR/ABVR experiments have allowed for mapping of the severity of the reaction, based on a variety of parameters. These findings have been quite useful in understanding the issues and hazards associated with fragment impact.

Given the understanding, the significant reduction in testing costs, and reduction in hazards associated with testing that the BVR/ABVR experiment has provided, it would be very beneficial to validate their accuracy in predicting the actual response of a full scale motor. Some efforts have been made to accomplish this, but they have been limited in scope and have focused on AP based propellants. While those efforts showed promise in validating the BVR/ABVR experiment for AP based propellants, no efforts have been made to validate them for detonable, nitramine-based, propellants.

As such, the focus of the current effort is to address this lack of subscale model validation for nitramine-based propellants. To accomplish this, multiple experiments were conducted using the ABVR setup, and parameters such as fragment velocity, propellant thickness, and air gap were investigated. These experiments were then repeated, but cylindrical sections of simulated rocket motors were used. The ABVR

experiment is validated by comparing its reaction response to that of the cylindrical sections. Further experiments and validation were completed by testing full-scale analog motors and comparing reaction responses.

EXPERIMENTAL METHODS

There were four separate test articles evaluated, including the ABVR experiment, cylindrical sections, and an analog full scale motor (see Figure 1). All experiments used a NATO STANAG 4496 Fragment Simulated Projectile (FSP), made from 1018 carbon steel. The FSP was sabot launched out of a 20 or 40 mm smooth bore cannon and passed through a sabot stripper and three break screens before impacting the test article. For all experiments, except those that used an analog motor, backlighting was provided via a Megga-Flash PF300 Slow Peak Flashbulb placed behind a 1"x1" square grid. For the analog motor tests, the same type of flashbulb was used to illuminate the test article. Multiple high speed Phantom cameras were used in each test to observe the overall reaction (slower frame rate) and the events occurring within the air gap between the propellant (faster frame rate). Images were recorded at a frame rate varying between 75,000-260,000 frames per second.

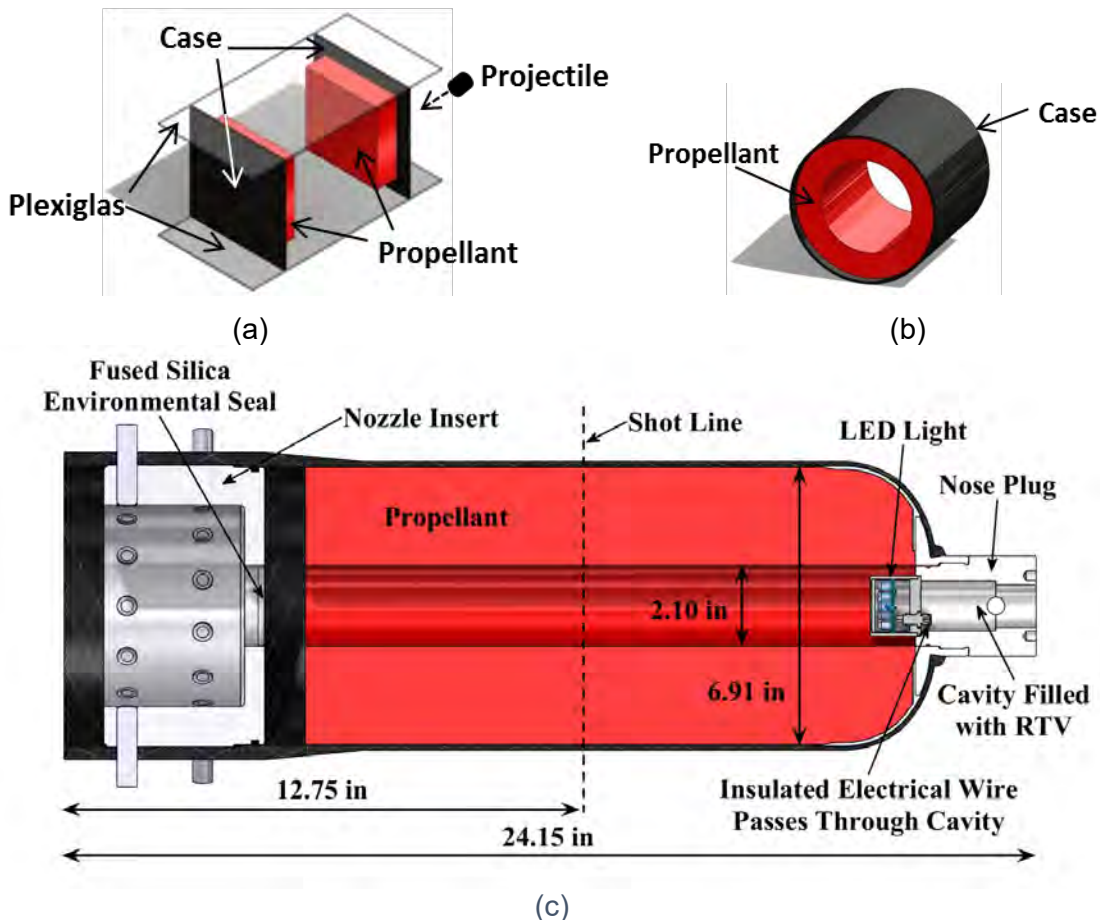


Figure 1 The various test articles used in this effort: (a) an ABVR experiment, (b) a cylindrical section, (c) full-scale analog motor

ABVR AND CYLINDRICAL SECTION

The ABVR test article, see Figure 1 (a), consisted of a 4.5 x 4.5 in square slab of MSP-1 propellant with a thickness of 1.25 or 2.5 ± 0.02 in. These were bonded to a casing material and placed in series, with the propellant slabs facing each other. The distance, or air gap, between the slabs of propellant was fixed by either gluing 0.093 in thick Lexan sheets (6 x 12 in) to the casing material or by attaching $\frac{1}{4}$ 20 nylon rods in each corner of the casing material. The air gap was set by using four stainless steel spacers of the desired length (tolerances of ± 0.005 in) – spacers were removed before tests. Details of the MSP-1 propellant can be found in previous publications. Fragment hit point was aimed at the center of the test article.

Two different casing materials were used in the ABVR experiments. The first was a 0.135 in thick IM7/8552 composite plate. The other consisted of a 0.10 in thick 7075-T6 aluminum plate that was prepped via grit blasting. After cleaning, a primer (Chemlok 205) layer was applied and then a bonding agent (Chemlok Bonder 234B). A layer of 0.030-0.035 in Kevlar filled EPDM Rubber (EP-701-02) insulation was then applied and cured to produce an aluminum casing plate. Both the composite and aluminum plates were adhered to the propellant using a hydroxyl-terminated polybutadiene (HTPB) liner (filled with carbon black).

Cylindrical sections of propellant bonded inside a composite case [see Figure 1 (b)] were also evaluated. These used the same IM7/8552 composite material with a thickness of 0.132 in. The web thickness was kept relatively constant between 1.038-1.135 in with an average of 1.09 in or between 2.288-2.375 in with an average of 2.34 in. The inner and outer diameters of the propellant varied for different air gaps. For some of the experiments, cylinders were quartered, see Figure 2. The outer diameter of the propellant for these samples was kept constant at 5.2 in for both web thicknesses of 1.09 and 2.34 in.

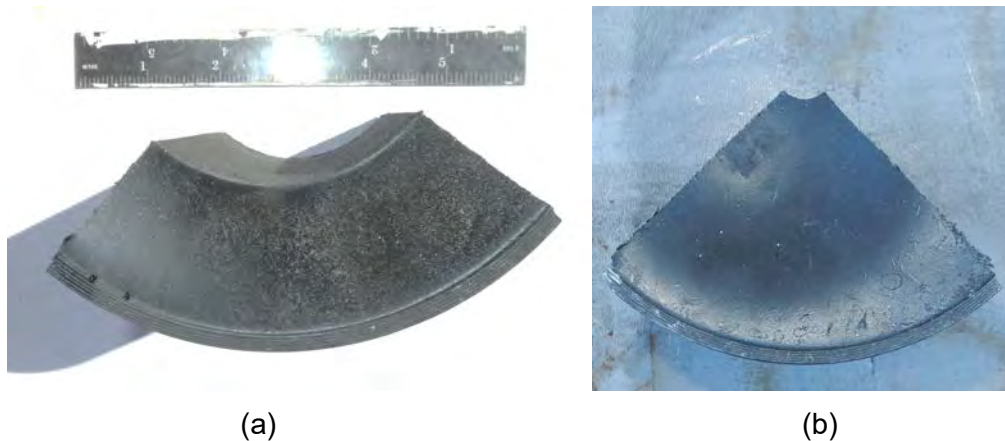


Figure 2 Quartered sections of cylindrical test articles used in experiments with a web thickness of (a) 1.09 in and (b) 2.34 in.

Both ABVR and cylindrical section experiments were evaluated using the same setup used in previous ABVR testing. Two rows of PCB Piezotronics pencil gauges for pressure measurements were placed at 45° off the shot line at 5, 9, and 13 ft away from the impact point, see Figure 3.

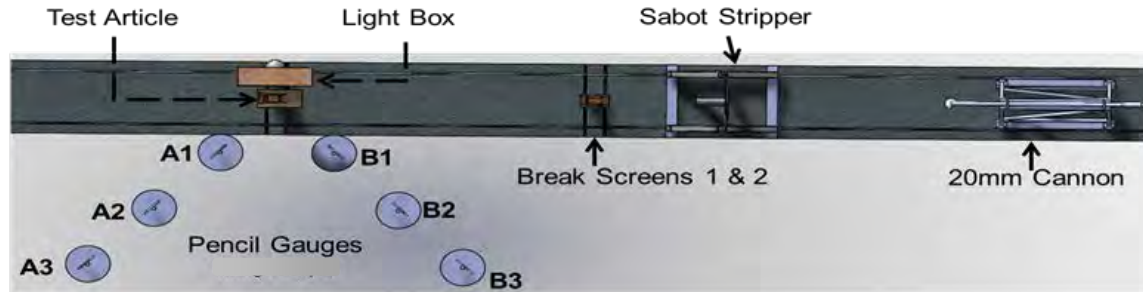


Figure 3 Test setup used to evaluate ABVR and cylindrical test articles.

ANALOG MOTOR

The full scale analog motor, see Figure 1 (c), consisted of a composite case, an aluminum 7075-T73 nozzle insert, and a stainless steel nose plug. The motor had a diameter of 7.18 in and was 24.15 in long. The MSP-1 propellant grain was a 6.91 in diameter cylinder with a 2.10 ± 0.04 diameter center bore perforation, resulting in a web thickness of 2.41 in and a propellant weight of approximately 31.3 lbs. The composite case was 0.135 in thick, at the fragment hit point, and made of IM-7 carbon/epoxy composite with S2 glass layers in the thicker aft closure joint. A layer of Kevlar-filled polyisoprene insulator was at the head end of the motor. An uncoated 1 λ fused silica window was inserted into the nozzle to act as a weather seal, provide confinement, and to allow optical access into the motor during testing. A Thorlabs LIUCWHA LED light was placed inside the motor at the head end and was used to illuminate the bore for optical measurements.

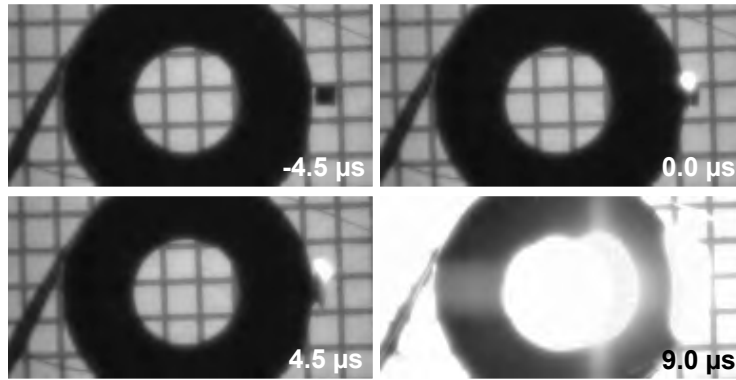
The analog motors were placed vertically, nose facing downward, on a 0.5 in thick plywood tabletop with a large enough hole to allow the nose plug to pass through. A 1 x 12 x 24 in steel witness plate was placed beneath the plywood tabletop, 4-4.5 in below the top of the table. A first surface mirror was placed above the motor at a 45° angle to allow a high speed monochrome Phantom camera (recording at 200,000 frames per second) to observe the reactions within the motor. To observe the exact fragment impact point, two grids were placed in line with the vertical and horizontal axis of the fragment shot line at the motor impact point. A high speed monochrome Phantom (recording at 12000 frames per second) camera was used to observe both grids simultaneously. A third high speed color Phantom camera (recording at 6200 frames per second) was used to observe the overall event.

The first two tests had eight and seven evenly spaced PCB Piezotronics pencil pressure gauges placed at a radius of 5 and 10 ft respectively. The second test resulted in a detonation that damaged the pencil gauges located 5 ft away from the test article. The remaining four tests had two rows of pencil gauges placed at 5, 10, 15 and 20 ft behind the test article at 45° offset from the fragment shot line. The shot line was aimed at the center of the motor, 12.75 in from the aft end of the motor.

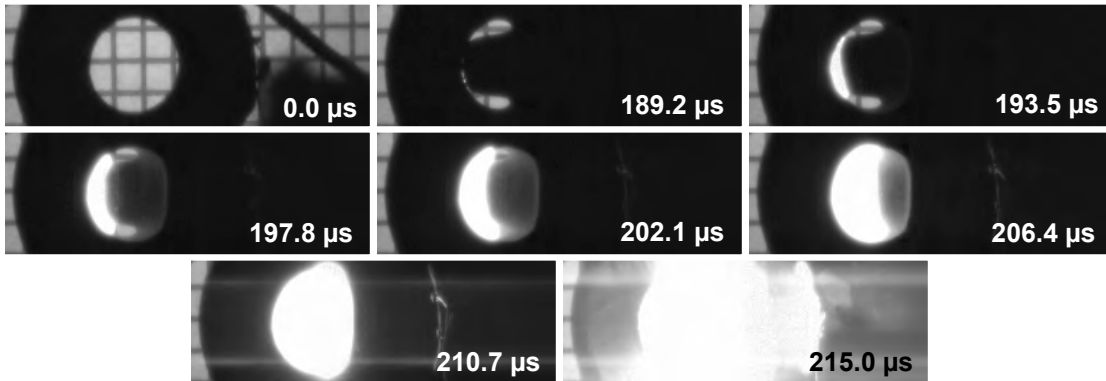
RESULTS AND DISCUSSION

Three types of reactions were typically seen throughout these tests, including Shock to Detonation Transition (SDT), Unknown Detonation Transition (XDT), and brief combustion events. An SDT event occurs when an insult provides sufficient impulse, over a minimum amount of time, that results in a prompt detonation to occur. In the

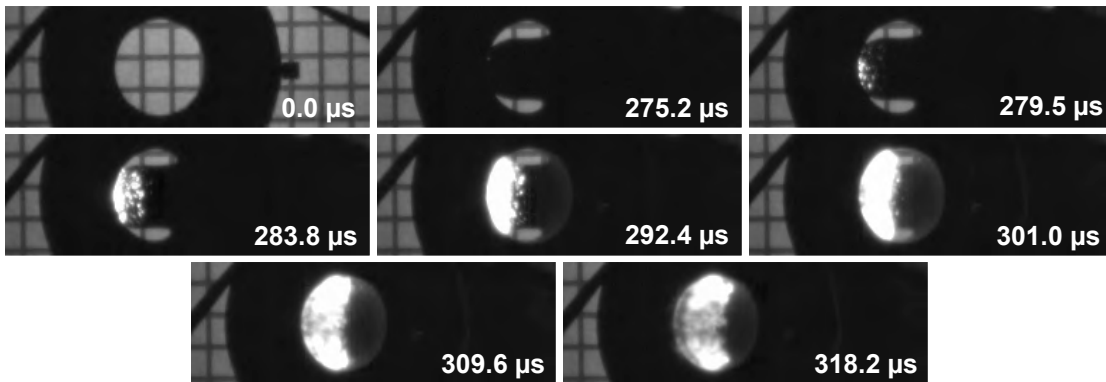
present scenario, this insult is provided by the fragment impacting the test article at high speeds, see Figure 4 (a). A detonation event typically commences less than 10 μs after the fragment touches the test article, commencing near the location of the impact point and propagating outwards through the rest of the article. Once a minimum fragment velocity threshold, unique to each test configuration, is achieved, an SDT event will occur. The detonation in both a SDT and XDT reaction results in notable increase in light emission from the test article, pressure measurements that are an order of magnitude or more larger than non-detonation events, and little to no recognizable remains of the test article.



(a)



(b)



(c)

Figure 4 Still images from three different reaction mechanisms typically observed in these tests: (a) SDT, (b) XDT, and (c) brief combustion.

If the fragment velocity drops below the SDT velocity threshold, then two other types of reactions can occur, XDT or brief combustion. Both reactions result from when the fragment passes through the case and one section of propellant, producing a debris cloud of propellant that propagates across an air gap/bore diameter. Once this propellant cloud impacts the other side of the air gap, it will initiate, and either produce an XDT [Figure 4 (b)] or brief combustion [Figure 4 (c)]. The dynamic properties of the propellant debris cloud control when one or the other reaction will occur. One of the dominating properties appears to be the porosity/continuity of the debris cloud. If the porosity is too low or high, a brief combustion event will occur. If the porosity is in between, a detonation can initiate at the leading edge of the debris cloud and propagate back through the cloud into the undamaged propellant, causing it to also detonate. Such a detonative/brief combustion behavior results in defined regions, dependent on fragment velocity and the test article air gap, where one or the other reaction will occur. This behavior was first noted by Finnegan et al.¹

ABVR VS. CYLINDRICAL

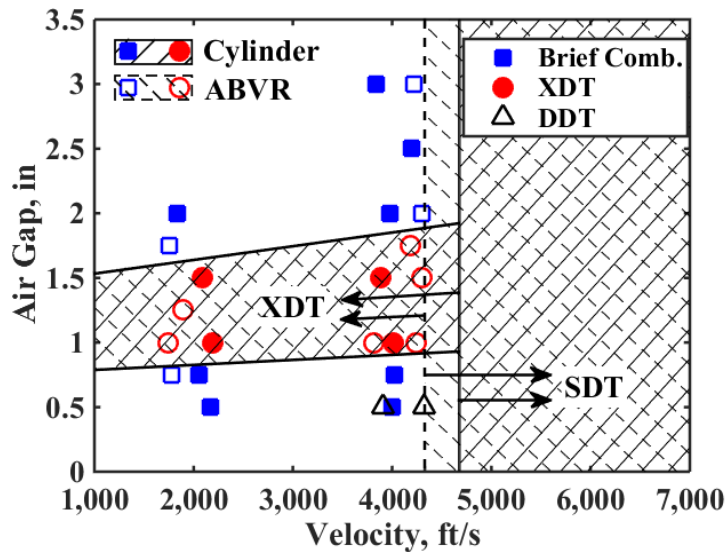
Comparison of the detonation reactions observed in the ABVR versus what was observed in the cylindrical experiments are provided in Table 1 and Figure 5. The data for the 1.25 in web thickness ABVR samples was obtained from previous efforts reported by Pfeil et al.⁵ Table 1 provides the fragment minimum velocity thresholds to produce an SDT reaction; the SDT thresholds are also represented by vertical lines in the plots provided in Figure 5. These thresholds are determined by taking the average velocity of the lowest velocity that produced an SDT reaction and the highest velocity that did not. The SDT thresholds of the ABVR and cylindrical samples, given the same web thickness, are within 334 ft/s or less, a rather minimal difference. Introducing curvature into the experiment causes the SDT threshold to increase slightly for the 1.25 in web thickness but decrease slightly for the 2.50 in web thickness. This discrepancy is likely a result of using quartered, instead of full, cylindrical samples. For the 2.50 in thick samples, detonation reactions were observed to begin on the cut surface, whereas the 1.25 in thick samples were not. Thus, it is likely that the threshold value observed for the quartered 1.25 thick sample is more accurate in representing a non-quartered sample than the 2.50 thick sample.

Table 1 SDT minimum fragment velocity thresholds for ABVR and cylindrical test configurations.

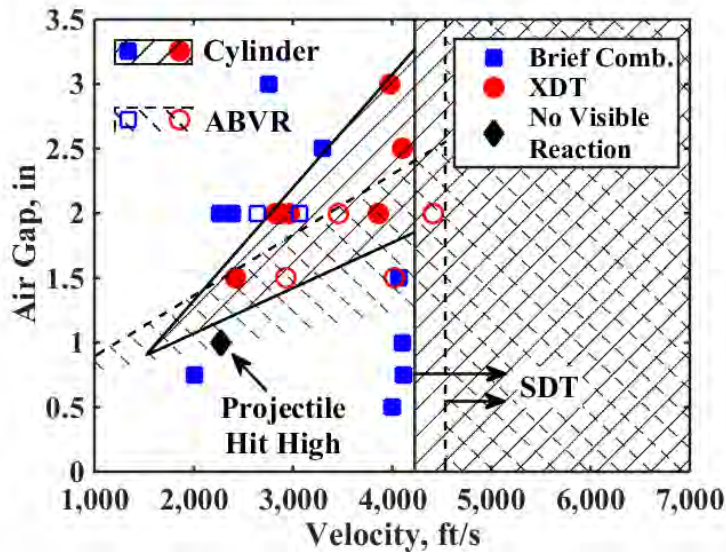
	SDT Threshold, ft/s
ABVR – 1.25 in Web	4329 ± 2
ABVR – 2.50 in Web	4536 ± 125
Quartered Cylinder – 1.09 in Web	4663 ± 63
Quartered Cylinder – 2.34 in Web	4219 ± 104

Both propellant web thickness configurations produced regions where XDT or brief combustion would occur, depending on fragment velocity and air gap. This region of XDT reactions was the same for both ABVR and cylindrical samples that had a web thickness of 1.25/1.09 in, see Figure 5 (a). Doubling the web thickness notably shifted the XDT reaction region and caused the ABVR and cylindrical data to diverge, see Figure 5 (b). Due to the limited data obtained for the ABVR setup with a web thickness

of 2.50 in, the XDT reaction region had to be inferred. The upper air gap limit was determined by the data obtained and by comparing against data provided by Pfeil et al.⁵ Their data indicated that using a steel plate, instead of propellant as the surface the debris cloud of propellant impacted, caused the slope of the upper air gap limit line to increase. Based on that observation and comparing against the data they obtained for a 2.50 in web thickness ABVR sample with a steel plate, a likely slope for the XDT upper air gap limit line can be inferred. There was not sufficient data to infer what the XDT lower air gap limit line could be.



(a)



(b)

Figure 5 Different detonation reactions as a function of fragment velocity and air gap for a web thickness of (a) 1.25 in (ABVR) and 1.09 in (cylindrical) or (b) 2.50 in (ABVR) and 2.34 in (cylindrical). Lined regions are where detonations occur.

The discrepancy between the XDT reaction region for the 2.50/2.34 in web thickness ABVR and cylindrical sections is most likely caused by the introduction of the

curved surface. The curvature likely allows the fragment to interact with more propellant as it passes through, as noted by Finnegan et al. This would cause more propellant to enter the propellant cloud, decreasing its porosity. Thus, cylindrical sections would require larger air gaps to obtain the correct porosity for XDT to occur and would be able to sustain an XDT reaction at even larger air gaps. It is likely that this also occurs for the thinner 1.25/1.09 thick samples, but the change in XDT limits must be less than the resolution of obtained data points.

ABVR VS. ANALOG MOTOR

The analog motor was designed based off the results obtained with the ABVR and cylindrical experiments. If those experiments were somewhat representative in predicting how a full scale motor would react, then the analog motor would have detonations nearing as low as 2700 ft/s, a velocity most would not have considered unlikely given fragment impact testing on motors with similar propellant. Furthermore, such a velocity would be very concerning, as statutory requirements indicate motors must pass fragment impact tests without detonating at a velocity over three times this velocity. In order to investigate the different detonation mechanisms and if the ABVR experiment is potentially representative of a full scale motor, six analog motors were impacted with FSP's at velocities near the different reaction thresholds identified in the previous experiments.

A comparison of SDT thresholds and XDT reaction regions for ABVR, cylindrical, and analog motor is provided in Figure 6. The SDT velocity threshold for the analog motor was found to be 4675 ± 118 , 139 ft/s higher than the ABVR experiment. Accounting for the \pm range of the SDT thresholds, it is possible that the difference between the ABVR experiment and the analog motor is even less than what is reported. The lowest velocity a detonation (XDT) occurred at was 2538 ft/s, resulting in a large fireball, see Figure 7, and pressures over 550 psi at 5 ft from the motor and 280 psi at 10 ft. This resulted in an XDT threshold velocity which was about 1000 ft/s slower than what was found in the ABVR experiments. Again, this is likely due to the curvature of analog motor and the resulting differences in the propellant cloud porosity. Despite this somewhat notable discrepancy, the ABVR experiment was quite valuable in identifying regions where detonations could occur at much lower velocities than would previously would have been suspected.

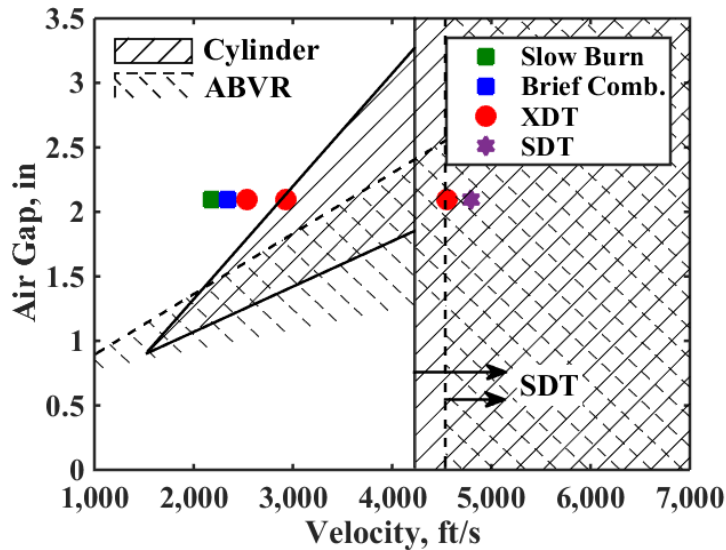


Figure 6 Data obtained for the analog motor compared to the SDT threshold and XDT reaction regions for the ABVR (2.50 in web thickness) and cylinder (2.34 in web thickness) experiments. Lined regions are where detonations occur.



Figure 7 The test article (a) before the e fragment impacted, and (b) the detonative response that followed after impact.

While the ABVR experiment appears to be a reasonable sub-scale test in predicting the detonative response of full scale motors, it is unclear on how well it is at predicting a non-detonative response for nitramine-based propellants. In the ABVR experiment, if a detonation did not occur, a brief combustion event would produce varying amounts of pressure (under 10 psi) and do little to no damage to the wooden table it was placed upon. In full-scale motor tests, explosions, burns, and brief combustion events have all been observed, and there is no apparent direct correlation between those tests and the amount of pressure or damage observed in the ABVR experiments. The only correlation that could be noteworthy is that the higher the pressure output observed in the ABVR experiments, the greater the violence observed in full scale motor tests; however, there is not enough data available to correlate those pressures to distinct reaction zones/mechanisms. Thus, it appears that the current ABVR experiment may be better suited to investigate detonative responses.

SUMMARY AND CONCLUSIONS

The ABVR experiments identified several regions, dependent of fragment velocity and air gap, where either SDT or XDT reactions would occur. These regions changed as propellant thickness and casing materials were changed. Similar reaction regions were observed when changing from ABVR to cylindrical experiments. For samples that had a propellant thickness of 1.09/1.25 in, both XDT and SDT regions were nearly identical, see Figure 5 (a). However, a measureable deviation was observed for the XDT regions when the propellant thickness was increased to 2.34/2.50 in, see Figure 5 (b). It is likely that this discrepancy is a result of more material entering the propellant cloud for the cylindrical samples, causing its porosity to differ from the propellant cloud produced in the planar ABVR experiments. Similar deviations were observed when comparing the reaction response of the analog motor and what was observed in the ABVR experiment (see Figure 6). The SDT thresholds were very similar, but the XDT reaction regions were measurably different.

ACKNOWLEDGMENTS

The authors would like to thank Bradley White and Keo Springer of Lawrence Livermore National Laboratory, Eric Harstad of Sandia National Laboratories, and Tom Mason of Los Alamos National Laboratory for their suggestions and input. They would like to recognize David Huebner, Joey Reed, William Delaney, Ray Klaver and Zachary Hoernschemeyer for their support in performing experiments. Finally, they would like to thank the Joint Insensitive Munitions Technical Program for the financial support to perform these efforts (Task 15-2-74).

REFERENCES

1. Finnegan, S. A., Pringle, J. K., Schulz, J. C., Heimdahl, O. E. R., and Lindfors, A. J., **Impact-Induced Delayed Detonation in an Energetic Material Debris Bubble Formed at an Air Gap**, International Journal of Impact Engineering, Vol. 14, pp. 241-254, 1993.
2. Finnegan, S. A., Pringle, J. K., Atwood, A. I., Heimdahl, O. E. R., and Covino, J., **Characterization of Impact-Induced Violent Reaction Behavior in Solid Rocket Motors Using a Planar Motor Test Model**, International Journal of Impact Engineering, Vol. 17, pp. 311-322, 1995.
3. Haskins, P. J., Cook, M. D., and Cheese, P. J., **Studies of XDT Phenomena Under Fragment Attack Impact Conditions**, Science and Technology of Energetic Materials, Vol. 66, 2005.
4. Haskins, P. J., and Cook, M. D., **On Delayed Detonation (XDT) Under Fragment Impact – An Analysis Of Experimental Data and a Simple Phenomenological Model**, AIP Conference Proceedings, Nashville, TN, June 28-July 3, 2009.
5. Pfeil, M. A., Stanfield, J. A., Neidert, J. B., Harstad, E. N., White, B. W., and Springer, H. K., **Parameters Influencing the Response of MSP-1 Propellant Subject to Fragment Impact**, NDIA IMEM, Nashville, TN, Sept. 12-15, 2016.



Presented to:
NDIA IMEM
Portland, OR
Paper #20136

*Validation of the Army Burn
to Violent Reaction (ABVR)
Test as a Tool to Predict Full-
Scale Motor Response to
Fragment Impact*



Distribution Statement A. Approved for Public Release. Distribution Unlimited

TECHNOLOGY DRIVEN. WARFIGHTER FOCUSED.

April 26, 2018

Presented by:
Dr. Jamie B. Neidert
Dr. Mark A. Pfeil & Jessica A. Stanfield
U.S. Army Aviation and Missile Research,
Development, and Engineering Center



Deliver collaborative and innovative aviation and missile capabilities for responsive and cost-effective research, development and life cycle engineering solutions.

~9,211
FY17 Strength



2,945
Civilian

16
Military

6,250
Contractor

907 / 5343
SETA Non-SETA

Core Competencies

- Life Cycle Engineering
- Research, Technology Development and Demonstration
- Design and Modification
- Software Engineering
- Systems Integration
- Test and Evaluation
- Qualification
- Aerodynamics/ Aeromechanics
- Structures
- Propulsion
- Guidance/Navigation
- Autonomy and Teaming
- Radio Frequency (RF) Technology
- Fire Control Radar Technology
- Image Processing
- Models and Simulation
- Cyber Security

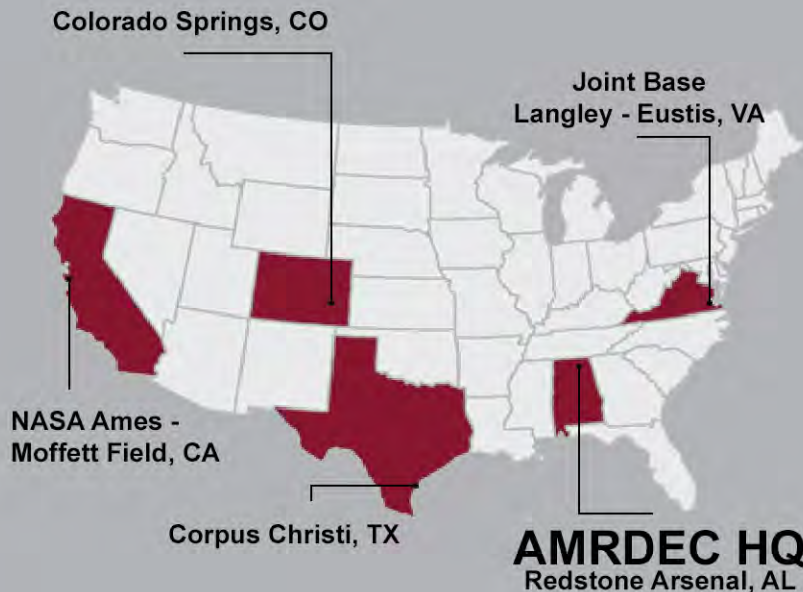
FY17
\$2,904M

6%
Aviation S&T

7%
Missile S&T

63%
Army

24%
Other



#1: Readiness

Provide aviation and missile systems solutions to ensure victory on the battlefield today.



#2: Future Force

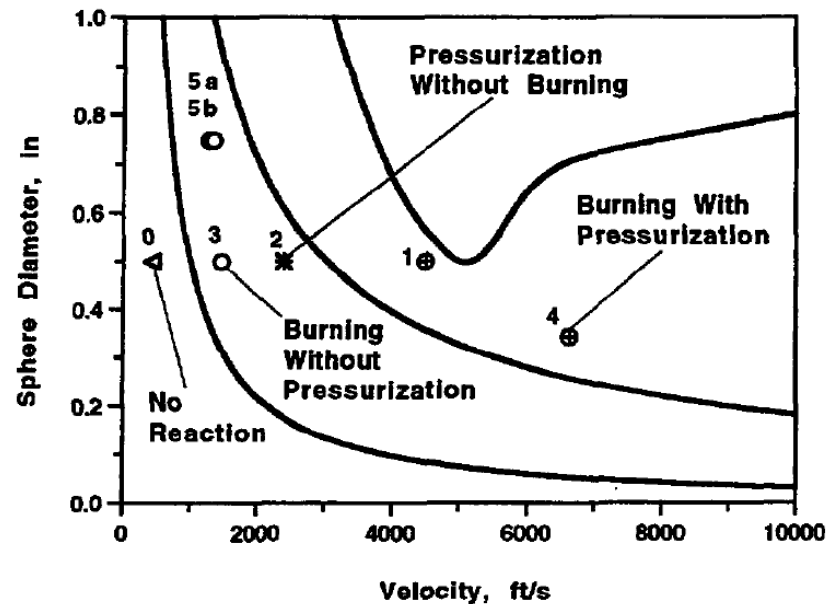
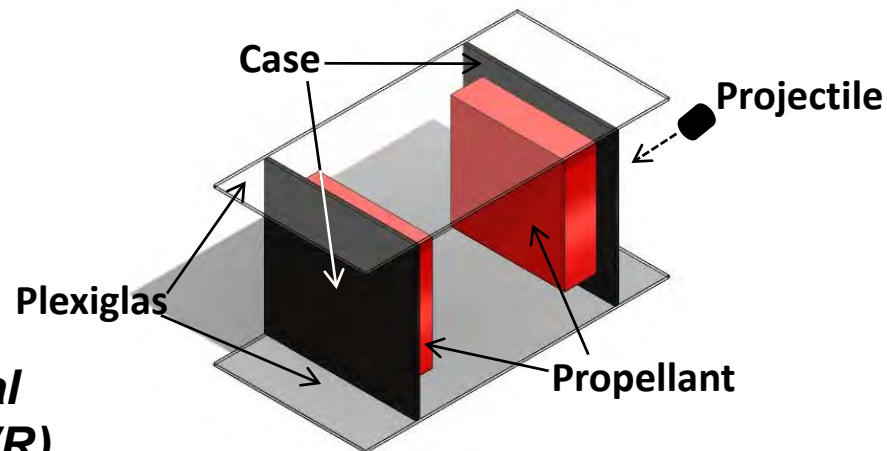
Develop and mature Science and Technology to provide technical capability to our Army's (and nation's) aviation and missile systems.

#3: Soldiers and People

Develop the engineering talent to support both Science and Technology and the aviation and missile materiel enterprise

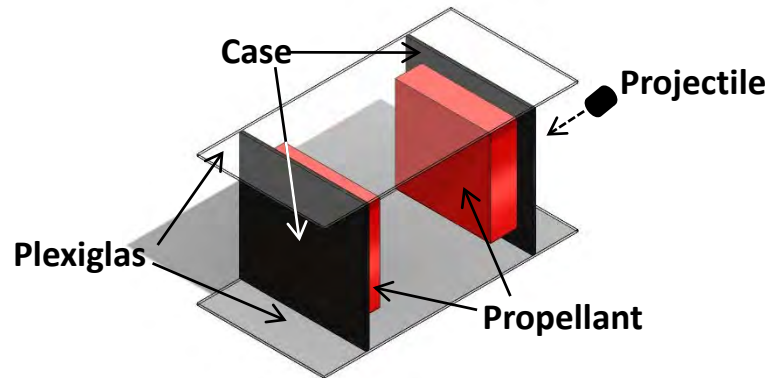


- **Burn to Violent Reaction (BVR)** developed in early 1990's at the US Navy/China Lake
 - Independently developed in UK around same time frame
 - Similar work at Redstone Arsenal in mid 1990's → Army BVR (ABVR)
 - Over 30 publications on efforts associated with BVR
- **Ammonium perchlorate propellants**
 - Relate reaction to ballistic behaviors
- **Nitramine based propellants**
 - Map out detonation regions
 - First (known) observed demonstration of XDT (unknown detonation transition) related to traversing damaged propellant

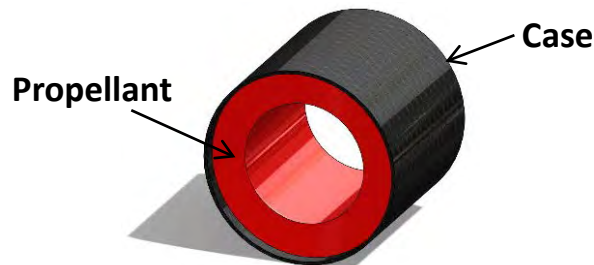


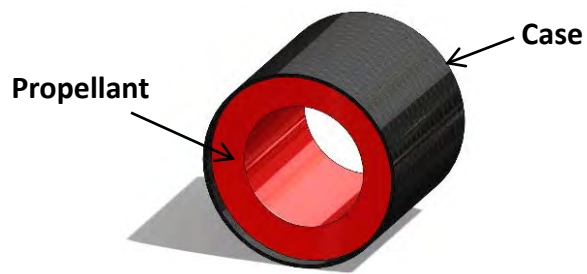
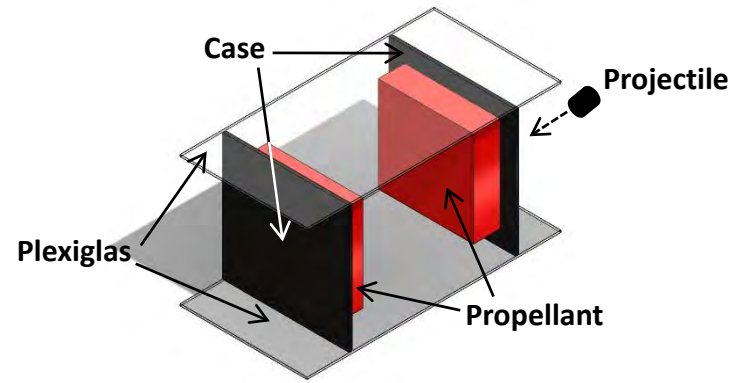
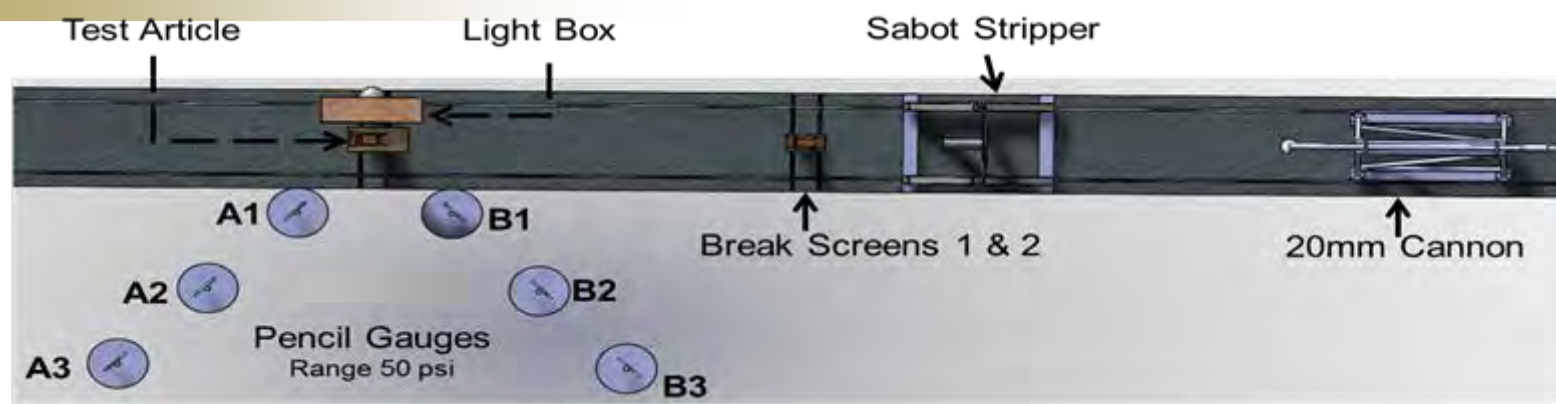
Finnegan et al., August, 1994

- Use subscale, simplified tests to identify important parameters influencing munition response to external stimuli (fragment impact)
 - Velocity, geometry, projectile, web thickness, materials, etc.



- Verify similar behavior observed in cylindrical sections
- Design motor to demonstrate different reaction mechanisms

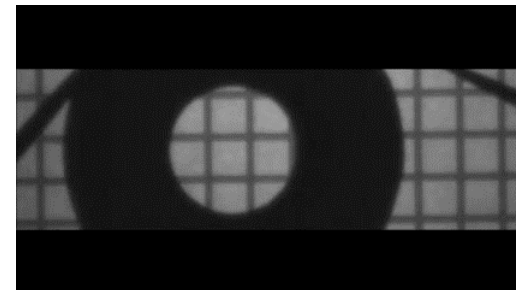
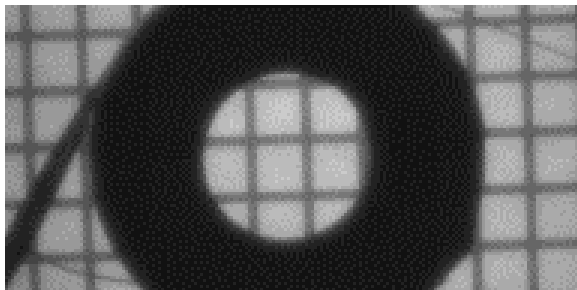




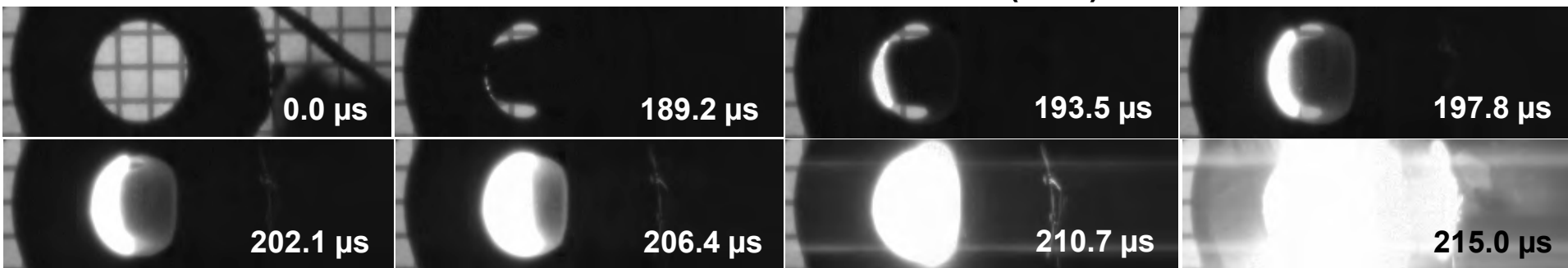
- **MSP-1 propellant**
 - ABVR web thickness – 1.25 or 2.50 in
 - Cylindrical web thickness – 1.09 or 2.34 in
- Pressure gauges set at a 45° offset
- Cylindrical tests that focused on Shock to Detonation (SDT) reaction used quartered samples



Shock to Detonation Transition (SDT)



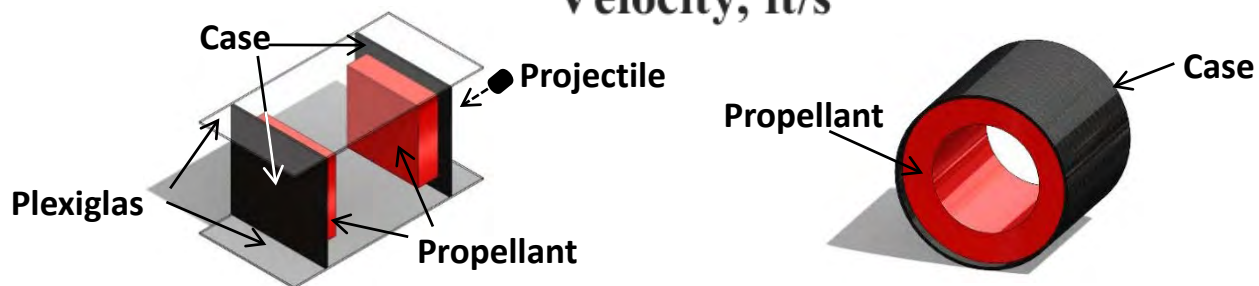
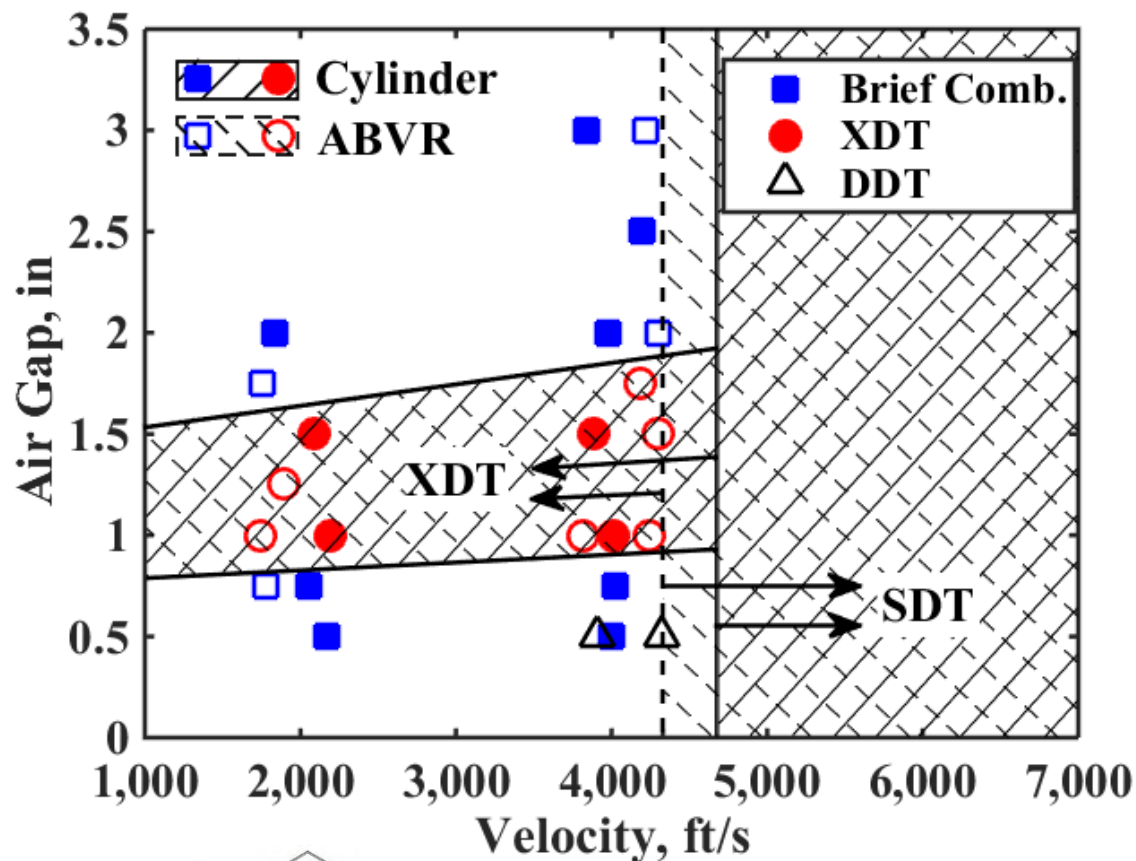
Unknown Detonation Transition (XDT)



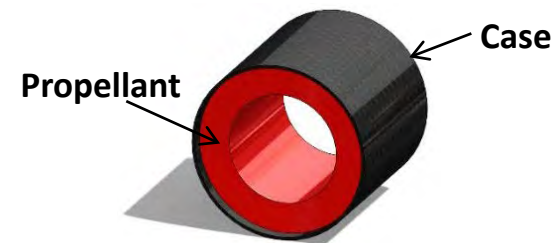
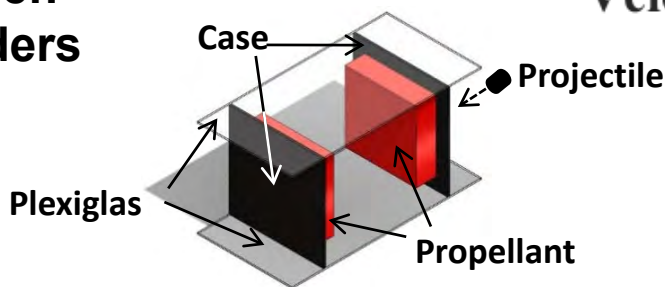
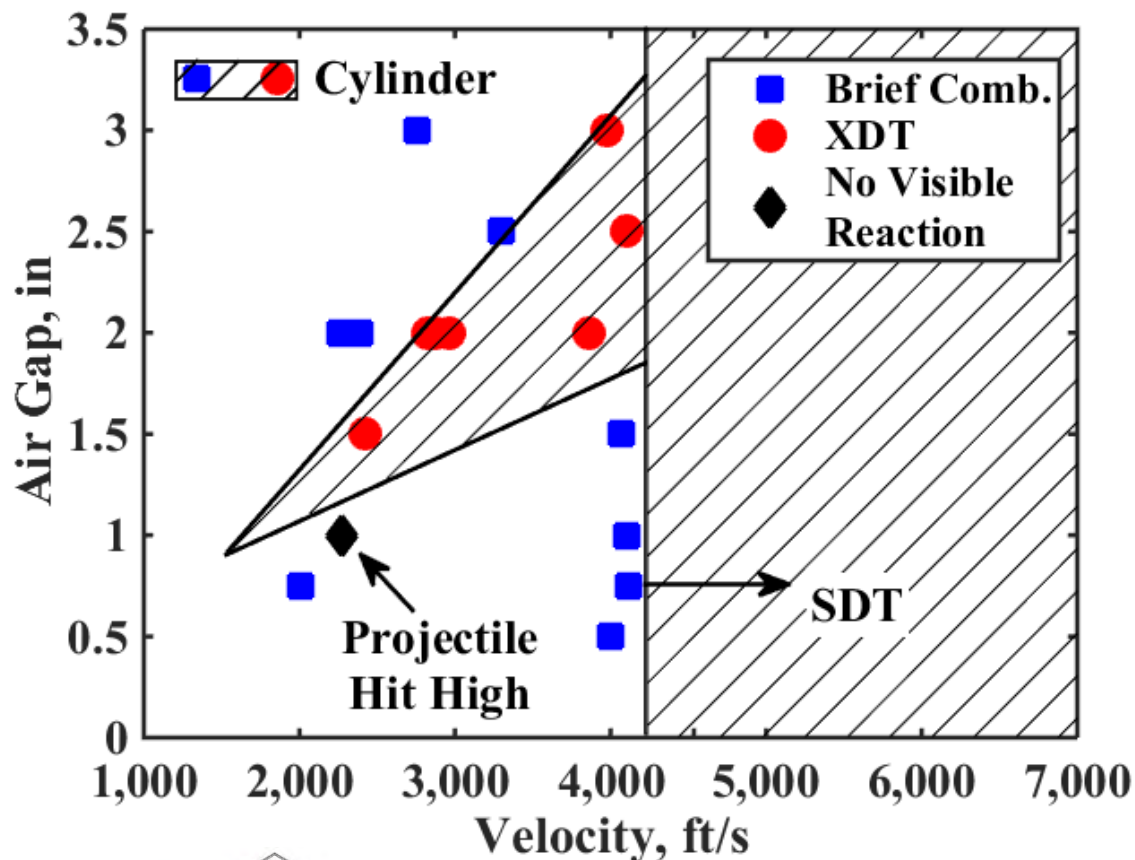
Brief Combustion



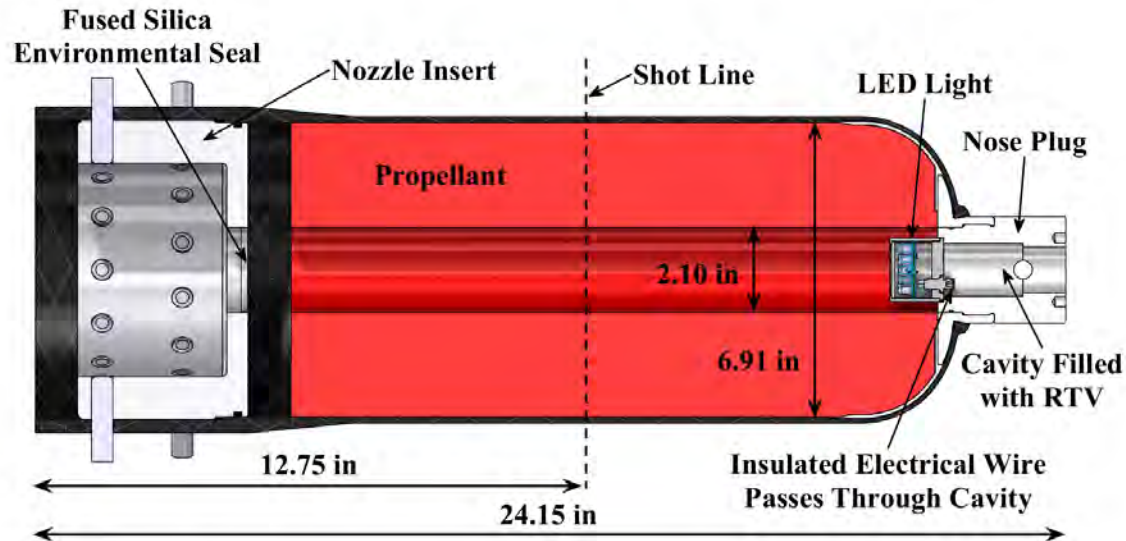
- **SDT thresholds**
 - ABVR – 4329 ± 2 ft/s
 - Cylindrical – 4663 ± 63 ft/s
- **XDT region includes 0.75-1.75 in air gaps (bore diameters) down to at least 2000 ft/s**
 - Varies with projectile velocity
 - Regions nearly identical for ABVR and cylindrical

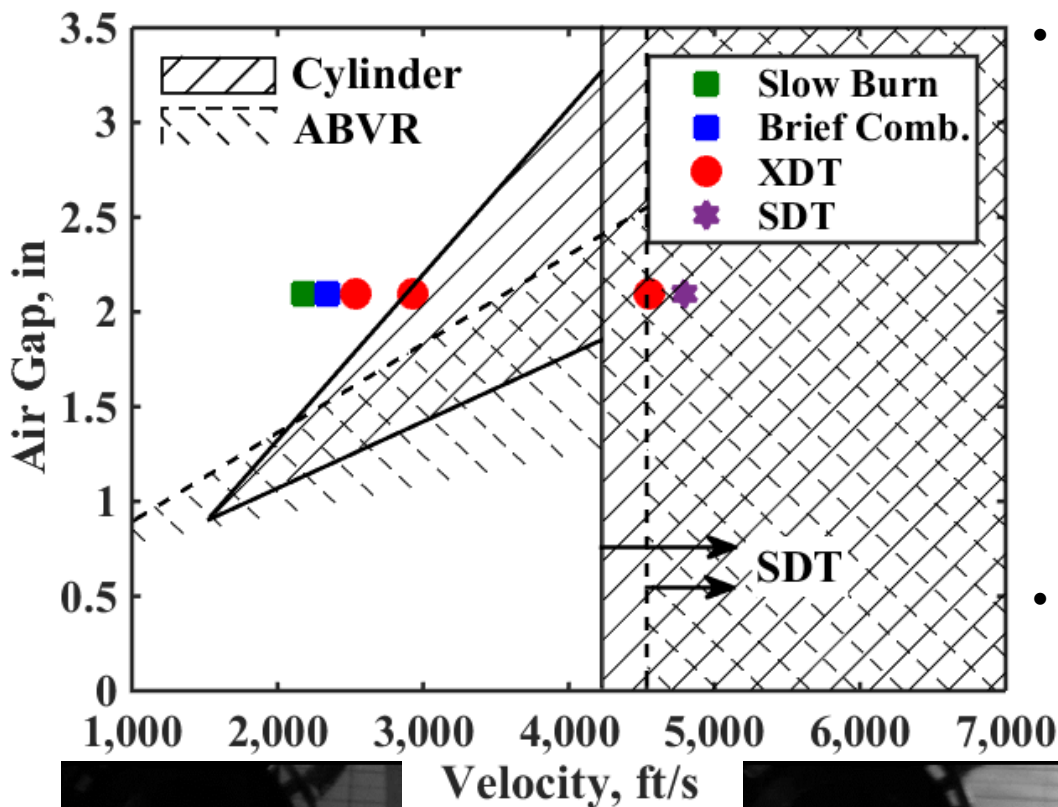


- **SDT thresholds**
 - ABVR – 4536 ± 125 ft/s
 - Cylindrical – 4219 ± 104 ft/s
- **XDT region includes 1.00-3.25 in air gaps (bore diameters) down to at least 2000 ft/s**
 - Varies notably with projectile velocity
 - Measurable difference between ABVR and cylinders
 - Region of no detonations

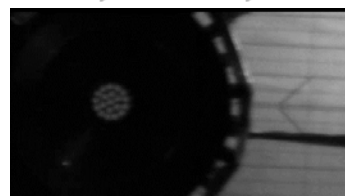
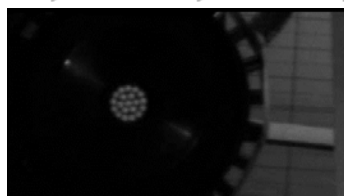


- **MSP-1 propellant (31.3 lbs)**
 - Web thickness of 2.41 in
- **Oriented vertically – nose down**
- **First surface mirror allowed for internal viewing of motor**
- **Pressure gauges set in circular patten or 45° offset**

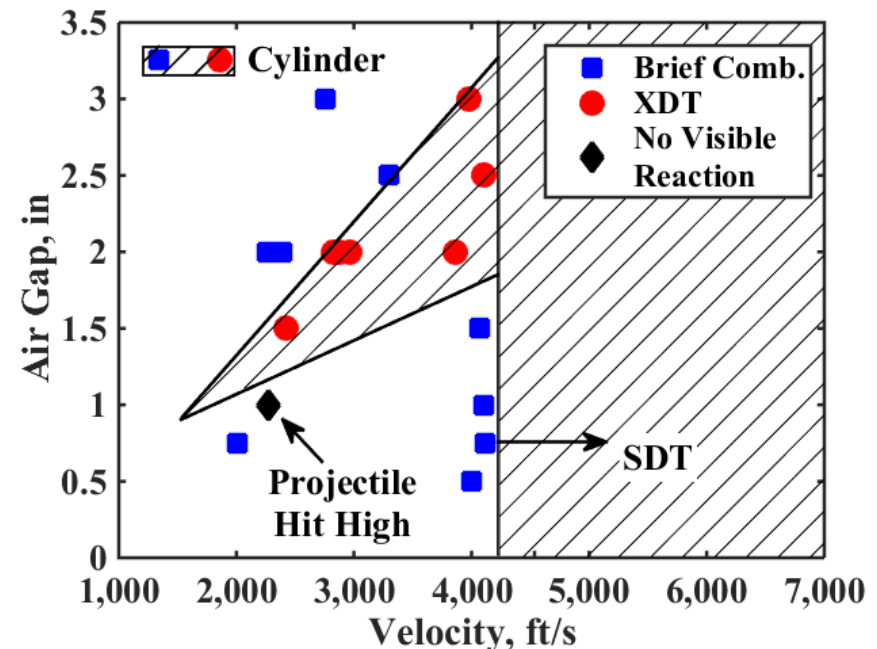




- SDT thresholds
 - ABVR – 4536 ± 125 ft/s
 - Cylindrical – 4219 ± 104 ft/s
 - Analog Motor – 4675 ± 118 ft/s
- XDT behavior very similar to cylinders



- ABVR reasonably predicts detonative behavior of a full scale motor
 - SDT threshold differs by <350 ft/s
 - XDT reaction region is the same for thinner web thickness
 - Thicker web causes some deviation
- Insufficient data available to compare non-detonative region
- Motors can detonate at lower velocities than what is typically expected
- Non-detonative regions may exist that are bounded by detonative regions at high and low fragment impact velocities





- **Joint Insensitive Munitions Technology Program – Task 15-2-74**
- **Technical input**
 - **Dr. Bradley White and Dr. Keo Springer of Lawrence Livermore National Laboratory**
 - **Dr. Eric Harstad of Sandia National Laboratories**
 - **Dr. Malcolm Cook of Atomic Weapons Establishment**
 - **Kenneth Graham of Aerojet Rocketdyne**
 - **Benji Staggs/Scott Riley at OATK**
 - **Dr. Soonyoung Hong of Naval Surface Warfare Center**
- **AMRDEC support**
 - **David Huebner, Joey Reed, William Delaney, Ray Klaver, Patrick Parsons, Zachary Hoernschemeyer, and Jeremiah Davidson**



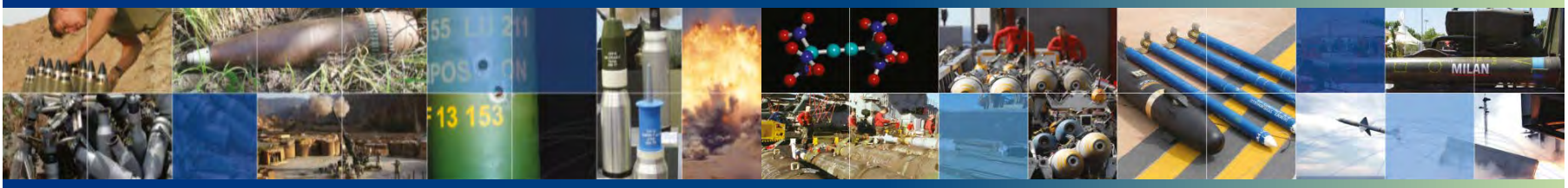
AMRDEC Web Site
www.amrdec.army.mil

Facebook
www.facebook.com/rdecom.amrdec

YouTube
www.youtube.com/user/AMRDEC

Twitter
[@usarmyamrdec](https://twitter.com/usarmyamrdec)

Public Affairs
AMRDEC-PAO@amrdec.army.mil



MSIAC Workshop 2018: Improved Explosives and Munitions Risk Management

IMEMTS, Portland, 23-27 April 2018

Martijn van der Voort
TSO - Munitions Transport and
Storage Safety
+32 2 707 5426
m.vandervoort@msiac.nato.int



Improved Explosives and
Munitions Risk Management

Granada, Spain | 10 - 14 September 2018





Improved Explosives and Munitions Risk Management

Granada, Spain | 10 - 14 September 2018



- Unclassified workshop open at no cost to government, industry and academia representatives from all MSIAC member nations

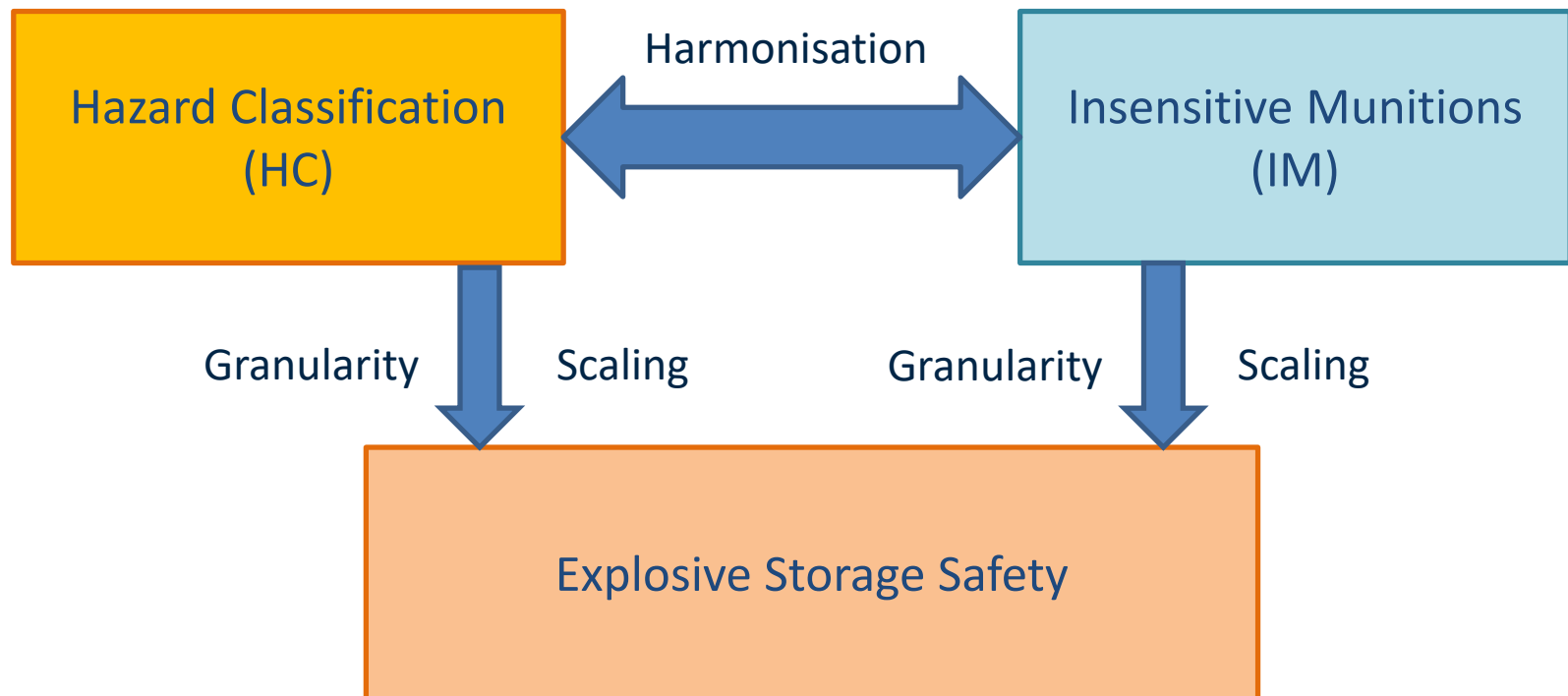
- Limited to 65 participants. In the event of oversubscription, MSIAC will work with the National Focal Point Officer(s) from the nations to balance participation.

- Visit MSIAC IEMRM workshop page!
 - Call for papers extended until April 30
 - Registration just opened
 - Take part in IEMRM Webinar, May 24, 15:00 CET

- Workshop will have various plenary sessions and parallel session (focus areas) and will host a dinner (Tuesday evening) and a visit to General Dynamics European Land Systems, GDELS (Wednesday afternoon)

Improved Explosives and Munitions Risk Management

This workshop seeks to exploit an improved understanding of munitions vulnerability and consequences to deliver improvements in munitions risk management



- **Support** the IM and HC harmonization initiative
 - Identify how response descriptors can be introduced in HC testing
 - Identify whether there's a need for revised definition of Hazard Divisions (HD) and Storage sub Divisions (SsD)

- **Develop** improved methods for explosives and munitions risk management
 - Exploit results from small- and full-scale testing
 - Manage risk with sufficient detail and granularity
 - Realize benefits of IM
 - Efficiently manage munitions presenting the greatest hazard

- **Recommend** improved methods for explosives and munitions safety risk standards
 - Ensuring they reflect the changing nature of the munitions stockpile
 - Balancing complexity versus ease of user application

Mon

REGISTRATION WELCOME AND PLENARY SESSION

**Improved
HC and IM Assessment**

**Improved
Consequence and Risk Analysis**

Tue

REVISED CRITERIA
FOR HC
ASSIGNMENT
PART 1

APPLICABILITY OF
HD ASSIGNMENT
TO STORAGE
PART 1

INTERNAL BLAST
AND DEBRIS

FRAGMENTATION

TUESDAY BRIEFINGS

Wed

REVISED CRITERIA
FOR HC
ASSIGNMENT
PART 2

APPLICABILITY OF
HD ASSIGNMENT
TO STORAGE
PART 2

EXTERNAL BLAST

THERMAL EFFECTS

WEDNESDAY BRIEFINGS

Thu

Implementation of IEMRM

DEPLOYED MISSIONS AND OPERATIONS

STORAGE IN HOME COUNTRY

Fri

CONCLUSIONS AND WAY FORWARD

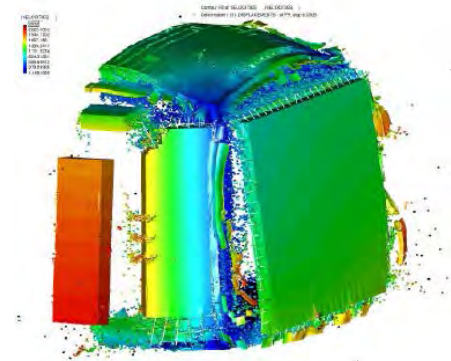
Plenary session presentations:

- Workshop introduction (MV)
- Lessons learned from Cook-Off Workshop & scaling effects (MA, MV)
- Operational aspects and limitations (MP)



Session papers and presentations:

- HC & IM harmonisation (MS, MP)
- Warhead fragmentation (EB, WB, MV, CC)
- Internal blast loads and debris (MV)
- External blast and TNT equivalence (CC)



Abstracts already received:

- The Detonative Reaction Behaviors of Minimum Signature Rockets Subjected to Fragment Impact (Mark Pfeil, AMRDEC, US)
- Numerical Modeling of Explosively Loaded Concrete Structure Using a Coupled CFD-CSD Methodology (Michael Giltrud, ASI, US)
- Characterization of debris throw from structural components subjected to dynamic loads (Johannes Schneider, EMI, DEU)
- Physics-based injury models for improved explosives and munitions risk management (Dr. Malte von Ramin, EMI, DEU)
- Many more have been discussed

And more....

- Lessons learned from International Explosives Safety Seminar (August 2018) by (Dr. Josephine Covino, DDESB, US)
- Input from the AASTP-4 Custodian Working Group by (Hans Oiom, NDEA, NOR)
-

Current HC system loosely defines explosive effects

Differences in Hazard Divisions (HD) between nations possible

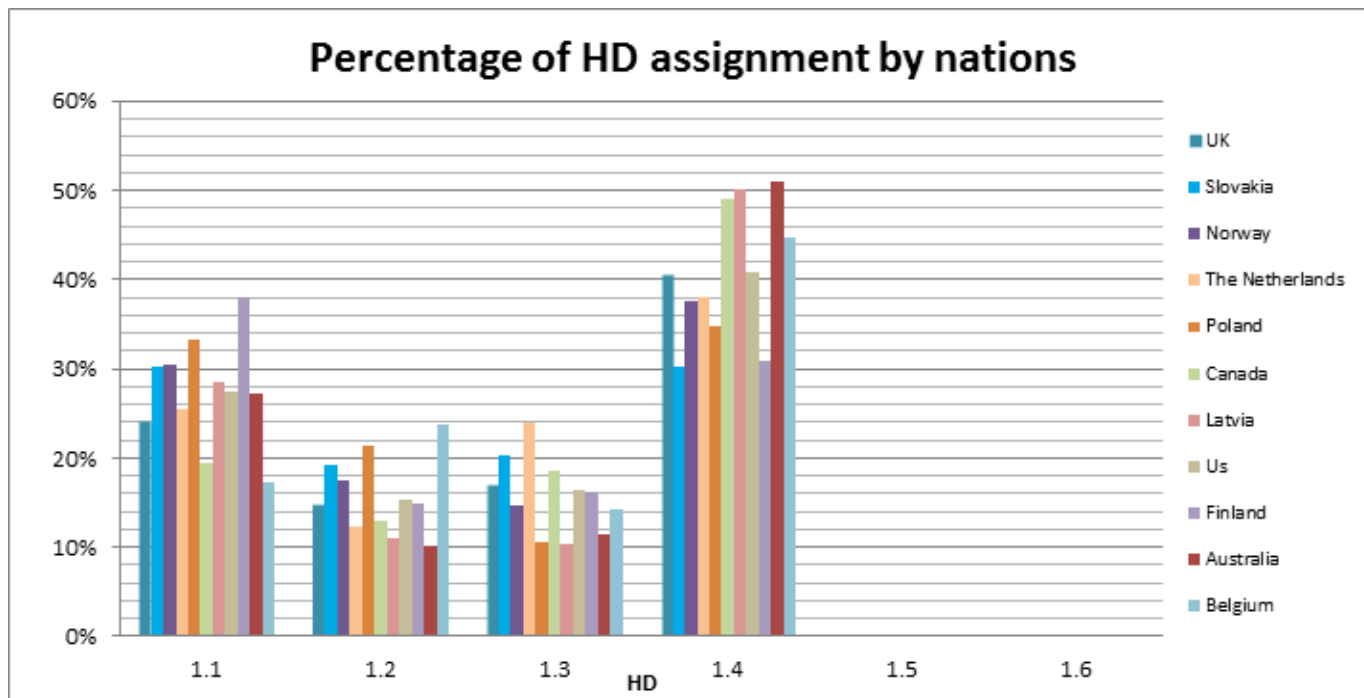


	Munitions Response
I	Detonation
II	Partial Detonation
III	Explosion
IV	Deflagration
V	Burn
VI	No Reaction

- Can IM response descriptors be introduced in HC testing* and what would be the implications?

**this was already done for test series 7 used to classify HD1.6*

Current HD & SsD may not be ideally representing the current and future munitions stockpile



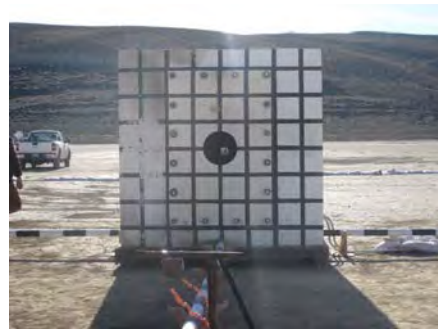
Study of International Hazard Classification, Leroy (2017)

- Is it necessary to revise the definitions of HD & SsD and what would be the implications?

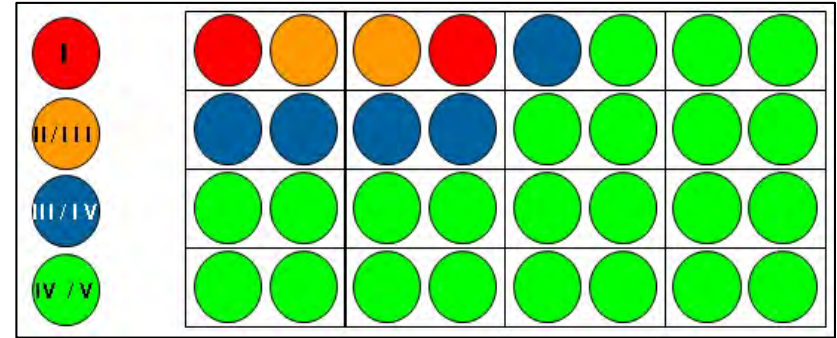
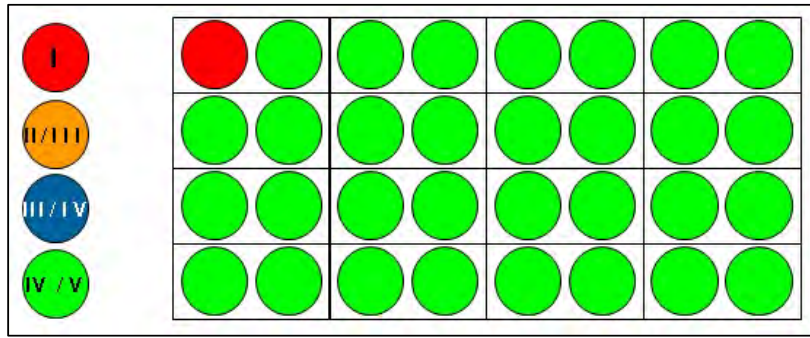
HC (UN orange book) for transport also adopted for storage



Scaling
Confinement



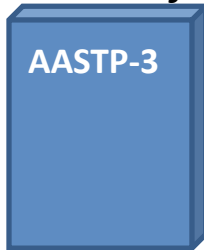
US propellant testing in concrete magazines, Farmer, et al. 2015



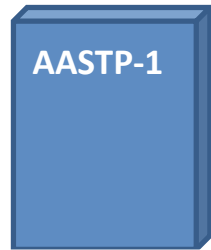
105 mm HE IM shells, Edwards (2011), single shell detonation (left), two shell detonation (right)

- Can we develop improved guidance to clarify the applicability of HC assessments?
- What complementary information (related to scale and confinement) is needed to make a reliable estimate of munitions response in storage conditions?
- What information from the explosive (storage) safety community is needed?
- What is a sufficient number of test repetitions?
- Are there best practices?

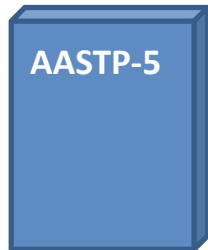
Hazard Classification



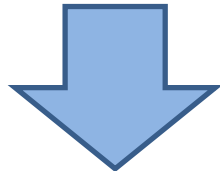
Guidelines for safe storage of ammunition



Home country:
Quantity Distances (QD)

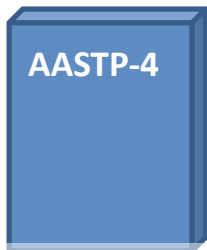


Deployed operations:
Field Distances (FD)

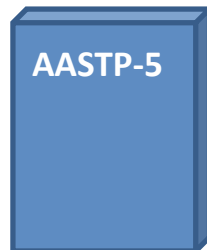


If these cannot be met:

Explosives Safety Risk Analysis



Detailed models



Practical method

Simple

Complicated

Explosives Safety and Munitions Risk Management (ESMRM)



Continuous process
To be conducted by ESO
As Low As Reasonably Practicable (ALARP)
Level of authority for risk approval

- Models primarily available for (mass) detonations
- Benefits of less violent munitions can't always be exploited

Munitions response descriptors (AOP-39)		Models available for consequence and risk analysis, e.g. AASTP-4?
I	Detonation	Yes
II	Partial Detonation	Yes/No (fraction that will detonate uncertain)
III	Explosion	No
IV	Deflagration	No
V	Burn	Yes
VI	No Reaction	NA

- What experimental data and models is required to quantify consequences and risks based on the response descriptors, in particular for Deflagration (type IV) and Explosion (type III)

- What models need to be developed in order to quantify fragmentation effects for less violent munitions responses?
- What experimental data is needed to develop and validate these models?
- Is the concept of Maximum & Hazardous Fragment Distance (MFD and HFD) still valid as a basis for safe separation distances?
- What information is needed from the HC/IM community?

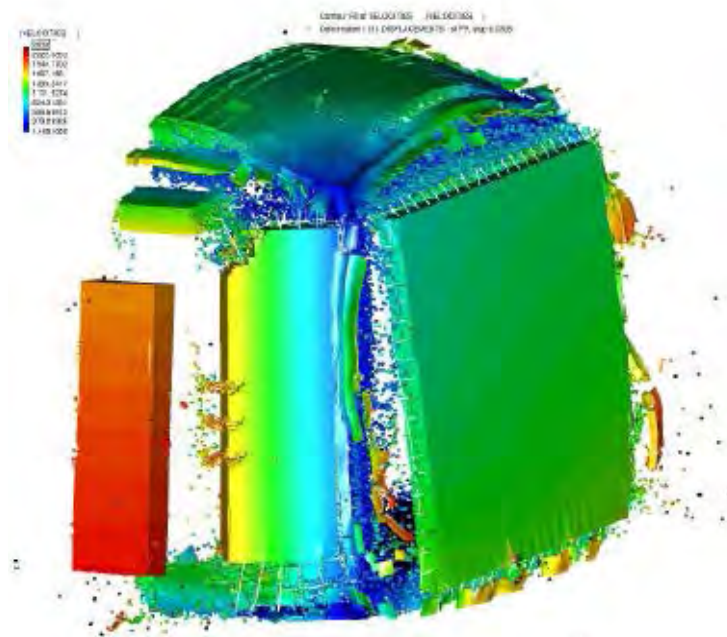


840 g steel fragment from a M107 155 mm artillery shell that reached 1824 m after a sub-detonative response.

- What models need to be developed in order to quantify internal blast and debris effects for less violent munitions responses?
- What experimental data is needed to develop and validate these models?
- What information is needed from the HC/IM community?

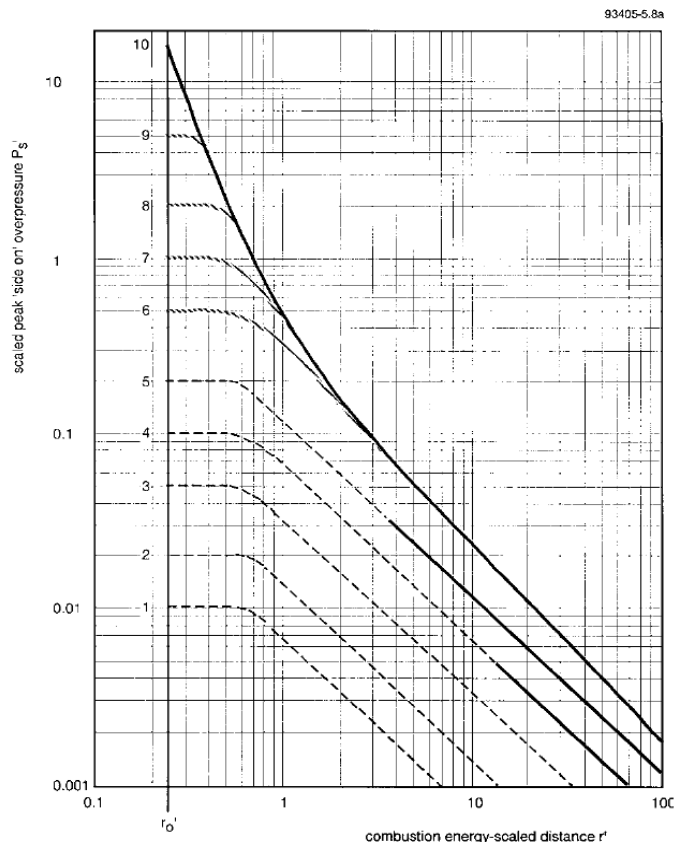


High speed frame from Kasun test (Grønsten)



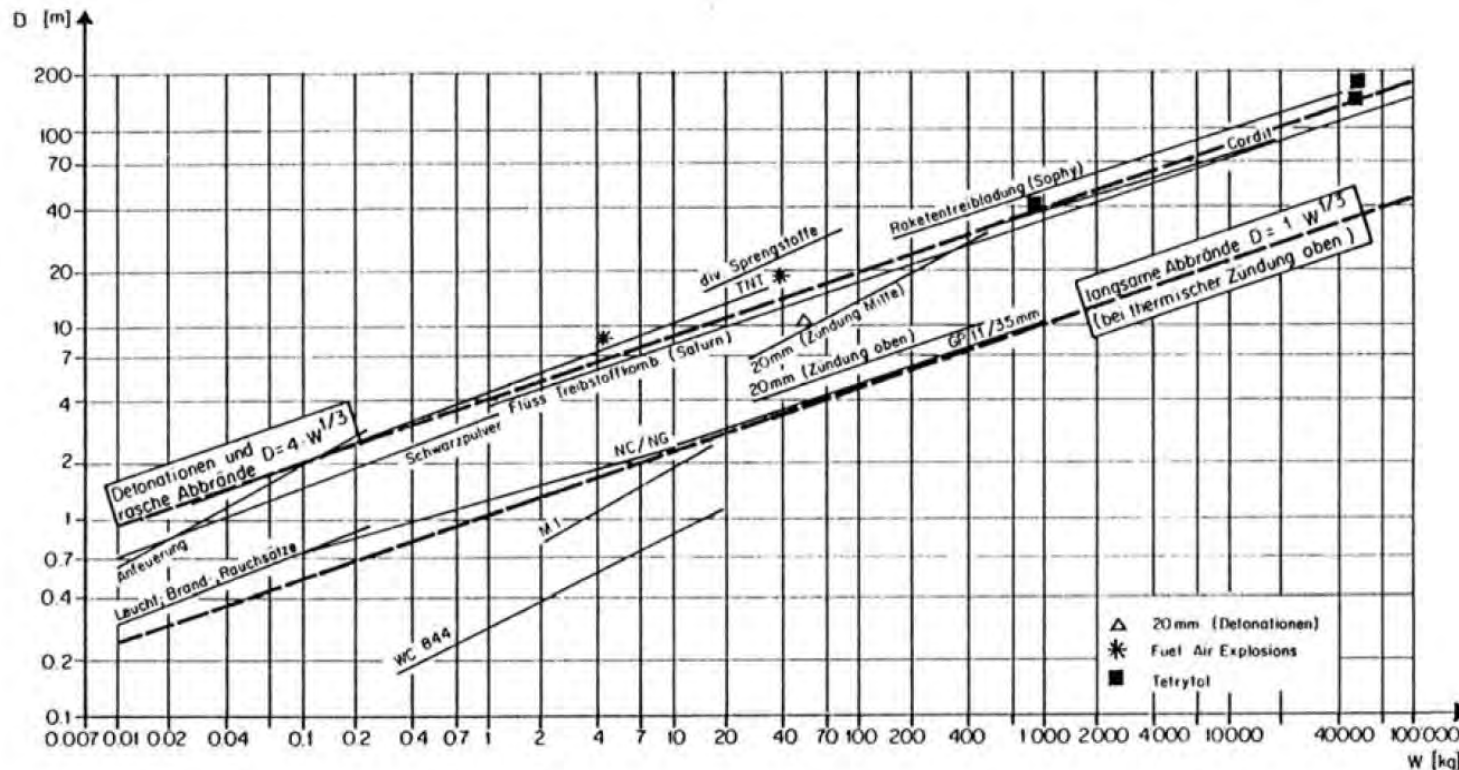
*Detonation in ammunition magazine (right)
by Applied Simulations, Inc (ASI)*

- What models need to be developed in order to quantify internal blast and debris effects for less violent munitions responses?
- Can TNT equivalency be used to model less violent responses?
- What experimental data is needed to develop and validate these models?
- What information is needed from the HC/IM community?



Multi-Energy blast charts [PGS2, van den Berg, 2004]. Curve 1 is a weak deflagration, curve 10 a detonation. Curves 6 to 9 (fast deflagrations) coincide with curve 10 in the far field.

- What models need to be developed in order to quantify thermal effects?
- What experimental data is needed to develop and validate these models?
- What information is needed from the HC/IM community?



Fireball diameters for various propellants and explosives
[AASTP-4, 2016]

- Areas to be addressed:
 - An increased granularity and detail could lead to more complex QD tables as well as consequence and risk analysis methods. As an alternative the introduction of **computer-based tools** into the standards could be considered. This will make application easier, and less prone to error, but also leads to a dependency on IT equipment which may be an issue e.g. during missions.
 - More detailed methods could also lead to **munition specific** consequence and risk analysis. This will improve the reliability of the results, but on the other hand also limits the range of applicability.

- In some cases assumptions made in standards prohibit progress. Currently AASTP-5 requires that all munitions are to be aggregated as HD1.1 in order to keep its application simple. This assumption should be challenged to **enable recognition of the benefits of IM and focus efforts on munitions which present the greatest hazard.**
- An **holistic approach** could be developed considering the cost and benefits of using **simplistic and conservative assessment** methods versus **more detailed quantitative assessment** methods. Dependent on the lifecycle phase and situation the most suitable approach could be selected.

The envisaged results of the workshop are:

- Revised approach to munitions hazards and risks in light of development and introduction of IM
- Improved methods for consequence and risk analysis
- Improved understanding of the true nature of hazards and risks and how this can improve ownership and associated costs

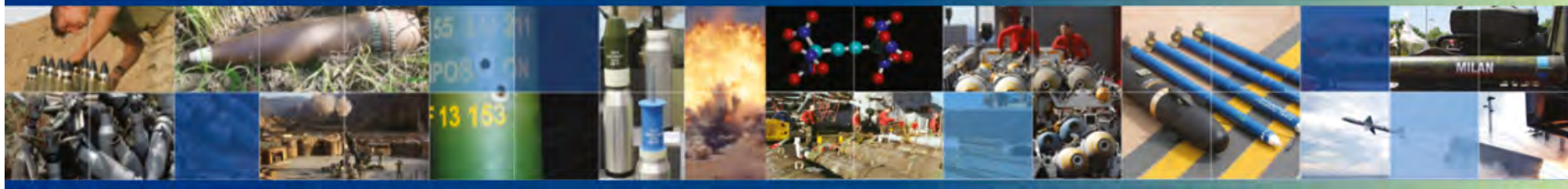


Improved Explosives and
Munitions Risk Management

Granada, Spain | 10 - 14 September 2018



Munitions Safety Information Analysis Center
Supporting Member Nations in the Enhancement of their Munitions Life Cycle Safety



Qualification and Energetic Materials Challenges

IMEMTS

Portland, OR, USA

23rd – 27th April 2018

Dr Matthew Andrews

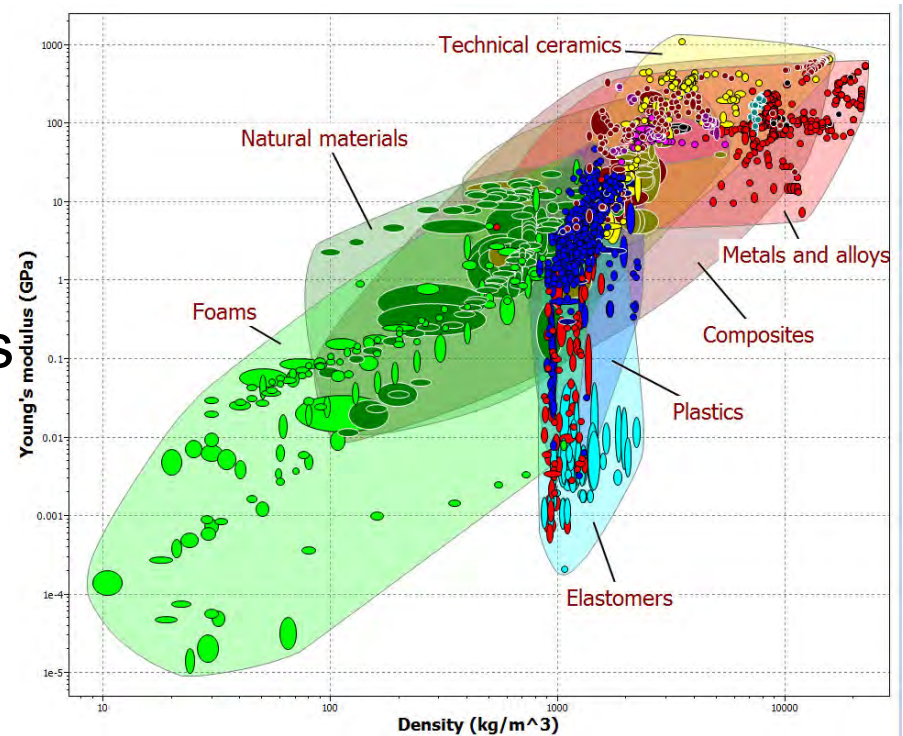
TSO Energetic Materials

+32.2.707.5630

m.andrews@msiac.nato.int



- Introduction
- MSIAC Workshops – The Repeating Issue
- Materials in Munitions
- Models & Benefits
- Current Testing Requirements
- How to Move Forward



Multiple materials present in munitions
 Visualising the bulk engineering materials in property space (ρ vs E)
<https://www.grantadesign.com/products/ces/find.htm>



■ NIMIC/MSIAC workshops

- Cook Off
- Shaped Charge Jet
- Fragment Impact
- XDT
- Sympathetic Reaction

■ Gaps highlighted

■ Few explosives have all experimentally determined observables¹

■ Why?

- Improved models
- Technology provides wider access to capability (Moore's Law)
- No data collection (needs don't match requirements)

Models

- Software exchange (1993)
- Lack of input conditions (1992)
- Improve models through collaboration (2004)

Material Characterisation - Mechanical

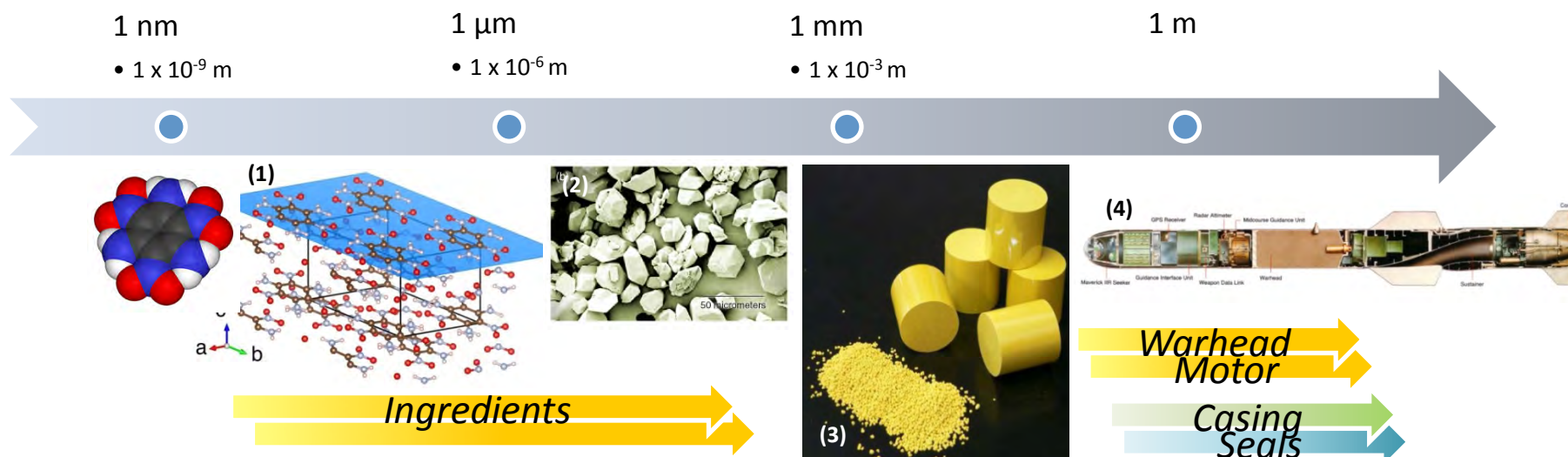
- Requirement for high strain rate properties (1992)
- Strain rates at temperature and pressures (2000)

Material Characterisation - Thermal

- Data needed at elevated temperatures (1993)
- Collaborative database on energetic & inert material properties (2004)
- Prioritise and identify standardised material data sets for SCJ (2014) and thermal (2016)

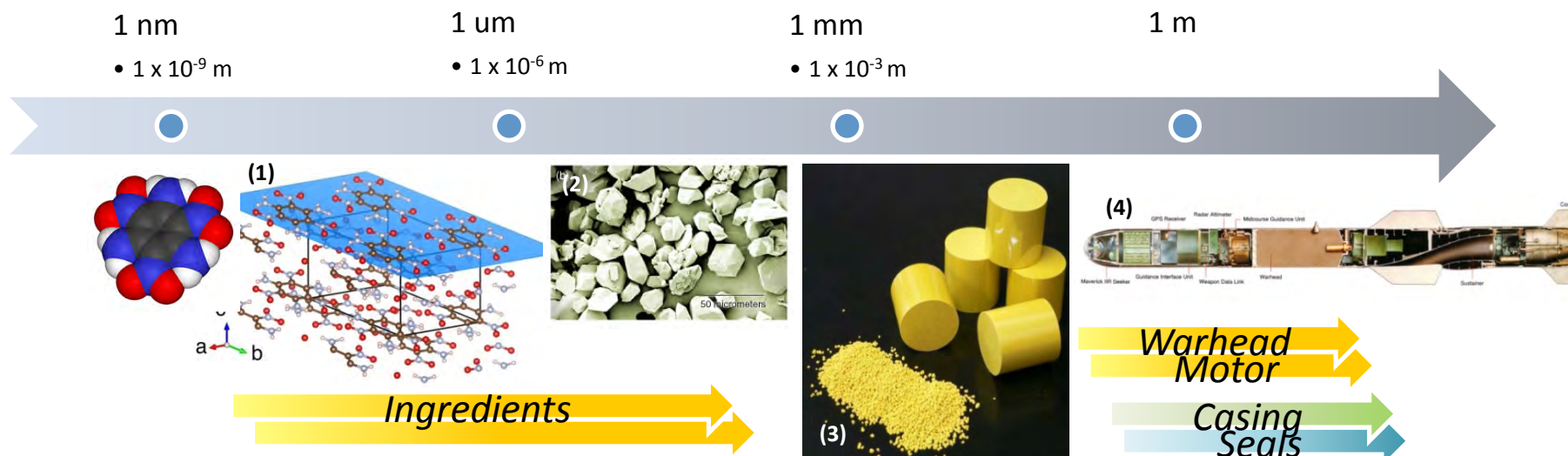
1. Peterson J. R., Wight, C. A. "An Eulerian-Lagrangian Computational Model for Deflagration and Detonation of High Explosives", (2012), 159, 2491-2499.

Physical	Chemical	Thermal	Mechanical
State (s, l, g)	Enthalpy of formation (kJ mol ⁻¹)	Thermal conductivity (W g ⁻¹ .K ⁻¹)	Tensile strength (MPa)
Density (g cm ⁻³)	Enthalpy of combustion (kJ mol ⁻¹)	CTE (μm m ⁻¹)	Compressive strength (MPa)
Molecular weight (g mol ⁻¹)	Enthalpy of detonation (kJ mol ⁻¹)	Specific heat capacity (J g ⁻¹ .K ⁻¹)	Complex modulus
Melting point (°C)	Solubility (mg L ⁻¹)		
Boiling point (°C)			
Decomposition temperature (°C)			
Hazard	Shock	Performance	
Impact (J)	Gap (GPa)	Detonation velocity (km s ⁻¹)	
Friction (N)	Shock velocity (km s ⁻¹)	Detonation pressure (GPa)	
ESD (J)	Particle velocity (km s ⁻¹)	Critical diameter (mm)	
	Run distance (mm)	Gurney energy (kJ kg ⁻¹)	



- Multiple materials present within munitions
 - Focus on energetic materials (this presentation)
- Understanding required across all scales
 - Material properties (physical, chemical, mechanical) to system response
- From single molecule to warhead
 - Scale – 10 orders of magnitude (nm to m)
 - Mass – 6 orders of magnitude (mg to kg)

1. Luscher, D. J. et al, *Crystals* **2017**, 7(5), 138
2. Heller, A. *Science & Technology Review* **2009**, 4-10
3. Price, D. *IMEMTS*, **2010**,
4. Kopp, C. *AGM-84E SLAM*, **1988**



- Testing focussed on performance and safety in storage, transport and service
 - STANAG 4123 / UN Hazard Classification
 - AOP-15 / Safety & Suitability for Service
 - STANAG 4439 / Insensitive Munitions
- Criteria for tests can be binary - usually pass/fail
 - Limited number of tests
 - High costs
- Reliance on 'whole body of evidence' for assessment

1 nm

• 1×10^{-9} m

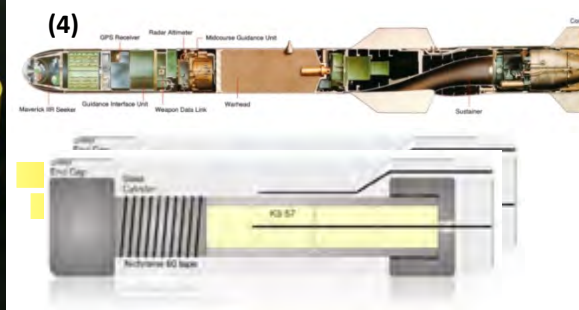
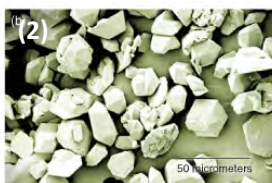
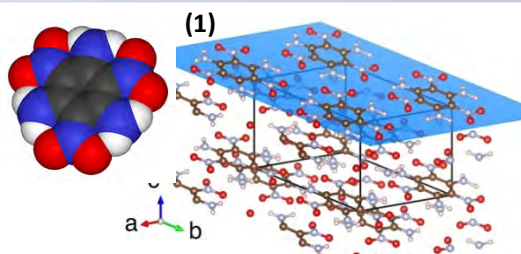
1 μ m

• 1×10^{-6} m

1 mm

• 1×10^{-3} m

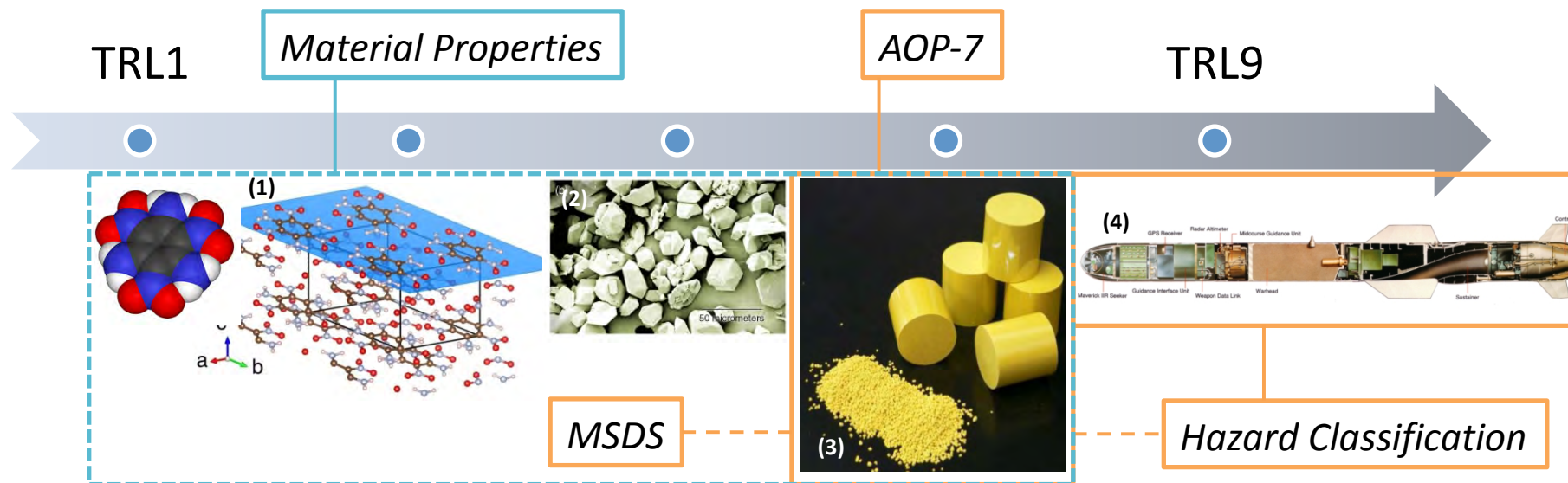
1 m



Ingredients

- Experiments performed to elucidate response to a hazard
- Some tests determine scientific understanding whilst other provide pass/fail
 - Friability
 - EMTAP 36 (UK Fragment Impact)
- All results are compared against existing EM knowledge
- Difficult to use information for prediction of munition response

Qualification



- Development cycle – no requirement to fully characterise materials
- Testing focussed on performance and safety
- AOP-7
 - Qualification for inclusion of energetic material in a military munition
- Hazard Classification
 - Assessment for transportation
- Material Safety Data Sheets
 - Some physical and chemical properties

Known Issues
EM down selection based on performance

AOP-7

- Qualification of new EM based on assessment of **safety and performance**
 - Agreed minimum data set
 - Whether the EM characteristics change during the lifecycle
 - Information on the chemical and physical properties shall be provided
 - Compliance with National H&S requirements shall be provided
 - MSDS
 - EHDS
- **Shall**
 - Can be interpreted as not mandated
- Chemical, Physical and Mechanical Properties:
 - **Stability & Thermal Characterization**, Variation of Properties with Age, **Compatibility**, Density, Melting Point, Thermal Characterisation, Glass Transition Point and **Mechanical/Rheological Properties**
- Hazard Assessment
 - **Ignition Temperature, Explosive Response when Ignited (Confined and Unconfined), Electrostatic Discharge, Impact, Friction, and Shock**
- Performance Assessment:
 - Detonation Velocity and **Critical Diameter**
- Those indicted in bold are mandatory qualification data or properties

Supporting Munitions Safety

Category	Test Performed	Criteria
Stability Characterisation	Vacuum Thermal Stability	< 2 cm ³ gas
	Thermal Stability	No change
Thermal Characterisation	Thermo gravimetric analysis	
	Self Heating (onset)	
	Compatibility	< 2 cm ³ gas
Ignition Temperature	Woods Metal Bath	
	Henkin Time to Explosion	
	Critical Temperature	> 82 °C
	1-L Cook Off	
Explosive Response	Variable Confinement (SCO)	Deflagration or less
	Variable Confinement (FCO)	Deflagration or less
	Small Scale Burn	Less than explosion
Sensitivity Tests	ESD	No reaction at 0.25 J
	Impact	
	Friction	> 96 N
	Shock Sensitivity	
	Cap Test	
Chemical, Physical, Mechanical	CTE	
	Density	
	Growth	1 %
	Exudation	0.1 %
	Young's Modulus	
	Compressive Strength	
	Strain @ Max Stress	
Cube Cracking	No fissures	
Variation with Age	Ageing protocol	
Toxicity Evaluation	MSDS	
Performance Properties	Detonation Velocity	
	Dent Depth	
	Explosivity of Dust	
	Critical Diameter	

- **US Example**
 - IMX-104 qualification
 - Zunino et al (IMEMTS 2012)
- **Greater testing requirements than AOP-7 minimum**
- **Tests**
 - Included chemical & physical parameters
- **Gaps**
 - Not reported
 - C_P
 - Wedge

- **Global Harmonised System**
 - EU requirement CLP (EU1272/2008)
 - Information gathered by manufacturer for Material Safety Data Sheet (MSDS)
 - 16 sections including Hazards, Transport and....

- **Chemical & Physical Properties**
 - Section 9
 - No consistency in reported information
 - From 0/20 to 18/20
 - Data usually only gathered at one temperature and/or pressure
 - 25°C (not consistent)
 - 133.3 hPa (also not consistent)

- **So how can we measure the parameters?**

SECTION 9: Physical and chemical properties
9.1 Information on basic physical and chemical properties

a) Appearance	Form: crystalline Colour: light yellow
b) Odour	No data available
c) Odour Threshold	No data available
d) pH	No data available
e) Melting point/freezing point	Melting point/range: 67 - 70 °C
f) Initial boiling point and boiling range	No data available
g) Flash point	155.0 °C - closed cup
h) Evaporation rate	No data available
i) Flammability (solid, gas)	No data available
j) Upper/lower flammability or explosive limits	No data available
k) Vapour pressure	133.3 hPa at 157.7 °C 1.3 hPa at 102.7 °C
l) Vapour density	No data available
m) Relative density	No data available
n) Water solubility	No data available
o) Partition coefficient: n-octanol/water	No data available
p) Auto-ignition temperature	No data available
q) Decomposition temperature	No data available
r) Viscosity	No data available
s) Explosive properties	No data available
t) Oxidizing properties	No data available

9.2 Other safety information

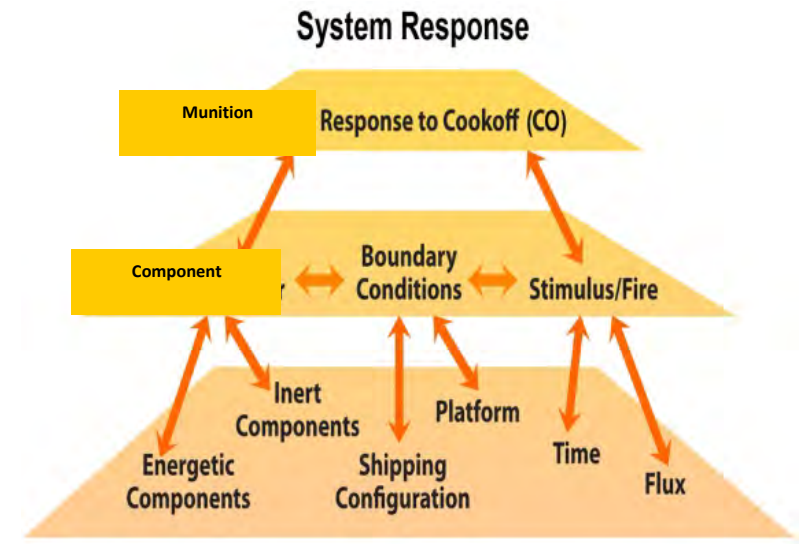
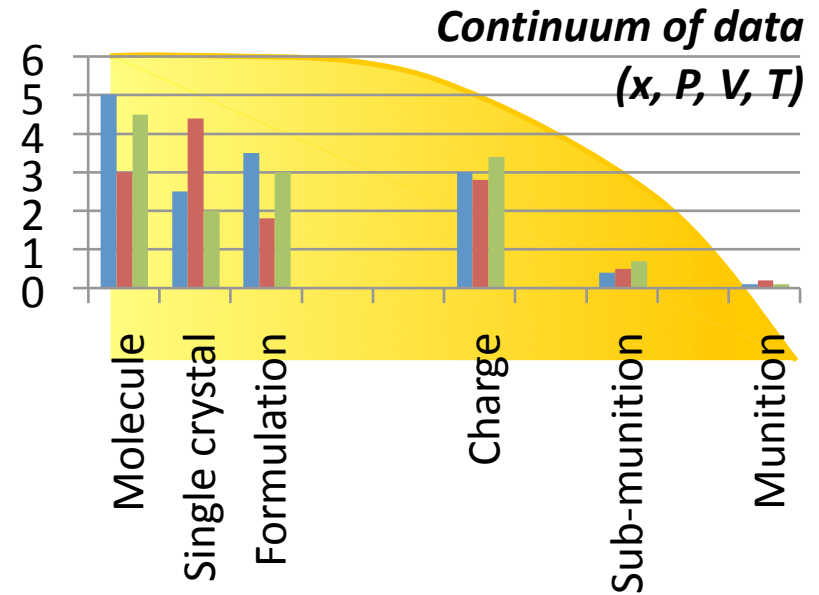
No data available

SECTION 10: Stability and reactivity

1. Sigma-Aldrich "2,4-Dinitrotoluene", (2015), Safety Data Sheet.

Whole Body of Evidence

- Understand munition response to key abnormal threats include
 - Thermal
 - Shock
 - Impact
- Discrete data sets available
 - Relates to specific tests
- Therefore we use
 - Models to test our understanding...but
 - Do we have the right information



Development of a scaling hierarchy for cook off hazards
Atwood, A. et al. (2010), IMEMTS, Munich

Models

■ Greater reliance on modelling for

- Simulation
- Safety assessment
- Ultimate aim →
 - Prediction

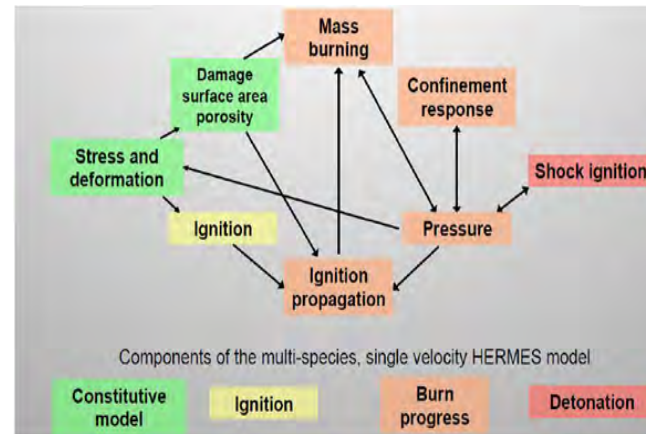
■ Development of computational tools for simulating abnormal thermal events (e.g.)

- Critical Temperature¹
- ALE3D²
 - LLNL
- Eulerian & Lagrangian³
 - University of Utah
- Multiple codes
 - SNL

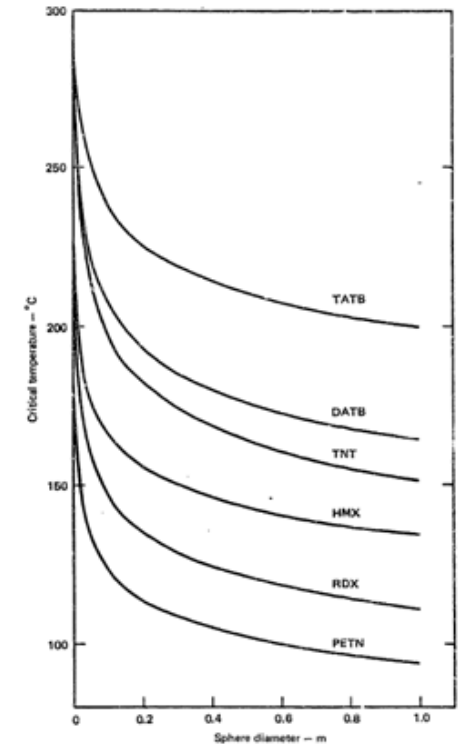
■ Thermal Hazards

■ Time to ignition

- Thermal & physical parameters
- Chemistry
- Confinement - complex



The HERMES model components
 Development of thermal violence cookoff tests at AWE
 Cook, M. (2016), SoCO, Atlanta

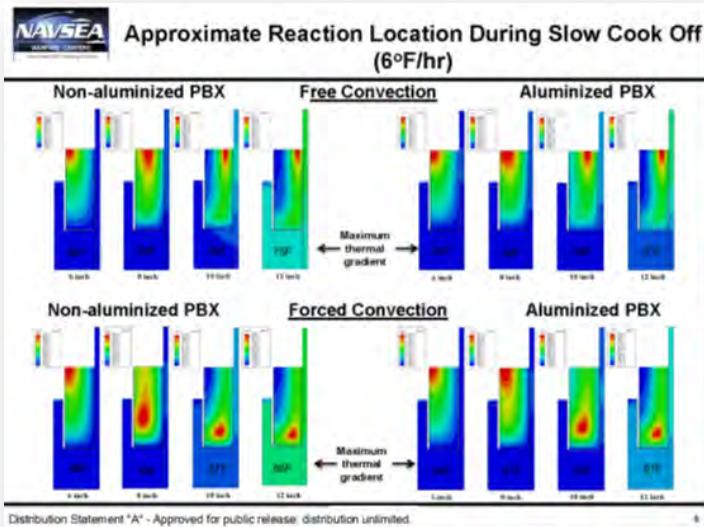


$$\frac{E_a}{T_m} = R \ln \left[\frac{a^2 \rho Q Z E_a}{T_m^2 \lambda \delta R} \right]$$

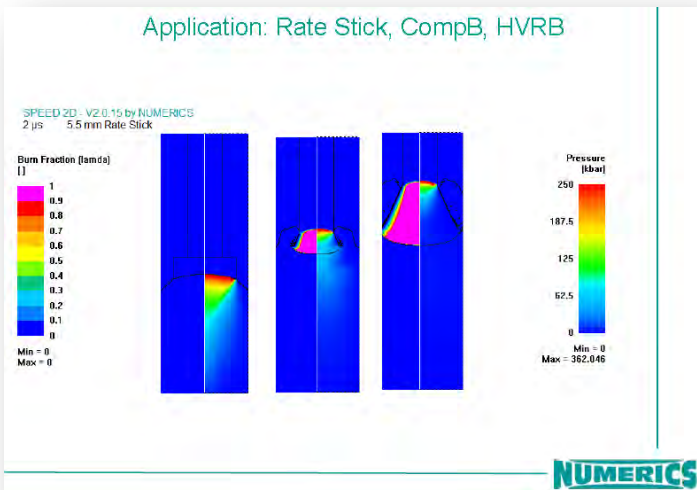
Critical temperature¹

1. Rogers, R. N. *Thermochimica Acta*, (1975), 11, 131-139
2. McClelland, M. A., Tran, T. D., Cunningham, B. J., Weese, R. K., Maienschein, J. L.. "Cookoff Response of PBXN-109: Material Characterization and ALE3D Model", (2000), JANNAF, Monterey, CA.
3. Peterson J. R., Wight, C. A. "An Eulerian-Lagrangian Computational Model for Deflagration and Detonation of High Explosives", (2012), 159, 2491-2499.

Supporting Munitions Safety



Clark, K. (2016), SoCO, Atlanta



Hartmann, T; Rottenkolber, E. (2014), SCJ, Brest

- Assess interdependence of, and sensitivity to changes in, variables
 - Size
 - Volume
 - Materials
 - External conditions
- Test mechanistic understanding
- Increases confidence in observed behaviour
- Provides insight into reaction that can not always be observed experimentally
 - Time to reaction
 - Location of reaction
 - Reaction growth
 - But cannot reliably predict reaction violence

Modelling Requirements

- Requirement to populate model(s) with experimental data as $[f_n(T)]$ and $[f_n(P)]$

- Coefficient of Thermal Expansion¹
- Specific Heat Capacity
 - Solid phase¹
 - Gaseous phase²
- Shear Modulus¹
- Bulk Modulus¹
- Reaction kinetics, detonation¹
- Condensed Phase Activation Energy²

Temperature
-60 °C to 500 °C
(model dependent)

Pressure
0.1 MPa to 50 GPa
(model dependent)

- Good models need

- Well defined experiments
- Information on the boundary conditions
- An iterative development cycle supported by progressive experimental design and testing programme

- Discussion

- Mismatch in requirement to obtain data

1. McClelland, M. A., Tran, T. D., Cunningham, B. J., Weese, R. K., Maienschein, J. L.. "Cookoff Response of PBXN-109: Material Characterization and ALE3D Model", (2000), JANNAF, Monterey, CA.

2. Peterson J. R., Wight, C. A. "An Eulerian-Lagrangian Computational Model for Deflagration and Detonation of High Explosives", (2012), 159, 2491-2499.



MSIAC Methods for Obtaining Parameters

Supporting Munitions Safety

- Chemical & Physical Properties
 - MSDS
 - Density, vapour pressure (if recorded)
 - AOP-7
 - Onset of decomposition; Ageing includes mechanical properties
- Parameters still required
 - Function of temperature (e.g. -60 to 120°C – material dependent)
 - Determine other factors from these selected parameters e.g. critical temperature, enthalpy of formation



MSIAC Methods for Obtaining Parameters

Supporting Munitions Safety

- Chemical & Physical Properties
 - MSDS
 - Density, vapour pressure (if recorded)
 - AOP-7
 - Onset of decomposition; Ageing includes mechanical properties
- Parameters still required
 - Function of temperature (e.g. -60 to 120°C – material dependent)
 - Determine other factors from these selected parameters e.g. critical temperature, enthalpy of formation

Thermal		Units
Vapour pressure	P_{vap}	hPa
Heat Capacity	C_p	J g ⁻¹ .°C ⁻¹
Thermal Conductivity	λ	W cm ⁻¹ .°C ⁻¹
Coefficient of Thermal Expansion	CTE	$\mu\text{m m}^{-1}$.°C ⁻¹
Activation Energy	E_a	kJ mol ⁻¹
Physical		
Density	ρ	g cm ⁻³
Enthalpy of Combustion	ΔH_c	kJ mol ⁻¹

ASTM D 4809	liquid hydrocarbon fuels	Bomb Calorimetry	17
-------------	--------------------------	------------------	----



MSIAC Methods for Obtaining Parameters

Supporting Munitions Safety

- Chemical & Physical Properties
 - MSDS
 - Density, vapour pressure (if recorded)
 - AOP-7
 - Onset of decomposition; Ageing includes mechanical properties
- Parameters still required
 - Function of temperature (e.g. -60 to 120°C – material & model dependent)
 - Determine other factors from these selected parameters e.g. critical temperature, enthalpy of formation

Thermal		Units	Existing Methods	Notes	Equipment
Vapour pressure	P_{vap}	hPa	ASTM E 1782		Differential Scanning Calorimetry or Differential Thermal Analysis
Heat Capacity	C_p	J g ⁻¹ .°C ⁻¹	ASTM E 1269		Differential Scanning Calorimetry
Thermal Conductivity	λ	W cm ⁻¹ .°C ⁻¹	ASTM E 1225		Longitudinal Heat Flow
			ASTM C 518		Heat Flow Meter Apparatus
Coefficient of Thermal Expansion	CTE	$\mu\text{m m}^{-1}$.°C ⁻¹	ASTM E 831 STANAG 4525	Thermochemical analysis	Thermal Mechanical Analyser (TMA)
			ASTM E 2716		Sinusoidal Modulated Temperature Differential Scanning Calorimetry
Activation Energy	E_a	kJ mol ⁻¹	ASTM E 1614 STANAG 4147		Thermogravimetry Using Ozawa/ Flynn/Wall Method
			ASTM E 698	Thermally unstable materials	Differential Scanning Calorimetry
Physical					
Density	ρ	g cm ⁻³	ASTM D 792		Displacement
			ASTM D 1217		Pycnometry
Enthalpy of Combustion	ΔH_c	kJ mol ⁻¹	ASTM D 4809	liquid hydrocarbon fuels	Bomb Calorimetry

MSIAC Unclassified. Distribution Unlimited

■ Data

- Capability exists to better characterise materials
- Request for chemical, physical and mechanical information is usually much later in the qualification process (type qualification)
- Propose at an earlier stage in development (pre-AOP-7)

■ Modelling

- Modelling is being used throughout munition development
 - Design
 - Safety assessment
 - Prediction
- Access to codes and models across most MSIAC nations
- Capability to run simulations is now faster and cheaper

■ Benefits

- Reduced time in development
- Greater insight into internal behaviour
- Improved assessment of time to reaction
- Well-posed models enable easier design modifications
- Increased confidence in assessed response level
- Helps assess programme risk

Stakeholders

Manufacturers
Design Authorities
Safety Authorities
Modellers
Experimentalist

How is MSIAC helping?

- Enabling exchange of information
 - Workshops
- Generating guidance on models and methodology
 - L-195 (Babcock & van der Voort)
 - L-213 (Babcock)
- Data reviews
 - L-198 (Andrews)
- Repository for data
 - Energetic Materials Compendium (EMC)
- Developing models
 - TEMPER
- Promoting discussion



Acknowledgements



Co-author:

Wade Babcock

MSIAC Team:

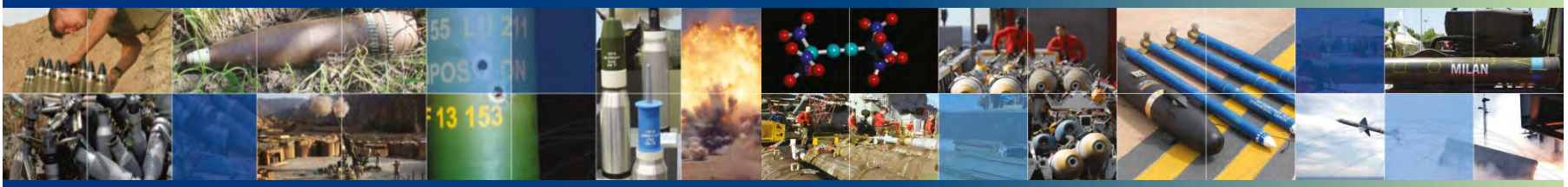
Dr Ernie Baker, Christelle Collet, Martin Pope,
Dr Michael Sharp, Martijn van der Voort



MSIAC

Munitions Safety Information Analysis Center

Supporting Member Nations in the Enhancement of their Munitions Life Cycle Safety



REACTION MECHANISMS FOR ROCKET MOTORS

Christelle Collet

Propulsion Technology TSO

+32 (0)2 707 5447

c.collet@msiac.nato.int

IMEMTS 2018

Portland, OR, USA

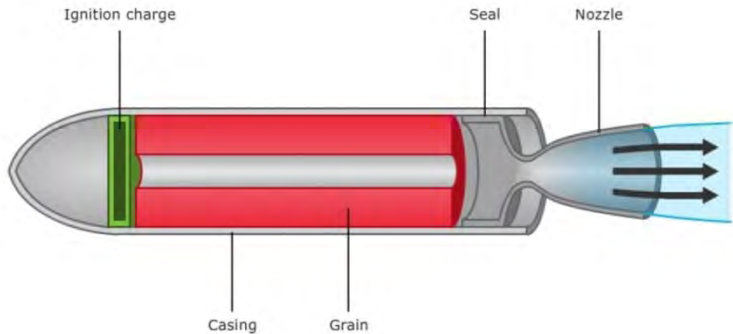


Introduction

1. Mechanical stimuli considered in this study
2. Decomposition Regimes
3. Transition pathways
4. Ways to improve SRMs' IM Signature of SRM

Conclusions

A Solid Rocket Motor configuration is simple... **But only at first sight!**



© Copyright. 2011. University of Waikato. All Rights Reserved.

Elements	Functions
Propellant grain	<ul style="list-style-type: none"> Burns and generates hot gases (typically 3,000 – 3,500 K) Controls rate and profile of hot gas generation Common propellant families used for SRM: mostly double base (CDB, EDB, CMDDB) and composite propellants (with active or inert polymer matrix)
Motor case	<ul style="list-style-type: none"> Withstands high pressure (up to 5 MPa), hot gases Solid propellants storage container
Nozzle	<ul style="list-style-type: none"> Accelerates hot gases to supersonic velocity Controls direction of hot gases
Igniter	Ignites propellant grain on command
Insulation	Prevents hot gases from burning through case
Skirts	Attach points to payload

Now what happens in case of accidental scenarios during the SRM's lifecycle?

- General SRMs' IM Signatures agreed by experts during the MSIAC workshop on IM Technology Gaps¹ :

Rocket Motor Type		IM Signature					
		FCO	SCO	BI	FI	SR	SCJ
Reduced Smoke		IV	IV	IV	IV	Pass	IV
Composite		III	I	III	III	Pass	III
Min Smoke Rocket Motor	XLDB	IV	I	I	I	I	I
	CDB	IV	III	IV	I	I	I
	EDB	IV	III	IV	I	I	I

→ This study aims to better understand the reaction mechanisms occurring under **mechanical threats** applied on Solid Rocket Motors

¹Sharp, M.W., MSIAC IM Technology Gaps Workshop – Output from the Rocket Motor Technology Discussion Group, MSIAC Report L-183, January 2014

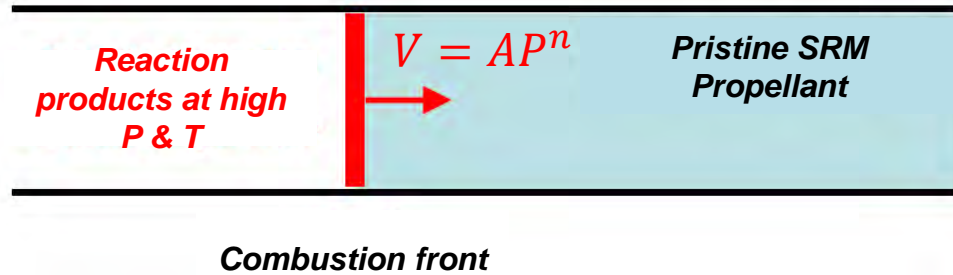
Only mechanical threats are considered in this study:

Threat	Bullet	Fragment	SCJ	EFP
Corresponding STANAG	4241	4496	4526	No existing STANAG
Projectile mass	42 g (12.7 mm M2 AP bullet)	18.6 g	Not relevant, continuous jet	A few hundreds of g
Material	Steel	Steel	Copper	Copper, Steel, Al
Diameter to impact	Not relevant. Perforating cone shaped	14.3 mm (conical shape)	1 to 5 mm	10 to 100 mm
Typical velocity at impact or velocity recommended by STANAG (when existing)	850 m/s	1830 and 2530 m/s	6000 to 8000 m/s for the jet tip	100 to 2000 m/s
Energy	20 kJ	30 and 60 kJ	V^2d between 100 and 300 $m^3 \cdot s^{-2}$	Between 100 and 200 kJ as an estimation for the average

Was considered as a credible mechanical threat for SRMs but not standardized

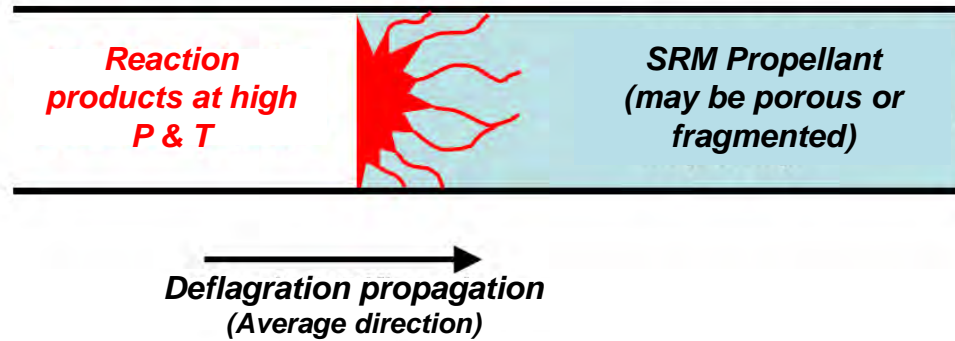
Design mode for a SRM:

Combustion

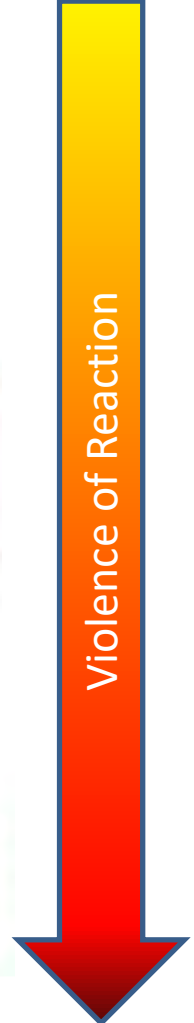
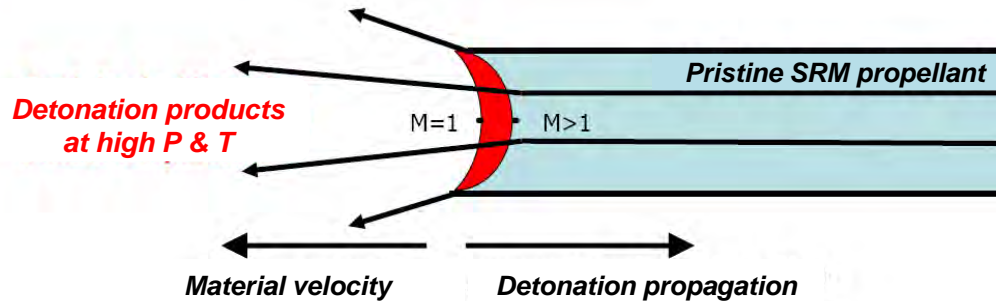


Abnormal regimes:

Deflagration



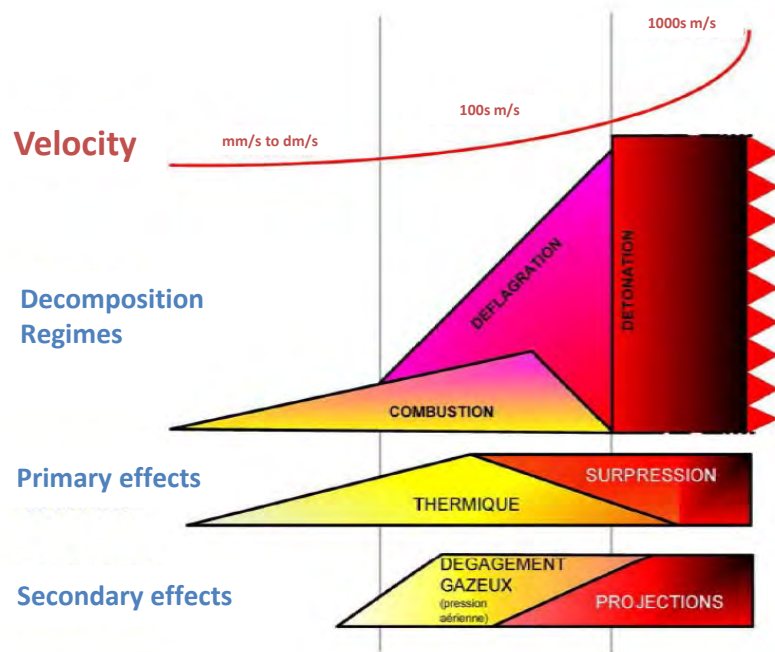
Detonation



- Characteristics of the different decomposition regimes

Decomposition Regime	Combustion	Deflagration	Detonation
Order of magnitude of propagation velocity within the material	$10^{-3} - 10^0$ m/s	10^2 m/s*	10^3 m/s
Primary effects	Thermal	Blast	Blast / fragments or debris (if light casing or no casing)
Secondary effects	Toxic	Thermal Possible fragments	Fragments / blast (if casing)

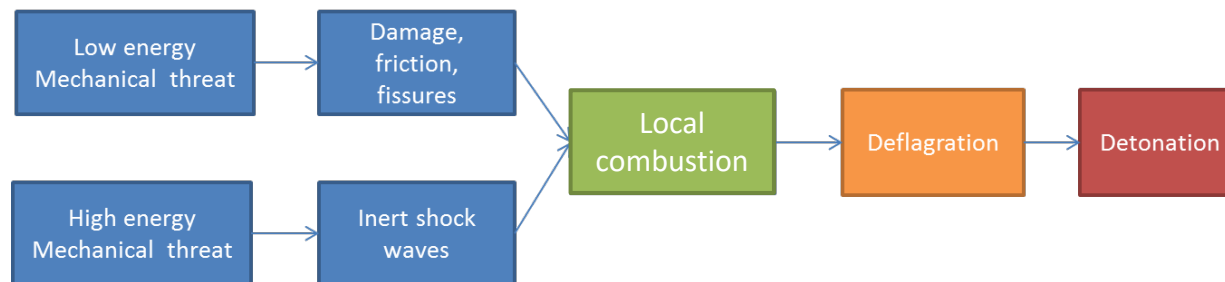
* contrary to combustion and detonation, the deflagration velocity is not an intrinsic parameter for the propellant



Guide de bonnes pratiques en pyrotechnie, Guide SFEPA n°9, 2009

In an SRM impacted by a mechanical stimulus, the Deflagration to Detonation Transition scenario is the following one:

1. The mechanical stimulus induces either damages, friction, fissures, or non reactive shock waves in the solid propellant
2. Depending on its ability to be ignited, the propellant locally burns in a **combustion** process but the combustion gases will infiltrate the damaged propellant, more gases are produced → the pressure increases → the burning rate increases → ... it becomes a **deflagration**
3. If nothing prevents the deflagration velocity to continuously increase inside the grain (self stabilization, increased damage or case break-up), then it will necessarily reach the sound velocity of the unreacted propellant → it becomes a **detonation**



Some key factors influencing the ability of a propellant to undergo DDT:

- A **too high value for coefficient n** (in Vieille's law) that prevents the combustion from stabilizing itself
- **Poor mechanical properties** for the propellant, that lead to fracture and therefore to an increased burning surface
- A **strong casing**, or no venting device that would allow the gas pressure to be released
- A value higher than **18 MPa/ms** for the maximum change in pressure as a function of time, obtained from friability tests
- A **small critical diameter in detonation**. Note that this concept is not trivial for SRMs → the hydraulic diameter is to be used to account for the bore effect

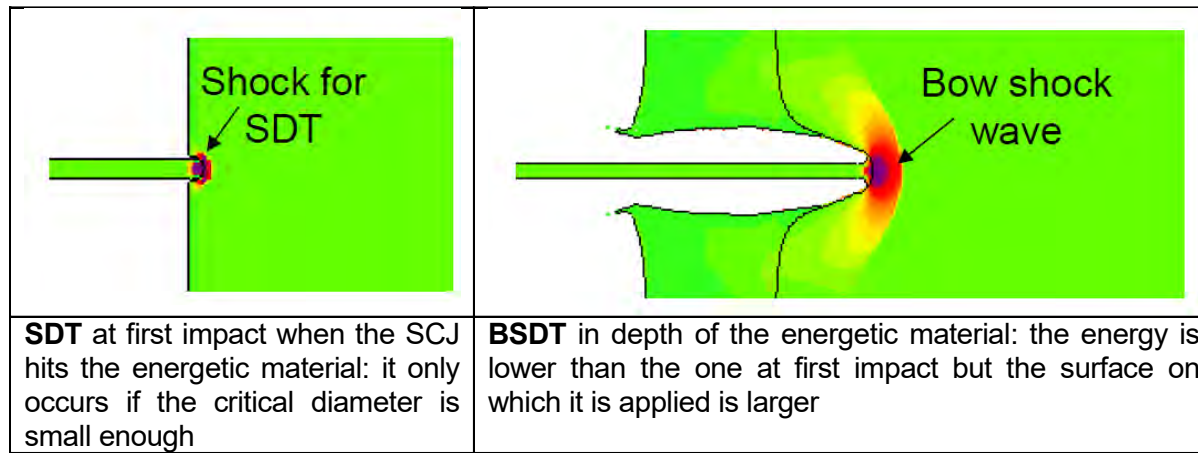
The scenario for Shock to Detonation Transition in an SRM impacted by a mechanical stimulus is the following one:

1. The high velocity impact induces a shock wave in the propellant
2. The propellant will detonate if and only if the 2 following conditions are met:
 - the **energy flux is greater than the energy threshold for ignition**. That is to say, the pressure level has to be higher than the initiation pressure and it must be applied over a sufficient duration
 - the above condition must be **applied on a surface greater than the propellant's critical diameter in detonation**



In the case of extremely high energy impacts such as EFP or shaped charge jet attacks, and depending on the critical diameter of the impacted energetic material, the detonation process may be either:

- **directly initiated** when the jet hits the energetic material → prompt SDT
- or, for larger critical diameters, **initiated at some distance from the first impact**, that is to say in the depth of the energetic material that was impacted → Bow Shock to Detonation Transition or BSDT

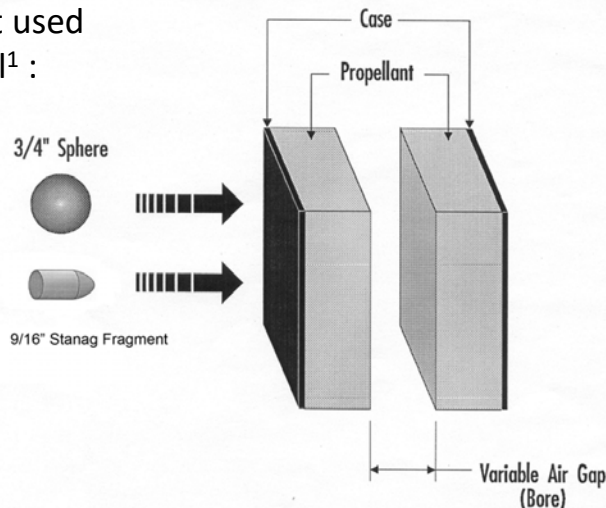


Although extensively studied, these processes remain misunderstood

In the case of SRMs, the Burn to Violent Reaction process may represent the first step of an Unknown (X) to Detonation Transition

Some relevant test set-ups were used in the US and in the UK to study the parameters related to BVR and XDT process:

Open configuration in the BVR test first used by Finnegan et al¹ :



Confined configuration used by Haskins & Cook² :



¹Finnegan, S., The bore effect and XDT, Joint NIMIC/TTCP KTA 4-20 Workshop on Cookoff and XDT Mechanisms, March 1996

²Cook, M.D., Haskins, P.J., Fragment Impact of Energetic Materials – A Review of Experimental Studies and an Analysis of Reaction Mechanisms, 14th International Symposium on Detonation, 2010

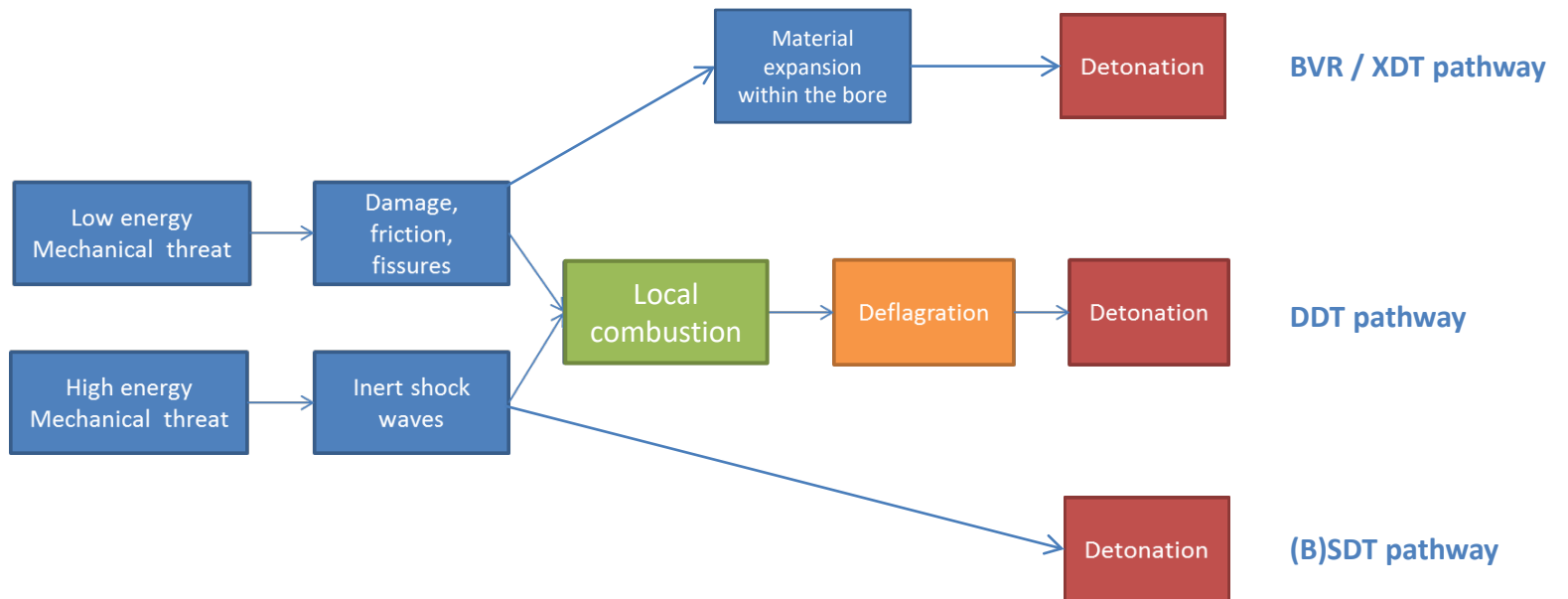
After several years of studies on this subject, and many relevant experiments Haskins & Cook were able to propose the key steps for BVR/XDT mechanisms:

1. A sufficiently fast impact (but below the SDT threshold) to generate rapidly moving damaged energetic material
2. A space into which the material can expand (e.g. the bore of a rocket motor)
3. A secondary surface for the damaged material to impact.
4. SDT of the damaged material following impact. Clearly, this will be dependent on the density and nature of the energetic material and the shock pressure generated on impact
5. Shock initiation (back detonation or “retonation”) of the main charge resulting from the detonation of the damaged material



Cook, M.D., Haskins, P.J., Briggs, R.I., Flower, H., Ottley, Ph., Wood, A.D., Cheese, Ph.J.,
An investigation into the mechanisms responsible for delayed detonations in projectile
impact experiments, International Detonation Symposium on Detonation, 2006

The BVR process would stop somewhere during step 4 of the above mechanism. If the conditions are met to initiate a detonation, then BVR is not appropriate anymore, it would then be called an XDT



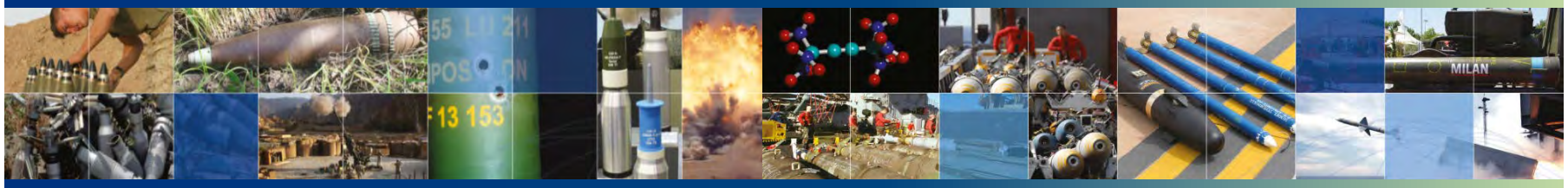
The IM community has been working on different and promising ways to decrease the response level of Solid Rocket Motors (SRMs) under mechanical solicitation

Some relevant examples have been found in the open literature on this subject:

	Examples	Complexity level	Advantages
Change the propellant	Use of low sensitivity composite propellant instead of Double Based propellant	Very high level of complexity, may need to re-qualify the whole system	The most efficient solution to decrease the reaction type under all IM threats
Change the munition design	Use composite or hybrid casings instead of metallic ones	High level of complexity	Very efficient to mitigate mechanical impacts, but also Fast Cookoff
Change the way to store the munitions	Use a bore mitigant, add barriers or deflectors between munitions, head-to-tail arrangements	Low level of complexity	Can be easily adapted to existing storage configurations

- Mechanical stimuli remain a major issue for solid rocket motors to be fully compliant with IM requirements, especially for Double Base propellants
- To improve the IM signature of SRMs, we need to better understand their reaction mechanism. Hopefully this study is of interest in this perspective
- Some promising ways were found to improve the IM signature for SRMs under mechanical impacts, either at the early stages of a future SRM's development, or for already in-service systems
- More details will be found in the upcoming MSIAC limited report on this topic. Coming soon...





MITIGATION TECHNOLOGIES FOR PROPULSION APPLICATIONS

Christelle Collet, Maud Cheneau, Emmanuel Schultz

IMEMTS 2018
Portland, OR, USA



Introduction

1. Passive Venting Devices
2. Active Mitigation Systems
3. Intumescent Coatings
4. Casing Materials
5. Barrier – Packaging – Arrangement

Analysis & Conclusions

General SRMs' IM Signatures agreed by experts during the MSIAC workshop on IM Technology Gaps* :

Rocket Motor Type	IM Signature					
	FCO	SCO	BI	FI	SR	SCJ
Reduced Smoke /Smokey	IV	I-IV	IV	IV	Pass	III
Min Smoke	IV	I-IV	I-IV	I	I-III	I

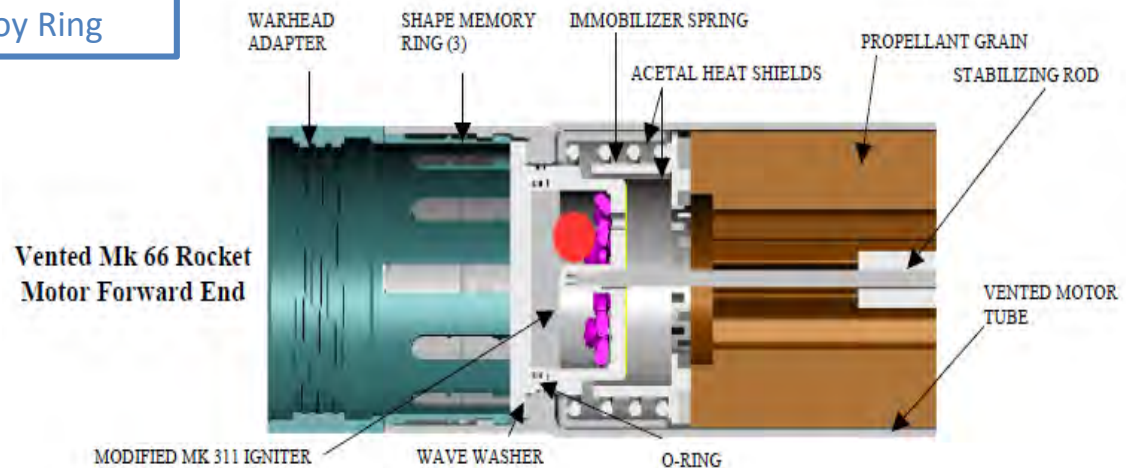
In 2016, in the frame of an MSIAC internship project, a review was done on mitigation technologies applied to SRMs

53 examples of mitigation techniques / examples / strategies were found during this study:

1. Passive venting devices: 8 examples
2. Active mitigation systems: 16 examples
3. Intumescent coatings: 15 examples
4. Casing materials: 8 examples
5. Packaging – Barrier – Arrangement: 6 examples

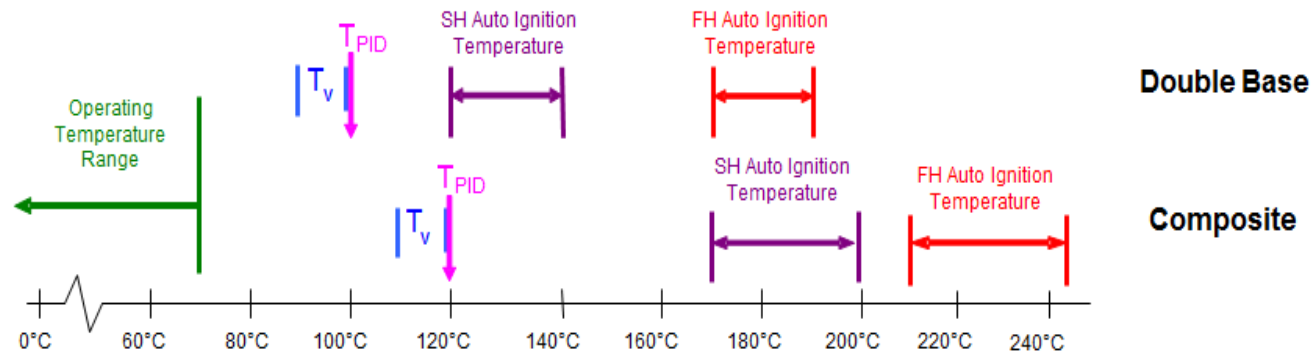
*Sharp, M.W., MSIAC IM Technology Gaps Workshop
 – Output from the Rocket Motor Technology
 Discussion Group, MSIAC Report L-183, January 2014

- Venting devices are designed to release the pressure in the casing created by an unexpected combustion before it transits into a more hazardous regime (in case of DDT for instance)
- Passive venting devices are mostly designed against FCO and SCO threats
- Example of a shape memory alloy ring for the MK66 motor: upon heating, the ring contracts, squeezing the tang fingers inward, and releasing the adapter

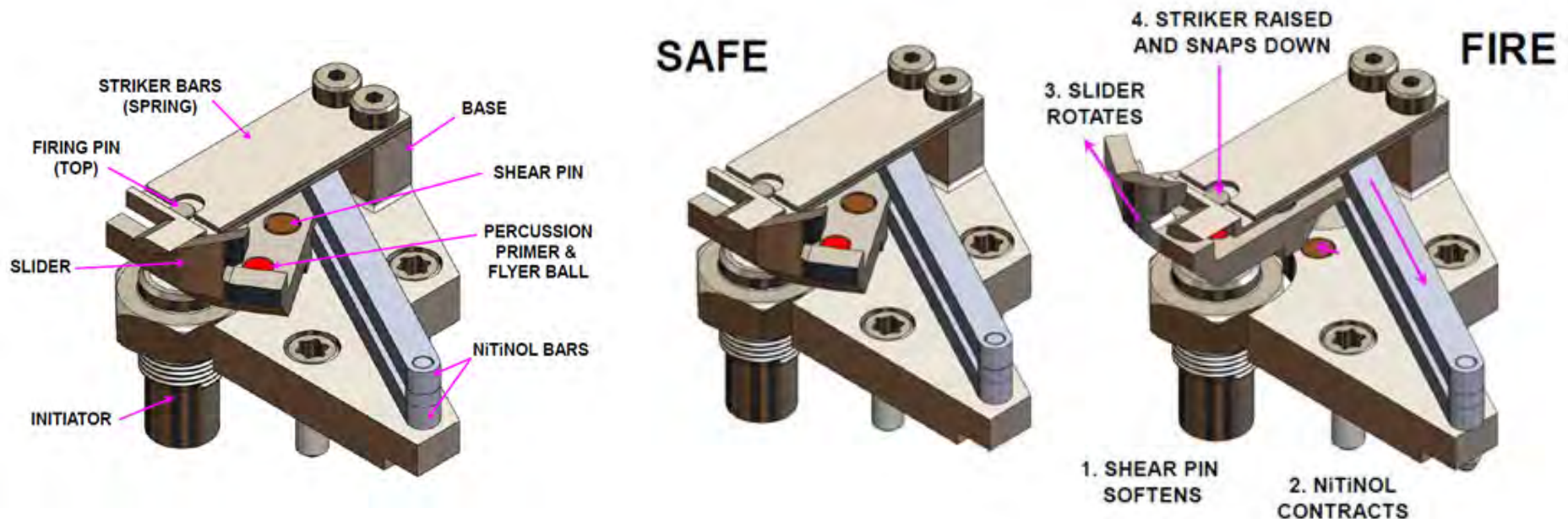


Functioning principle:

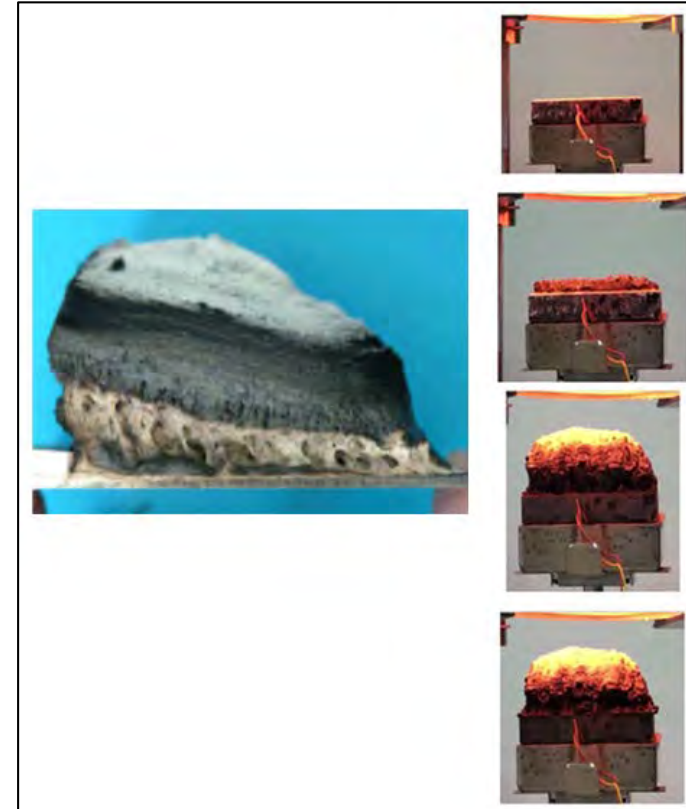
- 1) Temperature raises rapidly around the munition (FCO) or uniformly within the munition (SCO)
- 2) A venting device reacts, resulting in a rupture of the case
- 3) **Before** reaching its slow heating auto ignition temperature, **but after** the venting device has functioned, the propellant is ignited by a Pre-Ignition Device (PID)
- 4) The gases are evacuated through the vent, resulting in a controlled and low burning rate



A relevant example in this family: the RITA system designed for the MK22 rocket motor



- Intumescent coatings are materials that swell (i.e. intumesce) when subjected to heat, such as from a fire
- They expand to several times their original thickness, forming a foam-like insulating barrier with reduced thermal conductivity thus reducing the heat transfer rate
- Intumescent coatings are designed against FCO threats



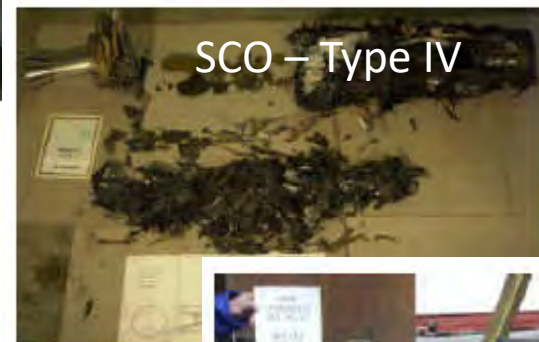
- Although intumescent coatings delay munitions' reaction, they generally do not make this reaction less violent!

→ used in association with other mitigation devices/strategies (e.g. apply intumescent coating everywhere except on one strip – bare strip - along the axis)

Results on MAGIC 1 for different coating configurations*

Outer thermal Insulation thickness (mm)	Outer thermal insulation weight (kg)	Bare strip width (mm)	Initial temperature (°C)	Reaction (Type)	Time before reaction (s)
0	0	0	15	III	100
0	0	0	40	IV - III	90
0	0	0	70	IV	60

- Composite and hybrid (composite & metal) casings have been progressively replacing metal casings to save weight in the munition system
- Their good ability in mitigating mechanical and thermal threats make them good candidates for IM



IM Tests on the ESSM Motor featuring a carbon fiber reinforced composite material*

Steel Strip Laminate: an association of steel strips and adhesive resin

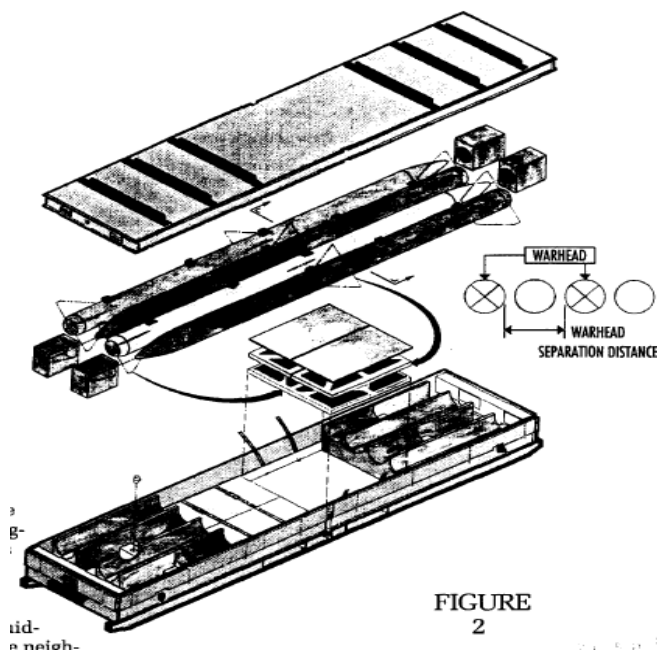


*Tenden, S., Fossumstuen, K., IM Improvement of Rocket Motor by Composite Case, Nammo Raufoss. Presented at the NATO RTO Applied Vehicle Technology (AVT) Panel Meeting in Aalborg, Denmark, September 2002

- These mitigation technologies are especially designed against mechanical threats that may occur during storage or transportation

Head to tail arrangement

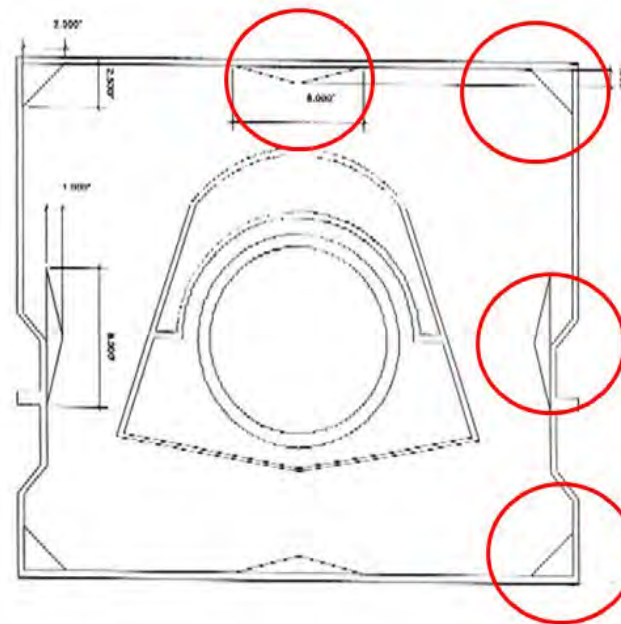
Example below with the AMRAAM container¹



¹Raevis, J., Inensitive Munitions Protection for the AMRAAM Missile Container, 1993

Diverter

Example below with the JASSM shipping container²



²Lobdell S.K., SMERF code analysis to examine the effect of diverters to prevent Sympathetic Reaction into JASSM shipping containers, IMEMTS, 1998

Even if no SRM featuring a bore mitigant has been yet qualified for in-service systems, this is considered as a promising technology against BI or FI threats. Indeed, this technology may prevent Burn to Violent Reaction transitions in SRMs.

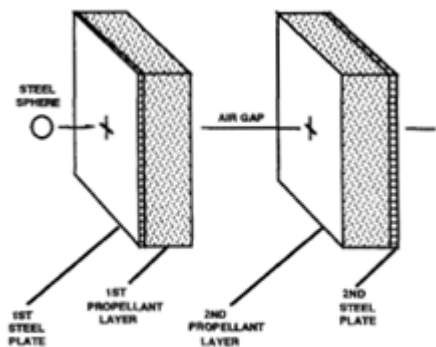
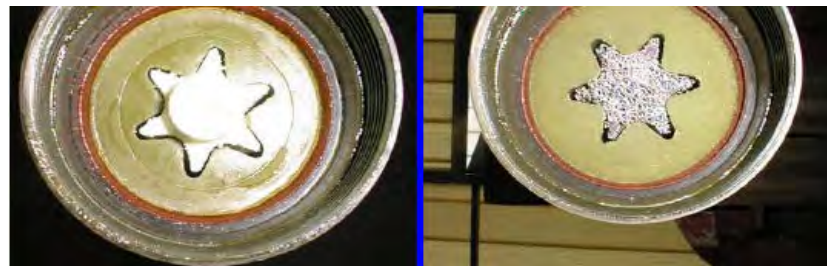


FIG. 1. Planar Rocket Motor Test Model.

TABLE II. Planar Model Test Results.

Test No.	Propellant	Air Gap Width, in	Material	Impact Vel., ft/s	Reaction
1	HEP-2	1.5	Air	3,970	detonation upon debris bubble impact
2	HEP-2	0.75	Foam	4,301	no reaction
3	HEP-2	1.5	Foam	4,121	no reaction
4	HEP-2	2.25	Foam	4,173	no reaction
5	HEP-2	1.5	Foam	3,084	no reaction
6	XLDB	1.5	Air	3,780	detonation upon debris bubble impact
7	XLDB	1.5	Foam	3,980	no reaction



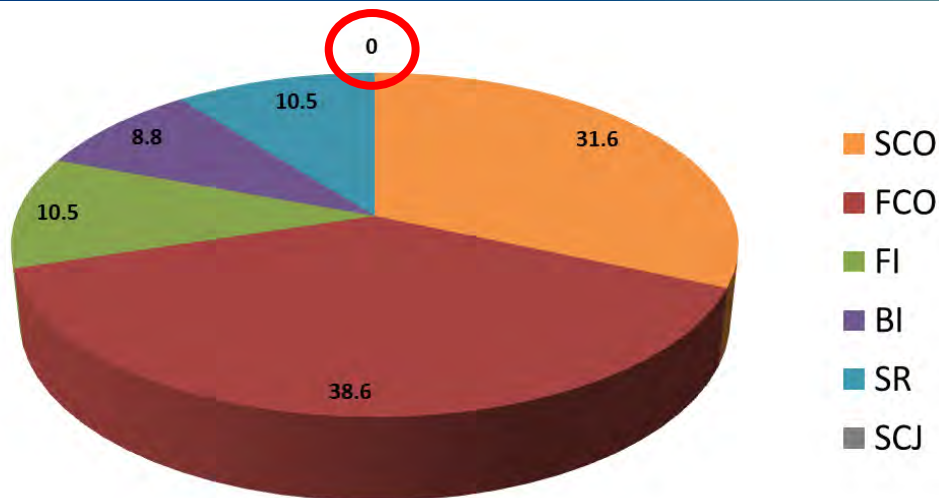
LSRM Response to Bullet impact (STANAG 4241 ; 12.7mm P, 850m/s)

Test label	Metal fragments	Blast overpressure		Response Type
		at 10 m (hPa)	at 15 m (hPa)	
Reference	3 fragments up to 50 m	28		IV
Reference with igniter	5 fragments up to 45 m	33	19	IV
Hybride case	6 fragments up to 10 m		13	IV
Weakened case	10 fragments up to 65 m	26		IV
Reference & Aluminium foam	6 fragments up to 12 m	27	20	IV
Reference & PEI Foam	5 fragments up to 7 m	23	12	V
	2 fragments on place	22	11	V

Finnegan, S, DeMay, S., Pringle, J., Heimdahl, O., Dimaranan, L., Smith, A., Use of Polymeric Foam Inserts for Mitigation of Impact-Induced Reactions in Solid Rocket Motors with A Center-Perforated Grain Design, 1994

The advantages and drawbacks for the 5 mitigation families found during this review are gathered here below

IM Family	Threats	Advantages	Drawbacks
Passive Venting Devices	FCO, SCO, BI, FI	Possibility to set the operating temperature	Useless against SCO if used alone Reliability level could be increased
Active Mitigation	FCO, SCO	Possibility to set the operating temperature	Use of EM adds safety issues Generally requires a combination of mitigation technologies
Intumescent coating	FCO	Ease of implementation Low cost	Requires surface pre-treatment Poor robustness Increased weight and diameter
Casing materials	FCO, BI, FI, (SR)	No additional part	Specific design of the case Relative high cost Not applicable for all types of missiles Not likely to respond under SCO
Packaging Barrier Arrangement	BI, FI, SR	Retrofittable for an existing munition	Requires a combination of IM technologies Increased weight and volume of packaged munitions

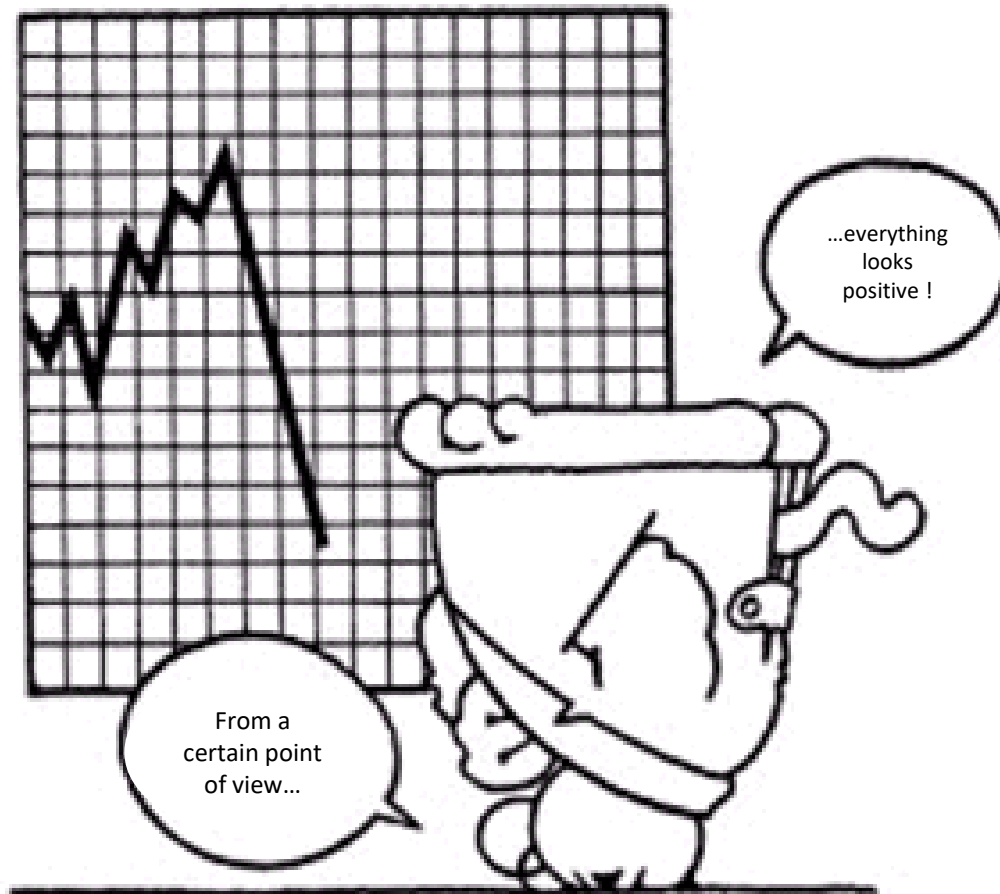


→ About 70 % of the existing mitigation technologies for SRMs are designed against thermal threats (FCO and/or SCO) although the impact threats (BI, FI, SR and SCJ) are considered as a critical issue for rocket motors, especially in the case of minimum smoke ones:

Rocket Motor Type	IM Signature					
	FCO	SCO	BI	FI	SR	SCJ
Reduced Smoke /Smokey	IV	I-IV	IV	IV	Pass	III
Min Smoke	IV	I-IV	I-IV	I	I-III	I

→ No existing mitigation technique against SCJ threats for SRMs

- Promising ways are existing to reduce or prevent high reaction levels from Solid Rocket Motors
- The review recently done by MSIAC on this topic revealed a total of 53 mitigation technologies, sorted into 5 families:
 - Passive Venting Devices
 - Active Mitigation Systems
 - Intumescent Coatings
 - Casing Materials
 - Packaging - Barrier - Arrangement
- These mitigation technologies are mostly designed against thermal threats (SCO, FCO) although mechanical threats remain a critical issue for SRMs, especially minimum smoke SRMs
- As a perspective, a summer project will be conducted in 2018 on mitigation technologies for warhead. The outputs from these summer projects will eventually result in an exhaustive and up-to-date online database of mitigation technologies available for the overall munition system. Coming soon in MTM...

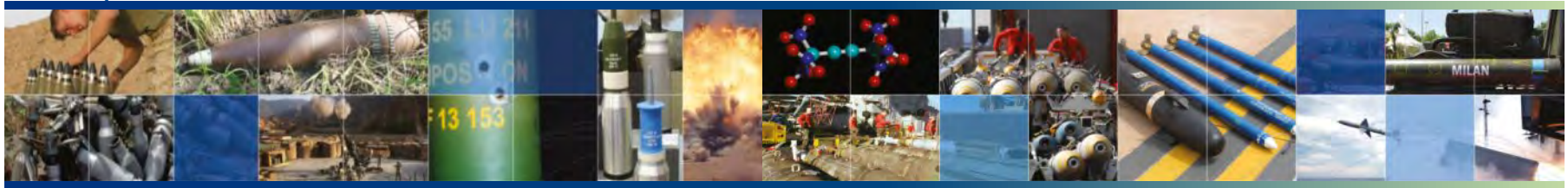




MSIAC

Munitions Safety Information Analysis Center

Supporting Member Nations in the Enhancement of their Munitions Life Cycle Safety



Property-Processing Implications in Additive Manufactured Materials for Munitions An MSIAC Limited Report

Wade Babcock

Materials Science Technical
Specialist

+32 2 707 56 36

w.babcock@msiac.nato.int

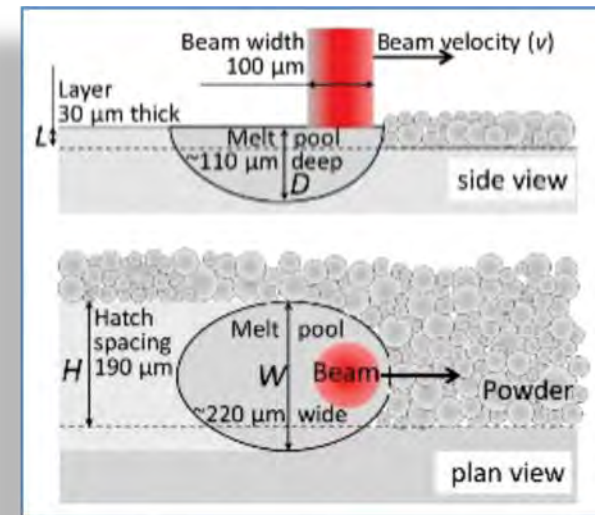




- A 2017/18 Work Element:
 - Novel Material Flaws & Processing/Property Implications of Additive Manufacturing (AM) for Energetics
- AM is being applied in energetics / munitions
- Unique processing creates novel flaws and failure modes
 - Heating, melting, re-melting, powder deposition, incomplete melting, extrusion/flow, curing, etc.
- Material selection in AM is still nascent
 - Availability, melting, processing

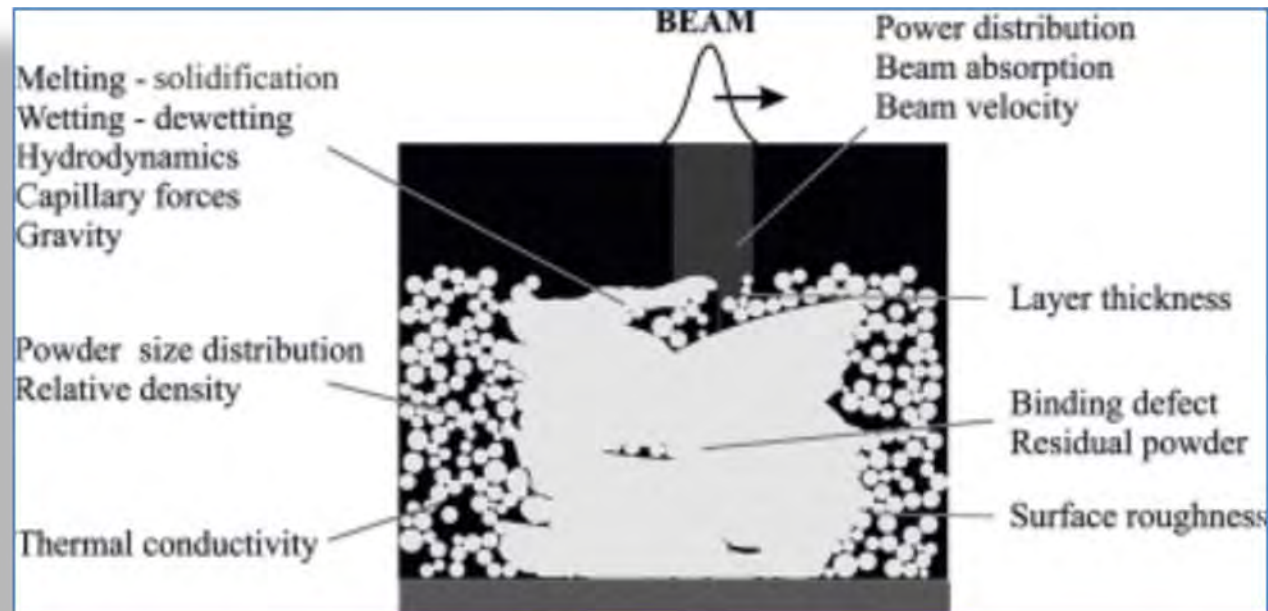
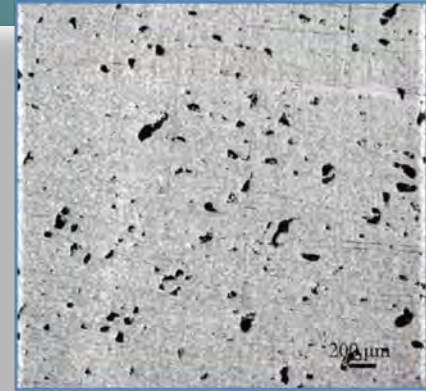
- Process rigidity has been a hallmark of energetics processing
 - Safety, repeatability: driving forces
 - Once a process is qualified, adhere to it!
- Flexibility is the primary virtue of AM
 - Ability to fabricate virtually any part
 - Variability from one part to the next
 - Compositional variation within a part...

- Variability at all levels
 - Within one build
 - Location and geometry dependent
 - Between multiple builds
 - Same machine, same settings
 - Same machine, varied settings
 - Different machines, same manufacturer
 - Similar machines, different manufacturers
 - Different users...



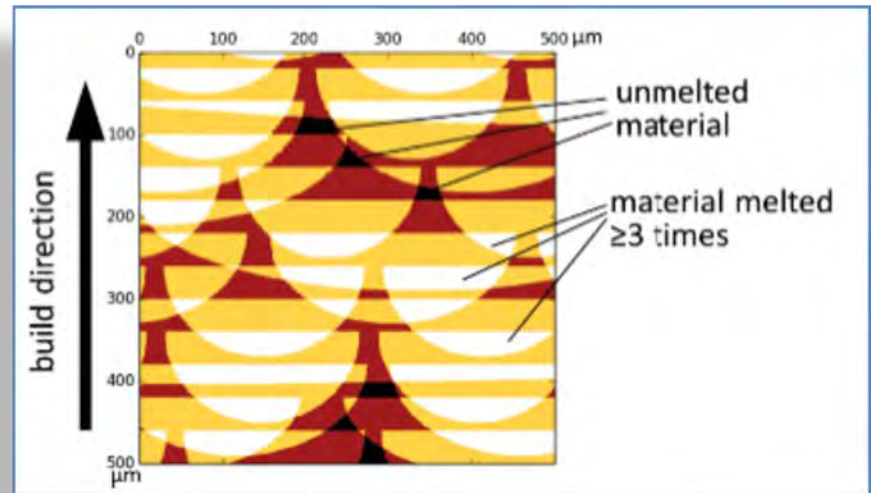
- Novel defects are being discovered
 - New processing methods bring new defects, flaws, failure modes
- Defects vary between processing methods
 - Need to match, catalog, and quantify
- Classical discovery of defects is through failure
 - Modern society seems to have a lower threshold for technical failure

- Porosity
- Voids
- Layer / Cross-layer Defects
- Under-melted / Under-consolidated
- Cracking
- Surface Finish



“Defect Generation and Propagation Mechanism During Additive manufacturing by Selective Beam Melting.”
 Bauereiss, A., Scharowsky, T., & Korner, C., Journal of Materials Processing Technology Vol. 214 Iss. 11 (2014)

- Processing, structure, properties, & performance are intimately linked
- Classical understanding arrived at through decades, centuries of experimentation
- Nascent AM techniques are not well-understood with respect to PSPP



- Fabricating replacement parts
 - Classical parts are qualified via statistical analysis, process controls, inspection
- AM Characteristics
 - Continually variable, local processing
 - Raw materials intended for radically different processing methods
 - Flexibility is a disadvantage – unconstrained process
 - Ability to create difficult-to-inspect geometries
 - Fab process may introduce heating and reheating
 - As-yet-difficult to establish post processing treatments

- Airframe manufacturers
 - Certify AM techniques to fabricate air-worthy parts
 - Constrained in high-risk, low-margin for error
 - Certification classically based on statistical analysis, process controls, inspections
 - ~10-year head-start
- Medical devices
 - Novel shapes, materials, surface finishes
 - Constrained in materials, life-cycle
 - Incredibly complex certification process
 - ~15 year head-start

- AM presents unique opportunities in the munitions design and fabrication space
- Many groups are working to implement AM in munition items
 - Some have created working parts and sub-systems
 - Complete munition items ...
- New processing technologies are always accompanied by new defects and failure modes
 - Not a show-stopper, just diligent effort and planning
- Other industries may provide good examples of qualification / certification processes applicable to munitions



- Solid rocket propellant grains usually have a hollow “bore”
- Engineering the shape of the bore, controls the thrust profile

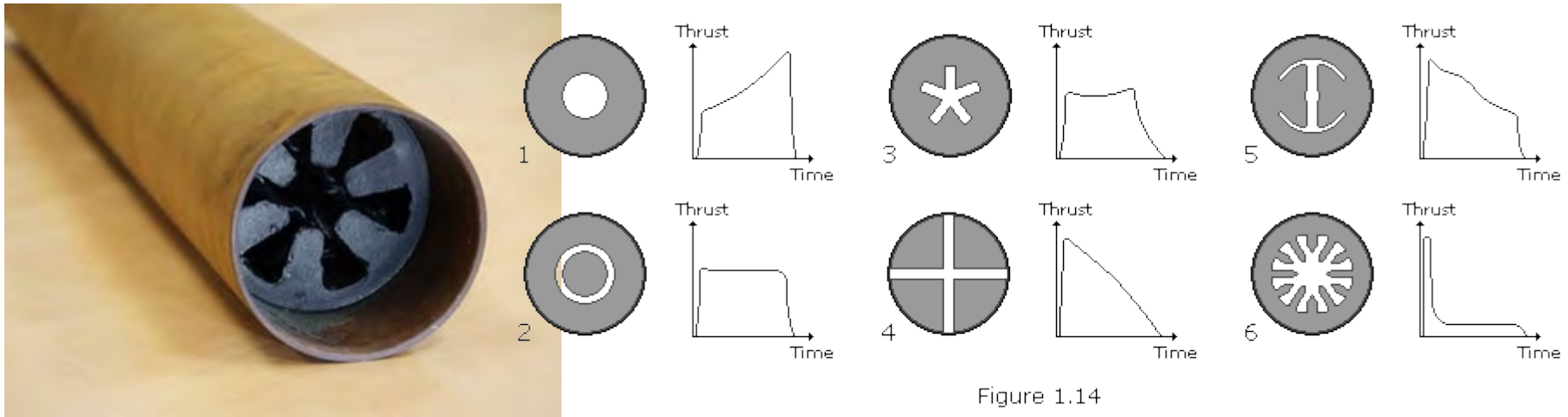
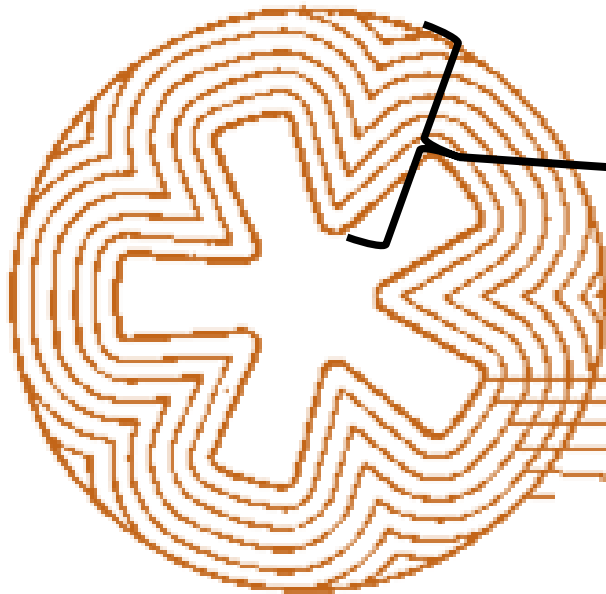


Figure 1.14

- Fabricate multiple materials at once
- Create materials that are difficult / impossible with traditional bulk mixing
- Alter composition of a material with respect to geometry



Change critical parameters such as burn rate, elasticity, or fracture toughness across grain dimensions.

Enable thrust profile to change not because of geometry, but because the propellant composition is changing as the burn front moves outward.



MSIAC

Munitions Safety Information Analysis Center

Supporting Member Nations in the Enhancement of their Munitions Life Cycle Safety



AGING AND MECHANICAL DAMAGE OF MUNITION MATERIALS

AN MSIAC LIMITED REPORT

Wade Babcock, MT TSO

+32 (0)2 707 5636

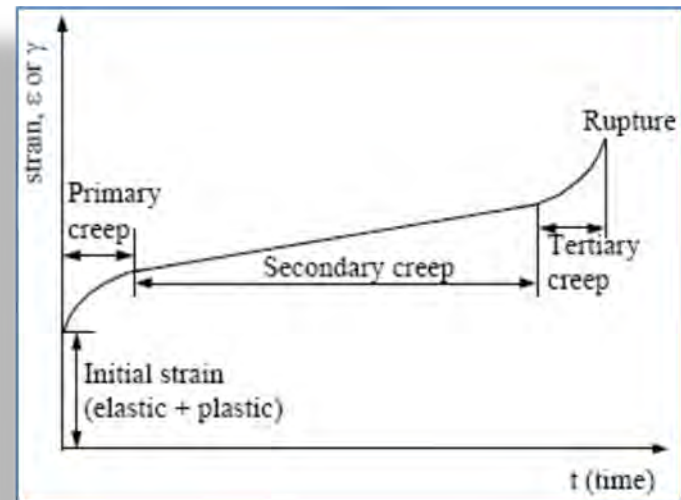
w.babcock@msiac.nato.int





- Two work element objectives:
 - Kno-Und-8 – Age-related Mechanical Damage
 - Mechanisms such as cracking, delamination, fiber breakage, particle/matrix and fiber/matrix debonding, etc.
 - Kno-Met-3 – Effect of Ageing on Materials and Munitions Safety
 - Review of IM and ageing studies, and applicability of latest R&D techniques to evaluate ageing
- Significant overlap of these two topics
 - Currently treating as one topic, with multiple distinct sub-sections

- Alteration of properties caused by exposure to service conditions
 - Sometimes routine, sometimes abnormal
- Aging alters properties gradually, over time
- Other insults may cause degradation suddenly or in “jumps”
- Implication is that aging is detrimental



- Aging → not always detrimental
 - I.e., if stiffness is critical to a component's performance and aging mechanisms cause the material's stiffness to increase over time...
- But, most changes in one property are accompanied by changes in another
 - Increasing stiffness is usually matched with reduced ductility
- The engineering design challenge: select appropriate materials, plan for changes

Multiple subsections based on material classes

Polymers

- Primer
- Organic fluid contamination
- Photo-induced degradation
- Chemical degradation
- Solvolysis
- Ozonolysis
- Oxidation
- Creep, fatigue
- Galvanic action



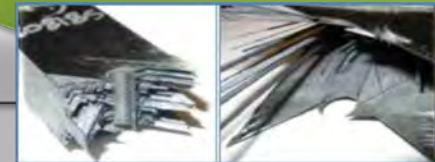
Metals

- Primer
- Environmental stress fracture
- Corrosion
- Fatigue, cyclic loading, vibration
- Irreversible deformation
- Stress-corrosion cracking
- Hydrogen embrittlement
- Hysteretic elastic/plastic deformation
- Galvanic action



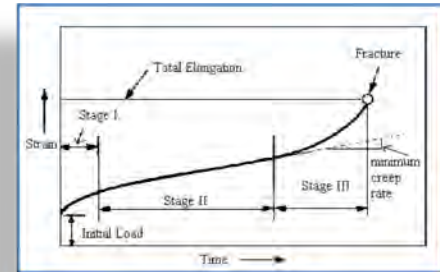
Composites

- Primer
- Constituents (polymer matrix, fiber, particulates, etc)
- Delamination, interlaminar cracks
- Fiber breakage
- Fiber pull-out
- Voids, bubbles
- Incomplete matrix penetration
- Stress concentrations at thickness changes, holes



Additional section on damage mechanisms referencing back to material damage morphologies

(Following structure of Ordnance Board Pillar P123(1) “Scientific Basis for the Whole Life Assessment of Munitions”)



And a few case studies

- Case Studies
 - Case I
 - Case II
 - Case III

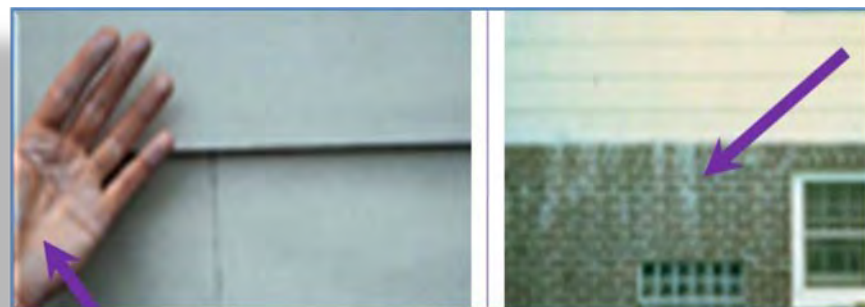
- Munitions Ageing
 - Insults
 - Transport
 - Rough Handling
 - Vibration
 - Climatic Conditions
 - Thermal Changes
 - Electromagnetic Insults

- Three most common uses for polymers in munitions:
 - Structural materials, pure form, with minor additives
 - Examples: brackets, straps, lugs, plugs, seals
 - Matrix for structural composites
 - Example: “(G)FRP” or (glass-)fiber-reinforced-polymer(epoxy)
 - Binders, components, and/or additives within energetics (aggregate composites)
 - Examples: plasticizers, coatings, binders

- Basics of polymer chemistry and nomenclature
- An understanding of chain architecture and interaction
- How bulk properties derive from molecular characteristics
- Common industrial polymers

- 97% of plastics in daily life
 - polyethylene (PE)
 - polypropylene (PP)
 - polyvinyl chloride (PVC)
 - polyethylene terephthalate (PET)
 - polystyrene (PS)
 - polycarbonate (PC)
 - polymethylmethacrylate (PMMA)
 - silicones (polysiloxanes)
- Plus, discussion of polymers typically used in energetics, such as hydroxyl-terminated polybutadiene (HTPB)

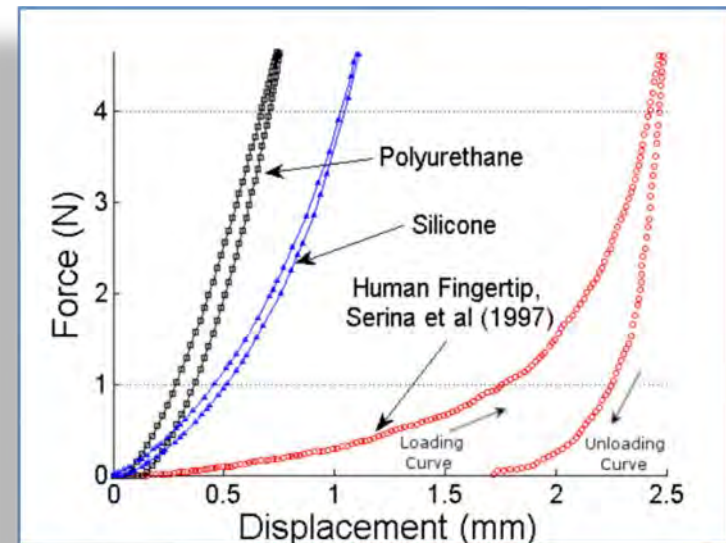
- Engineering properties
 - Strength, ductility, toughness
- Cosmetic / Appearance
 - Color, surface residue (chalking), cracking



- Examples:
 - Random chain scission in polyethylene
 - Specific chain scission in polyalphamethylstyrene

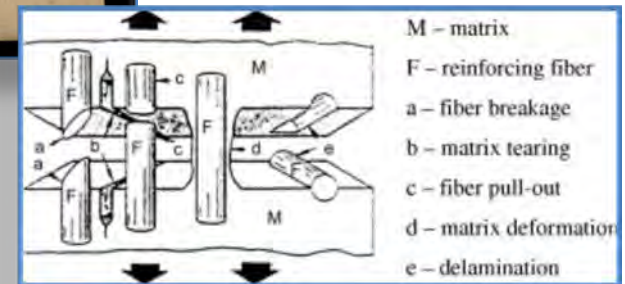
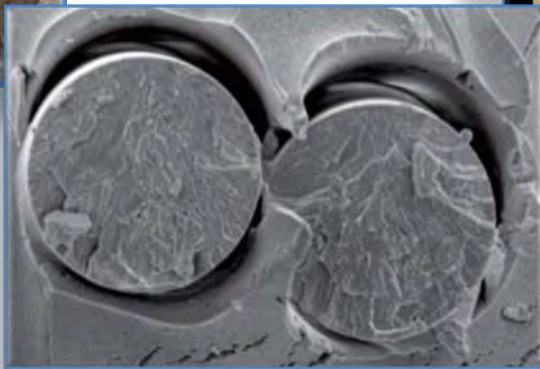
- Liquid-borne
 - Organic fluids
 - Chemical attack
 - Solvation / solvolysis
- Radiant Energy
 - Photo-induced damage
 - Thermally induced
- Gas-phase
 - Gaseous
 - Ozonolysis
 - Oxidation
 - Chlorine cracking

- Mechanically-borne
 - Creep / relaxation
 - Fatigue
 - Hysteretic elasticity reduction



- Swelling, debonding, loss of strength
 - When exposed to organic fluids and other corrosive environments, such as acids and alkali solutions
- Applied stress can accelerate process
- High strength polymers particularly sensitive
 - May become brittle and lose fracture resistance
 - Fracture toughness doesn't change but threshold stress intensity factor for crack propagation may be considerably lowered
 - Become prone to premature fracture because of sub-critical crack growth.

- Presentation here at IMEMTS
 - Includes overview of content and scope
 - Paper provides extract of Polymer section
- Final report published and available this summer



Stopping km/s Blunt Fragments and Limiting Shock Lensing with a New Advanced Energy Absorbing Composite

Gareth R Tear¹, Gianmaria Bullegas¹, Jose Videira¹

¹*Synbiosys Ltd., UK*

gareth@synbiosys.co

Abstract We are developing a lightweight ceramic/polymer composite for km/s fragment resistance. It uses a fundamentally new physical process for energy absorption that complements the conventional forms of energy dissipation of fracture and plastic deformation. This composite comes into its own against very high impact velocities, being able to provide protection in shock regimes where conventional materials like kevlar and steel can be considered incompressible fluids with zero protection capabilities.

This material can be used in rocket motor casings for increased IM compliance. It can absorb and dissipate energy extremely quickly (of the order of 100kJ/m²/μs). Crucially it limits shock lensing effects, augmenting current capabilities against blast and shaped fragments. The energy dissipation mechanism propagates at 7km/s inside the material and activates with minimal (<2%) overall strain of the structure. The design of the composite is flexible enough to be optimised for a range of projectile threats and velocities.

In practical terms, the composite has the same density as aluminium and is made from cheap raw materials. It can also be made transparent, enabling applications beyond rocket motor casings into protective blast windows.

We present here experimental verification of our fundamental energy absorbing process through plate impact experiments, taking measurements by interferometry (PDV) and high-speed videography. We demonstrate that this process does provide a significant (20m/s) decrease in rear surface velocity in plate impact experiments.

Introduction

Shock to Detonation Transition (SDT) is one of the phenomena limiting effective energetic materials for use in dangerous environments. Explosive efficiency, whether measured by weight, impulse or another metric, is sacrificed to achieve the low sensitivity demanded by Insensitive Munition (IM) requirements. Traditionally IM technology has focused on chemically developing explosives and compositions which have low intrinsic sensitivity. In this paper we present a mechanical mechanism for dissipating hot spot formation and attenuating shock fronts directly, allowing more efficient explosive compounds to be used, whilst maintaining the munitions overall IM compliance.

The mechanism has been implemented into a composite form of protection, offering the ability to absorb energy at the shock front, reducing the strain rate on the material behind the composite. It achieves this with less than 2% strain, making it a viable composite for protecting energetic material. The mechanism attenuates energy at the shock front, and can prevent the large transient impulses characteristic of shock waves and particularly dangerous to energetic material.

Vision for the composite technology

The composite has a density of around 2.5g/cm³. The raw materials can be considered abundant and will cost around \$2000 - \$5000 per ton to purchase, and the manufacturing involves traditional composite construction techniques with temperatures not exceeding 200°C.

This rocket motor casing composite will be the first of a family of composites developed by Synbiosys Ltd for impact protection. A transparent version can be made for window applications. High temperature performance of the composite is yet to be tested. Given the upper impact velocity is 7km/s, this composite family could be useful in certain space applications.

Experimental Method

One dimensional plate impact experiments are used to demonstrate the shock front attenuation and to characterise the material. Fragment impact experiments are used to validate the one dimensional behaviour into a more general and realistic loading scenario.

Sample Preparation and Geometry

The sample is manufactured from industrially sourced raw materials. The sample is polished on a lapping wheel to get flat and parallel sides (typically 2 sodium light bands) resulting in samples of around 20 mm to 30 mm in diameter and 5 mm to 15 mm thick. Low viscosity Hysol 9483 epoxy is used to bind the target material with any window or driver layers used on a per experiment basis.

Plate Impact Facility

Plate impact experiments are conducted on the Imperial College London 32 mm bore light gas gun. Using helium, velocities of up to 800 m/s have been achieved. The sample is mounted in a ThorLabs 3 inch optical mount, and aligned normal to the barrel. The alignment procedure is:

1. Align a laser diode coaxial to the barrel using an iris.
2. Align the target mount to be concentric with the barrel using a 3 inch iris mounted in the target holder.
3. Align the target mount to be normal to the barrel using a 3 inch planer mirror.

The sample is mounted to a three inch cast PMMA disk. This PMMA sample holder is verified to be flat over 75 mm to within 2 light bands using a sodium lamp. It is assumed that the sample holder is flat, so that the aligned target mount places the sample in the correct orientation.

The plate impact facility has a four channel fibre based generation one Photonic Doppler Velocimetry (PDV) system operating at 1550 nm (Strand 2006). Each channel has a dedicated laser diode. A 250 mm working distance probe with a 5 mm aperture and an achromatic doublet lens with -60dB back reflectance is used to launch the laser light into free space. The free space portion shown in figure 1 uses a projecting lens to focus the PDV onto the target and alignment mirrors to align the laser.

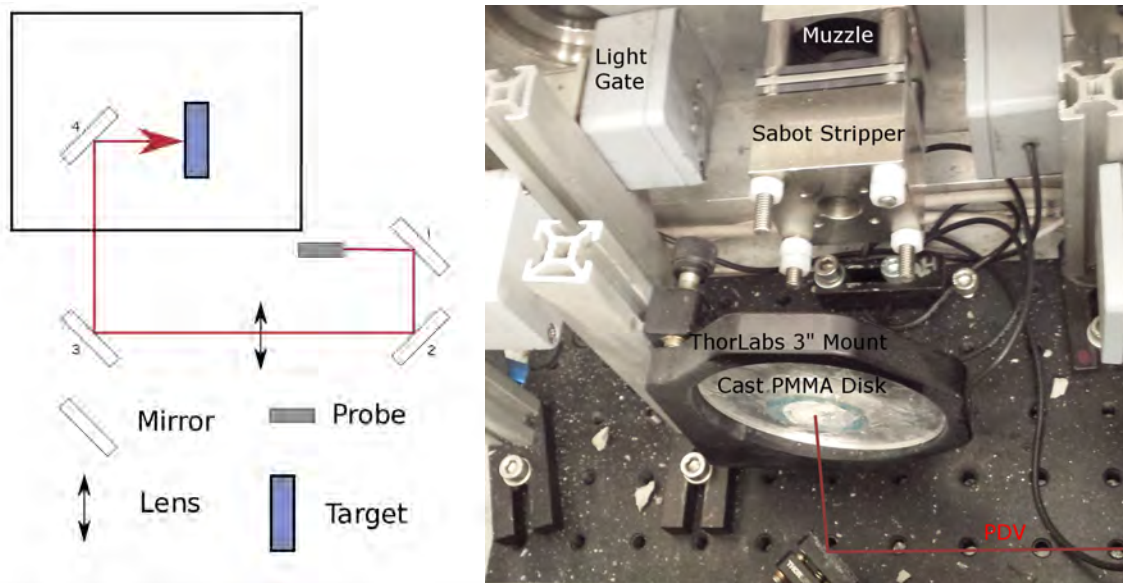


Figure 1 (Left): The PDV relay allows mirrors 1 and 2 to be used to align the beam along the axis of the lens. The lens is on a linear translation stage, allowing the lens to be moved along the beam path, changing the focal plane of the system for each new target. The mirrors 3 and 4 align the PDV onto the target. The barrel alignment laser is used to align the PDV with the centre of the target. Mirror 4 is sacrificial and must be replaced each experiment.

Figure 2 (Right): Target chamber of 32mm gas gun set up for fragment launch. To conduct plate impact experiments, the sabot stripper is removed from the muzzle.

Fragment Simulating Projectile (FSP) Impacts

FSPs conforming in geometry to STANAG 4496 are launched using the same 32 mm facility, however the sabot is stopped by a stripper plate attached to the muzzle. This stops the sabot whilst allowing the smaller fragment to pass. Velocity losses from the sabot speed to the fragment speed are minimal (typical less than 5 m/s). The stripper plate uses a sandwiched polycarbonate and aluminium structure to absorb energy, with a steel momentum trap as the last block. M6 studding is used to mount the blocks, and nylon nuts are used to hold the structure in place. Multiple sets of nuts are used, with clear space in-between, to ensure safe energy deposition into the target tank. A full description of the fragment launch capability is described in (Nguyen 2017, 2018). Figure 2 shows the target tank setup for fragment impact.

Results

Several impact experiments have been performed on plate impact and fragment impact scenarios. The results are separated into plate impact results, demonstrating the transient release phenomena, and fragment impact results demonstrating the capability.

Plate Impact

PDV data from the plate impact experiments shows a marked reduction in rear surface velocity when the transient release phenomena occurs. The plate impact experiments are used to determine the wave speed of this phenomena, and the optimal parameters of operation. The PDV spectrograms from two plate impact experiments demonstrating the reduction in velocity are shown in figure 3. A three point parabolic fit is used to determine the spectrogram peak, and the extracted velocity is shown in figure 4.

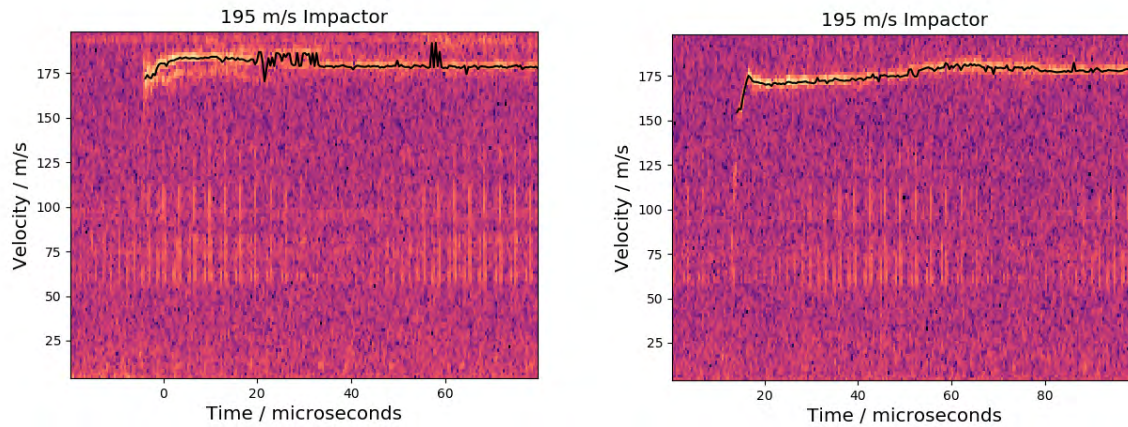


Figure 3: *Left* flyer impact at 195 m/s, demonstrating limited energy absorbing behaviour. The resulting shock peak is 185 m/s. *Right* improved energy absorption activated using a flyer impact at 195 m/s, showing an attenuation and ramping of the initial shock to 175 m/s peak, and the average absorbed impulse is $20\text{kJ/m}^2/\text{microsecond}$.

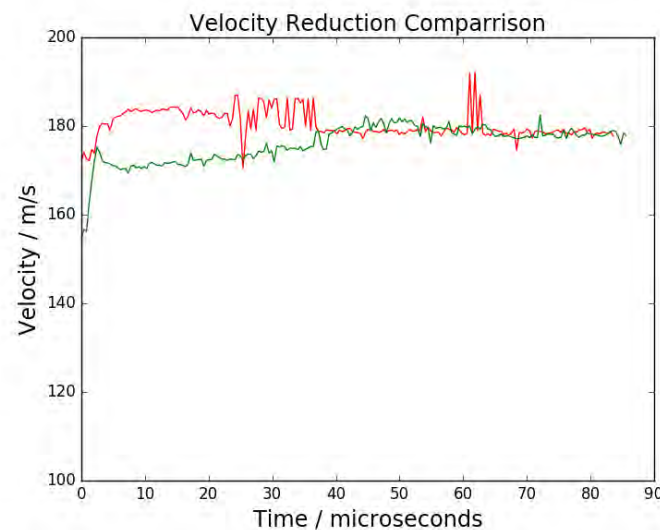


Figure 4: Extracted velocity curve from PDV, making the velocity reduction explicit. Note that the final velocity is the same, as these experiments are momentum equivalent. This ensures that, for an identical impulse, less energy is transferred (energy is dissipated by the release phenomena).

Using the reduction in velocity, an estimate of the energy absorbed, or effective toughness of the material, can be found. Using the pressure calculated from the Rankine-Hugoniot conditions, approximately $700 \pm 100 \text{kJ/m}^2$ has been absorbed in this 20 mm thick plate. Taking into account the timeframe of energy absorption over 35 microseconds, the energy absorption rate (or power) is $20\text{kJ/m}^2/\text{microsecond}$, or 20% of theoretical maximum.

Fragment Impact

A 430 m/s FSP was stopped using a 16mm thick non-optimised composite structure in figure 5, and an equivalent comparison carried out on toughened glass in figure 6. The FSP residual ricochet velocity was 20 m/s compared to toughened glass's 45 m/s. Glass was used in this instance as the composite can be made transparent, and comparison with transparent materials was desired.

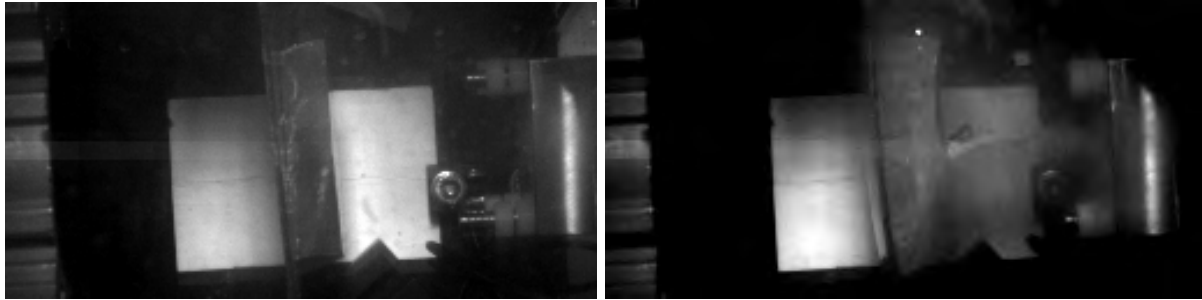


Figure 5: *Left* Energy absorbing composite target before impact. *Right* Target immediately after impact, with projectile bouncing off the surface at 20 m/s.



Figure 6: *Left* Typical toughened glass laminate target before impact, projectile approaching from right hand side. *Right* Target after impact, fracture to glass evident and fragment has ricocheted at 45 m/s.

Discussion

The present results demonstrate an ability to absorb energy at the shock front in one dimensional loading. This attenuation occurs from a transient release of the composite, preventing the high amplitude shock loading of the rear surface. Materials (e.g. energetic materials) bonded to the rear surface experience lower strain rates and so the impact velocity required to initiate an SDT event is increased. This allows more energetic materials to be used whilst maintaining IM compliance.

Three dimensional effects have yet to be fully characterised. In order to achieve this, multiple PDV channels are being deployed on future experiments, combined with rear surface imaging, to measure the effectiveness of this technique against converging shock geometries. As the attenuation of the shock front reduces its velocity as well as its pressure, regions of a converging shock front can be selectively slowed, to prevent the shockwaves reaching a focus.

There are two directions in which this technology can be developed.

Protective casings

As eluded to already, the development of a composite casing which attenuates shock waves is the primary focus. By preventing the initial shock being transmitted to the propellant, the IM threshold of the overall munition can be increased. This does not intrinsically lower the IM compliance of the energetic material, but as evidenced in the XDT phenomena, geometric and casing effects are an integral part of a munitions IM compliance testing.

Binder Additive

As the propellant is a composite, it is plausible to form an energetic composite that is resistant to SDT events. As the material is compressed, local hot spots are prevented by the rapid transient release phenomena, dissipating the build up of pressure in the hot spot. As the location of transient release can be engineered, an energetic structure can be designed with reduced sensitivity to anything except the designated detonator.

Conclusions

- One dimensional plate impact experiments demonstrate ability to directly absorb energy at the shock front.
- Initial low velocity fragment testing comparable to equivalent industry standard materials.
- Further development for high velocity fragments and three dimensional geometries is underway.

Synbiosys

Synbiosys is a materials innovation startup formed of alumni from Imperial College London. The company's expertise revolves around composites engineering, optical and solid state physics and shock physics. The advisors have a long history in working in academia, industry and government.

Organisations in which company members have been previously involved with are QinetiQ, Thales, AWE, the UK MoD (Department for Transport), the US DoD (DARPA and DTRA) and Imperial College's Institute for Shock Physics and Institute for Security Science and Technology.

Synbiosys as an entity has already a track record, having successfully delivered a project on time and on budget for DSTL for a different technology stream.

References

Strand, O. T., Goosman, D. R., Martinez, C., Whitworth, T. L., & Kuhlow, W. W. (2006). Compact system for high-speed velocimetry using heterodyne techniques. *Review of Scientific Instruments*, 77(8), 83108. <http://doi.org/10.1063/1.2336749>

Nguyen, T-T, Carpanen, D., Tear, G., Stinner, D., Clasper, J., Proud, W. & Masouros, S. (2018). Fragment Penetrating Injury to the Tibia. *Accepted*

Nguyen, T-T, Masouros, S., Tear, G. & Proud, W. (2017). Investigation of Ballistic Penetration through Tibia Soft Tissue Simulant. *20th Annual Conference on The Shock Compression of Condensed Matter (Accepted)*



Stopping km/s Blunt Fragments and Limiting Shock Lensing with a New Advanced Energy Absorbing Composite

Gareth R Tear, Gianmaria Bullegas, Jose Videira

Synbiosys Ltd.

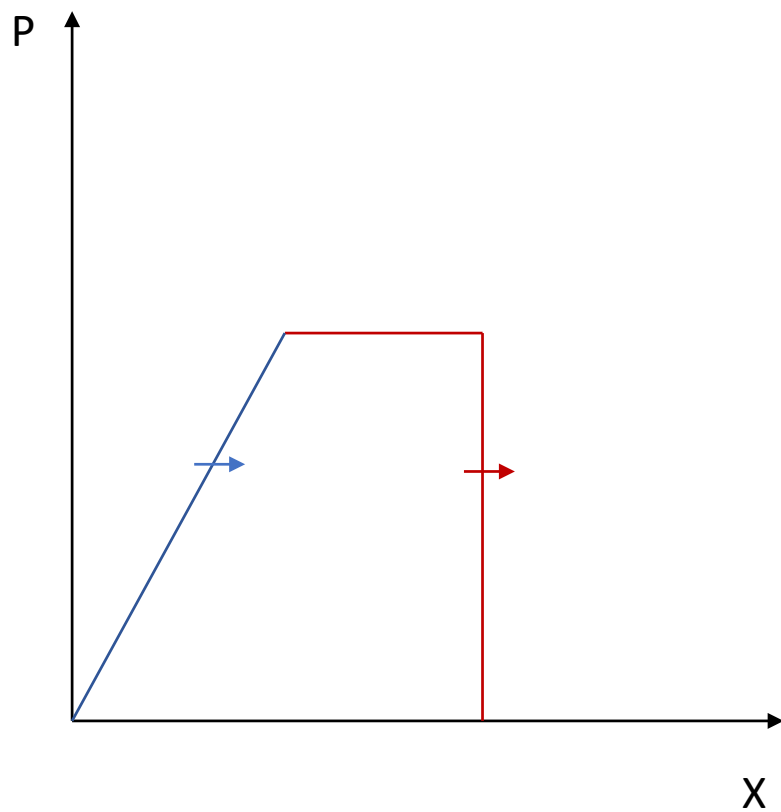
Overview

- Munition initiation usually occurs through hot spot formation during compression
- Currently two broad approaches to reduce hotspot initiation
 - Alter the chemical behavior of the explosive to reduce its sensitivity
 - Alter microstructure of the binder to reduce hotspot intensity
- We are presenting a new process to avoid hotspot formation

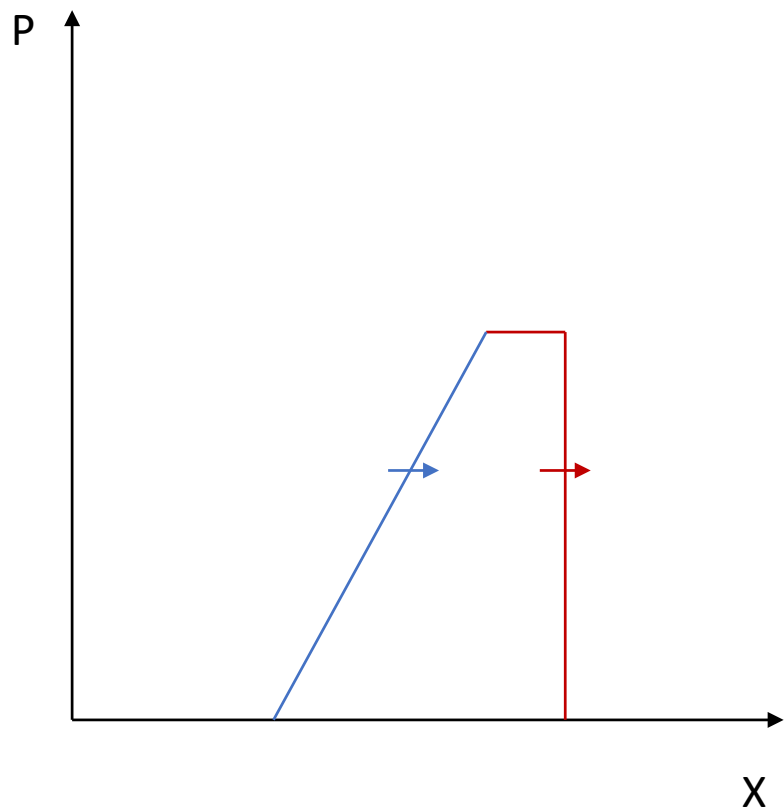
What is the process?

- Shock waves propagate very high transient pressures and temperatures very quickly.
- We need an equally fast energy dissipation mechanism to prevent the initial shock reaching the energetic material.
 - Plastic deformation and fracture aren't fast enough
- A new transient release phenomena has been proposed which allows the material to partially release at the shock front.

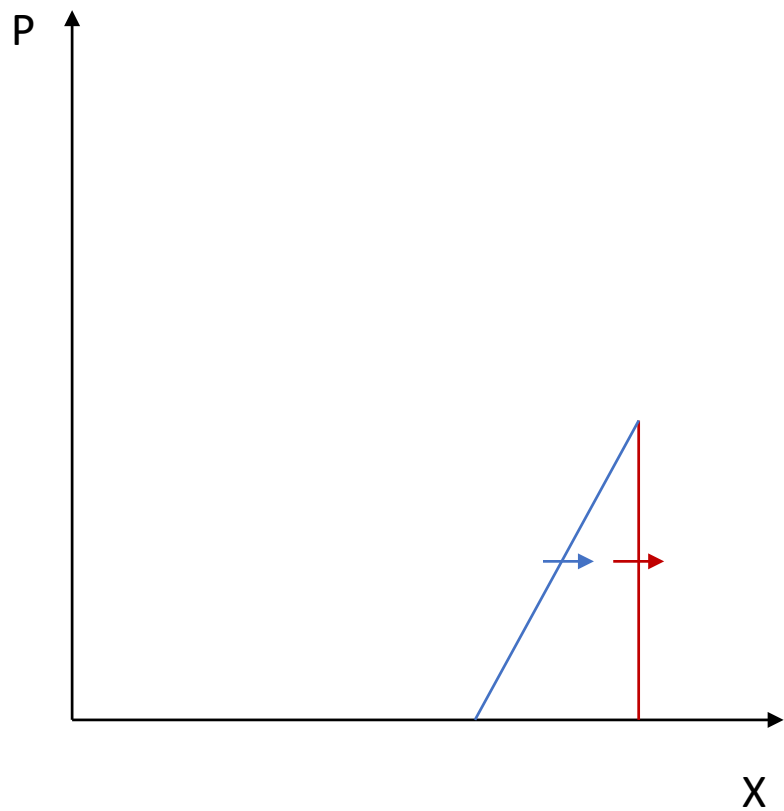
Typical Shock – Rarefaction Profile



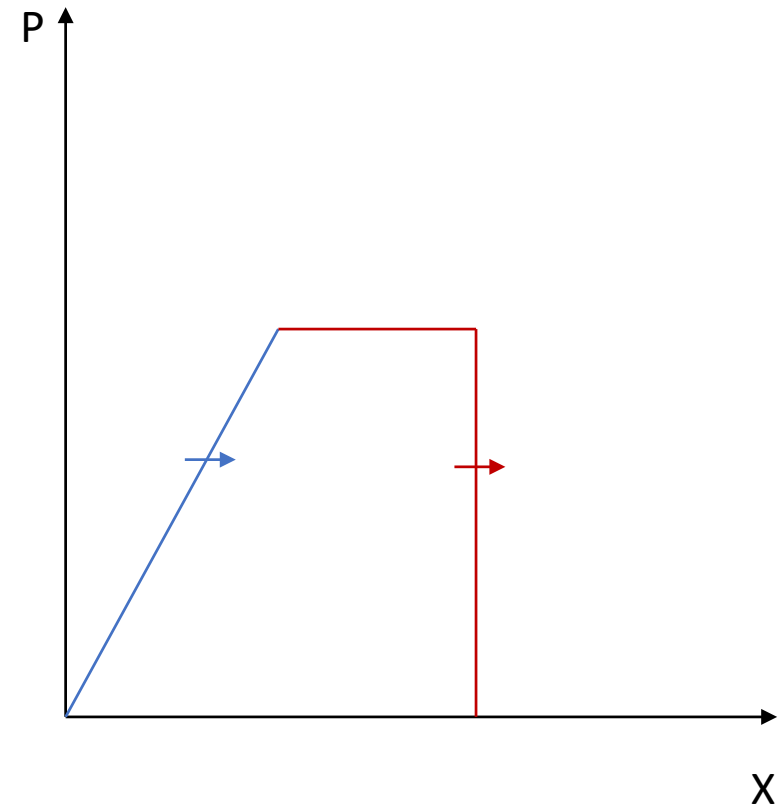
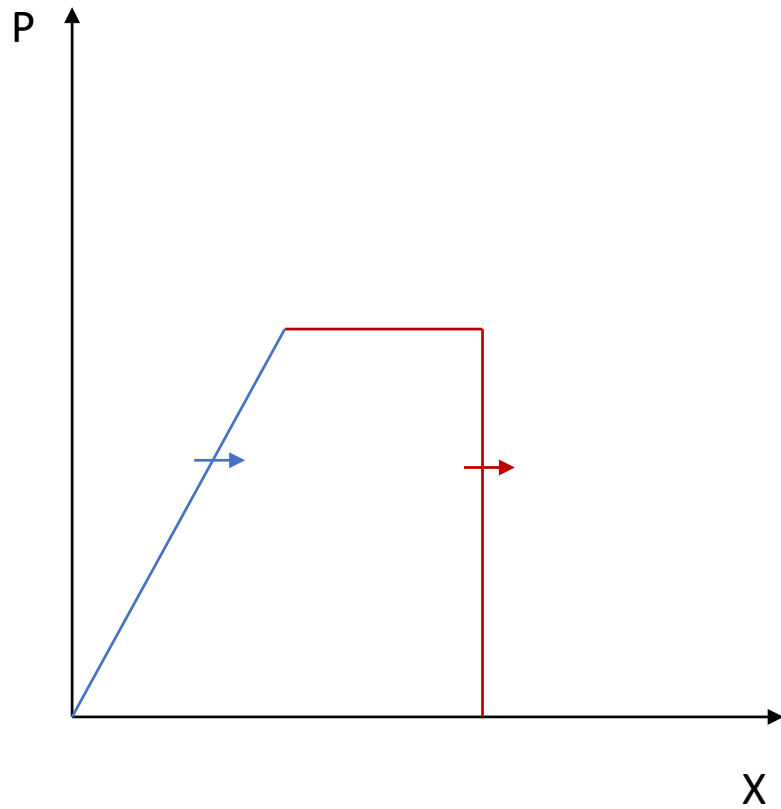
Typical Shock – Rarefaction Profile



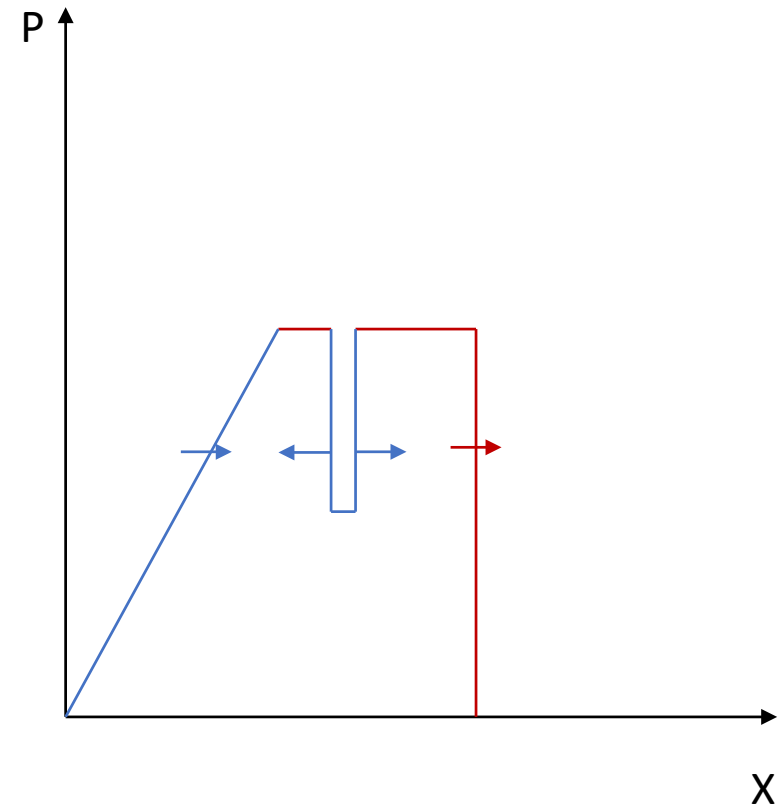
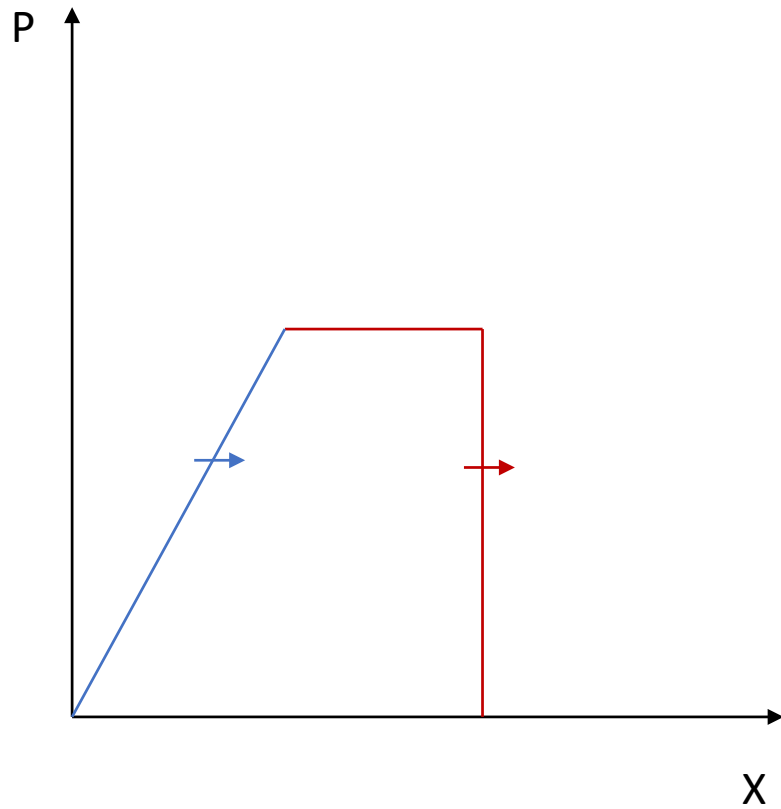
Typical Shock – Rarefaction Profile



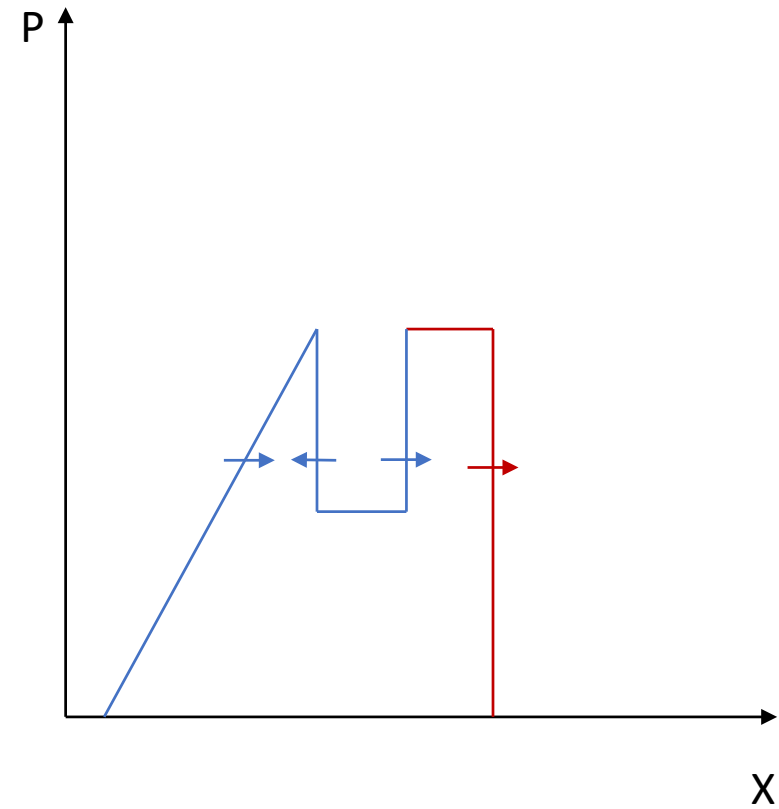
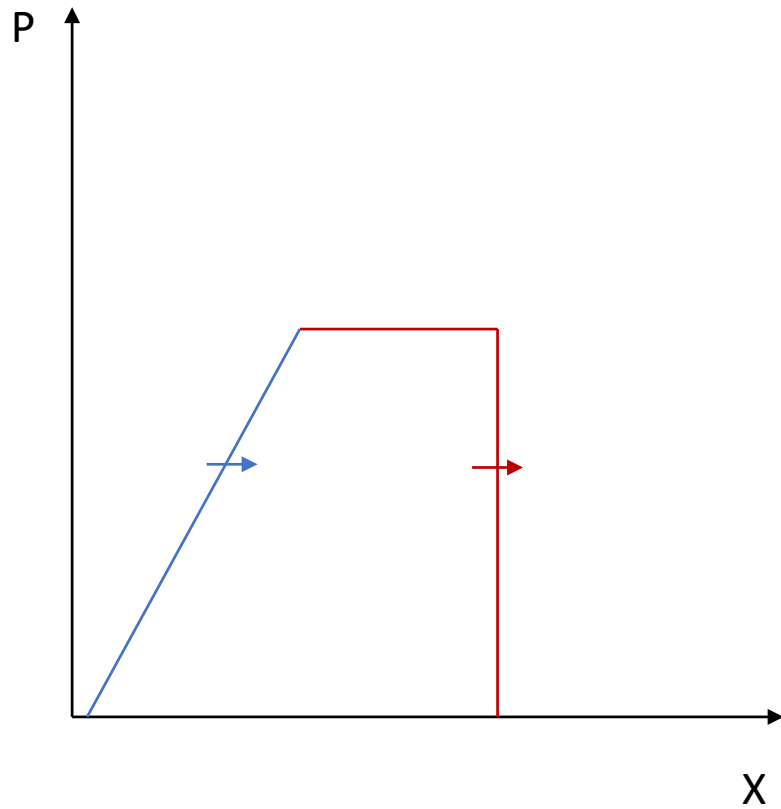
Including Transient Shock Release Phenomena



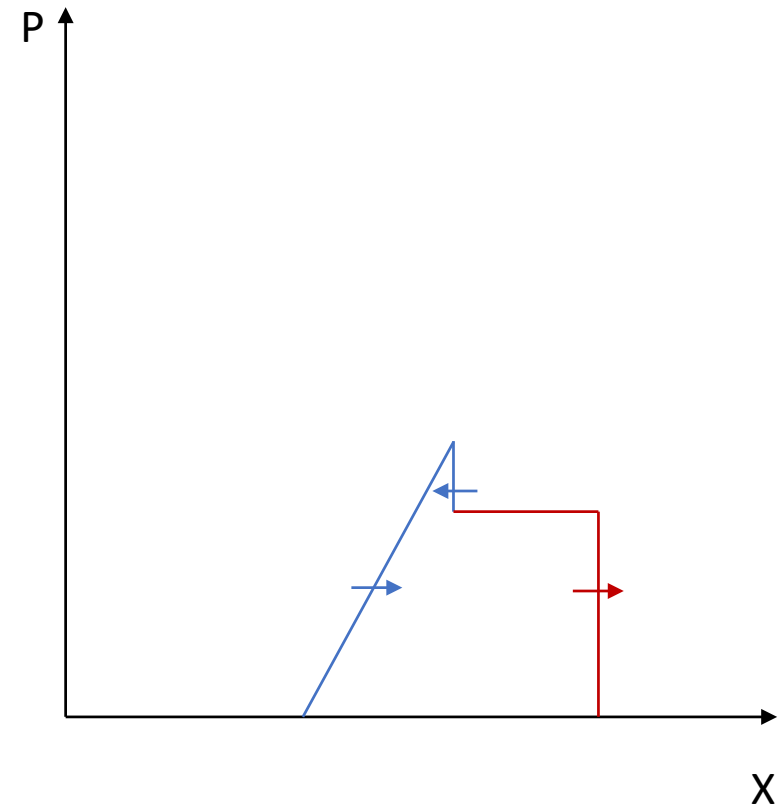
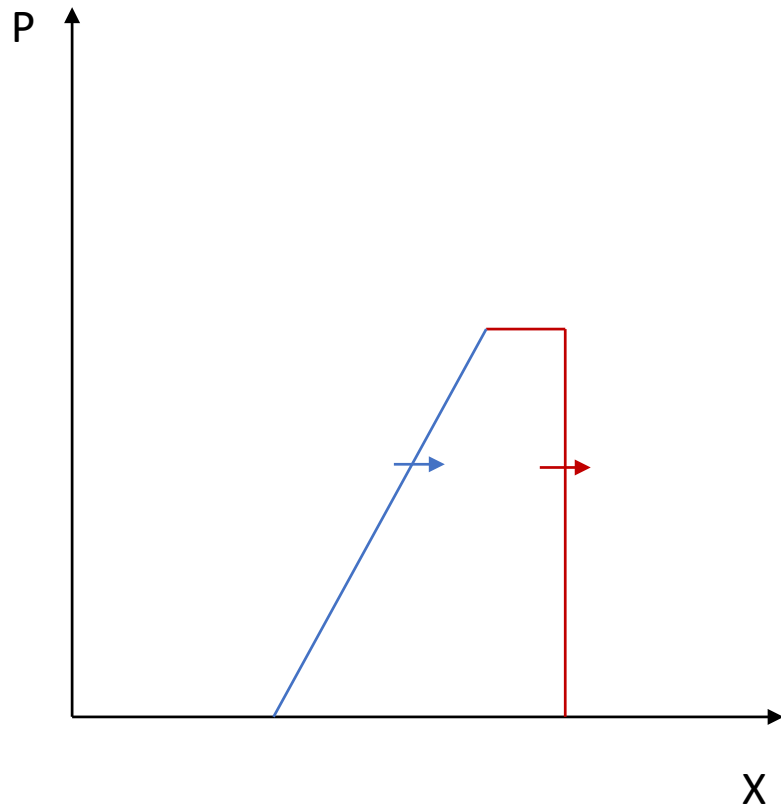
Including Transient Shock Release Phenomena



Including Transient Shock Release Phenomena



Including Transient Shock Release Phenomena



Including Transient Shock Release Phenomena

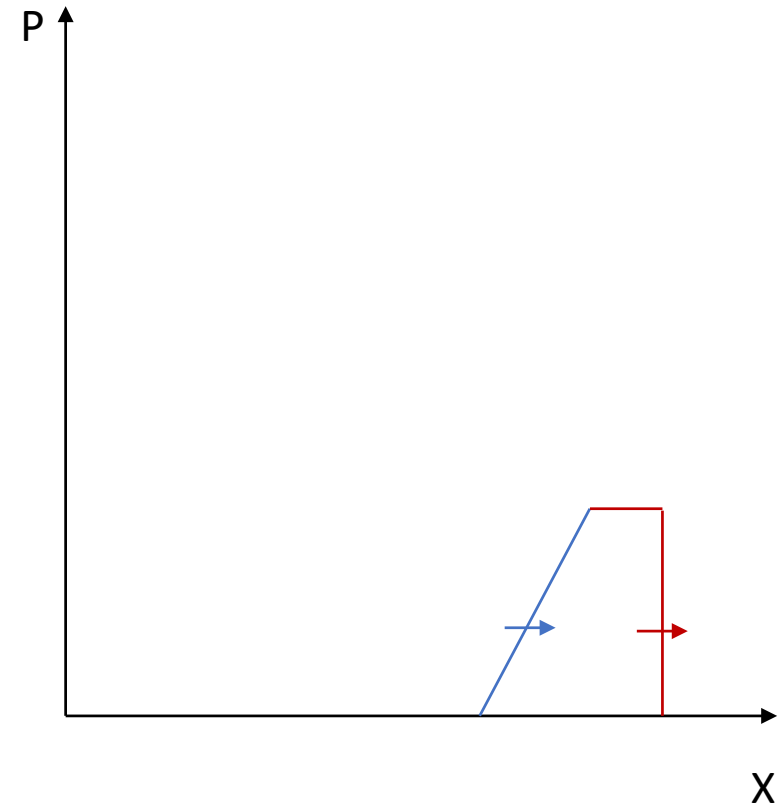
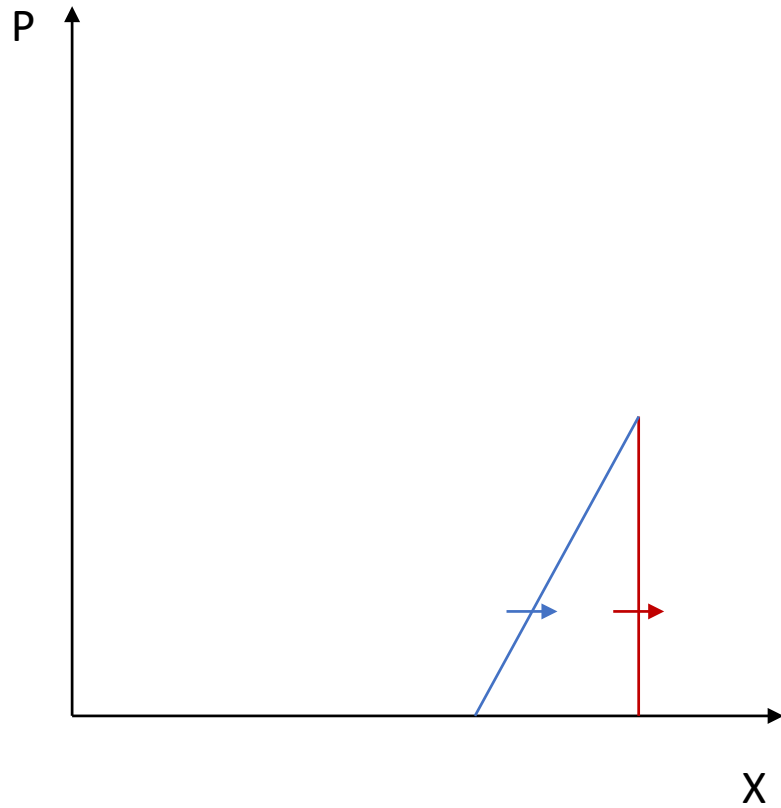


Plate impact experiments

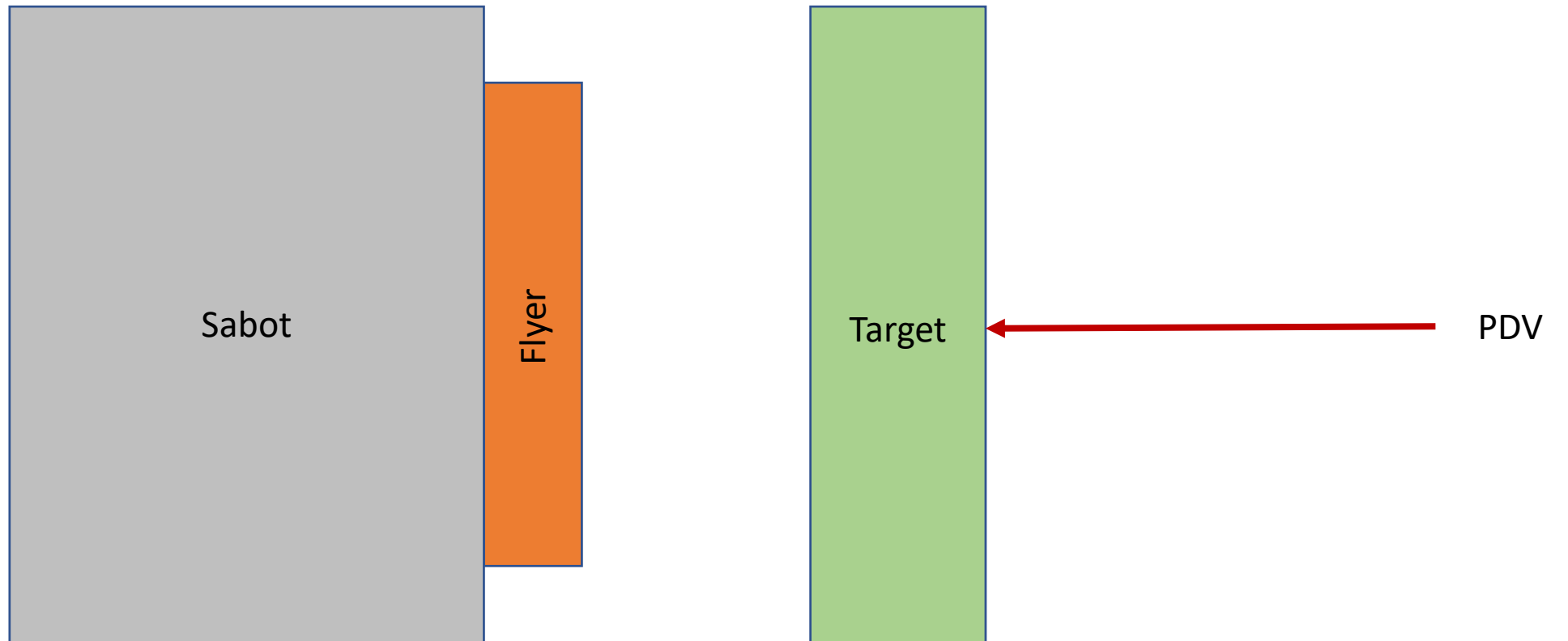


Plate impact experiments

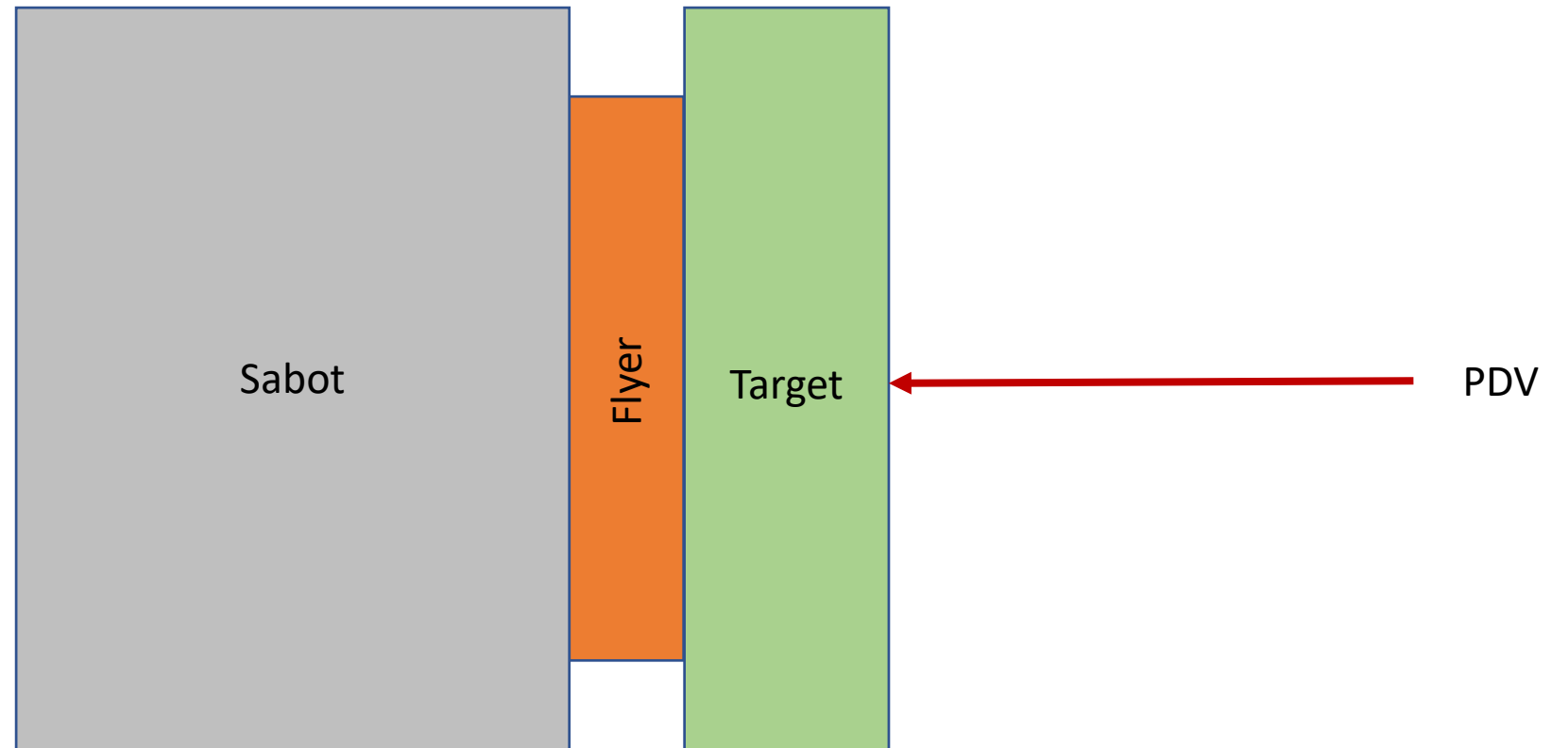


Plate impact experiments

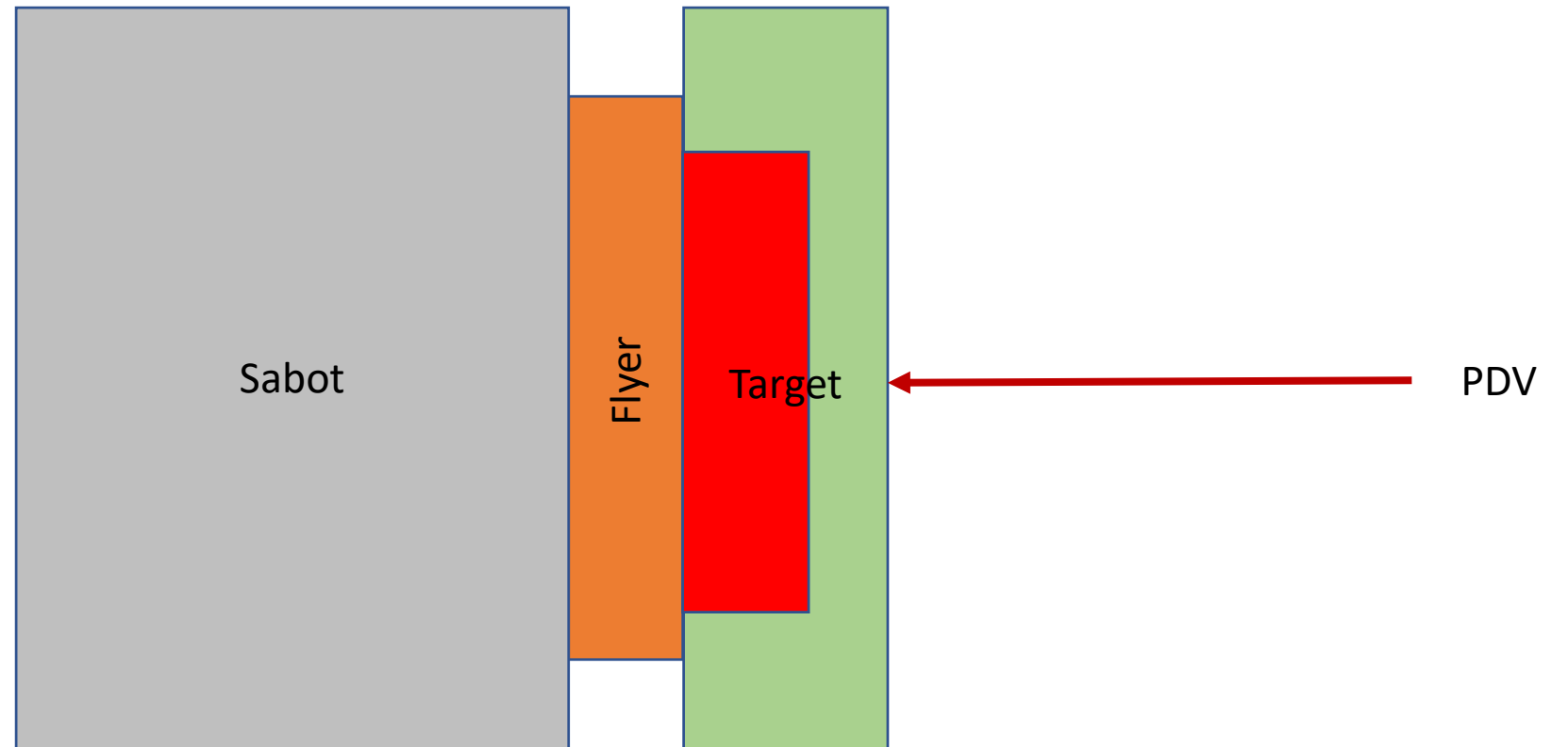


Plate impact experiments

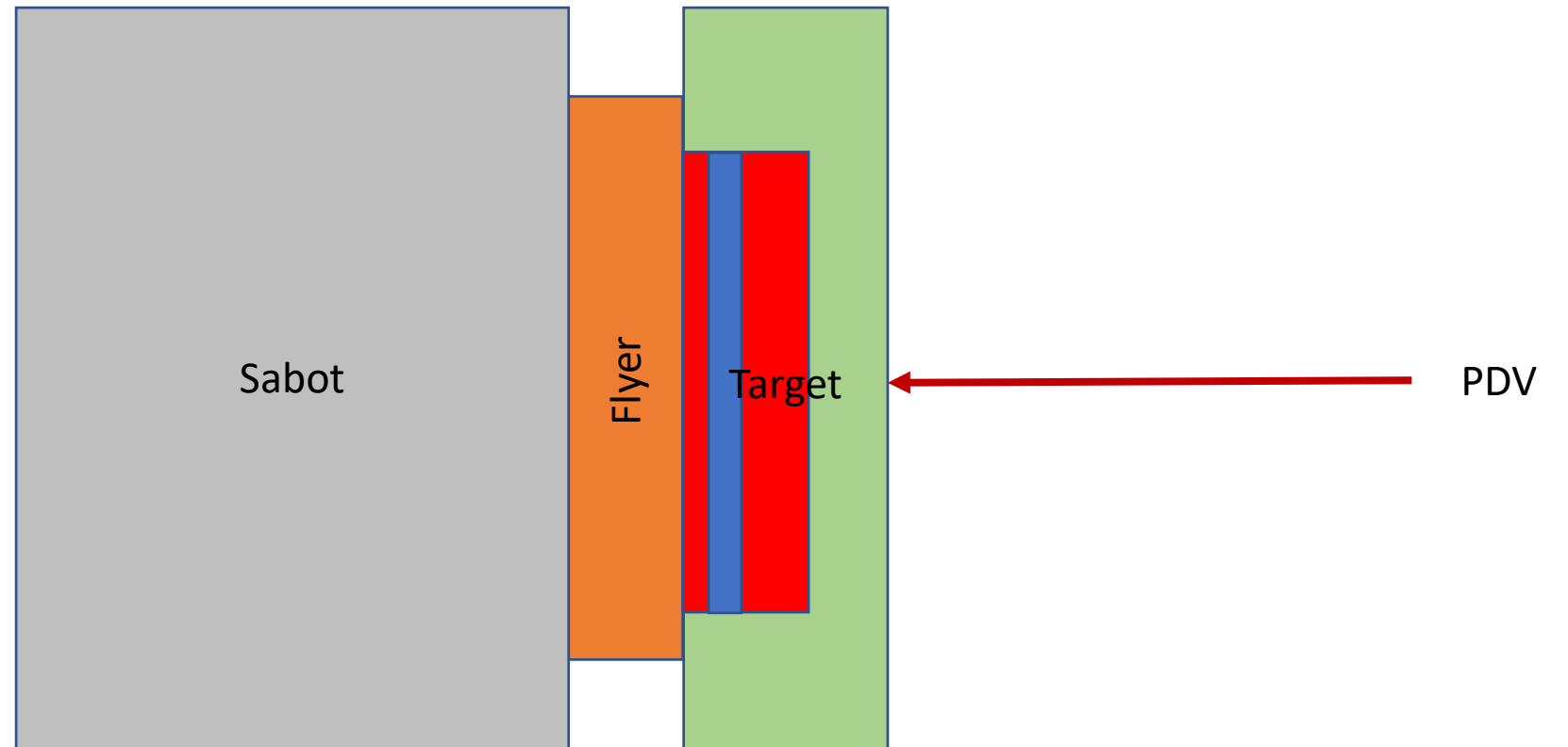


Plate impact experiments

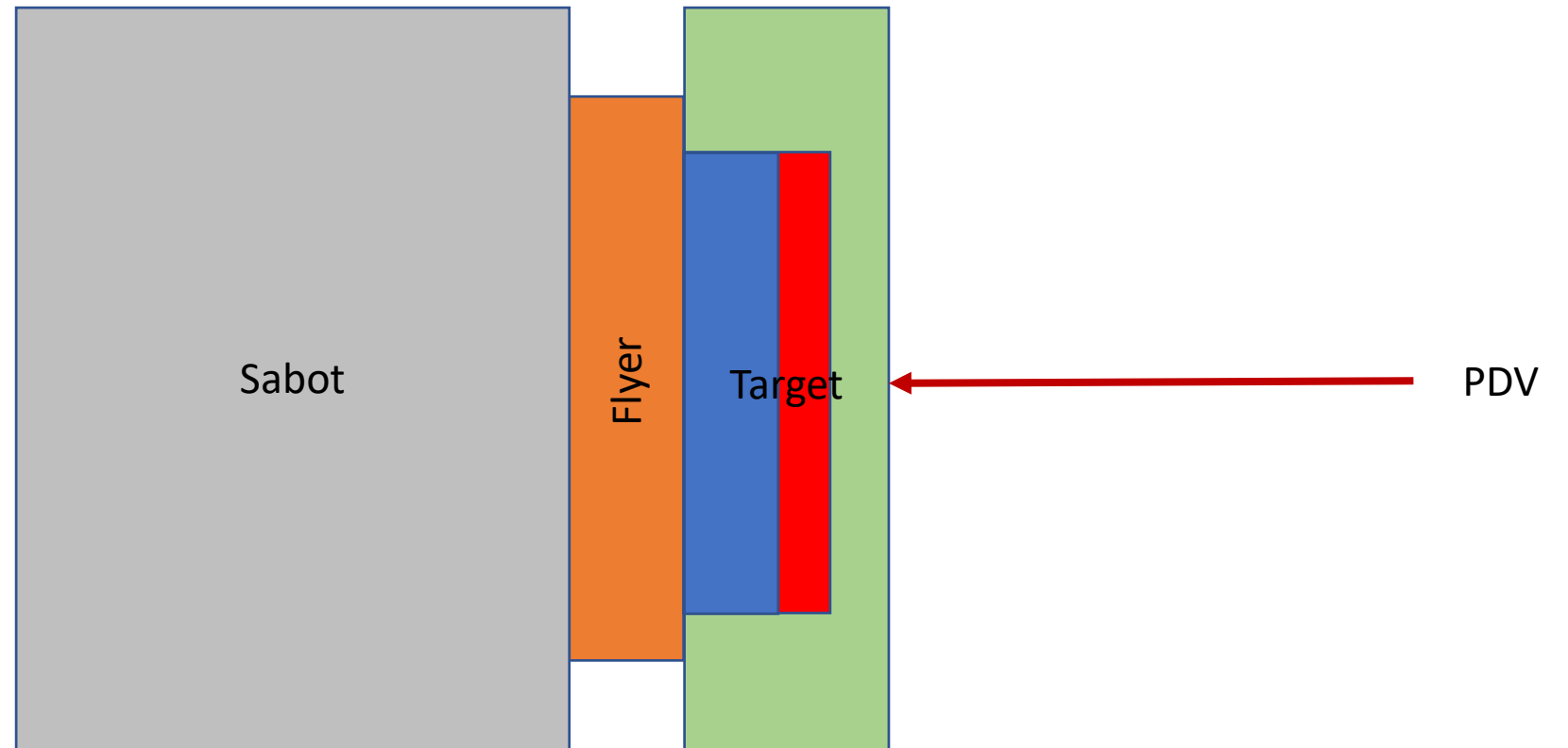


Plate impact experiments

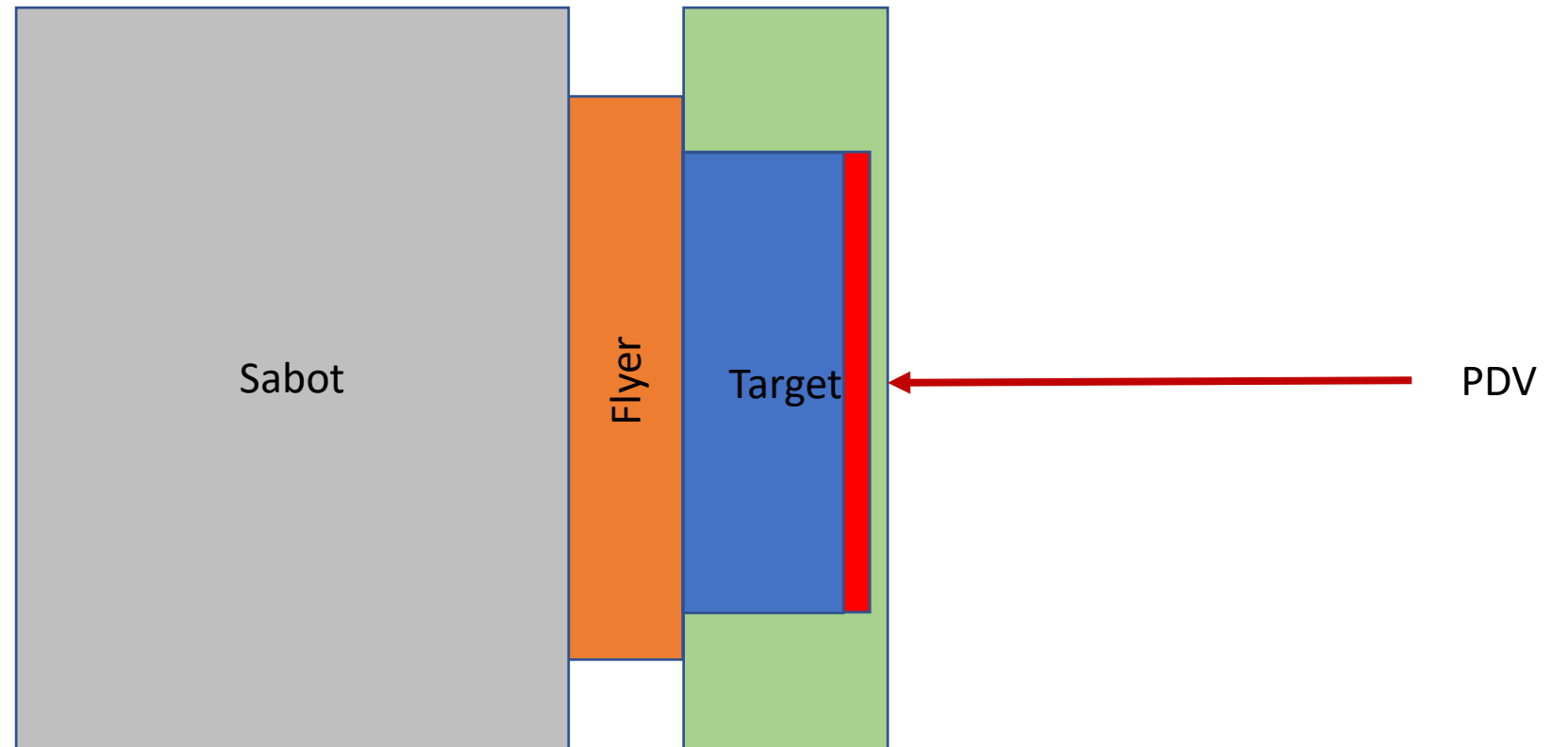
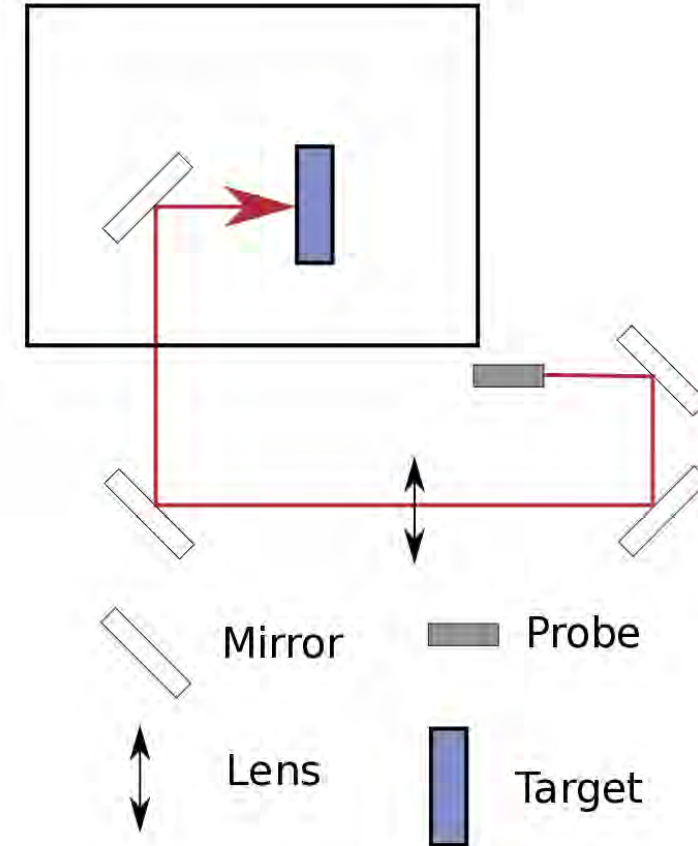
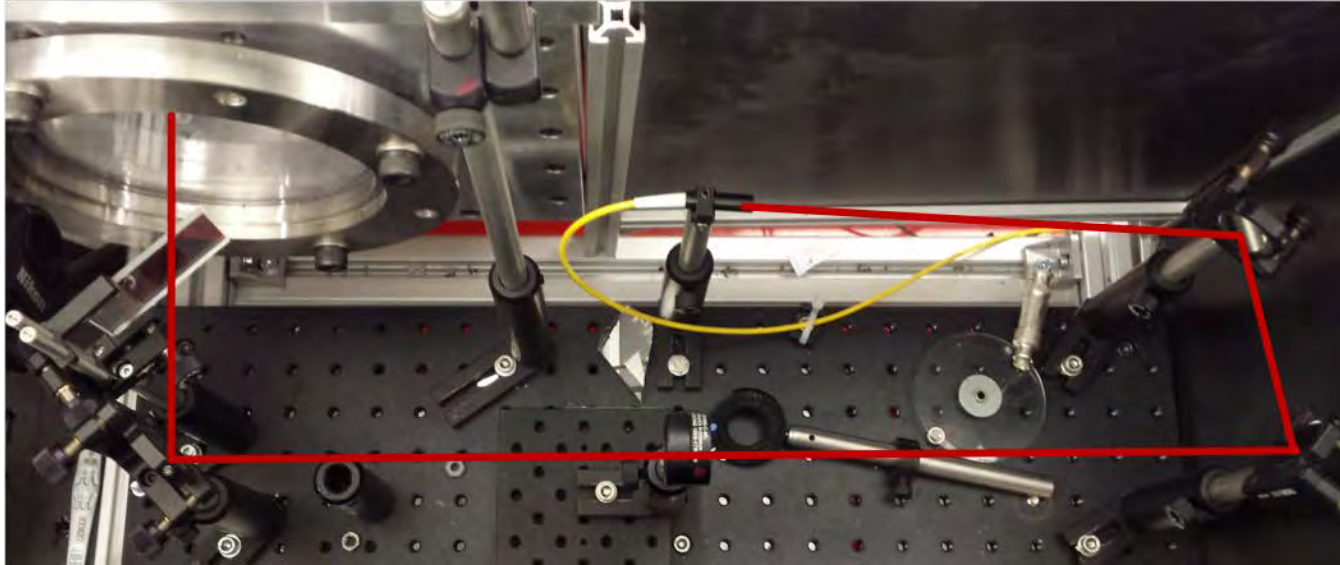
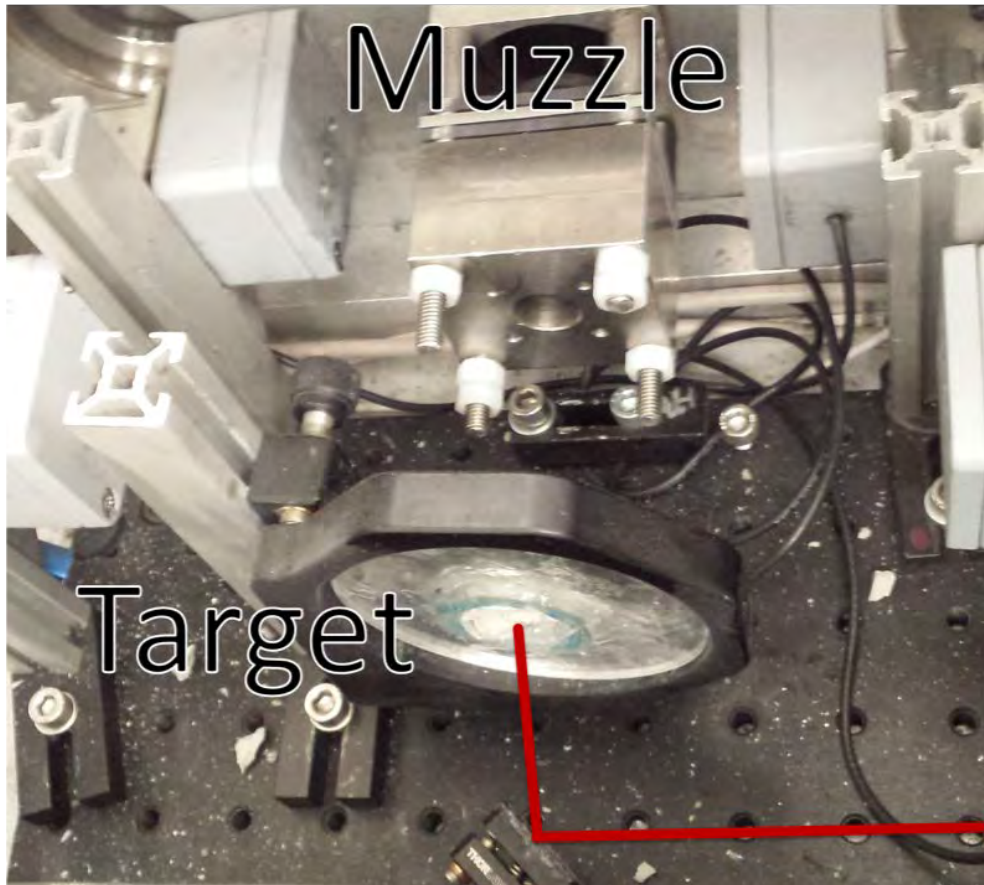


Plate impact experiments

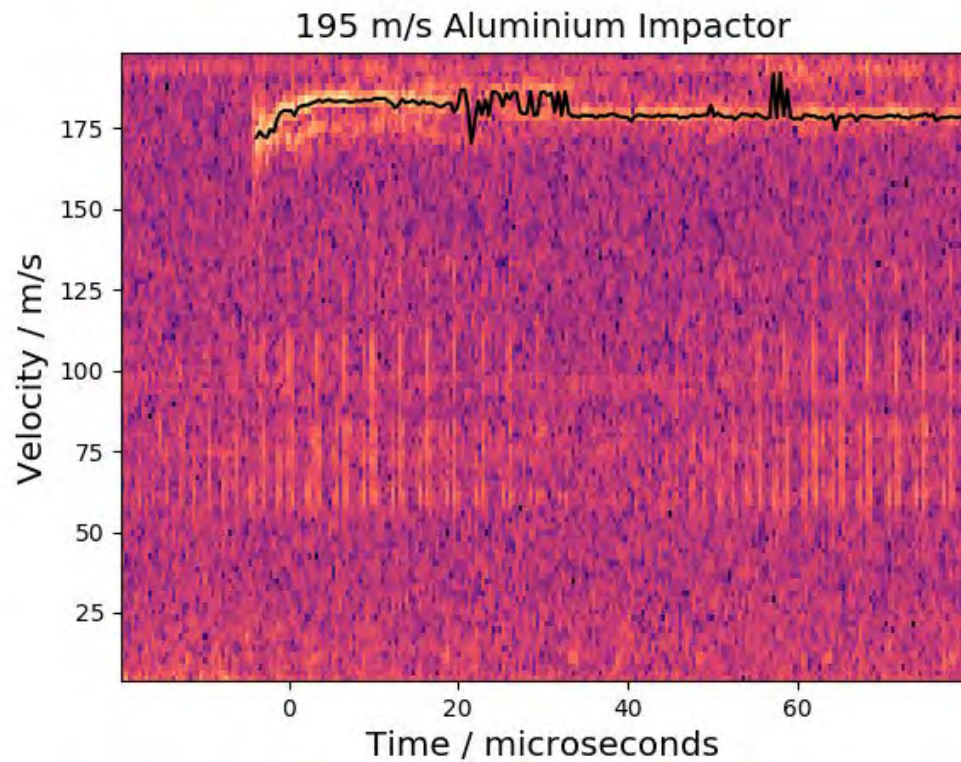


Target Chamber



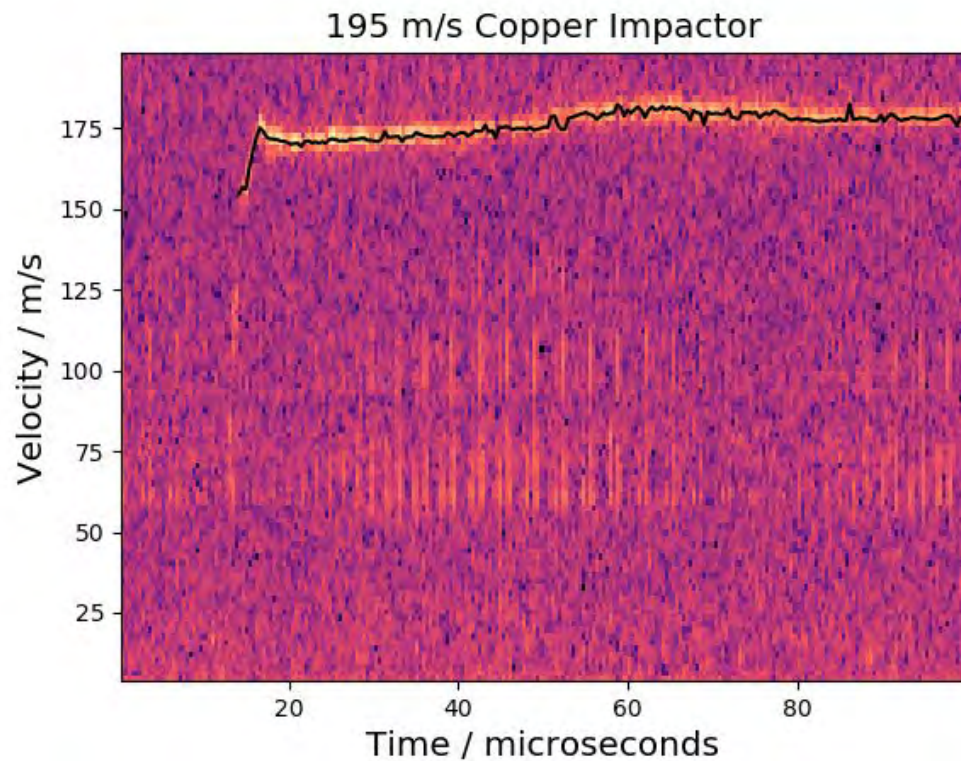
- Light gates measure velocity
- 3" ThorLabs optical mount used to align targets
- Polycarbonate/aluminium sabot stripper used for fragment experiments

Experimental Evidence



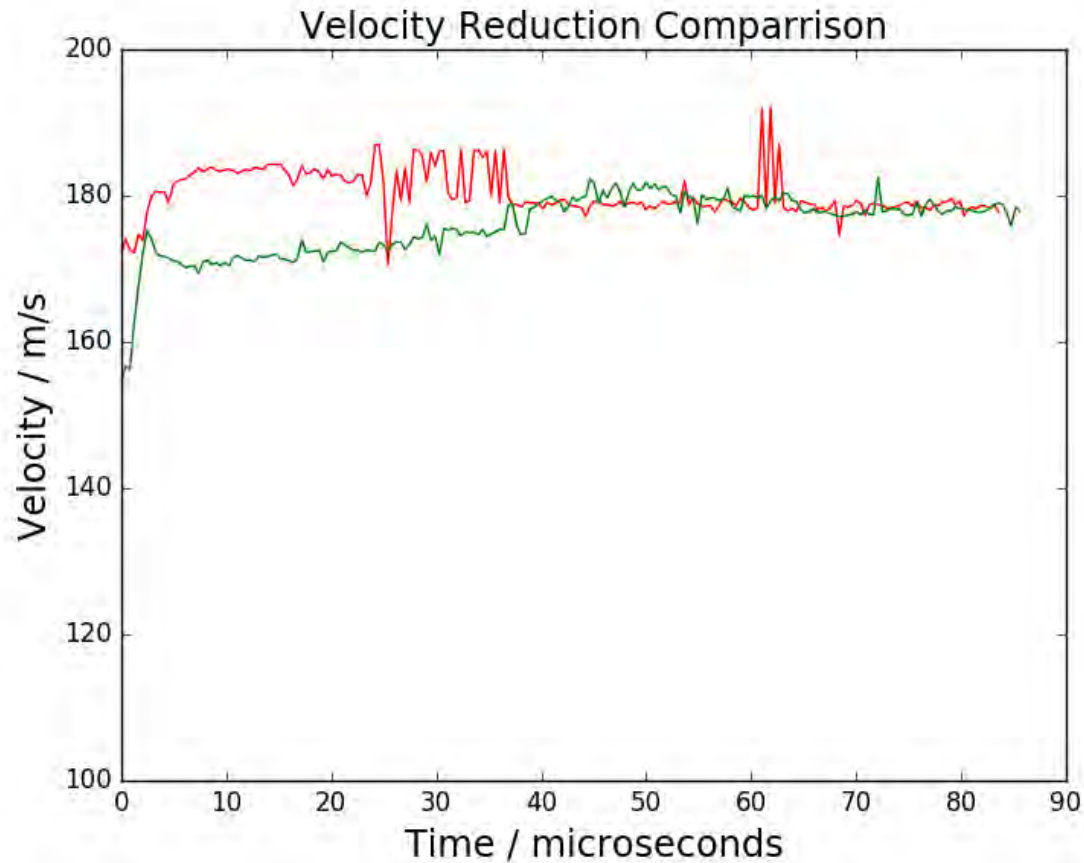
- 195 m/s impactor
- 185 m/s rear surface velocity
- No transient release

Experimental Evidence



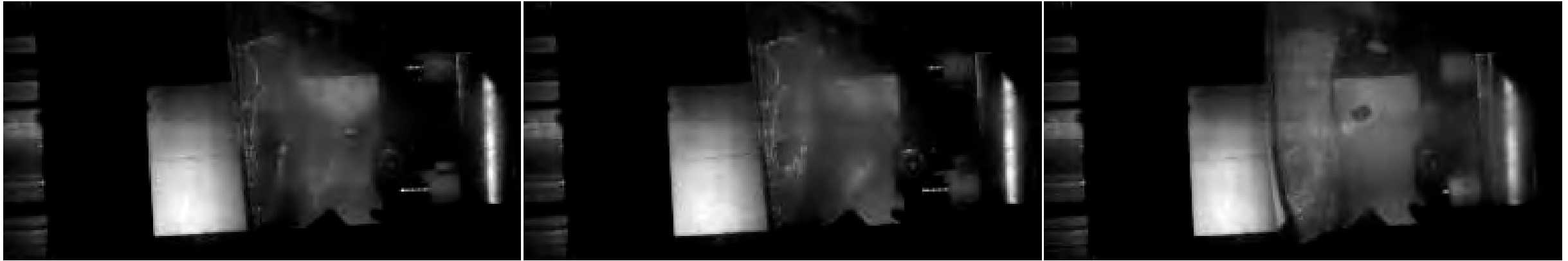
- 195 m/s impactor
- 175 m/s rear surface velocity spike, 160 m/s average
- Unoptimised transient release as evidenced by residual shock peak.

Experimental Evidence



- Same residual velocity – momentum conserved
- Reduced initial shock by 20 m/s
- Average reduction in velocity of 15 m/s for 35 microseconds
- Equivalent energy absorption to a material toughness of 1MJ/m^3

Experimental Evidence – Fragment Test



- 430 m/s steel STANAG fragment.
- Increasing velocity to work towards km/s protection

Next Steps

- Methodically increase fragment velocity to find maximum
- Investigate other materials
- Investigate 3D geometries
 - We can engineer the shape of the release phenomena
 - Converging shocks can be mitigated using a divergent release geometry

Conclusions

- Currently able to attenuate the shock front in plate impact experiments by 20 m/s
- Able to stop 430 m/s fragments
 - Need to optimize the transient release to get further improvement
 - Theoretical maximum is 7km/s
- Presented is a technology for a family of materials – we are investigating more suitable raw materials for km/s impacts.

Heavyweight Torpedo warhead IM assessment

R.FOUGEYOLLAS¹, D.COURRILLAUD¹, L.CHAFFOIS², P. CHABIN²

¹ NAVAL GROUP UNDERWATER WEAPONS BUSINESS UNIT, SAINT-TROPEZ (FRANCE)

²EURENCO, 1928 route d'Avignon, CS 90109 Sorgues – 84275 VEDENE, FRANCE

ABSTRACT

Thanks to its stealth, range and fire power, the F21 heavyweight torpedo gives client navies an unrivalled tactical advantage over all threat. Exploiting a range of innovations and advances in torpedo technology, a single F21 can knock out any surface combatant or submarine. The high energy density primary battery offers both high maximum speed and extended range while the new-generation acoustic head guarantees improved search efficiency from very shallow to deep waters. Fully digitalized technologies result in improved signal processing and enhanced overall performance.

The F21 complies fully with the demanding safety requirements applicable to nuclear-powered submarines. Regarding to the warhead insensitivity, this high requirement level is reached because the ammunition embeds live improved IM components such as an RDX/Al/AP cast cure substance for the main charge and thermal igniter. Moreover, its specific internal rubber based Thermal Protection gives some additional surviving characteristics against thermal threat such as external fire.

IM assessment was performed according to a rigorous process. This paper will describe the design principles and focus on results obtained against full scale tests such as shaped charge test.

1. INTRODUCTION

The Insensitive Munition (IM) assessment is realized according to STANAG 4439 in order to determine ammunition responses for threats defined in AOP 39. In case of F21 torpedo development, the IM assessment has been performed according to a rigorous process to respond to STANAG 4439, but also to all threats in operational situations. NAVAL GROUP and EURENCO have worked as a team on this project and have developed an IM warhead for the F21 heavyweight torpedo, currently in mass production.

This paper describes the design principles and focus on results obtained against full scale tests and especially shaped charge jet impact.

2. THE F21 HEAVY TORPEDO

The F21 torpedo is ending its development and is now in qualification step. It is the only torpedo development program today in the world. It benefits from all new technologies and permits to offer a great tactical advantage. Some characteristics are given in the table below:

Characteristics	Value
Length	6 m
Weight	1500 kg
Diameter	533,4mm
Range	> 50 km
Speed	> 50 knots
Propulsion	Electric
Guidance	Automatic or pilotage by optical fiber

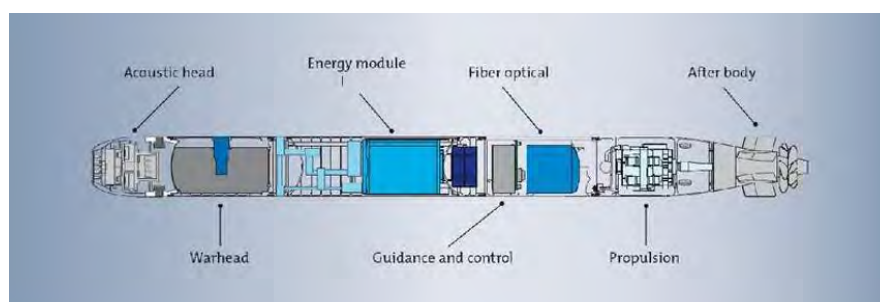
Thanks to its stealth, range and fire power, the F21 heavyweight torpedo gives client navies an unrivalled tactical advantage over all threats. The high energy density primary battery offers both high maximum speed and extended range while the new-generation acoustic head guarantees improved search efficiency from very shallow to deep waters. Fully digitalized technologies result in improved signal processing and enhanced overall performances .

The F21 torpedo has been developed with safety requirements applicable to nuclear-powered submarines. Besides great performances, all torpedo design drivers are thought on safety (warhead, primary battery...).

This paper focuses on the warhead section, which is qualified by French National Authority and already in service in one other client Navy, its design and security tests.

3. GENERAL DESCRIPTION OF THE WARHEAD

On the F21, the warhead is located in the front of the torpedo. The warhead section is mechanically and electrically connected with the Acoustic Head Section (AHS) in the front and with the Primary Battery in the rear.



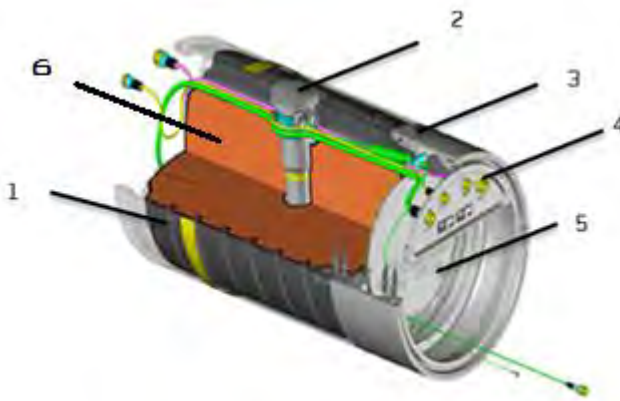
The F21 warhead is an anodized aluminium hull build in foundry. It contains three compartments:

- A chamber for the explosive loading,
- an impact fuze compartment
- a tunnel parallel to the axis for passing the electric cables between the acoustic head, in front of the torpedo, to the others torpedo sections. The crossing cables are located at the top of the hull. Its isolates cables and the explosive loading (Figure 1 : The F21 warhead).

This structure allows to resist to the pressure at the maximum depth.

The explosive loading is composed by :

- One cast-pbx main explosive charge B2211D (250 kg Net Explosive Weight),
- One thermal protection
- One fuze varnish



Mark	Designation
1	Aluminium hull
2	Impact Fuze
3	Cables
4	Connectors
5	Closing plate
6	Explosive loading

Figure 1 : The F21 warhead

Physical characteristics of the F21 warhead section are:

- Overall length : 1028 mm
- Diameter : 533,4 mm

4. MAIN EXPLOSIVE CHARGE CHARACTERISTICS

The explosive is designed by EURENCO, the Naval Group partner. It's an composite explosive B2211D composed by:

- ammonium perchlorate
- aluminium
- I-RDX® , insensitive grade designed by EURENCO
- HTPB based inert binder

The F21 warhead contains 250kg of B2211D (350kg equivalent TNT). Some performance characteristics of B2211D are given below are (MSIAC's database source):

Density (kg/m³)	1810
TNT equivalent (Peak pressure)	1,4
Detonation velocity (m/s)	5500

B2211D is an RDX/AP/Al HTPB-based cast-cure explosive, specifically designed for underwater applications and used in many warheads design since more than 30 years.

Results of some safety characteristics are given below (Source : MSIAC database):

B2211D	
Density	1810kg/m ³
Auto-ignition Temperature (STANAG 4491)	>200°C
Critical Diameter	76 mm
Friction sensitivity (AOP-7-STANAG 4489)	33J
Impact Sensitivity (AOP-7-STANAG 4487)	70N
Shock gap test (AOP-7-STANAG 4488)	80 cards
Capacity discharge (AOP-7-STANAG 4490)	No reaction

5. THERMAL PROTECTION

The thermal protection was developed in order to create thermal insulation between the aluminium hull and explosive. It delays temperature rising of the explosive in warhead section in case of external fire or any thermal attacks during life cycle.

The specific rubber material used has good thermal properties and thermal conductivity.

6. THERMAL FUZE VARNISH

The thermal fuze varnish was developed specially by EURENCO to prevent severe reactions under slow heating stimuli. Indeed, the live fuze compound auto-ignition temperature under slow heating conditions is far lower than B2211D's ignition temperature. So, burning initiation will start by fuze varnish in the rear part of the warhead and initiate the combustion of the main B2211D charge when external temperature reaches a certain threshold. The combustion start point prevents inner violent reaction of the main charge exposed to internal high temperature.

Moreover, burning gazes can escape with a weak closing plate between the warhead and the primary battery in the rear. So, two sections separate easily.

7. IM Assessment

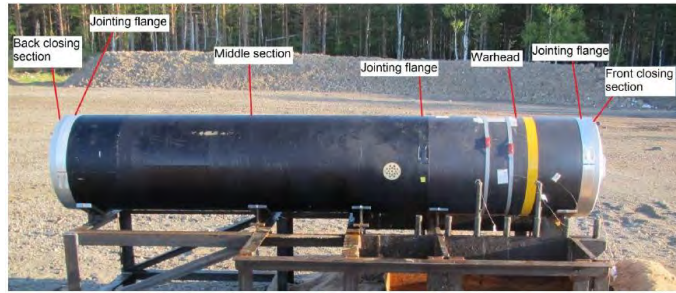
The F21 IM assessment was performed according to a rigorous process which combined analysis of experience feedback, simulations and tests.

Naval Group BU underwater weapons analyses F21 IM assessment according to STANAG 4439. Two tests are detailed in following paragraphs: fast cook-off and shaped charge jet impact.

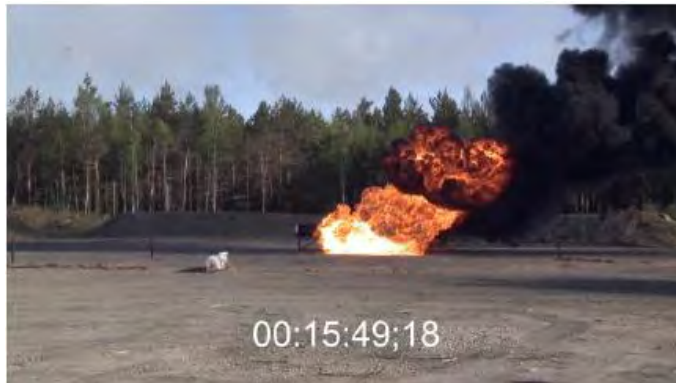
Fast Cook-Off Test

- Demonstration : full-scale trial,
- Scope : to assess the warhead reaction under a kerosene fire,
- Applicable standard : STANAG 4240,
- Configuration : warhead with primary battery.

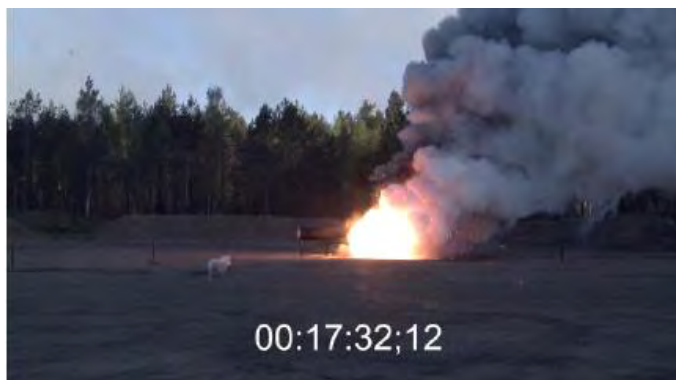
Warhead with primary battery



Fuel fire



Burning of main charge B2211D



End of burning



Figure 2 : Evolution in time of burning warhead

- Long burning time due to the total quantity of live material. Test performed with primary battery, no impact of the battery to the final reaction.
- No projection observed.
- Complete live material has burnt after the test
- **Conclusion : Type V (BURN)**

Shaped charge Jet Impact

Shape charge jet impact test is generally not performed because of most-likely expected Type II (partial detonation) or type III (explosion) reaction. Numeric simulations were predicting a possible type III or type IV reaction. The full-scale trial was performed to confirm or not this prediction.

- Demonstration : full-scale trial
- Scope : to asses the warhead reaction under a shaped charge jet impact
- Applicable standard : STANAG 4526
- Type of shaped charge used : RPG-7 (PG7M), see figure 3.
 - Caliber : 70mm
 - Steel armour penetration : 300mm
 - Main charge explosive : A IX-1 (96% RDX, 4% wax)
 - Net Explosive Weight : 320g
- Instrumentation :
 - steel witness plate,
 - pressure gauges,
 - high-speed camera.



Figure 3 : RPG-7 Shaped charge used for the trial

The nose cap of the RPG7 warhead was placed in direct contact with the test item and on a stand-alone of styrofoam, threaded rods and plywood. This was in the best way possible simulate a realistic scenario. The torpedo warhead was placed on steel witness plate.



Figure 4 : Trial configuration : test specimen and RPG-7 shaped charge

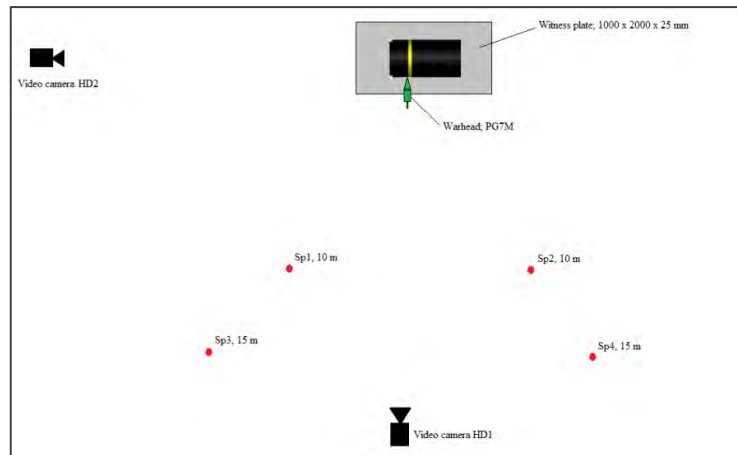


Figure 5 : Shaped charge Jet impact test layout

When the shaped charge jet hits the test item, parts and fragments from the test item are scattered around the test area (Figure6 : First seconds after shape charge ignition). The high explosive in the torpedo warhead is ignited and the test item burns with a white intensive flame for approximately 5 minutes (Figure 7 : Warhead burning).



Figure 6 : First seconds after jet has impacted the warhead



Figure 7 : warhead burning and after complete burn

Air blast pressure

The registered maximum air blast pressure values are shown in the following table. It is assumed that most part of this air blast pressure is caused by the PG7M warhead detonation itself.

Registered maximum air blast pressure values (kPa)			
Sp1, 10 m	Sp2, 10 m	Sp3, 15 m	Sp4, 15 m
10.1	10.7	6.0	6.4

Witness plate

No penetration holes or detonation evidence can be seen after the test, as shown in figure 9 below.



Figure 8 : witness plate after the test

Recovered fragments

Five pieces of unreacted high explosives were found, also some metallic pieces as well the front part of the warhead (Figure 10 : Front part of the warhead). This massive fragment can be observed on high speed camera, and is visible on Figure 7 (right) during the first seconds after shape charge initiation.



Figure 9 : front part of the warhead

Fragments distribution vs AOP-39 Energy / distance 20J criteria

The diagram below shows the recovered fragments : X-axis = mass of the fragment (g), Y-axis = Distance (m), compared to the 20J threshold criteria from AOP-39.

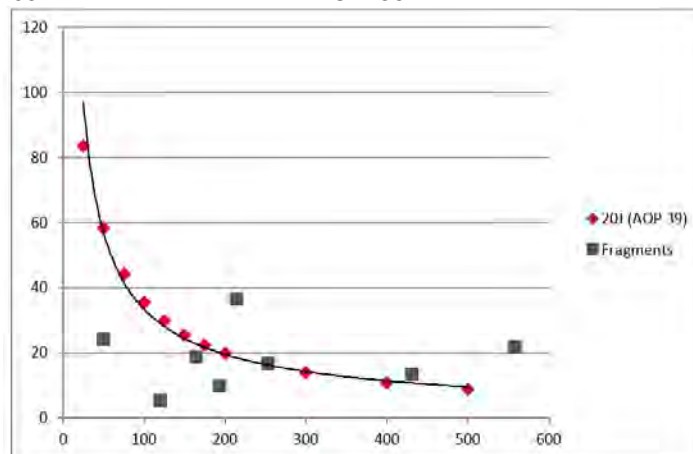


Figure 10 : Fragments distribution vs AOP-39 20J criteria

Test conclusion

According to AOP-39, the F21 warhead response is estimated as a Type IV reaction (Deflagration). Some fragments were thrown beyond 15m with an energy level greater than 20 J (Figure 10 : Fragments distribution based on the distance (m)/mass (g) AOP-39 relationship).

The maximum air blast pressure levels were relatively low and most likely caused by the PG7M warhead itself.

8. IM Signature

The IM signature was established using full-scale trials, analyses based on simulations or semi empirical tools as well as reading across experimental results obtained in equivalent configurations.

STANAG 4439 Requirements		FH	SH	BI	SR	FI-L	FI-H	SCJI
IM Signature	NR							
	V	●		○		○		
	IV		●					●
	III				○		○	
	II							
	I							

- Full compliance with STANAG 4439
- : Assessment by Full-scale trial
- : Assessment by analysis and/or read-across with other configurations

9. CONCLUSION

The warhead of F21 heavy torpedo was designed to meet the highest standard of IM specifications. The level of reactions observed during full-scale trials such as Fast Cook-Off and RPG-7 Shaped charge jet test demonstrates that the warhead can withstand very severe stimuli which are considered as critical regarding the Navy platform.

Heavy Torpedo warhead IM tests assessment

IMEMTS 2018, Portland
April 23-26, 2018

R. FOUGEYROLLAS¹, L. CHAFFOIS²
D. COURRILLAUD¹, P. CHABIN²

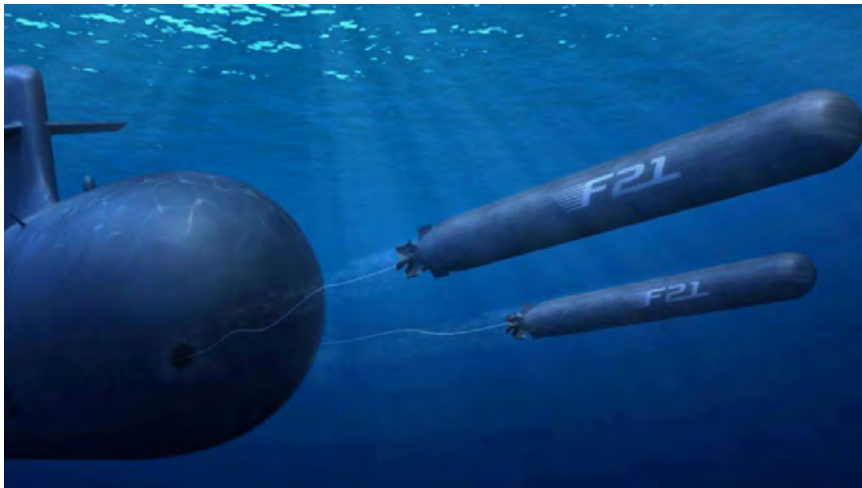
¹ : NAVAL GROUP

² : EURENCO

OUTLINE

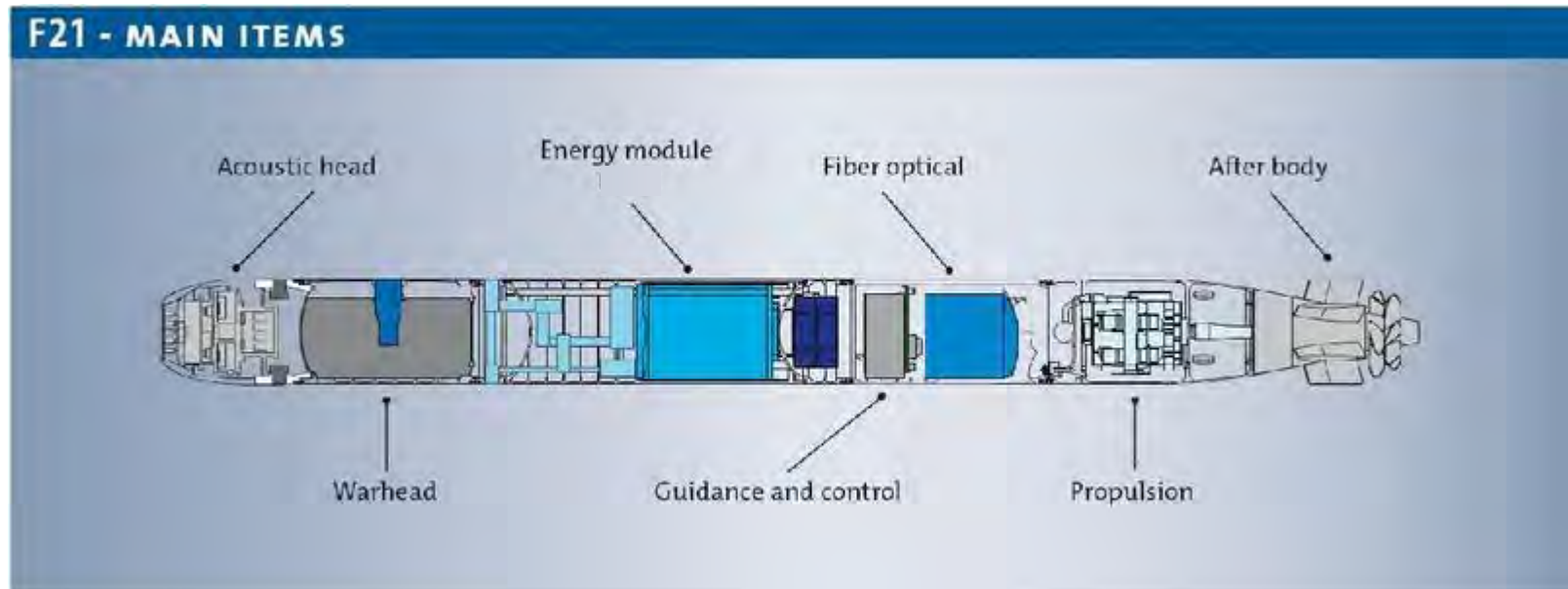
- **Presentation of the F21 heavyweight Torpedo**
- **Presentation of F21 Heavy Torpedo warhead design**
- **Fast Cook-Off and Shaped charge Jet Tests**
- **IM signature**

F21 Heavyweight Torpedo

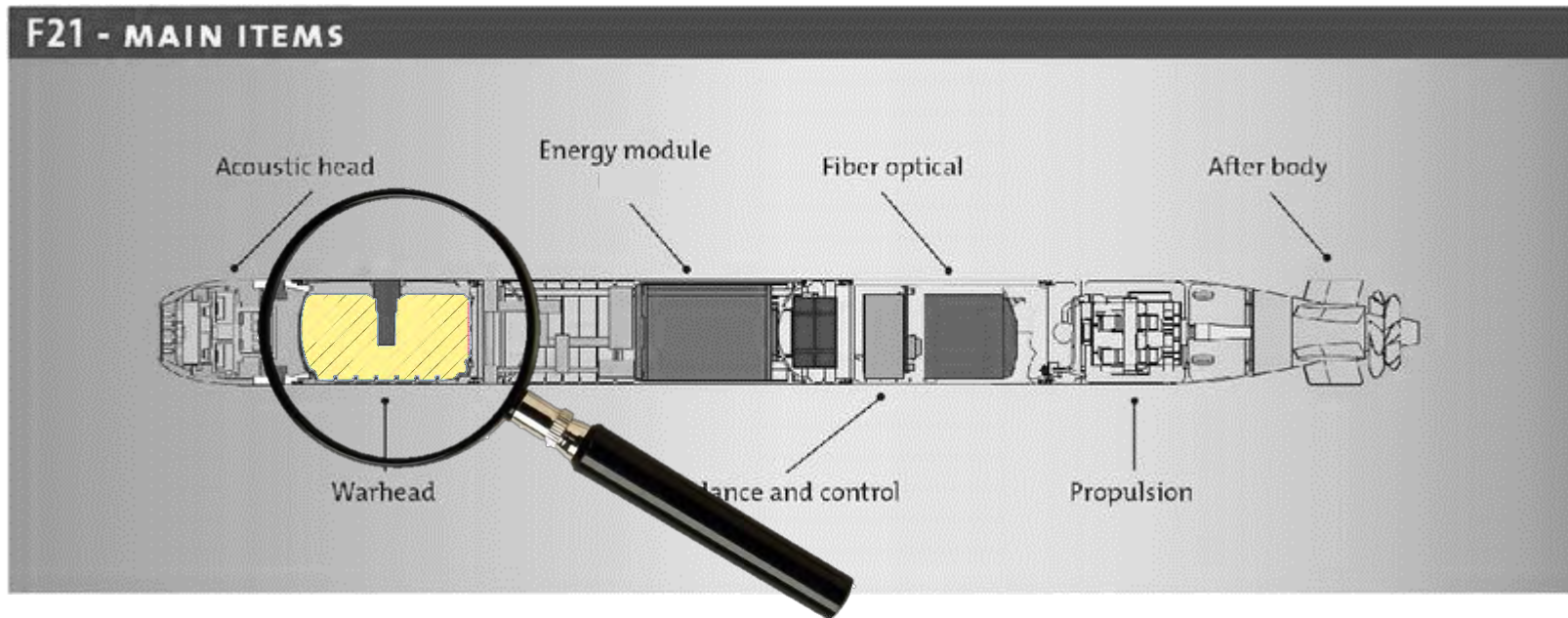


Characteristics	Value
Length	6 m
Weight	1 500 kg
Diameter	533,4 mm
Range	> 50 km
Speed	> 50 knots
Propulsion	Electric
Guidance	Automatic or optical fiber

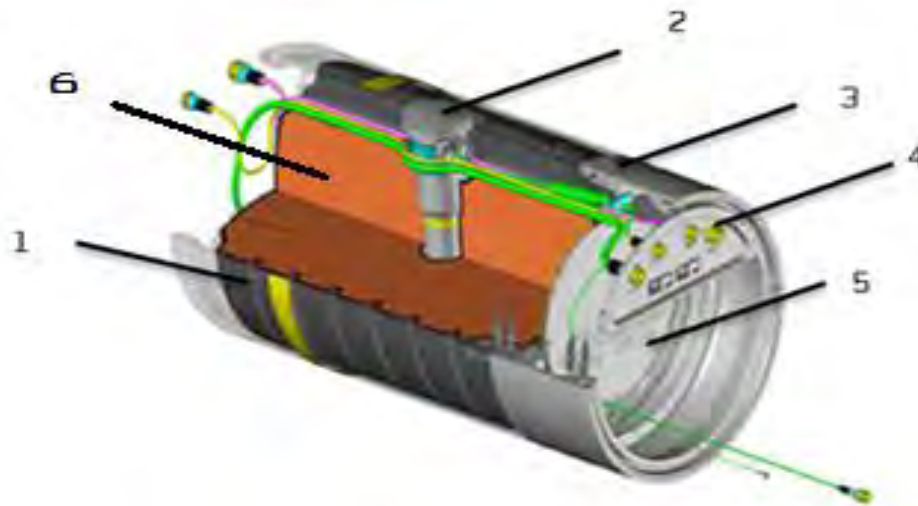
F21 Heavyweight Torpedo



F21 Heavyweight Torpedo



Warhead



Item	Description
1	Aluminum body
2	Impact Fuze
3 & 4	Cables & Connectors
5	Closing plate
6	Main charge Explosive + thermal protection + thermal fuze

Warhead

Main charge explosive

Characteristics	Value
Main charge Explosive Technology	Cast-cure PBX
Main charge Explosive	B2211D
Main charge Explosive components	I-RDX®/ AP / Al / IB HTPB-Based
Warhead Diameter	533,4 mm
Net Explosive Weight	250 kg
Warhead Gross Weight	348 kg

- Fully qualified to STANAG 4170
- Underwater applications : mines, torpedo warheads,
- Anti-ship missile warheads

Warhead

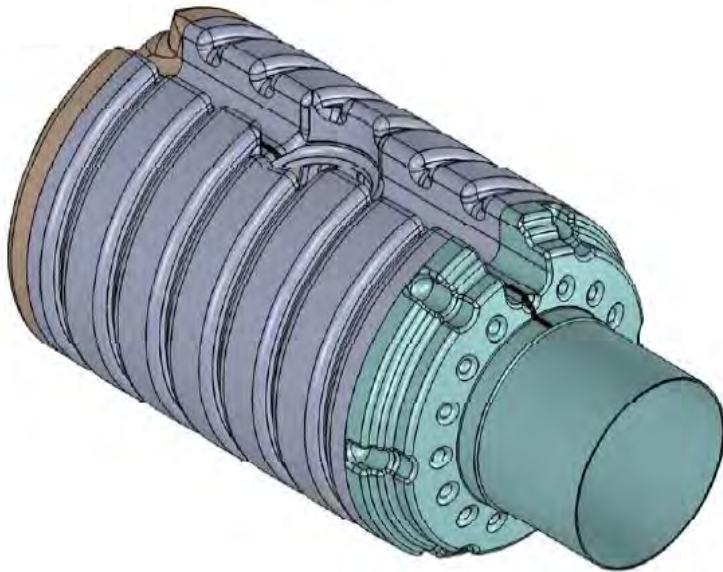
Main charge explosive : B2211D

Performance characteristics	Value
TNT Factor (Peak / Energy / Bubble effect)	1,4 / 1,4 / 2,1
Density	1,810
Detonation velocity	5 500 m.s ⁻¹
Safety characteristics	Value
Auto-ignition Temperature - STANAG 4491 (°C)	200 °C
Critical diameter	76 mm
Friction sensitivity - STANAG 4489	33 J
Impact Sensitivity - STANAG 4487	70 N
Card Gap Test Ø40mm - STANAG 4488	80 cards
Capacity discharge - STANAG 4490	No reaction

EIDS - Extremely Insensitive Detonating Substance

Warhead

Thermal Protection



- Rubber based technology
- Reinforced rubber material against thermal threats
- Composed of 5 sub-components
- Prevent mechanical friction of Main charge explosive with the metallic body
- Inserted into the empty warhead before filling

Warhead

Thermal Fuze varnish



- **HTPB-based live compound**
- **Density : 1,058**
- **Self-ignition temperature under slow-heating stimuli : approx. 165 °C**
- **Feature : locally initiate the main charge explosive when temperature reaches 165°C and prevent core-initiation of the main charge and related violent reactions**

Warhead

Thermal Fuze varnish : Slow Cook-Off test

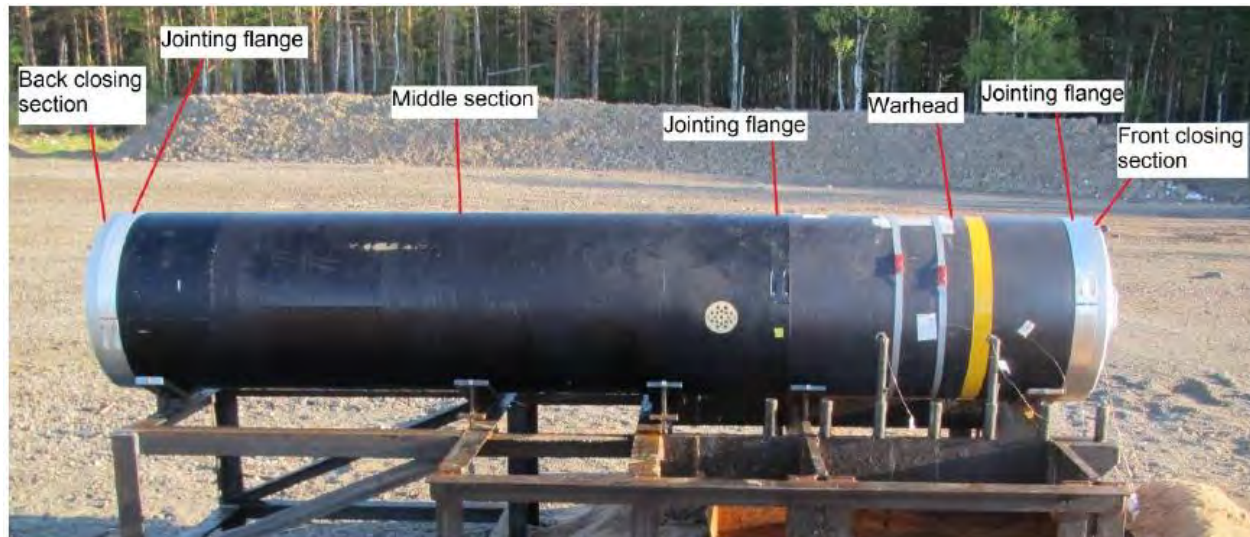


- **Application : Slow Cook-Off threat**
- **165 °C : initiation of thermal fuze located in the back end of the main charge**
- **Start of burning of main charge explosive**
- **Linear combustion of the main charge**
- **Fast burning and low level of reaction**

IM Assessment

Fast Cook-Off Test

- Test setup : IAW STANAG 4240
- Fuel fire stimuli
- Specimen configuration : Warhead section + battery section



IM Assessment

Fast Cook-Off Test

- T0 : burning of fuel
- T0 + 17' : burning of the main charge explosive
- T0 + 45' : complete warhead has burnt



Level of Reaction IAW STANAG 4439 : Type V (Burning)

IM Assessment

Shaped Charge Test

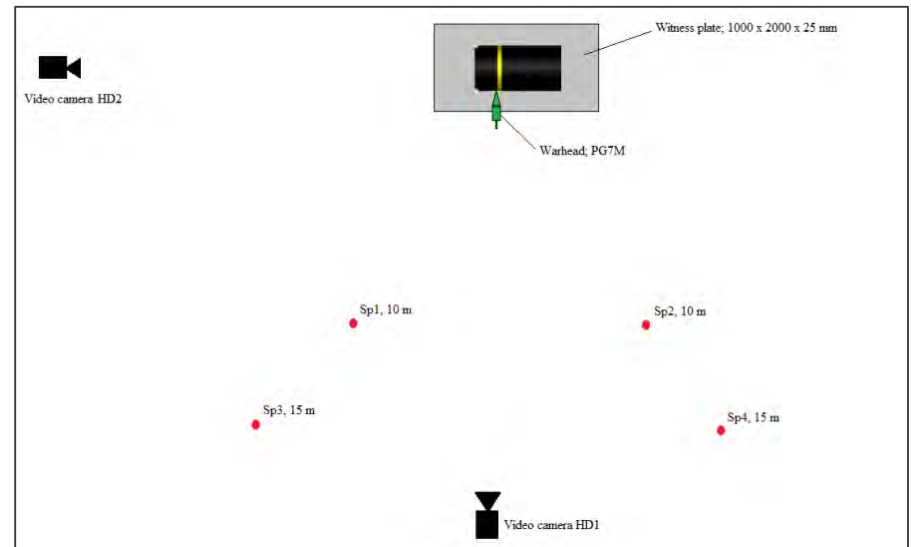
- **Test setup : IAW STANAG 4526**
- **Shaped charge warhead : RPG-7 (PG7M)**
 - Caliber : 70 mm
 - Steel armor penetration : 300 mm
 - Main charge explosive : A IX-1 (96% RDX, 4% wax)
 - Net Explosive Weight : 320 g



IM Assessment

Shaped Charge Test

- **Test setup : IAW STANAG 4526**
- **Instrumentation**
 - Measurement Pressure gauges
 - Steel witness plate
 - High Speed camera



IM Assessment

Shaped Charge Test

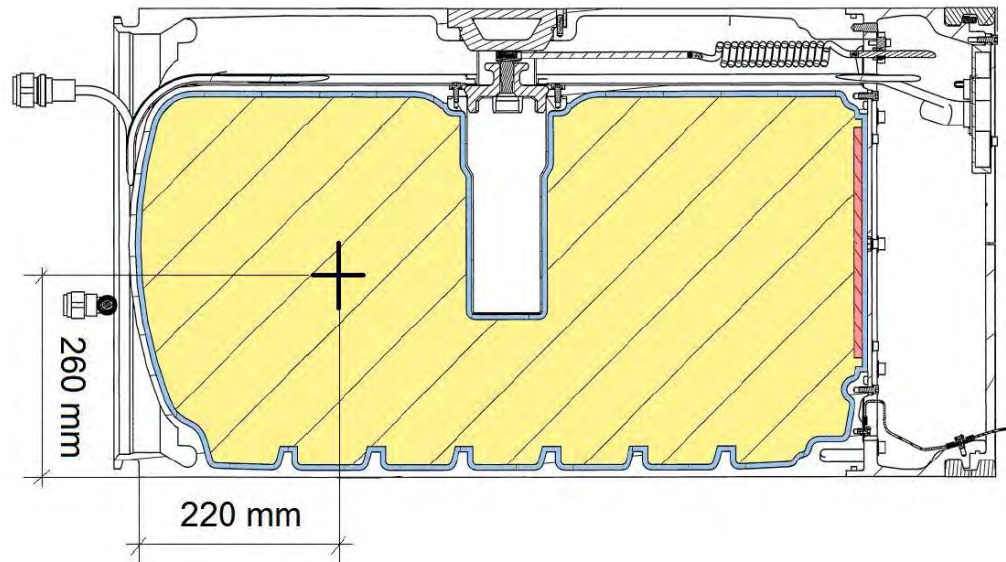
- Test setup : IAW STANAG 4526
- Test configuration : SC in contact with the warhead (no mitigation device)



IM Assessment

Shaped Charge Test

- Test setup : IAW STANAG 4526
- Test configuration : aim-point calculated to maximize the cross section of live material to be hit by the shaped charge jet



IM Assessment

Shaped Charge Test

- T0 : initiation of the Shaped charge.
- Front end of the warhead is cut from the body : massive fragment projected



IM Assessment

Shaped Charge Test

- **T0 + 3''** : start of burning of the main charge explosive.
- **T0 + 8'** : end of burning of the main charge explosive



IM Assessment

Shaped Charge Test

- **Maximum Air blast pressure measured**

Registered maximum air blast pressure values (kPa)			
Sp1, 10 m	Sp2, 10 m	Sp3, 15 m	Sp4, 15 m
10.1	10.7	6.0	6.4

- **Most part of air blast pressure probably due to the shaped charge itself, but no reference test performed**

IM Assessment

Shaped Charge Test

- Close-up view after the test. No impact/damage on witness plate.



IM Assessment

Shaped Charge Test

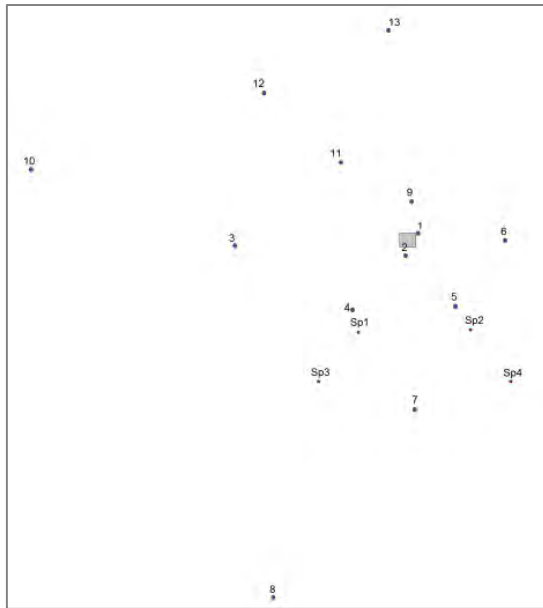
- Five pieces of unreacted high explosive recovered



IM Assessment

Shaped Charge Test

- Fragment distribution (not to scale)



No.	Description	Weight	Projection distance
		(g)	(m)
1	Rear part of the warhead.	46 500	1.15
2	Fragment from the warhead.	1 335	1.62
3	Unreacted high explosives.	164	18.96
4	Unreacted high explosives.	193	9.82
5	Fragment from the warhead.	1 655	8.30
6	Fragment from the warhead.	4 000	10.57
7	Unreacted high explosives.	253	16.82
8	Fragment from the warhead.	214	36.61
9	Unreacted high explosives.	120	5.47
10	Front part of the warhead.	14 500	34.06
11	Unreacted high explosives.	431	13.58
12	Unreacted high explosives.	558	22.04
13	Fragment from the warhead.	50	24.31

IM Assessment

Shaped Charge Test

- **Unreacted high explosive recovered : 1,7 kg**
- **Total weight of inert material recovered : 68,2 kg**
- **Massive fragment (front end) 14,5 kg recovered at 34 m from witness plate**
- **Low level of air blast measured**

Level of Reaction IAW STANAG 4439 : Type IV (Deflagration)

IM Signature

- IM Signature of F21 heavyweight torpedo warhead performed IAW STANAG 4439 / AOP-39

STANAG 4439 Requirements		FH	SH	BI	SR	FI-L	FI-H	SCJI
IM Signature	NR							
	V	●		○		○		
	IV		●					●
	III				○		○	
	II							
	I							



Full compliance with STANAG 4439



● : Assessment by Full-scale trial



○ : Assessment by analysis and/or read-across with other configurations

Acknowledgements

DGA



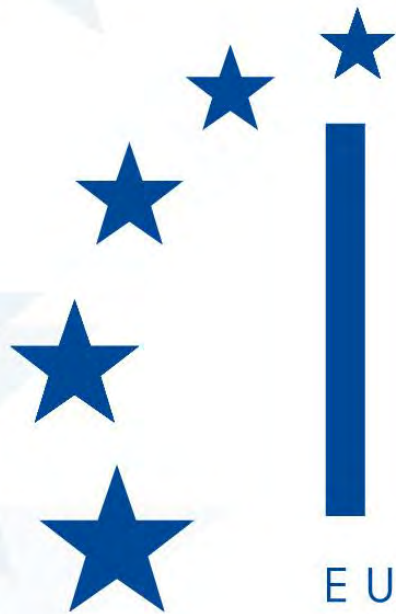
SAAB BOFORS TEST CENTER AB



ARIANE GROUP



Member of



INMEMG
MURAT

EUROPEAN MANUFACTURERS GROUP

20151

Influence of Ageing on the Properties of IHE

Dr. Hendrik Radies, Dr. Almuth Kessler

Introduction

In the last decades, operation areas of NATO partners have drastically changed. The times when ammunition was kept in air-conditioned bunkers for long-term storage until immediately before use are over. In practice, the ammunition is often stored in hot regions and in provisional rooms or containers under various conditions. In some cases, the ammunition may even be exposed to direct sun radiation without any protection. For example, in the next picture fully loaded vehicles and practice shooting in Afganistan are shown:



Figure 1: fully loaded vehicles and practice shooting in Afganistan

Accordingly, ammunition may experience extreme weather conditions and temperature loads. For example, in Kandahar (Afganistan) the typical average temperature in the summer is 86°F (30°C). Maximum temperatures of over 105°F (40°C) are often measured in June.

To assess the possible impact of extreme climate conditions on the ammunition - especially on the explosive charge - lab scale samples of two explosive types were aged and afterwards various investigations were performed with stressed and unstressed samples.

Investigations were carried out with respect to the mechanical properties, the shore A hardness, friction and impact sensitivity and thermal properties. Additionally, GAP tests were performed.

Samples

Three different high explosives used in tank and/or artillery munition were tested. Two of the three main charges are polymer bonded explosives based on RDX with an HTPB-Matrix. The third explosive charge is a TNT based explosive including RDX and NTO called MC-1.

All explosives were qualified as insensitive high explosive according STANAG 4170.

*Dr. Hendrik Radies
Rheinmetall Weapon Ammunition
Heinrich-Ehrhardt-Strasse 2, 29345 Unterluess, Germany
hendrik.radies@rheinmetall.com*

The samples were produced as cylinders, Janaf-samples and other geometries. After production the samples were stored at different temperatures for up to 12 months to simulate ≈ 25 years under depot conditions. The storage temperatures were:

- +21°C, up to 12 months (reference)
- +63°C, up to 12 months
- +71°C, up to 6 months

Parts of the PBX samples were stored packed (no interaction with the environment) and unpacked. The melt cast samples were stored only packed.

Investigations

The investigations were planned in different steps:

1. Determination of the properties of unaged explosives
2. Ageing of explosive samples
3. Determination of the properties of aged explosives
4. Comparison with unaged samples

Results

Change in Geometry

The biggest effects of changing the geometry, the weight and the density, were measured of the unpacked PBX samples.

After 6 months at +71°C a weight loss of nearly 4% was measured. At a temperature of +63°C the maximum weight loss after 12 months was 2.5%. It can be assumed that the weight loss results is due to loss of the plastisizer in the explosive charge. The investigated samples shrunk in the same time up to 2.35% in diameter and 2.1% in length at temperatures of +71°C. The effect was smaller at +63°C.

Because of the loss of weight and dimensions (diameter, length) of the samples showed an increase of the density from 1.66 g/cm³ to 1.71 g/cm³.

Without the possibility of interaction from the sample with the environment, the effect was nearly in the range of the measurement accuracy. In the following table a comparison of the weight loss and the change of the dimension of unpacked and packed PBX samples is shown.

Storage temperature	Storage time	Weight loss		Geometry change			
				Diameter		High	
		unpacked	packed	unpacked	packed	unpacked	packed
[°C]	[months]	[%]	[%]	[%]	[%]	[%]	[%]
+21°C	0	0	0	0	0	0	0
	12	-0,03	0,04	-0,05	0,16	0,04	0,12
+63°C	3	0,55	--	-0,49	--	0,18	--
	4	--	0,02	--	0,05	--	0,28
	6	0,79	--	0,53	--	0,38	--
	9	2,08	--	1,18	--	0,96	--
+71°C	12	2,5	--	1,14	--	1,17	--
	3	3,79	--	1,67	--	2,21	--
	4	--	0,02	--	-0,02	--	0,39
	6	3,88	--	2,35	--	2,13	--

Table 1: Comparison of the weight loss and the change of the dimension of unpacked and packed PBX

The TNT based explosive charges showed no effect concerning the changing of geometry and weight caused by the temperature storage.

Shore A Hardness

Based on the results of the weight loss it is expected that the Shore A hardness increase significantly provided the weight loss is based on the loss of plastisizer.

The results of the unpacked samples showed that the shore A hardness increased extremly at high temperatures. Already after 3 months at 71°C the shore A grew from 65° up to a level outside of the measuring range from maximum 100 Shore A.

In the same time the shore A of the packed PBX sample increased only 16 shore A and achieved the end level of polymerisation of the binder system. With longer storage time no change of the shore A values was detectable.

Because of the high value the measurement of shore A of the melt cast explosive was not possible.

Mechanical Properties

The change of the mechanical properties of the aged samples was tested by using a tensile test and compressive test at different temperatures (-40°C, +21°C, +63°C). The tensile tests were conducted only with the unpacked PBX samples; the compressive tests with packed and unpacked PBX samples as well as the melt cast samples.

The biggest change of the mechanical properties was detected in the unpacked PBX in the tensile and compressive tests. In Figure 2 results of the elongation tests are shown. At 21°C

only small changes were detected. A bigger change was measured after 6 months at 63°. The test samples stored for 3 and 6 months at 71°C as well as the sample stored for 12 months at 63°C were very hard/brittle so that no failure up to the maximum force of 200N of the apparatus was detected.

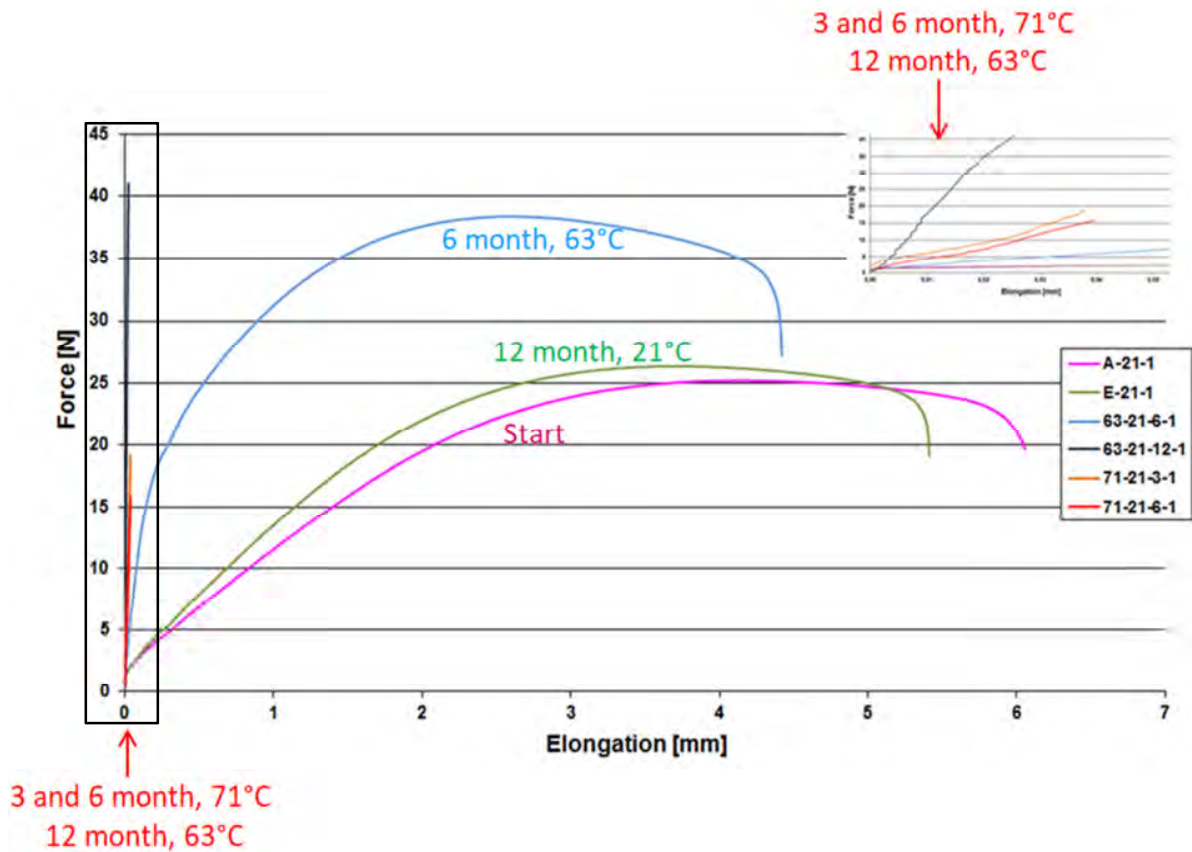


Figure 2: Elongation tests of aged PBX samples (unpacked)

A comparison of compressive tests of packed and unpacked samples is shown in Figure 3. The storage temperature of the samples was 71°C. It was shown that the compression curve of the packed sample at 71°C after 4 months is nearly the curve of the unaged sample. The unpacked sample showed a significant shift to higher forces at failure after 3 months at +71°C. The elastic deformation change is significant, as well. This results showed a drastic change of the mechanical properties when the samples were in contact to the environment.

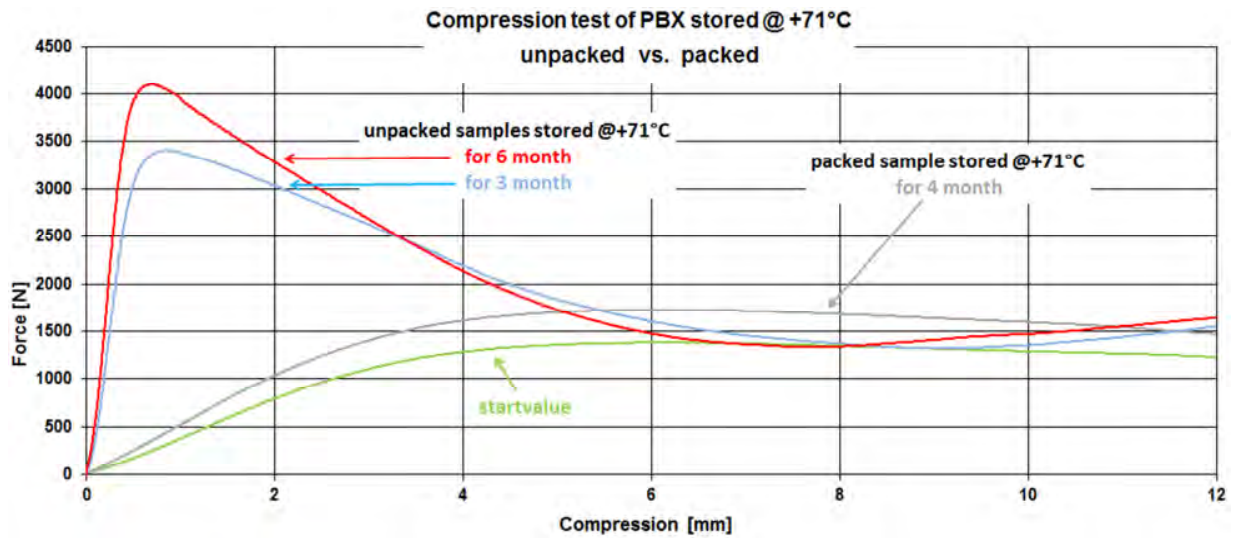


Figure 3: Compressive test of aged PBX samples (storage temperature +71°C packed and unpacked)

The following picture (Figure 4) shows the effect of the ageing process on the PBX samples. The fracture pattern shows a significant disparity between the unpacked and the packed samples.

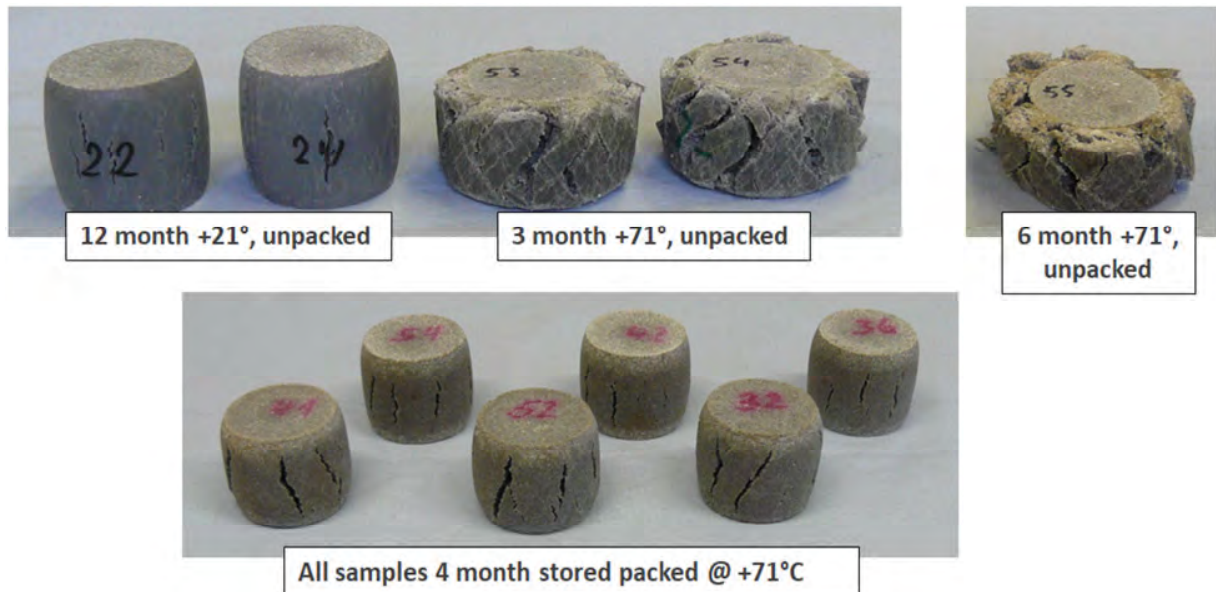


Figure 4: PBX samples after compression tests

The measurement of the melt cast explosive samples shows no influence of storage time and temperature.

Thermal Analysis

The decomposition point of the aged PBX explosive charges were measured. The results showed that the ageing process at different temperatures has no influence on the decomposition point of the samples.

The melt cast explosives were measured using two different methods. The first method was the determination of the melting and decomposition point of the explosives. In this case the results showed no influence of the ageing process on the decomposition point.

In the past, ammunition filled with TNT based explosives were qualified for storage and use up to 51°C. New ammunition shall be safe for storage and use up to 71°C. Under certain circumstances this can lead to problems based on sublimation of the TNT. Long term isothermic measurements with DSC were done under different temperatures (67°C, 71°C, 78°C).

For the measurements a defined surface is needed. Therefore the MC-1 was temporarily melted in a cup with a diameter of 6.2mm \approx 0.3cm² to get a nearly flat surface (see Figure 5).



Figure 5: MC-1 in a DSC cup, left side before melting, right side after melting

In the DSC Plot (Figure 6) a weight loss with temperature is measurable. With higher temperatures the weight loss grew. Based on this results the sublimation rates were calculated. The results are shown in Table 2.

Weight loss	Temperature	Sub Rate
[mg]	[°C]	[ng/cm ² *sec]
0,16	67	8,8
0,6	71	33,1
0,9	78	49,7

Table 2: Sublimation rate at different temperatures

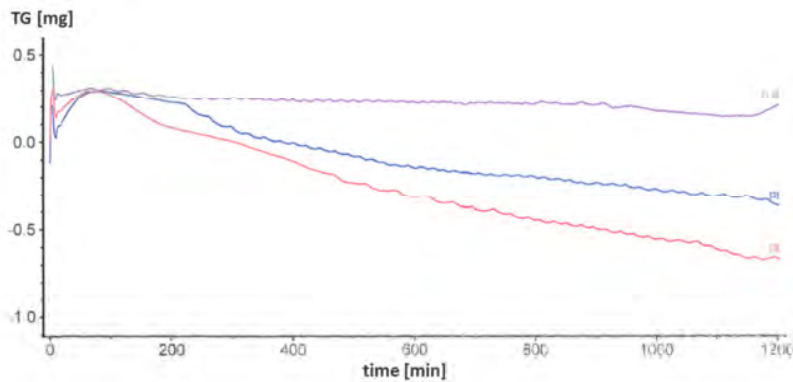


Figure 6: DSC Plot of MC-1 at constant temperature; red 78°C, blue 71°C, violet 67°C

Impact and Friction Sensitivity

Until now only the aged and unpacked samples of the PBX were measured using the BAM drop hammer and the BAM friction sensitivity tester.

The PBX samples which were aged at 63°C up to 12 months showed no influence on the impact sensitivity. But after 6 months at 71°C the impact sensitivity of the aged PBX decrease from 18J to 8J.

Concerning the friction sensitivity, the ageing process has no influence. All results of the impact and friction sensitivity are shown in Table 3.

Storage		Tests	
Temperature	Storage Time	Impact Sensitivity	Friction Sensitivity
[°C]	[month]	[J]	[N]
Start RT	0	18	240
+21°C	12	18	240
+63°C	12	22	240
+71°C	6	8	240

Table 3: Overview of results of friction and impact sensitivity

GAP Test

To test the shock wave sensitivity, various GAP tests were undertaken. For these tests only one PBX type was used. The samples were aged in the PMMA tubes, so that the samples were packed.

The tests were carried out before and after ageing. Freshly produced PBX showed the lowest sensitivity (GAP 8mm). After storage for 4 months at room temperature and under high

temperatures the GAP for no detonation grew to 11mm. No difference in GAP due to storage temperature was measurable. All data are shown Table 4.

Storage		GAP Test	
Temperature	Storage Time	Go	NoGo
[°C]	[month]	[mm PMMA]	[mm PMMA]
Start RT	0	7	8
+21°C	4	9	11
+63°C	4	10	11
+71°C	4	10	11

Table 4: Results of 21mm PMMA GAP test

Up to now, no test with the aged melt cast explosives were done.

Conclusions

Investigations with three different main charges concerning the ageing process were done. Two different RDX based PBX samples and one TNT based melt cast explosive were tested. The samples were stored under different temperatures (21°C (reference), 63°C, 71°C) for up to 12 months. All samples were stored packed, and one PBX sample was stored unpacked.

The results of the PBX samples showed, that the storage conditions (unpacked or packed) have a significant effect on the mechanical properties. The properties of the unpacked samples change extremely (density, weight loss, Shore A, tensile and compressive tests) compared to the packed samples. A difference between the two different PBX types were negligible. The TNT based explosive charge showed no influence on the mechanical properties due to the ageing process.

Measurements using the DSC showed no change of the decomposition point of all samples due to the ageing process. More relevant were the isothermic long term tests with the TNT based explosive. The samples were measured via DSC at constant temperatures of 67°C, 71°C and 78°C for period of 20h. A weight loss due to sublimation of the TNT material was detected. The effect grew with higher temperatures.

The investigated safety tests (friction and impact sensitivity) showed effects of ageing at 71°C of the unpacked PBX samples. At 63°C no effect was measurable. The packed samples were have not been measured yet. The GAP tests were done only with packed PBX samples. Here no negative influence caused by the ageing process was detectible.



Influence of ageing on the properties of IHE

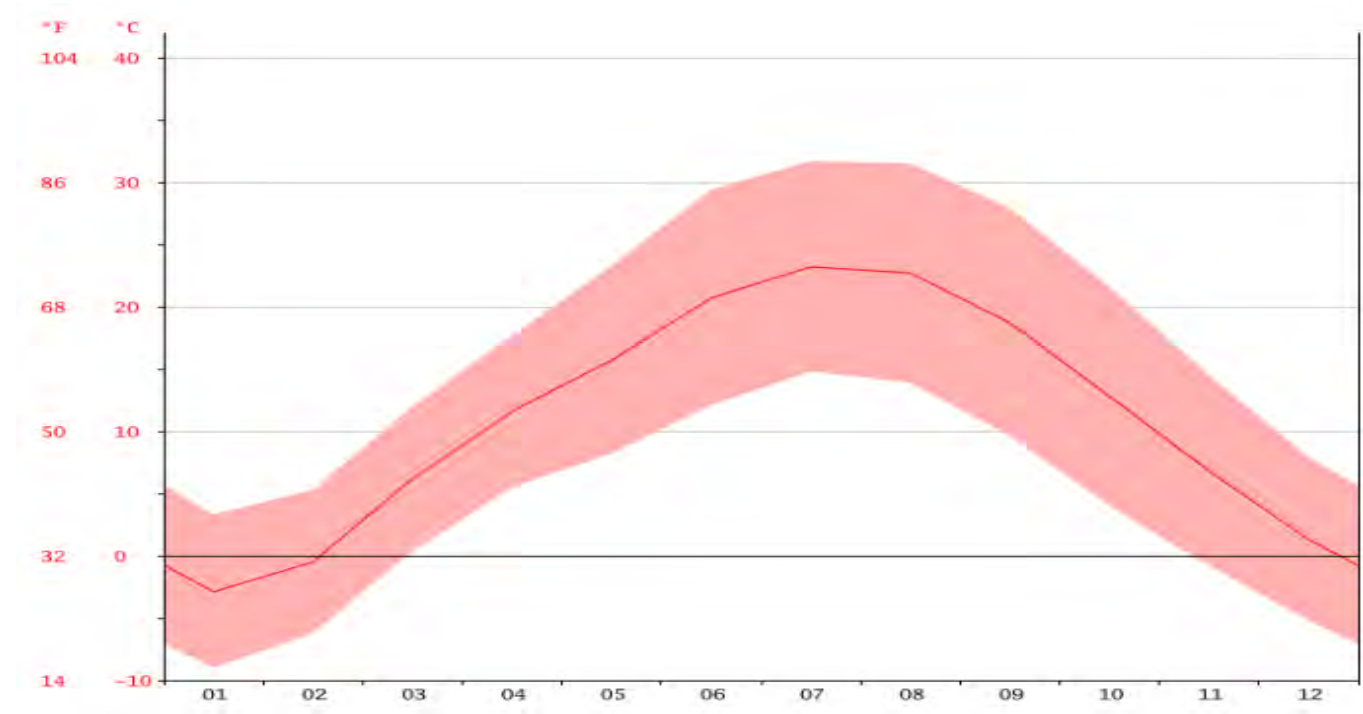
Rheinmetall WM, Development Department, Dr. Hendrik Radies

Motivation

- Modern scenario in NATO countries might be in very hot and also very cold regions
- The storage for ammunition in conflict area is under non-ideal conditions



Camp in Kabul



Temperature diagram Kabul

Motivation

- Handling of ammunition in battle zones is different to normal training
- In duty the unprotected vehicles with all their ammunition might be outside in the sun for some days or weeks



Practice shooting in Afghanistan



Fully loaded vehicles

Motivation

- To minimize risks of the handling of munitions, investigations concerning properties of aged high explosives were done
- Different explosives were prepared, aged and investigated
- The investigations were planned in different steps
 1. Determination of the properties of unaged explosives
 2. Ageing of explosive samples
 3. Determination of the properties of aged explosives
 4. Comparison with unaged samples

Status

- High explosives e.g. the binder system of PBX is subject to an aging process during life time
- Sublimation rate in TNT based explosives is also a part of the ageing process
- Different experiences conc. ageing of high explosives exists
- Different methods are written in literature

Goals

- Gain experience conc. ageing of PBX and additionally melt cast explosive
- Find a successful method for investigation of aged samples

Tested explosives

Three different explosive charges were tested

- Plastic bonded explosive
 - PBX-1 (RDX, Me, HTPB-binder)
 - PBX-2 (RDX, HTPB-binder), investigations partly still in progress
- Melt cast explosive
 - MC-1 (TNT based), investigations partly still in progress

Geometry of samples

- Cylinder 40x40mm, machined
- Janaf samples
- Miscellaneous



Ageing of samples and realized tests

Ageing

Storage at

- +21°C, 12 months (reference)
- +63°C, up to 12 months
- +71°C, up to 6 months

to simulate ≈ 25 years under depot conditions

Because of safety reasons no storage at higher temperatures!

Storage for PBX-1 partly unpacked and partly packed; for PBX-2 and MC-1 only packed

Tests

Change of geometry

Mass lost (loss of plasticizer)

Density

Shore A hardness

Thermal analysis (DSC)

Vacuum stability

IM-Properties

- Impact and Friction sensitivity
- GAP-Test

Mechanical properties

- Tensile testing and compressive testing

Change of geometry

Tested on cylinder (PBX packed and unpacked)

- Diameter
 - Biggest change $\approx 2.4\%$

- Length
 - Biggest change $\approx 2.1\%$

- Weight loss
 - Biggest weight loss $\approx 4\%$

- Density
 - Biggest change $1.66 \rightarrow 1.71 \text{g/cm}^3$

Storage temperature	Storage time	Weight loss		Geometry change			
		unpacked	packed	Diameter		High	
				unpacked	packed	unpacked	packed
[°C]	[months]	[%]	[%]	[%]	[%]	[%]	[%]
+21°C	0	0	0	0	0	0	0
	12	-0,03	0,04	-0,05	0,16	0,04	0,12
	+63°C	3	0,55	--	-0,49	--	0,18
	4	--	0,02	--	0,05	--	0,28
	6	0,79	--	0,53	--	0,38	--
	9	2,08	--	1,18	--	0,96	--
	12	2,5	--	1,14	--	1,17	--
+71°C	3	3,79	--	1,67	--	2,21	--
	4	--	0,02	--	-0,02	--	0,39
	6	3,88	--	2,35	--	2,13	--

Obvious change of geometry and weight in unpacked PBX samples, no influence on packed PBX and melt cast cylinders!

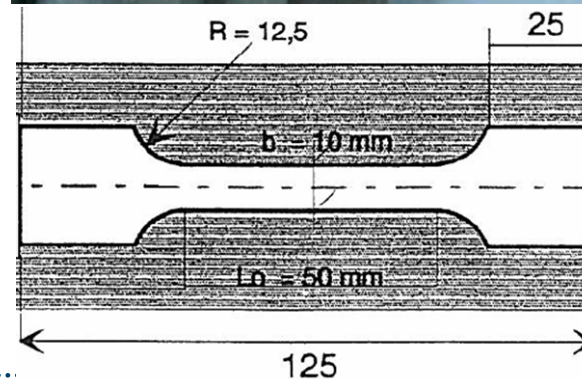
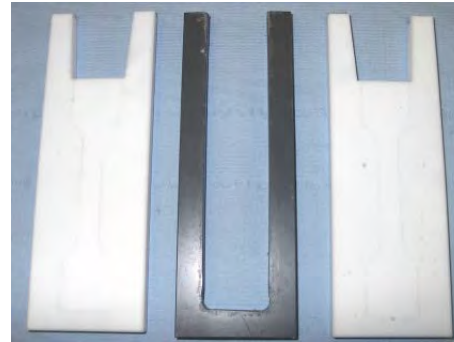
Shore A hardness

- Because of the high Shore A level of MC-1 investigations were only done with PBX
- The Shore A of the PBX sample increased with storage time
 - The changes of the shore A of the packed samples in a range of 15-20 Shore A
 - The Shore A values of the unpacked PBX samples increases so extremely that the values are outside of the measuring range (maximum 100 Shore A, start value 65 Shore A)

Obvious differences between unpacked and packed samples

Tensile Tests on PBX

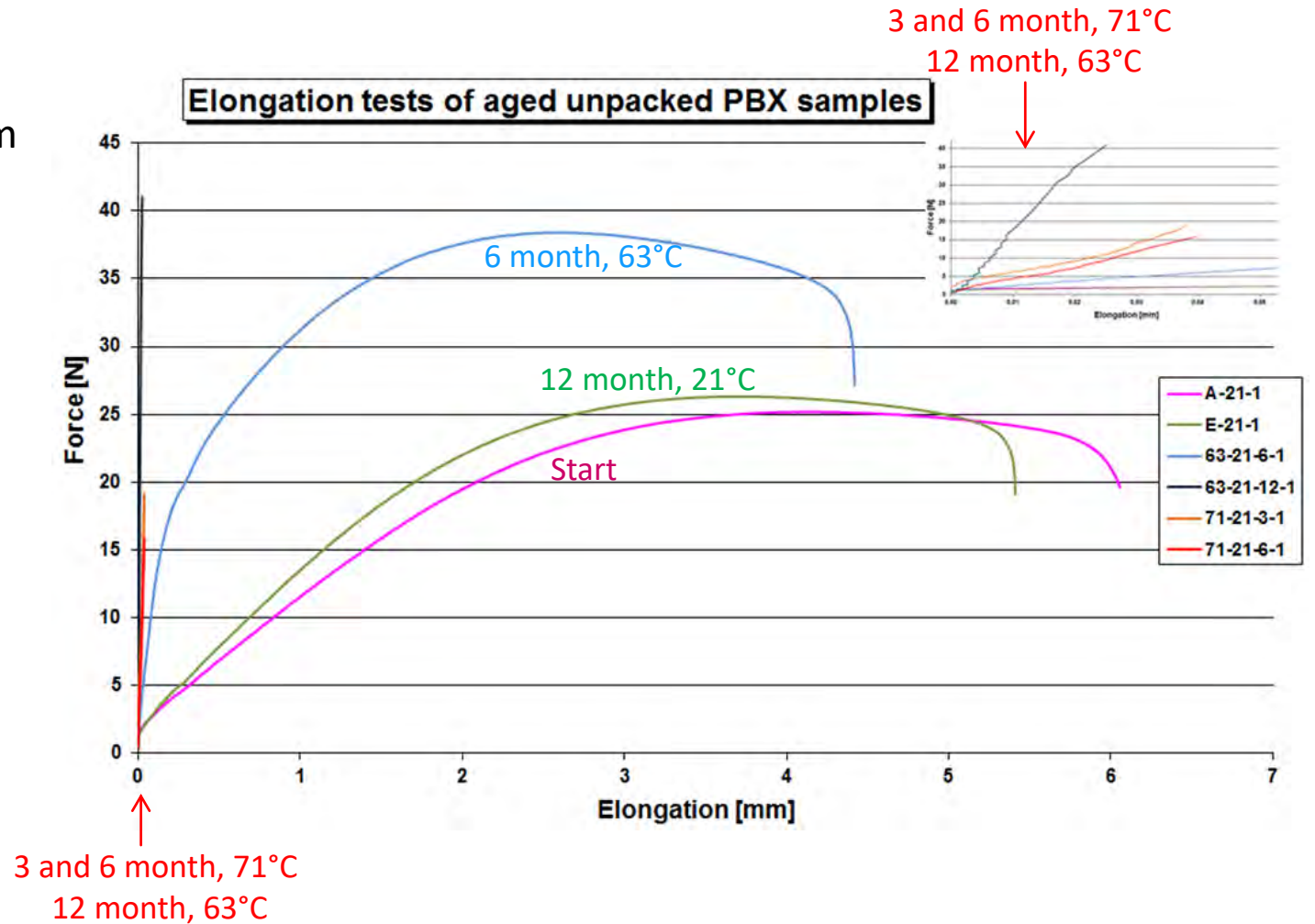
- Testing with unpacked samples
- Measurements in temperature range
- Sample preparation
 - Cast in special mould without machining
 - Cast in „U-Profile“, afterwards cutting
 - Cast as disc, afterwards cutting
 - Cast as bloc, afterwards shaping and cutting



Tensile Tests on PBX

Significant influence of storage conditions

- Storage +71°C => no failure up to force maximum
Samples were very brittle

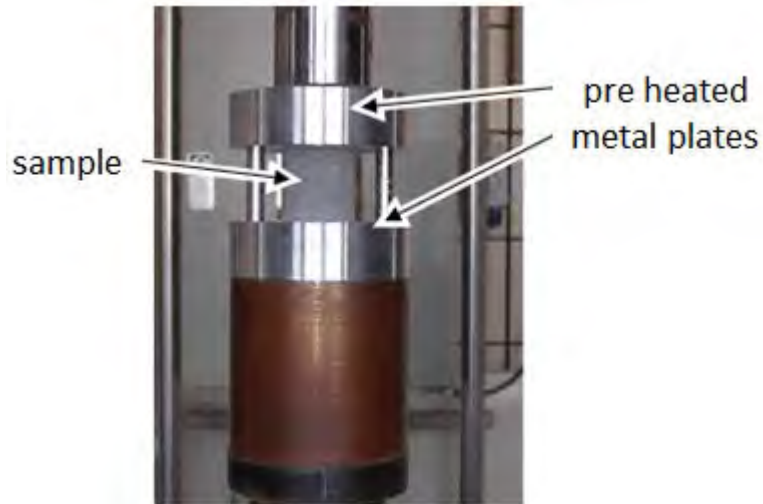


Compressive test

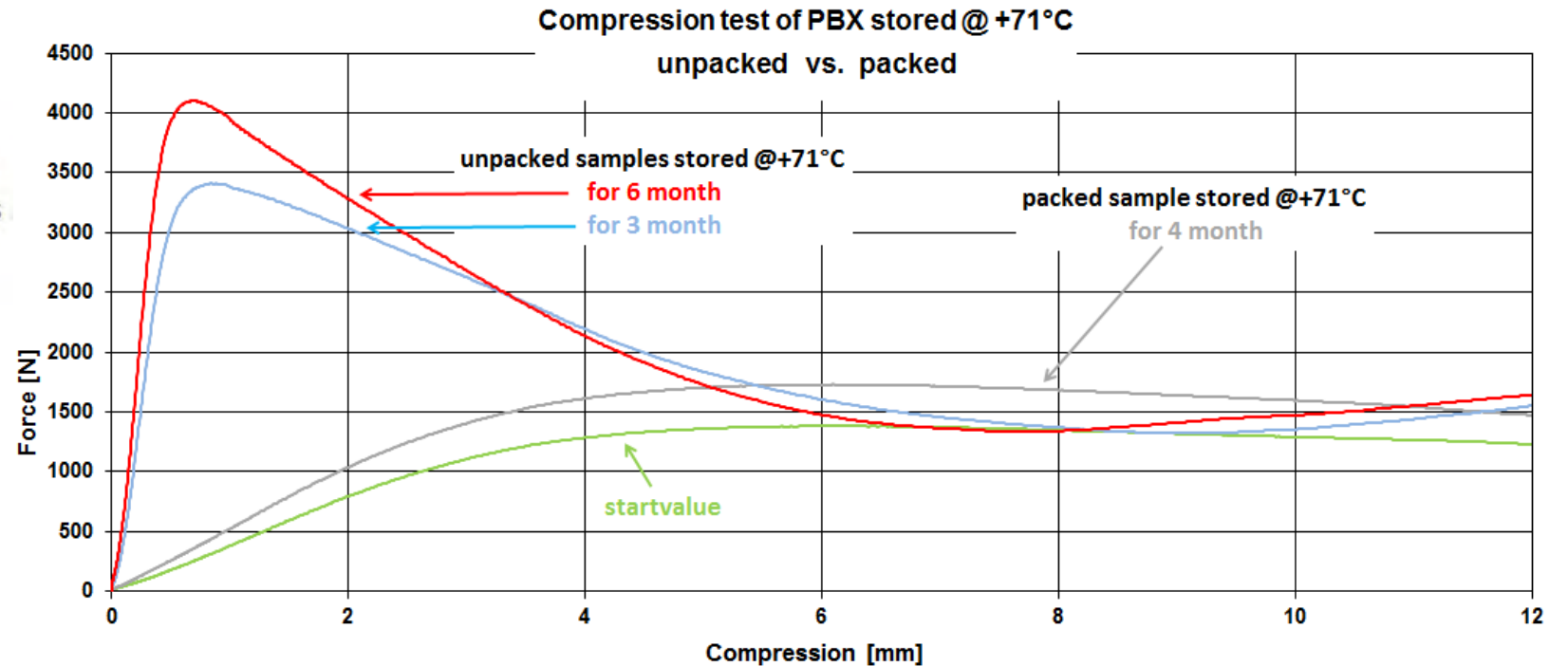
Measurements in temperature range (-46°C, +21°C and +63°C)

Samples: PBX-1 (unpacked and packed), PBX-2, MC-1

PBX-1 shows a significant influence of storage conditions

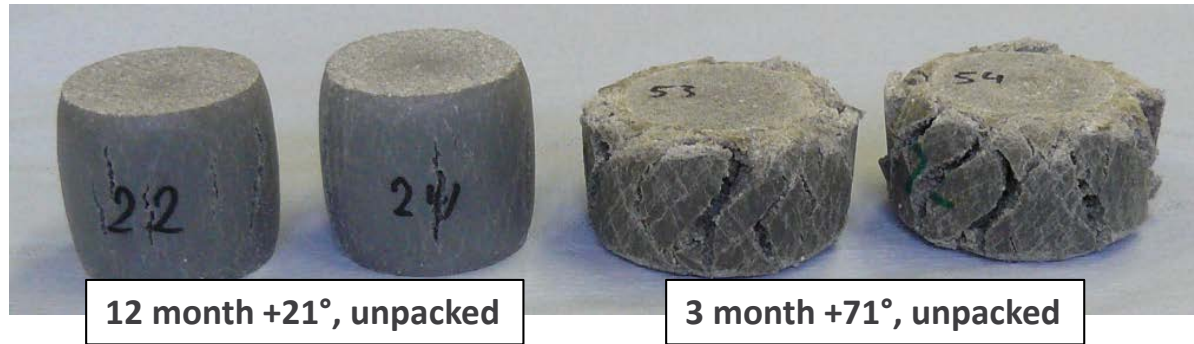


Set up compressive test



Compressive test

Unpacked, @71°C stored PBX cylinder showed significant optical differences after compressive tests

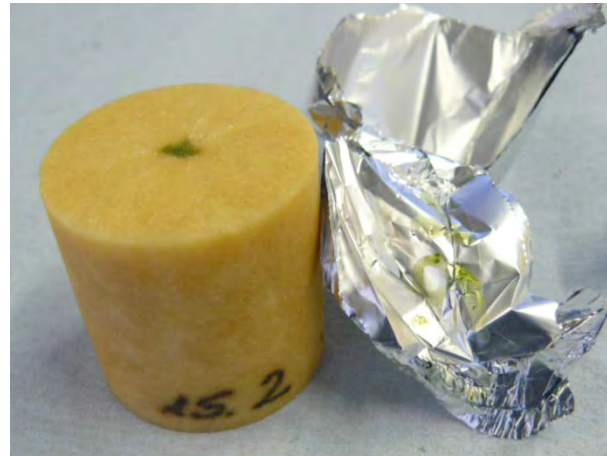


In comparison, packed PBX cylinders were more stable



Compressive test

- Compressive tests of the melt cast explosive shows a significantly different fracture to PBX but no influence of ageing



Vacuum stability

Testing of unpacked and packed stored PBX samples

- Hardly any change on vacuum stability

Storage		Vacuum Stability	
Temperature	Storage Time	unpacked	packed
[°C]	[month]	[cm ³ /2,5g]	[cm ³ /2,5g]
Start RT	0	0,12	0,08
+21°C	12	0,15	0,11
+63°C	3	0,27	0,11
	6	0,11	--
	9	0,26	--
+71°C	12	0,19	--
	3	0,24	--
	4	--	0,16
	6	0,19	--

Currently no measurements of the melt cast explosive are possible

Thermal analysis

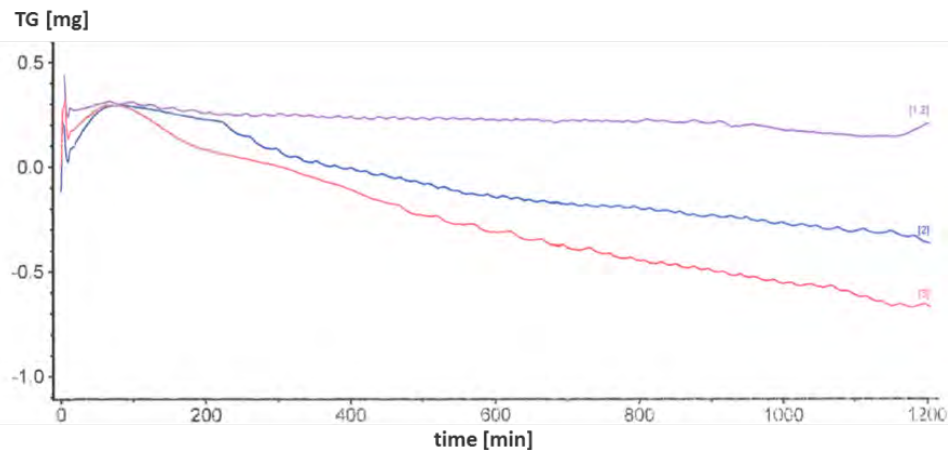
DSC (heat rate 5K/min up to 360°C)

- With PBX samples hardly any influence on decomposition point / weight loss



Sublimation rate with MC-1

- Tests of MC-1 via DTA at isotherm temperatures (67°C, 71°C and 78°C) for determination of sublimation rates*
- Melted MC-1 in a cup with a diameter of 6.2mm \approx 0.302cm² surface



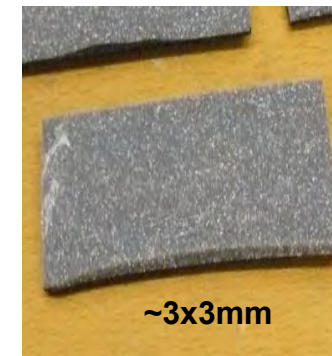
Weight loss [mg]	Temperature [°C]	Sub Rate [ng/cm ² *sec]
0,16	67	8,8
0,6	71	33,1
0,9	78	49,7

IM Properties of Explosive

Testing with unpacked PBX-1 samples

- No influence on friction sensitivity
- ***Important increase of impact sensitivity after storage at +71°C***

Storage		Tests	
Temperature	Storage Time	Impact Sensitivity	Friction Sensitivity
[°C]	[month]	[J]	[N]
Start RT	0	18	240
+21°C	12	18	240
+63°C	12	22	240
+71°C	6	8	240



Measurements of PBX-2 and MC-1 are still in progress

GAP Test

Testing with packed PBX samples

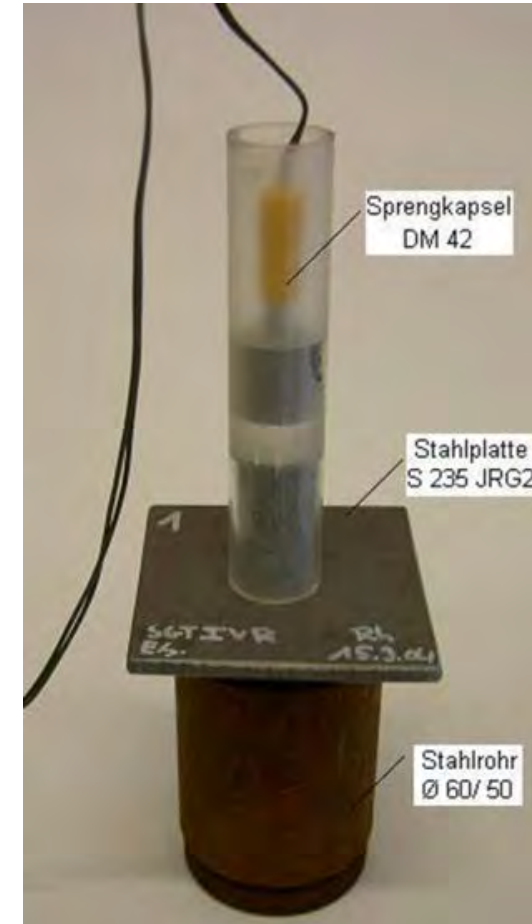
- 21mm GAP Test, GAP: PMMA
- Donor charge: HWC

Storage		GAP Test	
Temperature	Storage Time	Go	NoGo
[°C]	[month]	[mm PMMA]	[mm PMMA]
Start RT	0	7	8
+21°C	3	9	11
+63°C	3	10	11
+71°C	3	10	11

- Only small change during storage
- No influence of storage temperature

No tests with unpacked PBX

Measurements with MC-1 in progress



Conclusion

Important parameters for the PBX:

- Sample conditions (packed and unpacked)
- Storing conditions (+71°C the biggest effects)

No / small change after storage:

- Vacuum stability, thermal analyses, friction sensitivity
- GAP test (packed)

Significant change after storage (unpackaged samples)

- Impact sensitivity, tensile testing, compressive testing, Shore A hardness

Starting with 71°C significant sublimation can be detected

For testing of ageing phenomena of PBX the determination of mechanical properties (Shore A hardness (guide value) and tensile strength resp. compression tests) are favored

Because of the still running tests no final statement of the ageing of the melt cast can be given

FORCE PROTECTION IS OUR MISSION.

Increased impulse of solventless extruded double base rocket propellant by addition of high explosives RDX and FOX-7.

Erik Tunestål

EURENCO Bofors – 691 86 KARLSKOGA, Sweden
e.tunestal@eurenco.com – Phone: +46736683221

1- BACKGROUND

At Björkborn in Karlskoga propellants have been manufactured for more than a century. Thanks to Alfred Nobel's work in nitroglycerine it all started with double base formulations. Over the years several compositions have been developed and we have now passed 1400 serial production recipes.

An area of propellant manufacturing is the extruded solventless double base rocket propellants. These are smokeless propellant grains mainly used in short range systems like shoulder-launched systems, unguided rockets and surface-to-air missiles and rockets. These are propellants with ballistic modifiers which alter the burning characteristics of the propellant, the goal is to have a low pressure exponent around the design pressure of a system. This paper describes work done in the area of broadening the performance and possibilities of using high explosives in rocket propellant formulations to increase the specific impulse.

2- OBJECTIVE

This project's objective was to investigate if increasing the specific impulse in double base propellants by adding high explosives affects other apparent parameters of the propellant. The high explosives evaluated in the project is precipitated FOX-7 with an average crystal size of around 12 microns and RDX with an average crystal size of around 6 microns.

The experimental plan consisted of six tests described in the table below.

	RDX (NSH873)	FOX-7 (about 10 µm)	Specific Impulse (Ns/kg) Expansion 70 to 1 bar
Test nr 1	0	0	2326
Test nr 2	5	0	2335
Test nr 3	10	0	2344
Test nr 4	15	0	2352
Test nr 5	0	5	2335
Test nr 6	0	15	2352

The specific impulse is calculated from internal thermochemical codes. Since each gram of FOX-7 and RDX contains the same molecules the theoretical specific impulse is the same.

3- PREPARATION OF HIGH EXPLOSIVES

This segment describes the manufacturing techniques which Eurenco Bofors has developed for producing small size RDX and FOX-7 products.

3.1- RDX

The RDX crystals of propellant grade are produced in the standard RDX plant at Eurenco Bofors. The process consists of first producing normal hexogen in the plant. This hexogen

together with some NC and additives is dissolved and precipitated through an ejector based process to produce the small size particles. A representative particle size distribution is found in Figure 1. The additives facilitates the incorporation into the propellant formulation. The same method is used to produce the raw material for Eurenco Bofors LOVA-propellant production.

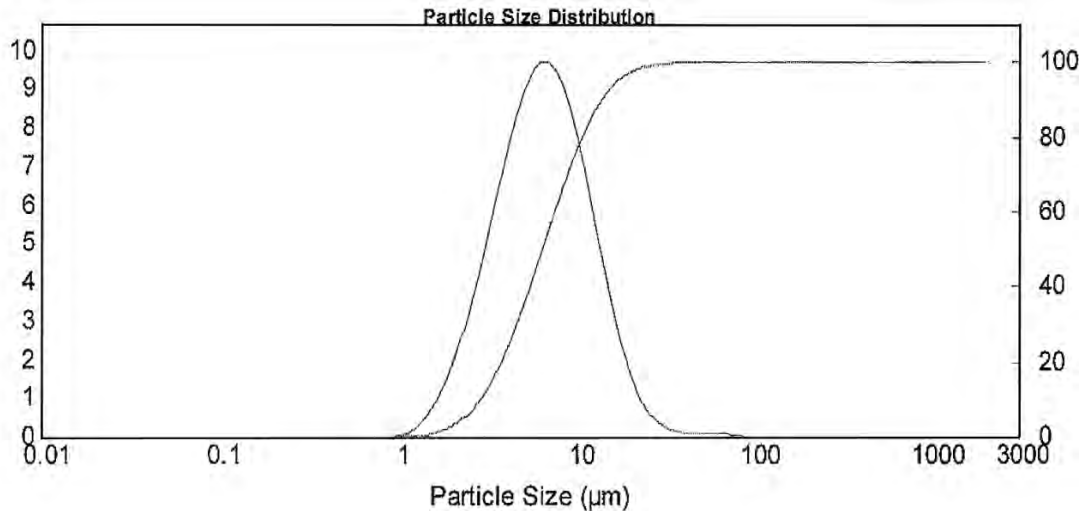


Figure 1 Particle size distribution of RDX, NSH873

3.2- FOX-7

Normal production process has been used to produce FOX7. It has been optimized to produce smaller crystals than normal. Smaller crystals are formed by adapting the process streams in the solvent/ non-solvent process. The main target is to achieve a faster feeding rate in the process. The particle distribution of the batch used is shown in Figure 2. There are several different qualities of FOX-7 in Eurenco's portfolio today, from 30 microns up to 300 microns, the quality now developed has an average particle size of 12 microns. SEM photos from the precipitated "raw" FOX-7 and the re-crystallized new quality is shown in Figure 3 and Figure 4 respectively.

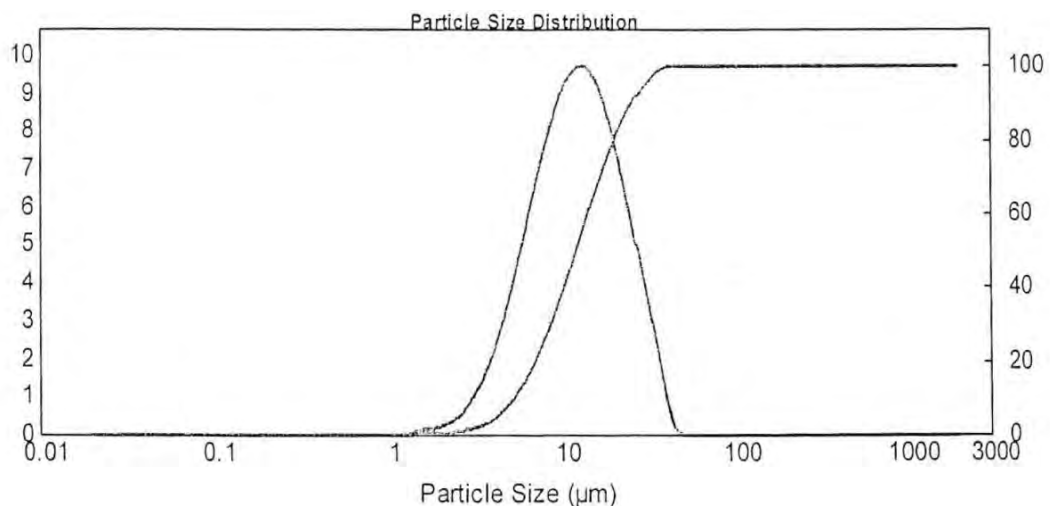


Figure 2 Particle size distribution of the FOX-7 batch used

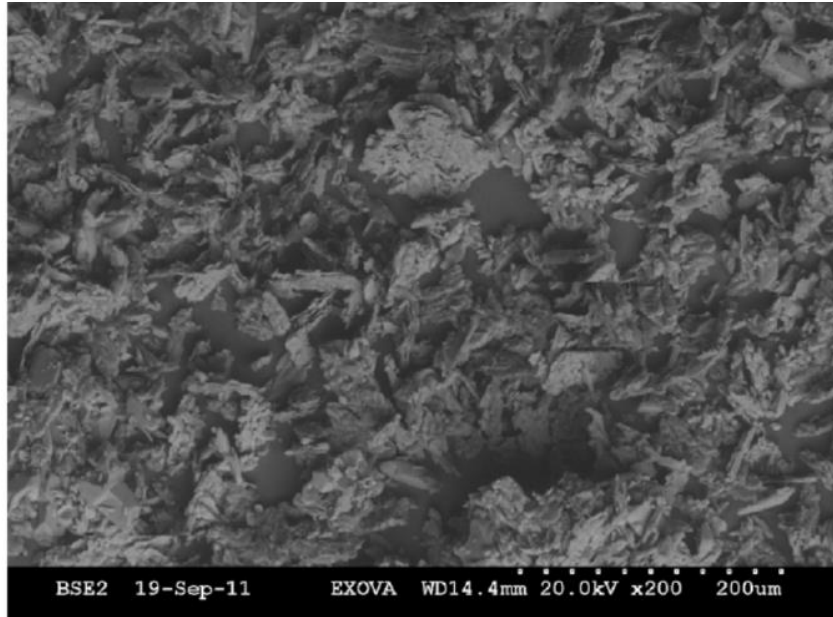


Figure 3 SEM photo of "raw" FOX-7 before re-crystallization.

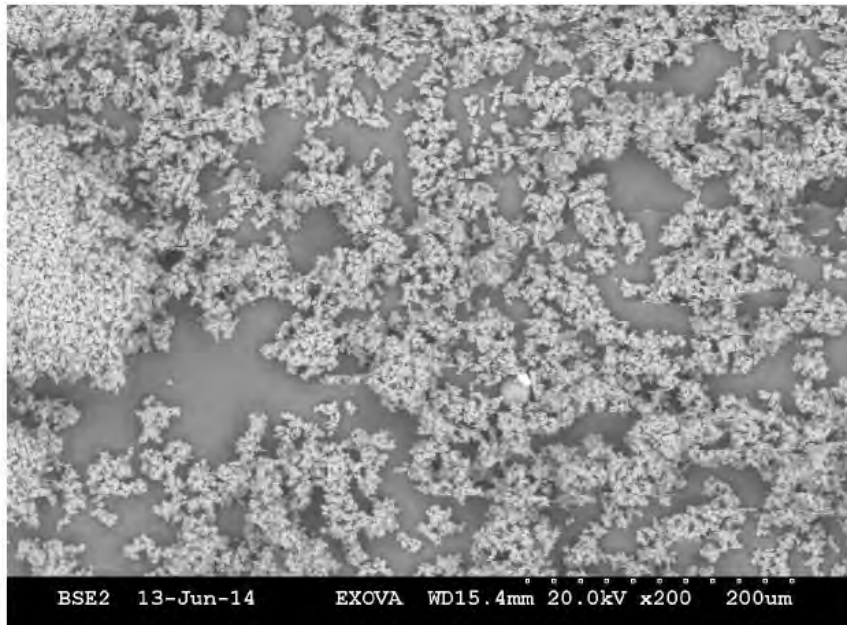


Figure 4 SEM photo of new small crystal size FOX-7 quality, 200x magnification

4- METHODOLOGY

This segment describes the ballistic analysis method and the way the propellant grains were prepared.

4.1- Production process

The production process used at Eurenco Bofors for producing extruded double base propellants is a solventless process described in the flow chart in Figure 5. In the current study the same operations were used but on a smaller scale. A homogenous mix of 100 kg without high explosives was prepared. This minimizes the variation in composition between the different tests. Up until this mixing step the process used is on full production scale.

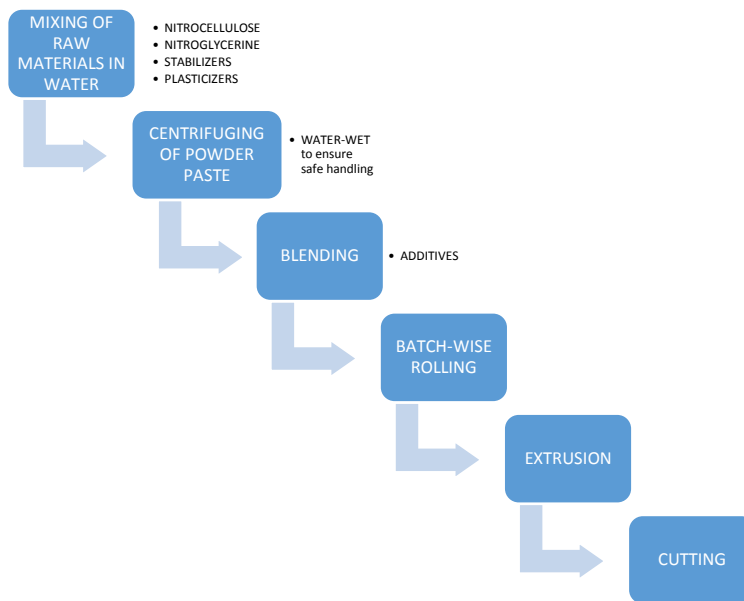


Figure 5 Flow chart of EDB production process

4.2- Composition

The composition which this study has been based upon is a 100% lead-free composition with a high specific impulse over 2300 Ns/kg. For an EDB rocket propellant this is in the upper regions of what can be achieved. This is obtained by having a relatively low additive and plasticizer content, 4.5% and 2% respectively.

The amount of additives in form of ballistic modifiers and processing aids were constant in all experiments. This has been achieved by using two different pre-mixes, with and without additives. 85% of the mix with additives has been used in all experiments.



Figure 6 Paste before and after final step of mixing. Pre-mix with additives (black), pre-mix without additives (white) and FOX-7 (yellow).

4.3- Propellant grains for experiment

A second blending step is required in order to thoroughly mix in the high explosives with the pre-mixed propellant paste. The second blending step is normally not performed in standard production. This final blending is performed in a 10-kg Z-blade mixer, see Figure 6.

The mixed paste is then rolled on differential rollers into a propellant carpet. The rolling is a process where the propellant paste is gelatinized into a plastic-rubber like material. This carpet is rolled into a carpet roll of a suitable diameter for the extrusion.



Figure 7 Photo from the rolling process at Eurenco Bofors.

The final processing step is to extrude the propellant. The carpet rolls are extruded in a ram press into their final shape as hollow cylinders with an outer diameter of 30 mm and inner diameter of 10 mm. They are cut into lengths of 100 mm, the weight of each grains is roughly 100 grams. Some of the grains used in this study is shown in Figure 8.



Figure 8 Photo of extruded propellant grains for ballistic testing

4.4- Ballistic analysis

The method used for the investigation is a standard rocket test which has been used in Eurenco Bofors for several years. In this method the burning rate of a composition is evaluated over a range of pressures. The results produced are the same as it would be generated with a Crawford Strand Burner. The design should resemble a rocket motor and has an exchangeable nozzle, the setup has been described more in detail in a previous conference (Tunestål, o.a., 2015).

The mock-up motors and propellant grains are conditioned for at least 12 hours in their respective temperature before firing.

The data output from this setup is a pressure time curve and the dimensions of the propellant grains are measured. The grains are measured manually with a calibrated caliper.

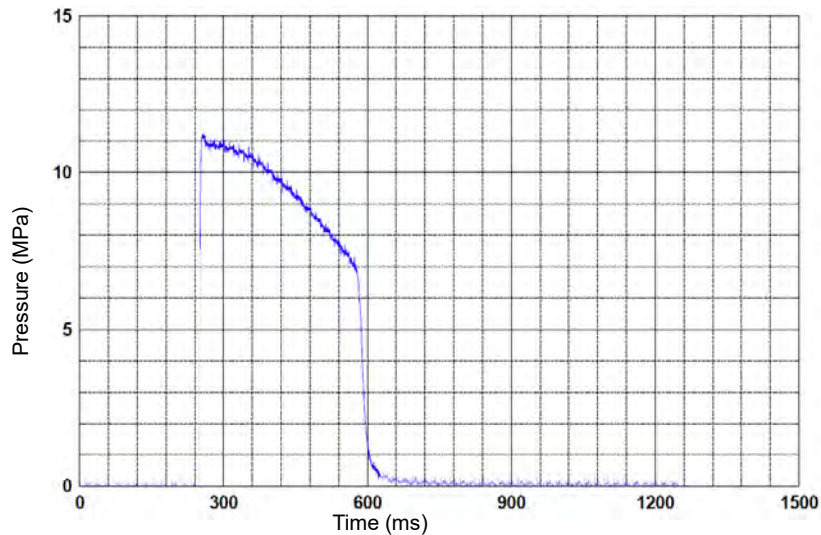


Figure 9 Representative result from a standard rocket firing

From the pressure-time curve and the dimension the burn rate at different pressures can be calculated. The results are normally presented as burn rate as a function of pressure or as a function of the ratio between propellant surface area and nozzle area.

5- RESULTS

This paragraph describes and discusses the results from the ballistic tests. The first part is regarding the base composition and the second and third subparagraphs discuss the RDX and FOX-7 enriched respectively. In this segment terminology from (Kubota, Ohlemiller, Caveny, & Summerfield, 1973) is used. The concept producing the catalytic effect in rocket propellant combustion is called super-rate burning. This occurs when the reaction rate in the fizz zone is increased.

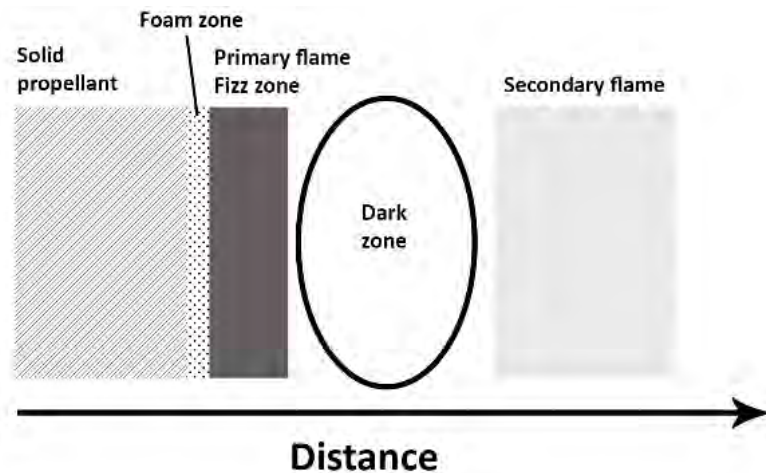


Figure 10 Description of the zones in propellant combustion

5.1- Base composition

The base composition has a relatively low amount of additives and a high energy content. This combination results in a composition which has smaller super-rate burning than what is characterizing an EDB rocket propellant. With an EDB composition you usually have a pressure region where the burn rate is constant (plateau burning) or even negative correlation (mesa burning) (Kubota, Ohlemiller, Caveny, & Summerfield, 1973). Comparing with other lead free compositions this composition shows less super-rate burning, see Figure 12. The same additive mixture used in the current formulation has also been used in another

propellant with a lower specific impulse, see Figure 11. In that formulation the specific impulse is around 2170 Ns/kg compared to 2330 Ns/kg for the current and the energy content is 870 cal/g and 1100 cal/g respectively. The composition with a lower energy content generates a very nice super-rate burning and exhibits a plateau and mesa burning between 10 and 20 MPa.

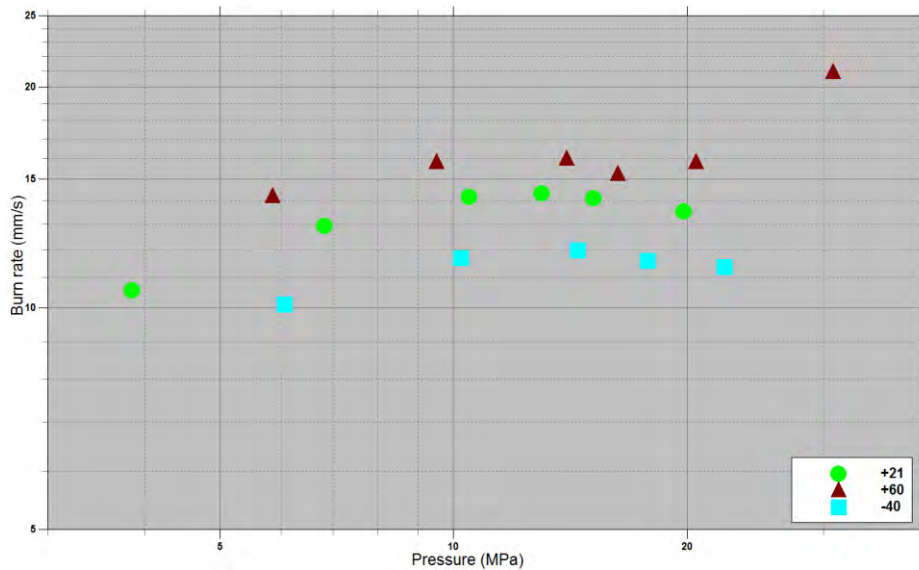


Figure 11 Burn rate results from lead-free propellant composition with 870 cal/g

For the current base composition there is not this pronounced behavior despite using the same mixture of additives. Though a plateau burning can be seen in the firings at -40°C from 12 to 16 MPa. At $+21^{\circ}\text{C}$ the pressure exponent is 0.297 using a curve fit to Vieille's law which is normally used to describe the pressure-burn rate relationship in propulsion technology (Kulkarni & Sharma, 1998).

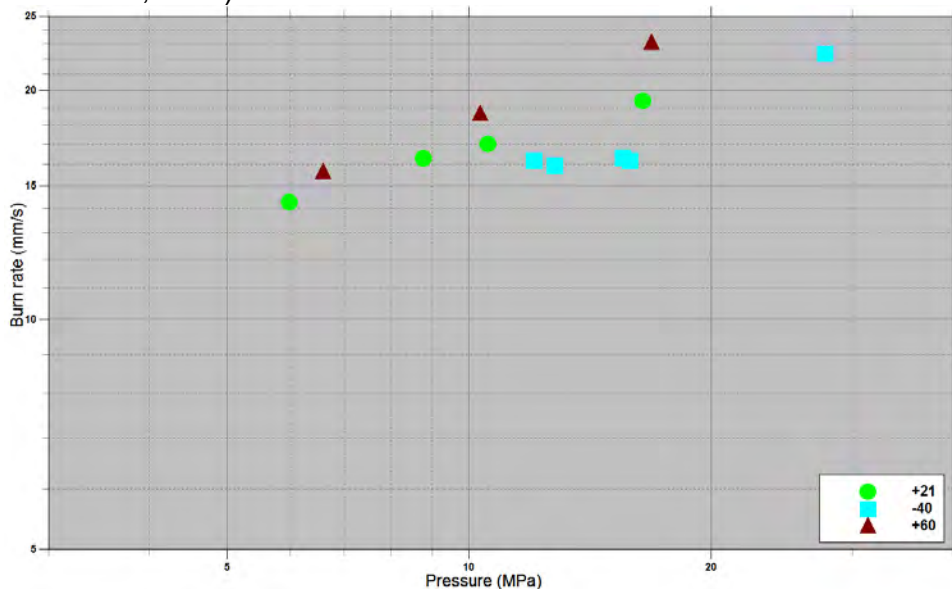


Figure 12 Burn rate results from lead-free propellant composition with 1100 cal/g

5.2- RDX enriched propellant

The addition of RDX into double base gun propellants is known to decrease the burn rate of the propellant. A theory to explain this is that the reaction rate in the fizz zone is decreased, due to becoming fuel rich when RDX is added to the composition (Yano & Gomi, 1986). The reactions in the fizz zone is also believed to be the cause of super-rate burning (Kubota,

Ohlemiller, Caveny, & Summerfield, 1973) of catalyzed rocket propellants. In this study the lowered burn rate associated with RDX addition is confirmed also for catalyzed rocket propellants. The burn rate is lowered over the entire pressure region but the pressure exponent remains constant. However the changed reactions in the fizz zone does not affect the super-rate burning. The effect of adding RDX seems to diminish with content. From 0 to 10% RDX-content the burn rate is reduced by 2% per percent of RDX but only 1% per percent of RDX with higher content.

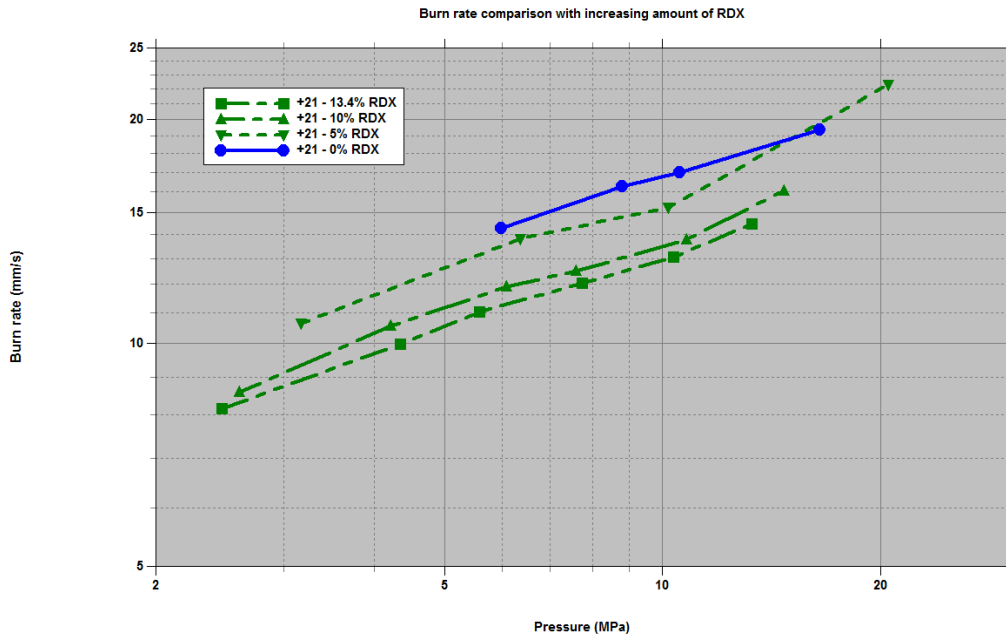


Figure 13 Burn rate with different amount of RDX content

When looking at the pressure exponent the test sample with 13.4% of RDX content has roughly the same slope as the nominal sample. When looking into details the average slope of all points at +21°C has an exponent of 0.330 and there is a pressure range from 5 to 10 MPa where it is a bit lower, 0.277. This should be compared to 0.297 for the entire test range for the nominal composition.

5.3- FOX-7 enriched propellant

No studies investigating burn rate when adding FOX-7 to propellant formulation has been found, but from the similar behavior of the molecules RDX and FOX-7 the hypothesis was that it would also decrease the burn rate. The results however show that the burn rate is not affected by the addition of FOX-7. A slight decrease can be noticed in the results for the 5%-sample but for the 15%-sample there is no difference. The results from the 5%-sample could be explained by experimental deviations.

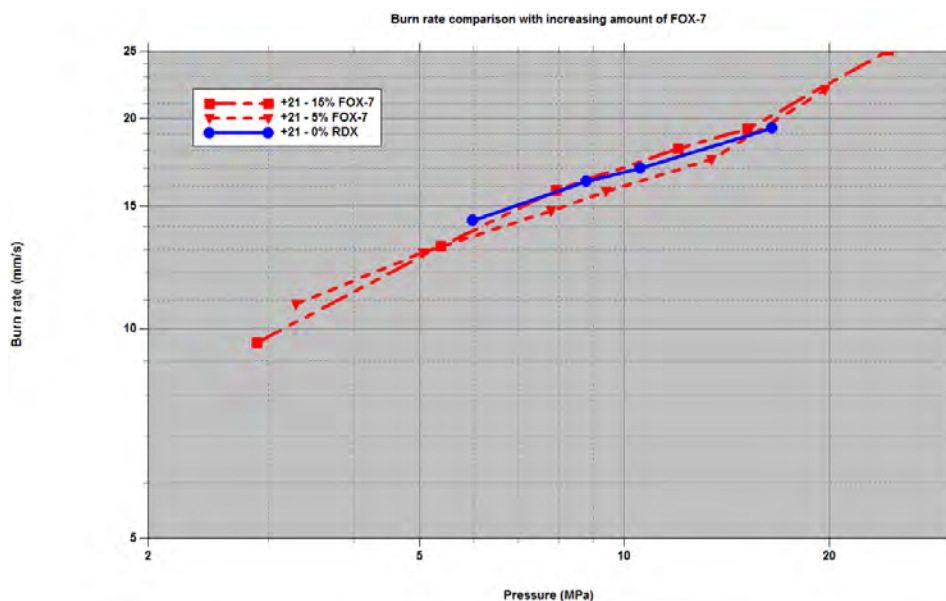


Figure 14 Burn rate with different amount of FOX-7 content

When looking at the pressure exponents for the test samples with FOX-7 there is overall a higher slope over the entire pressure range compared to the nominal, 0.431 compared to 0.297. But the evaluated pressure range is also much wider for the sample with FOX-7. The pressure exponent in the similar pressure region is 0.315 which is very close to the nominal.

6- DISCUSSION AND CONCLUSIONS

The significant difference between the FOX-7 and RDX behavior is not obvious to explain. The contents mentioned are weight-based which means that it is roughly the same amount of carbon, nitrogen, hydrogen and oxygen in the samples. This should result in the fizz zone chemistry remaining the same, the effect which is thought to cause the effect of decreased burn rate for RDX-propellant. The effects seen at +21°C also seems to be true for the samples evaluated at +60°C and -40°C since there is no significant difference in temperature coefficient for the tested samples.

The conclusion from these experiments are that you could indeed add high explosives to a propellant formulation in order to increase the specific impulse. The processing is not affected by the addition. When adding RDX the burn rate is decreased which could be used as a design parameter in order to reduce burn rate and still increase the specific impulse. In contrast FOX-7 does not seem to alter the burn rate which means it could be added to only increase the specific impulse.

REFERENCES

- Kubota, N., Ohlemiller, T. J., Caveny, L. H., & Summerfield, M. (1973). *The mechanism of super-rate burning of catalyzed double base propellants*. New Jersey: Princeton University.
- Kulkarni, A., & Sharma, K. (1998). Burn Rate Modelling fo Solid Rocket Propellants. *Defence Science Journal, Vol 48*, 119-123.
- Tunestål, E., Hafstrand, A., Lindborg, A., Krumlinde, P., Ek, S., Goede, P., & Schragen, C. (2015). New stabilizers for NC-propellants Evaluated in Rocket Propellants. *IMEMTS 2015 Rome, Italy*.
- Yano, Y., & Gomi, T. (1986). Burning Rate Characteristics of RDX-CMDB Propellants. *Journal of the Japan Society for Aeronautical and Space Sciences, 34*, 447-452. doi:10.2322/jjsass1969.34.447



INCREASED IMPULSE OF SOLVENTLESS EDB ROCKET PROPELLANT

- by addition of high explosives
RDX and FOX-7

www.eurenco.com

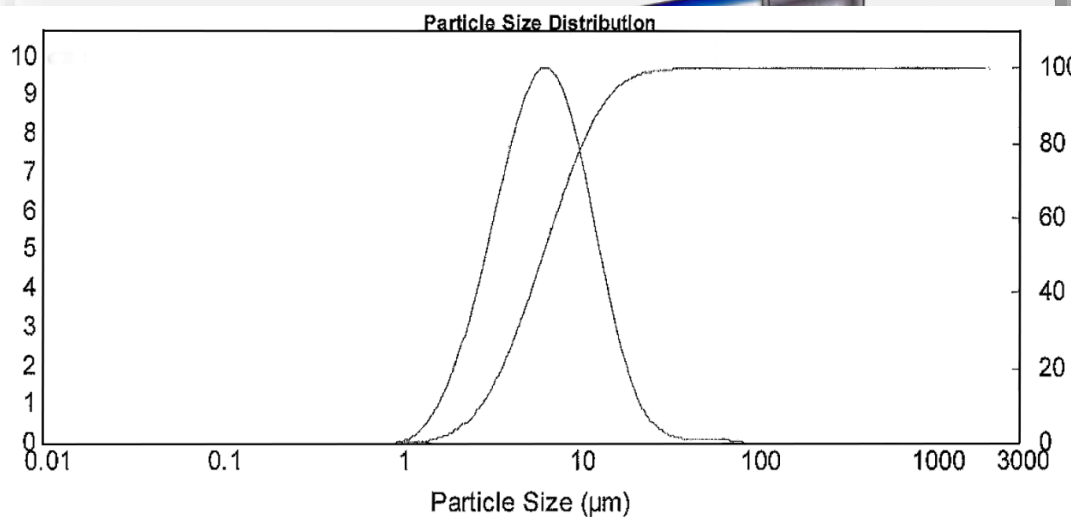
Objective

- Test addition of high explosives
 - Small size RDX and FOX-7

	RDX About 6 microns	FOX-7 About 12 microns	Specific Impulse (Ns/kg) Expansion 70 to 1 bar
Test no 1	0	0	2326
Test no 2	5	0	2335
Test no 3	10	0	2344
Test no 4	15	0	2352
Test no 5	0	5	2335
Test no 6	0	15	2352

RDX - Hexogen

- Propellant grade RDX
 - Particle size around 5 microns
 - Normal hexogen together with NC and additives
 - Precipitated with an ejector process



extremely high level of safety in handling.

Suction filter

FOX-7 - DADNE

- "Propellant grade" FOX-7
 - Particle size around 10 microns
 - Optimized parameters to produce smaller particles
 - > **Faster feeding rates**
 - Less sensitive

ERL drop hammer FOX-7

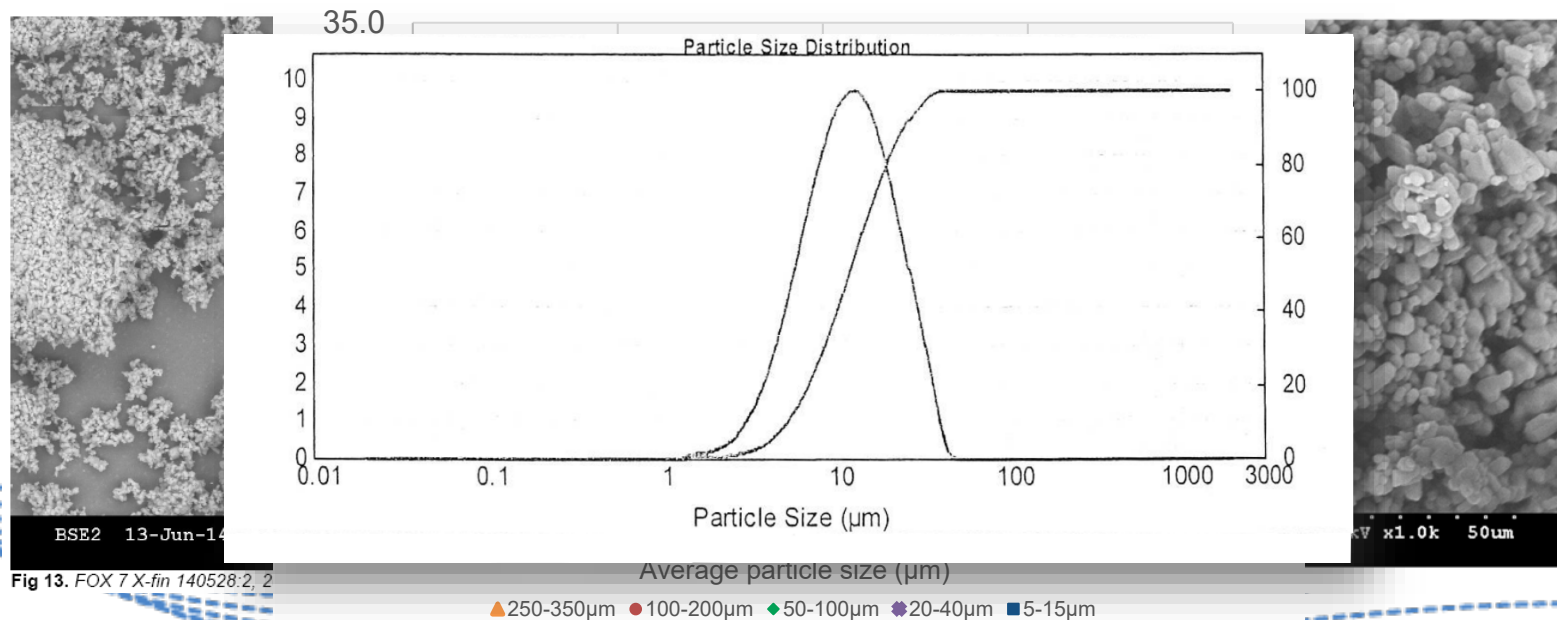


Fig 13. FOX 7 X-fin 140528:2, 2

FOX-7 - DADNE

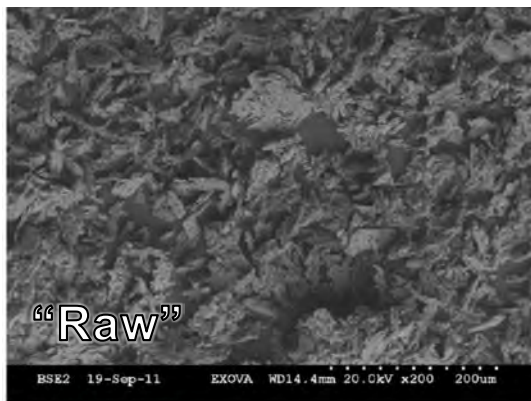


Fig. 2. Fox 7 rå 0124176. 200x.



Fig 13. FOX 7 X-fin 140528.2, 200x magnification.

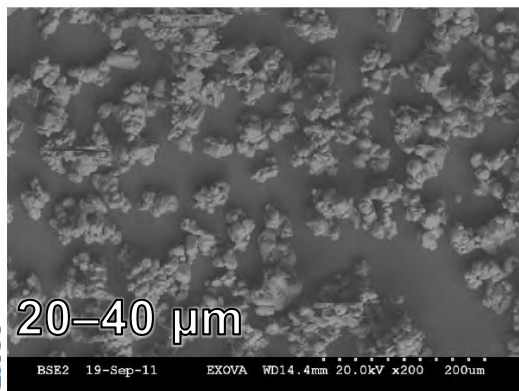


Fig. 5. NSF 110 10003. 200x.

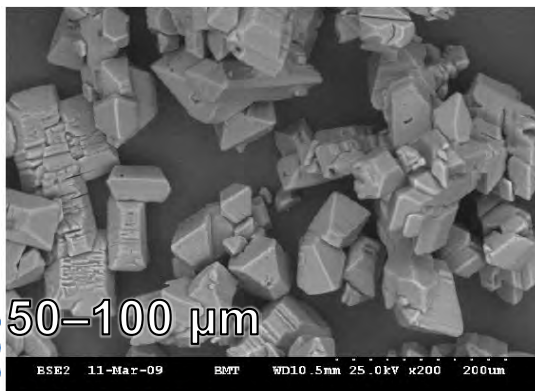


Fig. 12. FOX 7 NSF 120 0646299 (200x).

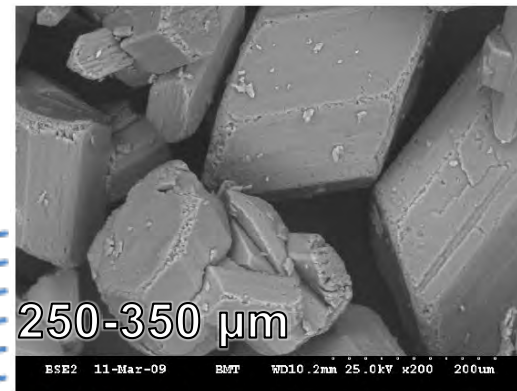
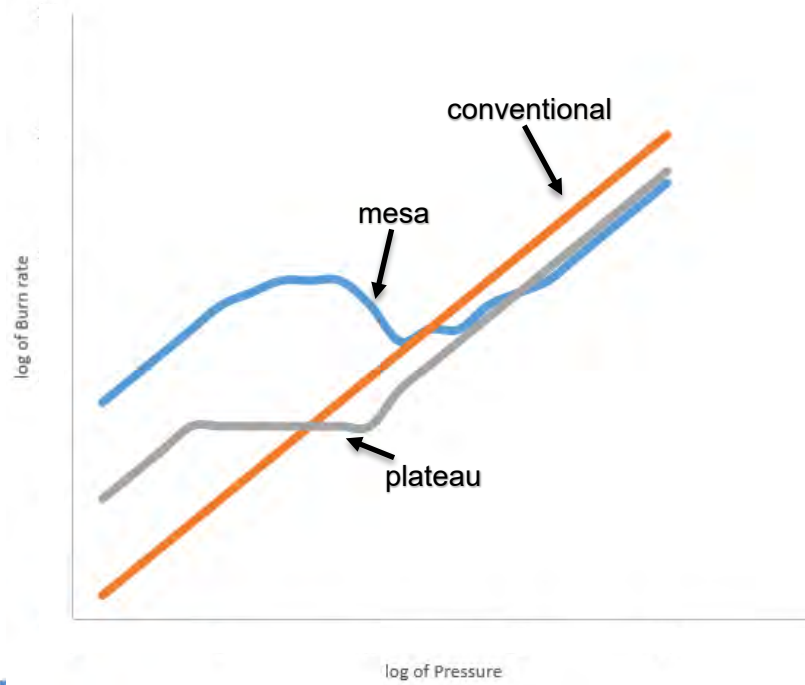


Fig. 20. FOX 7 NSF 140 0807038 (200x).

Combustion theory

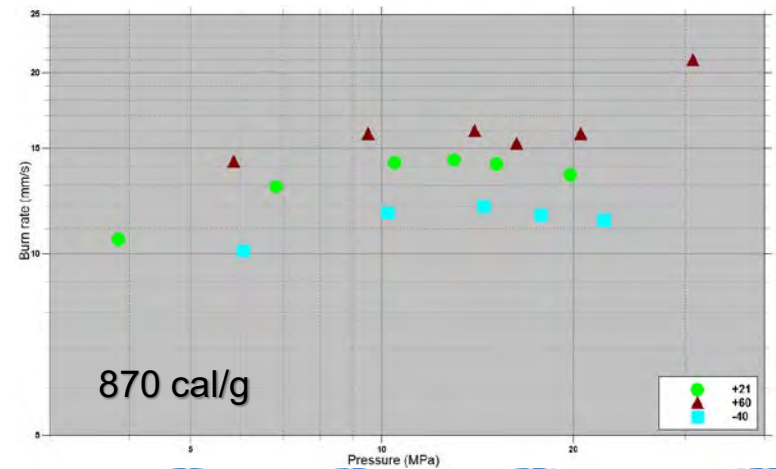
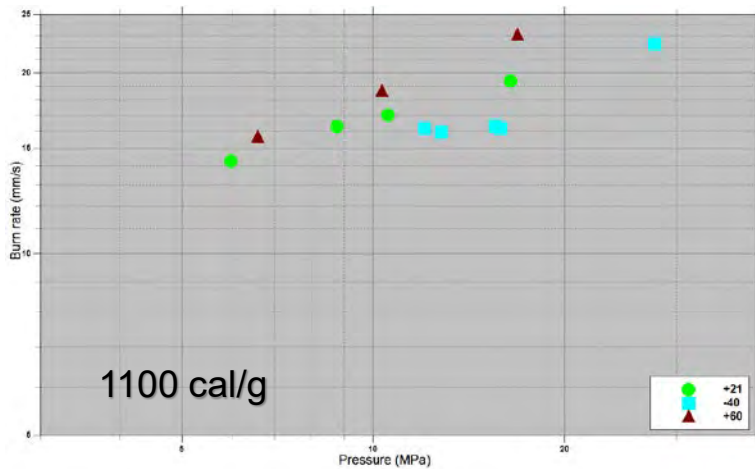
- Super-rate burning

$$r = a * P^n$$



Lead-free base composition

- High energy content (1100 cal/g)
 - Low super-rate burning
 - > **No plateau effect ($n = 0.297$ at +21°C)**
 - Same additive mix – different behaviour



Sample preparation

Pre-mixed propellant with additives

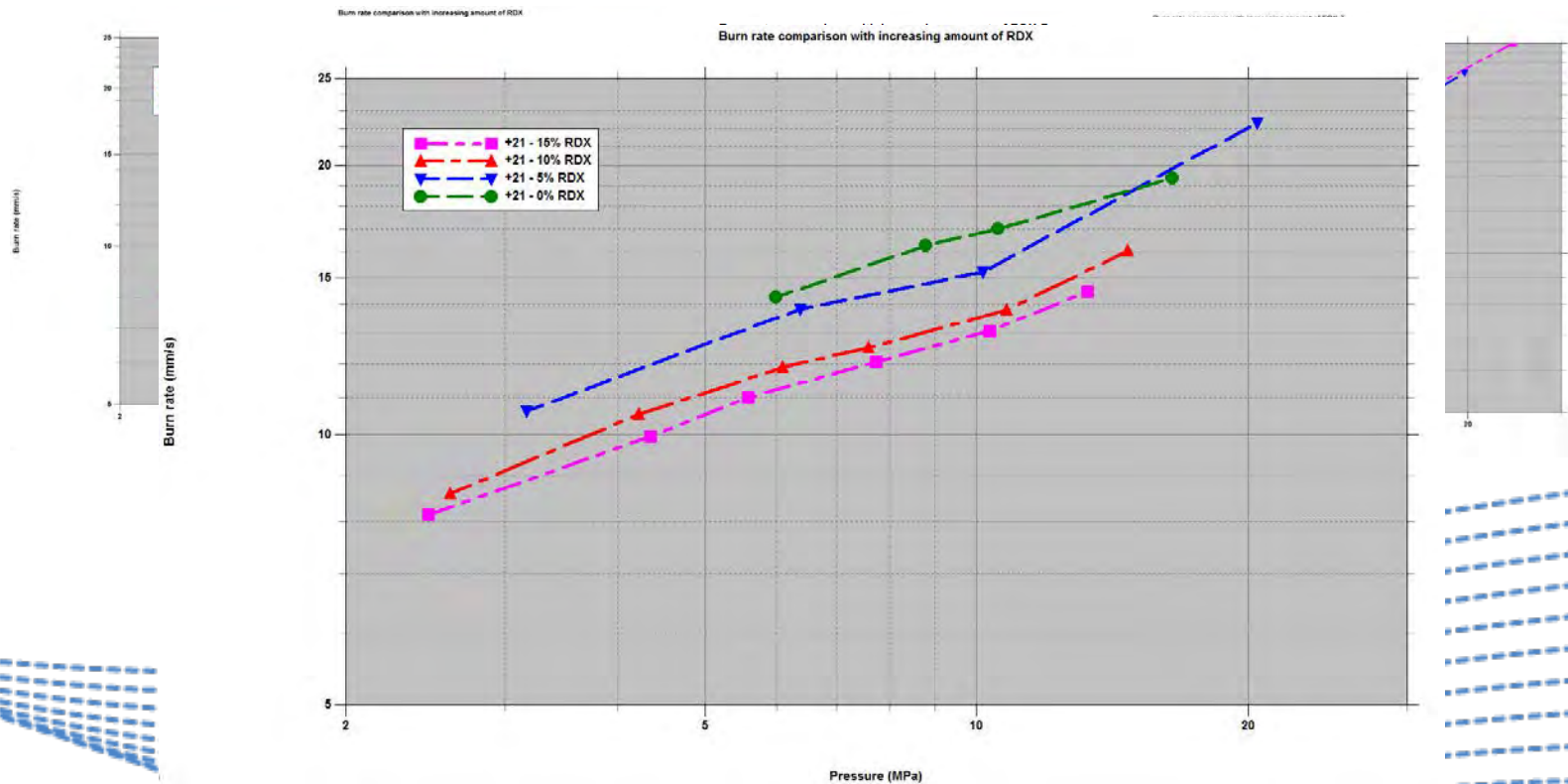
Second blending with high explosive addition

Propellant extruded into hollow cylinders and fired in mock-up motors



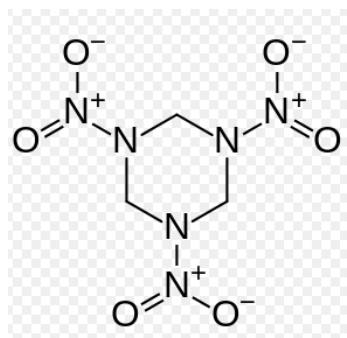
Results

Burn-rates at +21°C

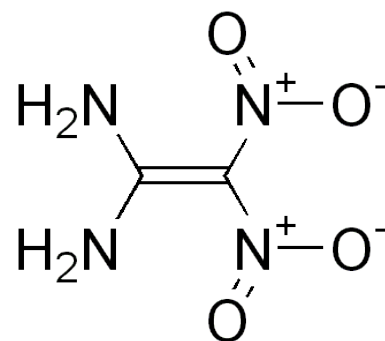


Results

Same



$C_3H_6N_6O_6$
MW = 222,12 g/mol



$C_2H_4N_4O_4$
MW = 148,08 g/mol

Conclusions

- Reduce gap to composite propellants.
- Reduce energetic plasticizers
- Complement burn rate modifiers

Further work

- Analyze non-ballistic effect on propellant
 - Glass transition
 - Mechanical properties
 - IM-signature



EUROPEAN LEADER IN ENERGETIC MATERIALS

Thank you for listening!

www.eurenco.com

QUALIFICATION OF MALLEABLE PLASTIC EXPLOSIVE HEXOMAX AND ITS APPLICATION IN A FLEXIBLE LINEAR SHAPED CHARGE SYSTEM

(1) C. SONGY, M. EL OTHMANI

(2) D. VINCI

(1) EURENCO, 1928 route d'Avignon, CS 90109 Sorgues- 84275 VEDENE, France

c.songy@eurenco.com – Phone : +33633472448

(2) SUPRAMECA SAS, Zone Portuaire Brégaillon, 663 avenue de la 1^{ère} armée française, 83500 LA SEYNE SUR MER, France

dominique.vinci@suprameca.com – Phone : +33620832608

ABSTRACT

Based on his know-how on cast-cure compositions, EURENCO developed several years ago a new generation of malleable plastic explosive blocks, called Hexomax [1]. Since 2014 the product has further been improved to meet the highest levels of requirements of Armies in term of performances, safety and malleability, and the French Army qualified Hexomax in 2016.

Thanks to its constant properties on the large range of temperatures recognized by the French Forces, Hexomax has been recently qualified by the French Army in the system Supraflex, a flexible linear shaped charge, designed and supplied by SUPRAMECA. Moreover, the preliminary test results, performed with Hexomax blocks combined with the specifically designed logistical box, demonstrated that a type VI reaction against the sympathetic reaction is achievable.

This paper presents available results in term of characteristics, performances and vulnerability of this improved Hexomax in tactical and logistical configurations.

INTRODUCTION

As leader in energetic materials, EURENCO develops and supplies IM solutions, from IM high explosive (HE) compositions to cast-cure compositions.

Based on its know-how on the cast-cure technology, EURENCO developed 10 years ago a new plastic explosive, containing RDX and an inert binder, in order to replace the previous PETN based plastic explosive known as PLASTRITE. Hexomax fulfills the Montreal Convention requirements. The development strategy was presented in 2012 at IMEMTS symposium in Las Vegas.

Since then, continuous works have been performed to further improve the material so that it now meets the highest requirements for military use in hot and cold countries.

Hexomax has been selected and qualified by the French Ministry of Defense to equip the French Forces. The Ministry of Defense has even extended the range of qualification of the product: Hexomax is now qualified to be used as the main explosive charge in the flexible linear shaped system Supraflex which is supplied by the French company SUPRAMECA, expert in designing and supplying shaped charges and breaching systems.

Latest results obtained with improved Hexomax will be presented in this paper.

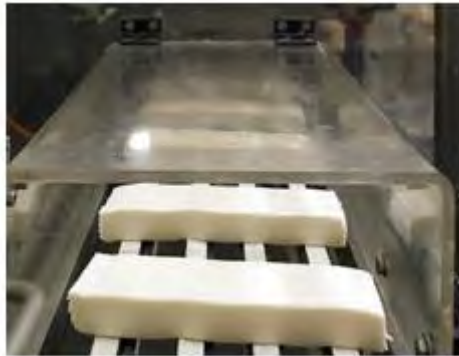
First, the properties of this plastic explosive, in term of performances, malleability and insensitivity will be described, as well as the effect of ageing. Regarding IM tests, preliminary tests undertaken with Hexomax blocks combined with the specifically designed logistical box Supracase, designed by SUPRAMECA, to reduce the sympathetic reaction between blocks, will be especially outlined. Moreover, environment tests performed on the product will be described. Then, the main performance results of the system Supraflex with Hexomax will be presented.

[1] *A new generation of malleable plastic explosive blocks, B. Mahé, IMEMTS, 2012*

1. PROPERTIES OF HEXOMAX

Hexomax is a malleable plastic explosive containing more than 85% RDX, maximum 14% inert binder and 1% tagging agent.

100 g to 1000 g blocks are produced at industrial scale. The cast-cure explosive composition is extruded, cut at the desired size and wrapped into a specific plastic film.



Picture 1: blocks on the production line

1.1. Performances

Using a detonator Nr 8 (or containing 800 mg PETN) is the easiest way to initiate Hexomax. The detonation velocity and critical diameter were measured. The detonation pressure was evaluated based on the measured density 1.56. The results are given in the following table.

Detonation velocity	7780 m/s
Critical diameter	~2 mm
Density	1.56
Detonation pressure (calculated)	>23GPa

Table 1: Detonation performance results

1.2. Sensitivity

Hexomax is fully qualified according to the STANAG 4170. In table 2 are reported the sensitivity data of the product against required tests.

	Results	Test references
Friction sensitivity	11+/30 at 353N	STANAG 4487 - annex A
Impact sensitivity	37 J	STANAG 4489 - annex C
Shock sensitivity (card gap test)	190 cards	STANAG 4488 - annex B

Table 2: Friction, impact and shock sensitivity results

These results are comparable with the values of the typical cast-cure composition B2238 used as booster in IM warheads (Impact sensitivity: 41J ; shock sensitivity : 180 cards).

In addition, Hexomax does not react against the 12m drop test and it is a good insulating material against electrostatic discharges: no reaction occurred when 300 kV was applied directly on the product (56 tests realized according to AECTP 250 method 253).

Regarding the stability in temperature, the self-ignition temperature by progressive heating is 214°C, this temperature corresponding to the RDX decomposition. Therefore, Hexomax is stable.

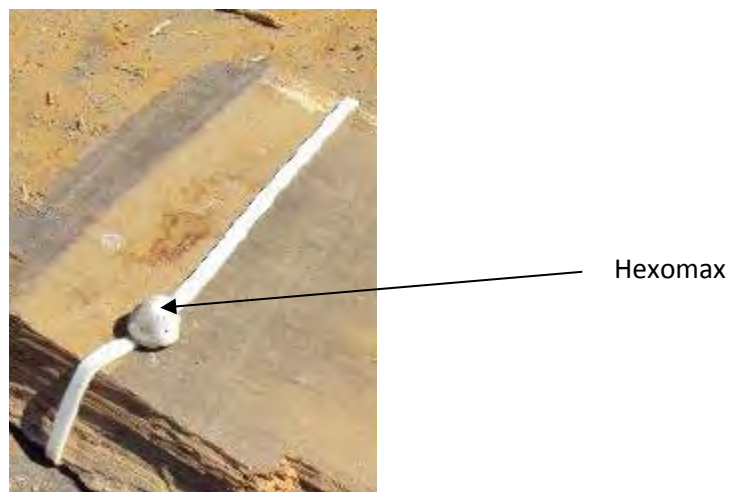
These results demonstrate that Hexomax is insensitive towards standard aggressions.

1.3. Malleability

Hexomax is very malleable on the complete range of temperature [-21°C;+55°C] and this characteristic is recognized by the French Forces. Therefore it can be used in various situations : around any round element to be destroyed or opened, as a booster to initiate another charge.



*Picture 2: Hexomax in various situations
(Courtesy of the Technical Service of French Army)*



Picture 3 : Hexomax used as booster

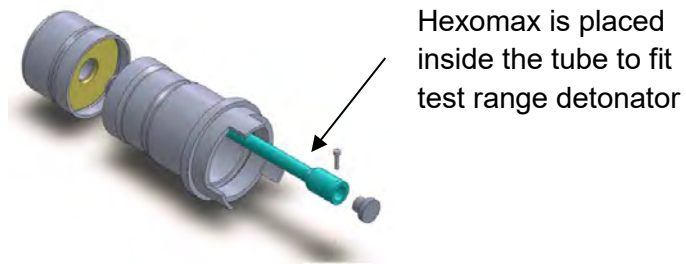


Figure 1 : Hexomax in modified fuze for test centers

1.4. Ageing effect

Blocks have been stored during 16.5 months at 60°C, which is equivalent to 22 years at 20°C according to Arrhenius law.

Characterizations were performed by DGA Techniques Terrestres on aged Hexomax and the results are compared with the initial product in the table 3.

	T0	After ageing
Self-ignition temperature by progressive heating	214°C	211°C
Impact sensitivity (BAM)	37 J	36 J
Friction sensitivity (BAM)	11+/30 at 353 N	0+/30 at 353 N

Table 3: Characterizations after ageing

Therefore, Hexomax remains safe for handling after more than 20 years ageing.

Moreover, it keeps its malleability property as shown in the picture 4.



Picture 4: Hexomax after ageing

1.5. IM properties

Fuel fire, slow cook off, bullet impact and fragment impact were performed on Hexomax. Three of them were presented in 2012 [1]. Hexomax blocks were placed in a logistic plywood box to realize the tests. As this type of box does not lead to any confinement, the results can be applied to Hexomax.

1.5.1. Fuel fire

The test was performed according to the STANAG 4240. The combustion of Hexomax was observed → type V.



Picture 5 : Fuel fire

1.5.2. Slow cook off

The test was performed according to the STANAG 4382. The combustion of Hexomax was observed → type V.



Picture 6: Hexomax in logistic plywood box after slow cook off

1.5.3. Bullet impact

The test was performed according to the STANAG 4241 (12,7 mm diameter bullet). No reaction was observed → type VI.



Picture 7: Hexomax after the bullet impact

1.5.4. Fragment impact

The test was performed according to the STANAG 4496: the mass of the fragment was 18,6g and the measured velocity 1830 m/s. Hexomax reacted and a type I reaction was observed.

1.5.5. Sympathetic reaction

In 2012, the performed tests showed that the reaction between 2 blocks is type I. Works were in progress to determine a design which guaranteed a non-transmission of detonation.

The French company SUPRAMECA has designed and developed a specific logistic box named Supracase which avoid the sympathetic reaction between Hexomax blocks by absorbing the detonation pressure.

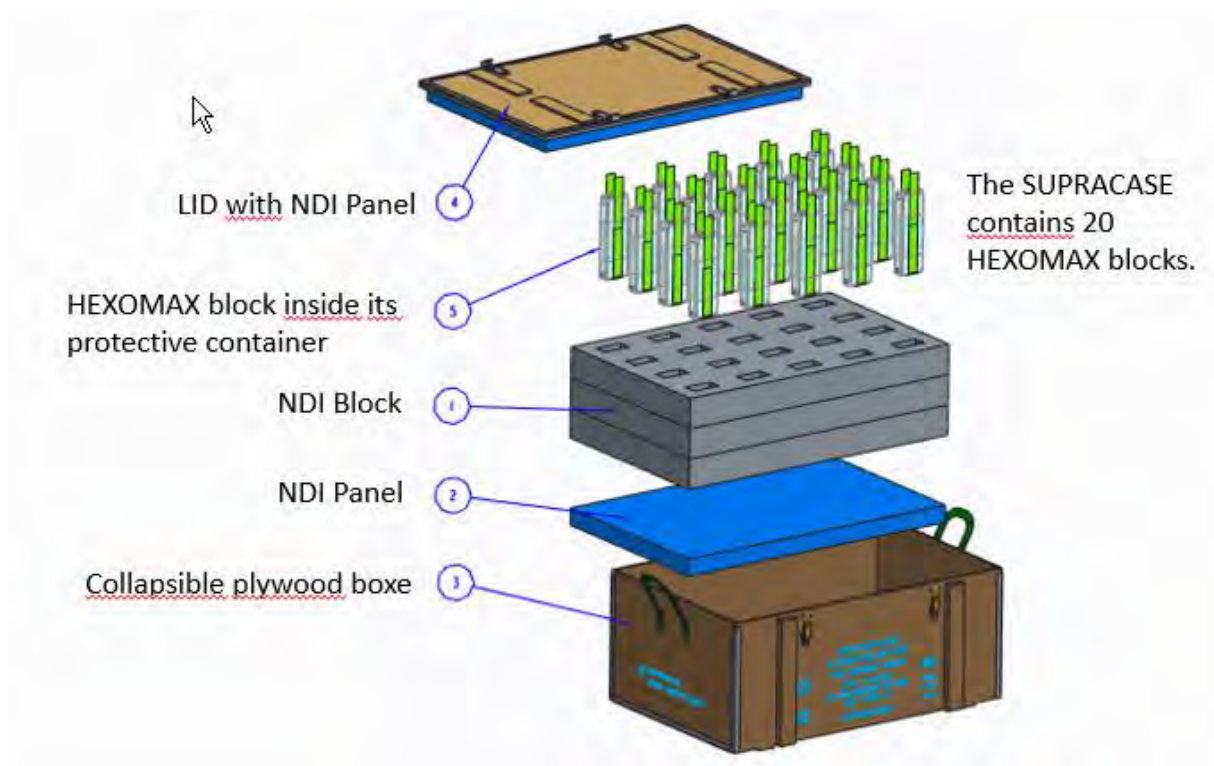


Figure 2: Description of Supracase

Preliminary tests were performed at EURENCO plant by measuring first the detonation over pressure of one block alone and then the detonation over pressure of blocks in Supracase.

Test 1 : Live blocks were inside the box which was placed on the wooden pallet. One block was initiated.



Figure 3: Configuration of the sympathetic test N°1

The measured detonation over pressure proves that only the initiated block detonated.

Test 2 : 4 boxes Supracase placed on a wooden pallet. Boxes 1 and 2 had live Hexomax blocks, while 3 and 4 had 1/5 live blocks (inert blocks for 4/5). Live blocks were placed close to the boxes 1 and 2. One block in box 1 was initiated.



Figure 4: Configuration of the sympathetic test N°2

After the test, the box 1 was completely destroyed but the blocks close to the initiated one did not react. Boxes 3 and 4 were not destroyed. Box 2 remained at its place and it was partially damaged but the live blocks are still inside.

These both results demonstrate that a type VI is achievable when Hexomax is placed in the Supracase.

1.5.6. Summary of IM behaviour

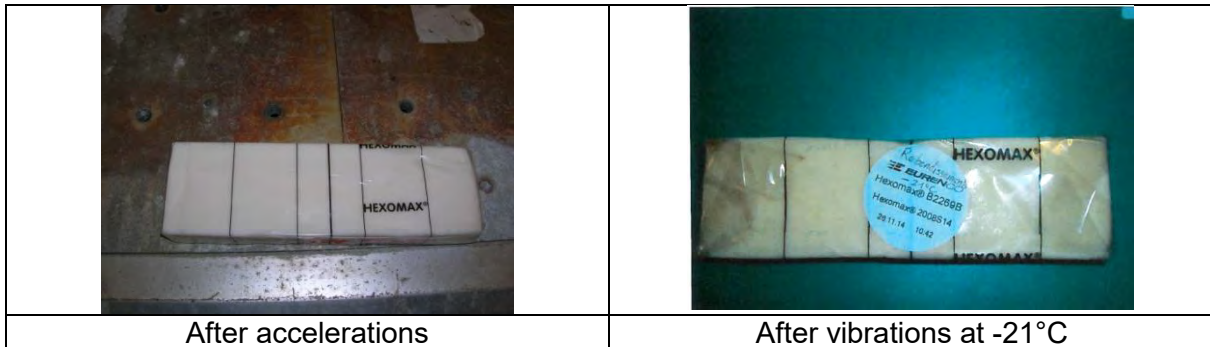
Tests	Reference	Results
Fuel fire	STANAG 4240	Type V
Slow cook off	STANAG 4382	Type V
Bullet Impact	STANAG 4241	Type VI
Sympathetic reaction		Type VI achievable by using Supracase
Fragment impact	STANAG 4496	Type I
Heavy fragment impact		Type I (assumption made according to other results)
Shaped charge		Type I (assumption made according to other results)

Table 4: IM signature

1.6. Environment testing

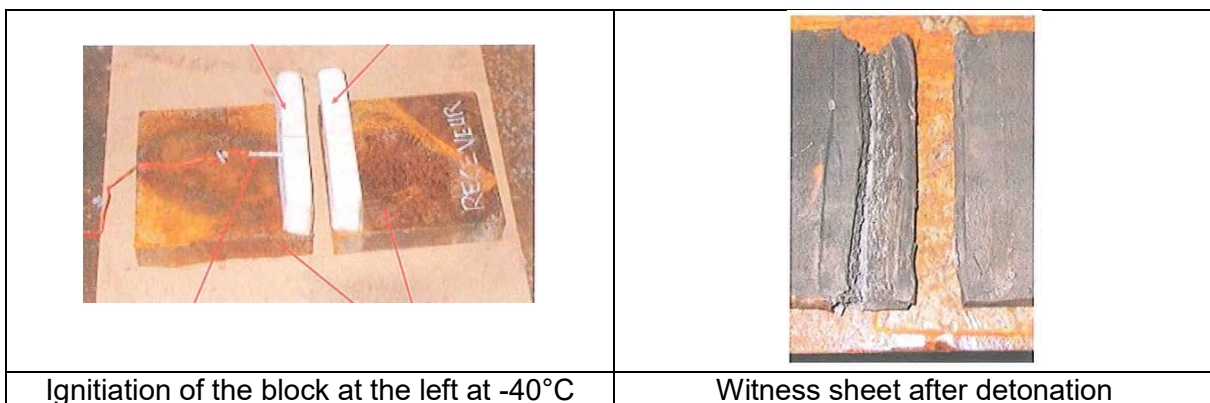
In the way of the qualification Hexomax has been tested under various environments it can face during its life. Environment tests were performed according to the standards AECTP 300 and 400.

- Storage and transport :
 - o Land transport vibrations
 - o Aircraft and Helicopter vibrations and accelerations up to 40g



Pictures 8: Hexomax after accelerations and vibrations induced by transport

- o Thermal shocks
- o Humid/hot/cold environments from -40°C to +71°C (5 cycles A1, 10 cycles A2 and 4 cycles B3 then 4 days at -40°C)
- o Solar radiations
- Use :
 - o Salted atmosphere
 - o Rain
 - o Dust wind
 - o Temperatures from -21°C to +55°C ; the ignition of the block has even been demonstrated until -40°C



Picture 9: Ignition of Hexomax at -40°C

All the results demonstrate that Hexomax keeps its properties after long storage worldwide and transport phases and it can be used in any of these environments. Moreover, Hexomax can be deployed under water.

2. QUALIFICATION IN THE SUPRAFLEX SYSTEM

Thanks to its performance, insensitivity and unique malleability and modeling, Hexomax can be used as the explosive charge for any system like Supraflex.

Supraflex has been designed by the French company SUPRAMECA to be able to cut large steel thicknesses. An adhesive is under the charge so that it sticks directly on the target during 30 min. Moreover, the system can be easily initiated thanks to the booster developed by SUPRAMECA, which can be placed anywhere along the charge. This ensures a reliable ignition.

Hexomax blocks are unwrapped and placed by modeling into the linear charge.



Picture 10: Hexomax into Supraflex



Picture 11: Supraflex on steel plate



Picture 12: Cut steel plate after ignition

The desired cutting form is obtained.

Based on the achieved performances, Supraflex 10, 25 and 40 combined with Hexomax have been qualified in 2017 by the French Ministry of Defense for breaching applications (walls, etc).

As described in the following table, the cutting performance in steel varies according to the type of Supraflex:

Type	Weight of explosive	Cut thickness in steel
Supraflex® 10	190 g/m	10 mm
Supraflex® 25	1161 g/m	25 mm
Supraflex® 40	2953 g/m	40 mm

Table 5: Performance of Supraflex

CONCLUSION

Hexomax is safe for handling, transport and use in the complete range of temperature and keeps its properties after 20 years ageing.

The IM properties of the product can be improved by using the logistic box Supracase as experimentally demonstrated: type VI is achievable for sympathetic reaction.

Its unique malleability allows Hexomax to be used alone for any cutting, opening or destruction operation. For more specific cutting work, it can be placed into any pre-formed shape, like the flexible linear shaped charge Supraflex. The French Ministry of Defense has qualified the product for these applications and further uses are already foreseen.

Sheet-metal Ammunition Packing Tray for Mitigation of Secondary Cook-off of Medium-caliber Ammunition

Presented by

Greg Little, J.P. Shebalin, Jim Fetsko, Joe Silber
Naval Surface Warfare Center Dahlgren Division, Dahlgren, Virginia
Email: greg.little@navy.mil
Phone: 540-653-0187

And

Jeb Brough
Matsys, Inc., Sterling, VA

Abstract

Bullet Impact (BI) and Fragment Impact (FI) Insensitive Munitions (IM) tests against unlinked, medium-caliber ammunition packaged in ammunition cans with high-density polyethylene (HDPE) packing trays have demonstrated a secondary hazard distinct from the rounds' initial reaction to impact. Specifically, the HDPE trays display a tendency to catch fire as a result of the impact and initial reaction of the ammunition. This fire begins a sustained series of secondary cook-offs of projectiles and cartridge cases that lasts until either the fire burns out or the contents of the ammunition can have reacted or been ejected due to secondary reactions.

This hazard has been witnessed in two types of 25mm ammunition, with two more due for demonstration testing in 2018. Any munitions packaged in similar trays may be vulnerable to this phenomenon due to the high energy density of the HDPE and its flammability properties. Secondary reactions often continue long after the initial impact with no obvious visual indication that combustion is taking place until a reaction occurs.

Replacement of these trays with a nonflammable alternative would mitigate this safety hazard. Preliminary testing of prototype sheet-metal ammunition packing trays has demonstrated favorable results in this regard without degrading the initial IM response. Currently, design refinements are underway to improve manufacturability of these trays. Once these refinements are complete, the trays are expected to meet all necessary packaging requirements (cost, weight, performance) while mitigating the secondary cook-off hazard.

Background

Prior BI and FI testing conducted on containerized, unlinked PGU-47/U Armor-piercing High-explosive (APEX) 25mm ammunition (developed and tested by Nammo) revealed an unexpected hazard—the ignition and slow burn of the HDPE packaging trays, resulting in a series of cook-off reactions, often occurring after a significant delay and continuing for many minutes afterward (the reaction furthest in time occurred 42 minutes after initial impact). Given the ubiquity of the HDPE trays in packaging unlinked, medium-caliber ammunition, the similarity of energetics across ammo types, and the long service life of commonly used medium caliber

ammo types, it was reasonable to expect that testing of common ammunition types under modern IM standards would reveal this hazard to be widespread. The Navy Insensitive Munitions Advanced Development (IMAD) Program funded a task to determine the extent of the delayed cook-off response and to develop and test possible replacement trays that would mitigate the hazard.

Unlinked 25mm rounds are packaged in the CNU-405/E, an ammunition can that holds one-hundred (100) rounds in fourteen stacked HDPE trays, thirteen alternating between seven and eight rounds per tray, with the top tray containing just two rounds to make the loadout an even one-hundred. Images of how alternating rounds nest together can be seen in Figure 1.

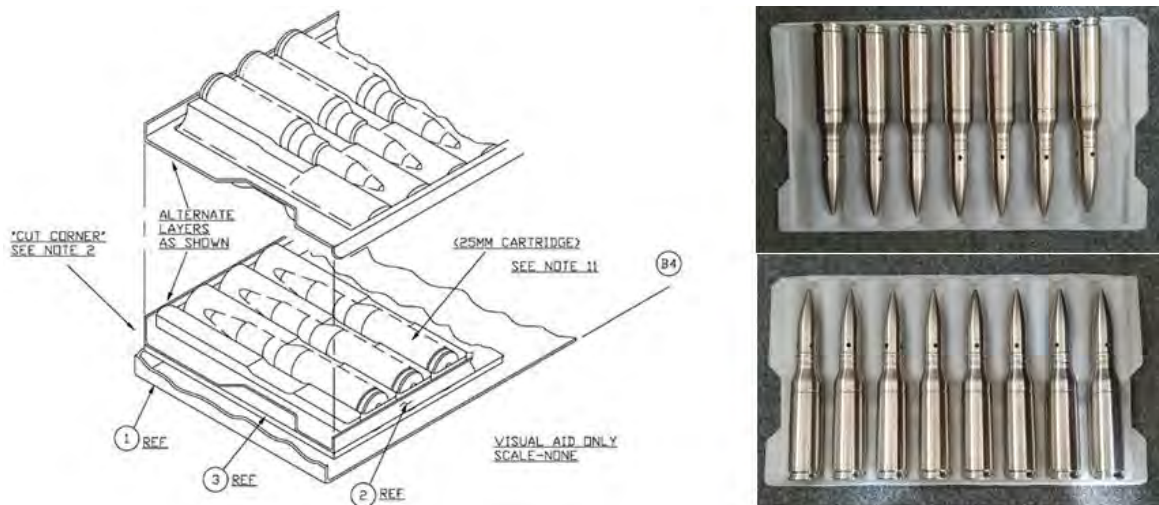


Figure 1: HDPE packing tray nesting (left) and 25mm round alternating tray layout (right)

2016 Progress

Due to availability issues with the PGU-47/U and a desire to characterize the extent of the hazard across different ammunition types, initial mitigation testing focused on the PGU-32/U Semi-Armor Piercing High-Explosive Tracered (SAPHEI-T) round, an all-purpose round in widespread use by the U.S. Navy and Marine Corps. The purpose of this testing was to determine whether the phenomenon occurs across different 25mm ammunition types and, if so, whether or not a nonflammable packing tray would mitigate the hazard.

The initial tested prototype was cut from 0.050" 5052 sheet aluminum. In addition to bending the edges to improve stiffness, a waterjet was used to cut slots for the nesting of the 25mm rounds, contrasting with the full cradles in the current HDPE trays. This offers two advantages. The first is a substantial weight savings over a solid tray, necessary as the new trays cannot weigh any more than the current HDPE trays. The second advantage is less obvious. The slots in each tray act as a path for gas pressure relief. When an impact occurs in the current packing arrangement, the sudden pressure rise forces every tray and round above the point of impact upward like a piston, ejecting the ammo can lid and much of the can's contents at high velocity. With the aluminum packing trays, the same impact pressure rise flows

through the slots between layers, attenuating throughout the can's entire volume. As will be seen in the test results section, this attenuation results in the ammo can lid remaining in place, containing most or all of the debris within the ammo can. The aluminum tray design can be seen in Figure 2.



Figure 2: Prototype aluminum tray (left); Three trays stacked with dummy 25mm rounds (right)

Initial testing against the PGU-32/U focused on testing with a single 0.50" armor-piercing (AP) bullet. Using a single bullet instead of three was deemed necessary during these early characterization tests due to the difficulty of controlling the impact point of the second and third rounds without restraint of the ammo can, which would be undesirable. Additionally, the aim point for all of these tests was the propellant center of mass. PGU-47/U and PGU-32/U rounds have dissimilar explosive fills but similar propellants, so targeting the propellant was deemed less likely to cause a reaction so violent that the can would lose all confinement. This would enable testing to focus on recreating the hazard seen in the initial PGU-47/U IM testing. Table 1 depicts the 2016 test matrix.

Table 1: 2016 Test Matrix

Test Description	Aim Point	Tray Type	Purpose
Single Bullet Impact (BI Test 1)	PGU-32 Propellant	HDPE	Test PGU-32 round for delayed cook-off vulnerability
Single Bullet Impact (BI Test 2)	PGU-32 Propellant	HDPE	Repeat of Test 1 to demonstrate repeatability
Single Bullet Impact (BI Test 3)	PGU-32 Propellant	Aluminum	Demonstrate that tray swap mitigates delayed cook-off hazard
Single Bullet Impact (BI Test 4)	PGU-32 Propellant	Aluminum	Repeat of Test 3 to demonstrate repeatability

BI Tests 1 and 2 demonstrated the transient nature of the delayed cook-off phenomenon. Test 1's impact ejected the ammo can's lid and resulted in clear signs of burning trays and a secondary cook-off reaction at 4 min 18 sec after impact. Conversely, despite an identical test setup, aimpoint and lid ejection, Test 2 trays did not sustain a burn and no secondary reactions were observed. Comparative pictures of the plastic trays from each test can be seen in Figure 3.



Figure 3: Comparison of plastic tray thermal degradation from Test 1 (left) and Test 2 (right)

BI Tests 3 and 4 repeated the test setup from 1 and 2, with the HDPE trays replaced by the prototype aluminum trays seen earlier in Figure 2. The difference in reactions was obvious. First, whereas the HDPE tests resulted in the ejection of the lid along with every tray and round above the point of impact, in the aluminum tests, the lid bowed upward but remained attached, keeping the trays and rounds inside which significantly limited the scattering of debris. This can be seen in Figure 4.



Figure 4: Comparison of post-test debris in BI Test 1 (left) and BI Test 3 (right).

Test 3 had a single round react and eject from the side of the ammo can one minute after initial impact, leaving a hole to the right visible in Figure 4. However, as there was no sign of tray burning in the post-test debris, this is most likely due to the initial heating caused by the impact and the immediate reaction of the propellant and/or explosive to that impact. There were no further reactions in Test 3 despite having roughly twice the energetic material remain inside the ammo can compared to Test 1 or 2. In Test 4 a pair of small, audible reactions that caused the ammo can to jump were observed in the first 25 seconds after impact, but nothing left the

can. Aside from some char residue from the burning energetic material and localized melting near the point of impact, the aluminum trays showed no signs of degradation (Figure 5).



Figure 5: BI Test 4 rounds and trays.

The 2016 testing demonstrated that both the understanding of the hazard’s root cause and the proof-of-concept solution devised were valid. In addition, the prototype aluminum tray design (shown in Figure 1) allows attenuation of internal pressure rises, limiting the scattering of debris seen consistently in HDPE testing.

2017 Progress

Continuing work to characterize the scope of the threat was undertaken in 2017. Full BI and FI tests of the PGU-32 were performed, with varying aim points and tray types. Table 2 depicts the 2017 test matrix.

Table 2: 2017 Test Matrix

Test Description	Aim Point	Tray Type	Purpose
Triple Bullet Impact (BI Test 5)	PGU-32 Projectile	HDPE	Test PGU-32 projectile for delayed cook-off vulnerability
Triple Bullet Impact (BI Test 6)	PGU-32 Propellant	HDPE	Determine vulnerability to IM test standard as compared to single bullet.
Fragment Impact (FI Test 1)	PGU-32 Propellant	HDPE	Test PGU-32 propellant for delayed cool-off vulnerability to FI
Fragment Impact (FI Test 2)	PGU-32 Propellant	Aluminum	Determine how aluminum trays affect overall FI response

BI Test 5 represented the first attempt to perform a full triple-bullet impact test against PGU-32/U rounds for the explicit purpose of observing packing tray burning and subsequent delayed cook-off reactions. Prior-year testing was performed entirely with single-bullet impact tests into the propellant, deemed the less likely energetic material to induce a violent reaction. In increasing to the full triple-0.50” AP bullet configuration as specified in STANAG 4241 and

setting the aim point at the more sensitive projectile, BI Test 5 can be considered a bounding, worst-case BI test for this ammunition type.

The results of the test validated the 2016 decision to target the propellant. The violence of BI Test 5 was sufficient to blow apart the ammo can and scatter the ammo and trays, providing no confined space in which a delayed cook-off event could take place. While these results did not provide useful data in categorizing the phenomenon in question, there was evidence of a tray that burned up almost entirely outside the ammo can, further illustrating the flammability of the HDPE under impact conditions. Evidence of these responses are shown in Figure 6.



Figure 6: Post-test debris of BI Test 5 showing catastrophic damage to the ammo can (left) and a burned HDPE packing tray (right)

The aluminum trays had already been proven not to burn under BI using this ammunition. Moreover, demonstrating the HDPE hazard under full triple 0.50" AP bullet threat was desirable. To avoid a repeat of the violence observed in BI Test 5 (and resulting lack of relevant data), BI Test 6 used three rounds to impact the original 2016 aim point of the propellant in the cartridge case. This test would conclude the BI characterization of the PGU-32/U delayed cook-off response.

BI Test 6 resulted in another clear indication of delayed cook-off responses. Two delayed responses occurred, one at 1:57 min. after impact and the other at 4:13 min. after impact. As can be seen in Figure 4, the can remained largely intact minus the typical ejection of the lid and upper layers of trays and ammunition. Figure 7 shows a burned and melted tray fused to an empty cartridge case.



Figure 7: Remains of cooked-off rounds and burned trays (left); A partially burned tray fused to empty cartridge case (right)

Initial testing focused exclusively on BI threats. However, because this delayed cook-off response was also seen in the PGU-47/U FI testing that inspired this work, characterizing both the likelihood of delayed cook-off response in the PGU-32 and the overall FI response in the presence of aluminum trays was deemed necessary.

For FI Test 1, a propellant cartridge aim point was chosen to lessen the possibility of catastrophic damage to the can such as that seen in BI Test 5. Despite this decision, the response was very similar to that of BI Test 5, with the can opening fully (Figure 8) and exposing the rounds and trays, leaving no confined conditions for the cook-off to take place. Rather than repeat a test where relevant data was unlikely to be acquired, focus turned to testing aluminum prototype trays under the same conditions. One important consideration for replacement packaging is that it should not worsen current IM reaction levels. FI Test 2 was therefore conducted to demonstrate that the reaction was no worse than FI Test 1.



Figure 8: Ammo can post-test, completely blown open

The test item response was very similar to that of FI Test 1, with a slight improvement in that max fragment distance decreased (from 216 ft. to 136 ft.) and fewer fragments exceeded the 20 J threshold (22 in FI Test 1 vs. 8 in FI Test 2). No worsening of the baseline reaction was evident, and it is possible that the slots in the aluminum trays allowed for pressure relief that would account for the response's mild improvement. These results are shown in Figure 9. Additionally, two other ammo types, the PGU-23 and PGU-25, were procured for 2018 testing to further demonstrate improved response to the threat.



Figure 9: Test stand post-test, showing scattered aluminum trays and rounds (left); Post-test debris that traveled farther than 50 ft (right).

Aluminum Tray Design Refinement

In parallel with the hazard characterization work, design improvements to the prototype tray are underway. The original design used waterjet-cut aluminum sheets, well-suited to quick, cost-effective production of test articles. However, the waterjet is not an efficient method of mass-producing trays.

Prototype manufacturing hardware has been fabricated to test a mass-production process in small-scale before the effort proceeds to large-scale fabrication. Once the procedure has been perfected and the improved design has been verified by testing to address both safety and logistical concerns, manufacturers will be approached to begin discussing mass-production options and expected costs going forward.

Conclusions

The slow burn-rate of the HDPE trays can provide the fuel for sustained fires. Secondary reactions have been observed as long as 42 minutes after impact when these trays are present. Replacement of the HDPE trays with nonflammable trays will result in a significant safety improvement in medium-caliber ammo cans. While secondary reactions can still occur due to the initial impact spilling propellant/explosive within the ammo can interior, the high burn rate of these energetic materials ensures such reactions will be confined to the immediate vicinity of the inciting event.

Additionally, showing that the aluminum trays do not worsen the immediate reaction in either Bullet or Fragment Impact events proves that one safety improvement isn't coming at the expense of another safety issue. Provided the logistical and basic safety packaging requirements can be met, the sheet-metal ammunition packing tray offers a solution to the safety hazard of delayed cook-off.

Path Forward

Testing of PGU-23 and PGU-25 rounds will occur in 2018 to characterize the phenomenon as completely as possible. Four BI tests are currently planned, one for each ammo/tray type combination. The test matrix is detailed in Table 3.

Further work will involve finalizing the tray design for manufacturability and weight constraints and subjecting it to final impact and environmental testing, as well as investigating potential sources of production as this initiative moves toward transition. Once a finalized design has been developed, a limited number of sets will be fabricated for environmental and BI testing, which should conclude the work no later than 2019.

Table 3: 2018 BI Test Matrix

Test Description	Aim Point	Tray Type	Purpose
Triple Bullet Impact (BI Test 7)	PGU-23 Propellant	HDPE	Test PGU-23 projectile for delayed cook-off vulnerability
Triple Bullet Impact (BI Test 8)	PGU-23 Propellant	Aluminum	Demonstrate that tray swap mitigates delayed cook-off hazard
Triple Bullet Impact (BI Test 9)	PGU-25 Propellant	HDPE	Test PGU-25 projectile for delayed cook-off vulnerability
Triple Bullet Impact (BI Test 10)	PGU-25 Propellant	Aluminum	Demonstrate that tray swap mitigates delayed cook-off hazard

Acknowledgements

This work was sponsored by the Navy Insensitive Munitions Advanced Development Program and coordinated through the Ordnance Technology Project. Material and technical support has also come from NAVAIR PMA-242, the NSWCCD Gun Weapon Systems Division (Code E30), and Navy Packaging, Handling, Storage, and Transportation (PHS&T). Initial testing in 2014 was performed by Nammo and all IMAD-funded testing was performed by the NSWCCD Test and Evaluation Division (Code E40).

References

1. Test Results of Fragment Impact Tests Conducted on PGU-32 Semi-armor-piercing-high-explosive Incendiary-traced Cartridges Using Plastic and Aluminum Dunnage; Crabtree, Donna; E40 Report 17-156; NSWCCD; July, 2017
2. Test Results for Bullet Impact of the PGU-32 Semi-armor-piercing High-explosive Incendiary-traced Cartridge; Crabtree, Donna; E40 Report 17-087; NSWCCD; April, 2017

3. Test Results for Bullet Impact Conducted on the PGU-32 Semi-armor-piercing High-explosive Incendiary-traced Cartridge; Ross, Daniel; E40 Report 16-117-A; NSWCCD; June 2016
4. Insensitive Munitions Test Results for the 25-mm APEX Cartridge; Sogstad, Einar; Nammo Test Report 2066777 Version 1; December, 2014

Sheet-metal Ammunition Packing Tray for Mitigation of Secondary Cook-off of Medium-caliber Ammunition

**2018 International Insensitive Munitions
and Energetic Materials Symposium
Portland, OR
April 23 - 26, 2018**

**Greg Little, JP Shebalin, Jim Fetsko, Joe Silber
Naval Surface Warfare Center, Dahlgren Division, Dahlgren, VA**

**Jeb Brough
Matsys, Inc., Sterling, VA**

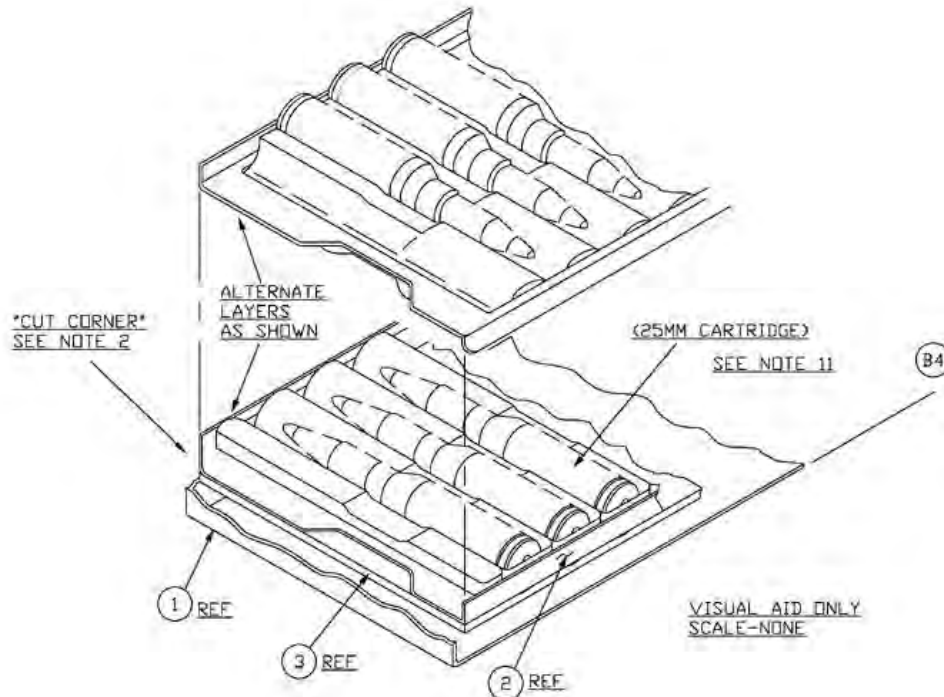
Email: greg.little@navy.mil
Phone: 540-653-0187

Background

- Insensitive Munitions (IM) testing of the 25mm PGU-47/U Armor Piercing High-Explosive Incendiary-Traced (“APEX”) Cartridge was performed by Nammo, the developer of the APEX, in 2014.
- In both Bullet Impact (BI) and Fragment Impact (FI) tests, delayed cook-off reactions of the ammunition remaining in the can were observed. These reactions occurred up to 42 minutes after the initial impact.
- This delayed cook-off is caused by the high-density polyethylene (HDPE) packing trays used to cushion rows of unlinked rounds.
- **This phenomenon was likely to impact other variants of ammunition stored in similar trays. A non-flammable replacement tray which still meets all packaging requirements will mitigate the subsequent cook-off reactions in impact scenarios.**

System Hardware – HDPE Trays

- Each CNU-405/E container contains 100 25mm rounds stacked in 13 alternating layers of 7 or 8 rounds, with a 14th layer of 2 rounds to round out the total to 100.
- Layers are separated by the molded HDPE trays.



7 rounds

8 rounds

A full set of HDPE trays (14 trays at 4.4 lbs total weight) contains the thermal energy equivalent of almost 0.75 gallons of gasoline.

PGU-47/U BI and FI Testing Results

- BI Test 1 (propellant aim point) resulted in minimal burning in the trays. Two post-impact reactions occur, at 4s and 21s after impact.
- BI Test 2 (projectile aim point) resulted in 24 delayed cook-off reactions over 11 minutes.
- FI Test 1 (propellant aim point) resulted in 2 reactions at approximately 3 and 8 minutes after impact.
- FI Test 2 (projectile aim point) resulted in 4 reactions at approximately 4, 12, 21, and 42 minutes after impact.



**Delayed Cook-off Reaction
due to burning HDPE trays**

Approach

- **Design replacement tray that mitigates hazard while fulfilling all packaging requirements**
 - **Cost**
 - **Weight**
 - **Basic Safety Series testing**
 - **Manufacturability**

- **Characterize extent of hazard across ammunition types**
 - **Focus on widely used ammo first**
 - **Limited by funding and test cost**

Designing a working prototype tray easy to produce in testing quantities allows these tasks to operate largely independent of one another.

System Hardware – Aluminum Tray



Aluminum tray mass will be no greater than HDPE tray mass

- Made of 5052 Aluminum. Folded edges improve stiffness compared with HDPE trays, which bow significantly when fully loaded.
- Alternating cutouts save weight while allowing rounds to nest in similar orientation to HDPE trays.
- Cutouts allow pressure to flow more easily between layers, reducing likelihood of ejecting the lid.

System Hardware – PGU-32 SAPHEI-T

- **Initial mitigation testing focused on the PGU-32/U Semi-Armor Piercing High Explosive Incendiary, Tracer round (SAPHEI-T)**
 - **This round currently sees wide use across services**
 - **Contains propellant similar to that of the PGU-47/U, already proven vulnerable to delayed cook-off**



Test Methodology

- **A limited first-year budget drove test scoping decisions.**
 - **Attempted to replicate, then mitigate, the phenomenon with the PGU-32/U.**
 - **Planned to repeat each test because the delayed burning reaction did not always occur in PGU-47/U testing.**
- **The cartridge case and similar propellant served as the aim point for BI testing.**
 - **A single 0.50 cal AP bullet was chosen to minimize the chance of a large scale reaction of projectiles that would destroy the confinement of the CNU-405/E.**
 - **Difficult to control the impact point of the second and third bullet without excessive confinement of the ammo can.**
 - **Only one bullet was required in the second BI test against PGU-47/U. Both other rounds missed due to the can jumping off the stand.**

FY16 Test Review

Test Description	Target	Tray Type	Result
Single Bullet Impact	PGU-32 Propellant	HDPE	Does observed hazard occur in PGU-32/U?
Single Bullet Impact	PGU-32 Propellant	HDPE	Repeat of Test 1
Single Bullet Impact	PGU-32 Propellant	Aluminum	Demonstrate that aluminum trays mitigate delayed cook-off.
Single Bullet Impact	PGU-32 Propellant	Aluminum	Repeat of Test 2

HDPE PGU-32 Test Results – BI Tests 1 & 2

• BI Test 1

- Violent initial reaction ejected lid and roughly half the trays and rounds
 - Bullet likely hit a projectile (one reacted projectile found)
- HDPE trays burned, resulting in a secondary reaction at 4 min 18 sec after impact.
- All cartridges were recovered within 50 ft., but several components of the lid exceeded 50 ft.



BI Test 1



• BI Test 2

- Can lid was blown clear, but the initial reaction was significantly less violent than in Test 1.
- Trays did not ignite. No secondary reactions were observed.
- Demonstrates the transient nature of the phenomenon – the hazard is present but does not always manifest.



BI Test 2



HDPE PGU-32 Tests Tray Comparison



Dunnage from
Test 1



Dunnage from
Test 2

- Thermal degradation of the trays in Test 1 is more pronounced than in Test 2, corresponding with the delayed reaction caused by tray burning witnessed in Test 1.

Aluminum PGU-32 Test Results – BI Tests 3 & 4

BI Test 3

- Some melting and charring in the impact vicinity, but the aluminum trays did not burn.
- The ammo can lid stayed attached due to the tray's slotted design.
- One secondary reaction occurred 1 minute after impact, ejecting a cartridge beyond 50 ft. All other debris remained inside can.



BI Test 3



BI Test 4

- Aside from localized melting/charring, no degradation was visible on the trays.
- The lid remained attached to the container.
- During the 25 second period after impact, two small audible reactions caused the container to jump.
- No additional reactions occurred. All rounds were recovered in the can.



BI Test 4



Test Matrix – FY17

Test Description	Target	Tray Type	Purpose
Triple Bullet Impact	PGU-32 Projectile	HDPE	Full BI Test of PGU-32 projectile for delayed cook-off vulnerability
Triple Bullet Impact	PGU-32 Propellant	HDPE	Full BI Test of PGU-32 propellant
Fragment Impact	PGU-32 Propellant	HDPE	Test PGU-32 Propellant for delayed cook-off vulnerability to FI
Fragment Impact	PGU-32 Propellant	Aluminum	Determine if Al trays worsen reaction violence

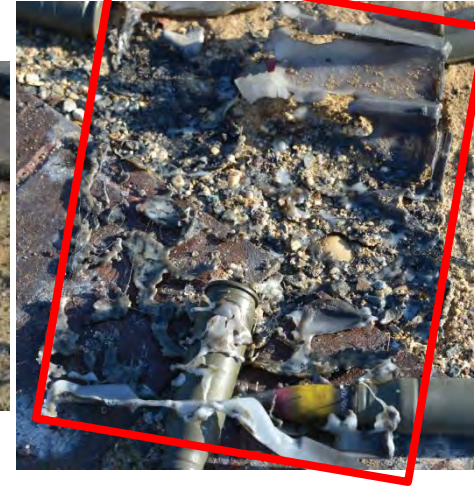
HDPE PGU-32 Test Results – BI Tests 5 & 6

BI Test 5

- Much more violent than BI aimed at cartridge case
- Entire can ripped apart, leaving no confinement to begin cook-off response.
- Despite the lack of delayed cook-off, there was evidence of trays having burned outside the can.



BI Test 5



BI Test 6

- The initial impact blew the lid off along with numerous trays and rounds. The container otherwise remained intact.
- Two delayed reactions occurred at 1 min 57 sec and at 4 min 13 sec. These ejected most of the can's remaining contents.
- One piece of tray debris was found partially burned and melted to the cartridge case.



BI Test 6



PGU-32 Test Results – FI Tests 1 & 2

FI Test 1 (HDPE Trays)

- The fragment combined with the initial reaction to completely blow open the can's structure, removing any confinement.
- No secondary cook-off occurred.
- Furthest fragment distance was 216 ft. 24 pieces of debris exceeded the 50 ft threshold (22 exceeded 20 J).



FI Test 1



FI Test 2 (Aluminum Trays)

- The fragment impact completely blew open the can's structure, removing any confinement.
- No secondary cook-off occurred.
- Furthest fragment distance was 136 ft. 15 pieces of debris exceeded 50 ft (8 exceeded 20 J).
- Aluminum trays may have mitigated violence compared to HDPE trays.



FI Test 2



Tray Design Refinement

- Design optimization with a focus on logistical factors and manufacturability is underway in parallel with the testing effort.
 - Current waterjet-cutting method is appropriate for test quantities, but not mass-production.
 - Prototype small-scale production hardware has been fabricated to test out improved design process.
 - Once scaled up, improved design will address both logistical and safety issues.
 - After the improved design has been verified by environmental and impact testing, manufacturers will be approached to discuss costs associated with mass-production.

The Navy filed patent application 104525 in May, 2017 for “SHEET-METAL AMMUNITION PACKING TRAY.”

Conclusions

- **Hazard**

- Testing of the PGU-32 demonstrates that the delayed cook-off phenomenon is not limited to a single medium-caliber ammo type.
- Delayed cook-off is a transient phenomenon, not occurring in every impact incident.
- Even without direct cook-off of rounds in the can, slow-burning plastic is a long-duration hazard that could transition fire to adjacent spaces or munitions.

- **Solution**

- BI and FI testing demonstrate that, in addition to addressing the specific hazard, the aluminum trays did nothing to worsen initial total item response and helped mitigate it in both cases.
- Total elimination of post-impact reaction may not be possible. Residual heat of both impact and the initial reaction can prompt a violent response in the immediate aftermath.
- HDPE trays are flimsy when fully loaded, frequently crack, and are typically discarded after a single use. Sheet-metal trays are stiffer and more durable, with greater potential for reuse.
- **Replacement of HDPE trays with non-flammable, sheet-metal trays can address both hazard-mitigation and logistical concerns.**

Path Forward

- **Hazard Characterization**

- Bullet Impact of PGU-23 and PGU-25 rounds to conclude hazard characterization.

- **Tray Design**

- Tray design will be finalized for production readiness.
- Environmental testing with intermediate/final tray design.
- Impact testing will be conducted with the final design

- **Transition**

- PMA-242 has been engaged throughout the process and has expressed interest in transition provided weight, cost, and packaging requirements are met with final design.

Acknowledgments

- **NOSSA**
 - Ken Tomasello, IMAD
Program Manager
 - Heather Hayden
- **NSWCDD**
 - Noel Colon-Diaz
 - Jim McConkie
 - Jacqui Williamson
 - Perry Fridley
 - Rachel Kramer
 - Donna Crabtree, Test
Engineer
 - Daniel Ross, Test Engineer
 - Gerhard Thielman, NSWCDD
Legal
- **PMA-242**
 - Pete Sweazy
- **IHEODTD PHS&T**
 - Elizabeth Lee
 - Earl Humphries

NEW NTO WORKSHOP AND ASSOCIATED PRODUCT CHARACTERIZATIONS

A. Delage, P. Chabin, G. Alvarez, V. Chauffour & G. Eck

EURENCO, 1928 route d'Avignon, CS 90109 Sorgues- 84275 VEDENE, France
a.delage@eurenco.com – Phone: +33629671952

ABSTRACT

NTO was produced for more than 25 years at the EURENCO Sorgues plant. However in 2016, the existing workshop was redesigned and rebuilt, to allow a continuous way of production, increase control on the process safety and improve the final product quality.

This paper will firstly describe the different steps of the NTO manufacturing showing some specific process improvements put in place in the workshop. Then will be presented the results of the characterizations of the different grades of NTO (Class II, III and IV) and the specific quality NTO CF which has a granular size distribution and a high bulk density designed for IM melt cast applications.

All the results obtained during this study allow our product to be qualified by the French MoD. The new NTO has then been also tested and checked in two IM compositions, one cast PBX B2214B and one for a pressed application P16945. The results obtained confirm that the main characteristics in performance, safety and vulnerability of this two IM products are kept with using the new NTO.

1- INTRODUCTION

3-Nitro-1,2,4-triazol-5-one (NTO) is mainly used by EURENCO's customers in Melt-Cast compositions for Insensitive Munitions (NTO CF), very Insensitive Cast-PBX formulations (B2214B, B2268A) as well as moulding powders for Pressed-PBX formulations (P16945). Their applications include Mortar and Artillery ammunition as well as munitions used from naval platforms such as aircraft carriers (bombs & penetrators).

NTO explosives production traces its roots back to the 1980s when EURENCO (at the time SNPE) patented NTO as an explosive for military use. After more than 25 years of production, it has been decided to redesign and rebuild the existing workshop to allow a continuous way of production, increase control on the process safety, reduce the environmental impacts of this type of production (waste acid, air) and improve the final product quality.

Different grades of NTO are produced in this new workshop, Class II, III and IV for cast-PBX formulations and also a specific quality NTO CF which has a granular size distribution and a high bulk density designed for IM melt-cast applications.

The challenge was to improve the process (robustness & reproducible) and to keep exactly the same qualities of NTO as those produced in the old workshop (already qualified for our customer's applications) without changing the technical specifications.

2- WHERE WE WERE...

Some pictures of the old workshop are gathered in the figure 1. This workshop was built in 1972, and before the NTO production which started in 1987, it was dedicated for PETN manufacturing. No specific instrumentation was automated and the control station and command control wasn't deported. Moreover, it was impossible to reach the required level regarding safety and environmental regulation.

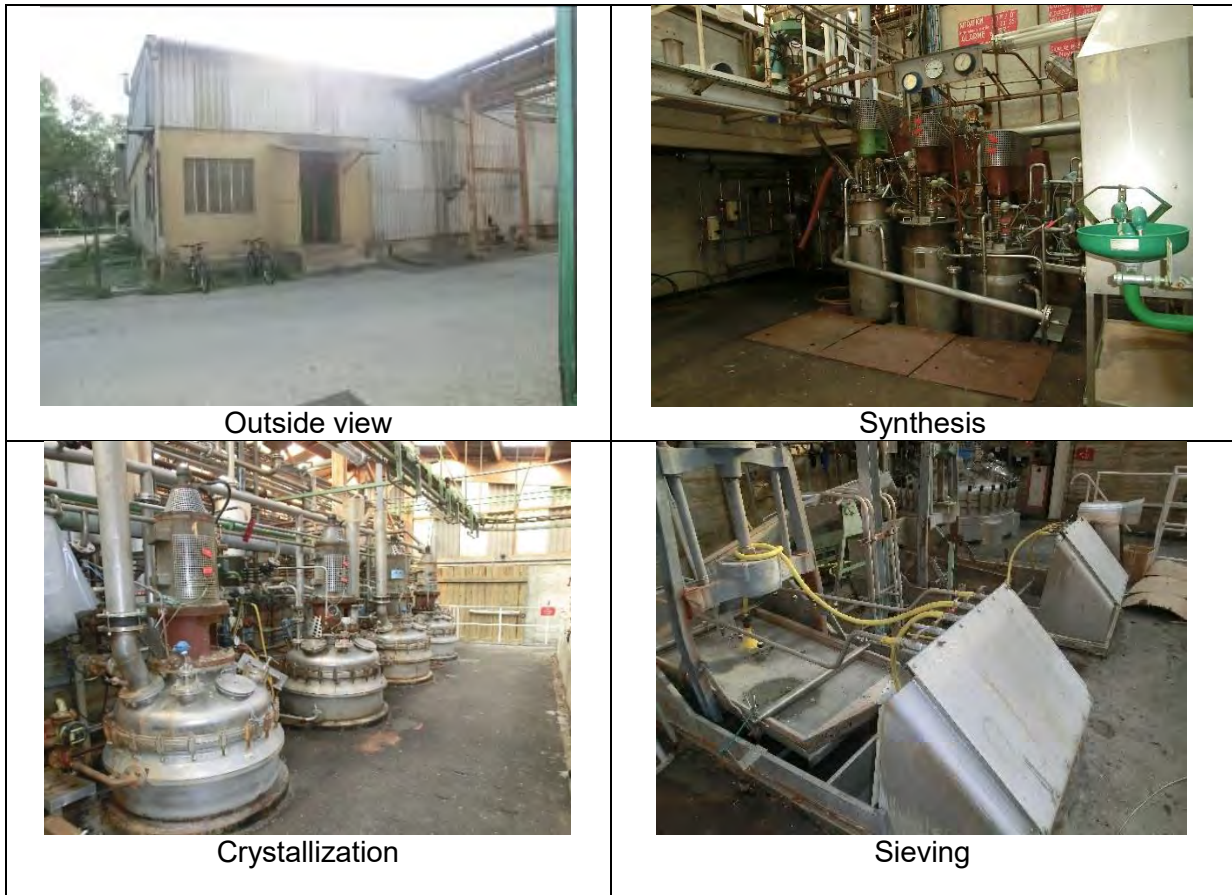


Figure 1: Old workshop views

3- WHERE WE ARE

EURENCO has commissioned in May 2016 the new workshop, figure 2, dedicated for the production of NTO insensitive explosives as part of its investment strategy in Sorgues (France) to modernize explosive production lines and answer current and future customer's needs. This new workshop is able to produce more than 200T/year.

Even if the production process has been kept (chemical process), each step has been improved, from the raw material supply (NA, TO) to the drying phase and the packaging cell. All these steps are completely instrumented which allow us to a fully masterized production.



Figure 2: New workshop

3.1- Production process

The production process includes different steps as shown in figure 3:

- Synthesis step: nitration of TO by nitric acid
- Dilution Step: to eliminate the impurities
- Crystallization: to purify the product & to determine the final quality of NTO
- Filtration using a new technology (banding filter)
- Drying using a new technology (fluidising drying)

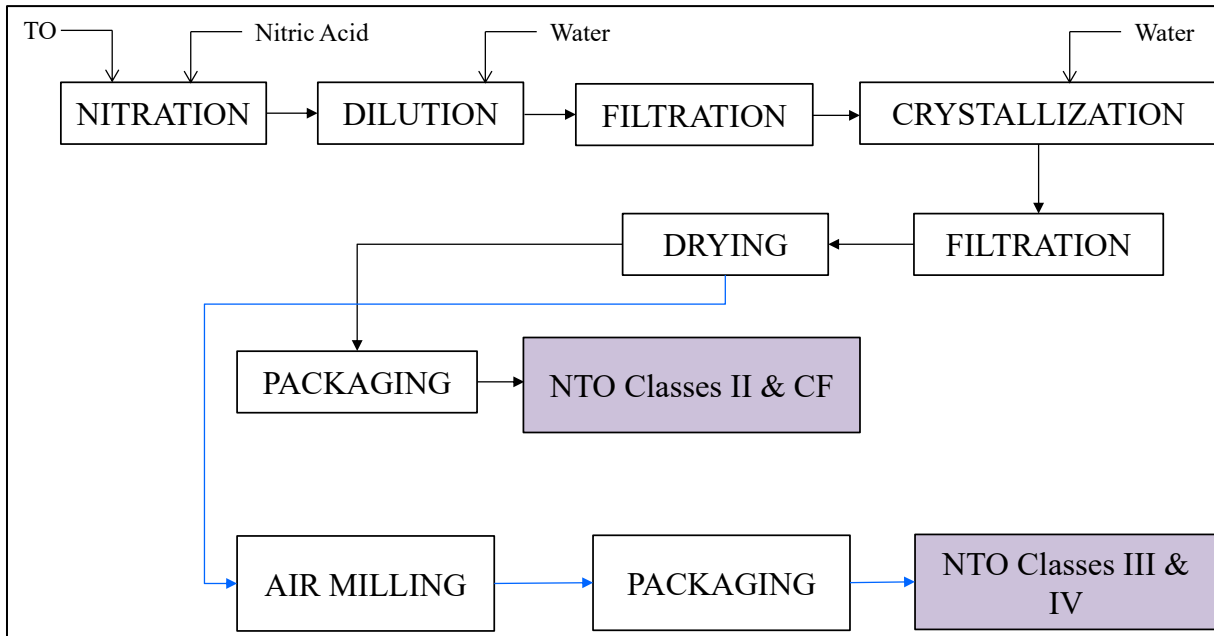


Figure 3: NTO production Flow-sheet

3.2- Synthesis & filtration cell

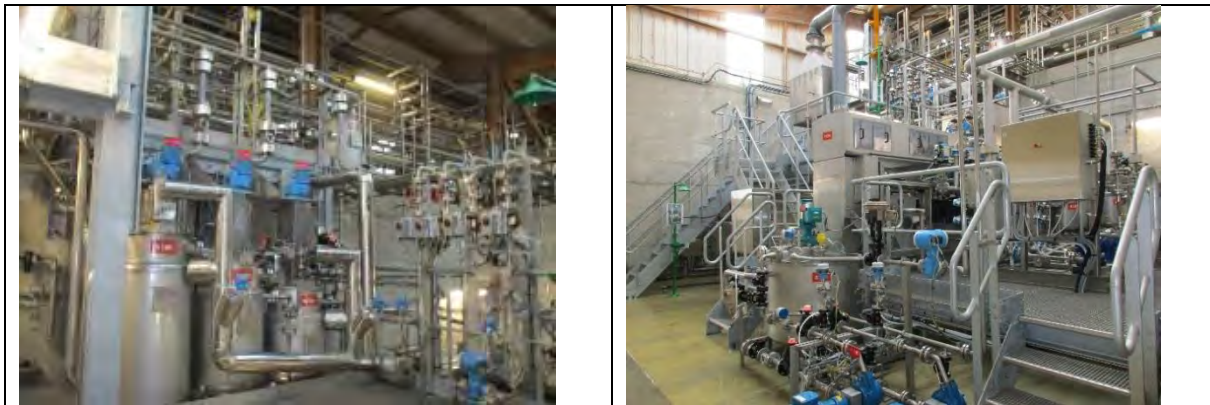


Figure 4: Synthesis cell

The raw materials are introduced in a continuous way with a controlled rate of flow, the synthesis phase, figure 4, has been optimized by adding instrumentation allowing the control station to be deported in a specific building outside the workshop.

The main improvement consists of the use of a dynamic band filter for the cleaning phase of the NTO (separation between acid and NTO) and which allows the continuous production. A perfect cleaning phase is important to ensure the NTO quality and to master the final crystallized product.

3.3- Crystallization

Before to be crystallized, the ratio NTO/water is exactly measured using a pycnometer. Through this step, we can choose the final quality of the NTO (NTO class II & CF) which depends on the accurate quantity of NTO in the crystallizer and a specific process (temperature, ramp...).



Figure 5: Crystallization cell

3.4- Drying & packaging cell.

The main improvement at this step is the use of the fluidizing technology, figure 6, a compress air is used to dry the NTO particles in movement inside the vessel, and this allows a continuous drying and effectively a continuous production.

Before to be automatically packed, detectors are used to ensure the no-presence of foreign matter or metallic particles in the product.



Figure 6: Drying & packaging cell

4- QUALIFICATION PROGRAM

In order to qualify the new plant of NTO, a characterization program was established and validated by the French MoD. It includes a characterization of the granular explosive (NTO Class II, III, IV & CF), Cast-PBX formulations (B2214B) and Pressed-PBX formulations (P16945).

4.1- Granular explosive

The characterization includes:

- Definition File Test (Technical Specifications)
- Safety & vulnerability test
- Others (Microscope, SEM...)

Two levels of characterization were selected: Level 1 corresponding to the products that will undergo a complete characterization and level 2 which corresponds to a limited characterization as shown in the table 1 below. It was selected to place at level 1: NTO class II, IV and CF and Level 2 would apply to Class III.

The results obtained will be compared with the reference (old process), specifications imposed by the definition files and the values from the control charts.

Analysis		NTO Class II	NTO Class III	NTO Class IV	NTO CF
	Humidity	x	x	x	x
	Purity	x	x	x	x
	Acidity (HNO ₃)	x	x	x	x
	TO Content	x	x	x	x
	Chlorine content	x	x	x	x
	Volatile matter	x	x	x	x
	Granulation	x	x	x	x
	Bulk density	x	x	x	x
Safety	Friction sensitivity (BAM)	x	x	x	x
	Impact sensitivity	x	x	x	x
	Progressive heating	x	x	x	x
	DSC	x	x	x	x
	Vacuum stability	x		x	x
	Gutter combustion	x		x	x
	Electric spark	x		x	x
Others	Optical microscope	x	x	x	x
	SEM	x		x	x
	Density	x		x	x
	Melting point	x		x	x

Table 1: Characterization program of the Granular Explosive (NTO)

4.2- Cast-PBX formulations

A B2214B composition (NTO, HMX, binder) was produced using the new NTO, the aim is to characterize this composition at t0 & t6month (table 2) in order to prove that there is no difference compared to the reference (B2214B using old NTO).

Analyses	B2214B
Bulk density	x
Constituent content	x
Mechanical properties at 20 °C	x
Impact sensitivity (t0 & t6month)	x
Friction sensitivity (t0 & t6month)	x
Hammer 30 Kg	x
Progressive heating	x
Gutter combustion	x
Electric spark	x
Vacuum stability	x
Card Gap test (t0 & t6 month)	x
Critical diameter (t0 & t6month)	x
DSC (t0 & t6month)	x
Friability	x
Velocity of detonation	x
Critical temperature for thermoinitiation	x

Table 2: Characterization program of the B2214B

4.3- Pressed-PBX formulations

A granular composition P16945 (NTO, RDX, binder & graphite) was produced using the new NTO, and characterized as shown in the table below. A comparison will be done with the reference (P16945 using old NTO).

Analyses	P16945
Bulk density	X
Constituent content	X
Volatile matter	X
Impact sensitivity	X
Friction sensitivity	X
Granulation	X
Progressive heating	X
Electric spark (ESD)	X
Vacuum stability	X
Card Gap test	X
Critical diameter	X
DSC	X
Friability	X
Velocity of detonation	X

Table 3: Characterization program of the P16945

5- TECHNICAL RESULTS

5.1. Granular explosive (NTO Class II, III, IV & CF)

In order to demonstrate the robustness of the new production line as well as the conformity of the NTO product, several batch's (> 10) have been analyzed according to definition file (technical specifications). Then, one operation was chosen for the series of tests of the qualification program.

5.1.1. NTO class II

The NTO class II was compared to the reference as shown in table 4. We note that the physicochemical & pyrotechnical results are similar to the reference. The NTO class 2 is compliant to the specifications.

Analyses	NTO Class II (New line)	NTO Class II (reference)	Definition File (Specifications)
Purity (%)	99.2	99.9	≥ 99
Acidity (HNO ₃) (%)	0.00	0.03	≤ 0.05
TO Content (%)	0.03	0.13	≤ 0.2
Chlorine content (%)	0.00	0.00	≤ 0.02
Volatile matter (%)	0.02	0.00	≤ 0.1
Bulk density (kg/m ³)	994	814	-
Friction sensitivity (BAM) (N)	5 + at 353 N	4 + at 353 N	-
Impact sensitivity (J)	18	19	-
Progressive heating (°C)	266	265	-
DSC (Onset point °C)	270.5	271	-
Vacuum stability (cm ³ /g)	0.38	0.4	-
Gutter combustion	No propagation	No propagation	-



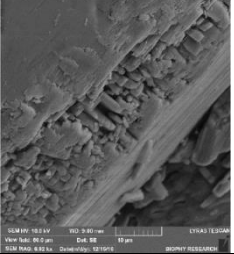
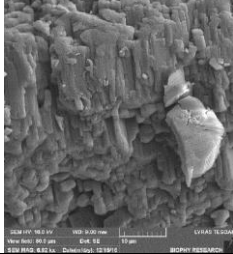
Electric spark (mJ)	> 792	> 792	-
Optical microscope			-
SEM			-
Melting point (°C)	Decomposition at 250°C	Decomposition at 250°C	-
Granulation (% retained on)			
> 0.800 mm	2	0	≤ 4
> 0.500 mm	18	5	≤ 20
> 0.315 mm	53	45	30/60
> 0.200 mm	88	88	≥ 85

Table 4: Characterization results of NTO Class II

5.1.2. NTO class III

The NTO class III was compared to the reference (table 5). We note that the physicochemical & pyrotechnical results are nearly identical. The NTO class III is compliant to the specifications.

Analyses	NTO Class III (New line)	NTO Class III (Reference)	Definition File (Specifications)
Humidity (%)	0.01	0.01	-
Purity (%)	99.1	99.3	≥ 99
Acidity (HNO ₃) (%)	0.03	0.03	≤ 0.05
TO Content (%)	0.03	0.07	≤ 0.2
Chlorine content (%)	0.00	0.00	≤ 0.02
Volatile matter (%)	0.02	0.02	≤ 0.1
Laser granulometry (µm)	55.2	56.5	50 ± 10
Bulk density (Kg/m ³)	560	510	-
Friction sensitivity (BAM) (N)	9 + at 353 N	8 + at 353 N	-
Impact sensitivity (J)	9.1	11	-
Progressive heating (°C)	267	266	-
DSC (onset point °C)	270.4	270.5	-

Table 5: Characterization results of NTO Class III

5.1.3. NTO class IV

Table 6 represents a comparison between the NTO class IV and the reference. We note that the physicochemical & pyrotechnical results are similar. The NTO class IV is compliant to the specifications.

Analyses	NTO Class IV (New line)	NTO Class IV (reference)	Definition File (Specifications)
Humidity (%)	0.01	0.02	-
Purity (%)	99.7	99.3	≥ 99
Acidity (HNO ₃) (%)	0.01	0.01	≤ 0.05
TO Content (%)	0.02	0.04	≤ 0.2
Chlorine content (%)	0.01	0.00	≤ 0.02
Volatile matter (%)	0.01	0.01-0.02	≤ 0.1
Laser Granulometry (µm)	12.5	11.7	12 ± 3
Friction sensitivity (BAM) (N)	3 + at 353 N	0 + at 353 N	-
Impact sensitivity (J)	13	8.1	-
Progressive heating (°C)	269	269	-
DSC (Onset point °C)	272.4	271.6	-
Vacuum stability (cm ³ /g)	0.16	0.26	-
Gutter combustion	No propagation	No propagation	
Electric spark (mJ)	> 792	> 792	-

Table 6: Characterization results of NTO Class IV

5.1.4. NTO CF

The NTO CF was compared to the reference as shown in table 7. We note that the physicochemical & pyrotechnical results are nearly identical. The NTO CF is compliant to the specifications.

Analyses	NTO CF (New line)	NTO CF (reference)	Definition File (Specifications)
Humidity (%)	0.03	0.02	-
Purity (%)	100	99.7	≥ 99
Acidity (HNO ₃) (%)	0	0	≤ 0.05
TO Content (%)	0	0.001	≤ 0.2
Chlorine content (%)	0	0	≤ 0.02
Volatile matter (%)	0.01	0	≤ 0.1
Bulk density (Kg/m ³)	927	939	> 900
Friction sensitivity (BAM) (N)	0 + at 353 N	0 + at 353 N	-
Impact sensitivity (J)	16	13	-
Progressive heating (°C)	266	265	-
DSC (Onset point °C)	272.4	271.6	-
Vacuum stability (cm ³ /g)	0.12	0.16	-
Gutter combustion	No propagation	No propagation	
Electric spark (mJ)	> 792	> 792	-

Table 7: Characterization results of NTO CF

5.2. Cast-PBX formulations

After analyzing the 3 grades of NTO (II, III & IV) a B2214B composition was produced and analyzed. The results are represented in table 8. We note that the B2214B is compliant to the specifications and there is no-difference between new B2214B (New NTO) and old B2214B (old NTO).

Analyses	B2214B (NTO New line)	Reference	Specifications
density (kg/m ³)	1630	1643	1605-1645
Constituent content (NTO, HMX, binder) (%)	72.2/12.5/15.3	72.2/11.6/16.2	
Mechanical properties at 20 °C (Stress Mpa)	0.89	0.75	0.7±0.3
Impact sensitivity (J)	31	27	-
Friction sensitivity (N)	15 + at 353N	4 + at 353 N	-
Progressive heating (°C)	234	232	233
Gutter combustion	No propagation	No propagation	-
Electric spark (mJ)	> 792	> 792	
Card Gap test (phi 75 mm)	35 mm	35mm	-
Velocity of detonation (m/s)	7414	7482	-

Table 8: Characterization results of B2214B

5.3. Pressed-PBX formulations

The NTO class II was produced and analyzed for the production of the P16945 (NTO, RDX, Binder & Graphite). The P16945 was analyzed as shown in table 9. We note that the P16945 is compliant to the specifications and there is no-difference between new P16945 (New NTO) and old P16945 (old NTO).

Analyses	P16945 (NTO New line)	Reference	Specifications
Bulk density (kg/m ³)	693	721	-
Constituent content (NTO, RDX, Binder & graphite) (%)	75.2/19.3/5/0.5	75.3/19.6/4.5/0.6	75±3/20±2/5±0.5/0.5±0.3
Impact sensitivity (J)	9.7	10	-
Friction sensitivity (N)	3 + at 353N	2+ at 353N	-
Granulation (% retained on)			
> 0.800 mm	43	49	-
> 0.500 mm	63	73	> 50
> 0.315 mm	81	88	> 80
> 0.040 mm	100	100	> 98
Progressive heating (°C)	210	209	-
Electric spark (mJ)	> 792	> 792	-
Vacuum stability (cm ³ /g)	0.14	0.31	-
Card Gap test (phi 40 mm)	200	190	-
DSC (Onset point °C)	202	205	-
Velocity of detonation	In progress	7893	-

Table 9: Characterization results of P16945

6- CONCLUSION

After more than 25 years, the workshop used for the NTO production has been designed and rebuilt, the new one is now able to more than 200 T per year. Different qualities of NTO are produced, class II, III, IV & CF for Cast-PBX IM applications but also a specific quality designed for IM Melt-Cast formulations.

The challenge was to demonstrate that with this new production line and with this optimized process, the quality of our NTO was the same of that produced before and already qualified for our customers.

The qualification program was established and validated by the French MoD. The results confirm that all grades of NTO (NTO class II, III, IV & CF) are compliant to the specifications and identical to the references. The new NTO has then been also tested and checked in two IM compositions, one plastic bonded explosive B2214B and one for a pressed application P16945.

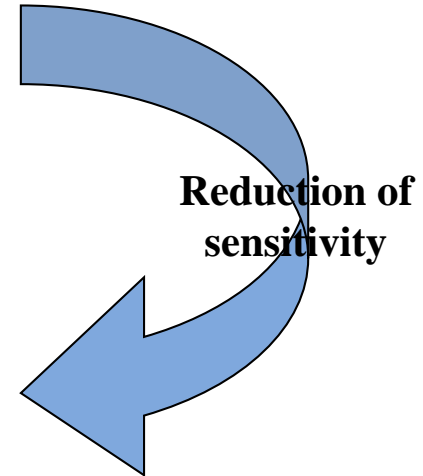
The line is fully qualified and commissioned.



NEW NTO WORKSHOP AND ASSOCIATED PRODUCT CHARACTERIZATIONS

A. Delage, P. Chabin, G. Alvarez, V. Chauffour & G. Eck

- **Introduction**
- **Applications**
- **Process**
- **New plant vs Old plant**
- **Characterization program**
- **Results**
- **Conclusion**

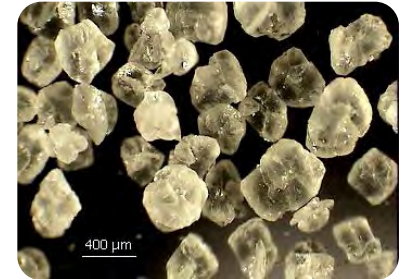
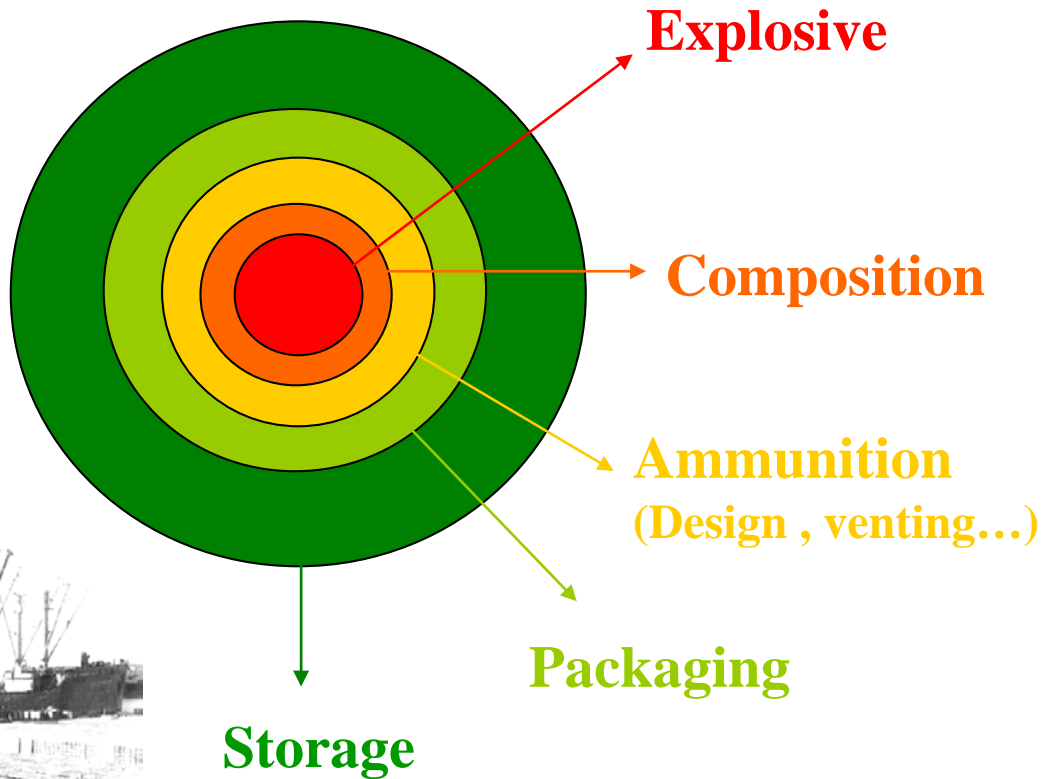


CAST CURED COMPOSITIONS



**PRESSED COMPOSITIONS
MELT CAST COMPOSITIONS**

□ Insensitive Munitions (IM) are to be considered as a whole



NTO



Composition P16945



NTO
Most well known IM explosive
Available from 10 µm up to 450 µm

Class 4
 $D_{50} \sim 10 \mu\text{m}$

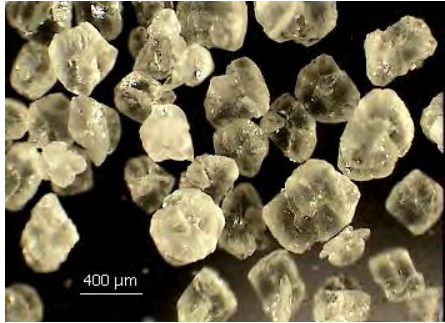
Class 3
 $D_{50} \sim 50 \mu\text{m}$

Class 2
 $D_{50} \sim 350 \mu\text{m}$

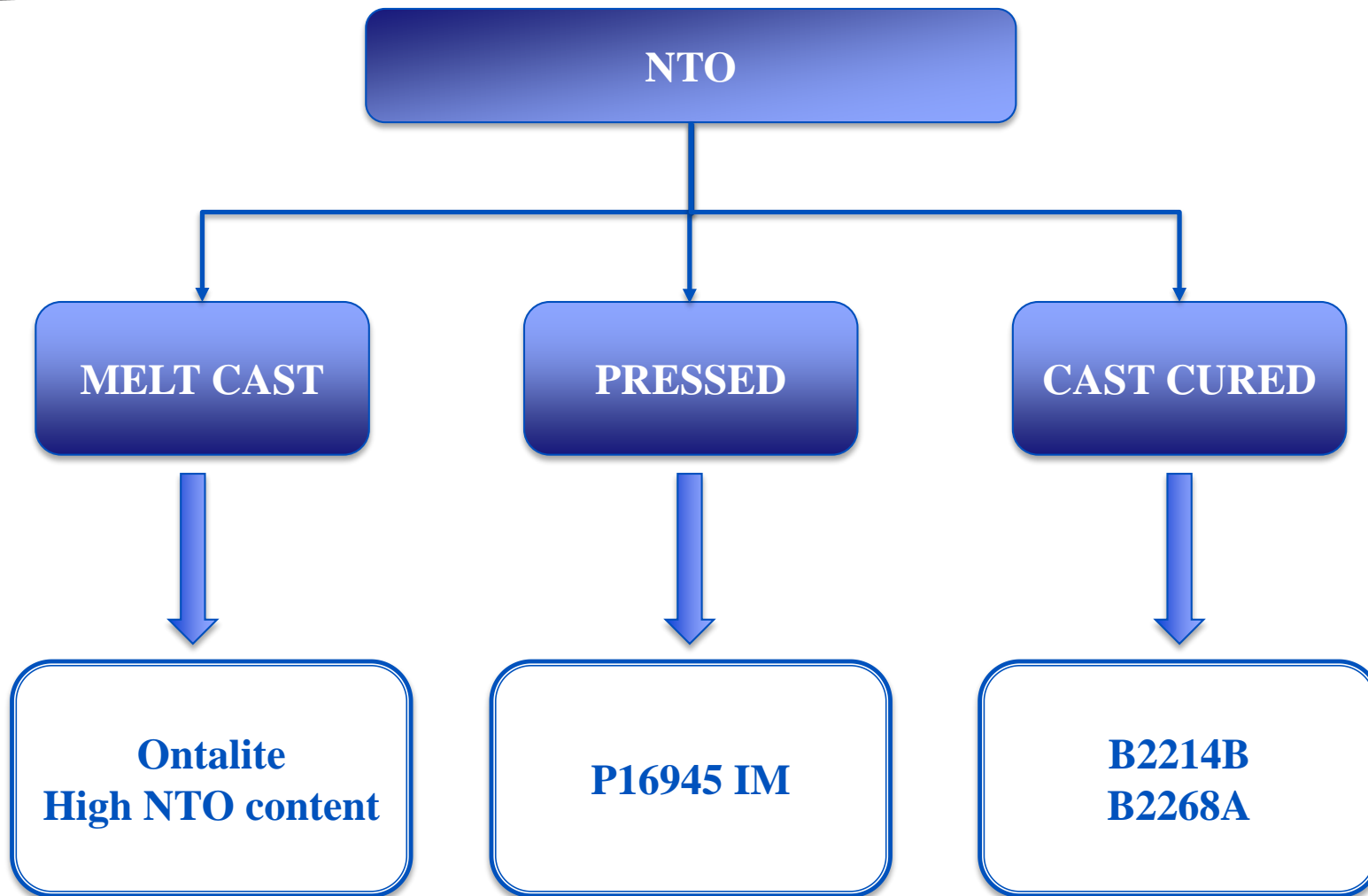
Class CF
(High Bulk de
 $D_{50} \sim 450 \mu\text{m}$



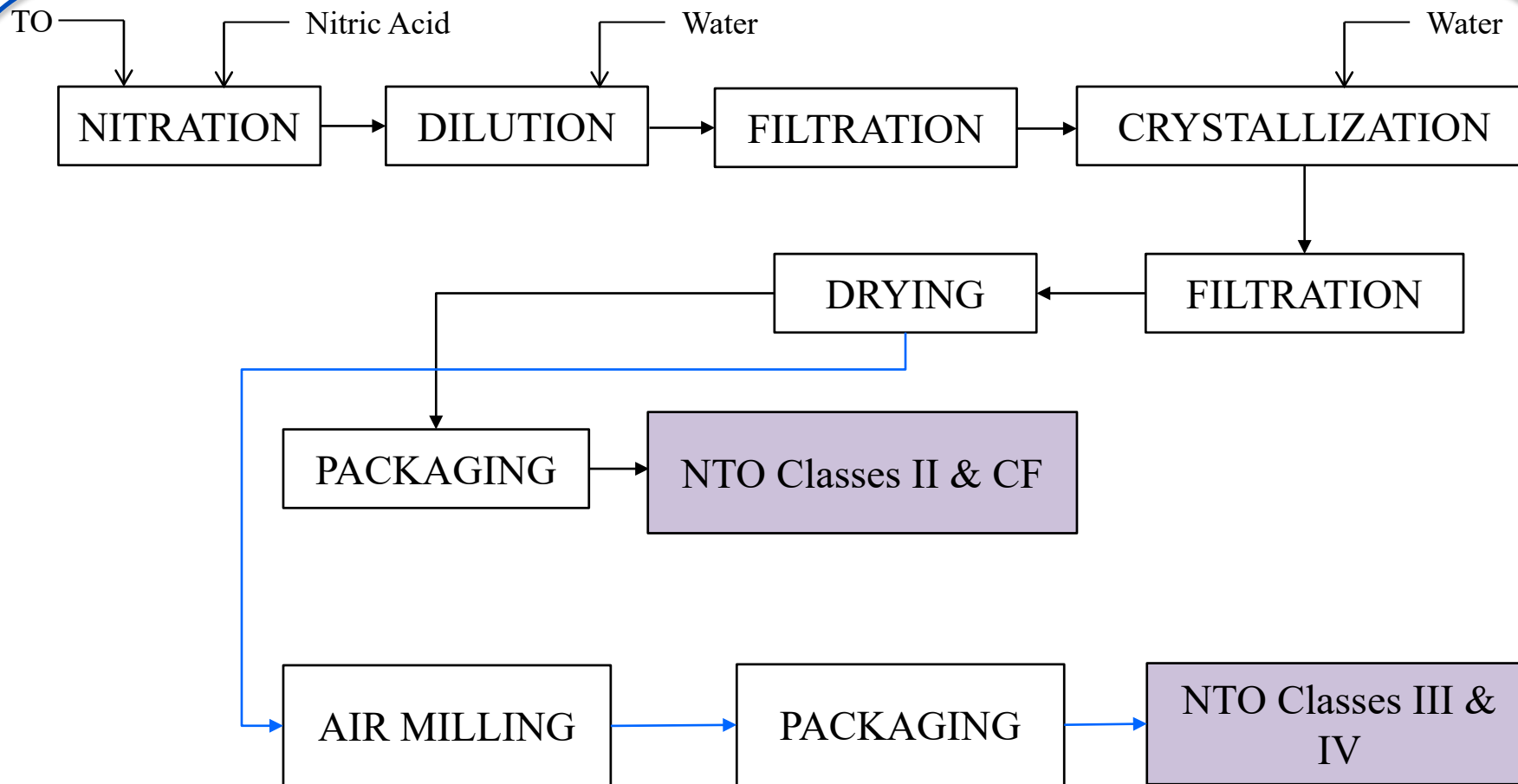
Cast cured compositions
Most of melt cast IM compositions
Pressed



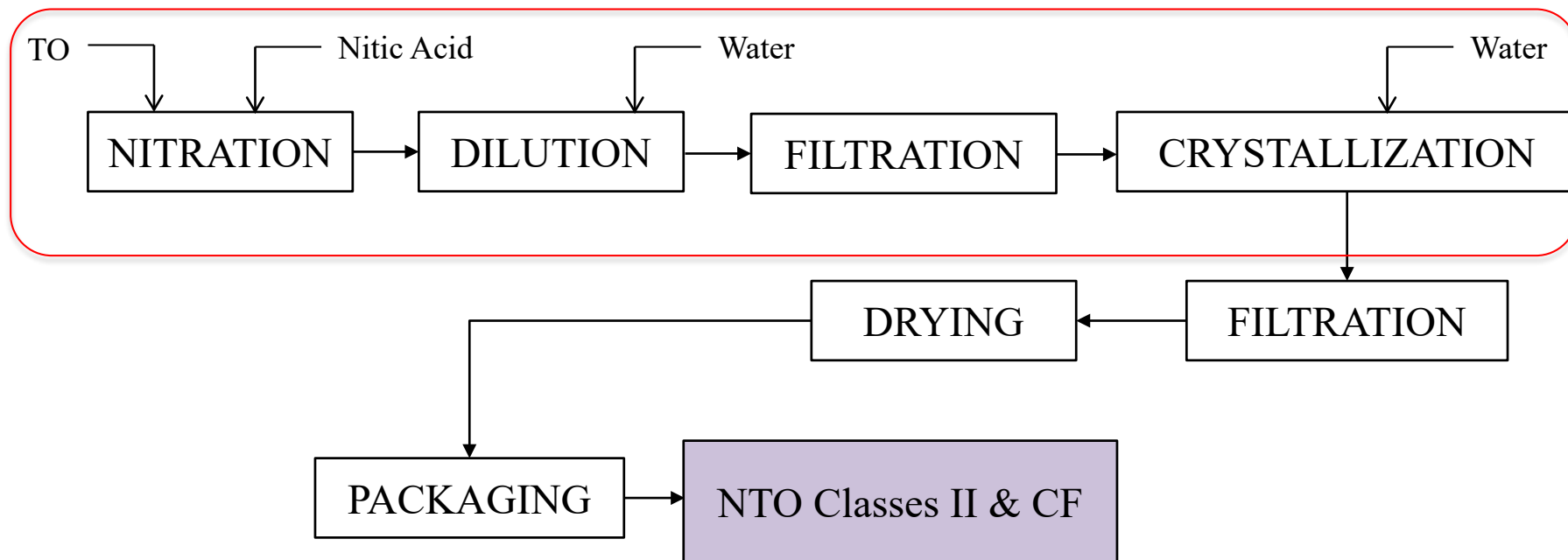
- **Introduction**
- **Applications**
- **Process**
- **New plant vs Old plant**
- **Characterization program**
- **Results**
- **Conclusion**



- **Introduction**
- **Applications**
- **Process**
- **New plant vs Old plant**
- **Characterization program**
- **Results**
- **Conclusion**



- **Introduction**
- **Applications**
- **Process**
- **New plant vs Old plant**
- **Characterization program**
- **Results**
- **Conclusion**



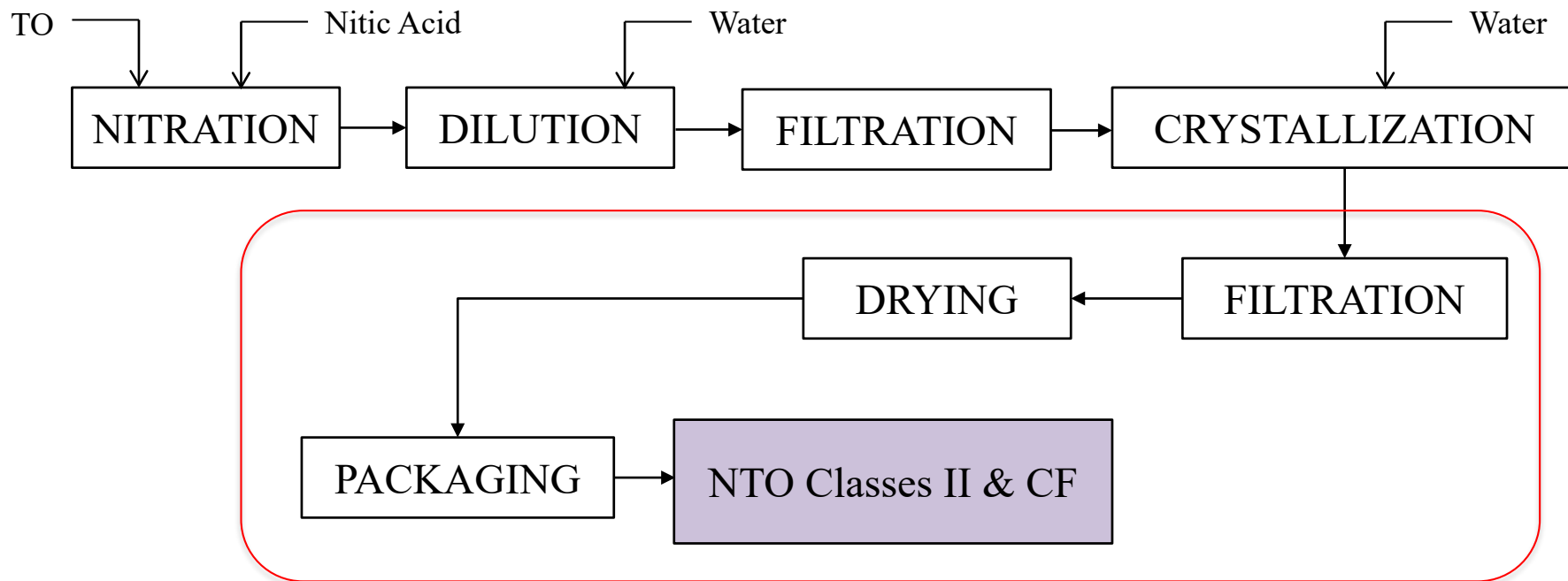
Workshop n° 320



Synthesis



Crystallization



Drying: workshop n° 362
 Packaging: workshop n° 205



Outside view

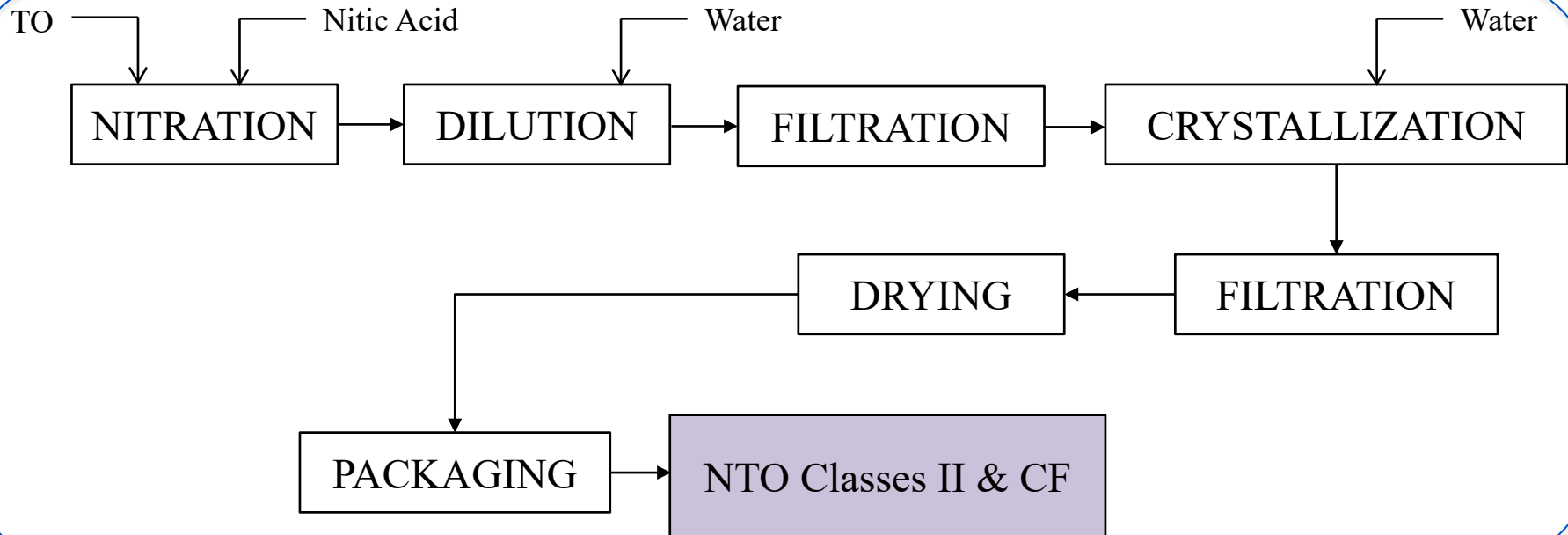


Sieving

No specific instrumentation was automated and the control station and command control wasn't deported

Impossible to reach the required level regarding safety and environmental regulation.

- **Introduction**
- **Applications**
- **Process**
- **New plant vs Old plant**
- **Characterization program**
- **Results**
- **Conclusion**



Workshop n° 320

From Raw materials to Packaging final product at the same plant

New technologies of: Filtration, Drying & packaging

Synthesis cell



- **Synthesis Step:** Continuous nitration of TO by nitric acid → NTO
- **Dilution Step:** Eliminating the impurities

Crystallization cell



Pycnometers



Crystallizers

- **Pycnometers:** ratio NTO/water
- **Crystallization:** purify the product & final quality of NTO

Drying & Packaging cell

Drying



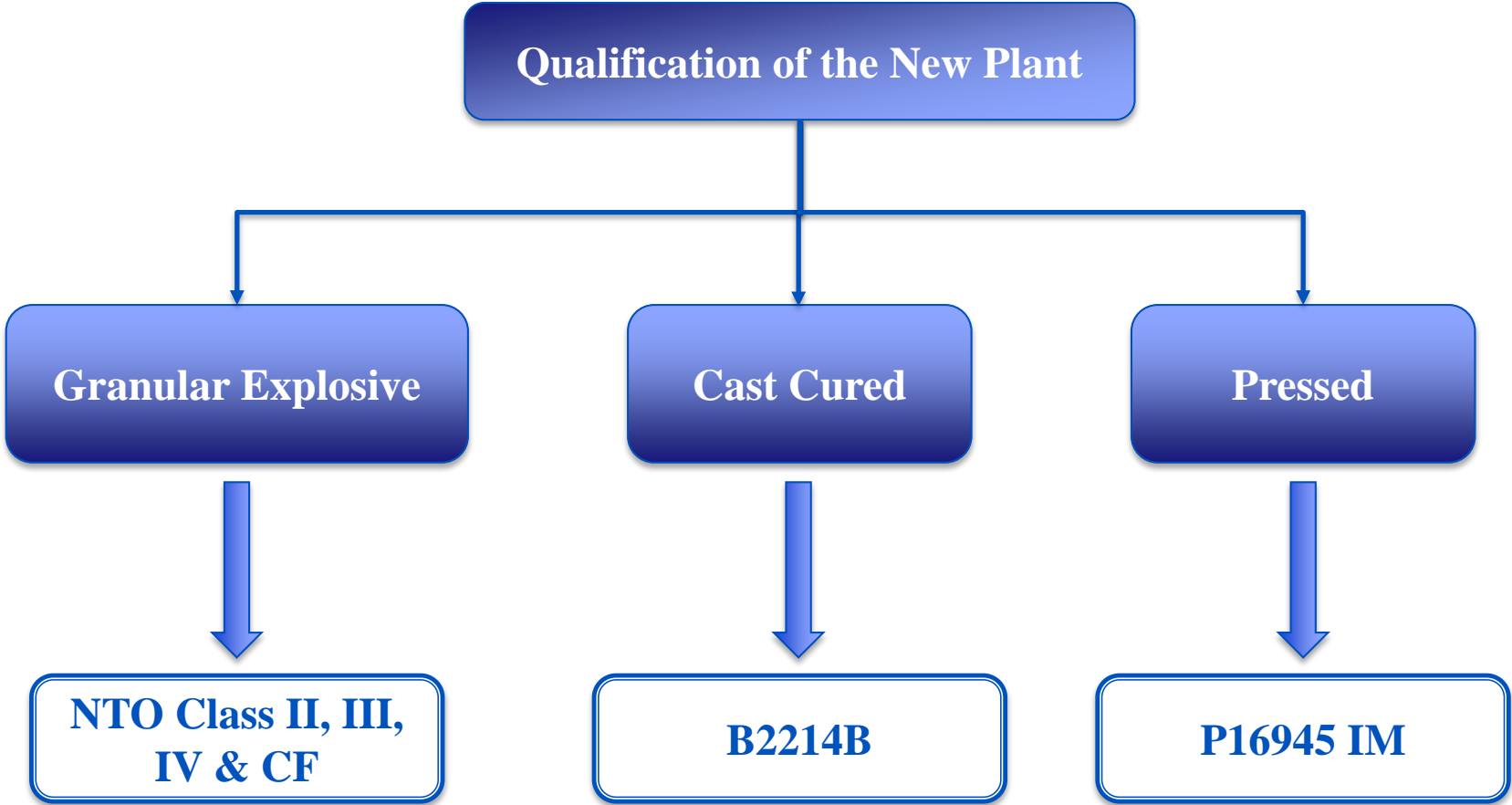
Packaging

- **Drying:** Fluidizing Technology

❑ Advantages of the New Plant:

- **Continuous & Integrated Process** from the introducing of the Raw material's to the packaging of the final product
- **New Process Technology:**
 - Filtration: dynamic band filter for the cleaning phase of the NTO (separation between acid and NTO)
 - Pycnometer: Ratio NTO/H₂O → final quality of the NTO
 - Filtration & Drying: fluidizing technology: a compress air is used to dry the NTO particles in movement inside the vessel
 - Packaging: detectors are used to ensure the no-presence of foreign matter or metallic particles in the product.
- All the specific instrumentation are **automated** and the control station and command control are **deported** 😊
- **Safety and environmental regulation** 😊
- **> 200T/Year** 😊

- **Introduction**
- **Applications**
- **Process**
- **New plant vs Old plant**
- **Characterization program**
- **Results**
- **Conclusion**



Characterization program Validated by the French MoD

Granular Explosive: NTO

Analyses		NTO Class II	NTO Class III	NTO Class IV	NTO CF
Technical Specifications	Appearance	x	x	x	x
	Humidity	x	x	x	x
	Purity	x	x	x	x
	Acidity (HNO ₃)	x	x	x	x
	TO Content	x	x	x	x
	Chlorine content	x	x	x	x
	Volatile matter	x	x	x	x
	Granulation	x	x	x	x
	Bulk density	x	x	x	x
Safety & Vulnerability	Friction sensitivity (BAM)	x	x	x	x
	Impact sensitivity	x	x	x	x
	Progressive heating	x	x	x	x
	DSC	x	x	x	x
	Vacuum stability	x		x	x
	Gutter combustion	x		x	x
	Electric spark	x		x	x
Others	Optical microscope	x	x	x	x
	SEM	x		x	x
	Density	x		x	x
	Melting point	x		x	x

Comparison between New NTO & The reference (old NTO), Technical specifications, Chart controls

Cast Cured Composition (B2214B) & Pressed Composition (P16945)

Analyses	B2214B
Density	x
Constituent content	x
Mechanical properties at 20 °C	x
Impact sensitivity (t0 & t6month)	x
Friction sensitivity (t0 & t6month)	x
Hammer 30 Kg	x
Progressive heating	x
Gutter combustion	x
Electric spark	x
Vacuum stability	x
Card Gap test (t0 & t6 month)	x
Critical diameter (t0 & t6month)	x
DSC (t0 & t6month)	x
Friability	x
Velocity of detonation	x
Critical temperature for thermoinitiation	x

Analyses	P16945
Bulk density	x
Constituent content	x
Volatile matter	x
Impact sensitivity	x
Friction sensitivity	x
Granulation	x
Progressive heating	x
Electric spark	x
Vacuum stability	x
Card Gap test	x
Critical diameter	x
DSC	x
Friability	x
Velocity of detonation	x

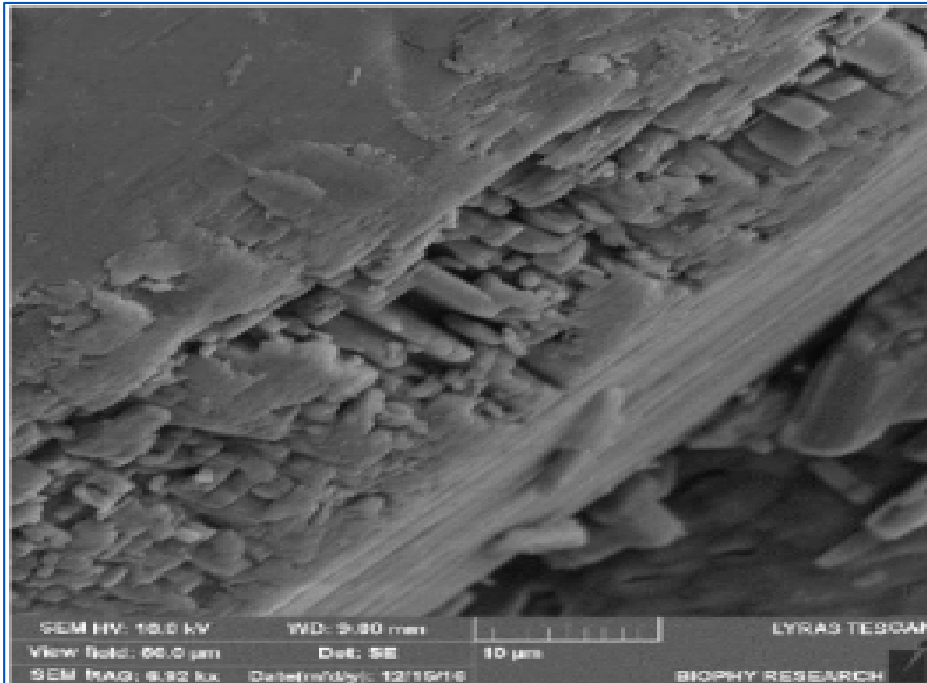
Comparison with Reference, Technical specifications & Chart controls

- **Introduction**
- **Applications**
- **Process**
- **New plant vs Old plant**
- **Characterization program**
- **Results**
- **Conclusion**

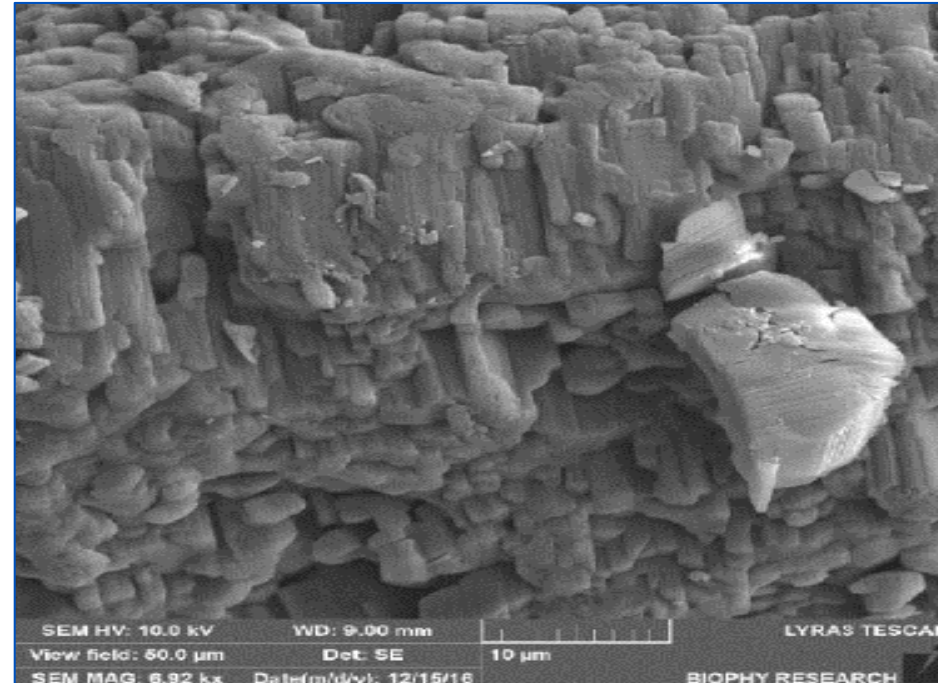
Granular Explosive: NTO Class II

Analyses	NTO Class II (New line)	NTO Class II (reference)	Definition File (Specifications)
Purity (%)	99.2	99.9	≥ 99
Acidity (HNO ₃) (%)	0.00	0.03	≤ 0.05
TO Content (%)	0.03	0.13	≤ 0.2
Chlorine content (%)	0.00	0.00	≤ 0.02
Volatile matter (%)	0.02	0.00	≤ 0.1
Bulk density (kg/m ³)	994	814	-
Friction sensitivity (BAM) (N)	5 + at 353 N	4 + at 353 N	-
Impact sensitivity (J)	18	19	-
Progressive heating (°C)	266	265	-
DSC (Onset point °C)	270.5	271	-
Vacuum stability (cm ³ /g)	0.38	0.4	-
Gutter combustion	No propagation	No propagation	-
Electric spark (mJ)	> 792	> 792	-
Melting point (°C)	Decomposition at 250°C	Decomposition at 250°C	-

□ Granular Explosive: NTO Class II



ONTA class II



Reference ONTA class II

NTO class II complies to the specifications & similar to the reference

□ Granular Explosive: NTO Class III

Analyses	NTO Class III (New line)	NTO Class III (Reference)	Definition File (Specifications)
Purity (%)	99.1	99.3	≥ 99
Acidity (HNO ₃) (%)	0.03	0.03	≤ 0.05
TO Content (%)	0.03	0.07	≤ 0.2
Chlorine content (%)	0.00	0.00	≤ 0.02
Volatile matter (%)	0.02	0.02	≤ 0.1
Laser granulometry (µm)	55.2	56.5	50 ± 10
Bulk density (Kg/m ³)	560	510	-
Friction sensitivity (BAM) (N)	9 + at 353 N	8 + at 353 N	-
Impact sensitivity (J)	9.1	11	-
Progressive heating (°C)	267	266	-
DSC (onset point °C)	270.4	270.5	-

NTO class III complies to the specifications & similar to the reference

□ Granular Explosive: NTO Class IV

Analyses	NTO Class IV (New line)	NTO Class IV (reference)	Definition File (Specifications)
Humidity (%)	0.01	0.02	-
Purity (%)	99.7	99.3	≥ 99
Acidity (HNO ₃) (%)	0.01	0.01	≤ 0.05
TO Content (%)	0.02	0.04	≤ 0.2
Chlorine content (%)	0.01	0.00	≤ 0.02
Volatile matter (%)	0.01	0.01-0.02	≤ 0.1
Laser Granulometry (µm)	12.5	11.7	12 ± 3
Friction sensitivity (BAM) (N)	3 + at 353 N	0 + at 353 N	-
Impact sensitivity (J)	13	8.1	-
Progressive heating (°C)	269	269	-
DSC (Onset point °C)	272.4	271.6	-
Vacuum stability (cm ³ /g)	0.16	0.26	-
Gutter combustion	No propagation	No propagation	-
Electric spark (mJ)	> 792	> 792	-

NTO class IV is conform to the specifications & similar to the reference

□ Granular Explosive: NTO Class CF

Analyses	NTO CF (New line)	NTO CF (reference)	Definition File (Specifications)
Humidity (%)	0.03	0.02	-
Purity (%)	100	99.7	≥ 99
Acidity (HNO ₃) (%)	0	0	≤ 0.05
TO Content (%)	0	0.001	≤ 0.2
Chlorine content (%)	0	0	≤ 0.02
Volatile matter (%)	0.01	0	≤ 0.1
Bulk density (Kg/m ³)	927	939	> 900
Friction sensitivity (BAM) (N)	0 + at 353 N	0 + at 353 N	-
Impact sensitivity (J)	16	13	-
Progressive heating (°C)	266	265	-
DSC (Onset point °C)	272.4	271.6	-
Vacuum stability (cm ³ /g)	0.12	0.16	-
Gutter combustion	No propagation	No propagation	-
Electric spark (mJ)	> 792	> 792	-

NTO CF complies to the specifications & similar to the reference

Cast Cured Composition: B2214B

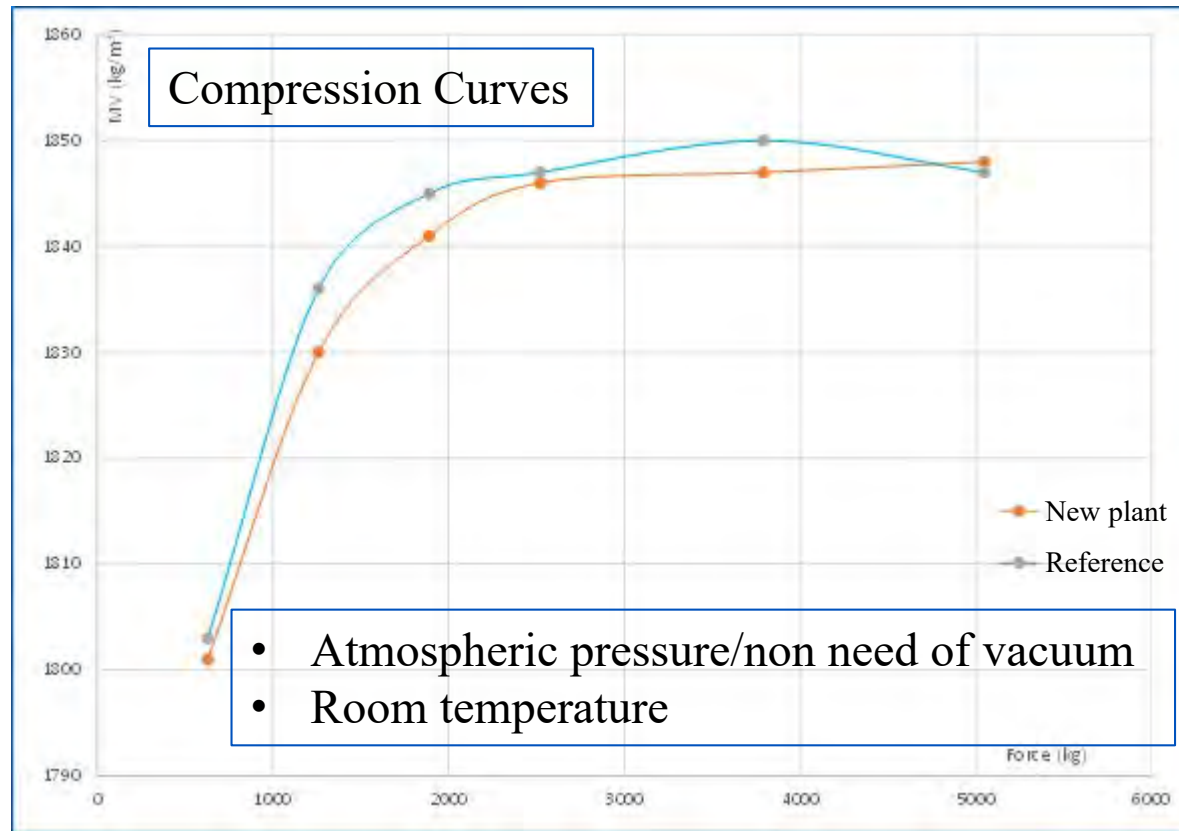
Analyses	B2214B (NTO New line)	Reference	Specifications
density (kg/m ³)	1630	1643	1605-1645
Constituent content (NTO, HMX, binder) (%)	72.2/12.5/15.3	72.2/11.6/16.2	
Mechanical properties at 20 °C (Stress Mpa)	0.89	0.75	0.7±0.3
Impact sensitivity (J)	31	27	-
Friction sensitivity (N)	15 + at 353N	4 + at 353 N	-
Progressive heating (°C)	234	232	233
Gutter combustion	No propagation	No propagation	-
Electric spark (mJ)	> 792	> 792	
Card Gap test (phi 75 mm)	35 mm	35mm	-
Velocity of detonation (m/s)	7414	7482	-

B2214B complies to the specifications & similar to the reference

Pressed Composition: P16945

Analyses	P16945 (NTO New line)	Reference	Specifications
Bulk density (kg/m ³)	693	721	-
Constituent content (NTO, RDX, Binder & graphite) (%)	75.2/19.3/5/0.5	75.3/19.6/4.5/0.6	75±3/20±2/5±0.5/0.5±0.3
Impact sensitivity (J)	9.7	10	-
Friction sensitivity (N)	3 + at 353N	2+ at 353N	-
Granulation (% retained on)			
> 0.800 mm	43	49	-
> 0.500 mm	63	73	> 50
> 0.315 mm	81	88	> 80
> 0.040 mm	100	100	> 98
Progressive heating (°C)	210	209	-
Electric spark (mJ)	> 792	> 792	-
Vacuum stability (cm ³ /g)	0.14	0.31	-
Card Gap test (phi 40 mm)	200	190	-
DSC (Onset point °C)	202	205	-
Velocity of detonation	In progress	7893	-

☐ Pressed Composition: P16945



P16945 complies to the specifications & similar to the reference

- **Introduction**
- **Applications**
- **Process**
- **New plant vs Old plant**
- **Characterization program**
- **Results**
- **Conclusion**

- Process: Robust, automated & Reproducible 😊**
- Safety and environmental regulation 😊**
- All the Grade of NTO (II, III, IV & CF) are conform to the specifications & identical to the references 😊**
- The new NTO has then been also tested and checked in two IM compositions, one cast PBX B2214B and one for a pressed application P16945 😊**
- > 200T/Year 😊**
- The line is fully qualified and commissioned 😊**

- G. Eck, P. Chabin, G. Alvarez & V. Chauffour who coauthored this work
- Process Engineering & production team who have worked intensively for the success of the new Plant
- Laboratory team who characterized the NTO & the compositions

Thank you for your attention
Questions?



EUROPEAN LEADER IN ENERGETIC MATERIALS

DEVELOPMENT OF A CONUS MANUFACTURING CAPABILITY FOR FOX-7

Bradley A. Sleadd, David T. Boruta

Naval Surface Warfare Center, Indian Head EOD Technology Division
Indian Head, MD

Joseph W. Clubb

Naval Air Warfare Center Weapons Division
China Lake, CA

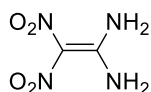
Abstract

1,1-diamino-2,2-dinitroethene, or FOX-7, is an insensitive energetic material originally developed by FOI Sweden. Theoretical thermochemical calculations indicate that FOX-7 should exhibit nearly equivalent performance with that of RDX, while being considerably less sensitive to unplanned stimuli. Much like TATB, FOX-7 contains amino and nitro groups which can participate in intra and intermolecular hydrogen bonding. This phenomenon is believed to provide both materials with their unusual stability. FOX-7 has been evaluated in both propellant and explosive applications with very promising results. As such, a domestic source of FOX-7 is highly desirable since the only current commercial supplier is the European conglomerate, Eurenco.

As part of a JIMTP program, NSWC IHEODTD has been tasked with developing a domestic manufacturing capability for FOX-7, as well as providing the four classes of material currently available from Eurenco. FOX-7 has been synthesized at NSWC IHEODTD at the 5, 20, 100 gram and kilogram scales, and there is currently an active SOP for the manufacture of FOX-7 at the multi-kilogram scale with yields typically in the 65-70% range. We have also produced all four classes/particle size distributions of FOX-7; Class 1 (20-40 μm), Class 2 (50-100 μm), Class 3 (100-200 μm) and Class 4 (250-350 μm) via recrystallization, and have produced Class 1 and Class 4 via recrystallization at the multi-kilogram scale.

Introduction

The objective of this effort was to develop a scalable process which would produce R&D quantities of 1,1-diamino-2,2-dinitroethene (aka FOX-7 or DADNE, Figure 1). The Chemical Scale-up Group at NSWC IHEODTD was selected for this process R&D effort to act as a continental United States (CONUS) source of R&D quantities of FOX-7 for JIMTP Task 14-2-68. Developing this capability would in turn provide the ability to support future programs requiring R&D quantities of FOX-7 synthesized in the CONUS.

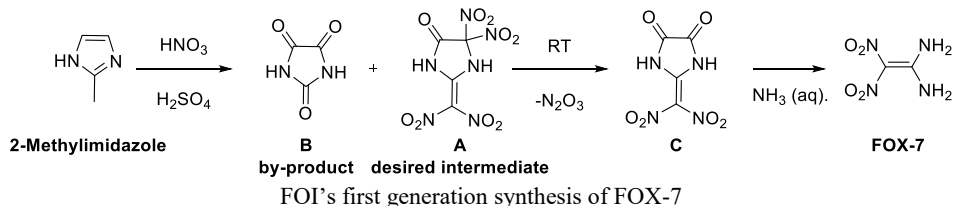


FOX-7

1,1-diamino-2,2-dinitroethene (FOX-7)

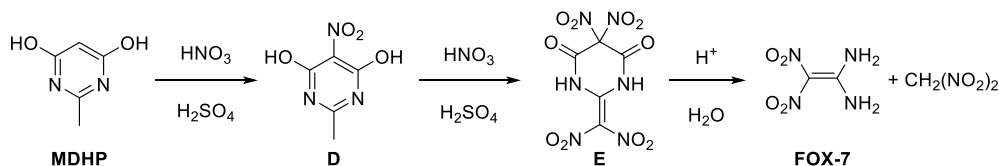
FOX-7 was first synthesized and reported by Latypov, Langlet, and Wellmar of the Swedish Defense Research Agency (FOI).¹ Currently, EURENCO Bofors AB is licensed by the Swedish government to synthesize pilot and production scale quantities of FOX-7.

As shown in Figure 2, FOI's first generation synthesis of FOX-7 proceeded from 2-methylimidazole in mixed acid containing up to 20% water to afford the desired intermediate, 2-dinitromethylene-4,4-dinitroimidazolidin-5-one (A), along with parabanic acid (B) as a by-product. Use of oleum afforded none of the desired intermediate, but rather 2-methyl-4-nitro-imidazole and parabanic acid (B). The desired intermediate would then hydrolyze at ambient temperature to form 2-dinitromethyleneimidazolidine-4,5-dione (C), which would then be exposed to aqueous ammonia to afford FOX-7.



FOI's first generation synthesis of FOX-7

An improved process to FOX-7 was also developed at FOI.² As shown in Figure 3, exposing 2-methyl-3,5-dihydroxypyrimidine (MDHP) to mixed acid proceeds through two stages of nitration. The first nitration is reported to be fast,³ which affords 4,6-dihydroxy-2-methyl-5-nitropyrimidine (D). The second nitration is the slow step,³ which gives access to 2-dinitromethylene-5,5-dinitrodihydropyrimidine-4,6(1H,5H)-dione (E). Intermediate E can either be isolated and hydrolyzed after separation from the mixed acid,⁴ or an *in-situ* quench can be performed to directly afford FOX-7 and dinitromethane,² which typically undergoes further hydrolytic decomposition.



FOI's second generation synthesis of FOX-7

FOX-7 has been reported to have a crystal density⁵ of 1.88 g/cm³. It has been reported to be significantly less sensitive than RDX with respect to impact⁶ and friction while maintaining RDX-like performance properties.⁷ EURENCO Bofors has produced FOX-7 in different particle sizes: Class I (20 – 40 μm),

Class II (50 – 100 μm), Class III (100 – 200 μm), and Class IV (250 – 350 μm).³ Unlike typical energetic molecules, FOX-7 has been observed to have increased shock sensitivity as particle size decreases. This phenomenon is still not well understood.^{9,10}

Results and Discussion

The NSWC IHEODTD Chemical Scale-up Group chose the MDHP process as a starting point for this effort. From a cost-savings perspective, this process would be an ideal starting point; the starting materials were readily available in bulk, and the process would be less labor intensive. An *in-situ* ice quench would avoid the need for a separate hydrolysis step and would eliminate the need to deal with the major by-product of the reaction, dinitromethane.

Scale-up from the 1 gram to 20 gram scale

Initial investigations into reproducing the conditions described by Latypov and Bellamy in the literature^{2,4} were performed at the 1g, 5g, and 20g scales in laboratory glassware. The reaction proceeded as described in the literature, and the exothermic behavior of the reaction was controlled using an ice water bath and by controlling the dose rate of the white fuming nitric acid. The *in-situ* ice quench often produced yellow NO_x fumes, heat, and moderate amounts of foam. The heat generated was largely due to acid-base chemistry occurring between the ice water and mixed acid, while the foam was generated from hydrolytic decomposition to NO_x and CO_2 by-products in addition to rapid precipitation of FOX-7 out of solution. The samples of FOX-7 were analyzed by NMR and DSC and were compared with an authentic sample and checked against data published in the open literature. The ^1H and ^{13}C NMR data for FOX-7 were consistent with those previously reported.

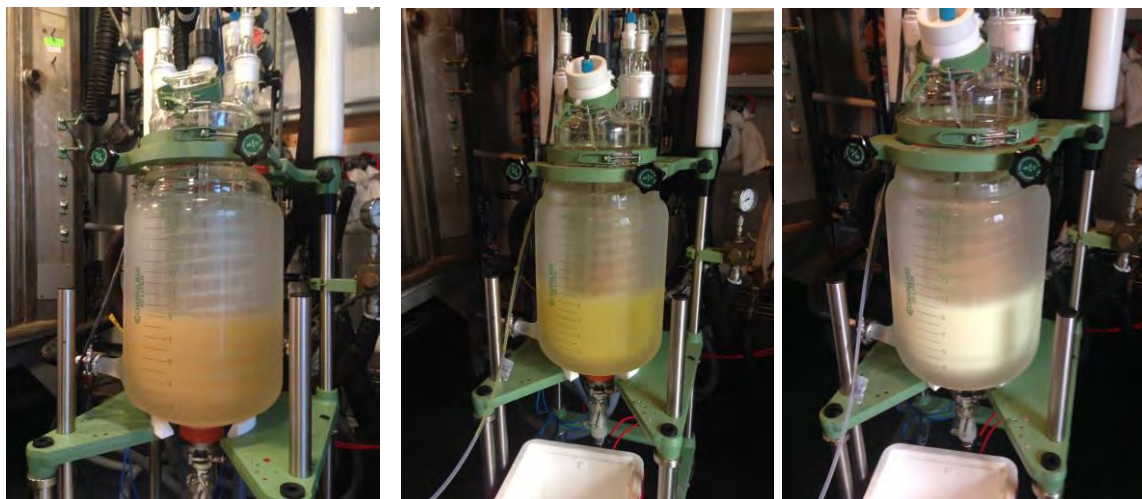
2-Liter RC-1 Scale-up to 100 grams

At the 100 gram scale, an initial thermal profile was developed using a Mettler Toledo RC1e reaction calorimeter. When the first 100 gram batch was performed, $T_R - T_J$ was observed to peak around 10K and began to fall off immediately after the dose stopped. The second 100 gram batch was used to obtain heat flow data on the reaction. The reaction typically behaved similarly to the smaller scale batches. Again, the *in-situ* ice quench often produced yellow NO_x fumes, heat, and foam. The Chemical Scale-up Group's evaluation of the amount NO_x , heat, and foam produced during the quench warranted a more delicate approach to quenching at larger scale, where the crude mixture in mixed acid would be dosed into a stirred quench reactor containing water while maintaining a desired temperature.

Scale-up synthesis to the 1 kilogram batch in the 20-liter reactor

The 1 kilogram batch synthesis of FOX-7 was performed in a Chemglass 20-liter reactor with Teflon-coated temperature controlling coils. The kilogram batch synthesis of FOX-7 began by dissolving MDHP in sulfuric acid in the 20-liter reactor. Temperature control was maintained through the use of a combination of the 20-liter reactor jacket along with the internal cooling coils, which were controlled by a separate, external chiller.

The dose rate and coolant feed to the reactor jacket and coils were continuously adjusted to maintain the desired nitration temperature. During the dose, the color of the material changed from a light brown, to a transparent yellow, and finally to a transparent white. The agitation was stopped to observe the material and the solids looked suspended in the liquid.



A

B

C

20-Liter reactor contents during nitration: A) MDHP dissolved in sulfuric acid; homogeneous. B) Reactor contents during nitric acid dose; homogeneous. C) Reactor contents near completion of nitric acid dose; color change, fine suspension, no longer homogenous.

The slurry containing E from the 20 L reactor was then pumped into warm water in a 50 L reactor for the quench decomposition to form FOX-7.



A

B

C

50-liter reactor during quench: A) Reactor at beginning of quench. B) Reactor 30 minutes into quench, particles suspended, color change, mostly translucent. C) Reactor 1 hour into quench, contents opaque.

The contents of the 50-liter reactor were then drained into a 1 micron filter bag. The solids were washed with water and air dried to give a 72% overall crude yield.

Recrystallization Method Development and Recrystallization of Kilogram Batches

Crystallization conditions used to obtain particle sizes and morphologies consistent with material produced by Eurenco Bofors was proprietary information given to Joseph Clubb, NAWC WD, and later shared with us with permission by Eurenco.⁸ Consequently, it will not be presented in this paper.

Safety and Thermal Characterization

In order to assess the CONUS material and compare against OCONUS source a series of round-robin safety and thermal evaluations were conducted by NSWC IHEODTD, NAWC China Lake, and ARDEC Picatinny. Each participant was shipped up to 1-kg batch of both the Class I and Class IV recrystallized CONUS FOX-7 from NSWC Indian Head. In order to avoid method or machine bias the round-robin participants made 'best attempt' to standardize the test protocol and stipulations were agreed upon prior to testing. The testing followed the Allied Ordinance Publication (AOP-7) 2nd edition MANUAL OF DATA REQUIREMENTS AND TESTS FOR THE QUALIFICATION OF EXPLOSIVE MATERIALS FOR MILITARY USE that calls out accepted methods via associated STANAGs for friction (4487), impact (4489), electrostatic discharge (4490), and thermal stability (4515). Where methods or testing equipment differed in the slightest, stipulations were agreed upon with respect to mass of testing samples, testing environment, data analysis and reporting. The testing equipment and stipulations are as follows:

Equipment

Impact – ERL

- Type 12 Tooling
- Mass of drop weight: 2.5 kg
- Mass of Striker: 520-540 gm
- 180A Garnet Paper

Friction – Safety Management System (SMS) supplied Alleghany Ballistics Laboratory (ABL) and BAM

- Wheels and Plates – verify hardness finish use hardened steel \cong 60 microinch
- Pressure Gauge Calibration – verify calibration is valid

Electrostatic Discharge – SMS and ABL

- Verify Ohm value of in-line resistor
- Needle distance-position approximate 0.0020" Hold voltage at 5.785 Kv
- Run using IH intervals – start at 0.326 joules

Differential Scanning Calorimetry – TA Instruments or Mettler Toledo models

- DSC to be run at 5°C/min per ASTM E3537

Additional Stipulations

- All test masses will be 35mgs \pm 2
- All tests to proceed with 'lights off' for observational effect
- Testing to proceed at 45-55% relative humidity or as close to it as possible - note Hr and T
- All sites used the older hemetic aluminum pans, closed pan vented

Test Results and Discussion

Each site conducted impact, friction via ABL and BAM, electrostatic discharge, and differential scanning calorimetry. Data analysis was to include a 50% failure point, low fire, and threshold initiation limit (TIL). Results were collated and compared to each other and to an 'as received' OCONUS source provided by Eurenco Bofors at the time. Test results from round-robin effort are shown below in Table 1. Table 2 shows the comparison with the OCONUS FOX-7 material.

Table 1: Round-Robin Safety and Thermal Test Results

Site	Sample Lot# Class	Impact (cm)			Friction		ESD (joules)			DSC (°C)
		50%	Low	TiL	ABL (lbf)	BAM (N)	50%	Low	TiL	
Indian Head	IHM170FX7-076 I	*55	51	32	708 (50%)	10/10 NF 216	TBD	0.095	0.037	Doublet 231,282
	IHM17FFX7-104 IV	*46	41	26	20/20 NF 1000	10/10 NF 216	TBD	0.095	0.037	Doublet 228, 282
Picatinny	IHM170FX7-076 I	**79	79	63	20/20 NF @ 1800	10/10 NF 324	TBD	0.095	0.037	Doublet 232, 261
	IHM17FFX7-104 IV	*71	63	32	20/20 NF @ 1800	10/10 NF 360	TBD	0.095	0.037	Doublet 232, 260
China Lake	IHM170FX7-076 I	**71	63	50	20/20 NF @ 1000	10/10 NF 360	8.37	3.80	1.50	Doublet 231, 289
	IHM17FFX7-104 IV	**51	40	32	20/20 NF @ 1000	10/10 NF 360	20/20 NF @ 8.0			Doublet 228, 288

*50% point determined by Brucon Method

** 50% point determined by either Probit or Modified Brucon Method

Table 2. Comparison of OCONUS and CONUS FOX-7 Material

Test	Class I		Class IV	
	OCONUS	CONUS	OCONUS	CONUS
ERL Impact (cm) (50%/LF/TiL)	60/40/20	71/63/50	34/32/13	51/40/32
ABL Friction (lbf)	20/20 NF 1000	20/20 NF 1000	20/20 NF 1000	20/20 NF 1000
BAM Friction (N)	10/10 NF 360	10/10 NF 360	288	10/10 NF 360
*ESD (joules) (50%/LF/TiL)	> 8.0/3.80/1.50	8.37/3.80/1.50	> 8.0	> 8.0
DSC (°C)	228, 286	231, 289	228, 286	228, 288

In general, the testing results from each round-robin site are similar with respect to impact and friction. Some small differences were noted on impact and friction values specifically with the test results between Indian Head and the other two sites Picatinny and China Lake. Indian Head observed impact 50% values of 55 and 46 centimeters (cm) for the two classes (I and IV), whereas, Picatinny and China Lake were in very close agreement with the Class I material (79 and 71cm) and Indian Head and China Lake were in better agreement for the Class IV material (51 to 46cm). Additionally, Indian Head found the BAM friction values to be lower than both Picatinny and China Lake (216 to 324/360 newtons). The ESD results from both Picatinny and Indian Head were in good agreement with respect to the low fire (0.095 j) and the TiL (0.037 j), no 50% values were determined. On the other hand China Lake observed a significant difference in the ESD values (order of magnitude) where both classes of material 50% initiation values were above 8.0 joules. At first glance, this would appear to be of great concern in the data, but closer inspection suggests the difference is based on the ‘interpretation’ of the data. China Lake follows the method protocol called out in AOP-7 2nd edition under the US Mil-Std-1751A category 201.03.002 entitled ‘Electrostatic Discharge Sensitivity – NAWC Method’. Under that method the description for a fire is outlined as ‘a test sample has a positive result, i.e., flash, spark, burn, odor, or noise other than instrument noise’. Upon discussion with the other sites it was found that they consider a ‘hot spot’ or ‘localized glow’ a positive result whereas NAWC does not consider that to be positive.

In comparing the CONUS material to OCONUS the data set used was conducted specifically by NAWC China Lake. For the CONUS material the data set from the round robin was used. For the OCONUS material prior safety and thermal testing data was used. Differences seen in the number of ESD testing shots was a result of using the prior safety data for in-house use. Only the minimum of 0.25 joules is

reported as the OCONUS material was not tested beyond that value. As can be seen both FOX-7 material showed no initiation at 0.25 joules and interestingly, the high values reported by China Lake during the round-robin study coincide with the literature value reported by FOI at > 8.0 joules. The impact data suggests that the CONUS material appears to show somewhat better results in sensitivity with 50% values of 71 and 51 for class I and IV compared to 60 and 34 for the OCONUS material. Both materials are insensitive to friction at 1000 pounds of applied force. Overall, the CONUS material is as good or better with respect to safety testing as the OCONUS material. The thermal profiles, measured by DSC, show no anomalies displaying well known decomposition peaks approximately 228 and 288°C.

Conclusion

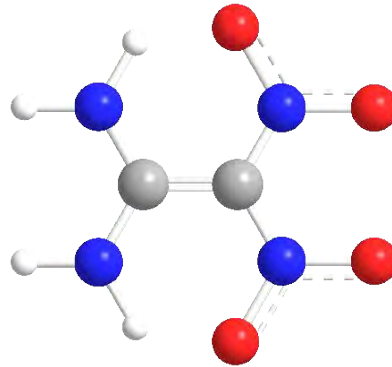
In summary, the synthesis and scale-up of FOX-7 was performed by the Chemical Scale-up group at NSWC IHEODTD. FOX-7 was successfully scaled up to the kilogram batch. The crude material was successfully recrystallized to access the Class I and Class IV particle sizes. Characterization and safety data acquired at all three sites including NSWC IHEODTD was found to be either in agreement or exceeded that of authentic samples of FOX-7.

References and Notes

1. Latypov, N. V.; Bergman, J.; Langlet, A.; Wellmar, U.; Bemm, U. *Tetrahedron* **1998**, *54*, 1152.
2. a) Latypov, N.V.; Langlet, A.; Wellmar, U. WO Patent 99/03818, 1999. b) Latypov N.V.; Langle, A.; Wellmar, U.; Goede, P.; Bergman, J. *Insensitive Munitions and Energetic Materials Technology Symposium (NDIA)* Bordeaux, France, **2001**, 620.
3. a) Astrat'ev, A. A.; Dashko, D.V.; Marshin, A. Y.; Stepanov, A. I.; Urazgil'deev, N. A. *Russian J. Org. Chem.* **2001**, *37*, 729. b) Latypov, N. V.; Bergman, J.; Langlet, A.; Wellmar, U.; Bemm, U.; Goede, P. *J. Org. Chem.* **2002**, *67*, 7833. c) Langlet, A.; Latypov, N. V.; Wellmar, U.; Goede, P. *Propellants, Explosives, Pyrotechnics* **2004**, *29*, 344.
4. Latypov, N.V.; Johansson, M.; Holmgren, E.; Sizova, E.; Sizov, V.V.; Bellamy, A. J. *Org. Proc. Res. Dev.* **2007**, *11*, 56.
5. a) Bemm, U.; Östmark, H. *Acta Cryst* **1997**, *C54*, 1997. b) Gilardi, R. Cambridge Crystallographic Data Centre, 1999, CCDC 127539. c) Evers, J.; Klapötke, T. M.; Mayer, P.; Oehlinger, G.; Welch, J. *Inorg. Chem.* **2006**, *45*, 4996-5007.
6. a) Lockert, I. J. DSTO-TR-1238, 2001. b) Östmark, H.; Bergmann, H.; Bemm, U.; Goede, P.; Holmgren, E.; Johansson, M.; Langlet, A.; Latypov, N. V.; Pettersson, A.; Pettersson, M.-L.; Wingborg, N. *International Annual Conference of ICT*, Karlsruhe, Germany, **2001**, *26*, 1–21.
7. Janzon, B.; Bergman, H.; Eldstätter, C.; Lamnevik, Östmark, H. *20th International Symposium on Ballistics* Orlando, FL, **2002**, 686.
8. EURENCO Bofors proprietary information given to Joseph Clubb, NAWC WD. Shared with NSWC IHEODTD with permission by EURENCO
9. Clubb, J.W., Turnbaugh, D., and White, D., "A Study on Shock Sensitivity Anomaly with respect to 1,1-Diamino-2,2-dinitroethylene (FOX-7) Particle Size", *5th International Dinitramide and FOX-7 Symposium*, Sept. 21-23, **2011**, Paris, France.
10. Clubb, J.W., Bramson, M., Wooldridge, D., Turnbaugh, D., White, D.; "The Use of Mixture Design of Experiment to Predict and Tailor Properties of an Aggregate Material", *9th International Symposium on Special Topics in Chemical Propulsion*, Quebec City, Canada, July 9-13, **2012**.

National Defense Industrial Association Insensitive Munitions Energetic Materials Technology Symposium

24 April 2018



Bradley A. Sleadd
David T. Boruta
Joseph W. Clubb



NDIA

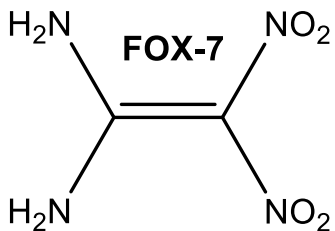
Funding provided by
**Joint Insensitive Munitions Technology
Program (JIMTP)**

- ❖ Develop a **Continental United States (CONUS)** manufacturing capability for FOX-7
- ❖ Demonstrate the capability to produce all 4 classes of FOX-7 currently available from EURENCO Bofors with equivalent purity/quality

EURENCO offers 4 different classes of DADNE (FOX-7) with different crystal sizes:

- o **Class 1: 20 – 40 μm**
- o **Class 2: 50 – 100 μm**
- o **Class 3: 100 – 200 μm**
- o **Class 4: 250 – 300 μm**

- ❖ 1,1-Diamino-2,2-dinitroethene (FOX-7) is an energetic material developed by FOI Sweden in the late 1990s as an insensitive RDX replacement
- ❖ Technology was then transferred to NEXPLO Bofors AB (now EURENCO Bofors AB) for pilot/production scale manufacture



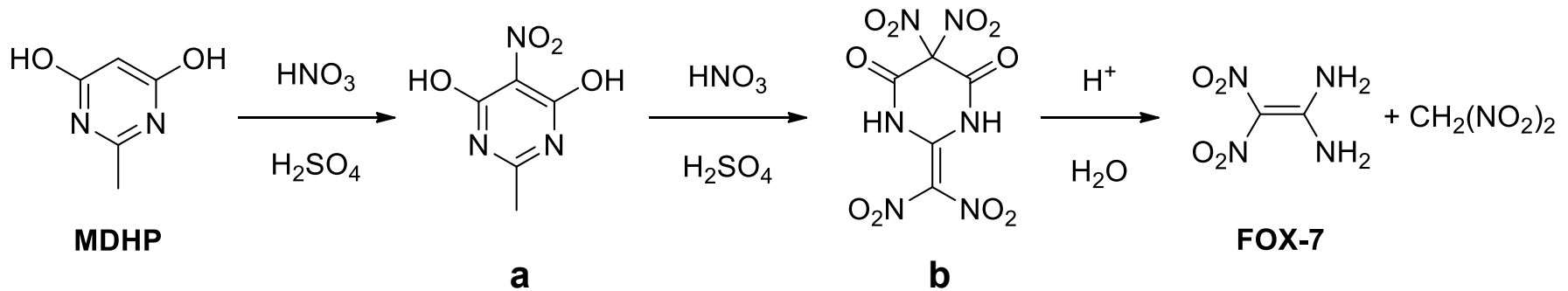
2,2-dinitroethene-1,1-diamine

Chemical Formula: $C_2H_4N_4O_4$

Exact Mass: 148.02

Appearance	Yellow crystals
Drop weight sensitivity	20-40 J (RDX 4-5J)
Friction sensitivity	> 350 N (RDX 120 N)
Small Scale Gap Test at 1.63 g/ml	6.22 mm (RDX 9.33 mm, HMX 10.3 mm, TNT 6.4 mm)
ESD	> 8 J (HMX 0.2 J)
Detonation velocity	8800 m/s
Density	1.885 (crystal)
Purity HPLC	> 99%
Vacuum stability	0.1 – 0.4 ml/g,h at 120°C
Measured detonation pressure	34 GPa (RDX 35 GPa).
Appearance	Yellow crystals

Synthesis



Mixed acid nitration conducted at 10-30°C

➤ **“b” is insoluble in mixed acid**

Resultant slurry was poured into ice water

Delayed foaming (dinitromethane decomposition) and NO_x generation

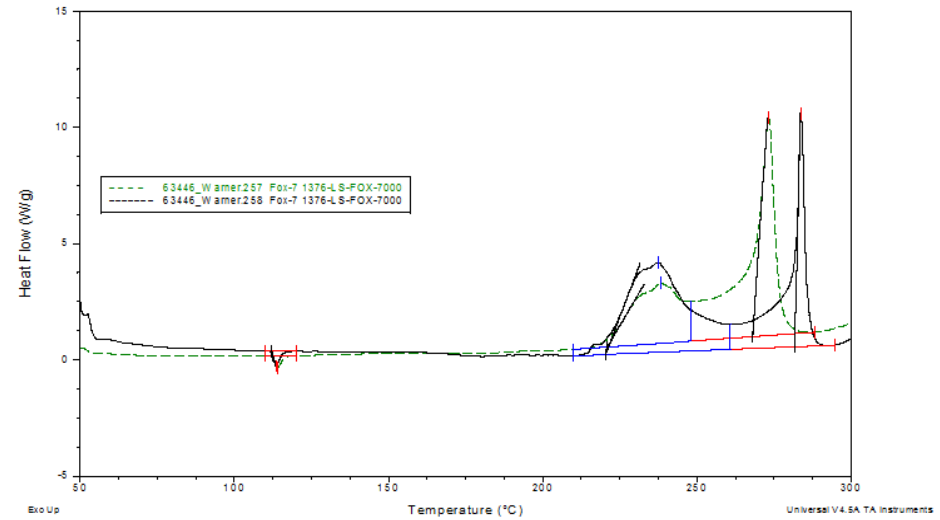
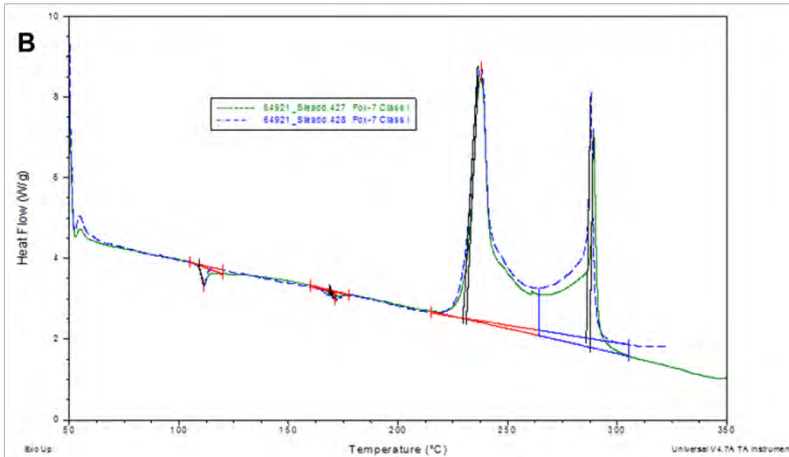
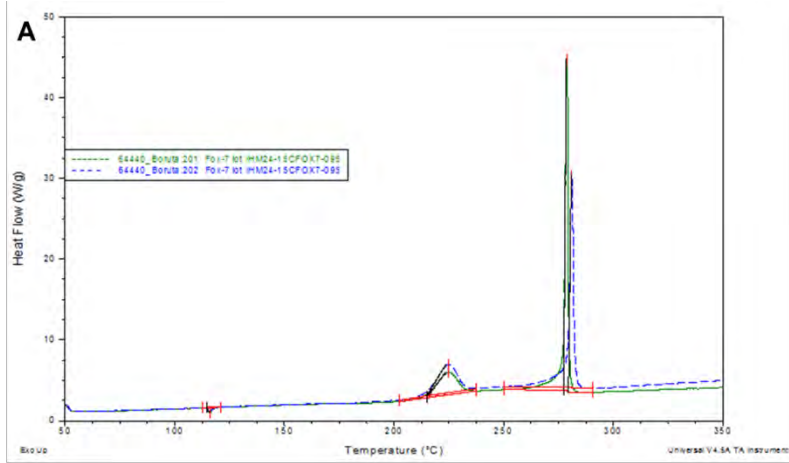
For larger scales, slurry will be dose-quenched into warm/hot water

Scale Up Protocol

Round-bottomed flask or MT EasyMax

- **5 gram theoretical yield**
 - **Small scale safety data**
 - **Impact, friction, ESD, DSC**
 - **Reproducibility & yield**
- **20 gram theoretical yield**
 - **Small scale safety data**
 - **Impact, friction, ESD, DSC**
 - **Reproducibility & yield**
 - **Recrystallization**
 - **SEM & PSD**



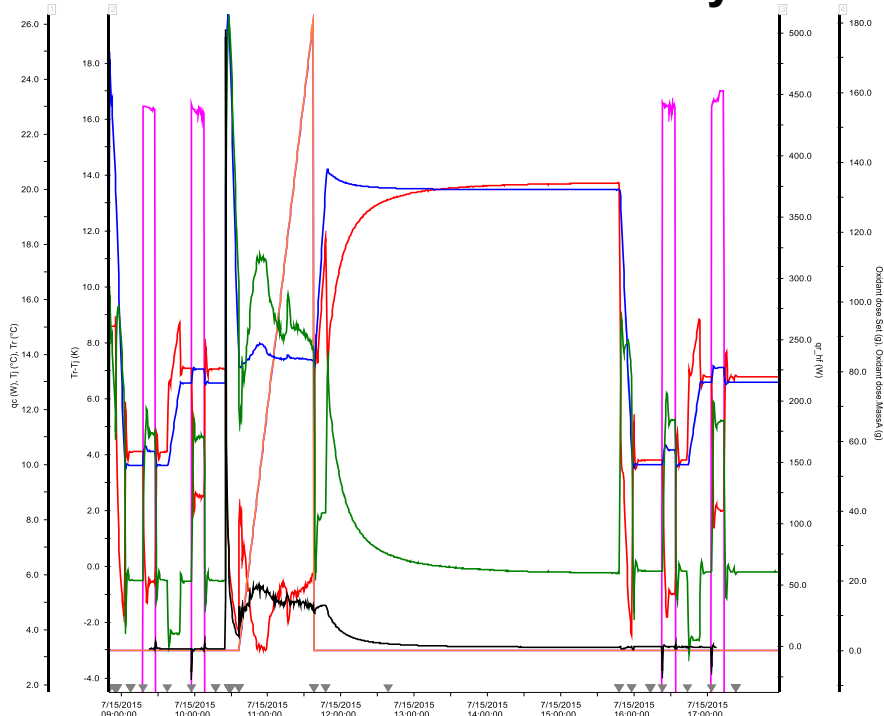


DSC trace of EURENCO Bofors FOX-7

Selected DSC traces of NSWC IHEODTD FOX-7: 5g recrystallized batches. A) FOX-7 recrystallized from hot water at IHEODTD. B) FOX-7 recrystallized from NMP/water at IHEODTD

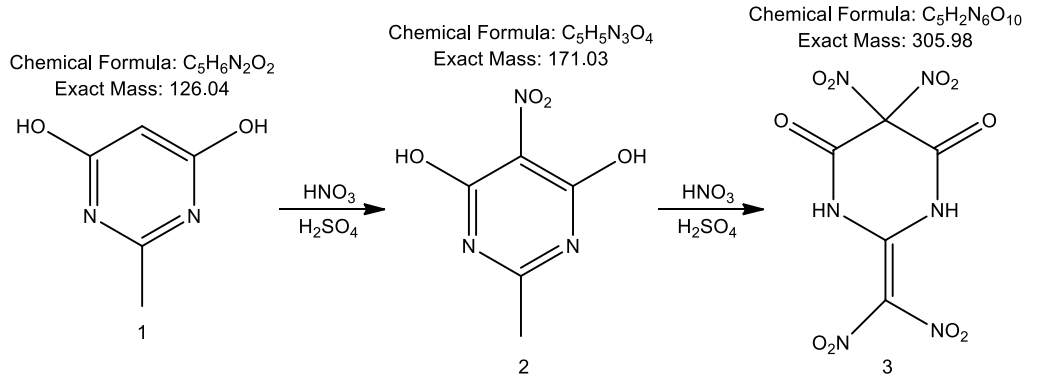
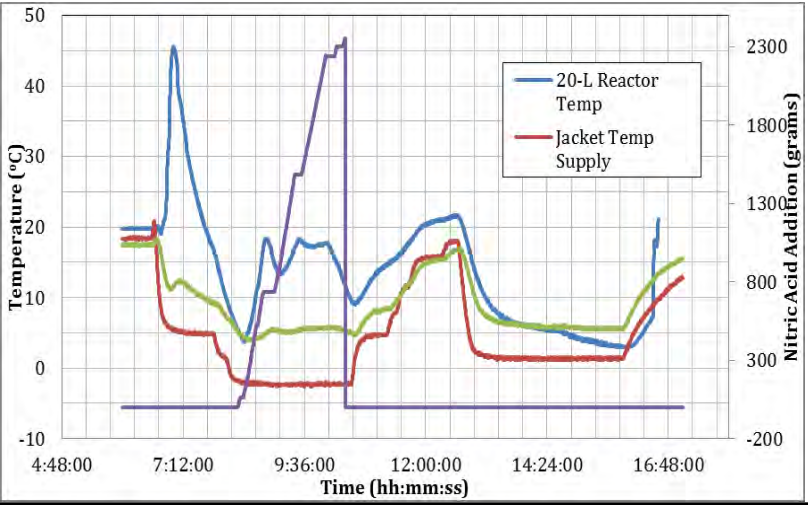
Mettler Toledo RC1e Reaction Calorimeter

- 100 gram theoretical yield
 - Small scale safety data
 - Impact, friction, ESD, DSC
 - Reproducibility & yield
 - Recrystallization
 - SEM & PSD
 - **Heat flow calorimetry**



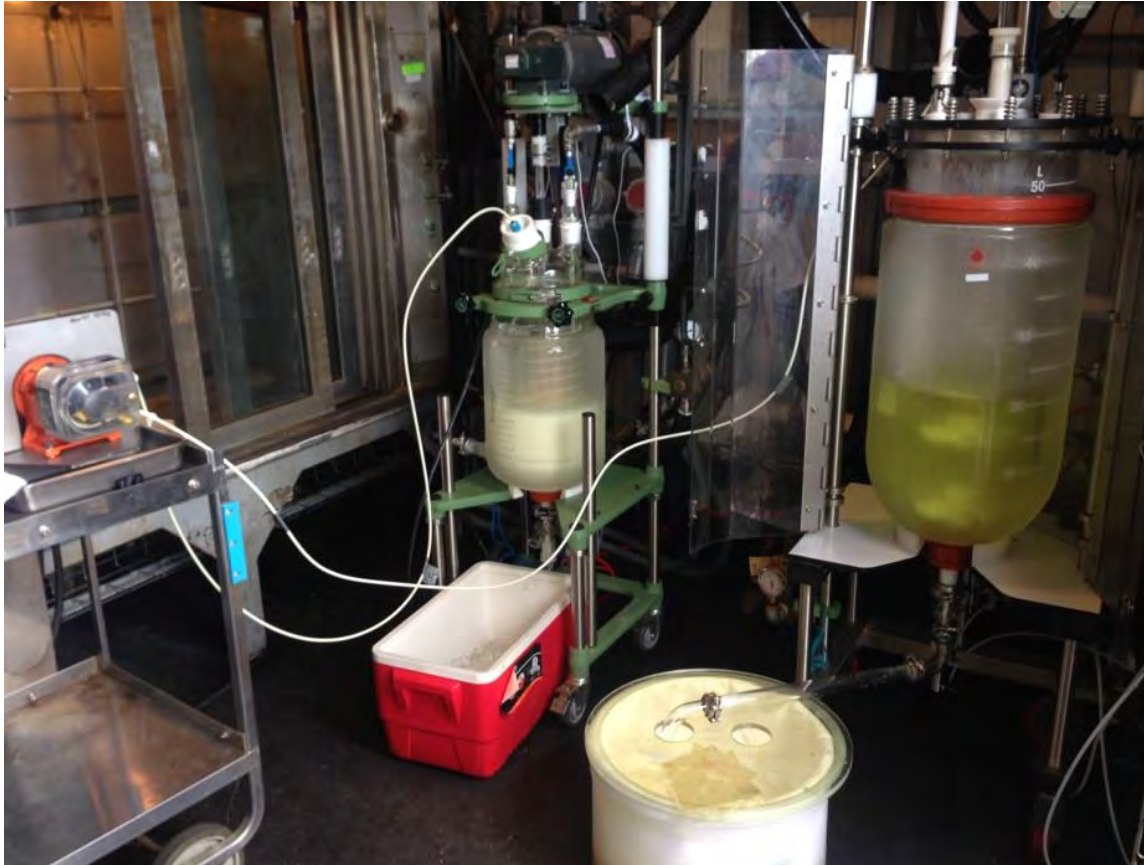
Scale Up: Nitration

1 kg theoretical yield

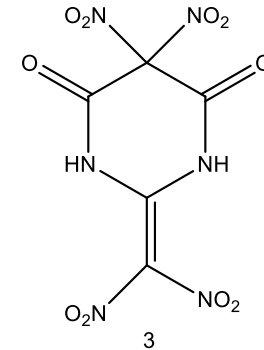


Solids mass increase x 2.4

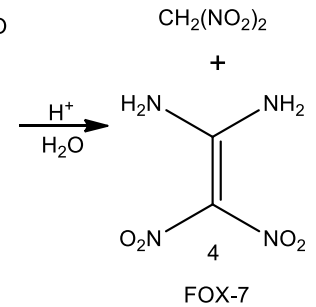
Solids mass decrease x 2.9



Chemical Formula: $C_5H_2N_6O_{10}$
Exact Mass: 305.98

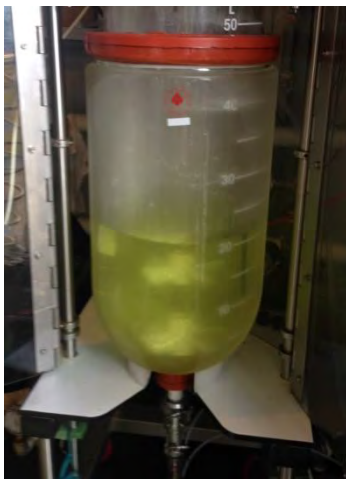


Chemical Formula: $CH_2N_2O_4$
Exact Mass: 106.00



Scale Up: Quench

Nitration mixture is pumped into warm water



Yields typically ~70%



Scale Up: Nitration

2 kg theoretical yield



Solids mass increase x 2.4!



Scale Up: Nitration

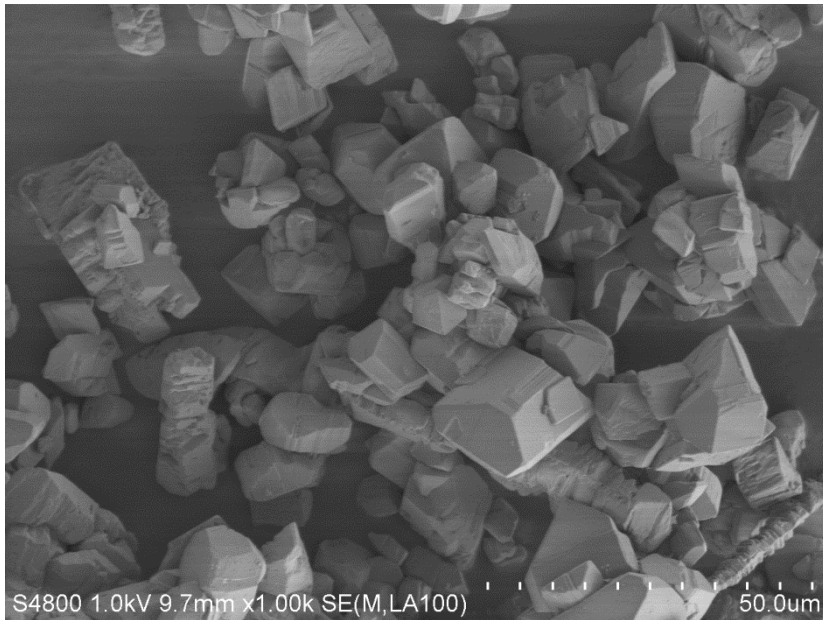
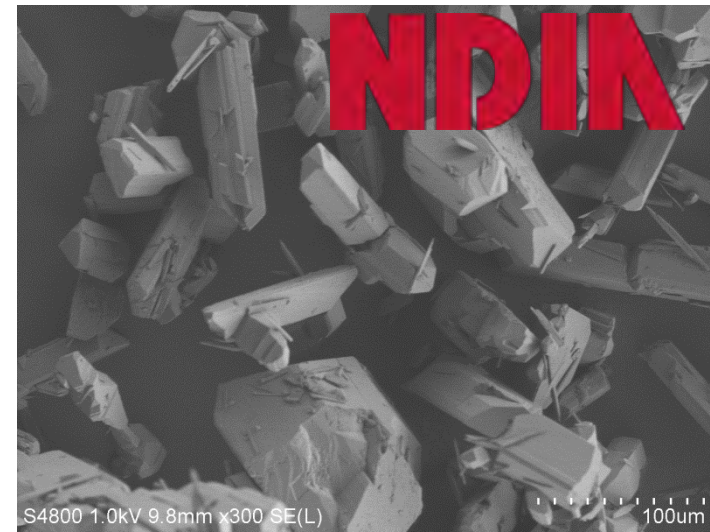
Subsequent batches were limited to 1.5 kg
Second “upper” impeller was installed on agitator shaft



Recrystallization

2 L Scale; RC1

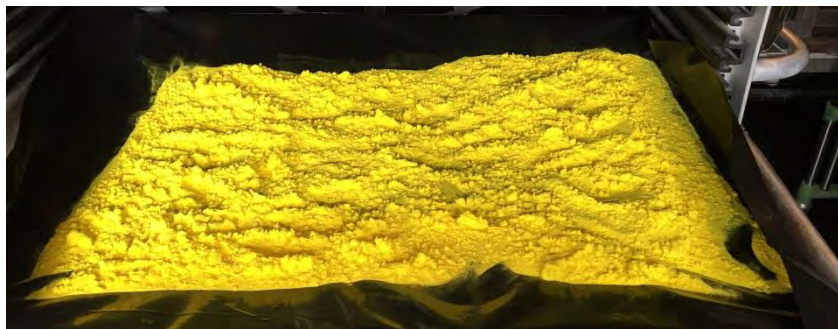
All four classes were obtained
At the 2 L scale



Recrystallization



2 kg scale



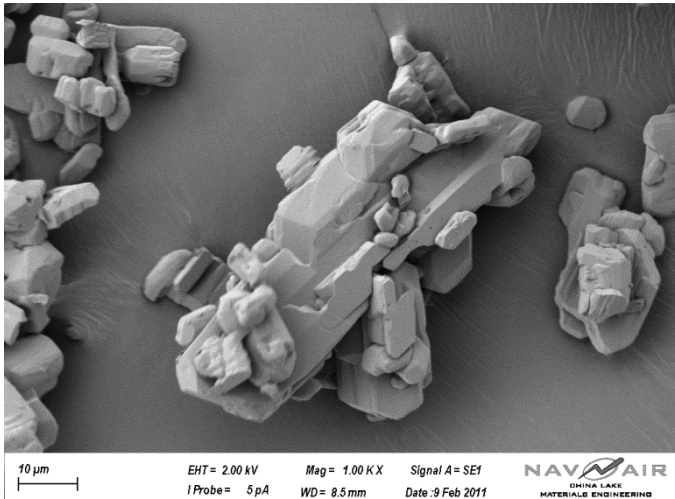
Recovery typically
>80%

Recrystallization

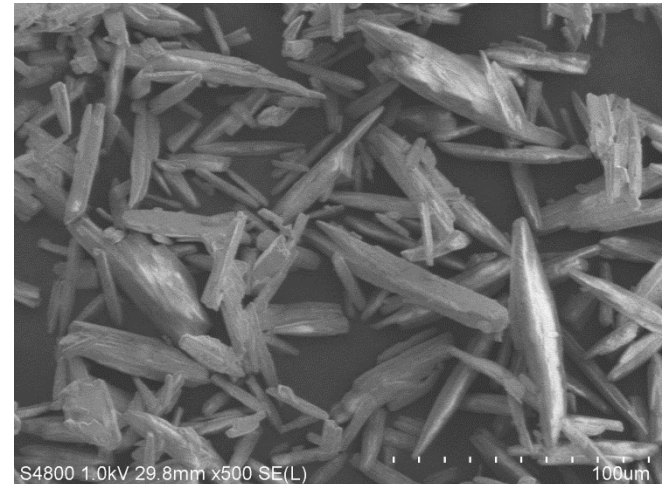
Recrystallization parameters did not scale!
Conditions that worked at the 2 L scale
Did not work at the 50 L scale (not surprising)

Class I: 20-40 μm

EURENCO Bofors Class I



CONUS Class I (bad solvent)



Recrystallization CONUS FOX-7

Class I; too large!

Class IV; too large!

Horiba LA950 for Windows [Wet] Ver7.02

2017.02.14 14:12:21

HORIBA

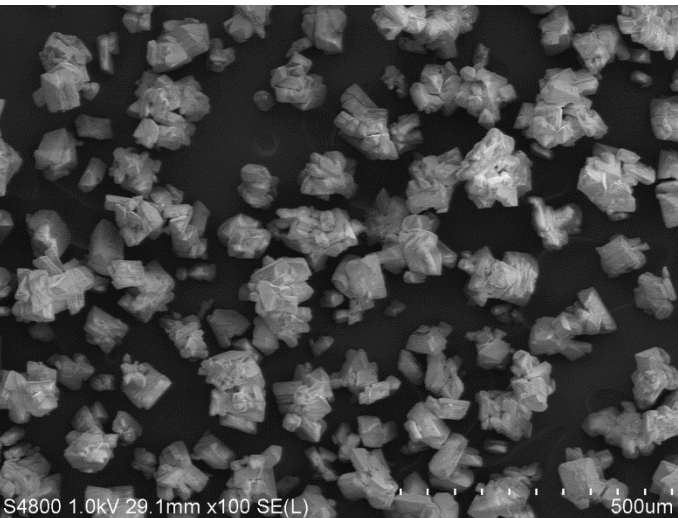
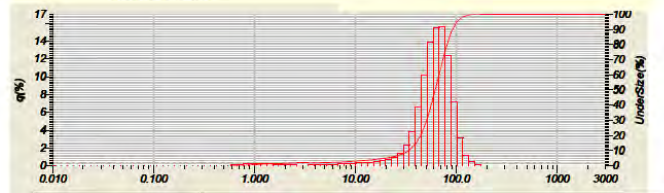
Mean Size : 62.28785(µm)

ID#	: 201702141411715	Circulation Speed	: 5
Sample Name	: FOX-7	Agitation Speed	: S
Material	:	Ultra Sonic	: OFF
Source	:	Transmittance(R)	: 92.4(%)
Lot Number	:	Transmittance(B)	: 88.5(%)
Test or Assay. Number	: D1M178FX7-292	Sample Data Acquisition Times (LD)	: 15000
Distribution Base	: Volume	Sample Data Acquisition Times (LED)	: 15000
Form of Distribution	: Auto		
Iteration Number	: 15		
Refractive Index (R)	: FOX-7(FOX-7) 1.810 - 0.100(Heptane) 1.390		
HIS No.	: D0004619		
Measure Condition File Name	: FOX-7		

Median Size : 61.85731(µm)
Mode Size : 71.3273(µm)
Variance : 684.21(µm²)
CV : 38.8044(%)
Std.Dev. : 24.1704(µm)
Span : OFF

Measure Condition File Name : FOX-7
Measure Condition File Name : FOX-7

Micro-Filter	Upper & VCL	Lower & VCL
0.10(µm)	0.10(µm)	0.10(µm)
0.20(µm)	0.20(µm)	0.20(µm)
0.50(µm)	0.50(µm)	0.50(µm)
1.00(µm)	1.00(µm)	1.00(µm)
2.00(µm)	2.00(µm)	2.00(µm)
5.00(µm)	5.00(µm)	5.00(µm)
10.00(µm)	10.00(µm)	10.00(µm)
20.00(µm)	20.00(µm)	20.00(µm)
50.00(µm)	50.00(µm)	50.00(µm)
100.00(µm)	100.00(µm)	100.00(µm)
200.00(µm)	200.00(µm)	200.00(µm)
500.00(µm)	500.00(µm)	500.00(µm)
1000.00(µm)	1000.00(µm)	1000.00(µm)
2000.00(µm)	2000.00(µm)	2000.00(µm)
5000.00(µm)	5000.00(µm)	5000.00(µm)



Horiba LA950 for Windows [Wet] Ver7.02

2017.02.15 13:56:30

HORIBA

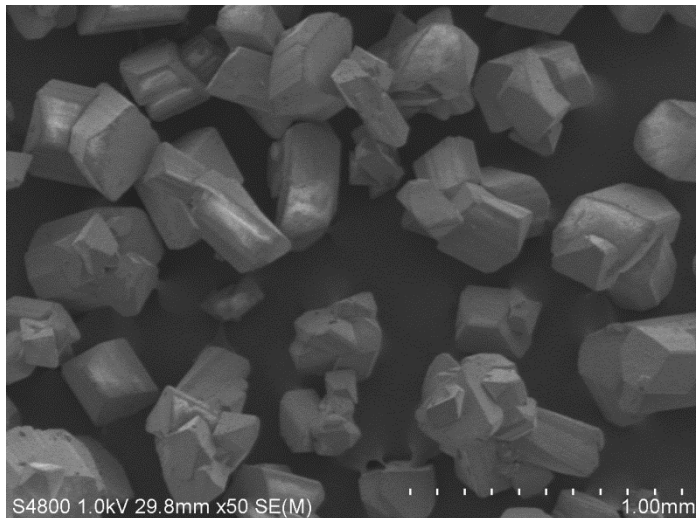
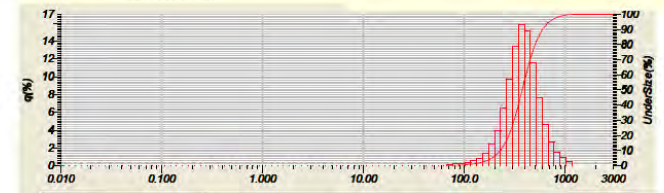
Mean Size : 399.87085(µm)

ID#	: 201702151355718	Circulation Speed	: 5
Sample Name	: FOX-7	Agitation Speed	: S
Material	:	Ultra Sonic	: OFF
Source	:	Transmittance(R)	: 90.1(%)
Lot Number	: D1M178FX7-291	Transmittance(B)	: 87.4(%)
Test or Assay. Number	: 67607	Sample Data Acquisition Times (LD)	: 15000
Distribution Base	: Volume	Sample Data Acquisition Times (LED)	: 15000
Form of Distribution	: Auto		
Iteration Number	: 15		
Refractive Index (R)	: FOX-7(FOX-7) 1.810 - 0.100(Heptane) 1.390		
HIS No.	: D0004619		
Measure Condition File Name	: FOX-7		

Median Size : 378.17499(µm)
Mode Size : 371.0867(µm)
Variance : 28008(µm²)
CV : 38.5461(%)
Std.Dev. : 158.1334(µm)
Span : OFF

Measure Condition File Name : FOX-7
Measure Condition File Name : FOX-7

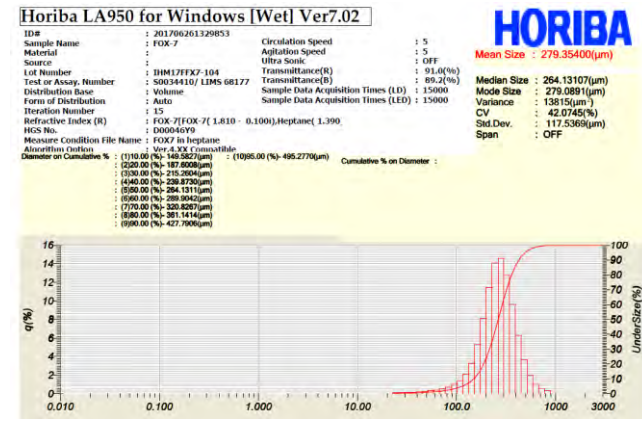
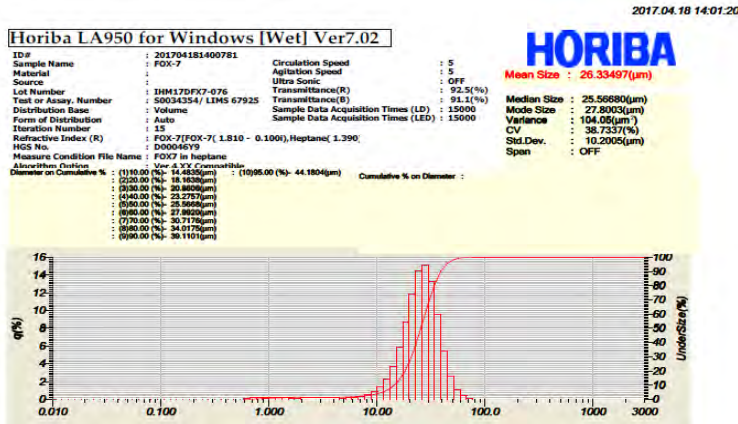
Micro-Filter	Upper & VCL	Lower & VCL
0.10(µm)	0.10(µm)	0.10(µm)
0.20(µm)	0.20(µm)	0.20(µm)
0.50(µm)	0.50(µm)	0.50(µm)
1.00(µm)	1.00(µm)	1.00(µm)
2.00(µm)	2.00(µm)	2.00(µm)
5.00(µm)	5.00(µm)	5.00(µm)
10.00(µm)	10.00(µm)	10.00(µm)
20.00(µm)	20.00(µm)	20.00(µm)
50.00(µm)	50.00(µm)	50.00(µm)
100.00(µm)	100.00(µm)	100.00(µm)
200.00(µm)	200.00(µm)	200.00(µm)
500.00(µm)	500.00(µm)	500.00(µm)
1000.00(µm)	1000.00(µm)	1000.00(µm)
2000.00(µm)	2000.00(µm)	2000.00(µm)
5000.00(µm)	5000.00(µm)	5000.00(µm)



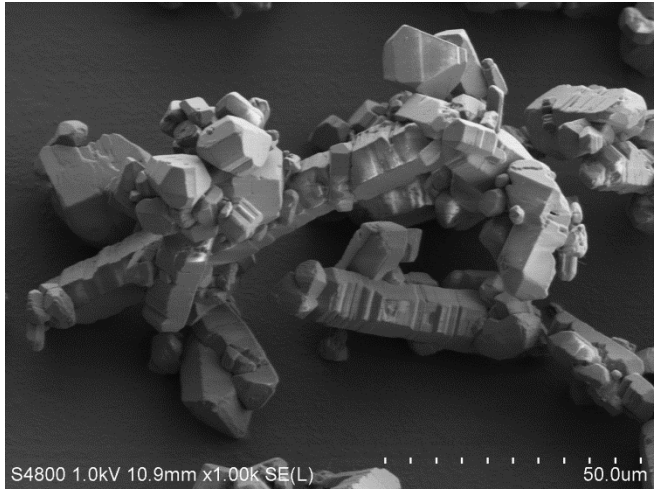
Recrystallization CONUS FOX-7

Class I

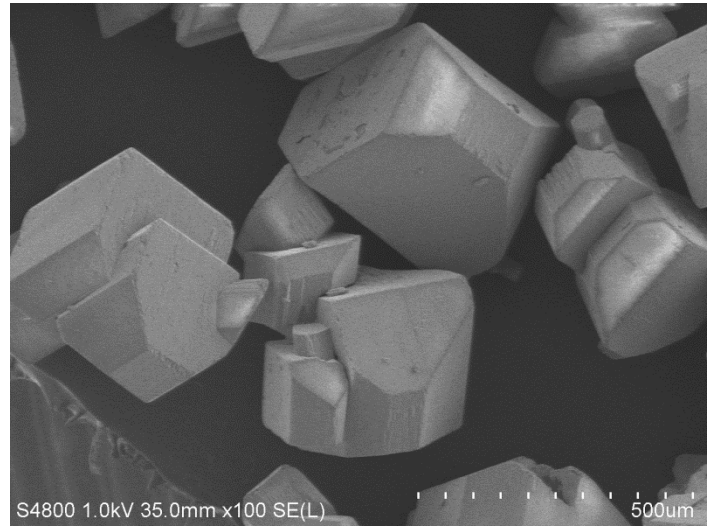
Class IV



27 µm



279 µm





Safety and Thermal Analysis CONUS Round-Robin Testing



➤ Machine and Method

▪ **ERL Impact:**

- ✓ Type 12 Tooling
- ✓ Mass of drop weight: 2.5kg
- ✓ Mass of Striker: 520-540gm
- ✓ 180A Garnet Paper

▪ **ESD: SMS Equipment (ARDEC CL), ABL (IH)**

- ✓ Verify Ohm value of in-line resistor
- ✓ Needle distance-position approximate 0.0020”
Hold voltage at 5.785Kv
- ✓ Run using IH intervals – start at 0.326joules

▪ **ABL Friction: SMS Equipment**

- ✓ Wheels and Plates – verify hardness finish use hardened steel \cong 60microinch
- ✓ Pressure Gauge Calibration – verify calibration is valid

▪ **BAM Friction:**

- ✓ Wheels and Plates – verify hardness finish (new wheels and plates)
- ✓ Pressure Gauge Calibration – verify calibration is valid

➤ Methods Stipulation:

1. All test masses will be 35mgs \pm 2
2. All tests to proceed with ‘lights off’ for observational effect
3. Testing to proceed at 45-55% relative humidity or as close to it as possible - note Hr and T
4. DSC to be run at 5°C/min per ASTM E3537
5. All sites use the older hemetic aluminum pans, closed pan vented

➤ Data Analysis

- ✓ Provide both Bruceton 50% and 20 TIL
- ✓ Provide description of reaction (sparks, pop, fire, consumption, smell) in comments section



Safety and Thermal Analysis CONUS Round-Robin Testing



Site	Sample Lot# Class	Impact (cm)			Friction		ESD (joules)			DSC (°C)
		50%	Low	TiL	ABL (lbf)	BAM (N)	50%	Low	TiL	
Indian Head	IHM170FX7-076 I	*55	51	32	708 (50%)	10/10 NF 216	TBD	0.095	0.037	Doublet 231,282
	IHM17FFX7-104 IV	*46	41	26	20/20 NF 1000	10/10 NF 216	TBD	0.095	0.037	Doublet 228, 282
Picatinny	IHM170FX7-076 I	**79	79	63	20/20 NF @ 1800	10/10 NF 324	TBD	0.095	0.037	Doublet 232, 261
	IHM17FFX7-104 IV	*71	63	32	20/20 NF @ 1800	10/10 NF 360	TBD	0.095	0.037	Doublet 232, 260
China Lake	IHM170FX7-076 I	**71	63	50	20/20 NF @ 1000	10/10 NF 360	8.37	3.80	1.50	Doublet 231, 289
	IHM17FFX7-104 IV	**51	40	32	20/20 NF @ 1000	10/10 NF 360	20/20 NF @ 8.0			Doublet 228, 288

*50% point via Bruceton Method

** 50% point determined by Probit or Modified Bruceton Method

Analysis:

- ✓ ERL Impact – IH values tend to trend lower, CL and ARDEC fairly similar
- ✓ ABL Friction – only IH Class I was observed to be lower than other sites
- ✓ BAM Friction – IH observations were a couple of logs lower, CL/ARDEC nearly the same
- ✓ ESD – IH and ARDEC same results, CL significantly different in observations (magnitudes)???

➤ *ESD differences are likely due to the 'interpretation' of the description of a fire found in AOP-7 edition 2, not the method or machinery. Under NAWC method a fire consists of 'flash, spark, burn, odor, or noise other than instrument noise'*



Safety and Thermal Analysis OCONUS vs. CONUS



Test	Class I		Class IV	
	OCONUS	CONUS	OCONUS	CONUS
ERL Impact (cm) (50%/LF/TiL)	60/40/20	71/63/50	34/32/13	51/40/32
ABL Friction (lbf)	20/20 NF 1000	20/20 NF 1000	20/20 NF 1000	20/20 NF 1000
BAM Friction (N)	10/10 NF 360	10/10 NF 360	288	10/10 NF 360
*ESD (joules) (50%/LF/TiL)	> 8.0/3.80/1.50	8.37/3.80/1.50	> 8.0	> 8.0
DSC (°C)	228, 286	231, 289	228, 286	228, 288

■ Analysis:

- ✓ ERL Impact – Recent CONUS values appear to be slightly higher than the ‘as received’ OCONUS material but follow the general trend of Class I less sensitive to impact than the larger Class IV material – in general fairly good correlation.
- ✓ ABL Friction – Both CONUS and OCONUS tested out at the same level with no friction sensitivity up to 1000 pound of applied force.
- ✓ BAM Friction – All but the OCONUS Class IV tested out to no initiation (fires) up to 360 newtons of force.
- ✓ ESD – All materials tested to no ignition to spark at 0.25joules of energy
 - * The ESD testing used the NAWC method and description called out in AOP-7 edition 2. As noted prior site differences are likely due to the ‘interpretation’ of the description of a fire per the NAWC method.



Conclusions



A CONUS Manufacturing Capability for FOX-7 has been developed

Need to optimize nitration for larger scales

- Eliminate “yogurt” formation

Recrystallization to match EURENCO classes eventually successful

- Trial and error for conditions when changing scale and equipment

ROM cost estimate at this scale is inadvisable

- Economy of scale not yet realized for MDHP
- Economy of scale not yet realized for nitration/quench
- Economy of scale not yet realized for recrystallization



Acknowledgments



Joint Insensitive Munitions Technology Program (JIMTP)

- Anthony DiStasio, Program Manager
- Jen Duchow, MATG III

JIMTP Task 14-2-68

- Joey Clubb, NAWC WD, Principal Investigator
- Philip Samuels, ARDEC, Co-Investigator

Navy Energetics Manufacturing Technology Center (EMTC)

- Chuck Painter, Director

NSWC IHEODTD Chemicals Development & Manufacturing Branch

- M24; Chemical Scale-up Group;
- Scientists, engineers and analysts at ARDEC, NAWC WD and NSWC IHEODTD for Round Robin testing



NDIA

QUESTIONS?

Filling the Gap between the Initiation Behavior of Shaped Charge Jets and Fragments

Werner Arnold¹, Thomas Hartmann², Ernst Rottenkolber²

¹ MBDA-TDW Gesellschaft für verteidigungstechnische Wirksysteme mbH, Hagenauer
Forst, D-86529 Schrobenhausen, Germany,

² NUMERICS GmbH, Mozartring 6, D-85238 Petershausen, Germany

Abstract

In the previous IMEMTS paper [10] the findings showed that for shaped charge jet (SCJ) attacks the critical stimulus $S = v^2 \cdot d$ (v = jet velocity; d = jet diameter) for the initiation of a munition is no longer constant ($S \neq \text{const.}$) and therefore a new initiation model is necessary. In this work the initiation scope should be extended from SCJs to fragments represented by STANAG projectiles. The original STANAG projectile with $L/D = 1$ and elongated ones with $L/D = 3$ made out of steel and copper were shot with a EMI powder gun against the TDW standard charge with the PBX KS32 (HMX/PB 85/15, $\rho = 1.64 \text{ g/cm}^3$). The results were in good agreement with those achieved during the SCJ trials. A new linear initiation model was proposed: $v = A - B \cdot d$.

1 Introduction

During more than one decade of studying initiation phenomenology numerous papers at previous IMEMTS and other symposia ([1] - [11]) were published. Most of them dealt with the hypervelocity impact initiation of plastic bonded high explosive charges by shaped charge jets (SCJ) and a few ones reported results in the ordnance velocity impact regime with STANAG projectiles [9] and explosively formed projectiles (EFP) [2]. A recent finding of our investigations of charge jet (SCJ) attacks suggests that the critical stimulus $S = v^2 \cdot d$ (v = SCJ / projectile velocity; d = SCJ / projectile diameter) for the initiation of a munition can no longer be seen as a constant ($S \neq \text{const.}$) Also, known equations, e.g. Jacobs-Roslund, are not capable to describe low velocity and hypervelocity impacts with the same parameter set.

Consequently, a new initiation model is needed taking these findings into account. The presented study shall therefore continue the investigations already launched in [10] under the title "Towards a Unified Initiation Model". On the way to such a new unified model further work has to be done trying to realize a "unifying link" between the initiation phenomenology of shaped charge jet impacts (in the hypervelocity regime) and of projectile impacts (in the lower velocity regime). The situation of today is that a larger number of experimental results are available in the hypervelocity regime of the SCJs and only a few ones in the lower velocity regime of STANAG / EFP projectiles. Therefore, a series of trials were planned and conducted to close the data gap in the low velocity regime.

2 From Shaped Charge to Fragments

For fragments the STANAG projectile is representative according to [12]. While making the transition from SCJ towards STANAG projectile impacts several changes of initiation phenomena are expected. This transition process starts from a continuous copper jet and ends up with the standard steel STANAG projectile with $L/D = 1$. The individual steps include:

- continuous Cu liner SCJ with velocity gradient
- particulated Cu liner SCJ with different jet particle velocities
- modified STANAG projectile: elongated ($L/D > 1$) and material changed to Cu
- modified STANAG projectile made of steel but elongated ($L/D > 1$)
- standard steel STANAG projectile ($L/D = 1$)

In the first step from a continuous to a particulated (Cu liner) SCJ a first change in the initiation phenomenology could be observed [10]: the second SCJ particle (and all the following ones) now hits moving, but bare high explosive (KS32) leading to a higher sensitivity (larger ERL). Taking the next step, only one elongated ($L/D > 1$) Cu projectile will be hitting the test charge instead of multiple SCJ particles. Then the next step towards the $L/D = 1$ STANAG steel projectile makes the transition from Cu to steel, and the final step is done when using an original STANAG steel projectile [12] with $L/D = 1$. Such a short projectile can erode very quickly while perforating the charge. This might lead to a higher required velocity to initiate the charge, as the initiation now - due to the quick erosion process - must take place at the entry side of the charge (instead of exit side). In any case an at least partial transition from a *penetration mode* to an *impact mode* initiation [4] must occur, which might be accompanied by a further change in required particle velocity.

This short summary of the initiation phenomena induced by the transition from SCJs towards STANAG projectiles already shows that it is not fully clear or foreseeable what will happen when this transition is actually executed. Therefore, further experimental trials with original STANAG-projectiles ($L/D = 1$ [12], Figure 1 top) and elongated ones made out of steel and copper were planned and conducted. The experimental work was supported by numerical simulations. Like in earlier tests (e.g. [10]) the so called “standard charge” filled with the TDW insensitive high explosive KS32 (HMX/PB 85/15, $\rho = 1.64 \text{ g/cm}^3$) was used in the investigations (Figure 1 bottom). The charge consists of a high explosive cylinder with 100 mm in diameter and 200 mm in length and a mild steel casing with 10 mm thickness and two screwed lids on both sides (standard threads).

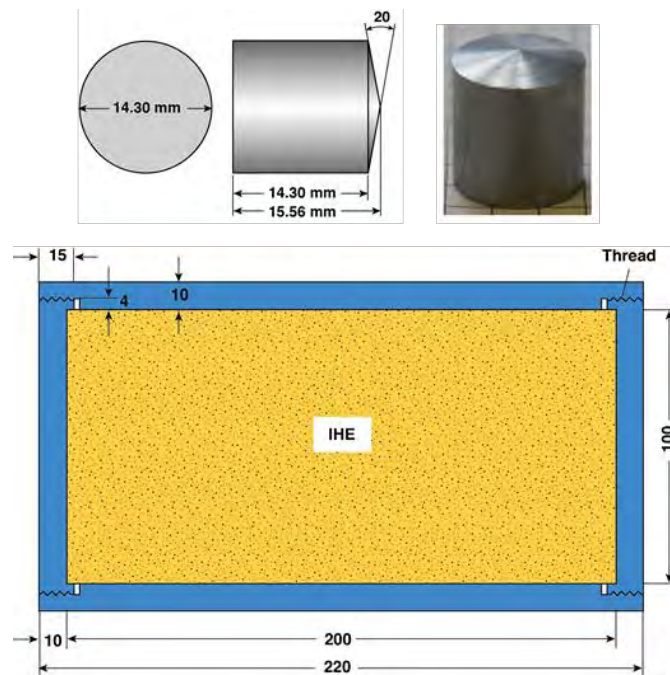


Fig. 1: Original STANAG-projectile ($L/D = 1$, top) and TDW standard charge (bottom).

3 Numerical Simulations

Numerical simulations were applied to determine the minimum projectile length required to perforate the complete charge and to investigate the erosion process, the velocity reduction during the penetration of the charge, acceptable maximum yaw angle ($< 6^\circ$), impact velocity vs. projectile velocity behind the steel casing, casing materials etc. The original STANAG projectile ($L/D = 1$) and elongated ones ($L/D = 2, 2.5$ & 3) were studied (Figure 2). Besides steel projectiles (in accordance with [12]) also Cu projectiles (making the link to copper SC jets) were regarded. The high explosive was modelled with an inert PBX-simili.

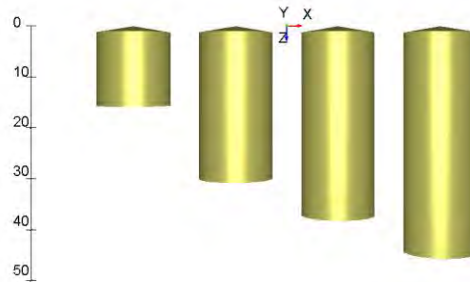


Fig. 2: Simulation models of the STANAG projectile ($L/D = 1$) and elongated ones ($L/D = 2, 2.5$ & 3).

A sequence of the penetration of an elongated Cu-projectile ($L/D = 3$) is shown in Figure 3. The impact velocity (on the steel casing) was 2000 m/s. After perforation of the 10 mm thick steel casing of the charge the projectile is already strongly eroded (ca. 40%). When arriving at the middle of the penetration velocity is close to 1000 m/s. In the simulation the length of the projectile is sufficient to reach the rear side of the charge but it is fully eroded and cannot completely perforate the casing.

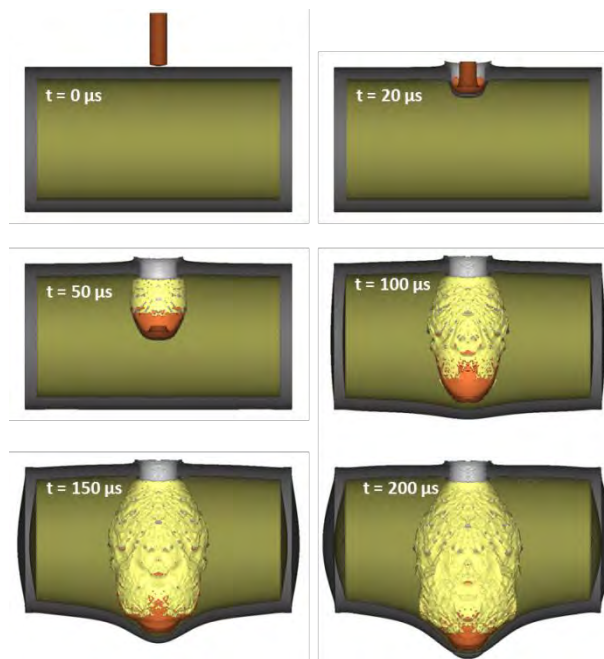


Fig. 3: Sequence from (0 – 200 μ s) of the penetration of an elongated Cu-projectile ($L/D = 3$).

4 Experimental Trials

Figure 4 shows all results of the trials with shaped charges with calibers ranging from 44 mm up to 200 mm (taken from [10]) against the standard charge carried out over the last years.

On abscissa, the parameter *velocity* is used instead of the *stimulus* $S = v^2 d$ as done in [10]. This is because the stimulus seems inappropriate as a ranking parameter when comparing ERL results of SCJ vs. STANAG-projectiles, which will be discussed later. On the ordinate the ERL (Explosive Reaction Level) is plotted describing the change in reactivity of the charge when the projectile velocity is increased. A definition of the six ERLs is given e.g. in [10]. The conducted tests shall now add curves for STANAG-projectiles to the chart and thus fill the missing gap between these two most important threats.

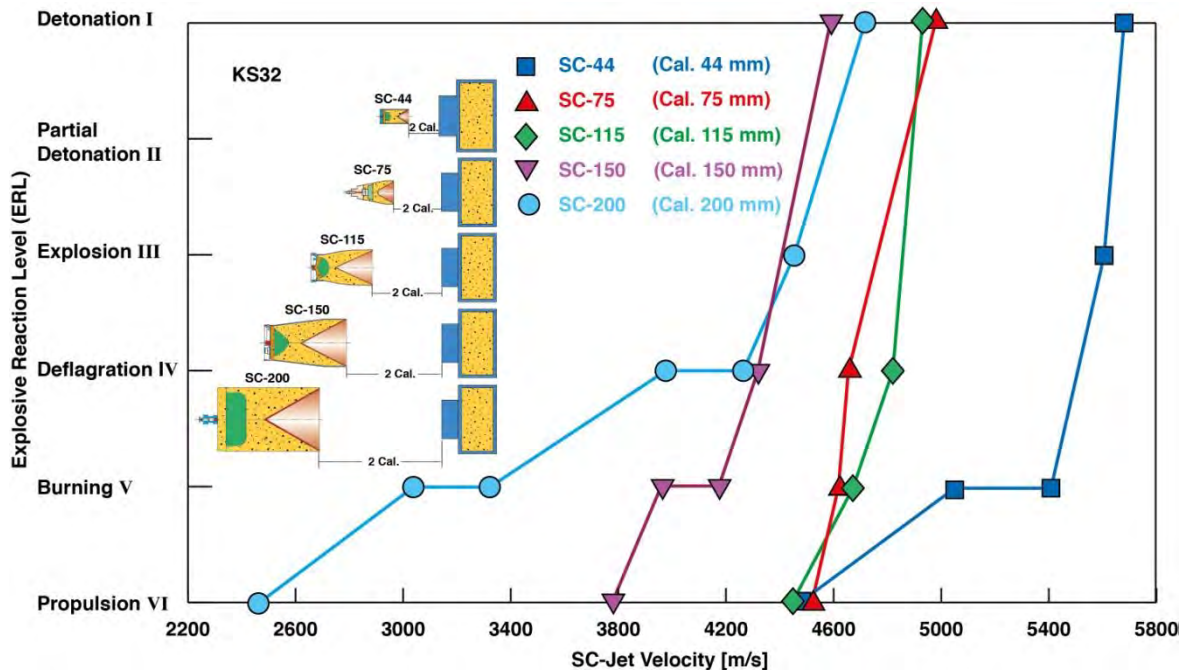


Fig. 4: ERL-curves of all investigated shaped charges (SC) with calibers from 44 mm up to 200 mm (from [10]).

4.1 Test Setup

Firing tests with STANAG-projectiles and their derivatives: L/D = 1 & 3, made from steel and copper materials were planned and carried out. The trials were conducted at the Fraunhofer Ernst-Mach-Institute (EMI) in Germany. A powder gun was used by the EMI to accelerate the projectiles. The projectiles were mounted into a standard sabot which was stripped-off before hitting the target. The upper velocity limit was about 2600 m/s. The larger two-stage light-gas gun (LGG) allowing much higher velocities was out of operation at that time.

The test setup was designed to be as close as possible to the setup used for the SCJ trials (see e.g. [10]). The pictures in Figure 5 (taken at the EMI impact chamber) illustrate the setup. The projectile enters the chamber through the opening on the left. A high-speed video camera records the projectile's flight path and permits to determine the impact velocity, the projectile pitch and the impact point on the charge. A mirror is applied to observe the shot from an orthogonal direction and to control projectile yaw. The Aluminum witness plate (2 mm thick) in the background is used to detect higher ERL levels (ERL = I & II). For the lower level reactions, the casing fragments and the KS32 residues respectively were collected and used for the ERL assessment as in the SCJ trials e.g. in [10]. The close-up on the right of Figure 5 shows the TDW standard charge mounted in the projectile's shot line.



Fig. 5: Test setup at the EMI impact chamber (left) and a close-up of the TDW standard charge (right).

4.2 Test Results

Most tests were performed with the elongated STANAG-projectiles with $L/D = 3$ with steel and copper materials and it was intended to shoot complete ERL curves with these projectiles. Unfortunately, the maximum velocity reached with the EMI powder gun ($v_{max} = 2600$ m/s) was too low to achieve a partial or full detonation (ERL = II or I) of the insensitive KS32. Therefore, these parts of the ERL curve had to be assessed by extrapolation. Within the available budget frame, it was not possible to conduct additional trials. However, to get at least an impression of what will happen when taking the last step in the above mentioned transition process, also one shot with the original STANAG $L/D = 1$ steel projectile was carried out.

4.2.1 Elongated STANAG $L/D = 3$ Steel and Copper Projectiles

The two diagrams in Figures 6 and 7 for steel and copper projectiles respectively were achieved by incrementally increasing the impact velocities. The impact velocities v_0 were measured with the EMI high speed camera and the ERL were assessed as described above. The photo insets (with respective test numbers) give a vivid illustration of the reaction behavior of the standard charges. In all tests, the impact angles were below the allowable maximum of 6° determined in the numerical simulations (see above).

The reaction behavior of the TDW standard charge with KS32 was mostly the same as that observed with the SCJ attacks described e.g. in [10]. The reaction levels increase in a step-wise way from low level reactions starting at about 2200 m/s to higher level where the casing breaks up into increasingly smaller fragments. The tests exhibit only marginal differences between steel and copper projectiles with a slight trend to lower velocities for the Cu material projectiles – presumably due to the higher mass (density). Extrapolating the available results, it can be anticipated that an impact velocity of about 2700 m/s will be required to reach a partial or full detonation. The differences between steel and copper projectiles are marginal with a slight trend to lesser velocities for the Cu material projectiles, presumably due to the higher mass (density).

4.2.2 Standard STANAG $L/D = 1$ Steel Projectile

The result of test with the original STANAG steel projectile is also plotted in Figure 6. As expected a distinctly higher impact velocity than with the $L/D = 3$ projectile was required to reach same ERL = V (~ 2600 m/s compared to ~ 2400 m/s). This was already shortly discussed in Section 2 in the context of the transition phenomenology. The quicker erosion pro-

cess requires higher projectile velocities at the impact / entry side to cause a reaction. In this context also the potentially enforced transition process from a *penetration mode* to an *impact mode* initiation discussed in [4] must be noted.

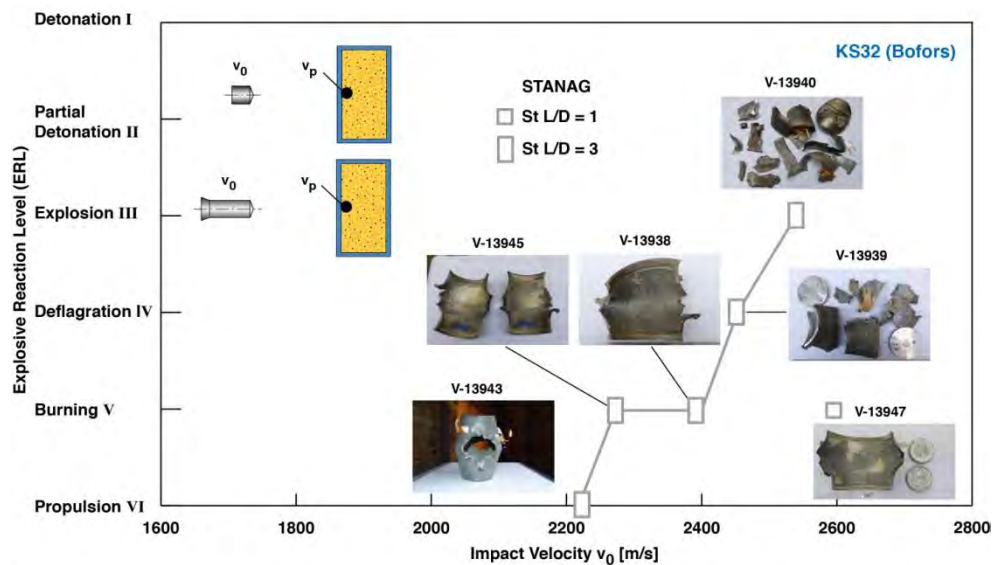


Fig. 6: Test results with steel projectiles with corresponding documentation of the residues.

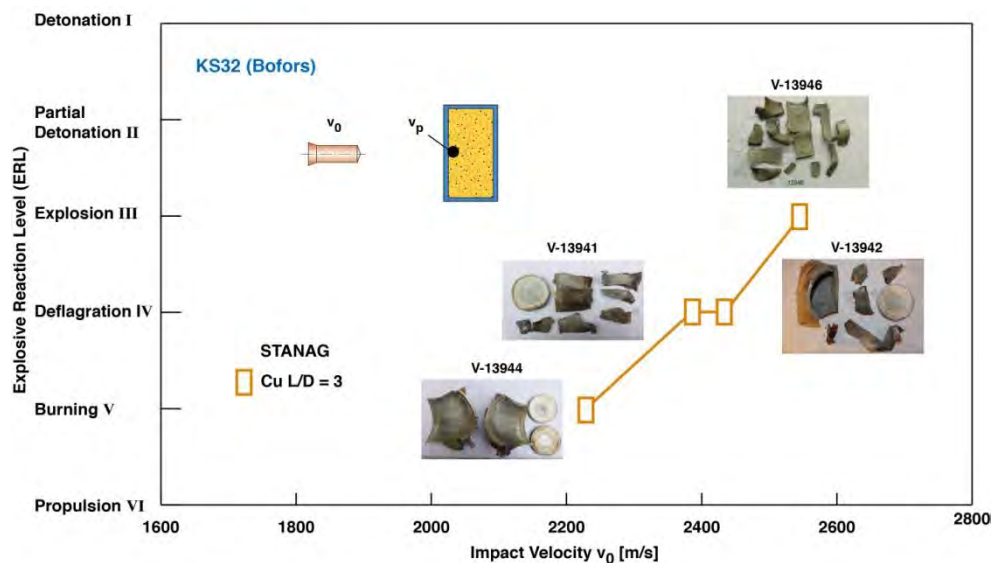


Fig. 7: Test results with copper projectiles with corresponding documentation of the residues.

4.2.3 Initiation Phenomenology

In Section 2, it was assumed that the transition from a *penetration mode* to an *impact mode* initiation process would occur when the projectile aspect ratio is reduced to $L/D = 1$. The detailed evaluation of the test results indicates that this transition can be already observed with the $L/D = 3$ projectile. V-13943 with $ERL = VI$ (Figures 6) was found to exhibit a clearly enlarged entry hole, which cannot be observed in the clear *penetration impact mode* situations with shaped charge jets (e.g. [10]). Figure 8 shows the casing after the test and makes clear that this entry hole is much larger and asymmetrical (width 75 mm and height 35 mm) than it could be expected from the STANAG projectile with 14.3 mm diameter. This means

(as numerical simulations showed) that chemical reactions started already at the entry side (characteristic of *impact mode* initiation). On the other hand, also the exit hole is very large (width 90 mm and height 60 mm) seemingly indicating a *penetration mode* initiation.

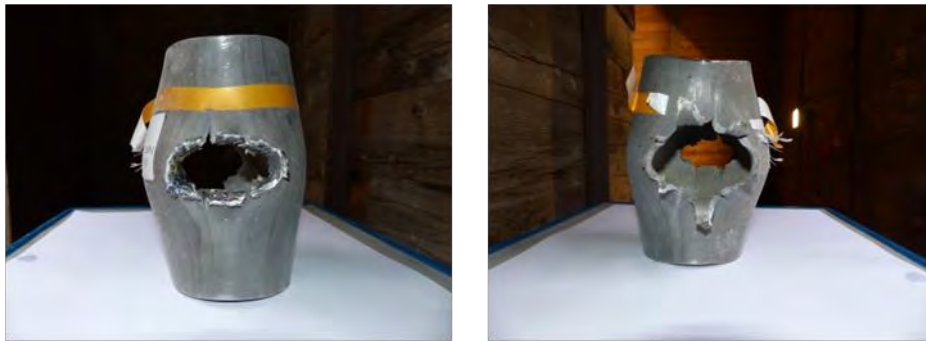


Fig. 8: Steel casing of test V-13943 with ERL = VI: entry side (left) and exit side (right).

4.3 Comparison with SCJ Results

In order to make the STANAG results comparable with the SCJ results in Figure 4 the measured impact velocity v_0 has to be converted to the velocity behind the 10 mm mild steel casing. The result of this transformation is the projectile velocity v_p , at which the projectile is entering the high explosive KS32 and which was used for the SCJ ranking (SCJ velocity behind the barrier). This conversion was accomplished by numerical simulations. Figure 9 exemplarily shows the model setup with an $L/D = 3$ projectile hitting the steel casing (left) and an $L/D = 1$ projectile after the perforation (right).

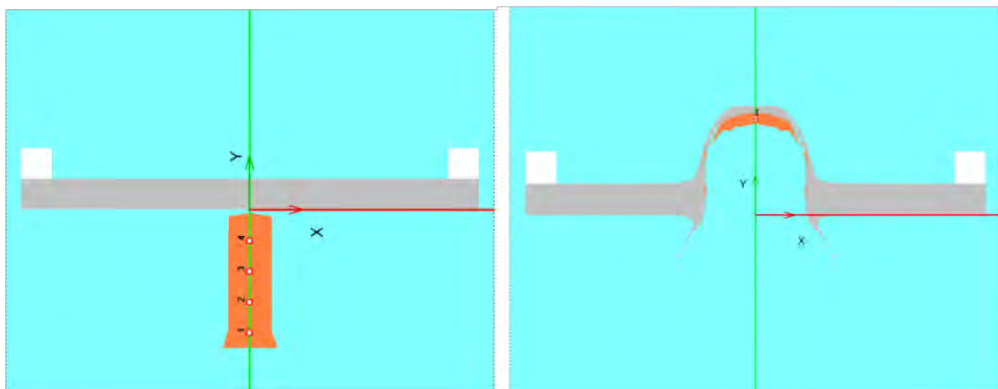


Fig. 9: Model setup: $L/D = 3$ projectile hitting the steel casing (left).
 $L/D = 1$ projectile after perforation of the steel casing (right).

The diagram in Figure 10 combines all the data of the SCJ trials with those from the STANAG projectile trials. The dashed lines from ERL = III to ERL = I thereby indicate the necessary extrapolation. The STANAG-projectile data fit well in into the overall ERL trends and the data generally look consistent.

It should be noted that this is not at all the case when the ERL is plotted over the stimulus $S = v^2d$ instead of the projectile velocity. In that case the STANAG projectile data would be completely super-positioned with the SCJ data, which would not make sense! Hence, also this result confirms that the stimulus $S = v^2d$ is not an appropriate parameter the description of initiation behavior.

Despite the fact that the STANAG data fit in very well there are still a couple of questions that remain unanswered for the moment, e.g.:

- Why are ERL-slopes different between SCJ and STANAG projectile results?
- What is the reason for the ramp-like ERL-slope especially for the SC-200?
- How does the gap between SCJ and STANAG projectile results look like?
- Why does the low velocity of the L/D = 1 steel projectile lead to an ERL = V initiation?
- Is there an influence of the critical diameter of KS32 ($d_f \sim 8$ mm) being very close to the jet diameter d_j of the SC-200?
- What is the influence of the transition between *impact mode* and *penetration mode* initiation?

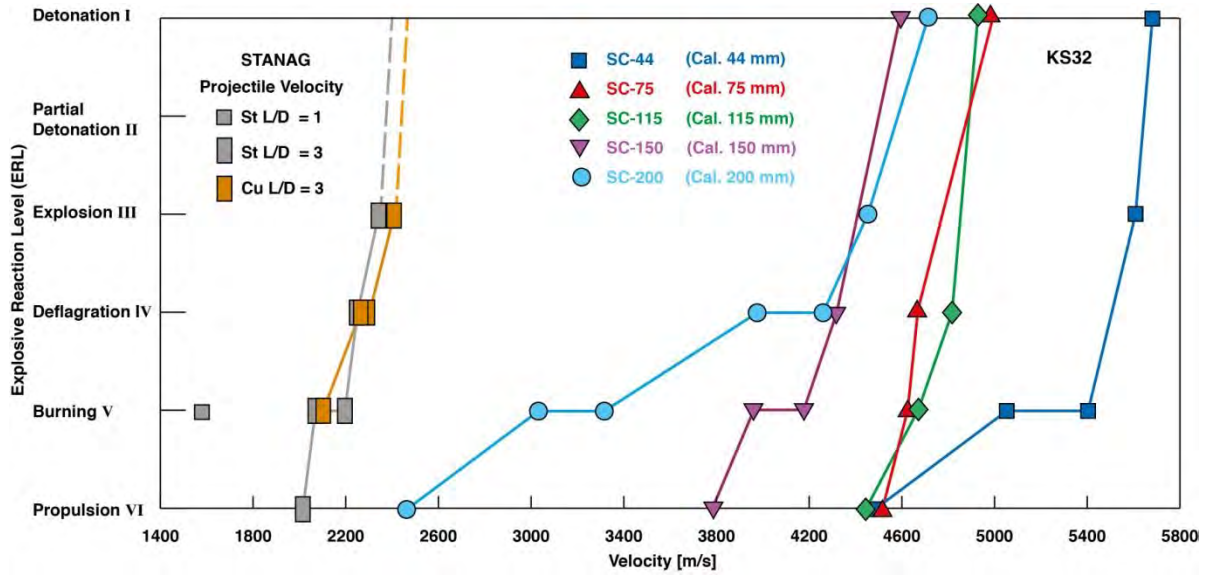


Fig. 10: Comparison of the SCJ results (from [10]) with the STANAG projectile results of this work.

5 New Unified Initiation Model

In [10] it was already realized that the stimulus $S = v^2 \cdot d$ is not an appropriate parameter for description of the observed initiation phenomena. Both parameters v & d (velocity & diameter of the jet / projectile) were used and it was assumed that instead of Eqn. (1) assuming $S = v^2 \cdot d = \text{const} = A^2$:

$$v = A/\sqrt{d} \quad (1)$$

$$v = A - B \cdot d \quad (2)$$

a linear relation as in Eqn. (2) might be a better description.

Using the ERL = I (detonation) and ERL = VI (low reaction / burning) from the data in Figure 10 as upper and lower limit for reactions, the diagram in Figure 11 can be drawn showing such an linear initiation behavior and supporting the proposed formula of (2). Data between the shaped charge SC-200 and the STANAG-projectile are still missing and this gap should be filled up the next years. A first step is already taken in [11].

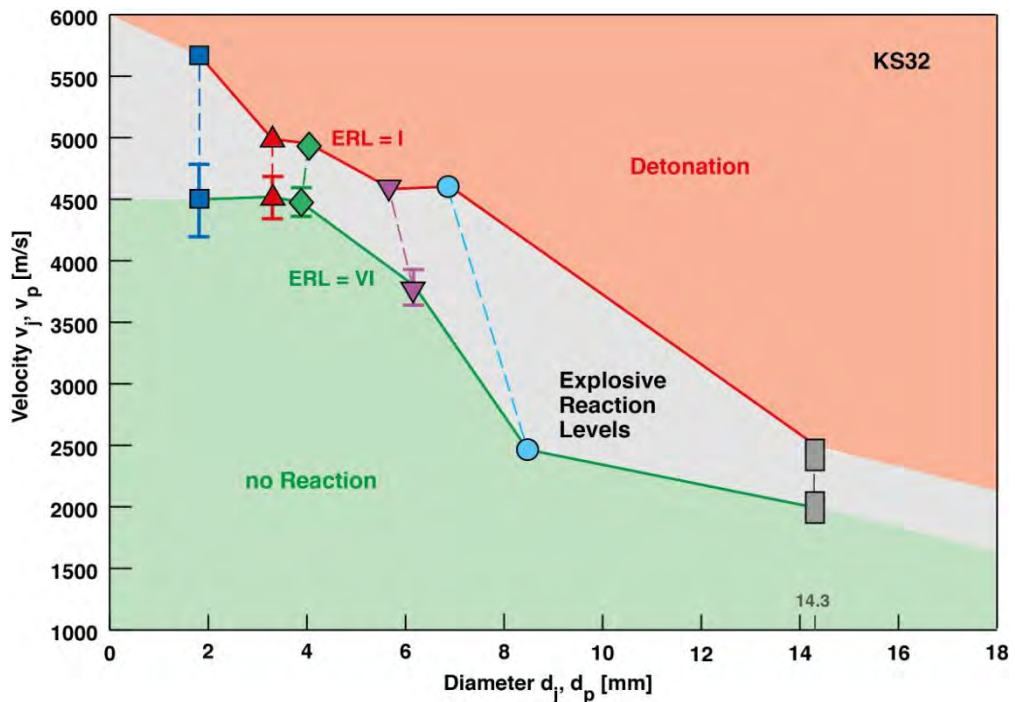


Fig. 11: Approximately linear initiation behavior of the data for ERL = I and ERL = VI.

6 Conclusions

In addition to the numerous initiation trials with SC jets also test campaigns with fragments represented by the STANAG projectile [12] were performed, based on the results achieved in [9]. The conducted experiments were supported by numerical simulations.

Original ($L/D = 1$) and elongated ($L/D = 3$) STANAG projectiles made out of steel and copper were shot from the EMI powder gun on the TDW standard charge with the PBX KS32 (HMX/PB 85/15, $\rho = 1.64 \text{ g/cm}^3$) – the charge already used in the SCJ trials. Since the EMI gun only reached a maximum projectile velocity of about 2600 m/s, the velocity to cause detonation had to be extrapolated and was found to be about 2700 m/s with the elongated projectile.

Obviously a transition process between a *penetration mode* initiation and an *impact mode* initiation [4] was enforced. This could be concluded from the observed reactions at the projectile entry side and from the fact that the $L/D = 1$ steel projectile erodes very quickly (not being able to reach the exit side of the charge) and requires higher impact velocities.

The new results fit in very well into the already available data set for shaped charge jets (SCJ). Once again the results showed very clearly that the stimulus $S = v^2 \cdot d$ is inappropriate as ranking parameter and that the “ $S = \text{const. rule}$ ” is not valid. The independent parameters v & d (velocity & diameter of the jet / projectile) rather exhibited a linear initiation behavior. Hence, a new initiation model is proposed: $v = A - B \cdot d$.

Acknowledgement

The authors would like to thank the BAAINBw Team K1.2 at Koblenz for the funding of this study and the EMI team at Kandern for conducting the powder gun trials.

References

- [1] W. Arnold, E. Rottenkolber, "Sensitivity of High Explosives against Shaped Charge Jets", Insensitive Munitions & Energetic Materials (IMEMTS) 2007, Miami, USA
- [2] W. Arnold, "High Explosive Initiation by High Velocity Pojectile Impact", HVIS 2010, Freiburg, GE
- [3] W. Arnold, M. Graswald, "Shaped Charge Jet Initiation of High Explosives equipped with an Explosive Train", IMEMTS 2010, Munich, GE
- [4] W. Arnold, E. Rottenkolber, "Shaped Charge Jet Initiation Phenomena of Plastic Bonded High Ex-plosives", IMEMTS 2012, Las Vegas, USA
- [5] W. Arnold, E. Rottenkolber, "High Explosive Initiation Behavior by Shaped Charge Jet Impacts", Hypervelocity Impact Symposium HVIS 2012, Baltimore, USA
- [6] W. Arnold, E. Rottenkolber, "Significant Charge Parameters influencing the Shaped Charge Jet Initiation", IMEMTS 2013, San Diego, USA
- [7] W. Arnold, E. Rottenkolber, T. Hartmann, "Analysis of Shock and Jet Initiation Tests of High Explosives", 15th Int. Symposium on Detonation ISD 2014, San Francisco, USA
- [8] W. Arnold, E. Rottenkolber, T. Hartmann, "Challenging v^2d ", IMEMTS 2015, Rome, IT
- [9] W. Arnold, E. Rottenkolber, T. Hartmann, "Testing and Modeling the Initiation of Insensitive Explosives by Projectile Impact", 11th EUROPYRO International Seminar 2015, Toulouse, France
- [10] W. Arnold, T. Hartmann, E. Rottenkolber, "Towards a Unified Initiation Model", IMEMTS 2016, Nashville, USA
- [11] W. Arnold, T. Hartmann, E. Rottenkolber, "Initiation Phenomenology from Hypervelocity to Low Velocity Impacts", 16th Int. Symposium on Detonation ISD 2018, Cambridge, USA (to be published)
- [12] STANAG 4496 (Edition 1), "Fragment Impact, Munitions Test Procedure", 2006

Impacts of REACH, ITAR and other regulations on Energetic Materials Sustainability

Geneviève Eck, Mohamed El Othmani, Julie Perouel, Delphine Dru, Bruno Nouguez

EURENCO, 1928 route d'Avignon, CS 90109 Sorgues- 84275 VEDENE, France
g.eck@eurenco.com – Phone : +33642117722

1- INTRODUCTION

EURENCO has for many years been producing a complete range of high explosives as well as the compositions based thereof.

Most of these compositions require the implementation of solvents or various components such as plasticizers, catalysts, binders or bonding agents. In the last years, the availability of these components has become more and more critical because of European or US regulations. Many European companies have to face to these regulation.

Thus EURENCO has identified the chemical components considered as critical in its production process. Some of them have been or will be banned by REACH (Registration, Evaluation, Authorisation and Restriction of Chemicals) regulation. The other products are subject to exportation limitations such as ITAR (International Traffic in Arms Regulations) and EAR (Export Administration Regulation) or sometimes by producers themselves which are reluctant to provide products for military applications.

Depending on the component and also the type of regulation, different strategies have been applied to deal with this new issue:

- Find new suppliers of the same component
- Replace the critical component by another one that is supposed to be chemically and/or functionally equivalent

Thus the impact of these regulations could be minor as well as of great importance which means that this can lead to the complete requalification of the composition.

The objective of this paper is to present a summary of the work performed in this area.

2- IDENTIFICATION OF THE CRITICAL COMPOUNDS

2.1- Components impacted by REACH regulation

REACH is a regulation of the European Union, adopted to improve the protection of human health and the environment from the risks that can be posed by chemicals.

In principle, REACH applies to all chemical substances except polymers; not only those used in industrial processes but also in our day-to-day lives, for example in cleaning products, paints as well as in articles such as clothes, furniture and electrical appliances. Therefore, the regulation has an impact on most companies across the EU.

Thus companies must identify and manage the risks linked to the substances they manufacture and market in the EU which means that companies could be involved as manufacturers, importers or even downstream users.

In the long run, the most hazardous substances should be substituted with less dangerous ones. Thus most of European companies need to anticipate.

EURENCO starts to make a list of critical compounds few years ago. The table 1 presents some of the more relevant compounds.

Impacted compounds	Use	Regulation impacts on the supply	Strategy
DBP Dibutyl Phtalate (CAS 84-74-2)	- Plasticizer	- Prohibited by REACH since 2015	- Replacement
DCE Dichloroethane (CAS 107-06-2)	- Polymerisation solvent	- Impacted by REACH - Not to be used after 2021	- Search for a new polymerization solvent
Tetrachloroethylene (CAS 127-18-4)	- Jellification solvent	- Prohibited by REACH since 2016	- Search for a new solvent

Table 1: EURENCO compounds impacted by REACH regulation

2.2- Components impacted by ITAR or EAR regulations

As for the components impacted by REACH regulation, a list of critical compounds impacted by ITAR or EAR regulation has been made. Some of these compounds are detailed in table 2.

Impacted compounds	Use	Regulation impacts on the supply	Strategy
HTPB R45HT2	- Polymer	- Produced in the USA under EAR licence - Difficulties for renewing the end user statement	- Find new suppliers
Copolymer SBS	- Thermoplastic copolymer	- Long supply period - Difficulties due to the final use (Military application)	- Find an European source
TEPAN tetramethylen pentamine acrylonitrile (CAS 68412-45-3)	- Bonding agent	- Impacted by ITAR regulation	- Find new suppliers
BiPh ₃ or TPB Triphenyl Bismuth (CAS 603-33-8)	- Polymerization catalyst	- Impacted by ITAR regulation	- Find new suppliers

Table 2: EURENCO compounds impacted by ITAR or REACH regulations

The problem is slightly different than the one for REACH regulation. The objective for components impacted par ITAR or EAR regulations is to find through a new European supplier the same chemical compounds.

3- TECHNICAL RESULTS

3.1- Components impacted by REACH regulation

Various compounds are impacted: two solvents and one plasticizer.

The difficulty is to find another chemical compound that should have an equivalent function to the old one and that does not have any impact on the final application.

3.1.1- DBP replacement

Dibutyl phthalate was used as a plasticizer in the nitrocellulose varnish used for final coating of modular artillery charges (MACS) and combustible cartridge cases (CCC). As DBP was part of Annex XIV with a sunset date in 2015, a new varnish has been formulated where DBP was replaced by a plasticizer widely used in the cosmetic industry.

Chemical compatibilities were successfully assessed against other products. Measured combustion quickness, ash percentage and permeability were consistent with former definition data.

The overall qualifications of MACS and CCCs were performed, taking into account not only the change in coating but also various changes in the product configuration and the production processes.

3.1.2- DCE replacement

Dichloroethane (DCE) is the solvent for the polymerization of epichlorhydrine (ECH) to get PECH Polyepichlorhydrine), the intermediate polymer in GAP (Glycidyle azide polymer) production. DCE is impacted by REACH regulation and will be authorized for use up to the end of 2021.

Polymerization reactions are based on active species which makes not easy to find a new solvent, furthermore if this new solvent has to be "green" and environmentally friendly.

That is why the replacement of DCE has been undertaken in two parts:

- ➔ Middle term replacement by a standard organic solvent:
 - Another organic solvent that is not yet impacted by REACH regulation and that is compatible with the polymerization reaction conditions and has been tested at lab scale and proved to yield to a polymer with characteristics (Mn / Mp and OH content) equivalent to those of an industrial polymer
 - Process file is also ready for scale up to the industrial workshop.

- ➔ Long term replacement: Research studies are carried on in order to find new ways to polymerize ECH (Epichlorhydrine). Up to now, the early results are very promising.

3.1.3- Tetrachloroethylene replacement

Tetrachloroethylene was used for the jellification of the copolymer SBS in the formulation C1322 used for the production of base-bleed grains. In 2013 this solvent was in the REACH candidate list with a sunset date in April 2016. The replacement of this solvent has been studied in collaboration with a bespoke solvent supplier:

- ➔ Drafting of specification
- ➔ Proposition of new candidates for tetrachloroethylene replacement
- ➔ Proposition by the solvent supplier of 3 alternatives (Biosane 161420, Biosane 1611165 and Butylal)
- ➔ Validation of Biosane 161420 based on physical characteristics such as the saturated vapor pressure and the enthalpy of vaporization.

3.2- Components impacted by ITAR / EAR regulations

To date, the components impacts by ITAR or EAR regulations are mainly polymers, bonding agents or catalysts.

3.2.1- HTPB R45HT2

HTPB R45HT2 is the most used polymer in EURENCO cast PBX compositions. Up to 2016, this product was supplied from a single supplier based in USA and thus impacted by EAR regulation. A new European supplier has been found. According to our specifications, the technical characterizations of the HTPB proposed by the European source are very close to those of US HTPB as presented in the table 3.

Characterizations	Units	Specifications	US HTPB	European HTPB
Viscosity at 30°C	mPa.s	< 6500	5000	4000-5500
OH content	mg KOH/g	/	47.1	44-51
OH content	meq/kg	0.73 < 0.90	0.84	/
Mn (g/mol)	g/mol	/	2800	2900
Density at 20°C	/	/	0.901	0.90-0.92

Table 3: Characteristics comparison between HTPB from 2 different suppliers

The qualification in composition of this new source of HTPB is in progress according to:

- ➔ Measurement of the chemical compatibilities with most important granular products (RDX, HMX, NTO)
- ➔ Evaluation in cast PBX compositions in 8 L mixer in order to check the implementation feasibility
- ➔ Evaluation in cast PBX compositions in 35 L industrial mixer to check the implementation feasibility and characterize the compositions
- ➔ Ageing studies at 60°C
- ➔ Evaluation in the proprietary bi-component process

The most relevant results are detailed hereafter.

3.2.1.1- Qualification at 8 L. scale

The qualification has been performed on 6 different cast cured compositions in order to scan a large set of ingredients (See table 4).

For all these compositions, characterization results on:

- Density
- Hardness
- Mechanical properties at +20°C, -45°C and +60°C
- Sensitivity to friction and impact

have been found conform to the specifications and equivalent to those for standard industrial compositions.

Ingredients	B2238B	B2211B	PBXN-109	B2214B	B2263A
RDX	✓	✓	✓		✓
HMX				✓	
NTO				✓	
PA		✓			
Al		✓	✓		
HTPB	✓	✓	✓	✓	✓

Table 4: Compositions for qualification of a new source of HTPB

3.2.1.2- Qualification at 35 L. scale

The next step was to scale up at a 35 L. mixer the following compositions: B2238B, B2263A and PBXN-109.

Results are available for the first two compositions and are in progress for the composition PBXN-109.

The results on both compositions show a good reproducibility from lab scale to pilot scale. Furthermore they are encouraging for scaling up to industrial mixer and make us confident to substitute the US source by the European source.

3.2.2- Copolymer SBS

SBS is a copolymer Styrene-Butadiene-Styrene. A second source of supply had to be found because of the end use (Military application) that is a problem with the current supplier.

The qualification of a new European source of SBS (Named "source n°2" in the following paragraphs) has been successfully done according to:

- ➔ Validation of SBS n°2 compliance with EURENCO specification
- ➔ Validation of SBS n°2 in the production process of C1322
- ➔ Validation of the final composition

3.2.2.1- Compliance of the new source of SBS with the specifications

SBS n°2 has been found compliant as presented in the table n°5.

Characterizations	Units	Specifications	SBS n°2 sample 1	SBS n°2 sample 2
IR	/	Conform to the reference	Conform	Conform
Glass T° by DSC	°C	$-98 \leq \leq -86$	-88.5	-88.4
Volatile matter	%	≤ 0.3	0.03	0.00
Ash content	%	≤ 0.25	0.00	0.00
Viscosity in solution	Poises	$9 \leq \leq 15$	13	14

Table 5: Characterization of SBS n°2

3.2.2.2- Validation of the new source in the final composition

No unexpected behavior has been observed in all production process steps of the composition C1322.

Physico-chemical characteristics as well as safety characteristics have been measured and compared to those obtained with the composition produced from SBS n°1.

The final composition is conform to the specifications and the results of the measurements are quite identical to those on the reference composition. The most important results are summarized in table 6.

Thus the new source has been fully qualified and approved for industrial use.

Characterization	Specification	SBS n°1	SBS n°2
Density (kg/m ³)	1540 / 1600	1560	1567
Glass temperature (°C)	≤ -84	-84	-90.5
Mechanical properties at 20°C <ul style="list-style-type: none">▪ Sm (MPa)▪ Em (%)	≥ 3.5 ≥ 5	4.3 11.9	4.5 17.2
Impact sensitivity (J)	/	34	50.1
Friction sensitivity (N)	/	27 + at 353	217
Vacuum stability 130°C/193h. (cm ³ /g)	/	0.47	0.21

Table 6: Final validation of SBS n°2

3.2.3- TEPAN

TEPAN (tetramethylen pentamine acrylonitrile) is used as a bonding agent in the formulation of cast PBX or composite rocket propellants. Since it is supplied from USA, it is impacted by ITAR regulation.

Two French alternative suppliers have been identified and samples of TEPAN have been supplied (Named "TEPAN n°2" and "TEPAN n°3" to be compared to TEPAN n°1).

The qualification of these two new sources of TEPAN according to:

- ➔ Characterization of TEPAN
- ➔ Validation of TEPAN at 8 liter mixer scale
- ➔ Validation of TEPAN at industrial scale

3.2.3.1- Characterization of TEPAN n°2 and n°3

Both TEPAN are conform to EURENCO specifications. As an example, the table 7 shows the results for TEPAN n°2.

Characterization	Specification	TEPAN n°1 (Reference)	TEPAN n°2
Total amine content	11/15 eq/kg	13.7	13.7
Water content	≤ 0.50 %	0.28	0.28
IR	Conform to the reference	See figure 1	See figure 1

Table 7: Compared characterizations of TEPAN n°1 and TEPAN n°2

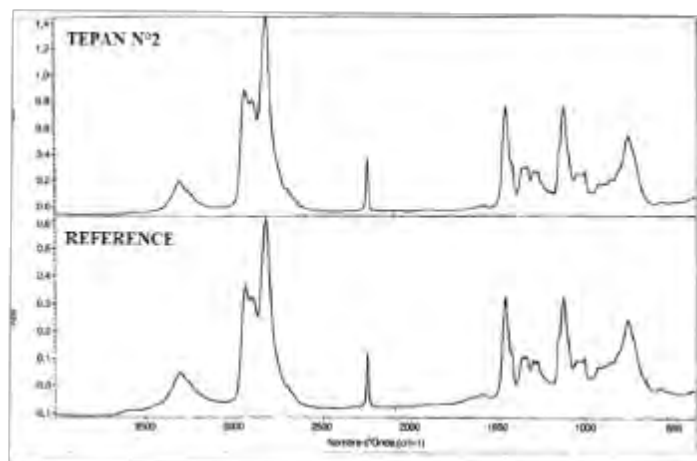


Figure 1: IR spectrum of TEPAN n°2 compared to the US reference

3.2.3.2- Validation of TEPAN in compositions

Both qualities have been tested in formulations at lab scale and the compositions based on TEPAN n°2 and n°3 have been found to be conform with the specifications.

The more relevant results for TEPAN n°2 are summarized in table n°8.

TEPAN quality	TEPAN n°2	
Formulation tested	B2238	B2214B
Viscosity	Compliant with industrial scale	Compliant with industrial scale
Density	1.572	1.636
Mechanical properties		
▪ Smt (MPa)	0.96	0.60
▪ Emt (%)	9.3	10.6

Table 8: Validation of TEPAN n°2 in composition

- The feasibility data such as the viscosity are compatible for scale up at industrial mixer.
- Densities are as expected for both tested compositions
- Mechanical properties for B2214B are consistent with those at industrial scale for B2214B
- Mechanical properties for B2238 are slightly different (emt little bit low) but it might be due to the scale at which the experiment has been performed.

3.2.4- TPB (Triphenyl bismuth)

TPB is a catalyst for polymerization of cast cured formulations. Up to 2012 it was supplied in USA. A new supplier has been qualified (Named later "TPB n°2"). TPB n°2 has been tested in PBXN-109 composition. The most relevant characteristics of PBXN-109 prepared with TPB n°2 are presented in the table 9.

Characteristics	PBXN-109 with US TPB ^(a)	PBXN-109 with TPB n°2 ^(b)
Density	1669/1683	1669
Mechanical properties at 20°C		
▪ Sm (MPa)	0.33/0.76	0.61
▪ Em (%)	19/55	19
Shore hardness	44/64	62

(a) Industrial results (36 mixes)

(b) Results at 8 liter scale

Table 9: Qualification of TPB n°2 on PBXN-109

4- CONCLUSION

Most of the issues encountered by EURENCO in France that are induced by the REACH regulation, have been solved, or are about to be solved. For some products (DCE as example) long term research studies are needed in order to find a sustainable replacement product. Since REACH is still updating, fundamental work will be always necessary to propose environment friendly solutions.

Among the products which are subject to ITAR or EAR authorizations, the most important remaining action is related to the HTPB European supplier, where a long term program is self-supported by EURENCO and remains to be completed.

Moreover, triphenyl bismuth (TPB) could constitute a critical product, even if a non US supplier has been qualified, as no European producer was found.



Impact of REACH, ITAR and other
regulations on Energetic Materials
Sustainability

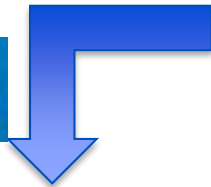
G. ECK, M. EL OTHMANI, J. PEROUEL,
D. DRU, B. NOUGUEZ

www.eurenco.com

- **Introduction**
- **Impact of REACH regulation**
- **Impact of ITAR / EAR regulation**
- **Conclusion**



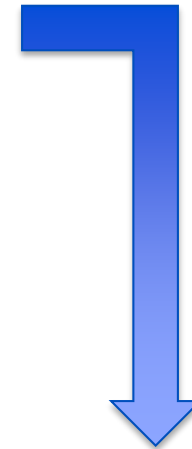
REACH



- **Registration, Evaluation, Authorization and Restriction of Chemicals**
- **Adopted to improve the protection of human health and the environment from the risks that can be posed by chemicals**



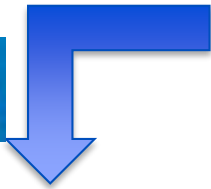
ITAR
(US/DoD or US/DoC regulations)
EAR



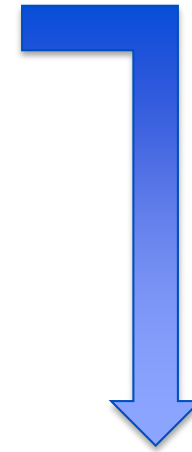
- **International Traffic in Arms regulations / Export Administration Regulation**
- **Designed to help ensure that defense related technology does not get into the wrong hands**

EUROPE has to face to different regulations

REACH



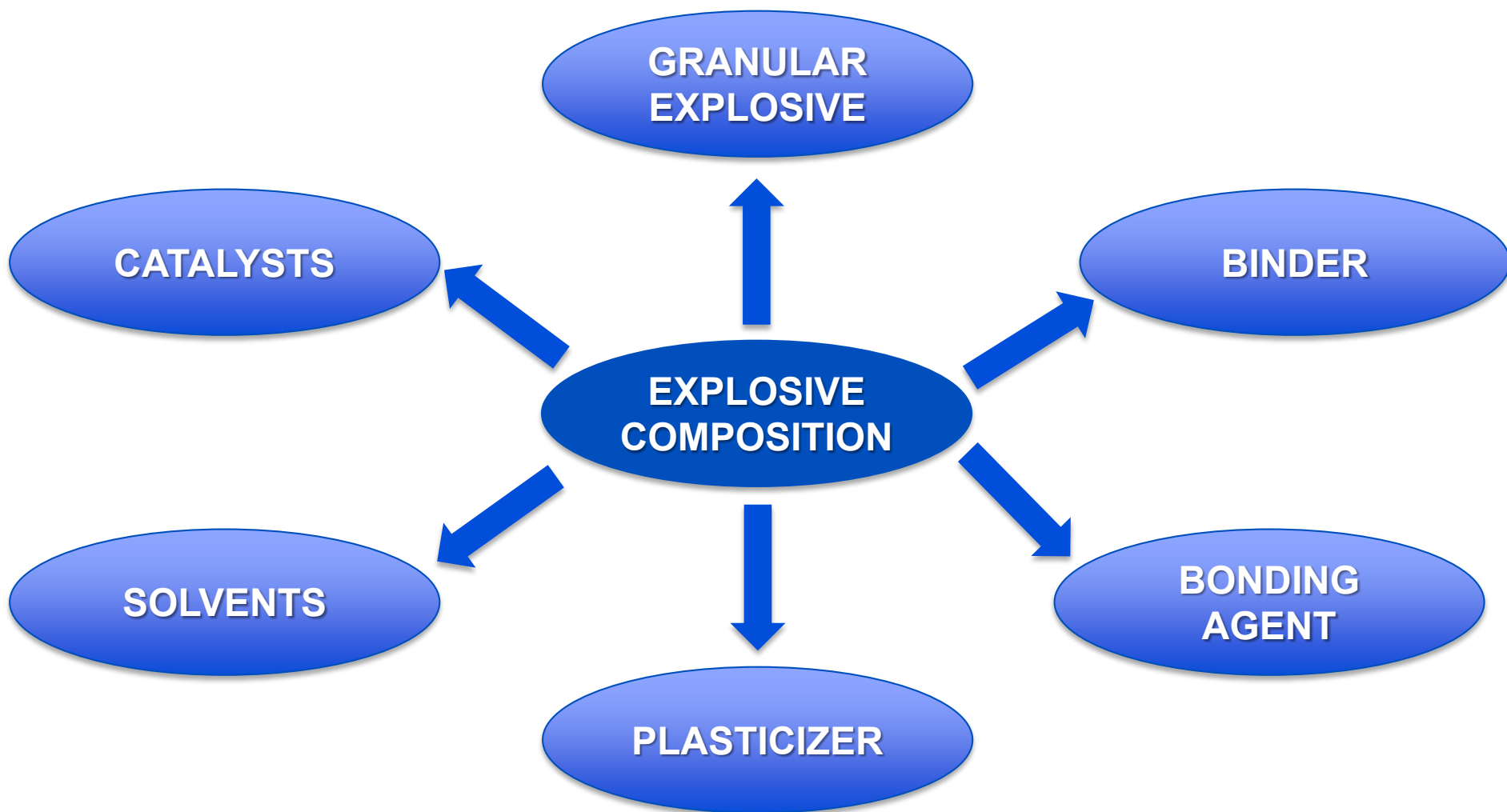
ITAR
(US/DoD or US/DoC regulations)
EAR

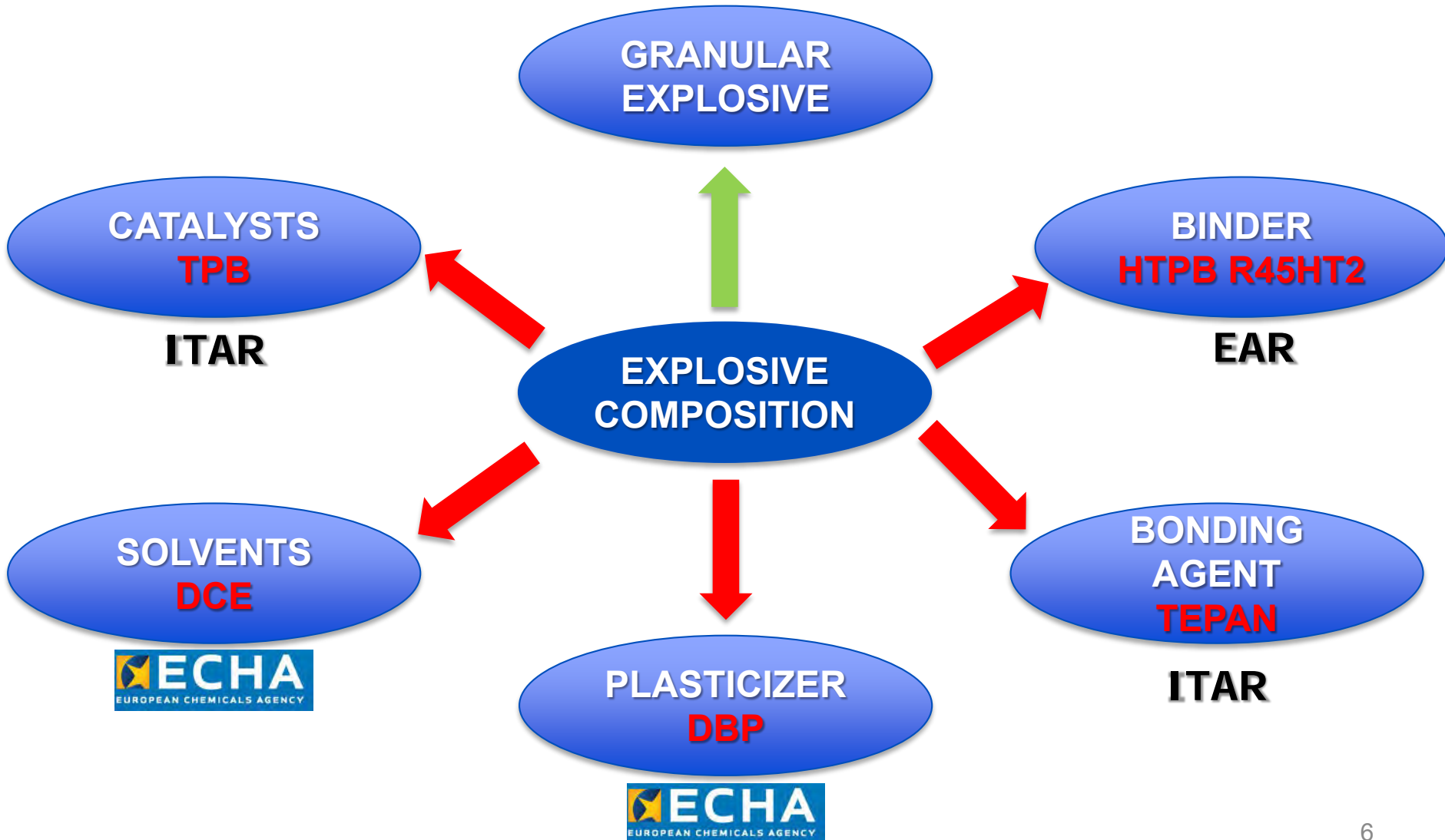


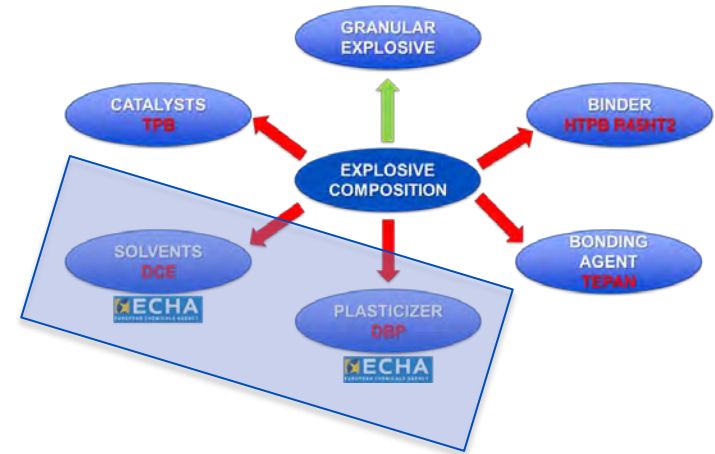
- **Replace the critical component by another one that is supposed to be chemically and/or functionally equivalent**

- **Find new suppliers of the same component**









- **Introduction**
- **Impact of REACH regulation**
- **Impact of ITAR / EAR regulation**
- **Conclusion**

List of critical compounds

Impacted compounds	Use	Regulation impact	Strategy
DBP Dibutyl Phtalate	Plasticizer	Prohibited by REACH since 2015	Replacement
DCE Dichloroethane	Polymerization solvent	Not to be in use after 2021	Search for a new polymerization solvent
Tetrachloroethylene	Jellification solvent	Prohibited by REACH since 2016	Search for a new solvent

DBP Dibutyl Phtalate

PLASTICIZER
in the nitrocellulose varnish used for final
coating of MACS and CCC

- Replaced by a plasticizer widely used in the cosmetic industry
- Qualification of this new compound completed
 - Chemical compatibilities
 - Combustion quickness
 - Ash percent
 - Permeability
 - Overall qualification of MACS and CCC

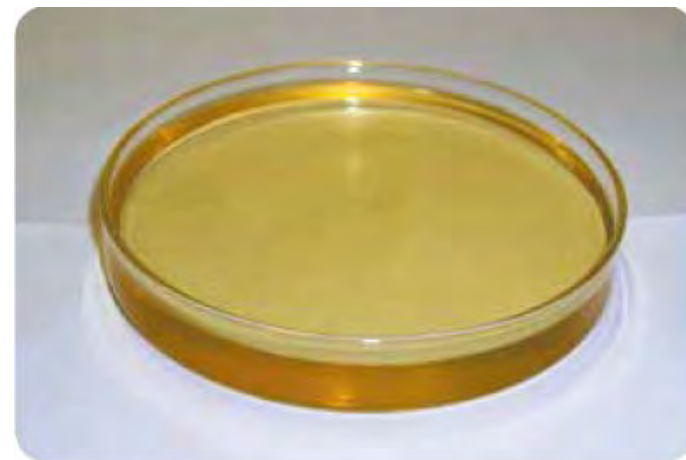


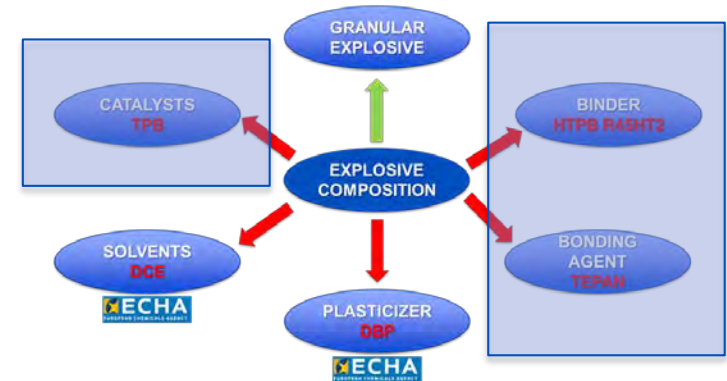
DCE
Dichloroethane

SOLVENT

Polymerization of ECH to get PECH, the
intermediate polymer in GAP production

- Middle term replacement by a standard organic solvent
 - Organic solvent not yet impacted by REACH
 - Process file ready for scale up to the industrial workshop
- Long term replacement: Research studies to find new ways to polymerize ECH





- Introduction
- Impact of REACH regulation
- Impact of ITAR / EAR regulation
- Conclusion

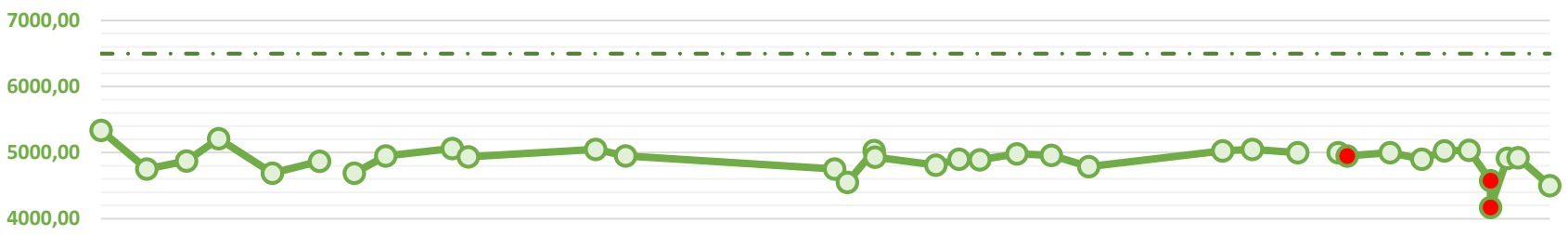
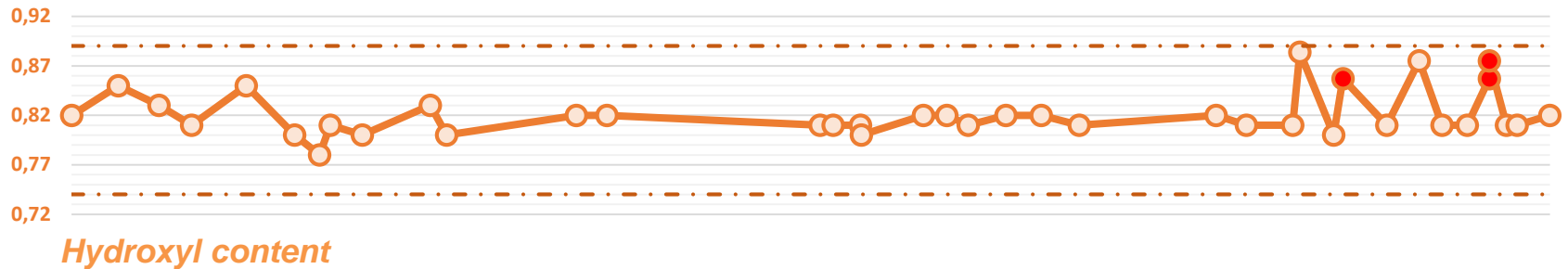
List of critical compounds

Impacted compounds	Use	Regulation impact	Strategy
HTPB R45HT2	Polymer	<ul style="list-style-type: none"> • Produced in the USA under EAR licence • Difficulties for renewing the end user statement 	Find new suppliers
Copolymer SBS	Thermoplastic copolymer	<ul style="list-style-type: none"> • Long period supply • Difficulties due to final use 	Find an European source
TEPAN Tetraethylen pentamine acrylonitrile	Bonding agent	<ul style="list-style-type: none"> • Impacted by ITAR regulation 	Find new suppliers
BiPh ₃ or TPB Triphenyl bismuth	Polymerization catalyst	<ul style="list-style-type: none"> • Impacted by ITAR regulation 	Find new suppliers

HTPB R45HT2

BINDER
Most used polymer in EURENCO cast PBX compositions

- Supplying oh HTPB from a new source and comparison with the current one



HTPB R45HT2**BINDER****Most used polymer in EURENCO cast PBX
compositions**

- **Qualification of this new source**
 - **Chemical compatibilities with most important granular products**
 - **Evaluation in cast PBX composition in 8 L. mixer → implementation feasibility**
 - **Evaluation in cast PBX composition in 35 L. mixer → implementation feasibility and composition characterization**
 - **Ageing studies at 60°C**
 - **Evaluation in 135 L. mixer**
 - **Evaluation in the proprietary bi-component process**

HTPB R45HT2**BINDER****Most used polymer in EURENCO cast PBX
compositions**

- **Qualification of this new source**
 - **Chemical compatibilities with most important granular products**
 - **Evaluation in cast PBX composition in 8 L. mixer → implementation feasibility**
 - **Evaluation in cast PBX composition in 35 L. mixer → implementation feasibility and composition characterization**
 - **Ageing studies at 60°C → In progress**
 - **Evaluation in 135 L. mixer → In progress**
 - **Evaluation in the proprietary bi-component process → In progress**

HTPB R45HT2

- Qualification at 8 L. scale on 6 cast cured compositions

	B2238B	B2211B	PBXN-109	B2214B	B2263A
RDX	✓	✓	✓		✓
HMX				✓	
NTO				✓	
PA		✓			
AI		✓	✓		
HTPB	✓	✓	✓	✓	✓

HTPB R45HT2

- Qualification at 35 L. scale on 3 cast cured compositions

	B2238B		PBXN-109		B2263A
RDX	✓		✓		✓
HMX					
NTO					
PA					
AI			✓		
HTPB	✓		✓		✓

HTPB R45HT2

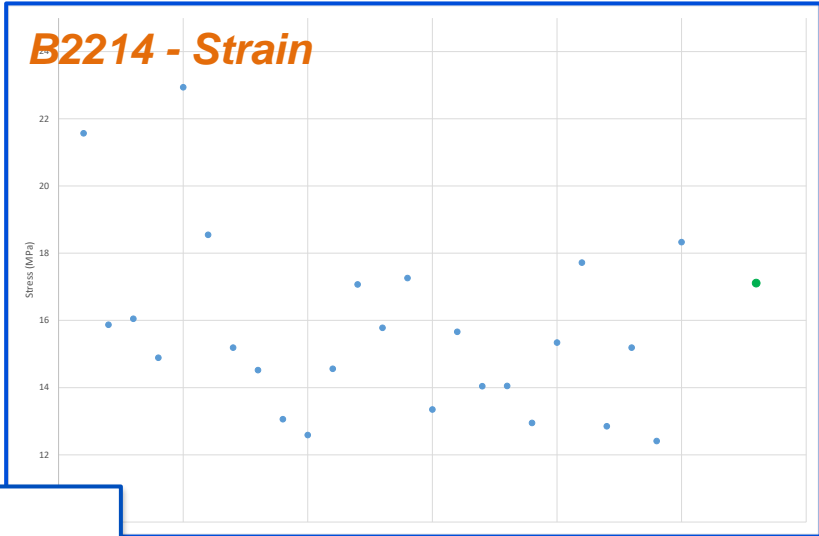
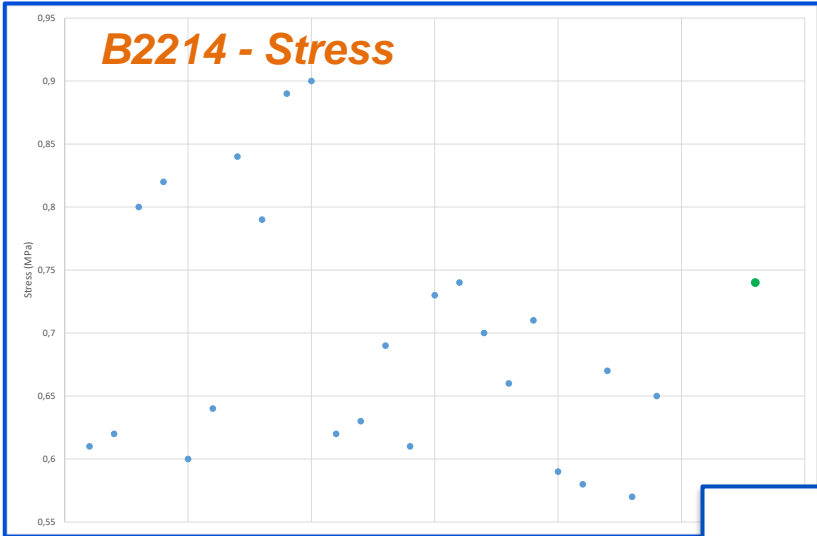
- **Qualification at 8 L. scale : Characterizations**
 - **Density**
 - **Hardness**
 - **Mechanical properties at +20°C, -45°C, +60°C**
 - **Sensitivity to friction (ISF) and impact (ISI)**



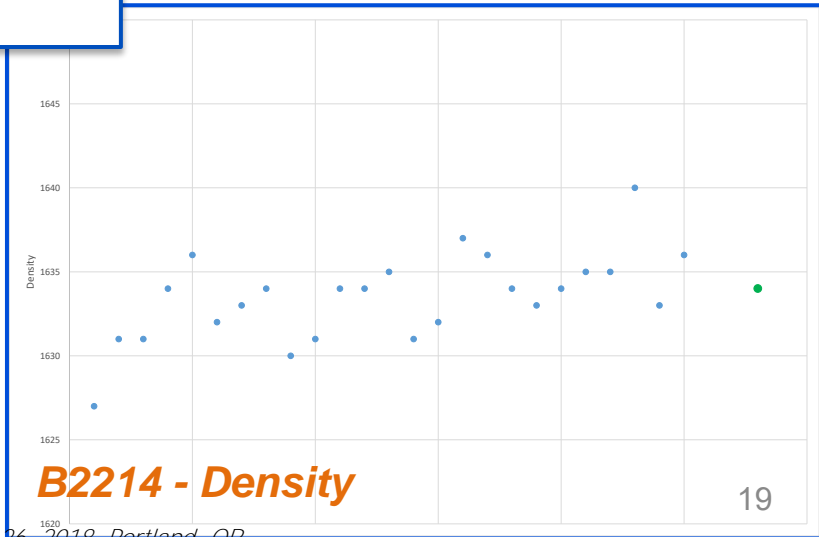
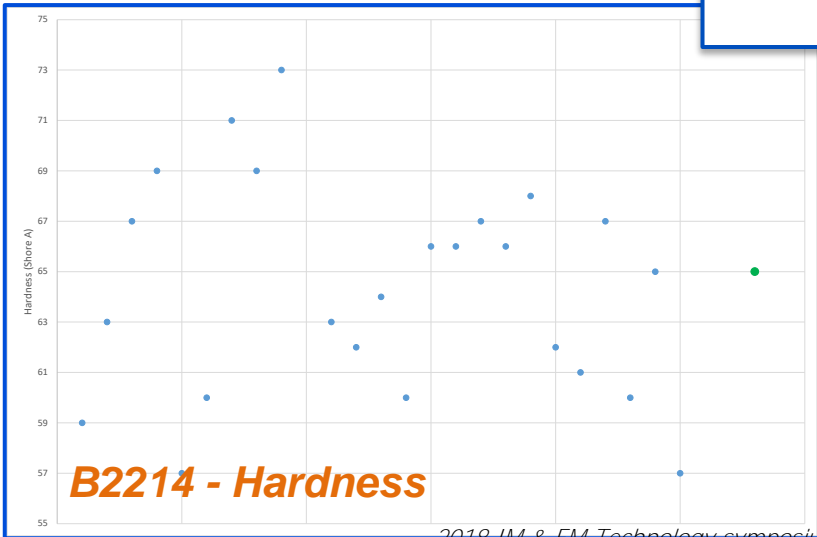
- ✓ **Conform to the specifications**
- ✓ **Results equivalent to those for standard industrial compositions**

- **Additive characterization at 35 L. scale**
 - **Friability**

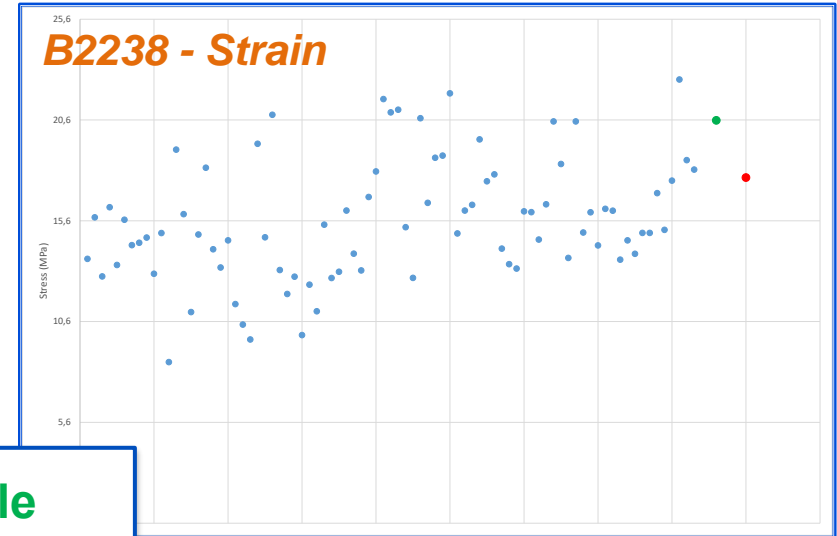
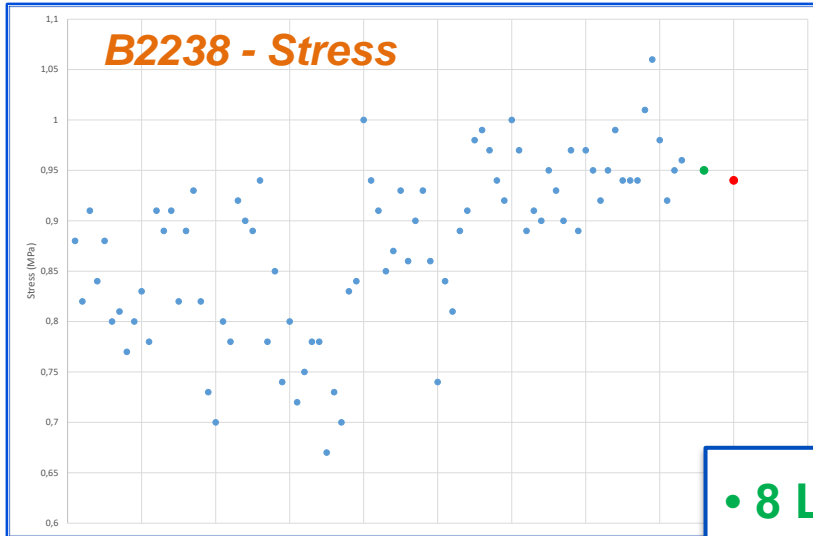
HTPB R45HT2



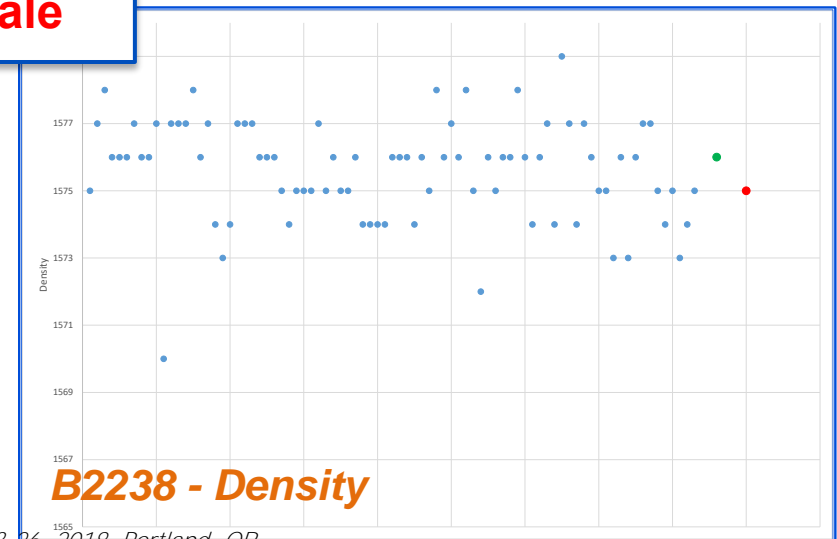
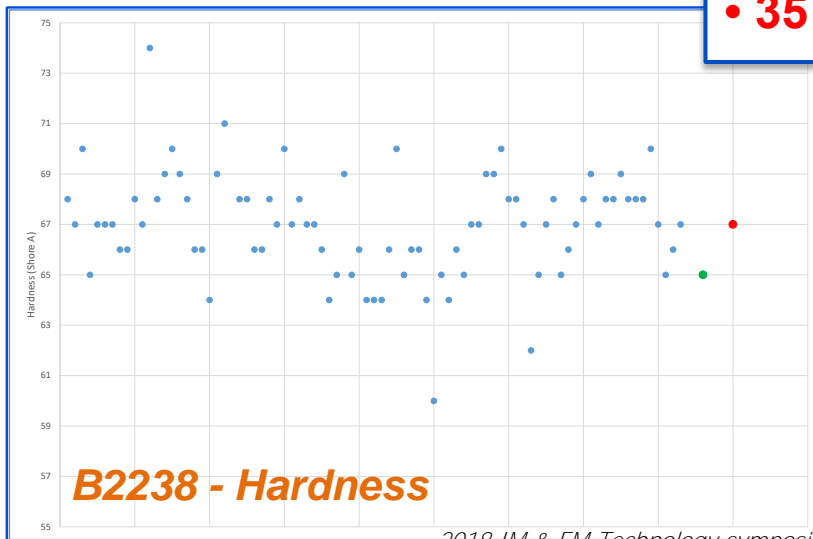
• 8 L. scale



HTPB R45HT2



- 8 L. scale
- 35 L. scale



TEPAN
Tetraethylen pentamine acrylonitrile

BONDING AGENT
In formulation of cast PBX or composite rocket
propellants

- **Supplying of 2 French alternatives (TEPAN N°2 and TEPAN N°3) and comparison with the reference (TEPAN n°1)**

Characterization	Specification	TEPAN n°1 (Reference)	TEPAN n°2
Total amine content	11/15 eq/kg	13.7	13.7
Water content	≤ 0.50 %	0.28	0.28

TEPAN
Tetraethylen pentamine acrylonitrile

BONDING AGENT
In formulation of cast PBX or composite rocket
propellants

○ **Validation in composition**

Formulation tested	B2238	B2214B
Viscosity	Compliant with industrial scale	Compliant with industrial scale
Density	1.572	1.636
Mechanical properties		
- Smt (MPa)	0.96	0.60
- Emt (%)	9.3	10.6

TPB Triphenyl bismuth

CATALYST For polymerization of cast cured formulations

- Supplying of TPB N°2 (Non European supplier)
- Validation in composition PBXN-109

Characteristics	PBXN-109 with US TPB ^(a)	PBXN-109 with TPB n°2 ^(b)
Density	1669/1683	1669
Mechanical properties at 20°C		
- Sm (MPa)	0.33/0.76	0.61
- Em (%)	19/55	19
Shore hardness	44/64	62

a) Industrial results (36 mixes)

b) Results at 8 L. scale

- **Introduction**
- **Impact of REACH regulation**
- **Impact of ITAR / EAR regulation**
- **Conclusion**

Impacted compounds	Regulation impacts on the supply	Status
DBP / Dibutyl Phthalate	REACH	✓
DCE / Dichloroethane	REACH	Long term research studies needed
Tetrachloroethylene	REACH	✓
HTPB R45HT2	EAR	Long term program to be completed
TEPAN	ITAR	✓
Copolymer SBS	« Reluctant » supplier	✓
BiPhi ₃ / TPB / Triphenyl bismuth	ITAR	✓

Most of the issues encountered by EURENCO

- ☺ **have been solved (DBP, TCE, TEPAN, SBS, TPB)**
- ☺ **or are about to be solved (HTPB)**

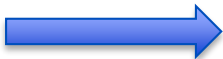


Of course these regulations cost money

But

- ➔ **They force us to find alternative solutions sometimes very innovative (DCE)**
- ➔ **They can significantly reduce the exposure of workers to dangerous substances**

Overall they are cost effective



- **J. PEROUEL, D. DRU, M. EL OTHMANI and B. NOUGUEZ** who coauthored this work
- **Process team and laboratory team** who performed and characterized the compositions
- **Bergerac team** for MACS and CCC related inputs

Thank you for your attention
Questions?



EUROPEAN LEADER IN ENERGETIC MATERIALS

www.eurenco.com



LAWRENCE
LIVERMORE
NATIONAL
LABORATORY

New Polycarbonate-Based Thermoplastic Polyurethane Binder for HMX Based Explosives

E.L. Robertson; D.M. Hoffman; P.F. Pagoria*

April 23-26, 2018

Insensitive Munitions and Energetic Materials Technology
Symposium

Portland, Oregon

LLNL-PROC-748964

This work was performed under the auspices of the U.S. Department of Energy by Lawrence Livermore National Laboratory under Contract DE-AC52-07NA27344.

Disclaimer

This document was prepared as an account of work sponsored by an agency of the United States government. Neither the United States government nor Lawrence Livermore National Security, LLC, nor any of their employees makes any warranty, expressed or implied, or assumes any legal liability or responsibility for the accuracy, completeness, or usefulness of any information, apparatus, product, or process disclosed, or represents that its use would not infringe privately owned rights. Reference herein to any specific commercial product, process, or service by trade name, trademark, manufacturer, or otherwise does not necessarily constitute or imply its endorsement, recommendation, or favoring by the United States government or Lawrence Livermore National Security, LLC. The views and opinions of authors expressed herein do not necessarily state or reflect those of the United States government or Lawrence Livermore National Security, LLC, and shall not be used for advertising or product endorsement purposes.

New Polycarbonate-Based Thermoplastic Polyurethane Binder for HMX Based Explosives

Emily L. Robertson*, D. Mark Hoffman, and Philip F. Pagoria

Energetic Materials Center
Lawrence Livermore National Laboratory, Livermore, CA USA 94550

robertson37@llnl.gov

Abstract:

Plastic bonded explosive formulations comprised of HMX are commonly used in expensive precision weapons platforms. Thermoset polyurethanes have been studied extensively as binders for these explosive charges. We chose to examine thermoplastic polyurethanes (TPUs) based on the processing advantages they promise, leading to their application in several established high explosive formulations. For example, aromatic polyester based thermoplastic polyurethanes under the trade name Estanes® have been used in several DOE explosives, including LX-14 (95.5% HMX and 4.4% Estane). Because of the attractive properties of TPUs and the availability of new commercially available polycarbonate polyurethane systems, we have undertaken a study of new HMX-based formulations using new TPUs, mainly derived from polycarbonates. To our knowledge there have been no published energetic material formulations using polycarbonate-based polyurethanes.

The polymers and multiple HMX formulations utilizing the polycarbonate-based thermoplastic polyurethanes (PC-TPU) have been produced and characterized. Commercially available polymers have been characterized by differential scanning calorimetry for glass and melt transition temperatures. Formulations comprised of 95% HMX and 5% binder with different polymers were produced and characterized for small scale sensitivity, pressing density, and processing feasibility. Based on these experiments we found that the isocyanate used to produce the polycarbonate polyurethane is important and believe aliphatic polyurethanes are a viable alternative to traditional thermoset polyurethane in explosive formulations.

Keywords: hmx; polycarbonate thermoplastic polyurethane; aliphatic; aromatic

Introduction

Plastic bonded explosive formulations comprised of HMX are commonly used in expensive precision weapons platforms. Thermoset polyurethanes have been studied extensively as binders for these explosive charges. [1] Thermoplastic polyurethanes (TPUs) were examined based on the processing advantages they promise, leading to their application in several established high explosive formulations. For example, aromatic polyester based thermoplastic polyurethanes under the trade name Estanes®¹ have been used in several DOE explosives, including LX-14 (95.5% HMX and 4.4% Estane). Because of the attractive properties of TPUs and the availability of new, commercially available polycarbonate polyurethane systems, we

¹® Estane and Pearlstick after a registered trademark of the Lubrizol Corporation. Estane is also known as Pearlstick.

have researched and herein report on HMX-based formulations using new TPUs, mainly derived from polycarbonates.

Polyurethane Background

Polyurethanes are a family of segmented co-polymers consisting of hard and soft “blocks” with urethane linkages (Figure 1). Polyurethanes can either be thermosets or thermoplastics depending on the composition.

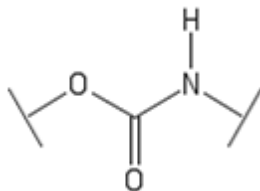


Figure 1. Urethane linkage

Polyurethanes have three distinct building blocks that dictate their properties: 1) the isocyanate, 2) the polyol, and 3) the chain extender diol (Figure 2, 3). The isocyanate is rigid and will contribute to the hard segment region while the polyol is flexible and contributes to the soft segment region. The chain extender can be either rigid or flexible. [2, 3]

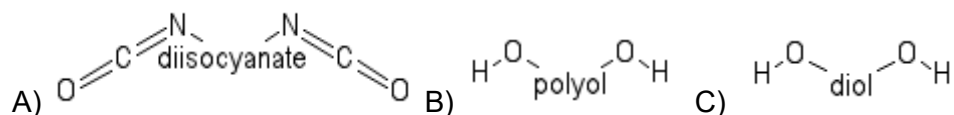


Figure 2. The components of a polyurethane: A) an isocyanate, B) a polyol, and C) a chain extender diol.

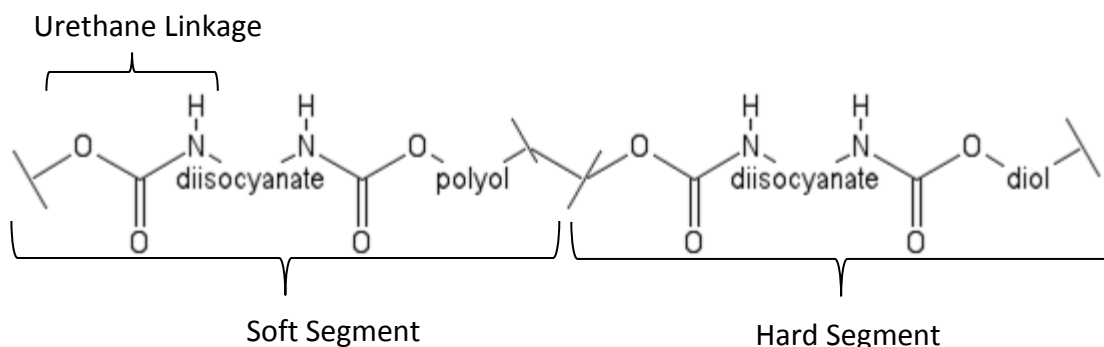


Figure 3. The repeating units of a polyurethane with 1 of the 4 urethane linkages highlighted along with the soft and hard segments.

Polyurethanes are identified based on the isocyanate and polyols used in their synthesis. Isocyanates are classed as either aromatic or aliphatic (non-aromatic). Aliphatic isocyanates are typically stable to photolysis and have excellent optical clarity and adhesion. Aromatic isocyanates are typically more flexible, stronger, and tougher. [2-4]

Commercially available polyols used in thermoplastic polyurethanes generally fall into 4 categories: 1) polyester, 2) polyether, 3) polycaprolactone, or 4) polycarbonate. Carbonate polyols are characterized by their excellent hydrolysis and chemical resistance at elevated temperatures and low compression set. [3, 5-10]

Materials

Based on commercial availability and batch sizes, three polycarbonate-based thermoplastic polyurethanes (PC-TPUs) were selected: two aliphatic and one aromatic (Table 1). Estane 5703 is an aromatic polyester-based thermoplastic polyurethane used in LX-14 that has been included as a comparison. The specific material compositions are proprietary.

Table 1: Polycarbonate-based thermoplastic polyurethane properties from vendors

Material	Quadrathane ARC-75A	Quadrathane ALC-75A	ChronoFlex AL 75A-Q	Estane 5703 [now Pearlstick 5703]
Manufacturer	Biomerics	Biomerics	AdvanSource	Lubrizol
Type	aromatic polycarbonate	aliphatic polycarbonate	aliphatic polycarbonate	<i>aromatic polyester</i>
Durometer (Shore Hardness)	75A	75A	75A	70A
Specific Gravity	1.17	1.14	ca 1.10	1.19
Ultimate Tensile Strength (psi)	6000	4500	ca 4000	4500
Ultimate Elongation (%)	550	500	350–750	630

Polymer Characterization

Thermoplastic materials are formed into usable parts in a pressing operation through the application of heat and pressure to melt the binder and form it into the desired shape. In general, the polymer flows and compacts more readily with increased temperature, however, thermal properties and stability of the explosive creates a maximum safe pressing temperature. As an upper limit, HMX goes through a phase transformation at 162 °C [11]. Process capabilities can also place limits. For example, LLNL allows pressing HMX formulations at up to 105 °C with in-die pressures up to 35 ksi.

An indication of the relative processing temperatures required for each binder is provided by consideration of glass transition (T_g) and melt transition (T_m) temperatures for hard and soft segments. Transition temperatures were measured using differential scanning calorimetry (DSC) on 20 mg specimens, sweeping from -80 °C to 205 °C at a rate of 5 °C min^{-1} . All samples were tested as received from the manufacturer, however, it should be noted that the thermal history can impact degree of sample crystallinity, potentially resulting in variations in the measured transition temperatures. [12] The as received condition represents a realistic worst-case scenario for the processability of the material since the final explosive molding powder is not always immediately used and may age prior to pressing. Thermal annealing the samples would have decreased the amount of crystallinity and lowered the transition temperatures. Results are summarized in Table 2.

Table 2: Transition temperatures for polycarbonate thermoplastic polyurethanes

Type	Polyurethane	Tg (SS)	Tg (HS)	Tm (SS)	Tm (HS)
Aromatic Polycarbonate	Quadrathane ARC-75A	-27.3 °C	not observed	72.4 °C	166.0 °C
Aliphatic Polycarbonate	Quadrathane ALC-75A	-33.3 °C	59.4 °C	118.8 °C	133.3 °C
Aliphatic Polycarbonate	ChronoFlex AL 75-A	-31.4 °C	not observed	68.2 °C	110.5 °C

The primary purpose of DSC testing was to verify that the polymers, in a realistic worst-case condition, would melt at a temperature that could be used in pressing operations. All of the polyurethanes tested had melting points, defined by the hard segments, above 105 °C, the temperature limit for pressing HMX based formulations at LLNL. It should be noted that Estane 5703 exhibits hard segment melting between 150 °C and 200 °C, depending on the thermal history and crystallite content. Furthermore, HMX based formulations with Estane 5703 exhibit acceptable pressing at 105 °C.[12].

Small quantities of 95 wt% HMX and 5 wt% polyurethane were hand mixed and pressed at 35 ksi and 105 °C to determine the maximum achievable density for these formulations. All three formulations reached over 98% of theoretical maximum density (TMD). The results are summarized in Table 3.

Table 3: Percent TMD achieved under maximum LLNL pressing conditions

	Quadrathane ARC-75A	Quadrathane ALC-75A	ChronoFlex AL 75A-Q
Percent theoretical maximum density	98.3%	98.5%	98.3%

To create molding powder for pressing operations, the polymers needed to be dissolved to allow coating of the HMX particles. The major concern with this process was finding a solvent that dissolved the polymers without dissolving significant quantities of HMX. It turns out PC-TPU have great chemical resistance which made it difficult to find a solvent that dissolved the polymers but did not also readily dissolve HMX. A subset of the solvents considered and evaluated along with their HMX solubilities are summarized in Table 4.

Table 4: Solubility of polymer and HMX in various solvents of interest (25 g in 100 mL of solvent)

Solvent System	ChronoFlex AL 75A-Q	Quadrathane ALC-75A	Quadrathane ARC-75A	HMX solubility
Chloroform	Readily dissolves	Readily dissolves	No	0.012 g/100 mL @ 20 °C [13]
Cyclohexanone	Dissolves with minimal heat	Dissolves with minimal heat	Dissolves	1.0 g/ 100 g @ 25 °C [14] 3.06 g/ 100 g @ 30 °C [15]

50% MEK: 50% Toluene	Dissolves with heat	Dissolves with heat	Dissolves with high heat	1.403/100 g: 0.011/100 g @ 30 °C [15]
Benzoflex 9-88 plasticizer + MEK	No	No	Dissolves with heat	Unknown + 1.403/100 g @ 30 °C [15]

Safety Testing

The polyurethanes were verified to be chemically compatible with HMX as determined by gas evolution using the Chemical Reactivity Test (CRT). CRT measures the amount of gasses produced from a 0.25 g specimen after 22 hours at 120 °C. The amount of gas produced by the mixture of HMX and polyurethane is compared to the sum of the gas evolved by the polymer and HMX individually. For all three polyurethanes, the mixture produced less than 0.75 cc g⁻¹ of gas beyond the sum of the individual components.

LLNL's standard small-scale safety tests (SSST) were performed to ensure that systems with lower than acceptable margin of safety were identified. Small-scale safety testing is always conducted on samples of candidate formulations before scaling to larger quantities as a best practice. The SSST suite of five tests at LLNL consists: impact (drop hammer), BAM friction, electrostatic sensitivity (ESD), differential scanning calorimetry (DSC), and chemical reactivity (CRT).

The CRT in combination with DSC measurements were used to evaluate both the thermal stability and chemical compatibility of the formulations. In the CRT experiment for a formulation, if the total gas evolved is less than 4.00 cc g⁻¹, the formulation is considered thermally stable for storage. The DSC was used to determine the formulations decomposition temperature with the DSC exotherm onset and peak temperature being reported.

Each of the polyurethanes were dissolved at 7 wt% in cyclohexanone and hand mixed with HMX at a 95:5 wt/wt% and then dried in a 60 °C oven to constant mass after which SSST and pressing studies were performed. A summary of the results is in Table 5 along with LX-14 (95.5 wt% HMX and 4.5 wt% Estane 5703) for comparison.

Table 5: LLNL small scale safety testing on 95 wt% HMX and 5 wt% PC-TPUs

Small Scale Safety Test	Quadrathane ARC-75A	Quadrathane ALC-75A	ChronoFlex AL 75A-Q	LX-14 (95.5% HMX 4.5% Estane 5703)
Impact (DH50), cm	66	49	53	69
BAM Friction	1/10 @ 36.0 kg	1/10 @ 32.4 kg	1/10 @ 32.5 kg	0/10 @ 36.0 kg
Electrostatic sensitivity	0/10 @ 1.0 J @ 510 Ω	0/10 @ 1.0 J @ 510 Ω	0/10 @ 1.0 J @ 510 Ω	0/10 @ 1.0 J @ 500 Ω
CRT Total gas release, 22hrs @ 120°C	0.05 cc g ⁻¹	0.04 cc g ⁻¹	0.10 cc g ⁻¹	0.03 cc g ⁻¹
DSC	Closed: 272.6 °C/278.1 °C (1722)	Closed: 276.6 °C/279.9 °C (1783)	Closed: 279.0 °C/282.1 °C (1605)	Closed: 276.6 °C/280.7 °C (1565)

Onset/Peak Temperature at 5°C, °C (ΔH , J/g)	Pin Hole: 274.0 °C/278.8 °C (1734)	Pin Hole: 278.2 °C/281.4 °C (1741)	Pin Hole: 279.3 °C/282.4 °C (1624)	Pin Hole: 275.1 °C/279.3 °C (1740)
---	--	--	--	--

Slurry Coating

To determine feasibility at meaningful scales, 50 g batches were slurry coated, in a 1 L vessel with an air driven propeller. The polyurethanes were 7 wt% in cyclohexanone.

The solubility of cyclohexanone in water is 9 g /100 g⁻¹ of water at 20 °C but increases with temperature to 78.6 g / 100 g⁻¹ of water at 96.6 °C, the boiling point of the azeotrope. [16] Molding powder was successfully formulated by suspending 47.5 g of HMX in 200 mL of water and adding the equivalent of 2.5 g of polyurethane dissolved in cyclohexanone at ambient. An additional 200 mL of water was added to form and solidify the molding powder and the slurry was increased in temperature to reduce the bead size and drive additional cyclohexanone into the water phase.

Using these slurry coating parameters, all three polycarbonate polyurethanes produced molding powder that were similar in size and polymer distribution to one another. However, unlike the Estane formulation LX-14, the molding powders were binder enclosed by HMX rather than the binder-coated HMX (Figure 4-6).

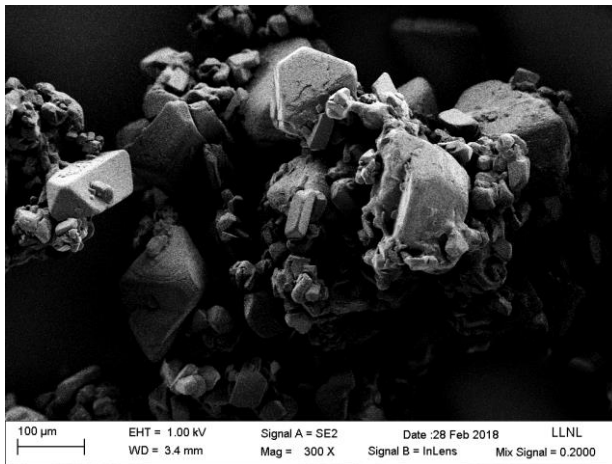


Figure 4. Quadtrathane ARC formulated HMX

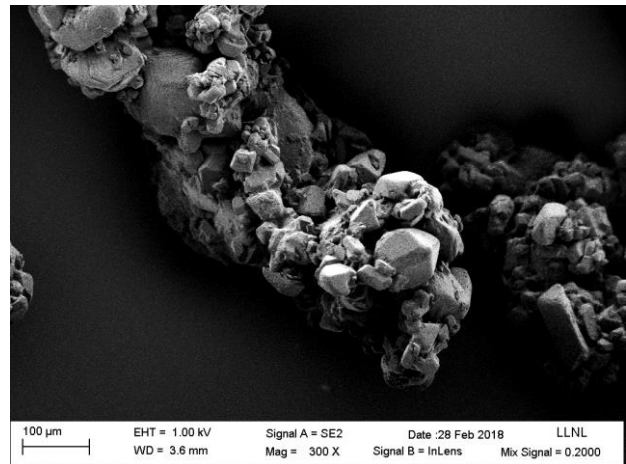


Figure 5. Quadtrathane ALC formulated HMX

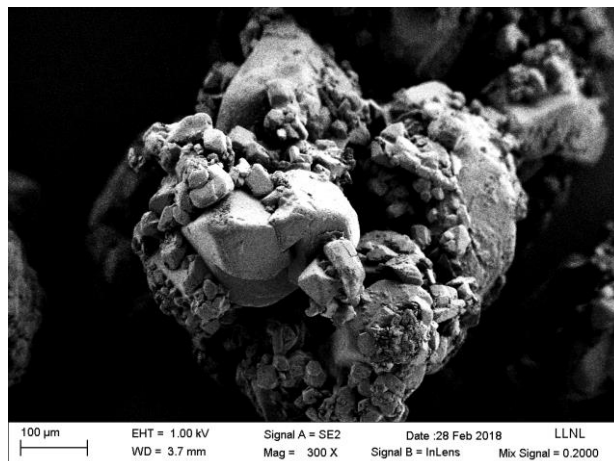


Figure 6. ChronoFlex formulated HMX**Discussion**

Three commercially available PC-TPUs were selected to determine their feasibility as a binder in an HMX formulation. Two of the PC-TPUs were made with aliphatic isocyanates while the third used an aromatic isocyanate. All three tested as compatible with HMX and had similar safety testing results as LX-14.

Under maximum temperature pressure conditions (105 °C, 35 kpsi), formulations made with each of the three polyurethanes achieved over 98% theoretical maximum density indicating the high melting temperature of the crystalline hard segments is not an issue.

All three polyurethanes formed molding powder using the slurry coating process. Using identical slurry coating parameters, beads were formed that were quite uniform throughout the batch as well as between the different polyurethanes. However, the beads formed were rough and had noticeable crystalline material on the surface as opposed to having a binder rich surface. The greatest difference thus far among the three polycarbonate polyurethanes has been the solubility in a variety of solvents to create a solution for coating HMX. The aliphatic polycarbonate polyurethanes have a variety of solvents they will dissolve in – some more readily than others. The aromatic polycarbonate polyurethane on the other hand, had very few options.

Future Work

These formulations will undergo thermal and explosive characterization. The coefficient of thermal expansion will be measured as well as the softening point. The detonation velocity and C-J pressure will be measured using the Disc Acceleration eXperiment (DAX). These tests will offer a more complete picture as to the feasibility of these PC-TPUs in HMX formulations.

Acknowledgements

The authors would like to thank Eric Bukovsky, Pat Harwood, and Nicole Anderson (LLNL) for their technical expertise. Special thanks are due to Jennifer Montgomery, Fowzia Zaka, Ginger Guillen, Steven Strout, and Peter Hsu (LLNL) for their measurements of the DSC, CRT, Drop Hammer, Spark, and BAM friction. This work performed under the auspices of the U.S. Department of Energy by Lawrence Livermore National Laboratory under Contract DE-AC52-07NA27344.

This document was prepared as an account of work sponsored by an agency of the United States government. Neither the United States government nor Lawrence Livermore National Security, LLC, nor any of their employees makes any warranty, expressed or implied, or assumes any legal liability or responsibility for the accuracy, completeness, or usefulness of any information, apparatus, product, or process disclosed, or represents that its use would not infringe privately owned rights. Reference herein to any specific commercial product, process, or service by trade name, trademark, manufacturer, or otherwise does not necessarily constitute or imply its endorsement, recommendation, or favoring by the United States government or Lawrence Livermore National Security, LLC. The views and opinions of authors expressed herein do not necessarily state or reflect those of the United States government or Lawrence Livermore National Security, LLC, and shall not be used for advertising or product endorsement purposes.

References

1. Hoffman, D.M., F.-M. Kong, and I.L. Chiu, *PRELIMINARY EVALUATION OF SOME COMMERCIAL POLYURETHANE ADHESIVES FOR POSSIBLE WEAPONS APPLICATIONS*. *Polym.-Plast. Technol. Eng.*, 1987. **26**(2): p. 95-142
2. Nozaki, S., et al., *Effect of chain architecture of polyol with secondary hydroxyl group on aggregation structure and mechanical properties of polyurethane elastomer*. *Polymer*, 2017. **116**: p. 423-428.
3. Hepburn, C., *Polyurethane Elastomers*. 1982, New York. NY: Elsevier Science Publishing Co. Inc.
4. C. Prisacariua, C.P. Buckley, and A.A. Caraculacu, *Mechanical response of dibenzyl-based polyurethanes with diol chain extension*. *Polymer*, 2005. **46** p. 3884-3894.
5. Eceiza, A., et al., *Structure–property relationships of thermoplastic polyurethane elastomers based on polycarbonate diols*. *Journal of Applied Polymer Science*, 2008. **108**(5): p. 3092-3103.
6. Poreba, R., et al., *Aliphatic polycarbonate-based polyurethane nanostructured materials. The influence of the composition on thermal stability and degradation*. *Composites Part B: Engineering*, 2014. **58**: p. 496-501.
7. Špírková, M., et al., *Novel polycarbonate-based polyurethane elastomers: Composition–property relationship*. *European Polymer Journal*, 2011. **47**(5): p. 959-972.
8. Kultys, A., et al., *The synthesis and characterization of new thermoplastic poly(carbonate-urethane) elastomers derived from HDI and aliphatic–aromatic chain extenders*. *European Polymer Journal*, 2009. **45**(9): p. 2629-2643.
9. Kultys, A., M. Rogulska, and H. Gluchowska, *The effect of soft-segment structure on the properties of novel thermoplastic polyurethane elastomers based on an unconventional chain extender*. *Polymer International*, 2011. **60**(4): p. 652-659.
10. Eceiza, A., et al., *Thermoplastic polyurethane elastomers based on polycarbonate diols with different soft segment molecular weight and chemical structure: Mechanical and thermal properties*. *Polymer Engineering & Science*, 2008. **48**(2): p. 297-306.
11. R. K. Weese, J.L.M., C. T. Perrino, *Kinetics of the b-d solid-solid phase transition of HMX, Octahydro-1,3,5,7-tetranitro-1,3,5,7-tetrazocine*. Lawrence Livermore Laboratory, Livermore, CA **UCRL-JC-145325**.
12. Hoffman, D.M., *Dynamic mechanical signatures of a polyester-urethane and plastic-bonded explosives based on this polymer*. *Journal of Applied Polymer Science*, 2002. **83**(5): p. 1009-1024.
13. Yasuda, S.K., *Microdetermination of estane in explosive mixtures*. *Journal of Chromatography A*, 1968. **37**: p. 393-397.
14. Sitzmann, M.E., et. al., *Solubilities of High Explosives: Removal of High Explosive Fillers from Munitions by Chemical Dissolution*.
15. B. Singh, L.K.C., P.N. Gadhikar, *A Survey on the Cyclotetramethylene Tetranitramine (HMX)*. *Defence Science Journal*, 1978. **28**: p. 41-50.
16. Musser, M.T., *Cyclohexanol and Cyclohexanone*, in *Ullmann's Encyclopedia of Industrial Chemistry*.

New Polycarbonate-Based Thermoplastic Polyurethane Binder for HMX Based Explosives

Lawrence Livermore National Laboratory
LLNL-PRES-748963

Insensitive Munitions and Energetic Materials Technology Symposium
Portland, Oregon
April 23-26, 2018

Emily Robertson



New commercially available TPUs may provide improved long-term stability over current TPUs

Advantages:

- More thermally and hydrolytically stable than Estane 5703
- Lower density compared to fluoropolymers – more desensitizing

Disadvantages:

- Limited solubility in solvents of interest
- T_m for hard segments tend to be above the traditional maximum temperatures pressing HMX-based formulations

Before we can test these properties of interest, we need to determine if it is feasible to formulate with these new materials.

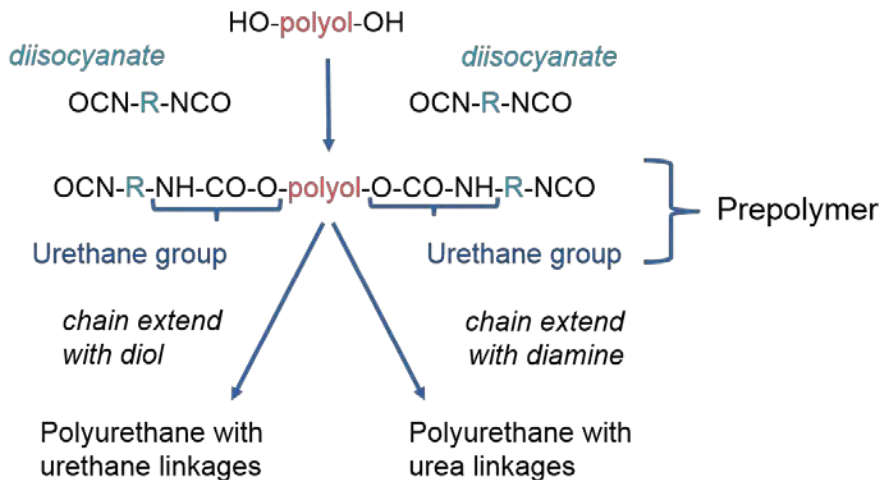
New TPUs are attractive but need to be tested for feasibility first

Selected 3 PC-TPU as binders of interest

Thermoplastic polyurethanes are classified by polyol and isocyanate type.

Urethanes have 3 basic building blocks:

1. Isocyanate (rigid)
2. Polyol (flexible)
3. Chain extender (rigid or flexible)



Known material – Estane

Estane 5703 (used in LX-14 and 9011) is an aromatic polyester-based TPU

Potential new binders – PC-TPUs

Polycarbonate as the **polyol**

- Excellent hydrolysis and chemical resistance at elevated temperatures
- Low compression set
- *No documented use in explosives*

Aliphatic and aromatic as the **isocyanate**

- Aliphatic have excellent adhesion
- Aromatic are known for toughness

Selected 3 PC-TPU as binders of interest

3 commercially available PC-TPU were purchased.

Type	Polyurethane	Manufacturer	Durometer (Shore Hardness)	Specific Gravity
Aliphatic Polycarbonate-based Polyurethane	Chronoflex AL 75A-Q	AdvanSource	75A	ca 1.10*
Aliphatic Polycarbonate-based Polyurethane	Quadrathane ALC-75A	Biomerics	75A	1.14
Aromatic Polycarbonate-based Polyurethane	Quadrathane ARC-75A	Biomerics	75A	1.17
<i>Aromatic Polyester-based Polyurethane</i>	<i>Estane 5703P [now Pearlstick 5703]</i>	<i>Lubrizol</i>	<i>70A</i>	<i>1.19</i>
<i>Fluoroelastomer</i>	<i>Viton A-100</i>	<i>Chemours</i>	<i>79A</i>	<i>1.82</i>

*TSD gives a large range of properties

Selected PC-TPUs with hardness values similar to Estane 5703

First concern – Is it safe?

A. Compatibility test of PC-TPUs with HMX

Determined by gas evolution using Chemical Reactivity Test (CRT).

Binder	Explosive	CRT Total gas release, 22 h @ 120 °C
Chronoflex AL 75A	HMX	0.01 cc g ⁻¹
Quadrathane ALC-75A	HMX	0.05 cc g ⁻¹
Quadrathane ARC-75A	HMX	0.08 cc g ⁻¹

Measuring gas produced by the mixture of HMX and polyurethane and comparing it to the sum of the gas evolved the individual components.

$$(\text{explosive} + \text{binder}) \leq 0.75 \text{ cc g}^{-1} + \text{explosive} + \text{binder}$$

All three mixtures produced $< 0.75 \text{ cc g}^{-1}$ – considered compatible

All three binders are compatible with HMX

First concern – Is it safe?

B. LLNL's 5 small scale safety testing of 95 wt% HMX: 5 wt% binder.

Binder	Impact Height for 50% Reaction (DH50), cm	BAM Friction	Spark	CRT Total gas release, 22 hrs @120 °C	DSC Onset/Peak Temperature @ 5 °C min ⁻¹ , °C (ΔH , J g ⁻¹)
Chronoflex AL 75A	66	1/10 @ 36.0 kg	0/10 @ 1.0 J @ 510 Ω TIL = 0.19 J @ 0 Ω	0.05 cc g ⁻¹	Closed: 272.6/278.1 (1722) Pin Hole: 274.0/278.8 (1734)
Quadrathane ALC-75A	49	1/10 @ 32.4 kg	0/10 @ 1.0 J @ 510 Ω TIL = 0.19 J @ 0 Ω	0.04 cc g ⁻¹	Closed: 276.6/279.9 (1783) Pin Hole: 278.2/281.4 (1741)
Quadrathane ARC-75A	53	1/10 @ 32.5 kg	0/10 @ 1.0 J @ 510 Ω TIL = 0.15 J @ 0 Ω	0.10 cc g ⁻¹	Closed: 279.0/282.1 (1605) Pin Hole: 279.3/282.4 (1624)
LX-14 (95.5% HMX 4.5% Estane 5703)	69	0/10 @ 36.0 kg	0/10 @ 1.0 J @ 500 Ω	0.03 cc g ⁻¹	Closed: 276.6/280.7 (1565) Pin Hole: 275.1/279.3 (1740)

All formulations are in the same general range (which is to be expected). Main variations are in their impact sensitivity.

All three binders register on the same safety scale as LX-14

Second concern – Could we press to high density?

LLNL has a limitation (for safety) of pressing HMX formulations at up to 105 °C with in-die pressures up to 35 ksi

Type	Polyurethane	Tg(SS)	Tg(HS)	Tm(SS)	Tm(HS)	Test Press
Aliphatic Polycarbonate-based	Chronoflex AL 75A	-31.4 °C	NO	68.2 °C	110.5 °C	98.8% TMD
Aliphatic Polycarbonate-based	Quadrathane ALC-75A	-33.3 °C	59.4	118.8 °C	133.3 °C	98.5% TMD
Aromatic Polycarbonate-based	Quadrathane ARC-75A	-27.3 °C	NO	72.4 °C	166.0 °C	98.3% TMD

Estane 5703 has a hard segment melting temperature between 150 °C and 200 °C, depending on the content and perfection of the crystallites¹

1. Hoffman, D.M., *Dynamic mechanical signatures of a polyester-urethane and plastic-bonded explosives based on this polymer*. Journal of Applied Polymer Science, 2002. **83**(5): p. 1009-1024.

All three binders have melting characteristics similar to Estane 5703 and are capable of pressing to high densities

Third concern – Can we formulate it?

A. Binders need to dissolve in a solvent that does not readily dissolve HMX as well to allow for coating the explosive

LX-14 uses MEK to dissolve the Estane binder.

Polyurethane	Chloroform	Cyclohexanone	50:50 MEK:Toluene	MEK + Benzoflex 9-88 (plasticizer)
Chronoflex AL 75A	Readily dissolves	Dissolves with minimal heat	Dissolves with heat	No
Quadrathane ALC-75A	Readily dissolves	Dissolves with minimal heat	Dissolves with heat	No
Quadrathane ARC-75A	No	Dissolves	Dissolves with high heat	Dissolves with heat
HMX Solubility	0.012 g/ 100 mL @ 20 °C ²	1.0 g/ 100 g @ 25 °C³ 3.06 g/100 g @ 30 °C⁴	1.403 g/ 100 g @ 30 °C ⁴ : 0.011 g/ 100 g @ 30 °C ⁴	1.403 g/ 100 g @ 30 °C ⁴ + Unknown

2. Yasuda, S. K. (1968). "Microdetermination of estane in explosive mixtures."
3. Sitzmann, M. E., et. al. "Solubilities of High Explosives: Removal of High Explosive Fillers from Munitions by Chemical Dissolution."
4. B. Singh, L. K. C., P.N. Gadhikar (1978). "A Survey on the Cyclotetramethylene Tetranitramine (HMX)."

Cyclohexanone selected for all three to reduce variability going forward



Third concern – Can we formulate it?

B. Slurry coating procedure utilized as it would be the most scalable

Cyclohexanone solubility in water starts out low but increases rapidly with temperature. As such, the lacquer addition must be done at ambient (20–25 °C).



Incorporated
HMX in water



Immediately after
lacquer addition



Immediately after
water addition



Slurry reached
~80 °C

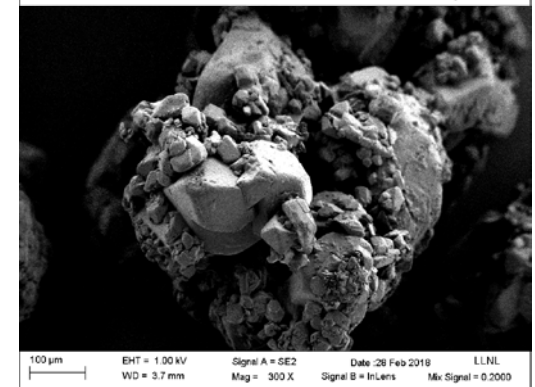
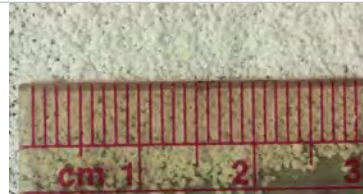
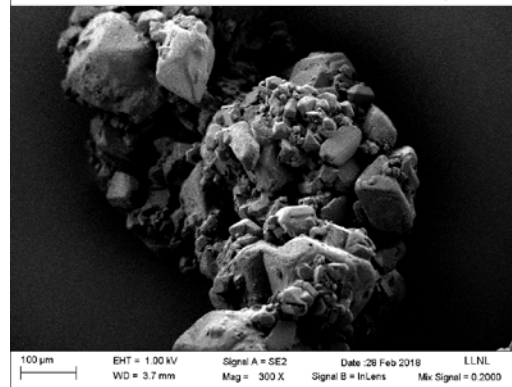
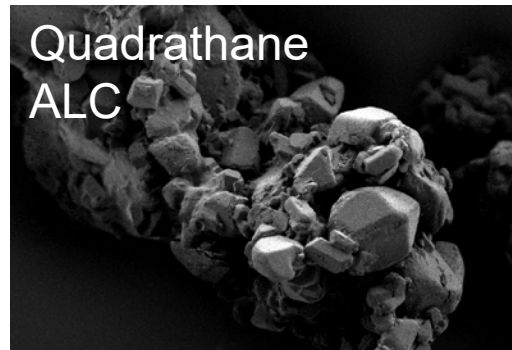
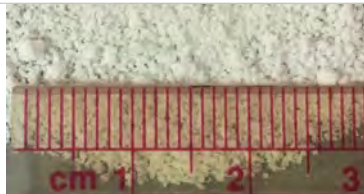
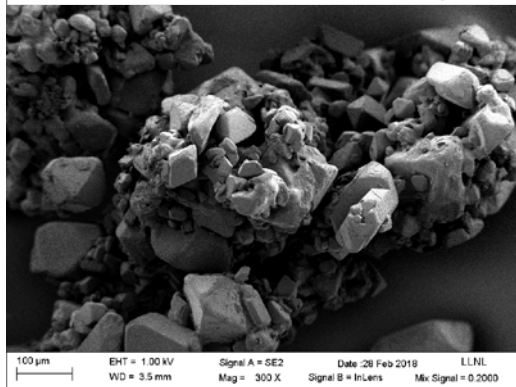


Resulting
molding powder



If lacquer was added to a warm (60 °C) slurry, the binder becomes associated with the water phase and coats the vessel rather than forming beads.

Molding powder is binder encapsulated by HMX



All three formed uniform molding powder

How do they measure up?

Type	Polyurethane	Safety	Pressability	Lacquers	Slurry Coating
Aliphatic	Chronoflex AL 75A	Similar	Slightly lower melting point (Tm (HS) 110 °C)	Multiple options to dissolve	Similar
Aliphatic	Quadrathane ALC-75A	Similar	Slightly lower melting point (Tm (HS) 133 °C)	Multiple options to dissolve	Similar
Aromatic	Quadrathane ARC-75A	Similar	Slightly higher melting point (Tm (HS) 166 °C)	Difficult to dissolve	Similar

All three have similar safety and pressability. Molding powders with similar particle sizes are achievable under identical parameters.

The aromatic PC-TPU was very limited in solvents. The aliphatic PC-TPUs were more flexible in their solvent options.

Aliphatic PC-TPUs have benefits over the Aromatic PC-TPUs

Future plans

Thermal characterization

- Coefficient of Thermal Expansion (CTE)
- Softening point



Thermal Mechanical Analysis (TMA)

Explosive Characteristics

- Detonation velocity
- C-J pressure

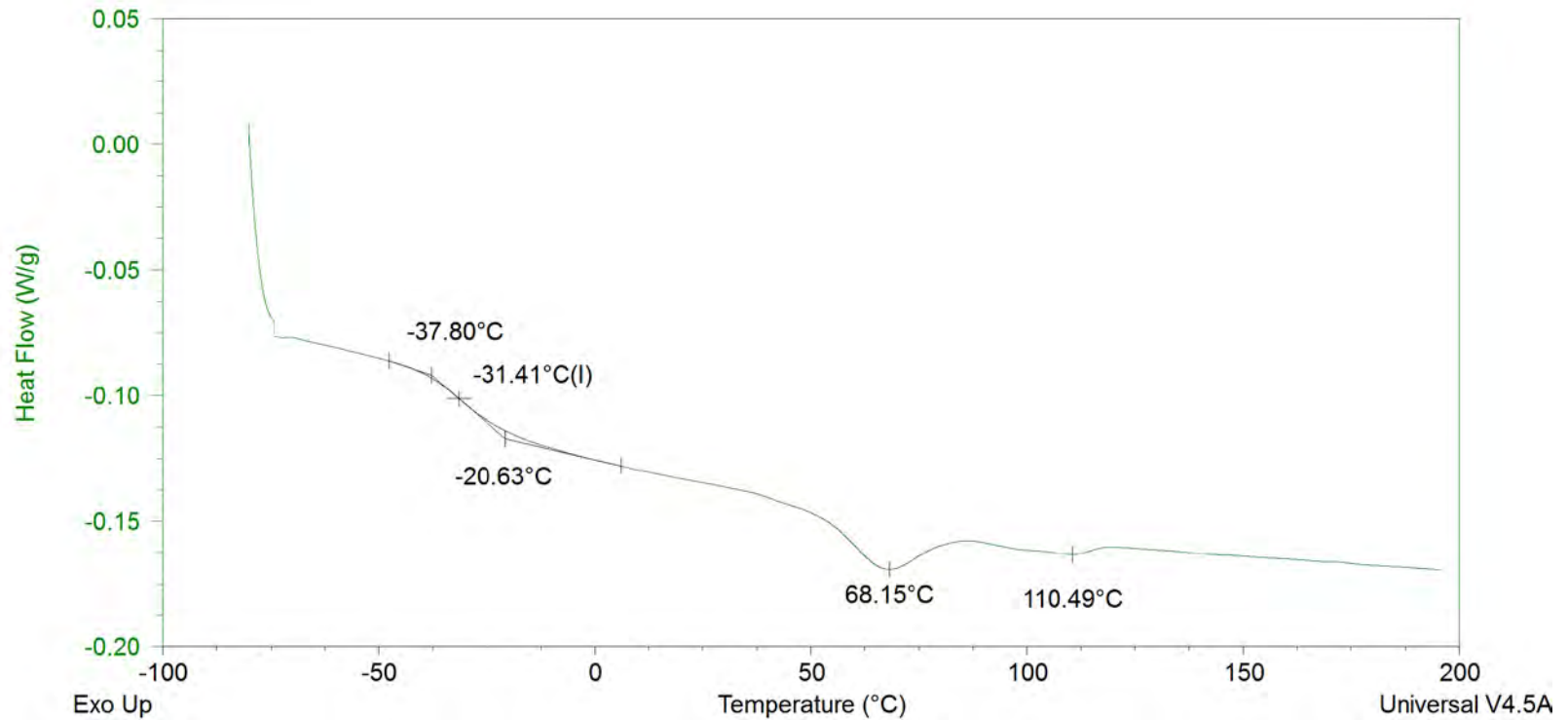


Disc Acceleration eXperiment (DAX)



**Lawrence Livermore
National Laboratory**

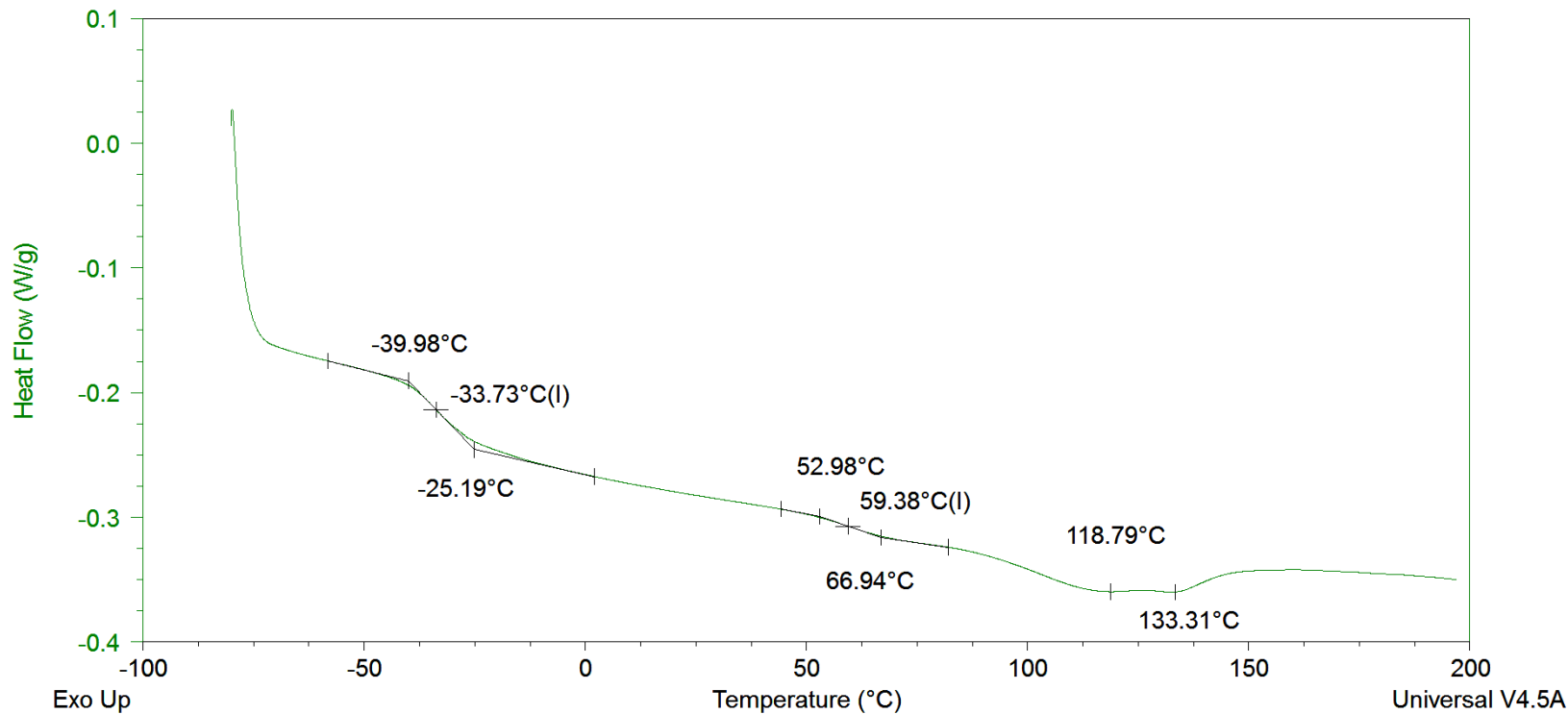
Chronoflex DSC



ChronoFlex AL 75A – aliphatic polycarbonate-based polyurethane.

20 mg tested in a closed hermetic dish from -80 °C to 205 °C at 5 °Cmin⁻¹

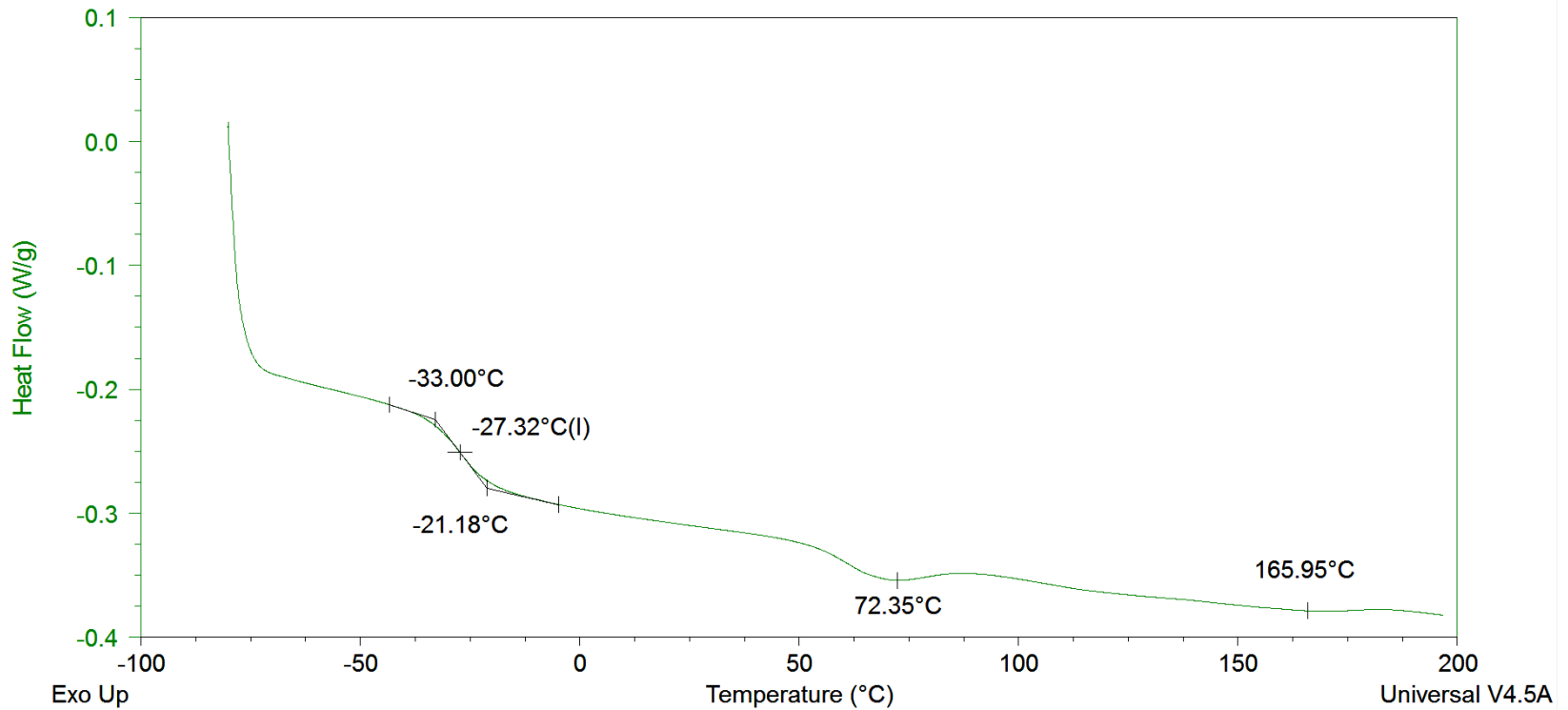
Quadrathane ALC DSC



Quadrathane ALC – aliphatic polycarbonate-based polyurethane.

20 mg tested in a closed hermetic dish from -80 °C to 205 °C at 5 °Cmin⁻¹

Quadrathane ARC DSC



Quadrathane ARC – aromatic polycarbonate-based polyurethane.

20 mg tested in a closed hermetic dish from -80 °C to 205 °C at 5 °Cmin⁻¹

Performance Evaluation of Reduced Sensitivity Explosives with Novel Applications

2018 IM & EM Technology Symposium

Elizabeth Francois, Bryce Tappan, Patrick Bowden, Rose Burritt, Rajesh Patel

Elizabeth Francois

4/25/2018





High Explosive Pellet Pressing Incident

Elizabeth Francois

Insensitive Munitions and Energetic Materials
Technology Symposium 4/25/2018
LA-UR-23440

UNCLASSIFIED

Overview

- The details of the Event
- Possible causes
- Lessons learned and the path forward

UNCLASSIFIED

A routine day of pressing explosives

- At 9am Monday 4/2/18 an operator was preparing to press 1" x 1" PBX 9501 pellets
- 930ish metal fatigue sound heard
- Event occurs

UNCLASSIFIED

Slide 4

25 Ton Carver press (not the Event press)



- The press has heated platens
- There is a secondary controller for the heat
- Shielding consists of 1/2" Lexan, 1/4" air gap and another 1/2" Lexan plate/
- 30g of HE can be pressed with the operator in the room.

UNCLASSIFIED

Slide 5

The Press involved in the Event



UNCLASSIFIED

Slide 6

The personnel present for the Event



- One worker and one escort were present.
- Both were 10-12 feet from the press.
- Both were OK!
- Both sustained hearing loss, possibly not permanent.
- Shielding worked. No frag escaped.

UNCLASSIFIED

One inch die, before and after



- The die was made of tool steel.
- The steel shattered, and showed no evidence of detonation.
- 23.6g of PBX 9501 was being pressed
- No HE was found after event.

UNCLASSIFIED

Slide 8

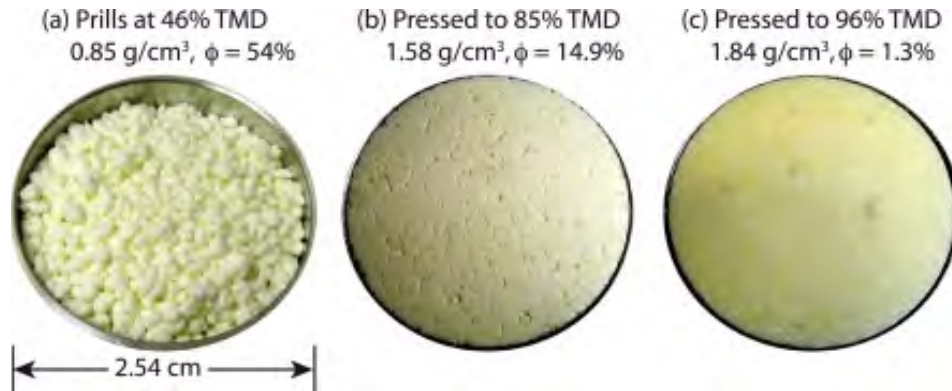
Causes and Hypotheses

- The cause may never be known
- Hypothesis #1
 - The PBX 9501 was at fault in some way
- Hypothesis #2
 - The stemple was cocked in the die, gouging the die polish and creating friction heating.
- Hypothesis #3
 - Metal fatigue sound heard just before Event was the die body or stemple cracking and failing.

UNCLASSIFIED

Slide 9

Hypothesis #1 PBX 9501



Was there something wrong with the molding powder that caused it to react violently?

- This was a well characterized, ex-WR lot from 1989 that has been extensively studied
- Thousands tests incorporating millions of pellets have been performed.
- No previous accident at LANL with 9501 has been recorded.
- Small scale safety testing (Impact, Friction, DSC, VTS) showed it to be within normal parameters.

UNCLASSIFIED

UNCLASSIFIED

memorandum

Explosive Science and Shock Physics
M-7: High Explosives Science & Technology

To/MS: Distribution
From/MS: Geoffrey W. Brown, M-7
geoffb@lanl.gov
Phone/Fax: 7-6718/Fax 7-0500
Symbol: M-7-AC-18-029 U
Date: April 18, 2018

Material Safety Release: PBX 9501 HOL89C730-010

The material PBX 9501 HOL89C730-010, submitted to M-7 Analytical Chemistry on April 3, 2018 meets the safe handling requirements for explosives as defined in P101-8, rev 4, section 3.2.13.

NOTE: This memo documents the results of M-7 high explosives safe handling and storage testing only and in no way certifies that this material meets all safety, compositional, or material requirements. All IWDs or other work control documents should be reviewed for suitability of this material for specific applications.

Lab Number 52753
Material Code PBX 9501 HOL89C730-010
Manufacturer Holston

Test	PBX 9501 HOL89C730-010	Reference
Impact (Type 12) H ₅₀ (cm) ^a	28.6	PETN (0601-02 L-298) 9.6
Friction Load ₅₀ (N) ^b	244.3	PETN (0601-02 L-298) 66.4
Spark Screen** or Til* (J) ^c	*0.125	PETN (0601-02 L-298) *0.0625
DSC (10°C/min ramp in N ₂ atmosphere)		
Onset of Decomposition (°C)	246	PETN (94-01B) 165
Peak Exotherm (°C)	280	PETN (94-01B) 205
Vacuum Stability (ml/g) (Gas evolved after 48hr @ 120°C)	0.16	N/A
a. Drop height resulting in a "go" in 50% of samples obtained through a Neyer D-optimal testing method. b. Force resulting in a "go" in 50% of samples obtained through a Neyer D-optimal testing method. c. TTL test: Highest level at which 20 consecutive No-Go results are observed. Screen test: 13 No-Go results at 0.25 J.		

Distribution:

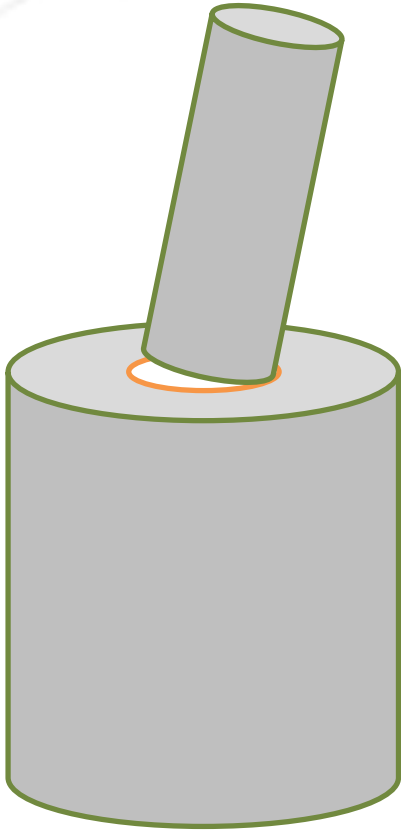
E. Francois, M-7,
elizabethf@lanl.gov
M-7 Group Office

Reviewed:


G. Brown 4/18/18
Date

UNCLASSIFIED

Hypothesis #2 The stemple was angled

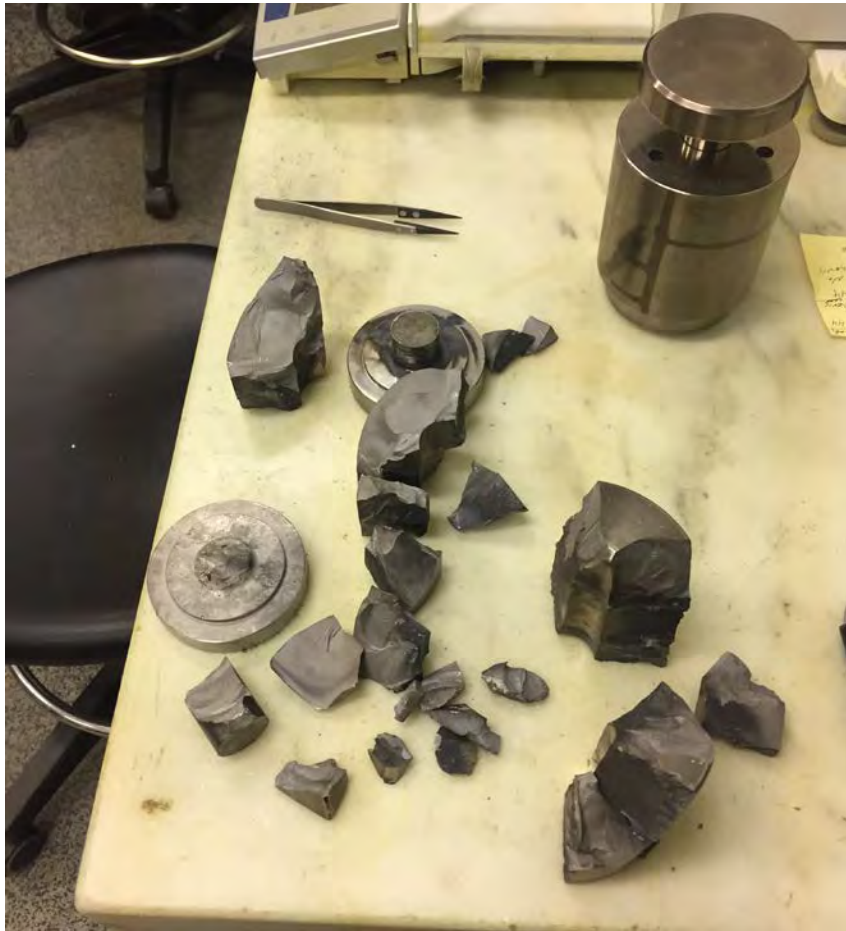


- Pellets are pressed in cycles
- A cycle consists of a pressing phase and a relaxation phase.
- This is done to increase density and pellet quality
- The stemple moves mostly during the first cycle only.
- The event occurred on the fifth cycle.

UNCLASSIFIED

Slide 12

Hypothesis #3 Metal Fatigue causing a die failure



- The operator heard a metallic sound immediately before the event occurred.
- The sound could have been from some failure of the die.

UNCLASSIFIED

Slide 13

Lessons learned

- The controls put in place worked.
- Improvements can be made:
 - Shielding Improvements
 - Formalized Non-Destructive Testing
 - Formalized die maintenance
 - Addressing hearing protection
- The path forward
 - Restart

UNCLASSIFIED

Slide 14

Shielding as defined by the DOE Standard Explosives Safety

Table II-6. Safety Shields for Explosive Laboratory Operations*

Shield	Minimum distance from explosive	Explosives limit
Leather gloves, jackets, or coats, and plastic face shields	----	.77 gr (50 mg)
.12 in (3 mm) tempered glass	3.15 in (8 cm)	.77 gr (50 mg)
.2755 in (7 mm) Lucite/equivalent material	5.905 in (15 cm)	.0882 oz (2.5 g)
.8 in (20 mm) Lucite/equivalent material	5.905 in (15 cm)	.3527 oz (10 g)
.6 in (15 mm) laminated resistant glass	7.874 in (20 cm)	.7054 oz (20 g)
.9999 in (25.4 mm) Lexan/Lexguard	11.81 in (30 cm)	1.764 oz (50 g)
2 units each of .9999 in (25.4 mm) plate glass laminated with .4882 in (12.4 mm) polycarbonate with a .374 in (9.5 mm) air gap between units (glass sides facing the explosive)	11.81 in (30 cm)	1.764 oz (50 g) (steel confined)

UNCLASSIFIED

Slide 15

Shielding improvements

- Lexan is good at stopping fragments, but what is better?
 - Thicker lexan?
 - Lexan with a tempered glass inner layer
 - Bulletproof glass? Bulletproof fiberglass?

UNCLASSIFIED

Slide 16

Non-Destructive Testing

12.2. Pressing

12.2.1 General

(c) Pressing mandrels, punches, and dies used in explosives operations shall be examined regularly during periods of use for evidence of structural failure. **Suitable nondestructive test methods shall be used to perform the examination.** Site management shall establish intervals between inspections for each tooling design before committing the tooling to use. The inspection interval and updating should be based on experience with similar tooling designs and configurations. All new or modified mandrels, punches, and dies shall be inspected before their first use. At least one pressing cycle should be completed with mock explosives before proceeding to explosives.

UNCLASSIFIED

Slide 17

NDE continued

AET-6 personnel assisted us with formalizing NDE

- Magnaflux: Ferrous materials, surface defects.
- Dye Penetration: Non-Ferrous materials, surface defects
- Radiography: internal defects, low resolution
- Visual inspection, Micrometry.

UNCLASSIFIED

Die Maintenance

- Inspect Die set before each use.
- Measure tolerance of body and stemples before each use.
- Reject die if scratches and chips are found on body mirror polished surfaces
- Reject die if tolerance is less than 0.001” or greater than 0.002”.
- Rejected Die sets may be re-machined if possible.

UNCLASSIFIED

Slide 19

Pantex process comparison

- Pantex small scale pressing managers visited LANL on 4/10 to view and discuss the event. LANL's process was walked down and dissected.
- LANL managers visited Pantex on 4/12 to view and discuss their operations.
- Differences exist but are due largely to the nature of the pressing. The adherence to the DOE safety standard is comparable.

UNCLASSIFIED

Slide 20

Industrial Hygiene and Hearing protection

- Calculations completed by Bruce Dahlquist (Industrial Hygiene) suggest blast over pressurization NOISE from the event to be 172-169 dB (10 feet and 15 feet respectively).
- This is well above the impulsive noise exposure limit of 140 dB (threshold for hearing loss).
- Hearing protection is recommended.

UNCLASSIFIED

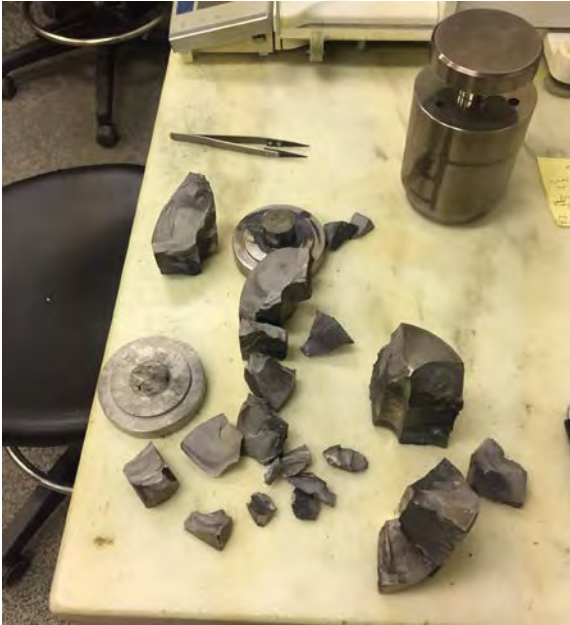
Slide 21

Restart

- TBD

UNCLASSIFIED

Acknowledgements



M-7

- Sean Bashaw
- Alice Branch
- Sheldon Larson
- Ken Laintz
- Laida Valdez

Pantex

- Monty Cates
- Lennon Mings
- Ed Patterson
- Tony Dutton
- Tori Gallier

M-DO and WFO

- Eric Brown
- Ellen Cerreta
- Joe Lloyd
- Ken Gillespie
- Brian Watkins
- Doug Tasker

Medical and IH

- Bruce Dahlquist
- Occupational Medicine

AET-6

- Yoshi Coe
- Steve Fresquez
- Dick Bingham
- David Harvey

Forensic Metallurgists

- Robert Hackenberg
- Kevin Bohn
- Jessica Lopez
- Joel Montalvo
- Andrew Richards
- Eric Tegtmeier
- David Alexander

Other

- Steve Malcolm
- Dan Hooks
- Doug Tasker

UNCLASSIFIED

Slide 23

Melt-pour Explosive Formulations Development Featuring TNBA

NDIA IMEMTS 2018 (Session 5B)

Virgil Fung *, Brian Alexander, Jacob Morris, PhD., David W Price, PhD., Robyn Wilmoth
BAE Systems, Holston Army Ammunition Plant, Kingsport, Tennessee, United States
25th April 2018

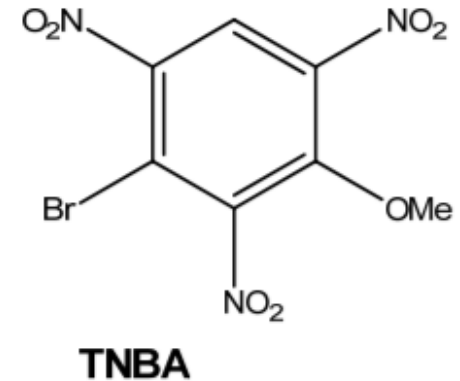


Briefing Outline

- TNBA Background
- TNBA Synthesis and Formulation Efforts
- Preliminary Sensitivity and Performance Testing
- Results and Conclusion
- Path Forward
- Acknowledgements

TNBA Background – The GrIMEX Program

- TNBA (2,4,6-Trinitro-3-bromoanisole) selected as an ingredient candidate from the Green IM Comp B Replacement Program, GrIMEX (presented previously at 2015 and 2016 IMEMTS)
- GrIMEX program objectives
 - Develop environmentally acceptable synthesis methods to produce environmentally sustainable, insensitive secondary explosives as alternatives to cyclotrimethylenetrinitramine (RDX), 2,4,6-trinitrotoluene (TNT), and ammonium perchlorate (AP)
 - Develop novel formulations utilizing the alternative materials to replace Composition B (without RDX and NTO)
- TNBA selected as one of the candidates to replace TNT due to its higher energy and relatively low melting point
 - Suitable for existing LAP infrastructure



TNBA Background – Toxicology Assessment

- Toxicology Assessment performed in accordance with the United States Army Public Health Center (USAPHC) Phased Approach concept ASTM E-2552-08
- TNBA is no worse than TNT as a melt-ingredient

Compound	Oral	Inhalation	Dermal	Ocular	Reproduction/ Development	Mutagenicity	Comments
TNBA	Moderate	Low	Moderate	Low	Moderate	High	
PIPE	High	Low	Moderate	Low	Moderate	Low	Possible carcinogen
DNMT	Low	Low	Moderate	Low	Low	High	
DNP	Moderate	Low	Moderate	Low	Low	High	
TNT	Moderate	Low	Moderate	Moderate	Low	High	Suspect human carcinogen

TNBA Background – Performance Comparison

	TNT replacements		
	TNBA	DNP	TNT
Impact Sensitivity, cm	(Naval) 79.43	55.0	88
Impact Sensitivity (RDX Std.), cm	23.3	39.0	
Friction Sensitivity, N	70.0	246.0	216
Friction Sensitivity (RDX Std.), N	144.0	164.0	
ESD, J	0.2900	0.2625	> 0.25
Detonation velocity (m/s)	6571	8251	7180
Detonation pressure (GPa)	23.98	29.24	20.02
V/V0 7.20	-5.87	-7.93	-5.42
Oxygen balance	-44.72	-30.37	-73.96
Density, g/cm ³	1.948	1.773	1.654
Melting Point °C	97	87	
Heat of Formation (kJ/mol)	18.88	120.5	-63.2

TNBA Background – BAE Systems IRAD Program

- BAE Systems IRAD program to develop TNBA melt-cast formulations
 - Unlike the GRIMEX program, there is no restriction on HE filler selection
- Program Strategy
 - Leveraging the improved performance aspect of TNBA, the new TNBA melt-pour formulations can potentially out-perform existing candidates containing 2,4-Dinitroanisole (DNAN)
 - Direct replacement of DNAN in IMX formulations
 - IMX-104 (DNAN/RDX/NTO)
 - PAX-48 (DNAN/HMX/NTO)
 - Preliminary formulation effort to assess IM response in comparison to baseline candidates
- Relatively new and continuing effort

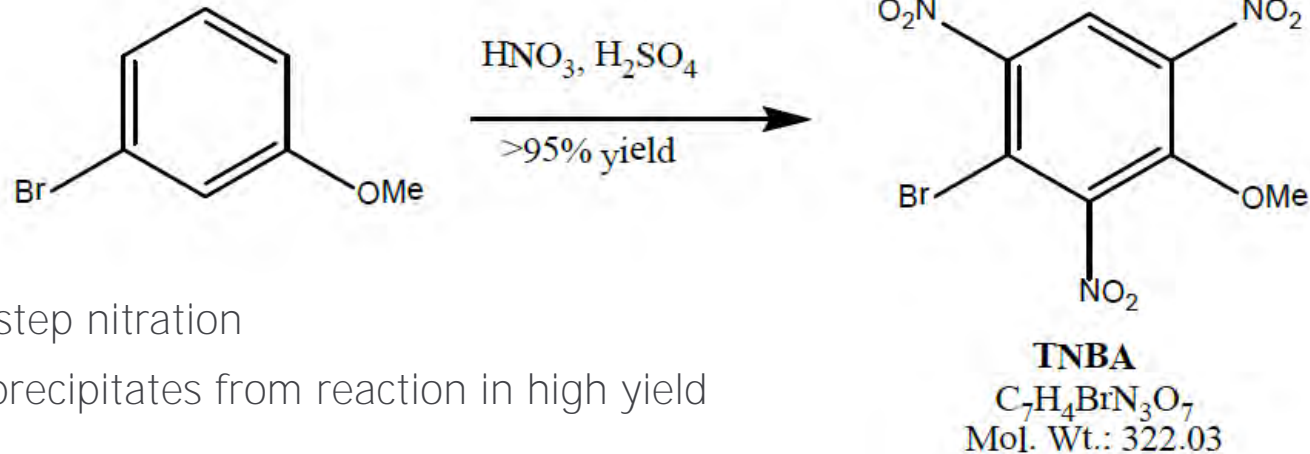


TNBA Background – BAE Systems IRAD Program

- TNBA was selected due to:
 - Robust/mature chemistry
 - Insensitive compare to TNT
 - One Synthetic Step
 - Higher performance than DNAN
 - Relatively cheap to produce
 - Similar thermal properties to existing melt-pour formulations – suitable for processing at current LAP facilities
- TNBA had been successfully scaled up to Pilot and Full Production Scale Manufacture
 - Batch size ranging from 300 – 2,000 lbs.



TNBA Synthesis



- Synthesis route is one step nitration
 - Crystalline solid precipitates from reaction in high yield
- Robust Process:
 - Many nitrations have been performed (lab and pilot scale)
 - Yields ranged from 96.5% to 100%
 - Purity ranged from 98.69% to 99.92%
- Preliminary data show TNBA has a shock sensitivity (NOL LSGT) of 164 cards
 - TNT is usually ~ 130 cards
 - Could be due to high degree of crystallinity, may improve with solid fills added (or better casting)

TNBA Formulation Efforts (1)

- Use TNBA as a replacement for DNAN in IMX-104 (RDX/NTO) and PAX-48 (HMX/NTO)
 - Increased performance of new TNBA candidates expected
- Initial formulation screening using 50 grams melt kettle to evaluate viscosity (ease of pouring)
- Attempted to maximize solids loading level to maintain high performance
- As the melting point of TNBA is higher, the processing temperature is more effective at $>100^{\circ}\text{C}$
- Promising candidates were scaled to 500 grams batch
 - Physical assessment of viscosity
 - Samples for hazard and thermal analysis
- Final candidates were cast into tubes for limited LSGT and plate dent firing



50 grams melt-kettle



1-gallon melt-kettle

TNBA Formulation Efforts (2)

- Direct replacement of DNAN with TNBA, same solids ratio
- Initial compositions:
 - TNBA-IMX104 (~32% TNBA / 68% solids)
 - TNBA-PAX48 (~35% TNBA / 65% solids)
- Both candidates exhibited very high viscosities – more TNBA was needed, plus increase in processing temperature
- Final candidates (considered as processable for melt-pour)
 - TNBA-IMX104 (~ 41% TNBA / 59% solids)
 - TNBA-PAX48 (~ 44% TNBA / 56% solids)
- Thermal and Hazard Analysis conducted



Candidate	Melting (°C)	DSC Peak Max (°C)	Impact (cm) RDX Std. = 16.2 cm	BAM Friction (N)	ESD (J) RDX Std. = 0.0888 J
TNBA-IMX104	97.3	235.5	59.57	314.0	> 9.4875
TNBA-PAX48	98.8	242.5	49.17	270.0	> 9.4875

TNBA Formulations Sensitivity Testing

- Limited NOL LSGT conducted on both candidates (3 shots)
 - Shock sensitivity a good indication on the overall IM properties in confined environment

Candidate	Shot 1	Shot 2	Shot 3	50% Card Gap	Pressure (kbar)
TNBA-IMX104	150 Cards (NO GO)	125 Cards (GO)	137.5 Cards (GO)	137.5 -150.0 Cards	38.9 – 45.1
TNBA-PAX48	150 Cards (NO GO)	125 Cards (GO)	137.5 Cards (NO GO)	125.0 – 137.5 Cards	45.1 – 48.8

- Limited LSGT results more shock sensitivity than DNAN based baseline (~ 120 cards, 50.1 kbar) which is expected
- Still significantly less shock sensitive than Composition B (~ 200 cards, 20.7 kbar)
- Both candidates should have similar shock sensitivity properties – full LSGT firing (8-12 shots) can confirm



NOL LSGT Set Up



"GO"
Witness Plate



"NO GO"
Witness Plate

TNBA Formulations Performance Testing (1)

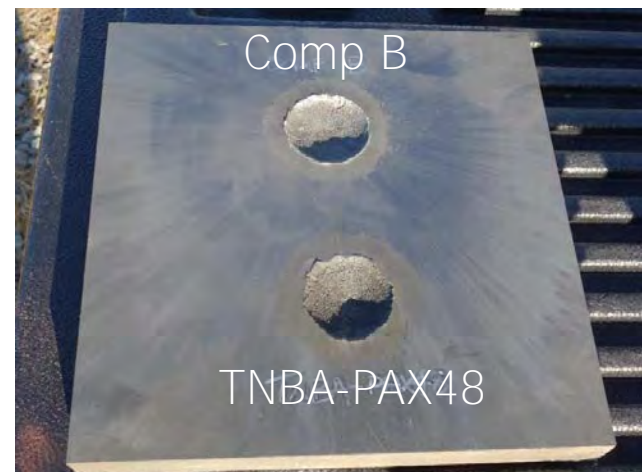
- Compare relative performance of candidates against IMX-104 and Composition B
 - Unconfined LSGT charge (~ 250 g) with no Pentolite booster placed on 10" × 10" × 1" witness plate
 - Dent on witness plate quantified using 3D Scanning Technique
 - Pressure probes @ 5, 10 and 15 feet from test charge
 - Shock Overpressure
 - Peak Impulse Pressure



TNBA Formulations Performance Testing (2)

- Plate Dent Comparison

Candidates	Visual Dent Observation	3D Scanning Result	
		IMX-104	Comp B
TNBA-IMX104	Larger than IMX-104	125% of IMX-104	93.7% of Comp B
TNBA-PAX48	Larger than IMX-104; Same size as Comp B	134% of IMX-104	100% of Comp B

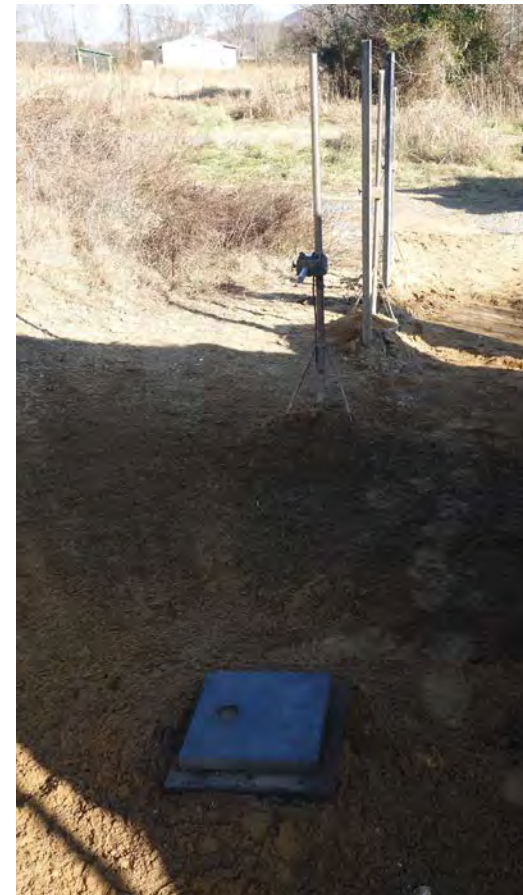


TNBA Formulations Performance Testing (3)

- Detonation Pressure Comparison
 - Normalized against IMX-104 baseline

Candidates	Shock Overpressure			Peak Impulse Pressure		
	@ 5 ft.	@ 10 ft.	@ 15 ft.	@ 5 ft.	@ 10 ft.	@ 15 ft.
IMX-104	1.00	1.00	1.00	1.00	1.00	1.00
TNBA-IMX104	1.32	1.20	1.07	1.27	1.32	1.25
TNBA-PAX48	0.97	1.10	1.18	0.95	1.89	1.26

- Overall, the detonation pressures of the candidates are 20-30% higher than the baseline of IMX-104



Results / Conclusion

- Base on limited LSGT firing, both TNBA candidates exhibited good shock sensitivity (50% card gap = 150 cards or less).
- Performance comparison from Plate Dent and Det. Pressure suggested both TNBA candidates will out-perform existing DNAN-based IM explosives (IMX-104/PAX-48)
- From the limited available data, TNBA had proven to be a worthy melt ingredient candidate to replace DNAN in the current family of IM Melt Cast explosive
 - Robust chemistry at all scales
 - Readily available / CONUS manufacturing
 - Improvement in performance over existing IM melt-cast explosives (plate dent/det. pressure)
 - Adequate IM properties
 - Similar thermal characteristics of end product to current IM melt-cast explosive (no new investment required on LAP operations)

Path Forward

- Continuation of the current IRAD program to further develop these TNBA formulation candidates:
 - Complete full Large Scale Gap Test on both TNBA formulation candidates
 - Optimize formulations base on efflux viscosity and degree of settling
 - Conduct in-depth, instrumented determination of explosive performances
 - Detonation Velocity & Pressure
 - Disc Acceleration eXperiment (DAX)
 - Cylinder Expansion (CYLEX)
 - Preliminary exudation / accelerated aging study
 - Mass loss / irreversible growth
- Formulation efforts involving novel energetic fillers already planned in the SERDP Green IM Explosive (GrIMEX) Program
- More to report at the IMEMTS 2019

Summary

- TNBA has shown great potentials to be used in a family of new IM melt-cast explosives
- TNBA can be manufactured in production quantities (robust process at HSAAP)
- TNBA melt-cast explosives can be processed with existing manufacturing equipment at LAP facilities
- TNBA melt-cast explosives exhibited good IM properties and performance matching or greater than existing baseline (IMX-104 / PAX-48), confirming that TNBA is a suitable replacement for DNAN as the melt ingredient
- Further IM and Performance improvement can be expected from further formulation optimization efforts
- Potential product TRL higher than other high-performance IM melt-cast explosives (e.g. DNP based)
 - Great stop-gap improvement to current DNAN based explosives

Acknowledgements

- BAE Systems OSI – Holston Army Ammunition Plant
 - Dr. Neil Tucker
 - Mr. Matt Hathaway
 - Dr. Jeremy Headrick
 - Ms. Kelly Smith
 - Ms. Denise Painter
 - Mr. Todd Dye
 - Mr. Tracy Kelly
 - Mr. Paul Lucas



MDNT: IM MELT PHASE ENERGETIC BINDER

Omar Abbassi, Philip Samuels, Paul Anderson, Daniel Iwaniuk, Christopher Choi
US Army ARDEC
Picatinny Arsenal, NJ

ABSTRACT

As the push for Insensitive Munition (IM) compliancy in munition systems continues, the maturity of DNAN-based High Explosive (HE) solutions have contributed to significant improvements over their legacy counterparts. However, a technology gap still exists as the output of the DNAN-based IM HE formulations limits their ability to meet the lethality requirements of several munition systems. A promising high-output melt-phase energetic binder that has been evaluated in recent years is 1-methyl-3,5-dinitro-1,2,4-triazole (MDNT). In screening tests MDNT was demonstrated to have detonation velocity similar to that of Composition B, while simultaneously having shock sensitivity below that of TNT. Follow-on testing confirmed the performance output of MDNT, and additional shock sensitivity testing illustrated very promising trends. Pushing the envelope for high-output formulations capable of being utilized in shaped charge applications, formulations with HMX demonstrated exceptional performance; comparable to PBXN-9 and approaching LX-14. Characterization and demonstrations included a side-by-side comparison to LX-14 in testing utilizing a 3.2" Generic Shaped Charge Testing Unit (GSTCU). Although ARDEC views MDNT as an energetic melt phase material capable of bridging the technical gap between performance and sensitivity, it is no longer being pursued due to repeated dermal sensitization occurrences.

INTRODUCTION

MDNT was first synthesized in lab scale quantities by one of the national lab partners of the Army, and was selected for further evaluation under an OSD joint funding program. Further quantities of MDNT were produced by ARDEC synthetic chemists and BAE Holston supporting small scale performance and sensitivity characterization. A subsequently funded effort focused on a scalable synthetic process to produce MDNT. That process was developed and matured at the lab scale at Nalas Engineering, and subsequently demonstrated at intermediate and pilot scales at BAE Holston. A total of approximately 45 lbs of MDNT was produced to support the latter phases of the effort; the development and characterization of a meltable IM formulation for anti-armor warhead (AAW) applications.

Formulation efforts with HMX demonstrated a melt-cast explosive with performance properties rivaling legacy explosives such as PBXN-9 and LX-14. However, due to the limited quantities of MDNT available, a processing method was never fully realized to achieve high quality casts. Shock sensitivity and performance remained un-optimized due to the relatively low casting densities achieved and it was anticipated that similar un-optimized results would be observed in larger-scale IM and performance demonstrations without a formal casting study and analysis.

RESULTS AND DISCUSSION

MDNT Melt-Phase Characterization

MDNT has been characterized via several sensitivity and performance tests, and although the casting density was not optimal, the results illustrate benefits to sensitivity without drawbacks to performance.

Diameter (inches)	Type	% TMD	DV (km/s)	CJ (GPa)
0.50	Cast	90.0	> TNT < Comp B	> TNT < Comp B
0.75	Cast	94.7	> TNT < Comp B	> TNT = Comp B

Table 1 – Detonation Velocity Comparison

Formulation	TMD%	Gap (in)	Shock (kbar)
MDNT (IHE)	83%	= TNT	= TNT
MDNT (LSGT)	89%	< TNT	> TNT

Table 2 – Shock Sensitivity Comparison

Although the samples that were cast for testing were lower than 95% TMD (Table 1), the output for detonation velocity and detonation pressure resulted in values at or exceeding predictions. Additionally, the 0.50" diameter test resulted in a high order detonation. This indicates that the critical diameter is below 0.50 inches. This also validates the result of the LSGT below that of TNT (Table 2), and allowed for shock sensitivity evaluation in an IHE gab tube as the diameter of 0.50 inches for that test is larger than the critical diameter of MDNT.

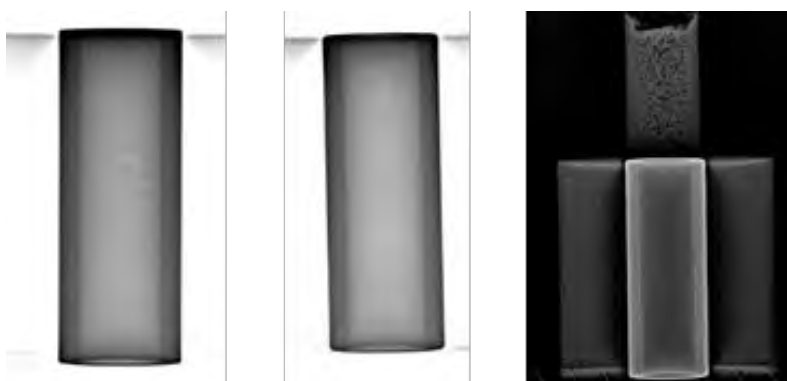


Figure 1 – MDNT IHE Tube X-Rays

The IHE tubes had a lower than desired density at only 83% of TMD. Generally this has a negative effect on shock sensitivity; however, the testing proceeded forward. Testing showed a shock sensitivity on par with that of TNT. The LSGT data previously showed more favorable results with a TMD of 89%. Although the IHE shock sensitivity is higher than preferred, it was not unexpected given the density and porosity in the test assets.

Figure 2 illustrates that for multiple materials or formulations, density/TMD is a critical parameter to reduce shock sensitivity. The increased slope for MDNT and TNT illustrate that this effect is more pronounced for melt-phase casted samples. MDNT is in need of a casting study to determine and optimize the processing parameters for all tests and applications. Once

optimized, an accurate characterization of the shock density can be performed. Extrapolating the data for MDNT in Figure 2 illustrates that a superior shock sensitivity may be expected at a TMD above 90%.

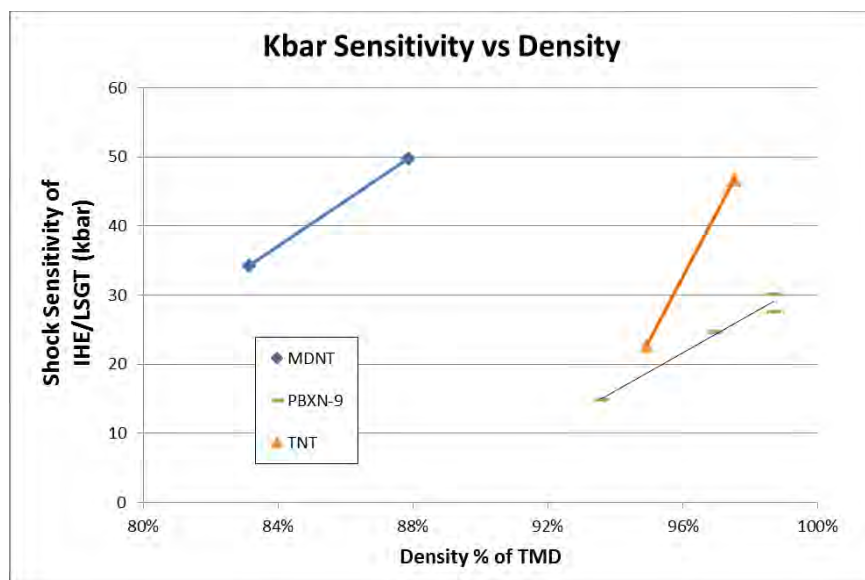


Figure 2 – Shock Sensitivity vs Density

MDNT Melt-Phase Formulation Characterization

Similar to what was observed with casting density for neat MDNT characterization, the formulation test assets for characterization also showed porosity, resulting in casting densities at or below 92% TMD.

A formulation with a significant amount of HMX was selected for characterization. Assets were prepared to evaluate detonation velocity, detonation pressure, cylinder expansion, and IHE shock sensitivity. Testing at the low density levels illustrated performance at PBXN-9 and LX-14 levels with similar shock sensitivity. Although the performance should be further optimized, the real advantage with improved casting densities would be the shock sensitivity gains, as the results are likely indicative of the porosity in the test samples.

Formulation	Gurney E (cal/g)	VoD (km/s)	Pressure (Gpa)
MDNT	NA	= Comp B	= Comp B
MDNT-HMX	= PBXN-9 < LX-14	= PBXN-9 < LX-14	> PBXN-9 > LX-14

Table 3 - Performance Comparison to PBXN-9, LX-14

The shock sensitivity of the MDNT-HMX formulation was characterized by the IHE gap test. Testing at a density of 92% TMD had a shock sensitivity equivalent to that of PBXN-9.

Formulation	TMD %	Gap (in)	Shock (kbar)
MDNT	83%	= TNT	= TNT
MDNT-HMX	92%	= PBXN-9 < LX-14	= PBXN-9 > LX-14

Table 4 – Formulation IHE Comparison

Prior to performing full scale engineering FI testing on the MDNT-HMX formulation, samples were subjected to a sub-scale fragment impact testing developed and performed by the Navy. The sub-scale FI test was developed under a Joint OSD funded effort in which the thickness of a cover plate can be varied and is tested against a Self Forming Fragment (SFF).

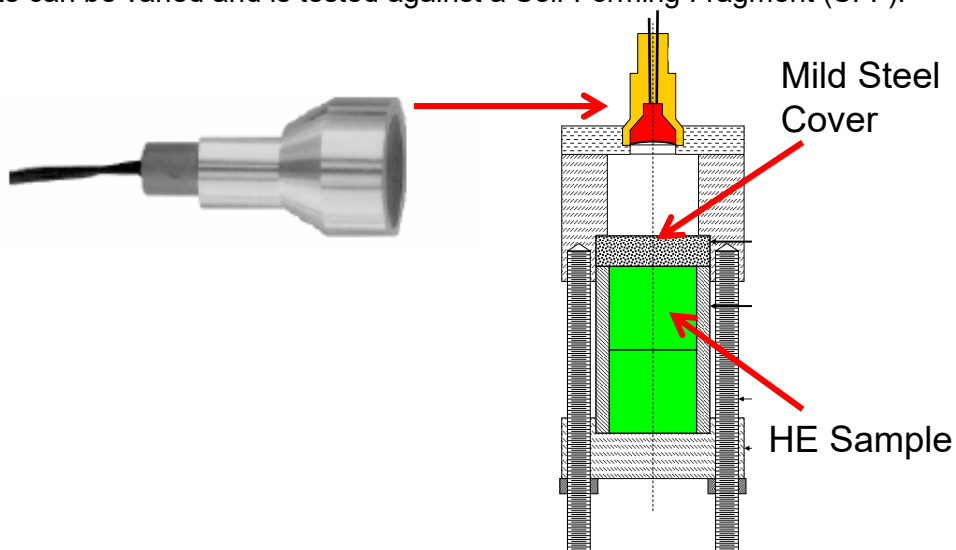


Figure 3 – Sub Scale FI Screening Test Setup

The sub-scale FI test results (Table 5) were performed on MDNT-HMX samples at 92% TMD. The samples (figure 4) had relatively high levels of porosity, which would likely make it difficult to mitigate a penetrating threat. At plate thicknesses of 0.375” and 0.5,” the MDNT-HMX formulation reacted similarly to what was observed for LX-14. The data suggests that the formulation was expected to perform similarly to LX-14 in mitigating a fragment impact threat.

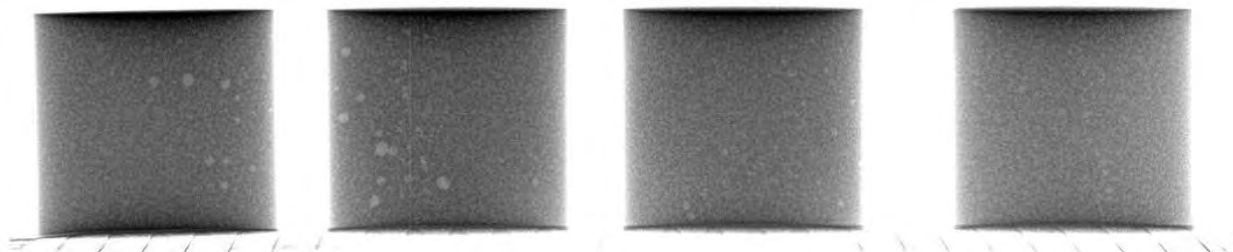


Figure 4 – X-ray of MDNT-HMX samples with visible porosity

Formulation	Results w.r.t. Cover Plate Thickness (inches) for Single Liner in SFF		
	1/4	3/8	1/2
MDNT-HMX		Explosion	Explosion
LX-14	Deflagration	Explosion	Explosion, 17% of sample recovered

Table 5: Sub-Scale FI Testing Comparison

Final testing of the MDNT-HMX formulation was to demonstrate its ability to mitigate FI in a generic shaped charge testing unit (GSTCU) engineering IM test, and to push a 3.2 inch GSTCU. The formulation was loaded into the GSTCU, then encased in both a thin 0.5 mm aluminum liner and a thicker 12.5 mm aluminum outer casing (Figure 5).

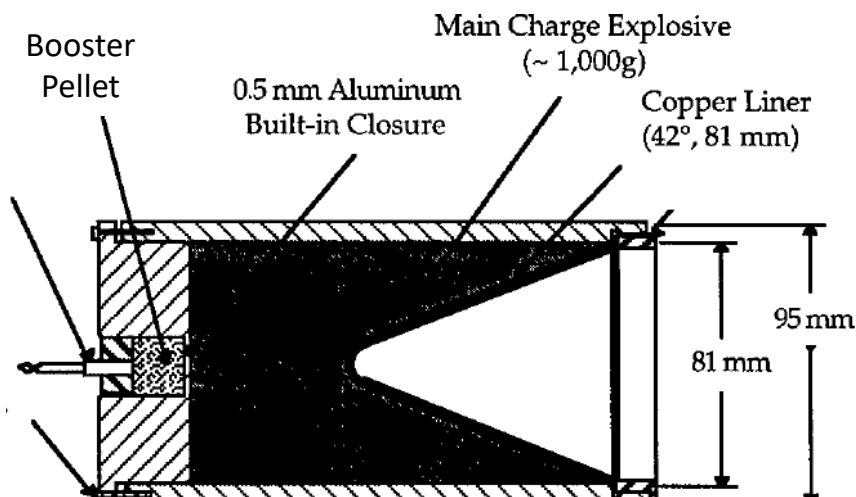


Figure 5 – 3.2" GSTCU encased in 12.5 mm aluminum

The fragment impact testing was conducted at 6000 fps and was performed in a side-by-side comparison to LX-14. Testing was performed with the test assets in a horizontal position, with the shaped charge directed towards a stack of two 2-inch witness plate. Both the MDNT-HMX and the LX-14 test articles initiated high order when impacted by the 6000 fps fragment. In both cases, the shaped charge formed and penetrated through or into the 2nd witness plate. Pressure traces from both tests provided further evidence of a full Type I detonation.

As both assets detonated high order, the fragment speed was maintained at 6000 fps for the remainder of the test series rather than increasing to the current standard of 8300 fps. The first series of tests was duplicated, with the inclusion of a plastic 6mm Particle Impact Mitigation Sleeve (PIMS) liner. The PIMS technology was developed under a separate Joint OSD funded effort, using plastic sleeves to mitigate the fragment threat. In this configuration, the LX-14 test resulted in a splatter of high explosive (HE) onto the witness plates with no evidence of the shaped charge liner forming. The liner was recovered, as were several pieces of the casing. For the MDNT-HMX test article, the test was very similar to the baseline test shot with a high order reaction; the liner slug formed and penetrated the 2nd side witness plate, with pressure traces indicative of a high order Type I detonation.

The testing with the 6mm PIMS liner was repeated and the test results were essentially duplicated, with the LX-14 test article resulting in an estimated Type IV reaction and the MDNT-HMX test article displaying a full Type I detonation reaction.

Test Asset	PIMS	Steel Plates	P1/4 20ft (psi)	P2/5 40ft (psi)	P3/6 60ft (psi)	Estimate Rxn
LX-14-581	None	Through Hole	4.73/6.78	2.42/2.44	1.21/1.80	Type (I)
MDNT-HMX-1	None	Slug in 2 nd plate	4.22/5.30	2.23/2.45	1.02/1.30	Type (I)
LX-14-587	6mm	HE Splatter	0.46/0.31	0.18/0.21	0.14/0.14	Type (IV)
MDNT-HMX-4	6mm	Slug in 2 nd plate	3.44/3.77	1.91/2.03	1.18/1.19	Type (I/II)
LX-14-593	6mm	HE Splatter	0.53/0.35	0.25/0.25	0.17/0.13	Type (IV)
MDNT-HMX-2	6mm	Through Hole	3.40/3.58	2.21/2.13	1.26/1.15	Type (I)

Table 6: FI Testing Summary

The FI testing series illustrated that although the shock sensitivity was reduced as compared to LX-14, the explosive in combination with the PIMS liner did not mitigate the FI threat. As the

same combination mitigated the threat with LX-14, the data suggests the Type I detonation results were attributed to the porosity within the test articles.

The final testing conducted was a performance demonstration within the 3.2-inch GSTCU. The generic shaped charge measures penetration through steel at a stand-off distance of a given number of charge diameters (CDs). It is meant to be a down-selection tool that leads into a liner design program for a given HE. The plan was to conduct the penetration performance test at 5 CDs to minimize variability. An in-house LX-14 baseline was conducted as well.

The penetration depth of the MDNT-HMX loaded GTSCUs was approximately 86% of the depth of the LX-14 in-house tests at a stand-off of 5 CDs. This was a positive result considering the formulation contains less HMX by weight, as compared to the LX-14 formulation. It is understood that the liner design is not optimized for the explosives being compared, but it is a good indicator of how well the formulation performed. An MDNT formulation with a higher concentration of HMX, coupled with a proper liner redesign effort, may meet or exceed PBXN-9 and LX-14 penetration.

Explosive	Avg Penetration Depth	Shot 1 Depth	Shot 2 Depth
MDNT-HMX	86% of LX-14	81% of LX-14	91% of LX-14
PBXN-9*	90% of LX-14	NA	NA
LX-14*	91% of LX-14	NA	NA

Table 7: 3.2" GSTCU Penetration Depth at 5CD in Steel as compared to ARDEC LX-14 Results. *PBXN-9 and LX-14 from IMAD Report

With the conclusion of the testing performed, two things were evident. First, the performance output of a MDNT-HMX formulation was approaching LX-14 levels. Second, for the true IM benefits to be obtained, a process to eliminate/reduce porosity to achieve higher density, higher quality assets was paramount.

The MDNT and MDNT-HMX formulation show higher than anticipated shock sensitivities, due to the low density of the samples. Data exists with several explosives where a shift in as little as 3% density results in a 25 to 47 card difference.

Efforts to Increase Density and Eliminate Porosity

The transition to a follow-on effort was to demonstrate an MDNT-HMX based HE in AAW performance applications, against fragment impact and slow cook-off IM threats. The initial focus was placed on methods to increase the density of test assets through improved casting processes.

Lab pours were conducted on MDNT where the pouring temperature was reduced to the melting point of MDNT, between 94°C and 95°C. Additionally, the metal parts were pre-heated to 90°C to minimize the delta-T in the process. Two sets of pours were conducted: first on neat MDNT and second on MDNT with a processing additive.

Water density measurements were used to determine the density of the casts. A 100% TMD baseline was established by HE pycnometry. Discounting the riser sections, the density of the neat MDNT cast was calculated to be 98.3% of TMD (Figure 6). For the MDNT containing the processing additive, the baseline TMD was also determined by HE pycnometry. The casting disregarding the riser sections had a measured density of 97.6% of TMD (Figure 6). In both scenarios, lab pours illustrated a much high density than previous pours (83-92% TMD).

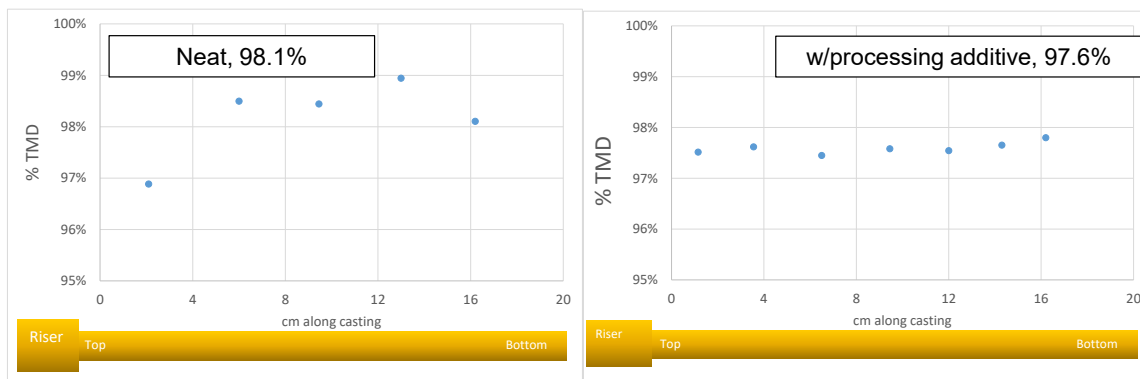


Figure 6 – Density of Lab Pours: MDNT (left), MDNT with processing additive (right)

Vapor Pressure and Dermal Sensitization

Casting quality results in the lab were not able to be duplicated on the pilot scale utilizing similar pouring and metal parts temperatures on the initial trial. Plans were set to continue with a set of experiments varying pouring temperature, metal parts temperature and cooling conditions. However, cases of dermal sensitization and irritation were investigated prior to continuing.

One of the major factors likely contributing to both the poor casting quality and the dermal sensitization is the vapor pressure of MDNT (DNMT in Figure 7). The vapor pressure exceeds that of most other melt phase materials. In previous investigations, efforts with another novel high vapor pressure melt-phase material were terminated as the high vapor pressure was causing crystallization outside of the melt kettle. While MDNT was not crystallizing outside of the melt kettle, operators did note that MDNT was quite volatile as the MDNT fumes were present throughout the melt-pour facility after handling and processing with MDNT. Furthermore, this phenomenon was evident even when opening a bag containing dry powder in preparation for pours.

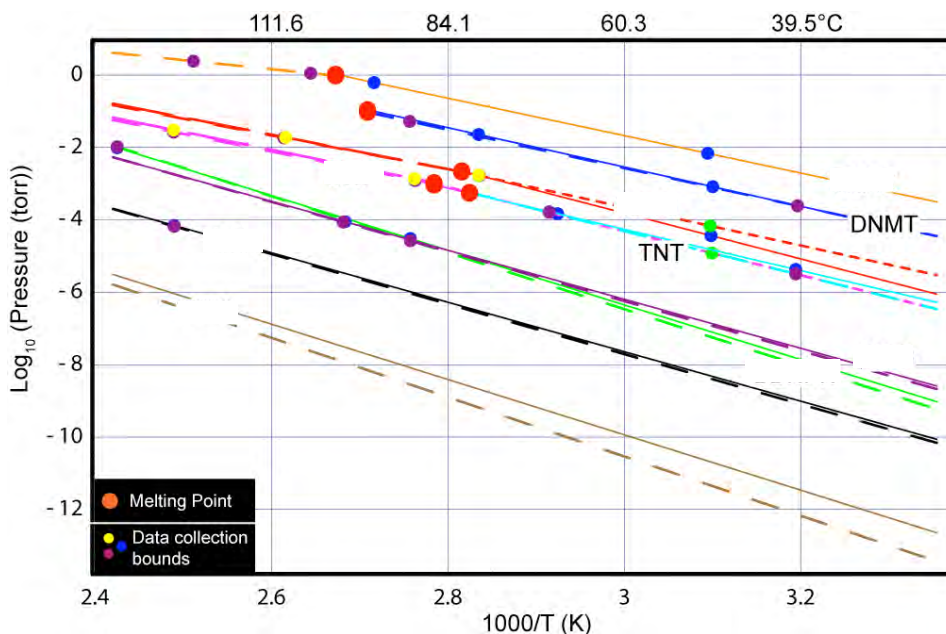


Figure 7 – Vapor Pressure of Explosives

The high vapor pressure of MDNT may explain the difficulty in obtaining high quality casts. As the temperature required for melt casting MDNT is increased, the vapor pressure becomes sufficient to overcome atmospheric pressure, thus, causing the liquid to form vapor bubbles inside the bulk of the material. However, since the temperature for casting is not dramatically increased above the melt temperature of MDNT, and the melt pour was done at atmospheric pressure, the vapor bubble formation is limited to shallow depths within the castings. This could explain the voids and porosity evident in X-rays of testing assets and why the porosity is only seen in the top-half of these assets (Figures 1, 4). Similar materials were cast side-by-side in grenades with similar casting parameters, and the excess porosity of MDNT in comparison to other materials is evident.

In addition to the porosity, multiple cases of dermal irritation had occurred with effects being heightened to subsequent exposures. This is mitigated with proper PPE during processing and handling, however, cases of skin sensitization were evident even during post-inspection procedures. After a visual inspection of the booster cavity of a finished grenade at room temperature, symptoms of skin irritation were present on an employee's neck. The sensitization during such limited exposure raises health concerns during the entire life-cycle of the material in a munition system or application.

SUMMARY AND CONCLUSIONS

MDNT has been demonstrated in several performance tests to have output similar to Composition B. In formulations with HMX, performance testing has demonstrated output rivaling PBXN-9 and approaching LX-14. In addition to performance, the shock sensitivity of MDNT projects well, although it was not realized in the engineering FI testing completed to date.

The major technical challenge and detriment was the processing optimization for preparing test assets with MDNT. Lab pours have illustrated that by controlling and tailoring the temperature of the process, high density casts can be achieved. This was never realized on pilot scale equipment as vapor pressure and dermal sensitization issues were prohibited. Although ARDEC views MDNT as an energetic melt phase material capable of bridging the technical gap between performance and sensitivity, it is no longer being pursued due to repeated dermal sensitization occurrences.

ACKNOWLEDGMENTS

The authors would like to thank the personnel at ARDEC for their efforts in planning, supporting and executing the testing of MDNT and its formulations in this effort. The authors would also like to thank the teams at Nalas Engineering and BAE Systems for their efforts in developing and scaling-up the synthesis of MDNT, as well as the Joint Insensitive Munition Technical Panel program office and the Program Executive Office for funding the majority of this work.



MDNT IM Melt Phase Energetic Binder

NDIA IMEM Technology Symposium
Portland, OR
April 23-26, 2018

Omar Abbassi
US Army ARDEC

UNPARALLELED
**COMMITMENT
& SOLUTIONS**

Act like someone's life depends on what we do.

DISTRIBUTION A: Approved for public release; distribution unlimited.



U.S. ARMY ARMAMENT
RESEARCH, DEVELOPMENT
& ENGINEERING CENTER

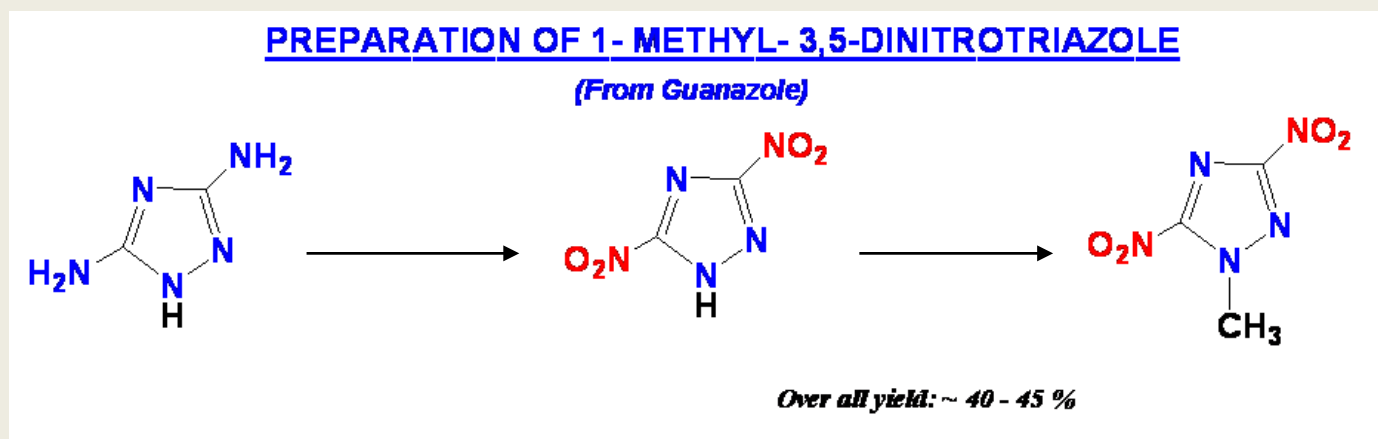


- Introduction
- Synthesis
- Characterization
- Formulation
- Porosity
- Vapor Pressure
- Summary
- Acknowledgements



- MDNT (1-methyl-2,4-dinitrotriazole) is an explosive binder with a melting point below 100°C
- Due to promising theoretical calculations and estimates, this material was investigated as a potential melt cast alternative
 - Less sensitive than TNT
 - Performance greater than DNAN
 - Performance greater than TNT

- MDNT was synthesized in ARDEC labs in a 2-step process from Guanazole



- Overall yield was 40-45%
- Prepared on the 10 to 25g scale



- Small scale safety testing was conducted
 - ERL Impact > 100cm
 - BAM Friction > No reactions at 252N
 - ESD > No reactions at 0.25J
 - Vacuum Stability: Total excess of gas evolved < 2mL
- Synthesis was scaled up providing quantities to support additional testing



- Series of rate sticks were prepared for detonation velocity testing

- 0.50"
- 0.75"



- Densities were 90-95% of TMD
- Testing at 0.50" and 0.75" illustrated performance exceeding TNT, and equivalent to Comp B levels



- Shock sensitivity testing was conducted
 - Partial LSGT (3 tubes) at 89% of TMD
 - IHE at 83% of TMD



LSGT, 150 cards = No Go



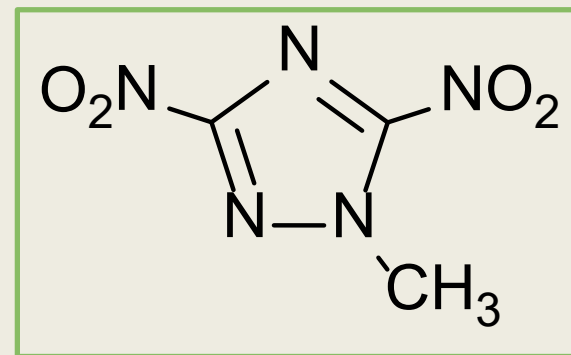
IHE, 160 cards = No Go

- Testing illustrated sensitivity improvements over TNT



- MDNT (1-methyl-2,4-dinitrotriazole) is viewed as a promising melt phase energetic material for both its performance and insensitivity attributes
 - Comp B level performance without solids
 - Less shock sensitivity than TNT

- **Formula:** $C_3H_3N_5O_4$
- **Density:** 1.68 g/cm³
- **Melting Point:** 94 – 97 °C
- **Detonation Pressure:** = **Comp B**
- **Detonation Velocity:** = **Comp B**
- **Shock Sensitivity:** < **TNT**

**MDNT**

(1-methyl-2,4-dinitro-1,3,5-triazole)



- Objectives: to develop a formulation with...
 1. Det Velocity and Det Pressure equal to or greater than LX-14
 2. Gurney Energy equal to or greater than PBXN-9

- Initial Path Forward:
 - Select formulation based on loading study to determine amount of HMX to maintain ideal viscosity for melt-cast operation
 - Addition of additives to aid in casting quality
 - Perform performance and sensitivity testing

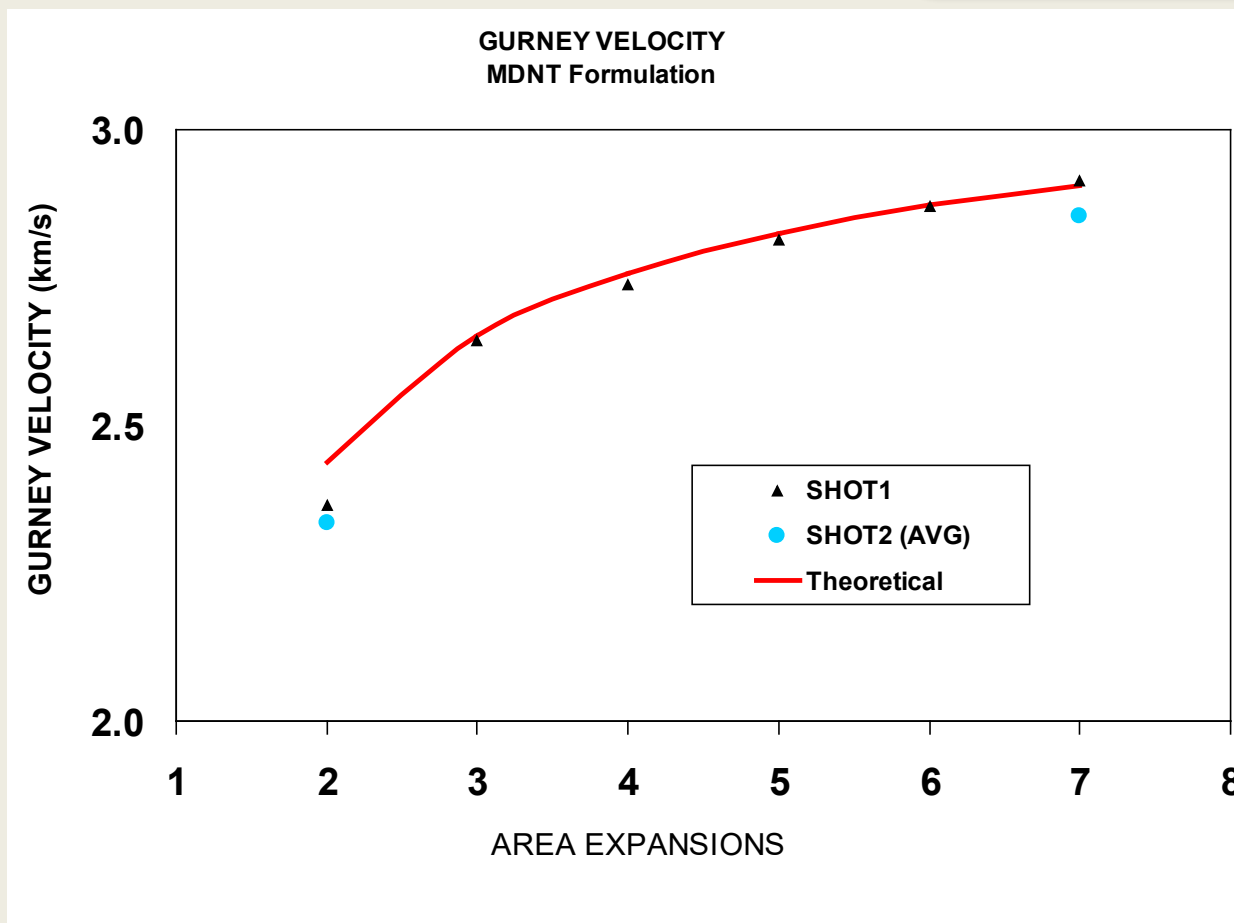


- Initial castings resulted in assets with 96.7% TMD
- Safety Testing:
 - ERL impact 50% point = 28.8 cm
 - BAM friction → 10 NO GO @252N
 - ESD → 20 NO GO @0.025 joule
 - Thermal Stability → **PASS**
 - Small Scale Burn → **PASS**



- Cylinder expansion testing was performed
- Gurney energy was near PBXN-9 levels

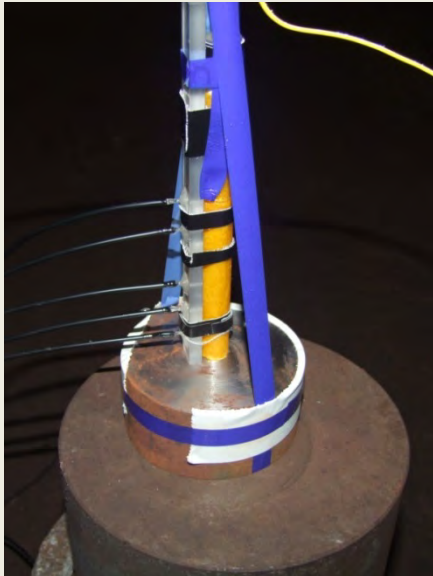
Theoretical data is in very close agreement to the streak data from Shot #1





- Performance testing in 0.75" Unconfined rate stick testing
 - Detonation Velocity = PBXN-9
 - Detonation Pressure > LX-14

0.75" Rate Sticks of MDNT-HMX Formulation

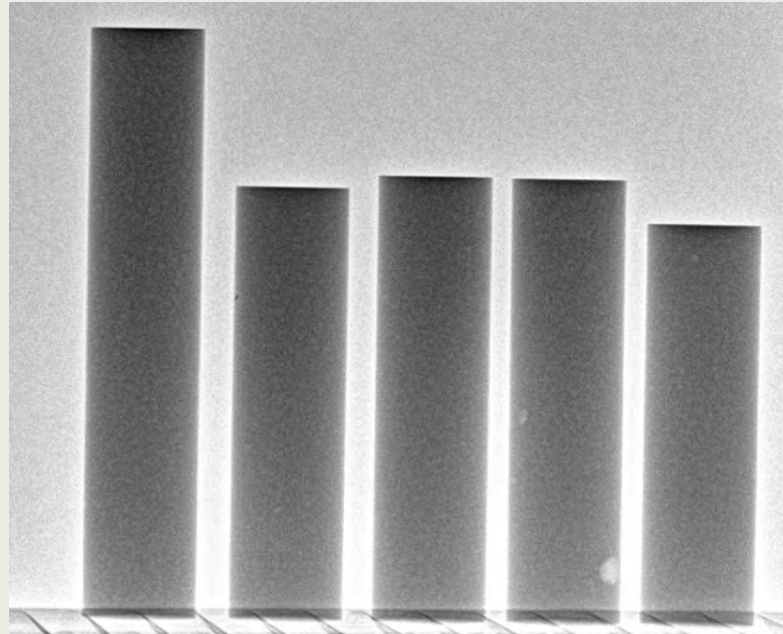
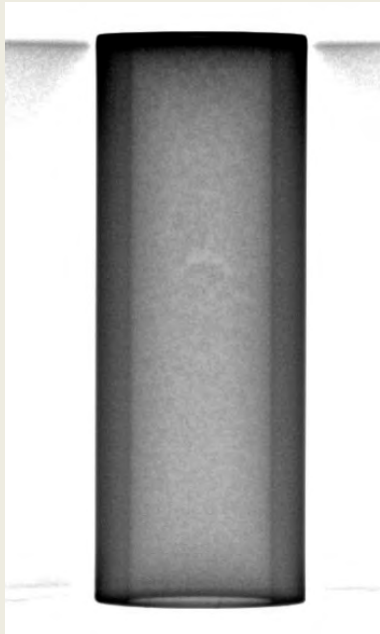




SHOCK SENSITIVITY



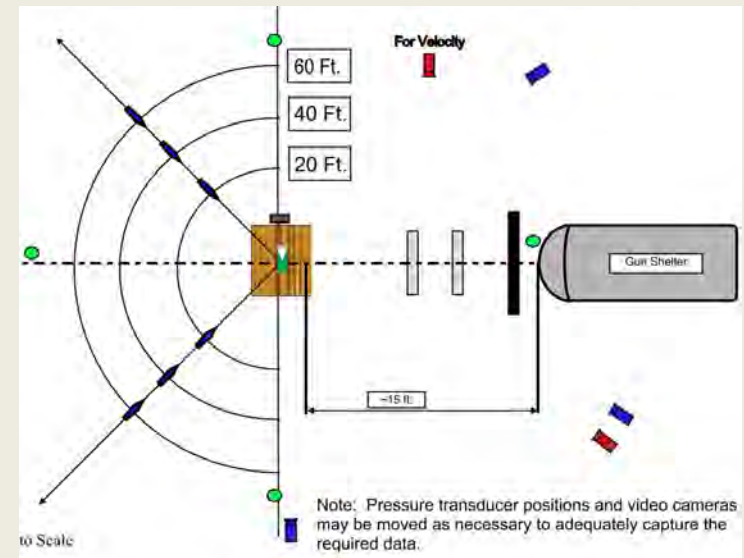
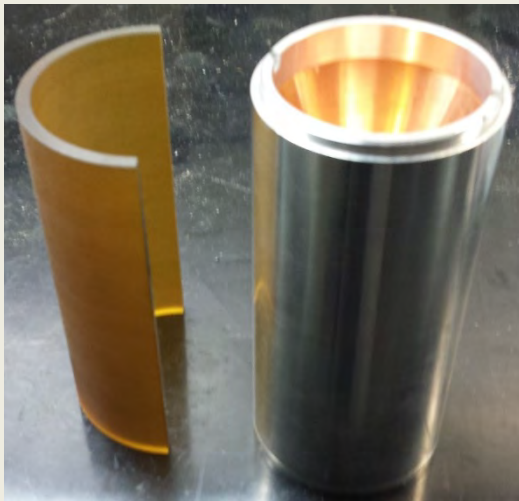
- IHE assets for MDNT-HMX:
 - ~92% TMD
 - Shock sensitivity was $<$ LX-14 and $=$ PBXN-9
- Shock sensitivity testing may have been negatively affected by the porosity and low density of the test assets





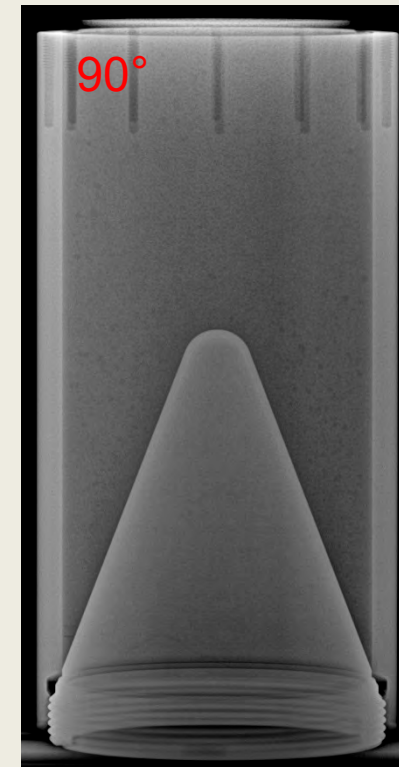
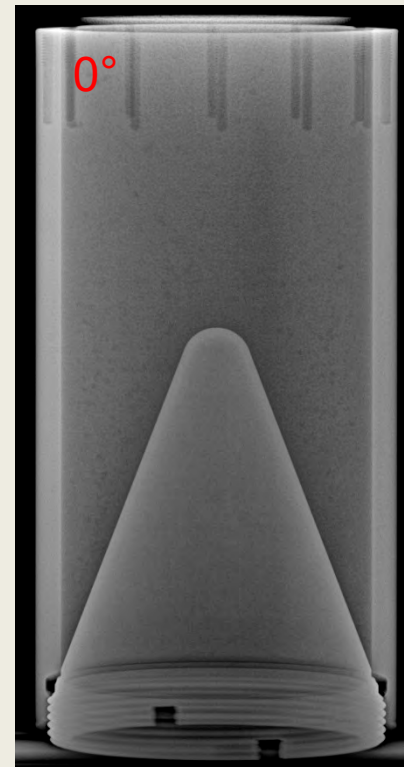
- Testing performed in a 3.2" Generic Testing Unit

- MDNT-HMX Formulation
- LX-14
- Impact Mitigation Liner
- 6000 fps





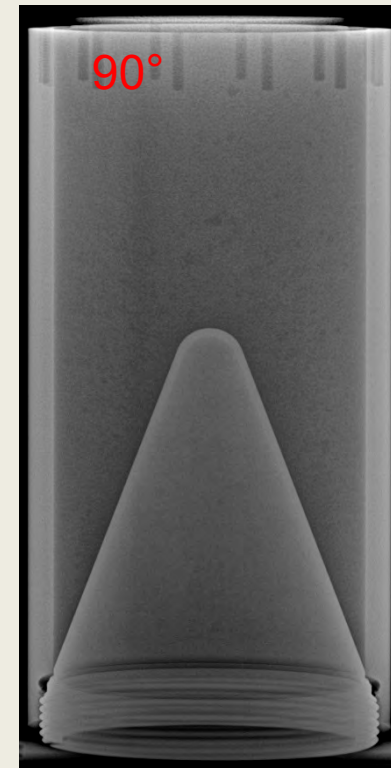
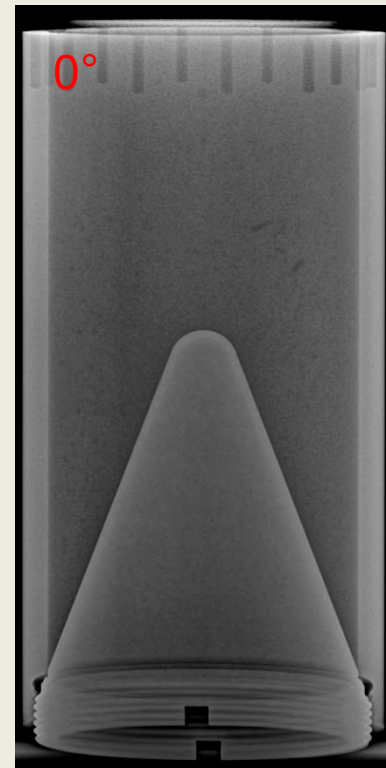
- No liner, 6000 fps
 - LX-14 High Order Rxn
 - MDNT-HMX High Order Rxn

LX-14**MDNT-HMX**

Test	Liner	Velocity (fps)	Steel Plates	Largest	Furthest	P1/4 20ft (psi)	P2/5 40ft (psi)	P3/6 60ft (psi)	Estimate
LX-14	None	5353	Through Hole	NA	NA	4.73/6.78	2.42/2.44	1.21/1.80	Type I
MDNT-HMX	None	5968	Slug in 2 nd plate	NA	NA	4.22/5.30	2.23/2.45	1.02/1.30	Type I



- 6mm Liner at 6000 fps
 - LX-14 Type III/IV
 - MDNT-HMX High Order Rxn

LX-14**MDNT-HMX**

Test	Liner	Velocity (fps)	Steel Plates	Largest	Furthest	P1/4 20ft (psi)	P2/5 40ft (psi)	P3/6 60ft (psi)	Estimate
LX-14	6mm	5954	HE splatter	Copper Liner	Aluminum Casing	0.53/0.35	0.25/0.25	0.17/0.13	Type III/IV
MDNT-HMX	6mm	5990	Through Hole	NA	NA	3.40/3.58	2.21/2.13	1.26/1.15	Type I



- MDNT-HMX formulation FI testing had violent reactions at 6000 fps with a 6mm Liner
 - 6mm of liner mitigated LX-14 to Type III/IV
 - MDNT-HMX assets had several voids and porosity
 - Casting quality and densities a concern





- Penetration tests were conducted
 - Copper Liner, through steel stack
 - Two LX-14 baselines
 - Two MDNT-HMX tests
 - Compare to historical LX-14 and PBXN-9 data
 - 5 CDs Standoff

Explosive	Avg. Penetration Depth	Shot 1 Depth	Shot 2 Depth
MDNT-HMX	86% of LX-14	81% of LX-14	91% of LX-14
PBXN-9*	90% of LX-14	NA	NA
LX-14*	91% of LX-14	NA	NA

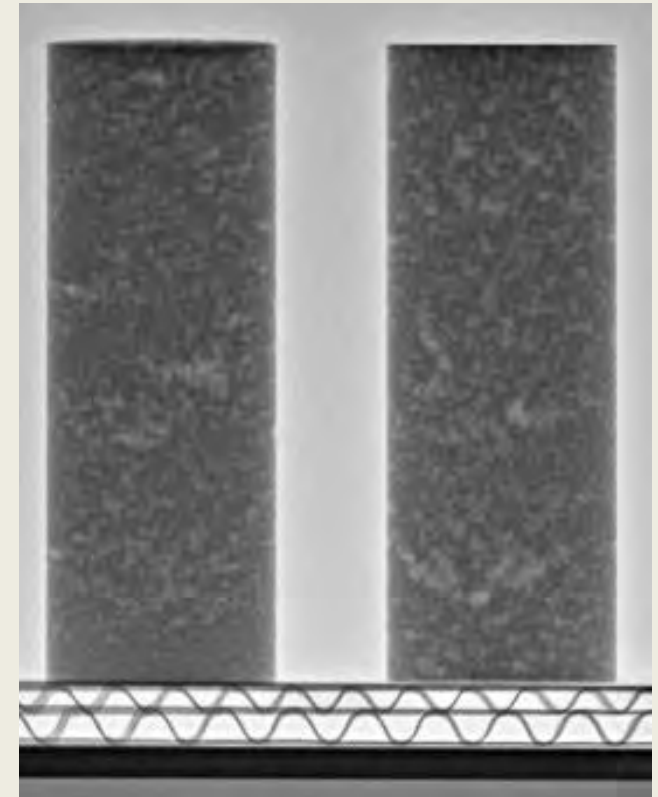
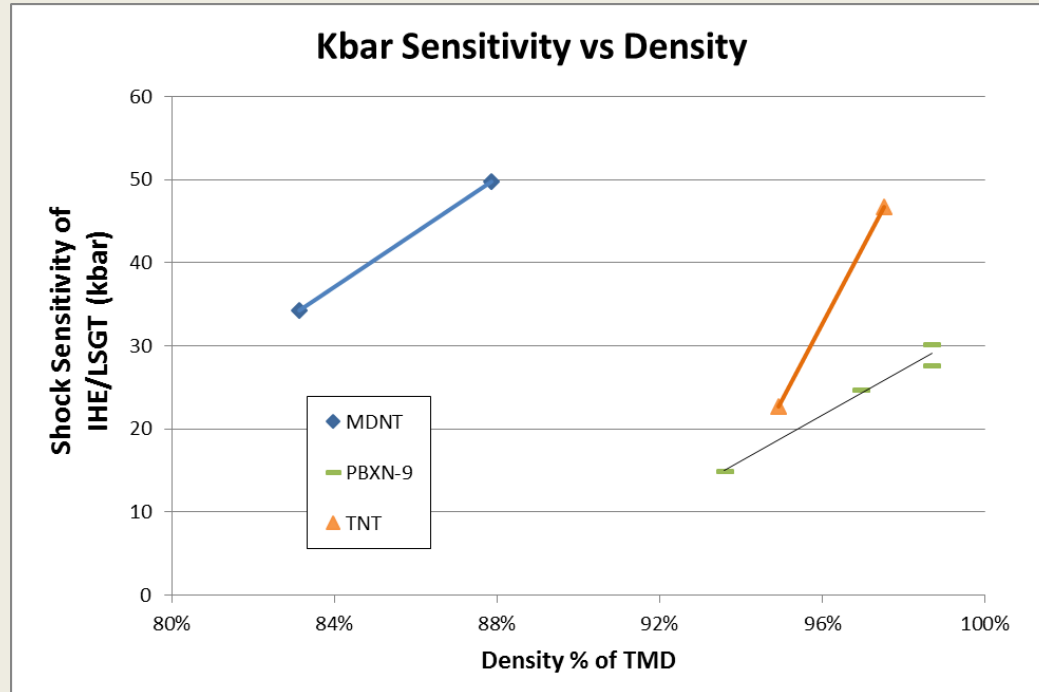
*PBXN-9 and LX-14 historical data

- Liner design is not optimized for the explosives being compared
- Still a good barometer of how well the MDNT-HMX performs
- MDNT modified formulation coupled with a proper liner redesign effort may meet or exceed LX-14 penetration





- Trends illustrate that at higher density, sensitivity to shock is improved.
- Extrapolating the trend for MDNT projects extremely favorably for shock sensitivity at higher density





- Barrier with MDNT has been the casting quality. Low density of casting:

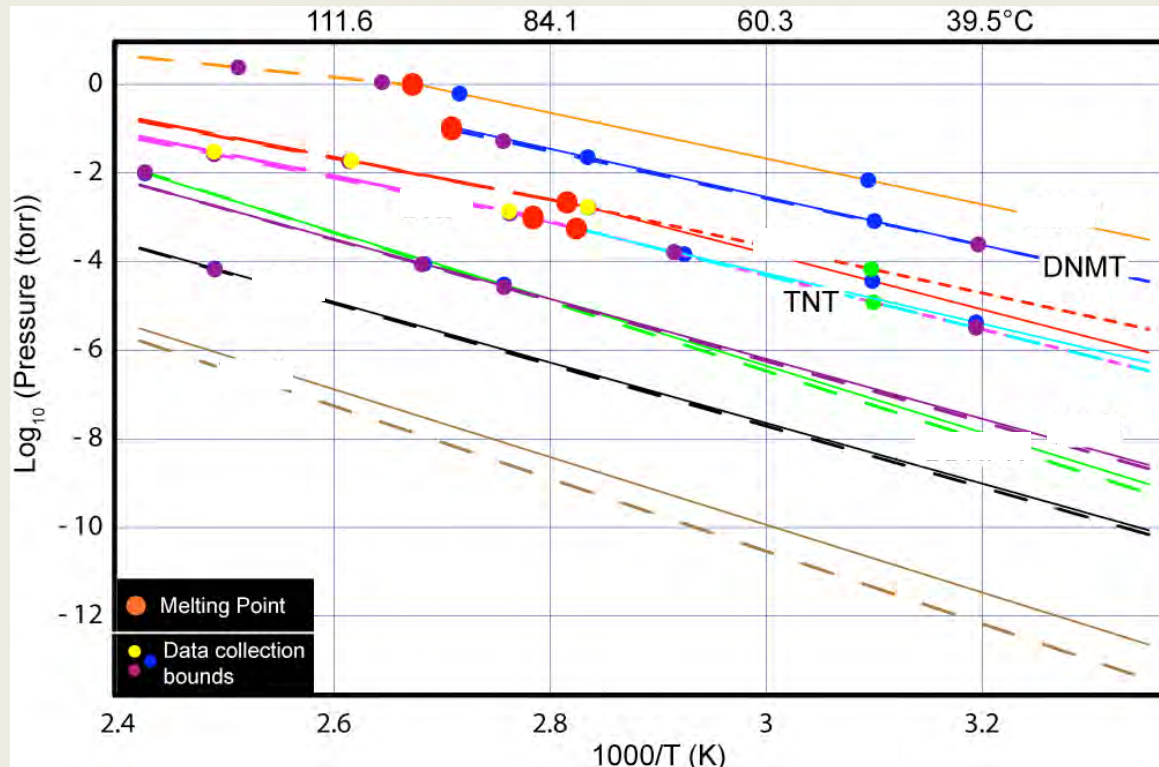
1. Limits the performance

- At low densities (~90% TMD) the Det Vel of MDNT was comparable to Comp B
- MDNT-HMX ~92% TMD was comparable to PBXN-9
- Higher densities should improve the performance

2. Negatively effects shock sensitivity

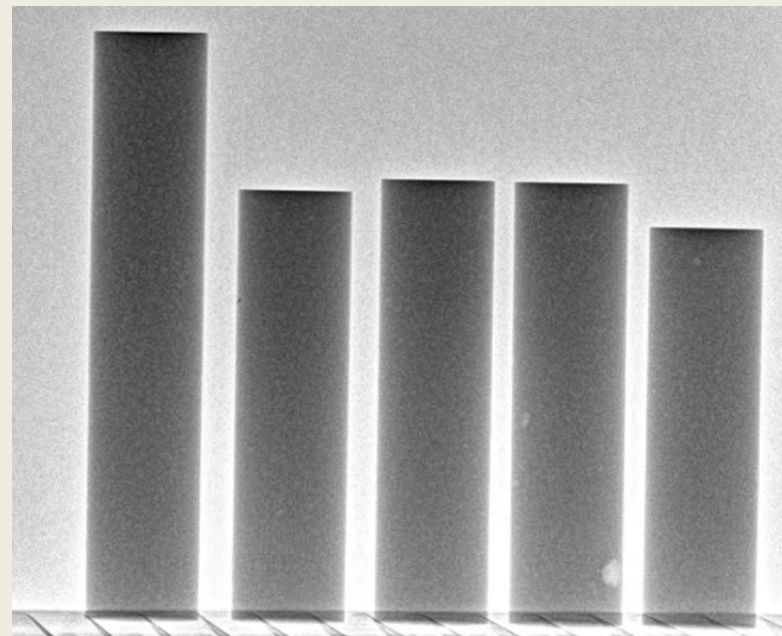
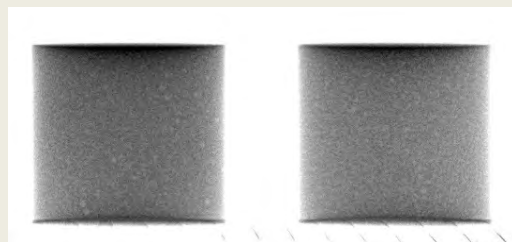
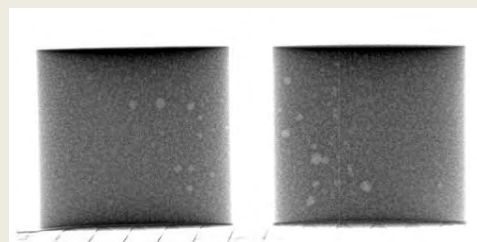
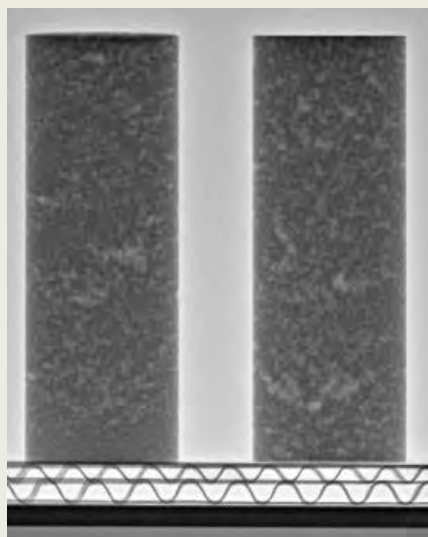
- Increase in voids and hot spots, a cleaner cast will result in an improved shock sensitivity.

- A casting study was setup to improve casting quality of MDNT:
 - Use of processing additives to address porosity and cast quality
 - Optimization of pouring temperature and temperature of metal parts
- Possible cause for voids and porosity is high vapor pressure of MDNT





- Off-gassing may be occurring during casting/cool-down procedures, resulting in voids and porosity
- With similar conditions, MDNT exhibits excess porosity in comparison to other melt-phase explosives





- MDNT is a skin irritant and sensitizer, with subsequent exposures resulting in heightened symptoms
 - During melt-phase and lab operations
 - All users were not affected
 - Mitigated with proper PPE
- Dermal irritation symptoms were present without direct exposure to the solid form
 - Bag of dry powder
 - Post processing inspection
 - High vapor pressure
- Efforts evaluating MDNT at ARDEC were halted due to recurring dermal irritation and sensitization



- MDNT (pure material):
 - MDNT tested with performance up to Comp B levels in detonation velocity and detonation pressure
 - Shock sensitivity below TNT
- MDNT-HMX Formulation:
 - MDNT-HMX formulation at or exceeding PBXN-9 output levels, and approaching LX-14
 - Shock Sensitivity was similar to PBXN-9
- Sensitivity and Performance are both negatively affected by porosity that may be pronounced due to high vapor pressure and off-gassing during melt-pour procedures
- High vapor pressure and dermal sensitization ultimately led to termination of MDNT efforts at ARDEC.



- ARDEC Team for testing and analysis
- ARDEC/BAE Labs for initial synthesis scale-up
- Nalas Engineering for developing scalable synthesis route
- BAE Holston for scale-up in pilot plant facilities
- PEO Ammo IM TTA
- JIMTP Program Office
- Dr Leonard Stiel for theoretical calculations



QUESTIONS?

Robust Enhanced Blast Explosive Manufacturing at Holston Army Ammunition Plant **NDIA IMEMTS 2018 (Session 4B)**

Virgil Fung *, Brian Alexander, Erica Lotspeich, PhD., Robyn Wilmoth
BAE Systems, Holston Army Ammunition Plant, Kingsport, Tennessee, United States
24th April 2018



Briefing Outline

- Background
- EB Explosive Overview
- EB Explosive Process Development
- EB Explosive Manufacturing at HSAAP
- EB Explosive Manufacturing Capabilities
- Other EB Explosive Manufactured at HSAAP
- Summary
- Acknowledgements

Background – Enhanced Blast Explosives Overview

- Enhanced Blast (EB) Explosives offer performance characteristics of both aluminized and non-aluminized formulations for target defeat
- The incorporation of aluminum powder achieved high shock overpressure for longer duration than non-aluminized composition
- EB Explosive is formulated to optimize the balance of detonation velocity and total mechanical energy, resulting in desirable metal pushing capability as well as high blast energy
- EB Explosives are typically selected for multi-purpose warheads in shoulder-launched weapon or direct-fire applications
- EB Explosives of interest:
 - PBXIH-18 (Aluminized HMX Based EB with inert plasticizer; ~ 30% aluminum)
 - PAX-3 (Aluminized HMX Based EB with energetic plasticizer; ~ 20% aluminum)
 - PAX-30 (Aluminized HMX Based EB with energetic plasticizer; ~ 15% aluminum)
 - PAX-42 (Aluminized RDX Based EB with energetic plasticizer; ~ 15% aluminum)

Background – EB Explosive Processing (1)

- Multiple ways to manufacture EB Explosive
 - Granulation via Aqueous Slurry Coating
 - One step process similar to standard Holston PBX manufacturing process
 - Production equipment readily available
 - Twin Screw Extrusion
 - Multi-steps process; incorporation of aluminum powder with nitramine precursor; granulator
 - Production Twin Screw Extruder not available at HSAAP
 - High Shear Mixer
 - Multi-steps process; dry or coated nitramine required
 - High Shear Mixer not available at HSAAP



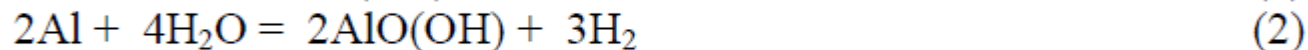
Background – EB Explosive Processing (2)

- Aqueous Slurry Coating is preferred at HSAAP
 - Most efficient and cost effective process
 - Most suited for existing infrastructure without major investment
 - All processing steps conducted at HSAAP
- Choose between Water Replacement (WR) Fluid & Water
 - WR Fluid
 - Non reactive with aluminum powder
 - similar boiling point as water
 - High cost (purchase/recovery) for Production
 - Water
 - Significantly lower cost than WR Fluid
 - No special delivery or handling equipment
 - Standard aqueous source for HE manufacturing at HSAAP



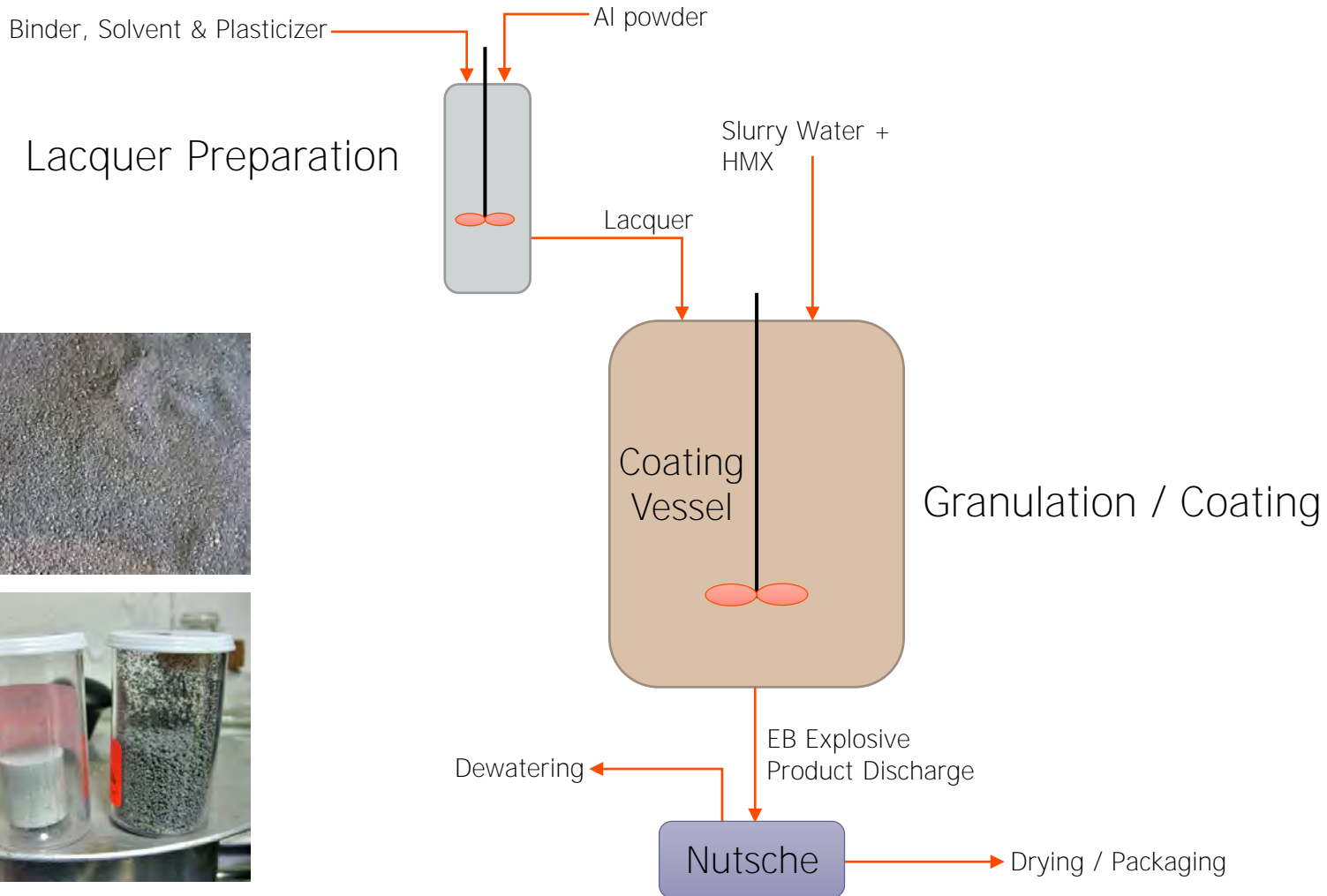
EB Explosive Process Development

- Hydrogen Generation from Aluminum/Water Interaction



- BAE Systems developed a water slurry coating process to encounter potential Hydrogen generation via
 - Suitable additives
 - Specific temperature during key stages of the process (granulation & distillation)
 - Process Configuration Changes (e.g. solvent removal / lacquer preparation)
- Hydrogen monitoring conducted at various stages of the process (coating / dewatering / drying) and none was recorded, suggesting no hydrogen generation was detected throughout the process
- The new EB Explosive Water Slurry Process was successfully scaled from Lab (5 lbs.) to Production (300 – 350 lbs.)

EB Explosive Water Slurry Process - Overview



EB Explosive Manufactured in Production at HSAAP (1)

- PAX-3
 - Developed & Qualified by US ARMY ARDEC
 - HMX based EB with aluminum and energetic plasticizer (BDNPA/F)
 - Previously manufactured at HSAAP via Slurry Coating with WR Fluid
 - Produced PAX-2 (precursor without Aluminum) for Twin Screw Extrusion (3rd party facility) in 2011
 - Robust Process for Slurry Coating with Water developed in 2015
 - Over **5,500 lbs.** manufactured in Production to date
 - PAX-3 fielded in shoulder launched weapon and under evaluation in the 120mm Advanced Multi-Purpose (AMP), XM1147 Tank Cartridge



EB Explosive Manufactured in Production at HSAAP (2)

- PAX-3 (from 2017 Production Campaign)



EB Explosive Manufactured in Production at HSAAP (3)

- PAX-3 vs. PBXN-9



EB Explosive Manufactured in Production HSAAP (4)

- PBXIH-18
 - Developed & Qualified by US NAVY Indian Head
 - HMX based EB with aluminum and inert plasticizer (DOA)
 - Previously manufactured at HSAAP via Slurry Coating with WR Fluid
 - Current process involved Twin Screw Extrusion (3rd party facility) of precursor (e.g. PBXN-9)
 - Robust Process for Slurry Coating with Water developed in 2016
 - Over **2,100 lbs.** manufactured in Production to date
 - BAE Systems water slurry material performed identically to WR slurry material (presented at IMEMTS 2016)



EB Explosive Manufactured in Production HSAAP (5)

- PBXIH-18 (from 2017 Production Campaign)



EB Explosive Manufacturing Capability at HSAAP (1)

- Manufacturing Equipment – R&D Pilot Plant



Lacquer Preparation Vessel



Coating/Granulation Vessel (Small)
~ 50-100 lbs.



Coating/Granulation Vessel (Large)
~ 300 lbs. or more

EB Explosive Manufacturing Capability at HSAAP (2)

- Manufacturing Equipment – Production Facility



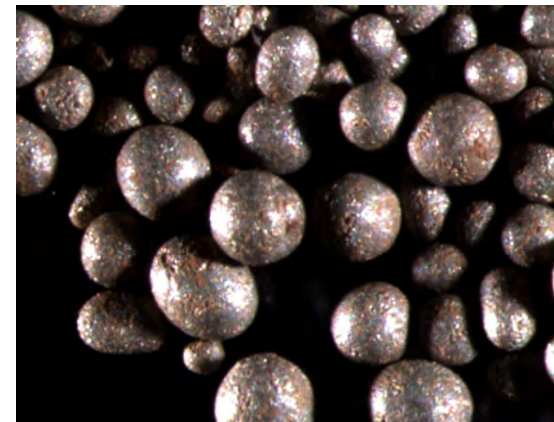
Lacquer Preparation Vessel



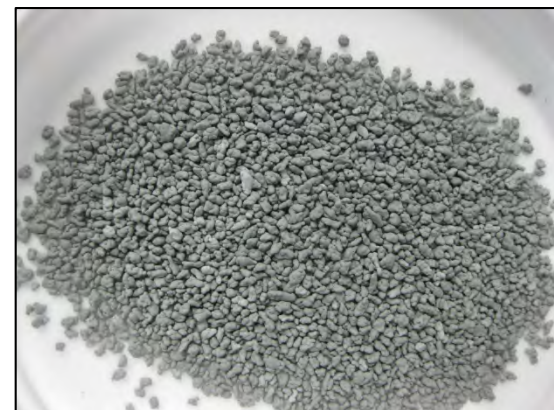
Coating/Granulation Vessel (Large) ~ 300 lbs. or more

Other EB Explosive Manufactured at HSAAP

- PAX-3 with alternate Energetic Plasticizer (R8002)
 - ~ 2,000 lbs. manufactured with water slurry coating production process
 - R8002 plasticizer replacing BDNPA/F in order to address limited supply issue
 - R8002 readily available (HSAAP product)
- PAX-30
 - High HMX Content (>75%) EB Explosive
 - BAE Systems developed lab-scale coating process for both energetic plasticizer (BDNPA/F & R8002)
 - 2 lbs. batch size (Scale-Up Ready)
 - Samples under end-use evaluation
- PAX-42
 - High RDX Content (>75%) EB Explosive using BDNPA/F
 - Robust lab scale process developed under IRAD effort
 - 2 lbs. batch size (Scale-Up Ready)



PAX-3 w R8002 (Production)



PAX-42 (Laboratory)

Summary

- BAE Systems had developed a **ROBUST, SAFE & COST EFFECTIVE** one-step water slurry coating process to manufacture aluminized EB Explosive at HSAAP
- Water-Replacement Fluid is no longer needed to mitigate the risk of Hydrogen Generation
- PAX-3 (**5,500 lbs.**), PBXIH-18 (**2,100 lbs.**) and PAX-3 w R8002 (**2,000 lbs.**) have been successfully manufactured with Production Equipment
- Both PAX-3 and PBXIH-18 made in this process are qualification-ready
 - PAX-3 will be subjected to explosive qualification later this year
- No difference in material characteristics between Water and WR Fluid
- R&D Pilot Scale Coating Vessel available for Process Development and Optimization with current and new EB Explosives
- Other pressable EB Explosives such as PAX-30 and PAX-42 ready to “Scale-Up”

Acknowledgements

- BAE Systems OSI – Holston Army Ammunition Plant
 - Dr. David Price
 - Dr. Neil Tucker
 - Mr. Matt Hathaway
 - Mr. Chris Long
 - Ms. Kelly Smith
 - Ms. Denise Painter
 - Mr. Todd Dye
 - Mr. Tracy Kelly
 - Mr. Paul Lucas
 - Mr. Myles Donegan
 - Mr. Greg Krieger
 - Mr. Sam Littlejohn
 - Dr. Tess Kirchner
 - Dr. Jeremy Headrick



Characterization of LX-14 FEM and PBXN-9 FEM High Energy Explosives

NDIA IMEMTS 2018

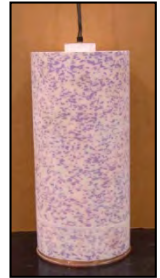
Brian Alexander*
BAE Systems
Holston Army Ammunition Plant
Kingsport, Tennessee, USA

April 24, 2018



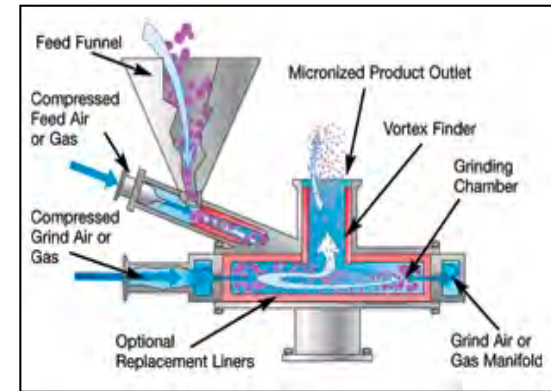
Program Overview

- Reduce the shock sensitive properties of established high energy explosives
 - LX-14
 - HMX, Estane Binder
 - PBXN-9
 - HMX, Hytemp ,Diocetyl Adipate (DOA)
- High Nitramine containing explosives utilized to achieve target defeat
 - Exceptional Explosive Energies
 - Tend to be shock sensitive due to nitramine content
- BAE Systems Internally Funded Research Project (IRAD)
 - Integration of IM Technology into legacy formulations
 - Modification of the HMX component
 - Fluid Energy Milled HMX (FEMHMX)

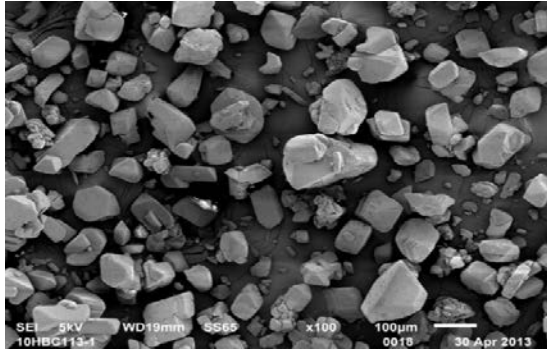


FEM Technology

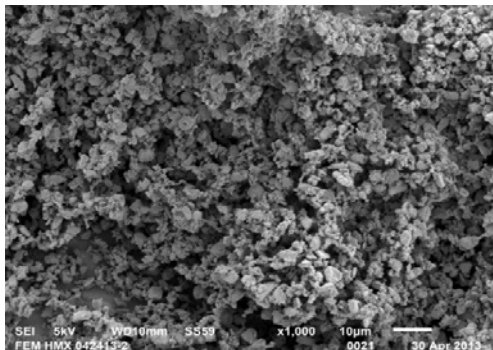
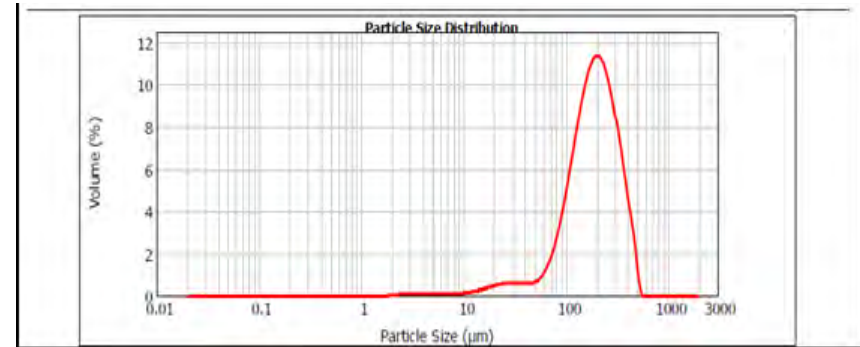
- Traditional mechanical size reduction technology
 - Particles mechanically milled
 - Rough, irregular shapes of produce crystals
- **Innovation of the technology resides in its simplicity:**
 - Compress air employed to move explosive in mill chamber
 - Particle-to-particle impacts reduce size of explosive
 - Ability to reach 1 micron
- No moving parts associated with the energetic processing
 - No sensitized handling of explosives
 - Removal of “pinch points”, extended friction
 - No hazardous collection of explosive dust in system



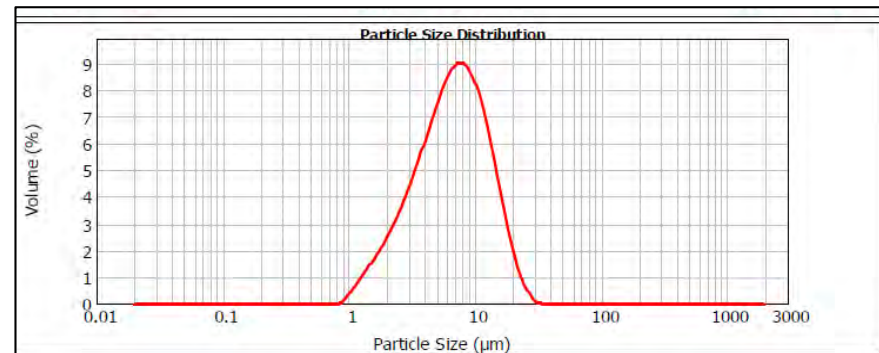
PSD Reduction



HMX Class 1 (X100)



FEM HMX (X 1,000)

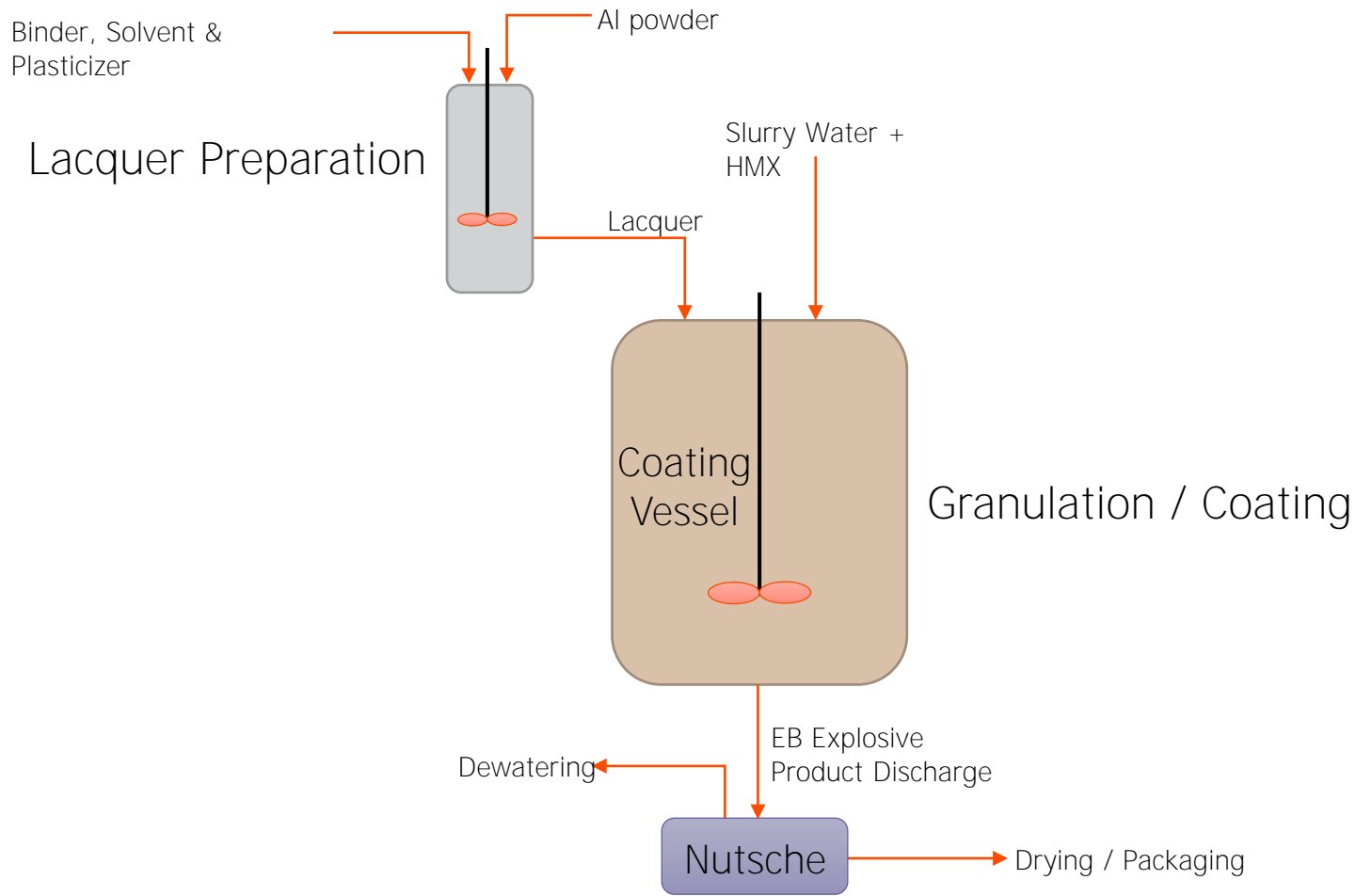


PBXN-9 FEM Laboratory Processing

- BAE Systems, OSI (HSAAP)
 - R&D Laboratory Facilities
- Trials Conducted:
 - 1 Liter PBX Slurry Still
 - 10 Liter PBX Coating Still
- HSAAP Slurry Coating Technology
 - HMX mixed in a water system (Slurry)
 - Hytemp/DOA binder dissolved in organic solvent (Lacquer)
 - Lacquer fed into slurry to achieve a precipitation of the binder
 - Solvent recovered via distillation
 - Product cooled, filtered and dried
- Experimental Plan
 - Standard PBXN-9 processing
 - Varied HMX Class 1 / FEM HMX Ratio



Slurry Coat Processing

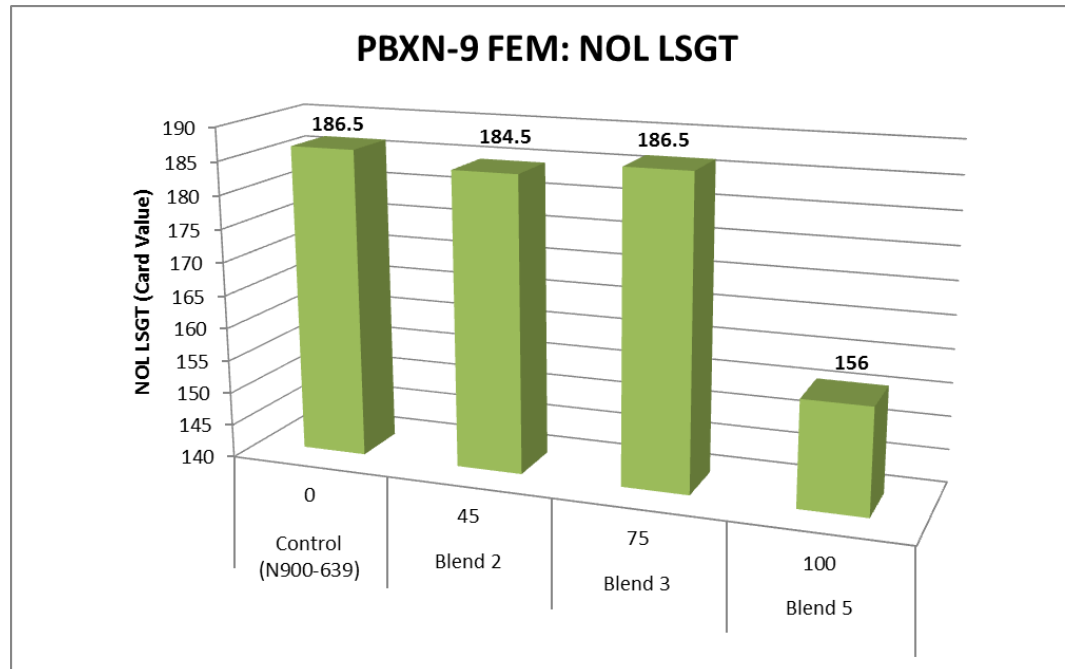


PBXN-9 FEM: Analysis

PBXN-9 with FEM HMX								
Spec	Target					% Passing		
Batch	% FEM	DOA	% HMX	Hytemp	Cup BD	6	8	40
		5 - 7	91 - 93	1.5 - 3	> 0.8 g/cc	99 - 100	95 - 100	0 - 5
1154-55	25	1.54	96.06	2.40	0.953	100.0	99.3	1.7
1154-56	25	1.51	95.92	2.57	0.945	99.3	98.6	4.2
1154-57	25	5.59	92.26	2.15	0.925	99.8	98.8	1.0
1154-69	25	5.45	92.70	1.85	0.914	100.0	96.9	2.5
1154-70	25	5.47	92.85	1.68	0.940	100.0	98.0	4.5
1154-43	45	6.26	91.77	1.97	0.982	100.0	99.9	1.6
1154-44	45	6.24	91.82	1.90	0.936	99.9	99.1	4.0
1154-45	45	5.78	92.34	1.88	0.954	100.0	98.9	3.2
1154-49	75	5.79	92.24	1.97	0.842	99.0	98.6	3.0
1154-50	75	6.08	91.91	2.01	0.846	99.8	99.3	2.2
1154-51	75	5.89	92.02	2.09	0.877	99.4	98.7	3.6
1154-52	90	6.14	91.79	2.07	0.806	99.8	99.6	6.3
1154-53	90	6.25	91.67	2.08	0.784	99.9	99.8	7.4
1154-54	90	6.16	91.82	2.02	0.780	99.8	99.6	56.2
1154-46	100	6.08	92.02	1.90	0.688	100.0	100.0	56.0
1154-47	100	6.13	91.89	1.98	0.702	100.0	100.0	57.5
1154-48	100	5.96	92.09	1.95	0.711	100.0	100.0	41.0

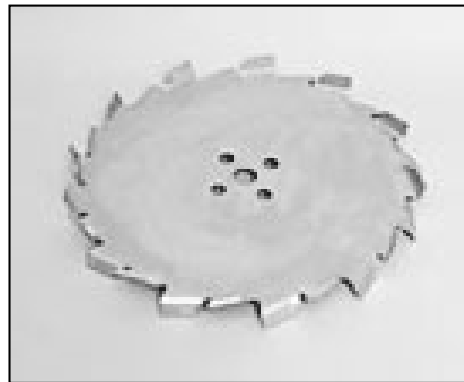
PBXN-9 FEM: NOL LSGT

Batch #	% FEM	DOA	% HMX	Hytemp	Bulk Density	%Pass #6	%Pass #8	%Pass #40	NOL LSGT	Pressed Density	% TMD
		5 - 7	91 - 93	1.5 - 3	> 0.8 g/cc	99 - 100	95 - 100	0 - 5	> 1.73 g/cc		
Control (N900-639)	0	6.30	91.90	1.80	0.83	100	100	0	186.5	1.694	95.2
Blend 2	45	6.24	91.82	1.90	0.94	99.9	99.1	4.0	184.5	1.6756	94.1
Blend 3	75	6.08	91.91	2.01	0.85	99.8	99.3	2.2	186.5	1.6528	92.9
Blend 5	100	6.13	91.89	1.98	0.70	100.0	100.0	57.5	156	1.6487	92.6

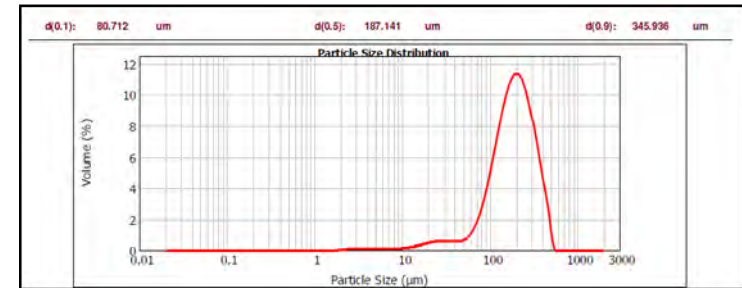


LX-14 Explosive

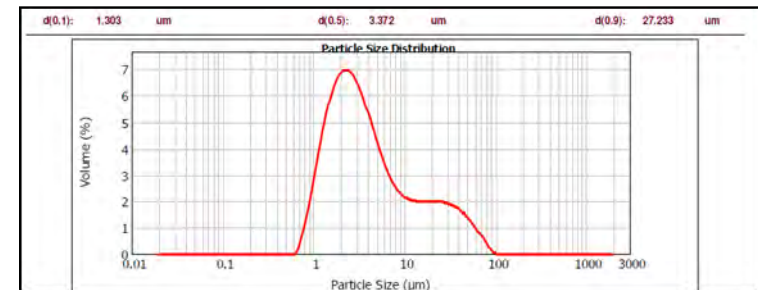
- High Nitramine (HMX) based explosive
- Composition
 - Estane Binder
 - HMX Explosive
 - HMX Class 1
 - HMX Class 2
 - HMX Class 2 (Cowles)
- HMX Cowles Grind
 - Serrated blade induces hydrodynamic shear



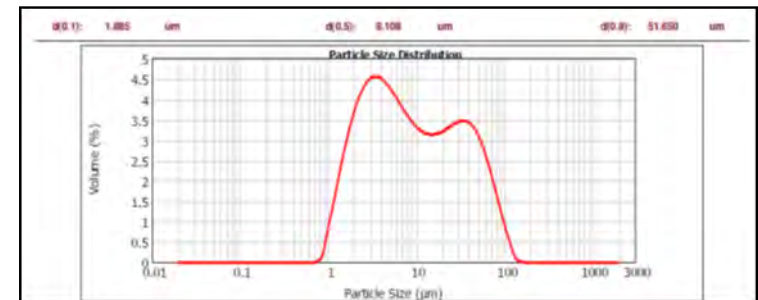
HMX Class 1



HMX Class 2

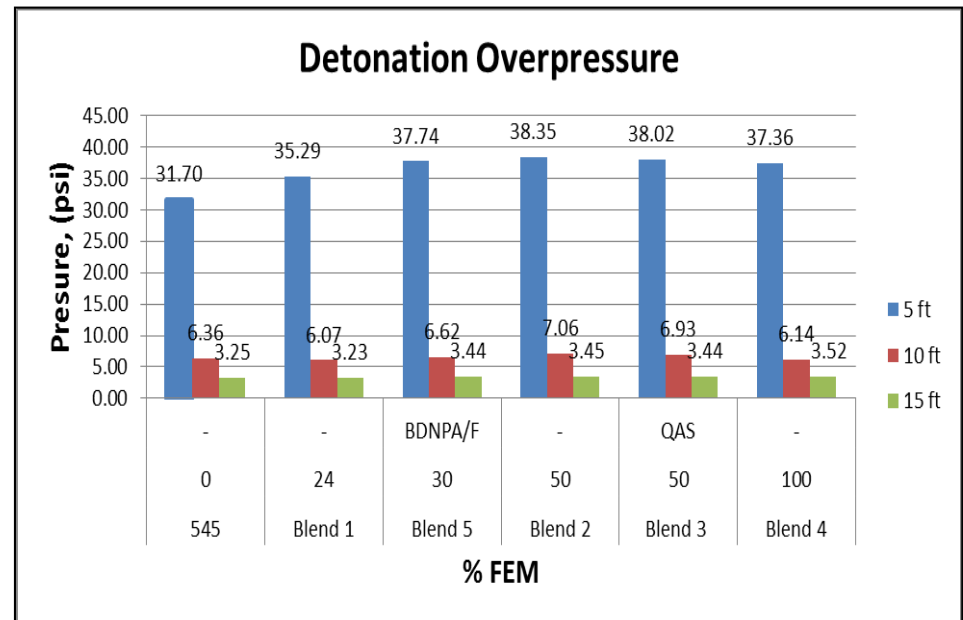


HMX Class 2 Cowles



BAE Systems: Explosive Performance

- Blast Overpressure assessment
 - Conducted at BAE Systems (Kingsport, TN) HSAAP facility
- Test Configuration
 - 3 PCB piezoelectric pencil gauge
 - Axial oriented with test charge
 - 5ft, 10ft and 15ft
 - LX140-545 used as baseline comparison of output performance
- Results
 - All experimental formulations exceed pressure of baseline



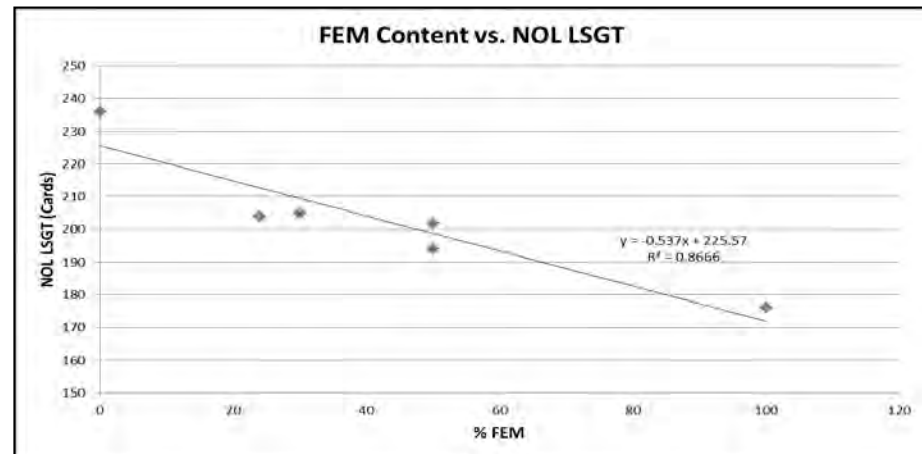
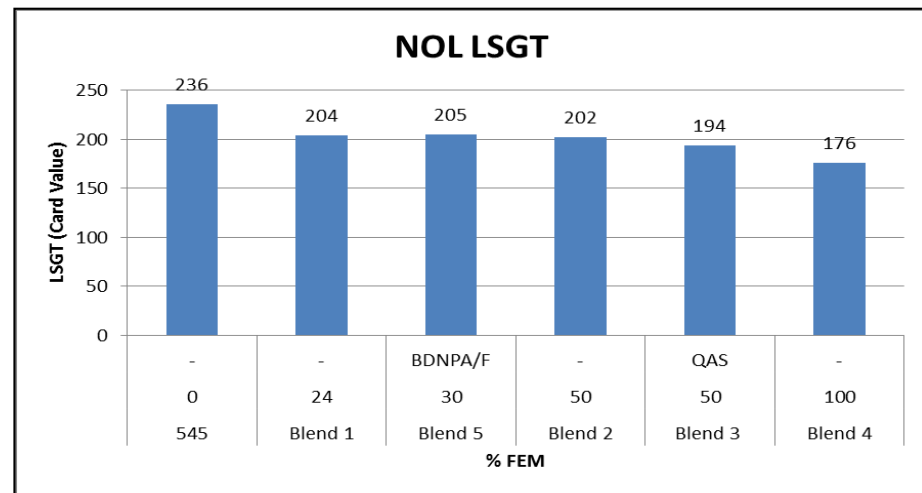
LX-14 FEM

- Prototype Explosive Formulations Consisted:

- 0% FEM (Baseline Formulation)
- 24% FEM
- 30% FEM
- 50% FEM
- 100% FEM

- NOL LSGT

- Card gap value decreases with increase in FEM content
- 60 Card Reduction (25.4%)
 - Batch 545 = 236 cards
 - 100% FEM = 176cards



US ARMY: ARDEC Evaluation

- Preliminary press data
 - Increase in density during press cycle
 - Additional decrease in NOL LSGT Card Gap Value

80% FEM

Material: LX-14 (mod) 80FEM				
Lot #: RDD17E011-059				
Date: 5/23/2017				
Density: 1.81 g/cc				
Shot #: 11-743				
Shot	Pellet #s	Gap (in.)	Result (GO/NOGO)	Notes
1	22,33,28	1.80	NO-GO	
2	45,1,35	1.67	NO-GO	
3	31,10,15	1.60	GO	
4	17,39,4	1.64	GO	
5	25,38,14	1.66	NO-GO	N+1
6	44,32,43	1.65	GO	N
7	23,20,16	1.65	GO	N
8	12,41,37	1.66	GO	N+1
9	5,42,29	1.67	NO-GO	N+2
10	6,26,8	1.67	GO	N+2
50% point = $N + 1.5 = 1.665$ " = 166.5 cards				

Data shows ~29.4% in shock reduction as compared to BAE Systems Baseline data

100% FEM

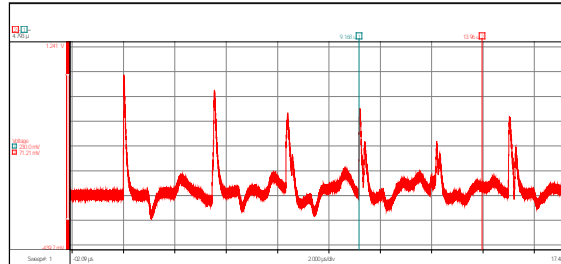
Material: LX-14 (mod) 100FEM			
Lot #: RDD17E011-056			
Date: 5/23/2017			
Density: 1.80 g/cc			
Shot #: 11-742			
Pellet #s	Gap (in.)	Result (GO/NOGO)	Notes
1,12,30	2.00	NO-GO	
32,20,2	1.50	GO	
26,5,28	1.80	NO-GO	
44,25,19	1.65	NO-GO	
4,8,23	1.55	GO	
10,18,42	1.61	GO	N
6,36,24	1.64	NO-GO	
33,17,9	1.62	NO-GO	N+1
14,31,37	1.61	NO-GO	N
22,15,3	1.62	GO	N+1
t = $N + 1/2 = 1.615$ " = 161.5 cards			

Data shows ~31.5% in shock reduction as compared to BAE Systems Baseline data

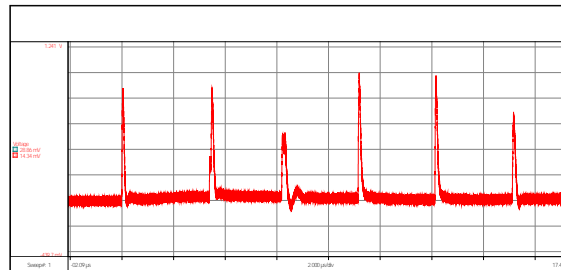
Detonation Velocity: 80% FEM

Nammo Talley

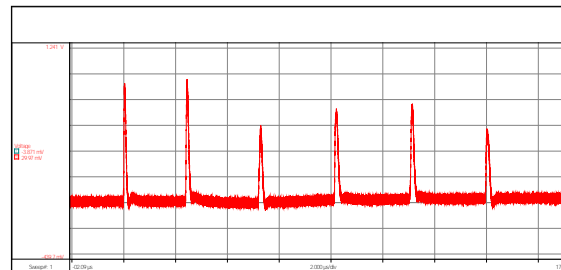
VoD = 8675 m/s



VoD = 8526 m/s



VoD = 8637 m/s



ARDEC

LX-14 (mod) LSDV Testing

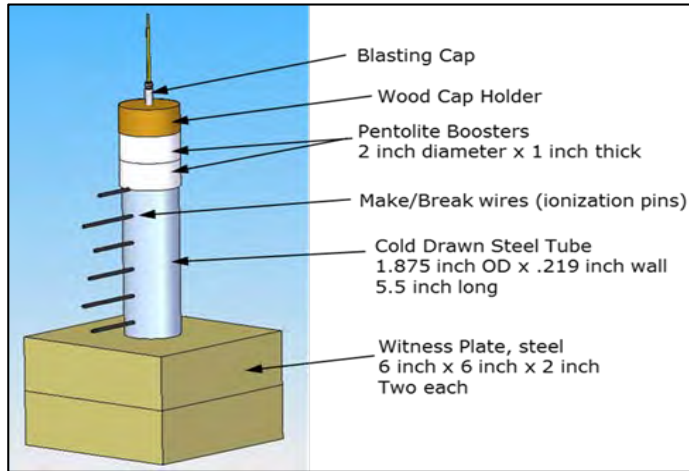
5/26/2017

Material	Shot #	Det. Vel. (mm/us)
LX-14 (mod) 80 FEM	11-750	8.63
	11-751	8.65
LX-14 (mod) 100 FEM	11-752	8.63
	11-753	8.63

Detonation Calorimetry

Sample	Date	Lot	Net Heat (cal/g)
BAE lx-14 50-50 fem	6/22/2016	Batch 30	1378.03
BAE lx-14 50-50 fem	6/23/2016	Batch 30	1339.99
BAE lx-14 50-50 fem	6/22/2016	Batch 30	1378.03
BAE lx-14 100 fem	6/23/2016	Batch 31	1332.58
BAE lx-14 100 fem	6/23/2016	Batch 31	1339.55

Plate Dent



Nammo Talley

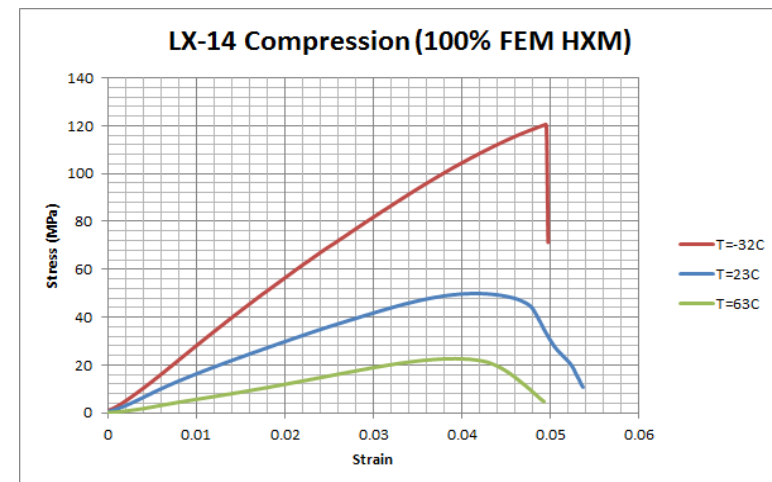
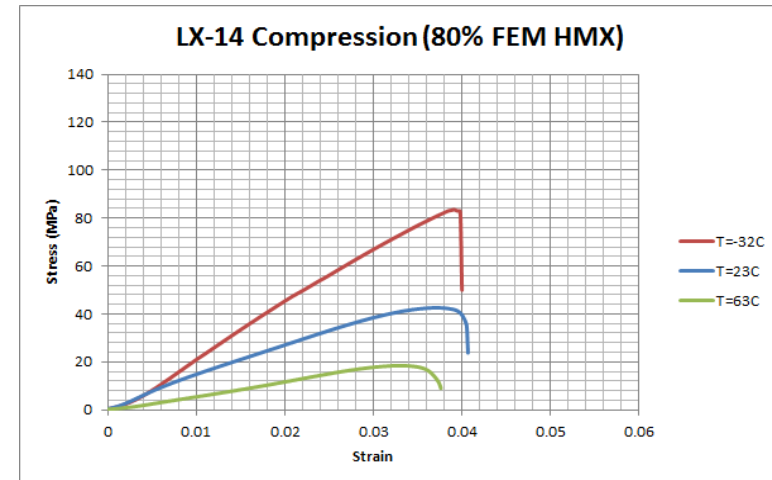
Sample #	Explosive	Avg Depth (in)
DRT-002*	BAE LX-14	0.47065
DRT-015*	BAE LX-14	0.4749
DRT-016*	BAE LX-14	0.4722
DRT-001	PBXN-110	0.429325
DRT-003	PBXN-110	0.4258
DRT-004	PBXN-110	0.414925

ARDEC

LX-14 (mod) LSDV Testing		
5/26/2017		
Material	Shot #	Dent (in.)
LX-14 (mod) 80 FEM	11-750	0.419
	11-751	0.419
LX-14 (mod) 100 FEM	11-752	0.421
	11-753	0.415

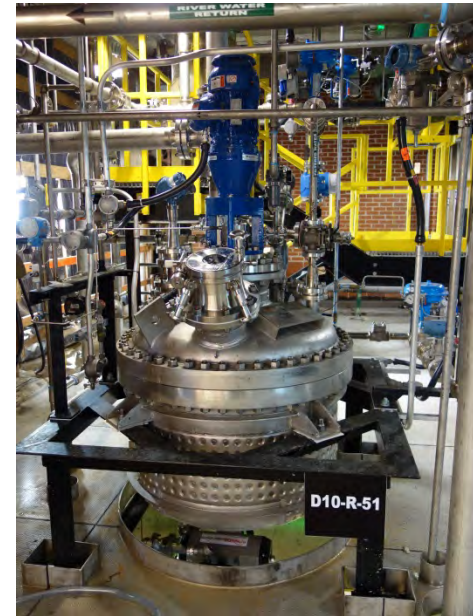
Uniaxial Compression

Temp (deg C)	Sample	Yield Stress (MPa)	Strain @ Yield	Modulus (MPa)
63C	80% FEM	18.4	0.0327	631
	100% FEM	22.6	0.039	568
23C	80% FEM	42.5	0.0371	1233
	100% FEM	49.8	0.042	1286
	Ref (Legacy)	19.4	0.028	940
-32C	80% FEM	83.5	0.0395	2333
	100% FEM	120.5	0.0495	2529



HSAAP Pilot Plant

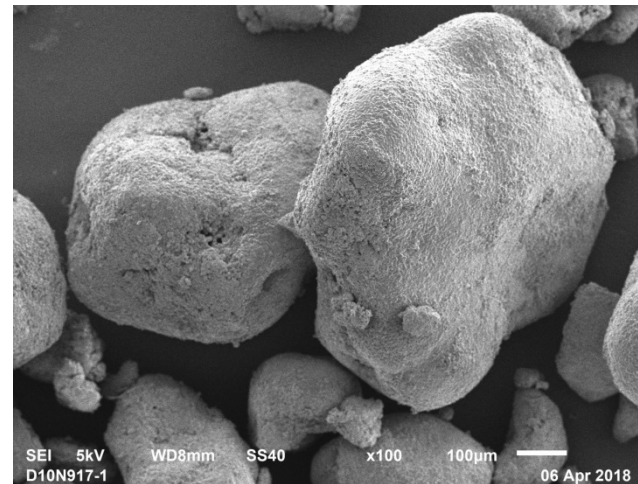
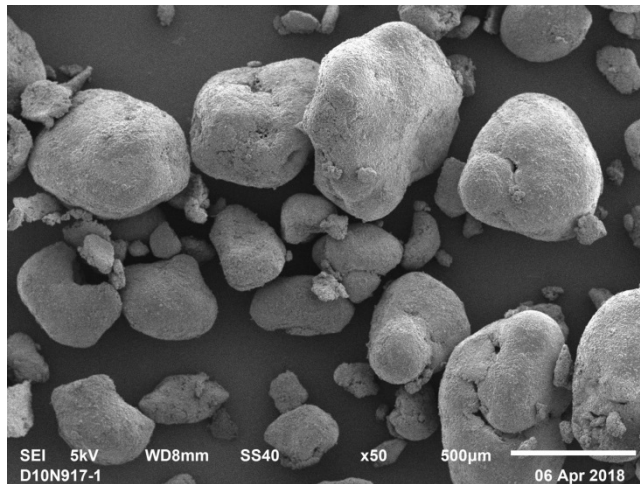
- Building D-10: R&D Pilot Formulation Center
- PBXN-9 FEM (90% FEM)
 - 590 Lbs. produced to date
- LX-14 FEM
 - 536 Lbs. produced to date



Pilot Plant: PBXN-9 FEM

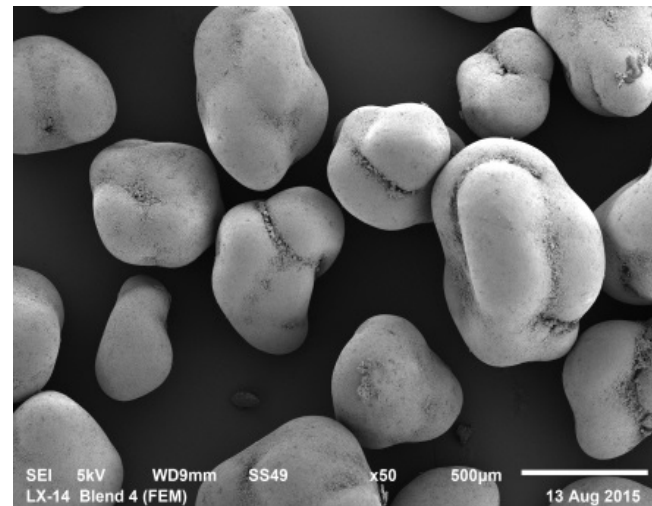
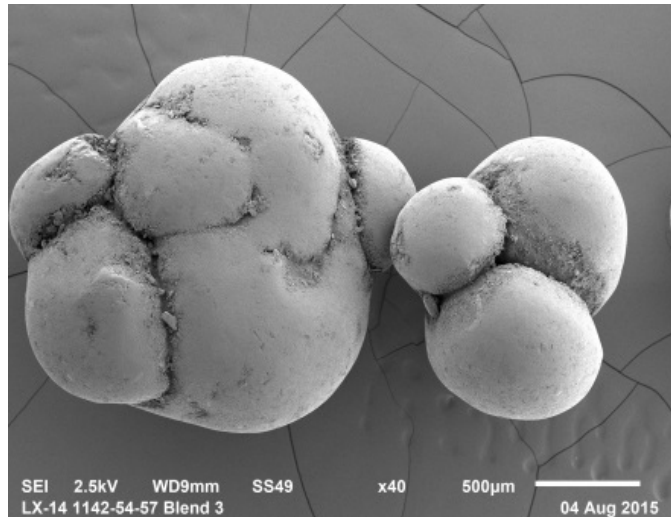
PBXN-9 with FEM HMX - Analytical Result Summary

Batch/ Notebook #	Lab/Pilot	Batch Size (lbs.)	% FEM HMX	Composition			Bulk Density	Pressed Density	Flowdex	Friction Co-eff	Granulation			Naval Impact		VTS
				HMX %	DOA %	Hytemp %					Pass #6	Pass #8	Pass #40	N-9	RDX Std	
				91.0-93.0	5.0-7.0	1.5-3.0					>0.80 g/cc	>1.73 g/cc	<220	99-100	95-100	
D10N917-1	Pilot	145	90	92.02	5.77	2.21	0.71	1.69	12	208.74	99.8	98.1	45.2	84.14	12.12	0.0304
D10N917-2	Pilot	145	100	91.66	5.83	2.50	0.71	1.677	7	121.77	99.9	99.3	5.1	89.13	12.12	0
D10N917-3	Pilot	300	90	91.78	5.88	2.34	0.67	1.692	9	147.74	99.6	98	9.2	39.81	13.14	0.0247



Pilot Plant: LX-14 FEM

LX-14 with FEM HMX - Analytical Result Summary														
Batch/ Notebook #	Lab/Pilot	Batch Size	% FEM HMX	Composition		Bulk Density (g/cc)	Volatiles	Granulation				Insolubles		Color
				HMX %	Estane %			Retain 5/16"	Retain #4	Retain #50	Retain #80	USSS #40	USSS #60	
				94.9 - 96.1	3.9 - 5.1	> 0.85 g/cc	0.10% Max	None	1 max	95 min	98 min	0 max.	5 max.	
D10LX14FEM17-1	Pilot	118 lb.	80	96.1	3.90	0.878	0.071	0	0	84.4	13.2	0	0	White
D10LX14FEM17-2	Pilot	300 lb.	80	95.36	4.64	0.85	0.06	0	0	91.8	72	0	0	White
D10LX14FEM17-3	Pilot	118 lb.	80	95.33	4.67	0.877	0	0	0	94	6	0	0	White



Conclusion

- **Reduction of shock sensitivity in PBXN-9 and LX-14**
 - Sensitivity reduction can be tailored with amount of FEM
- PBXN-9 FEM (Containing 90% FEM)
 - Card Gap
 - 186 Cards (Baseline HSAAP Data) / 156 Cards (HSAAP Data)
- LX-14 FEM (Containing 80% FEM)
 - Card Gap
 - 236 Cards (Baseline HSAAP Data) / 166.5 Cards (ARDEC Data)
- No degradation in lethality
- Current IM technology employed
 - No new or exotic cost prohibitive compounds
 - No change in HSAAP manufacturing techniques
- Materials successfully produced to the HSAAP Pilot Plant
- Products currently being assessed in the industrial base LAP infrastructure
- DOD Weapon Platforms
 - Technology could limit expensive full qualification costs for implementation of FEM

Acknowledgements



- Phil Samuels

- R&D Analytical Group
- David Price, Jacob Morris, Paul Lucas, Neil Tucker, Erica Lotspeich, Robyn Wilmoth

- Andy Davis
- Kyle Mychajlonka

Synthesis, Formulation, and Testing of 3,4-DNP

NDIA IMEMTS 2018

*Dr. Jacob Morris, Jim Phillips, Dr. Neil Tucker, Dr. David Price
BAE Systems Ordnance Systems Inc.
Holston Army Ammunition Plant, Kingsport TN, USA



Melt-Pour Ingredient Objectives

Ingredient Development Overview

- Identify and Prepare New Melt Pour Ingredients with ~Comp B Performance
- Evaluate Using Small Scale Safety and Performance Testing
- Evaluate Scalability of Synthesis
- Evaluate Formulation Characteristics

Selection Criteria

- Melting Point in Desired Range (80-110 °C)
- Sufficiently High Density /Performance
- Ease of Preparation
- Scalability
- Environmental / Handling Issues



What's Wrong with Comp B?

Environmental

- DoD utilizes a large amount of Comp B in artillery and mortar rounds
- RDX and TNT have known toxicity concerns and contaminate soil and groundwater
 - RDX has become an undesirable component of new munitions formulations because it causes neurological effects in personnel, and is a possible human carcinogen.
 - RDX has also become an environmental contaminant of concern

Performance

- Comp B does not meet current “IM” (Insensitive Munitions) requirements mandated by DoD
 - Both RDX and TNT contribute to the lack of IM

IM Test:	Fast Heating	Slow Heating	Bullet Impact	Fragment Impact	Sympathic Reaction	Shaped Charge Jet Impact
Passing Criteria	V	V	V	V	III	III
120mm (Comp B)	II	I	I	I	(I)*	(I)*

Analytical Requirements

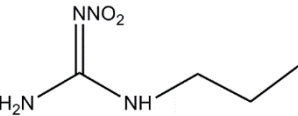
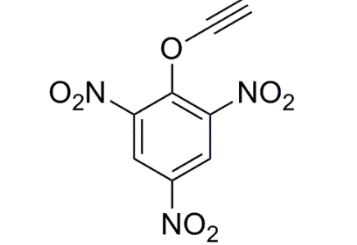
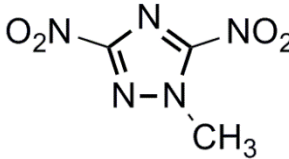
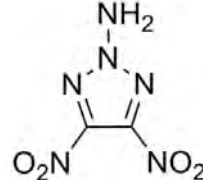
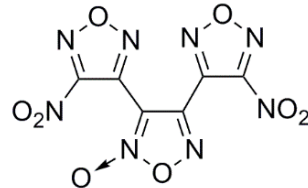
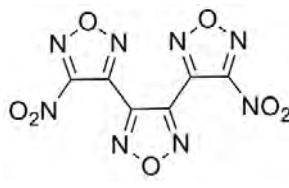
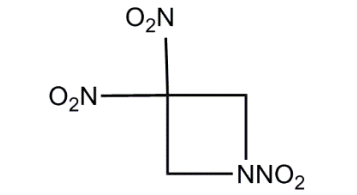
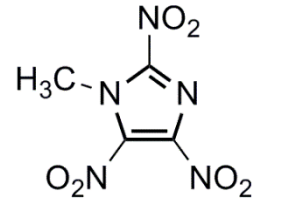
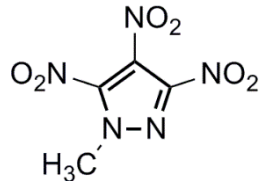
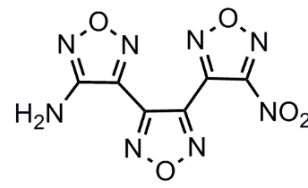
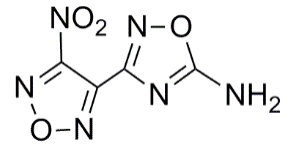
<i>Properties</i>	<i>Method</i>	<i>Minimum</i>	<i>Maximum</i>
Density (g/cm ³)	Gas Pycnometry	1.7	-
Exotherm Onset	DSC	150°C	-
Thermal Stability	VTS (48h@100°C)	-	2 cc/g
Purity	Chromatography (GC or HPLC) or NMR	95%	-
Det. C-J Pressure	Calculated by Cheetah 7.0	30 GPa	-
Detonation Velocity	Calculated by Cheetah 7.0	8.0 km/s	-

Additional Data Requirements:

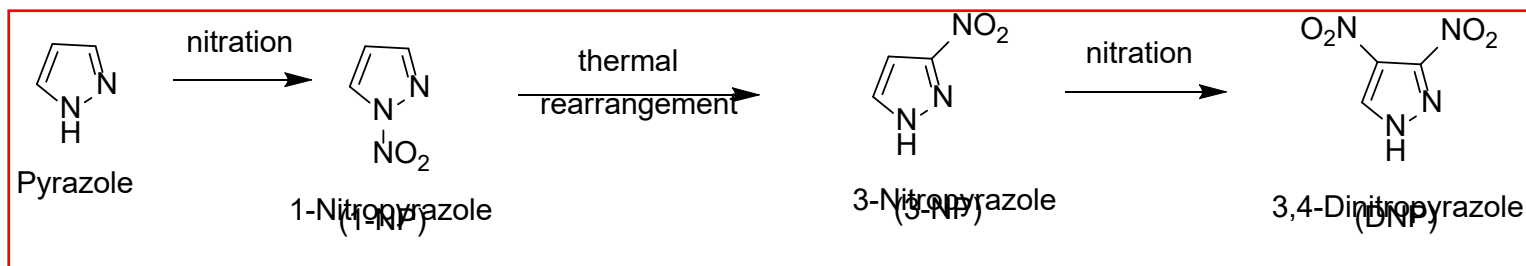
- Sensitivity (Impact, Friction, ESD)
- Heat of Formation
- Compatibility (DSC or VTS)

Melt-Pour Candidates

Issues Encountered:

Performance	Toxicity / Vapor Pressure	No. of Synthetic Steps / Reaction Conditions			
 <p>PrNQ</p>	 <p>PiPE</p>	 <p>MDNT</p>	 <p>DNAT</p>	 <p>BNFF (DNTF)</p>	 <p>LLM-172</p>
 <p>TNAZ</p>	 <p>MTNI</p>	 <p>MTNP</p>	 <p>LLM-175</p>	 <p>LLM-201</p>	

3,4-DNP Overview



DNP Advantages

- Insensitive to impact, friction, ESD
- Performance exceeding Comp-B
- Inexpensive starting materials
- High yielding, 1-step synthesis
- Chemistry can be readily scaled at HSAAP

Property	Comp. B	DNP
Melting Point (°C)	80	87
Density (g/cm ³)	1.68	1.79
Exotherm Onset (°C)		276
VOD (m/s)	7960	8115
Detonation Pressure (GPa)	29.2	29.4
Oxygen Balance (%)	-43.0	-30.4
Impact Sensitivity h _{50%} (cm)	75	147

DNP Sensitivity

Impact

Sample	Holston Short Impact (cm)	Navy Impact (cm)
DNP (Purified)	>80	94.8
RDX Standard	42.8	21.9

Friction

Sample	Friction (N)
DNP (Purified)	246
RDX Standard	164

ESD

Sample	ESD (J)
DNP (Purified)	0.26
RDX Standard	0.03

✓ DNP less sensitive than RDX

VTS Compatibility

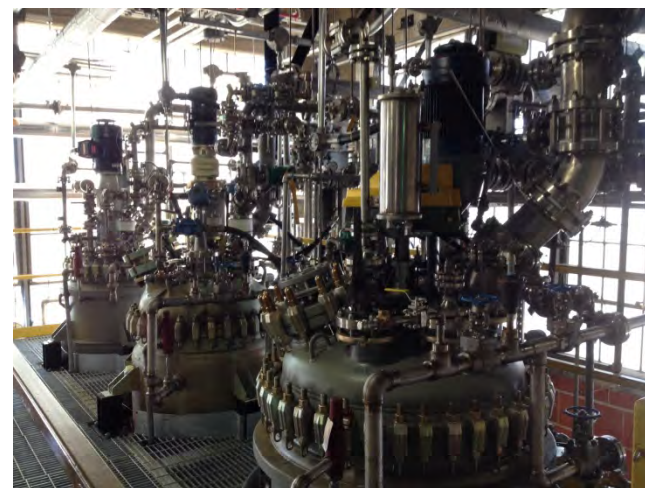
	Neat	RDX	HMX	NTO	LLM-105	HK-56	DNGU	Aluminum	Carbon Steel
DNP	---	Pass	Pass	Pass	Pass	Pass	Pass	Pass	Pass

- VTS Compatibility by STANAG 4147 Test 1B:
 - 2.5 g of DNP mixed with 2.5 g other ingredients
 - Total gas evolved after 40 hrs at 100 °C must be less than 5 cc of neat material
- **All materials were compatible as tested**

DNP – Pilot Plant

- Process scaled from lab to pilot plant at Holston
- Process:
 - Mixed acid nitration of 3-NP to DNP
 - Solvent recrystallization
 - Isolated and dried
- Total Yield: **>300 lbs**
- Material for further formulation/testing at BAE Systems and ARDEC

Purity	Nitrate wt%	Sulfate wt%
>99.5%	<0.02	<0.02



USPHC Toxicity Testing

- Early DNP Testing from USPHC:
 - Ames Salmonella Assay: Positive
 - Mouse Micronucleus Test: Negative

USAPHC Phased Approach Testing (ASTM E-2552-08)

	Oral	Inhalation	Dermal	Ocular	Reproduction/Development	Mutagenicity
DNMT	Low	Low	Moderate	Low	Low	High
DNP	Moderate	Low	Moderate	Low	Low	High
TNT	Moderate	Low	Moderate	Moderate	Low	High
RDX	Moderate	Unknown	Low	Low	Low	Moderate

Compound	Green algae	Daphnia	Fish	Earthworms	Transport	Persistence	Bioaccumulation
TNBA	Moderate	Low	Low	Unknown	Low	High	Low
PiPE	Low	Low	Low	Unknown	Low	High	Low
DNMT	Low	Low	Low	Unknown	High	High	Low
DNP	Low	Low	Low	Unknown	High	High	Low
TNT	Low	Low	Moderate	High	Moderate	High	Low

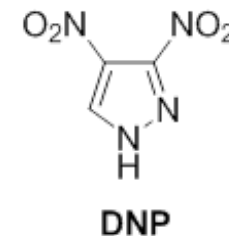
- No unusual DNP environmental toxicity issues

Results-Ingredient Testing (ARL)

- Ingredients were sent to Army Research Lab for Kow, Koc, water solubility, and vapor pressure testing:

Sample	VP (torr; estimated)			$\Delta H_{\text{vap (est)}}$ kJ/mol
	25°C	70°C	100°C	
DNP	2.42×10^{-11}	1.57×10^{-08}	2.72×10^{-06}	141.4
TNBA	1.59×10^{-07}	6.66×10^{-05}	3.08×10^{-03}	121.7
TNT	5.50×10^{-06}	2.31×10^{-03}	5.77×10^{-02}	114.1
RDX	3.30×10^{-09}	2.76×10^{-06}	9.92×10^{-05}	127.1
HMX	3.01×10^{-15}	3.14×10^{-11}	4.37×10^{-09}	174.7

- ✓ DNP has lower vapor pressures than TNT
- ✓ Soluble in water but low tendency to bioconcentrate in aquatic life.



DNP Dermal Testing

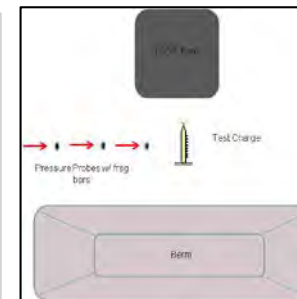
- “DNP was found to elicit a low-to-mild hapten formation response by DPRA (direct peptide reactivity assay). Thus, DNP is found to be **mildly sensitizing** by analysis with DPRA.”
- “The mild reaction by DPRA indicates that exposure to DNP in an occupational setting should be considered **generally safe with appropriate precautions**. Sensitization to the compound could potentially occur over an extended period of exposure, but with adequate PPE, this can be mitigated. The DPRA is best analyzed in conjunction with additional in vitro skin sensitization assays and in correlation with in silico analysis of the physical and chemical properties in order to accurately predict its sensitizing potential.”
- “DNP was found to elicit a positive reaction for both sensitization markers in the THP-1 monocytic leukemia cell line, a dendritic cell surrogate. Both CD54 and CD86 expression levels were increased as a result of 24-hour exposure to DNP. Thus, **DNP is a sensitizer according to the h-CLAT test.**”-(Toxicology Study No. S.0024589d-15)
- BAE is requiring R&D personnel to **wear Tyvek suits and full-face respirators** while handling DNP in heated, molten phase and when handling solid DNP outside of adequate ventilation and engineering controls (i.e. hood).

Proper Engineering Controls and PPE for safe handling

DNP Performance Testing

DNP Explosive Performance Testing:

- Rate Stick / Plate Dent (ARDEC)
- Critical Diameter (BAE Systems)
- Shock Overpressure (BAE Systems)
- LSGT (BAE Systems)



Performance Rate-Stick / Plate-Dent

- Detonation velocity and pressure of DNP tested
- DNP pressed to a density of 1.75 g/cc
- Results compared to Comp. B and DNMT

	Pressure (Calc) GPa	Pressure (Exp.) GPa	VOD (Calc) m/s	VOD (Exp.) m/s
DNP	29.1	30.2	8,246	8,115
DNMT	27.5	24.8	7,710	7,800
Comp. B	26.1	27.6	7,900	8,018

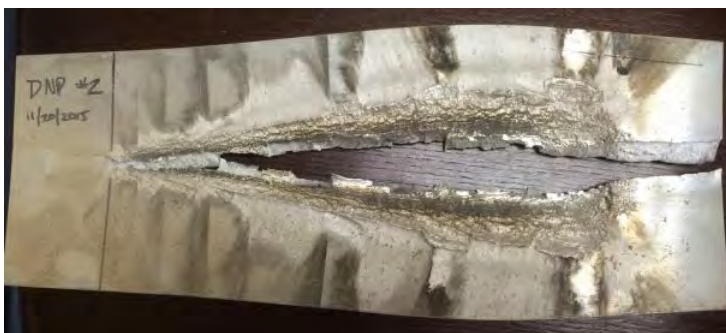


Critical Diameter Testing

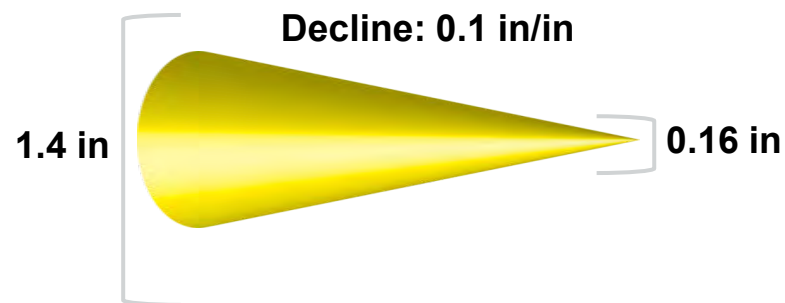
- Critical Diameter was determined by pouring conical charges of DNP into a split-mold
- Cone Parameters:
 - Maximum Diameter: 1.4 Inches
 - Minimum Diameter: 0.16 Inches
 - Declining Angle: 0.1 Inches per Inch
- Charges set on aluminum plate (16" x 6" x 0.5")
- **Critical diameter < 0.16 inches**
 - Propagation through length of explosive



DNP w/ #8 Detonator



Witness Plate



Large-Scale Gap Testing – DNP

- DNP poured into 6” steel tubes (~0.5 lbs of material, 96% TMD)

- Heated tubes required to obtain quality pours:

- No Visible Cracking/Crystalline Domains

- Steel Witness Plate used to provide a clear go/no-go indication:

- Calculated 50% Go/No-Go point based upon firings

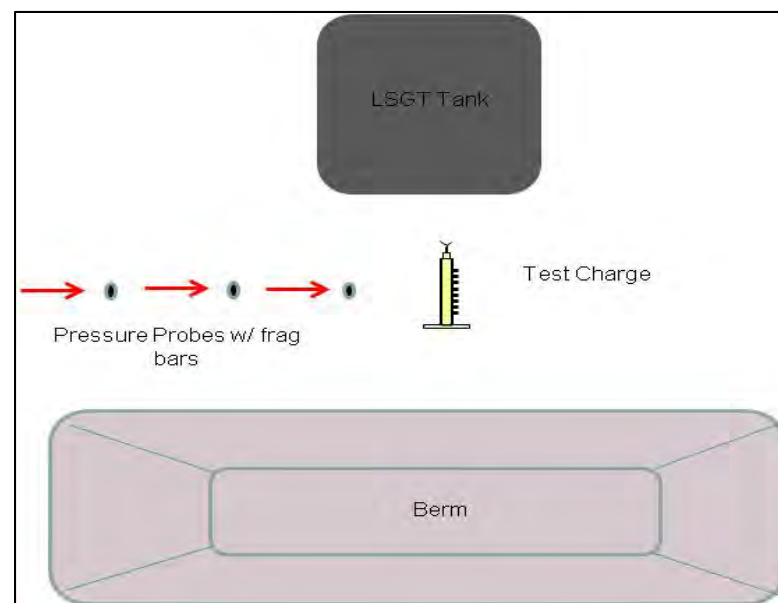
DNP: 193-195 cards (22.8-22.2 kbar)

Comp B: 215-225 cards (17.9-16.2 kbar)



Shock Overpressure Testing

- Degree of damage to surroundings related to:
 - Shock Overpressure
 - Shock Duration
 - Peak Impulse
- Overpressure measured by Piezotronic pressure probes
 - Oriented axially at 5, 10, and 15 ft
- DNP poured into tubes:
 - Sample size: 0.5 lbs
 - Density: 1.67 g/cc



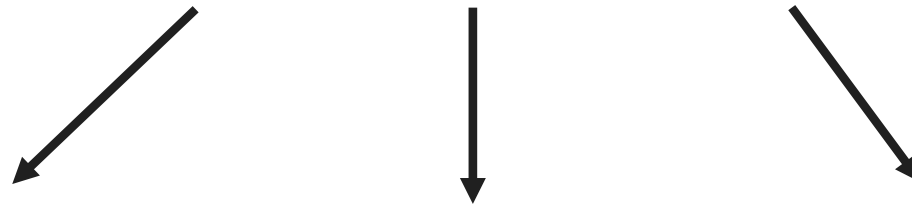
Shock Overpressure Testing

- Comparison testing shows that DNP is an extremely powerful explosive
- Better performance than current melt-pour explosives
- Performance close to LX-14 (95.5% HMX)

Shock Overpressure (Psi)

	<u>5 ft</u>	<u>10 ft</u>	<u>15 ft</u>
DNP	30.8	6.5	3.3
Comp. B	27.7	6.3	3.1
IMX-104	28.1	6.1	3.2
PBXN-7	27.5	6.4	3.2
LX-14	31.7	6.4	3.3

DNP Formulations



Octol
Replacement

IMX-101/104
Replacement

DNP w/ New
IM Ingredients

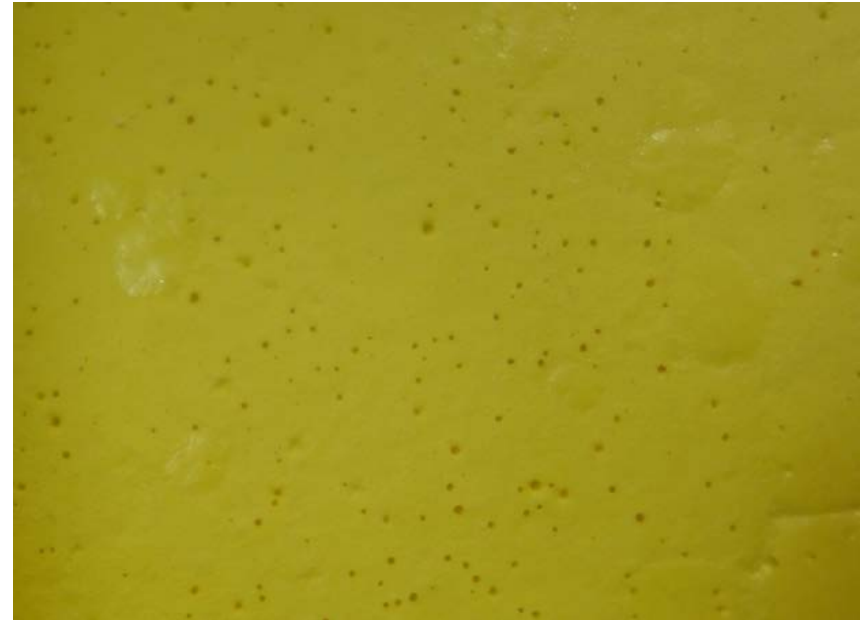
Octol Replacement

	Density (g/cc)	Pressure (GPa)	Det. Velocity (km/s)	Estimated Gurney
DNP: HMX (50:50)	1.84	33.4	8.65	2.95
Octol (25:75)	1.83	32.4	8.57	2.89

- Ability to get high solids loading with molten DNP
- 40-60% HMX gives similar performance as Octol (Type 1)
- Use of FEM/Nano HMX would help reduce shock sensitivity



New IM Ingredients Formulations



Composition	P _{cj} (Cheetah 7.0)	V/V _o (7.20) (Cheetah 7.0)	ERL Impact, cm	BAM Friction, N
DNP/DNGU/LLM-105	31.0	-7.78	82	328
Comp. B	27.0	-7.55	38	150

■ New IM Ingredients Formulations

- Fairly easy to get high solids loadings in DNP
- Due to high performance of DNP, LLM-105 was replaced with DNGU:
 - High DNGU solids loading
 - DNGU helps lower potential costs,
 - DNGU helps lower shock sensitivity
 - "Coarse" grade DNGU can be balanced by normal "fine" grade DNGU or FEM HMX.



Formulation	Composition	Pcj (Jaguar)	Gurney 7 vol (Jaguar)	ERL Impact, cm	BAM Friction, N
OSX-15	DNP/DNGU/HMX	31.3	2.78	50.6	277.2
Comp B	TNT/RDX (40:60)	26.4	2.81	38	150

Conclusion and Path Forward

Synthesis:

- Scalable synthesis route: DNP currently synthesized on pilot-scale
- >300-lbs of DNP synthesized to date
- Optimization of purification/recrystallization currently ongoing
- Inexpensive / High-Yield Process

Formulation:

- Formulation efforts are just beginning
- DNP has Comp. B performance: Formulations could have explosive performance greater than Octol

Testing:

- Additional Explosive Testing (BAE Systems/ARDEC)
- Formulation Testing (BAE Systems)
- Weapons Testing (ARDEC)



Great Potential as the Next-Generation Melt-Pour Base

Acknowledgements



US ARMY – ARDEC / ARL

Anthony DiStasio, Kate Maier, Phil Samuels, Omar Abbassi, Paul Anderson, Dr. Rose Pesce-Rodriguez
- Program Funding (FREEDM) and DNP Development Efforts



Strategic Environmental Research and Development Program

Robin Nissan
- Program Funding



US ARMY Public Health Command

Dr. Mark Johnson, Dr. William Eck, Dr. Emily Reinke
USA Public Health Command (USAPHC)



BAE SYSTEMS

Bowman Potter, Matt Hathaway, Dr. Jeremy Headrick, Dr. Tess Kirchner, Robyn Wilmoth, Kelly Guntrum, Chris Long, Brian Alexander, Todd Dye, Tracy Kelly

Improving knowledge of tactical rocket motor response under Insensitive Munitions threats

IMEMTS PORTLAND - April 2018

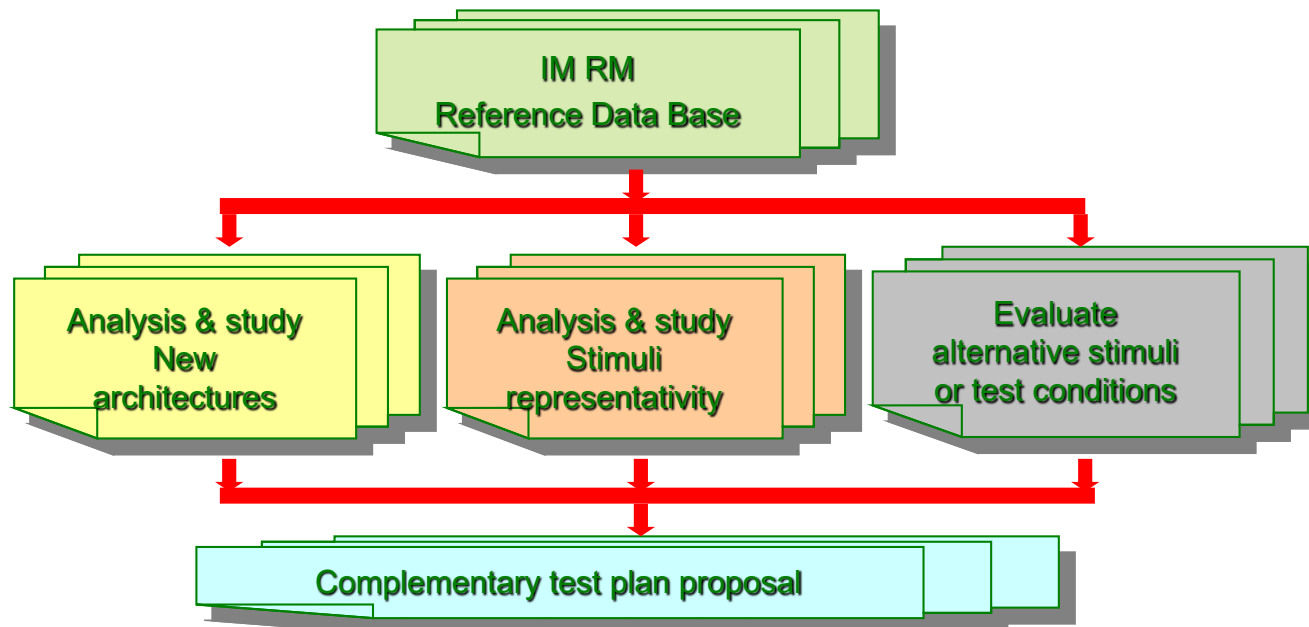
Laurent BONHOMME
Jean-Michel LARRIEU
Florian PECHOUX



- **INTRODUCTION**
- **IM ADVANCED RESEARCH PROGRAMME APTE**
- **FRENCH IM TACTICAL SRM DATABASE**
- **NEW GLOBAL IM PROTOCOL FOR TACTICAL SRM FAILURE MODE ANALYSIS**
- **TEST PLAN OUTCOME OVERVIEW**
 - **Test conditions (BI)**
 - **Alternative stimuli (BI)**
 - **New architecture (FH)**
 - **Lesson learned : Test Set-up influence (BI)**
- **CONCLUSION**

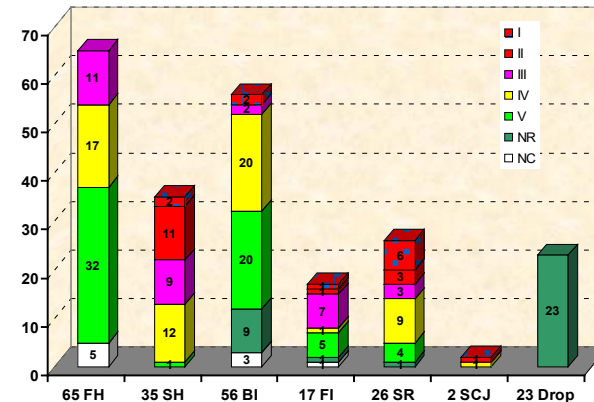
IM ADVANCED RESEARCH PROGRAMME APTE

- Over last 10 years, French MOD funded the Advanced Research Programme “APTE” (Tactical Propulsion Improvement).
- Advanced Research Programme conducted by French Rocket Motor manufacturers ROXEL and ARIANEGROUP.
- The IM part of the programme was devoted to:
 - Search the best IM compromise for solid rocket motor hardware,
 - Analysis of the standard stimuli representativeness and results interpretation,
 - Evaluate the impact of alternative stimuli or test conditions



FRENCH IM TACTICAL SRM DATABASE

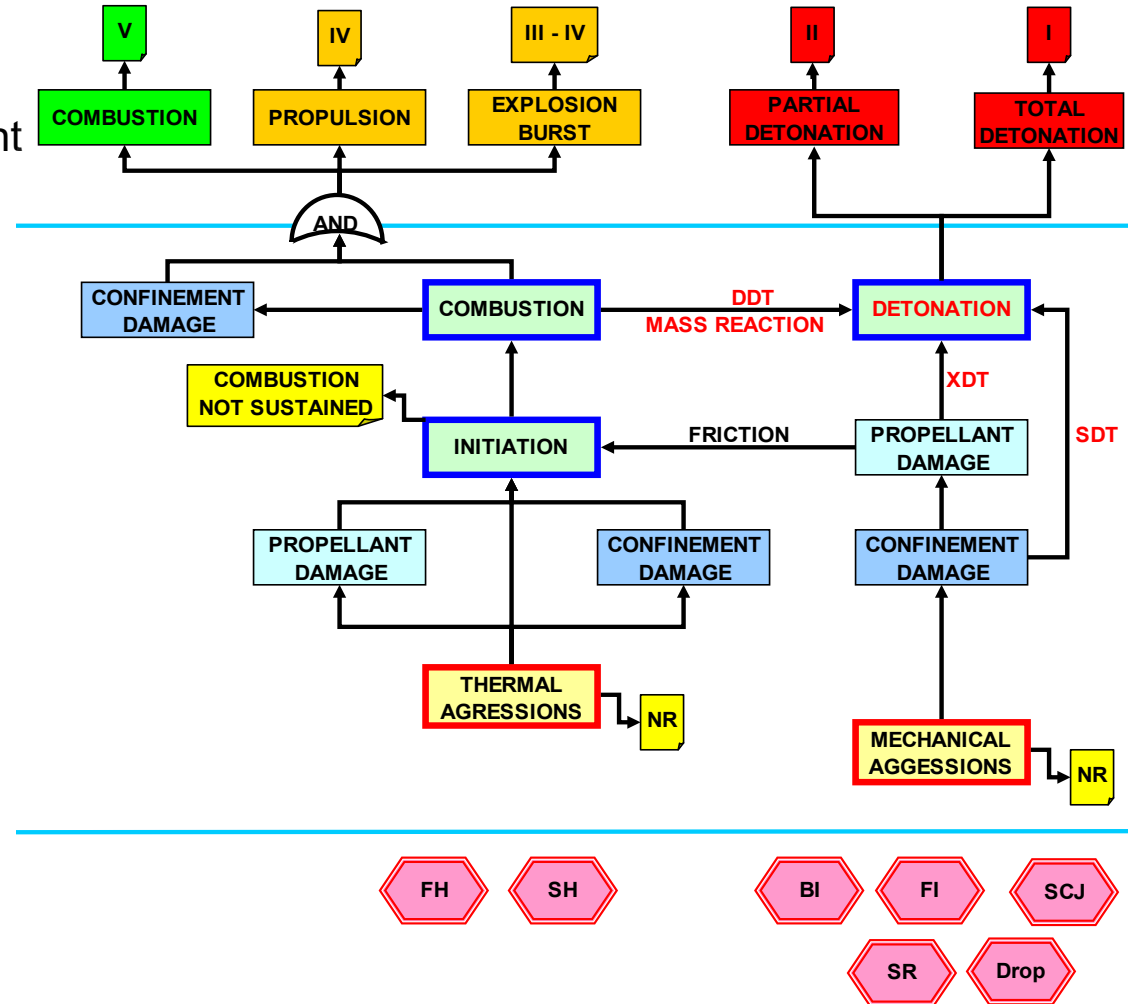
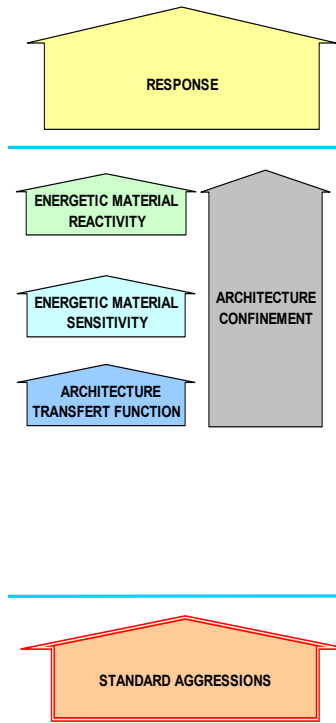
- A database has been populated with more than 220 different test results conducted on Solid Rocket Motors (SRM) and mock-ups in France since the 80's, and is continuously populated with new results.
- Characteristics of the tested objects are :
 - Diameter up to 350 mm
 - Metallic, composite and hybrid cases
 - All propellants and igniters types
 - Propellant mass up to 200 kg
- Tests characteristics, compliance or not with corresponding STANAG test procedure
- Tests Results with main measurements and hazard classification (reaction level)
- Database contents :
 - 65 Fast Heating tests (FH)
 - 35 Slow Heating tests (SH)
 - 56 Bullet Impact tests (BI)
 - 17 Fragment Impact tests (FI)
 - 2 Shape charge jet tests (SCJ)
 - 26 Sympathetic Reaction tests (SR)
 - 23 Drop tests



→ Identification of deficiencies and gaps in the technology and knowledge

NEW GLOBAL IM PROTOCOL FOR TACTICAL SRM FAILURE MODE ANALYSIS

- New protocol is based on AOP39 ones but :
 - dedicated for tactical Solid Rocket Motors (SRM)
 - applicable for all stimuli
- SRM architecture effects are detailed :
 - SRM materials design and confinement
 - Propellant sensitivity and reactivity
 - Stimuli

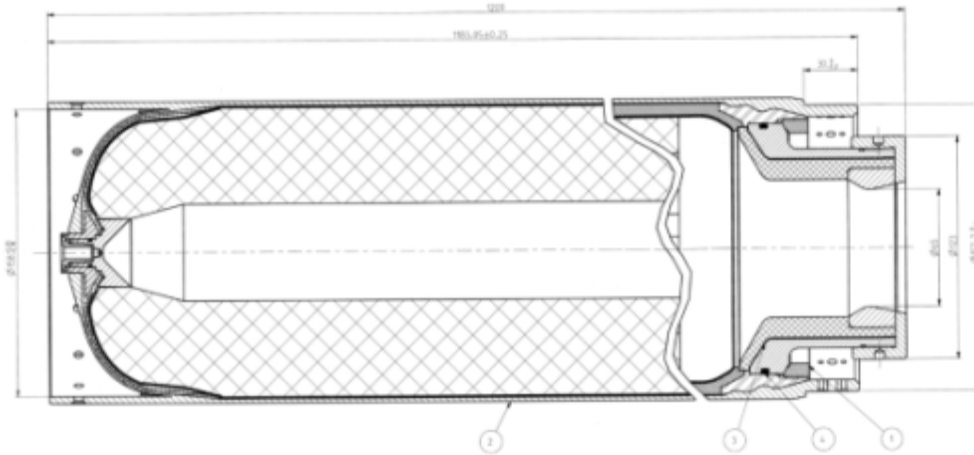


TEST PLAN OUTCOME OVERVIEW : Test conditions (BI)

➤ Effect of the temperature on SRM response to BI aggression:

- Three temperature evaluated : Ambient, -40°C, +70°C

➤ Specimen tested :



➤ Main characteristics :

- Composite carbon fibre case (external diameter : 160 mm / Length: 1209 mm)
- High Burning Rate Propellant (Finocyl shape / about 30 Kg)

➤ BI Tests results :

- Test conditions : 20°C, Bullet impact velocity = 843 m/s



→ **Type Iv** (Fragments < 15 m but rear end total displacement > 15 m)

- Test conditions : -40°C, Bullet impact velocity 838 m/s



→ **Type III** (Fragments and burning propellant up to 110 m)

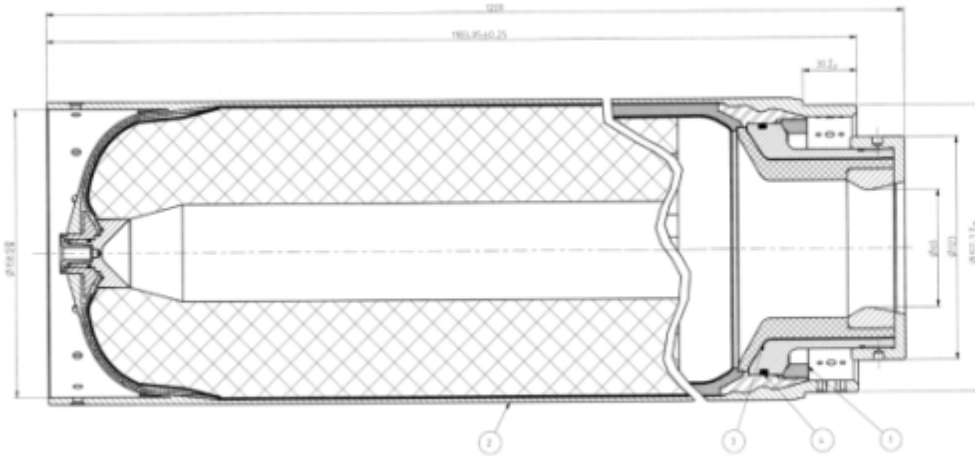
- Test conditions : 70°C, Bullet impact velocity 830 m/s



→ **Type Iv** (Fragment < 15 m but rear end total displacement > 15 m)

TEST PLAN OUTCOME OVERVIEW : Alternative stimuli (BI)

- **Alternative stimuli** : Explosive armor piercing 12,7 mm Bullet
- **Specimen tested** :



- **Main characteristics** :

- Composite carbon fibre case (external diameter : 160 mm / Length: 1209 mm)
- High Burning Rate Propellant (Finocyl shape / about 30 Kg)

TEST PLAN OUTCOME OVERVIEW : Alternative stimuli (BI)

➤ BI Tests results :

- Test conditions : 12.7 mm AP Bullet at 843 m/s (Reference)



→ **Type IVp** (Fragments < 15 m but rear end total displacement > 15 m)

- Test conditions : 12,7 mm explosive AP Bullet at 863 m/s (Alternative)

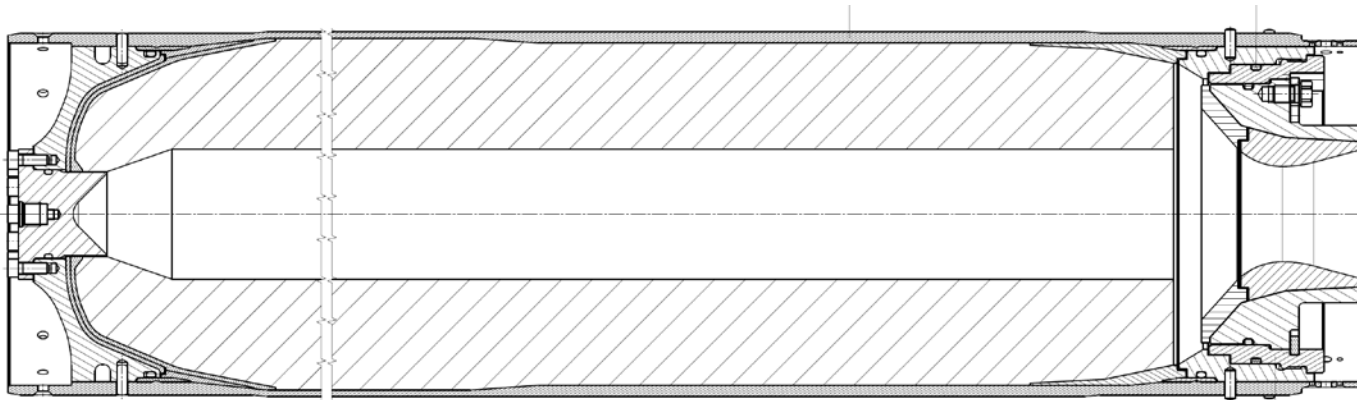


→ **Type IVp/III** (Rear end moved and stopped at 43 m , burning propellant up to 200 m)

➤ New architecture :

- Optimised confinement release to FCO aggression

➤ Specimen tested



➤ Main characteristics :

- Composite kevlar/carbon/Kevlar fibre case with 180°C resin (external diameter : 165 mm / Length: 1200 mm)
- Passive venting rear end
- IM advanced propellant (30 Kg)

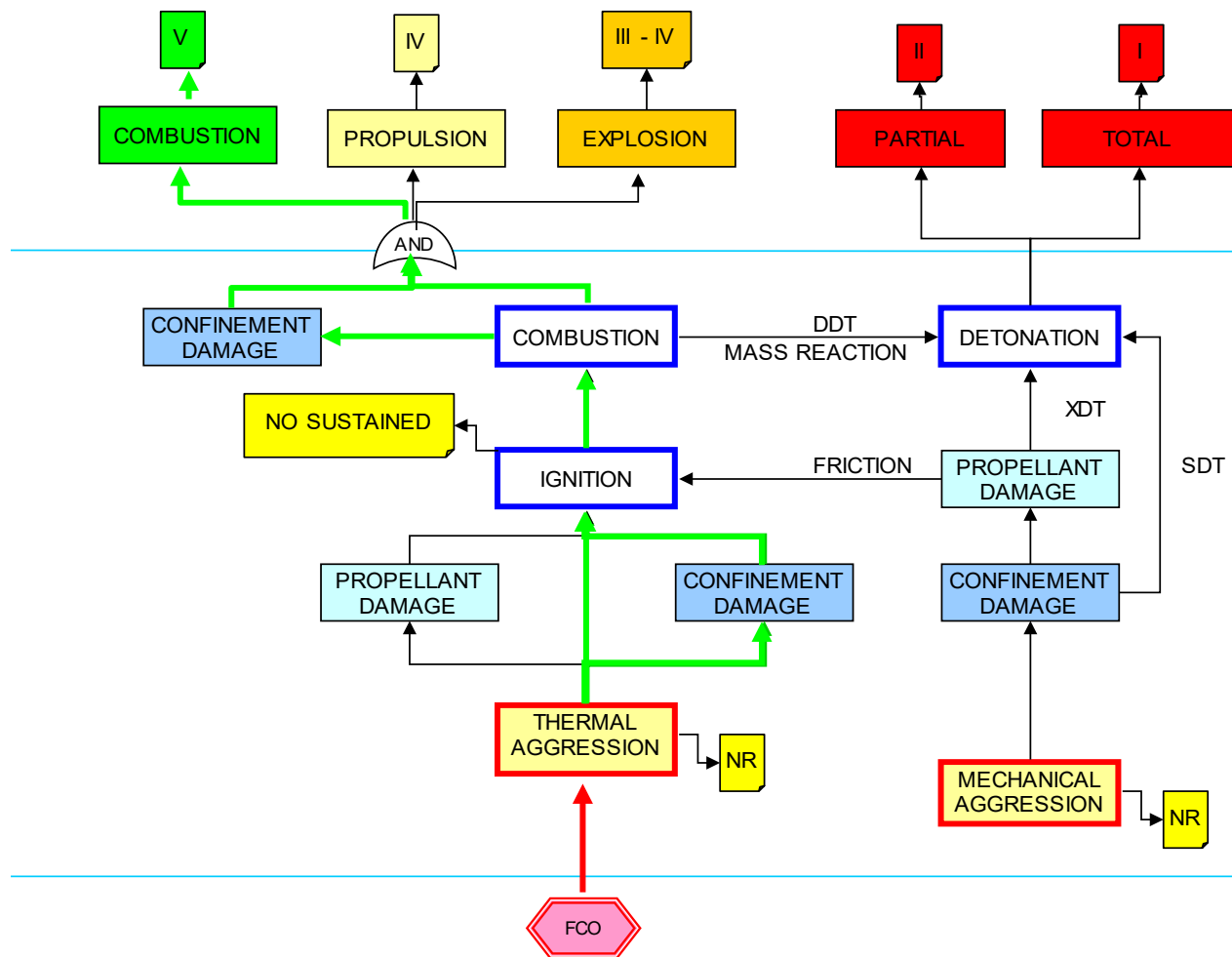
➤ FH Test results :

- Average temperature : 950°C
- Results :
 - Reaction at 74s
 - Overall deconfinement of the structure at low pressure (composite case and rear end passive venting)
 - No thrust
 - Fragments :
 - Passive venting rear end recovered in the pool
 - Inert fragment < 15m
 - Unburned propellant < 30m

→ Classification : Type V



➤ Application of the global IM protocol for SRM :



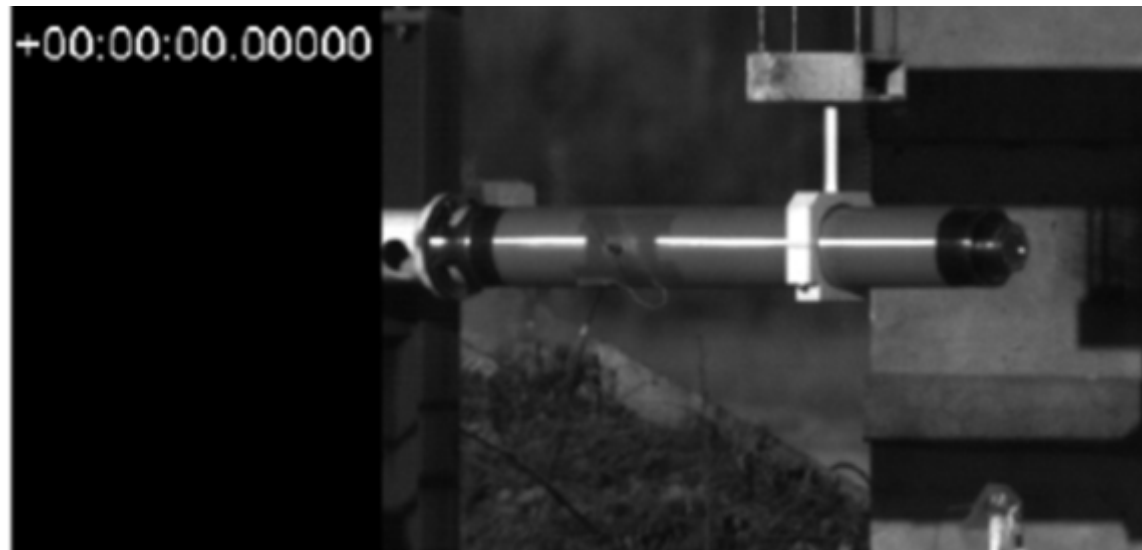
TEST PLAN OUTCOME OVERVIEW : Lesson learned – Test set-up influence (BI)

➤ Specimen overview :



- Kevlar over-wrapped grooved steel case (external diameter : 165 mm / Length: 1340 mm)
- High Burning Rate Propellant (Finocyl shape / about 30 Kg)

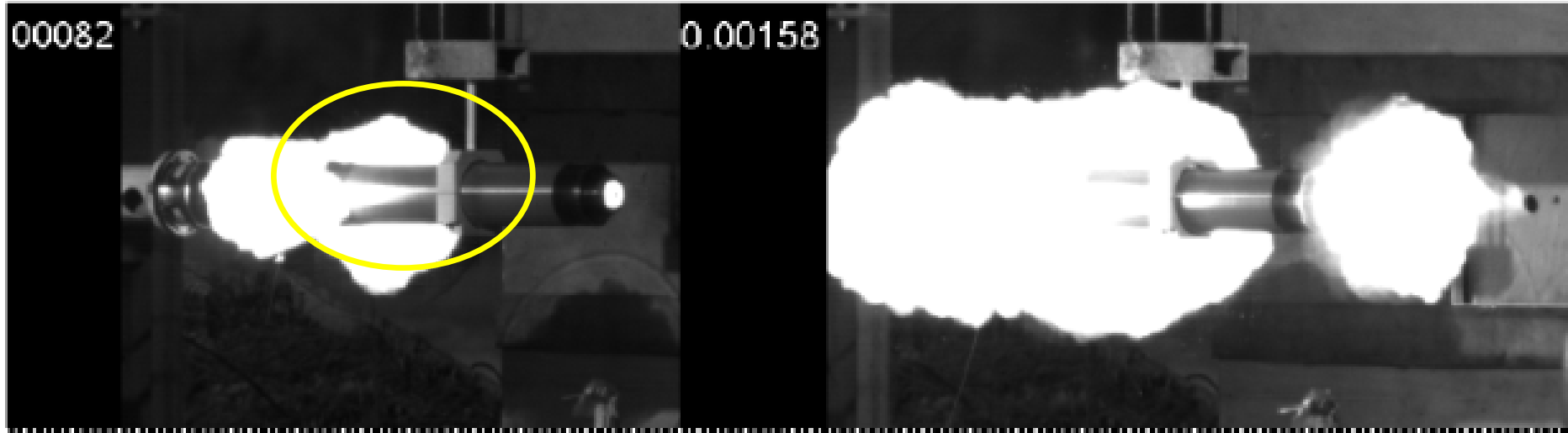
➤ BI Test Set-up :



TEST PLAN OUTCOME OVERVIEW : Lesson learned – Test set-up influence (BI)

➤ BI Test results :

- Test bench rear belt support prevented full venting of the case at low pressure :



➔ **Classification : Type IV instead of Type V expected** due to test bench attachment mean

CONCLUSION

- Identification of deficiencies and gaps in the technology and knowledge to be evaluated in IM ARP APTE.
 - Simple and unique SRM protocol for all IM aggressions has been established
 - About 40 full scale tests performed by DGA French test centre
 - Knowledge gap filled
- Interest of new architecture to upgrade the reaction level classification
 - Some architectures have been identified to be used for future applications
- Alternative stimuli and test conditions impact evaluated
- Lesson learned : Take care about test set-up influence



Acknowledgements & Questions



Members of



Any Questions ?

UNCLASSIFIED

**2018 Insensitive Munition and Energetic Materials Technology Symposium
Portland, OR, 23-26 April 2018**

Fragment Impact Testing of the XM25

Nausheen Al-Shehab*, Kevin Miers

U.S. Army RDECOM-ARDEC, Picatinny Arsenal, NJ 07806-5000
Nausheen Al-Shehab, E-mail: nausheen.m.alshehab.civ@mail.mil

The developmental XM25 Counter Defilade Target Engagement (CDTE) is a shoulder-fired weapon designed to provide U.S. Soldiers with the capability of engaging targets under cover. Current cartridges include the XM1083 High Explosive Airburst (HEAB) and XM1081 Target Practice (TP) rounds. Baseline IM tests were conducted against the packaged configuration and showed that HEAB cartridges react violently when subjected to fragment impact (FI). This is consistent with modeling predictions that the first impacted round will likely react violently as the induced shock strength for small caliber items is particularly sensitive to fragment attitude and hit location error even though the fragment likely breaks up on perforation. Continuum modeling also suggest significant mechanical insult to adjacent rounds should only a single round detonate, both in FI and Sympathetic Reaction (SR) scenarios. This is consistent with engineering level SR tests performed for packaged rounds which indicate violent reactions for adjacent and diagonally adjacent acceptor rounds. Several FI mitigation strategies are discussed and modeled to predict their effectiveness. FI testing of the TP cartridges (inert warhead with live propellant) were conducted to determine how much of the reaction was due to the propulsion vice how much was the result of the warhead. While these responses were generally benign, in all these tests the lid was repeatedly thrown a significant distance from the initial test location. FI tests against containers with inert simulants were conducted to determine how far debris was expected to be thrown as a function of fragment momentum alone. These results were compared with those determined via high-rate continuum modeling. It was determined, both experimentally and computationally, that the propellant alone was sufficient to project hazardous debris.

Distribution Statement A: Approved for public release; distribution is unlimited.

UNCLASSIFIED

Introduction

As part of an ongoing, developmental 25mm program, a host of complete rounds are under development. Efforts to improve the Insensitive Munition (IM) response of these all up rounds (AUR) are currently under way and include the XM1081 target practice (TP) and XM1083 High Explosive Air Burst (HEAB) AUR (Figure 1). The XM1083 HEAB is a next generation of medium caliber technology with fore and aft, air bursting warheads. The propulsion for both the XM1083 HEAB and XM1081 TP cartridges features a standard percussion primer and a small amount of small caliber gun propellant. Both warheads in the XM1083 projectile are loaded with PBXN-5. The XM1081 TP fires a projectile with ballistically similar performance to the HEAB cartridge, but without any energetic filler.

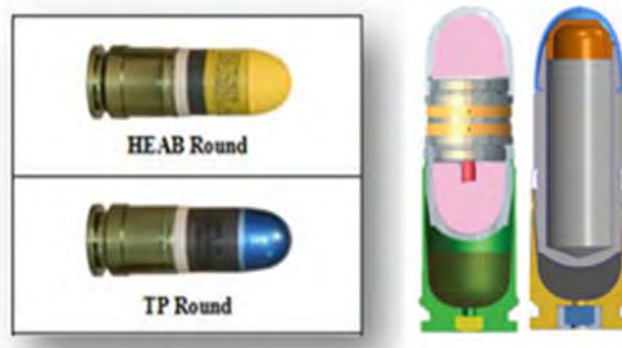


Figure 1. HEAB and TP Cartridges.

HEAB AUR FI Testing

Fragment Impact (FI) tests were conducted as per MIL-STD-2105D and NATO STANAG 4496 [1]. For these experiments, test articles were placed less than 15m from the muzzle in order to reduce impact variability [2, 3], including pitch, yaw, hit location, and velocity. An example of the setup can be seen below in Figure 2. Fragment impact velocity of 2530 ± 90 m/s, with an alternate velocity of 1830 ± 60 m/s, are specified in the STANAG. The 14.3mm mild, steel fragment has an aspect ratio (L/D) of approximately 1 with a conical ogive possessing a 160° included angle.



Figure 2. Typical fragment impact test setup

HEAB Packaged Configurations

FI tests were conducted in both the tactical, that is operational, and logistical configurations. In the tactical configuration, the 40 XM25 AURs are loaded in a single PA108 metal ammunition can containing two fiberboard boxes. These boxes are stacked one on top of the other with all of the noses of the AUR pointed

Distribution Statement A: Approved for public release; distribution is unlimited.

down with each round separated from its neighbor with fiberboard dividers. The two boxes are subsequently offset, so that the primers do not line up with the cartridges above or below. The PA108 container is roughly 20 cm long, 32 cm high and 32 cm wide. The logistical configuration consists of two full PA108 ammunition containers packed in a wire-bound, wooden crate. Both configurations are shown below in Figure 3.



Figure 3. Closed tactical (left), open tactical (center) and logistical configurations (right).

FI testing is performed against both the warhead and the propellant to determine the participation of each in the overall reaction. For the logistical and tactical configurations, the shot line is determined by the longest line-of-site of the cartridges. In the tactical case with only a single container, the fragment is fired into the end. In the logistical configuration, with two ammo containers packed side-by-side, the fragment is fired into the side of the container. Aim point heights and shot line are shown in Figure 4.

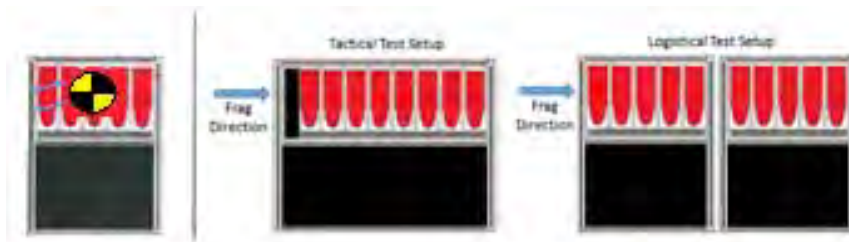


Figure 4. Fragment impact aim points and firing direction

HEAB AUR Engineering Tests

Two engineering tests were conducted against the explosive and propellant in the tactical configuration. Figure 5 shows the results of both tests. The state of the test arena after both tests was very similar. Some XM1083 cartridges traveled more than 30m and landed outside of the arena. The fragment velocities for both tests were measure by high speed video (HSV) and determined to be within the allowable velocity tolerance: 2448m/s for the propellant test and 2527m/s for the explosive. In both tests, the packaged cartridges did not mass detonate and most of the individual cartridges survived intact but were strewn around at various distances in and around the arena. The witness plate from Test 2 (along the explosive shot line) shows more scarring and slight bowing. The witness plate for the propellant shot line exhibited minimal damage. Based on this data, the results from the fragment impacting the explosive were found to be more violent than those achieved from propellant impact.



Figure 5. Engineering Tests: (a) Recovered witness plates; (b) Post Test Images

Distribution Statement A: Approved for public release; distribution is unlimited.

Formal HEAB Testing

Formal FI testing was conducted against both the HE and propellant of the HEAB AUR. The first test, fired against the HE as shown below in Figure 6 a., was in the logistical configuration. The fragment impacted at a velocity of 2461 m/s. The lid of the first container was thrown a significant distance from the test stand and cartridge and container fragments were scattered throughout the arena. The second container exhibited a very different response. It survived intact and none of the cartridges contributed to the response. The farthest fragment recovered was 27m from the test stand with no visible damage to the witness plate.

The second single container FI test was conducted in the tactical configuration against the propellant. This time the fragment achieved a slightly higher velocity of 2517m/s. The container was torn to pieces, with only a few large portions recovered (Figure 6b.). The witness plate showed damage from both the container and cartridges and the farthest fragment recovered was a cartridge case with fuzed projectile found over 46m from the test stand.



Figure 6. Formal Tests: (a) Explosive Impact- test setup, Post-test, Recovered debris; (b) Propellant Impact- Post-test stand/witness plate and recovered debris

These were officially scored packaged tests, in contrast to engineering or component tests conducted previously. The FI test against the propellant was determined to have resulted in a Type II reaction and against the explosive, it was scored as a Type III. Both engineering level tactical configuration and formal logistical configuration FI tests of packaged HEAB cartridges showed that impacting the explosive resulted in an explosion reaction. Tactical configuration tests of the packaged HEAB cartridge, including both engineering level and formal impacts conducted against the propellant resulted in mixed scores. There are a number of variables that can affect the response of munitions subjected to FI testing [3, 4]. These include fragment attitude, both pitch and yaw, velocity variation and aim point errors. Given that the fragment size is on the order of the explosive and propellant cross sectional diameter, it is possible that only slight variations in aim point result in greater violence when the shot line is through the propellant than when it is through the explosive.

Formal TP Testing

In addition to the formal testing conducted against the HEAB AURs as discussed in the previous section, five additional FI tests were conducted against packaged TP AURs. Since the TP cartridges contained only propellant, these tests were conducted with the goal of isolating the contribution of the propellant to the reaction of the HEAB AUR when impacted through the propellant shot line. Four of these tests were conducted at the standard velocity of 2530 ± 90 m/s with two each conducted in the tactical configuration, and the remaining two conducted in the logistical configuration. One tactical test was conducted at a velocity of approximately 2000m/s. Although all responses were generally benign, the lid was repeatedly thrown over 30m in each test. Figure 7a are HSV images that clearly show the lid being launched as a result of the system response. At the lowest impact velocity, the lid bowed but was not perforated. In all the other tests that achieved a satisfactory mean velocity, the lid was perforated between the first and second cartridges. Generally the lids were thrown farther when tested in the tactical configuration than in the logistical configuration, owing their different response, at least in part, to the additional confinement offered by the wooden packaging. It is important to note however, that the lowest velocity tactical test resulted in the lid being thrown the farthest. This is in contrast to the high velocity tests, potentially due to the uninhibited

pressure build-up of the burning propellant as the lid was not perforated by fragmentation as it was in the higher velocity tests. Figures 7b and 7c show the container and lid for these tests.



Figure 7. TP FI Test Results: (a) HSV images; (b) logistical configuration; (c) tactical configuration

Modeling Inert Cartridges

FI modeling utilizing inert cartridges was conducted using the Lawrence Livermore National Laboratories (LLNL) developed code ALE3D. This was done in an attempt to understand the interaction between the fragment and the container, independent of any contribution from an energetic reaction. Modeling results, shown below in Figure 8, suggest that the holes in the lid are caused by debris thrown when the fragment impacts the cartridge, and that the lid is likely thrown due to a hydraulic effect as suggested above.

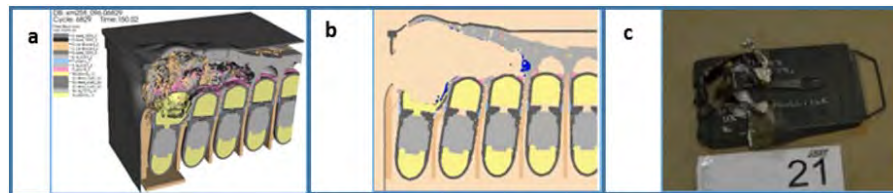


Figure 8. Inert propellant model compared to live propellant TP response.

Inert Simulant Modeling and Testing

Tests were conducted against PA108 containers with inert simulants to evaluate debris thrown exclusively as a function of fragment momentum. Solid aluminum cylinders were used as projectile simulants. Two tests were conducted at the mean velocity of 2530 ± 90 m/s, and in both tests the lids were thrown from the test stand but not as far as in the previous TP tests. In addition, there were also no holes in the lids as a result of these tests. This also suggests that the holes are caused by the debris field from the cartridge case fragments. Figure 9a shows the output from modeling conducted using the Elastic Plastic Impact Code (EPIC) [4] with pictures of the inert simulants from each test. These results do not indicate that the lids would likely be launched. HSV was also used to record the event and selected frames are shown in Figure 9c. These frames show the event and again, the lid appears to have been very violently separated and thrown from its original location.



Figure 9. Inert Surrogate: (s) EPIC model; (b) FI test debris; (c) High Speed Video frames of lid projection.

UNCLASSIFIED

Based on these results, the hypothesis is that as the fragment entered the confined container volume, it generated a significant hydraulic effect that subsequently propelled the lid. A scored or vented container might function to minimize this. Modeling the non-detonative response of a shocked granular propellant bed was impossible within the confines of time and funding afforded this project, so no attempt was made to model this complexity. Due to the lid being thrown five times farther in the TP tests than in the inert tests, the propellant reaction is believed to be the single most important contributing factor as to why the lid was thrown so far.

FI/Sympathetic Reaction (SR) Spacing Designs and Modeling

The chemical energy of an individual aft warhead is roughly half the kinetic energy of the incoming fragment, so it is conceivable that shock initiation of the first warhead under fragment attack, in conjunction with the residual fragment energy, is a more severe threat to adjacent cartridges than that which would result from SR alone. Assuming that the first warhead in the shot line always promptly detonates upon impact, SR test data can be used to help provide a lower bound for the reaction violence in adjacent cartridges.

Two SR tests were conducted, one with HEAB AURs, and another with TP AURs. Each test utilized a total of six live cartridges (one donor and five acceptors) per test, utilizing two layers of packaging. The acceptors were placed in the following positions: adjacent-1, diagonal-1, below-2, adjacent-2, and diagonal-2 (the numbers denote the top (1) or bottom (2) of the packaging). All of the cartridges were painted in order to determine the severity of reaction for each acceptor placement (Figure 10a.).



Figure 10. SR Test: (a) HEAB Engineering SR Test Cartridge Configuration; (b) HEAB Results

A detonator was used to initiate a donor HEAB round. The acceptor test items in the HEAB SR test reacted with a Type III explosion level of violence. Figure 10b shows the blast chamber and the collected debris. In particular, the adjacent and diagonal acceptor cartridges appeared to have deflagrated, and the bottom row warheads appeared not to have reacted. In light of these results, it was determined to be necessary to measure exactly how much more severe the FI threat was than that posed by SR. In addition, this information is desirable from the perspective of considering potential mitigation schemes. Within the model, an augmented CJ volume burn was used to light the explosive region in the first grenade warhead at the point of impact, and a Jones-Wilkins-Lee (JWL) equation of state (EOS) was used to describe the adiabatic expansion of the detonation products. Modeling predictions are shown in Figures 11 and 12.

These results indicate a directionality to the shock input to the adjacent cartridges, as would be expected for a completely inert target. The peak pressure in the second cartridge in the shot line is calculated to be substantially greater than the LSGT pressure threshold for this explosive. Although this criterion is not sufficient in and of itself, it is a qualitative benchmark useful for the purpose of making comparisons. The results also show that a reduction in the induced peak pressure of adjacent cartridges can be achieved by using a higher density separator material than corrugated fiberboard, such as a common polymer. Other efforts are ongoing in order to reduce sympathetic reaction violence in the event that prompt detonation of the first cartridge cannot reasonably be prevented. These include evaluation of different round to round spacing and packaging configurations.

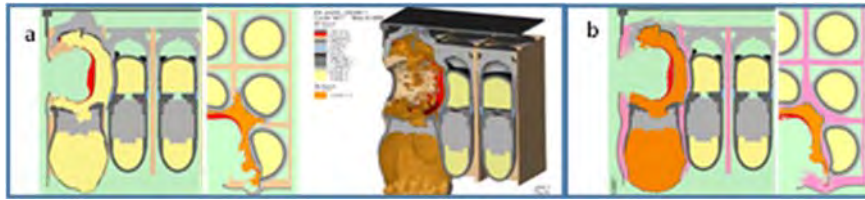


Figure 11. Material plots for first live cartridge subjected to FI: (a) baseline; (b) plastic separator configuration (right)

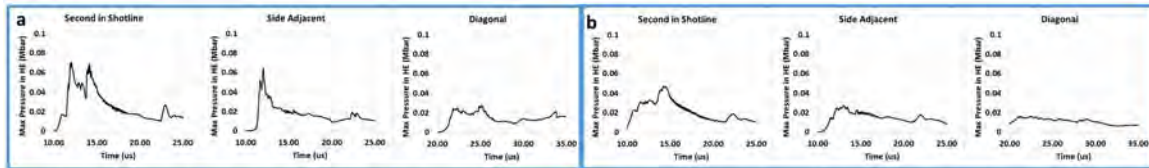


Figure 12. Maximum pressure in HE region (Mbar) vs. time (us) plots for cartridges, (a) baseline and (b) plastic barrier configurations

Barrier Designs and Hydrocode Modeling

Particle Impact Mitigation Sleeves (PIMS) are one technique that has been successfully used in the past to mitigate violent response of ordnance subjected to FI [5]. PIMS may be used on the outside of the packaging, on the inside of the packaging but on the outside of the munition, internally between the munition case and energetic material, or in any combination of these scenarios. For a variety of reasons, not the least of which includes cost minimization, a PIMS liner is planned to be integrated within the PA108 container external to the rounds. The PA108 ammunition container is lined with corrugated fiberboard with the two boxes stacked one on top of another with some space to incorporate PIMS in lieu of the corrugated fiberboard dunnage currently used.

High-rate continuum modeling, using ALE3D, was utilized to identify barrier configurations that would reduce the initial shock within the weight and volume constraints [6]. Two dimensional axisymmetric modeling was used as it allowed appropriate resolution of the shock fronts. Several combinations of materials of varying thicknesses occupying this space were modeled, including the baseline corrugated fiberboard packaging, wood, plastic, aluminum, porous aluminum, and 4340 steel. These were modeled using standard Mie-Gruneisen equations of state [7] and Steinberg-Guinan strength models. Spall failure was modeled with a tensile hydrostatic stress criterion, and void seeding was used to remove excessively strained, and subsequently failed material, from the calculation.

Several shock initiation criteria were considered in evaluating the merit of various protection schemes. These included wedge test data, critical energy fluence, the NOL LSGT pressure, as well as several variants of the James criterion [10]. The usefulness of any of these models is dependent upon the availability of experimental data with which to parameterize them. Wedge test data, from a similar explosive to PBXN-5 at a roughly equivalent density, was used as a tentative criterion [8]. This data is shown below in Table 1. Since the critical diameter of this explosive is equivalently small [9], it is assumed that the pressures are essentially planar for pass/fail determinations even though the shock is diverging and the pressure field behind it is non-uniform.

Table 1. Wedge test data

Pressure (kbar)	Run to Detonation (mm)
48	4.6
68	2.9
101	1.7
164	--

The LSGT pressure threshold criterion was also considered. The go/no-go threshold pressure transmitted to the acceptor explosive was obtained via a shock impedance matching calculation. Exceeding this pressure over is often used as a qualitative benchmark in the absence of better data. However, rational use of this criterion requires discerning between pressure spikes due to shock and isentropic compression. A secondary goal is to reduce the overall mechanical insult to the warhead to the greatest extent practical so as to avoid shear initiation and reduce any subdetonative response [11-13]. A reasonable strategy would be to model the scenario in an attempt to keep the shock pressure low, and experimentally test progressively heavier barrier designs until the desired reduction in reaction violence is achieved. Figure 13 shows typical centerline pressure profiles (in blue) compared to experimental data (in red). By comparison with the wedge test data, improvements over the baseline are hypothesized to occur using various PIMS configurations. Figure 14 shows material and pressure plots for several of these.

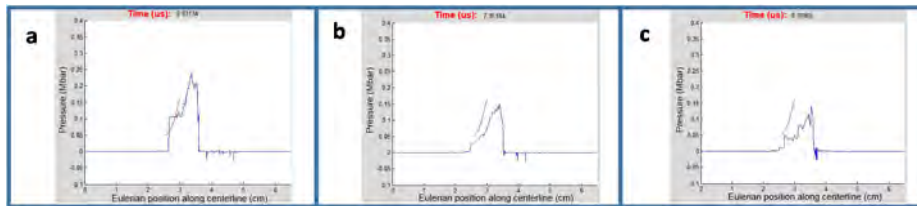


Figure 13. Shock run distance compared to wedge test data (a) baseline configuration; (b) Polymer PIMS; (c) Metal/polymer PIMS.

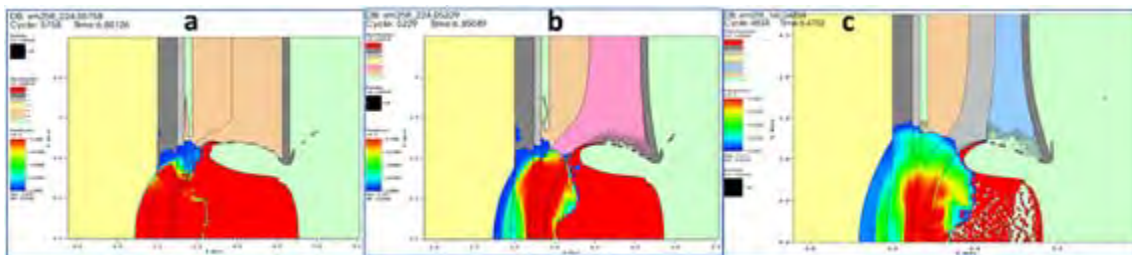


Figure 14. Pressure plots (a) baseline (b) Polymer PIMS (c) Metal/Polymer PIMS

The results of the modeling are summarized in Table 2. The wedge test criterion pass/fail rating indicates whether the centerline input shock was of sufficient pressure and duration to shock initiate based on experimental data, and the gap test criterion is based on whether the pressure ever exceeded the NOL LSGT go/no-go threshold.

UNCLASSIFIED

Table 2. Modeling results.

Configuration	Wedge Test Criterion	Gap Test Criterion
Baseline CF	Fail	Fail
Wood	Marginal	Fail
Polymer	Marginal/Pass	Fail
Polymer/Metal 1	Pass	Fail
40% Porous Al	Pass	Fail
Solid Al	Fail	Fail
Polymer/Metal2	Marginal/Pass	Fail
Steel	Fail	Fail

As can be seen in the table above, there are several configurations that appear feasible for lowering the shock pressure enough for the initial input shock to pass the wedge test criterion, with several caveats. Primarily the pressure pulse generated by FI is likely more severe than the flat-top shocks generated via wedge test. Alternative techniques such as a volume-averaged pressure might be used to remedy this although they are not entirely free from other complications. Sufficiently refined, fully three-dimensional models need to be set up and run in order to predict a higher fidelity response. Another potential pitfall is response variability. Specifically, spall failure is an important feature of the response as this projectile has been experimentally verified to break up into several pieces upon impact with steel sheet used in ammo containers.

Conclusions

Both engineering level tactical configuration and official logistical configuration FI tests of packaged 25mm HEAB cartridges show that impacting the explosive results in a moderately violent reaction. Tactical configuration tests, engineering and formal, of the packaged cartridge where FI was conducted against the propellant resulted in mixed responses. Potential aim point variation related to challenges associated with the FI test methodology may have also contributed to the different reaction levels. FI tests of TP cartridges, in both packaging configurations, and inert simulants, in the tactical configuration, resulted in the container lid being launched over appreciable distances. The distance that the lid was thrown was greater for the tactical configuration than for the logistical when the TP cartridges were tested. In addition, in most of the TP tests the lids were also perforated. Modeling indicates that the holes in the lid may be caused by debris resulting from impact, and that the lid itself is likely thrown due to a hydraulic effect. Engineering SR testing shows that detonation of a single warhead causes adjacent cartridges in the same row to explode, but does not cause cartridges in the lower level to react violently. Modeling was used to evaluate various PIMS materials (wood, plastic and metal) as replacements for the existing corrugated cardboard dunnage. This modeling showed that a polymer and/or some combinations of polymer and metal has the potential (based on wedge test pass/fail criteria) to lower the shock pressure enough to prevent initiation of the explosive fill. Based on these results, there are several potential candidates for replacement dunnage that may provide a reduction in the level of reaction violence.

Acknowledgements

The authors would like to thank the following individuals and organizations for their support and participation in this development program: Andrew Cline, PdM IW; Bob Phung, APO, Robert Greenfield, US Army ARDEC 25mm System Engineer; Stanley DeFisher and Anthony DiStasio, the Joint IM Technology Program (JIMTP); Ed Mooney, US Army Test Facility; Matt Brian, National Testing Service; Vince Martinez, Orbital ATK; David Hunter, GD-OTS for FI gun image. Furthermore, Tim Madsen, US Army ARDEC is thanked for his insightful discussions of the engineering test data.

Distribution Statement A: Approved for public release; distribution is unlimited.

UNCLASSIFIED

UNCLASSIFIED

References

- [1] "Fragment Impact, Munitions Test Procedure", STANAG 4496 Ed. 1, NATO Standardization Agency, Brussels, Belgium, 2006.
- [2] E.L. Baker, N.M. Al-Shehab, K. Tomasello, K. Kennision and D. Hunter, "Fragment Impact Gun Testing Technology and Issues", 2015 Insensitive Munitions & Energetic Materials Technology Symposium, May 18-21, Rome, Italy, 2015.
- [3] E.L. Baker, N. Al-Shehab, K. T., Miers, K. T., D. J. Pudlak, "Insensitive Munitions Fragment Impact Gun Testing Technology Challenges", *Propellants, Explosives, Pyrotechnics* 41, 572-579, 2016.
- [4] G.R. Johnson, R. A. Stryk, T. J. Holmquist, S. R. Beissel. "Numerical Algorithms in a Lagrangian Hydrocode". WL-TR-1997-7093, Wright Laboratory, Armament Directorate, June 1997.
- [5] A. Daniels, J. Pham, K. Ng, and D. Pfau, "Development of Particle Impact Mitigation Sleeves to Reduced IM Response", 2007 Insensitive Munitions & Energetic Materials Technology Symposium, October 15-17, Miami, FL, USA, 2007.
- [6] A.L. Nichols III, Editor. "ALE3D User's Manual". LLNL-SM-681737, Lawrence Livermore National Laboratory, November 2015.
- [7] S.P. Marsh, Editor. "LASL Shock Hugoniot Data". University of California Press, 1980.
- [8] L.G. Green, R.J. Wasley, P.E. Kramer, "Shock Initiation of LX-07-2". UCRL-50851, Lawrence Radiation Laboratory.
- [9] C.M. Tarver, J.S. Christensen, K.J. McMullen, S.K. Chidester, "Overcoming LX-17 Failure Diameter Size by High Pressure Shock Initiation using Ultra Fast, Thin, Small Diameter Flyer Plates".
- [10] M. Gresshoff, C.A. Hrousis, "Probabilistic Shock Threshold Criterion". 14th International Detonation Symposium, Coeur d'Alene, Idaho, April 11-16, 2010.
- [11] R.B. Frey, "The Initiation of Explosive Charges by Rapid Shear". Ballistic Research Laboratory, Aberdeen Proving Ground, MD, June 1980.
- [12] R.B. Frey, P. Howe, J. Trimble, G. Melani, "Initiation of Explosive Charges by Projectile Impact". Ballistic Research Laboratory, Aberdeen Proving Ground, MD, June 1979.
- [13] P.C. Chou, D. Liang, W.J. Flis, "Shock and Shear Initiation of Explosive". *Shock Waves* (1991) 1:285.



FRAGMENT IMPACT TESTING OF THE XM25

APRIL 2018

IM&EM: REAL WARFIGHTER ADVANTAGE AND COST EFFECTIVE SOLUTIONS THROUGHOUT THE LIFECYCLE

PRESENTED BY NAUSHEEN AL-SHEHAB

UNPARALLELED
COMMITMENT
& SOLUTIONS

Act like someone's life depends on what we do.



U.S. ARMY ARMAMENT
RESEARCH, DEVELOPMENT
& ENGINEERING CENTER



BACKGROUND



- The Counter Defilade Target Engagement (CDTE) is a shoulder-fired weapon system that gives Soldiers the ability to engage personnel targets behind cover
- The XM1083 High Explosive Air Burst (HEAB) projectile has dual steel warheads
- The XM1081 target practice (TP) fires an inert projectile with similar performance to the HEAB cartridge
- Both the TP and the HEAB rounds contain approximately 1.2 grams of commercial off the shelf shotgun propellant.

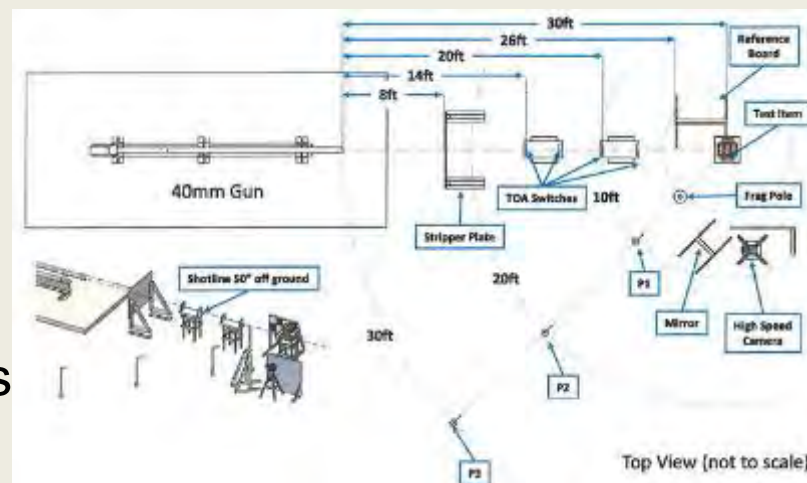
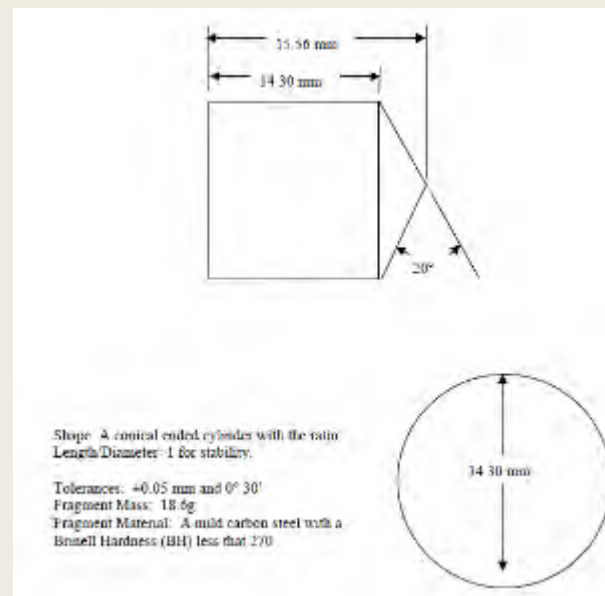




FRAGMENT IMPACT GUN TESTING



- U.S. IM fragment impact testing
 - MIL-STD-2105D
 - NATO STANAG 4496, Ed. 1
- Standard test: 2530 ± 90 m/s
 - Alternate test of 1830 ± 60 m/s
- Standard fragment (projectile) geometry
- Several loosely defined and undefined characteristics can affect the test item response
 - Velocity variation
 - Projectile tilt upon impact
 - Aim point variation
 - Fragment material characteristics





U.S. ARMY
RDECOM

FI Test Configurations Tactical vs. Logistical



UNCLASSIFIED



Tactical configuration consists of the cartridges packed inside of a PA108 container. Each container contains 2 trays of 40 cartridges



“Wirebound” logistical shipping consists of two PA108 containers inside of a wooden shell

1x PA108 Container

Top View

Orthogonal View

Pallet Straps



Tactical Configuration

2x PA108 Container

Wire-bound
Wood Crate



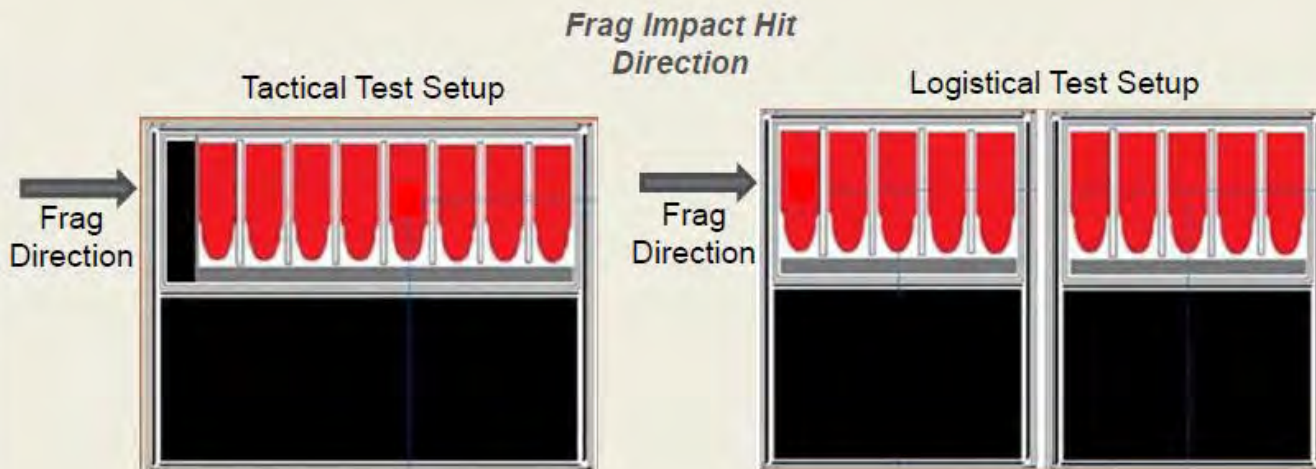
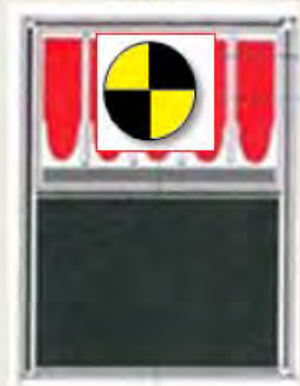
Logistical Configuration

Distribution A: Approved for Public Release. Distribution is Unlimited

UNCLASSIFIED



Frag Impact Aim Point



Test Setup



Test Setup



U.S. ARMY
RDECOM

HEAB ENGINEERING FI TESTS



Propellant Shotline (Tactical Configuration)



Propellant Impact - Bottom

Explosive Shotline (Tactical Configuration)



Explosive Impact - Bottom



Explosive Impact - Side



Type IV



Type III

2448m/s

2527m/s



HEAB FORMAL FI TESTS



Propellant Shotline (Tactical Configuration)



Test Setup



Container severely damaged



Results

2517m/s

Explosive Shotline (Logistical Configuration)



Test Setup



Second Container intact

Results

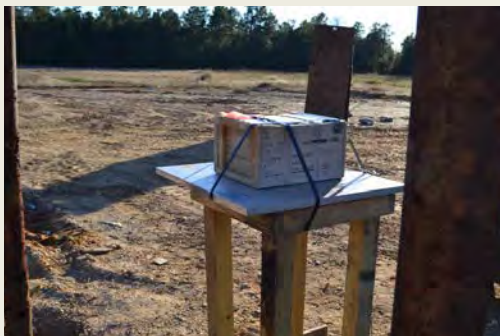


2461m/s

Tactical Configuration



Logistical Configuration



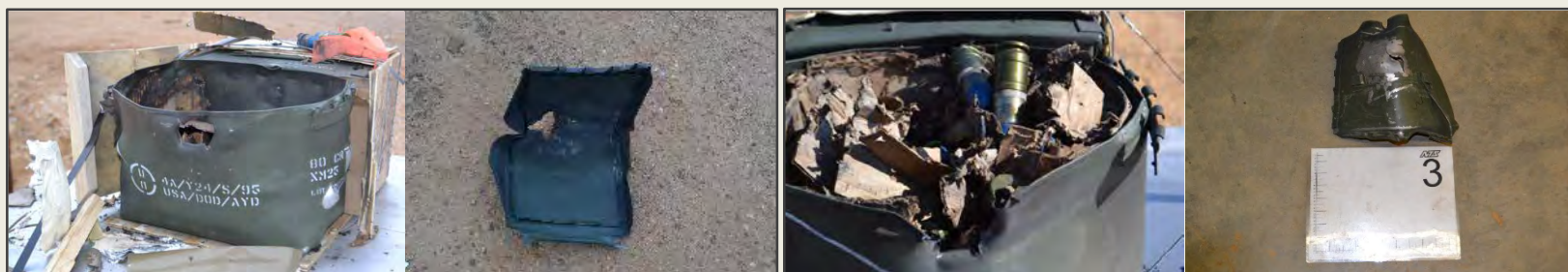
High Speed Video Footage



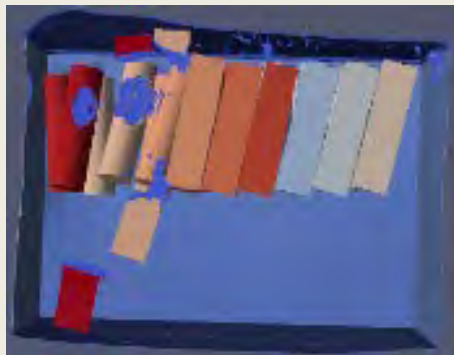
Inert cartridge Modeling



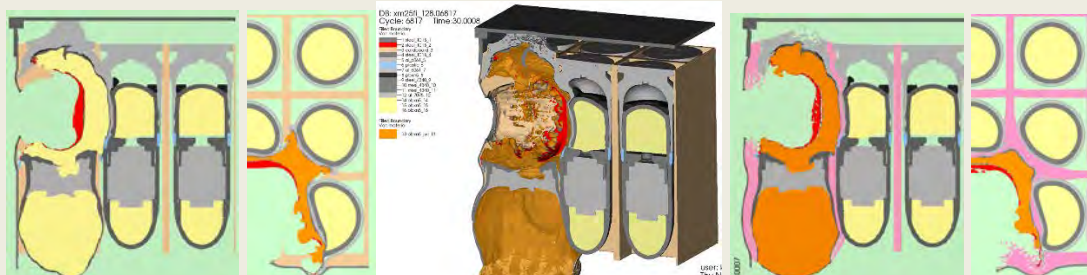
*Holes in lid likely caused by debris
Lid likely thrown due to hydraulic effect*

***Tactical Configuration***Shot 1
(2004m/s)Shot 2
(2486m/s)Shot 5
(2500m/s)***Logistical Configuration***Shot 3
(2525m/s)Shot 4
(2495m/s)

All lids are bowed and thrown > 30 meters
All lids are perforated, except for the lower velocity tactical configuration



- *EPIC modeling of inert simulants suggests damage to lid may be from cartridge fragmentation.*
- *Inert simulant testing results also show no holes in lids, suggesting that, in the TP configuration tests, holes may be caused by debris field from the cartridge case fragments*
- *Lids were thrown from the test stand, although not as far as in the TP tests*



- Significant directionality to shock generated in adjacent cartridges
- Reduced peak pressure induced in adjacent cartridges

SR Test Results - HEAB





U.S. ARMY
RDECOM

FI BARRIER DESIGNS HYDROCODE MODELING

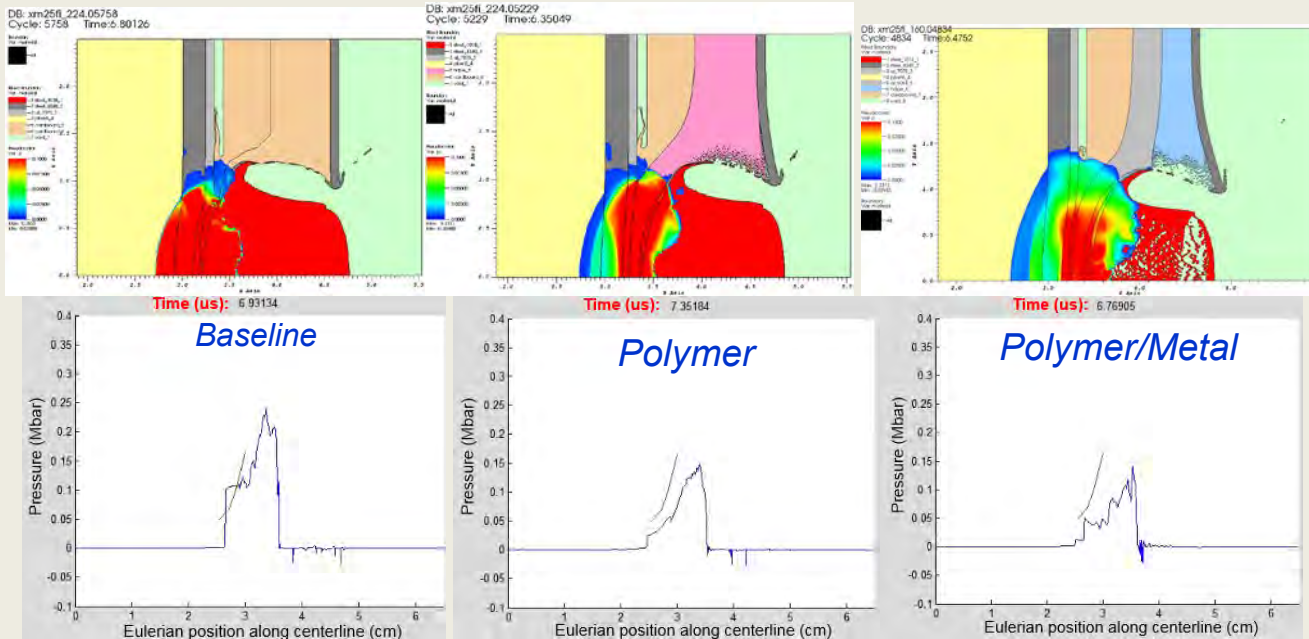


Pop plot data

Pressure (kbar)	Run to Detonation (mm)
48	4.6
68	2.9
101	1.7
164	--

Configuration	Wedge Test Criterion	Gap Test Criterion
Baseline CF	Fail	Fail
Wood	Marginal	Fail
Polymer	Marginal/Pass	Fail
Polymer/Metal1	Pass	Fail
Porous Al	Pass	Fail
Solid Al	Fail	Fail
Polymer/Metal2	Marginal/Pass	Fail
Metal2	Fail	Fail

Several candidate barrier configurations



Designs explored to mitigate initial impact shock



Summary



- Both engineering level tactical configuration and formal logistical configuration FI tests show that impacting the explosive results in an explosion.
- Tactical configuration tests, engineering and formal, of the packaged cartridge impacting the propellant had mixed results.
 - Potential aimpoint variation due to challenges with FI testing
- TP cartridges and inert simulants caused the lid to be thrown
 - Lids were thrown farthest and were perforated in tests with TP cartridges
 - Modeling suggests that lid perforation is likely caused by cartridge debris throw and the lid is thrown due to hydraulic effects
- SR testing causes cartridges in the same row to explode, however, this is not transmitted to the row below. Based on modeling results of the PIMS, there are several potential candidates for replacement dunnage that may reduce reaction violence.



- **PdM IW** – Andre Cline
- **APO** - Bob Phung
- **ARDEC 25mm System Engineer** - Robert Greenfield
- **JIMTP** – Anthony DiStasio and Stanley DeFisher
- **US Army Test Facility** – Ed Mooney
- **National Testing Service** – Matt Brian
- **Orbital ATK** – Vince Martinez
- **GD-OTS** – David Hunter
- **ARDEC** – Tim Madsen



Thank You!





IM PLANS AND JIMTP FUTURE IN THE UNITED STATES



Mr. Anthony Di Stasio
Program Manager
US Army ARDEC
973-724-4547
Anthony.r.distasio.civ@mail.mil
OUSD(AT&L)/TWS/LW&M



Joint Insensitive Munitions Technology Program

Mission - Develop, mature and transition Joint Insensitive Munition science and technologies to improve the response of the DoD munitions portfolio to threats from combat, terrorists, and accidents.

Purpose – to provide a Science and Technology base to support the Secretary of Defense in ensuring that munitions under development or procurement are safe throughout their lifecycle when subjected to unplanned stimuli to the maximum extent practicable.



Why the “J”? (Historically)

- Historical incidents and existing vulnerabilities dictate need to improve the response of our DoD-wide munition portfolio
- Technology gaps and potential solutions cut across services/agencies and specific munitions
- Addressing/evaluating munitions on an item-by-item basis resulted in an inefficient investment of both intellectual capital and \$
- Combination of JIMTP and IM Strategic Plans (IMSPs) represents a Departmental strategy to invest in a combination of priority critical technologies and munition response improvements
- Ensure and increase combat capability through increased safety, reduced shipping and storage burdens, and increased force protection/survivability

NATO STANAG 4439 DEFINITION

Munitions which **reliably fulfill their performance**, readiness and operational requirements on demand and which **minimize the probability** of inadvertent initiation and **severity** of subsequent collateral damage to weapon platforms, logistic systems and personnel when subjected to **unplanned stimuli**.



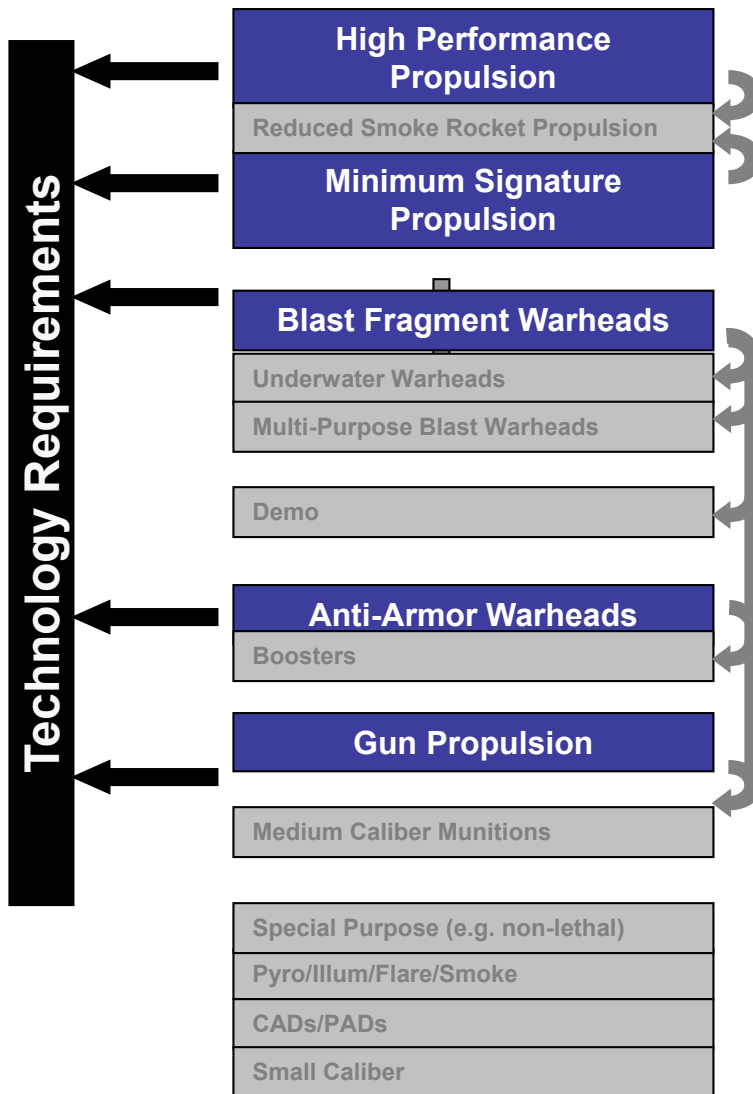
USC, Title 10, Chapter 141, Section 2389 December 2001

“§ 2389. Ensuring safety regarding insensitive munitions. The Secretary of Defense shall ensure, to the extent practicable, that insensitive munitions under development or procurement are safe throughout development and fielding when subject to unplanned stimuli.”



JIMTP S&T Focuses on DoD Munitions Portfolio

Munition Area
Technology
Groups
(MATG)



➤ DoD Portfolio contains five primary areas where Non-compliant munitions are identified for procurement



IM Success

- 60mm mortar
- 81mm mortar
- 120mm mortar
- 105mm Artillery
- 155mm Artillery
- Air-to-air weapons
- 500lb general purpose bomb
- 1000lb general purpose bomb
- Demolition charges (2 sizes)




- Future will focus on the acquisition cycles and strategies of new weapons
- “Fixing” legacy systems was step 1
 - Addressing the challenges of “TBD” systems requires broad research




Energetics Enterprise

MIBP




NAC

- Novel Synthesis
- Scale up
- Production



TTCP

- Novel synthesis
- Scale up
- Evaluation



ARL/ARO

- Novel Synthesis



SMCA

- PD-JP
- PD-JS



JMP/JFTP

- Novel Synthesis
- Tool Development




ARDEC

- Explosives
- Gun Propulsion




JIMTP

- Energetic material
- IM Evaluation




AMRDEC

- Propulsion
- Propellant




AFRL-RQ

- Propulsion



ONR/NRL

- Novel Synthesis
- Scale up




AFRL-HERD

- Explosives



NSWCIEHODTD

- Scale up
- Implementation




AFOSR

- Basic Research



NAWCWD

- Synthesis
- Implementation

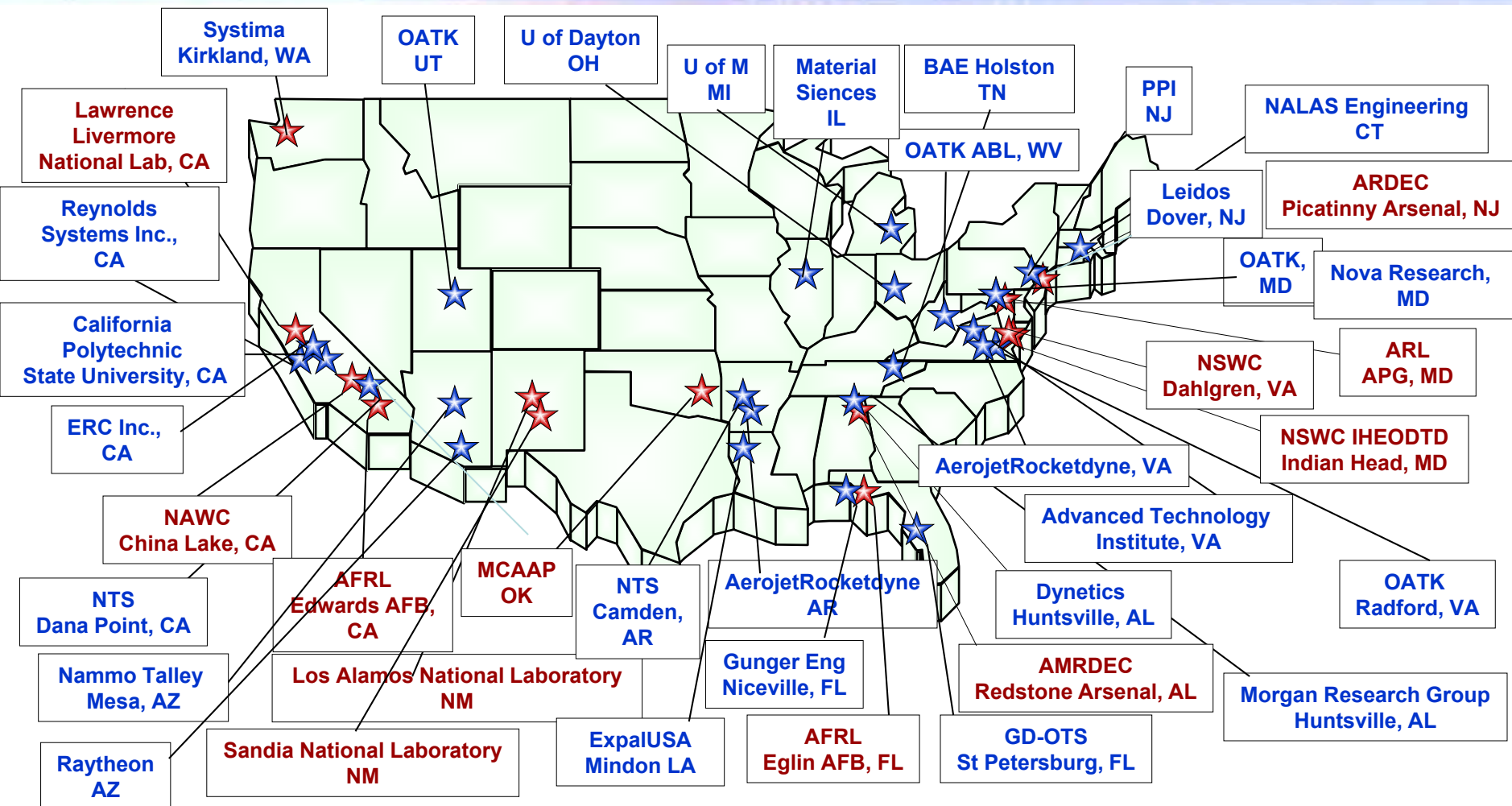


EOD





FY16/17 Joint Munitions Technology - Performers -



JIMTP is strengthening government-industry partnerships



Challenges

- **Range extension in multiple systems**
- **Understanding of relationship between short duration shock vs long duration shock (HJ criteria vs wedge test)**
- **Understanding “damage” (cracks, voids, porosity, thermal) generation and propagation during insult**
- **Understanding the science behind SCO/FCO challenges**



Summary

- **Technology and capability gaps continue to drive our focus**
 - **JIMTP mission remains with dynamic weapon portfolio**
- **Fundamental understanding challenges remain**
 - **Trying to address highest priorities with Directed Studies and partners (labs, SBIR, DOE etc.)**
- **Transition environment is complex and applicable technology is available for integration**



Questions



Synthesis Development of Novel Energetic Ingredients

NDIA IM/EM 2018

Sarah Headrick, PhD; David Price, PhD; Jacob Morris, PhD; Rycel Uy, PhD; Jim Phillips
BAE Systems Ordnance Systems Inc.
Holston Army Ammunition Plant, Kingsport TN, USA



Acknowledgements



Strategic Environmental Research and Development Program

Robin Nissan, PhD
-Program funding



US Army Research and Development Engineering Center

Anthony DiStasio, Paul Anderson, PhD and Alexander Paraskos, PhD
-Technical input and program funding



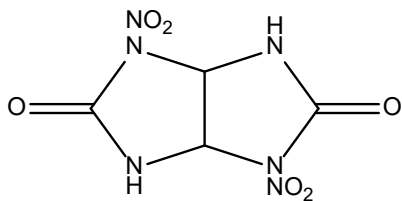
BAE Systems

Matt Hathaway, Dr. Jeremy Headrick, Robyn Wilmoth, Kelly Smith, Chris Long, Dr. Tess Kirchner
-Analytical testing

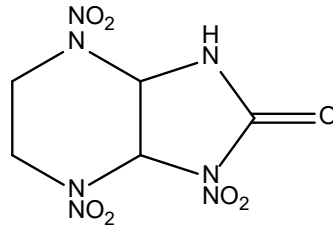
Overview

- Defense scientists constantly scour the literature for new explosive ingredients to fulfill their needs
- Individual needs can vary widely based on system requirements
- Possible material requirements can include:
 - Sensitivity
 - Energetic performance
 - Thermal stability (greater than 300 °C)
 - Crystal morphology
- Today's presentation will highlight BAE Systems' orphan explosive ingredients
 - Synthesis from the gram scale up to pilot scale
 - Did not meet requirements for original intended purpose
 - Could be desirable for future applications

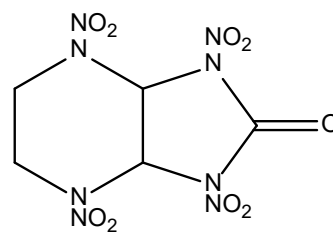
Orphan Ingredients



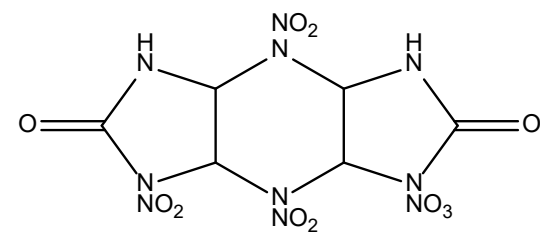
DNGU



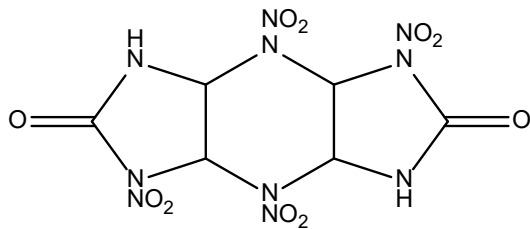
HK-56



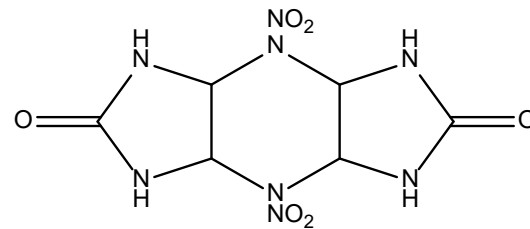
TNABN



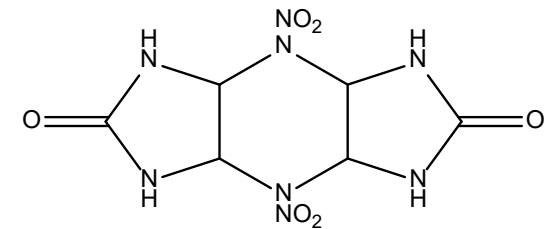
c-TNTC



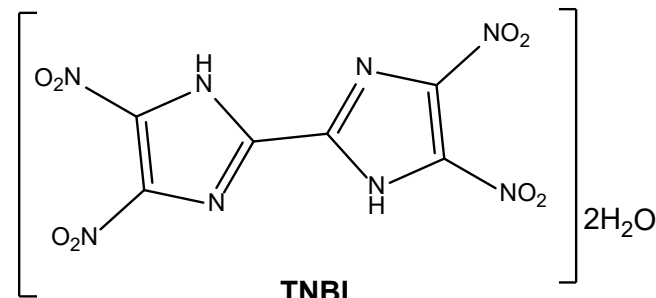
s-TNTC



DNTC



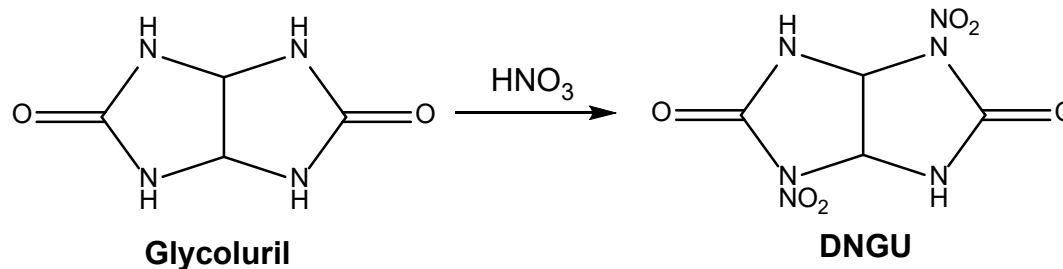
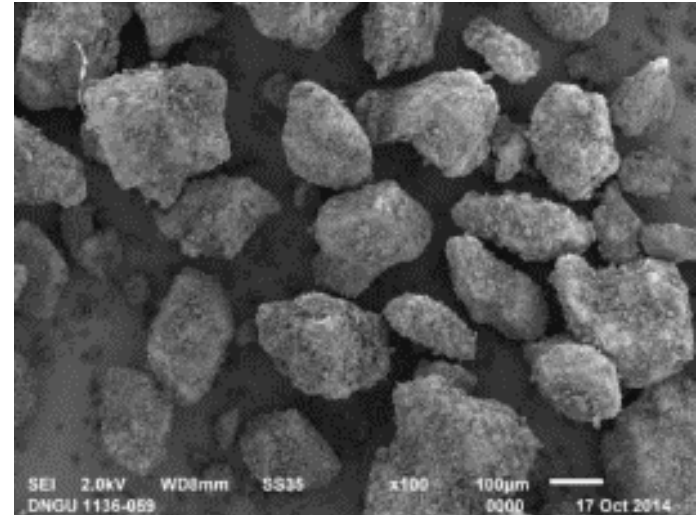
TriTNTC



TNBI

DNGU Synthesis and Optimization

- DNGU produced through nitration of glycoluril
 - Glycoluril is commercially available & inexpensive
- DNGU cost estimated to be between RDX and HMX
- DNGU has been synthesized on the pilot scale
- Synthesis process has been optimized:
 - Original DNGU was ~15-20 microns
 - Optimized DNGU much larger (~200-300 microns)
 - Yields typically 90-95% with purities >99%



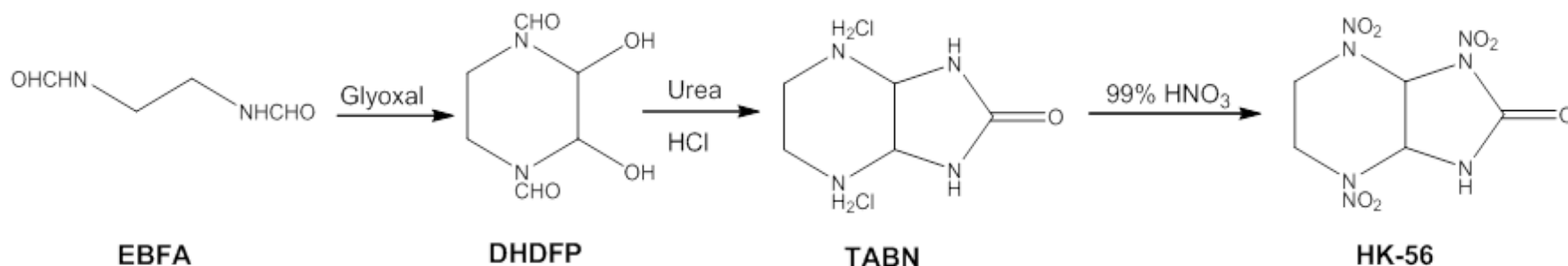
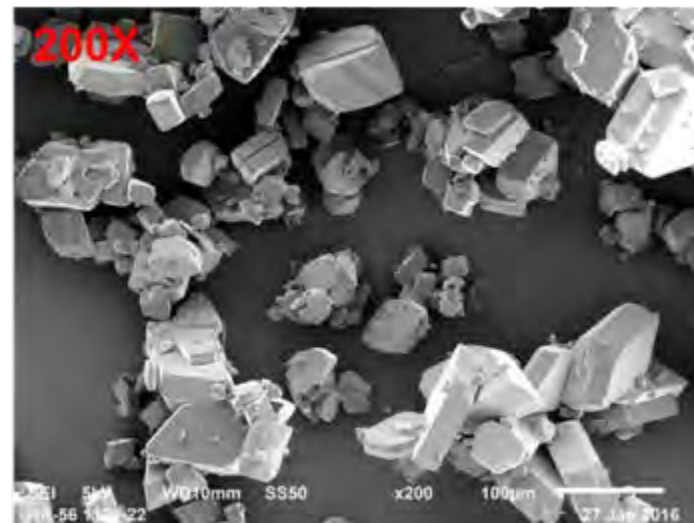
DNGU Properties

Property	Value
Impact (Naval, cm)	58.64 (18.84)
BAM Friction (N)	>360 (164.0)
ESD (J)	0.0366
DSC Exotherm (°C, 5 °C/min)	241.54
Density (g/cc)	1.94
Heat of Formation (kJ/mol)	-359.4
Oxygen Balance	-27.6
VOD (calcd, km/s)	8.67
CJ Pressure (calcd, GPa)	33.3

- Exceptionally insensitive to impact & friction
- Very high density (similar to HMX)
- Higher DSC exotherm than RDX
- Predicted performance parameters similar to RDX

HK-56 Synthesis

- Simple reactions to produce DHDFP and TABN
 - Commercially available starting materials
 - Yields ~65-70%
- Facile nitration to produce HK-56
- Initial HK-56 particle size quite small (5-10 microns)
 - Plate-like particle shape
- Process improvements yielded larger, more cubic crystals suitable for formulation efforts



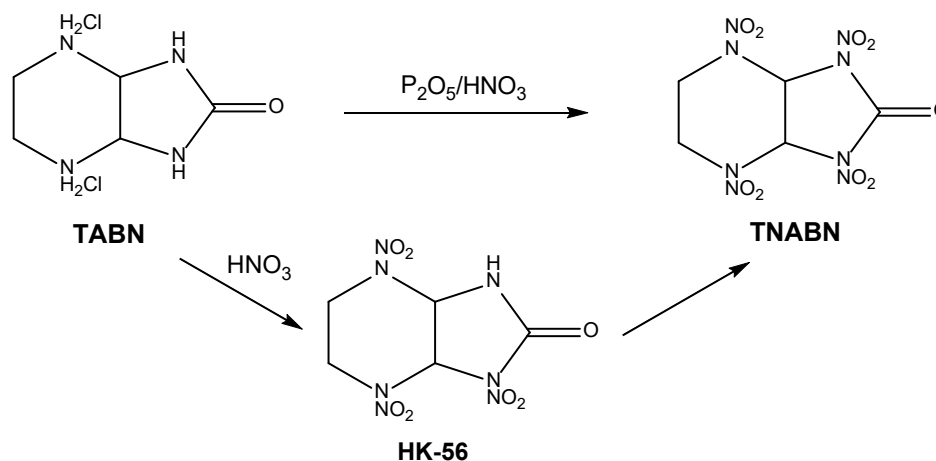
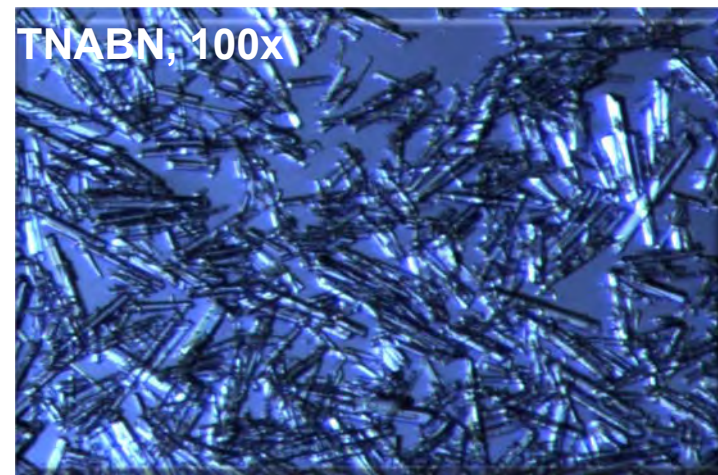
HK-56 Properties

Property	Value
Impact (Naval, cm)	79.35 (56.67)
BAM Friction (N)	>360
ESD (J)	0.0829
DSC Exotherm (°C, 10 °C/min)	203.84
Density (g/cc)	1.86
Heat of Formation (kJ/mol)	-129.9
Oxygen Balance	-37.5
VOD (calcd, km/s)	8.38
CJ Pressure (calcd, GPa)	31.2

- HK-56 is very insensitive to impact, friction and ESD
- Density very similar to RDX
- DSC exotherm similar to RDX
- Predicted performance slightly below that of RDX

TNABN Synthesis & Optimization

- TNABN synthesized from either TABN or HK-56
 - HK-56 nitration yields ~98% pure product
 - HK-56 route is readily scalable
- Multiple crystallizations completed using numerous solvents
 - All yielded highly crystalline needles



Non-Export Controlled Information

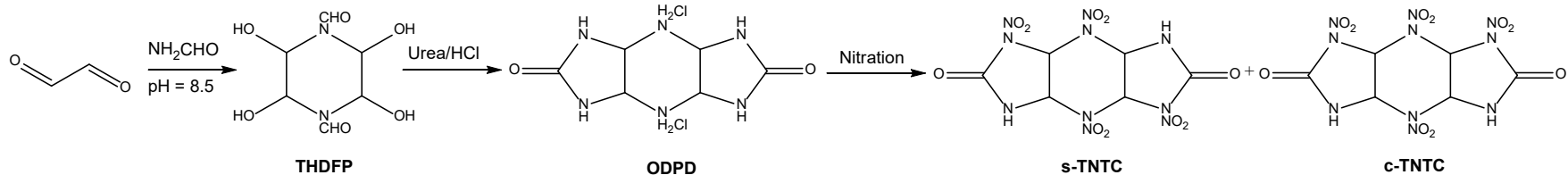
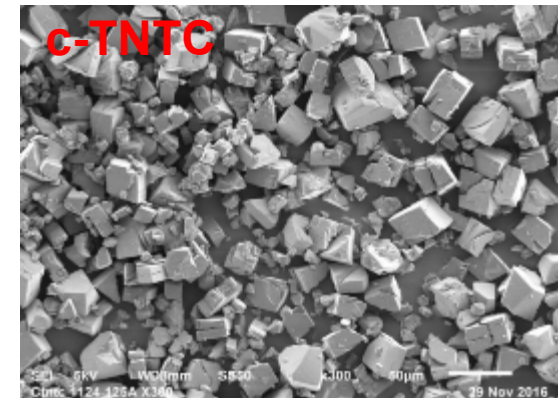
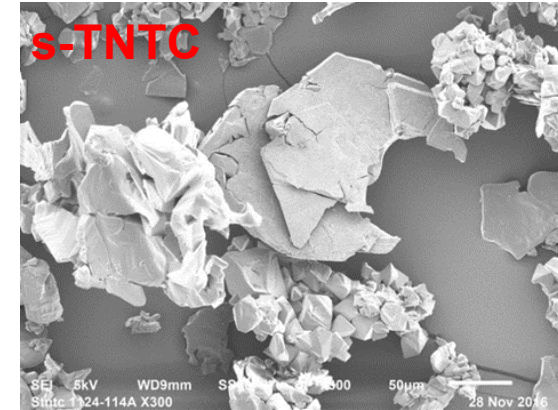
TNABN Properties

Property	Value
Holston Impact (50%, cm)	20 (51.3)
BAM Friction (N)	132.4 (134.2)
ESD (J)	0.4000 (0.0366)
DSC Exotherm (°C, 10 °C/min)	248.58
Density (g/cc)	1.97
Heat of Formation (kJ/mol)	70.31
Oxygen Balance	-19.9
VOD (calcd, km/s)	9015
CJ Pressure (calcd, GPa)	38.12

- TNABN very similar to HMX with the following comparable properties:
 - sensitivity
 - DSC exotherm
 - density
 - predicted performance

TNTCs Synthesis

- Precursor THDFP has been produced on the kilogram scale (Gottlieb et al)
- ODPD synthesis process uses inexpensive ingredients
 - Optimization of process needed
- Reaction to product TNTC is uncomplicated using scalable materials
 - Highly pure products can be acquired
 - Optimization of process needed
 - Literature indicates s-TNTC may be a more stable product than c-TNTC
- Overall synthesis route has potential for scalability



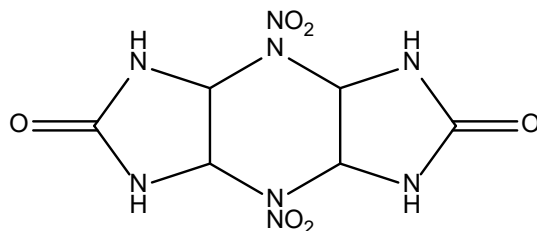
TNTCs Properties

Property	s-TNTC	c-TNTC
Holston Impact (50%, cm)	<12 (33.1)	<12 (33.1)
BAM Friction (N)	301.2 (224.6)	334.0 (224.6)
ESD (J, TIL)	0.0425 (0.0888)	0.0366 (0.0241)
DSC Exotherm (°C, 10 °C/min)	247.73	250.18
Density (g/cc)	1.97	1.96
Heat of Formation (kJ/mol)	-137.7	-163.35
Oxygen Balance	-21.2	-21.2
Predicted VOD (calcd, km/s)	9.02	8.98
CJ Pressure (calcd, GPa)	36.9	37.1

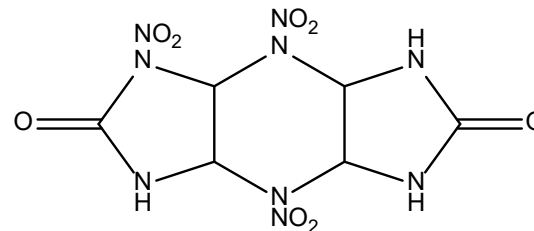
- TNTCs are very sensitive to impact!
- TNTCs are very like HMX in terms of:
 - Density
 - DSC Exotherm
 - Predicted performance

TNTC Intermediates: DNTC & TriINTC

- Two TNTC intermediates were isolated & characterized during TNTCs synthesis activities
- DNTC was previously characterized by Boyer et al.
- DNTC has high DSC exotherm: 311 °C
- TriINTC does not appear in the literature
 - Discovery of TriINTC was surprising & exciting
- TNTC intermediates could be used in the future to selectively produce the TNTCs
- TriINTC predicted performance similar to RDX



DNTC



TriINTC

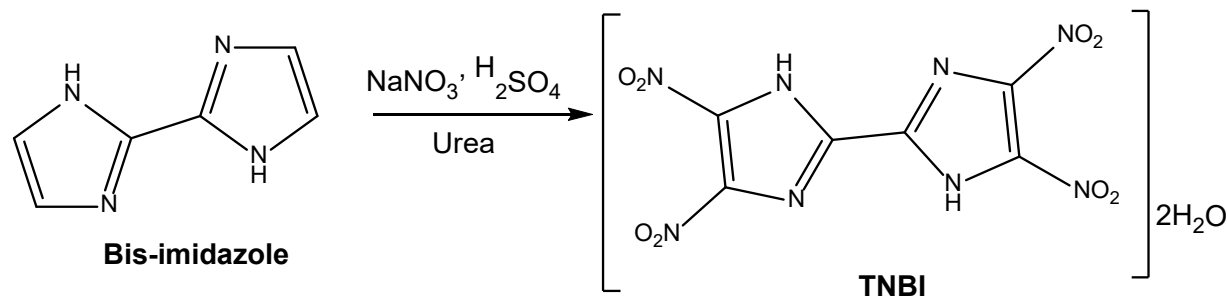
DNTC & TriNTC Properties

Property	DNTC	TriNTC
Holston Impact (50%, cm)	31.9 (41.8)	24.17 (41.8)
BAM Friction (N)	>360 (260.4)	>360 (260.4)
ESD (J, TIL)	0.1375 (0.0241)	0.0738 (0.0241)
DSC Exotherm (°C, 10 °C/min)	311.01	244.3
Density (g/cc)	ND	1.95
Heat of Formation (kJ/mol)	ND	ND
Oxygen Balance	-55.5	-36.0
Predicted VOD (km/s)	7.43	8.13
CJ Pressure (GPa)	ND	ND

- DNTC & TriNTC both fairly sensitive to impact
- TriNTC possesses HMX-like density
- DNTC has a high DSC exotherm; could be useful in applications requiring high thermal stability?

Synthesis of TNBI

- Synthesis of TNBI completed using known synthesis methods
 - Reaction is un-complicated and uses inexpensive ingredients
 - No optimization was completed
- Reaction yield approximately 50-60%
 - In agreement with literature values
- Purification process developed to provide TNBI in 99% organic purity
 - Purification also reduces sulfates content of product



TNBI Properties

Property	Value
Holston Impact (50%, cm)	60.9 (56.7)
BAM Friction (N)	311.5 (251.1)
ESD (J)	0.1375 (0.1375)
DSC Exotherm (°C, 10 °C/min)	288.9
Density (g/cc)	1.80
Heat of Formation (kJ/mol)	-417.07
Oxygen Balance	-22.8
VOD (calcd, km/s)	8182
CJ Pressure (GPa)	27.86

- TNBI appears to be insensitive to impact and friction
- Density is similar to RDX
- DSC exotherm is higher than RDX
- Performance properties slightly lower than that of RDX

Summary

- Eight orphan explosive compounds were presented
 - All were synthesized through potentially scalable and inexpensive synthesis routes
- DNGU, TNBI and HK-56 have potential applications for insensitive munitions purposes
- TNTCs, TriNTC and TNABN may be suitable for applications requiring higher sensitivity
- DNTC possesses a DSC exotherm above 300 °C
 - Suitable for high temperature applications



Effect of Insensitive HE on Shaped Charge Jets

Werner Arnold¹, Thomas Hartmann², Ernst Rottenkolber²

¹ MBDA-TDW Gesellschaft für verteidigungstechnische Wirksysteme mbH, Hagenauer Forst, D-86529 Schrobenhausen, Germany,

² NUMERICS GmbH, Mozartring 6, D-85238 Petershausen, Germany

Abstract

Two different trends can be observed in the warhead community: on the one hand the demand for increased insensitive munition (IM) is still growing. This finally led to the replacement of TNT-bonded charges by plastic bonded ones (PBX). Contrary to TNT, a standard (inert) plastic binder cannot react within the very short times of a detonation front and thus leads to an increased roughness of the detonation front. On the other hand, there is also a demand for an increased performance of shaped charges with 10 calibers depth of penetration for Cu liners or even 12 calibers for Mo liners. This requires thin and usually not constant wall thickness liners. The possible conflicts of these two objectives were investigated in experimental studies, which are summarized in the present work.

1 Introduction

A few decades ago, shaped charges were typically filled with TNT-bonded explosives. Already at that time, it was tried to measure the roughness of the detonation front resulting from the inhomogeneity of the explosive ([1] & [2]) and the question was raised if this roughness has an impact on the performance of a shaped charge jet (SCJ). However, experiments showed that the influence was only marginal (e.g. [2] & [3]) and only little further attention was given to the topic.

The question re-emerged when the classical TNT bonded explosives were replaced by plastic bonded explosives (PBX) to make the charges more insensitive [4]. While the TNT binder was detonable and the detonation front could propagate with approximately the same velocity in the explosive and in the binder, this is not the case with the inert plastic binder. Consequently, the use of PBX increases the roughness of the detonation front.

At the same time, the developers of shape charges are striving for higher performance by the application of higher density liner materials and / or non-constant thickness liners – both measures at least partly decreasing the liner thickness and thus making the shaped charges (theoretically) more sensitive towards a rough detonation front. Facing these trends, the detonation front roughness became an issue again and an experimental program was launched to investigate its effects on the liner material and to quantify its influence on a shaped charge jet.

2 High Explosive Types

Three batches of the TDW PBX KS32 (HMX/HTPB 85/15, $\rho = 1.64 \text{ g/cm}^3$) with different HMX grain size distributions were manufactured:

- Standard: bimodal with mean grain sizes of 30 μm (fine mode) and 500 μm (coarse mode),

- Coarse: unimodal with mean grain size of 500 μm ,
- Fine: unimodal with mean grain size of 30 μm .

With these three different KS32 batches both the roughness of the detonation front and the influence of this roughness on the SCJ behavior should be measured in the following two test series.

3 Roughness of a Detonation Front

In [1] and [2] the roughness of the detonation front was measured optically with a rotating mirror camera in streak mode. In [5], the authors studied shock wave interactions in multi point initiation systems by direct measurements of indentations in Oxygen Free High Conductivity (OFHC) copper, which is also used for SC liners. This technique was applied in this work as well. The principle of the test setup is sketched in Figure 1. The different KS32 types were initiated by a detonator and a Hexogen/Wax/Carbon (HWC) booster. An additional HWC disk of 10 mm thickness should ensure a safe initiation for all three KS32 types. The Cu plate below was used to witness the roughness of the detonation front. A final big steel block was added to trap the shock waves (avoiding reflections) and to stabilize the setup. The idea was to “print” the structure of the detonation front onto the Cu plate surface without significant lateral motion of this surface after the passage of the detonation front wave.

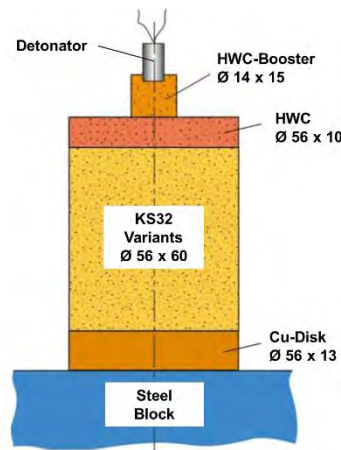


Fig. 1: Sketch of the test setup to measure a rough detonation front with a Cu witness disk.

To achieve these objectives three different configurations were investigated in numerical simulations. The models for these setups are shown in Figure 2. In the first configuration on the left side, a model as shown in Figure 1 was used. In the second configuration in the middle of Figure 2, the radial extension of the Cu witness plate was increased to avoid lateral movements of the Cu surface. In the third and final configuration on the right side, the Cu plate and a part of the KS32 were placed into a 20 mm deep milled hole in the steel block to largely avoid any radial movement of the Cu surface.

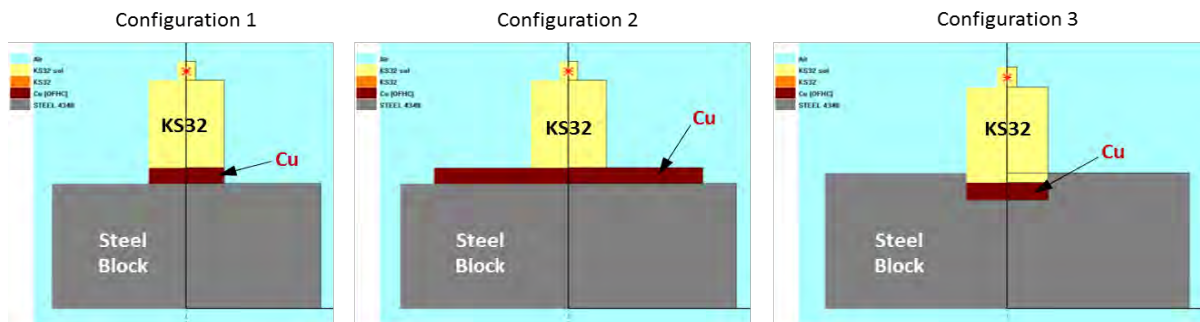


Fig. 2: Numerical simulation models for the three different configurations.

The numerical simulation studies clearly showed too large lateral flow of the copper in configuration 1, while the lateral movements of the Cu surface were already limited to between 2 – 8 mm (middle to edge) in configuration 2. The best results were achieved with configuration 3 with only 1 – 3 mm (middle to edge) radial shift of the Cu surface. Tests with all three configurations were conducted but with the focus on configuration 3.

3.1 Cast on Cu Disk

In a first test series the three types of explosives were cast onto extended and confined copper plates and detonated. The sample deformations were in close agreement with the predictions obtained from the numerical simulations. Figure 3 shows configuration 2 & 3 after the test, where in #3 the shock loaded Cu disk was already taken out of the setup.



Fig. 3: Cu witness plate of configuration 2 (left) and steel block of configuration 3 without Cu sample (right) after the firings.

For each sample, the roughness of the copper surface, i.e. the indentations caused by the detonation front, was evaluated visually (optical microscopy) as well as by roughness measurement. Finally, the results of the different HE batches were compared to each other.

Typical results of the microscopic evaluation of the Cu surfaces are shown in Figure 4, where the roughness achieved with KS32-fine (left) and KS32-coarse (right) are highlighted. The difference between the two batches can already clearly be seen. The roughness of the fine grain sample is relatively low and partially even below the sensitivity of the meter, whereas the roughness measurement of the coarse grain sample yields maxima of 50 – 70 μm and 5 – 10 μm average. In Section 4, an SC liner with a thickness of 0.4 mm (400 μm) will be presented. The max. roughness could thus reach up to 10 – 15 % of the liner thickness.

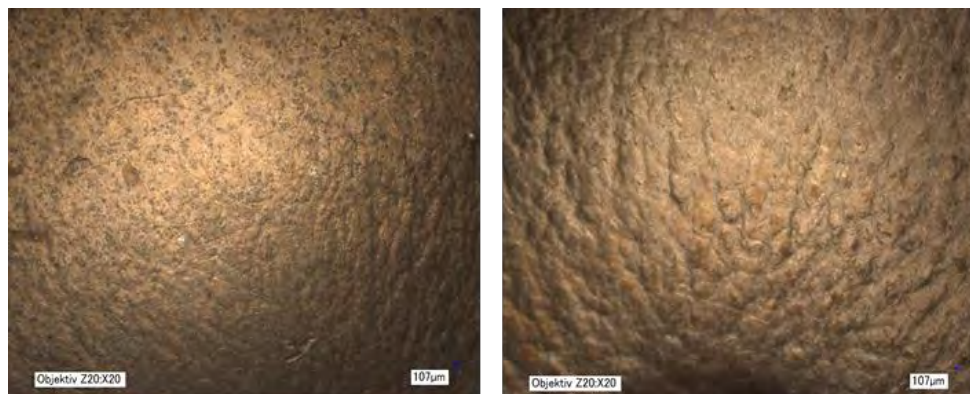


Fig. 4: Microscopic evaluation of the Cu surface roughness with KS32-fine (left) and with KS32-coarse (right).

3.2 Machined and glued on Cu Disk

The standard process for manufacturing shaped charges is casting the HE onto the SC liner. But sometimes, in more special cases, the HE is machined to fit onto a ready SC liner. Therefore, a second test series in configuration 3 was conducted with the KS32 explosive surface machined and then glued onto the Cu disk. Figure 5 shows in a series of pictures illustrating the surprising results – here exemplarily depicted for the KS32-standard. The left picture shows a micrograph of the machined, polished and further prepared surface of the KS32 sample. The yellow colored HMX-grains were thereby cut in a statistical manner. The corresponding test result is presented in the middle picture. The evaluation with an optical microscope shows many deep craters with diameters comparable to the cut HMX grain size distribution. Finally, a scanning electron microscope (SEM) picture of some of the craters is shown on the right. It was found that the crater depths are in roughly the same order of magnitude as the grain diameters.

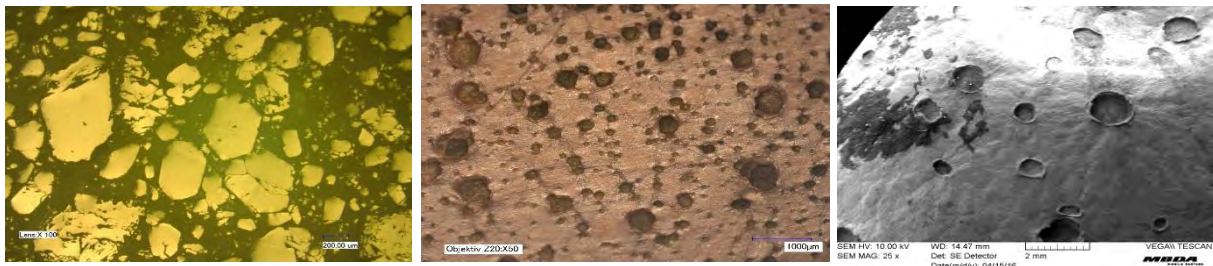


Fig. 5: Micrograph of cut and polished KS32-standard surface (left, HMX grains in yellow), Cu surface with craters after firing (middle) and SEM close-up picture of some craters (right).

From these results it must be concluded that machining the HE is not an appropriate process when thin high-performance SC liners are involved. Consequently, no further trials applying this technique were performed.

4 Influence of Roughness on the SC Jet

Based on the results obtained with the Cu surface roughness trials SC tests with the three KS32 types were planned. In a first step, an appropriate SC charge had to be designed. Thereby, several design requirements should be met:

- High tip-velocity were thought to be reasonable to achieve differences in the results,
- Thick enough SC jet to obtain an accuracy level high enough to see these differences,
- Simple and cost-effective design without detonation wave shaper
- Availability of the equipment to manufacture the SC selected liners

In numbers, the tip velocity should be as high as possible but not higher than 10.000 m/s (to keep it in a stable region) and the SCJ diameter should be at least 1.5 mm to ensure an accurate evaluation. Having these requirements in mind several SC liner designs were simulated and finally down-selected. In a second step, the candidate design of the shaped charge was then manufactured and filled with the three different KS32 types.

4.1 SC Design based on Numerical Simulations

Several SC designs and liners were taken into account and studied by numerical simulations for their usability in the planned test campaigns. The following parameters were varied:

- SC caliber: 44 mm and 64 mm
- Liner angle: 50°, 55° and 60°

- Liner wall thickness depending on liner angle

In total 12 simulations were performed and assessed by mainly analyzing the different mass profiles of the jets. Figure 6 exemplarily shows results with a caliber of 64 mm, liner angles of 50° and 60° and various liner thicknesses. The corresponding mass profiles are presented in Figure 7. In summary, tip velocities > 8000 m/s could only be reached with 50° liner angle for both calibers, but the required jet diameter could only safely be achieved with 64 mm caliber.

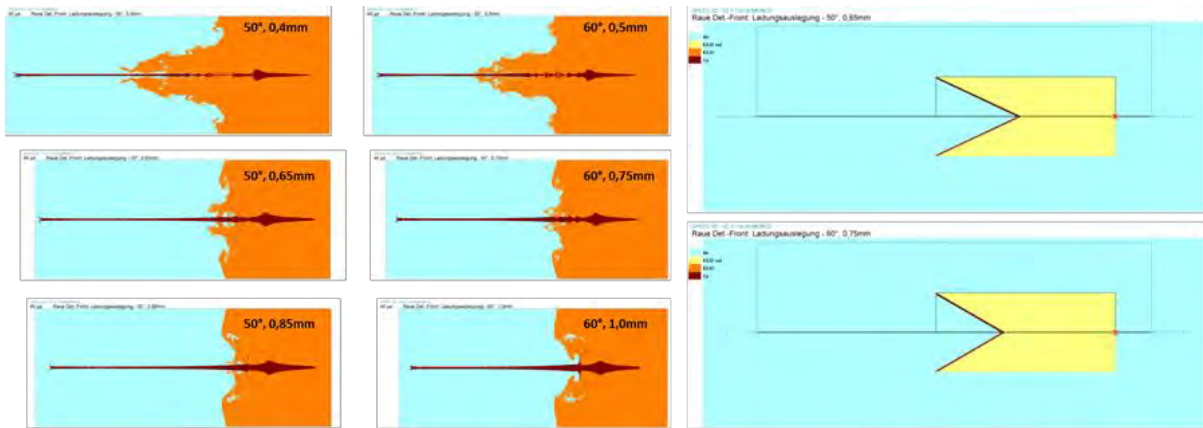


Fig. 6: Simulation model (right) and results (left) for a SC charge with caliber of 64 mm at $t = 50 \mu\text{s}$.

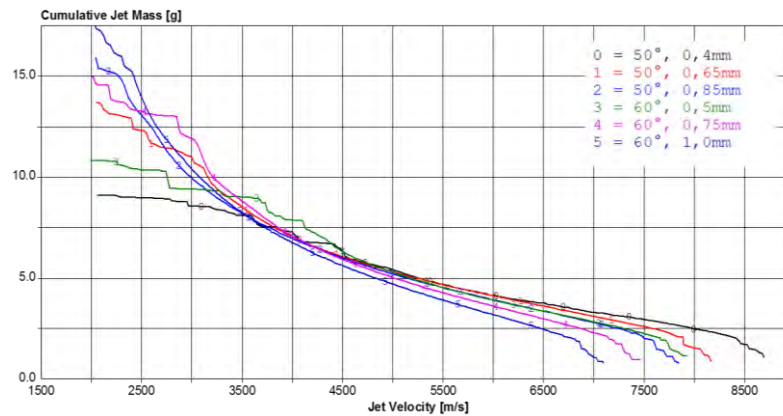


Fig 7: Mass profiles for the SC jets at $t = 50 \mu\text{s}$.

4.2 Selected SC Design

Following the simulation results and the underlying requirements, the SC design shown in Figure 8 was selected and manufactured. All three KS32 types were cast onto the liner and an additional HWC disk diameter 64 mm and thickness 10 mm (as introduced in Section 3) was applied to guarantee the same initiation conditions (run distances to detonation) for all three KS32 types. The explosive train was the same as in the roughness measurement test setup of section 3.

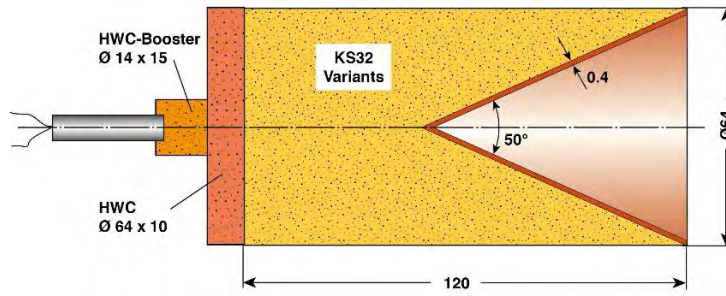


Fig. 8: Sketch of the test SC with a caliber of 64 mm.

The charges were fired in front of a double flash X-ray (FXR) camera and evaluated with respect to tip velocity, jet breakup, jet length and particle drift allowing a quantitative comparison of the influence of the grain size distribution and the detonation front roughness, respectively. Figure 9 shows a typical FXR picture with the nominal trigger times of $t_1 = 160 \mu\text{s}$ and $t_2 = 230 \mu\text{s}$. Supplementary a reference Cu wire was added to the setup for a better assessment of the jet thickness.

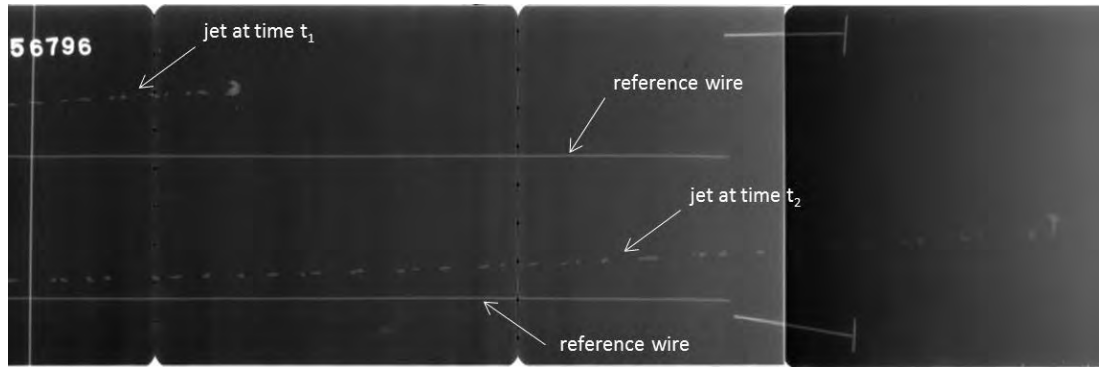


Fig. 9: FXR picture of the SC-Jet at two different times with a reference copper wire (HL56796).

4.3 Achieved SC-Jets and Evaluation procedure

In total, nine tests were conducted with the SC test charge containing the three different KS32 types (twofold repetition of each trial). Table 1 summarizes the test campaign showing the test numbering.

Tab 1: Summary of conducted SCJ test campaign

HMX grain size	standard	coarse	fine
series 1	HL56794	HL56795	HL56796
series 2	HL56797	HL56798	HL56799
series 3	HL56800	HL56801	HL56802

Figure 10 shows three FXR pictures of the tip (right) and rear part (left) of the SC jets with the three different KS32 types. Prior to the actual evaluation process these pictures shall be visually inspected.

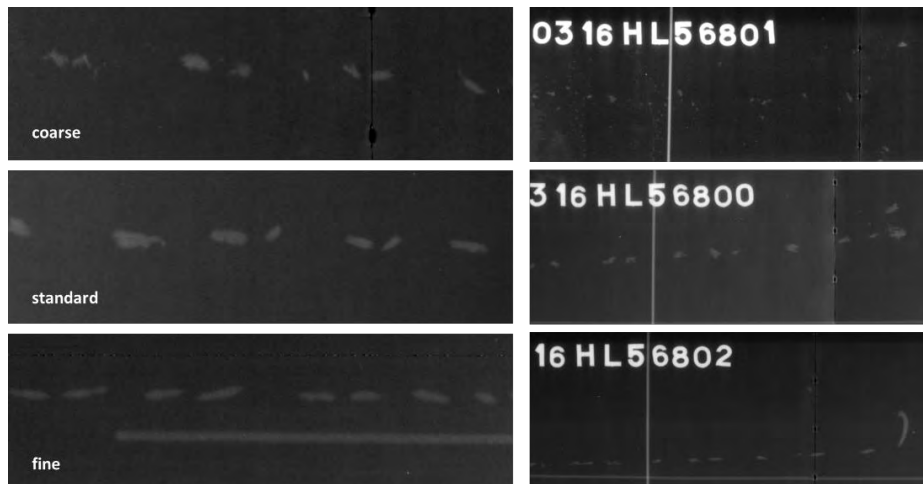


Fig. 10: Particulated SC jets: front part (right) and rear part (left) for the different KS32 types

The qualitative influence of the different the HMX grain sizes on the particles can be clearly seen in both parts of the jet: with KS32-fine the SCJ breaks up into well-defined particles, whereas with KS32-coarse these “particles” appear more like small fragments. With KS32-standard the behavior is somewhere in between.

All FXR pictures were electronically evaluated applying our in-house software EDI (Edge Detection in Images) [6]. EDI automatically detects the edges of the individual particles at the two FXR exposure times and determines tip velocity, jet breakup, jet length and particle drift. This data then allowed a quantitative assessment of the influence of the grains size distribution and thus of the roughness of the detonation front on these parameters. As an example for the EDI evaluation, Figure 11 shows a close-up of a part of a jet evaluation in an FXR picture for both tracks. Additionally, this detail highlights another aspect. From the comparison of the marked particle at t_1 and t_2 , it can be concluded that the particles are spinning around their axes and that they are not always rotationally symmetric but are often flattened.

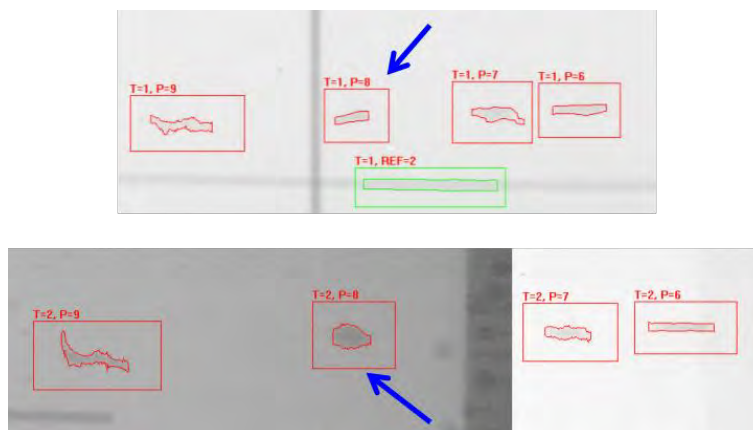


Fig. 11: Typical close-up of an EDI evaluation with a flat rotating particle (arrow).

4.4 Test Results

For the final quantitative assessment of the influence of the detonation front roughness on the SC jet behavior, all evaluation results were averaged over the three conducted trials per HMX grain size and compared to each other. This comparison is discussed in the following.

4.4.1 SCJ Velocity

Figure 12 shows the evaluation of the SCJ tip velocity for the three KS32 types (fine, standard and coarse). The open symbols indicate the three individual results of the trials whereas the full ones mark the mean values. All in all, the figure makes clear that no influence of the grains size on the tip velocity can be ascertained.

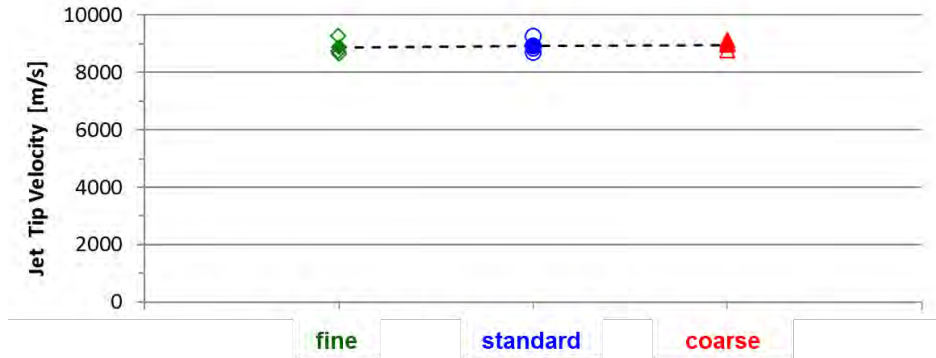


Fig. 12: Individual (open symbols) and averaged (closed symbols) SCJ tip velocities

4.4.2 Time and Position of SCJ Particulation

Figure 13 and Figure 14 illustrate the evaluation of all SCJ particles with respect to time and position of particulation. The assessment of mean breakup times in Figure 13 resulted in 78 μs for the fine, 64 μs for the standard and 62 μs for the coarse grained KS32 type with a standard deviation of ca. 22 μs . Due to the nearly identical jet velocities, the comparison of the particulation positions in Figure 14 shows practically the same behavior with 514 mm, 415 mm and 395 mm, respectively.

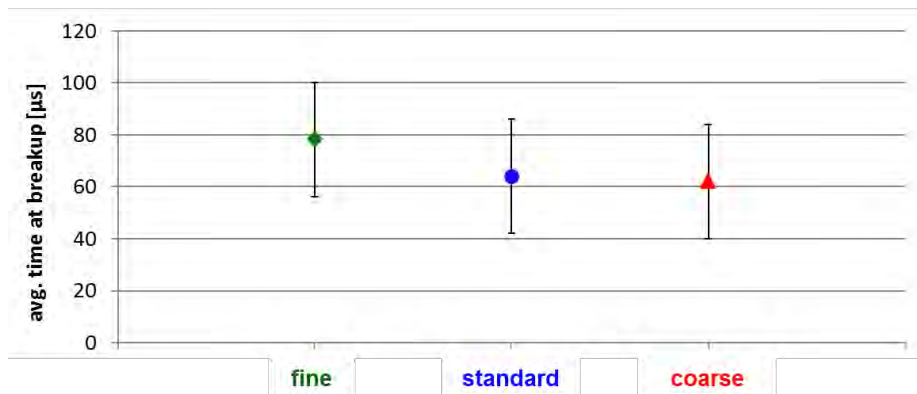


Fig. 13: Test results for the averaged particulation times.

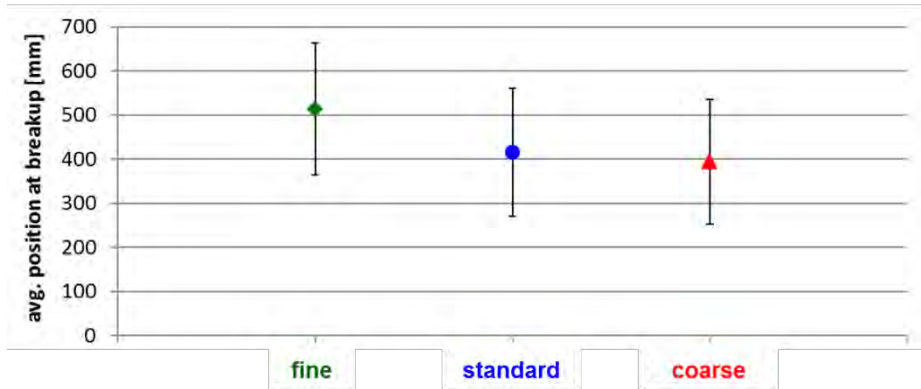


Fig. 14: Test results for the averaged particulation positions.

Even when the scattering in the data is taken into account, the tests clearly indicate that with the fine HMX grain size the particulation occurs at a larger distance and at a later time, respectively.

4.4.3 SCJ Cumulative Length

The cumulated length of the jet can be regarded as the most important parameter for the SCJ jet performance. The influence of the grain size distribution on this parameter is thus of particular importance.

Figure 15 shows the comparison of the averaged results. A significant influence of the grain size distribution on the jet length can be observed. Comparing the cumulated lengths at an exemplary jet velocity of 5000 m/s to KS32-fine, a 14% lower length can be observed with the KS32-standard charge and an even 18% lower length with the KS32-coarse charge.

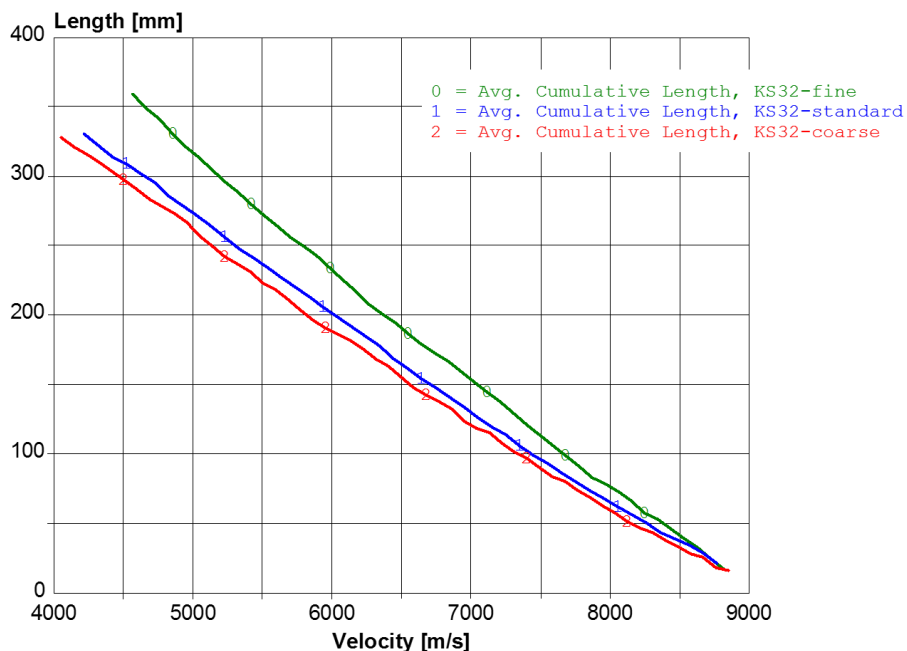


Fig. 15: Test results for the averaged cumulative jet lengths.

5 Conclusions

Three batches of KS32 (HMX/HTPB 85/15) with different distributions of the HMX grain size were manufactured:

- Standard: bimodal with mean grain sizes of 30 μm (fine mode) and 500 μm (coarse mode),
- Coarse: unimodal with mean grain size of 500 μm ,
- Fine: unimodal with mean grain size of 30 μm .

With these three KS32 types test setups for the measurement of the roughness of the detonation front were developed. The roughness was directly measured by the indentation (“footprint”) of the detonation front on Cu witness plates. In these tests with charges cast on the witness plates, a clear trend to an increased roughness with increased grain size could be observed. The roughest Cu surfaces showed maximum differences of 50 – 70 μm and 5 – 10 μm on average. It could further be found that the detonation front causes massive cratering in the CU surface, when the charge is machined and glued onto the Cu witness plates. This type of manufacturing process thus seems inappropriate for thin-walled SCJ liners.

Based on the results of this first study, a test shaped charge was designed to investigate the influence of this detonation front roughness on a shaped charge jet. In total nine SC charges were manufactured and shot in front of a FXR facility to study the particulated jets. An in-house software EDI was applied to evaluate and assess the SCJ characteristics. The SCJ velocity, particulation time and position and finally the cumulative length were evaluated. A significant influence of the roughness of the detonation front especially on the cumulative SCJ length was observed. At a jet velocity of 5000 m/s and compared to the KS32-fine charge, a 14% length decrease with KS32-standard and even 18% with KS32-coarse charge could be measured.

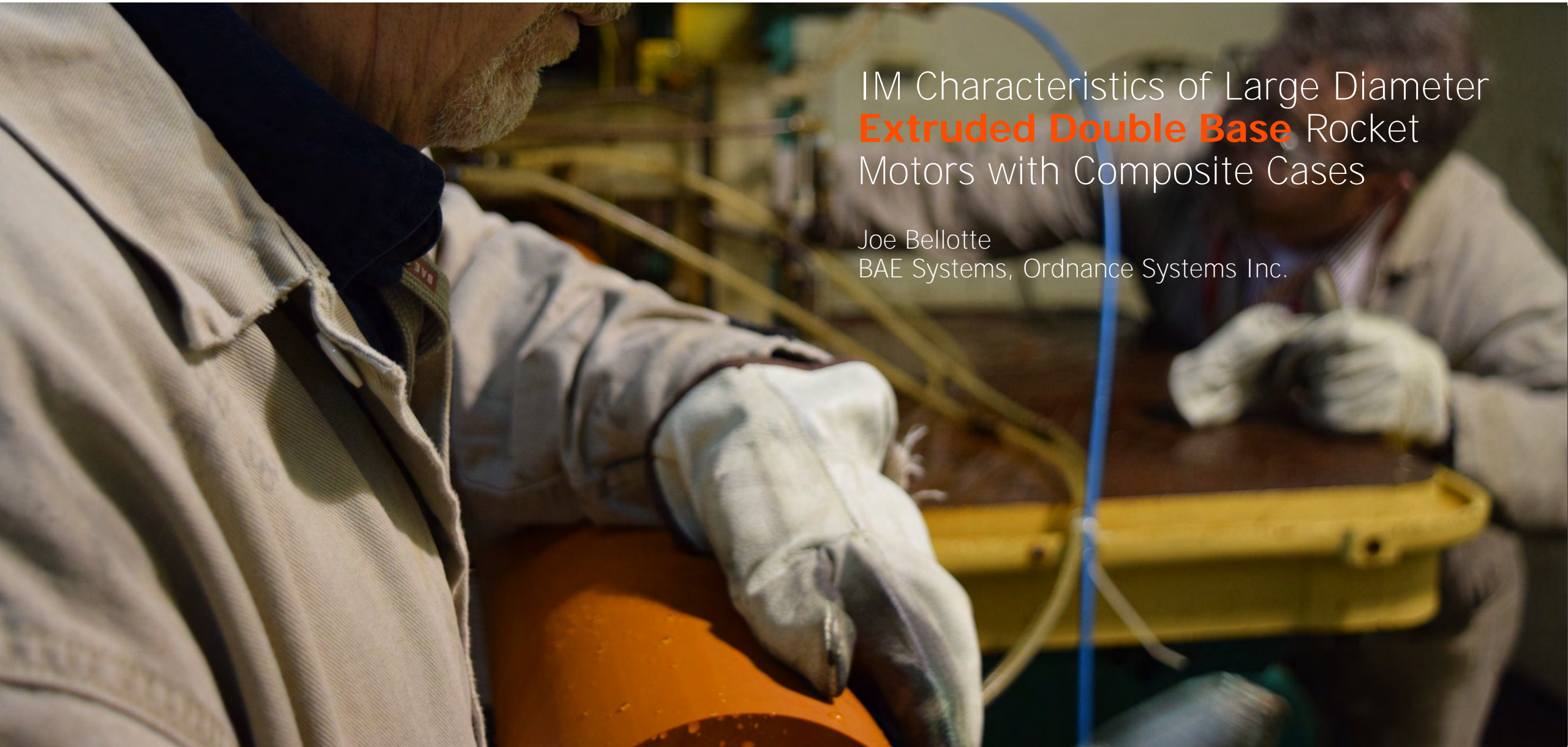
If the observed effects on the tested laboratory charge can also be found for practical (high-performance) shaped charges, however, is yet to be investigated. This will be part of future work.

Acknowledgement

The authors would like to thank the BAAINBw Team K1.2 at Koblenz for the funding of this study.

References

- [1] M. Held, “Roughness of the Detonation Front”, TDW-Report TDW-TN-AG41-134 (in German), 1984
- [2] P. Chanteret, A. Becuwe, A. Kerdraon, “A Study of the Influence of HE Grain Size on Shaped Charge Jet Fragmentation”, Proc. 13th Int. Symp. on Ballistics, Stockholm, Sweden, 1992
- [3] P. Chanteret, A. Lichtenberger, “About varying Shaped Charge Liner Thickness”, Proc. 17th Int. Symp. on Ballistics, Midrand, South Africa, 1998
- [4] I. Plaksin, R. Guirguis, L. Rodrigues, R. Mendes, S. Plaksin, E. Fernandes, C. Ferreira, „Effects of Meso-Scale Perturbations in the Detonation Reaction Zone on Shaped Charge Liner Response“, Proc. 28th Int. Symp. on Ballistics, Atlanta, GA, USA, 2014
- [5] W. Arnold, M. Graswald, E. Rottenkolber, “A Novel Technology for Switchable Modes Warheads”, 26th Int. Symp. on Ballistics, Miami, FL, USA, 2011
- [6] NN, „EDI 4.2 – User Manual“, TDW, NUMERICS, 2014



IM Characteristics of Large Diameter **Extruded Double Base** Rocket Motors with Composite Cases

Joe Bellotte
BAE Systems, Ordnance Systems Inc.

Traditional Extruded Double Base IM Response

- Typical IM response of extruded double base motors well characterized
 - Violent reactions for metal combustion chambers
 - Bullet Impact*
 - Frag Impact
 - Slow Cookoff
 - Fast Cookoff*
- Larger diameters are typically less favorable
 - Critical diameter can be a factor
 - Long L/D may present additional challenges

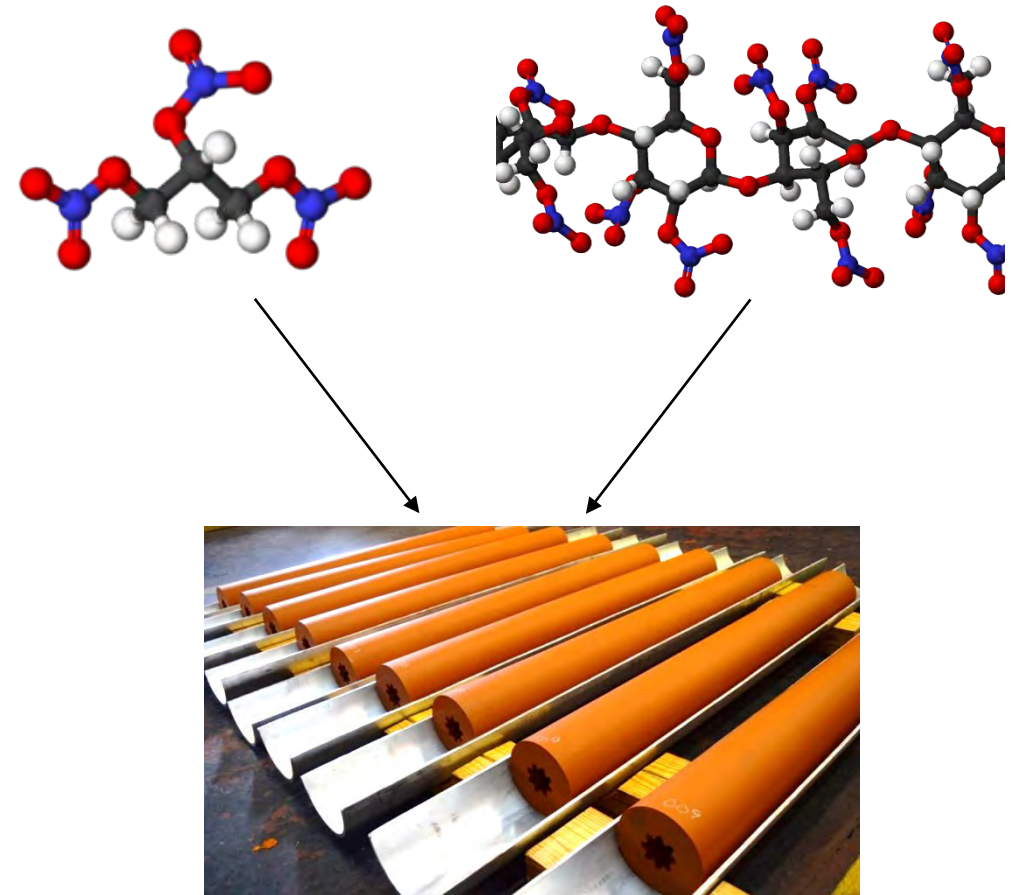


USS Forrestal Fire

*Not all EDB motors exhibit a violent response to this stimulus

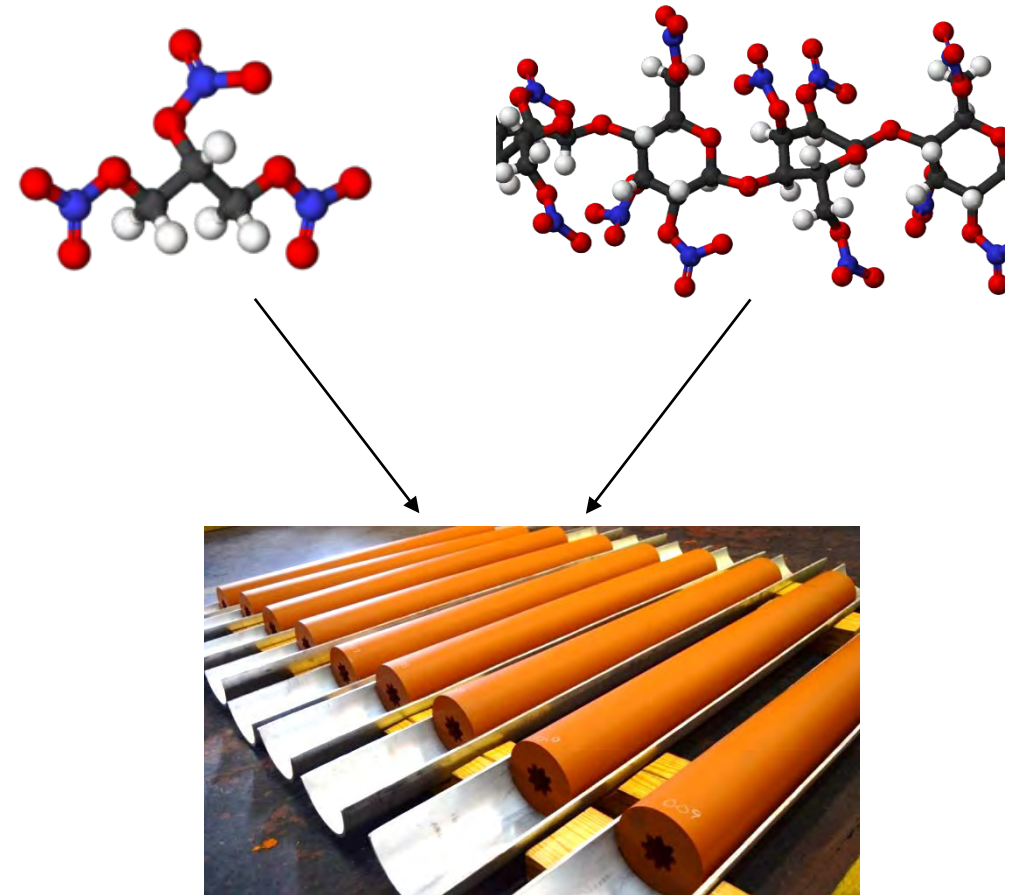
The Root of the Problem

- Inherent properties of EDB propellants
 - Both NG and NC are sensitive as individual components
 - The combination **REDUCES** the sensitivity of the materials
 - EDB propellants are the lowest card gap (least shock sensitive) in the Army production inventory
- Confinement
 - Confinement of double base is a known hazard
 - Metal cases provide minimal release in the event of a bullet or frag impact
 - Without bulkhead release mechanisms, cookoff results in the same issue



The Root of the Problem

- Lethal Fragments
 - Even less violent energetic reactions are a problem in the presence of lethal fragmenting materials
- Diameter
 - Even small diameters (less than 2") result in violent reactions



Previous Work on Composite Cases

- Hydra Missile (2.75" Diameter)
 - Previous work on the Mk. 66 motor shows improved IM response with composite cases
 - Simulated release mechanisms improved responses to cookoff environments
 - Tests may improve by performing system level test (including payload on the forward interface)
- Conclusions and Questions
 - Violent IM response not inherent to the energetic in the Mk. 66 configuration
 - Composite cases are a viable mitigation for EDB propellants
 - Is there a diametric limitation?



IM Test w/MK-66	Aluminum Case	Composite Case
Frag Impact (Army)	III – IV	IV**
Bullet Impact (.50 cal)	V	V
Fast Cook-Off	IV	V
Slow Cook-Off	III	IV**

*All information from IMEM 2006, Paper 7A, Farabaugh et. Al.

Extension to Large Diameter

- Large Diameter Tactical Motors
 - Development of large diameter tactical motors using EDB propellants ongoing
 - Benefits in cost, volume, complexity, manufacturability
 - Can IM properties be retained?



Recent Large Diameter Tactical Work

- Design and Manufacturing Development
 - Composite case EDB motors up to 6" in diameter have recently been developed for tactical application
 - More than double the web of the Mk. 66 rocket motor
 - Grain extrusion, machining, inhibition as well as motor performance in static testing have all been successfully demonstrated



Demonstrated IM Properties of Large Diameter EDB Motors

- Technologies incorporated for IM
 - Low shock sensitivity EDB propellant
 - Filament-wound graphite epoxy motor case
 - Shape memory alloy retention rings for forward and aft bulkheads

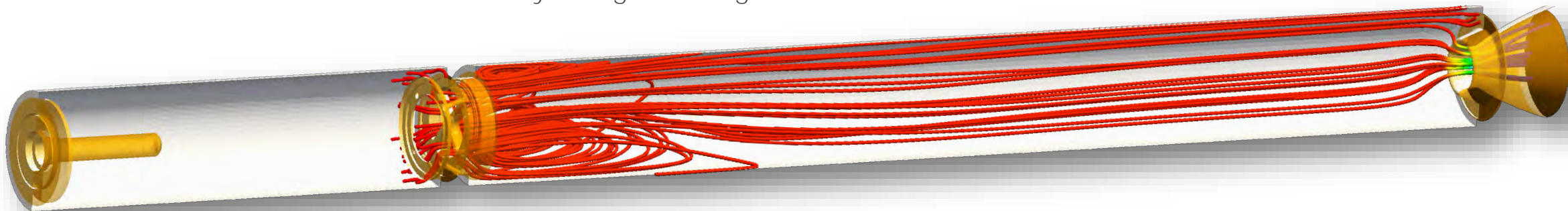


Demonstrated IM Properties of Large Diameter EDB Motors

- Tests
 - Fragment Impact
 - Slow Cookoff
 - Fast Cookoff
- Results
 - Even at the larger diameter and length, the composite case motors retain the IM properties demonstrated in the 2.75" size

Future Large OD Motor Work

- Larger Diameters
 - Demonstration of manufacturing and diameters larger than 6"
 - Evaluate IM response at thicker webs
- Additional IM mitigation
 - Evaluate IM response at a system level (payload, packaging)
 - Investigate IM response as a function of grain design (perf, L/D etc.)
 - Additional reduction in propellant shock sensitivity
 - Maintenance of shock sensitivity at higher energies



U.S. Navy Insensitive Munitions Handbook

Ken Tomasello and Heather Hayden, PhD
Insensitive Munitions Office
Naval Ordnance Safety and Security Activity, Indian Head, MD

Jerry Ward, PhD, Don Porada, and Mark Peterson, CSP
Booz Allen Hamilton, Arlington, VA

ABSTRACT

The Naval Ordnance Safety & Security Activity (NOSSA) is developing a “U.S. Navy Insensitive Munitions Handbook” as a comprehensive source of information tailored for the Navy Insensitive Munitions (IM) community, specifically for the munitions Program Offices that are required to develop and conduct IM Programs for their munitions. This paper is intended as an advance introduction to the Handbook and provides summary discussions of handbook contents, such as: (a) Selected history of the IM Program, (b) Navy IM policy and guidance, (c) The Navy IM development process, (d) The Joint IM Strategic Planning (IMSP)/Plans of Action and Milestones (POA&Ms) process (e) Selected IM research projects, (f) Threat Hazard Assessments, (g) IM qualification, and (h) IM compliance. The IM research projects and the relevant points of contact are based on information, from the FY17/18 IMSP/POA&Ms and documentation from technology programs with IM related efforts (Joint Munitions Program (JMP), Joint IM Technology Program (JIMTP), IM Advanced Development (IMAD) Program, and IM Technology Transition Program (IMTTP). The 2017 information is included in the Handbook to provide recent examples of the extent of IM research and collaboration that is indicative of the range of possibilities for future areas for IM research and development. Upon completion of the Handbook, NOSSA plans are to issue and maintain the Handbook on its secure website.

Introductory Sections of the Handbook

The Navy Goals for the IM Program

The Navy's goal is to fully implement the Department of Defense (DoD) IM Program. The Navy's approach is to address:

- a) **IM Technology** - Identify IM technology shortfalls for Navy and Joint munitions, conduct a robust Science and Technology (S&T) program to develop solutions for the shortfalls, and identify windows of opportunity for the Program Offices (POs) to insert the solutions in their munitions improvement/development programs.
- b) **IM Improvements** – Without regard to program acquisition category, all Department of Navy (DON) munitions are to be designed/improved to meet IM requirements. Operational capabilities and performance are to be attained without compromising system and platform safety.
- c) **IM Compliance** – A munition is certified to be IM compliant when it is assessed/scored by the Navy Munitions Response Evaluation Board (MREB) or by another appropriate Service Review Authority, to pass all required IM tests. The

Statement A: Approved for public release; distribution is unlimited.

Navy Munitions POs are to conduct coordinated IM/Hazard Classification (HC) testing that addresses the passing criteria for the six IM Threats (Fast Cook-off (FCO), Slow Cook-off (SCO), Bullet Impact (BI), Fragment Impact (FI), Sympathetic Reaction (SR), and Shaped Charge Jet (SCJ)). Achieving IM compliance is to be viewed over the munition program's entire life cycle. Passing all IM tests (full IM compliance) for a munition requires: **a)** A Burn Reaction or better (No Sustained Reaction) for the FCO, SCO, BI, and FI IM tests and **b)** An Explosion Reaction or better (Deflagration Reaction, Burn Reaction, or No Sustained Reaction) for the SR and SCJ tests.

Objectives of the Handbook

The objective of the Handbook will be to provide the Navy IM community with a reference and tutorial guide for executing a Munition's IM Program. The document addresses: **a)** A brief history of the IM program, **b)** The current IM policy and guidance as implemented by the Navy (**NOTE:** Copies of the current IM related Navy Instructions are provided in the Appendices, **c)** A description of the Navy's IM development process, **d)** Guidance on how to implement the Joint IMSP/POA&Ms process for the munitions in their portfolio, **e)** Information on sources of Navy, Joint, and other Service IM technology solutions and developments that can address IM technology shortfalls identified in the Munitions POs' POA&Ms, **f)** Guidance on preparing an IM Threat Hazard Assessment (THA), **g)** Guidance on complying with Qualification and Final (Type) Qualification requirements for Navy explosives (explosives, propellants, and pyrotechnics), **h)** Guidance on complying with the harmonized IM /HC testing and analysis requirements, and **i)** Guidance on evaluating the results of the harmonized IM/HC test results to assess a munition's compliance with IM criteria.

IM Background

In 1994, Ray Beauregard wrote an excellent paper entitled "History of the U.S. Navy Insensitive Munitions Program," <http://www.insensitivemunitions.org/> on the history of the Navy's IM program, which was subsequently revised in 2005 and 2009. Starting with the Chief of Naval Operation (CNO) issuing OPNAVINST 8010.13, the Handbook provides a selected listing (23) of DoD, Joint, and Navy guidance and policy issuances related to the U.S. Joint and DoD IM program.

IM Policy and Guidance

The Handbook provides the Navy Munitions Program Managers (PMs) and their program development teams the relevant U.S. law and DoD, Joint, and Navy policy and guidance regarding IM. The Handbook provides excerpts of important IM policy and guidance for executing the DoD IM Program, which are taken from the U.S. Law and DoD, Joint Chiefs, and MIL-STD issuances listed below:

U.S. Law - **USC, Title 10, Chapter 141, Section 2389** December 2001.

DoD Policy - **DoDD 5000.01**, The Defense Acquisition System May 12, 2003, Certified Current as of 20 November 2007, E1.1.23. Safety and **DoDI 5000.02**, Operation of the Defense Acquisition System, Encl. 3, System Engineering, January 7, 2015.

Joint Chiefs Policy - **CJCSI 3170.01I**, Joint Capabilities Integration and Development System, 23 January 2015.

MIL-STDs - **MIL-STD-882E**, Department of Defense Standard Practice, System Safety, 11 May 2012. and **MIL-STD-2105D**, Hazard Assessment Tests for Non-Nuclear Munitions, 19 April 2011. (Appendix C in Handbook.)

Navy IM Policy - The Navy implements the DoD/Joint IM Program via three Navy instructions: **OPNAVINST 8010.13E**, Department of Navy Policy on Insensitive Munitions, 14 January 2014. (Appendix D in Handbook.)

NAVSEAINST 8010.5C, Insensitive Munitions Program Planning and Execution, 15 September 2015. (Appendix E in Handbook.) – This instruction:

- a) Promulgates procedures and the Navy organizational structure for planning and executing an integrated DON IM Program, and amplifies IMSP policy and guidance provided in the DoD Standard Operating Procedure (SOP) for Insensitive Munitions Strategic Planning (IMSP) and Plans of Action and Milestones (POA&Ms) Defined by Joint Services Business Rules.
- b) Provides procedures for out-of-cycle waiver requests.
- c) Explains Joint Staff's Joint Requirements Oversight Council (JROC) responsibility to approve munitions procurement.
- d) Explains Navy's Weapon System Explosives Safety Review Board (WSESRB) responsibility for approval for service use.
- e) Establishes responsibilities, with respect to the IMSP/POA&M process, for the Commander, Marine Corps Systems Command (COMMARCORSSYSCOM) Project Manager for Ammunition (PM AMMO).
- f) Establishes responsibilities, with respect to the IMSP/POA&M process, for the IM Council (IMC) and its members, NOSSA N8 (Weapons Assessment Directorate), and the Naval Warfare Centers.
- g) Establishes responsibilities for Navy Munitions Program Executive Officers (PEOs) to comply with Navy IM policies and procedures for conducting an IM Program.
- h) Requires that:
 - i. All energetic material be qualified and undergo Final (Type) qualification per NAVSEAINST 8020.5C Qualification and final (Type) Qualification Procedures for Navy Explosives (High Explosives, Propellants, Pyrotechnics, and Blasting Agents), 05 May 2000 (Appendix I in Handbook).
 - ii. IM be integrated into a total system safety program per MIL-STD-882E.
 - iii. Each munition address FCO, SCO, BI, FI, SR, and SCJ threats per MIL-STD-2105D and applicable NATO Standardization Agreements (STANAGs). To be considered IM compliant, a munition item must, at a minimum, satisfy the passing criteria for the Joint Requirements Oversight Council/Office of the Under Secretary of Defense (JROC/OUUSD) Joint Standard IM Tests.

NOSSAINST 8010.1A, Munitions Reaction Evaluation Board (MREB), 30 August 2017.

(Appendix F in Handbook.) - This instruction states the mission, authority, responsibilities, and membership of the DON MREB. The MREB major responsibilities are to review for concurrence (in conjunction with the DoD Explosives Safety Board (DDESB) for HC testing): **a)** Detailed IM/HC test plans in concert with NOSSA N8's approved THAs and **b)** IM and basic safety test results to obtain an official (score) assessment of record of the reactions. NOSSA N8 renders a decision on final approval with MREB recommendation for approval of test plans and findings/recommendations.

Navy IM Development Process

The elements of the Navy's IM development process for planning and conducting an IM program, which generally takes from 1 to 15 years, is portrayed in Figure 1 and discussed below:

- a) Navy Weapons PEOs/PMs
 - i. PEOs/PMs initiate planning a munition development program.



Figure 1. The Navy IM Development Cycle

- ii. PMs are given a requirement from the Fleet or otherwise determine that there is a requirement for a new or improved munition.
 - iii. Munition design solutions are selected based on many factors including cost, schedule, warfighter and performance requirements, safety (including IM), THA, technology availability, reliability and maintainability, etc.
 - iv. One of the steps for planning a munition development is preparing an abbreviated or full IM POA&Ms.
- b) Weapons Life Cycle
- i. Based on requirements documentation, the PM determines (or validates if the development program is for improvement of an existing munition) the munition's life cycle and establishes:
 - (i) Operational environment - Where will the munition be used? — **(i)** Surface (land or sea), **(ii)** Underwater, **(iii)** Air launched from fixed wing or rotary aircraft and **(iv)** Continental United States (CONUS) or Outside the United States (OCONUS).
 - (ii) Logistical environment – How and where will the munition be stored and transported? — **(i)** Truck, ship or air transportation or **(ii)** Depots and/or ship storage.
- c) IM THA
- i. PM evaluates the life cycle environmental profile of a munition to determine the threats and hazards to which it may be exposed throughout its entire life cycle. The THA:
 - (i) Identifies the threats and hazards that the munition may be exposed to during its life cycle.
 - (ii) Analyzes the underlying causes, and assesses the potential results of exposure to these threats and hazards. — **(i)** This assessment of the potential threats and hazards includes those posed by friendly munitions, enemy munitions, accidents, handling, environmental lifecycle conditions, etc. and **(ii)** Provides rationale for which of the standard IM tests should be conducted on the munition, which tests may be deleted, as unnecessary/not appropriate and what additional testing that may be required to assess the basic safety of the munition.

- ii. Preparation of a THA is a required step in the development of an IM Program for an IM priority munition. (Section **7.2. Definitions of Terms for the Joint IMSP and POA&M Process**. of the Handbook) in the DoD SOP.
 - iii. A summary of the THA, or updated changes as necessary, is a required element of the munitions' POA&M.
- d) IM Tests
- i. Based on the approved THA and harmonized IM/HC Test Plan, the PM conducts the Joint Standard IM Tests per the JROC/OUUSD and required by MIL-STD-2105D. The Tests include FCO, SCO, BI, FI, SR, and SCJ.
 - ii. Note: In a harmonized IM and HC test program, there are two additional HC-only required tests: Thermal Stability Articles and 40 Ft Drop.
- e) Consequences of Reaction
- i. Based on the IM test results, what is the impact of the IM reactions on the warfighter, weapons platform, or logistical environment (storage or transportation)? Would the IM results lead to an event that could be catastrophic, resulting in potential loss of life and equipment? Or is the impact of the IM reactions so low such that there are little or no injuries or equipment damage? In other words, were the IM test results passing or failing the Joint Standard IM Tests pass/fail criteria?
 - ii. Is there technology available to reduce the severity of the IM reactions or is new IM technology needed?
- f) Vulnerability and Hazard Classification
- i. The reactions of munitions to the IM/HC threats/tests are used to determine the vulnerability of munitions in the environments (platform / transport / storage) that are encountered during the munitions life cycle.
 - ii. PMs must hazard classify their munitions per DoD 6055.09-M, DoD Ammunition and Explosives Safety Standards: General Explosives Safety Information and Requirements and NAVSEAINST 8020.8C (TB 700-2 / TO 11A-1-47), DoD Ammunition and Hazard Classification Procedures, to address threats to munitions during transport and storage.
- g) IM Science and Technology (S&T)
- i. The Office of Naval Research (ONR) programs and OUSD's JIMTP and the DoD/Department of Energy (DOE) JMP evaluate the munition program IM deficiencies as identified in IM testing and establish programs to address those deficiencies. If new less sensitive energetic molecules or binder materials are needed, efforts to fund such research would be funded by Basic Research, 6.1 Research, Development, Test & Evaluation (RDT&E) funding. If more advanced solutions are needed such as new energetic (explosive or propellant) formulations, new case materials or designs, or modeling and simulation to predict munition energetic responses in lieu of destructive testing, then research efforts would be funded by Applied Research, 6.2 RDT&E funding, and/or Advanced Technology Development, 6.3 funding.
 - ii. The PMs work closely with the Office of Naval Research (ONR), JIMTP and JMP so that those S&T programs can develop the technologies to address munitions' IM deficiencies and Fleet operational requirements.
- h) IMAD and IMTTP
- i. As S&T IM technologies mature and are successful, the next step is demonstration and validation, with 6.4 RDT&E funding, prior to implementation and transition to the Navy PMs' munitions. IMAD and IMTTP are the Navy's 6.4 Demonstration and Validation programs with the goal of maturing and transitioning 6.3 IM technologies for application by PMs in their munition development programs.
 - ii. The focus of IMTTP is Air-launched weapons. IMAD was established to develop, mature and transition IM technology for all DON munitions.

- iii. The IM technologies available for transition include new explosives and warheads, new propellants and rocket motors, advance gun propulsion systems, new container materials and shielding. Successful IM technologies from IMAD and IMTTP reduce the munitions sensitivity to the IM threats while maintaining or exceeding operational requirements.
- i) Return to Navy Weapon PEOs/PMs
 - i. The PM's IM POA&M documents their munition programs' IM approach and progress and is included in the PEO's biennial IMSP.
 - ii. When deficiencies are found for a given developmental munition in IM testing, the development cycle may be repeated if the IM technologies do not exist to effectively address the IM deficiencies and meet operational requirements.

Joint IMSP/POA&Ms Process

OUSD (Acquisition, Technology and Logistics), OUSD (AT&L), issued the initial policy for IMSP in 2004. DoD SOP for IMSP and POA&Ms, 3rd Revision, March 2017 is the current issuance that promulgates the policy and mandatory requirements for IMSP. In addition, the SOP provides the IM community "business rules," additional business processes, to enhance the overall management of the IMSPs, to include assigning roles and responsibilities for conducting reviews of the IM POA&Ms. The objective of Section 7. **Joint IMSP/POA&Ms Process** of the Handbook is to provide Navy Munitions PEOs/PMs and their munitions program development teams with a summary of the mandatory guidance in the SOP. The policy and mandatory guidance for the IMSP process provided in the SOP is summarized in the Handbook. Specifically, the Handbook addresses:

- a) **Schedule** - Provides a notional Navy IMSP schedule for the preparation of the IMSPs developed by the Navy Munitions PEOs, which include the relevant POA&Ms developed by the munitions PMs as appendices. The IMSPs/POA&Ms are submitted to the JROC for approval biennially to address the planning process for a two-year period starting with an odd numbered year.
- b) **Approval Process** - Describes the Navy-specific IMSP approval process.
- c) **Development Process** - Describes the IMSP/POA&M Development Process. Several important points include:
 - i. Each DON Munitions PEO/PM is responsible for developing and maintaining a munitions Portfolio containing all munitions they procure, as well as for all munitions for which they have a Configuration Management (CM) role whether they are being actively procured or not.
 - ii. Approval of the IMSP by the JROC constitutes the authority to procure non-IM compliant items for the two-year period covered by the IMSP.
 - iii. The authority to procure a non-IM compliant item not contained in any Service IMSP requires an "out-of-cycle waiver," which must be obtained from the JROC through a separate process.
- d) **Preparing IMSP/POA&Ms** - To support the Navy Munitions PEOs/PMs and their teams in preparing their IMSP and POA&Ms, NOSSA IMO (N855) maintains an IMSP/POA&Ms Scorecard Template on the NOSSA Secure Website for reviewing/scoring IMSP Key Elements prescribed in the SOP (Part A, Section 4.0) and summarized in the Handbook. The Scorecard Template is an excellent tool/guide that should be used by the Navy Munitions PEOs/PMs and their teams in their development of acceptable / approvable IMSPs/POA&Ms.
 - i. **IMSP Key Elements** - The format for the IMSP is left to the discretion of the reporting PEO/PM. However, specific key elements (Section 7.8.2 **IMSP Key**

Elements. of the Handbook). are to be included in the development of the IMSP.

- ii. **POA&M Formats** - Prescriptive formats (Section **7.8.3 POA&M Formats.** of the Handbook) have been established by the JSIMTP and the DoD IM IPT for the POA&Ms to ensure uniformity in documenting the IM efforts across the Joint Service IM community.

IM Technology

As per NAVSEAINST 8010.5C policy, Munitions PMs under cognizant PEO or Systems Command authority, are to seek every window of opportunity to incorporate appropriate technologies developed by the JMP, JIMTP, IMAD Program, and IMTTP, and similar programs of other Services, to provide IM-compliant munitions for the Naval Fleet. The objective of Section **8. IM Technology** of the Handbook is to provide Navy Munitions PMs and their munitions program development teams with a broad overview of the resources available to them that has IM RDT&E technology concepts and data that may have applicability to the IM Improvement Programs for their priority munitions. The IM efforts span Applied Research (6.2), Advanced Technology Development (6.3), and Demonstration and Validation (6.4) RDT&E funding as well as international projects, and seek solutions to gaps in IM technology that inhibit development of IM-compliant munitions. Identifying research projects that have application to the Program's specific munition can lead to collaborative efforts to pursue, and/or leverage, relevant solutions to successfully address the standard IM threats or any additional threats identified by the munitions' THA. The Handbook:

- a) Provides brief descriptions of the IM technology programs JMP, JIMTP, IMAD Program, and IMTTP, discusses the missions and IM technology focus areas and provides recent (Fiscal Year 17 (FY17)) example IM research project titles, as available, and identifies the POCs. References are provided for the FY17/18 Navy, Army, Missile Defense Agency (MDA), and U.S. Special Operations Command (USSOCOM) IMSP/POA&Ms.
- b) Discusses partnering agreements that describe an understanding of mutual interest regarding an IM technology.
- c) Describes existing (and under development) web-based repositories/portals for data generated by the IM technology programs.

Threat Hazard Assessments

A THA is an evaluation of the life cycle environmental profile of a munition to determine the threats and hazards to which it may be exposed throughout its entire life cycle. The munitions life cycle covers the years-long period from concept development to final disposition, whether the end state is operational employment against a target, expenditure in training or testing, or demilitarization/disposal. The THA identifies the threats and hazards that the munition may be exposed to during its life cycle, analyzes the underlying causes, and assesses the potential results of exposure to these threats and hazards. The THA provides rationale for which of the standard tests should be conducted on the munition, and which tests may be deleted, as unnecessary. The THA may also propose additional testing that may be required to assess the basic safety of the munition. The preparation of a THA is a required step in the development of an IM Program. And a summary of the THA, or updated changes as necessary, is a required element of the munitions' POA&M. To support the Navy Munitions PEOs/PMs and their teams in preparing THAs, NOSSA IMO (N855) is preparing a THA Template to be maintained on the NOSSA Secure Website.

IM Qualification

NAVSEAINST 8010.5C requires that “IM must be successfully integrated into a total system safety program” per MIL-STD-882E. As stated in NAVSEAINST 8020.5C, *“Qualification is the assessment of the explosive material to determine whether it possesses properties that make it safe and suitable for consideration for use in its intended role. Final (Type) Qualification is granted when the qualified explosive has been assessed as part of the design of a specific munition and predicted to be safe and suitable for military operational or training use.”*

NAVSEAINST 8020.5C applies to explosives at Navy installations and aboard Navy ships or aircraft, whether designed and built by the Navy or developed by other Services, private industry, or foreign sources and whether intended for operational use, testing, training, or transport. Fleet ballistic missile strategic weapons and nuclear weapons are excluded.

The Qualification and Final (Type) Qualification, per NAVSEAINST 8020.5C, of all energetic material in Navy munitions is essential to the Navy implementation of the IM program. This ensures that the energetic materials are safe and suitable for use in Navy munitions before operational, safety and IM evaluation of the end item munition. The Naval Sea Systems Command (NAVSEASYS COM) is assigned the Navy-wide responsibility for energetic materials, explosives safety and IM policy. Lead Systems Command responsibilities include the approval authority for Qualification and Final (Type) Qualification of explosives.

IM Compliance

IM Requirement., USC, Title 10, Chapter 141, Section 2389 December 2001 states “§ 2389. Ensuring safety regarding insensitive munitions. The Secretary of Defense shall ensure, to the extent practicable, that insensitive munitions under development or procurement are safe throughout development and fielding when subject to unplanned stimuli.”

As per OPNAVINST 8010.13E, all DON munitions, without regard to program acquisition category are to be designed to meet IM requirements. Operational capabilities and performance are to be attained without compromising system and platform safety. IM should be integrated using a systems safety approach. Achieving IM compliance or incremental improvement in IM compliance is considered over the program's entire life cycle.

Munition POs’ IMSP/POA&Ms, which are submitted to the JROC and OUSD(AT&L) (now OUSD (Acquisition and Sustainment (A&S)) biennially, document the program, progress and status of the POs’ munitions IM improvement program for achieving IM compliance.

Harmonized Joint IM/HC Testing, Requirements, and Passing Criteria - The Joint IM community began to coordinate IM testing with the Joint Hazard Classifiers with the publication of MIL-STD 2105B in January 1994. OUSD Memo dated 01 February 2010 approved the set of IM standardized tests and criteria.

Table 10-1. in Section **10.2.1 Joint Standard IM Tests** of the Handbook, lists the JROC/ OUSD approved set of Joint standardized IM tests and the additional two HC-only required tests, the passing criteria, the required number of tests, and the test munition configuration (whether logistical or operational). Figure 2 defines the IM threats associated with each of the six Joint IM Tests, the potential munition responses (reaction types) to the IM tests, and the passing criteria for each test to obtain IM compliance.

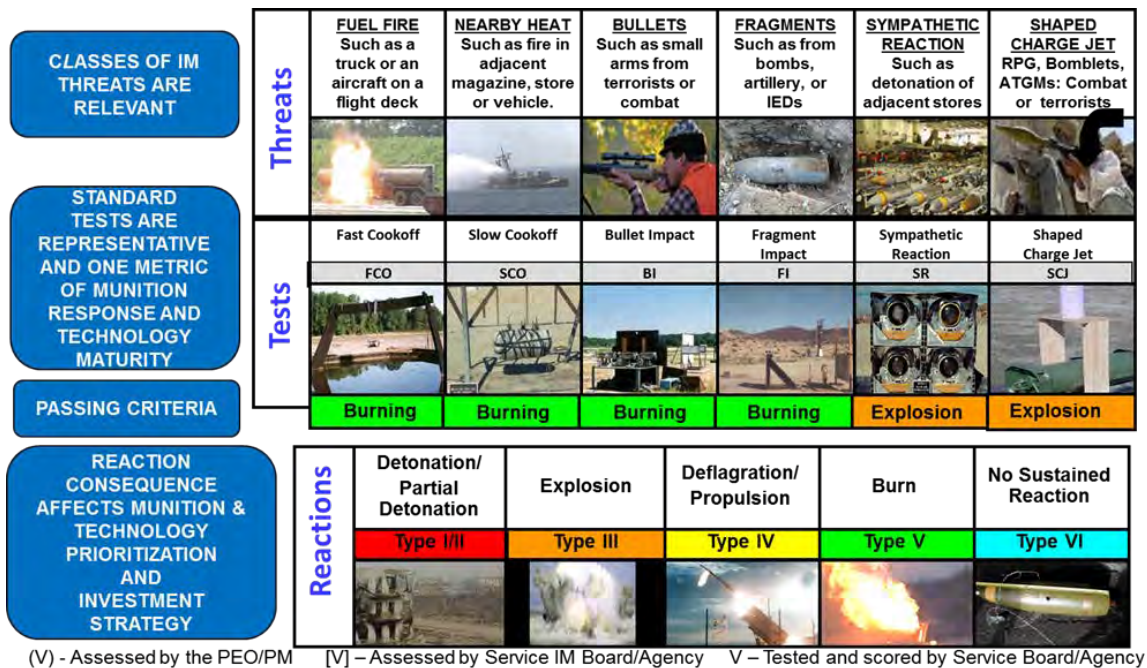


Figure 2. IM Threats, Standard Tests, and Reaction Types

Munitions POs are responsible for preparing an approved munition-specific harmonized IM/HC test plan that is based on the Joint Standard IM and the HC tests, and obtaining the approval of the test plan prior to IM and HC testing. Upon approval of the munition-specific harmonized IM/HC test plan, Munitions POs are responsible for conducting the required IM tests. Final test reports must be submitted to NOSSA IMO N855. Test responses to the IM tests must be validated by the MREB for munitions programs led by the DON or by the appropriate Service board if led by another Service. Test responses to the IM and HC tests must be validated by the Navy (NOSSA N851) and other Service Joint Hazard Classifiers and the DDESB.IM Compliance section.

IM/HC Test Plan Template - NOSSA IMO (N855) has developed a template, the **U.S. Navy Munition Test Plan Template for Combined Insensitive Munitions/Final Hazard Classifications**, to provide a tool for the Navy IM and HC communities to prepare coordinated IM and HC test plans with test requirements, guidance, and best practices combined into one harmonized test document. The Template is maintained on the NOSSA Secure Website.

Verifying IM Compliance - The MREB, whose mission, authority, responsibility, and membership is prescribed in NOSSAINST 8010.1A, is the responsible body to approve Navy IM/HC test plans for IM, to concur that the IM/HC tests were conducted as approved by the MREB, and to score the munitions' reaction types during the IM/HC tests.

Reporting IM Compliance - Munition POs report the status of their program to achieve IM compliance in their required biennial munition-specific POA&Ms, which accompany their IMSP submission to the JROC and OUSD(A&S). Specifically, the status of IM compliance for a specific munition is reported in a POA&M "IM Reaction Table." Table 11-1 in the Handbook is an example IM Reaction Table, which is taken from the DoD SOP. Table 11-1. was developed for the DoD SOP for IMSP and POA&Ms to portray the progress of the POs' IM Improvement Programs to achieve IM compliance for their munition in their munition specific POA&M.

Concluding Remarks

This paper is an advance introduction to the Handbook, which, upon completion, will be issued by NOSSA on its secure website. NOSSA plans to update the Handbook on its secure website, as necessary. The Handbook will be a comprehensive source of information tailored for the

Navy IM community. The IM research projects and the relevant POCs are based on information from the FY17/18 IMSP/POA&Ms and documentation from technology programs with IM related efforts (e.g., JMP, JIMTP, IMAD Program, and IMTTP). Information on 2017 research programs is included in the Handbook to provide recent examples of IM related research and collaboration that is indicative of the range of possibilities for future areas for IM research and development.

Acknowledgements

The Naval Ordnance Safety & Security Activity sponsored the development of the “U. S. Navy Insensitive Munitions Handbook” and the preparation and presentation of this paper.



U.S. Navy Insensitive Munitions Handbook

*Presented by Jerry M. Ward, Ph.D.
Booz Allen Hamilton
Arlington, Virginia*



Acknowledgements

SPONSOR

Naval Ordnance Safety and Security Activity (NOSSA)

NOSSA co-authors

Ken Tomasello and Heather Hayden, PhD

Booz Allen Hamilton co-authors

Don Porada and Mark Peterson



Outline

- **BLUF**
- **Navy Goals for IM Program**
- **Handbook Objectives**
- **IM Policy and Guidance**
- **Navy IM Development Process**
- **Joint IM Strategic Planning (IMSP)/Plans of Action & Milestones (POA&Ms) Process**
- **IM Technology**
- **Threat Hazard Assessment (THA) – Backup slide**
- **IM Qualification – Backup Slide**
- **IM Compliance**
- **Concluding Remarks**



BLUF

- To inform the international IM and Munitions Safety communities that NOSSA is developing a U.S. Navy Handbook as a source of information tailored for the Navy IM community, specifically for the munitions Program Offices (POs) that are required to develop and conduct IM programs for their munitions.
- This paper is intended as an advance introduction to the Handbook and provides selected summary discussions of the Handbook contents.
- Upon completion of the Handbook, NOSSA plans are to issue and maintain the Handbook on its secure website.



Navy Goals for IM Program

- **IM Technology** – Identify IM Technology shortfalls and conduct Science & Technology (S&T) program to develop solutions.
- **IM Improvements** – All Navy munitions are to be designed/improved to meet IM requirements. Operational capabilities and performance are to be attained without compromising system and platform safety.
- **IM Compliance** – A munition is certified to be IM compliant when it is assessed/scored by the Navy Munitions Response Evaluation Board (MREB) or by another appropriate Service Review authority, to pass all required IM tests. Navy Munitions POs are to conduct coordinated IM/Hazard Classification (IM/HC) testing.



Handbook Objectives

- Brief history of IM program
- Current IM policy/guidance as implemented by the Navy
- Description of the Navy's IM development process
- Guidance on how to implement the Joint IMSP/POA&Ms process
- Information on sources of Navy, Joint, and other Service IM technology solutions and developments that address IM technology shortfalls
- Guidance on preparing IM Threat Hazard Assessments (THAs)
- Guidance on complying with Qualification and Final (Type) Qualification for Navy explosives
- Guidance on complying with harmonized IM/HC testing and analysis requirements
- Guidance on evaluation results of the harmonized IM/HC test results to assess a munition's compliance with IM criteria



IM Policy and Guidance

- USC, Title 10, Chapter 141, Section 2389 December 2001 – **§ 2389**. *Ensuring safety regarding insensitive munitions*
- DoDD 5000.01, The Defense Acquisition System and DoDI 5000.02, Operation of the Defense Acquisition System, Encl. 3, System Engineering
- CJCSI 3170.01I, Joint Capabilities Integration and Development System
- MIL-STD-882E, Department of Defense Standard Practice, System Safety
- MIL-STD-2105D, Hazard Assessment Tests for Non-Nuclear Munitions (Appendix C in Handbook)



IM Policy and Guidance

- **OPNAVINST 8010.13E**, Department of Navy (DON) Policy on Insensitive Munitions (Appendix D in Handbook)
- **NAVSEAINST 8010.5C**, Insensitive Munitions Program Planning and Execution, (Appendix E in Handbook)
- **NOSSAINST 8010.1A**, Munitions Reaction Evaluation Board (MREB) (Appendix F in Handbook)
- **NAVSEAINST 8020.5C**, Qualification and Final (Type) Qualification Procedures for Navy Explosives (High Explosives, Propellants, Pyrotechnics, and Blasting Agents) (Appendix I in Handbook)
- **NAVSEAINST 8020.8C**, (TB 700-2/TO 11A-1-47, Joint Technical Bulletin), Department of Defense Ammunition and Explosives Hazard Classification Procedures

Navy IM Development Process





Joint IMSP/POA&Ms Process

- The Department of Defense (DoD) Standard Operating Procedure (SOP) for IMSP and POA&Ms provides the policy and mandatory guidance for the Joint IMSP/POA&Ms process.
- The U.S. Navy Handbook provides the Navy Munitions Program Executive Officers/Program Managers (PEOs/PMs) and their munitions development teams with a tailored (Navy specific) summary of the DoD SOP.
 - Schedule
 - Approval process
 - Policy and mandatory guidance for IMSP/POA&Ms preparation



IM Technology

- NAVSEAINST 8010.5C (IM Program Planning and Execution) – Munitions PMs are to seek every window of opportunity to incorporate appropriate technologies to provide IM-compliant munitions for the Naval Fleet.
- The Handbook addresses:
 - IM technology programs
 - Joint Munitions Program (JMP)
 - Joint IM Technical Panel (JIMTP)
 - IM Advanced Development (IMAD) Program
 - IM Technology Transfer Program (IMTTP)
 - Other PM/Service/Agency/Combatant Command Programs
 - Web-based repositories/portals for data generated by IM technology programs
 - Partnering agreements.



IM Compliance

- The requirement - USC, Title 10, Chapter 141, Section 2389 December 2001 states “§ 2389. *Ensuring safety regarding insensitive munitions. The Secretary of Defense shall ensure, to the extent practicable, that insensitive munitions under development or procurement are safe throughout development and fielding when subject to unplanned stimuli.*”
- The Handbook summarizes the procedure for ensuring IM compliance:
 - The Munitions PO develops/obtains a MREB/Joint Hazard Classifiers (JHC)/DoD Explosives Safety Board (DDESB)) approved Harmonized IM/HC test plan
 - The Munitions PO conducts the IM/HC tests
 - The MREB scores the IM tests and the JHC/DDESB assesses the IM/HC test results and determines the munition Final HC (FHC)
 - The Munitions PO reports the status of their program to achieve IM compliance in their required biennial munition-specific POA&Ms.













IM Threats, Standard Tests and Reaction Types






CLASSES OF IM THREATS ARE RELEVANT

STANDARD TESTS ARE REPRESENTATIVE AND ONE METRIC OF MUNITION RESPONSE AND TECHNOLOGY MATURITY

PASSING CRITERIA

REACTION CONSEQUENCE AFFECTS MUNITION & TECHNOLOGY PRIORITIZATION AND INVESTMENT STRATEGY

Threats	<u>FUEL FIRE</u> Such as a truck or an aircraft on a flight deck 	<u>NEARBY HEAT</u> Such as fire in adjacent magazine, store or vehicle. 	<u>BULLETS</u> Such as small arms from terrorists or combat 	<u>FRAGMENTS</u> Such as from bombs, artillery, or IEDs 	<u>SYMPATHETIC REACTION</u> Such as detonation of adjacent stores 	<u>SHAPED CHARGE JET</u> RPG, Bomblets, ATGMs: Combat or terrorists 
	Fast Cookoff FCO	Slow Cookoff SCO	Bullet Impact BI	Fragment Impact FI	Sympathetic Reaction SR	Shaped Charge Jet SCJ
Tests						
	Burning	Burning	Burning	Burning	Explosion	Explosion

Reactions	Detonation/ Partial Detonation	Explosion	Deflagration/ Propulsion	Burn	No Sustained Reaction
	Type I/II	Type III	Type IV	Type V	Type VI
					

(V) - Assessed by the PEO/PM [V] – Assessed by Service IM Board/Agency V – Tested and scored by Service Board/Agency



Concluding Remarks

This paper is an advance introduction to the Handbook, which, upon completion, will be issued by NOSSA on its secure website. NOSSA plans to update the Handbook on its secure website, as necessary.



Backup Slides

THA

- A THA is an evaluation of the life cycle environmental profile of a munition to determine the threats and hazards to which it may be exposed throughout its entire life cycle.
- The THA provides rationale for which of the standard tests should be conducted on the munition, and which tests may be deleted, as unnecessary. The THA may also propose additional testing.
- The preparation of a THA is a required step in the development of an IM Program.
- To support the Navy Munitions PEOs/PMs and their teams in preparing THAs, NOSSA IMO (N855) is preparing a THA Template to be maintained on the NOSSA Secure Website. The THA Template will be summarized in the Handbook.



IM Qualification

- The Handbook summarizes the requirements/guidance from:
 - NAVSEAINST 8010.5C (IM Program Planning and Execution):
 - “IM must be successfully integrated into a total system safety program” per MIL-STD-882E (DoD System Safety)
 - Qualification and Final (Type) Qualification of all energetic material in Navy munitions per NAVSEAINST 8020.5C is essential to the Navy IM program.
 - OPNAVINST 8010.13E (DON Policy on IM):
 - Lists the Joint Requirements Oversight Council (JROC)/Office of the Under Secretary of Defense (OUSD) approved set of standardized IM tests and the additional two HC (only) required tests and their passing criteria.
 - IM/HC Test Plan Template developed by NOSSA IMO (N855) to be tool for the Navy IM and HC communities to prepare coordinated / standardized IM/HC test plans.



Table 10-1 Joint Standard IM Tests (2017)

TESTS	REFERENCES	# OF TESTS	TEST CONFIGURATIONS
LF/EF (FCO)	STANAG 4240, E2 (Revision in process)	2	1 Test Logistical 1 Test Operational
SLOW HEATING (SCO)	STANAG 4382,E2, Procedure 1	2	2 Tests Logistical
BI	STANAG 4241, E2, Procedure 1 (HD1.2.3/ 1.6) (Revision in process)	2(3)	1(2) Logistical 1 Test Operational
FI	STANAG 4496, E1, Standard Procedure	2	1 Test Logistical 1 Test Operational
SR	STANAG 4396, E2	2	2 Tests Logistical (1 Test w/confinement, 1 Test w/o confinement)
SCJ	STANAG 4526, E2, Procedure 2 (Revision in process)	2	1 Test Logistical 1 Test Operational
THERMAL STABILITY ARTICLES	NAVSEAINST 8020.8C	1	1 Test Logistical
40 FT DROP	NAVSEAINST 8020.8C	3	3 Tests Logistical



Table 11-1 IM Reaction Table (Example)

	FCO	SCO	BI	FI	SR	SCJ	HC	FY	Remaining IM Investment (\$K)	
Baseline										
XXX	III	III	I	I	[F]	[F]	1.1E	FY02		
XXX	IV	V	V	III	P	[F]	1.2.1E	FY02		
XXX	[III]	III	IV	III	[P]	[P]	1.2.2H	FY02		
Current										
XXX	III	III	I	I	[F]	[F]	1.1E	FY09		
XXX	IV	V	V	III	P	[F]	1.2.1E	FY09		
XXX	[III]	III	IV	III	[P]	[P]	1.2.2H	FY09		
Alternative Configurations										
XXX	IV	V	V	III	P	II	1.1E	FY12		
XXX	III	III	[IV]	[III]	P	P	1.1E	FY12		
Projected										
XXX	(III)	(III)	(I)	(I)	(F)	(F)	1.1E	FY15		
XXX	(V)	V	V	(IV)	P	(P)	1.2.1E	FY15		
XXX	(IV)	(V)	IV	(IV)	(P)	(P)	1.2.2H	FY15		

Cost of Propane Fast Cook-Off Testing

Jon J. Yagla and David Hubble

Naval Surface Warfare Center Dahlgren Division, Dahlgren, Virginia

Ephraim Washburn

Naval Air Warfare Center Weapons Division, China Lake, California

ABSTRACT

The cost of fast cook-off testing with propane has been obtained by careful tracking of expenses over a significant number of tests. These costs are compared to liquid fuel fire testing. The costs consist of nonrecurring costs, the costs directly attributable to a given test, and recurring costs of damage repair, maintenance, and environmental compliance. The nonrecurring costs are design, siting, materials, chamber fabrication, fuel distribution systems, fabrication, and calibration. The costs attributable to a given test are mainly planning, construction of test stands, instrumentation, field crews, fuel, data analysis, and reporting. Recurring costs of damage repair, maintenance of the cook-off facility including fuel equipment, and environmental compliance are itemized.

These costs have been compared to the corresponding costs of liquid fuel fire testing. The cost of testing with propane is shown to be significantly less than with liquid fuels. The total cost of the propane fast cook-off test was found to be \$25,886, compared to \$36,791 for the liquid fuel test. The paper explains the development of the cost model and cost of each item, and how the costs were obtained.

INTRODUCTION

A cost assessment was performed to compare the total operating costs associated with performing fast cook-off testing. Both the propane fast cook-off (FCO) burner and the traditional jet fuel pool fire were analyzed (Figure 1 and Figure 2).



Figure 1. US Navy FCO 3.7 m by 3.7 m propane burner located in Dahlgren, Virginia

The total operating cost of the propane burner is based on data from the burners that were developed and operated at Dahlgren (2.4 m by 2.4 m and 3.7 m by 3.7 m square burners). Annualized recurring cost data are more limited, as the Dahlgren burners are the only ones that have been operational long enough to obtain data. The regulatory compliance costs are very site-specific, as regulations vary from state to state in the U.S., and by country internationally. The per-test costs vary according to the test site's labor rates and safety rules, but the hours of work required should be accurate anywhere.



Figure 2. The liquid fuel pool fire at Dahlgren

Costs are compared to liquid fuel fire testing. Standard test cost estimating templates are used by test ranges. The cost of conducting liquid fuel fire tests and propane fire tests can be accurately obtained with the templates. However, cost is only one element of the decision as to what type of burner to use or build. Liquid fuel burners have a large environmental liability, which can make them impractical no matter what the cost. Propane burners have a very small environmental impact and should be able to be used almost anywhere.

COST MODEL

The cost assessment was performed by breaking the costs down into three categories:

- (1) Nonrecurring costs of engineering, manufacturing, construction, and calibration
- (2) Per-test cost of daily operations
- (3) Annualized recurring costs of maintenance and regulatory compliance

Nonrecurring Costs. The nonrecurring costs are the one-time costs associated with obtaining a burner. The nonrecurring costs include the engineering costs to design the burner, the manufacturing and construction cost to fabricate and build the burner, and the costs associated with calibrating and certifying the burner. The majority of the nonrecurring cost is the labor required to fabricate and assemble the facility. Dahlgren's labor rate of \$149 per hour was used throughout the cost assessment whenever labor hours were involved.

Per-test Cost. The per-test costs include all recurring costs that are repeated for each additional test performed. The per-test costs include the requirements and documentation, all pre-test preparations and fabrication, the labor involved in test execution, all post-test activities (i.e., clean up), material surcharges (i.e., fuel), and non-labor costs (i.e., test stand material). Significant savings in the per-test costs are due to the lower cost of propane per gallon, as well as the need for less total fuel per test. Additionally, there are savings from not requiring a commercial driver to deliver the fuel truck on the day of the test. Instead, the propane tank is filled as a routine operation when all other tanks are filled at the test site and the delivery fee is factored into the fuel cost. Finally, per-test savings are realized with the propane burner by requiring fewer weather-call man hours. The weather call is factored into the cost of the test because historically, a certain percentage of tests are cancelled due to high wind. It is anticipated that the shorter time required to set-up for a propane test (no delay for fuel to be pumped) will decrease the likelihood of a weather-related cancellation.

Annualized Recurring Costs. Finally, the annualized recurring costs include all recurring costs that are not specifically tied to test execution. These recurring costs would include regular maintenance to the system and the costs associated with maintaining regulatory and safety compliance. It is assumed here that the truck used to transport jet fuel is owned by the test site, while propane will be delivered by a truck owned by the propane supply company. There are significant costs associated with maintaining fuel delivery capability as will be presented in the following section.

NONRECURRING COSTS

Engineering Costs. Drawings of the 3.7 m by 3.7 m burner at Dahlgren are provided in Figure 3 and Figure 4. This burner has been carefully developed and calibrated and is made from readily available materials that are inexpensive and easy to assemble. The parts list with suppliers is shown in Table 1. The engineering has been done and is not a cost item should this burner be selected by a test facility.

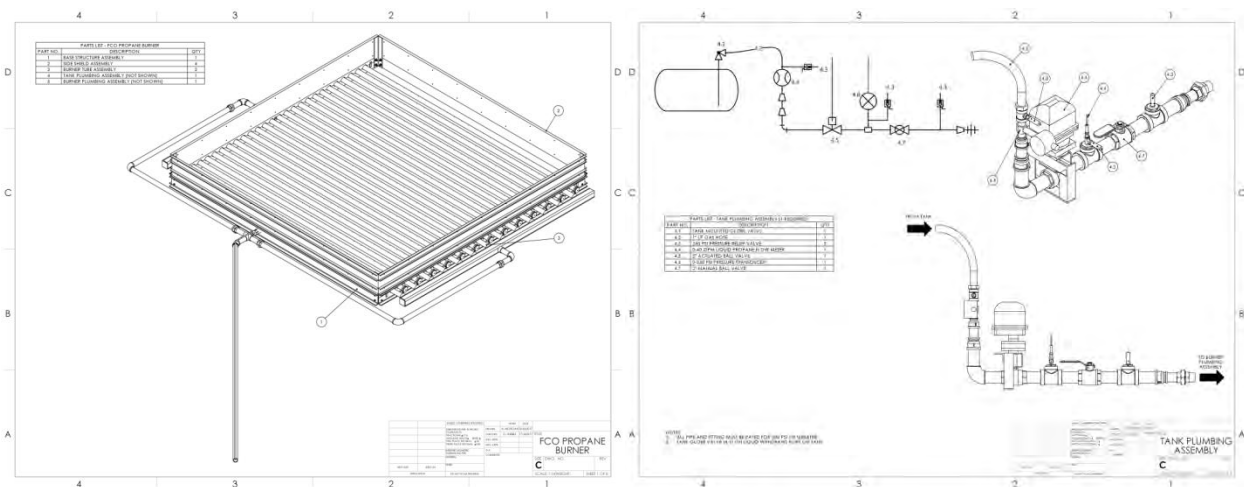


Figure 3. Dahlgren propane burner and propane burner tank piping assembly

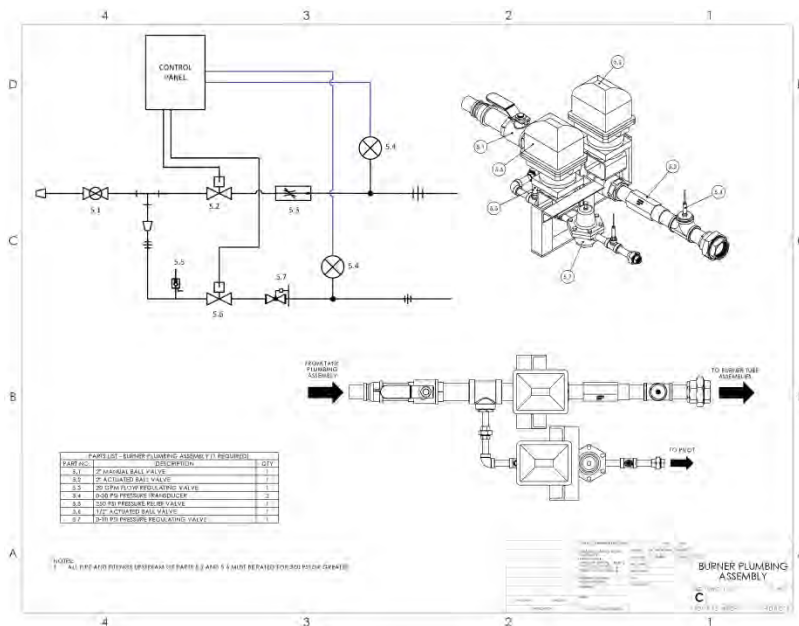


Figure 4. Dahlgren burner piping assembly

Table 1. Material costs and labor for constructing a propane burner

Electrical Panel at Tank								
Part	Quantity	Source	Item ID #	CY 17 price	Total			
Mil Spec Connector receptacle 3 pole female QuickConnect	1	McMaster Carr	6134T31	\$18	\$18			
Mil Spec Connector receptacle 6 pole female QuickConnect	1	McMaster Carr	6134T33	\$14	\$14			
Mil Spec Connector receptacle 10 pole female QuickConnect	1	McMaster Carr	6134T34	\$25	\$25			
Mil Spec Connector receptacle 15 pole male QuickConnect	1	McMaster Carr	6134T25	\$22	\$22			
Category 5E Keystone Style Coupler	1	McMaster Carr	3243T2	\$11	\$11			
1 ft. 5E cord	1	McMaster Carr	9953K21	\$3	\$3			
Terminal Block 2 circuits	3	McMaster Carr	7527K42	\$2	\$6			
Terminal Block 10 circuits	1	McMaster Carr	7527K51	\$5	\$5			
IEC 320-C14 with switch	1	Digikey	CCM1915-ND	\$9	\$9			
110V AC to 10V DC transformer	1	Omega	PST-10	\$200	\$200			
110V AC to 24V DC transformer	1	McMaster Carr	7009K35	\$116	\$116			
Ignition transformer 1092-F	1	Grainger	23M557	\$103	\$103			
Enclosure	1	McMaster Carr	8261K31	\$100	\$100			
Ethernet Daq	1	National Instruments	9184	\$100	\$100			
Digital relay module	1	National Instruments	9481	\$232	\$232			
+10V voltage module	1	National Instruments	9215	\$540	\$540			
+500mV module	1	National Instruments	9238	\$1,100	\$1,100			
Relay socket	1	McMaster Carr	7266K17	\$13	\$13			
Relay	1	McMaster Carr	7266K65	\$16	\$16			
Labor CY17	50			\$149	\$7,450			
				Sum:	\$10,083			
Electrical Panel at Burner								
Part	Quantity	Source	Item ID #	Price	Total			
110V AC to 10V DC transformer	1	Omega	PST-10	\$200	\$200			
Enclosure	1	McMaster Carr	8261K31	\$100	\$100			
Relay socket	3	McMaster Carr	7266K17	\$13	\$39			
Relay	3	McMaster Carr	7266K65	\$16	\$48			
Terminal Block 10 circuits	2	McMaster Carr	7527K51	\$5	\$10			
IEC 320-C14 with switch	1	digikey	CCM1915-ND	\$9	\$9			
Mil Spec Connector receptacle 10 pole female QuickConnect	1	McMaster Carr	6134T31	\$25	\$25			
Mil Spec Connector receptacle 3 pole male QuickConnect	1	McMaster Carr	6134T21	\$12	\$12			
Mil Spec Connector receptacle 15 pole male QuickConnect	1	McMaster Carr	6134T25	\$22	\$22			
Labor	50			\$149	\$7,450			
				Total Electrical	\$17,533			
Burner								
Part	Quantity	Source	Item ID #	Price	Total			
2" sch 40 gal pipe	30	Discount Steel		\$75	\$2,250			
6" X 8.2lb Channel 12' Long	4	Discount Steel		\$103	\$412			
2" union	30	Plumbing Supply		\$20	\$600			
2" Tee	25	Plumbing Supply		\$15	\$375			
2" ellbow	2	Plumbing Supply		\$11	\$22			
2" caps	30	Plumbing Supply		\$5	\$150			
2" nipple (5" length)	60	Plumbing Supply		\$7	\$420			
Windscreens	22	various		\$4	\$88			
labor	80			\$149	\$11,920			
				Total burner:	\$16,237			
Pipe-system from tank to burner								
Part	Quantity	Source	Item ID #	Price	Total			
30psi pressure gage	2	Omega	MMG030V1P4D01	\$420	\$840			
250 psi pressure gage	1	Omega	MMG250V1P4D01	\$420	\$420			
2" Regulator	0	Flomec	8580	\$1,530	\$0			
Propane hose 10', 1"	1	McMaster	45835K653	\$158	\$158			
2" to 1" reducer (300 psi)	4	McMaster	4627K196	\$37	\$147			
1" to 1/2" reducer (300 psi)	2	McMaster	4627K143	\$14	\$29			
2" Tee (300 psi)	4	McMaster	4627K258	\$44	\$174			
2"X6" Nipple (300 psi)	10	McMaster	4550K289	\$12	\$120			
1 1/2" to 1/2" reducer (300 psi)	2	McMaster	4627K193	\$31	\$61			
1 1/2" nipple (300 psi)	2	McMaster	7727K313	\$5	\$10			
1/2" nipple (300 psi)	5	McMaster	4550K197	\$3	\$15			
1/2" to 1/4" reducing tee (300 psi)	3	McMaster	4627K322	\$14	\$42			
2" to 1 1/2" reducing tee (300 psi)	2	McMaster	4627K332	\$60	\$120			
2" Ball valve	2	McMaster	47865K28	\$64	\$127			
2, 2" ball vales and 1/2" ball valve with three actuators	1	Indelac Controls, Inc		\$10,619	\$10,619			
labor	120			\$149	\$17,880			
				Total pipe:	\$30,762			
				Total Cost:	\$64,532			

Manufacturing and Construction Costs. The manufacturing and construction costs are provided in Table 1 above. The burner at Dahlgren sits on a 2.5 cm thick steel plate that is covered with hand-placed bricks without mortar. Options at other sites would be an existing concrete slab, a fabricated slab, or tamped crushed rock. If a bare steel plate is used, the heat from the fire will cause it to warp during the test and not return to its original shape. Some tests spill molten aluminum onto the bricks, which is easily cleaned. The plate and bricks were already available at the test site and are not included in the cost. The burner at Dahlgren uses a 1900 liter propane tank. It is on a skid for easy transport to and from the range. There is a quick-disconnect coupler for connecting the tank to the equipment in the shelter. It is rented from a propane supplier and not considered to be a part of constructing the system.

Fuel Delivery and Control System. There are several options for controlling a gas burner. The first and least expensive is manual control. Dahlgren burners were operated manually while under development. Manual operation consists of opening valves to start the gas flow, operating a switch to start the igniter, and turning the valves off after the test. The operations have to be performed in a shelter when energetic materials are being tested. The fuel supply tank also has to be sheltered. The shelters for the Dahlgren burner and equipment are shown in Figure 5.



Figure 5. Shelter for the fuel delivery and pressure regulation system equipment and shelters for propane tank and fuel

With a manually operated system, the shelters need to be close enough to the burner to allow reasonably short runs of pipe or hose, but still provide safety for the operators. Pipe runs on the order of 9.1 m worked fine and were used for all of the development testing (probably 100 or more tests). With the passive evaporation burner design, only liquid flows through most of the

pipe and the pressure drops are small. The Dahlgren liquid and gas fuel fast cook-off tests are only part of the testing going on at the range. Other tests such as bullet impact, fragmentation arenas, and rocket motor restrained firings are conducted there as well. There are central, collocated shelters for test control and data acquisition. Pipe runs from these shelters would be on the order 305 m, making manual operation impractical. Therefore, a personal computer (PC)-based electrical system, based on an existing system being used to control a propane burner for treating explosive debris, was developed. Figure 6 shows the PC-based system at Dahlgren. Simulated dial gauges are shown for the tank pressure, the burner pressure, and the pilot ignition flame. The valves are controlled by touch screen rectangular buttons. The status of each valve is indicated by the color of the simulated lamp next to each button.

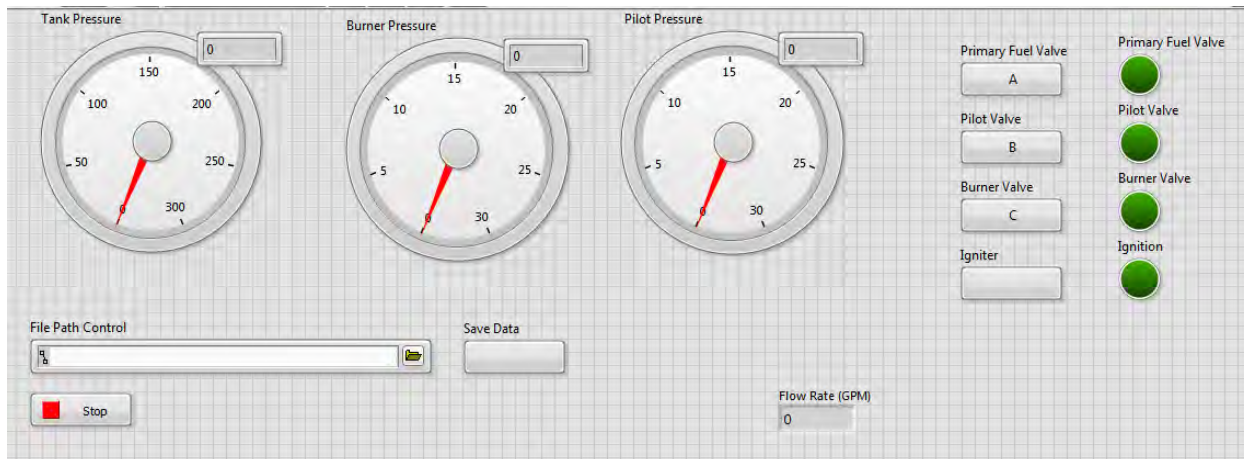


Figure 6. This is a screen shot of the LabView display for the PC-based burner control system at Dahlgren

The Dahlgren burner PC uses LabView software. PCs and the software are available at most large test centers and laboratories, and are not included in the cost estimate. The computer uses a network connection to remotely control the test from a test control shelter. Network connections can have problems with reliability and latency. Should a more reliable control system be desired, a PLC should be used instead of a PC on a network. A PLC is an industrial digital computer which has been ruggedized and adapted for the control of manufacturing processes, such as assembly lines or any activity that requires high-reliability control, ease of programming, and process fault diagnosis.

The cost of materials for constructing a propane burner is \$20,300. The labor cost (at \$149 per hour) at Dahlgren was \$44,700. The cost of a fully operational burner is \$65,000 with PC control, or \$65,300 with dedicated PLC control. The system costs are shown in Table 1 above.

CALIBRATION COST

The cost of burner calibration, as required in References 1 and 2, depends on the skills and equipment available at the test center. Calibration testing requires collection of forty-eight (48) channels of thermocouple and heat flux data during a number of tests. Figure 7 shows possible equipment for calibrating a burner with thermocouples placed at forty positions in the burner. Many test centers have personnel and equipment suitable for the testing. Dahlgren personnel have calibrated burners in Virginia, California, the Netherlands, and Sweden. Using Dahlgren personnel to perform the calibration for the test site, the calibration cost is \$29,764 as shown in Table 2.

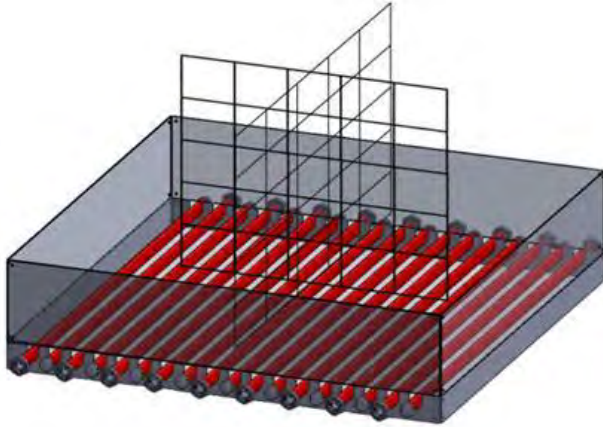


Figure 7. Burner calibration arrangement and test

Table 2. Calibration testing cost worksheet

Calibration Testing Cost Worksheet					
Item	No. persons	Duration (hrs)	rate	total	
Checkout and pack	1	40	150	6000	
Conduct tests	2	40	150	12000	
Return, clean equipment	1	20	150	3000	
Analyze & report	1	40	150	6000	
			Labor	27000	
Materials					
Materials			Materials	1000	
Travel:	Unit cost	Days	Total		
Per diem	67	2	6	804	
Hotel	100	2	6	600	
Car rental	60		6	360	
Transportation	xxx	2			
			Travel	1764	
			Total calibration	29764	

PER-TEST COST OF BURNER OPERATIONS

There are two basic types of fast cook-off tests performed at Dahlgren. The first are tests conducted on items with energetic materials in compliance with STANAG 4240. These tests are scored for reaction type by a national authority. The tests may require preapproval by the authority, instrumentation to measure blast overpressure, video, or high-speed photography to monitor the fire, fragments, debris, and six thermocouples located near the top, bottom, ends, and sides of the test item. The final positions of the fragments and debris that are projected out of the pit are mapped, and the fragments are collected, weighed, and photographed. The data are compiled into a report and video clips for the reviewing officials.

The second type of test is performed for engineering purposes. These are sometimes performed during the research and development of new munitions. These tests are used to see

what might happen if a test of an item were conducted for score, to develop and improve mitigation systems for items under development, fire research to characterize fast cook-off fires, and materials research to study new materials and improve existing materials. These tests are usually less complete in regards to the instrumentation in STANAG 4240 tests, but may have more instrumentation in and around the test item. Sometimes, the test items are inert. These tests are so diverse that only the costs for the basic facility and operation are provided.

The liquid fire costs are well characterized and form the basis for estimating the costs of conducting tests with the propane burner. A standard template is used to plan a STANAG 4240 liquid fuel test and calculate the cost, as shown in Table 3. The table is organized into sections for producing and organizing documents, test site preparations, conducting the test, analyzing and reporting the data, instrumentation expenses, and materials and surcharges. The elements of the table in the context of the liquid fuel fire and propane burner are discussed below.

Requirements and Documentation. The first block of data is for meeting with the customer, learning his requirements, learning about the test item, handling the test item, any special safety requirements, preparing the test plan, preparing other safety documents such as the threat hazard analysis, and designing the test stand. This requires 29 man hours at a cost of \$4,321 and is the same for both the liquid pool test and the propane test.

Pre-test Preparations. This section covers fabrication of the test fixtures, installing them into the burner, and setting up the thermocouples, blast overpressure gauges, and video cameras. For a liquid pool fire, the pan is inspected and any required repairs are made and fuel is delivered to the test site. For a propane test, the fuel tank is brought out and connected to the burner supply lines. The burner tube ports are cleaned, fittings are checked for leaks, propane is flowed through the system, and depending on how much time has lapsed since the previous test, a short checkout burn may also be conducted. For the liquid pool test, this requires 50 man hours for a cost of \$7,450.

Test Execution. The test requires calm or very low wind speeds, as the test item must be engulfed in the flame until it reacts, and the fire is very susceptible to wind. The wind is usually at its lowest speed in the early hours of the morning before sunrise, and then builds as the sun rises. Therefore an early start is required. The instrumentation team makes final checks of the blast overpressure gauges, videos, and thermocouples. The test engineer and the test director monitor the wind speed and decide whether or not to conduct the test. The test item is brought out to the test site and put on the test stand. Thermocouples are installed 5.1 cm from the front, back, left, and right sides of the test item. The new STANAG 4240 will require thermocouples also at the top and bottom. The only persons allowed to touch the test item on Dahlgren ranges are ones who have special qualifications and certifications for handling explosive items. Two ordnance handlers are required. There must also be a certified firing director and a certified lookout (safety observer) present. For tests in a liquid fuel fire, the ordnance handlers also install thermite grenades in the corner of the pit (required to ignite the liquid fuel). For liquid fuel fires, fuel must be transferred from a pumper truck into the pit. Once the fuel transfer is complete, gasoline is poured in the corners as an accelerator to achieve the required rise rate of temperature on the test item. The test personnel retire to a shelter, and once instrumentation is confirmed to be ready, the test is conducted. After the test item reacts and the fire is completely out, a minimum hold time (minimum of 30 minutes) is started and all personnel must remain in the shelter. After the hold time has elapsed, the firing director and ordnance handlers go to the pit and confirm it will be safe for the others to come out to begin the post-test operations. This requires 63 man hours for a total cost of \$9,387.

Post-test Activities. Fragments and debris from the test are catalogued as to range and bearing from the test stand, description, and mass. The items are arranged by type and then photographed. Instrumentation and video data are played back to confirm the test setup and correct any obvious errors. The videos are edited into clips from each view and compiled into a single DVD. Electronic data are reduced to plots with engineering units and put onto a DVD. These materials are used by the test engineer to prepare a final report, and shared with the customer at the test site. Finally, there is test debris to clean up and possible repairs for the burner. The clean costs are often significant. Post-test costs are assumed to be the same for both the propane and liquid pool test. These activities require 36 hours for a cost of \$5,364.

Materials and Surcharges. There are fixed charges for fuel, technical writers, and the range control console operators that are billed to the test. Fuel makes up the bulk of the material cost of a liquid pool fire. Total costs for this section are \$9,275.

Non-labor Costs. The cost of expendable items such as the firing leads, thermocouples, and test stand are billed to the test. The total is \$995 per liquid pool test.

Total Liquid Fuel Fire Cost. The total cost of the example liquid fuel fire test in Table 3 is \$36,791.

Propane Fire Costs. The pre-test requirements and documentation costs for the two types of fires are the same. The post-test activities are the same. However, there are significant differences in the pre-test preparation, test execution, and materials.

Changes in Pre-test Preparations. Part of the cost of the liquid fuel fire test is inspecting and repairing the water-tight pit that holds the fuel. The pit is required to be water tight to ensure that fuel does not escape onto the ground. The propane burner does not require this inspection, which saves \$745 per test. A fuel delivery cost of \$1,192 is also avoided resulting in a total pre-test savings of \$1,937.

Changes in Test Execution. The weather call is not so critical, as the test can be conducted very quickly once the test item is in place on the stand. This will save on average 6 man hours (\$894) per test due to fewer test cancellations. Further, the test can be aborted at any time. An hour or more may elapse between the start of fuel delivery and closing the firing key on the liquid fuel test, with no abort possible once fuel is introduced to the pan. Also, the labor required to pour the fuel and wire and place the thermite grenades is eliminated. Together, this results in a savings of an additional 10 man hours (\$1,490) per test, for a total of \$2,384.

Changes in Materials and Surcharges. For the liquid fuel fire, the test requires a quantity of fuel that will burn for 150% of the expected reaction time. Fuel quantities in the range of 2,000 to 3,000 gallons are normal, with 2,000 gallons used in this analysis. With the gas fuel fire, the fuel can be shut off at any time, which saves a lot of fuel. Liquid JP-5 fuel costs \$3.50 per gallon. This leads to a normal fuel expense of \$7,000. A typical propane fast cook-off test can be performed using a single 500-gallon fuel tank. The current price delivered for the last test that was conducted was \$0.99/gallon. One full tank would cost \$500. This results in a fuel savings of \$6,500.

Total Cost and Savings. The total cost of the example propane fast cook-off test depicted in Table 3 is \$25,886 compared to \$36,791 for a total per-test savings of \$10,905.

Table 3. Cost of burner operations

Requirements & Documentation						Propane	Savings
	People	hr/Day	Days	Labor Hours	Labor Cost(\$)		
Customer interface & Requirements	1	4	1	4	\$ 596.00	\$ 596.00	\$ -
Preparation of test plan(s)	1	4	1	4	\$ 596.00	\$ 596.00	\$ -
Preparation of safety documents	1	8	1	8	\$ 1,192.00	\$ 1,192.00	\$ -
Schedule coordination	1	4	1	4	\$ 596.00	\$ 596.00	\$ -
Fixture design & procuremnt	1	2	1	2	\$ 298.00	\$ 298.00	\$ -
Planning meeting(s) support	2	2	1	4	\$ 596.00	\$ 596.00	\$ -
Review Test Plan	2	1	1	2	\$ 298.00	\$ 298.00	\$ -
Review Test Plan	1	1	1	1	\$ 149.00	\$ 149.00	\$ -
Subtotal				29	\$ 4,321.00	\$ 4,321.00	\$ -
Pre-Test Preparations							
	People	hr/Day	Days	Labor Hours	Labor Cost(\$)		
On-site technical direction (range coordination)	1	4	1	4	\$ 596.00	\$ 596.00	\$ -
Fabrication of fixtures/targets (range crew)	2	4	1	8	\$ 1,192.00	\$ 1,192.00	\$ -
Pan Checkout and Setup	2	5	1	10	\$ 1,490.00	\$ 745.00	\$ 745.00
Build up Thermocouples (4)	1	4	1	4	\$ 596.00	\$ 596.00	\$ -
Set up gauges, cameras, and TCS	2	8	1	16	\$ 2,384.00	\$ 2,384.00	\$ -
Fuel Delivery	1	8	1	8	\$ 1,192.00	\$ -	\$ 1,192.00
Subtotal				50	\$ 7,450.00	\$ 5,513.00	\$ 1,937.00
Test Execution							
	People	hr/Day	Days	Labor Hours	Labor Cost(\$)		
On-site technical direction	1	5	1	5	\$ 745.00	\$ 745.00	\$ -
Weather Call	1	2	1	2	\$ 298.00	\$ 298.00	\$ -
Lookout / firing director	2	4	1	8	\$ 1,192.00	\$ 1,192.00	\$ -
Weather Call	7	2	1	14	\$ 2,086.00	\$ 1,192.00	\$ 894.00
Test Setup (leaving during test)	5	2	1	10	\$ 1,490.00	\$ 596.00	\$ 894.00
Ordnance Support during test	2	2	1	4	\$ 596.00	\$ 596.00	\$ -
Weather Call	2	2	1	4	\$ 596.00	\$ 596.00	\$ -
Instrumentation Setup	4	2	1	8	\$ 1,192.00	\$ 1,192.00	\$ -
Instrumentation Support during test	2	2	1	4	\$ 596.00	\$ 596.00	\$ -
Public works support	1	4	1	4	\$ 596.00	\$ -	\$ 596.00
Subtotal				63	\$ 9,387.00	\$ 7,003.00	\$ 2,384.00
Post Execution Activities							
	People	hr/Day	Days	Labor Hours	Labor Cost (\$)		
Test Engineering							\$ -
On-site technical direction	1	3	1	3	\$ 447.00	\$ 447.00	\$ -
Quick-Look Report(s)	1	4	1	4	\$ 596.00	\$ 596.00	\$ -
Engineer meeting with I.E.	1	2	1	2	\$ 298.00	\$ 298.00	\$ -
Site/ mount cleanup (range personnel)	3	2	1	6	\$ 894.00	\$ 894.00	\$ -
Equipment breakdown/storage	2	2	1	4	\$ 596.00	\$ 596.00	\$ -
Film/video editing	1	4	1	4	\$ 596.00	\$ 596.00	\$ -
CD/DVD reproduction (labor)	1	1	1	1	\$ 149.00	\$ 149.00	\$ -
Data Analysis	1	6	1	6	\$ 894.00	\$ 894.00	\$ -
I.E. Meeting with Test Engineer	1	2	1	2	\$ 298.00	\$ 298.00	\$ -
Post-test ammo expenditure documentation	2	1	1	2	\$ 298.00	\$ 298.00	\$ -
Test Engineer generates deliverables for I.E.	1	2	1	2	\$ 298.00	\$ 298.00	\$ -
Subtotal				36	\$ 5,364.00	\$ 5,364.00	\$ -
Materials and Surcharges							
Item			Unit Cost(\$)	Qty	Cost (\$)		
JP-5 fuel			3.5	2000	\$ 7,000.00	\$ 500.00	\$ 6,500.00
Tech Writer (per document- TP, OPS, RHA)			605	3	\$ 1,815.00	\$ 1,815.00	\$ -
Range Control (per range day)			460	1	\$ 460.00	\$ 460.00	\$ -
					\$ 9,275.00	\$ 2,775.00	\$ 6,500.00
Burdened Non-Labor Costs							
Item			Unit Cost (\$)	Qty	Cost (\$)		
Firing lead			60	1	\$ 84.00	\$ -	\$ 84.00
Thermocouples (4)			100	4	\$ 560.00	\$ 560.00	\$ -
Table Materials			250	1	\$ 350.00	\$ 350.00	\$ -
					\$ 994.00	\$ 910.00	\$ 84.00
Total					Liquid	Propane	Savings
					\$ 36,791.00	\$ 25,886.00	\$ 10,905.00

Annualized Recurring Costs. The recurring costs of maintenance and regulatory compliance for the liquid fuel fast cook-off and the propane gas fuel fire are presented here and in Table 4. The annualized recurring cost for liquid fuel fire testing is \$45,382. The annualized recurring cost for gas fire testing is \$8,784. Many costs are identical between the two systems, such as anticipated repair costs per year and the cost to update and maintain safety documentation. The liquid pool fire does have some significant yearly costs that the propane burner does not. Environmental requirements to collect and analyze the containment area, as well as the environmental reporting required, make up \$5,561. Maintaining the fuel delivery truck is also expensive at \$19,380 per year. Finally, the thermite grenades required to ignite the liquid pool fire and the associated ammunition transfer fees that go along with them total \$14,213 per year. This results in a total annualized recurring savings of \$36,598.

Table 4. Annualized recurring cost of FCO testing

Item	Liquid Fire	Frequency	Cost/year	Propane Fire	
Repair and replace expanded metal grates	2 man days materials	1/per year	\$ 2,384	n.a.	
Burner tube replacement	n.a.	1/year		2 man days	\$ 2,384
Repair wind screens	n.a.	1/year		2 man days materials	\$ 2,384
Propane tank rental	n.a	1/year		2- 500 gallon	\$ 176
Liquid waste pump and haul		5 years		n.a.	\$ 100
Collect samples	4 man days		\$ 954		
Laboratory analysis	3 man days		\$ 715		
Vendor contract	2 man days		\$ 477		
Award contact	1 man day		\$ 238		
Schedule range	.2 man day		\$ 48		
Meet vender, transfer liquid	5 man days		\$ 715		
Fuel Truck with Pump					
Parts			\$ 1,500		
Maintenace of SOPs-Inert	2 man days	4 years	\$ 596	2 man days	\$ 596
Maintenace of SOPs-Energetic	3 man days	4 years	\$ 894	3 man days	\$ 894
Post test clean up w/hazmat	4 man days	1/year	\$ 4,768	n.a.	
Environmental reporting	2 man days	1/year	\$ 2,384	n.a.	
Thermite grenades				n.a.	
receive shipment	1250	1/yr	\$ 1,250		
ammo transfer to EEA	2500	2/year	\$ 5,000		
grenade unit cost	34	72/year	\$ 2,448		
squib unit cost	29	72/year	\$ 2,088		
storage					
requisitions(alocate, expend)	.5 man days	1/year	\$ 745		
expenditure forms	.125 man days	1/test	\$ 2,682		
		Total	\$ 45,382	Total	\$ 6,534

SUMMARY AND CONCLUSIONS

The cost of fast cook-off testing with propane has been obtained by careful tracking of expenses over a significant number of tests. These costs are compared to liquid fuel fire testing. The costs consist of nonrecurring costs, the costs directly attributable to a given test, and recurring costs of damage repair, maintenance, and environmental compliance. The nonrecurring costs are design, siting, materials, chamber fabrication, fuel distribution systems, fabrication, and calibration. The costs attributable to given test are mainly planning, construction of test stands, instrumentation, field crews, fuel, data analysis, and reporting. Recurring costs of damage repair, maintenance of the cook-off facility including fuel equipment, and environmental compliance are itemized.

These costs have been compared to the corresponding costs of liquid fuel fire testing. The cost of testing with propane is shown to be significantly less than with liquid fuels.

Once the costs were itemized over several years and a significant number of tests, the propane test was compared with liquid fuel test. The costs of environmental impacts were not calculated. The costs having a "no test" result as a consequence of weather changes between commitment to do the test and executing the "no test" (which can include the cost of a very expensive test item), has not been included. This happens because once the fuel is poured and the thermite grenades are in place, safety rules prevent the test from being stopped.

The total cost of the propane fast cook-off test was found to be \$25,886, compared to \$36,791 for the liquid fuel test.

REFERENCES

1. MIL-STD-2105D, Department of Defense Test Method Standard. *Hazard Assessment Tests for Non-Nuclear Munitions*, 19 April 2011.
2. STANAG 4240 edition 2, NATO *Liquid fuel/External Fire, Munition Test Procedures*, 15 April 2003.

Cost of Propane Fast Cook-Off Testing



Jon Yagla and David Hubble
NSWCDD, Dahlgren, VA

Ephraim Washburn
NAWCWD, China Lake, CA

2018 Insensitive Munitions and Energetic
Materials Technology Symposium
Portland, Oregon





Background



- Fast cookoff (FCO) is an international standard safety test required for all explosive ordnance
- Environmental concerns
 - Tests use large pools of hydrocarbon fuel such as JP5, JP8, kerosene, etc.
 - Emissions from one test: 200 kg CO, 35 kg NO_x, 30 kg SO_x, 225 kg soot, 125 kg unburned HC, and 20,000 kg CO₂
 - Ground water concerns
 - Public relations
- Propane viable substitute fuel
 - Gas at atmospheric conditions
 - Cleaner burning
 - Readily available
 - Sufficient heat content





Cost Assessment



- Compare cost of propane burner FCO test to jet fuel pool fire FCO test
- 3.7 m by 3.7 m propane burner built at Dahlgren, VA used for comparison
- Three categories
 - Non recurring costs
 - Per-test costs
 - Annualized recurring costs



Nonrecurring Costs



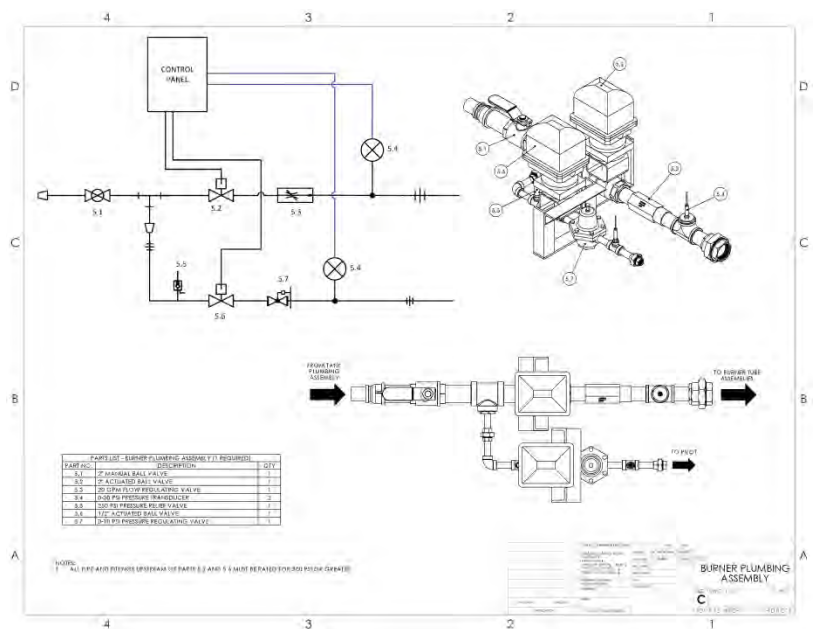
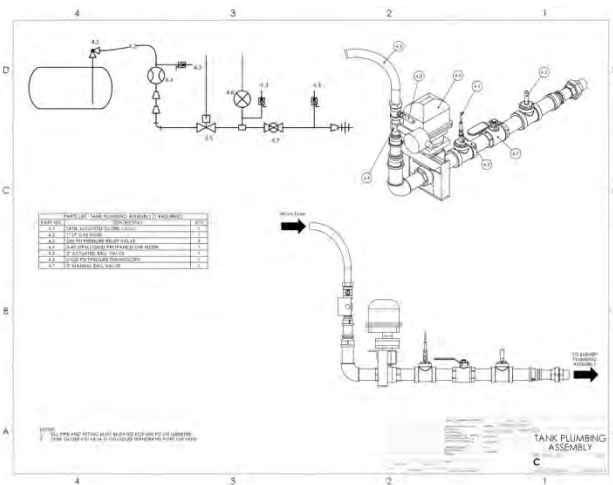
- Engineering design
 - Initial design cost high (>\$500K)
 - Tried multiple design iterations
 - Developed and designed to be made from inexpensive readily available supplies
 - Adaption of 3.7 m by 3.7 m propane burner at Dahlgren, VA to 6.1 m by 4.6 m propane burner at China Lake, CA <\$100K
 - Considerable work done, future adaptation costs even less



Nonrecurring Costs



- Engineering design
 - 3.7 m by 3.7 m propane burner technical drawing package available upon request





Nonrecurring Costs



- Material and labor for construction of burner

Location	Category	Cost
Electrical Panels	Material	\$2633
	Labor	\$14900
Burner	Material	\$4317
	Labor	\$11920
Pipe System from tank to burner	Material	\$12882
	Labor	\$17880
Total	Material	\$19832
	Labor	\$44700



Nonrecurring Costs



- Material and labor costs
 - Only \$16237 is susceptible to damage
 - Multiple test possible on one burner

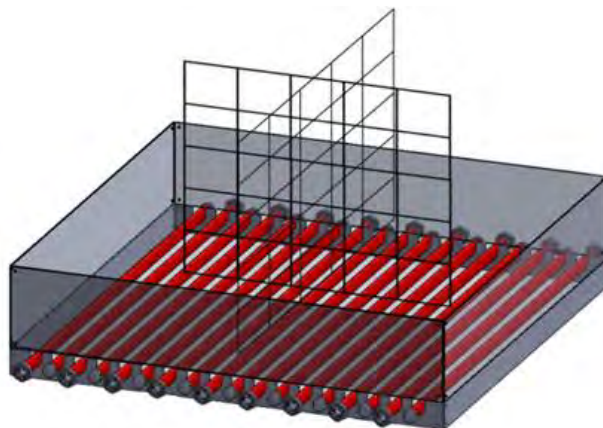




Nonrecurring Costs



- Calibration costs
 - Directed by STANAG 4240
 - Costs dependent on skill of operators
 - NSWCCD Personnel costs for testing
 - Preparation, testing, clean-up, analysis, and reporting - \$27000
 - Materials - \$1000
 - Calibration setup shown below

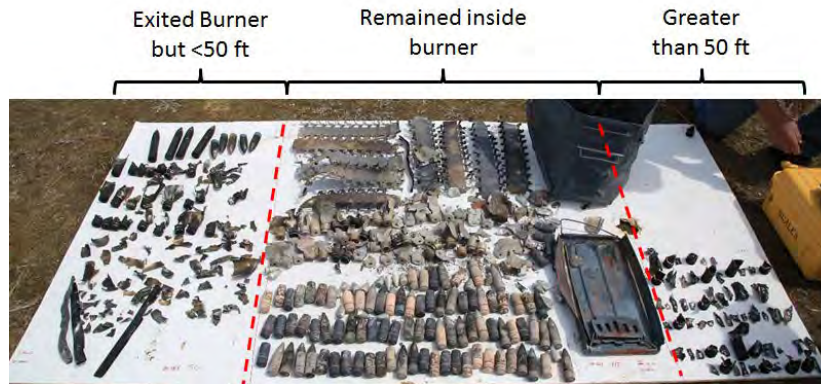




Per-Test Costs



- Different types of tests
- Tests to officially “score” item



- Engineering tests





Per-Test Costs



- Comparison of costs of official FCO tests with jet fuel pool fire and propane burner
- Requirements and documentation
 - Meet with customer and determine requirement
 - Safety research and test stand design
 - Same cost for both types, \$4321



Per-Test Costs



- Pre-test preparations
 - Fabrication of test fixtures
 - Preparation of area
 - Instrumentation installation
- Savings of \$1192 with propane burner
 - No lengthy pit inspection
 - No fuel delivery cost



Per-Test Costs



- Test execution
 - Follow STANAG 4240
 - Savings of \$2384 with propane burner
 - Fewer test cancellations from weather
 - No need to wait for fuel pouring
- Post-test activities
 - Fragment and debris mapping
 - Clean up
 - Compiling, editing, and delivering data
 - Little costs difference between tests
 - Big difference in comfort of personnel (no fumes)



Per-Test Costs



- Material and surcharges
 - Biggest cost difference between tests
 - Fuel savings is \$6500
- Total costs
 - Jet fuel pool fire FCO test: \$36791
 - Propane burner FCO test: \$25886
 - Savings of \$10905 per test



Annualized recurring costs



- Significant savings compared to the jet fuel fire FCO tests
 - Liquid fuel hauling and maintenance costs
 - Environmental costs
 - Thermite grenade costs

Item	Liquid Fire	Frequency	Cost/year	Propane Fire	
Repair and replace expanded metal grates	2 man days materials	1/per year	\$ 2,384	n.a.	
Burner tube replacement	n.a.	1/year		2 man days	\$ 2,384
Repair wind screens	n.a.	1/year		2 man days materials	\$ 2,384 \$ 176
Propane tank rental	n.a	1/year		2- 500 gallon	\$ 100
Liquid waste pump and haul		5 years		n.a.	
Collect samples	4 man days		\$ 954		
Laboratory analysis	3 man days		\$ 715		
Vendor contract	2 man days		\$ 477		
Award contact	1 man day		\$ 238		
Schedule range	.2 man day		\$ 48		
Meet vender, transfer liquid	5 man days		\$ 715		
Fuel Truck with Pump					
Parts			\$ 1,500		
Maintenace of SOPs-Inert	2 man days	4 years	\$ 596	2 man days	\$ 596
Maintenace of SOPs-Energetic	3 man days	4 years	\$ 894	3 man days	\$ 894
Post test clean up w/hazmat	4 man days	1/year	\$ 4,768	n.a.	
Environmental reporting	2 man days	1/year	\$ 2,384	n.a.	
Thermite grenades				n.a.	
receive shipment		1250 1/yr	\$ 1,250		
ammo transfer to EEA		2500 2/year	\$ 5,000		
grenade unit cost		34 72/year	\$ 2,448		
squib unit cost		29 72/year	\$ 2,088		
storage					
requisitions(allocate, expend)	.5 man days	1/year	\$ 745		
expenditure forms	.125 man days	1/test	\$ 2,682		
Total			\$ 45,382	Total	\$ 6,534



Conclusions



- Compared cost of propane burner FCO test to jet fuel pool fire FCO test
- Non recurring costs are significantly reduced
 - Sharing of past engineering design work
 - Protection of expensive components
- Per-test costs reduced by 30% with propane burner
- Annualized recurring costs reduced by 86% with propane burner



Acknowledgments



Funded by:

The Environmental Security Technology
Certification Program (ESTCP)



The Inert Munitions Advanced
Development (IMAD) Program





Fast Cook-Off Modeling and Simulation

Jon J. Yagla and Saul Hernandez-Valle
Paper No. 20259

*Gun and Electric Weapon
Systems (E)*



Introduction and Background

Modeling with experimental confirmation was the subject of our IMEMTS paper and poster presented in Nashville in 2016 [1]. We showed a very accurate time to reaction for a Navy rocket booster motor in a 25 x 25 inch square missile launcher canister made out of a carbon fiber composite material. A reaction time of 14 minutes was predicted *before the test*. The test showed the reaction to occur at 14 minutes. Since that time, the computer simulation was run for a 21-inch-diameter second stage rocket motor in an open fire. The prediction *before the test* was 244 seconds to reaction; the test showed 225 seconds to reaction. Calculations were then carried out for a very complicated third stage rocket motor with a composite case. The predicted time was 260 seconds; the experimental time was 240 seconds.

Finally, we had an opportunity to model the fast cook-off test of 110 rounds of 30-millimeter (mm) gun ammunition contained in an ammo can with a thermal protection system. We did not have accurate reaction rate chemistry data, so we used a generic values for an Arrhenius reaction rate for nitrocellulose/nitroglycerin propellant from a French paper, and computed a reaction time of 163 seconds, compared to 150 seconds from the experiment. We made no changes in the input or property data to converge the model on the experimental time.

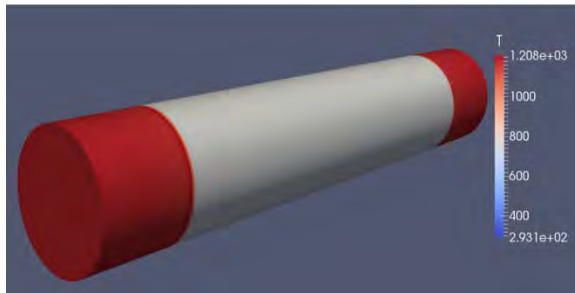
In this problem, each cartridge case was modeled with its own propellant and primer. The thermal protection system consisted of fiberboard panels around the inner surface of the can. There also was a wide strip of canvas wound back and forth in the can separating the layers of cartridges. Having modeled the time to reaction, and realizing the model is likely to be predicting the evolution of decomposition products accurately, we are ready to start work on predicting the violence of the reactions. Results from the models will help our understanding of fast cook-off and lead to safer weapons.

This paper reviews the rocket motor calculations, then shows the work done on the ammunition can. A concept for how the method can be extended to the computation of reaction violence is shown.

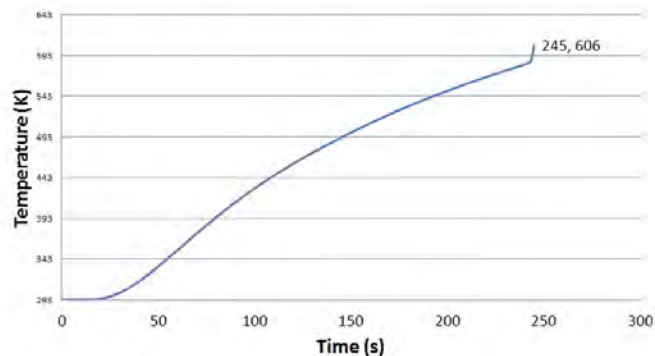
Second Stage Rocket Motor

Predicted Reaction Time: 244 seconds, 20 seconds more than the test data time of 225 seconds

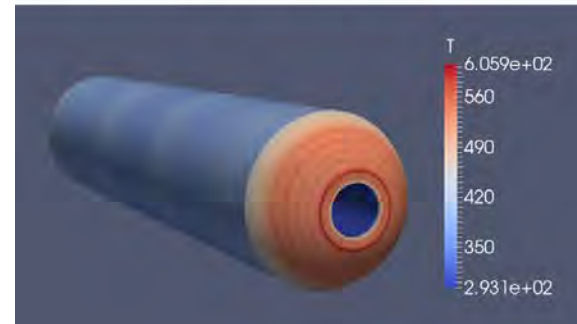
COMPOSITE CASE TEMPERATURE (K)
AT REACTION TIME



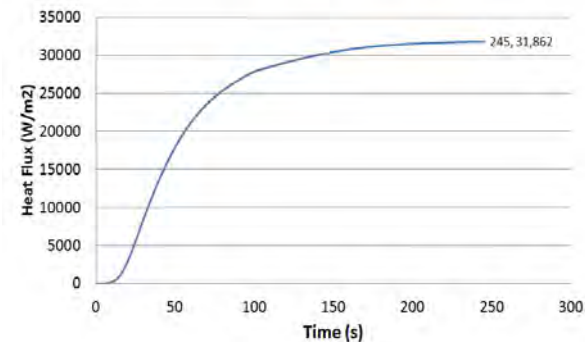
Propellant Maximum Temperature



Propellant Temperature (K) at
Reaction Time

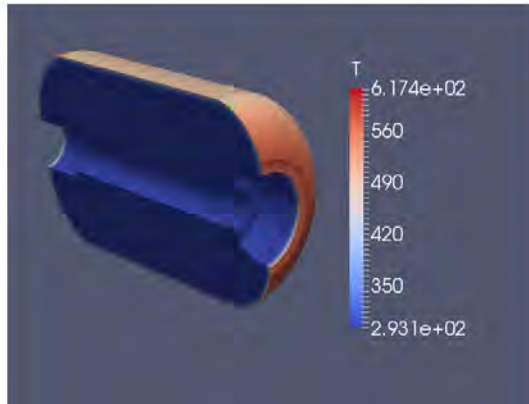


Heat Flux Reaching the Propellant

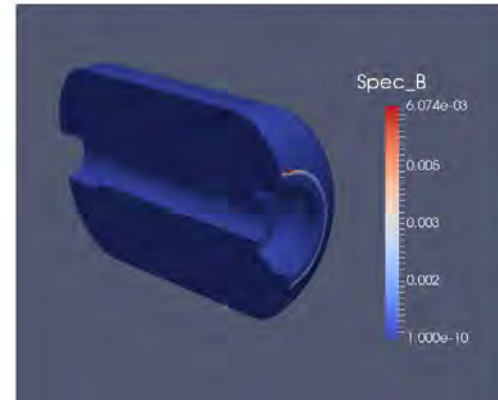


Third Sage Rocket Motor

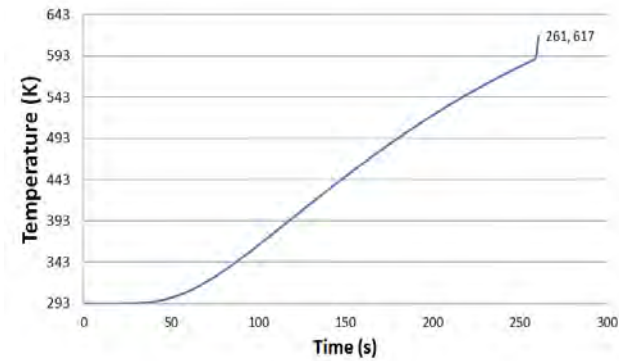
Propellant Temperature



Gas Phase Concentration

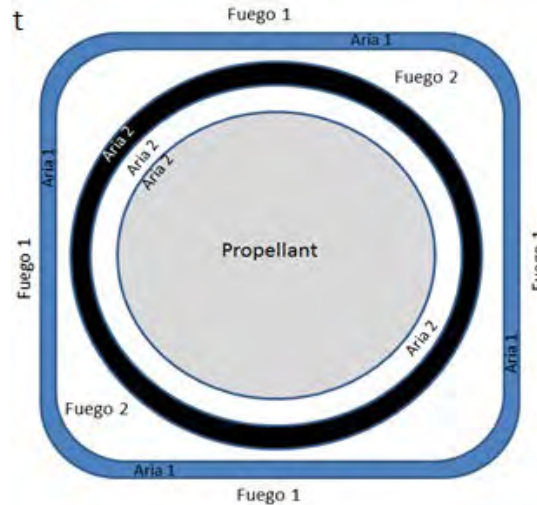


Propellant Maximum Temperature



Predicted Reaction Time for TSRM :
260 seconds, 20 seconds more than
the test data time of 240 seconds

Modeling Strategy



No one computer model is available to solve the problem of heat flow from the fire, through a container, into the rocket motor, and finally the response of the propellant. Our model consists of four sub models using the Sandia Fuego and Aria computer codes. Fuego is a reactive flow gas dynamics code that was used to model the fire with one application, and natural convection in the space between the container, or launcher canister, and the motor with a second application. These are both flows where the fluid motion is caused by buoyancy. The conduction of heat and pyrolysis of epoxy is converted to gaseous products and char. This process was modeled with Aria. The radiative heat input to the rocket motor was calculated using Aria inner-surface temperatures of the canister walls. Convective heating inside was computed using heat transfer coefficients determined from the second Fuego model. The heat flow through the chamber, insulation, and on into the propellant was computed with a second Aria model. The heat flow into the propellant causes self-heating of the propellant, which suddenly greatly exceeds the material's ability to conduct heat to the outside, resulting in an explosion.

Missile Launching Canister in Fast Cook Off Pit Ready for Test



Instruments Inside Canister

Instruments on Rocket Motor

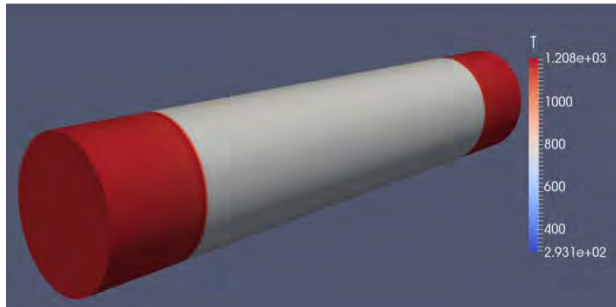


Pre-test model predictions and the test both showed cook-off at 15 minutes after ignition of the fire

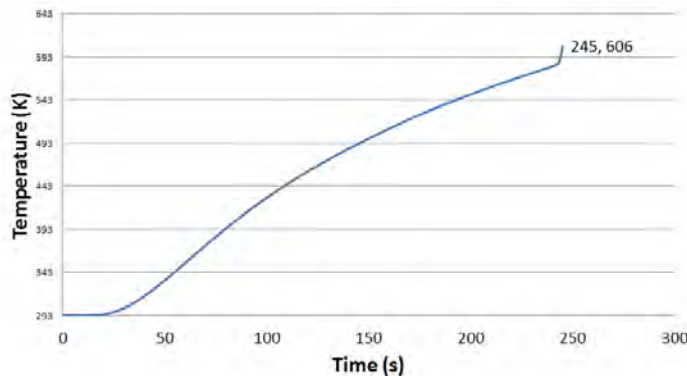
Second Stage Rocket Motor

Predicted Reaction Time: 244 seconds, 20 seconds more than the test data time of 225 seconds

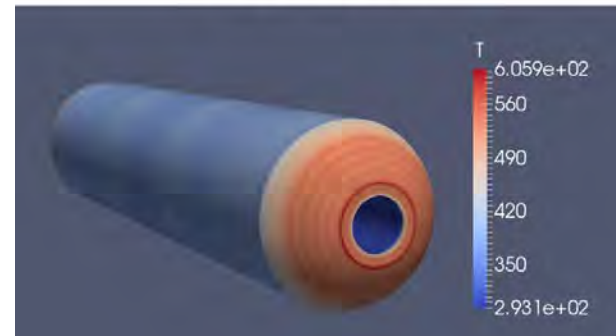
COMPOSITE CASE TEMPERATURE (K)
AT REACTION TIME



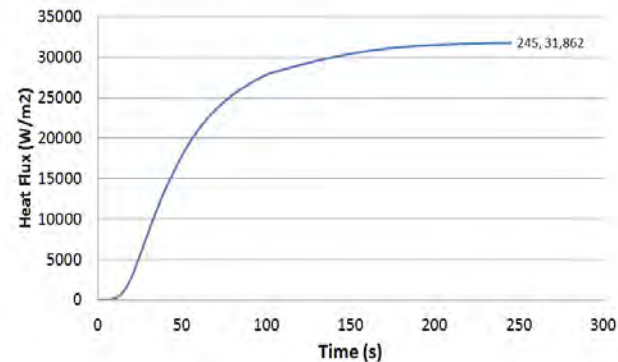
Propellant Maximum Temperature



Propellant Temperature (K) at
Reaction Time

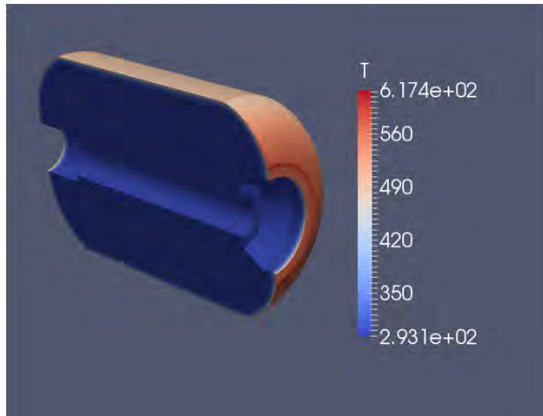


Heat Flux Reaching the Propellant

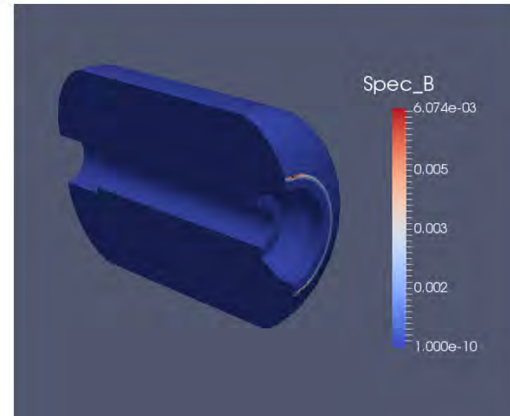


Third Stage Rocket Motor

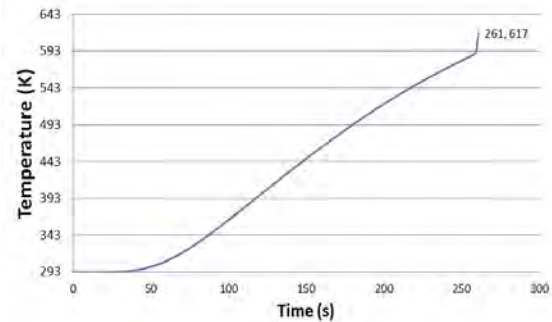
Propellant Temperature



Gas Phase Concentration



Propellant Maximum Temperature

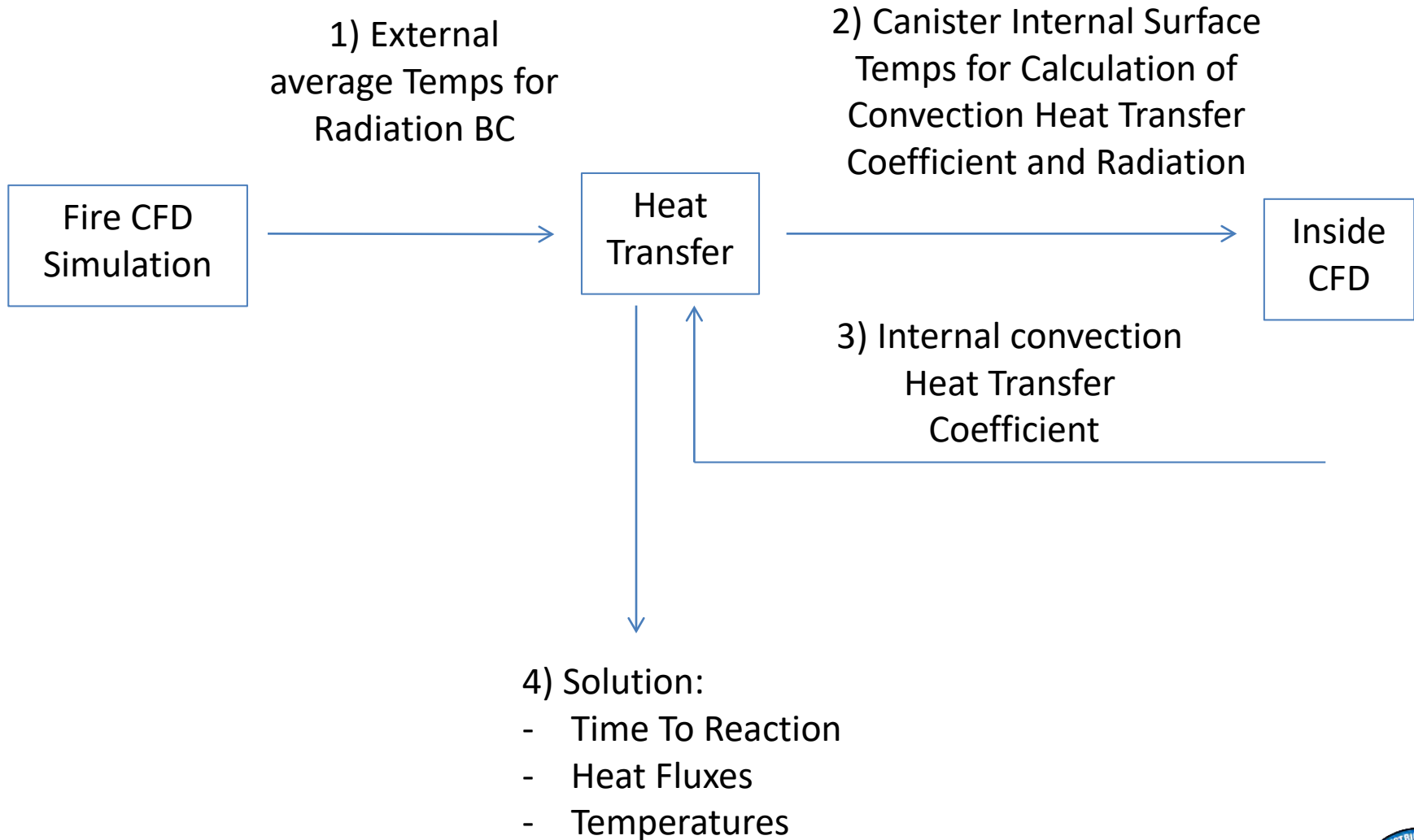


Predicted Reaction Time for TSRM :
260 seconds, 20 seconds more than
the test data time of 240 seconds

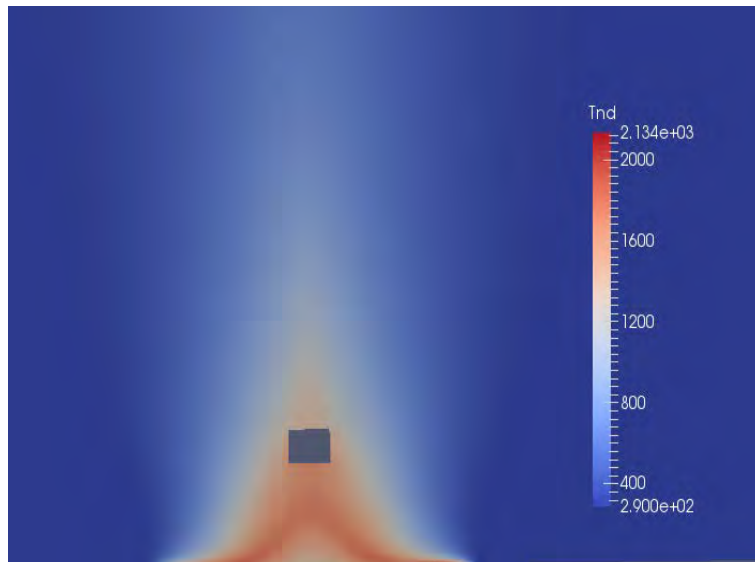
Fast Cook-Off of 110 30 mm Cartridges in an Ammo Can in a Propane Fire



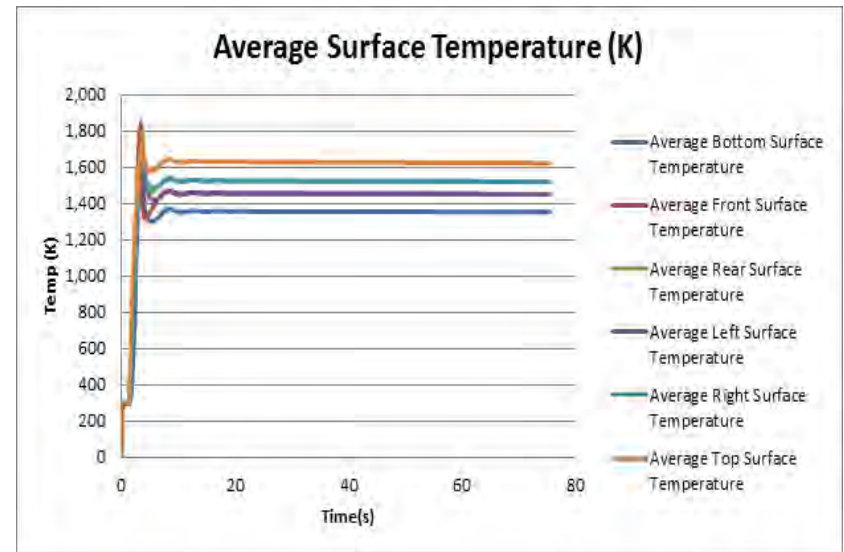
Modeling Flow Chart for Ammunition Can



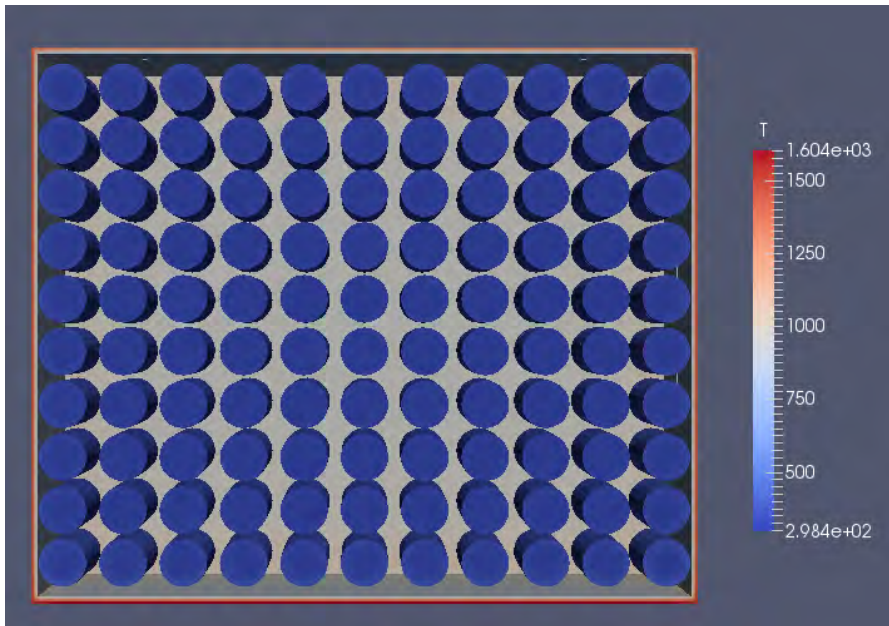
Surface and Steady State Temperature for the Ammo Can



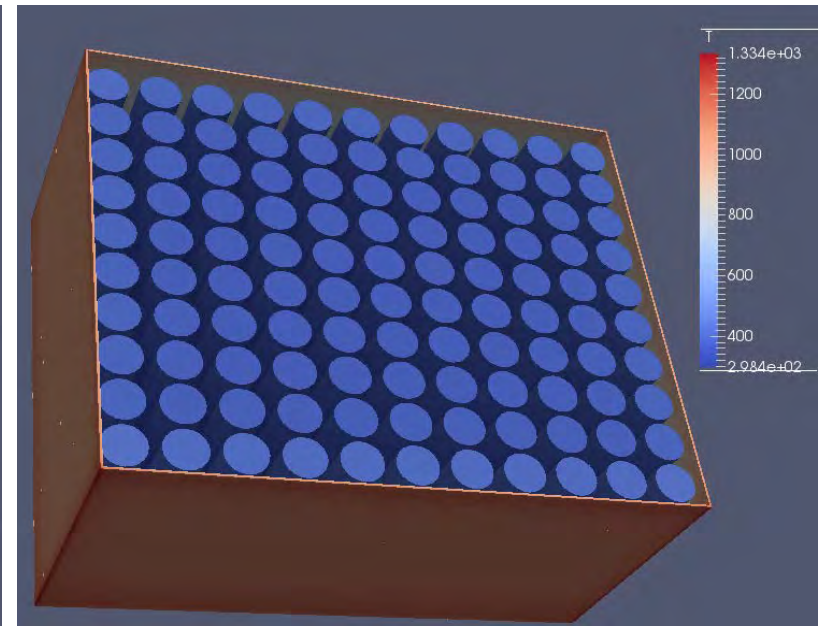
Steady state temperature field around ammo can at 75 seconds



After about 10 seconds steady state temperatures are attained

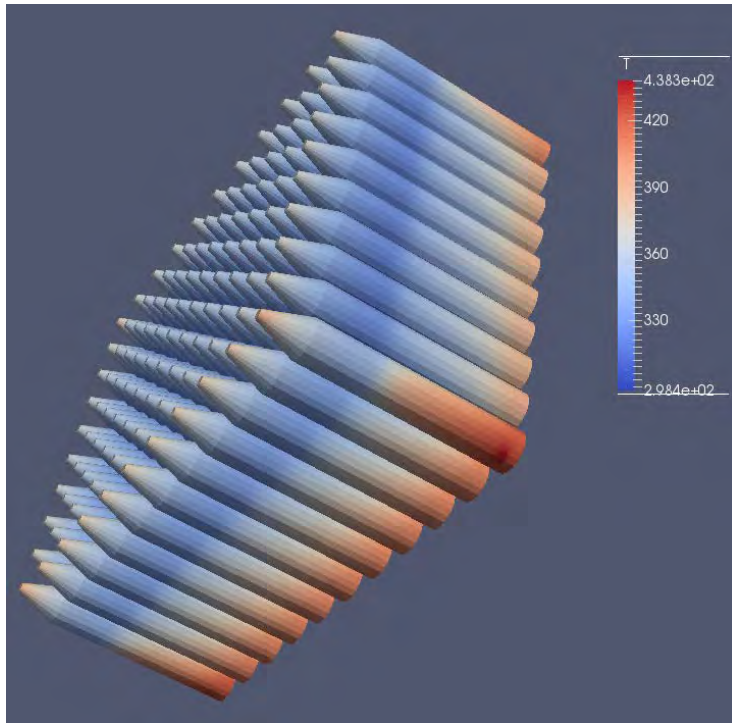


Metal, fiber board, and canvas

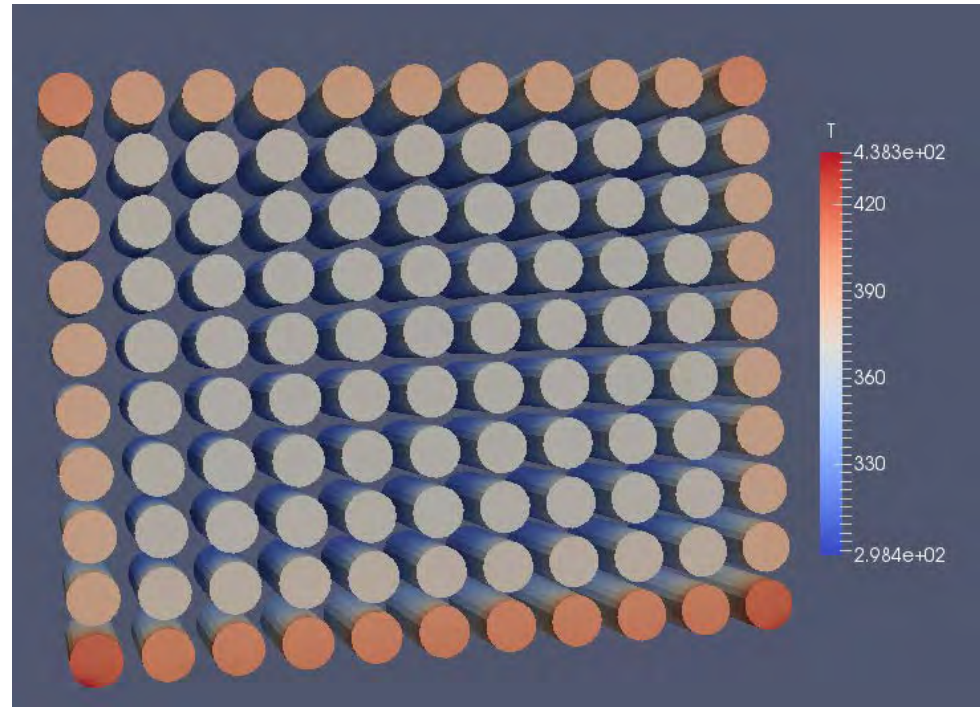


Fiberboard, canvas and packed rounds

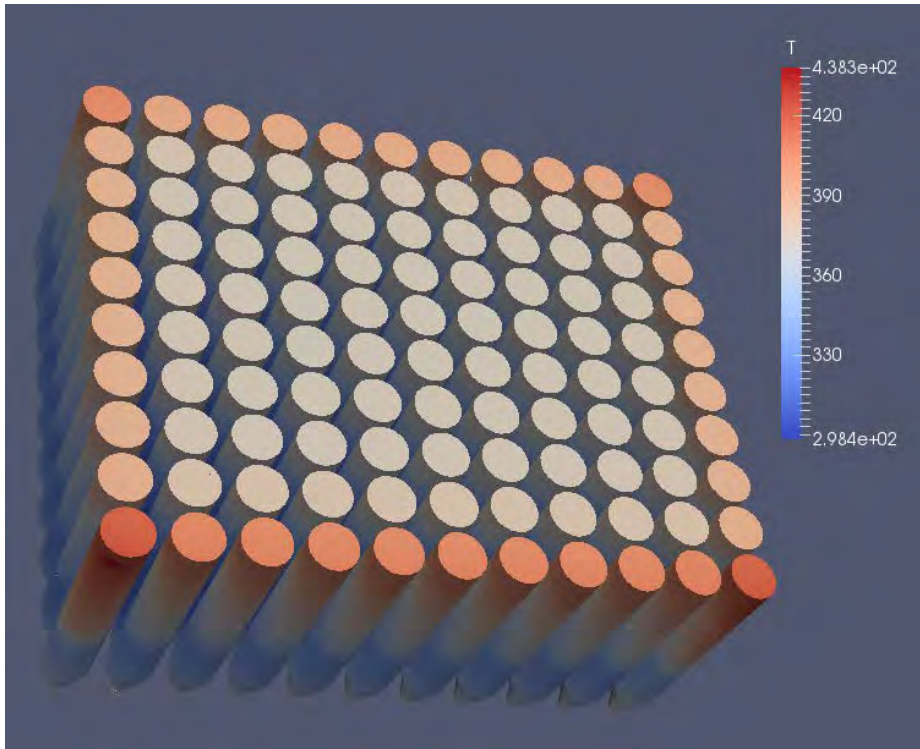
Temperatures of Cartridge Cases Shortly After the Reaction Began in the Lower Corners



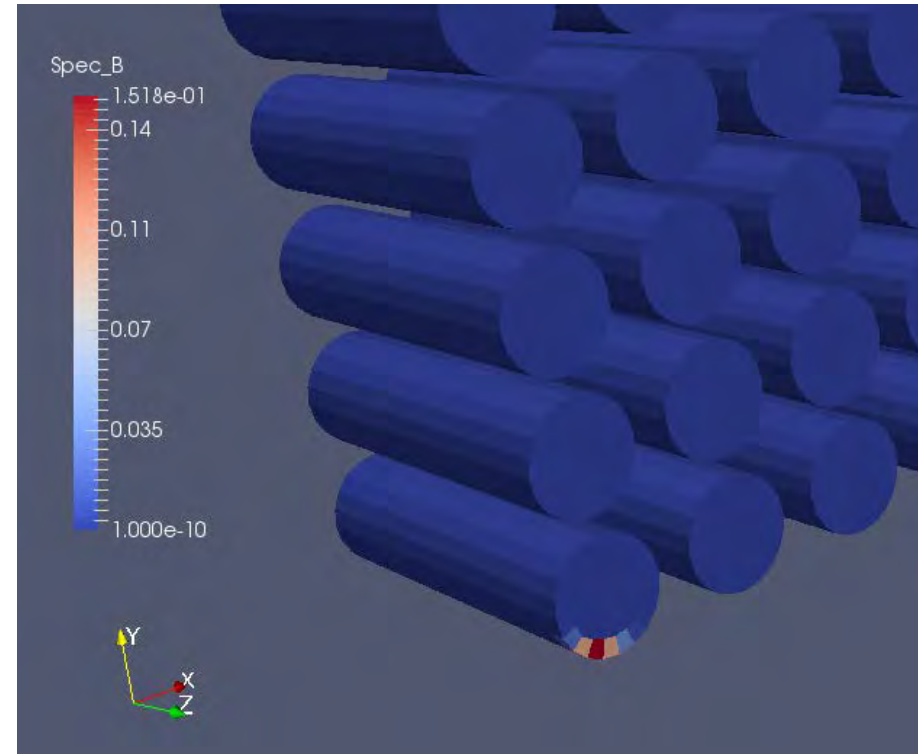
Cartridge case temperatures during ramp up to the reaction. The bottom corner projectiles are starting to show more heating.



Case head temperatures during the ramp up. Temperatures are rising in the lower corner case heads at a higher rate.

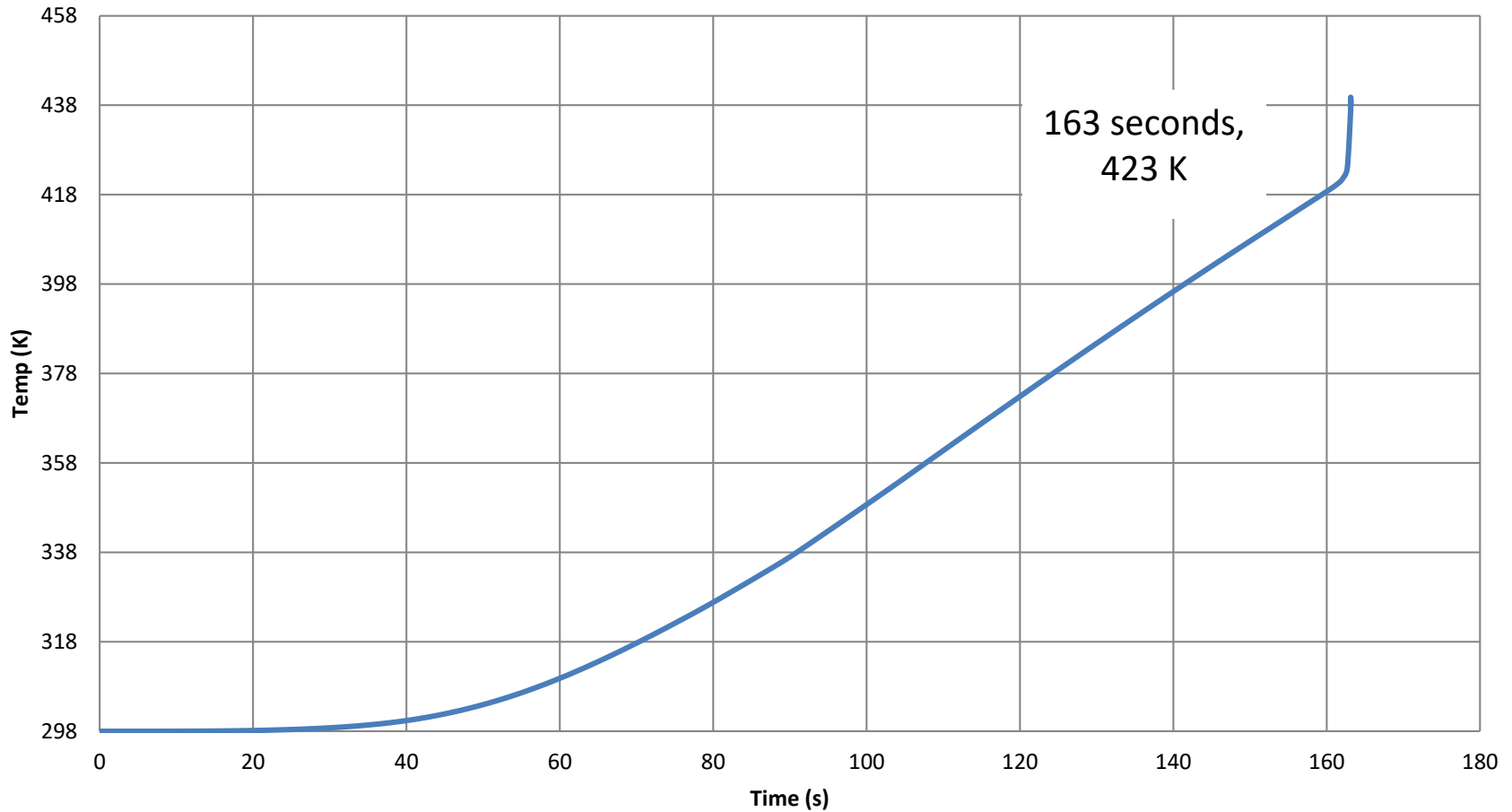


Cartridge Cases

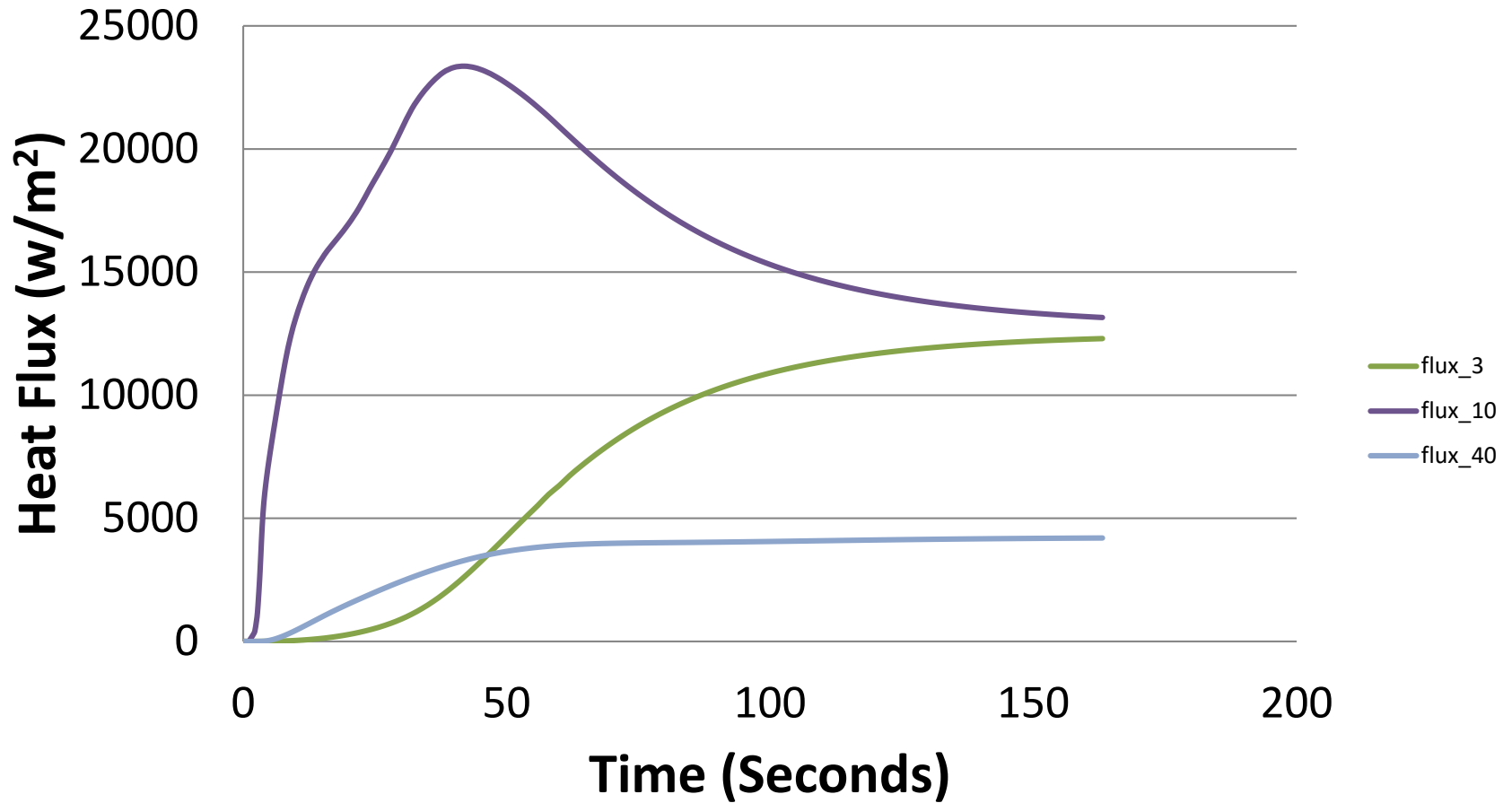


Propellant inside of cartridge cases. The charge in the corner is evolving gaseous decomposition products (species B), 0.151 moles per liter.

Propellant Temperature in First Round to React



Heat Fluxes Along Thermal Path to Propellant



Debris from Reaction

Exited Burner
but <50 ft

Remained inside
burner

Greater
than 50 ft



Summary and Conclusions

Fast cook-off models have produced very good agreement with experiments for the time to reaction. The models also produce very useful data that could not be obtained otherwise, especial heat flux along the path from the fire to the reactive material. The models have been validated with data from three different rocket motors in conditions varying from a bare motor in the fire to a motor inside of missile launching canister made out of carbon fiber composite material. The models also predicted the explosion of an ammunition can full of live cartridges. The model showed the heating to be most severe in the lower corners of can. The model also included mitigation materials and could be used to further improve similar systems. The evolution of pyrolysis products was also calculated.

The next logical step in development of the technology is to augment the present models with another code we have experience with to calculate reaction violence.

The computer models could also be used to predict the reaction time for slow cook-off. The heating is mainly free and forced convection in ovens. Some of the fast cook-offs we have calculated for encanistered munitions start at the point of maximum natural convection. It would not be difficult to simulate all the heat flow paths in slow cook-off, including source and sink elements to simulate internal blowers.

Comparing Fire Response of Simulated Rocket Motors in Steel and Carbon Fiber Composite Missile Launching Canisters

Jon J. Yagla, PhD.

Insensitive Munitions and Energetic Materials Technology Symposium

Portland, Oregon USA

April 2018

NSWCDD-PN-18-00179; Distribution Statement A: Approved for Public Release, distribution is unlimited

NSWCDD-PN-18-00179; Distribution Statement A: Approved for Public Release, distribution is unlimited

Abstract

The paper explains the results from a two-part experiment that was designed to provide data on the thermal response of encanistered missiles in fast cook-off testing. The first part is the fire response in a liquid fuel fire. The second part will be a propane fuel fire. A steel canister and a carbon fiber composite canister were used. The test and data analysis are complete for the liquid fuel fire and are the subject of the paper.

The tests were designed to document the complete thermal path from the fire, through the missile launching canister, and into propellant in simulated rocket motors. The thermal path starts in the fire with radiation and forced convection heating of the canister, then conduction through the canister wall, radiation and natural convection between the canister and the rocket motor case, conduction through the case, conduction through a thin layer of insulation, and into the propellant. Temperature versus time was measured in the fire and at each interface all the way to the propellant.

Each canister contained three simulated rocket motor segments separated by insulating partitions. The motors used different materials for the cases. Some of the motors used steel cases; the others used aluminum, titanium, and carbon fiber composite cases. Two types of insulation between the case and the propellant were represented, EPDM rubber and cork. Two propellant simulants were used, one a careful representation of an operational motor, the other an inexpensive mineral based material.

The results show the time-dependent fire temperature, the temperature at each interface, and calculations of the heat flux into the simulated propellant. There was a thermal event inside the carbon fiber composite canister. All but one of the simulated propellants received heat in the range of 20–25 kW/m². The outlier was an aluminum chamber with cork insulation. Calculations showed the heat flux would have been in the same range had the motor used EPDM insulation.

1 PURPOSE OF EXPERIMENT

The purpose of the experiment was as follows:

- Gather comparative data on steel and carbon fiber composite missile launching canisters
- Assess relative performance of steel, aluminum, and carbon fiber composite rocket motor chamber materials
- Obtain data for converging and validating finite element models
- Obtain data for later comparison to propane gas fuel fire cook-off fires

As shown in Figure 1, two canister segments were insulated from each other and joined in the middle of the pit, one meter above the fuel. Approximately eighty (80) channels of thermocouple and displacement data were recorded during the test.



Figure 1. Steel and carbon fiber canisters in Dahlgren fast cook-off pit.

As shown in Figure 2, thermocouples were placed inside and outside each face of the canisters to measure the temperature and calculate the heat flux. The inner and outer thermocouples were aligned to measure along a straight path from the fire to the propellant. The fire thermocouples were placed on the line 50 millimeters (mm) from the canister. The instrumentation cables were brought out through a conduit. A linear variable distance transformer (LVDT) measured the sagging deformation of the composite canister. The horizontal pipe was for a string to pull the movable element of the LVDT, which was located outside of the fire.



Figure 2. Thermocouples on canisters.

Figure 3 is a pictorial view of the assembly on the test stand. The actual arrangement as tested is shown in Figure 4. As shown in Figure 5, the canisters were assembled into modules for insertion into the canister segments. The motors were of the center perforation type, with one cylindrical perforation. The perforations were aligned and thermocouples were installed in free air in the perforations.

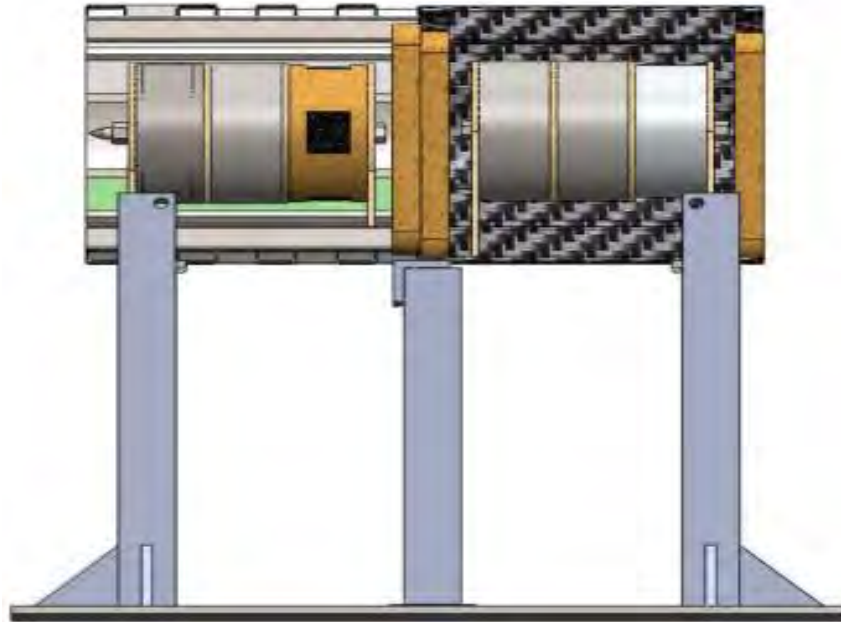


Figure 3. Representative rocket motor chambers.

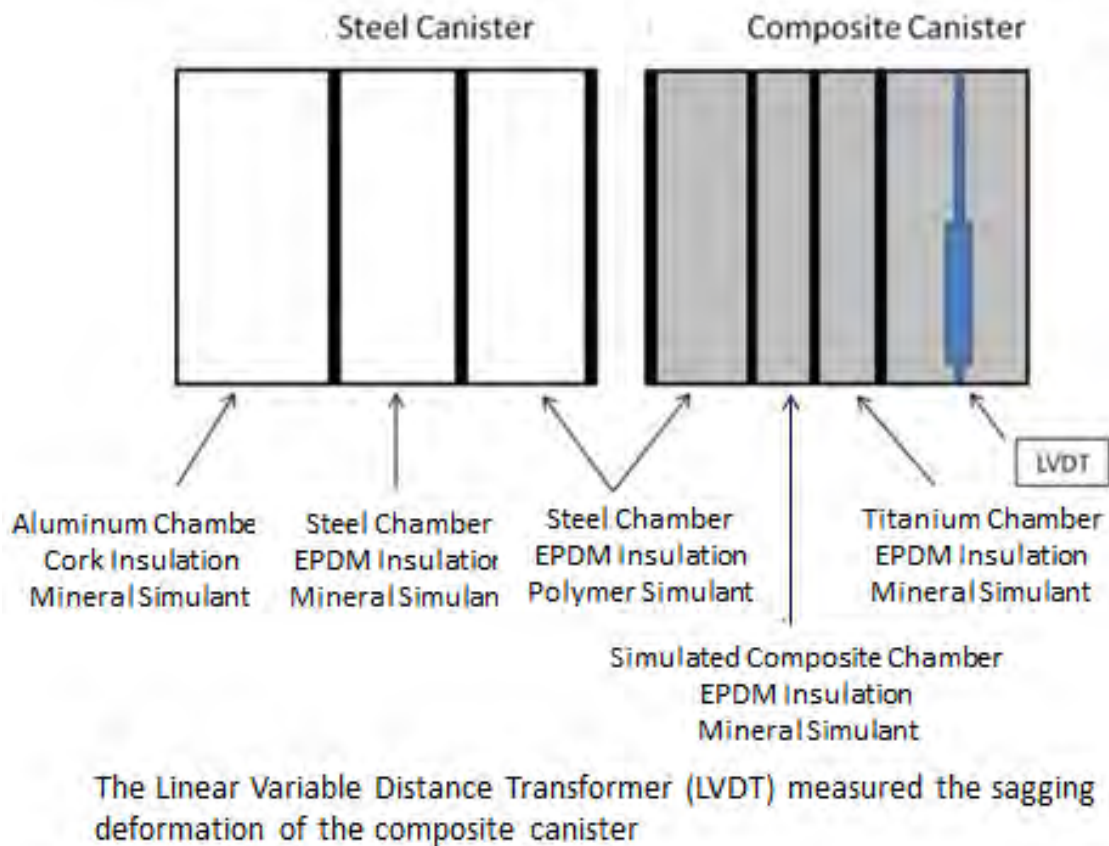


Figure 4. Simulated motor chamber segments.

Figure 5 shows the motor segments with instrumentation.

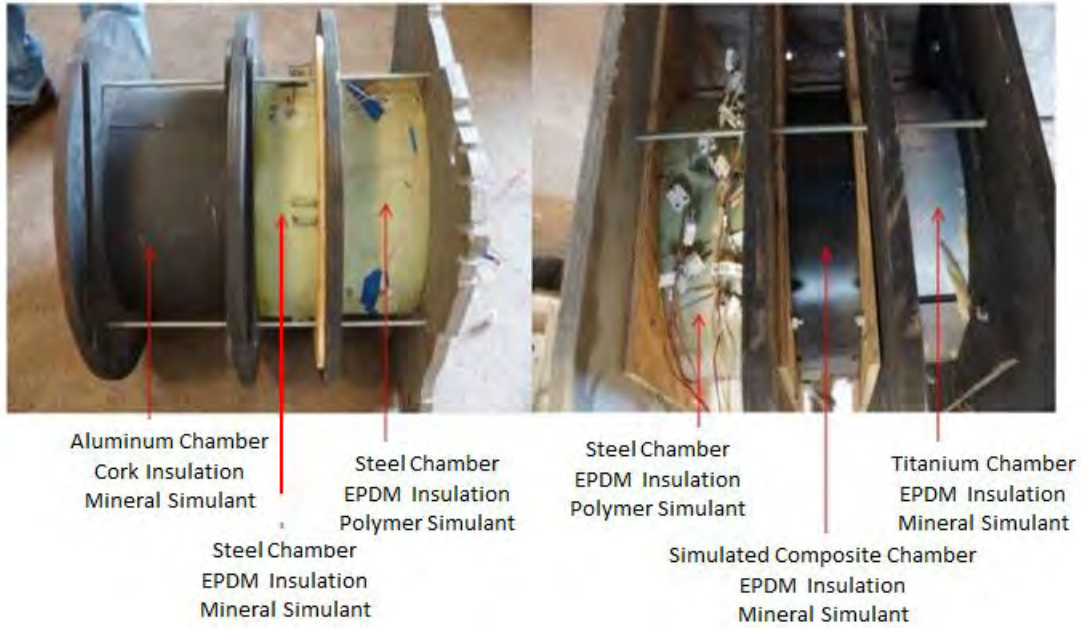


Figure 5. Motor segments with instrumentation.

2 EXPERIMENTAL DATA

The flow of heat from the fire through the four faces of each canister was measured. A thermal event occurred in the carbon fiber composite canister, as shown in Figure 6. As can be seen in the internal surfaces plot, there was a thermal event inside the canisters. This was attributed to the carbon fiber epoxy material igniting at the known auto ignition temperature for the material.

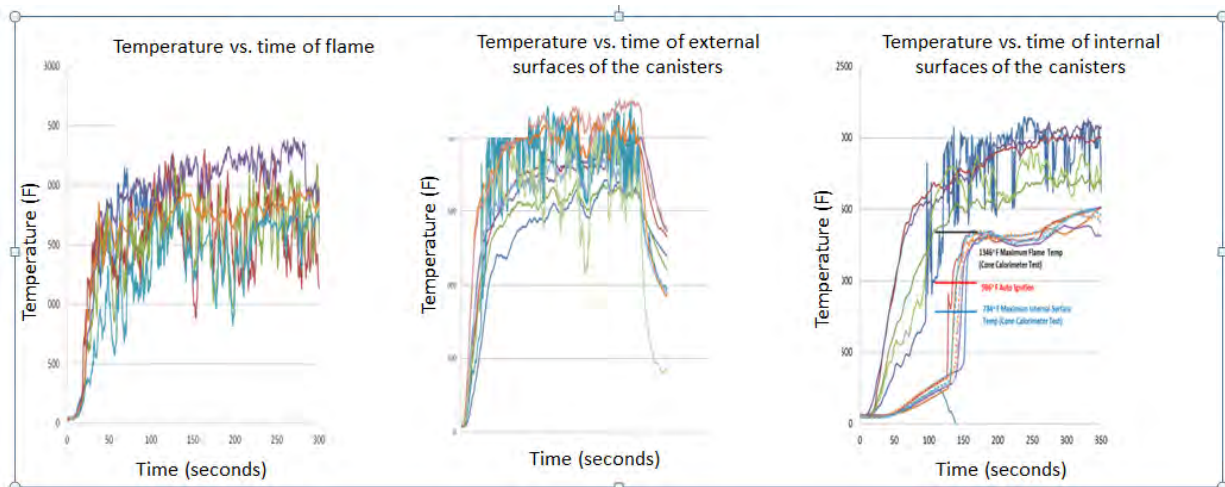


Figure 6. Temperatures versus time along the path from the fire to the internal surfaces of the canisters.

Figure 7 shows the temperatures along thermal paths into a motor with a steel chamber in the steel canister. The details along the paths are different, but all converge on 1,250 to 1,300°F at a time of 180 seconds. The differences in the fire and canister walls, mainly due to wind, are all averaged out inside the canister. This is not to say that the wind has no effect on the results, it only says that the effects of the wind condition during the test aren't sensed by the motor after 3 minutes in the fire. The wind generates turbulence, which increases the efficiency of combustion, increases the temperature, increases radiation according to T^4 , and increases the convective heating by the fire.

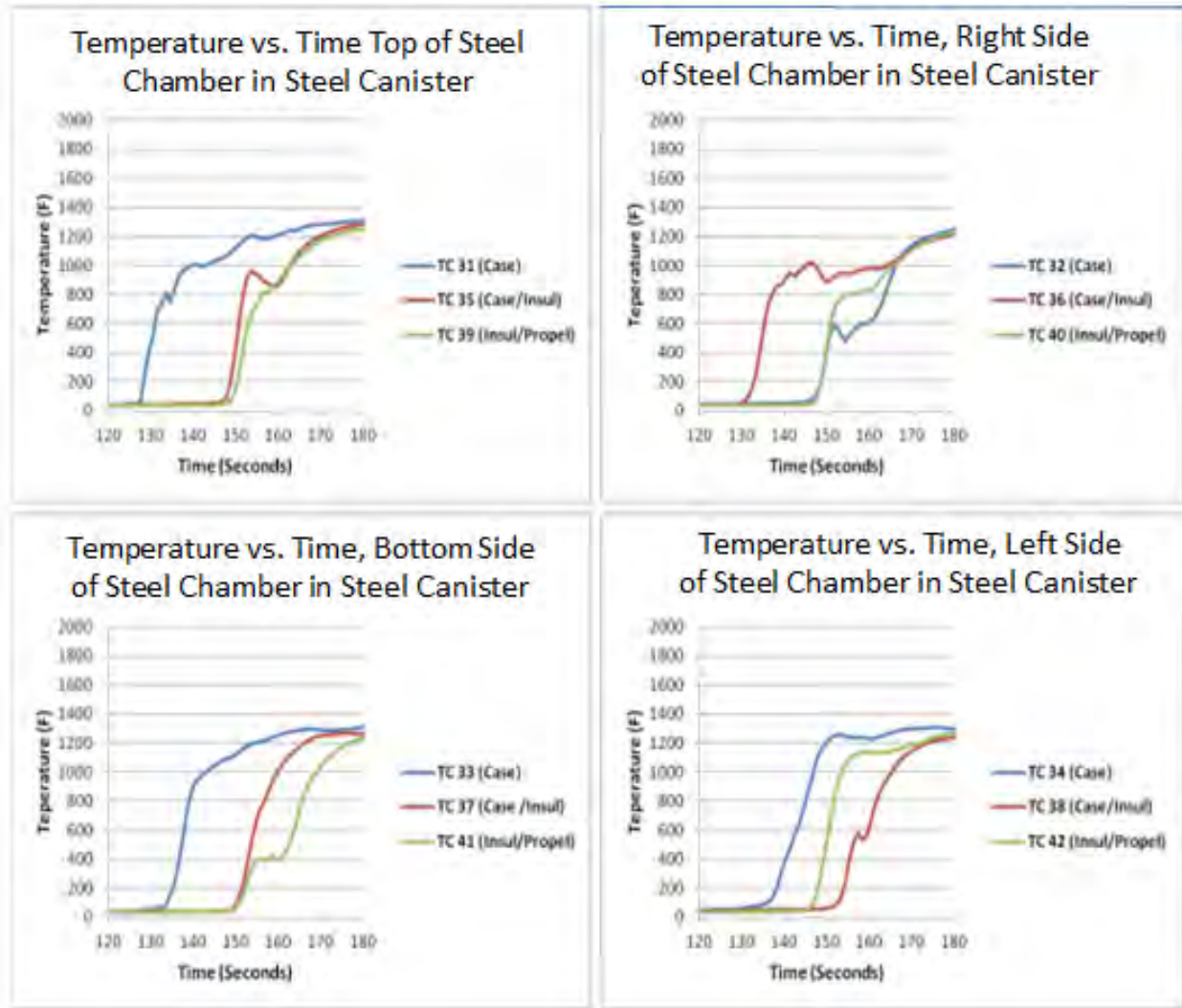


Figure 7. Temperatures along thermal paths into a motor with a steel chamber in the steel canister.

Figure 8 shows temperatures along similar paths to an identical motor with a steel chamber in the carbon fiber composite canister. Again, there are differences along each path, but the temperatures converge on 1,250°F after 3 minutes in the fire.

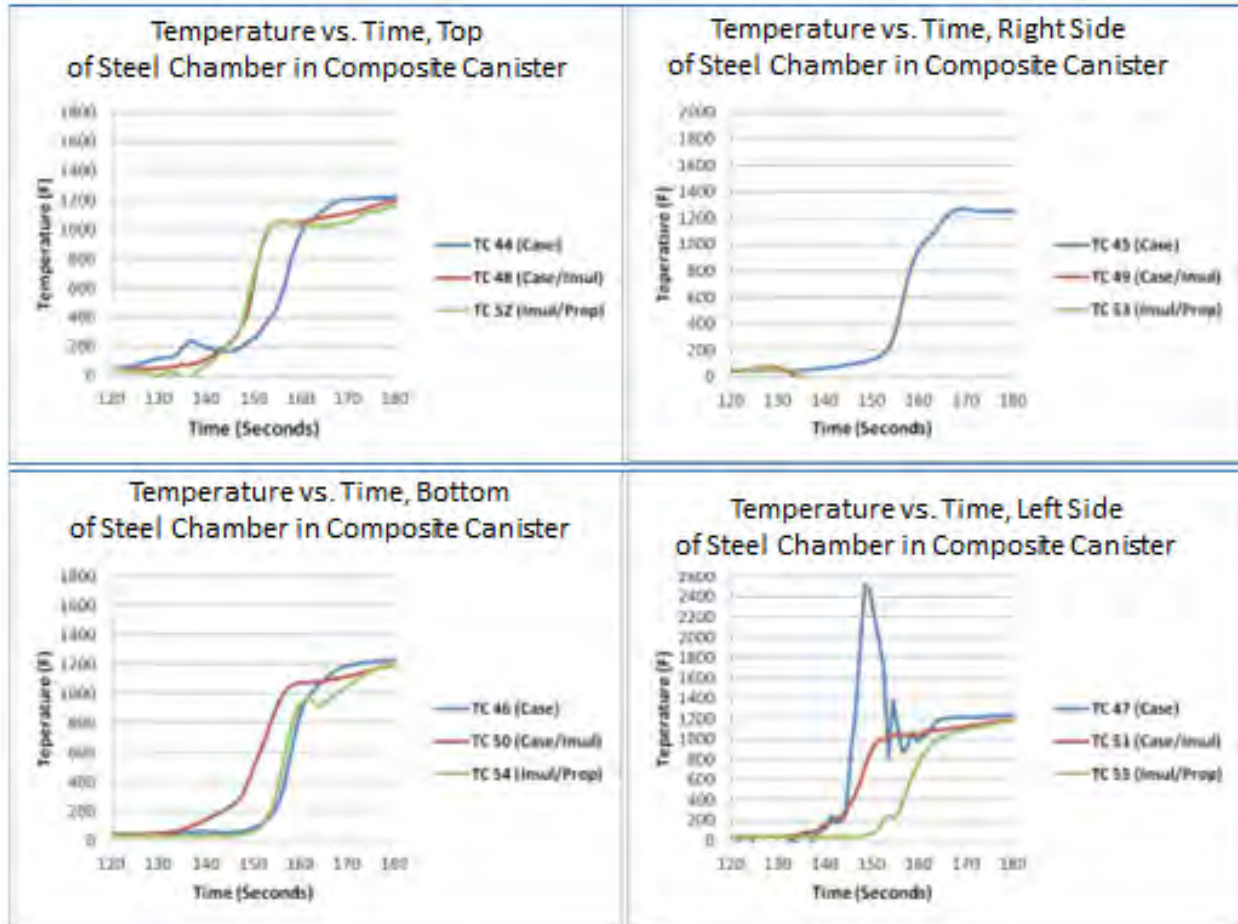


Figure 8. Temperature versus time along thermal paths into a motor with a steel case in the carbon fiber composite canister.

The effects of the thermal event are apparent in the data traces from the left side of the canister (Figure 9). There was a sudden temperature rise to 2,400°F, which quickly dropped back down to 1,000°F. Two data traces from the right side were lost at the time of the thermal event. Perhaps they were casualties. Again, all the temperatures converge to 1,250°F after 3 minutes in the fire. Therefore, it does not seem to matter to the motor whether it was in a steel canister or a composite canister.

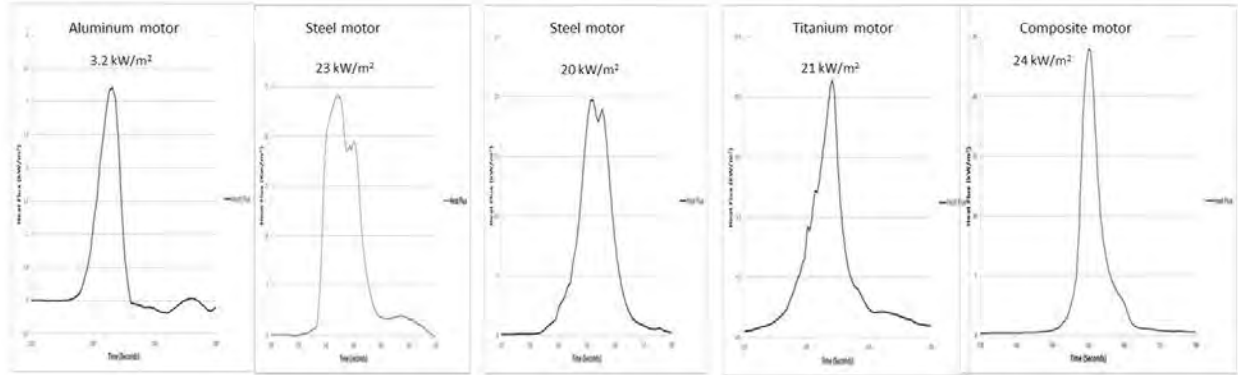


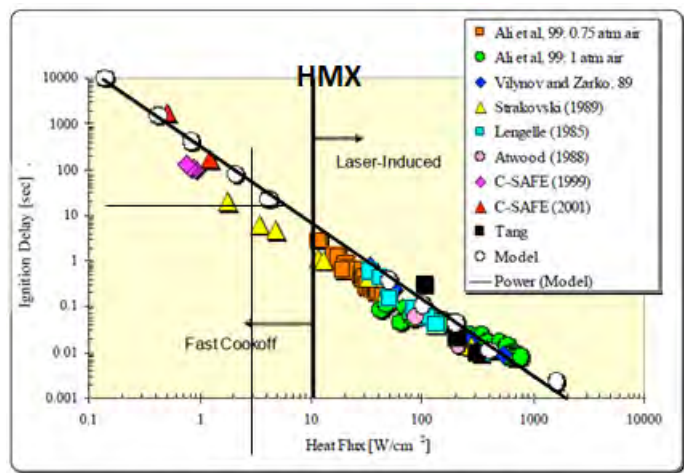
Figure 9. Heat fluxes into propellant.

The heat fluxes into the propellant were all around 20–24 kW/m². Figure 10 shows a curve for time to cook-off versus heat flux for HMX explosive. This would cause cook-off at approximately 1 minute after this heat flux is attained, in either canister, for a propellant like HMX.

Calculations showed the heat flux into the propellant of the aluminum chamber motor would have been in the 20–24 kW/m² if the insulation would have been EPDM.

There was not much difference between the heat flux into the sophisticated propellant simulant and the inexpensive mineral-based simulant.

Data for heat flux versus time to reaction is needed for other energetic materials. The very tight clustering of the data along a straight line, as shown in Figure 10, suggests this may be a very fundamental property of explosives. If so, all cook-off reaction times could be classified by one data point on the curve (e.g., time to reaction for heat flux of 1 w/m²), and the slope of the curve.



Ignition delay versus heat flux

K. V. Meredith and M. W. Beckstead
Brigham Young University

Figure 10. Estimated time to cook-off for HMX explosive.

As shown in Figure 11, the canisters retained their shapes throughout the fire.



Figure 11. Post-test remains.

3. SUMMARY AND CONCLUSIONS

The summary and conclusions are as follows:

- Experimental data for six simulated rocket motors were obtained using a steel missile launching canister and a carbon fiber composite canister.
- The data showed similar rocket motor thermal responses in either canister type, and all motor types with EPDM insulation.
- The peak heat fluxes into the motors were in the range of 20 –24 kW/m².
- There was little deformation of the carbon fiber composite canister.
- Data are now available to validate computer models of fast cook with a variety of chamber materials and steel and carbon fiber canisters.



Comparing Fire Response of Simulated Rocket Motors in Steel and Carbon Fiber Composite Missile Launching Canisters

Jon J. Yagla, PhD.

Insensitive Munitions and Energetic Materials Technology Symposium

Portland, Oregon USA

April 2018

*Gun and Electric Weapon
Systems (E)*



NSWCDD-PN-18-00179; Distribution Statement A: Approved for Public Release, distribution is unlimited

Purpose of Experiment

- Gather comparative data on steel and carbon fiber composite missile launching canisters
- Assess relative performance of steel, aluminum, and carbon fiber composite rocket motor chamber materials
- Obtain data for converging and validating finite element models
- Obtain data for later comparison with propane gas fuel fire cook-off fires

Simulated Steel and Carbon Fiber Composite Canisters in Dahlgren Fast Cook-off Pit



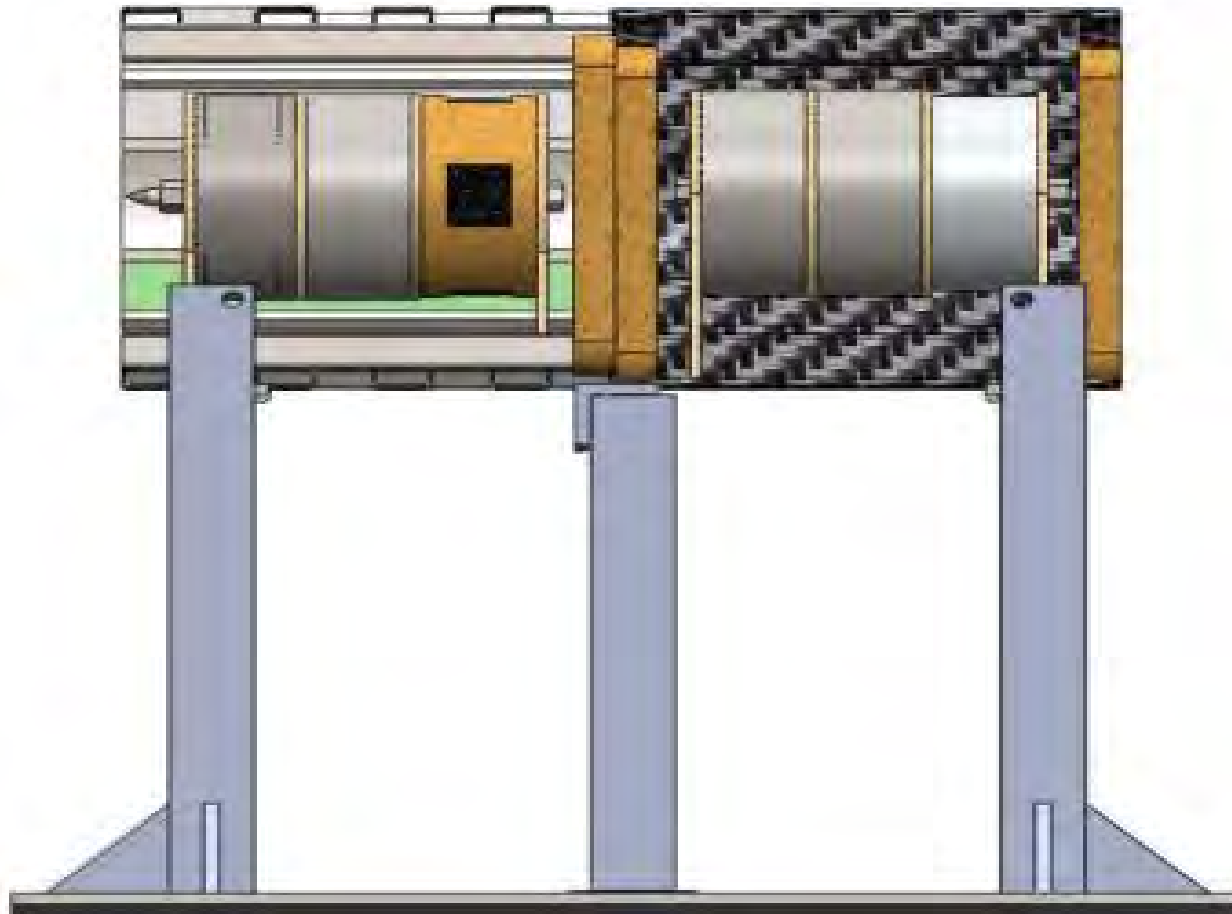
Two canister segments were insulated from each other and joined in the middle of the pit one meter above the fuel. Approximately 80 channels of thermocouple and displacement data were recorded during the test.

Canisters on Test Stand

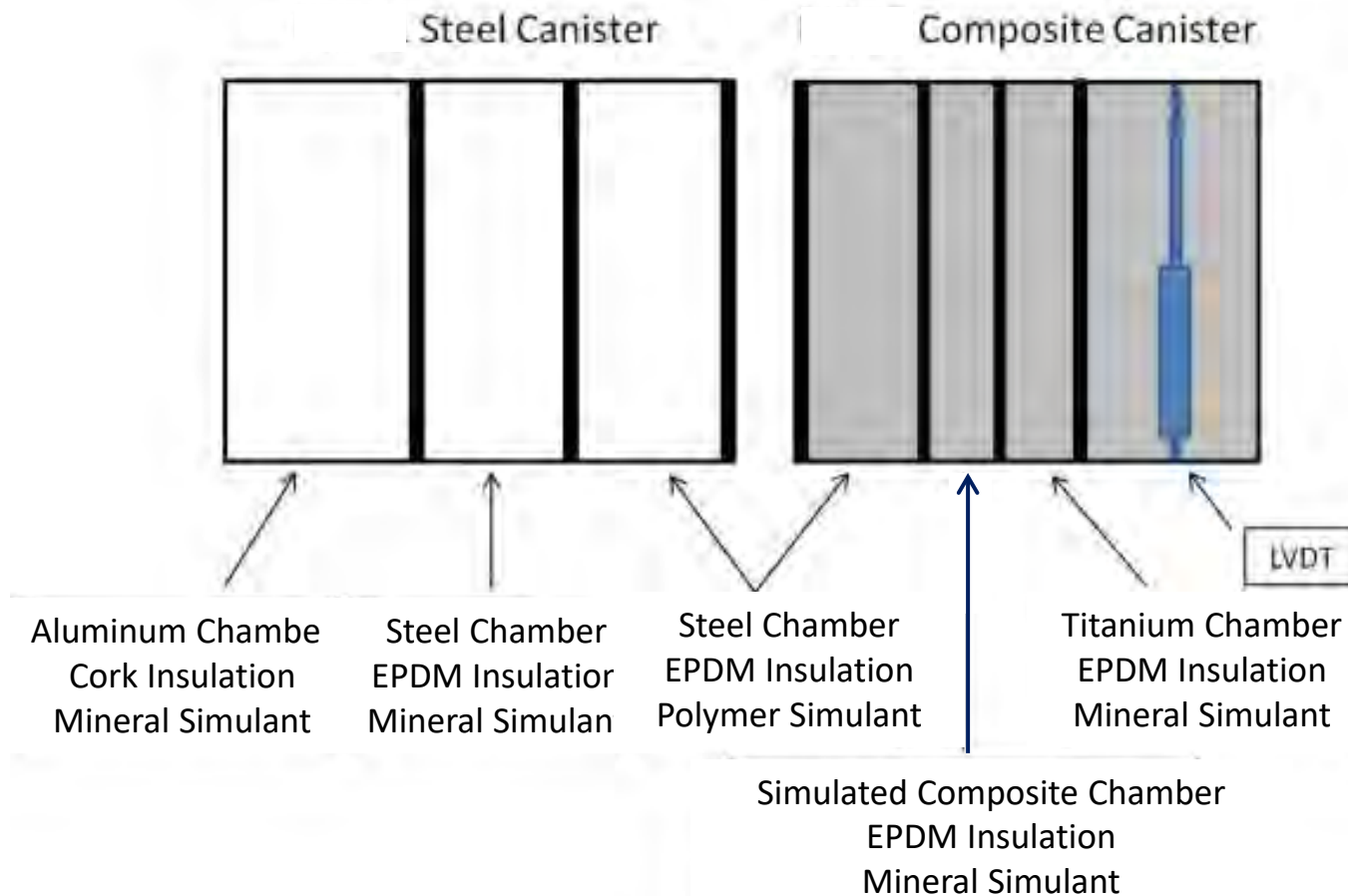


Thermocouples were placed inside and outside each face of the simulated canisters to measure the temperature and calculate the heat flux.

Representative Rocket Motor Chambers



Simulated Motor Chamber Segments



The Linear Variable Distance Transformer (LVDT) measured the sagging deformation of the composite canister

Motor Segments with Instrumentation



Aluminum Chamber
Cork Insulation
Mineral Simulant

Steel Chamber
EPDM Insulation
Polymer Simulant

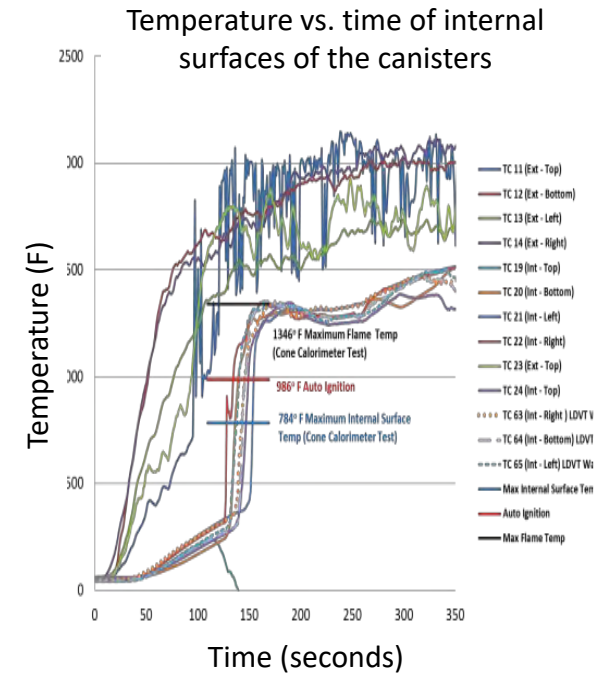
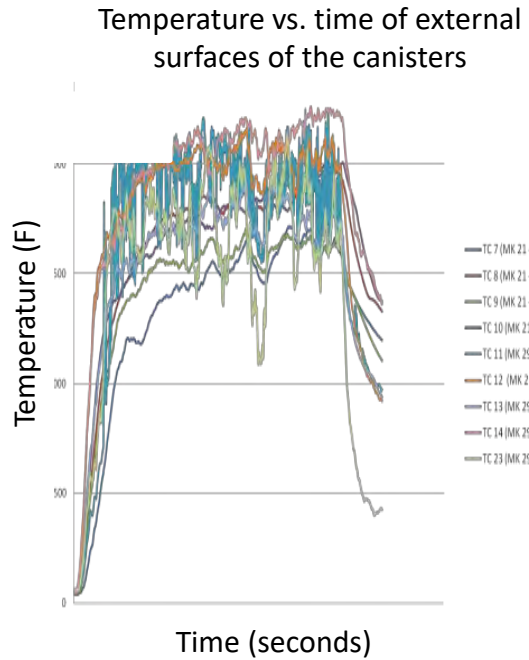
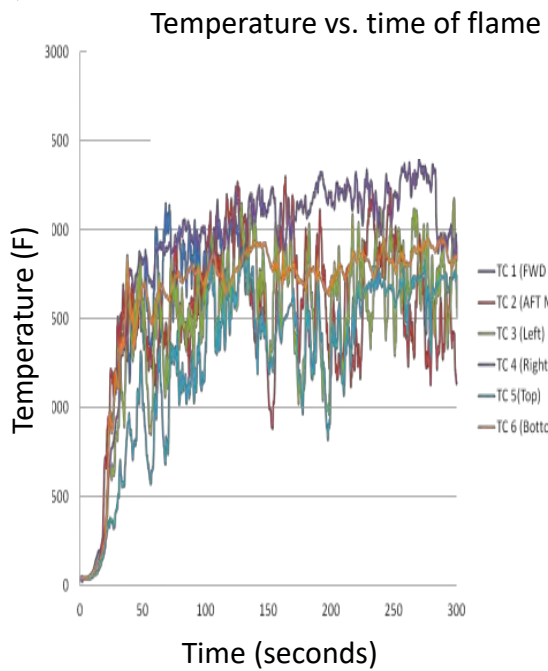
Steel Chamber
EPDM Insulation
Mineral Simulant

Steel Chamber
EPDM Insulation
Polymer Simulant

Simulated Composite Chamber
EPDM Insulation
Mineral Simulant

Titanium Chamber
EPDM Insulation
Mineral Simulant

Heat Flow from Fire Through the Canister Walls

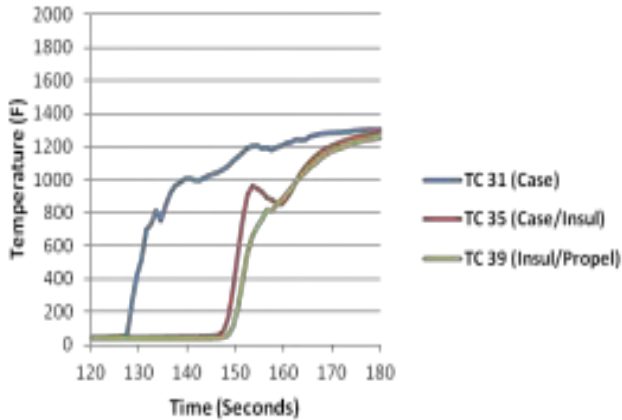


The flow of heat from the fire through the four faces of each canister was measured. A thermal event occurred in the carbon fiber composite canister.

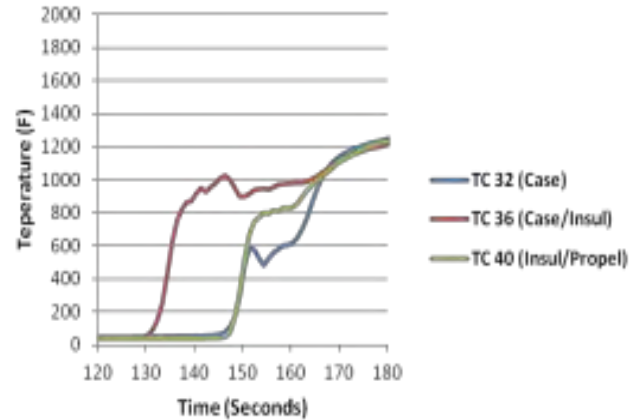


Heat Flows Through Steel Chamber, Insulation, and into Propellant

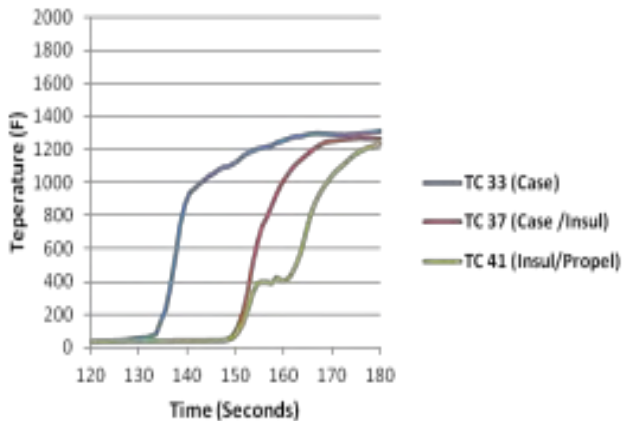
Temperature vs. Time
Top of Steel Canister



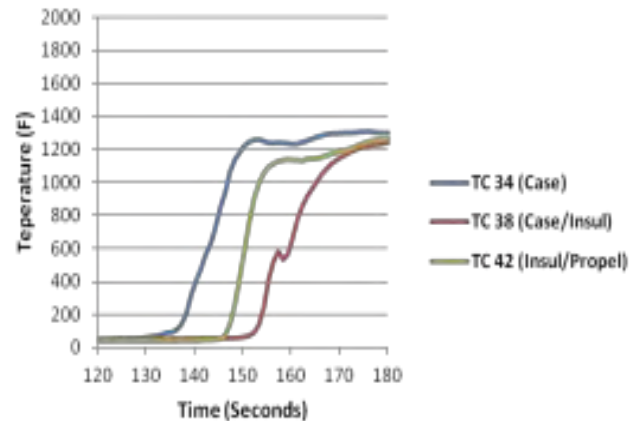
Temperature vs. Time, Right Side
of Steel Chamber in Steel Canister



Temperature vs. Time, Right Side
of Steel Chamber in Steel Canister

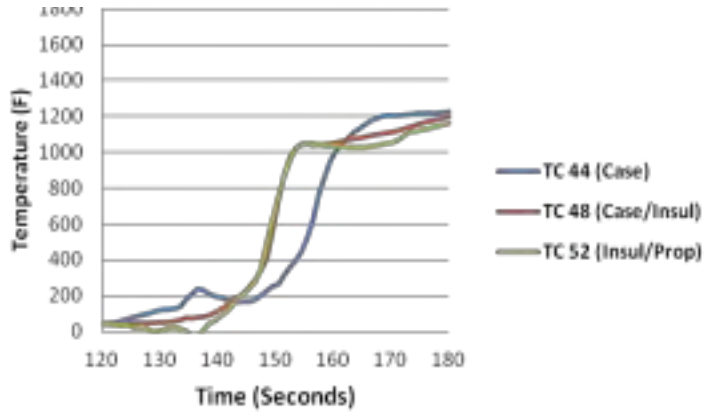


Temperature vs. Time, Left Side
of Steel Chamber in Steel Canister

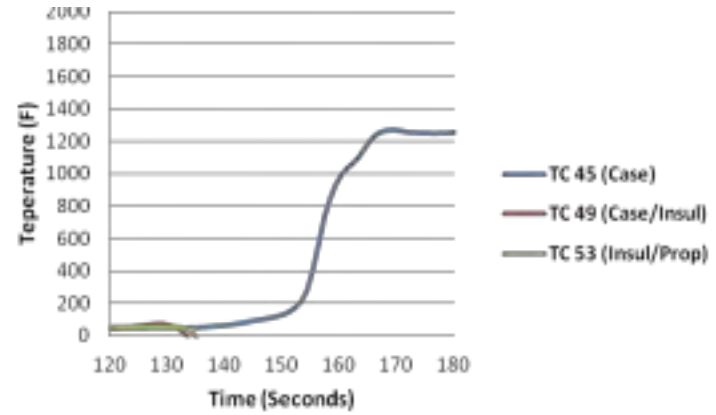


Heat Flow Through Composite Chamber, Insulation, and into Propellant

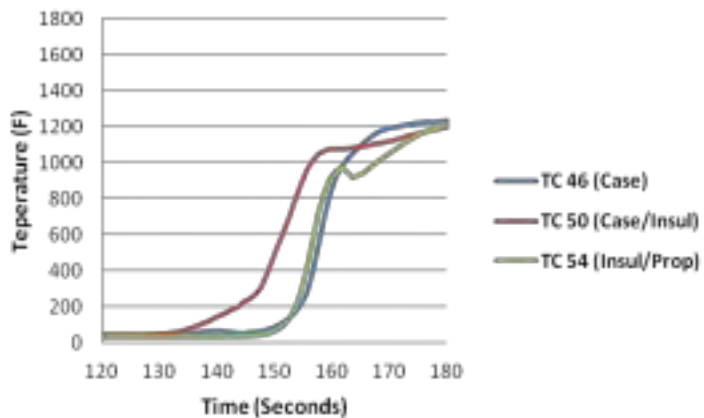
Temperature vs. Time, Top of Steel Chamber in Composite



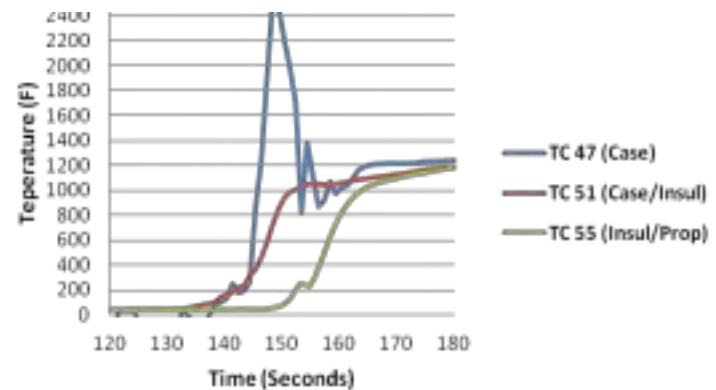
Temperature vs. Time, Right Side of Steel Chamber in Composite



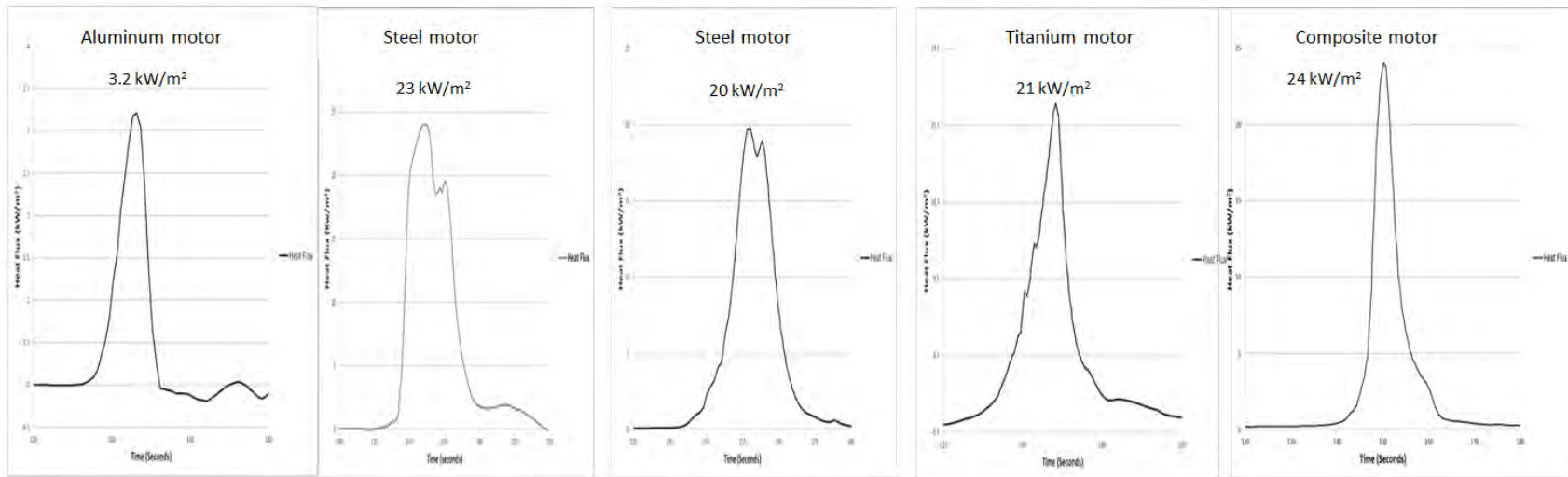
Temperature vs. Time, Bottom of Steel Chamber in Composite



Temperature vs. Time, Left Side of Steel Chamber in Composite



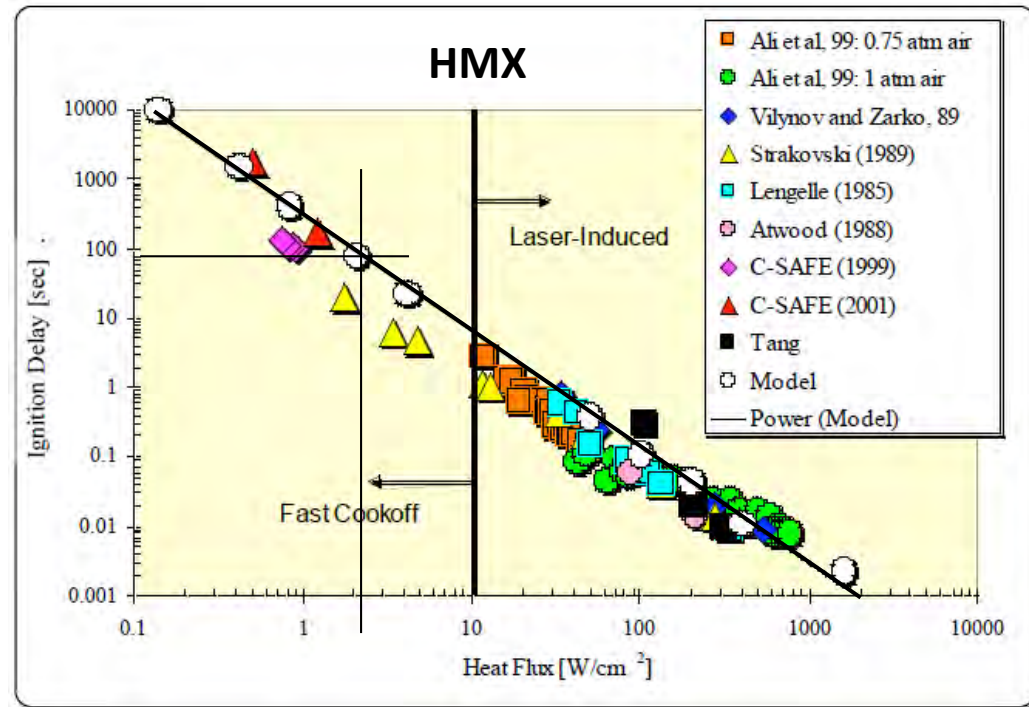
Heat Fluxes into Propellant



Except for the aluminum motor with cork insulation, the heat fluxes were all in the range of 20–24 kW/m².

Estimated Time to Cook-Off

The heat fluxes were all around 20–24 kW/m² (2-2.4W/cm²). This would cause cook off at approximately a 90 seconds after this heat flux is attained in either canister for a propellant like HMX. Data for heat flux versus time to reaction data is needed for other energetic materials. The very tight clustering of the data along a straight line, spanning five orders of magnitude, suggests this may be a very fundamental property of explosives.



Ignition delay versus heat flux

K. V. Meredith and M. W. Beckstead
Brigham Young University

Post-Test Remains



The canisters retained their shapes throughout the fire.

Summary and Conclusions

- Experimental data for six simulated rocket motors was obtained using a steel missile launching canister and a carbon fiber composite canister
- The data showed similar rocket motor thermal responses in either canister type and all motor types with EPDM insulation
- The peak heat fluxes into the motors were in the range of 20 to 24 kW/m²
- There was little deformation of the carbon fiber composite canister
- Data are now available to validate computer models of fast cook-off with a variety chamber materials and steel and carbon fiber canisters
- The experiment should be repeated in a propane fire

Radiant Chambers for Fast Cook of Testing and Simulation

Joh J. Yagla, PhD and Joseph Plaia, PhD

Paper No. 20262

2018 Insensitive Munitions and Energetic Materials Technology Symposium

Portland, Oregon

23–27 April 2018

NSWCDD-PN-18-00173; Distribution Statement A: Approved for Public Release; distribution is unlimited

1 INTRODUCTION

Two radiant chambers have been built and tested, Figure 1. They provide a uniform radiation field for testing small items. They have been calibrated with thermocouple rakes and cylindrical steel calorimeters. The radiation fields are unexpectedly uniform and have axial and circumferential uniformity. The chambers use eight 250-Watt cylindrical halogen bulbs. The bulbs are enclosed in inexpensive work light housings readily available at home centers. A variac has been used to control the heat flux. Since fast-cook heating of test items is believed to be 90% radiative, the chambers provide good tests for many items.

The chambers have been used to test instruments before putting them in large fuel fires. They have also been used to obtain highly controlled laboratory data for development of computer simulations, explaining experimental data from equipment being tested during development, and converging computer simulations when there was uncertainty in material property data.

Calibration data are presented along with results from testing a 7-inch (180-millimeter (mm)) rocket motor chamber with insulation and simulated propellant. Temperature versus time data was recorded by fifteen (15) thermocouples to measure the heat flow along each of five thermal paths from the outer surface of the motor, through the insulation, and into the propellant. The data were used to resolve problems caused by uncertainty in property data for the motor chamber and insulation in a finite element model used to analyze a restrained firing of a missile in a shipboard launcher.



Figure 1. Radiant chamber set up for testing a segment of a rocket motor with inert propellant. The test item has thermocouples to measure the temperature along three thermal paths to the propellant. Temperatures are measured on the outer surface of the motor, the inner surface between the motor and insulation, and between the insulation and the propellant. The computer screen shows the data traces which were viewed in real time as the test evolved. The power was turned off when the motor would have cooked off, which is when the traces turn down and the motor cools.

2 TEMPERATURE AND HEAT FLUX CALIBRATION

Calibration data for a single 250 Watt halogen lamp is shown in figure 2.

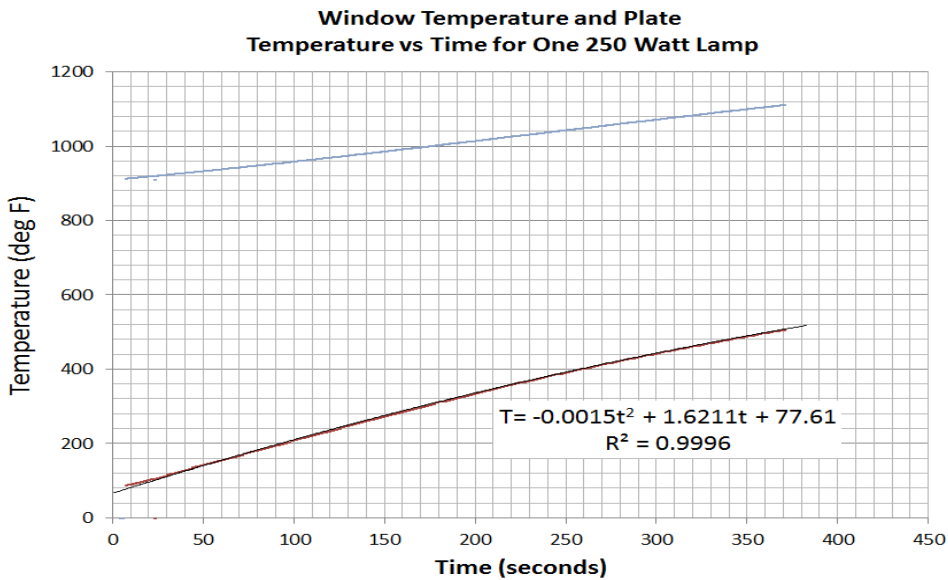


Figure 2. Window temperature and plate temperature versus time for one 250 Watt lamp.

The following paragraphs show how the combined radiation from the octagonal array of heat lamps can produce a uniform radiation field in a chamber. For the testing a set of calorimeters were made from standard 2-inch (trade size) pipe nipples 4 inches long. The first calorimeter had circumferential thermocouples on the inside. The temperature was measured at nine locations in a mid-plane through the calorimeter, figure 3. With nine locations being radiated by eight lamps, any circumferential variation should be detected. The data show there is very little variation around the circumference, figure 4.



Figure 4. Calorimeter for showing angular uniformity of temperature. Thermocouples are welded to the calorimeter at nine locations around the inner circumference.

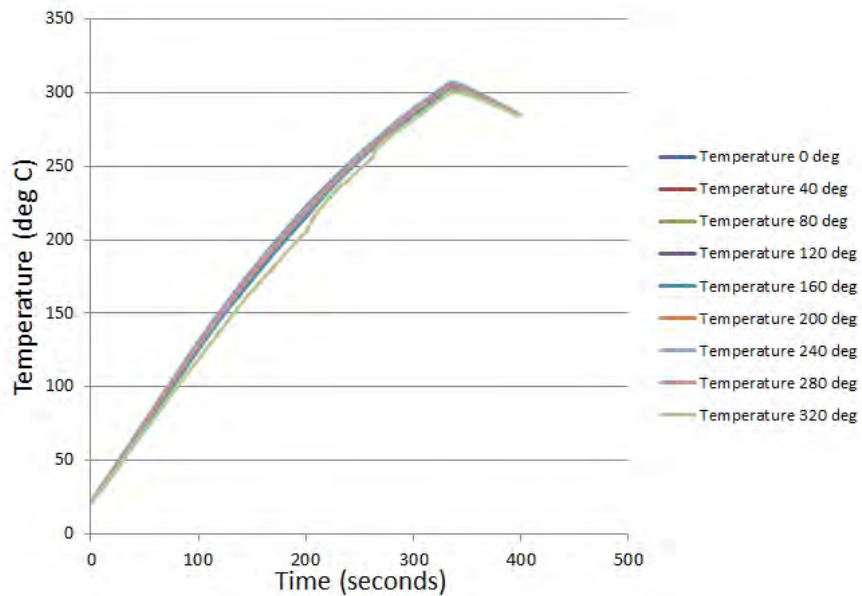


Figure 5. Temperature around the circumference of calorimeter at 40 degree intervals. Since there are eight lamps at 45 degree intervals, any aliasing of the data due to uneven radiation from the lamps would have been apparent in the data.

The temperature was measured at three locations along the surface of a calorimeter in the axial direction, figure 6. Measurements were made inside and outside of the calorimeter. The

temperature versus time traces fall neatly on one line for the entire time of exposure. At any time the temperatures are nearly the same everywhere, indicating good axial uniformity. The average temperature at each was calculated and plotted. Figure 7 is a graph showing a formula for the average temperature versus time. The value of r is a measure of the accuracy of the equation, with $r = 1$ being perfect.



Figure 6. Calorimeter for calibrating heat flux and showing uniformity of temperature and heat flux. Three axial stations were monitored on both surfaces of the calorimeter.

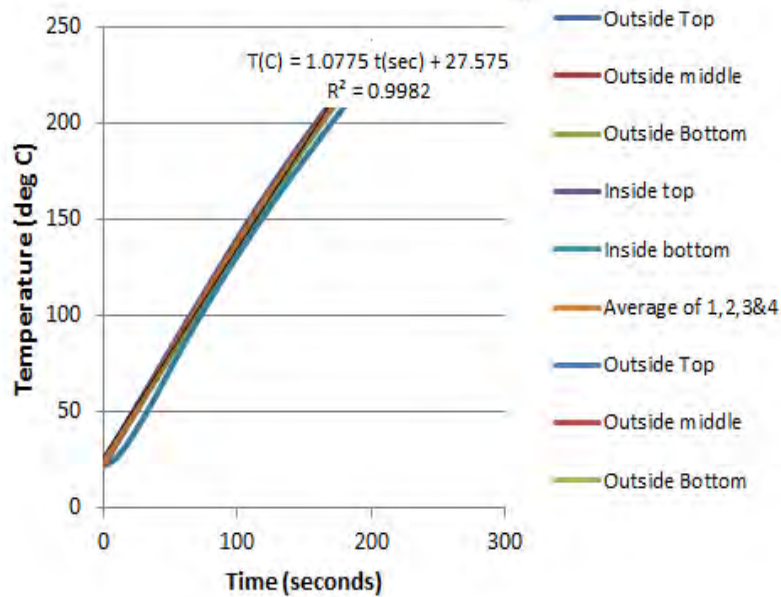


Figure 7. Temperature versus time from calorimeter thermocouples.

The absorbed heat flux was calculated. The results are shown figure 8. The formula for the heat flux versus time was differentiated to get the heating rate. Q is the heat absorbed. This was used to calculate a heating power of 499 Watts. The absorbed heat flux was 30.4 kW/m², which is very useful for designing and testing systems for STANAG 4240, Fast Heating (cook-off) Test.

Compute Heat Flux			
dT/dt		1.078	Kelvins/sec
mass		0.517	kg
specific heat		896	j/kgK
C heat capacity		463	j/K
dQ/dt=mcdT/dt		499	J/s watts
		0.499	kw
diameter		2.391	in
		0.0607	m
circumference		0.191	m
length		3.391	in
		0.0861	m
area		0.01642	sq m
absorbed heat flux		30.4	kw/sq m

Figure 8. Heat flux calibration. The figure shows how the absorbed heat flux was calculated for the calorimeter. The absorbed heat flux was 30.4 kW/m². This is representative of the heat flux into the energetic material in fast cook off testing.

Checking and calibrating instruments

Figure 9 shows a Differential Flame Thermometer (DFT) being checked out in the radiant chamber prior to an important test in a fast cook-off pit. The DFT is an instrument for measuring heat flux. The DFT has a thermocouple on the back face of a thin Inconel plate, with insulation. The temperature can be differentiated, and the heat flux calculated using properties of the plate as provided by the manufacturer.

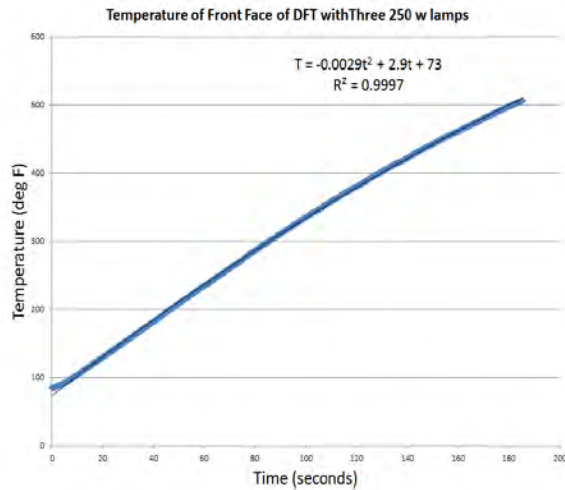


Figure 9. Differential Flame Thermometer (DFT) being tested in a radiant chamber, and resulting temperature versus time on the inside face of the DFT.

Figure 10 shows a cylindrical calorimeter with thermopiles on two diametrically opposed faces to measure the heat flux into the instrument. The thermopiles provide a direct measurement of the heat flux, not requiring differentiation of temperature data. A thermocouple was placed on the centerline in the middle of the cylinder. The instruments were used in fast cook off tests in the propane fuel fast cook-off facility at WTD-91 in Meppen, Germany.

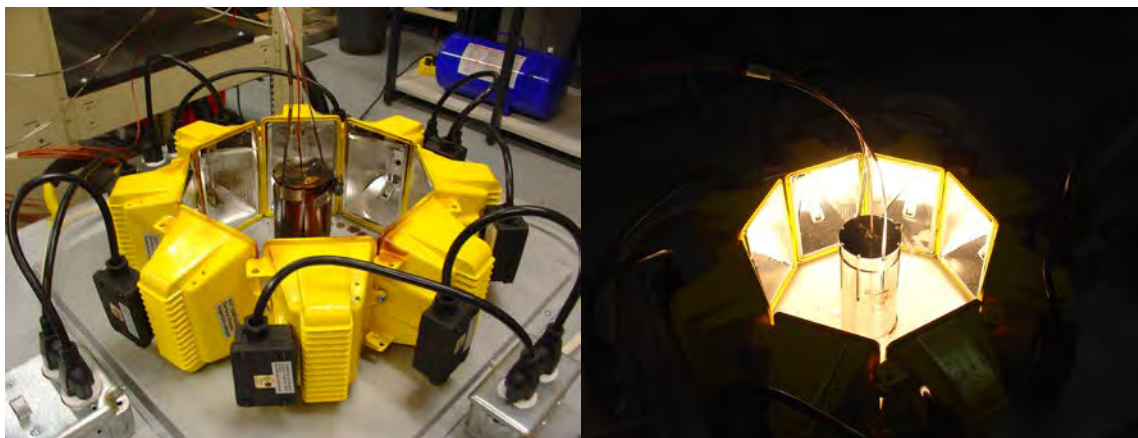


Figure 10. Thermopile calorimeter being checked out in radiant chamber

The data from the calorimeter is shown by figure 11.

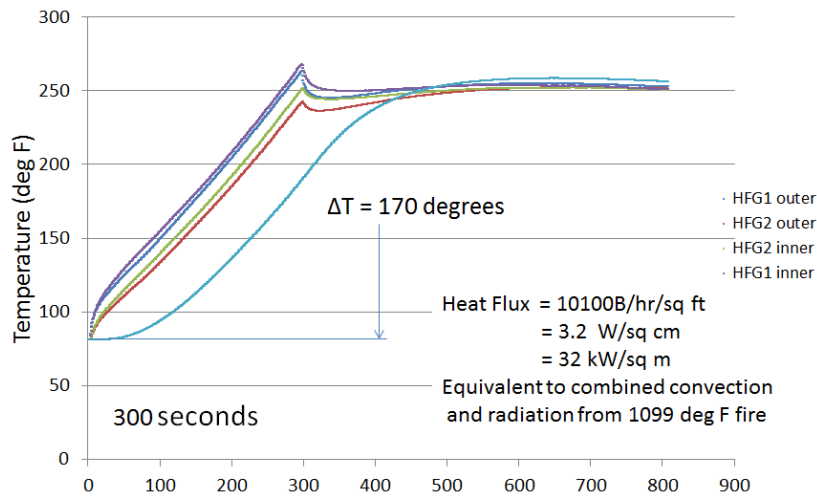


Figure 11. Signals from the four thermopiles signals of the heat flux calorimeter. Each thermopile has two places to extract a measurement. The fifth signal is from a thermocouple on the centerline of the instrument. Heat fluxes in the range of 20-30 kW/m² are typical of the heat fluxes into the energetic material at cook-off for many items that have been tested. Figure 12 shows a calorimeter in a radiant chamber with the heat flux set at 25 kW/m².

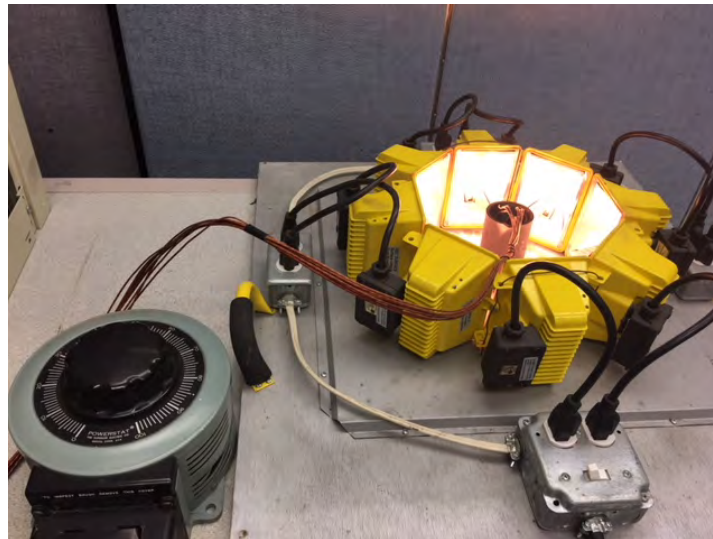


Figure 13. Calorimeter in a radiant chamber set to produce a heat flux of 25 kW/m².

3. Magazine Safety Test

There was a full-scale test of a rocket motor undergoing a restrained firing in a missile launcher. A restrained firing is a shipboard casualty in which a missile is fired, but for some reason does not leave the ship. There is a concern that the heat produced could cause ignition of an adjacent round. There were problems interpreting the data from the test. A unit was built-up using a segment of the aluminum motor that was actually used in the test. The motor was instrumented with thermocouples and loaded with inert propellant simulant.



Figure 14. Interior instrumentation showing thermocouples to measure the temperature at the interface between the insulation and propellant.



Figure 15. Motor with simulated propellant.

The test in the radiant chamber yielded material property data for the “as built” rocket motor. It was then conclusively determined that the adjacent round in the magazine safety test would not have cooked off.

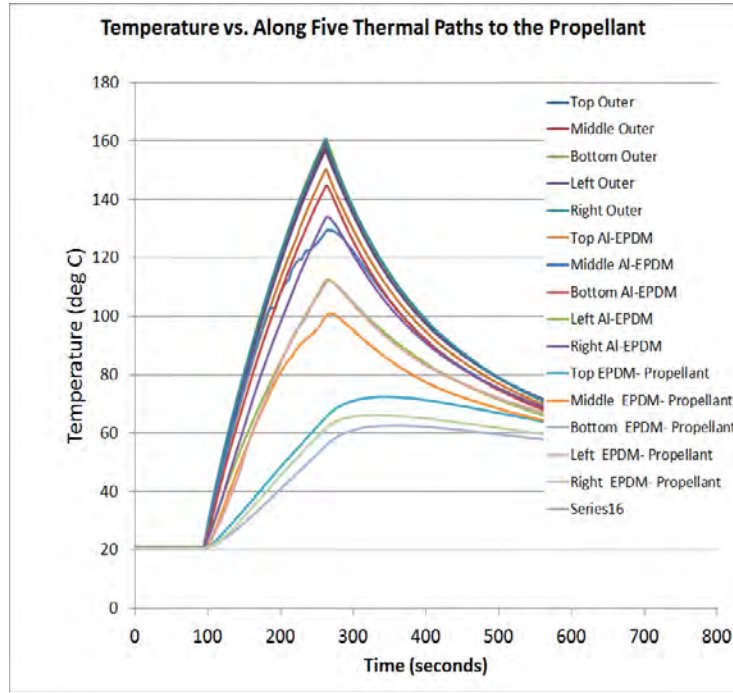


Figure 16. Records from thermocouples on five thermal paths to propellant.

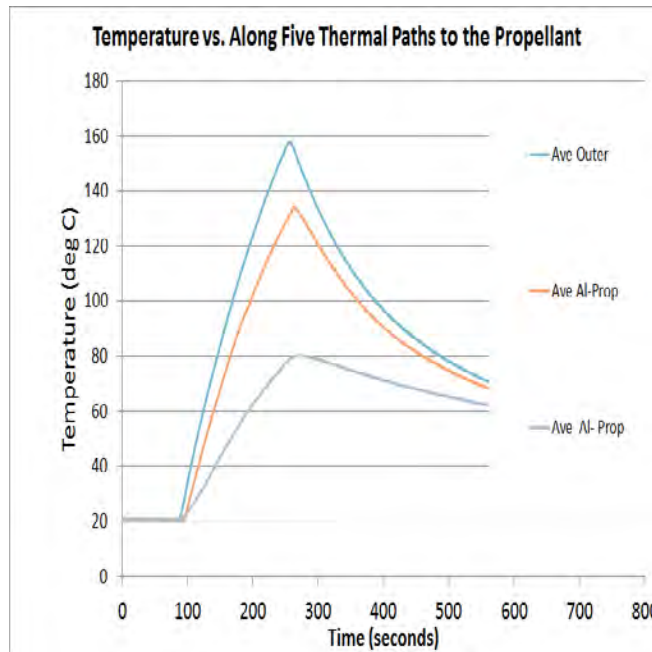


Figure 17. Average values of temperature versus time at the interfaces for heat flux calculations.

3 SUMMARY AND CONCLUSIONS

- Radiant chambers have been built to simulate the radiant heating in fast cook-off fires.
- The radiant chambers show good uniformity in temperature.
- The chambers provide a broad range of heat fluxes, which span the range of heat flux into propellant in enclosed systems (20–25 kw/m²) to absorbed radiation on the outer surface of test items in fuel fires 90 kw/m².
- The heat flux meets the heat flux requirement for STANAG 4240 Fast Cook-Off Testing.
- The chambers have been used for testing instruments and test items prior to exposure to fires.
- The chambers have been used to solve complex problems in fast cook-off and magazine safety testing.



Radiant Chambers for Fast Cook-Off Testing and Simulation

Jon J. Yagla, PhD and Joseph Plaia, PhD

Paper No. 20262

2018 Insensitive Munitions and Energetic Materials
Technology Symposium

Portland, Oregon USA

April 2018

*Gun and Electric Weapon
Systems (E)*



Radiant Chamber and Data Acquisition Equipment



- Two radiant chambers built and tested
- Uniform radiation field for testing small items
- Calibrated with thermocouple rakes and calorimeters
- ✓ Used to test instruments before putting them in large fuel fires
- ✓ Highly controlled laboratory data for development of computer simulations
- ✓ Explaining experimental data from equipment being tested during development

Organization of the Paper

Calibrating the chambers

Checking and calibrating instruments

Checking and calibrating for test items

Testing a rocket motor



Temperature and Heat Flux Calibration

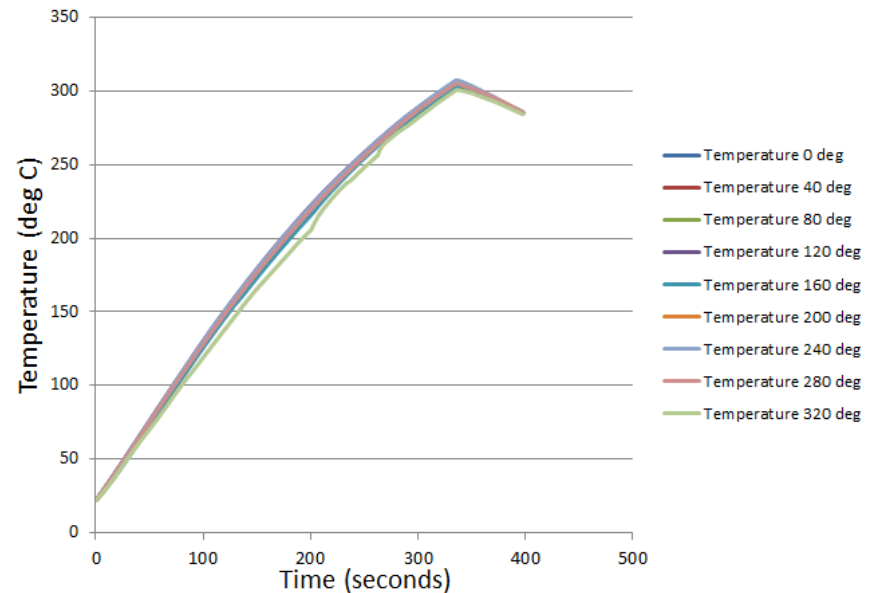


Temperature Around Circumference of Calorimeter



Calorimeter for showing angular uniformity of temperature

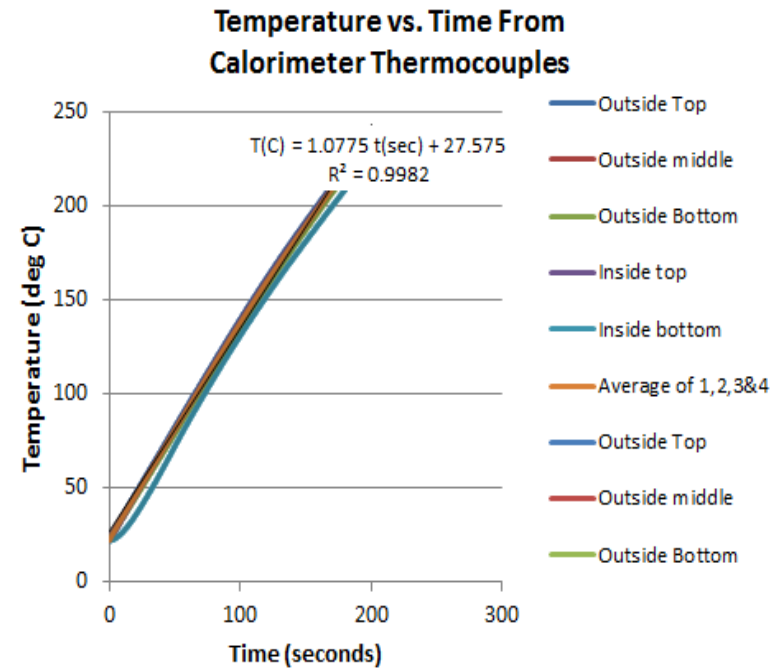
Temperatures Around the Circumference of Calorimeter at 40 degree Intervals



Nine locations radiated by eight lamps

Circumferential variation should be detected

Very little variation around the circumference



Temperature at three axial locations

Measurements inside and outside of the calorimeter

The temperature verses time traces on one line

Heat Flux Calibration

Compute Heat Flux			
dT/dt		1.078	Kelvins/sec
mass		0.517	kg
specific heat		896	j/kgK
C heat capacity		463	j/K
dQ/dt=mc dT/dt		499	J/s watts
		0.499	kw
diameter		2.391	in
		0.0607	m
circumference		0.191	m
length		3.391	in
		0.0861	m
area		0.01642	sq m
absorbed heat flux		30.4	kw/sq m

Absorbed heat flux 30.4 kW/m

Spans range of the heat flux for encanistered missiles



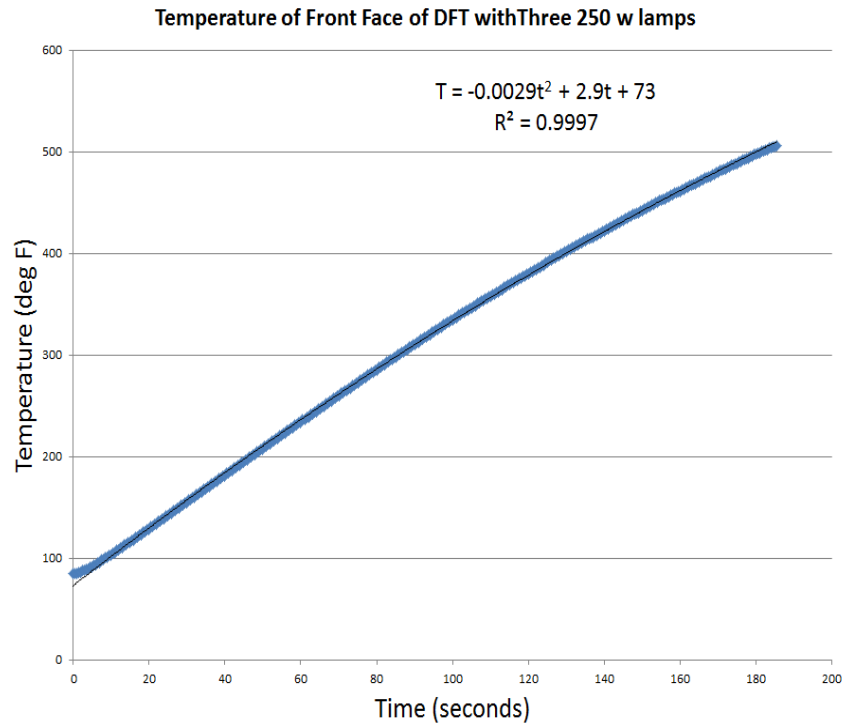
Checking and Calibrating Instruments



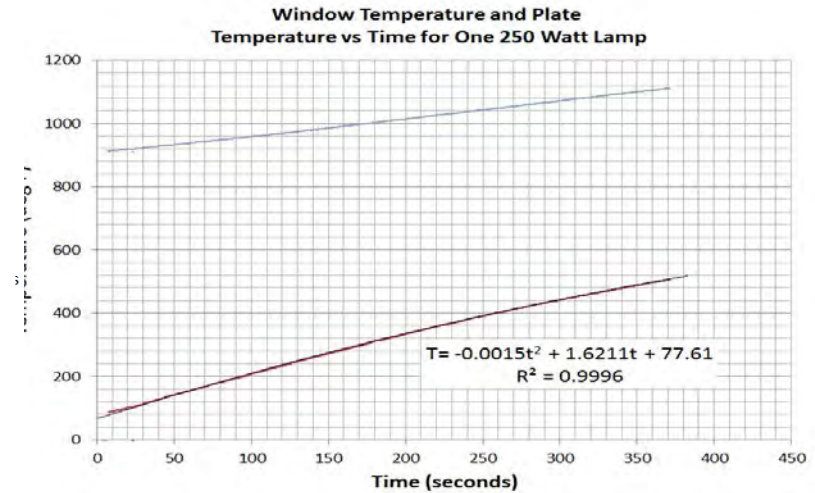
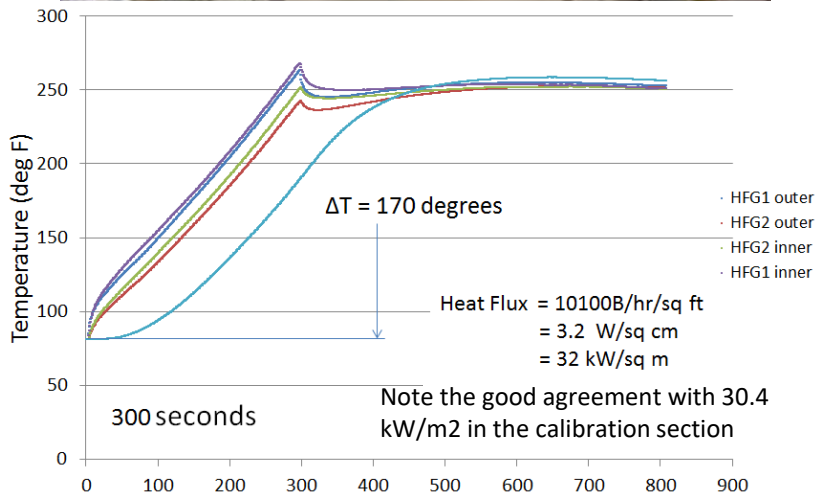
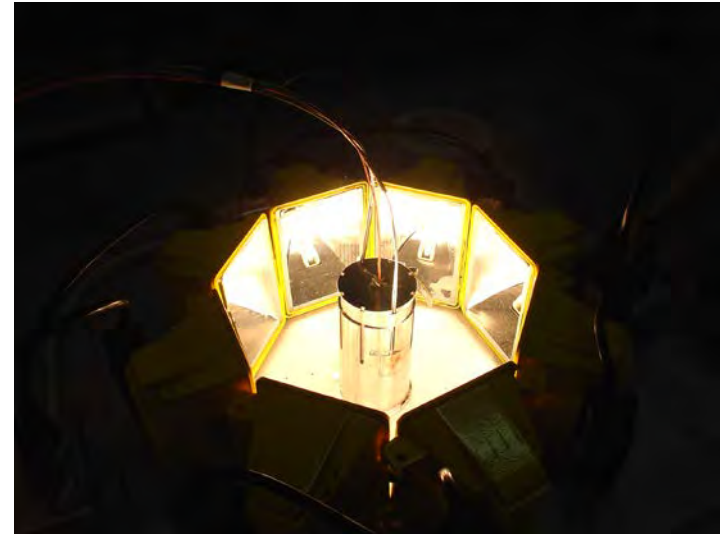
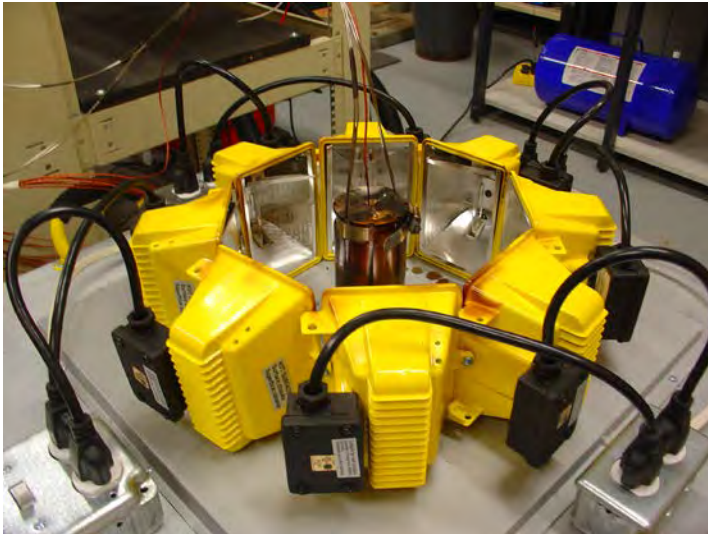
Differential Flame Thermometer Being Checked Out in Radiant Chamber



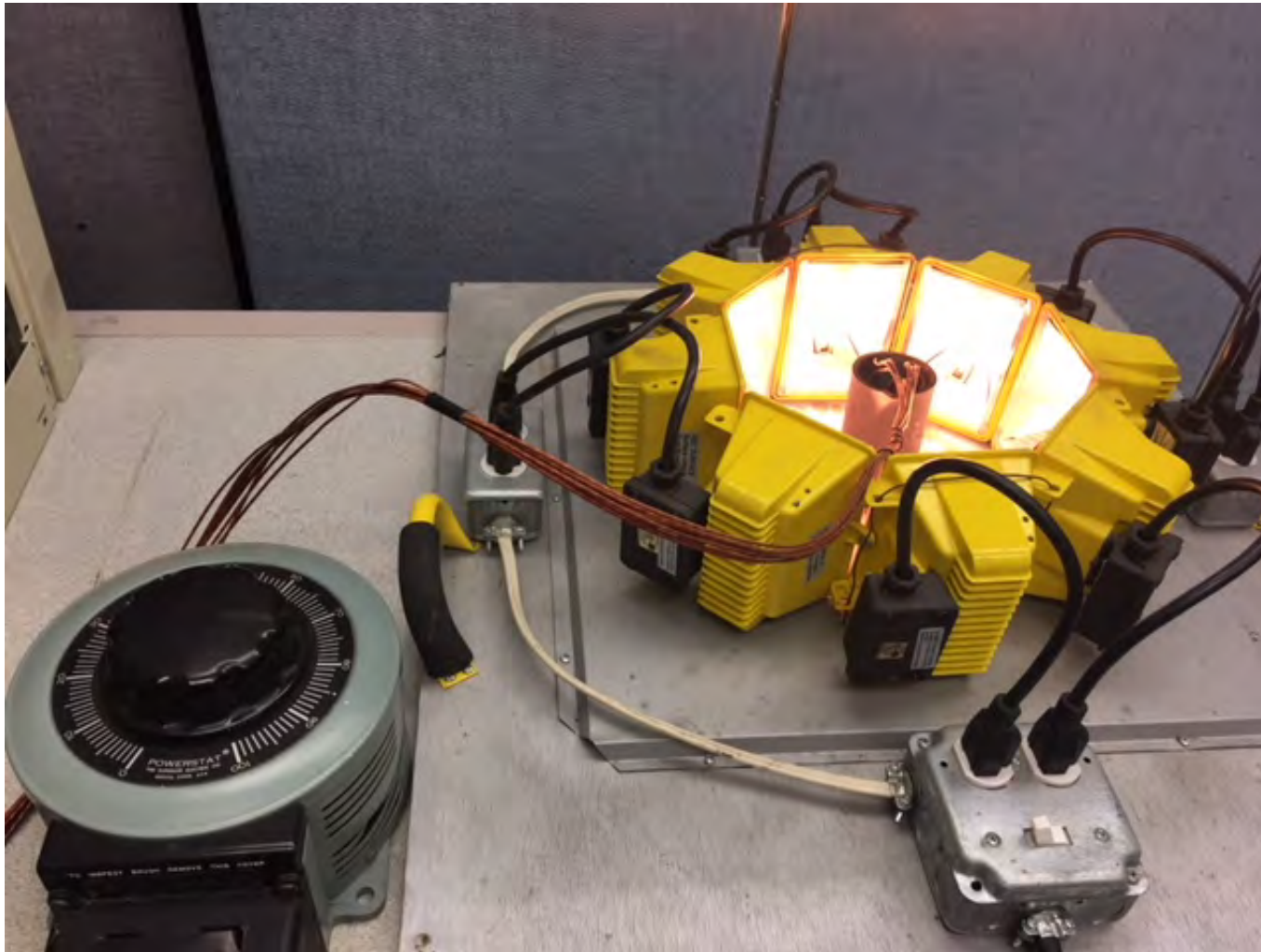
Differential Flame Thermometer



Heat Flux Calibration with a Low-Emissivity Thermopile Calorimeter



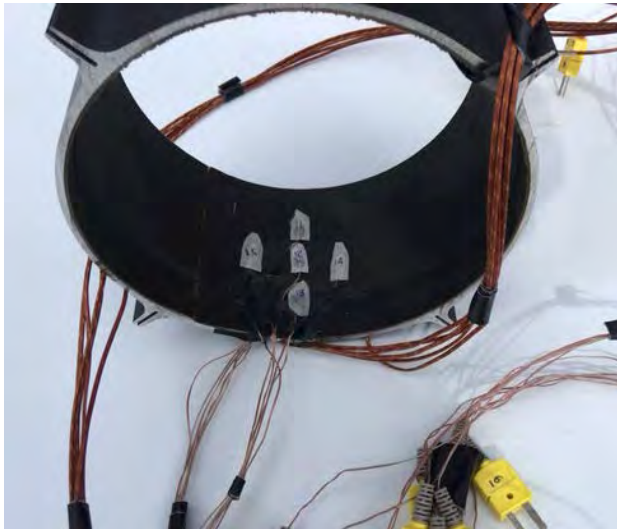
Variable Transformer Allows Adjustment of Heat Flux



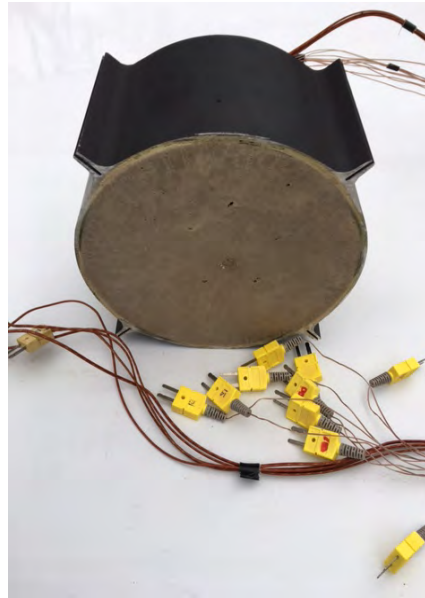
Magazine Safety Test



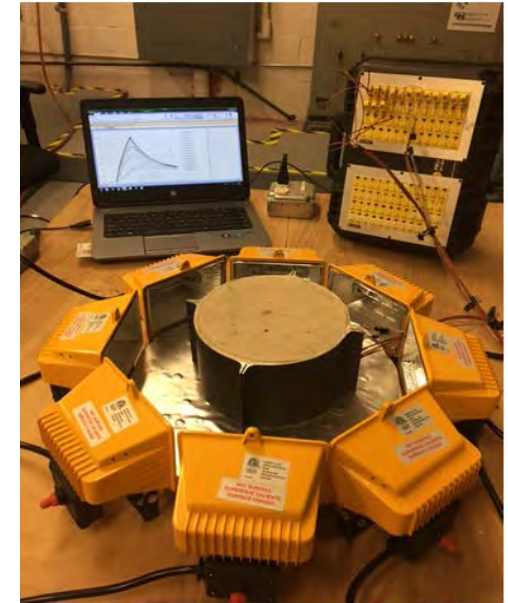
Empty Rocket Motor Casing



Motor Case Filled with Inert Propellant

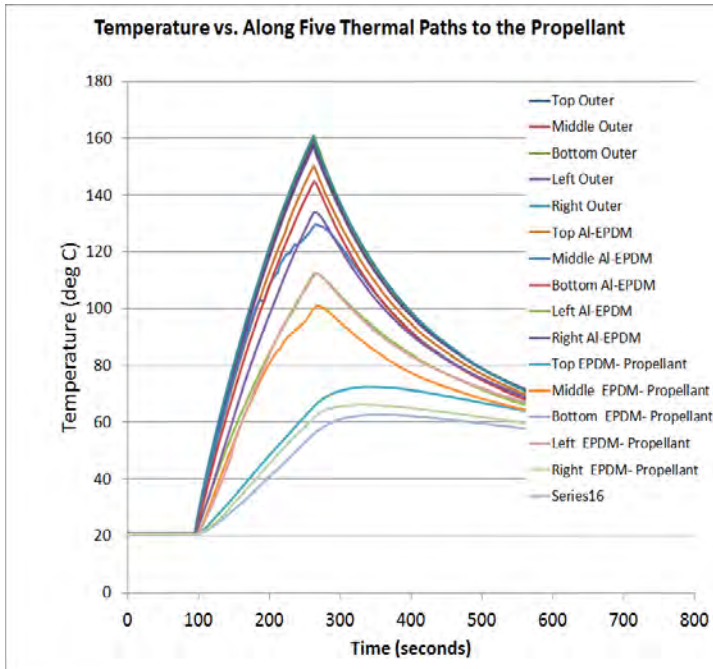


Full Setup with Instrumentation

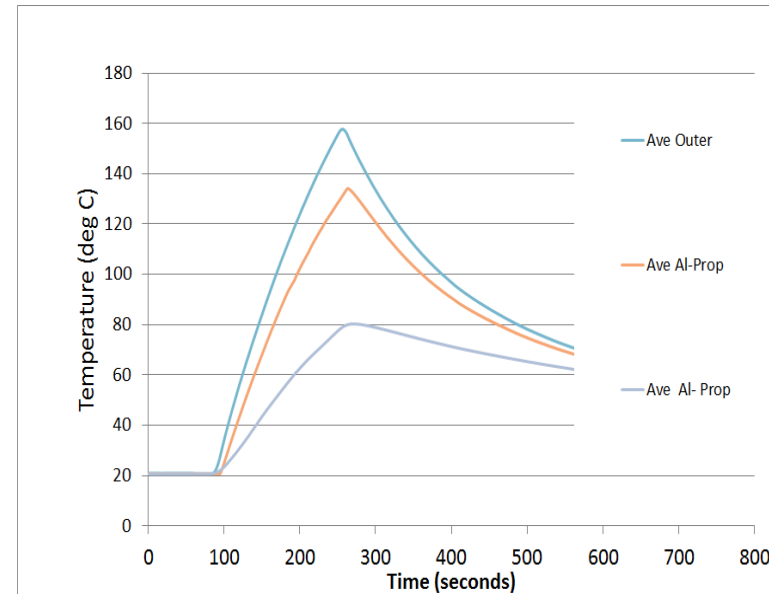


- Section of a real test motor
- Inert propellant simulant
- TCs along five thermal paths to propellant
- TCs on outer casing, between case and insulation, between the insulation and the propellant

Temperature Versus Time for All Fifteen (15) Thermocouples



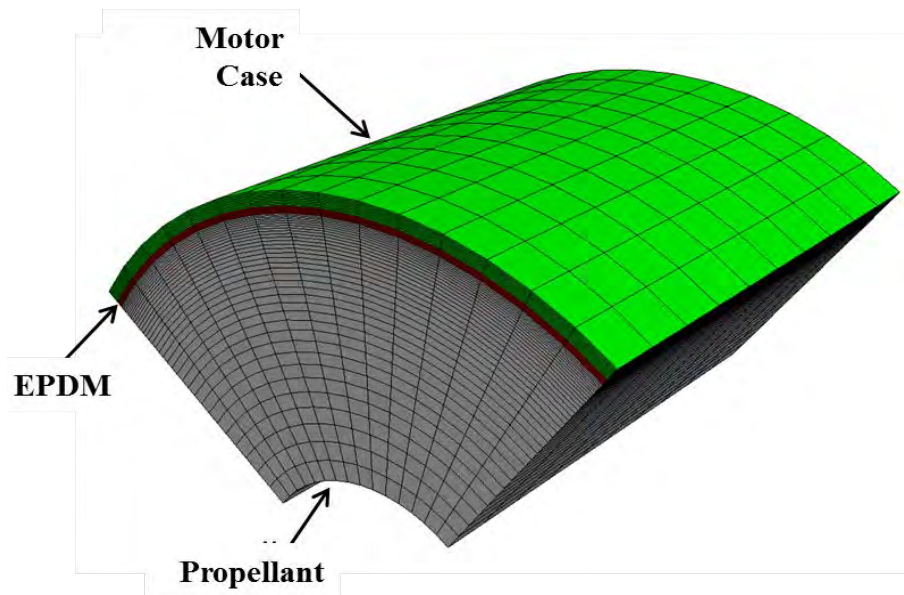
Average Temperature Versus Time at Three Stations



- Data recorded at fifteen (15) thermocouples
- Motor was heated for approximately 160 seconds
- Solved inverse heat transfer problem to determine material thermal properties

- Finite volume model of the rocket motor
- Heat transfer problem was solved using Aria
- Constant heat flux applied to outer surface to mimic radiant heat flux from chamber
- Convection was assumed negligible compared to radiation
- Initial material thermal properties assumed from similar materials
- Optimization method used to iteratively improve values for material properties

Rocket Motor Finite Volume Model



Iterative Improvement of Material Property Values

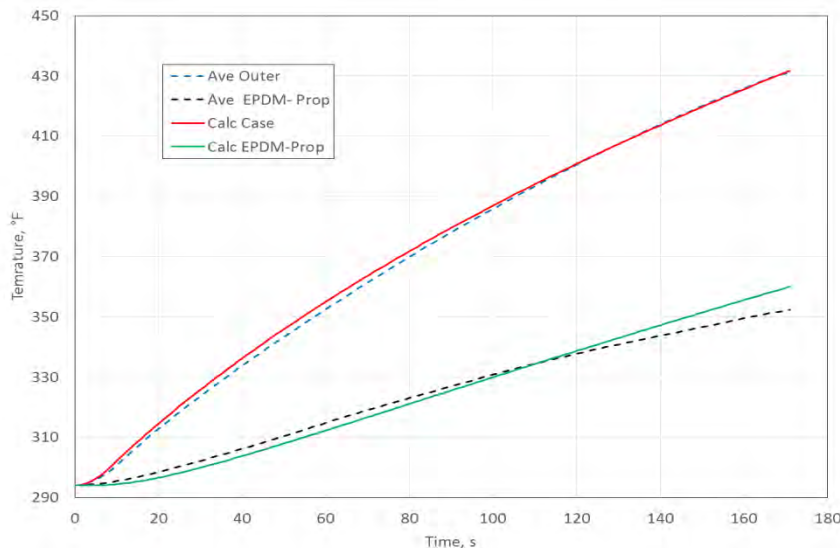
	Variable	Units	Case 1	Case 2	Case 3	...	Case 8
Motor Case	ρ	kg/m ³	2770	2500	2191.8		2191.8
	k	W/m ² K	130	130	130		130
	c_p	J/kgK	1047	1047	1047		1047
Insulation	ρ	kg/m ³	1000	1000	1000		900
	k	W/m ² K	0.13	.013	0.13		0.13
	c_p	J/kgK	2010	2010	2010		1700
Propellant	ρ	kg/m ³	1500	1500	1500		1786
	k	W/m ² K	0.16	0.16	.016		0.16
	c_p	J/kgK	4190	4190	4190		4190
L²-norm			183.4	119.0	48.33		39.64

- Modified Newton method used for optimizing material properties
 - L2 norm of temperature versus time curves
 - $$L^2 = \sqrt{\sum_{i=1}^n (\hat{T}_i - T_i)^2}$$
- \hat{T} is the test data at each i time, T is the modeled temperature at time i
- Newton method provided predictions for property values from case to case

Optimized Material Properties

- Final results show good agreement between calculated and measured temperatures
- Provides confidence that material properties are correct
- Data from radiant chamber instrumental in development of these values

Calculated and Measured Temperature Data
Using Optimized Material Properties



Final Calibrated Material Properties

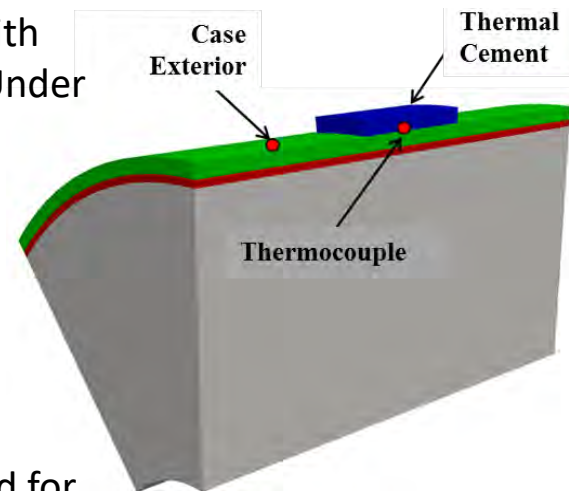
Property	ρ	k	c_p
Units	kg/m ³	W/m ² K	J/kgK
Motor Case	2192	130	1047
EPDM	900	0.13	1700
Propellant	1786	0.16	4190



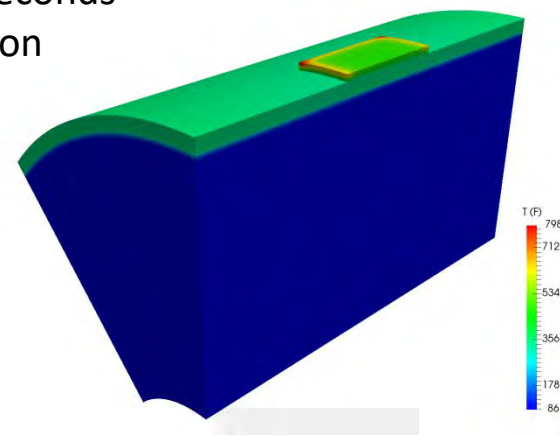
Rocket Motor Restrained Firing Model

- During RF test, TCs were covered with thermal cement with known properties
- Cement included in model with other three layers
- Thermal properties of other materials determined using radiant chamber data
- Thickness of cement was estimated, and multiple cases were run to determine sensitivity of results to cement thickness

Finite Volume Model of Rocket Motor with Thermocouple Under Cement



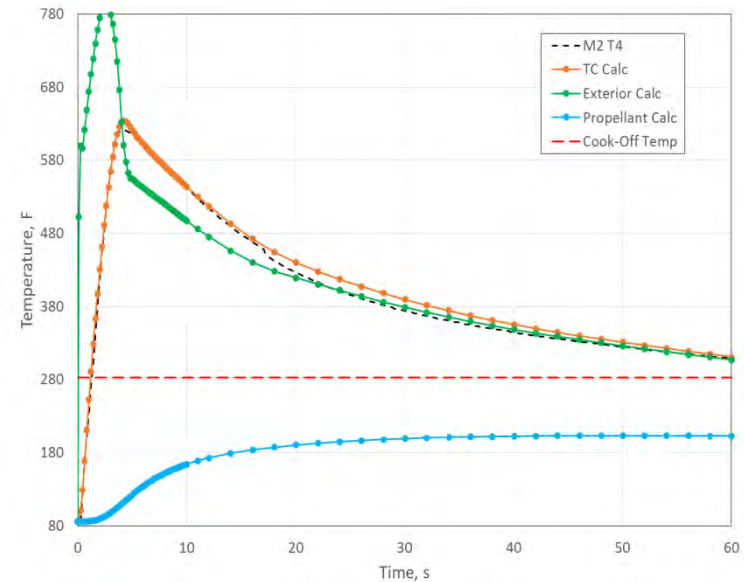
Cut-Away View of Temperature Predicted for One Case at 3.1 Seconds After Motor Ignition



Check for Rocket Motor FCO

- Finite volume model of rocket motor created to duplicate the previous restrained firing test
- Calibrated material properties used in model
- Temperatures measured on rocket motor case used to determine time-varying heat flux from restrained firing
- SCO temperature data used to estimate propellant cook-off temperature
- Plot indicates
 - Good agreement between calculated and measured TC temperature
 - Propellant temperature remains well below cook-off temperature

Temperature versus Time for RF
Thermocouple Location and Propellant



- M2T4 is measured data from TC mounted on the rocket motor case
- TC Calc is the calculated temperature of the TC
- Propellant case is the calculated temperature of the motor case
- Propellant Calc is the peak temperature of the modeled propellant
- Cook-Off Temp is the cook-off temperature of the propellant derived from SCO data

Summary and Conclusions

- Radiant chambers have been built to simulate the radiant heating in fast cook-off fires
- The radiant chambers show good axial and circumferential uniformity in temperature
- The chambers provide a broad range of heat fluxes which easily span the range of heat flux into propellant in enclosed systems (20–25 kW/m²)
- The heat flux is in the range for developing enclosed systems to qualify under STANAG 4240
- The chambers have been used for testing instruments and test items prior to exposure to fires
- The chambers have been used to solve complex problems in fast cook-off and Navy launcher safety testing

Backup



Introduction

Two radiant chambers have been built and tested. They provide a uniform radiation field for testing small items. They have been calibrated with thermocouple rakes and cylindrical steel calorimeters. The radiation fields are unexpectedly uniform and have axial and circumferential uniformity. The chambers use eight 250-Watt cylindrical halogen bulbs. The bulbs are enclosed in inexpensive work light housings readily available at home centers. A variac has been used to control the heat flux. Since fast cook heating of test items is 90% radiative, the chambers provide good tests for many items.

The chambers have been used to test instruments before putting them in large fuel fires. They have also been used to obtain highly controlled laboratory data for development of computer simulations, explaining experimental data from equipment being tested during development, and converging computer simulations when there was uncertainty in material property data.

Calibration data are presented along with results from testing a 7-inch (180 mm) rocket motor chamber with insulation and simulated propellant. Temperature versus time data was recorded by fifteen (15) thermocouples to measure the heat flow along each of five thermal paths from the outer surface of the motor, through the insulation, and into the propellant. The data were used to resolve problems caused by uncertainty in property data for the motor chamber and insulation in a finite element model used to analyze a restrained firing of a missile in a shipboard launcher.

Introduction, continued

The chambers have been used to test instruments before putting them in large fuel fires. They have also been used to obtain highly controlled laboratory data for development of computer simulations, explaining experimental data from equipment being tested during development, and converging computer simulations when there was uncertainty in material property data.

Calibration data are presented along with results from testing a 7-inch (180 mm) rocket motor chamber with insulation and simulated propellant. Temperature versus time data was recorded by fifteen (15) thermocouples to measure the heat flow along each of five thermal paths from the outer surface of the motor, through the insulation, and into the propellant. The data were used to resolve problems caused by uncertainty in property data for the motor chamber and insulation in a finite element model used to analyze a restrained firing of a missile in a shipboard launcher.

Insensitive Minimum Smoke Propellants for Tactical Missiles

Thomas Deschner¹, Eirik A. Løkke¹,
Tor E. Kristensen², Tomas L. Jensen², Erik Unneberg²

1. *Aerospace Propulsion, Nammo Raufoss AS,
P.O. Box 162, NO-2831 Raufoss, Norway*
2. *Land Systems Division, Norwegian Defence Research Establishment (FFI),
P.O. Box 25, NO-2027 Kjeller, Norway*

thomas.deschner@nammo.com

Abstract

Modern weapon systems have a high demand for insensitive minimum smoke propellants that are not inflicted by REACH regulations. In that respect, the development of new minimum smoke propellants has to be pushed towards less hazardous and less sensitive energetic fillers and plasticizers. Additionally, its successful implementation is also dependent on replacing existing hazardous ballistic modifiers based on lead and copper compositions while maintaining the good ballistic and mechanical properties at the same time.

In this work, FFI and NAMMO are presenting the extension of their family of GAP-nitramine-NENA propellants with different insensitive energetic fillers like FOX-7 or AN. In these formulations, the nitramine was partly or completely substituted by FOX-7 or AN.

The results are compared to previously tested minimum smoke propellants with special emphasis on the developed specific GAP-RDX-Bu-NENA propellant for the LMM boost motor.

Even though seen as a promising candidate as well due to preliminary results with good prospects, the tested FOX-7 formulations unfortunately only show similar shock sensitivity performance as pure nitramine based GAP-Bu-NENA propellants. Strain and strength of the propellant is reduced compared to pure GAP/nitramine propellant while the modulus is increased. However, tensile testing at -40°C indicate a better low temperature behavior of the GAP/FOX-7 propellant compared to pure GAP/nitramine propellant. Burn rates are reduced and pressure exponents increased by incorporation of FOX-7.

Propellants containing AN show the best mechanical properties, also the best low temperature behavior, of all tested formulations. However, on the downside, the burn rate dropped dramatically for the pure GAP/AN propellant compared to a GAP/nitramine propellant. Shock sensitivity is reduced by incorporation of AN in the propellant.

Introduction

In Norway, the systematical investigation of minimum smoke rocket propellants based on glycidyl azide polymer (GAP) and energetic fillers such as cyclotrimethylenetrinitramine (RDX), cyclotetramethylenetetranitramine (HMX), hydrazinium nitroformate (HNF) and hexanitrohexaazaisowurtzitane (CL-20) was initiated in the early 1990s, as a close collaboration between Norwegian Defence Research Establishment (FFI) and Nammo Raufoss AS (NAMMO). Although promising in many respects, issues associated with sensitivity, stability, mechanical characteristics and production costs hindered industrial scale-up of such formulations based on these compounds.

Since 2011, FFI and NAMMO have made renewed and intensified efforts to develop a family of minimum smoke composite propellants based on reduced sensitivity nitramines (RS-RDX and RS-HMX), GAP binder and low sensitivity nitroethylnitramine (NENA) energetic plasticizers. The development effort has been reported by Kristensen *et. al.* [1].

In 2013, NAMMO was awarded a contract for the development and qualification of the propulsion section of the Lightweight Multirole Missile (LMM). LMM is developed by Thales Land & Air Systems as a precision lightweight weapon for light platforms to counter the modern and emerging threats of land, sea and air targets. Results from the LMM propellant qualification effort were shared on the 2016 IM & EM Technology Symposium [2,3].

1,1-diamino-2,2-dinitrotoluene (FOX-7 or DADNE) is a promising candidate due to an explosive performance similar to RDX. Additionally, it is inherently less sensitive than RDX and HMX which allows for a safer handling of the material. On the downside, the current price of FOX-7 is high and the availability of ground material has been limited. This is mainly caused by the absence of demand as HTPB/AP-based rocket propellants are still the workhorse for the rocket industry.

Ammonium nitrate (AN) on the other hand is cheap and like FOX-7 less sensitive than nitramines, but possesses on the downside lower energy content and a lower explosive performance than RDX or HMX.

Composition and thermochemical performance

The propellant compositions and calculated thermochemical performance are shown in Table 1. All formulations contained 65% energetic solids. As its performance is comparable to double-base (DB) propellants, the GAP propellants presented here are free from certain undesirable DB compounds, such as sensitive nitrate ester plasticizers and burn rate modifiers based on lead and copper. The propellants exhaust signature has been classified as AA according to STANAG 6016, which is a minimum smoke signature classification. The main combustion products are CO, CO₂, N₂ and H₂O.

Table 1: Composition and thermochemical performance of the investigated GAP propellants. The thermochemical performance has been calculated using standard software (described in NASA RP-1311 part I and II), applying standard conditions (chamber pressure = 6.9 MPa, equilibrium expansion to 1 atm = 0.101 MPa).

Propellant	GAP/HMX	GAP/RDX	GAP/RDX/ AN	GAP/AN	GAP/FOX-7
Composition					
RS HMX, 50-60 micron and RS HMX, ground	65	-	25	-	-
RS RDX kl. 8 and RS RDX, ground	-	65	-	-	-
AN and AN, ground	-	-	20	65	-
FOX-7, class 2, FOX-7, class 3 and FOX-7, ground	-	-	-	-	65
GAP, di- and polyfunctional isocyanates, Bu-NENA, stabilizers, burn rate modifiers and additives	35	35	35	35	35
Calculated thermochemical performance					
Characteristic velocity, c^* [m/s]	2234	2243	2213	2148	1290
Theoretical specific impulse, I_{sp} [Ns/kg]	1430	1437	1414	1365	2061

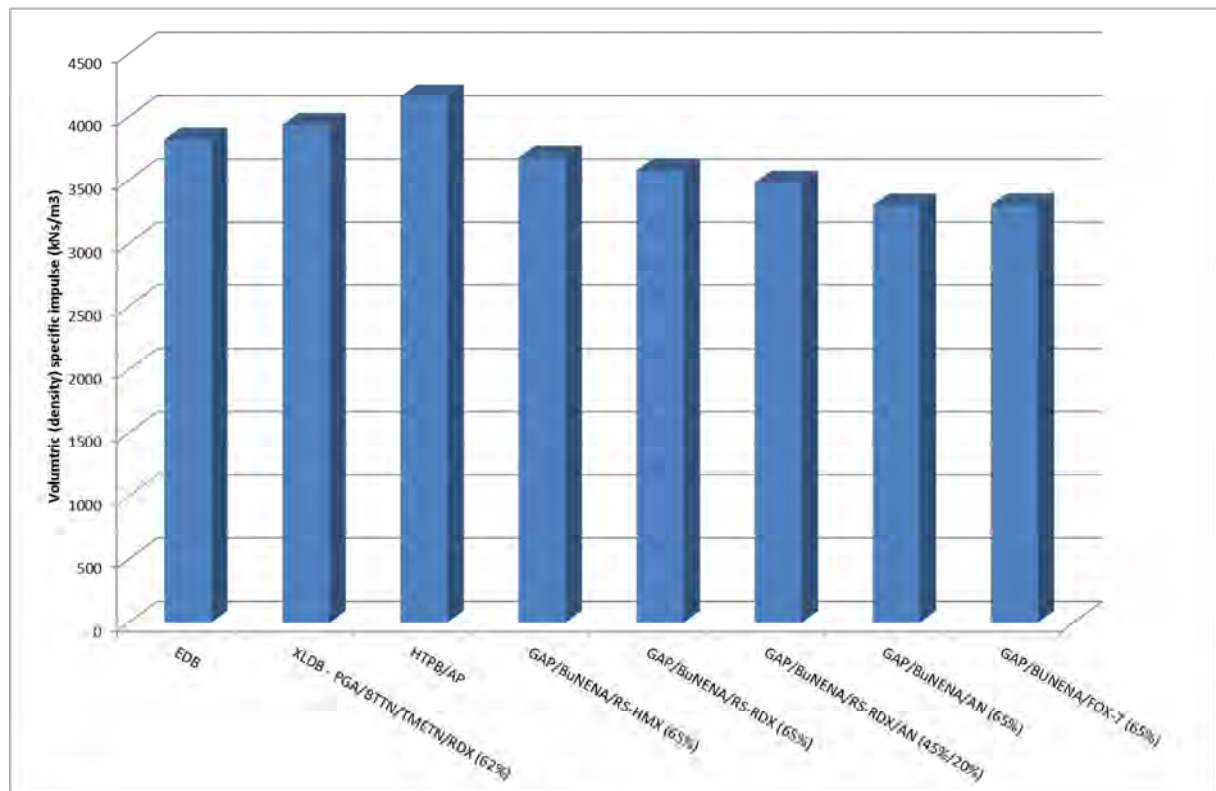


Figure 1: Volumetric specific impulse of investigated GAP propellants. The thermochemical performance has been calculated using standard software (described in NASA RP-1311 part I and II), applying standard conditions (chamber pressure = 6.9 MPa, equilibrium expansion to 1 atm = 0.101 MPa).

The use of conveniently handled Bu-NENA energetic plasticizer is a trade-off between sensitivity and performance. The reduction in sensitivity of the propellants is also favored by incorporation of reduced sensitivity (RS) nitramines. Both materials are delivered by Chemring Nobel AS, Norway, and are manufactured at their plant in Saetre, just south of Oslo. GAP and FOX-7 are delivered by the European Energetics Corporation (Eurenc), and the first is manufactured at their Sorgues plant in Southern France and the second is manufactured at their Karlskoga plant in Sweden. AN used in the formulations were two types, the coarse quality was spray crystallised AN manufactured by ICT Karlsruhe in Germany and the fine quality was from grinding of crystalline grade AN from Yara Rostock in Germany.

It is vital to balance the processing properties during mixing and casting operations with the optimization of mechanical and ballistic properties. This is achieved by adjusting the formulation with respect to the binder/curatives, bonding agent system, burn rate modifier system, and the type and particle size distribution of the energetic fillers.

FFI has developed a number of neutral polymeric bonding agents (NPBAs), each tailor-made for its certain application in GAP-nitramine propellants [2,4]. Mixed isocyanate curatives have been used to adjust crosslinking and to tailor chain extension.

FFI and NAMMO have developed a lead-free burn rate modifier system that is compliant with existing and upcoming environmental regulations (REACH). The system provides adequate ballistic properties, while it at the same time opens up for industrial scale propellant processing through the attainment of a sufficient pot life.

FOX-7 characteristics

FOX-7 is a high explosive with similar performance as RDX. At the same time, FOX-7 exhibits a significantly lower sensitivity towards shock friction and heat than RDX. As well, FOX-7 is stable towards hydrolysis and can therefore tolerate humidity. According to data published by Eurenc Bofors and FOI, FOX-7 has excellent compatibility with most materials used in energetic compositions. Prior to application, compatibility towards all propellant ingredients was tested and no incompatibility was found. FOX-7 is desensitized in water and has to be dried prior to use. Table 2 summarizes some of the available data on FOX-7.

Table 2: FOX-7 characteristics based on published data from Eurenco Bofors and FOI.

Property	Unit	Value
Density	[g/cm ³]	1,885
Detonation velocity	[m/s]	8870
Heat of formation	[kcal/mole]	-32
Activation energy	[kcal/mole]	58
Vacuum stability at 120°C	[ml/g]	0.1-0.4
Koenen Test, according to UN	[mm]	6, type F reaction
Measured detonation pressure	[GPa]	34
Calculated detonation pressure (Cheetah)	[GPa]	36.6
Friction sensitivity, typical	[N]	< 350
Impact sensitivity, typical	[J]	20-40
ESD	[J]	> 8

The particle sizes that are commercially available for FOX-7 are given in Table 3 and are compared to the particle sizes of the other energetic fillers used in this study.

Table 3 Commercially available particle sizes of FOX-7 and comparison to the particle sizes for the other energetic fillers used in this study. Particle size analysis was conducted by a MALVERN 2000 particle size analyzer.

Material	Typical particle size, d ₅₀ [microns]	Particle size, d ₅₀ used [microns]
FOX-7, class 1	20-40	38
FOX-7, class 2	50-100	87
FOX-7, class 3	100-200	120
FOX-7, class 4	200-350	-
FOX-7, ground	~10	10-13
RS-HMX, 50-60 micron, Grade B	50-60	44
RS-HMX, ground, Grade B	9-15	9
RS-RDX, class 8	40-60	49-55
RS-RDX, ground	5-8	6-9
AN	160	158
AN, ground	10-20	16

The friction and impact sensitivity of the energetic fillers used in this study is shown in Table 4. As can be seen, FOX-7 class 1, class 2 or class 3 are more insensitive than the BAM apparatus is able to measure. However, FOX-7 ground to 10 microns has a similar sensitivity as RS-RDX class 8.

Table 4: Friction and impact sensitivity of the energetic fillers used in this study. All values are determined in BAM equipment according to UN Test 3 (a)(ii) for friction sensitivity and UN Test 3 (b)(i) for impact sensitivity.

Material	Impact sensitivity, BAM Fallhammer [J]	Friction sensitivity, BAM [N]
FOX-7, class 1	> 49	> 353
FOX-7, class 2	> 49	353
FOX-7, class 3	> 49	> 353
FOX-7, ground	15	141
RS-HMX, 50-60 micron	N/D	N/D
RS-HMX, ground	N/D	N/D
RS-RDX, class 8	11	126
RS-RDX, ground	4,5	94
AN	N/D	N/D
AN, ground	47	283

Processing characteristics

The GAP propellants have been prepared in a 5-gallon (10 kg) Baker-Perkins twin-bladed planetary vertical mixer. All propellants have good flow through all mixing cycles, and exhibits a creamy behaviour at the end-of mix and during casting. The viscosity is around 150 – 200 Pa·s at end-of-mix (at 35°C), with lowest value for the propellants containing RS-HMX or FOX-7 and the highest value for the propellant containing RS-RDX. The propellants have an acceptable pot life of 10 hours at 35°C and the cure time is 168 hours at 60°C.

Mechanical properties

The mechanical properties of the investigated GAP propellants are shown in Table 5. Except for the GAP/AN propellant, the strength is rather low but still acceptable for small rocket motors. The GAP/FOX-7 propellant displays a high elastic modulus and low elongation properties at room temperature. GAP propellants containing AN as a minor or main oxidizer exhibit a lower degree of de-wetting and better low temperature properties than nitramine or FOX-7 based GAP propellants. As well, they show the highest strength at room temperature. This is due to the fact that a traditional bonding agent known from HTPB/AP propellants can be used for the GAP/(RDX)/AN propellant, while neutral polymeric based bonding agents (NPBA) are used in case of the GAP/nitramine and GAP/FOX-7 propellants.

Table 5: Mechanical and physical properties of the GAP propellants. Uniaxial testing of the propellant was performed according to STANAG 4506, using a crosshead speed of 50 mm/min. All values are reported as the mean value calculated from testing of five propellant specimens from the same batch. Engineering values are presented. DMA and TMA have been performed according to STANAG 4540 and 4525 respectively.

Propellant	GAP/HMX	GAP/RDX	GAP/RDX/AN	GAP/AN	GAP/FOX-7
Composition	65% RS-HMX	65% RS-RDX	45% RS-RDX 20% AN	65% AN	65% FOX-7
Mechanical properties at +21°C					
Max / break stress [MPa]	0.6 / 0.5	0.4 / 0.4	0.4 / 0.4	0.8 / 0.8	0.6 / 0.6
Strain at max / break	25 / 28	26 / 43	33 / 44	24 / 25	11 / 13
Elastic modulus [MPa]	3.1	2.9	3.2	5.6	9.0
Mechanical properties at -40°C					
Max / break stress [MPa]	2.6 / 1.8	2.3 / 1.6	2.0 / 1.9	2.9 / 2.8	2.2 / 1.8
Strain at max / break	40 / 91	27 / 80	20 / 27	57 / 62	25 / 65
Elastic modulus [MPa]	14.7	29.5	24.2	15.8	37.2
Physical properties					
Density [kg/m ³]	1646	1597	1573	1535	1601
Glass transition temperature by DMA, T _g [°C]	-52	-50	-51	N/D	N/D
Coefficient of thermal expansion, CTE [$1 \cdot 10^{-4}$ m/mK]	1.4	1.3	1.4	N/D	N/D

Burn rate characteristics

Table 6 summarizes the burn rate characteristics of the different GAP propellants at 21°C as evaluated through static firing of 2x4-inch test motors. Propellants with RS-RDX and RS-HMX show similar properties and burn rates of around 11 mm/s at 10 MPa are achieved together with pressure exponents of around 0.5. However, if the nitramine is partly or fully replaced by an insensitive energetic filler like AN or FOX-7, burn rates are greatly reduced and pressure exponents are significantly increased to values above 0.6. A propellant containing 65% AN only shows a burn rate of around 6 mm/s at 10 MPa while a propellant with 65% FOX-7 exhibits a burn rate of around 9 mm/s at 10 MPa. However, replacing only 20% of the nitramine with AN results in only 17% drop in burn rate and only in a slightly higher pressure exponent.

Table 6: Reference burn rates and pressure indices of the GAP propellants calculated from firing data of 2x4-inch test motors, using Vieille's burn rate law and least square method. Data recorded at +21°C.

Propellant	GAP/HMX	GAP/RDX	GAP/RDX/AN	GAP/AN	GAP/FOX-7
Composition	65% RS-HMX	65% RS-RDX	45% RS-RDX 20% AN	65% AN	65% FOX-7
Ballistic properties at +21°C					
Burn rate at 6.9 MPa [mm/s]	8.8	9.1	7.5	4.8	6.7
Burn rate at 10 MPa [mm/s]	10.7	10.8	9.2	6.1	8.8
Burn rate at 15 MPa [mm/s]	13.1	13.2	11.5	7.9	11.9
Pressure exponent (~ 5-15 MPa)	0.52	0.48	0.55	0.66	0.74

Safety characteristics

The safety characteristics of the investigated GAP propellants are shown in Table 7. Compared to traditional DB propellants and composite propellants based on inert binders, the GAP propellants demonstrate lower impact and friction sensitivities. It is expected that the sensitivity is lowest for the GAP propellant containing AN as the solid filler, but the impact sensitivity is quite similar for all propellants regardless of type of solid filler. The GAP propellant with FOX-7 has somewhat lower friction sensitivity than the propellants containing nitramines, which is expected based on the lower sensitivity of the coarse FOX-7 compared to both RS-HMX and RS-RDX. The temperatures for the peak maximum exotherms denote the decomposition of the respective solid fillers.

Table 7: Safety characteristics for GAP propellants.

Propellant	GAP/HMX	GAP/RDX	GAP/RDX/AN	GAP/AN	GAP/FOX-7
Composition	65% RS-HMX	65% RS-RDX	45% RS-RDX 20% AN	65% AN	65% FOX-7
Impact energy ^(a) [J]	20 J	19 J	22 J	23 J	18 J
Friction load ^(b) [N]	192 N	184 N	192 N	342 N	240 N
Initial onset exotherm ^(c) [°C]	200	191	163 / 187	N/D	224
Peak maximum exotherm ^(c) [°C]	221	218	180 / 208	N/D	248

(a) UN test 3(a)(ii), BAM lowest impact energy;

(b) UN test 3(b)(i), BAM lowest friction load

(c) STANAG 4515(B2), differential scanning calorimetry (DSC), heating rate 2 °C/min

The shock sensitivity of the GAP propellants have been evaluated by the intermediate-scale gap test according to STANAG 4488, annex B. Figure 2 depicts the detonation threshold pressure. Although initial small-scale gap test (21mm diameter water gap test) showed good

prospects with reduced shock sensitivity with increasing content of FOX-7 as reported by Kristensen et.al. [5], the tested GAP propellant with FOX-7 unfortunately show similar shock sensitivity as pure nitramine based GAP propellants. The shock sensitivity is reduced by incorporation of AN in the propellant. The results indicate that the GAP propellants can propagate a detonation, but compared to data reported by others [6,7] the GAP propellants are at least as insensitive to SDT as Azamite[®] and Azalane[®] propellants and good insensitive explosives such as I-PBXN-109. The results also demonstrate that the GAP propellants can withstand a somewhat higher shock initiation pressure compared to traditional NEPE propellants plasticized with nitroglycerin.

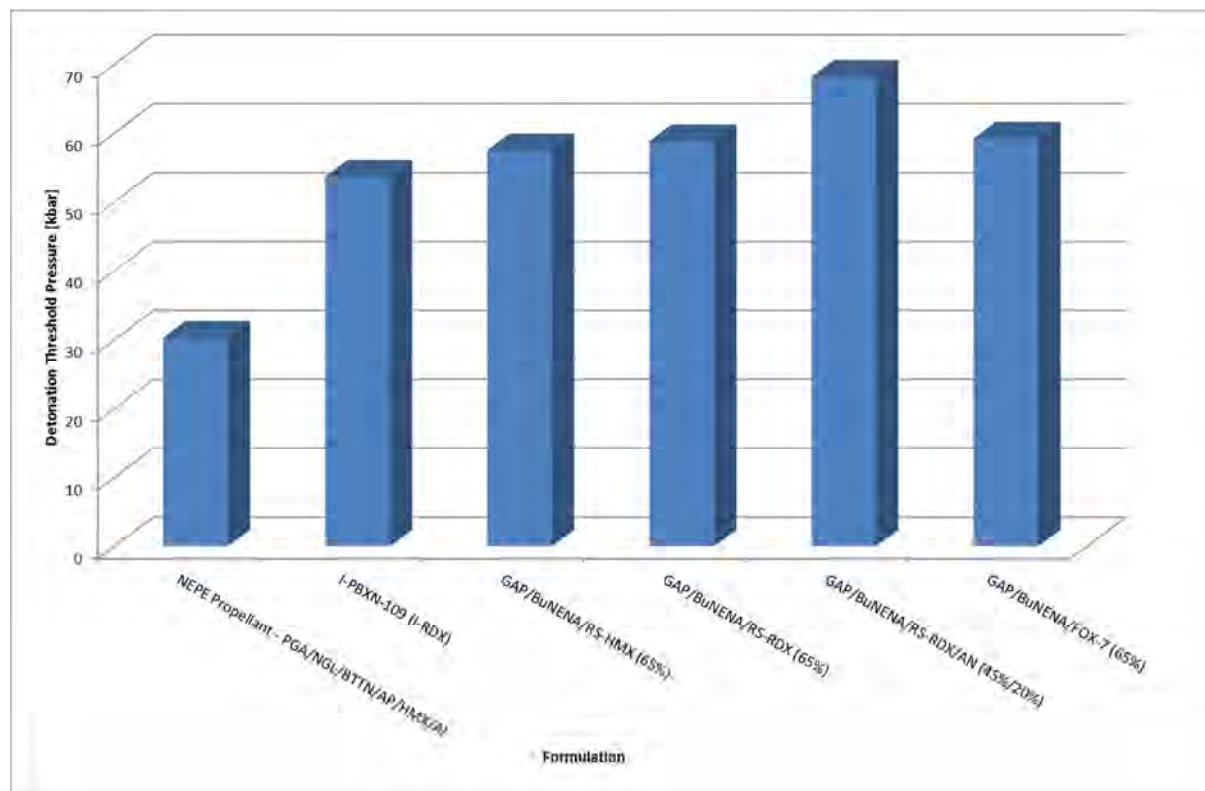


Figure 2: Intermediate scale gap test according to STANAG 4488, annex B. The detonation threshold pressure value is calculated from the acetate card barrier thickness giving the 50% point for GO/NO GO reactions. Twelve trial shots in accordance with the standard Bruceton statistical approach are performed. The diameter of the acceptor charge (test sample) is 40mm and the length is 200mm. The explosive charge used as donor and witness charges, is 95% RDX / 4.5% Wax / 0.5% Graphite and the detonator contains 0.6 g of PETN as the base charge. The reference values for a standard NEPE propellant and I-PBXN-109 are from Nguyen et. al. [7].

Conclusions

FFI and NAMMO have studied sensitivity, and ballistic and mechanical properties of GAP propellants containing 65% energetic fillers. The difference in properties between propellants containing either RS-RDX or RS-HMX is only marginal. Shock sensitivities according to the intermediate scale gap test can only be reduced by incorporation of Ammonium nitrate. GAP/FOX-7 propellants exhibit similar shock sensitivities as GAP propellants containing reduced sensitivity nitramines. Impact and friction sensitivity of either AN or FOX-7 based GAP propellants are in the lower region compared to nitramine based GAP propellants. Both insensitive fillers FOX-7 and AN dilute the energy content of the propellant and reduce burn

rates significantly. The use of only AN or FOX-7 as energetic filler indicates a too low energy content for propellant purposes. Due to the usage of traditional bonding agents, GAP propellants containing AN as a minor or main oxidizer exhibit a lower degree of de-wetting and show better low temperature properties than nitramine or FOX-7 based GAP propellants.

Acknowledgements

FFI and NAMMO are grateful for the continuous financial support provided by the Norwegian Ministry of Defence for the fundamental missile propulsion technology. Acknowledgement goes to Eurenco Bofors for supplying FOX-7 and expertise. Chemring Nobel AS is acknowledged for supportive expertise and expedited development of tailored nitramine products.

References

1. T. E. Kristensen, T. L. Jensen, E. Unneberg, T. Deschner, E. A. Løkke, Development of Smokeless Nitramine Composite Rocket Propellants at FFI and NAMMO, *45th Int. Annual Conference of the ICT*, Karlsruhe, Germany, June 24 – 27, **2014**, p. 7/1-10.
2. E. A. Løkke, T. Deschner, T. E. Kristensen, T. L. Jensen, E. Unneberg, A New Generation of Minimum Smoke Propellants for Tactical Missile Propulsion, *Insensitive Munitions and Energetic Materials Technology Symposium*, Nashville, TN, USA, September 12 – 15, **2016**, Abstract # 18731.
3. S. Holden, C. Stennet, P. Cheese, Small Scale Fragment Attack Testing on the LMM Missile Boost Motor and the Influence of the Conduit Form on XDT Threshold, *Insensitive Munitions and Energetic Materials Technology Symposium*, Nashville, TN, USA, September 12 – 15, **2016**, p.1/1-10.
4. E. Landsem, F. K. Hansen, E. Unneberg, T. E. Kristensen, Neutral Polymeric Bonding Agents (NPBA) and Their Use in Smokeless Composite Rocket Propellants Based on HMX-GAP-BuNENA, *Propellants, Explos. Pyrotech.* **2012**, 37, 581-591.
5. T. L. Jensen, E. Unneberg, T. E. Kristensen, Smokeless GAP-RDX Composite Rocket Propellants Containing Diaminodinitroethylene (FOX-7), *Propellants, Explos. Pyrotech.* **2017**, 42, 381-585.
6. F. Morin, M. Golfier, C. Nguyen, New Solid Rocket Propellants for Tactical Missile Propulsion – Smokeless and Aluminized GAP-Based Propellants, *Technical Advances and Changes in Tactical Missile Propulsion for Air, Sea and Land Application, NATO RTO AVT-208 Symposium*, San Diego, CA, USA, April 16-20, **2012**, p. 1/1-14.
7. C. Nguyen, F. Morin, F. Hiernard, Y. Guengant, High Performance Aluminized GAP-based Propellants – IM Results, *Insensitive Munitions and Energetic Materials Technology Symposium*, Munich, Germany, October 11 – 14, **2010**.

2018 Insensitive Munitions & Energetic Materials Technology Symposium
Portland, OR

Fragment Impact Standardization Historical Review

Kathryn E. Hunt¹ and Ernest L. Baker²

- 1) OUSD/AT&L, Land Warfare and Munitions, Pentagon, Washington DC, USA
2) Munitions Safety Information Analysis Center (NATO), Brussels, Belgium

This report describes the results of a review of the history and development of NATO STANAG 4496 Fragment Impact Munitions Test Procedures related to the origin of the threat fragment characteristics and requirements that were first cited in the initial edition of STANAG 4496. The review was performed by completing a literature search of historical papers and documents surrounding the original development for the STANAG. The purpose of the fragment impact test is to assess the reaction, if any, of munitions and weapon systems to impact by a high velocity fragment. The review discusses the technical rationale behind the following aspects of the STANAG requirements: (1) Fragment shape, both a discussion of the effect of yaw at impact as well as a discussion of the merit of various designs and shape factors (2) Fragment size (3) Fragment velocity and (4) Multiple fragments. This study was used to inform the NATO AC/326 SG/B Fragment Impact Custodial Working Group (FI CWG).

INTRODUCTION

As part of the documentation for a revised edition of NATO STANAG 4496 Fragment Impact Munitions Test Procedure, it is important to recognize the basis for previous decisions on modifications of the standard. To that end, this paper covers some historical fragment impact (FI) information as well as the origin of the threat fragment characteristics and requirements that were first cited in the initial edition of STANAG 4496. Prior to the publication of the standard, a variety of different test methodologies existed for evaluating fragment impact.

Number, size, shape, velocity, and the method for projecting the fragment(s) have long been the dominate considerations when discussing fragment impact testing. The earliest fragment impact safety requirement appeared in NAVSEA Instruction 8010.5 in 1985. Multiple half-inch square mild steel cubes were required to be projected at the test item with 3-5 hits recorded and a striking velocity of 8300 fps. This was intended to simulate general purpose bomb fragments [1]. The most commonly used procedures in the 1980's and 90's relied on explosively projected the fragments. A mat of preformed fragments were placed on the front face of the explosive charge which was detonated. Neither number of fragment hits nor the fragment orientation were controlled, leading to inconsistent test results. Starting in the mid-1990s the test methods were improved to use gas guns to launch individual fragments to the target.

Table 1 gives an overview of various NATO nations FI test policy and procedure requirements that were in place in 2001 [2]. This represented the Nations' baseline for the evolution of STANAG 4496.

Table 1: Summary of Policy and Procedure Requirements prior to 2001

	NATO	France Light Fragment	France Heavy Fragment	UK	US Preferred	US Alt #1
Geometry	Conical Tipped cylinder	Cube (NATO fragment used)	Parallelepiped (sphere is used)	Cylinder Ø 12.7mm h=12.7mm	12.7 mm cube	Conical tipped cylinder
Mass, g	16	20 (16)	250	13.5	16	16
# of Fragments	1	3 (1)	1	1	2-5	1
Launcher Type	Undefined	Undefined (gun)	Smooth bore gun	RARDEN gun	Fragment Projector	Undefined (gun)
Velocity Range, m/s	2000	0<v<2000	0<v<1600	400<v<2500	2530 ± 90	1830 ± 60

REPRESENTATIVE THREAT FRAGMENTS

The archival data used to examine the generic threat fragment in STANAG 4496 are summarized in tables 2 and 3 below. The data in table 2, developed by Victor [3] in the 1980s, includes the characteristics of typical fragments projected from several classes of munitions. It is important to note that approximately 26% of all fragments are greater than the average fragment mass, and therefore basing a threat fragment on average fragment mass represents neither the worst case nor the most credible one. The second table shows fragment mass and velocity data for specific weapons were a “worst case” threat scenario [4].

Table 2. Computed Fragments Characteristics (Mott & Gurney)

Threat Weapon	Mass	Ø	Source Velocity		Nominal Range ⁽¹⁾		Avg. Frag. Mass ⁽²⁾	Frag. > 15g ⁽³⁾	Cube Velocity of cube at Nominal Range	
	kg	cm	ft/s	(m/s)	ft	(m)	g	%	ft/s	(m/s)
Grenade	1.46	7.6	3700	(1128)	31	(9.4)	2.3	1.4	3191	(973)
Missile	32.8	17	5000	(1524)	125	(38.1)	3.0	2.6	2763	(842)
Artillery/ Missile	41.8	17	3890	(1186)	80	(24.4)	10.4	21.5	3216	(980)
Missile	100.4	32	5939	(1810)	135	(41.1)	4.3	5.5	3125	(952)
Missile/ Artillery	118.2	32	4920	(1500)	100	(30.5)	14.0	15.1	3876	(1181)
Missile	365.5	50	5188	(1581)	111	(33.8)	29.9	29.7	4235	(1291)
Missile	1003.	75	5814	(1772)	140	(42.7)	38.0	47.6	4500	(1372)

⁽¹⁾ Range at which main fragment beam delivers 3 fragments per square foot

⁽²⁾ About 26% of fragments are larger than the average mass for each warhead

⁽³⁾ Comparable to Army IM test fragment or Navy IM test fragment (16g)

Table 3. Various Munition Worst Case Fragment Characteristics

Munition	Design fragment	
	Mass (g)	Velocity (m/s)
Mk81	12.76	2396
Mk82	18.43	2402
Mk117	38.61	2386
Mk83	52.16	2259
Mk84	63.79	2365
155mm M107	64.55	1030
8" M106	97.52	1152
105mm M1	13.13	1237

VELOCITY

During the time period in which the original fragment impact standard was written, the U.S. utilized the highest fragment velocity, 2530 m/s, which has now become the standard. This fragment velocity, as defined in MIL-STD-2105B and STANAG-4240, Draft 10, originated from a US Navy survey dated 1987 [5]. The velocity chosen for the ½-inch steel cube was 8300 ft/s (2530 m/s) because it represented the upper range of the threat fragment velocity spectrum for a general-purpose bomb. MSIAC (NIMIC at the time) also looked at various munitions fragment velocities and reached a similar conclusion that 2530 m/s is at the very upper bound of possible threat fragments [6]. It is also important to note that fragment velocities above 2000 m/s were not observed for ground munitions. Additional work by MSIAC and also work done by J. Starkenburg [7] indicates that fragment velocities for artillery type weapons may only be near 2530 m/s when detonated in a stack configuration as initial fragment velocities for stacks of ammunition have been observed to be almost twice as high as for fragments from single-item ammunition.

FRAGMENT GEOMETRY

Because several Nations used differently shaped threat fragments, agreement on the shape of the threat fragment was critical for the STANAG test procedure. The cube shape resembles a preformed fragment present in some munitions. The lighter sphere shape is used in characterizing explosive formulations. The conical type cylinder was created to allow easier launch from a fragment gun. Although the cube most closely represents fragmentation, its angle of attack is not repeatable with face, edge and corner impacts resulting in significantly different shock loadings. Conversely, the advantage of spherical fragments is repeatability, however the spherical fragments were not perceived as a credible threat. Spherical fragments also require either a higher initial velocity or greater mass for the same input of shock duration to the target. As seen in figure 1 [4], the sphere had to be five times more massive than the NATO/MIL-STD-2105B alternate 1 fragment at 10° yaw, in order to maintain a given shock threshold. This was deemed too high for practical testing or to be representative of anything but rogue fragments.

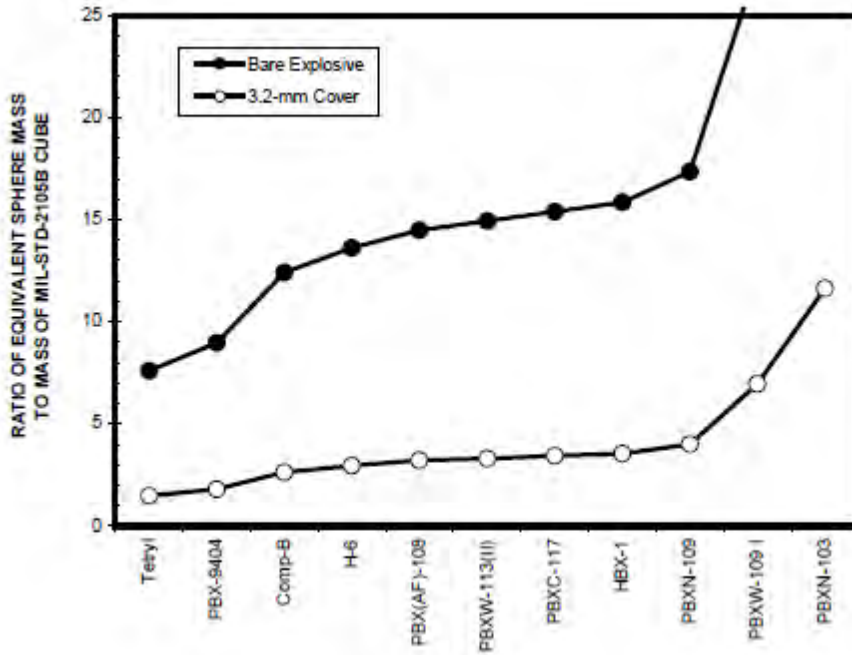


Figure 1. The ratio of sphere mass and the mass of a 10° yawed cube that have the same critical velocity for detonation using the Jacobs-Roslund formula

Returning to look at the cube, the primary disadvantage remained repeatability. An issue which can be mitigated by using a conical tipped cylinder with its 160° included angle face (10° to normal) [4,8]. A cylinder with these characteristics is considered comparable to the cube because approximately 95% of the time a randomly oriented cube will have an impact yaw of greater than 10° with the impact surface. J.Starkenbug created figure 2 which illustrates that a conical tipped cylinder (denoted in the figure as Army Frag) significantly reduces yaw effects as compared to the cube.

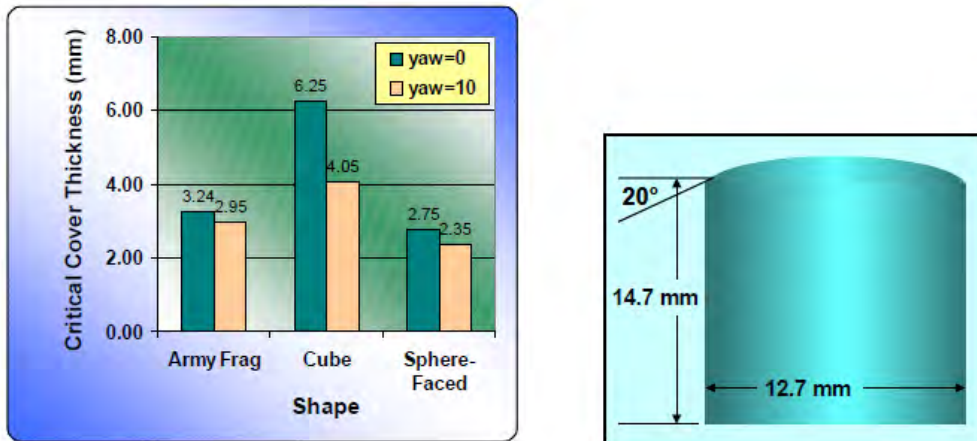


Figure 5. (

Figure 2. Critical cover thickness as computed by CTH for a Comp-B target impacted at 1830 m/s [8]

In the end, it was determined that the conical tipped cylinder provided the best compromise between fragment realism and repeatability. However, the original authors of this STANAG wanted to ensure that the chosen NATO threat fragment maintained the shock generated by a cubical fragment. Looking back at figure 2, the NATO/ MIL-STD-2105B alternate 1 detonates at a lower cover plate thickness and represents a lower shock level than the cube. Starkenburg completed

additional calculations proposing the current STANAG 4496 fragment shape and mass (18.6g) as equivalent to the shock stimulus of the cube.

MULTIPLE FRAGMENTS

In a threat scenario it is perhaps unrealistic to believe that a single fragment will be the only impact, therefore several legacy test procedures called for the impact of multiple fragments. However, for non-detonation reactions, the effect of multiple fragments is un-predictable, sometimes decreasing the reaction severity and sometimes increasing it, providing inconclusive results. This gives no advantage to testing with multiple fragment projections. Thus, there was no advantage to testing with multiple fragment projections. For SDT of damaged material, as in a rocket motor, it was decided at the time that the reaction severity of multiple depended on the degree of damage, the timing, and system conditions. It was felt that a multiple fragment impact test would not be repeatable enough to address these concerns, and that “multiple impacts at a single velocity do not represent reality” [4]. For SDT of neat material, it was shown that any effects of multiple fragment impact are unlikely since the fragments space out very rapidly and then slow rapidly with distance. Figure 3 below shows that the fragment spacing reaches 3 fragment diameters at less than 13-m distance for a representative munition, so the effect of multiple fragment impact on SDT can be neglected [4].

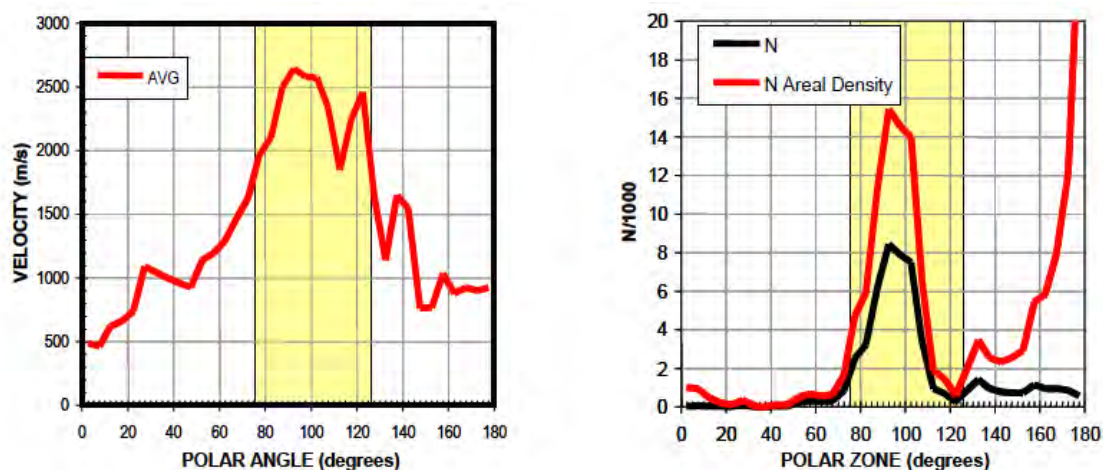


Figure 3. Velocity vs. polar zone (left) and number of fragments vs. polar zone (right) for a particular representative munition.

CONCLUSION

This report describes the results of a review of the history and development of NATO STANAG 4496 Fragment Impact Munitions Test Procedures related to the origin of the threat fragment characteristics and requirements that were first cited in the initial edition of STANAG 4496. In the end, it was determined that the conical tipped cylinder provided the best compromise between fragment realism and repeatability. However, the original authors of this STANAG wanted to ensure that the chosen NATO threat fragment maintained the shock generated by a cubical fragment. The current STANAG 4496 fragment shape, mass and velocity was chosen to provide an equivalent to the shock stimulus of a worst case fragment representative cube. This historical review was used to inform the NATO AC/326 SG/B Fragment Impact Custodial Working Group (FI CWG). The working group has used the review results as part of their process to update NATO STANAG 4496, the technical content of which will be migrated into a new AOP 4496. The historical review are being included in Annex A of the new AOP 4496.

ACKNOWLEDGEMENTS

The authors would like to acknowledge Dr. Pat Baker for providing much of the basis of this work as well as all of the original contributors to STANAG 4496. Ms. Hunt would also like to acknowledge Dr. Brian Fuchs for encouraging her to publish this paper.

REFERENCES

- [1] Beauregard, Raymond, "*History of the US Navy's IM Program*", 24 January 2005
- [2] Fisher, M., and Peugeot, F., "Fragment Impact Testing Requirements, Methods and Issues Part 1: Representativeness," 2001 Insensitive Munitions & Energetic Materials Technology Symposium.
- [3] Victor, A.C. "Useful Data and Methods Related to Insensitive Munitions Threat Hazard Assessments", Victor Technology, San Rafael, California, ADPA Insensitive Munitions Symposium (1996)
- [4] Baker, P. "Summary of JANNAF review of MIL-STD-2105B Fragment Impact Test Procedure", 2002.
- [5] Johnson, C.E., "Insensitive Munitions Fragment Impact – Assessment of Fragment Threats, Aug 87." Naval Sea Systems Command, 1987.
- [6] "Fragment Impact Testing: NIMIC's Review and Proposal." NIMIC L-86, April 2002. Michael Fisher and Frédéric Peugeot.
- [7] Starkenburg, J., Benjamin, K., Frey, R. "Predicting fragmentation Propagation Probabilities for Ammunition Stacks", Aug 1996.
- [8] Starkenburg, J., "Simulations of the Effects of Fragment Shape and Orientation on the Shock Initiation of Covered Composition B Targets," JANNAF Fragment Impact Workshop, 2001.
- [9] NATO, STANAG 4496, "Fragment Impact, Munitions Test Procedure" Edition 1, 13 December 2006.
- [10] MIL-STD-2105B, "Military Standard, Hazard Assessment Tests for Non-Nuclear Munitions,"AMSC N6037, Department of Defense, 1994.



History of the Fragment Impact STANAG

*Insensitive Munitions and Energetic Materials Technology
Symposium
23-26 April 2018*

Presented by: Kathryn Hunt

Purpose

- This review was done to support a revised edition of NATO STANAG 4496 Fragment Impact Munitions Test Procedure
- Areas for Consideration
 - Fragment Threats
 - Fragment Velocity
 - Fragment Geometry
 - Multiple Fragments

Policy and Procedure Requirements (2001)

	NATO	France Light Fragment	France Heavy Fragment	UK	US Preferred	US Alt #1
Geometry	Conical Tipped cylinder	Cube (NATO fragment used)	Parallelepiped (sphere is used)	Cylinder Ø 12.7mm h=12.7mm	12.7 mm cube	Conical tipped cylinder
Mass, g	16	20 (16)	250	13.5	16	16
# of Frags	1	3 (1)	1	1	2-5	1
Launcher Type	Undefined	Undefined (gun)	Smooth bore gun	RARDEN gun	Fragment Projector	Undefined (gun)
Velocity Range, m/s	2000	$0 < v < 2000$	$0 < v < 1600$	$400 < v < 2500$	2530 ± 90	1830 ± 60

Representative Frag Velocities

Table III: Computed Fragments Characteristics (Mott & Gurney)

Threat Weapon	Mass	Ø	Source Velocity		Nominal Range ⁽¹⁾		Avg. Frag. Mass ⁽²⁾	Frag. > 15g ⁽³⁾	Cube Velocity of cube at Nominal Range	
	kg	cm	ft/s	(m/s)	ft	(m)	g	%	ft/s	(m/s)
Grenade	1.46	7.6	3700	(1128)	31	(9.4)	2.3	1.4	3191	(973)
Missile	32.8	17	5000	(1524)	125	(38.1)	3.0	2.6	2763	(842)
Artillery/ Missile	41.8	17	3890	(1186)	80	(24.4)	10.4	21.5	3216	(980)
Missile	100.4	32	5939	(1810)	135	(41.1)	4.3	5.5	3125	(952)
Missile/ Artillery	118.2	32	4920	(1500)	100	(30.5)	14.0	15.1	3876	(1181)
Missile	365.5	50	5188	(1581)	111	(33.8)	29.9	29.7	4235	(1291)
Missile	1003.	75	5814	(1772)	140	(42.7)	38.0	47.6	4500	(1372)

⁽¹⁾ Range at which main fragment beam delivers 3 fragments per square foot

⁽²⁾ About 26% of fragments are larger than the average mass for each warhead

⁽³⁾ Comparable to Army IM test fragment or Navy IM test fragment (16g)

- When looking at primarily ground launched systems fragments do not reach even 1830 m/s in velocity

Representative Frag Velocities

Munition	Design fragment	
	Mass (g)	Velocity (m/s)
Mk81	12.76	2396
Mk82	18.43	2402
Mk117	38.61	2386
Mk83	52.16	2259
Mk84	63.79	2365
155mm M107	64.55	1030
8" M106	97.52	1152
105mm M1	13.13	1237

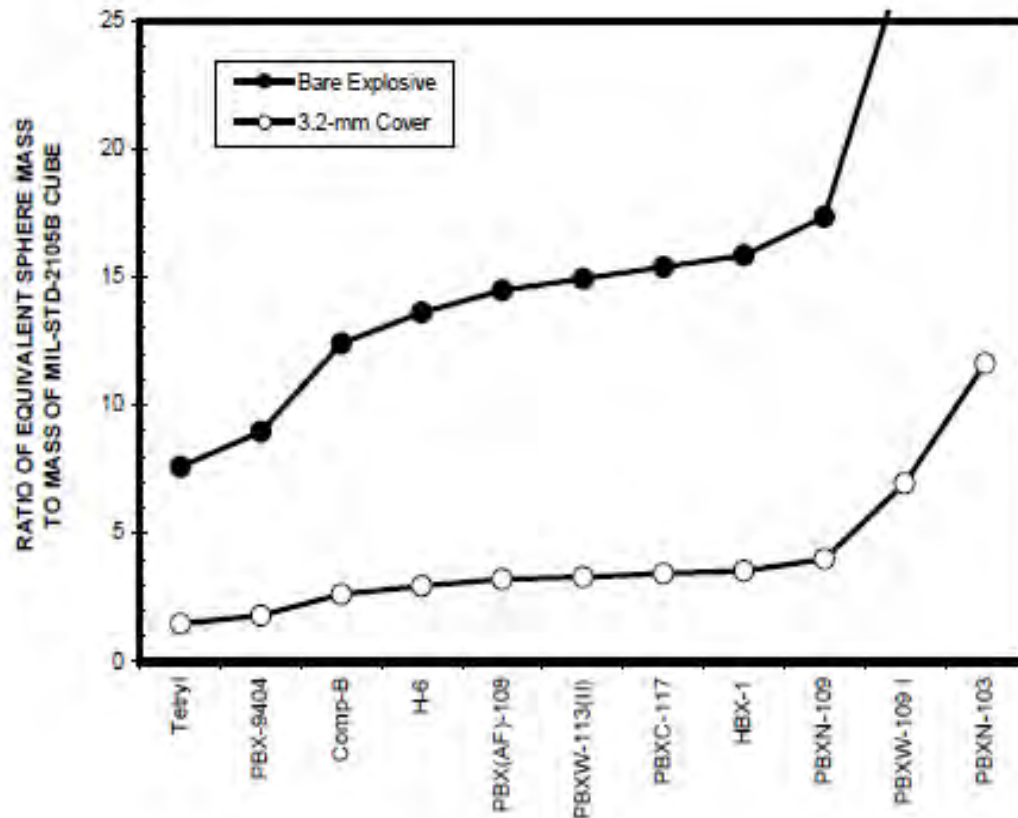
- Compiled by MSIAC (NIMIC at the time) to support the original STANAG
- Additionally, the fragment velocity, as defined in MIL-STD-2105B and STANAG-4240, Draft 10, originated from a US Navy survey dated 1987. The velocity chosen for the ½-inch steel cube was 8300 ft/s (2530 m/s) because it represented the upper range of the threat fragment velocity

Fragment Shape Pros and Cons

- The cube shape resembles a preformed fragment
 - angle of attack is not repeatable
 - Flat impact is anomalous
- Sphere shape is used in characterizing explosive formulations.
 - Repeatable
 - Not threat representative
- Conical type cylinder was created to allow easier launch from a fragment gun.
 - More repeatable than cube
 - Eliminates flat impacts

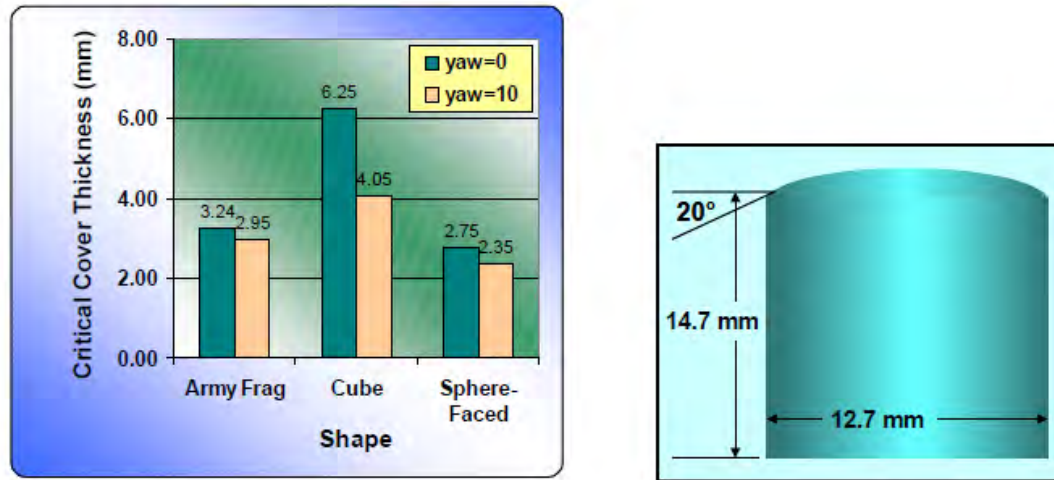
Sphere versus Cube

- Spherical fragments also require either a higher initial velocity or greater mass for the same input of shock duration to the target
- Equivalent sphere must be 5x more massive than cube



- An equivalent sphere is defined as that sphere that will give the same detonation threshold velocity as a cube at 10° yaw

Conical vs Cube



- Conical tip on the end of a cylinder reduces yaw effects compared to the cube.
- An edge-on cube at 10° yaw has a 35% drop in critical thickness, much larger than the conical-tipped fragment.

Fragment Weight/Shape Factor

- Maintain the cube's stimulus at 10° yaw
- Give the same critical cover thickness of the cube at 10° impact a Comp-B charge covered with a mild-steel plate (18.6g conical cylinder)
- 95.6% of the fragments in zones with velocities faster than 1830 m/s are smaller than the recommended fragment
 - Looked at as the high end of credible threat spectrum

Multiple Fragments

- For Non-detonation reactions, effect of multiple fragments unpredictable
- For SDT of damaged material
 - Complex issue
 - Multiple fragment impact test not repeatable enough
 - Multiple impacts at a single velocity do not represent reality.
- Finally, for SDT of neat material
 - Effects of multiple fragment impact are unlikely since the fragments space out very rapidly and then slow rapidly with distance.

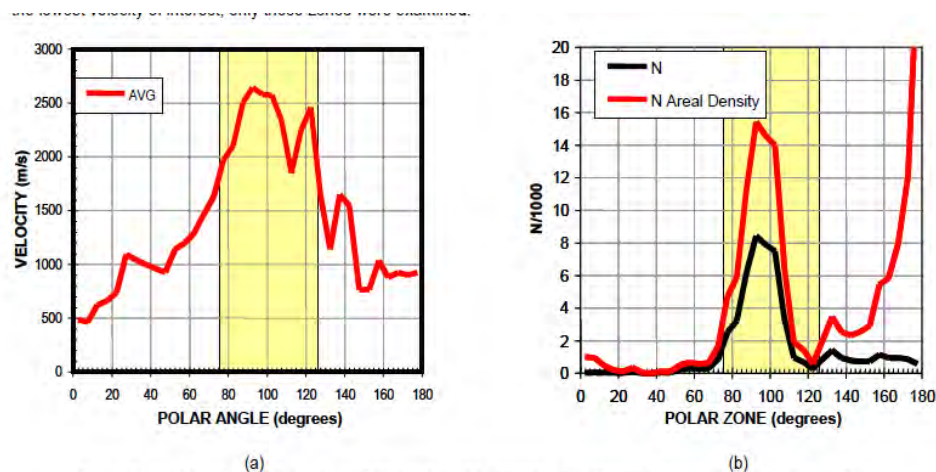


Figure 6. (a) Velocity vs. polar zone and (b) number of fragments vs. polar zone for a particular analog system.

Acknowledgements

- My co-author Dr. Ernie Baker
- Dr. Pat Baker and the original authors of STANAG
- Dr. Brian Fuchs for pushing me to write this paper



An Approach to Predict the Slow Cook-off Response of Confined and Vented Full-Scale Munitions Based on Small Scale Tests

N. Albert Moussa and Vijay V. Devarakonda, BlazeTech Corp., Woburn MA; Michael J. Kaneshige, Sandia National Laboratories, Albuquerque, NM; and Lori Nock, NSWC IHEODTD N00174

NDIA Insensitive Munitions and Energetic Materials Technology Symposium, April, 2018, Portland, OR

Abstract

We have developed an approach to predict the cook-off response of confined and vented full-scale munitions based on small scale testing and analysis. This approach has 4 steps: (1) Measure the thermal degradation rates of confined and vented explosive versus temperature through small scale tests (~2 g of explosive per test), (2) Measure the burn rates of pristine, heated and thermally degraded explosive in a strand burner (~3 g of explosive/test), (3) Capture the above processes in a fast running cook-off model that includes algorithms for thermal degradation kinetics versus temperature and venting (from step 1), and burn rate versus temperature, pressure, extent of thermal degradation and venting (step 2), and (4) Validate the model by comparing its predictions with cook-off test data.

A summary of key findings from the implementation of the above approach to PBXN-111 follows:

- The rate of thermal degradation depends on temperature and confinement. For example, the mass loss of confined PBXN-111 due to thermal degradation increases from 0.74% in 32.6 hours at 151.8°C to 13.2% in 5.8 hours at 175.7°C. The initial thermal degradation rates of confined and vented PBXN-111 are almost identical, but at later times the rate of reaction is higher in confined systems.
- Up to 2000 psig, the burn rate of PBXN-111 is almost independent of temperature, pressure and time but it increases marginally (up to 7.5 times) with the extent of thermal degradation. Above 2000 psig, the burn rate increases significantly with the extent of thermal degradation and pressure. We observed up to ~3 orders of magnitude increase in burn rate due to a combination of thermal degradation and pressure.
- The wall temperature required for ignition increases with heating rate.

BlazeTech's thermal degradation, burn rate and cook-off tests with PBXN-111 are presented along with the data analysis and model development. We find that tracking the pressure evolution (while ignored by others) is critical to proper modelling of slow cook-off.

Introduction

Historical data (USS Oriskany 1966, USS Forestall 1967, USS Enterprise 1969 and USS Nimitz 1981) suggest that accidents involving energetic materials and munitions can lead to large scale damage during regular military operations. This has prompted the DOD and DOE to develop Insensitive Munitions (IM) that are safe under normal conditions but can be activated on-demand under a narrow range of conditions. However, the explosive formulations being evaluated as IMs can cook-off when exposed to heat. Cook-off response is commonly studied using full scale tests that are time and resource intensive. In addition to developing safer chemistries, the research community is examining safety methods such as latent venting to protect against various types of hazards. We developed an innovative approach to evaluate the safety of new formulations to cook-off and develop vent design parameters. Our approach consists of a coordinated set of small scale tests and modeling covering thermal degradation, ignition, combustion and venting. It was implemented on the slow cookoff of PBXN-111 through a Phase II SBIR project funded by the US Navy and it can be applied to other munition formulations. PBXN-111 consists of 43% ammonium perchlorate, 25% aluminum, 20% RDX, and 12% HTPB/IDP binder system. Our models can also be used to design vents to lower the cook-off violence and are equally valid to fast cook-off. Our approach consists of four steps described in this paper.

Thermal Degradation of PBXN-111

The first step is to develop thermal degradation kinetics through controlled tests and analysis. PBXN-111 undergoes exothermic thermal degradation reactions at increasing rates when heated causing it to self-heat and eventually ignite. Focusing on these pre-ignition reactions, we developed a small-scale test where the thermal degradation rate can be measured accurately through controlled tests on ~2 g of explosive per test. The explosive is loaded into a steel casing and placed in a larger aluminum oven shown in Figure 1 (mid and right photographs). It is heated to a target temperature between 150° and 180°C where it is held for several hours either under completely confined or vented conditions and the heat was turned off before the material can ignite. The small size ensures that the entire test setup heats up uniformly with no temperature gradients during the test. We used 3 thermocouples (TC1, TC2 and Control) to measure the steel casing temperature and one to measure the explosive temperatures during the tests. The confined test setup is also equipped with a pressure sensor to measure the pressure-time history due to thermal degradation. In each test, we carefully measured the dimensions and masses of about 6 cylindrical PBXN-111 pellets which were then loaded into the test fixture. We measured the temperature-time histories during the test, the overall mass loss after the test and for the confined tests the pressure-time histories.

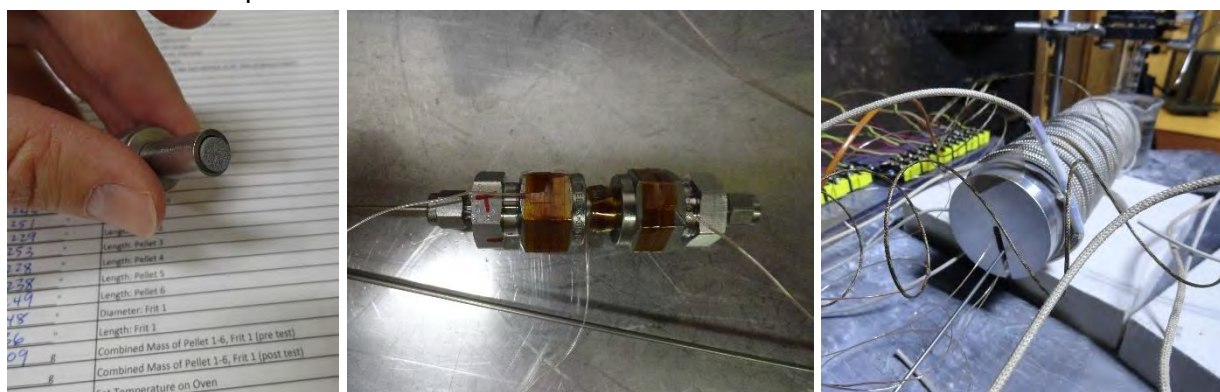


Figure 1: Photographs of apparatus assembly for the thermal degradation tests on confined and vented PBXN-111.

We performed 8 tests each with confined and vented PBXN-111 varying the temperature and exposure time. Sample data from one of these tests (Con-114) in which confined PBXN-111 was heated to 160.3°C for 17.2 hours are shown in Figure 2. At the start of each test, we heated the oven to a slightly higher temperature than the target value to ensure that the steel casing and the explosive reach the target temperature in only a few minutes as shown in Figure 2 (a). RDX-based explosives like PBXN-111 degrade slowly below 130°C, so we focused on the duration for which the test apparatus remains hotter than 130°C. The close agreement between the temperature-time histories recorded by the 4 thermocouples shows that the temperature was uniform throughout the test setup. The explosive heated up more than the casing at later times suggesting the occurrence of exothermic reactions. We turned the oven off at ~1000 minutes and allowed the system to cool down to ambient temperature. The pressure increased slowly with time initially, before accelerating later due to rapid gas and heat release from thermal degradation reactions reaching a maximum of 723 psig when the heat was turned off as shown in Figure 2 (b). The pressure then decreased gradually as the system cooled down. Focusing on the period when the explosive remained hotter than 130°C, we determined the time-averaged temperature. The test conditions as well as the measured mass losses from the confined tests are summarized in Table 1. These results show that at a given temperature, the mass loss due to thermal degradation (i.e., the extent of reaction) increases with time. The mass loss rate is slow initially, but increases with time. The mass loss rate increases with temperature from 151.8°C (Con-108) to 175.7°C (Con-116). We performed 8 such tests on vented PBXN-111 and the results from

these tests are presented in Table 2. The initial mass loss rates are comparable in confined and vented PBXN-111, but later the confined PBXN-111 degraded faster than the vented material.

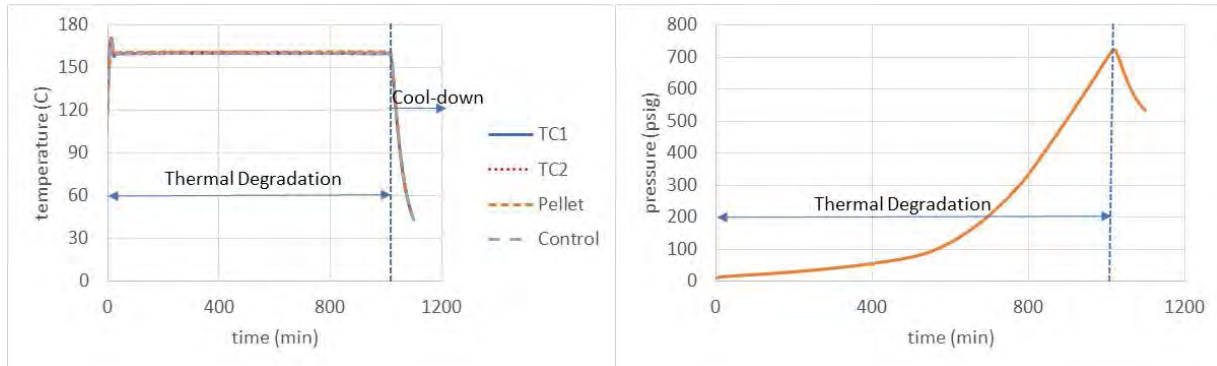


Figure 2: Temperature and pressure versus time data collected from thermal degradation test Con-114 in which confined PBXN-111 heated to 160.3 C for 17.2 hours.

Table 1: Summary of test conditions and key results from thermal degradation tests on confined PBXN-111.

Test No. Con-	t (min)	Temperature (°C)			P (psig)			Explosive Mass (g)		Mass Loss, %
		T_{mean}	T_{peak}	T_f	P_i	P_{peak}	P_f	Initial	Final	
108	1955	151.8	156.5	31.2	2.4	80.7	48.6	2.109	2.078	0.74
102	246	160.1	163.4	160.1	3.2	30.5	NM	2.120	2.112	0.41
104	500	160.1	165	21.6	4.2	65.2	32.2	2.136	2.126	0.47
114	1031	160.3	170.6	43.8	4.9	723	534	2.065	1.960	5.05
106	266	168.9	174	35.8	2.7	130	81	2.162	2.134	1.27
110	506	169.6	174.9	33	3.1	1220	953	2.164	1.947	10.0
112	267	174.3	184.7	54.8	10.4	888	697	2.017	1.890	6.3
116	349	175.7	182.2	25.6	2.5	1104	NM	2.129	1.847	13.2

Table 2: Summary of test conditions and key results from thermal degradation tests on vented PBXN-111.

Test No.	Duration (min)	Temperature (°C)	Mass Loss (%)
Con109	1955	147.4	0.86
Con103	246.3	158.4	0.52
Con105	502.2	159.9	0.68
Con115	1030	160.1	2.93
Con107	264.4	167.5	1.4
Con111	505.6	169.3	4.7
Con113	266	173.2	6.8
Con117	350.2	174.2	11.9

We converted the pressure-time histories from each confined test into residual explosive mass versus time data, fitted a two-step first order reaction model through these data, and determined the rate constants for each step. The logarithmic rate constants from the two steps are plotted as functions of reciprocal temperature in the left of Figure 3 and determined the Arrhenius rate parameters from the slope and the y-intercept. The rate constant increased with temperature, but we obtained close agreement in the rate constants of various tests conducted at a given temperature. For vented PBXN-111, we fitted a global one-step reaction model through the overall mass loss versus time data and these rate constants are plotted versus reciprocal temperature in the right of Figure 3. The confined and vented PBXN-111 reacted at similar rates at the beginning,

but the pressure buildup with time increased the reaction rate of the former. The reaction rates were very slow below 150°C, but they increased significantly at higher temperatures: the rate constants (for both confined and vented PBXN-111) increased by more than 1 order of magnitude with temperature from 151.8°C to 175.7°C.

We have presented an innovative approach based on small scale tests and analysis to develop the thermal degradation reaction rate kinetics of confined and vented explosives. The rate kinetics models for PBXN-111 are now ready for integration into the cook-off model.

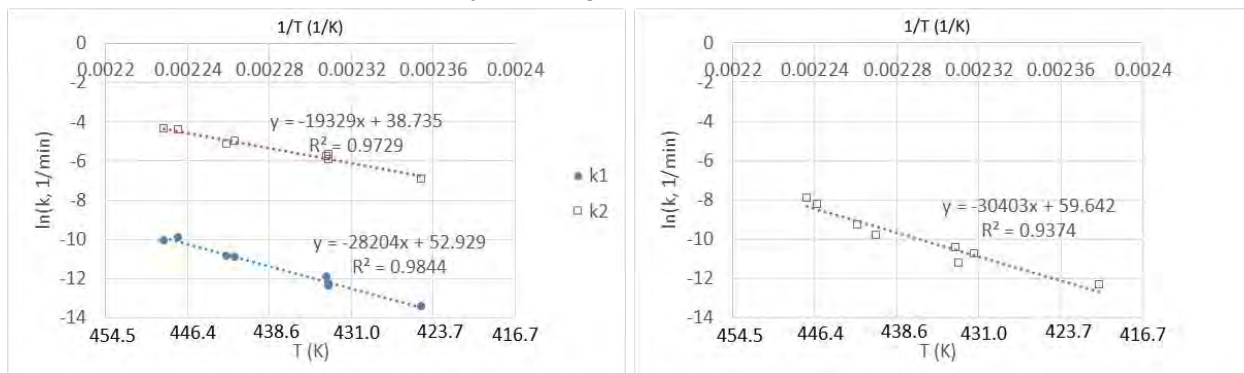


Figure 3: The rate constants for thermal degradation of confined (left) and vented (right) PBXN-111.

Combustion of PBXN-111

Upon ignition, the combustion front propagates through the explosive raising the pressure rapidly. Focusing on these fast processes, we performed burn rate measurements on pristine, heated (but undegraded), and heated and degraded PBXN-111 as functions of pressure in a strand burner. We made three key changes to the traditional strand burner measurements and the data analysis: (i) we reduced the empty space inside the burner chamber to improve confinement and facilitate secondary reactions of PBXN-111 thermal degradation products, (ii) we inserted thermocouples and break wires inside the explosive strand to track the strand temperature as well as the burn front location versus time during the burn test, and (iii) we used both the pressure-time histories and the thermocouple/break wire data to generate $x-t$ diagrams for the burn front. We attached the individual explosive pellets, ignitor, thermocouples (yellow wires in the left of Figure 4) and the break wires (red wires) to the sample holder before installing the sample holder inside the strand burner. A schematic of the overall setup is shown in the right of Figure 4. In each test, we measured the pressures (3 sensors), temperatures (2 locations along the strand) and signals from 5 break wires versus time, and the time of ignition (from ignitor data).

We conducted 10 burn tests varying the temperature, extent of degradation and initial pressure at ignition. Sample data from test HPSB-049 in which the strand was heated to 160°C for 17 hours prior to ignition are shown in Figure 5. It took ~3 hours to heat the strand burner and the explosive pellets from room temperature to ~160°C due to the large thermal mass of the strand burner (equipped with thick walls to withstand pressures generated during the burn test). The system remained close to 160°C during the thermal degradation phase, with the top of the strand being slightly warmer than the bottom. Once the strand was ignited, the burn test lasted only about 2 s. The strand burner was filled with an inert gas to generate an initial pressure of ~1000 psig before the onset of heating. The 3 pressure transducers responded differently to the temperature rise and exhibited some variability as shown in the figure. The pressure increased slightly during the 17-hour thermal degradation due to the release of thermal degradation products and the temperature becoming more uniform in the strand burner. Upon ignition, the pressure increased rapidly as shown in Figure 5 (b).

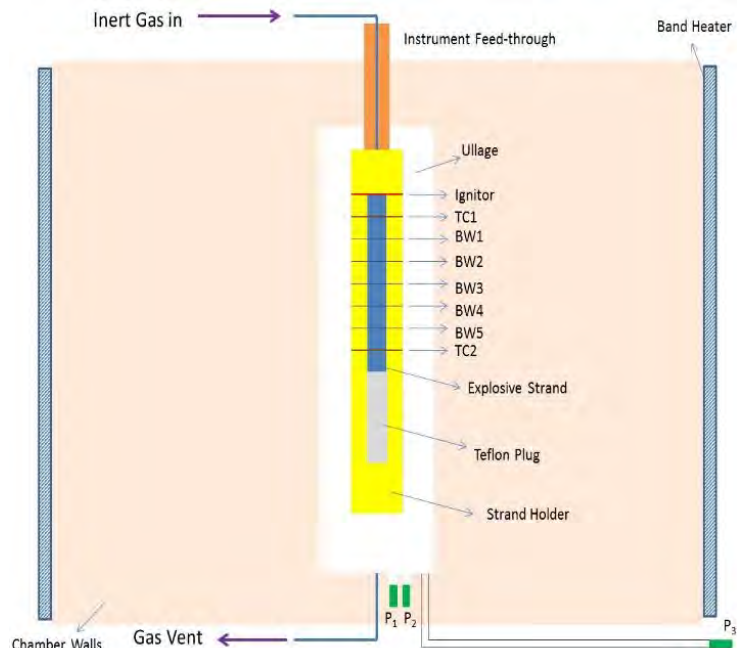
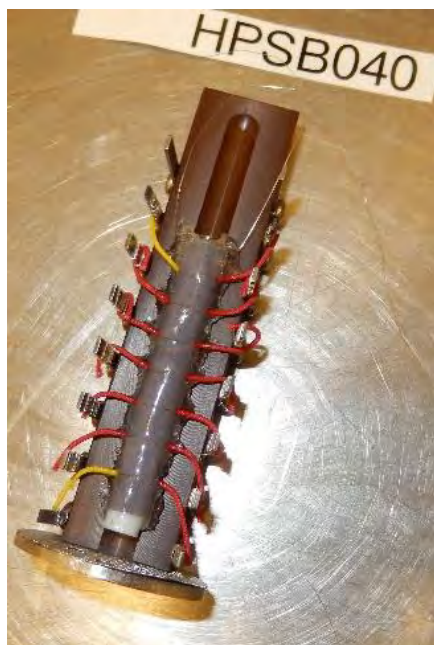
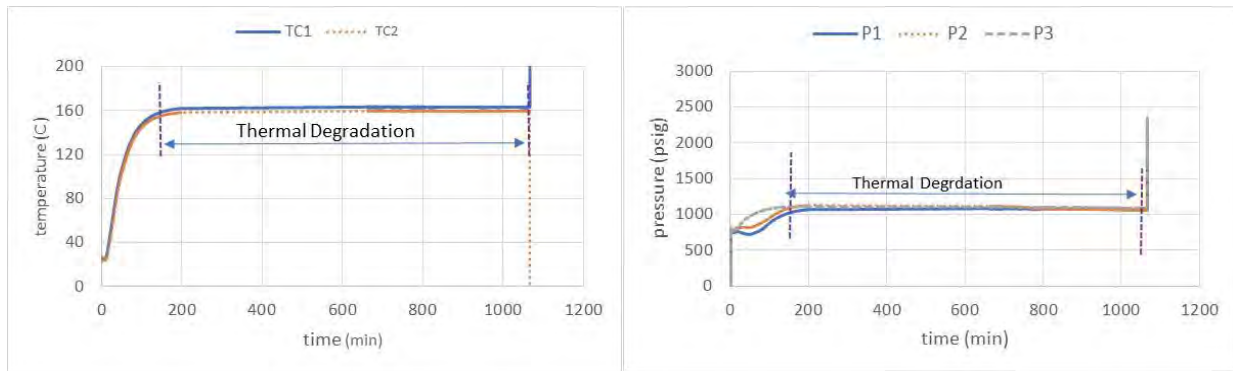


Figure 4: Installation of explosive pellets, ignitor, thermocouples, and break wires inside the sample holder; and the schematic of the strand burner apparatus.

The normalized signals from the ignitor located at the top of the strand, 2 thermocouples (TC1 located between the top 2 explosive pellets and TC2 between the bottom two), and the 5 breakwires, plotted in Figure 5 (c), show that the burn front moved from the top of the strand (ignitor location) to the bottom sequentially triggering each sensor along the way. The burn rate was slow initially and consumed the top pellet in 0.45 s, but accelerated later as it consumed the bottom pellet in only ~0.1 s. This acceleration is also evident from the narrowing of the gap between the triggering times of successive sensors as shown in Figure 5 (c). The pressure increased from ~1080 psig at ignition to ~2550 psig at the end of combustion as shown in Figure 5 (d). The rate of pressure rise increased during the test, also suggesting burn front acceleration. The small discontinuities in the pressure plots could be due to the small gaps between successive pellets introduced by the insertion of sensors. We interpreted the signals from the ignitor, thermocouples and the break wires in each test to track the burn front versus time. In a few tests, the break wires did not get triggered sequentially possibly due to electronic cross-talk and/or failure of the epoxy coating that caused the burn front to run down the sides of the explosive. We developed an alternate technique based on the pressure data to generate the $x-t$ plots for the burn propagation. We fitted second order polynomials through these plots and determined the burn rates and accelerations from first and second time derivatives of these fits.

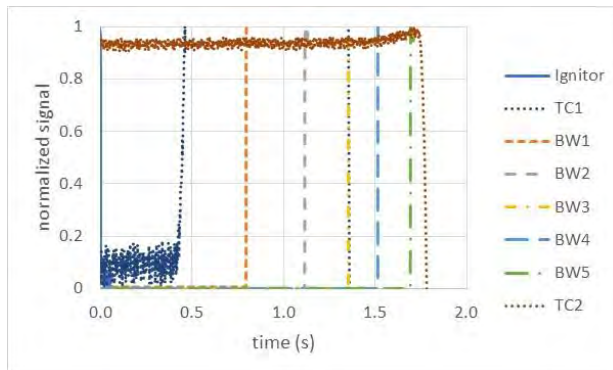
The test conditions such as the test id, strand temperature at ignition, time averaged strand temperature, duration for which the strand remains above 130°C, pressure at ignition and the peak pressure at the end of combustion are presented in the first 6 columns of Table 3. The extents of thermal degradation at ignition (ϕ calculated using our kinetics model) are presented in column 7. We fitted the power law model (below) through the burn rate versus pressure data obtained from each test and determined the burn rate parameters A and n . The burn rate increases significantly when the pressure exceeds ~2000 psig (13.8 MPa), so we generated separate fits for the data below and above 2000 psig. The fit parameters are presented in columns 8, 9, 11 and 12 of Table 3 for the following equation with u given in cm/s, P in MPa and ϕ in %:

$$u = A(\phi) \times P^{n(\phi)}$$

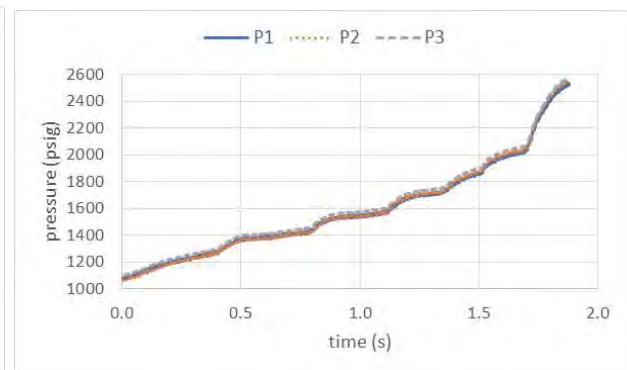


(a) Temperature-time history.

(b) Pressure-time histories.



(c) Ignitor, thermocouples and break wires data.



(d) Pressure-time histories after ignition.

Figure 5: Burn test HPSB049 in which PBXN-111 strand was thermally degraded for 17.2 hours at 160°C before ignition.

Pristine PBXN-111 at room temperature burned at a constant speed of 0.55 cm/s. Four tests with heated, but un-degraded explosive showed that the burn rate increased to 0.87 cm/s at 160°C and further to 0.93 cm/s at 175°C. These data suggest that the burn rate remains constant at 0.9 ± 0.03 cm/s and is almost independent of temperature between 160° and 175°C. Pressure has almost no effect on burn rate of undegraded PBXN-111 below 2000 psig, and so the value of n remains at 0 as shown in column 9. Above 2000 psig, the burn rate of undegraded PBXN-111 is weakly dependent on pressure (i.e., $n \sim 0$), while that of degraded material becomes increasingly sensitive to pressure (i.e., n increases with the extent of degradation). Since the burn rate increases with pressure, the combustion front accelerates with time in degraded PBXN-111, the magnitude of acceleration increasing with the extent of thermal degradation as shown in column 10 of the table. We observed increases of ~ 3 orders of magnitude in burn rate due to thermal degradation and pressure. We generated fits for the burn rate parameters A and n as functions of the extent of thermal degradation ϕ (which can be improved with additional data). These fits are used in our combustion model.

Models for Ignition, Combustion and Venting

We developed two separate fast-running engineering models to capture cook-off: ignition model to track the various processes that occur until ignition, and the combustion model to track the burn propagation through the explosive after ignition. The ignition model tracks the heat conduction from the casing walls to the explosive as well as within the explosive; thermal expansion of the explosive that in turn compresses the gases; thermal degradation and resulting porosity generation; changes in the rate of thermal degradation reactions due to venting; changes in the pressure due to heating, heat and gas generation from thermal degradation reactions, and gas loss due to venting; and ignition of the explosive when the local temperature significantly exceeds the externally imposed wall temperature. The model inputs include: dimensions of the explosive, ullage and the casing, heating profile (including the soak), and the vent parameters (pressure

needed for vent activation and the vent diameter). The model outputs the pressure, temperature and extent of reaction profiles throughout the explosive versus time until ignition, occurrence of ignition, and the time and location of ignition.

Table 3: Summary of conditions and key results from burn rate tests with pristine, heated and degraded PBXN-111.

Test	Measurements					Analysis					
	T# (°C)		t _{soak} [§]	P (psig)		φ	Initial		Later		
HPSB	T _{ign} ^{&}	T _{ave} [*]	(min)	P _{ign}	P _{final}	(%)	A (cm/s)	n	a (cm/s ²)	A (cm/s)	n
040**	22	22	0	0		0.00	0.23	0	0	NA	NA
041**	22	22	0	990	1880	0.00	0.55	0	0	NA	NA
046	161.8	156	7.1	1020	2110	0.00	0.87	0	0	NA	NA
049**	163	162.5	950	1080	2550	4.50	1.81	0	13.3	0.22	1.23
048	170	160.7	13.3	1050	2210	0.01	0.87	0	0	NA	NA
051	170.1	160.9	11.4	2630	5080	0.01	1.59	0	0	NA	NA
047	173.8	171.7	485	1450	3130	18.2	3.5	0	79.4	0.22	1.57
050**	171.1	169.3	480	2090	4240	6.35	1.96	0	42.7	0.22	1.23
043	175	172.7	3.5	1190	2650	0.03	0.93	0	2.34	0.22	0.96
044	177.3	175.8	239	1590	4510	7.38	6.5	0	27,784	0.22	2.34

* time averaged temperature near the strand top over the duration of thermal degradation reactions

temperatures near the strand top between pellets 1 & 2

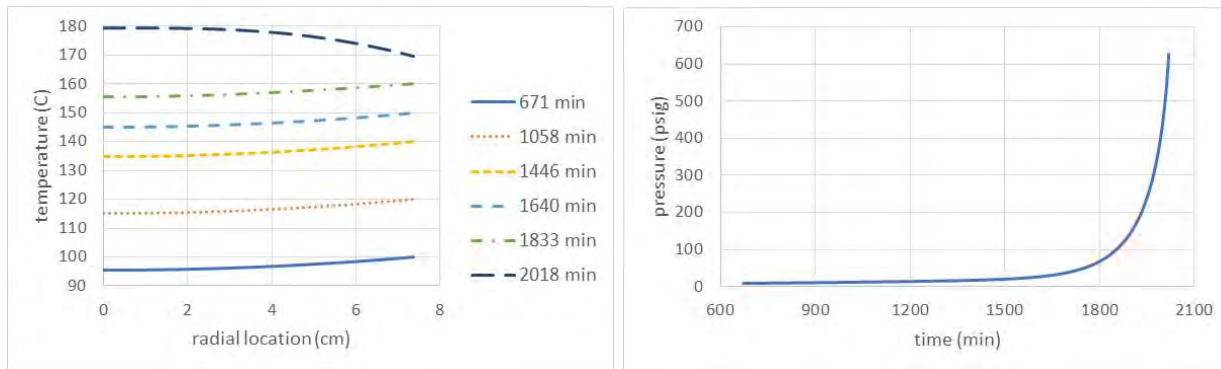
& at the time of ignition

§ duration for which the strand remains above 150°C

** leaks occurred during the test

We performed several parametric calculations with this model, and we present the results from one calculation here for illustration. We considered the Navy sub-scale test 1 [Refs. 1 and 2]) with 6690 g of PBXN-111 with a diameter of 14.74 cm and a length of 21.9 cm and heated in 3 steps: (i) rapid heating from $T_{ambient}$ to 65.6°C, (ii) 8 hour soak, and (iii) slow heating at 0.052°C/min until ignition. We assumed a confined system with no vent here. In the test, the explosive material ignited about 1960 min after soak when the explosive wall reached 166.5±1°C. The model predicts the temperature and extent of thermal degradation reaction distributions throughout the explosive as well as the quasi-static pressure versus time until ignition. The model assumes that the explosive surface remains in thermal equilibrium with the casing. Initially, the casing is hotter than the explosive, so heat is transferred from the explosive surface to the center. When the explosive reaches ~150°C, it undergoes exothermic reactions causing the material to self-heat. The casing wall quenches the surface of the explosive, but the heat released in the inner core remains trapped locally in the explosive. This causes the inner regions of the explosive to heat up more than the surface at later times changing the direction of heat transfer. We assumed that ignition occurs when the hottest region in the explosive exceeds the externally imposed wall temperature by >10°C. Our model predicts that this occurs when the wall temperature reaches 169.6°C about 2018 minutes after the end of soak. The ullage pressure predicted by our model (Figure 6 (b)) shows a small initial increase due to the temperature rise of the gases in the ullage. The heat and the gas release from exothermic reactions when the explosive reaches ~150°C at 1640 minutes, raises the pressure at increasing rates as shown by the sharp rise in the pressure-time history in Figure 6 (b). The model predicts a pressure of 626 psig (4.3 MPa) at ignition.

Our combustion model uses the results from ignition calculations presented above as inputs and tracks the burn front propagation accounting for the heat and gas generation from combustion and the energy losses from the burned gases. The model inputs include: dimensions of the explosive, casing and the ullage; location of ignition; conditions at ignition such as the pressure and the mean extent of thermal degradation averaged across the explosive; and the vent parameters (onset pressure for venting and the vent diameter). The model outputs the time



(a) Temperature profiles in the explosive until ignition. **(b) Quasi-static pressure versus time.**

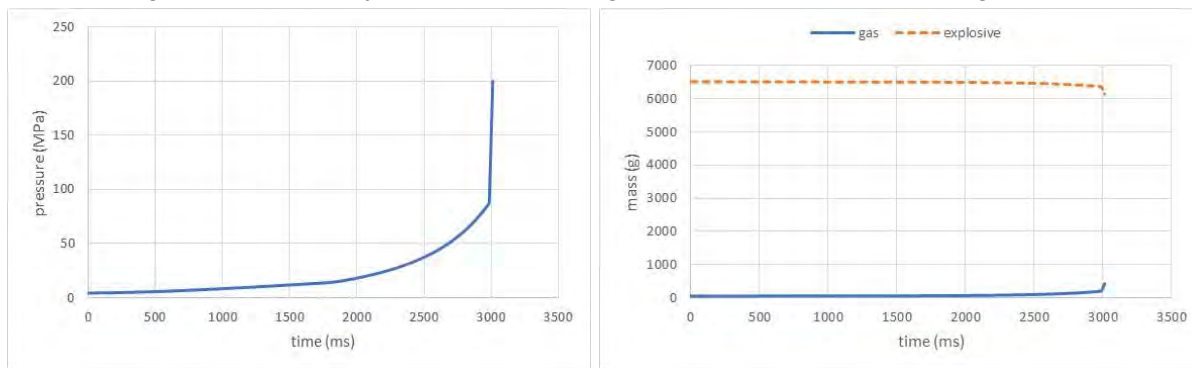
Figure 6: Results from sample calculation with the ignition model for the conditions of the Navy sub-scale test 1 with 6690 g of PBXN-111 heated at 0.055°C/min until cookoff.

dependent pressure, burned gas temperature, masses of residual explosive and gases, and the dimensions of burned region. We present here the results from one calculation for the conditions of Navy sub-scale test 1 for illustration. We used the ignition results (ignition at center 2018 minutes after the end of soak when the wall reaches 169.6°C, pressure at ignition of 4.3 MPa, and the mean porosity of ~0.4%). We assumed that the container had no leaks and that it could withstand a pressure of 200 MPa. The pressure-time history predicted by the model is plotted in Figure 7 (a). Given that the extent of thermal degradation at ignition is small and the pressure is low, the initial burn rate is low and pressure-independent. Since ignition occurs at the center, the burn front propagates in the radially outward direction. The mass burning rate (defined as the product of the burn rate and the surface area of the burned region) increases steadily with time causing a similar increase in the heat release and gas generation rates, raising the pressure steadily with time to 13.8 MPa (or 2000 psig). The burn rate then becomes pressure dependent and increases with pressure. The increases in the burn rate as well as the surface area of the burned region then increase the mass consumption rate of the explosive. ~3 s after the ignition, the burn front reaches the external wall. Then the burn front propagates axially in both directions away from the center rapidly raising the pressure, burn rate and the mass consumption rate. The pressure soon reaches 200 MPa, the assumed failure pressure for the casing. The casing may fail at a lower pressure due to the potential weakening of the wall caused by heat. The masses of the residual explosive and the gases generated from combustion are plotted versus time in Figure 7 (b). The residual explosive mass decreases slowly with time as the burn front travels from the center to the explosive surface. It then decreases rapidly as the mass burning rate increases sharply with time. Similarly, the mass of gas generated increases slowly with time initially, before speeding up later. The results from the ignition and the combustion models appear reasonable and internally consistent and serve as model verification.

Model Validation

Limited PBXN-111 SCO test data are available in the literature to validate our ignition model but none for our combustion model. These involved ~6690 g (D = 2.9" and L = 8.6") used in each of the Navy sub-scale tests [1,2] and ~57.6 g (diameter = 1" and length = 2.5") in the Variable Confinement Cook-off Test (VCCT) [3]. In these tests, the explosive was heated at a constant rate until cook-off while monitoring the temperatures at select locations. We performed 9 small scale cook-off tests with ~2.1 g of PBXN-111 per test (D = 0.25" and L = 1.5") to generate additional data at heating rates between 0.02° & 0.406°C/min and confinement levels. The input conditions as well as key results from all the cook-off tests (literature & BlazeTech) are summarized in Table 4. They cover ~1 order of magnitude variability each in size and heating rate for scaling analysis. Predictions from our ignition model for each set of test conditions are presented at the bottom of the table. Our predictions agree within ~3°C of the measurements

despite the large ranges in heating rates and sizes. These data show that at a given size, the wall temperature at ignition increases with heating rate. At a given heating rate, the wall temperature at ignition is (a) independent of radius up to ~0.5" and decreases as size increases above 0.5" (for slow heating rates that are commonly used in SCO tests), and (b) is independent of radius for fast heating rates. This serves as validation of our model. The utility of our model is that it yields additional information that is difficult to characterize such as the ignition location, extent of thermal degradation/porosity distribution until ignition, and the pressure at ignition.



(a) Pressure-time history after ignition.

(b) Masses of residual explosive and gases.

Figure 7: Results from sample calculation with the combustion model for the conditions from the Navy sub-scale test 1 with 6690 g of PBXN-111 heated at 0.055°C/min until cookoff.

Effect of Venting on Cook-Off

Latent venting can reduce the violence of cook-off as it affects both the thermal degradation reactions before ignition and the rate of combustion propagation after ignition of PBXN-111. A vent that opens early can discharge gaseous thermal degradation reaction intermediates and products from the munition into the atmosphere. Removal of these products eliminates their secondary reactions with the residual explosive as indicated by the fact that the thermal degradation rates are comparable in both the confined and vented PBXN-111 initially, but the confined material reacts faster than the vented one at later time. This suggests that when the munition is being heated slowly (under SCO conditions), a small vent that opens early should be adequate to reduce the pressure rise, because the rate of thermal degradation reaction is modest initially (provided the vent does not get clogged). In addition to reducing the extent of thermal degradation, venting reduces the pressure at ignition, which in turn affects the burn rate. If the vent gets activated at high pressures and opens after ignition, it can still help lower the violence of cook-off. This is because upon ignition, the burn rate of PBXN-111 depends mainly on pressure and the extent of thermal degradation. Burn rate remains low and constant for pressures below 2000 psig, but it increases significantly and becomes dependent on pressure and the extent of thermal degradation above 2000 psig. Therefore, a properly sized vent which ensures that the pressure remains below 2000 psig will reduce the violence of cook-off. Small-scale cookoff tests performed by BlazeTech/SNL have shown that completely confined PBXN-111 underwent cook-off leading to casing fragmentation. Exothermic reactions and mild self-heating occurred in a system with small leaks or a vent, but it did not cook-off. This suggests that venting is effective in reducing the violence of PBXN-111 cook-off. However, the vent needs to be designed and placed properly to ensure that it does not get clogged and remains effective.

Conclusions

We presented the implementation of our approach based on small scale tests and analysis to predict the slow cook-off violence of confined and vented PBXN-111. Our study showed that:

- The thermal degradation rate of PBXN-111 increases with temperature, time and confinement. Venting does not prevent self-heating, but it lowers the pressure at ignition.

- The burn rate of PBXN-111 is almost independent of temperature (if the material does not degrade during heating) and pressure below 2000 psig. Above 2000 psig, the burn rate becomes pressure-dependent in thermally degraded PBXN-111. Burn rate can increase by orders of magnitude due to pressure and thermal degradation.
- PBXN-111 cook-off can be captured using two models: (i) the ignition model predicts the temperature and extent of thermal degradation profiles and the pressure until ignition. Model predictions of ignition temperatures agree well with test data covering ~1 order of magnitude variability each in heating rates and size: serves as model validation. For slow heating rates (i.e., SCO conditions), the ignition temperature increases with heating rate (for a given size) and is independent of size below ~0.5", but it decreases with size above 0.5". For fast heating rates (FCO conditions), the ignition temperature is almost independent of size. The location of ignition shifts from the center towards the walls as the heating rate is increased. (ii) The combustion model predicts the burn front propagation, pressure, burned gas temperature, and residual explosive mass versus time.

The model presented here can be used to characterize the cook-off hazard, design vents to reduce the cook-off violence, and design future tests.

Table 4: Summary of test conditions and key results from the cook-off tests

Parameter	BlazeTech SCO Tests (CCO-)			VCCT [3]	Sub-Scale [1,2]	
	100a, 100b, 101a	103a, 103b, 104b	102a, 102b		Test 1	Test 2
Test Conditions						
$T_{ambient}$ (°C)	22	22	22	20*	20*	20*
Initial dT/dt (°C/min)	1.7	1.7	1.7	10*	10*	10*
T_{soak} (°C)	130	130	130	75	65.6	65.6
t_{soak} (min)	30	30	30	240	480	480
Final dT/dt (°C/min)	0.406	0.1	0.05	0.055	0.0515	0.479
Explosive Mass (g)	2.09	2.09	2.09	57.6	6690	6690
Ullage Volume (%)	45	45	45	10*	10*	10*
Explosive Radius (cm)	0.309	0.309	0.309	1.27	7.37	7.37
Explosive Length (cm)	3.8	3.8	3.8	6.35	21.9	21.9
Test Measurements						
T_{wall} at Ignition (°C)	195–197.2	185.5–188	178.9–179.2	177 – 183	166.5	197.7
$t_{ignition}$ after soak (min)	160–166	548–589	976	1854- 1963	1960	276
Model Predictions						
T_{wall} at Ignition (°C)	197.1	187.1	181.7	176.0	169.6	194.8
$t_{ignition}$ after soak (min)	165	573	1029	1837	2018	270
Ignition Location	center	center	center	center	center	6.64 cm from center

References

1. Beckett, K.M., Oetjen, M., Gibson, K., Nock, L., and K. Clark, "Effect of heating rate on munition thermal profile, hotspot location and reaction violence",
2. Beckett, K.M., Oetjen, M., and K.D. Gibson, "The effects of heating rate and reaction location on violence in monolithic energetic configurations",
3. Nock, L.A., Lawrence, G.W., Sherlock, M.H., Gibson, K.D. and D.N. Sorensen, "Effect of binder systems on underwater explosive slow cook-off violence and interactions with warhead venting".

All 3 papers were presented at the 39th PEDCS, JANNAF, Salt Lake City, Utah, 12/7-10/2015.

An Approach to Predict the Slow Cook-Off Response of Confined & Vented Munitions Based on Small Scale Tests

by

N. Albert Moussa and Vijay Venkat Devarakonda

BlazeTech Corp.

29B Montvale Ave. Woburn, MA 01801. Tel. 781-759-0700

Michael J. Kaneshige

Sandia National Laboratories, NM

&

Lori Nock

NSWC IHEODTD N00174

Contract N68335-16-C-0038

NDIA Insensitive Munitions and Energetic Materials Technology Symposium

April 23 - 26, 2018

Approach for Scaling

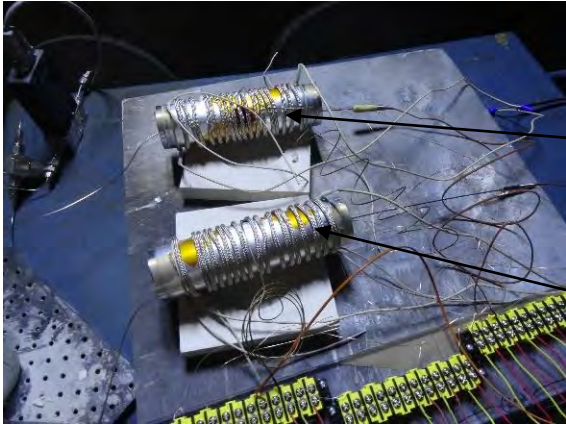
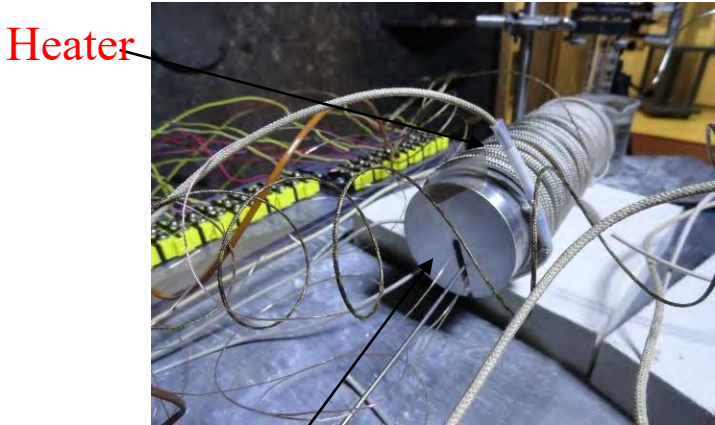
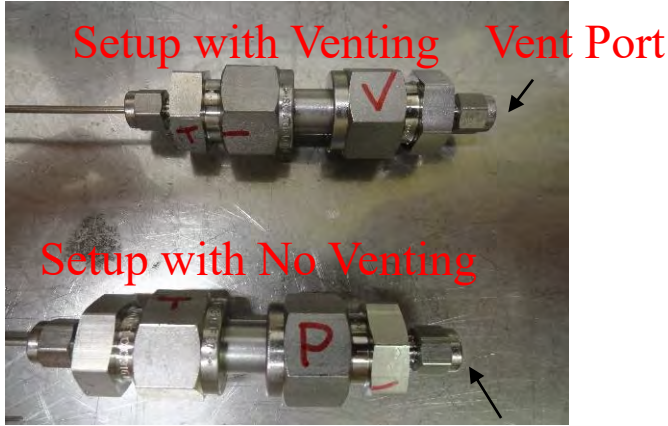
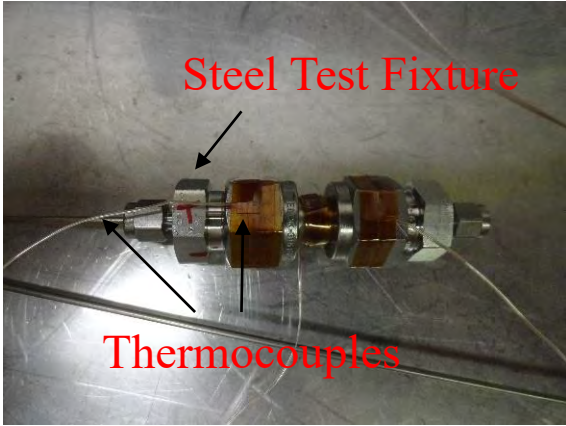
1. Characterize the thermal degradation kinetics of PBXN-111 (before ignition)
 - Small scale tests to measure degradation rates of confined & vented material vs. $T(t)$
 - Develop degradation kinetics models from test data accounting for dependence on T and venting
2. Examine the rate of combustion propagation in PBXN-111 (post-ignition)
 - Measure burn rates of pristine, heated and thermally degraded PBXN-111 in a strand burner vs. P
 - Develop models for burn rate vs. extent of thermal degradation (ϕ), P , and T
3. Develop fast running engineering models for
 - Ignition: predict $T(x,t)$ & $\phi(x,t)$ until ignition, and T_{wall} & P at ignition accounting for venting
 - Combustion: predict $P(t)$, $dP/dt(t)$ and dimensions of burned region accounting for the effects of T , P , ϕ & venting on burn rate
4. Model validation: compare T_{wall} at ignition predicted by the model with
 - Small scale cook-off tests by BlazeTech/Sandia
 - Larger scale tests by the Navy

The BlazeTech model can be used to predict the cook-off response of full-scale munitions loaded with PBXN-111 to heat accounting for venting

Step 1. Thermal Degradation of PBXN-111

- PBXN-111: 43% AP, 25% Al, 20% RDX, and 12% HTPB/IDP binder system
- Measure thermal degradation rates vs. $T(t)$ to generate easy-to-use kinetics data
- Test setup
 - Small scale, 1/4"×1/4" pellets (~2 g/test) & slow heating → uniform temperature throughout
 - Two configurations: confined (8 tests) and vented (8 tests)
- Test procedure
 - Heat to 150 – 175°C and hold for 4 – 32 hours (conditions designed to preclude ignition)
 - Measure five $T(t)$ (3 on casing), explosive, oven, and when confined $P(t)$
 - Turn heater off. Monitor $T(t)$ (and $P(t)$) during cool down
 - Measure mass loss due to thermal degradation by comparing pre- and post-test masses
- Data analysis: For each test,
 - Determine the time for which the explosive is hotter than 130 C
 - Determine the time-averaged temperature for that duration
 - Calculate the % mass loss from pre-test and post-test mass measurements
 - Develop kinetic model to calculate $m(t)$ from measured $P(t)$ and $T(t)$

Assembly Procedure

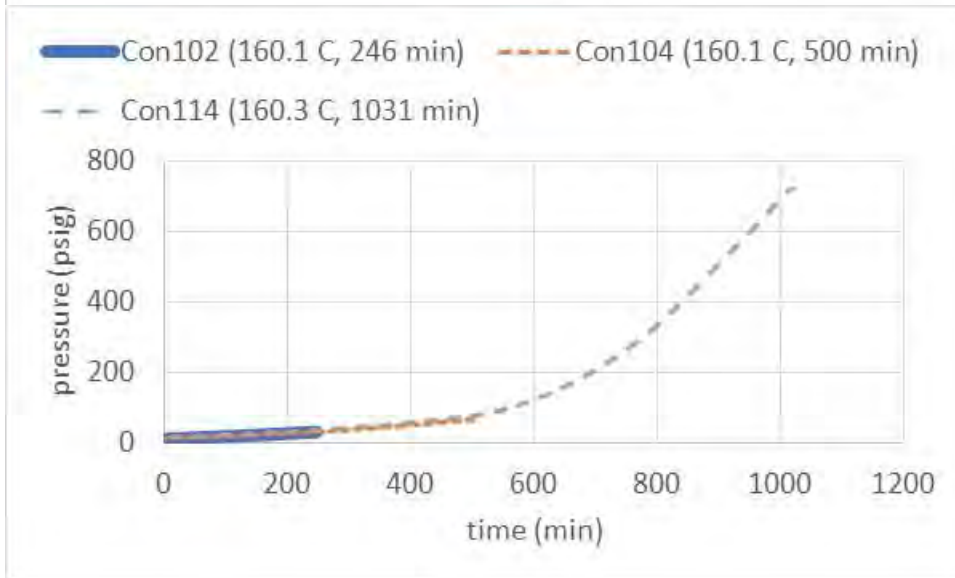
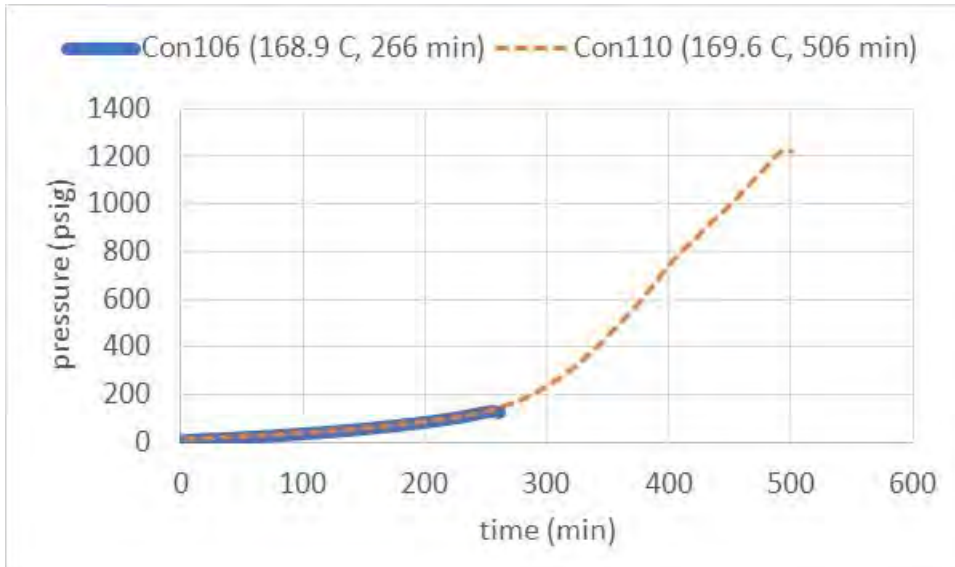


Al Oven
4

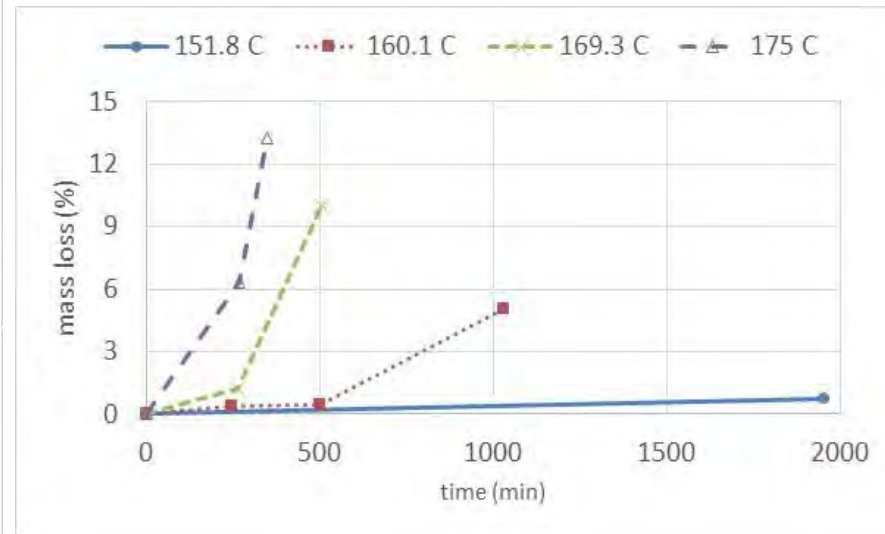
Approved for public release: distribution unlimited..

Confined Tests: Effects of $T(t)$ on $P(t)$ and $m(t)$

Pressure Rise, $P(t)$



Mass Loss, $m(t)$



Thermal Degradation Kinetics of PBXN-111

Post-Test Photographs After Exposure to ~160 C for 1030 minutes



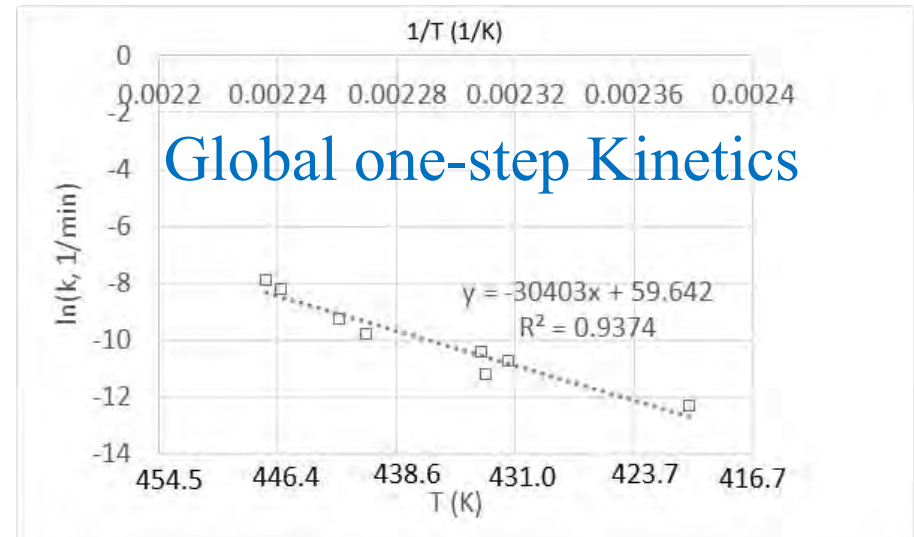
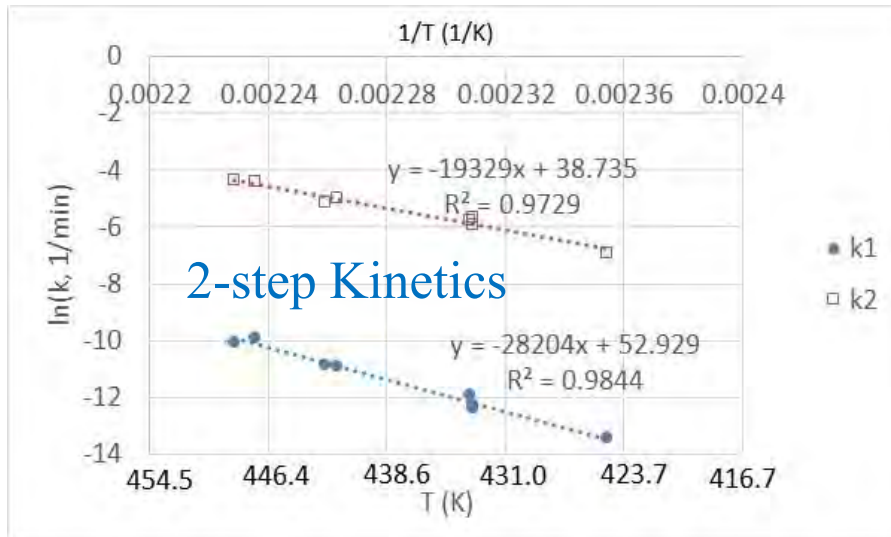
Confined Test Con114: 5.05% mass loss

Confined



Vented Test Con115: 2.93% mass loss

Vented

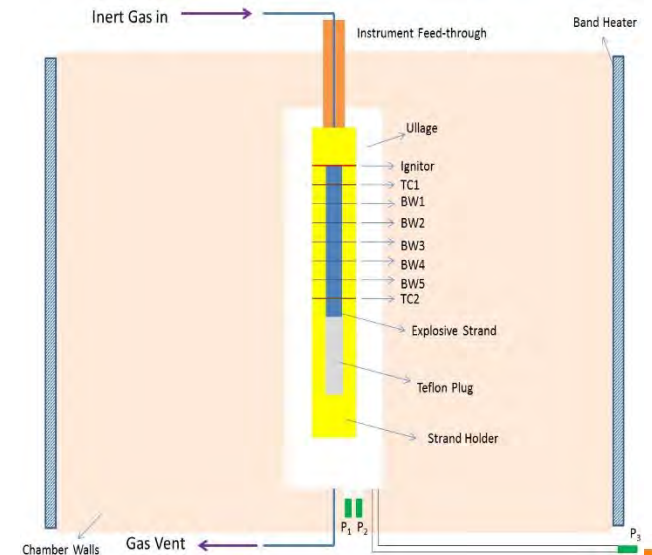
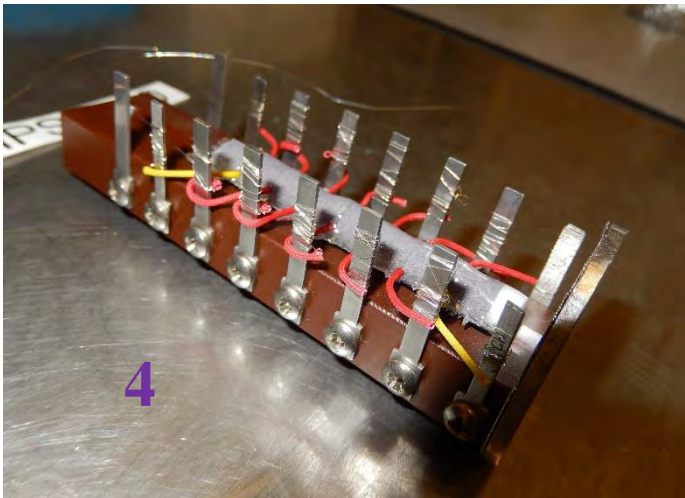
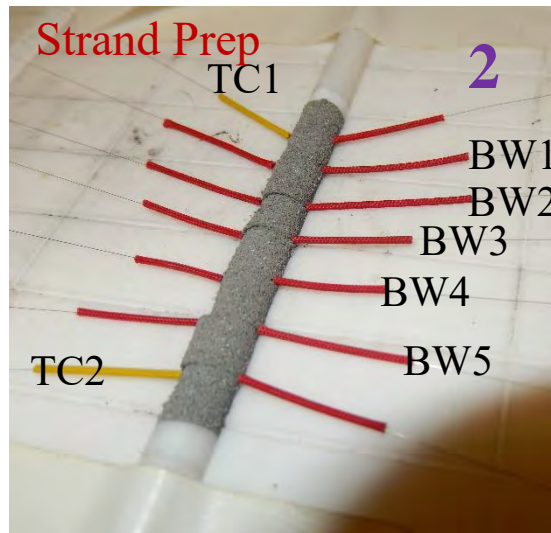
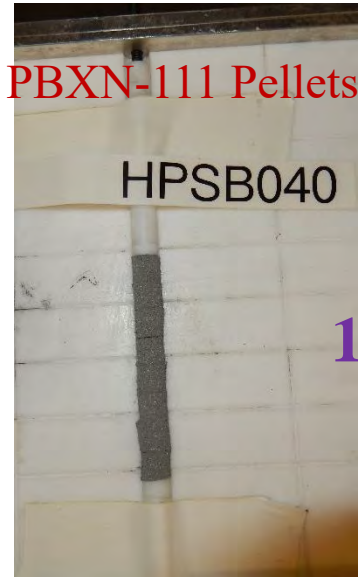


Thermal degradation rate increases with confinement

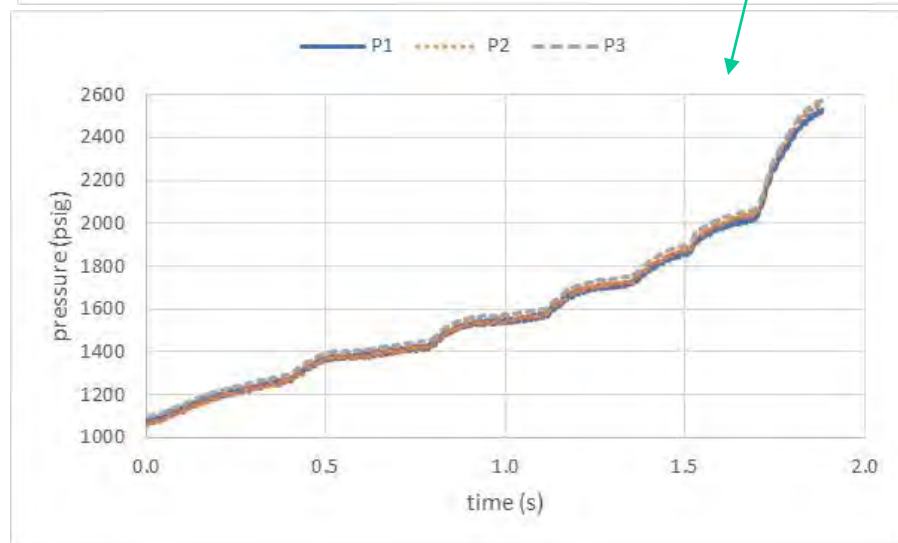
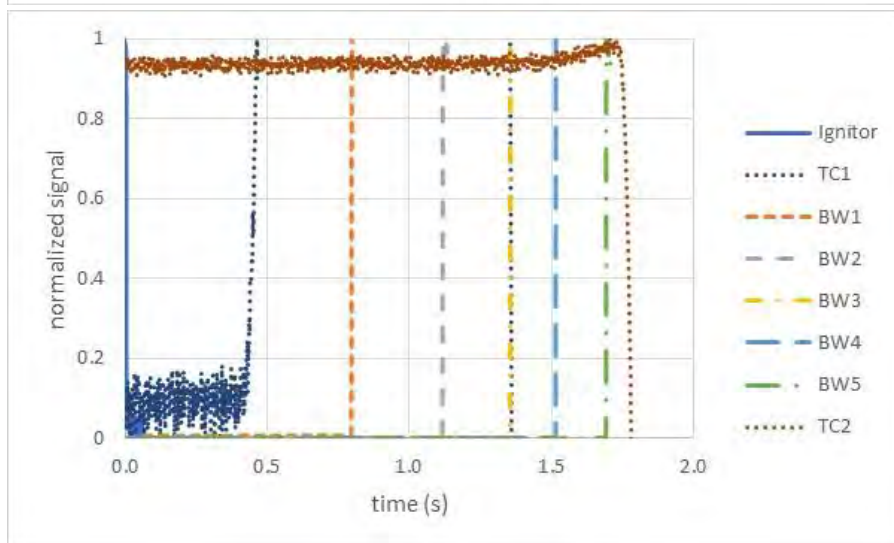
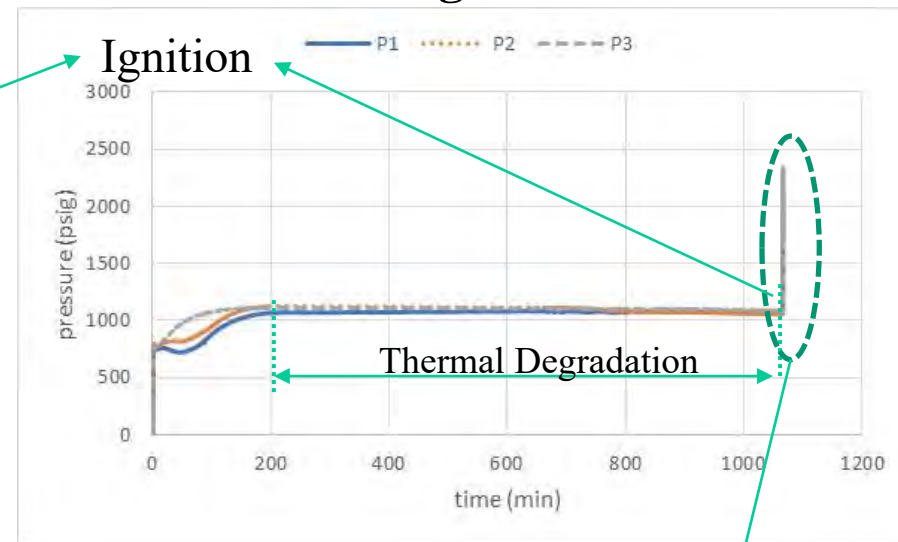
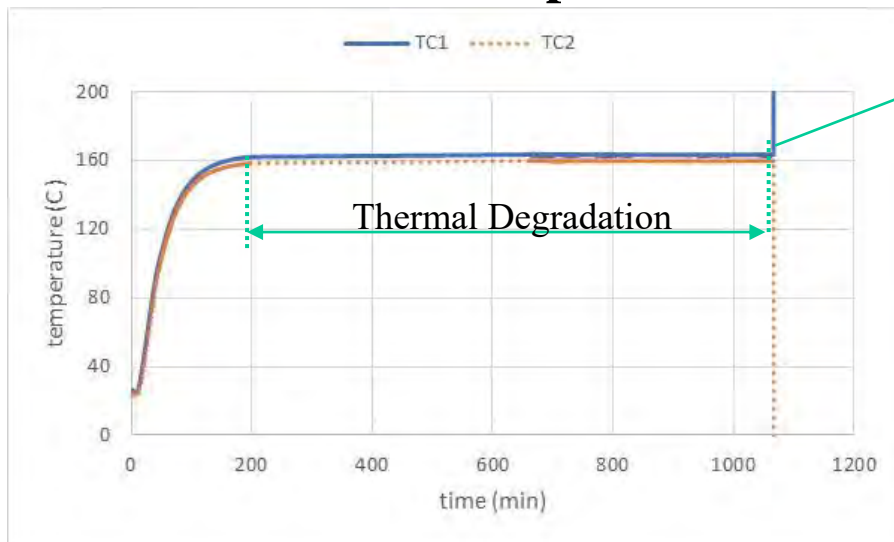
Step 2. Burn Rate of PBXN-111

- Measure burn rates vs. T , P and extent of thermal degradation (ϕ) in a strand burner
- 3 types of PBXN-111: pristine (2 tests), heated (4 tests) and thermally degraded (4 tests)
- Test procedure
 - Install ignitor, 2 thermocouples and 6 break wires in a PBXN-111 strand made from 8 cylindrical (1/4"×1/4") pellets
 - Fill strand burner with an inert gas to target initial pressure
 - Heat the entire strand burner to a desired temperature and hold to induce thermal degradation
 - Ignite the vertically oriented explosive strand at the top
 - Detect burn front arrival at various locations, $x(t)$, using the thermocouples and break wires
 - Record $P(t)$, $T(t)$ and $x(t)$
- Data analysis: In each test,
 - For various $T(t)$, calculate ϕ at end of heating period using the kinetic rates model
 - Generate $x-t$ plots for the combustion front for various P and for ϕ at end of heating period
 - Fit appropriate curves through the $x-t$ plots. Determine the burn rates and accelerations

Assembly Sequence

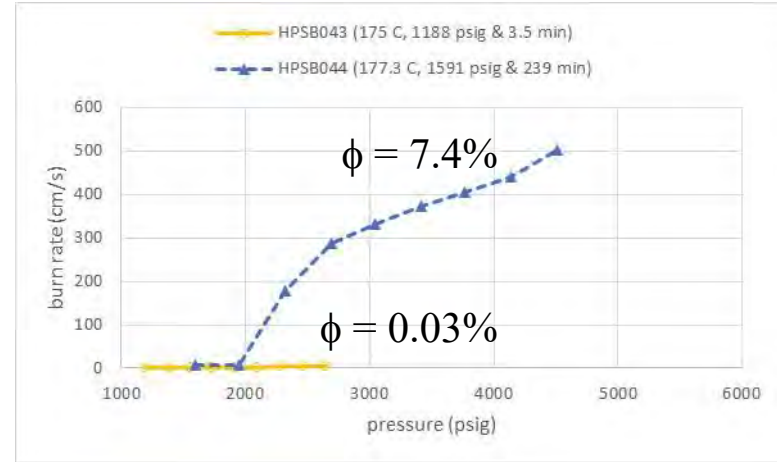
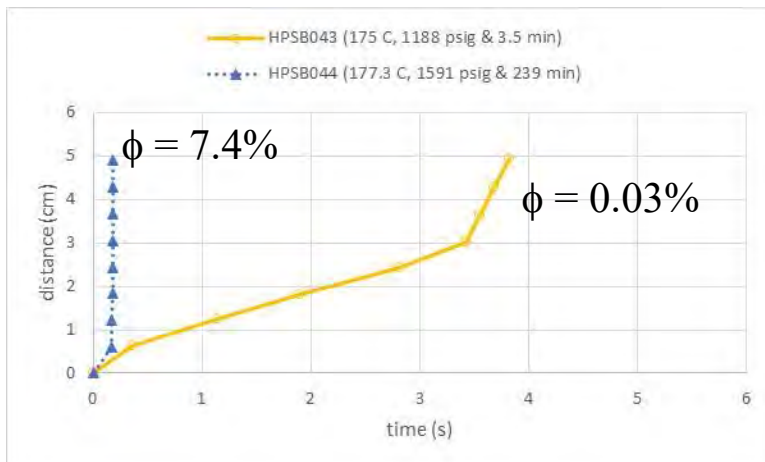
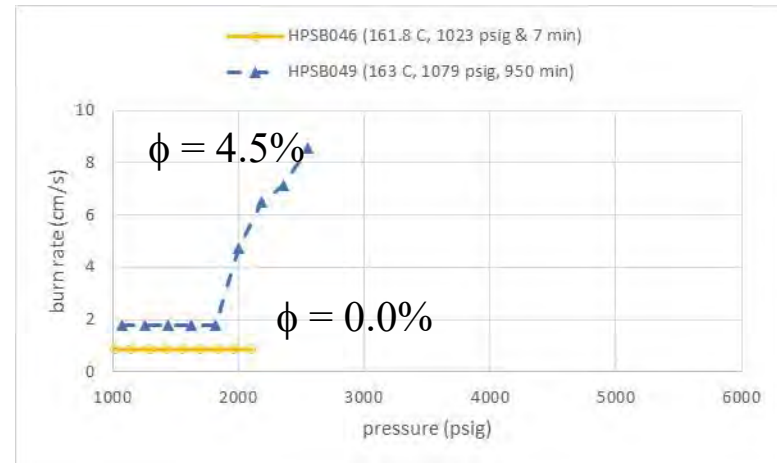
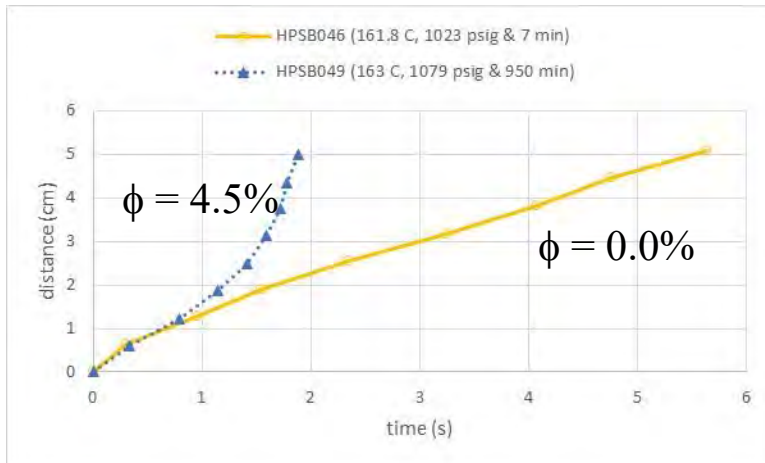


Sample Data from PBXN-111 Burn Test Strand Exposed to 160°C for 16 hours before ignition



Rates of burn propagation & pressure rise increase with time

Effect of Thermal Degradation on Burn Rate



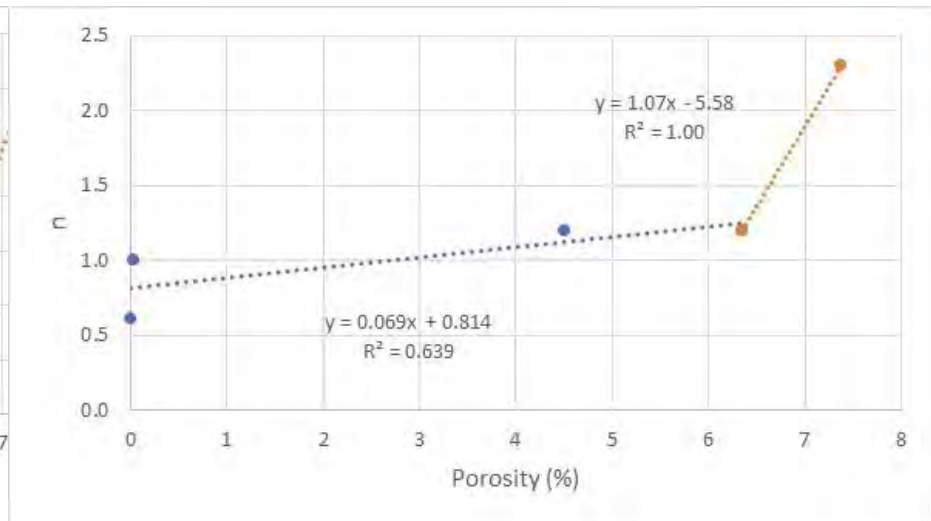
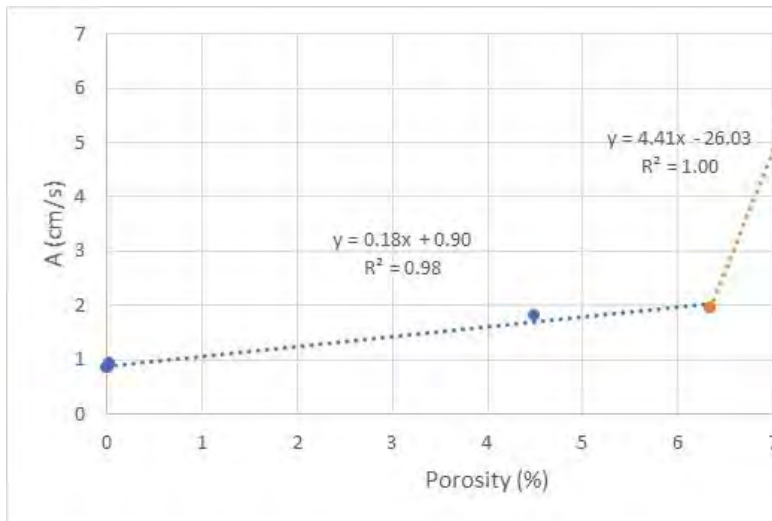
- Extent of thermal degradation (ϕ) estimated for each test using our kinetics model
- Undegraded PBXN-111: burn rate constant, but increases at 2000 psig
- Degraded PBXN-111: (i) $P < 2000$ psig: constant burn rate; (ii) $P > 2000$ psig: burn front accelerates with increasing ϕ and P

Burn Rate Model

$$u = A(\phi) \times P^{n(\phi)}$$

$$P < 2000 \text{ psig} \begin{cases} A = f(\phi) \\ n = 0 \end{cases}$$

$$P > 2000 \text{ psig} \begin{cases} A = 0.22 \text{ cm/s/MPa}^n \\ n = f(\phi) \end{cases}$$



- ϕ = extent of thermal degradation related to porosity (%) assuming uniform mass loss
- Slopes of burn rate parameters vs. P curves increase significantly at $\phi > 6.35\%$
- u : cm/s, P : MPa

Step 3. Model Development

A. Ignition Sub-Model

- Fast running 1-d model

- Inputs

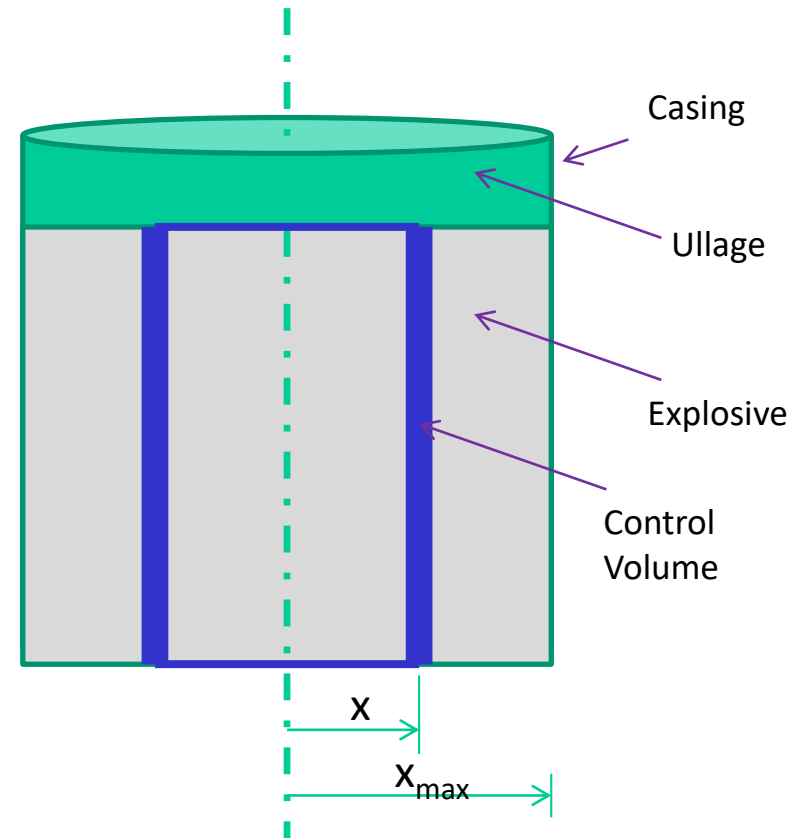
- Geometry: explosive & casing
- Heating: $T_{\text{initial}} \rightarrow T_{\text{soak}} \rightarrow T_{\text{final}}$ and durations
- Venting: onset P for venting and vent diameter

- Model tracks

- Heat conduction, thermal expansion
- Thermal degradation and morphology changes
- Venting: shift in reaction kinetics
- Changes in P : (i) heat & gas generation from degradation reactions, and (ii) venting losses
- Ignition when T inside explosive $\gg T_{\text{wall}}$

- Outputs

- $T(x,t)$, $\phi(x,t)$ and $P(t)$
- Occurrence of ignition: its time and location

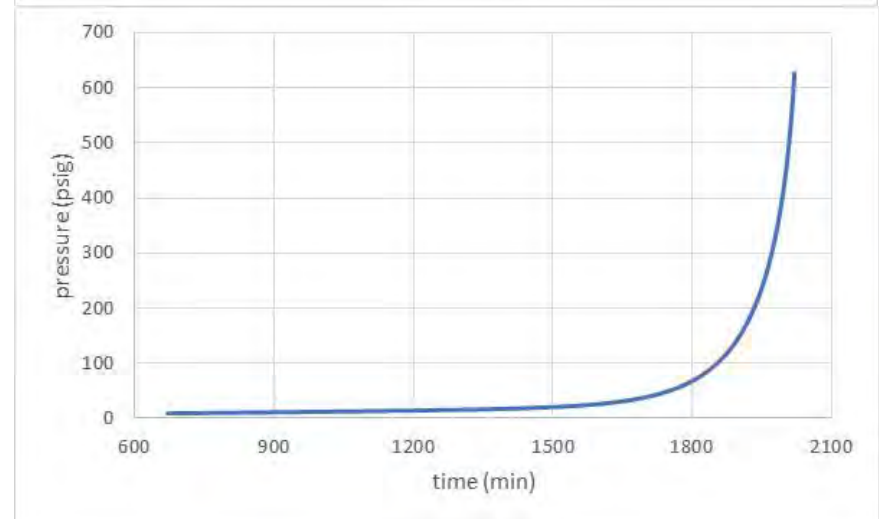
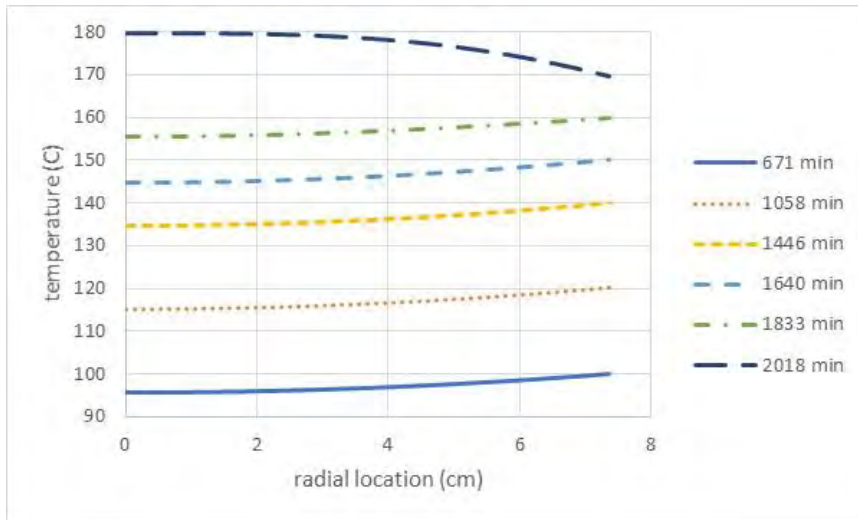
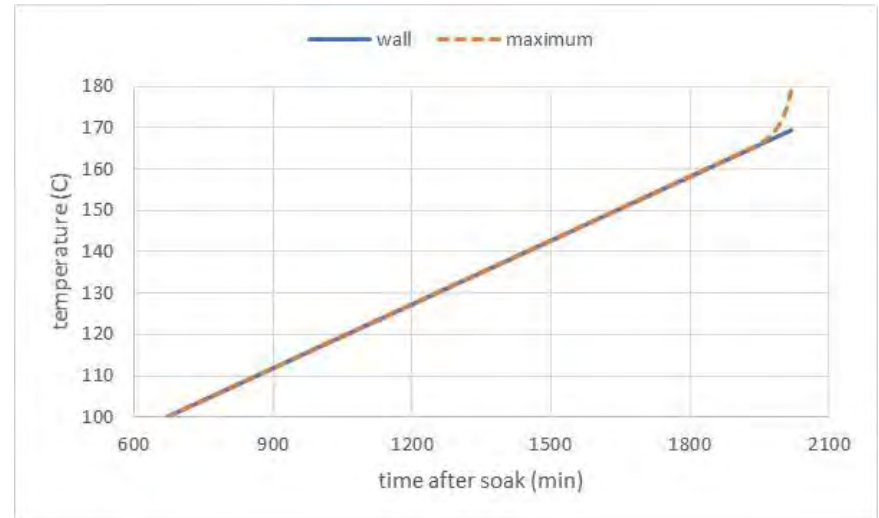


Sample Calculation: Navy Sub-Scale Test 1

- 6690 g (D ~ 14.74 cm, L ~ 21.9 cm) [1,2]
- Heating Profile: 8 hour soak at 65.6°C, then 0.052°C/min until ignition

	Test	Model
Ignition Time, min	1960	2018
T_{wall} @ ignition, °C	166.5	169.6

- Model predicts $T(x,t)$, P and ϕ that are difficult to measure accurately



[1, 2] Beckett, et al, 39th PEDCS, JANNAF Meeting, Salt Lake City, Utah, 12/7-10/2015.

B. Combustion Sub-Model

- Fast running engineering model

- Inputs

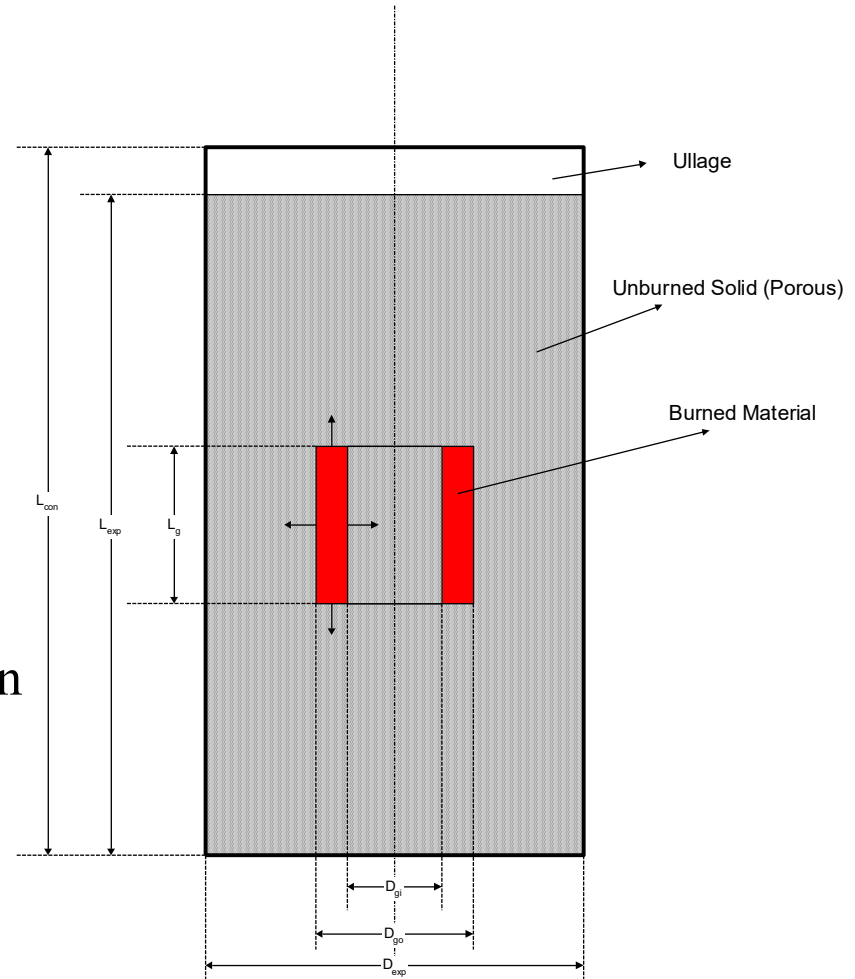
- Geometry: explosive & casing
- Ignition location
- Conditions at ignition: T , P , ϕ
- Vent onset pressure and diameter

- Model tracks

- Burn front propagation
- Heat/gas generation by combustion
- Energy losses from burned region

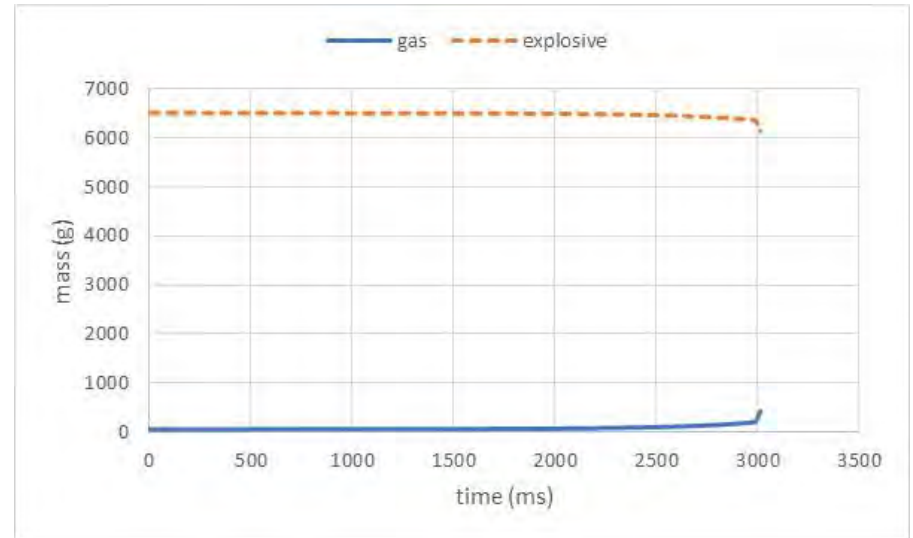
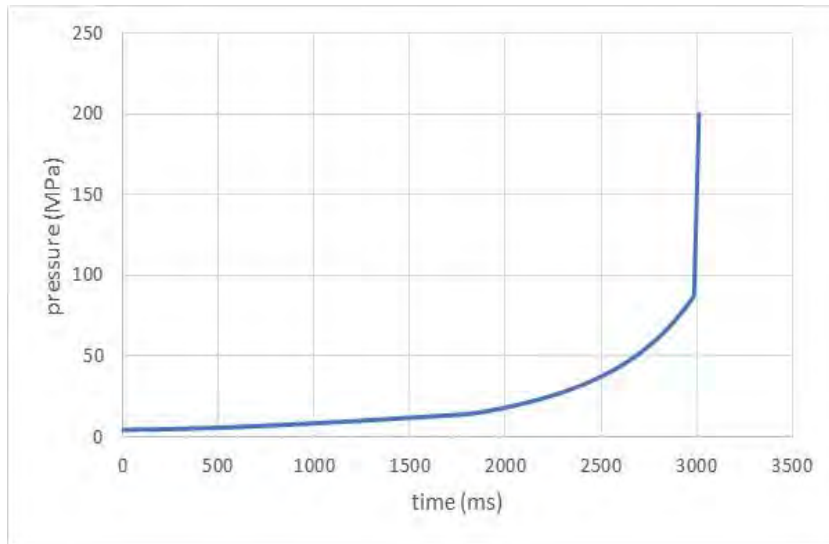
- Model outputs

- $P(t)$, $T_{burned}(t)$, $m_{exp}(t)$, dimensions of burned region vs. t



Sample Calculation: Navy Sub-Scale Test 1

- 6690 g of PBXN-111 (D ~ 14.74 cm, L ~ 21.9 cm) [1,2]
- Ignition location: explosive center
- Conditions at ignition:
 - Pressure = 626 psig (4.3 MPa)
 - Mean porosity ~ 0.4%
- Container assumed to fail at 200 MPa → we stopped the combustion calculation



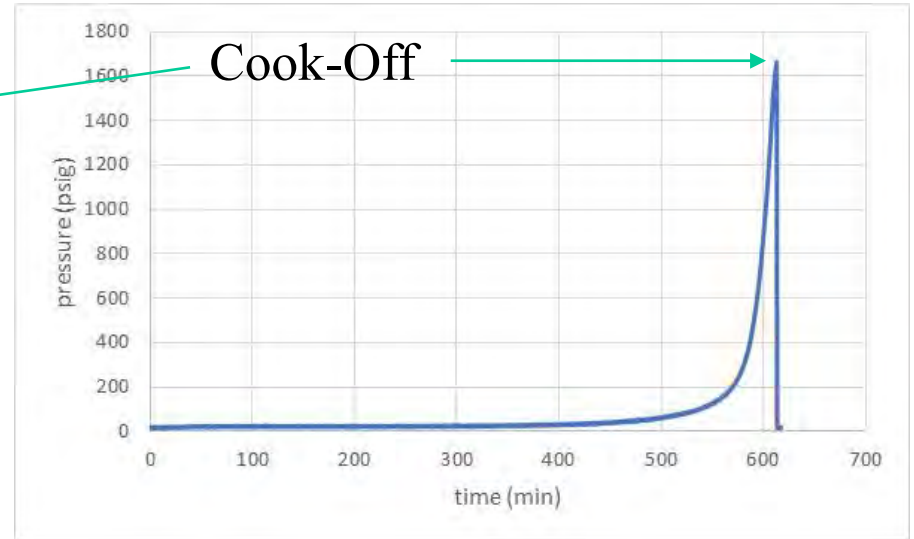
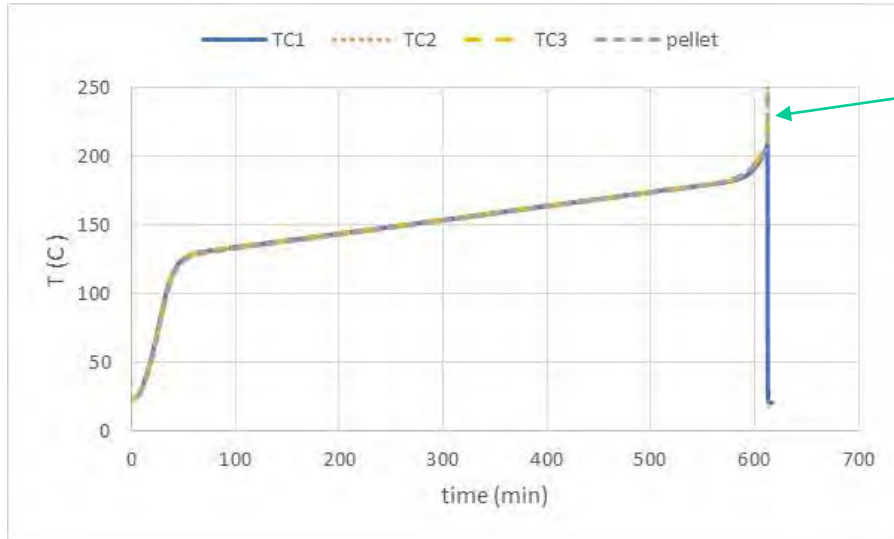
[1, 2] Beckett, et al, 39th PEDCS, JANNAF Meeting, Salt Lake City, Utah, 12/7-10/2015.

Step 4. Model Validation

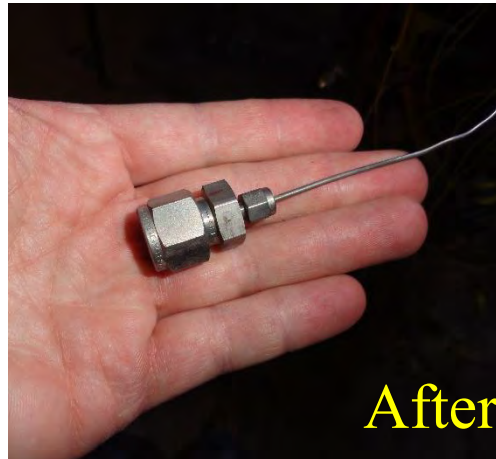
- **Limited literature data to validate ignition model and none for combustion model**
- **BlazeTech/SNL performed 8 small-scale cook-off tests to generate additional data:**
 - 2 confined, 2 vented, 4 small leaks. Violent cookoff did not occur in tests with venting: we used the occurrence of significant self-heating as indicative of ignition

	BlazeTech/SNL	VCCT [3]	Sub-scale [1, 2]	Max/Min of Range
Explosive Mass (g)	2.09	57.6	6690	3200
Explosive Radius (cm)	0.309	1.27	7.37	24
Explosive Length (cm)	3.8	6.35	21.9	5.8
Ullage Volume (%)	45	~10	~10	4.5
Final Heating Rate (°C/min)	0.05 to 0.406	0.055	0.0515 to 0.479	9.6

Data from Cook-Off Test at 0.1°C/min

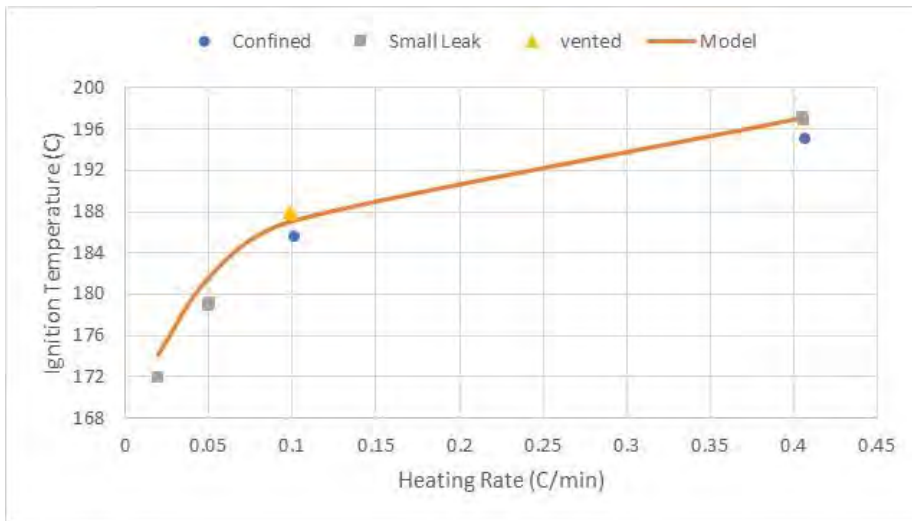


Before Test

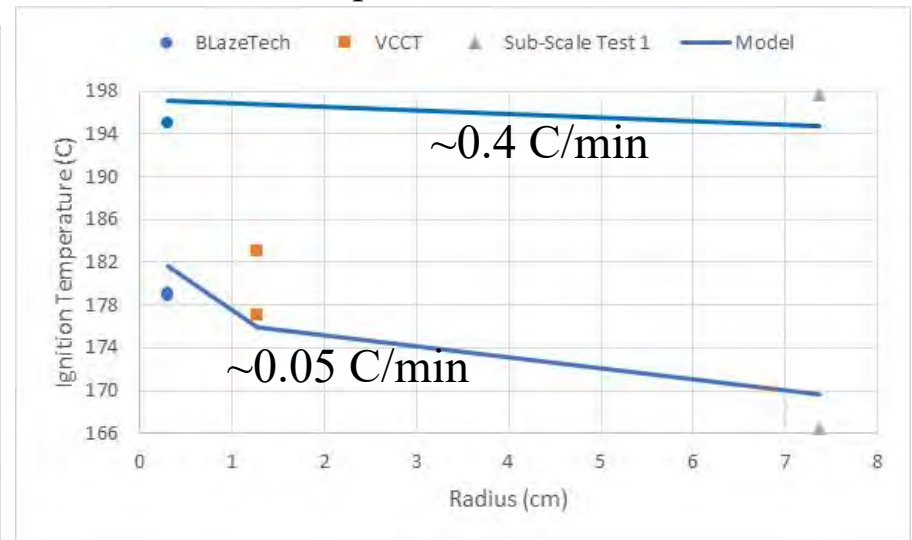


T_{ignition} for Various Sub-Scale Cook-Off Tests: Model Predictions vs. Measurements

Effect of Heating Rate on T_{ignition}
BlazeTech/SNL Tests, $R = 0.309$ cm



Effect of Scale on T_{ignition}
Three Separate Studies



- Ignition temperature (i) is almost independent of venting, (ii) increases with heating rate, and (iii) decreases with increasing size
- Model predictions agree well with a range of test data

Effect of Venting on Slow Cook-Off

- Venting affects thermal degradation reactions and combustion of PBXN-111
- Effects on thermal degradation (before ignition)
 - Gaseous reaction intermediates/products are released from the munition
 - Thermal degradation at a given T is slower for vented than confined material
 - A small vent at a low P could prevent pressure buildup
- Effects of venting on burn rate, u (after ignition)
 - u depends on extent of thermal degradation and P which is lowered by venting
 - $P < 2000$ psig, u remains constant
 - $P > 2000$ psig, u increases and may accelerate (depends on degradation)
 - Early and adequate venting to ensure that $P < 2000$ psig will reduce SCO violence
- Our small-scale cook-off tests on PBXN-111 have shown that
 - Completely confined material underwent violent cook-off (case fragmentation)
 - Vented material (leak in casing) underwent self-heating but not violent cook-off

Conclusions

- **From testing and analysis, we have quantified:**
 - The pre-ignition thermal degradation rates = $f(T, t$ and confinement)
 - The post-ignition burn rate, $u = f(P \ \& \ \phi$ at ignition), u can vary by orders of magnitude with a threshold in sensitivity ~ 2000 psig
- **We developed an engineering model of cook-off using these rates. It predicts:**
 - The time and spatial evolution of T , thermal degradation, burn front, unburnt and burn mass as well as $P(t)$, the latter is indicative of severity
 - The ignition temp. increases with heating rate (for a given size) and decreases with size (for a given heating rate), which is validated by the available data
 - We seek additional data for model validation
- **The model outputs can be coupled to a structural code to predict case fragmentation and collateral damage**
- **Our work can be extended to other munitions and used in the design of future tests and of vents**

INSENSITIVE MUNITIONS INDUSTRY CONTRIBUTION FOR NEW STANAG-AOP 4382 EDITION OF THE SLOW HEATING TEST

IMEMG's Expert Working Group on
Hazard Assessment & Classification

www.imemg.org

*Prepared by Yves Guengant
Presented by Dr Paul Deacon*

- European Organisation assembling twenty one leading armament groups working with Insensitive Munitions technologies



IMEMG express the armament industry's viewpoint with regards to relevant transnational regulations and requirements.

Expert Working Groups:

- Computer Models for IM Performance,
- Cost & Benefit Analysis,
- Effects of Ageing,
- Fast Cook-off Test Procedure,
- Hazard Assessment & Classification.

Hazard Assessment & Classification Expert Working Group presents this analysis

IMEMG's Expert Working Group on Hazard Assessment & Classification

- **ArianeGroup SAS** FRANCE
Yves GUENGANT
- **CEA-DAM**
Frank DAVID-QUILLOT
- **MBDA-France**
Michel VIVES
- **NEXTER Munitions**
Frederic NOZERES
- **ROXEL France**
Laurent BONHOMME
- **THALES LAS France SAS**
Carole FOURNIER

- **TDW GmbH** GERMANY
Dr Werner ARNOLD
- **Rheinmetall Waffe Munition GmbH**
Dr Gerhard HUBRICHT

- **RWM Italia SpA** ITALY
Massimo CASTIGLIA

- **AWE Plc.** UK
Pr Malcolm COOK
- **BAE Systems – Land UK**
David SIMMONS
- **MBDA (UK) Ltd**
Sean RANDALL

INTRODUCTION

- Various works are conducted by AC326 National Experts in the aim to define the new edition of STANAG-AOP 4382
- Technical arguments for changes can be extracted from the MSIAC Survey Questionnaire on the Slow Heating Test (December 2016) and the MSIAC Science of Cook-off workshop (March 2017)

- The most important question is about the heating rate value : $3,3^{\circ}\text{C}/\text{h}$
 - *Reasons for a change ? If modification, which new value ? And why ?*
 - *Must heating rate represent the most severe accident scenario or the most severe munition response ?*
- STANAG-AOP are under responsibility of National Experts, nevertheless IM Manufacturer Designers can bring feed-back and improvement suggestions

- IM Manufacturer Designers are concerned about objectives of the Slow Heating Test
 - *Must test represent the most severe accident scenario or most severe munition response ? It implies various test parameters ...*
 - » *heating rate value : unique value or according to munitions size*
 - » *heating system : forced airflow or natural convection*
 - » *preconditioning temperature and duration : today unclear rules*

- Major question is about the maximum response to slow heating : Type V
 - *It is pertinent if we consider that this threat can occur only in a closed space ?*
 - *projections and propulsion effects will be confined in this space without any external effect*
 - **Type IV** response requirement appears to be more appropriate

THE HEATING RATE VALUE

THE HEATING RATE VALUE

- Slow Heating Test is performed with 3,3°C/h rate for 3 decades and ...
 - Is change really necessary ?
 - Why not, if the new heating rate is representative of the **most severe accident scenario**, it is the responsibility of AC326 National Experts
 - But, really there is a real concern if it must be representative of the **most severe munition response**, because :
 - » it depends on munition size and architecture
 - » it depends also on energetic material (cast-cured, melt-cast ...)
 - » that it could introduce disconnectedness between nations and test centers

HEATING DEVICES

HEATING DEVICES

- STANAG 4382 ed2 “The test is **usually** performed by placing the test item in a disposable oven and heating the item with circulating heated air”
 - Is forced airflow the most representative of accidental scenario (circulating steam) ? Or is it the natural convection (battleship magazine) ?
 - It would be preferable to define more precisely the heating devices

PRECONDITIONING PHASE

PRECONDITIONING PHASE

- STANAG 4382 ed2 “precondition the test item **at 50°C for 8 hours** or until the test item reaches thermal equilibrium at 50°C, whichever occurs first”
 - Why this preconditioning phase ? Maximum ambient temperature ?
 - This requirement is not pertinent for large munitions because 8 hours are insufficient to reach thermal equilibrium ...
 - It would be more simple to start test at room temperature, global test duration would be more or less same

THE TYPE V RESPONSE TO SLOW HEATING

RESPONSE TO SLOW HEATING

- Slow Heating Threat corresponds to "Fire in an adjacent magazine, store or vehicle" with heating rate from 1°C to 30°C per hour"
- if an accidental scenario is able to heat munitions:
some ten hours, higher than 150 to 300°C (300 to 500°F),
- this scenario requires a **closed space**: magazine battleship, armored vehicle, storehouse, bunker, igloo... **but not in open field conditions**



RESPONSE TO SLOW HEATING

- is it pertinent to require a Type V response ?
 - No-hazardous effects beyond 15 meters.
- i.e. it is reminded that the “20 Joules fragment” is not able to go through only 2 mm thick aluminum sheet (*test 6c UN Orange Book ST-SG-AC10-11 Rev6*).
- i.e. Typical walls of warships ammunition stores are some 8 mm thick steel sheets ...
 - ➔ **Type IV seems be a sufficient requirement for such a threat !!!**

CONCLUSIONS AND PERSPECTIVES

CONCLUSIONS

- Concerns about objectives of heating rate modification
- Need for more precise STANAG-AOP 4382 requirements
- Change the maximum response from **Type V to Type IV**
 - because the **Type V effects are contained** inside the confined space (battleship magazine, underground store, armored vehicle ...) where the slow heating threat can occur (some ten hours up to higher than 150 to 300°C)

www.imemg.org

For PowerPoint distribution

yves.guengant@ariane.goup

An Explosive Fragment Projector for IM testing

G.G. Goviazin, R.E. Ceder, T. Eliash
Rafael, Manor – Advanced Defense Technologies Division
ISRAEL
Email: talel@rafael.co.il

Abstract

Fragment Attack (FA) testing, as described in STANAG 4496, calls for a specific fragment shape, material and velocity. Usually this is achieved by accelerating a fragment in a long barrel, powder or light gas gun. This method requires heavy infrastructure, binding FA tests to stationary facilities. At Rafael, the need for a mobile FA test apparatus had led us to use specially designed Explosively Formed Projectiles (EFP) as substitutes for the STANAG fragment. We call this method Modified Fragment Impact or MFI. In this method the EFP has the needed mass and velocity but is roughly spherical in shape and made of copper rather than steel. Another advantage of this method, besides being portable, is its accuracy both in velocity and in aim.

The objective of this work is to develop a new explosive charge and test set-up that will have the advantages of our EFP test method while projecting a fragment at the velocity, with shape, mass and material as required by the STANAG. The design process includes both hydrocode calculations and characterization of the performance through testing of selected designs.

Introduction

The Fragment Attack (FA) test is described in STANAG-4496 [1]. This procedure specifies a steel fragment of 18.6 g, made of mild steel, 14.30 mm in diameter and 15.56 mm in length, with a conical nose. The specified impact velocity is 2530 m/s. An alternate velocity of 1830 m/s is also specified in the STANAG. The means for accelerating the fragment to the desired velocity is usually a long barrel powder gun or a light gas dual stage gun. While this is a precise and common method, it requires a considerable investment in heavy infrastructure and maintenance. Typical setup time needs to account for activities such as sighting shots, propellant conditioning etc. [2, 3]. In addition, cost considerations require the gun to be protected from the detonation of the test item.

An alternate method which is relatively low-cost and mobile is the use of Explosively Formed Projectiles (EFP). This method was suggested for IM testing in the past for both copper and mild steel projectiles [4,5,6]. The disadvantage of this method is that the shape of the fragment differs from the STANAG requirements. At Rafael, the need for a mobile FA test apparatus has led us to use this method which we call Modified Fragment Impact or MFI [7]. In addition to its mobility, the tight manufacturing tolerances of the EFP charge yields consistent fragment velocity and shape thus reducing the need for a pre-test shot.

Several other designs were suggested as explosive fragment projectors such as the explosively driven light gas gun [8] or an explosive charge specifically designed for this purpose [9] which was based on the work of Held [10, 11]. These designs have the advantages of being portable and inexpensive but used a large explosive charge of ~4 kg and ~5-8kg respectively, resulting in an undesirable parasitic blast in the test arena.

The need to decrease the amount of high explosive incorporated in the test, served as motivation for the present work. By maximizing the effect of the charge confinement, we aimed to accomplish this goal. This approach, however, can decrease the explosive amount up to a certain physical limit. In order to decrease the explosive mass beyond this limit, we employed the Munroe effect by constructing a shaped charge like design. We will present the hydrocode simulations and experimental results achieved.

1830 m/s charge

This design aimed to maximize the use of the explosive's energy by placing a thick confinement around the charge. Thus one can utilize the detonation products' pressure on the fragment for a longer duration. The preliminary design was modeled, using The Autodyn® 2D Lagrangian-Eulerian coupled solver, and had a charge of 1.2 kg of LX07 with an infinite rigid boundary condition, in order to achieve the standards' alternate velocity of 1830 m/s. Later on we replaced the boundary condition with a steel case (Figure 1).

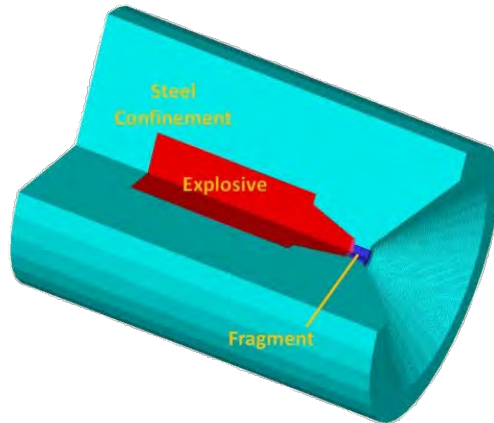


Figure 1 – Preliminary Autodyne model for a 1830m/s charge

The results of the simulation are shown in Figure 2: The fragment's shape after the acceleration process is unaltered and as can be seen from the time-velocity curve, the final velocity is ~1830m/s as required.

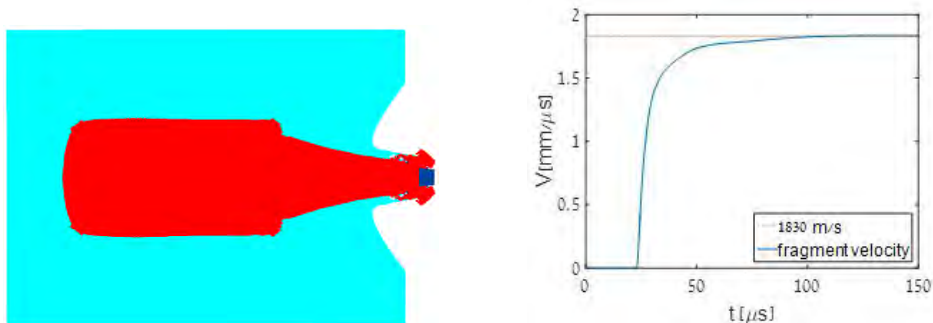


Figure 2 – 1830 m/s charge simulation result

This design performance was evaluated in a live test. In the detailed design we replaced the explosive fill from LX07 to a cure-cast explosive– PX91 (a formulation similar to PBXN110) and added the required features needed for the detonation chain and handling (Figure 3).

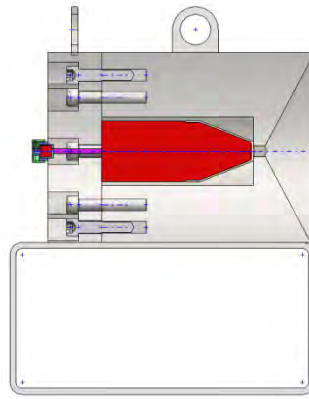


Figure 3 – 1830 m/s charge design

The test setup consisted of water containers placed around the charge due to safety requirements. Two flash x-rays were used to evaluate the shape and velocity of the fragment (see Figure 4).



Figure 4 – 1830 m/s charge test setup

The fragment velocity measured from the x-ray image was only 1650m/s. It is presumed that the front part of the confinement came apart sooner than predicted and as a result the pressure was released earlier. However, as can be seen in Figure 5 the fragment kept its shape.

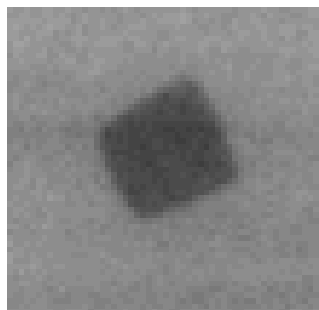


Figure 5 – 1830 m/s fragment test X-Ray image (1650m/s measured velocity)

This design shows a proof of concept regarding the efficiency of thick confinement in reducing the mass of explosive in the charge. Even though the velocity was not fully achieved, a high velocity was achieved with much less explosive than was done previously.

The fact that the fragment's shape was preserved is also a positive sign, since it already suffered its maximum loading at the beginning of the acceleration process. Further refinement of the confinement should achieve our design goals.

2530 m/s charge

The second effort we took was to achieve the standard velocity of 2530 m/s. First attempts of doing so with the same basic configuration did not achieve the desired velocity and an increase of the charge diameter (and mass) seemed necessary. We decided to take a different approach and instead of enlarging the charge we thought on using the Munroe effect to "focus" the detonation products' effect on the fragment. The preliminary design was modeled as before and showed the desired velocity with a charge of 0.8 kg of LX07 under the same boundary configuration as the previous design. The efficiency of this approach is evident when we compare the explosive mass of 0.8 kg to 1.2kg needed to achieve the lower velocity described above, and more so compared to ~8 kg in [9] or ~4 kg in [8].

The preliminary model is shown in Figure 6.

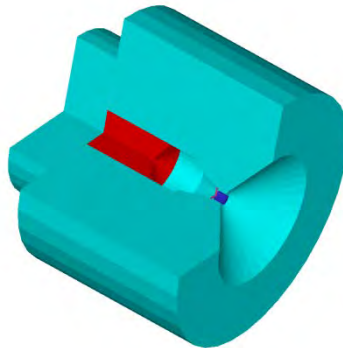


Figure 6 – Preliminary Autodyne model for a 2530m/s charge

The simulation results at two different times and the time-velocity curve as shown in Figure 7 demonstrate that the focused stream of detonation products on the fragment achieves the desired velocity.

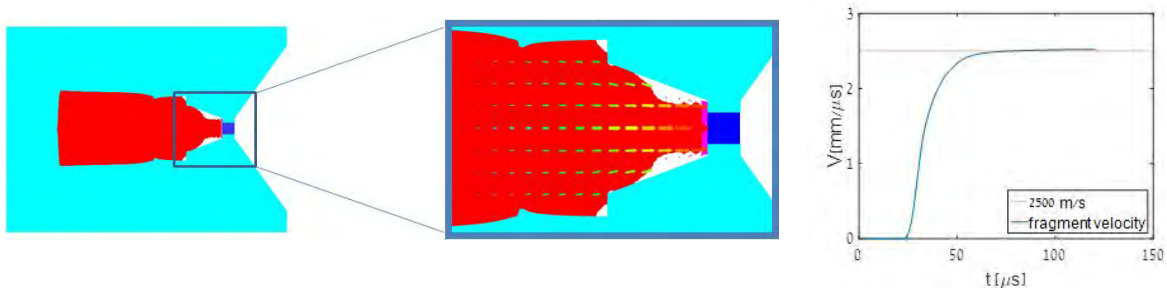


Figure 7 – 2530 m/s charge simulation result

This version was manufactured and tested after a detailed design process. We used PX91 explosive fill and redesigned the casting jigs to form the needed explosive shape. The design can be seen in Figure 8.

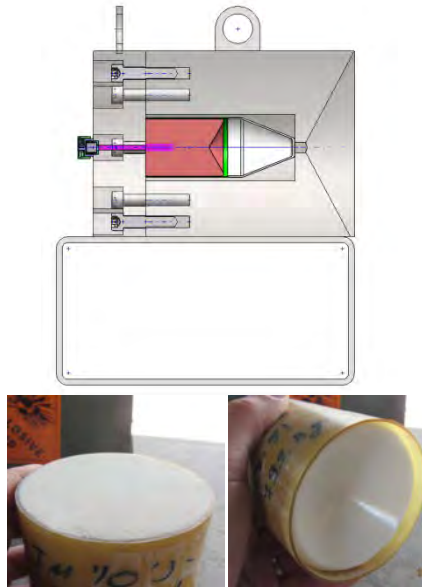


Figure 8 – 2530 m/s charge design

The charge's performance was also evaluated in a live test. The test setup was similar to the one used for the 1830m/s charge.

The fragment's velocity measured from the x-ray image was 2540m/s – well within the standard requirement. However, as can be seen in Figure 9, the fragment deformed beyond what could be regarded as an acceptable shape.

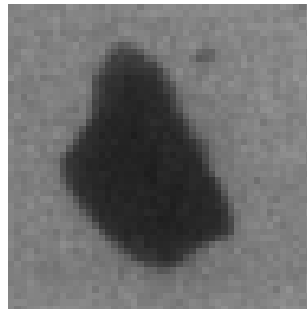


Figure 9 – 2530 m/s fragment test X-Ray image

Again this design shows proof of concept regarding the use of the Munroe effect in accelerating a fragment to the required velocity. With further refining of the design correct fragment shape could also be achieved.

Summary

Fragment Attack tests require test apparatus to accelerate the threat fragment. While a powder gun is the common way of achieving the fragment shape, velocity and accuracy requirements, it also has its limitations in terms of mobility and cost.

In this work we presented two designs aimed at achieving the STANAG requirements with an explosive charge using a much smaller charge than was demonstrated before. This was done by using the kinetic energy encompassed in the detonation products more efficiently. Two methods were employed: one based on heavy confinement and the other on a focused stream of detonation products (Munroe effect).

It was found that the second method has a greater potential for accelerating fragments for high velocities using relatively small amount of explosive (an order of magnitude smaller than previous attempts [9]). The challenge of preserving the fragment's shape in this method will be addressed in future work.

Acknowledgments

We would like to thank D. Henig and G. Kleiminz for assisting us in performing the experiments and for numerous fruitful discussions.

References

1. Fragment Impact, Munitions Test Procedure, STANAG 4496 Ed. 1, NATO Standardization Agency, Brussels, Belgium, 2006
2. Schultz, E. (2015) An international review of the STANAG 4496, Fragment Impact Test, 2015 Insensitive Munitions & Energetic Materials Technology Symposium, Rome, Italy, May 2017
3. Baker, E. L., Al-Shehab, N., Miers, K. and Pudlak, D. (2016), Insensitive Munitions Fragment Impact Gun Testing Technology Challenges. *Propellants, Explosives, Pyrotechnics*, 41: 572–579. doi:10.1002/prop.201600045
4. Tsur, D., and Miller, S., and Avnon, I., and Henik, D. (1994) EFP Charge as a Fragment Launcher in FI Test, Insensitive Munitions Technology Symposium, Williamsburg VA, 6-9 June 1994.
5. Lam, C. (Chanphu), McQueen, D. (Darren), Liersch, T (1997) Defence Science and Technology Organisation (Australia) and Aeronautical and Maritime Research Laboratory (Australia) An investigation into an alternative fragment projector for insensitive munitions qualification. DSTO Aeronautical and Maritime Research Laboratory, Melbourne, 1997.
6. Held, M. (2001), Fragment Tests after MIL-STD 2105 B. *Propellants, Explosives, Pyrotechnics*, 26: 144–147
7. Yarom, T. Blumberg Y., Rav-Hon M, (1999) Parametric study of explosive impact sensitivity using modified fragment impact method, Insensitive Munition & Energetic Material Symposium, Tampa FL, USA, November 1999.
8. Tanuay V., Brousseau, Sziri D., Batcheler P., Loiseau J., and Higgins A.J. (2007) Explosively Driven Gas Gun for Fragment Impact Test, 2007 Insensitive Munitions & Energetic Materials Technology Symposium, Miami, FL, USA, October 2007
9. Konig P.J and Smit B.T (2006) Establishment and Implementation of a Fragment Impact Test Capability, 2006 Insensitive Munitions & Energetic Materials Technology Symposium, San Francisco, CA, USA, November 2006
10. Held, M. (2000), Single Fragment Generator. *Propellants, Explosives, Pyrotechnics*, 25: 8–12
11. Held, M. (2000), Tests of Unconfined Single Fragment Generators. *Propellants, Explosives, Pyrotechnics*, 25: 3–7.

Thermal modeling of fast cook-offs

Markus Graswald and Raphael Gutser

TDW Gesellschaft für verteidigungstechnische Wirksysteme mbH
Hagenauer Forst 27, 86529 Schrobenhausen, Germany

Abstract

Being fully compliant to Insensitive Munitions (IM) requirements is of utmost importance for today's and future munitions. The IM approach as defined in AOP-39 is typically performed by using insensitive plastic-bonded high explosives (PBX) and assessing IM states and mitigation technologies on warhead system, munition, and, if necessary, munition packing level. Among other IM hazards listed in STANAG 4439, thermal stimuli through fast cook-off heating are usually of particular interest for large warheads and bombs, since they may strongly drive the warhead system design and shall be evaluated at the earliest opportunity.

A simplified approach applies a transient FE model in ANSYS with a typical flame temperature profile that allows predicting temperatures and times during a fast cook-off. Such investigations are used to evaluate potential areas of hot spot forming and critical components that may indicate the need for specific mitigation measures.

In a new approach, a reaction kinetic model originally developed for modeling self-heating of explosive charges at slow cook-offs and implemented into COMSOL is adapted for fast cook-off simulations. Differential scanning calorimetry (DSC) tests of small explosive samples at fast heating rates provide input data required. Parameters for self-heating of the explosive charge are derived with AKTS-Thermokinetics software fitted to such experimentally determined heating curves. This data is eventually implemented into COMSOL simulating fast cook-off behavior of full-scale warheads. This results in an accurate prediction of spatial temperature profiles as well as reaction times and temperatures. In addition, mitigation potential through intumescent coatings on the casing are assessed that provide an effective insulation layer and lead to significant reaction time delays.

1 Introduction

Insensitive Munitions (IM) requirements are very relevant for today's and future munitions. Among all IM hazards listed in STANAG 4439 [1], thermal stimuli such as slow and fast cook-off (SCO / FCO) heating are particularly interesting, since they may have a significant impact on the design of warheads using large and / or strongly confined high explosive (HE) charges. A number of fast cook-off studies investigate the heat transfer of a fire on test vessels through both experimental and modeling means, e.g. [2, 3, 4]. The influence of wind on flame temperatures in a large-scale experiment of a truck-sized nuclear waste transport package are reported in [5]. Recent thermal analysis and modeling efforts apply

For further information: markus.graswald@mbda-systems.de, +49 (8252) 99-7264.

single-phase or multi-physics finite element (FE) models. Hunter et al. [6] couple an Arrhenius rate equation for self-heating with convection as primary heat transfer mechanism. In a multi-physics finite element (FE) approach using COMSOL [7], time-dependent temperature profiles of experiments with variable confinement cook-off tests (VCCT) and a 105 mm artillery projectile using melt-cast Comp B charges are predicted.

TDWs IM assessment approach for thermal stimuli as outlined in Fig. 1 is based on AOP-39 [8] and starts with material tests for small HE charge samples followed by small-scale thermal testing, and a modeling & simulation phase. This helps to mitigate technical risks early in development programs and reduce both time and costs before full-scale IM tests are eventually performed on subsystem or system level for demonstrating IM compliance. [9] Results of an experimental and modeling slow-cook off study using confined small-scale test vessels filled with various high explosive (HE) charges have been published in [10, 11].

This paper presents a modeling and simulation study of a full-scale MK-82 warhead filled with TDWs insensitive and blast-enhanced KS22 (RDX/Al/Binder 67/18/15) high explosive charge. The fast-cook off modeling approach with heat transfer from the fire into the warhead and Arrhenius reaction kinetics for the HE charge is described in detail. A simplified approach of transient FCO simulations without reaction kinetics using ANSYS Mechanical provides initial results of critical parts and components. In a new approach, a reaction kinetic model is implemented into COMSOL and adapted for fast cook-off simulations. It provides an accurate prediction of reaction times, temperatures, and spatial temperature profiles and allows assessments of potential mitigation technologies.

2 Thermal modeling approach

Heat transfer from fires into solid media takes place through by conduction, convection, and radiation. At fast cook-off tests, the test vessel needs to be fully surrounded by flames. This results in heat transfer through radiation of the gaseous-solid mixture as major part and an inward convective flux as minor part, while an outward convective flux into the atmosphere can be neglected. Within the test vessel, conduction acts as main heat transfer process. When certain conditions are met, energetic materials inside the test vessel start to react resulting in burning or even more violent reactions that depend upon the high explosive properties, as well as confinement and venting conditions. Figure 2 visualizes this general heat transfer process.

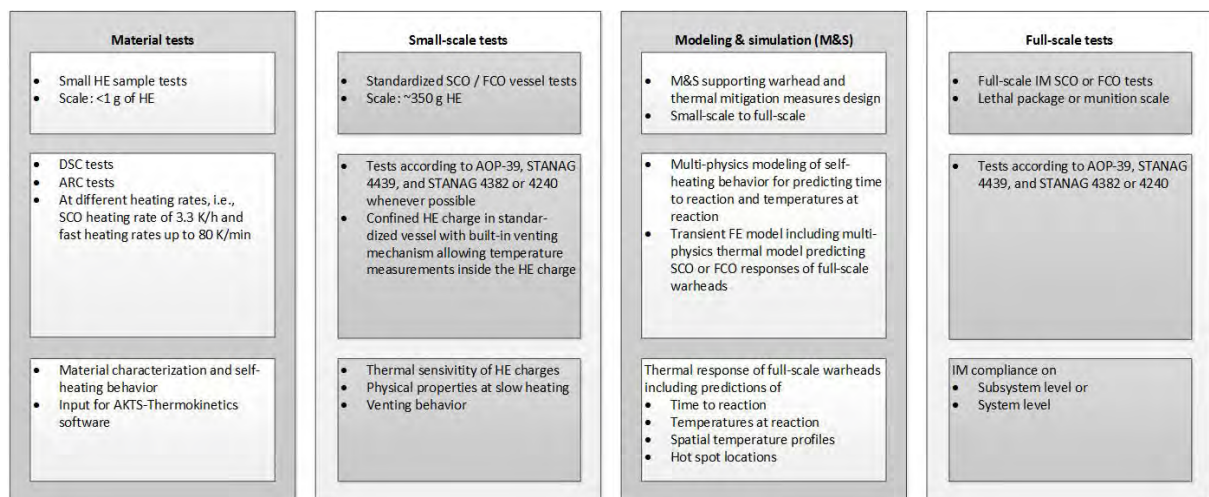


Figure 1. TDWs IM assessment approach for thermal stimuli.

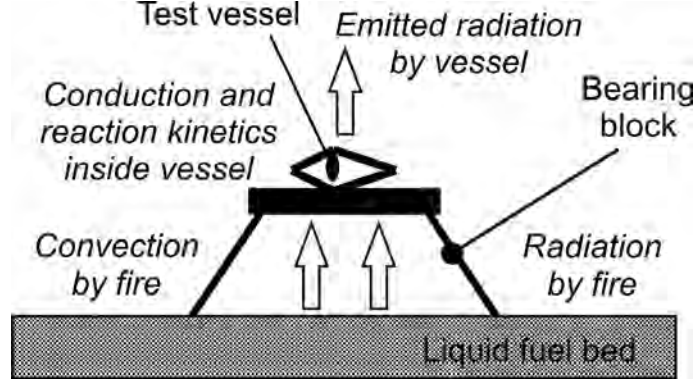


Figure 2. Schematic heat transfer process at fast cook-off tests.

Models simulating thermal responses can be mathematically described by coupling heat conduction with Arrhenius reaction kinetics via heat flux of the exothermal reaction [12]. Heat transport for thermal reactions of a high explosive charge can be modeled through a transient heat transfer equation in cylindrical coordinates r , since the test vessel is rotationally symmetric with its ends typically thermally isolated [13]:

$$\rho c_p \frac{\partial \theta}{\partial t} = \frac{1}{r} \frac{\partial}{\partial r} \left(r k \frac{\partial \theta}{\partial r} \right) + Q(r, t) \quad (1)$$

where ρ is the density, c_p is specific heat capacity, k is thermal conductivity, Q is the heat flux, t is the time, and θ is the temperature.

Heat transfer into solid media by conduction, convection, and radiation is simulated with ANSYS Mechanical 15.0 [14] and COMSOL Multiphysics 5.3a [15]. The latter allows the use of a global equation model for implementing reaction kinetics. Quadratic shape functions are used for the Lagrangian elements. Temperature dependent thermal conductivities and specific heat capacities were used for most materials in the simulation. Various boundary conditions were applied to account for the heat exchange with the environment. The inward convective heat flux q_{con} from the atmosphere is defined by

$$q_{con} = h(\theta_{ext} - \theta) \quad (2)$$

where θ_{ext} is the ambient temperature within the atmosphere. The temperature dependent heat transfer coefficient h is determined using an analytical equation for the turbulent heat transfer through the gas media in the flame profile close to the boundary. The ambient-to-surface radiative flux is the difference between absorbed and emitted radiation and described by:

$$q_{rad} = \varepsilon \sigma (\theta_{ext}^4 - \theta^4) \quad (3)$$

where ε is the emissivity and σ is the Stefan-Boltzmann constant. Emissivity of the fire is one according to black bodies. Table 1 gives an overview on boundary conditions applied.

Multi-physics coupling to global equation (1) is realized by adding a volumetric heat source term Q through the following equation:

$$Q(r, t) = q \frac{\partial \alpha}{\partial t} = q A_\alpha f(\alpha) e^{-\frac{E_\alpha(\alpha)}{R\theta}} \quad (4)$$

Table 1. Thermal properties as boundary conditions and for energy release.

Material	Parameter	Value
Steel	Convective heat transfer coefficient	h in $W/(m^2 K)$ 15
Steel	Surface emissivity	ε in 1 0.7
KS22	Effective reaction rate	q_{eff} in K/s 10^4

where q is the heat of reaction ($q_{eff} = \frac{q}{\rho c_p}$), $A_\alpha f(\alpha)$ is a pre-exponential factor, $E_\alpha(\alpha)$ is an activation energy function for model-free reaction kinetics, R is the universal gas constant, and α describes the reaction progress. This reflects the self-heating of the system which is reproduced through internal heat generation coupling with model-free reaction kinetics.

AKTS-Thermokinetics software [16] was used to determine the corresponding functions for $A_\alpha f(\alpha)$ and $E_\alpha(\alpha)$ through differential scanning calorimetry (DSC) tests of small explosive samples with fast heating rates up to 80 K/min. Figure 3 shows these (normalized) curves for a KS22 charge. Further input data for simulations can be found in Tab. 2.

3 FCO simulations in ANSYS Mechanical

Transient FCO simulations of a MK-82 warhead were conducted in ANSYS Mechanical 15.0 [14]. A simplified approach without reaction kinetics was used assessing critical parts of such warhead designs and mitigation technologies within the scope of a prototype development phase. Figure 4 shows a simplified flame temperature profile applied for transient simulations.

Figure 5 visualizes a FCO response of the complete warhead and its high explosive charge after ten seconds. Due to the short time nature of such fast cook-offs, heat generated by the fire is absorbed primarily by the casing and the high explosive charge underneath. This high explosive charge made of KS22 features a comparably low thermal conductivity and, therefore, is effectively isolating the inner core within FCO timeframes. Maximum temperatures are, hence, observed in the HE layer directly underneath the casing. A fast cook-off reaction is expected being ignited within this layer.

4 FCO simulations in COMSOL Multiphysics

A more detailed analysis of FCO processes is possible using a multi-physics approach through COMSOL [15] with heat generation of hot spots forming and eventually inducing a chemical reaction. A flame temperature profile according to STANAG 4240 [17] as shown in Fig. 6 was applied enabling a predictive simulation capability. This temperature profiles reaches an ambient temperature of 550 degrees C after

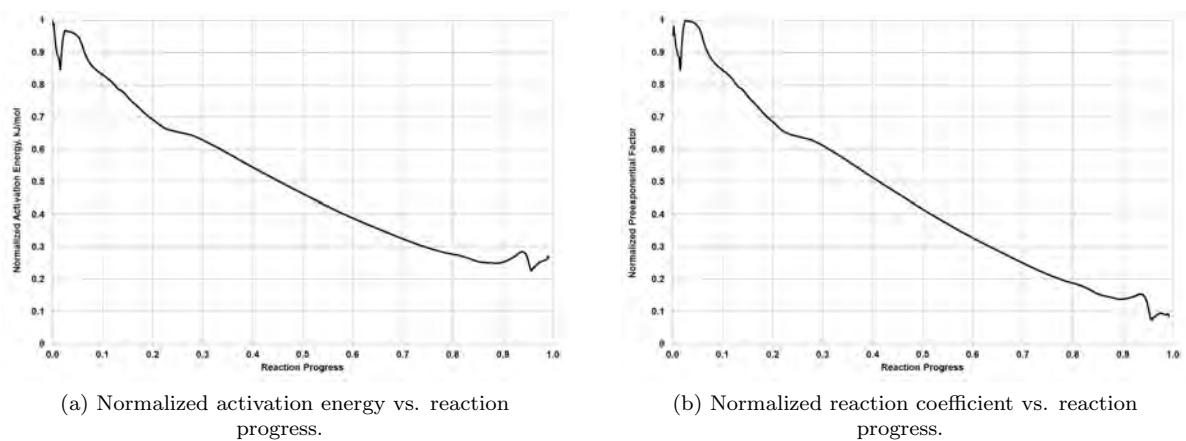


Figure 3. AKTS input data for a KS22a charge.

Table 2. Further input data for thermal simulations.

Material	Density ρ in kg/m^3	Thermal conductivity k in W/(m K)	Specific heat capacity c_p in J/(kg K)
Steel	7850	60.50	434
KS22	1650	0.40	1140
Coating A	270	0.25	840
Coating B	270	0.10	840

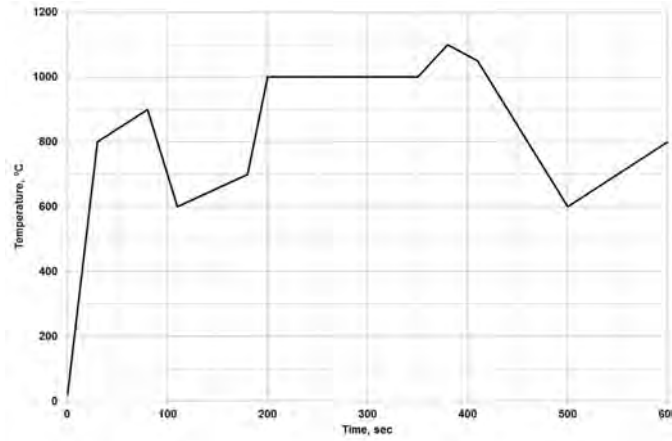
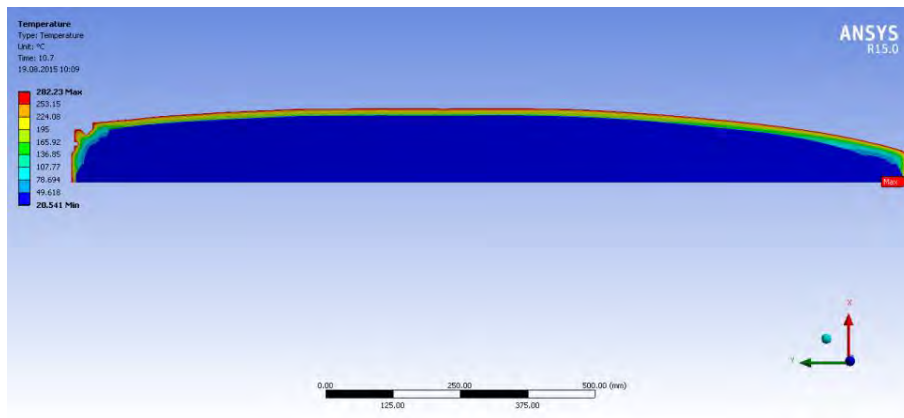
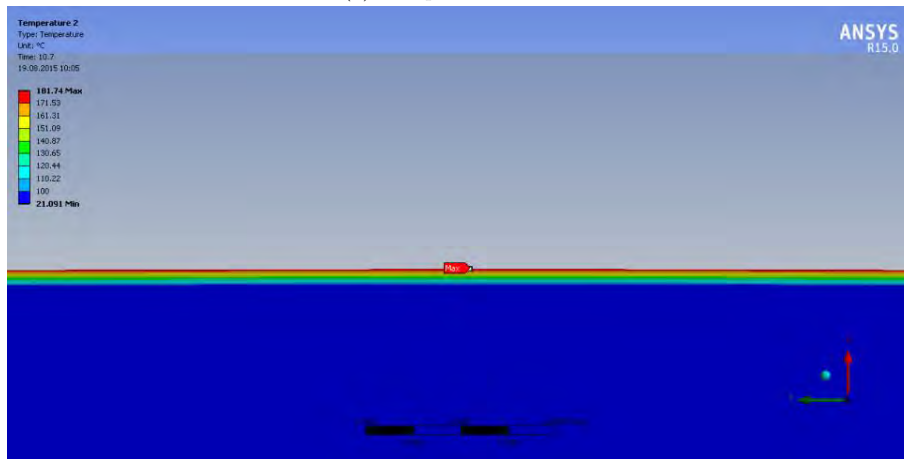


Figure 4. Flame temperature profile for transient simulations.



(a) Complete warhead.



(b) HE charge.

Figure 5. Resulting thermal FCO response of a MK-82 warhead after 10 seconds.

30 s and provides an average ambient temperature of 800 degrees C for the remaining test period as required.

A sensitivity analysis was performed of the simulation model regarding mesh sizes and numerical solvers as well as thermal boundary conditions for radiative and convective heat flux. Significant parameters such as surface emissivity of the casing and convective heat transfer coefficient were varied between 0.2 and 0.9 [2, 5] as well as 5 and 50 W/(m² K) [3], respectively. In addition, a simplified calculation of burning 4000 l of jet fuel for approx. 30 min results in approx. 15 W/(m² K) used as an estimate. The

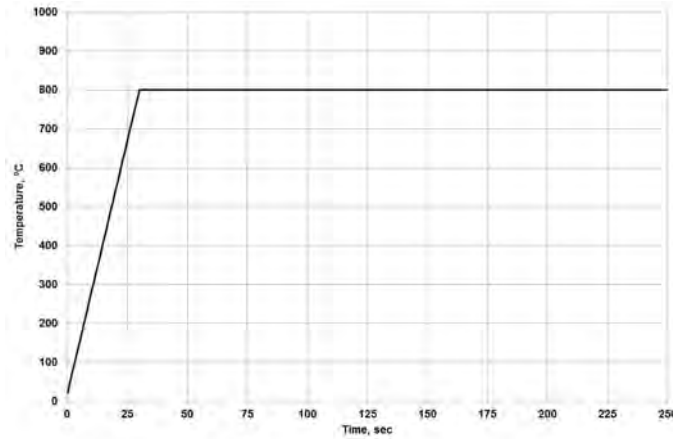
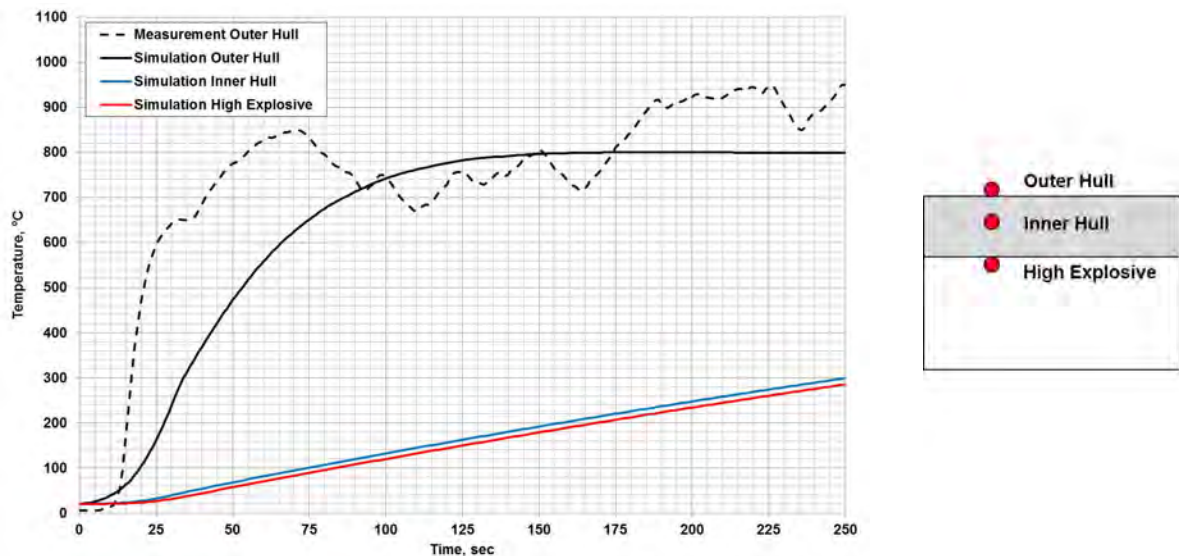


Figure 6. Flame temperature profile according to STANAG 4220 applied for COMSOL simulations.

analysis confirmed the earlier assumption with radiation as major heat transfer and revealed a significant impact of the emissivity on simulated casing temperatures, while the effect of the convective heat transfer coefficient was less significant. Last not least, values given in Tab. 1 were chosen for further simulations.

COMSOL simulation results excluding reaction kinetics are given in Fig. 7 with temperature-time profiles of gauge points located at outer casing, inner casing, and adjacent HE charge. It also includes a measured curve of a temperature sensor attached to the outer casing of a typical FCO test. Deviations between experimental and simulated data is relatively small reflecting results of the sensitivity analysis as discussed and considering random environmental conditions such as wind. Temperatures of the inner casing and inside the high explosive charge are significantly below the ambient temperature since this is based on the heat flux from gaseous to solid materials. Differences between temperatures of the inner casing and high explosive charge are small as a result of the high thermal conductivity of the steel casing compared to the HE charge.



(a) Simulated temperature-time profiles.

(b) Gauge locations.

Figure 7. COMSOL simulation with temperatures at the outer casing, inner casing, and in the adjacent HE charge.

4.1 Applying reaction kinetics

An in-depth analysis of a COMSOL model including reaction kinetics was also performed. Figure 8 presents corresponding results of temperature profiles of the casing and within the high explosive charge as well as the reaction progress. A significant reaction progress is observed after 200 s through a significant increase in reactive heat in the outer layer of the high explosive charge. This results in a rapid temperatures rise at approx. 215 s with high explosive temperatures exceeding casing temperatures. This marks the event of an ignition of the HE charge leading to a reactive warhead output.

Figures 9 and 10 provide spatial temperature contour plots of a such a MK-82 warhead in 2D and 3D, respectively, at three different instances in time. They show well that heat is absorbed at the long cylindrical casing section and transferred to high explosive layers directly underneath. The major volume of the high explosive charge, however, remains unaffected at temperatures below 30 degrees C through fast cook-off time regimes of a few minutes.

4.2 Assessing mitigation potentials through coatings

Mitigation potential by intumescent coatings was assessed with thermo-kinetic COMSOL simulations. Thermal exposition results in a swelling of such coatings creating an effective barrier against the heat flux through a small heat transfer coefficient. The objective is to provide an additional time delay between 200 and 300 s until the reaction threshold is reached [9]. Two different coating materials of carbonizing foams were assessed considering a thickness of one millimeter of effective insulation layer. Material properties of this effective intumescent layer are given in Tab. 2.

Figure 11 provides thermo-kinetic simulations results of these coating materials. A reaction delay of less than one minute is obtained in case of coating material A. Coating material B, however, features better insulation properties resulting in delay times of approx. two minutes. Although these low-price materials provides an effective mitigation method, their application process is time-consuming and requirements for environmental temperature ranges and life times may be critical.

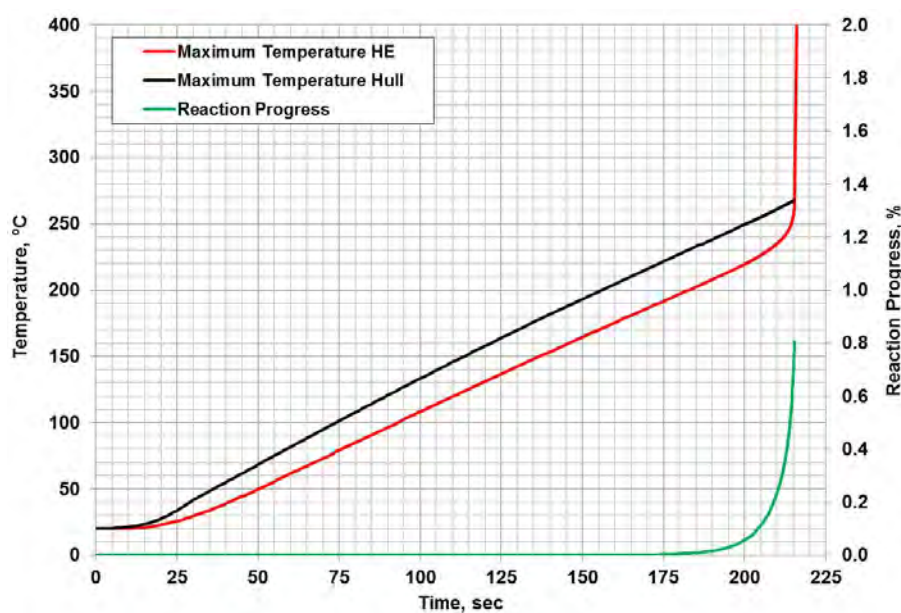


Figure 8. Temperature-time profiles showing formation of hot spots and resulting steep temperature increase in the HE charge.

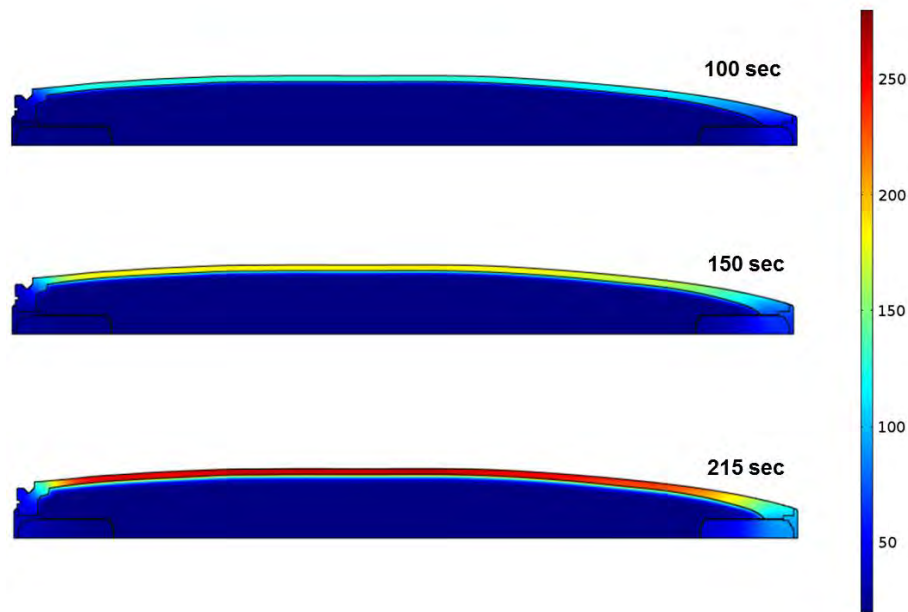


Figure 9. 2D contour plots of spatial temperature distributions (in degrees C) of a MK-82 bomb at different instances in time.

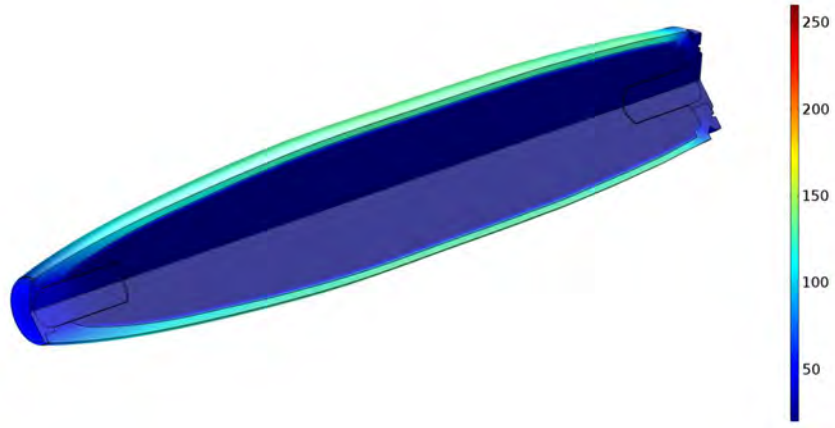
5 Conclusions

A fast-cook off modeling and simulation study was performed using at first a simplified thermal model without reaction kinetics that was implemented into ANSYS Mechanical and allowed an initial assessment of critical parts and components of warheads. A new modeling approach including reaction kinetics using COMSOL Multiphysics provides an accurate prediction of spatial temperature profiles and hot spot forming of full-scale warheads. This allows prediction of reaction times and temperatures and allows, in addition, an assessment of potential mitigation technologies such as intumescent coatings. These thermal models can be easily applied to other full-scale warhead systems allowing a prediction of their IM conformance.

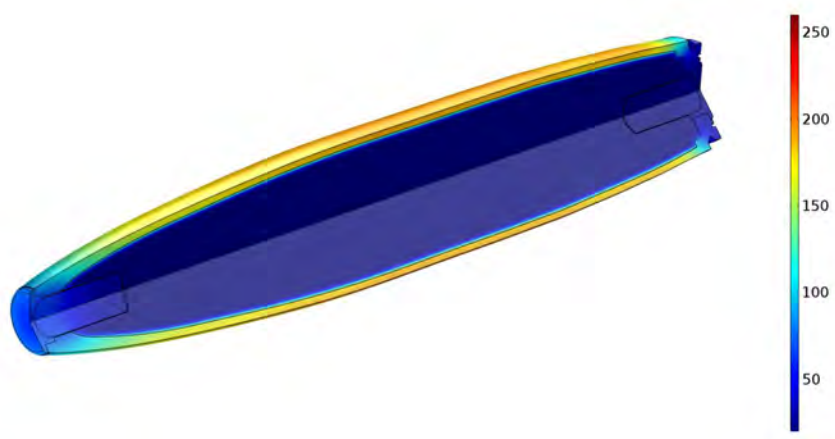
In future, applying temperature sensors inside or underneath the casing and inside the high explosive charge of small-scale or full-scale test vessels will allow further verification and optimization of thermal simulation models. Resulting effects such as burning or deflagration reactions may be predicted by including conservation equations and considering gas pressures and the mechanical behavior of inert warhead components in simulations.

References

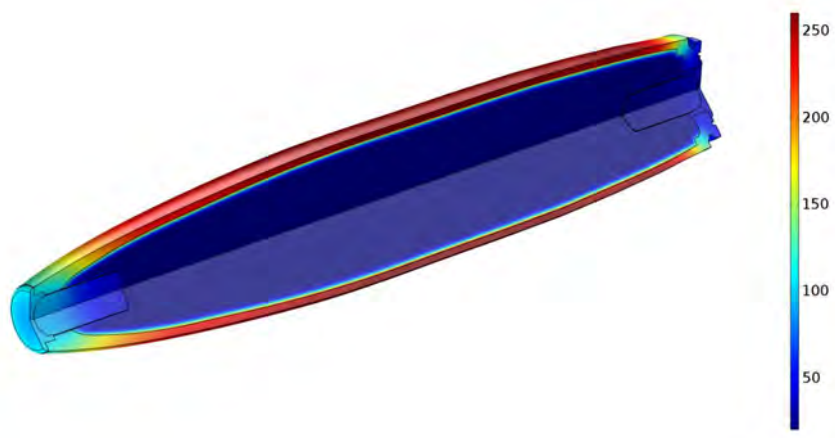
1. NATO. *STANAG 4439: Policy for Introduction and Assessment of Insensitive Munitions (IM)*. 2 edition, 2009.
2. B. Evers and P. Möllerström. *Fast cook-off test with a sand bed burner*. Luleå University of Technology, Luleå, Sweden, 2013. Bachelor's thesis.
3. C. Zhang and A. Usmani. Heat Transfer Principles in Thermal Calculation of Structures in Fire. *Fire Safety Journal*, 78:85–95, November 2015.
4. W. Ciro. *Fast Cookoff Tests Report*. University of Utah, Salt Lake City, UT, October 2003.
5. M. A. Kramer, M. Greiner, J. A. Koski, C. Lopez, and A. Suo-Anttila. Measurements of Heat Transfer to a Massive Cylindrical Calorimeter Engulfed in a Circular Pool Fire. *Journal of Heat Transfer*, 125:110–117, February 2003.
6. D. Hunter, L. Pitts, E. Colvin, M. Steinberg, K. Huddleston, N. Peterson, N. Al-Shehab, and E. L. Baker. Thermal Modeling the SCO Response of a TOW2B EFP. In *Proceedings of the Insensitive Munitions & Energetic Materials Technology Symposium*, Rome, Italy, 2015.



(a) After 100 seconds.



(b) After 150 seconds.



(c) After 215 seconds.

Figure 10. 3D temperature plots (in degrees C) of a MK-82 warhead simulated with COMSOL.

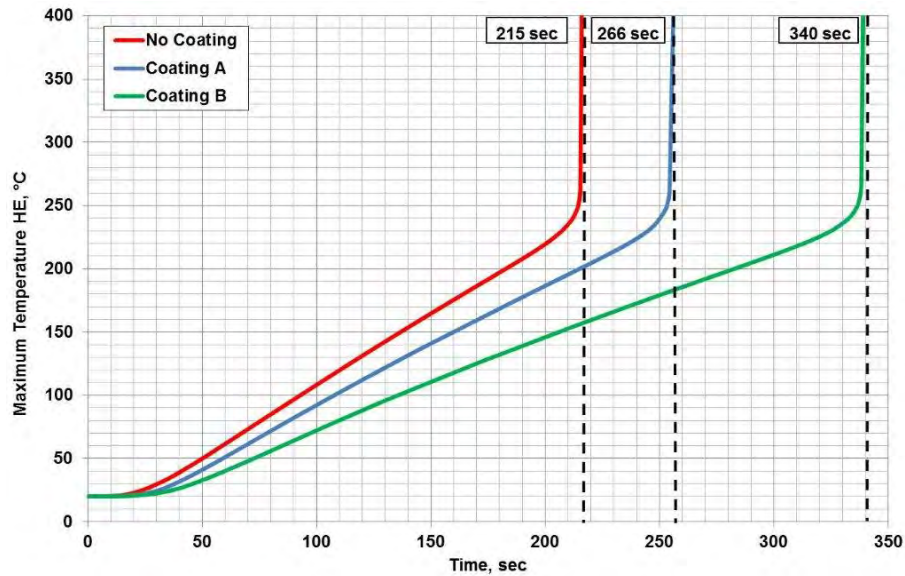


Figure 11. Temperature-time profiles showing effects of coatings applied on MK-82 bomb casings.

7. M. Pelletier and C. Dubois. Multiphysics Modelling of Variable Confinement Cook-off Test (VCCT). In *Proceedings of the Insensitive Munitions & Energetic Materials Technology Symposium*, San Diego, CA, 2013.
8. NATO. *AOP-39: Guidance on the Assessment and Development of Insensitive Munitions (IM)*. 3 edition, March 2010.
9. M. Graswald, R. Gutser, and R. Gleichmar. *FFE IM-Verbesserung: Ergebnisbericht 2014 / 2015 / 2016*. Number TDW-TN-EN-16-0008. TDW GmbH, Schrobenuhausen, 2016.
10. M. Graswald, R. Gutser, and E. Waldner. Modeling of thermal reactions and associated events. In *Proceedings of the 30th International Symposium on Ballistics*, Long Beach, CA, 2017.
11. M. Graswald and R. Gutser. Thermal modeling of slow cook-off responses. In *Proceedings of the Insensitive Munitions & Energetic Materials Technology Symposium*, Nashville, TN, 2016.
12. B. W. Asay. *Non-shock Initiation of Explosives*, volume 5, chapter Cookoff. Springer-Verlag, Berlin, Heidelberg, 2010.
13. J. P. Holman. *Heat Transfer*. The McGraw-Hill Companies, Inc., New York, NY, 10 edition, 2010.
14. N. N. *ANSYS Mechanical Release 15*. ANSYS Inc., Canonsburg, PA, 2013.
15. N. N. *COMSOL Multiphysics version 5.3*. COMSOL AB, Stockholm, Sweden, 2017.
16. N. N. *AKTS-Thermokinetics Software Version 4.15*. AKTS AG, Siders, Switzerland, 2015.
17. NATO. *STANAG 4240: Liquid Fuel / External Fire, Munition Test Procedures*. 2 edition, April 2003.

MICROFLUIDIC SYNTHESIS OF ENERGETIC COMPOUNDS

Dr. Joe Scavuzzo and Dr. Melissa Mileham

Abstract #20271

Orbital ATK
Corinne, Utah

ABSTRACT

Microfluidic synthesis is the use of microliter scale flow reactors to manipulate reactive liquids or solutions to produce chemical transformations. Microfluidic synthesis processes have some advantages over traditional batch processes, particularly when producing energetic molecules. For example, microfluidic reactors contain only microliters of reactive solution, which greatly reduce risks associated with large volumes of energetic material. Further, because of the high surface area-to-bulk ratio in microfluidic reactors, heat is efficiently transferred away from the system. This is of particular importance for the synthesis of energetic molecules where exothermic nitrations and oxidations are common. The simplicity of microfluidic reactors also allows for easy scale-up and automation for remotely controlled processes. The present work deals with the design and fabrication of a microfluidic reactor used to produce energetic molecules. A nitrated precursor for an energetic polymer was chosen as the target molecule. The synthetic process contains two steps where organic molecule X1 is first nitrated to produce NO₂-X1. In the second step, NO₂-X1 undergoes an exothermic rearrangement to give the final product, NO₂-X2. Each step was performed and optimized individually on the microfluidic reactor. The optimized conditions were then used to perform the two steps in series on a single reactor.

INTRODUCTION

MICROFLUIDIC REACTOR BACKGROUND

Microfluidic reactors manipulate reactive liquids or solutions to produce chemical transformations under geometrically constrained environments with internal dimensions on the scale of micrometers.^[1] Microfluidic reactors contain microliter volumes of reaction solution, therefore only micrograms of energetic material are in process at any given time. This is particularly advantageous during the development stage of a new chemical process. Developmental operations involving new energetic materials and/or processes are inherently higher risk because of unknown behaviors and the potential for explosion. Accepting these risks can be reasonable if the consequence of an unexpected behavior is low. Because the process volumes of microfluidic reactors are restricted to microliters/gram scale, the consequences of unexpected behavior are more acceptable.

Microfluidic reactors provide some unique advantages over traditional synthesis methods. The reactor's high surface area-to-volume ratio allows for very efficient heat transfer from the reactor to the reactor's external environment. Highly exothermic reactions are commonplace in energetic material synthesis and efficient heat transfer translates to safer operations by mitigating the risk of self-heating runaway reactions.

Precise temperature control can also lead to higher purity reaction products by decreasing side reactions. [1]

These advantages are amplified in many self-contained commercially available systems because of the extensive characterization of reactor capabilities. Further, many commercially available systems are specifically designed for rapid process development (10 to 25 reaction conditions per day) and simple scale-up to the kilo or pilot-scale. It should be noted that scale-up is typically accomplished by operating reactors in parallel and/or extending the length of the microfluidic pathway. Kilo-scale operations can produce between 6 and 12 liters/hour of reaction solution while maintaining an active reactor volume of only ~200 μL .

Though commercially available reactors are impressive and offer many advantages, for the purposes of the research outlined in this work, a simple reactor was constructed in-house using basic laboratory equipment as a proof of concept. A target energetic molecule was chosen that requires two chemical reactions. The first reaction is the nitration of molecule X1 with 98% nitric acid to give NO₂-X1. Compound NO₂-X1 is then chemically transformed in a second reaction to give the target molecule NO₂-X2.

DEVELOPMENT STRATEGY

The development of the reactor was a three-step process as outlined in Fig. 1:

1. Optimize reactor parameters for nitration to produce NO₂-X1 (reaction step 1)
2. Optimize reactor parameters for chemical transformation of NO₂-X1 to NO₂-X2 (reaction step 2)
3. Perform reaction step 1 and reaction step 2 in series to transform X1 to NO₂-X2 in a single reactor

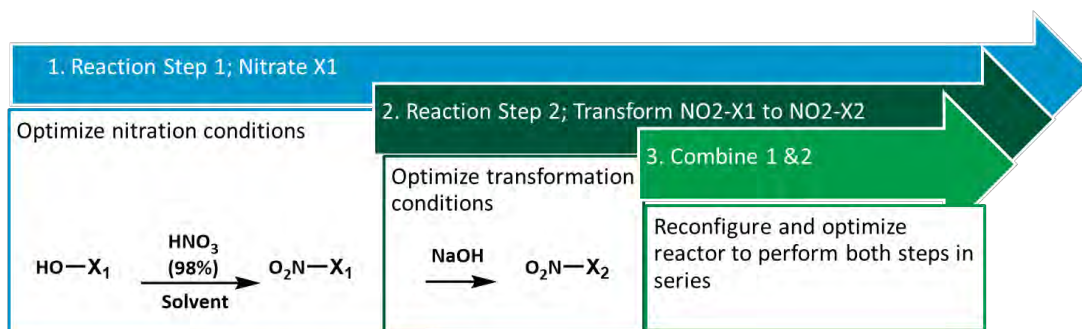


Fig. 1: Development strategy flow chart

RESULTS AND DISCUSSION

REACTOR DESIGN

The reactor is designed around critical design parameters and with flexibility in areas that allow for control over critical process control variables (Table 1). Reagents A and B are introduced to the system using syringe pumps set to constant flow rates. These reagents are pushed through acid resistant tubing (fluoropolymer) with an inner diameter of 0.79 mm to a T-Joint that combines reagents A and B into a single resonance tube. The resonance tube varies in length (30 to 140 cm) depending on the

operation and is coiled and submerged in a controllable constant temperature bath. Reagent feed ratios are controlled with different syringe sizes (Fig.2), or simply by using separate syringe pumps set to the desired flow rates. Resonance time is controlled by either resonance tube length or the combined flow rate of reagents A and B. Reaction product C is collected from the terminal end of the resonance tube into a glass vial for final analysis.

Table. 1: Reactor Design Parameters and Process Control Variables

Critical Design Parameters
Reagents A and B shall mix to produce product C ($A + B = C$).
Reagents A and B shall be introduced at a constant flow rate.
All wetted materials shall be resistant to oxidizing acids.
Reactor tube diameters shall be restricted to < 1mm diameter.
Reactor tube length must be of sufficient length to allow for reasonable resonance times.
Process Control Variables
Reaction temperature
Reagent feed ratios
Reaction solution resonance time

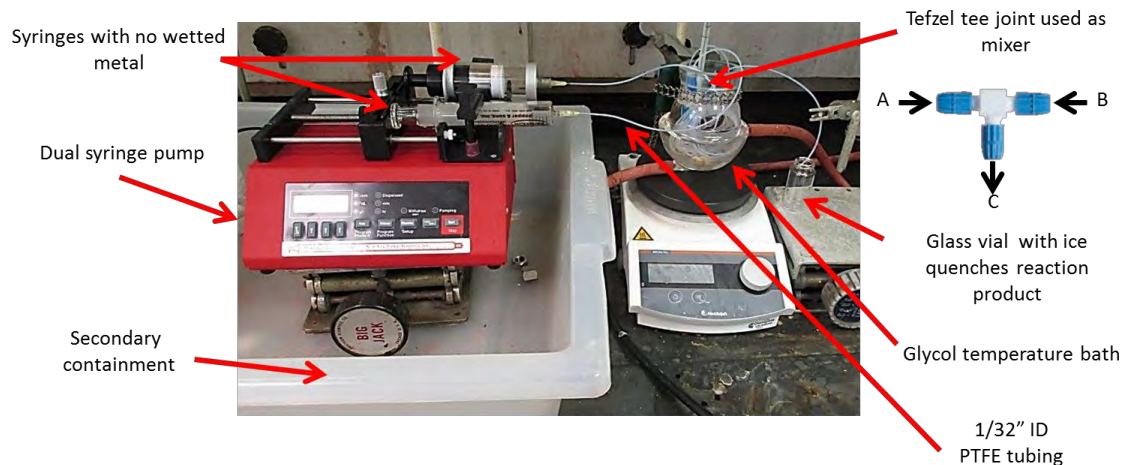


Fig. 2: Reactor design

REACTION STEP 1; X1 Nitration

The production of NO₂-X1 has traditionally been performed as a batch reaction, which requires extensive cooling to manage the exothermic nitration. Precise control over the reaction temperature, acid concentration and reaction time are required to ensure X1 is not under or over nitrated. The batch reaction conditions were used as a starting point for the microfluidic reactor conditions.

The reactor was configured as shown in Fig. 3 for the X1 nitration. Compound X1 was injected as reagent A and nitric acid or nitric acid/solvent solutions were injected as reagent B (Fig. 2 and 3). Reaction products were collected and analyzed by nuclear magnetic resonance (NMR) spectroscopy for percent conversion to NO₂-X1 and side products. Table 2 shows the process variables that were explored and the NMR analysis results. The first three experiments did not show any conversion of the starting material; it was determined that significantly longer reaction times are required. The resonance tube was extended from 30 cm to 412 cm for the remaining experiments. The data also shows higher acid concentrations are required for sufficient conversion to NO₂-X1. However, high acid concentrations also increase side reactions somewhat. Experiments 11 and 12 were conducted in order to demonstrate repeatability.

Statistical analysis was completed using JMP software to further understand the effects of changing process control variables. The analysis was a main effect analysis only for screening, which showed the acid concentration being the most significant factor, where lower amounts of solvent are best. The reactor size and retention time are close to significant ($P < 0.05$) and indicate smaller reactors and longer retention times are better. The results are shown in Tab. 2 and Fig. 4. The percent conversion and amount of side reaction product 1 present are in the same ranges expected for a batch reaction.

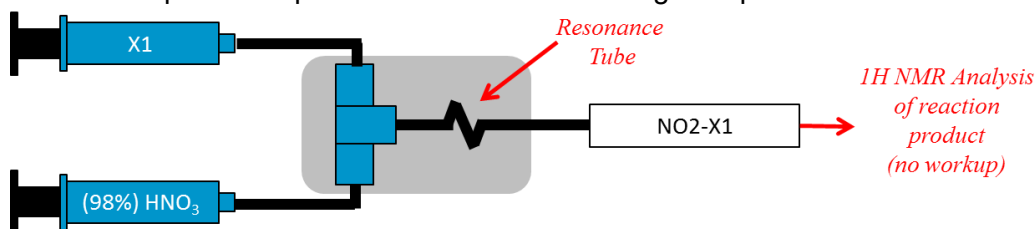


Fig. 3: X1 nitration reactor configuration

Table 2: X1 Nitration

Experiment	Temp (°C)	Acid Concentration (Solvent:HNO ₃)	Acid:X1	Flow Rate (mL/min)	Retention Time (min)	Molar % Conversion	% Side Rxn Product 1
1	15	2:3	4:1	0.11	2.05	0	0
2	25	2:3	4:1	0.11	2.05	0	0
3	30	2:3	4:1	0.11	5.65	0	0
4	20	1:3	4:1	0.15	21.6	19	14
5	20	1:5	4:1	1.23	2.68	13	12
6	20	1:5	4:1	0.25	13.4	14	12
7	20	1:5	4:1	0.125	26.0	54	13
8	27	1:5	4:1	1.23	2.68	22	13
9	20	0:1	4:1	1.23	2.68	68	14
10	20	0:1	4:1	0.25	13.4	43	7
11	20	0:1	4:0.68	0.76	4.23	78	39
12	20	0:1	4:0.68	0.152	21.0	74	18
11b	20	0:1	4:0.68	0.76	4.23	80	41
12b	20	0:1	4:0.68	0.152	21.0	75	27

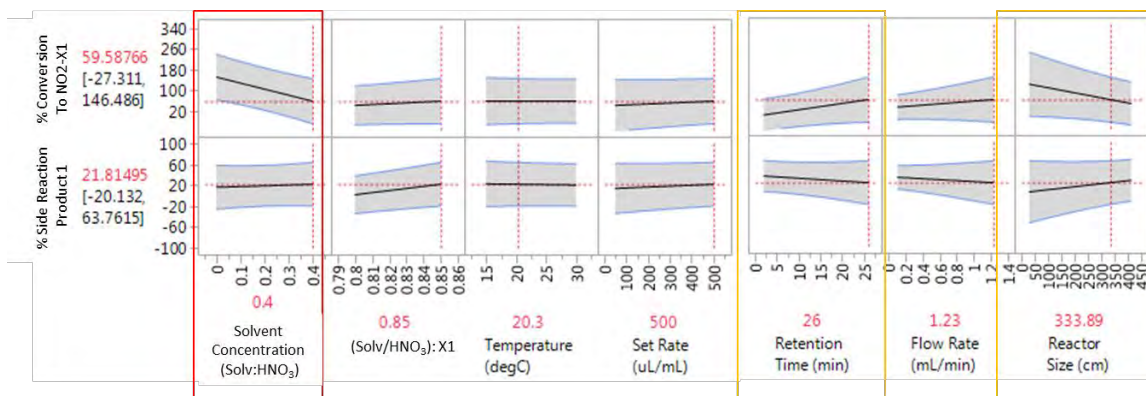


Fig. 4: Statistical analysis of NO2-X1 conversion

NO2-X2 STEP 2; NO2-X1 CAUSTIC TREATMENT

The reactor configuration used for the nitration of X1 was also used for the NO2-X1 transformation to NO2-X2. However in this case, reagent A (Fig. 2) is an organic solution of NO2-X1 and reagent B is a caustic solution. The reaction product of this step is the target material, X2-NO2. For the experiments outlined in Table 3, the NO2-X1 solution was prepared separately using a batch reaction set-up. The step 2 chemical transformation proved much easier in the microfluidic reactor than the nitration, with up to 100% conversion being achieved. It was also noted during the experiments that the reactor isothermal temperature bath remained at a constant temperature, indicating no apparent thermal runaways during the reaction. This is a key finding because the reaction involves the neutralization of any excess nitric acid from the previous step, which is an extremely exothermic reaction. Samples from each experiment were analyzed by NMR spectroscopy, with the percent conversion to NO2-X2 and side products shown in Table 4. Statistical analysis was also completed for this data set, and determined the concentration of the NaOH, retention time and temperature were all important factors. The prediction model based on this analysis is shown in Fig. 5 and shows that maximizing NaOH concentration will increase NO2-X2 conversion and yield with little impact on the amount of side product produced. Also, temperature offers minor improvements and a lower retention time increases yield while lowering the amount of side product.

Table. 3: Experiments conducted for conversion of NO₂-X1 to NO₂-X2

Experiment	NaOH:NO ₂ -X1	Temperature (°C)	Actual Flow Rate (mL/min)	Retention Time (min)
1	4:1	14	0.57	1.13
2	4:1	14	0.11	5.65
3	2.7:1	14	0.63	1.02
4	2.7:1	14	0.126	5.10
5	2.7:1	20	0.63	1.02
6	2.7:1	20	0.126	5.10
7	2.7:1	20	0.63	5.10
8	2.7:1	20	0.31	7.30
9	2.7:1	20	0.126	25.0
10	2.7:1	20	0.95	2.50
11	2.7:1	20	0.63	5.10

Table. 4: Conversion of NO₂-X1 to NO₂-X2 using a microfluidic reactor

Experiment	%Conversion (To NO ₂ -X2 or Side Product)	%Side Products	% Yield
1	20	0	20
2	20	0	20
3	83	0.6	82.4
4	92.4	2.6	89.8
5	94.7	2.2	92.5
6	97.3	3.9	93.4
7	100	5	95
8	100	9.3	90.7
9	100	40	60
10	93	6	87
11	97	13	84

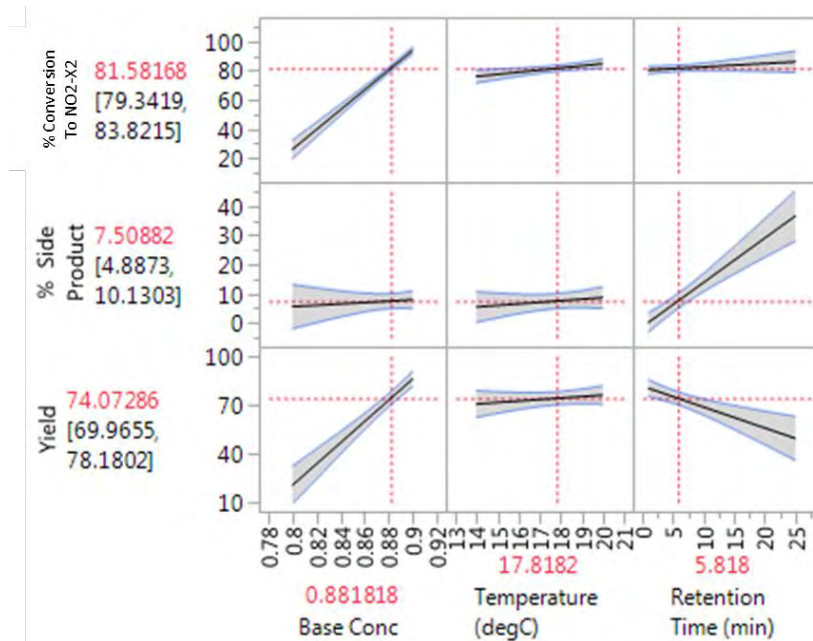


Fig. 5: Prediction model for ring closure step producing NO2-X2

STEP 1+2 IN SERIES; NITRATION AND CAUSTIC TREATMENT IN SERIES

In a final experiment, both steps of the NO2-X2 synthesis were performed in series on a single reactor. A schematic of the reactor is shown in Fig. 6. Compound X1 and nitric acid were injected into the T-joint under the optimized conditions discussed above to produce NO2-X1. The resonance tube containing NO2-X1 was then plumbed directly into a second T-joint where it was mixed with caustic and chemically transformed to NO2-X2. The specific conditions and results for each of the reactors are shown in Tables 5 to 7. NO2-X2 was produced at >75% yields. However, it is likely that additional optimization of process control variables would increase the reaction yield further. It should be noted that a 75% yield is in a similar range observed for batch conditions.

Table 5: Nitration conditions

<i>Experiment</i>	<i>HNO3:X1</i>	<i>Temperature (°C)</i>	<i>Actual Flow Rate (mL/min)</i>	<i>Retention Time (min)</i>
1	4:0.68	21	0.76	2.68
2	4:0.68	22	0.76	2.68
3	4:0.68	22	0.38	5.36

Table 6: Ring closure conditions

<i>Experiment</i>	<i>NaOH Concentration</i>	<i>Temperature (°C)</i>	<i>NaOH Flow Rate (mL/min)</i>	<i>Retention Time (min)</i>
1	3.4	22	0.774	1.2
2	7.2	22	0.774	1.2
3	7.2	32	2.4	0.7

Table 7: Experimental results from two-step microfluidic reactor producing NO₂-X₂

Experiment	%Conversion	% Side Products	Yield/Notes
1	N/A	N/A	Insufficient base
2	N/A	N/A	Inorganic precipitates
3	83	5.5	77.5

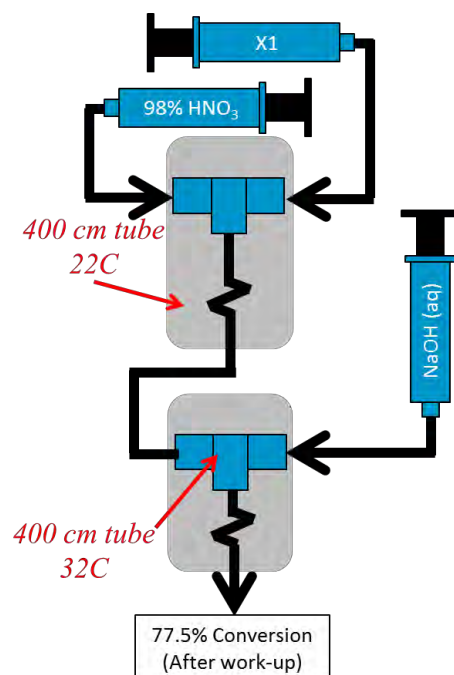


Fig. 6: Microfluidic reactor setup of two-step NO₂-X₂ synthesis

SUMMARY AND CONCLUSIONS

A microfluidic reactor was successfully constructed to meet the design parameters and required degree of control outlined in Table 1. The nitration of X₁ and caustic induced transformation of NO₂-X₁ have all been successfully completed using the current setup. Current methods for the nitration of X₁ are able to achieve at least an equivalent yield to the batch process, however, further optimization may increase the yield. The caustic induced transformation of NO₂-X₁ performed on the microfluidic reactor gave high yields of pure NO₂-X₂. When the reactor was reconfigured to perform both steps in series, NO₂-X₂ was successfully synthesized at a reasonable purity and yield. The in-house microfluidic reactor discussed here serves to prove that molecule NO₂-X₂ can be synthesized with microfluidics. Additional improvements in quality, and safety could be achieved with a more robust and properly characterized reactor.

REFERENCES

1. Elvira, K. S., Solvas, C. I., Wootton, R. C. R., deMello, A. J., ***The Past, Present And Potential For Microfluidic Reactor Technology In Chemical Synthesis***, Nature Chemistry, Vol 5, 905-915, (Nov 2013).

AUTHORS

Dr. Joe Scavuzzo

Email: Joe.Scavuzzo@OrbitalATK.com

Office Phone: (435)863-8148

Address:

Orbital ATK

Building M-3

9160 UT-83

Corinne, UT 84307

Dr. Melissa Mileham

Email: Melissa.Mileham@OrbitalATK.com

Office Phone: (435)863-8399

Address:

Orbital ATK

Building M-3

9160 UT-83

Corinne, UT 84307



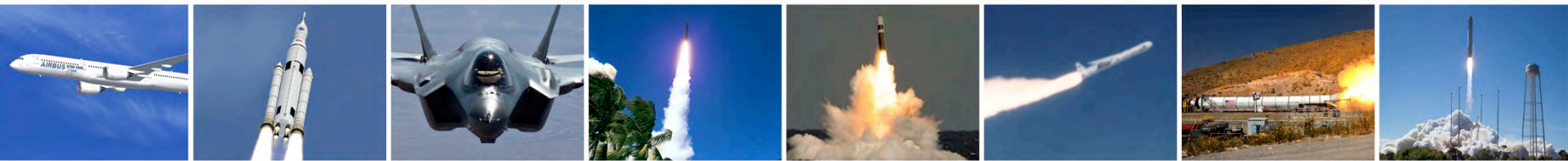
Microfluidic Synthesis of Energetic Materials

Joe Scavuzzo, PhD

Melissa Mileham, PhD

April 2018

Abstract # 20271

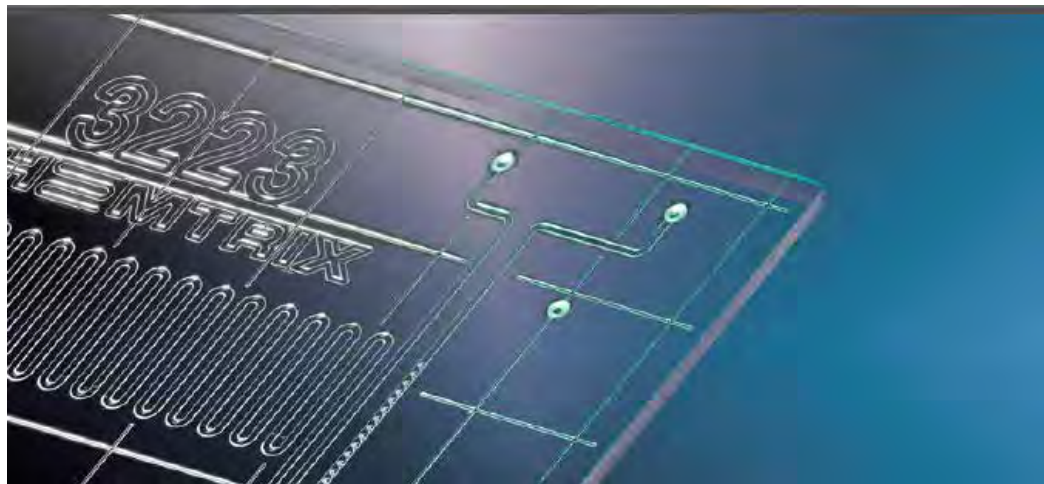


UNCLASSIFIED

Distribution A: Approved for Public Release. Distribution is unlimited.

What is Microfluidic Synthesis?

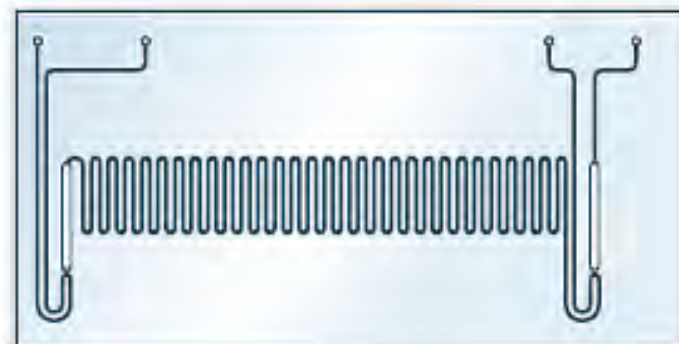
- **Microfluidics:** “Microfluidic systems manipulate and control fluids that are geometrically constrained within environments having internal dimensions, or hydrodynamic diameters, on a scale of micrometers” – Nature Chemistry, 2003
- **Microfluidic Synthesis** uses microfluidic technology to manipulate reactive liquids or solutions to produce chemical transformations



DESIGN 3223
Reactor with three inlets and one outlet:
 $A+B=P1+Q=P$

- Width channel: 300 μm
- Depth channel: 120 μm
- Reactor Volume: 10 μl

~2 in.



~1 in.

Advantages Of Microfluidic Reactors



- Efficient heat exchange between reactor and environment
 - Highly exothermic, reactions are common in energetic synthesis (nitration, oxidation, acid neutralizations, etc.). If exotherms are not properly managed, run-away reactions can occur.
- Low reactive volume (microliters of solution)
 - Low consequence hazard
- Easy scale-up
 - Very high throughput at lab scale (20 conditions/day)
 - Scale is increased by lengthening reactor path or including parallel reactors
 - ~5 μ L reactor can produce ~ 50 g of material/day
 - ~200 μ L reactor can produce at pilot scale levels

Lab Scale Work Station



Kilo Scale Work Station



Chemical Synthesis Methods



Batch Operation	Continuous Operation	Microfluidic Operation
High flexibility; preferred for multi-product/purpose operation, useful for a large range of reaction scale	Low flexibility; designed for a single process, not practical for development-scale production	Mid flexibility; lab and pilot scale reactor modifications are simple, reactors cannot handle all types of reaction media, useful for development to pilot plant scale
Low capital cost	High capital cost	Low capital cost
High consequence hazard; Large volumes of energetic materials being processed	High consequence hazard; large volumes of energetic materials being processed	Low consequence hazard; μL to mL volumes of energetic materials being processed
Reasonable scale-up from lab scale	Reasonable scale-up from lab scale – involves engineering/modeling	Simple scale-up from lab scale
Not suitable for unattended operation \rightarrow labor intensive \rightarrow high operating cost	Simple conversion to unattended operations \rightarrow low operating cost	Simple conversion to unattended operations \rightarrow low operating cost

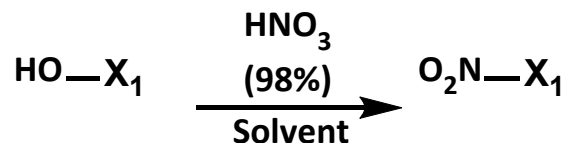
Development Path



Goal: Build a microfluidic reactor from lab materials and use it to perform a two step reaction and make compound NO₂-X₂

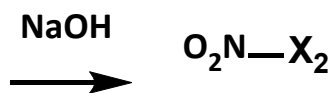
1. Reaction Step 1; Nitrate X₁

Optimize nitration conditions



2. Reaction Step 2; Transform NO₂-X₁ to NO₂-X₂

Optimize transformation conditions



3. Combine 1 & 2

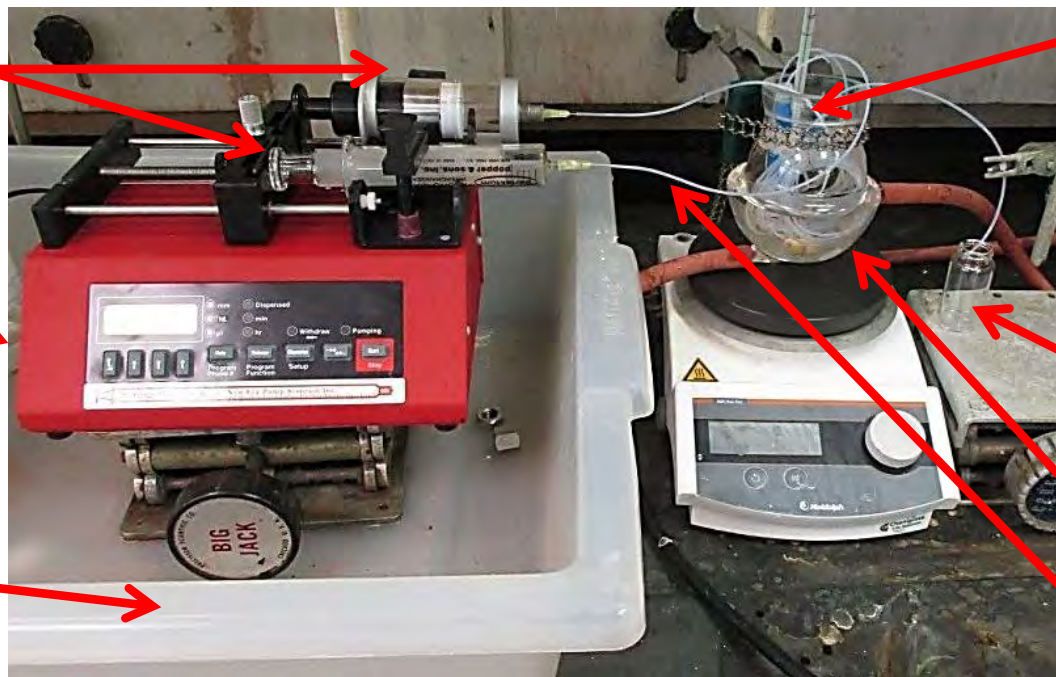
Reconfigure and optimize reactor to perform both steps in series

Reactor Design

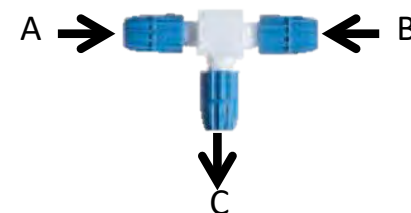
Syringes with no wetted metal

Dual syringe pump

Secondary containment



Tefzel T-joint used as mixer



Glass vial with ice quenches reaction product

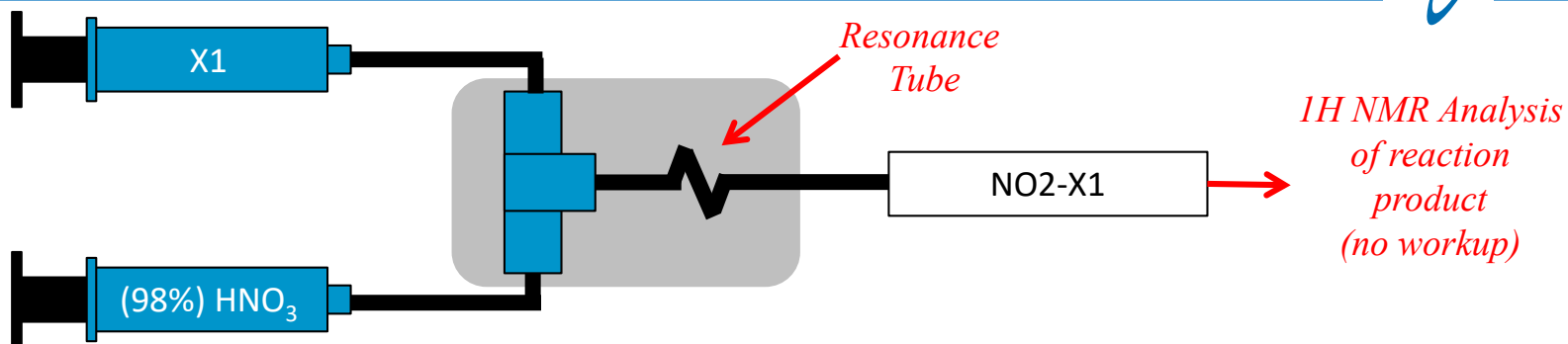
Glycol temperature bath

1/32-in. ID PTFE tubing 30cm

Process Controls

- Reagent feed ratios controlled by syringe size or dilution
- Reaction temperature controlled by temp bath
- Residence time controlled by plunger rate or reactor tube length

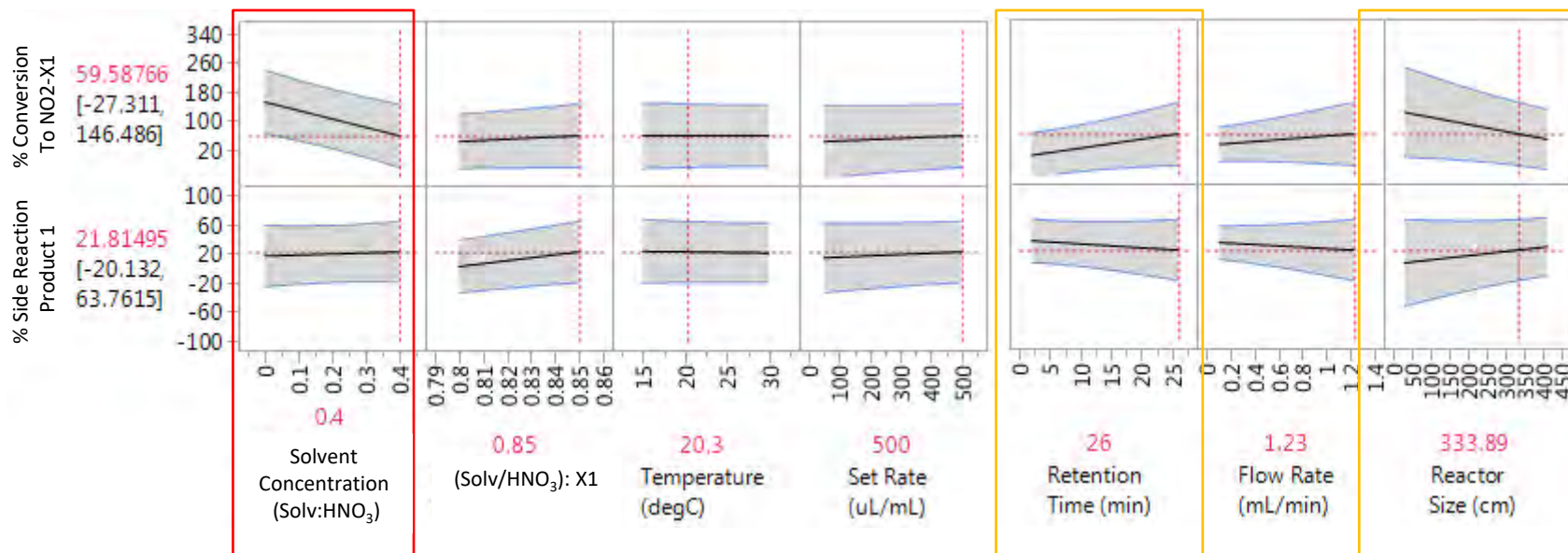
Nitration



Experiment	Temp (°C)	Acid Concentration (Solvent:HNO ₃)	Acid:X1	Flow Rate (mL/min)	Retention Time (min)	Molar % Conversion	% Side Rxn Product 1
1	15	2:3	4:1	0.11	2.05	0	0
2	25	2:3	4:1	0.11	2.05	0	0
3	30	2:3	4:1	0.11	5.65	0	0
4	20	1:3	4:1	0.15	21.6	19	14
5	20	1:5	4:1	1.23	2.68	13	12
6	20	1:5	4:1	0.25	13.4	14	12
7	20	1:5	4:1	0.125	26.0	54	13
8	27	1:5	4:1	1.23	2.68	22	13
9	20	0:1	4:1	1.23	2.68	68	14
10	20	0:1	4:1	0.25	13.4	43	7
11	20	0:1	4:0.68	0.76	4.23	78	39
12	20	0:1	4:0.68	0.152	21.0	74	18
11b	20	0:1	4:0.68	0.76	4.23	80	41
12b	20	0:1	4:0.68	0.152	21.0	75	27

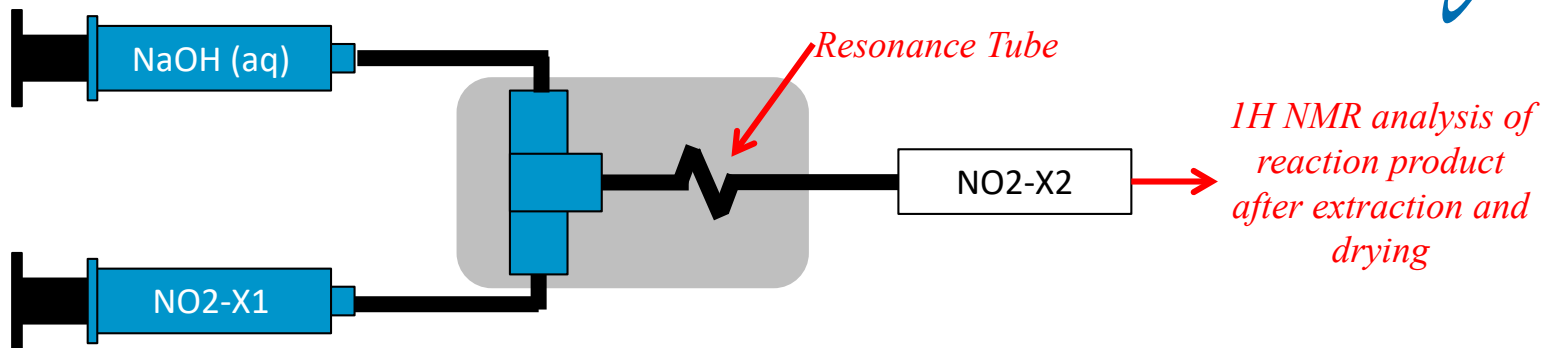
This method is capable of producing NO₂-X1 at conversions and purity levels similar to batch

Nitration Statistical Analysis



Acid concentration, reactor size, and retention time are the most significant variables

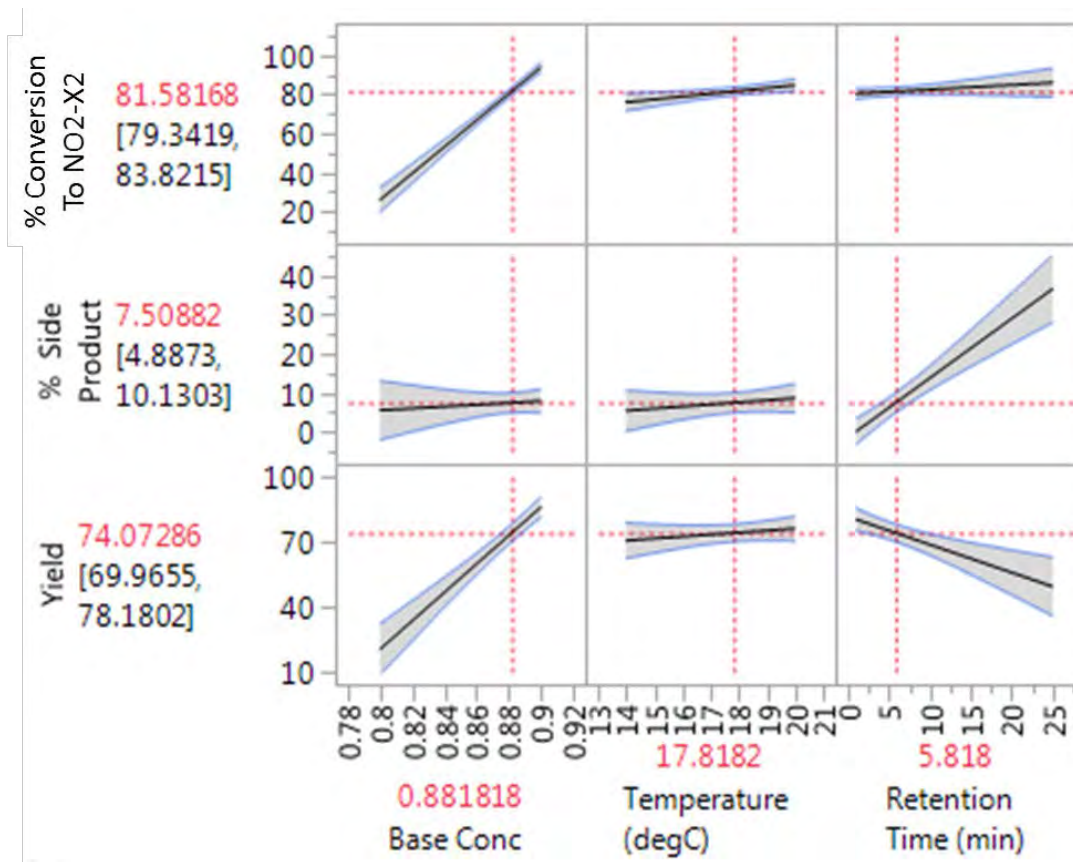
Step 2 (Caustic) Reaction



Experiment	NaOH:(NO2-X1)	Temp (°C)	Actual Flow Rate (mL/min)	Retention Time (min)	%Conversion From NO2-X1	%Side Products	% Reaction Yield
1	4:1	14	0.57	1.13	20	0	20
2	4:1	14	0.11	5.65	20	0	20
3	2.7:1	14	0.63	1.02	83	0.6	82.4
4	2.7:1	14	0.126	5.10	92.4	2.6	89.8
5	2.7:1	20	0.63	1.02	94.7	2.2	92.5
6	2.7:1	20	0.126	5.10	97.3	3.9	93.4
7	2.7:1	20	0.63	5.10	100	5	95
8	2.7:1	20	0.31	7.30	100	9.3	90.7
9	2.7:1	20	0.126	25.0	100	40	60
10	2.7:1	20	0.95	2.50	93	6	87
11	2.7:1	20	0.63	5.10	97	13	84

This method is capable of neutralizing all acid and producing NO2-X2 with complete conversion

Caustic Reaction Statistical Analysis

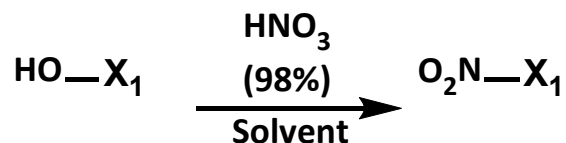


Increased base concentration increases conversion and yield without increasing side reaction

Development Path

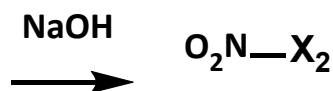
1. Reaction Step 1; Nitrate X1

Optimize nitration conditions



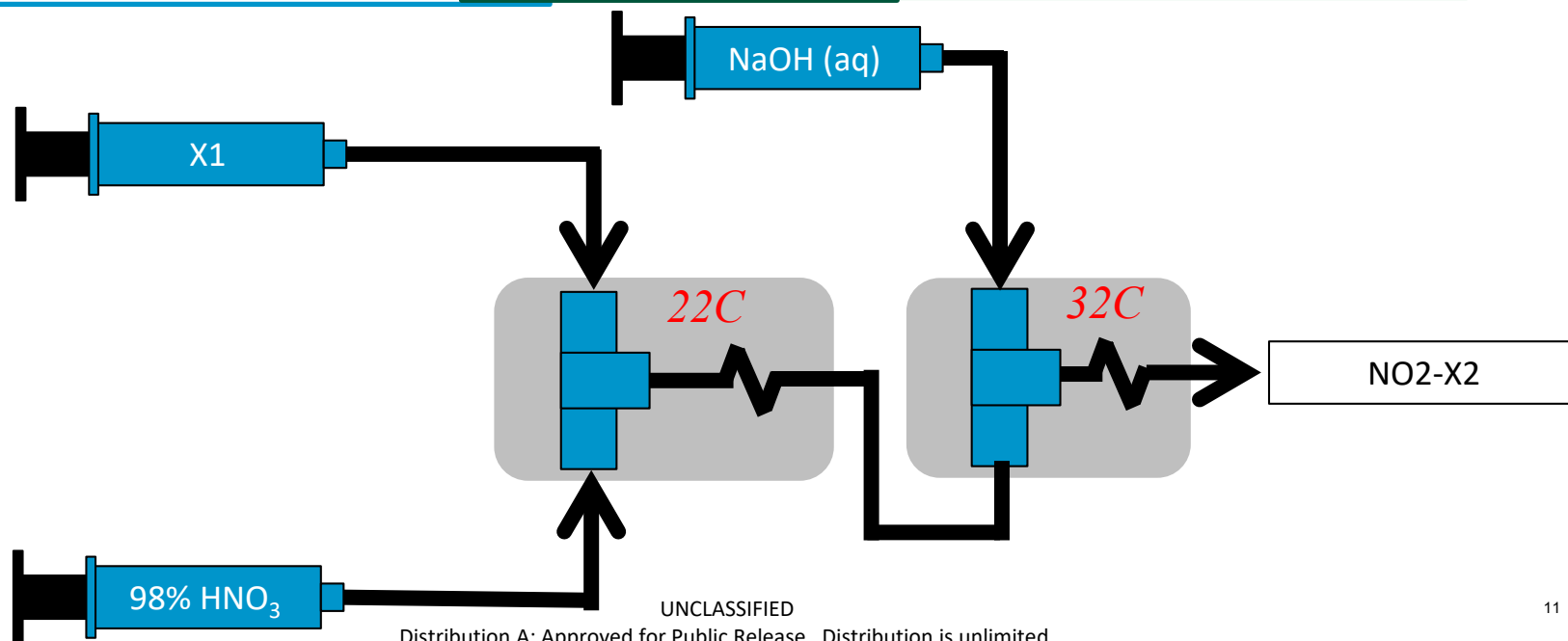
2. Reaction Step 2; Transform NO₂-X₁ to NO₂-X₂

Optimize transformation conditions



3. Combine 1 & 2

Reconfigure and optimize reactor to perform both steps in series



UNCLASSIFIED

Distribution A: Approved for Public Release. Distribution is unlimited.

Two Step Reaction



Two Step Reaction

Nitration Step Reactor Conditions (1st Segment)

Experiment	HNO ₃ :X1	Temperature (°C)	1st Segment Retention Time (min)	1st Segment Flow Rate (mL/min)	1st Segment Length (cm)
1	4:0.68	21	2.68	0.76	400
2	4:0.68	22	2.68	0.76	400
3	4:0.68	22	5.36	0.38	400

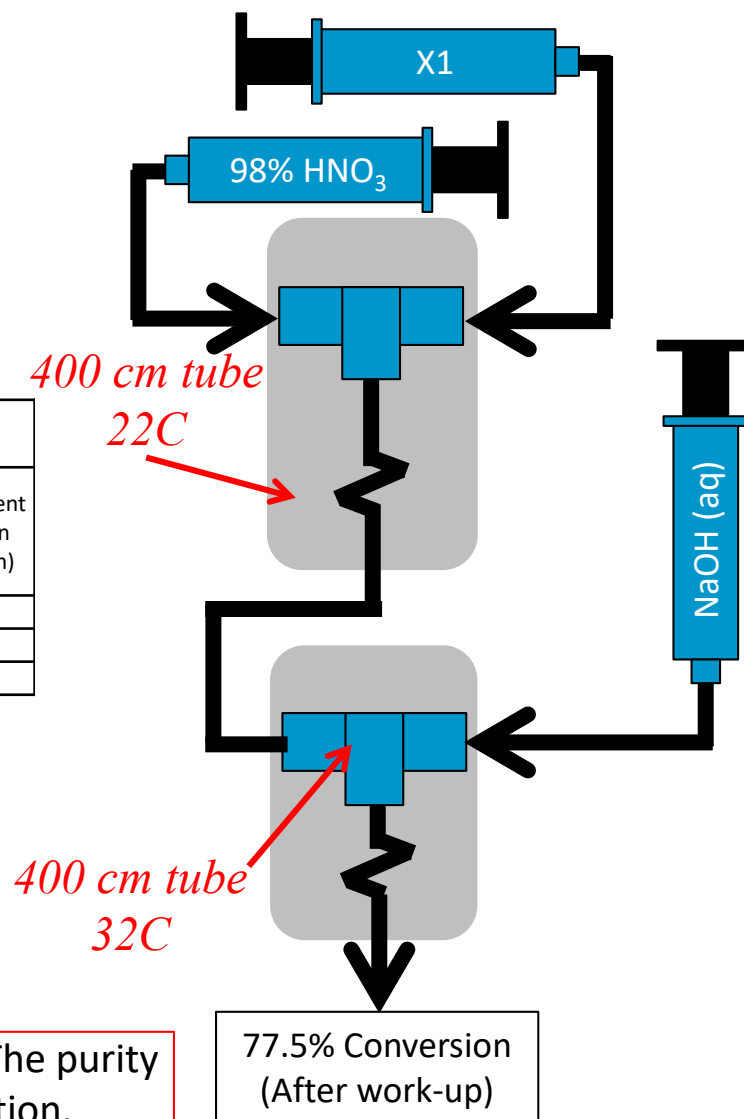
Ring Closure Reactor Conditions (2nd Segment)

Experiment	NaOH Concentration	Temperature (°C)	NaOH Flow Rate (mL/mL)	2nd Segment Length (cm)	2nd Segment Flow Rate (mL/min)	2nd Segment Retention Time (min)
1	3.4	22	0.774	400	1.7	1.2
2	7.2	22	0.774	400	1.7	1.2
3	7.2	32	2.4	400	2.9	0.7

Experimental Results

Experiment	% Conversion to X ₂ -NO ₂	% Side Product	Yield/Notes
1	NA	NA	Insufficient Base
2	NA	NA	Inorganic Precipitates
3	83	5.5	77.5

NO₂-X₂ was produced with a two step microfluidic reactor. The purity and yield were similar to that expected for a batch reaction.



- A microfluidic reactor was successfully built with inexpensive lab materials and could withstand nitration conditions
- The two step synthesis of NO₂-X₂ was carried out on the microfluidic reactor successfully
- Very useful for optimization because of quick variable adjustments and high throughput
 - 28 conditions in several days
 - Less exposure of equipment and personnel to hazardous processes (14 batch nitrations vs 14 microflow conditions)

Questions?

Explosives Ordnance Disposal (EOD) of Insensitive Munitions: Challenges and Solutions

Patrick Brousseau, Sonia Thiboutot and Emmanuela Diaz
Defence R&D Canada - Valcartier Research Center
2459 de la Bravoure road
Québec, Québec
Canada G1T 2C1
Patrick.Brousseau@drdc-rddc.gc.ca

Abstract

Over the last five years, Defence R&D Canada has explored efficient and clean methods to dispose of Insensitive Munitions. Those munitions, that were designed to withstand various aggressions, are bound to be more difficult to destroy. The results of the work performed to date lead us to believe that the amount of explosives spread during an EOD operation is directly proportional to the insensitiveness of the explosive. Some explosives, such as 3-Nitro-1,2,4-triazol-5-one (NTO) or Ammonium Perchlorate, appear to be difficult to detonate completely during blow-in-place operations. Another observation is related to the difficulties encountered using the current EOD methods when Insensitive Munitions must be destroyed in the field. Results of deposition tests ran on snow will be presented and discussed for their significance. During the tests, snow samples are collected and analyzed to determine the residual amounts of IM ingredients after either a high-order scenario, usually obtained when the munition is fired, or a blow-in-place reaction, occurring when a round is destroyed by a donor charge to eliminate the safety risk. During those tests, many different disposal methods were explored, i.e. one or many blocks of Composition C-4, placed at various locations, and shaped charges aimed at various points on the munitions. For some items tested, only a large shaped charge was efficient enough to eliminate any significant spread of explosives, and results obtained with other configurations always showed larger amounts of explosives residues at the detonation point for blow-in-place scenarios. Our conclusion is that new methods have to be designed to efficiently destroy Insensitive Munitions (IM). Those methods will include shaped charges, cutting charges, thermite mixes, high-power lasers and any other technology that will promote clean high order detonations or clean burning reactions. Our efforts identify those new methods will be presented, including one where the formulations are slightly modified to promote clean disposal. It appears that the EOD operators will have to be better equipped, but also possess higher skill levels than in the past to implement those clean methods.

Introduction

Insensitive Munitions, as per the definition of the term, are designed to be able to withstand external stimuli without adverse reactions, usually in the form of a violent event such as a detonation or, in some cases, an explosion. The energetic materials in the munitions were selected such that they were less sensitive to shocks and thermal aggressions. Intuitively, it was easy to predict that they would be more difficult to destroy in the field when a malfunction would occur. The first generations of energetics for Insensitive Munitions were less sensitive, but to a point which still allowed standard explosive ordnance disposal methods to be applied without great problems. However, the new generation of Insensitive Munitions is now able to withstand stronger aggressions. One good example is the development of IMX-101 [1] which is able to

resist to a large shaped charge jet attack. Such new and performant formulations now require tailored methods for the destruction of unexploded ordnance (UXO).

At the same time, in the last decade, a significant amount of work was dedicated to the measurement of the amount of explosives remaining on the ground following the high-order detonation of explosives or the destruction of UXO's using current EOD methods [2-5]. Without any surprise, it was realised that the high-order detonation of IM explosives created larger amounts of residues than standard explosives, albeit at the forensic level in many cases [3]. This was expected of less sensitive ingredients. However, the blow-in-place scenarios (EOD scenarios) of IM explosives were often found to produce amounts of explosive residues that were considered problematic by experts in the field. Percent quantities of the original material were sometimes found [3], or worse, a low-order detonation, which can spread hundreds of grams of explosives. This was a cause for concern for the sustainability of our local training ranges because of intensive use by military personnel combined with the UXO rates of some items. It is also coupled with a tightening of the environmental regulations. There was a realization that new methods are necessary to properly address the EOD problem of IM.

Following decades of developmental work, the fielding of Insensitive Munitions was occurring at a significant rate in the last decade. While IM technology was mostly applied to missile warheads, torpedoes and air dropped bombs before, there are now artillery shells and mortars of all sizes filled by IM explosives. The United States have been a precursor in the world by making the first important step by identifying its IM munitions [6]. The operator finding a shell in the field will now be able to know that it is IM. This is seen by the authors as an absolute necessity. Subsequently, as the development of very insensitive explosives is made, there is a need for new EOD methods for the efficient and clean destruction of IM.

The objective of this paper is to present the work that was performed at our research establishment to identify clean disposal methods for insensitive munitions. Our approach of coupling the testing of EOD methods with residue measurements will be presented. It is felt that it provides information that did not exist before and suggests a way forward for the development and testing of EOD methods for IM munitions.

Experimental Method

The objective was to find a suitable EOD method for one particular round, selected because of the current need for identifying an efficient EOD method for this round in Canada. It is a large-calibre Army round filled by a DNAN-based explosive developed at US ARDEC (PAX family), and containing NTO and a nitramine. One particular round was selected, but we feel that it representative of many other IM rounds. It was decided to couple the tests with measurements of post-detonation traces of explosives produced using each tested method. The method used for the collection of explosive residues on snow during an EOD operation was already reported in the past [7-10]. It was based on years of testing performed in the USA and Canada starting in the mid-90's, and it was used extensively in SERDP Project ER-2219 [11], which was a collaboration between the USA and Canada on the characterization of residues from the detonation of Insensitive Munitions. Briefly, the method involves performing detonations on snow, and collecting post-detonation samples after a careful delineation of the area of deposition, using the soot as the marker for the given area. Snow samples are collected using a systematic and multi-incremental approach and the snow samples are melted, filtrated

and both fractions are sent to chemical analysis [7]. The detonation is often made on a block of ice to prevent a crater from forming and reaching the ground, to avoid cross-contamination coming from the soil under the snow. Figure 1 presents a generic munition, from a past test, on a block of ice. The black soot trace is a good marker for the extent of the particles produced during the detonation. To ensure that the area delineated was large enough to collect all residues, a wider area is also delineated and sampled as shown in Figure 2.

The chemical analysis of DNAN and the nitramine were performed by High Pressure Liquid Chromatography (HPLC) with a photodiode array detector. When no detectable limits were found, extracts were re-analyzed using a gas chromatographic (GC) method on a DB-1 column of 7.4 m to increase the sensitivity. NTO was analyzed following a method obtained from Ms. Marianne Walsh from CRREL [12].



Figure 1: A munition on a block of ice ready for detonation (past test, not the current munition)



Figure 2: Sampling of area post-detonation

Both full-order detonations and EOD of munitions (attack from the outside) were made on the munition, for comparison. The number of repetition was kept from one to five for each scenario, given the significant costs and resources necessary for the chemical analysis of all the samples.

Different methods were tested for the EOD of the rounds, in order to find the ones that would produce the smallest amounts of explosive residues. They were selected using past experience, or through suggestions made by scientific staff or military EOD personnel. It should be noted that no simulation of these scenarios has been performed yet at DRDC-Valcartier Research Center. The explosive used to attack the round was Composition C-4, commercially available shaped charges or a military shaped charge. The list of scenarios tested is given in Table 1.

Table 1: Scenarios used for the EOD of an IM round

Scenario number	Scenario	Comment
1	Full-order detonation	Explosive (C-4, 100g) in the fuze well for initiation. Five repetitions.
2	5 blocks of C-4 around the charge	Simultaneous detonation of the five blocks, causing the shocks to meet inside the round. Four repetitions.
3	2 blocks of C-4	Test to try to reduce the amount of explosives for EOD. Only one repetition.
4	2 blocks of C-4, at the nose, optimized	Targeting the booster from the

	configuration	outside. Simultaneous detonation on each side, causing the shock to meet inside the round and compress the booster. Three repetitions.
5	67-mm shaped charge on the side	Going through the largest diameter, perpendicular to the axis of the shell. Three repetitions.
6	33-mm shaped charge aimed at the booster	Targeting the booster. Two repetitions.
7	67-mm shaped charge aimed at the booster	Targeting the booster. Two repetitions.
8	67-mm shaped charge aimed at the back	Going through the round from the back. Two repetitions.
9	84-mm shaped charge aimed at the back	Going through the round from the back. Military shaped charge. One repetition.

The idea of using shaped charges came from DRDC work with a commercial product (SM-EOD series from Saab Bofors) for the destruction of conventional ammunition (TNT-based). This method worked extremely well with 33-mm shaped charges, and produced high-order detonations every time. It was also appreciated by the EOD workers that performed the tests because of the stand-off offered and the ease of setting up the EOD operation. However, since we only had 20-mm and 33-mm shaped charges, it was found difficult to apply with IM explosives. It created partial detonations. The decision was then made to either seek a larger shaped charge (67- and 84-mm), or attack the booster. From IM shaped charge jet tests reported in the literature, it was found that a number of recent IM formulations could not pass the test with large shaped charges (RPG-7 size) that had significant v^2d values. There appeared to always be a shaped charge that would be large enough to obtain a detonation. The second option, attacking the booster, comes from the fact that a more sensitive explosive is usually placed in the explosive train, as the booster for the main charge, or as a supplementary charge. By targeting this explosive, which should be more sensitive, there is a good chance to initiate the booster and then detonate the complete round.

Results and Discussion

To assess the performance of each scenario at destroying the explosives, two ratios were defined. The first one is the Deposition Rate (DR). The DR is in percentage, and it is defined as:

$$DR = (\text{total mass of ingredient deposited} / \text{initial mass of ingredient in the round}) * 100 \%$$

It is calculated for each separate explosive species in the composition. However, in this paper, only the Deposition Rates of NTO and DNAN are reported and compared. These were the most relevant, since the nitramine is more sensitive.

The second ratio is called the Detonation Efficiency (DE). It is also reported in percentage, and it is defined as:

DE = 100 – ((the total masses of products deposited divided by the original total mass of ingredients in the round) X 100).

Both are useful to analyze the data collected. In an ideal world, the deposition rate of all ingredients would be zero and the detonation efficiency would then be 100%. While it is known that all detonations release at least forensic traces of explosives, we should try to reach as close as possible to this 100%, in order to minimize the contamination on training ranges and increase the sustainability of those ranges.

The results are presented in Table 2 for the various scenarios. It is very interesting to note that the full-order detonation of this round appears very efficient, with only traces of explosives being present. It is then possible to have clean detonations of IM rounds, when they are properly initiated. At 99.999% efficiency, the round compares well to conventional rounds filled in Composition B [3].

The second general observation that can be made is that the deposition rate of NTO is almost always larger than that of DNAN. This is a little counter-intuitive, given that DNAN is more a flammable solid than an explosive and does not detonate well. NTO is a good explosive in itself, with a good performance.

Table 1: Results of the deposition rates and detonation efficiency for the EOD scenarios of an IM round

Scenario	Number of replicates	DNAN DR (%)	NTO DR (%)	Detonation Efficiency (%)
1. Full-order detonation	5	0.001	0.002	99.999
2. 5 blocks of C-4 around the charge	5	6	26	83.7
3. 2 blocks of C-4, one on each side	4	13	43	72.1
4. 2 blocks of C-4, at the nose, optimized configuration	3	6	0.3	97.4
5. 67-mm shaped charge on the side	3	1	10	93.9
6. 33-mm shaped charge aimed at the nose	2	0.6	1	99.1
7. 67-mm shaped charge aimed at the nose	2	53	74	40.5
8. 67-mm shaped charge aimed at the back	2	29	26	74.3
9. 84-mm shaped charge aimed at the back	1 3	0.4 0.001	0 0.0001	99.8 99.999

Repetition of the test in following year				
--	--	--	--	--

The results of EOD scenarios using C-4 were rather discouraging. While it appeared, during the tests, to create full-order detonations and get rid of the rounds, the detonation efficiency was rather low for two of the scenarios, despite the fact that no large fragments were found at detonation point and everything indicated that they were high order events. Our modification (scenario 4) raised the efficiency to 97.4%, which is much better. However, it is rather low compared to the blow-in-place results of Walsh et al. for 60 mm mortars and 81mm mortars filled in Composition B, as examples (99.93% and 99.998%, respectively) [3]. However, at those levels of efficiency, the difference would be difficult to catch in practice, even with pressure sensors. It is only by performing those deposition rates studies at the same time as the EOD testing that we were able to identify the problem. Scenario 4 still releases tens of grams of explosives on the range for each detonation. Depending on the range location, use, hydro-geological behaviour, this could compromise the sustainability of the range. The other two methods with Composition C-4 (scenarios 2 and 3) generate hundreds of grams of explosives residues.

The results using C-4 encouraged the exploration of alternative methods for EOD of IM rounds. The use of shaped charges was already being investigated for conventional rounds at DRDC. It was decided to try with IM rounds as well. A 67-mm shaped charge on the side of the round produced promising results, with a detonation efficiency of 94%. This was still not the ideal result, but it was a step in the right direction. A 33-mm shaped charge pointed at the booster gave very good results in scenario 6 (detonation efficiency of 99%), but a 67-mm shaped charge doing the same job did very poorly. We assumed that we did not aim correctly and missed the booster, hitting instead the dummy fuse, or that the large amount of explosives was making the munition move on the block of ice during the attack. This demonstrated how complicated this operation would be in practice, to try to target the booster. Finally, a shaped charge aimed at the back of the round produced also mixed results. The 84-mm shaped charge gave a spectacular detonation efficiency, at 99.8% (repeated the following year and finding 99.999%), while the 67-mm shaped charge at the back only produced a detonation efficiency of 74.3%. The 67-mm shaped charge may have missed the explosive in the round. This method, using an 84-mm shaped charge, is, as far as we are concerned, the best way of disposing of UXO's of those rounds in the field, but if the booster can be targeted, a smaller shaped charge can be used to obtain a good efficiency detonation.

Other results have also shown similar trends [3]. The use of plastic explosives (or TNT) in blocks, outside of explosive shells, will meet limitations with very insensitive explosives (and propellants). It seems obvious now that shock-insensitive explosives would resist better to a shock through a metal wall coming from a plastic explosive. We believe that we are already there with the current IM explosives. And it is imperative that those new methods are developed to reduce or eliminate any future accumulation of contaminants in the training ranges.

DRDC - Valcartier Research Center has already started working on those new EOD methods for IM. The shaped charge approach was presented in the paper. In addition, here are some of the ideas that have been explored or are being explored:

- An optimal shaped charge for EOD. This tool is being developed with the objective of being tailored for EOD operations, and not necessarily for penetration of metal.
- Cutting charges for very insensitive explosives. When C-4 fails, when shaped charges would have to be monstrous in order to be efficient, a two-step process may be used, especially for tank and artillery rounds. The first step is to separate the fuse from the shell using a cutting charge. The main explosive and/or the booster explosive now become exposed. The second step is to place plastic explosives to initiate the charge from the booster well. Given the high detonation efficiency for high-order of IM rounds, this could work well to reduce the contamination.
- Thermite torches or any other device to initiate a burning reaction. Explosives burn well, and burning is often a rather clean process that at least does not generate large amounts of explosives residues.
- Modifications to the IM formulations to optimize the detonation efficiency while preserving the IM character. Tests have just been performed to that effect and the results will be known in the following months.
- High-power lasers. Tests have been performed using high-power lasers on IM rounds and the results are very promising. This will be the topic of another paper at a future meeting.

Conclusion

Different ways of destroying UXO's containing an IM explosive based on DNAN and NTO have been explored. The results showed that, in that case, the attack using C-4 blocks on the side of the round were not efficient (detonation efficiency of 72-84 %) and created large amounts of explosive residues. An optimal way of applying the C-4 was tested, but reached a detonation efficiency of 97%, which could be problematic for some ranges. An EOD method using shaped charges was tested. It was found that, if the shaped charge is precise enough, attacking the booster with a shaped charge can produce 99% efficiency of detonation using a 33-mm shaped charge. However, the best results were found using an 84-mm shaped charge aimed at the back of the round, in the base plate, perpendicular to the axis of the round, so that the jet would run all the way to the front through the explosive.

Those results indicate that, even if visually a high-order reaction appeared to have been created in an EOD operation, in practice it may still spread significant amounts of explosive on the ground. This was not the case with conventional rounds filled in Composition B. The results also indicate that new EOD methods for IM rounds need to be developed, that may not involve the traditional application of plastic explosives. It would be wise to couple deposition rate tests with the development of these new EOD methods for IM, to ascertain the success of the operation.

Acknowledgements

The staff at DASPM 4-3-4C, especially Mr. Stu McCulloch are acknowledged for their leadership and advisor role. Dr. Dana Pantea from the Director Land Equipment Program Staff is acknowledged for her support and leadership role in promoting the conduct of deposition rate tests and ensuring range sustainability. The Directorates of Ammunitions and Explosives Management and Engineering and of Land and Environmental are also acknowledged for their support. GD-OTS Canada is acknowledged for their essential collaboration by providing rounds, supplementary charges and inert fuses for our trials, in particular Mr. Pierre Pelletier and Ms. Isabelle Laroche. The DRDC technical staff is also greatly acknowledged for the trial and laboratory work, namely Ms. Annie Gagnon, Mr. André Marois, Ms. Annie Martinet and Mr. Charles Nicole. Mr. Nicole as well as Mr. Pascal Béland are also acknowledged for producing the booster charges in 2015.

References

- 1- Patel, C., Common Low-Cost IM Explosive Program, Presented at the Partners in Environmental Technology Technical Symposium & Workshop, 30 Nov 2011, Washington, DC, USA.
- 2- Thiboutot, S., Brousseau, P. et Ampleman, G., Deposition of PETN following the detonation of Seismoplast plastic explosive, *Propellants, Explosives, Pyrotechnics*, Special Issue: 40 Years of PEP, Volume 40, Issue 3, April 2015, pp. 329–332.
- 3- Walsh, M.R., Walsh, M.E., Ramsey, C.A., Zufelt, J., Thiboutot, S., Ampleman, G. et Zunino, L., Energetic residues from the detonation of IMX-104 insensitive munitions, *Propellants, Explosives, Pyrotechnics.*, Vol. 39, Jan 2014, pp. 243-250.
- 4- Walsh, M.R., Walsh, M.E., Ramsey, C.A., Brochu, S., Thiboutot, S. et Ampleman, G., Perchlorate contamination from the detonation of insensitive high-explosive rounds (U), *J. Hazardous Mat.*, vol. 262, Aug 2013, pp. 228-233.
- 5- Walsh, M.R., Walsh, M.A., Taylor, S., Ramsey, C.A., Ringelberg, D.B., Thiboutot, S., Ampleman, G. et Diaz E., Characterization of PAX-21 insensitive munition detonation residues, *Propellants, Explosives, Pyrotechnics*, 38 (3), May 2013, pp. 399-409.
- 6- Joint Ordnance Test Procedure (JOTP)-070, Identification Marking for Munitions, Joint Services Munition Safety Test Working Group, Department of Defence, USA, July 2013.
- 7- Walsh, M.R., Walsh, M.E., and Ramsey, C.A”, “Measuring energetic contamination deposition rate on snow”, *Water, Air and Soil Pollution*, 223 (7), pp. 3689-3699, DOI: 10.1007/s11270-012-1141-5, 2012.
- 8- Walsh, M.R., Walsh, M.E. and Ramsey C.E., *Measuring Energetic Residues on Snow*, 2007, ERDC/CRREL report TR-07-19.
- 9- Walsh, M. R., Walsh, M. E., Ramsey, C.A., Thiboutot, S. and Ampleman, G., “ Energetics Residues Deposition from Training with Large Caliber Weapon Systems”, *Proceedings of the European Conference of Defence and the Environment*, June 2015, Helsinki, Finland.

- 10- Walsh, M. E. Walsh, M. R., Ramsey, C.A., Thiboutot, S. and Ampleman, G., “ Sample Collection, Processing, and Analytical Methods for the Measurement of Post-Detonation Residues from Large Caliber Ammunition”, Proceedings of the European Conference of Defence and the Environment, June 2015, Helsinki, Finland.
- 11- <https://www.serdp-estcp.org/Program-Areas/Environmental-Restoration/Contaminants-on-Ranges/Characterizing-Fate-and-Transport/ER-2219>, accessed in March 2018.
- 12- Walsh, M.E., “Analytical Methods for Detonation Residues of Insensitive Munitions”, Journal of Energetic Materials, 34:1, 76-91, DOI:10.1080/07370652.2014.999173.



Explosives Ordnance Disposal (EOD) of Insensitive Munitions: Challenges and Solutions

P. Brousseau, S. Thiboutot, E. Diaz
DRDC Valcartier Research Centre



DRDC | RDDC

Outline

- Introduction: The Problem
- Test Method
- Results
- Future Work
- Conclusion

Introduction: The Problem

- Insensitive Munitions were developed to resist external stimuli
 - Such as shock
- Most munitions have a dud rate
 - They require destruction on military training ranges during training
- Traditional methods use plastic explosives on the side of the round
 - Applying shock

- Insensitive Munitions will be more difficult to destroy
 - Obtain partial detonations
 - Material spread on the training ranges

- We want to avoid contamination of the ranges

Introduction: The Problem



We observed that:

Amount of explosives spread \propto Insensitiveness

We need new EOD methods for IM !

Test Method

- Test EOD methods coupled with Deposition Rate tests
- Tests on snow
- Collect the snow and analyze the residues



Test Method



Test Method

- Army warhead
- Large calibre
 - Generic for this study
 - Method applicable to mortars, artillery and other ammo
- Explosive contains
 - NTO
 - DNAN
 - Nitramine
- The residues post-detonation were analysed for those products

Test Method

- Two parameters defined

- Deposition rate (of each energetic material)

$$DR (\%) = \frac{\text{Mass of ingredient deposited}}{\text{Initial mass of ingredient}} \times 100\%$$

- Detonation efficiency

$$DE (\%) = 100 - \left(\frac{\text{Mass of products deposited}}{\text{Total mass of products}} \times 100 \right)$$

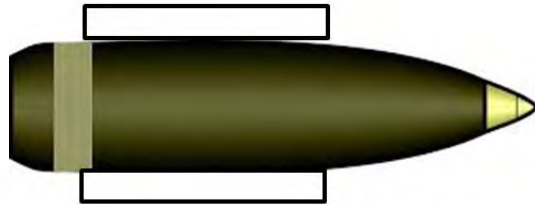
Test Method

- We tested different EOD methods
 - Plastic explosives on the side of the round (different configurations)
 - Shaped charges aimed at the side of the round
 - Shaped charges aimed at the booster
 - Shaped charges aimed at the back of the round
- We like shaped charges for EOD
 - Previous project
 - Good results with conventional rounds and small shaped charges
 - Poor results in the past with IM and small shaped charges
 - “There is always a shaped charge large enough”



Results

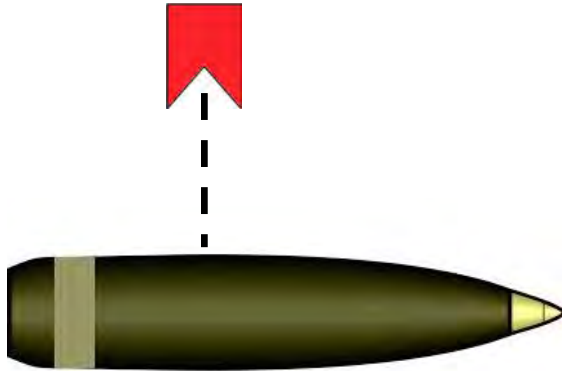
- First tests are normal functioning rounds, in static
 - Our IM round
 - Detonation efficiency = 99.999%
 - Compares well with Composition B in mortar and artillery rounds (literature)
- EOD Method 1: Using plastic explosives
 - 3 different methods
 - All looked full-order
 - The results are lower than EOD of Comp. B filled rounds (60-mm and 81-mm)
 - DE = 99.93% and 99.998%



DE = 72%, 83%, and 97%

Results

- EOD Method 2: Medium (67-mm) commercial shaped charge on the side
 - Interesting detonation efficiency



DE = 94%

Results

- EOD Method 3: Small (33-mm) and Medium (67-mm) commercial shaped charges aimed at the booster
 - Small shaped charge better than medium shaped charge
 - More precise?



DE = 99.1%, 40.5%

Results

- EOD Method 4: Medium (67-mm) commercial and large (84-mm) military shaped charges aimed at the back of the round
 - Medium shaped charge also gives bad results
 - Large shaped charge performs exceptionally well
 - As good as the EOD of Comp. B



DE = 74.3%, 99.8%

Results

- EOD Method 4: Large (84-mm) military shaped charges aimed at the back of the round
 - Tests repeated
 - Even better results



DE = 99.999%

Results

- NTO often gave higher deposition rates than DNAN
 - Counter-intuitive
 - NTO is a good IM ingredient
- NTO results are often variable in those tests on snow
 - High water solubility
 - Disappearance in snow

Future Work

- Alternative EOD methods being tested
 - Shaped charge tailored for EOD operations
 - Cutting charges for very insensitive explosives
 - Thermites to initiate a burning reaction
 - Burning may be cleaner
 - Modifications to the IM formulations to optimize the detonation efficiency
 - High-power lasers

Conclusions

- EOD methods of IM with plastic explosives can be deceiving
 - Low detonation efficiencies
- EOD methods with shaped charges gave variable results
 - On the side, good results
 - At the booster, promising results
 - At the back, some great results with a large shaped charge
- New EOD methods are being tested
- EOD operators may have to be more knowledgeable



DRDC | RDDC

SCIENCE, TECHNOLOGY AND KNOWLEDGE
FOR CANADA'S DEFENCE AND SECURITY

SCIENCE, TECHNOLOGIE ET SAVOIR
POUR LA DÉFENSE ET LA SÉCURITÉ DU CANADA



New generation Influence Mine classified as 1.6N

B. Granqvist, H. Hytti
OY FORCIT AB Forcit Defence
P.O.Box 19, FIN –10901 Hanko, Finland
Bjorn.granqvist@forcit.fi

Introduction

A new underwater Influence Mine, BLOCKER, is a cost effective Influence Mine equipped with advanced sensor systems (acoustic-, pressure- and magnetic sensors, optionally UEP), customer programmable algorithms/parameters and Insensitive Munitions Plastic Bonded Explosives, exercise systems and an impressive total energy output equivalent of over 1000 kg of TNT.

The Blocker is operational in Climate Categories C1 (Cold -33 °C) to B2 (wet warm +63 °C) and the operational depth is down to 100 meters (optionally to 200 meters). Operational time underwater is 1 year (optionally to 2 years) and the shelf-life is 25 years.



This Mine fulfils all the IM requirements, it has no mass explosion hazard and therefore hazard classification 1.1 does not make justice to this system. During the last years after completing the extensive testing, the work to reclassify the Underwater Influence Mine to 1.6N has started in Finland.

BLOCKER PHYSICAL CHARACTERISTICS	
Shape	Barrel
Height	Max. 1300 mm
Length	Max. 900 mm
Width	Max. 900 mm
Gross weight	~750 kg
Net explosive quantity	~600 kg
OPERATIONAL CHARACTERISTICS	
Shelf-life	25 years
Climate categories	C1-B2, -33 °C up to +63 °C
Main charge (EIDS)	FOXIT-Plastic Bonded Explosive
Booster charge	FPX R1- Plastic Bonded Explosive
Life in water	Minimum 1 year (option min 2 years)
Underwater Shock energy (50 m)	1,4 x TNT
Underwater Bubble energy (50 m)	2,2 x TNT
Maximum operational depth	100 meters (option 200 meters)

The BLOCKER is manufactured by OY FORCIT AB in Finland. It was developed for the Finnish Navy with serial production starting in 2013. Explosives in this product are plastic bonded explosives FOXIT (main charge) and FPX R1 (booster). Both of these explosives are widely tested and qualified.

The main charge FOXIT has been tested according to UN Recommendations on the Transport of Dangerous Goods, Manual of Test and Criteria and qualification testing has been performed by Finnish Defence Forces Research Agency. Based on the tests, FOXIT meets the requirements of EIS-material (Extremely Insensitive Substance).

Qualification for the explosive in the booster FPX R1 has been performed by both Swedish Defence Forces and Finnish Defence Forces. Sensitivity and quality tests for the booster explosive FPX R1 have been performed at Finnish Defence Forces research Agency (FDRA). Swedish Defence Materiel Administration's FSD 0214 standard test methods for booster explosives were used as test guidelines. Underwater Influence Mine, BLOCKER system and its main charge (FOXIT) and booster (FPX R1) combination have proven to be insensitive enough to be classified to class 1.6N.

The current transport classification for the Underwater Influence Mine, BLOCKER is UN 0137 1.1D. The aim is to get international transport classification in hazard division 1.6 and compatibility group N under the UN 0486.

Tests performed

In addition to STANAG IM tests, the UN Tests 7 (g) - 7(k) have been conducted to the whole Underwater Influence Mine (Article) and series 3, 5 and 7 (a) – 7(f) tests have been made on the FOXIT (Substance). According to tests performed by FDRA, the Underwater Influence Mine is not too dangerous to transport (the Manual of Tests and Criteria, Series 4) and it is thermally stable (the Manual of Tests and Criteria, Series 3). The Underwater Influence Mine passes all the test series 7 tests, and therefore the Underwater Influence Mine could be assigned to division 1.6.

The technical information of Underwater Influence Mine, test results (FOXIT) from UN Test series 3, 5 and 7, other performed tests and FPX R1 (qualification tests according to FSD 0214 and AOP-7):

FOXIT-properties:

PERFORMANCE/PROPERTY	RESULT
DENSITY	1.78 g/cm ³
VELOCITY OF DETONATION	5 500 m/s
CRITICAL DIAMETER (in plastic pipe)	>110 mm
MINIMUM BOOSTER TEST	150-200 g
SCB-TEST (12 °C/min)	168 °C / fire
HYGROSCOPICITY (57 % / 6 weeks)	< 0.06 %
HEAT EXPANSION (-47 ... +83 °C)	0.01 %
HARDNESS (Shore A. 24 °C)	62
TENSILE STRENGTH	0.93 Mpa
ELONGATION	39

Performed tests on the main explosive, Foxit:

Test results from UN Test series 3 and 5

TEST	RESULT	
3 (a)(iv) 30 kg Fall hammer Test	3,6 m, OK	Passes
3 (b)(i) BAM Friction Test	92 N	Passes
3 (c) Thermal Stability at 75 °C	OK	Passes
3 (d) Small-scale Burning Test	Burning	Passes
5 (a) Cap Sensitivity Test	-	Passes
5 (b)(i) DDT Test	-	Passes
5 (c) External Fire Test	-	Passes

Test results from UN Test series 7 (EIDS test result)

TEST	DESCRIPTION	RESULT
7 (a) EIDS Cap test	Shock test to determine the sensitivity to detonation by a standard detonator.	no reaction – pass
7 (b) EIDS Gap test	Shock test with defined booster and confinement to determine the sensitivity to shock. The gap is defined as thickness of PMMA. The substance will pass the test if there is no transmission with the gap thickness of 70 mm or less with the used test assembly.	50 mm - pass
7 (c) EIDS Impact Sensitivity	Test to determine the sensitivity of the explosive substance to deteriorate under the effect of an impact.	Not applicable since the diameter of test charges is well below the critical diameter.
7 (d) EIDS Bullet Impact Test	Test to determine the degree of reaction of the explosive substance to impact or penetration resulting from a given energy source.	Fire - pass
7 (e) EIDS External Fire Test	Test to determine the reaction of	Pressure burst – pass

Close to SCB-test (Stanag 4491)	the explosive substance to external fire when the material is confined.	
7 (f) EIDS Slow Cook-off Test Close to SCB-test (Stanag 4491)	Test to determine the reaction of the explosive substance in an environment in which the temperature is gradually increased to 365 °C.	Pressure burst – pass

Properties of FPX R1:

PERFORMANCE/PROPERTY	RESULT
COMPOSITION	RDX, binder
DENSITY	1,50 g/cm ³
CRITICAL DIAMETER	< 7 mm
VELOCITY OF DETONATION	7 600 m/s

Qualification tests performed on FPX R1:

Test results according to FSD 0214 for FPX R1

TEST	RESULT
NOL LSGT	59 mm
Fall hammer test	20 J (Powder form 20J, chip form 22,5)
Ignition temperature	216°C (1 min)
Friction sensitiveness	>360N
Shooting test	~900 m/s (no detonation 876 m/s, detonation 990 m/s)
Koenen test	< 1,5 mm
Electric spark test	0,5 – 5 J (lower reaction level than with reference material, tetryl)
Detonation velocity	7 598 m/s
Vacuum stability	0,3 ± 0,01 ml/g

Performed tests on Influence Mine

Test results from UN Test series 7 (EIDS test result)

TEST	ARTICLE	DESCRIPTION	RESULT
7 (g) 1.6 Article External Fire Test	Complete influence mine	Test to determine whether there is a mass explosion or a hazard from dangerous projections, radiant heat and/or violent burning when involved in a fire.	Burning - pass
7 (h) 1.6 Article Slow Cook-off Test	Complete influence mine	Test to determine the reaction of the article in an environment in which the temperature is gradually increased to 365 °C.	Burning - pass
7 (j) 1.6 Article Bullet Impact Test	Tests performed separately on booster and main charge	Test to determine the degree of reaction of the article to impact or penetration resulting from a given energy source.	<u>FPX R1 booster:</u> Burning – pass <u>Foxit -main charge:</u> Burning - pass
7 (k) 1.6 Article Stack Test	Complete influence mine	Test to determine whether a detonation of an article, as offered for transport, will initiate a detonation in an adjacent, like article.	30 cm – detonation 40 cm - pass

Additional tests performed on Influence Mine

TEST	RESULT
4 (b) (ii) 12 meter drop test	No fire or explosion - pass
4 (a) Thermal stability test	No external effects, no temperature rise exceeding 3 °C – pass
SCJ Impact test according to STANAG 4526	Deflagration/burning - pass

Current status

The concept has been discussed with the Finnish Safety and Chemicals Agency and also with the Finnish Transport Safety Agency. The Sub-Committee of Experts on the Transport of Dangerous Goods (Committee of Experts on the Transport of Dangerous Goods and on the Globally Harmonized System of Classification and Labelling of Chemicals) had this topic on their agenda during their meeting in Geneva November 2017. There was an international consensus, providing that if all the tests required has been performed acceptably, the classification to 1.6N should be possible for the system. According to the decision of the Sub-Committee of Experts on the Transport of Dangerous Goods, the package type (ADR P101) does not exclude the possibility to classify the article as 1.6N.

At the moment the application is under evaluation by the Finnish Safety and Chemical Agency. We expect to have the approval by summer 2018.

New generation Influence Mine classified as 1.6N

B. Granqvist, H. Hytti

OY FORCIT AB Forcit Defence

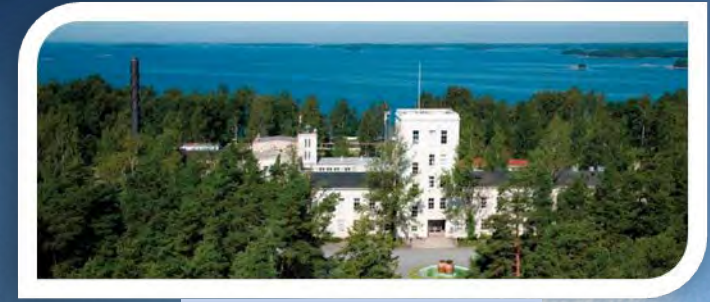
P.O.Box 19, FIN –10901 Hanko, Finland

Bjorn.granqvist@forcit.fi

New generation Influence Mine classified as 1.6N

History:

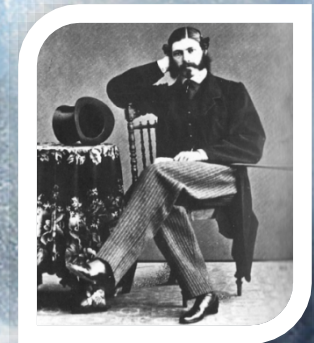
- Forcit was founded in 1893, Finland
- Since 1920's been a manufacturer for armed forces: ammunition, TNT -> PBX -> Defence System supplier
- Development and production of PBX's since 1983



Hanko plant

Today:

- Forcit is the largest explosives producer in Nordic countries
- Own R&D programmes and PBX family, also commonly known PBXN-109 etc.
- One of the largest PBX manufacturers in Europe



Forcit founder
John Malcom
Lewin 1893

New generation Influence Mine classified as 1.6N

- BLOCKER, is a cost effective Influence Mine equipped with advanced sensor systems (acoustic-, pressure- and magnetic sensors, optionally UEP)
- The BLOCKER is manufactured by OY FORCIT AB in Finland. Development was initiated by the Finnish Navy with serial production starting in 2013.
- Insensitive Munitions Plastic Bonded Explosives, FOXIT and FPX R1M as a booster.
Total underwater energy output equivalent to over 1000 kg of TNT



New generation Influence Mine classified as 1.6N

BLOCKER PHYSICAL CHARACTERISTICS	
Shape	Barrel
Height	Max. 1300 mm
Length	Max. 900 mm
Width	Max. 900 mm
Gross weight	~750 kg
Net explosive quantity	~600 kg
OPERATIONAL CHARACTERISTICS	
Shelf-life	25 years
Climate categories	C1-B2, -33 °C up to +63 °C
Main charge (EIDS)	FOXIT-Plastic Bonded Explosive
Booster charge	FPX R1- Plastic Bonded Explosive
Operational in water	Minimum 1 year (option min 2 years)
Underwater Shock energy (50 m)	1,4 x TNT
Underwater Bubble energy (50 m)	2,2 x TNT

New generation Influence Mine classified as 1.6N

- Both main charge and booster explosives widely tested and qualified (STANAG).
- FOXIT has been tested according to UN Recommendations on the Transport of Dangerous Goods and testing has been performed by Finnish Defence Forces Research Agency. Based on the tests, FOXIT meets the requirements of EIS-material (Extremely Insensitive Substance).
- Qualification of the booster explosive FPX R1 has been performed by UK MOD, Swedish Armed Forces and Finnish Defence Forces.
- Underwater Influence Mine, BLOCKER system and its main charge (FOXIT) and booster (FPX R1) combination have proven to be insensitive enough to be classified to 1.6N.
- The aim was to get international transport classification in hazard division 1.6 and compatibility group N under the UN 0486.

New generation Influence Mine classified as 1.6N

- This Mine fulfils all the IM requirements.
- Tests and classification for 1.6N was initiated.
- After completing the extensive testing, the work to classify the Underwater Influence Mine to 1.6N was finalized in Finland 2018.

New generation Influence Mine classified as 1.6N

- In addition to STANAG IM tests, the UN Tests 7 (g) - 7(k) and series 4 have been conducted to the whole Underwater Influence Mine (Article). Series 3, 5 and 7 (a) – 7(f) tests have been made on the FOXIT (Substance). According to tests performed by FDRA, the Underwater Influence Mine is not too dangerous to transport (the Manual of Tests and Criteria, Series 4) and it is thermally stable (the Manual of Tests and Criteria, Series 3).
- The Underwater Influence Mine passes all the test series 7 tests, and therefore the Underwater Influence Mine could be assigned to division 1.6.
- Booster less than 0,25 vol-% and hence no need for EIS, according to Transport of Dangerous Goods Manual of Tests and Criteria 6th edition.

New generation Influence Mine classified as 1.6N

- 7 (a) – 7 (f) tests on FOXIT

TEST	DESCRIPTION	RESULT
7 (a) EIDS Cap test	Shock test to determine the sensitivity to detonation by a standard detonator.	no reaction – pass
7 (b) EIDS Gap test	Shock test with defined booster and confinement to determine the sensitivity to shock. The gap is defined as thickness of PMMA. The substance will pass the test if there is no transmission with the gap thickness of 70 mm or less with the used test assembly.	50 mm - pass
7 (c) EIDS Impact Sensitivity	Test to determine the sensitivity of the explosive substance to deteriorate under the effect of an impact.	Not applicable since the diameter of test charges is well below the critical diameter.
7 (d) EIDS Bullet Impact Test	Test to determine the degree of reaction of the explosive substance to impact or penetration resulting from a given energy source.	Fire - pass
7 (e) EIDS External Fire Test Close to SCB-test (Stanag 4491)	Test to determine the reaction of the explosive substance to external fire when the material is confined.	Pressure burst – pass
7 (f) EIDS Slow Cook-off Test Close to SCB-test (Stanag 4491)	Test to determine the reaction of the explosive substance in an environment in which the temperature is gradually increased to 365 °C.	Pressure burst – pass

New generation Influence Mine classified as 1.6N

Performed tests on Influence Mine

Test results from UN Test series 7 (EIDS test result)

TEST	ARTICLE	DESCRIPTION	RESULT
7 (g) 1.6 Article External Fire Test	Complete influence mine	Test to determine whether there is a mass explosion or a hazard from dangerous projections, radiant heat and/or violent burning when involved in a fire.	Burning - pass
7 (h) 1.6 Article Slow Cook-off Test	Complete influence mine	Test to determine the reaction of the article in an environment in which the temperature is gradually increased to 365 °C.	Burning - pass
7 (j) 1.6 Article Bullet Impact Test	Tests performed on sea mine and separately on booster	Test to determine the degree of reaction of the article to impact or penetration resulting from a given energy source.	<u>FPX R1 booster:</u> Burning – pass <u>Sea mine:</u> Burning - pass
7 (k) 1.6 Article Stack Test	Complete influence mine	Test to determine whether a detonation of an article, as offered for transport, will initiate a detonation in an adjacent, like article.	30 cm – detonation 40 cm - pass

New generation Influence Mine classified as 1.6N

7 (h) 1.6 Article Slow Cook-off Test



Result: Burning - Pass



New generation Influence Mine classified as 1.6N

Performed tests on Influence Mine

Test results from UN Test series 7 (EIDS test result)

TEST	ARTICLE	DESCRIPTION	RESULT
7 (g) 1.6 Article External Fire Test	Complete influence mine	Test to determine whether there is a mass explosion or a hazard from dangerous projections, radiant heat and/or violent burning when involved in a fire.	Burning - pass
7 (h) 1.6 Article Slow Cook-off Test	Complete influence mine	Test to determine the reaction of the article in an environment in which the temperature is gradually increased to 365 °C.	Burning - pass
7 (j) 1.6 Article Bullet Impact Test	Tests performed on sea mine and separately on booster	Test to determine the degree of reaction of the article to impact or penetration resulting from a given energy source.	<u>FPX R1 booster:</u> Burning – pass <u>Sea mine:</u> Burning - pass
7 (k) 1.6 Article Stack Test	Complete influence mine	Test to determine whether a detonation of an article, as offered for transport, will initiate a detonation in an adjacent, like article.	30 cm – detonation 40 cm - pass

New generation Influence Mine classified as 1.6N

7 (k) 1.6 Article Stack Test



No propagation at 35cm →
7(k) tests at 40cm

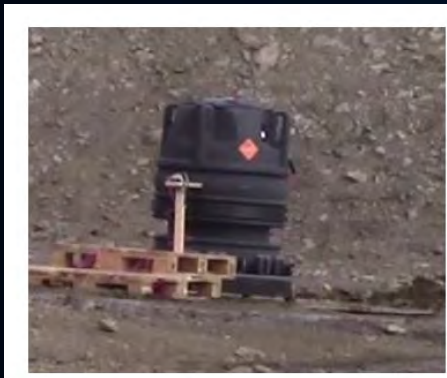
Booster, SAU with detonator etc.



New generation Influence Mine classified as 1.6N

IM testing example: SCJ Impact test according to STANAG 4526

TEST	RESULT
SCJ Impact test according to STANAG 4526	Deflagration/burning - pass



66mm hollow charge

New generation Influence Mine classified as 1.6N

Transport and storage configuration



New generation Influence Mine classified as 1.6N

Current status

The concept has been discussed with the Finnish Safety and Chemicals Agency and also with the Finnish Transport Safety Agency. The Sub-Committee of Experts on the Transport of Dangerous Goods (Committee of Experts on the Transport of Dangerous Goods and on the Globally Harmonized System of Classification and Labelling of Chemicals) had this topic on their agenda during their meeting in Geneva November 2017. There was an international consensus, providing that if all the tests required has been performed acceptably, the classification to 1.6N would be possible for the system. According to the decision of the Sub-Committee of Experts on the Transport of Dangerous Goods, the package type (ADR P101) does not exclude the possibility to classify the article as 1.6N.

New generation Influence Mine classified as 1.6N

Current status

The application was approved by the Finnish authority (Finnish Safety and Chemicals Agency) in April 2018, and the Blocker Influence Sea Mine is now classified as 1.6N

tukes
Terveystieteiden tutkimuskeskus
Suomen Terveystieteiden tutkimuskeskus

Päätös: 1 (2)
11.4.2018 15M/37/2018

ty: FORCIT AB, ForcIT Defence
PL 07
00001 Helsinki
FINLAND

Häätymäaikana 13.5.2018

Käijäheiden kuljetusluokituksen ja pakkaamattomana kuljetuksen hyväksynnän

Tuote: **1.6N** ja **1.6N** -merkitseminen
Tämä on ajateltavissa olevan vaaran, hyljintöiden, vaurioiden ja heikentämisen vaara. Lisäksi voidaan todeta myös muita haittoja.

Kuljetusluokitus
Tässä hyväksyntä edellyttää väkivallan väkivallan pakkaamattomana IMDG-koodin luvun 4.2.4 pöytäkirjan F201 vaatimusten pohjalta perustettua suojaa. Muutoksia, jotka koskevat sen valmistusta ja käytettyjen erityisvarusteiden käyttöä, on otettava huomioon. Tuotteen pakkaus on täytettävä täysin ilman lähtevä tuuletus ja tuuletus on säilytettävä tuuletusta toiseen etäällä.

Käijäheiden hyväksyntä luokitus

Kuljetusluokka:	6
Vaaranluokitus:	1.6
Tuotteenryhmä:	1.6
Y-tunnus:	1.6
Aiheeseen liittyvät koodit:	1.6N1, 1.6N2, 1.6N3, 1.6N4, 1.6N5, 1.6N6, 1.6N7, 1.6N8, 1.6N9, 1.6N10, 1.6N11, 1.6N12, 1.6N13, 1.6N14, 1.6N15, 1.6N16, 1.6N17, 1.6N18, 1.6N19, 1.6N20, 1.6N21, 1.6N22, 1.6N23, 1.6N24, 1.6N25, 1.6N26, 1.6N27, 1.6N28, 1.6N29, 1.6N30, 1.6N31, 1.6N32, 1.6N33, 1.6N34, 1.6N35, 1.6N36, 1.6N37, 1.6N38, 1.6N39, 1.6N40, 1.6N41, 1.6N42, 1.6N43, 1.6N44, 1.6N45, 1.6N46, 1.6N47, 1.6N48, 1.6N49, 1.6N50, 1.6N51, 1.6N52, 1.6N53, 1.6N54, 1.6N55, 1.6N56, 1.6N57, 1.6N58, 1.6N59, 1.6N60, 1.6N61, 1.6N62, 1.6N63, 1.6N64, 1.6N65, 1.6N66, 1.6N67, 1.6N68, 1.6N69, 1.6N70, 1.6N71, 1.6N72, 1.6N73, 1.6N74, 1.6N75, 1.6N76, 1.6N77, 1.6N78, 1.6N79, 1.6N80, 1.6N81, 1.6N82, 1.6N83, 1.6N84, 1.6N85, 1.6N86, 1.6N87, 1.6N88, 1.6N89, 1.6N90, 1.6N91, 1.6N92, 1.6N93, 1.6N94, 1.6N95, 1.6N96, 1.6N97, 1.6N98, 1.6N99, 1.6N100

Tämä päätös on annettu IMDG-koodin perusteella. Tässä ei kuitenkaan ole esitetty mitään erityistä suojaa. Aikaa, jona tämä päätös on voimassa, on 10 vuotta. CAD-Tuote on valmistettu ja pakkaaminen on suoritettu mukaisesti kuljetukseen, eikä jatkossa Y-tunnus käytettävissä jatkuvasti käytettävissä ole. Tuotteen pakkaus on täytettävä täysin ilman lähtevä tuuletus ja tuuletus on säilytettävä tuuletusta toiseen etäällä.

Yhteyshenkilö: **FORCIT AB**
Puhelin: +358 (0)10 300 3000
Sähköposti: **forcit@forcit.com**

1 (2)

Lisäohjeita: Tämä päätös on annettu IMDG-koodin perusteella. Tässä ei kuitenkaan ole esitetty mitään erityistä suojaa. Aikaa, jona tämä päätös on voimassa, on 10 vuotta. CAD-Tuote on valmistettu ja pakkaaminen on suoritettu mukaisesti kuljetukseen, eikä jatkossa Y-tunnus käytettävissä jatkuvasti käytettävissä ole. Tuotteen pakkaus on täytettävä täysin ilman lähtevä tuuletus ja tuuletus on säilytettävä tuuletusta toiseen etäällä.

Pakkaamattomana kuljetuksen hyväksyntä

Tämä päätös on annettu IMDG-koodin perusteella. Tässä ei kuitenkaan ole esitetty mitään erityistä suojaa. Aikaa, jona tämä päätös on voimassa, on 10 vuotta. CAD-Tuote on valmistettu ja pakkaaminen on suoritettu mukaisesti kuljetukseen, eikä jatkossa Y-tunnus käytettävissä jatkuvasti käytettävissä ole. Tuotteen pakkaus on täytettävä täysin ilman lähtevä tuuletus ja tuuletus on säilytettävä tuuletusta toiseen etäällä.

Päätöksen voima
Tämä päätös on annettu 11.4.2018 klo 15:00. Tämä päätös on voimassa 10 vuotta.

Muutokset
Tässä päätöksessä ei ole esitetty mitään erityistä suojaa. Aikaa, jona tämä päätös on voimassa, on 10 vuotta. CAD-Tuote on valmistettu ja pakkaaminen on suoritettu mukaisesti kuljetukseen, eikä jatkossa Y-tunnus käytettävissä jatkuvasti käytettävissä ole. Tuotteen pakkaus on täytettävä täysin ilman lähtevä tuuletus ja tuuletus on säilytettävä tuuletusta toiseen etäällä.

Luokitellut säännökset ja määräykset
IMDG-koodin luvun 2.3 kohta 2.3.2.2 ja luvun 4.3 kohta 4.3.4
Aikaa, jona tämä päätös on voimassa, on 10 vuotta. CAD-Tuote on valmistettu ja pakkaaminen on suoritettu mukaisesti kuljetukseen, eikä jatkossa Y-tunnus käytettävissä jatkuvasti käytettävissä ole. Tuotteen pakkaus on täytettävä täysin ilman lähtevä tuuletus ja tuuletus on säilytettävä tuuletusta toiseen etäällä.

Liitteet
Valtuutus
Määräykset

Tuotteet
1.6N1, 1.6N2, 1.6N3, 1.6N4, 1.6N5, 1.6N6, 1.6N7, 1.6N8, 1.6N9, 1.6N10, 1.6N11, 1.6N12, 1.6N13, 1.6N14, 1.6N15, 1.6N16, 1.6N17, 1.6N18, 1.6N19, 1.6N20, 1.6N21, 1.6N22, 1.6N23, 1.6N24, 1.6N25, 1.6N26, 1.6N27, 1.6N28, 1.6N29, 1.6N30, 1.6N31, 1.6N32, 1.6N33, 1.6N34, 1.6N35, 1.6N36, 1.6N37, 1.6N38, 1.6N39, 1.6N40, 1.6N41, 1.6N42, 1.6N43, 1.6N44, 1.6N45, 1.6N46, 1.6N47, 1.6N48, 1.6N49, 1.6N50, 1.6N51, 1.6N52, 1.6N53, 1.6N54, 1.6N55, 1.6N56, 1.6N57, 1.6N58, 1.6N59, 1.6N60, 1.6N61, 1.6N62, 1.6N63, 1.6N64, 1.6N65, 1.6N66, 1.6N67, 1.6N68, 1.6N69, 1.6N70, 1.6N71, 1.6N72, 1.6N73, 1.6N74, 1.6N75, 1.6N76, 1.6N77, 1.6N78, 1.6N79, 1.6N80, 1.6N81, 1.6N82, 1.6N83, 1.6N84, 1.6N85, 1.6N86, 1.6N87, 1.6N88, 1.6N89, 1.6N90, 1.6N91, 1.6N92, 1.6N93, 1.6N94, 1.6N95, 1.6N96, 1.6N97, 1.6N98, 1.6N99, 1.6N100

New generation Influence Mine classified as 1.6N

Thank you!

Questions?



Comparing Fires Using Scaling

Jon J. Yagla, PhD.

Insensitive Munitions and Energetic Materials Technology Symposium

Portland, Oregon USA

April 2018

*Gun and Electric Weapon
Systems (E)*



NSWCDD-PN-16-00187; Distribution Statement A: Approved for Public Release, distribution is unlimited

Fires Studied



Swedish JP5

~ 3ft x 4ft
(.9 x 1.1 m)



Swedish Sand Burner

~ 3ft x 4ft
(.9 x 1.1 m)



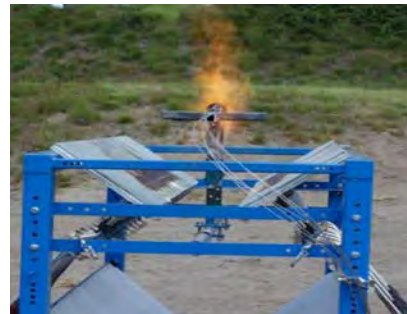
Swedish Torch

~ 1.5ft x 3ft
(.5 x .9 m)



Meppen Propane

~26ft x 16ft
7.9 x 4.9 m



Dutch Torch

~1.5ft x 3ft
(.5 x .9 m)



Dahlgren JP5

30ft x 30ft
(9.2 x 9.2 m)

Fires Studied, Cont.



Dutch Diesel
~6 ft diameter
(1.8 m)



Dahlgren JP5
12ft x 12ft
(3.8 x 3.8 m)



Dahlgren Propane
8ft x 8ft (2.4 x 2.4 m)
and 12ft x 12ft (3.6 x 3.6 m)

Fires Studied, Cont.



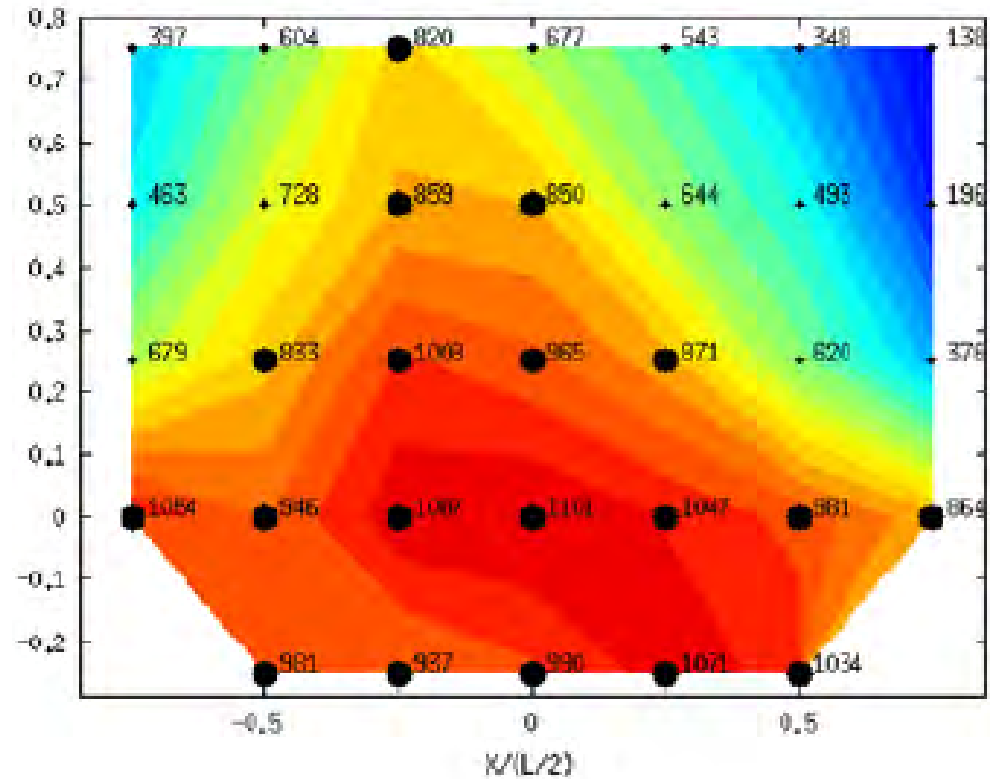
Sandia JP-4
62 f (19 m) Diameter



Meppen Propane
15 x 28 ft (5 x 8 m) Propane

Fires Studied, Final

Dahlgren .6 x 1.2 m propane demo burner



This is the smallest burner in the comparison using scaling study

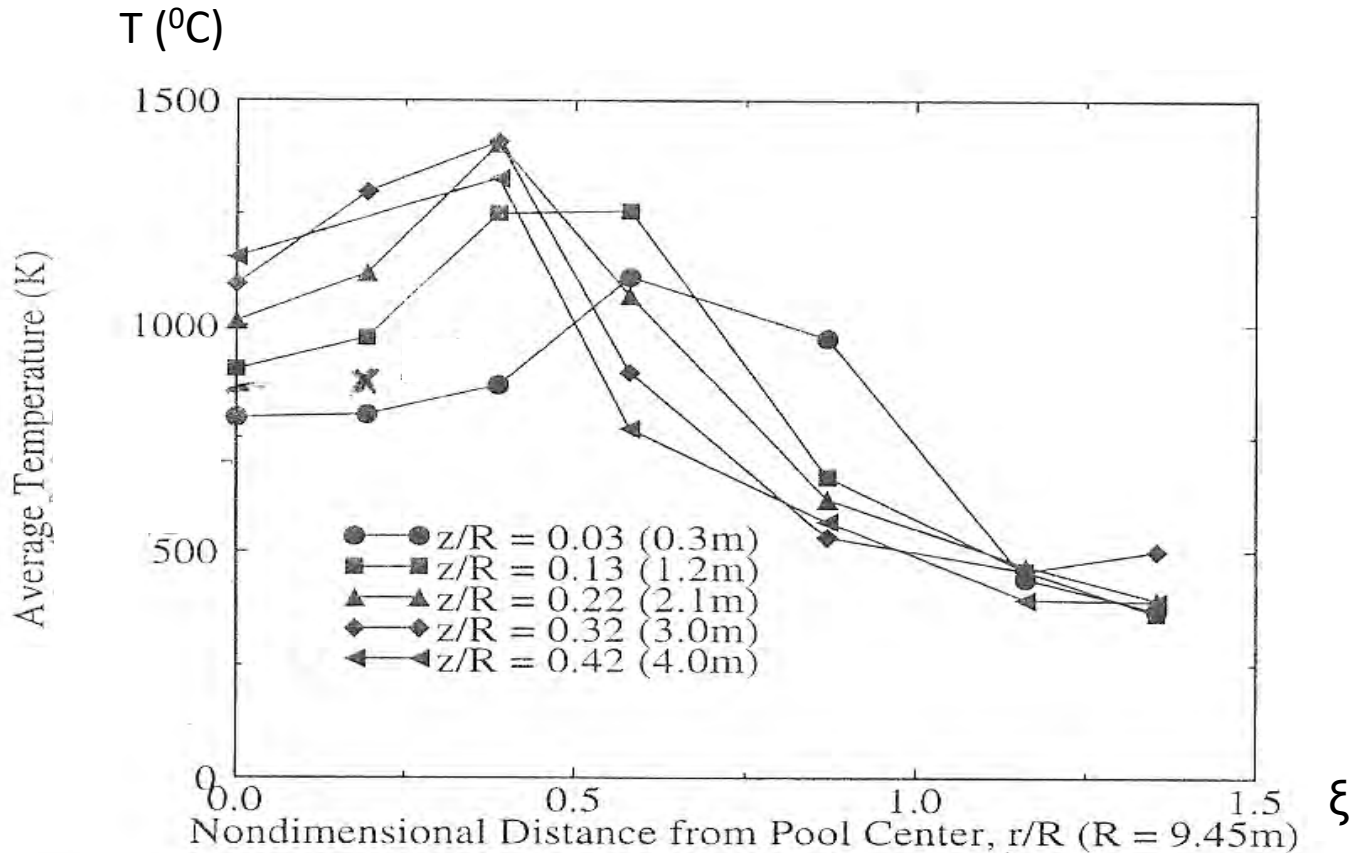


FIG. 1 -- Time-Averaged Thermocouple Temperature Profile for JP4 Pool Fire

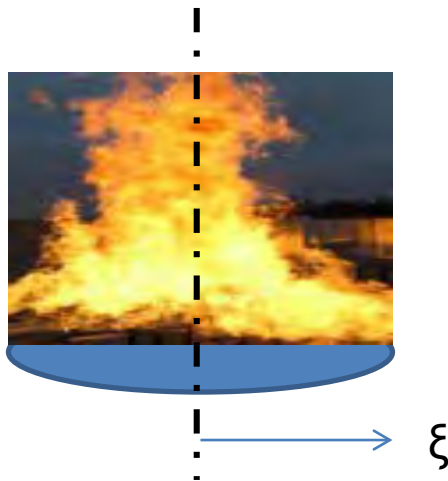
This is the largest burner in the comparison using scaling study



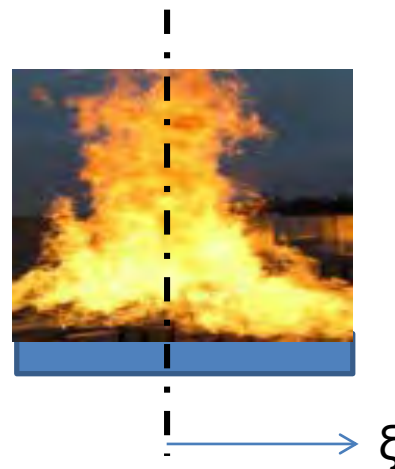
Objective

Compare fires at Dahlgren (Propane, Kerosene, and JP-5), with Propane fire at Meppen, and a JP-4 fire at Sandia

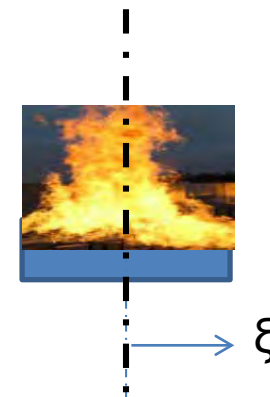
The approach is to compare fires by plotting temperature fields using non dimensional lengths



Round, $\xi = r/R$
Sandia ~19 m dia.



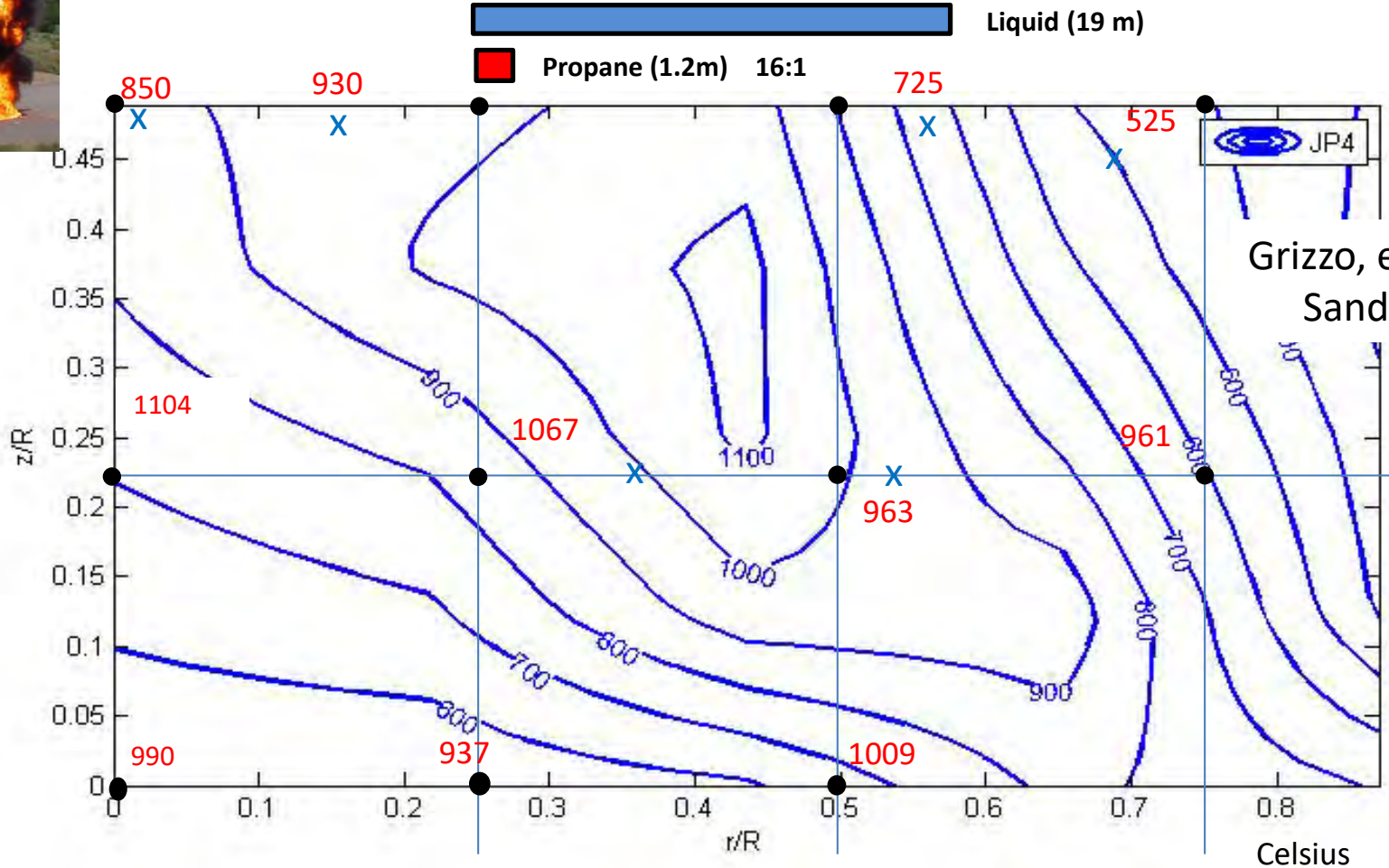
Square $\xi = x/(W/2)$
Dahlgren 9 x 9 (m)



Rectangle $\xi = x/(L/2)$
Dahlgren 2.5 x 4 ft
(0.6 x 1.2 m)

Sandia 10m Radius JP4 Fire Temperature Contours with Dahlgren Demo .6m Wide Burner Temperature Contours

This is the most extreme scale factor:



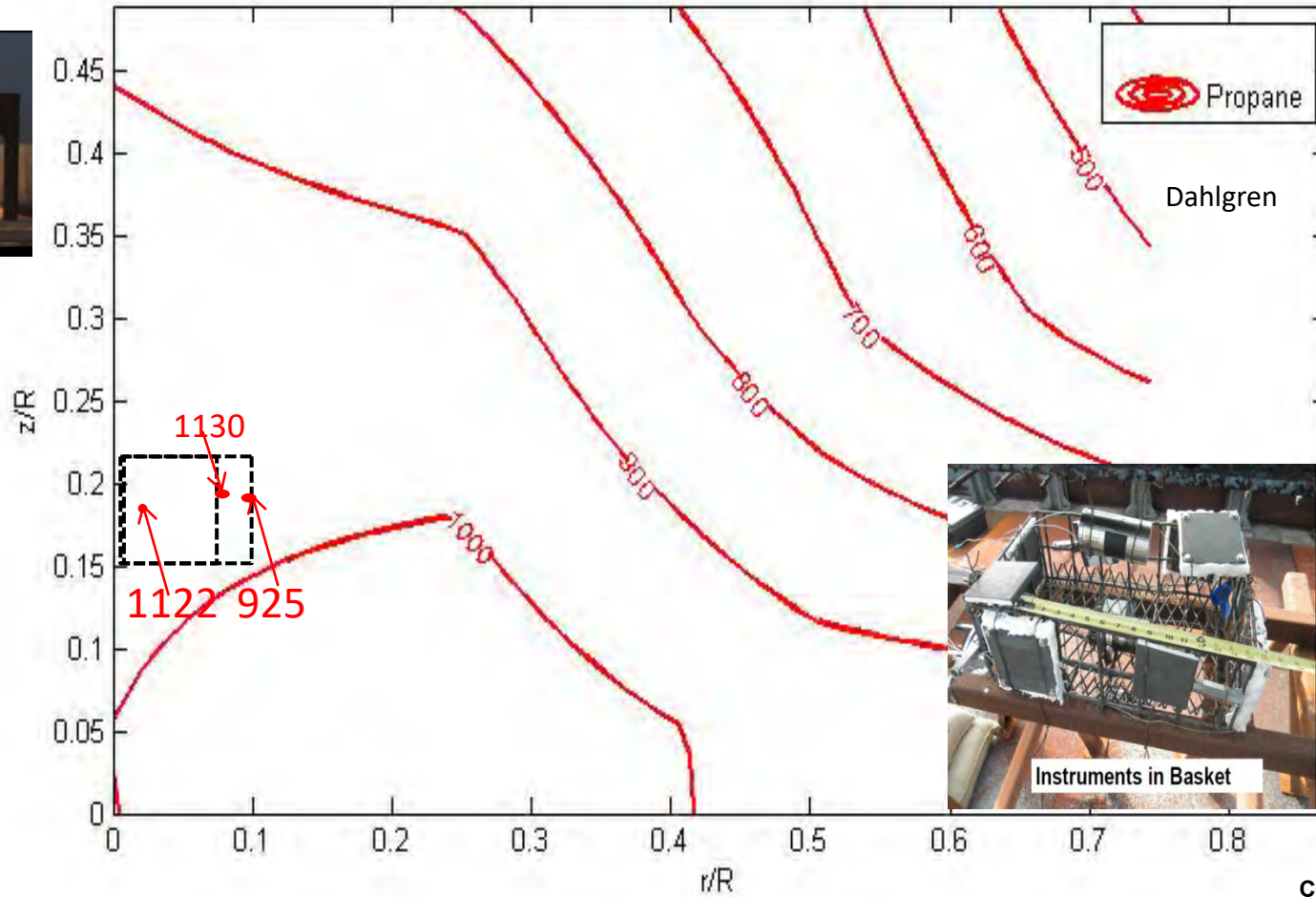
Grizzo, et. al.
Sandia

And it is trying to work!

X denotes place where interpolated JP-4 data gives same value as propane



Dahlgren Scale Demo Propane Burner Temperature Contours with Data from Meppen Fire

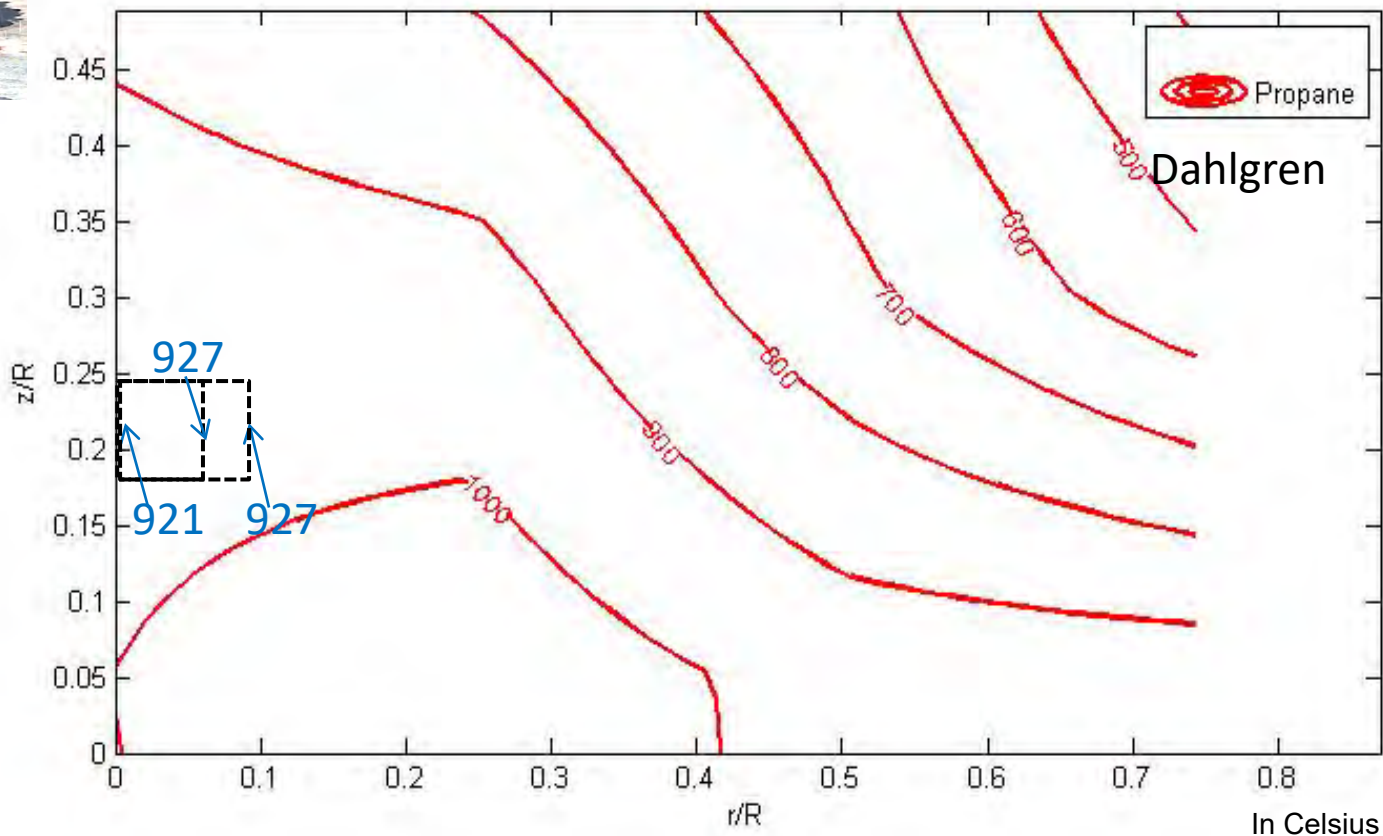


Basket of
instru-
ments

This shows the Dahlgren demo burner temperatures are a little lower than the temperatures in the burner at Meppen.

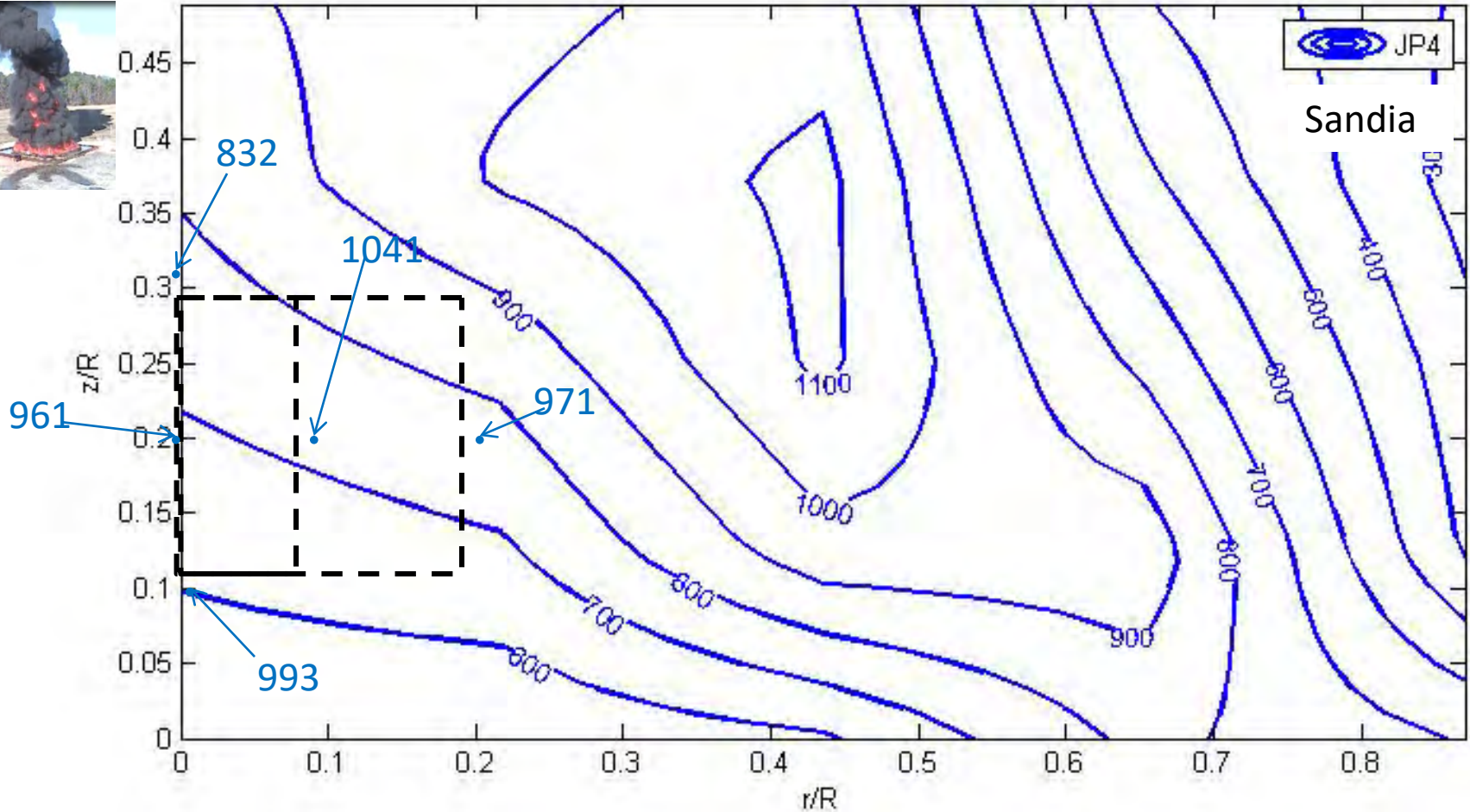
The Dahlgren fire temperatures have since been increased.

Dahlgren Scale Demo Propane Burner Temperature Contours with Data from Dahlgren JP-5 Fire



This shows the Dahlgren JP-5 fire was around the same temperature as the Demo Propane Burner

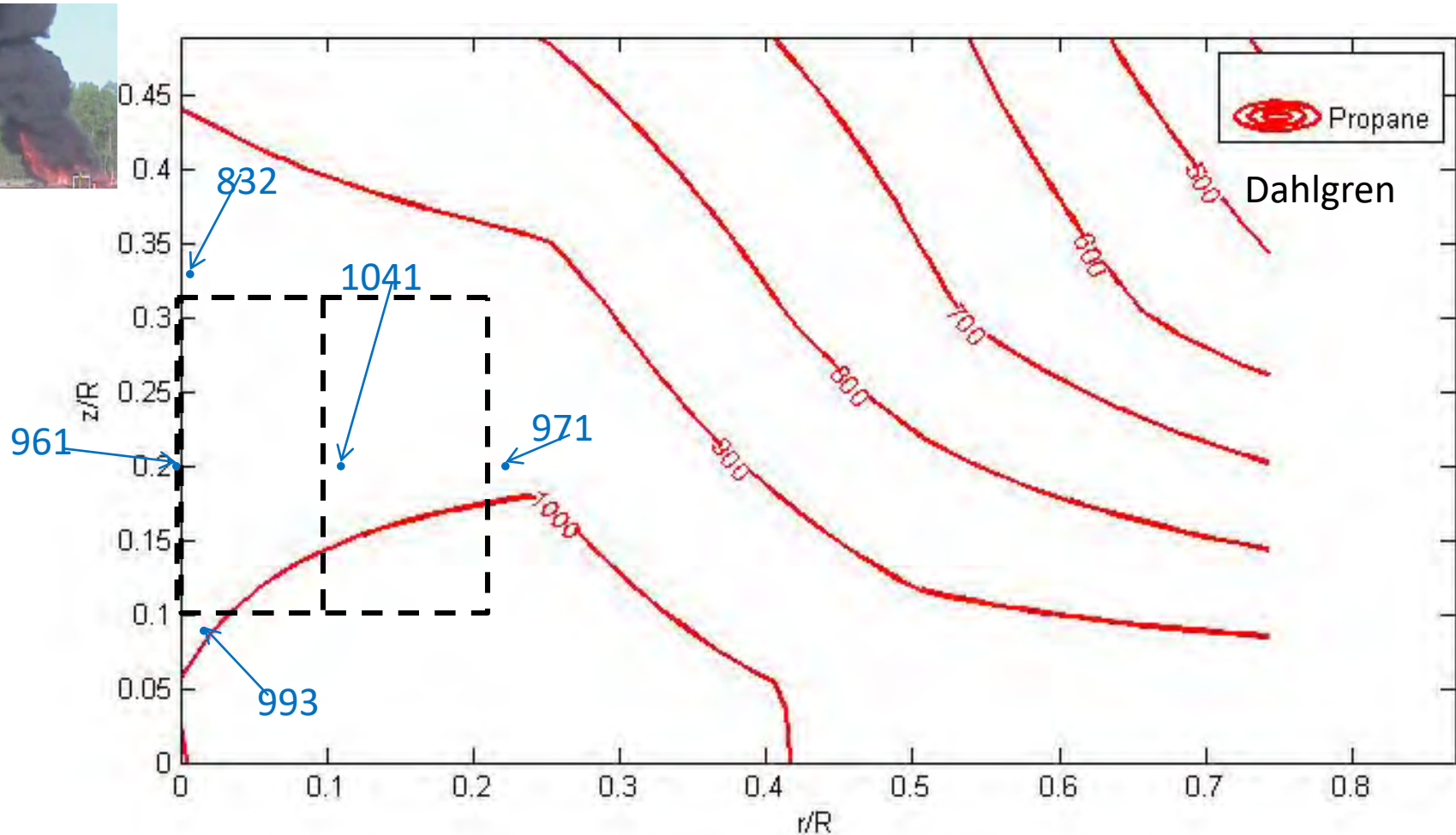
Sandia Round JP-4 Fire Data Temperature Contours with Data from SM-3 MK 21 Canister in Dahlgren SM-3 JP-5 fire



This shows the Dahlgren JP-5 fire was hotter than the Sandia JP-4 fire in the scaled location of the canister



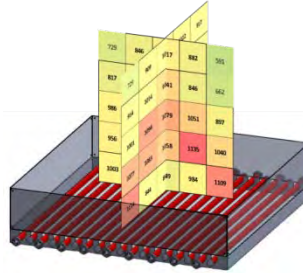
Dahlgren Scale Demo Propane Burner Temperature Contours with Data from SM-3 MK21 Canister in Dahlgren SM-3 JP-5 fire



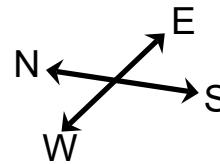
This shows the Dahlgren SM-3 fire was about the same temperature as the propane burner fire

8 ft x 8 ft Propane Average Temperature Measurements

8 ft x 8 ft (2.4 m) burner
Instruments 5 ft x 5 ft (1.5m) cube



Ensemble Average	999
Standard dev.	87



729	846	1017	882	591
817	909	1041	846	662
986	979	1079	1051	897
956	1054	1058	1135	1040
1003	1010	849	984	1109

Looking West



5'

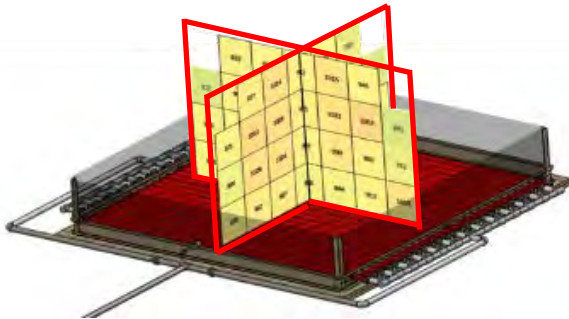
729	909	1017	1022	917
914	1014	1041	1037	1012
1001	1094	1079	1060	1064
1077	1083	1058	1092	1122
1114	844	849	950	1100

5'

Looking North



12 ft x 12 ft (3.6 m) Propane Average Temperature Measurements



Average	907°C
Maximum	1047°C
Co. Var.	8%



8'



	801	894	897	938	938	
749	842	906	928	951	882	817
899	936	933	900	956	923	847
944	940	911	827	834	932	967

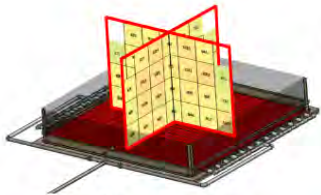
	870	920	897	997	1047	
658	929	990	928	961	987	952
910	1003	955	900	962	988	897
1012	871	903	827	850	859	814

6'



Side by Side Comparison of 8 x 8 and 12 x 12 Propane Burners

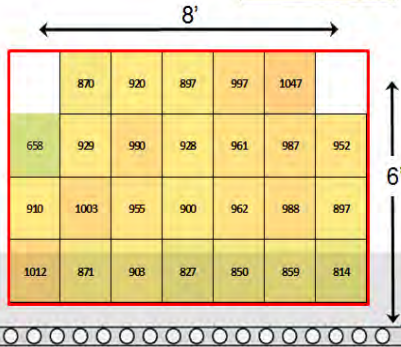
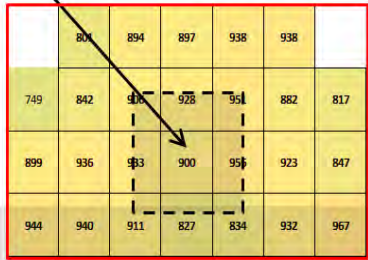
12 ft x 12 ft Propane Average Temperature Measurements (°C)



Average	907°C
Maximum	1047°C
Co. Var.	8%



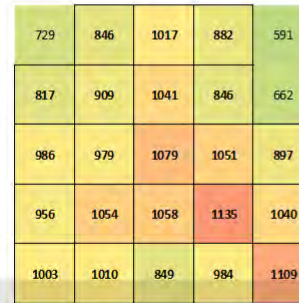
Square meter for reference



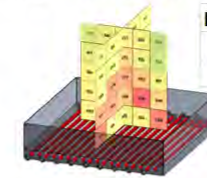
13

8 ft x 8 ft Propane Average Temperature Measurements (°C)

Calm wind conditions are needed for qualification testing



Looking West



Ensemble Average	999
Standard dev.	87

8ft x 8ft burner
Instruments 5Ft x
5ft cube



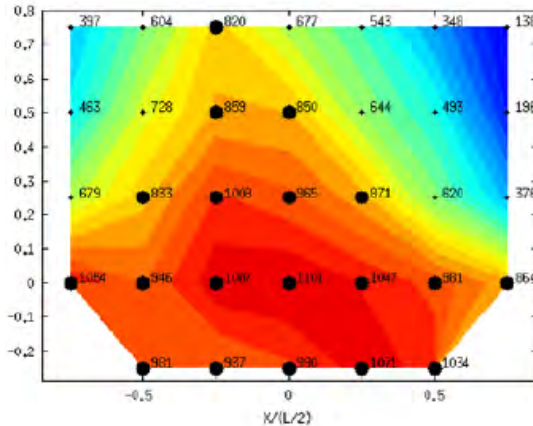
Looking North

12

The propane fires nicely fill out the space above the burner and don't have much structure. There isn't much difference between these two fires in a statistical sense



Non Dimensional Propane Temperature Fields



1:1

2.5 x 4 rectangle

729	846	1017	882	591
817	909	1041	846	662
986	979	1079	1051	897
956	1054	1058	1135	1040
1003	1010	849	984	1109

1:2

8 x 8 square

	801	894	897	938	938	
749	842	906	928	951	882	817
899	936	933	900	956	923	847
944	940	911	827	834	932	967

1:3

12 x 12 square

Again, the propane fires nicely fill out the space above the burner and don't have much structure. There isn't much difference between these three fires in a statistical sense.

Value of Flame Filling Flame Space Above Burner:
The average temperature on 12 thermocouples surrounding
container was 863°C (1585°F)



Summary

- Scaling the length axes shows temperature contours over a wide range of lengths (1.2 to 19 meters) and provides a means of comparing fires
- The JP-5 fire in Dahlgren and propane fires in Meppen and Dahlgren are reasonably the same at homologous positions near the test item
- Scaling may be used to predict the temperature field in large fire from temperature measurements in a small fire

Future Work

- The baseline liquid fuel fire at Sandia showed low temperatures in the inner core of the fire as compared to the other fires. Therefore a complete mapping of a liquid fuel fire in a large pit such as at Dahlgren is needed. This fire would become the baseline for scaling up or down, as much as 16:1 to 1:16. Pans for 12 ft. x 12 ft and 30 ft x 30 ft are readily available.
- Scaling for rectangular fires needs further development. This would facilitate developing modular fires consisting of arrays of basic modules.
- Square fires are prismatic near the pan, but quickly become cylindrical. Need to work out length scaling based on pan area^{1/2}.
- Estimate velocity fields from temperature fluctuations using signal processing techniques. Try to detect wave like motions and get group velocities as in acoustics.
- Apply turbulence methods to characterize time dependent fluctuations, $\langle u, v, w \rangle$.
- Study vertical direction using momentum length scaling from buoyant plume theory.
- Attempt large eddy simulations to determine the unstable, nearly chaotic swirling motions seen in large fires. Also check limits of scaling.

Manufacturing of PAX-3 High Explosive

Authors: Sean Swaszek, Phil Samuels, Dr. Paul Anderson, Katherine Guraini

Abstract

The manufacturing methods of processing controls of explosives play an important role in maintaining the quality of explosive formulations. PAX-3 is an explosive formulation that is of interest to the Army for use in gun launch munitions and grenades. PAX-3 shows improved shock and Insensitive Munition (IM) response as compared with traditional explosive fills. ARDEC developed the explosive formulation PAX-3 utilizing a twin screw extrusion mixing method. This is a continuous process in which a two part mixture is fed into the extruder, which uses high shear mixing to produce PAX-3. Currently, ARDEC is also pursuing an alternate formulation process of PAX-3 production in a single batch 500 gallon slurry coating process. Efforts for qualification of explosives often requires a significant amount of resources to complete all required testing. ARDEC is evaluating the material produced from these two methods to assess PAX-3 safety, long-term aging, and maintaining similar sensitivity and performance characteristics according to AOP-7. Cost and acquisition time are also responses of interest.

Background

The explosive composition PAX-3 is a high blast explosive that maintains metal pushing capability for applications. The formulation is composed of HMX, aluminum, binder, and plasticizer. In processing the material, the HMX and aluminum is coated in the polymer binder. The PAX-3 molding powder is pressed into items achieving high densities for specific applications. Efforts to produce and qualify PAX-3 molding powder using a slurry coating is being pursued by ARDEC. The ingredients such as final granule particle size and composition for the PAX-3 remains the same between both processes. Standards such as AOP-7 dictate that undergoing any process change may cause for requiring a requalification of a process.

The method of twin screw extrusion was pursued as a larger scale manufacturing method to produce PAX-3 high explosive. Early laboratory studies had shown the capability to produce PAX-3 using twin screw extrusion process using a non-aluminized analogous formulation and Aluminum. This is a 2 step process in which the non-aluminized analogous formulation is first produced using a slurry coating process and then used as part of a feed mix with aluminum in the twin screw. The twin screw extrusion process is a continuous method in which the ingredients are fed at a constant rate to produce the final product. This allows for flexibility to produce variant formulations containing different ratios of constituent materials. Efforts to transition the twin screw technology to larger scale manufacturing was funded under the ManTech program in 2009. Using a 19mm die twin screw extruder at Milan AAP, PAX-3 was produced in large scale quantities and used for characterization testing at ARDEC. This batch of material was used for qualification efforts and is now an accepted process to produce PAX-3.

Recently, work was pursued to produce PAX-3 using the slurry coating in a one-step single batch process. BAE Holston developed a process to produce 500gallon batches of PAX-3 using this method. Slurry coating is a process in which a binder-lacquer is dissolved in a solvent.

UNCLASSIFIED

Distribution Statement A: Approved for public release; distribution is unlimited

Energetic materials such as RDX or HMX along with Aluminum are mixed in an aqueous solution with the dissolved mixture in solvent. Upon heating the solution, the solvent is distilled off and the binder-lacquer mix coats individual particles. The benefit of this reduces the process from a 2-step using twin screw extrusion to a 1-step procedure for cost savings. The final product of the slurry process appears to be similar to material made in the twin screw extruder shown in figure 1.



Figure 1: Granules of PAX-3 produced in a twin screw extruder (left) and slurry process (right)

When undergoing changes to a production process for explosive such as PAX-3 there is concern materials will have different properties or characteristics. Examples of parameters that could affect the behavior include varying amounts of polymer coating of energetic particles, residual solvents or water remaining in the composition, foreign contaminants, or a physical change such as particle size or morphology. To ensure that the PAX-3 produced in the 1-step slurry process is comparable to the 2-step twin screw extrusion, it is being evaluated through a series of characterization tests. Running a complete series of qualification testing requires a significant amount of time and costs associated with the effort. ARDEC has therefore chosen a reduced set of tests to show the slurry produced PAX-3 maintains similar characteristics to the qualified twin screw extrusion process.

Scanning Electron Microscopy (SEM)

SEM images were obtained using a JEOL JCM 5700 tungsten filament scanning electron microscope using palladium/gold-coated samples in high vacuum mode. SEM images from PAX-3 water slurry method are shown in figure 2.

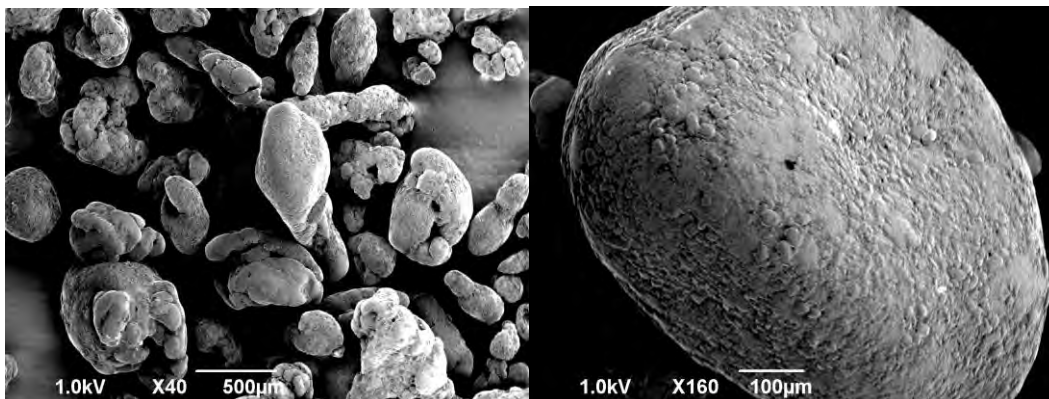


Figure 2: SEM images of PAX-3 granules produced using the slurry process

UNCLASSIFIED

Distribution Statement A: Approved for public release; distribution is unlimited

SAFETY TESTS

The basic sensitivity tests to evaluate a materials sensitivity include impact, friction, ESD, and shock sensitivity were conducted on PAX-3. Tests were performed according to AOP-7 and STANG 4489 ED1. Samples were prepared by grinding raw material in a Wiley Mill until it passed through a 25 mesh screen and dried at 120°F to a constant weight. The results of the sensitivity tests

Explosives Research Laboratory (ERL) Impact Test

The ARDEC ERL type 12 impact tester using a 2 ½-kg drop weight was used to determine the impact sensitivity of the sample. The drop height corresponding to the 50% probability of initiation measures impact sensitivity. The test method is described in STANAG 4489 Ed.1 "Explosives, Impact Sensitivity Tests." The PAX-3 did not react at a drop height of 21.6 cm for the water slurry material and 40 cm for the twin screw extrusion material. This range of results is on par with secondary explosive materials.

BAM Friction

The large BAM friction test method is described in AOP-7, 201.02.006, "BAM Friction Test." The porcelain pin is lowered onto the sample, and a weight placed on the arm to produce the desired load. The tester was activated, and the porcelain plate was reciprocated once to and fro. The results are observed as either a reaction (i.e., flash, smoke, and/or audible report) or no reaction. Testing begins at the maximum load of the apparatus (360 N) or lower if experience warrants it. If a reaction occurs in ten trials, the load is reduced until there are no reactions observed in the ten trials. The slurry material had 0/10 no-go reactions at 288N and a go reaction at 320N. The BAM impact was conducted on the twin screw extrusion material and results were 0/10 no-go reactions at 288N and a go reaction at 320N.

Shock Sensitivity (LSGT)

Large Scale Gap Testing (LSGT) was performed in accordance with AOP-7, 201.04.001. The PAX-3 test samples were pressed into free standing pellets and then stacked up into a 1.5" diameter by 5.0" long steel tubing which was supported a 0.375" thick witness plate. A detonator sat on top of booster pellets that were separated from test sample by a series of card gaps as shown in Figure 3. The clear cut hole on the witness plate determines whether the test is a "go" or "no go". The 50% point between "go" and "no go" for PAX-3 water slurry method was 155 cards (36.8 kbar). The result of the PAX-3 from the twin screw extrusion method was 143 cards (43.4 kbar).

Safety Test Results		
Test	PAX-3 Slurry	PAX-3 Twin Screw
ERL Impact	21.6cm (0/10) no-go	40cm (0/10) no-go
BAM Friction	288 (0/10) no-go	288 (0/10) no-go
BAM Friction	320 reaction	320 reaction
LSGT	155 cards	143 cards

Figure 3: Results from sensitivity testing on PAX-3

UNCLASSIFIED

Distribution Statement A: Approved for public release; distribution is unlimited

Thermal Characterization

Additional thermal characterization tests were performed to determine the materials response undergoing heating. Specific tests chosen were to look at off-gassing, residual solvents, reaction due to heating, and compatibility. The vacuum thermal stability, thermal stability, small scale burn, and differential scanning calorimetry were performed on the PAX-3 produced by the slurry process.

The vacuum thermal stability test was performed in accordance to AOP-7 202.01.01. A 5g sample of PAX-3 to 80°C for 48hrs. Post test results showed a 0.1% change in mass due to off-gas which is considered a passing score, the twin screw extrusion material had a similar score of 0.1% change in mass. These results are below the 2mL/g of gas evolved passing criteria.

The thermal stability test was conducted in accordance with TB700-2 where a 50g sample of explosive molding powder. The sample was heated to 75°C for a duration of 48 hours. Visual inspection of the PAX-3 explosive showed no signs of reaction or burning due to heating similar to the twin screw extrusion material.

Differential Scanning Calorimetry (DSC) testing was conducted on PAX-3 powder in accordance with STANAG 4515 where a small sample had undergone heating of 5°C per minute. The average onset and peak temperatures were 277.4°C and 279.2°C for slurry PAX-3. The reference results from PAX-3 produced using the twin screw extrusion method were 275.4°C for onset and 277.1°C for reaction.

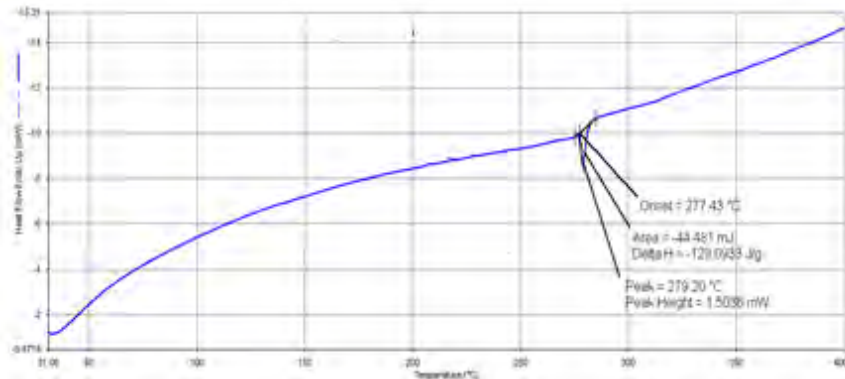


Figure 4: DSC results of PAX-3 subject to heating rate of 5°C/min.

Physical Characteristics

Using the twin screw extrusion process the PAX-3 was extruded continuously from a 19mm diameter die, cut and grouped to achieve smaller agglomeration of particles, and then used in molding powder for pressing. In the slurry coating process, the individual particles crash out of solution and range over a size distribution. The bulk density of molding powder produced using the slurry process batches 0.76-0.78g/cc compared to 0.85g/cc from the produced the twin screw extrusion. The composition analysis of the slurry material has the HMX, aluminum, binder, and plasticizer contents within the spec. Compression testing was performed to evaluate the mechanical behavior of the materials. The material was evaluated in accordance to the uniaxial

UNCLASSIFIED

Distribution Statement A: Approved for public release; distribution is unlimited

compression test STANAG 4443. The PAX-3 molding powder was pressed into billets and machined into samples with a 1.5" length and 0.75" diameter. The material was conditioned at 23°C and placed on an Instron 5969 material testing device. The samples were compressed at a rate of 0.015in/min recording the displacement and load. The data was used to calculate stress and strain profiles characterizing the behavior of PAX-3 under compression. The peak compressive strength for slurry PAX-3 was 2848PSI and the twin screw extrusion PAX-3 was 3002PSI. The PAX-3 molding powder was shown to achieve similar densities under similar pressing conditions.

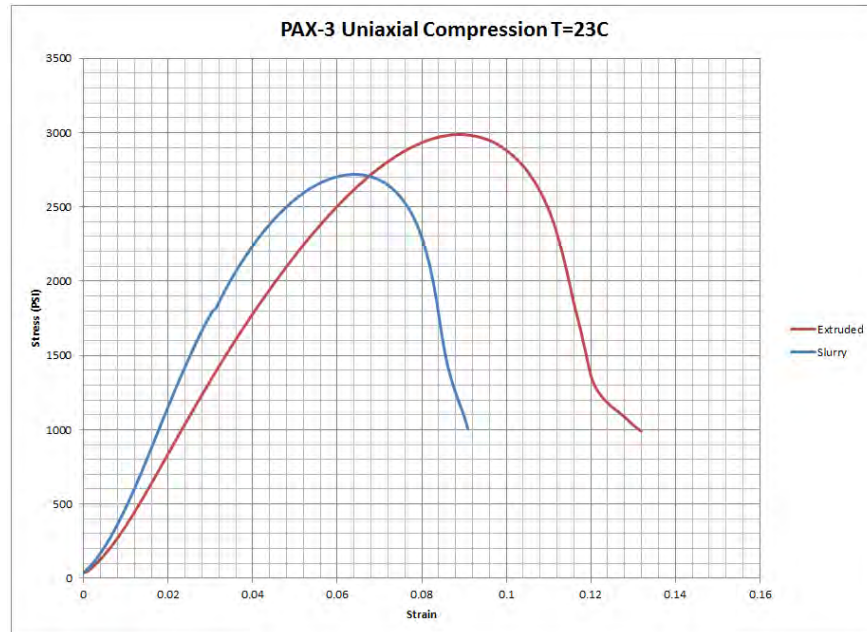


Figure 5: Uniaxial compression stress-strain plot of PAX-3

The formulation PAX-3 is currently of interest and being evaluated in grenade and tank ammunition applications. Gun launch munitions undergo significant loading during the acceleration of the projectile. Additional studies were performed to evaluate the response of potential defects under loading due to setback. The PAX-3 produced using the twin screw extrusion process was tested in the ARDEC Setback Test Equipment. The new PAX-3 produced in the slurry process has been evaluated in using the Indian Head setback test. The devices can apply loading rates on explosives samples. Cavities are machined into explosive billets to resemble defects such as gaps, cavities, and cracks. The loading rate and defect sizes are increased in order to obtain a reaction from the explosive.

Summary

While undergoing different processing methods to produce the PAX-3 formulation, initial testing results shows slurry produced material maintains similar characteristics to the twin screw extrusion produced material. Standard tests used to look at the thermal behavior, sensitivity, and

UNCLASSIFIED

Distribution Statement A: Approved for public release; distribution is unlimited

Unclassified

physical characteristics were evaluated and showed no notable differences in results changing the processing method between twin screw extrusion and slurry coating. Additional studies are being conducted on aged samples of PAX-3 slurry material. Using this data, ARDEC will qualify the slurry process by the "delta qualification" process with a reduced amount of testing. This will provide additional cost savings reducing additional testing while maintaining the rigor associated with the energetics qualification process. Results thus far show that the PAX-3 molding powder from the slurry process maintains its sensitivity and key characteristics after undergoing the processing method change.

UNCLASSIFIED

Distribution Statement A: Approved for public release; distribution is unlimited

References

- 1) Novel Manufacturing Process Development and Evaluation of High Blast Explosive PAX-3 with BDNPA/F and R8002 Plasticizers. Alexander, B. NDIA IMEM 2009
- 2) Twin Screw Extrusion of Thermobaric Explosives. Fair, M. 2006 IMEM
- 3) Development, Optimization, and Application of Combined Effects Explosives, Anderson, P. NDIA IMEM 2009
- 4) AOP-7: Manual of Data Requirements and Tests for the Qualification of Explosive Materials for Military Use. Edition 2 Rev. 2. April 2008.
- 5) STANAG 4170: Principals and Methodology for the Qualification of Explosive Materials for Military Use. Edition 2. Feb 2001
- 6) 7) Characterization of Picatinny Arsenal Explosive PAX-3. Katherine Maier. ARDEC-TR-16002. 2016.
- 7) STANAG 4443 Explosives Uniaxial Compressive Test. Edition 1. 1998

UNCLASSIFIED

Distribution Statement A: Approved for public release; distribution is unlimited

Unclassified

Acknowledgements

RDECOM – ARDEC

BAE Holston

PM-MAS

PEO AMMO

ATK Plymouth

UNCLASSIFIED

Distribution Statement A: Approved for public release; distribution is unlimited



Manufacturing of PAX-3 High Explosive

Presented to:

NDIA IMEM 2018

April 2018

UNPARALLELED
**COMMITMENT
& SOLUTIONS**

Act like someone's life depends on what we do.



U.S. ARMY ARMAMENT
RESEARCH, DEVELOPMENT
& ENGINEERING CENTER



- PAX-3 is a high blast explosive with metal pushing capabilities
- Developed to replace Aluminized Comp-A3
- Used in pressed applications for warheads
- Molding powder composed of
 - HMX
 - Aluminum
 - BDNPA/F
 - CAB
- Looking to requalify PAX-3 manufactured under a new process
- Formulation & constituents remain the same



- Back in 2000's the method of Twin Screw Extrusion (TSE) was evaluated as a manufacturing process for PAX-3
- TSE is a 2-step continuous mixing process
- It utilizes high shear mixing through a screw machine
- Components added to feed stock that extrude the final produce through an orifice
- ARDEC had studied mixing compositions and flexibility for the process to control



PAX-3 QUALIFICATION



- The TSE process was as a manufacturing method in which ARDEC qualified the process back in 2015
- A 19mm Die TSE located at Milan was used to produce over 2000lb using
 - Feed material was a non-aluminized analogous formulation & Aluminum in a performance fluid



Extrusion



Granulation



Molding Powder (Final Product)



PAX-3 SLURRY PROCESS



- BAE has scaled up manufacturing of PAX-3 at Holston
 - 500 gallon batch scale
 - Uses water solution
- Single step process where HMX & Aluminum is coated with binder/laquer
- Manufactured over 2000lbs to date



Molding Powder (final product)



- Changes in processing could lead to variation in final product
 - Residual solvents/water
 - Achieving correct % of constituents
 - Foreign materials added during the process
 - Source materials or replacement ingredients
- Potential impact on changes in material?
 - safety & handling
 - loading conditions
 - performance degradation
 - aging concerns



➤ **DoD Energetic Materials Qualification Process Test Protocol:**

- (1) Allied Ordnance Publication Seven (AOP-7) (Edition 2 Rev. 3), “Manual of Data Requirements and Tests for the Qualification of Explosive Materials for Military Use”, December 2007
- (2) Standardization Agreement (STANAG) 4170 (Edition 3), “Principles and Methodology for the Qualification of Explosive Materials for Military Use”, 2007.
- (3) DoD Energetics Qualification Program Matrix for Main Charge Explosives



QUALIFICATION TESTING



❖ Thermal Stability & Compatibility

- ✓ VTS
- ✓ Thermal Stability
- ✓ DSC
- ✓ VTS Generic Material Testing
- ✓ TGA
- ✓ Woods Metal Bath (5-sec explosion temperature)
- ✓ Critical Temperature Calculation
- ✓ Variable Confinement Cook-off Test (fast and slow)
- ✓ Small scale burn

❖ Sensitivity

- ✓ Small Scale ESD
- ✓ ERL/Bruceton Impact
- ✓ BAM Friction
- ✓ LSGT Shock Sensitivity
- ✓ Cap Sensitivity
- ✓ Setback

❖ Chemical/Physical/Mechanical Properties

- ✓ Coefficient of Thermal Expansion
- ✓ Comprehensive Strength
- ✓ Density/Bulk Density
- ✓ Irreversible Growth
- ✓ Exudation

❖ Aging

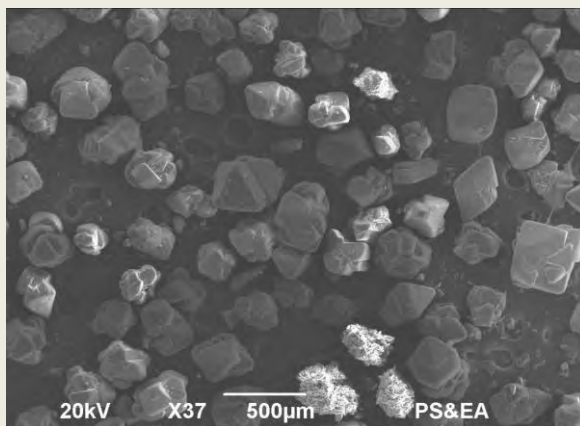
- ✓ Safe shelf Life
- ✓ Sensitivity Tests
- ✓ Mechanical Properties (on un-aged and aged material)

❖ Toxicity Evaluation

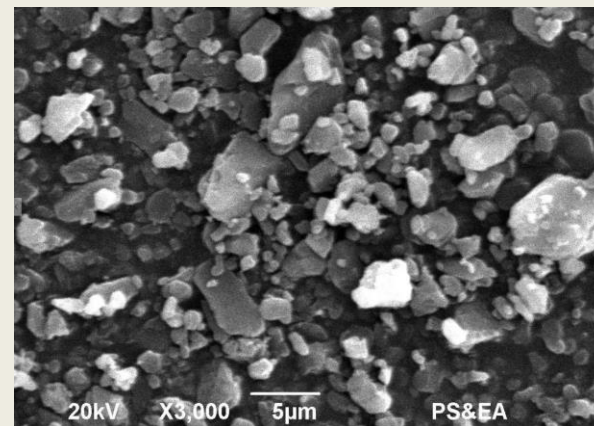
- ✓ Products of Combustion/Detonation
- ✓ Toxicity Clearance Report

❖ Performance Properties

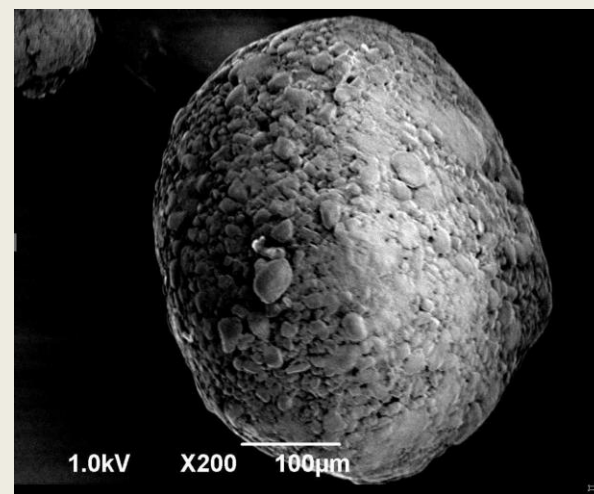
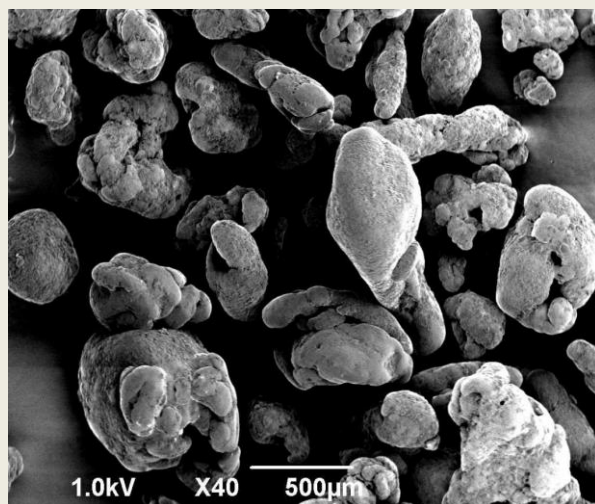
- ✓ Detonation Velocity/Detonation Pressure
- ✓ Critical Diameter



HMX Class 1



HMX Class 5



PAX-3 Slurry material under different magnification



	TEST TITLE	TEST METHOD	TEST CONDITION	TEST RANGE OR LIMIT	TEST RESULT (SLURRY PAX-3)	REFERENCE (EXTRUDED PAX-3)
1	STABILITY CHARACTERIZATION					
1.1	Vacuum Thermal Stability (VTS or MVTs)	AOP-7	5.00±0.01g	≤ 2 ml/g of gas evolved	0.0660 ml/g	0.0740 ml/g
		202.01.001	100 °C/48 h	(100 °C/40 h)		
			Or			
			100 °C/40 h			
1.2	Thermal Stability at +75 °C	TB 700-2	50g	Evidence of Self Heating	Start 49.9700g	Start 49.4041g
		UN Test 3c	75 °C/48 h		Final 49.9219g	Final 49.3558g
					(0.10% change)	(0.10% change)
					No evidence of instability	No evidence of instability

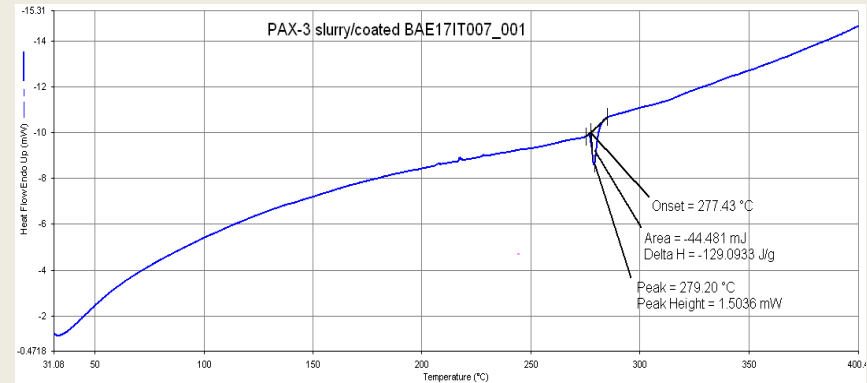


- Vacuum Thermal Stability (VTS) Test
 - 5g sample held at 100°C for 40hrs
 - Gas evolved 0.066 ml/g (0.074ml/g ref)
 - Pass, criteria – explosives will no exceed 2ml/g

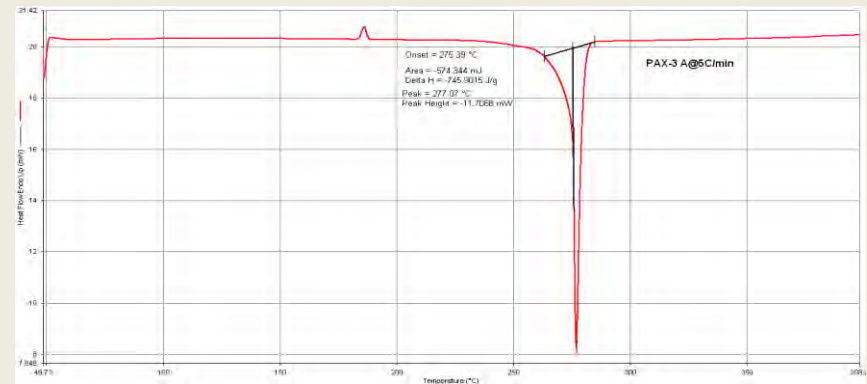
- Thermal Stability
 - 50g sample held at 75°C for 100hrs
 - Result - no indication of reaction (mass loss, color change)



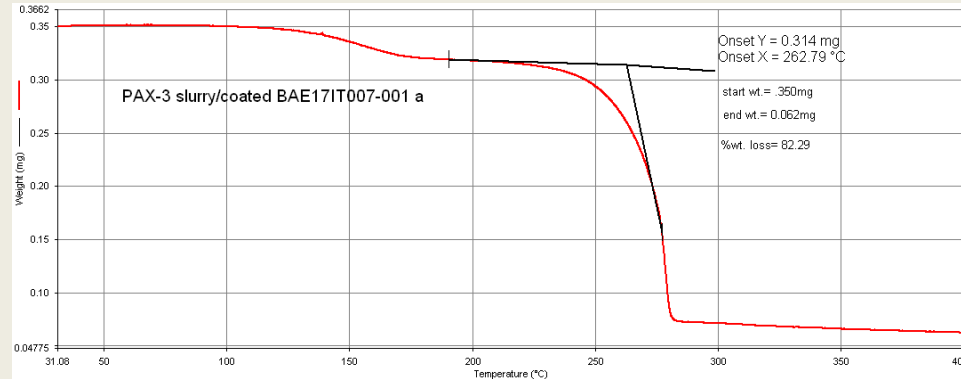
- DSC Testing
 - Heating rate of 5°C/min
 - Thermal run away event
- PAX-3 Slurry
 - Onset 277.43°C
 - Peak 279.2°C
- PAX-3 Reference
 - Onset 275.39°C
 - Peak 277.07°C



PAX-3 Slurry



PAX-3 Reference



• TGA Results

- Onset Temp – 262°C (Slurry), 258°C (Reference)
- Reaction – approx. 80% of material reacted



SENSITIVITY RESULTS



	TEST TITLE	TEST METHOD	TEST CONDITION	TEST RANGE OR LIMIT	TEST RESULT (SLURRY PAX-3)	REFERENCE (EXTRUDED PAX-3)
4	Sensitivity					
4.1	Electrostatic Discharge (ESD)				0/20 at 0.0063J (No-Go) 0.009J (Go)	0/20 at 0.25J (No-Go)
4.2	ERL/Bruceston Impact				24.6cm (50%)	42.1cm (50%)
4.3	BAM Friction				0/10 at 288N (No-Go) 324N (Go)	0/10 at 288N (No-Go) 324N (Go)
4.4	ABL Friction				0/20N at 578N (No-Go) 800N (Go)	no data no data
4.5	LSGT Shock Sensitivity				155 Cards	143 Cards
4.6	Cap Sensitivity				fail	fail

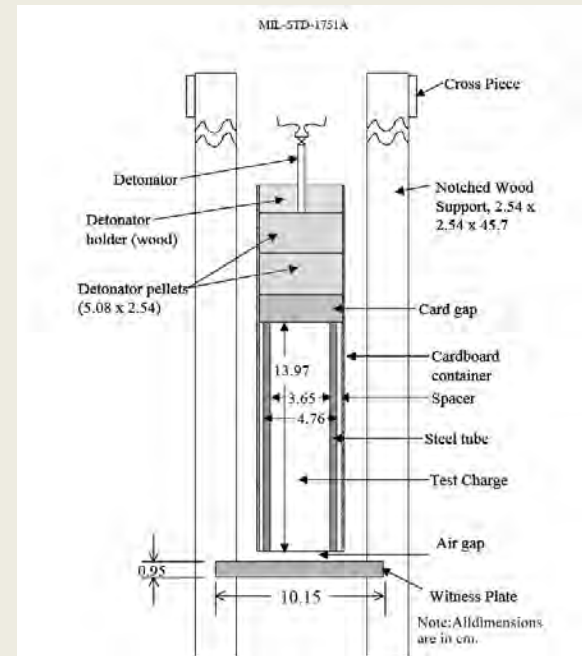
- ESD Tests were conducted on the new device for Slurry PAX-3 and old device for extruded PAX-3. All other materials appear more ESD sensitive when run on the new equipment
- Drop height for impact does appear to have a lower 50% point. This is still in the range of secondary explosives.
- ABL Friction was never conducted on Extruded PAX-3



SHOCK SENSITIVITY



- Large Scale Gap Test (LSGT)
 - 50% point for shock sensitivity
 - Pentolite donor pellets
 - PMMA gap to PAX-3 acceptor
- Slurry Process
 - 155 Cards (36.8kbar)
- TSE Process
 - 143 Cards (43.4kbar)

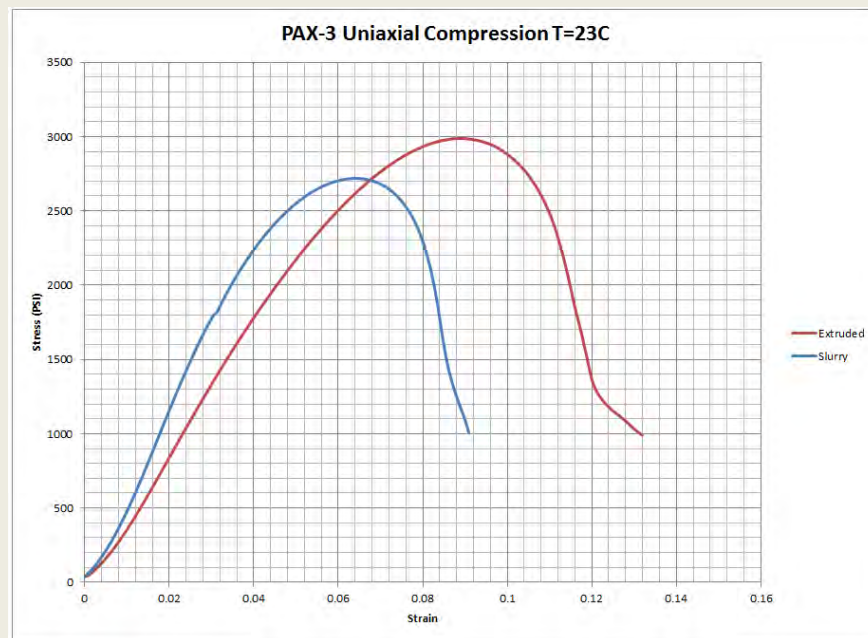




MECHANICAL PROPERTIES



- Uniaxial Compression
 - 1.5" x .75" cylinders
 - Strain Rate = 0.01/s
- Similar behavior under loading
 - Peak Compressive Stress
 - 2848PSI (Slurry)
 - 3002PSI (TSE)
 - Modulus
 - 67,400PSI (Slurry)
 - 51,200PSI (TSE)





- Initial testing shows no signs of concern based on results
 - Particles appear to be well coated
 - Similar characteristics & response
 - Thermal
 - Sensitivity
 - Physical
 - Awaiting Aged sample results
 - Composition Analysis shows no foreign materials
 - PAX-3 Slurry should maintain similar performance



- Currently PAX-3 is of interest to be used in tank ammo and grenade applications
- Testing to investigate material response when subject to setback is being conducted at Indian Head
 - Explosive samples are subject to accelerating loading to evaluate defect sizes and response



THE END



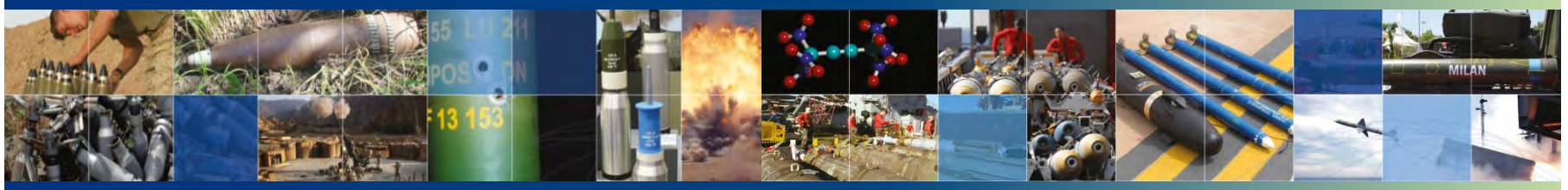
Questions?



MSIAC

Munitions Safety Information Analysis Center

Supporting Member Nations in the Enhancement of their Munitions Life Cycle Safety



STANAG 4396

Review of Sympathetic Reaction Tests

Insensitive Munitions and Energetic Materials
Technology Symposium
Portland, OR, USA - April 2018

Ernie Baker

TSO Warheads Technology

+32.(0)2.707.38.44

e.baker@msiac.nato.int

MSIAC Office

+32.(0)2.707.54.16

info@msiac.nato.int

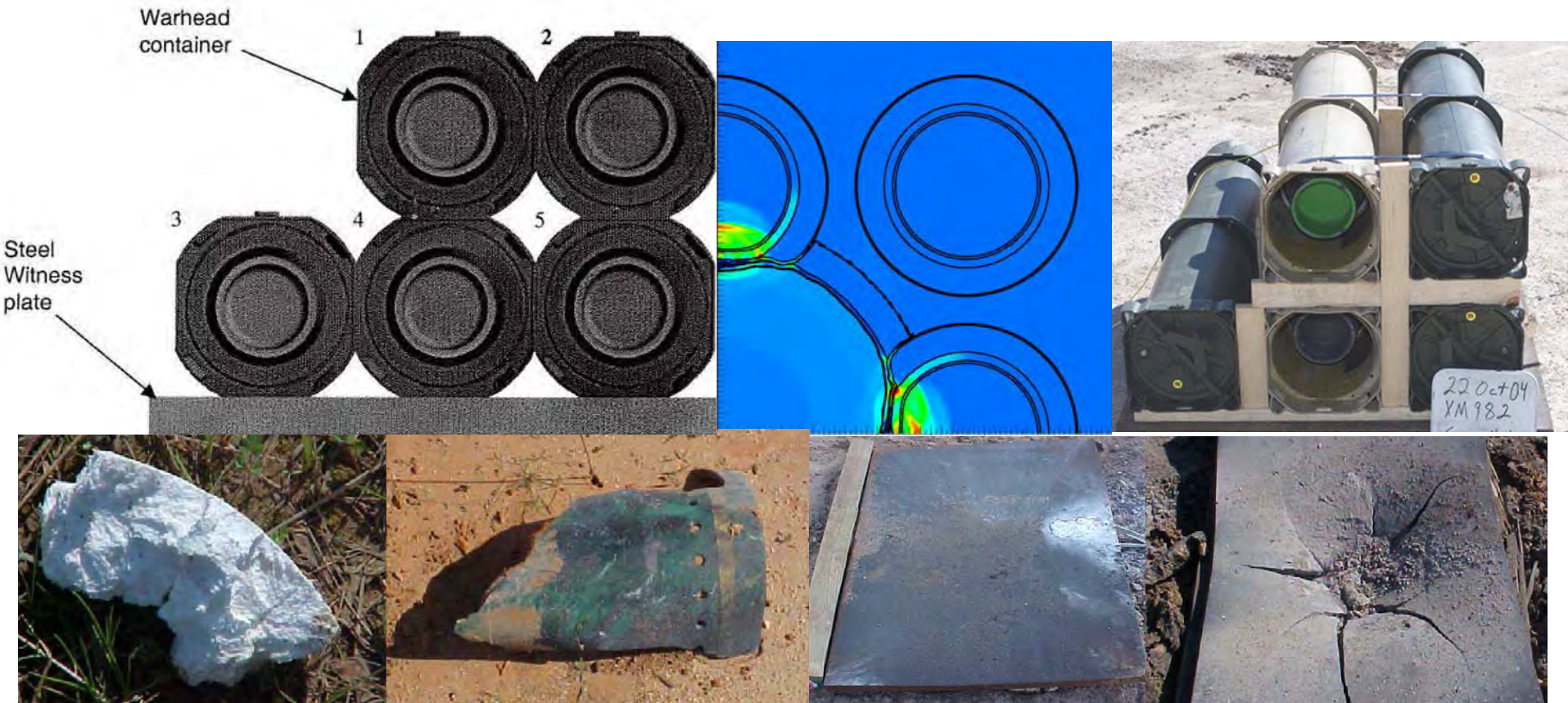
<http://www.msiac.nato.int>



- Background
- Process / Questionnaire
- Standards
- Analysis and Comments
- Conclusion

- In 2016, MSIAC initiated a review of STANAG 4382 (Slow Heating Tests) that led to a list of recommendations to update the document.
- NATO AC/326 SG/B tasked MSIAC to initiate the same type of review for the IM Sympathetic Reaction test.

To provide a standard test procedure to assess the potential for a munition to sympathetically react to the initiation of an adjacent munition.

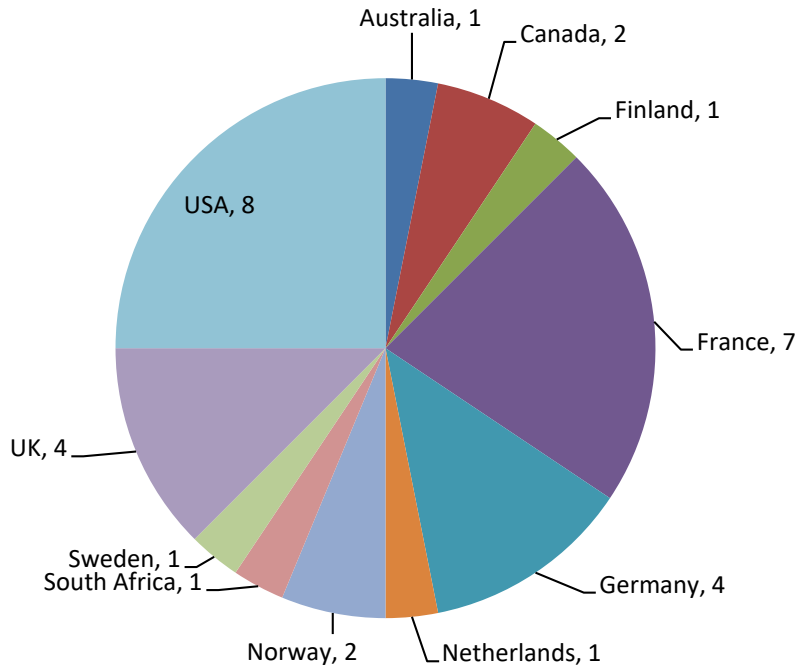


- MSIAC has written a survey related to the Sympathetic Reaction Test
- The survey was reviewed by the custodian of STANAG 4396 (France)
- The survey was sent to the nations
- After reception & analysis of the answers and other related documents, MSIAC is summarizing the results in a report.

- The sympathetic reaction test is defined within several documents.
 - In NATO:
 - STANAG 4396 ed.2 (Reaction level)
 - AOP-39 ed.3 (Requirements and Guidance)
 - In UN, for HC 1.6:
 - Test 7 (h) of UN Recommendations on the transport of dangerous goods – Manual of tests and criteria, 6th revised edition

32 responses from 10 nations.
59%/41% government /private

Answers by nations



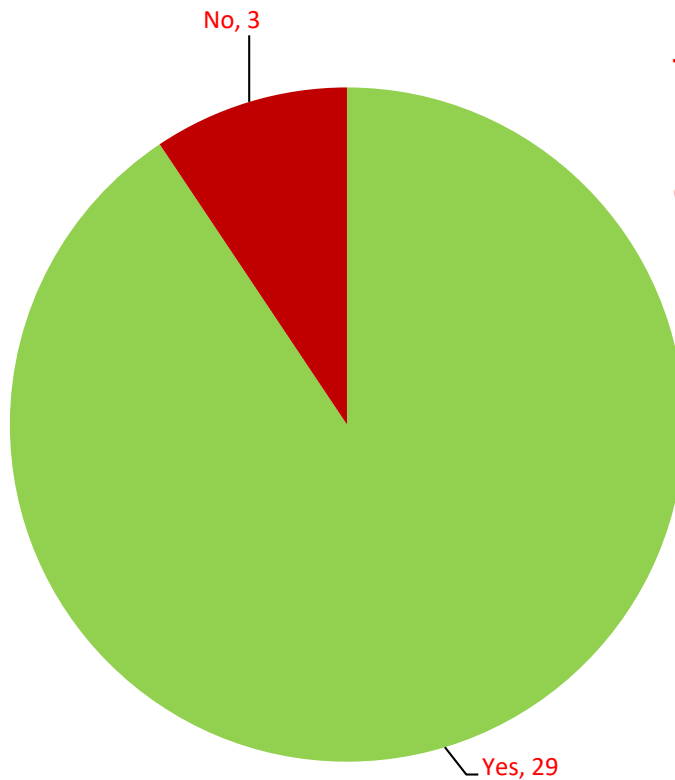
THANK YOU

for the number and the quality of your answers

Organisation	Country	IM Function
Directorate of Ordnance Safety	Australia	Other: Government
Consultant - Defence R&D Canada	Canada	Test Scorer
Defence R&D Canada - Valcartier Reserach	Canada	Other: Government
FDI/Explosives Centre	Finland	Test Center
ArianeGroup SAS	France	Test Center
DGA	France	Other: Government
DGA Missile Testing	France	Test Center
DGA Techniques Terrestres	France	Test Scorer
DGA/INSP/SM	France	Other: Government
THALES LAS FRANCE	France	Munition Developer
THALES LAS France - domaine VTS France	France	Munition Developer
Bundeswehr	Germany	Test Center
Diehl Defence	Germany	Munition Developer
MBDA-TDW	Germany	Munition Developer
Rheinmetall Waffe Munition GmbH / EZU	Germany	Test Center
MOD / KCW&M	Netherlands	Test Center
Forsvarets forskningsintutt	Norway	Government Oversight
Nammo	Norway	Test Center
RDM & National IM Steering Committee	South Africa	Test Center, Munition Developer
Bofors Test Center	Sweden	Test Center
BAE Systems Land UK	UK	Munition Developer
Health and Safety Laboratory	UK	Test Center
MBDA	UK	Munition Developer
Ordnance Test Solution Ltd	UK	Test Center
Navy Munitions Reaction Evaluation Board	USA	Test Scorer
96 Test Wing/Systems Safety Office	USA	Test Scorer
780TS Eglin AFB FL	USA	Other: Government
AF Research Laboratory	USA	Test Scorer
Air Force Live Cycle Management Center,	USA	Munition Developer
Army IM Board	USA	Test Scorer
NSWC/Hart Technologies	USA	Other: Government
Redstone Test Center, ATEC	USA	Test Center

Many responses are organizational, rather than of an individual

**What is the purpose of conducting the SR test?
To provide a standard test procedure to assess the potential for a munition to sympathetically react to the initiation of an adjacent munition.**

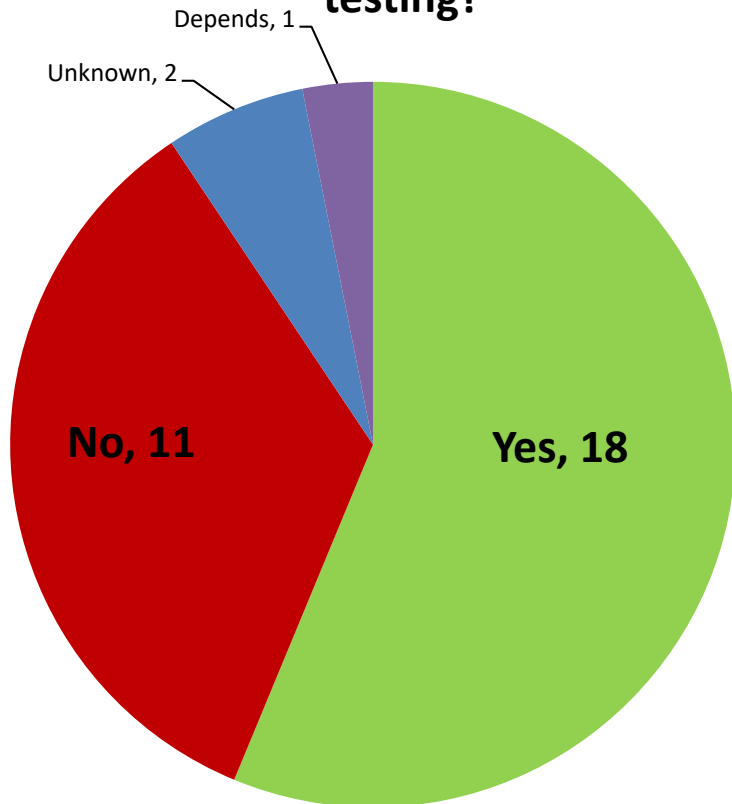


To evaluate the severity of an SR event for purpose of improving the Hazard Classification of a munition for storage and shipping.

To provide input for IM signature evaluation and HC evaluation

To characterize a munitions sympathetic reaction profile from the initiation of an adjacent munition representative of the users storage, transport or deployed configuration using a generic test procedure.

Should the test be fully harmonized with the Hazard Classification testing?



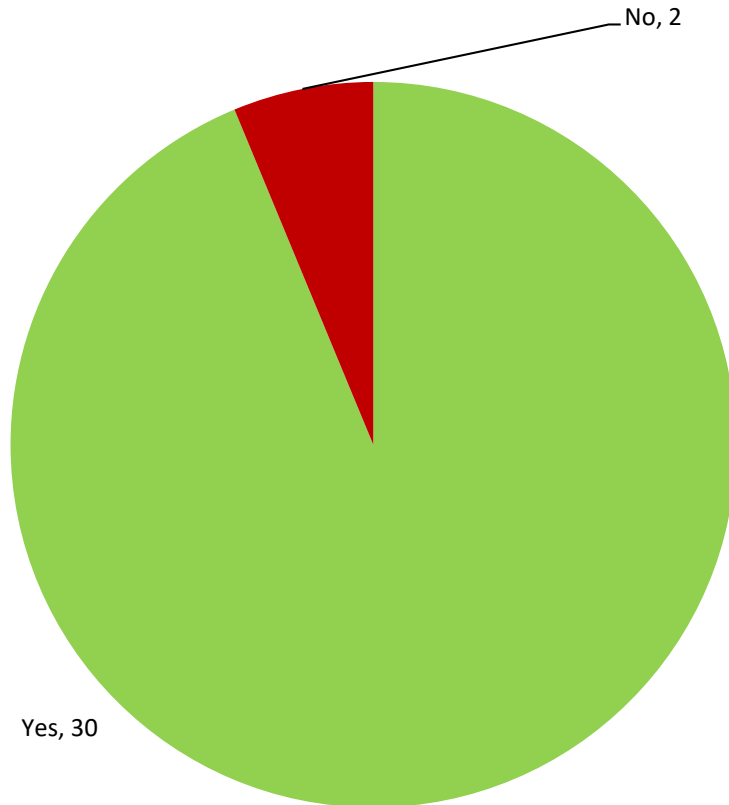
There should be two procedures,

- *Standard Test - that does not have variations on setup, therefore providing comparable results where ever it is done, this could be in line with the HC testing.*
- *Tailorable/Generic Test - that allows variance for user configurations that will provide an output depending on other factors such as storage, packaging etc."*

The test setup should allow for evidence gathering which can be used for both IM and Hazard Class scoring. This should ensure that only one test is needed.

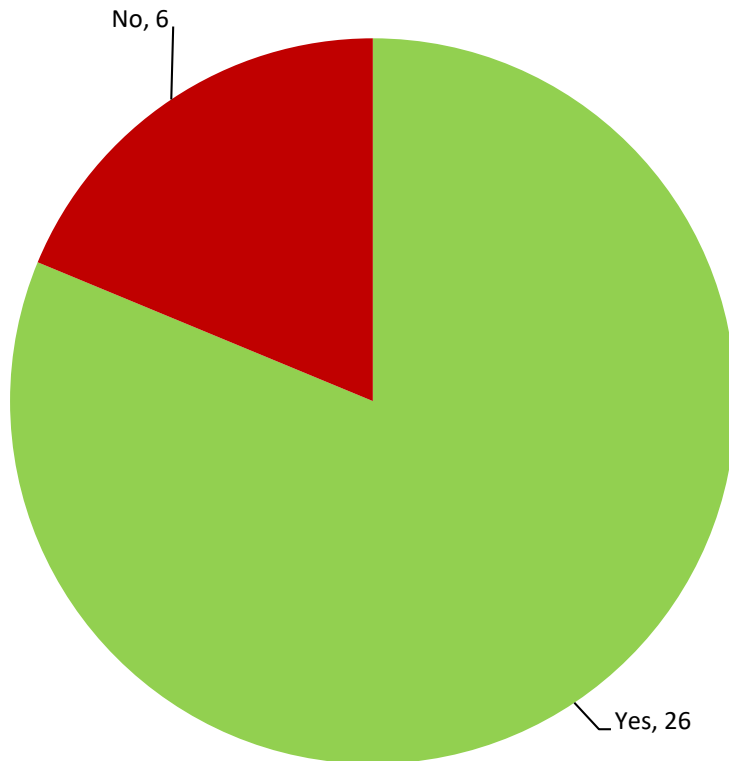
IM sympathetic reaction test must not be merged with the transportation stack test, because their objectives are different and not compatible.

Do you conduct your SR tests as required by the STANAG 4396 test procedure?



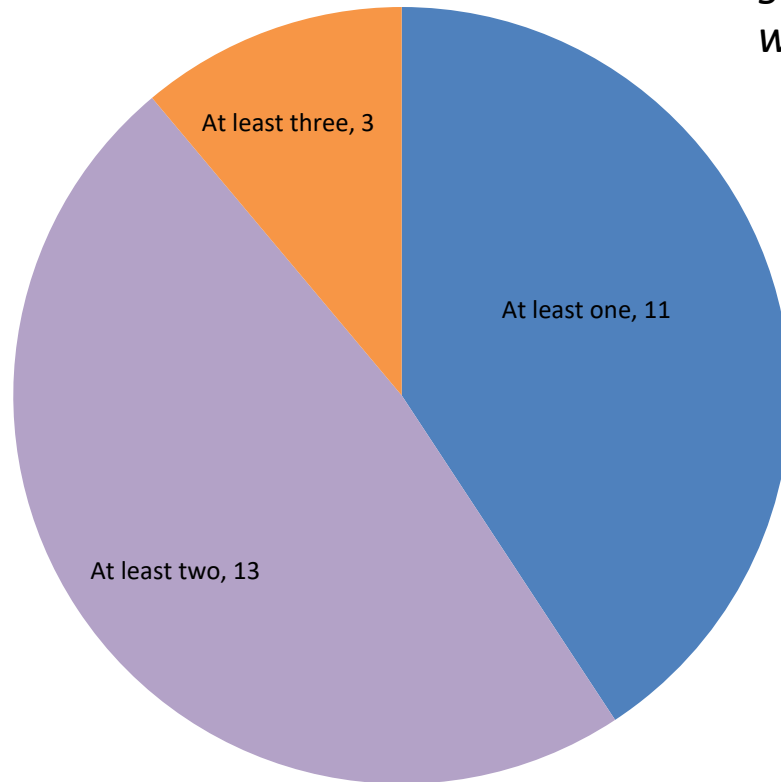
*1) Variation always required due to customer requirements or item particularities (UK).
2) Conducts HC SR testing ...not IM (USA).*

Should the test configuration be determined by a Threat Hazard Assessment (THA)



- 1) Variation always required due to customer requirements or item particularities (UK).
- 2) Conducts HC SR testing ...not IM (USA).

How many tests should be conducted?

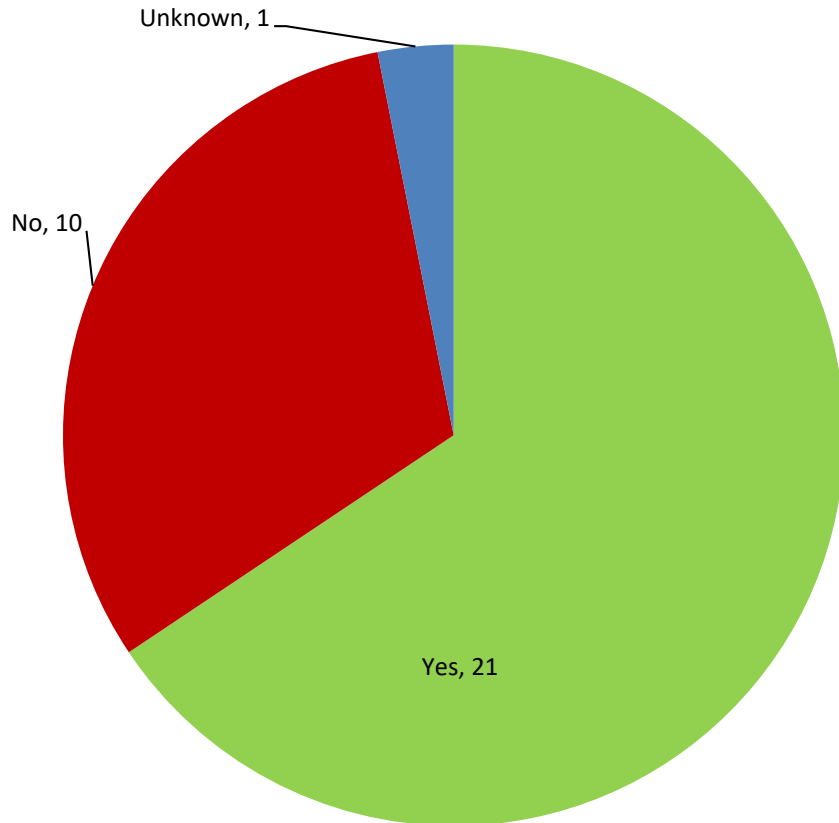


Good statistical question, and one that could get quite expensive. I would suggest that 3 without failure should provide good confidence

minimum of 1, if a pass, then a 2nd to confirm/validate the result.

One, to prevent excessive costs

Should a confined test be conducted?



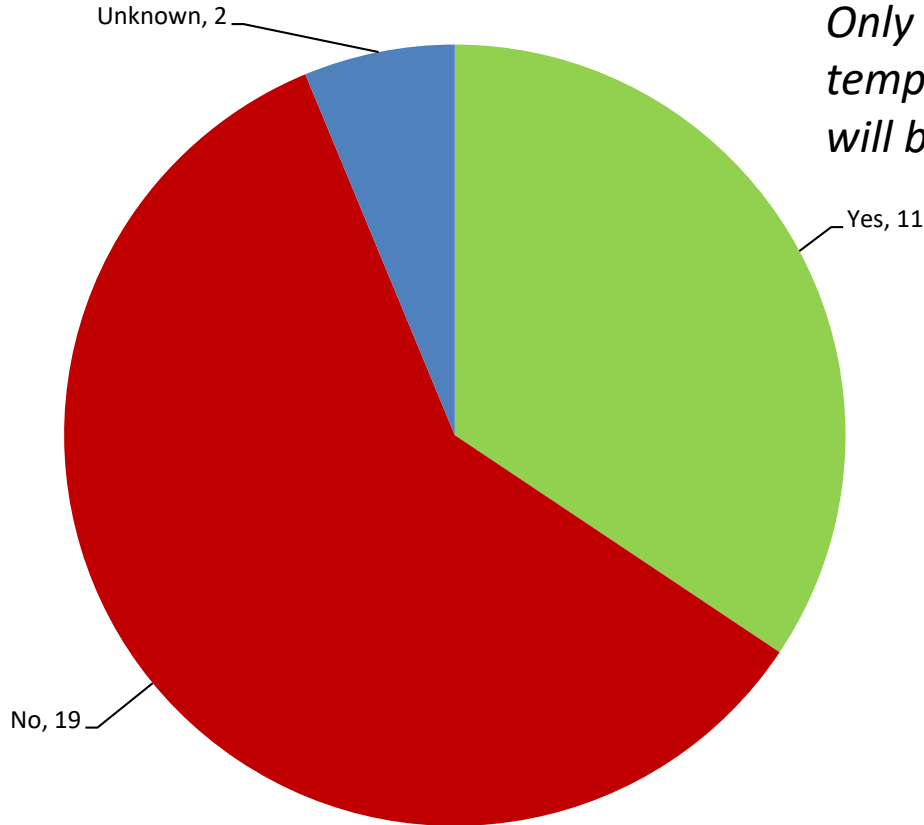
Potential Safety Issue: Sand Confinement

The confinement should be established in the threat hazard assessment for realistic scenarios. An equivalent confinement can then be designed.

When is it acceptable to replace live items with inert items?

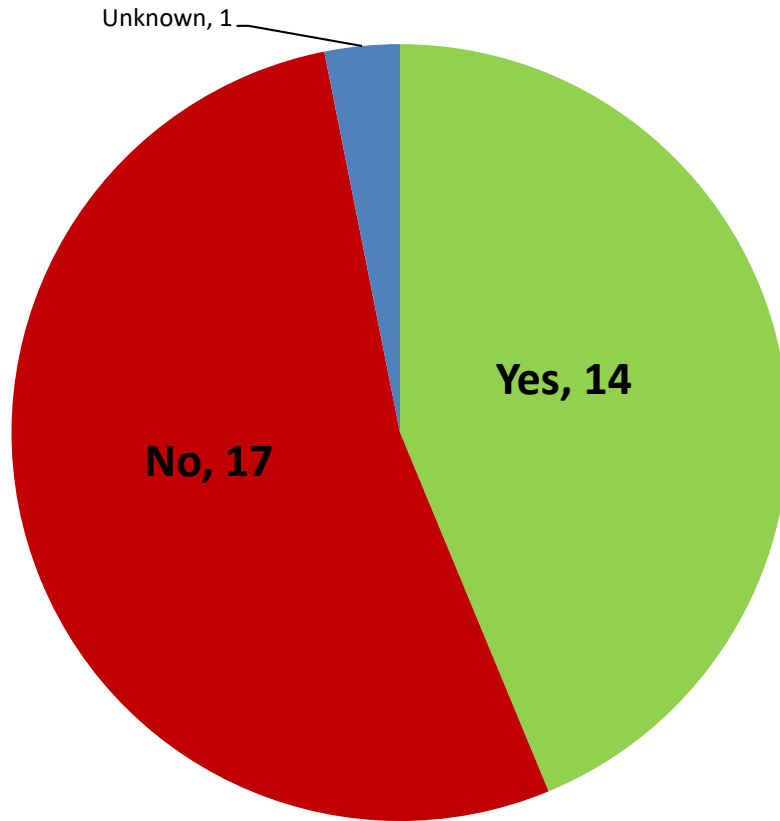
- 1) When confinement is needed to replicate actual storage/tactical environments but it is unnecessary to add extraneous live rounds to obtain a pass/fail result. For example a situation where the adjacent round is likely to detonate but not continue to propagate the detonation further.*
- 2) When used as confinement.*
- 3) When trying to differentiate the response from 2 parts of a munition, i.e. the warhead vs. the propellant or motor.*

Should preconditioning be used?



Only when the item tested has sensitivity to temperature and there is likelihood that this will be seen as defined by a THA

Should restraining devices be defined in the STANAG?



As per current STANAG: They shall not disturb the result analysis.

*To replicate in service configurations
These should be mentioned as suggestion for organizations facing space limitation*

Could be used sometimes but should depend on the test item configuration. Shouldn't be a mandatory requirement.

How should the donor be initiated?

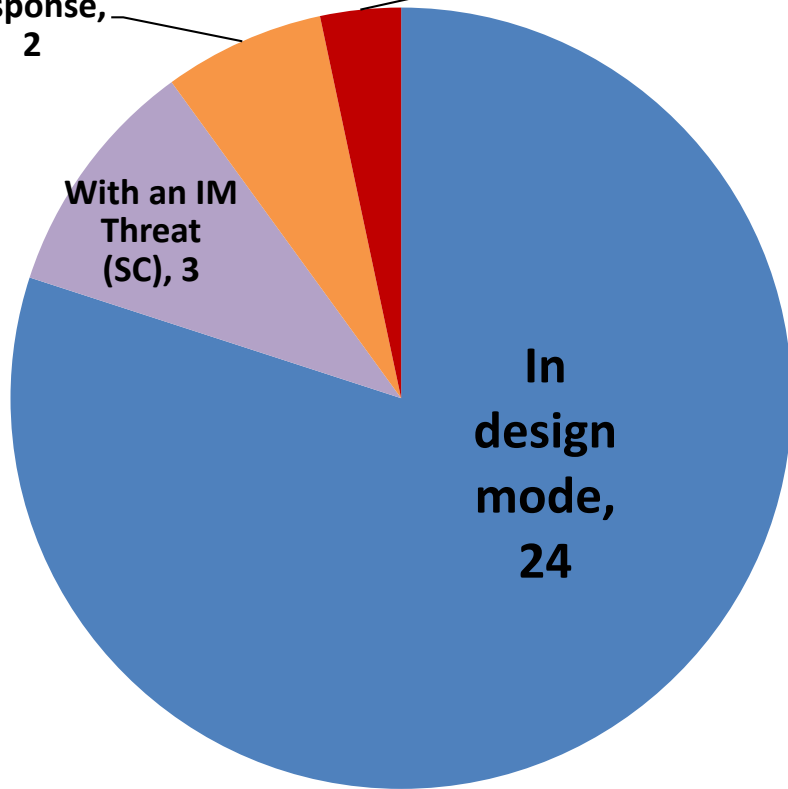
Warhead

To produce
a worst
case
response,
2

Unknown, 1

With an IM
Threat
(SC), 3

In
design
mode,
24

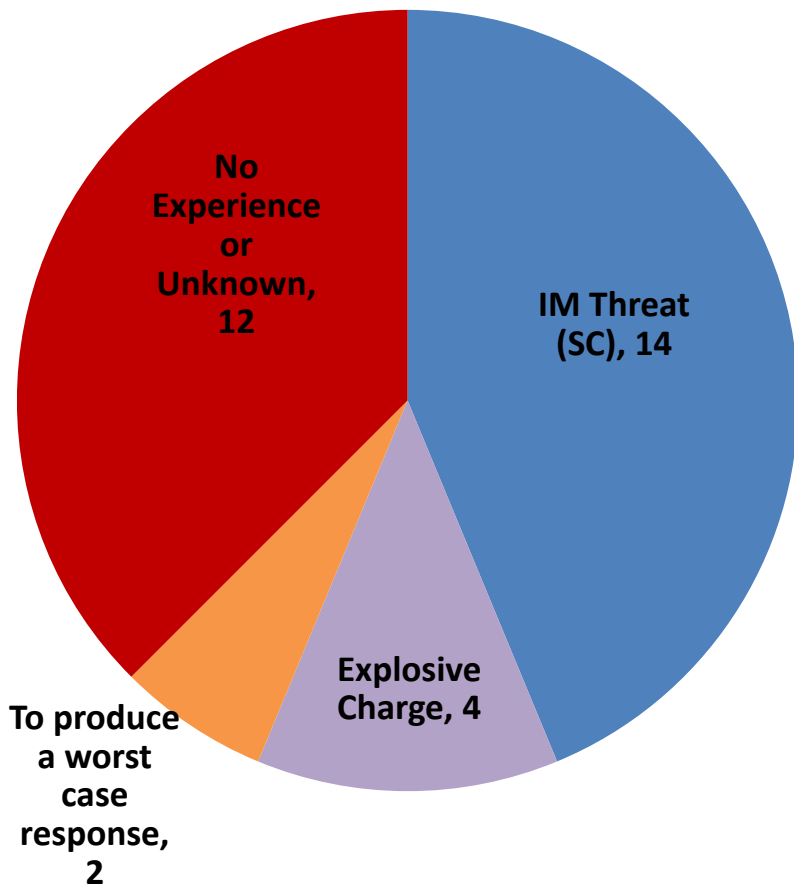


In a way that is closest to the real initiation, without compromising safety at the site. A dummy fuze with a hole and a small representative booster would be my recommendation.

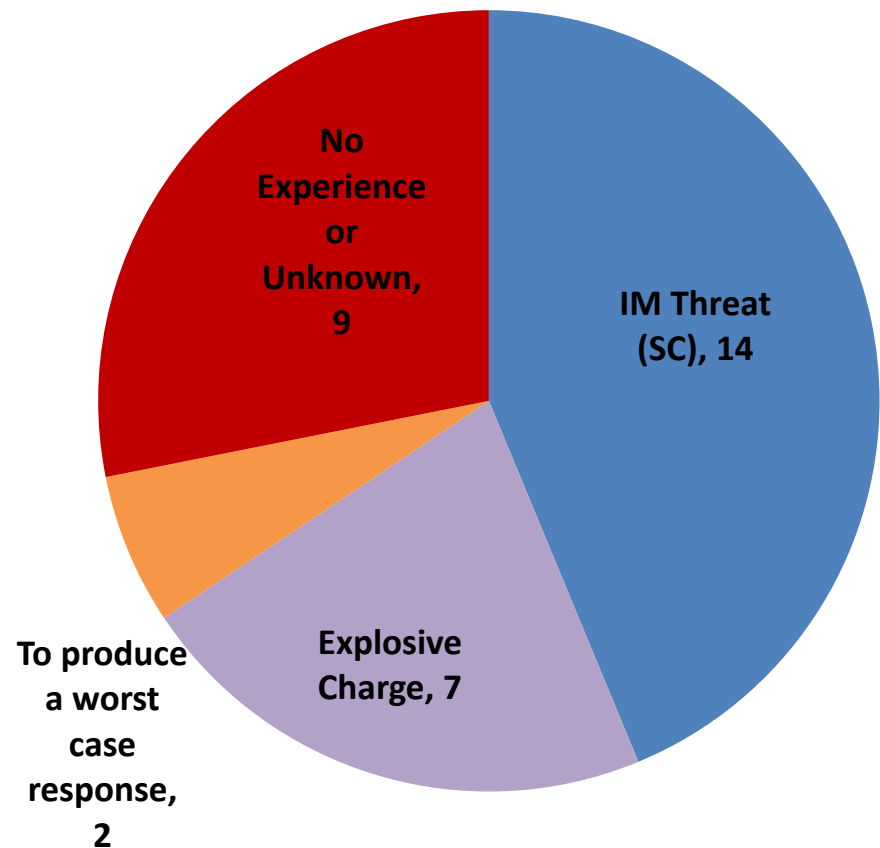
If the fuzing device is equipped with two or more independent effective protective features, then fuze disfunctioning could be excluded. Then the initiation of the donor with a credible IM threat that produces the worst case donor reaction, in general the Shaped Charge Jet (SCJ). If the fuze is not safe then it in logic to use the normal means of initiation.

How should the donor be initiated?

Rocket Motor



Gun Propellant

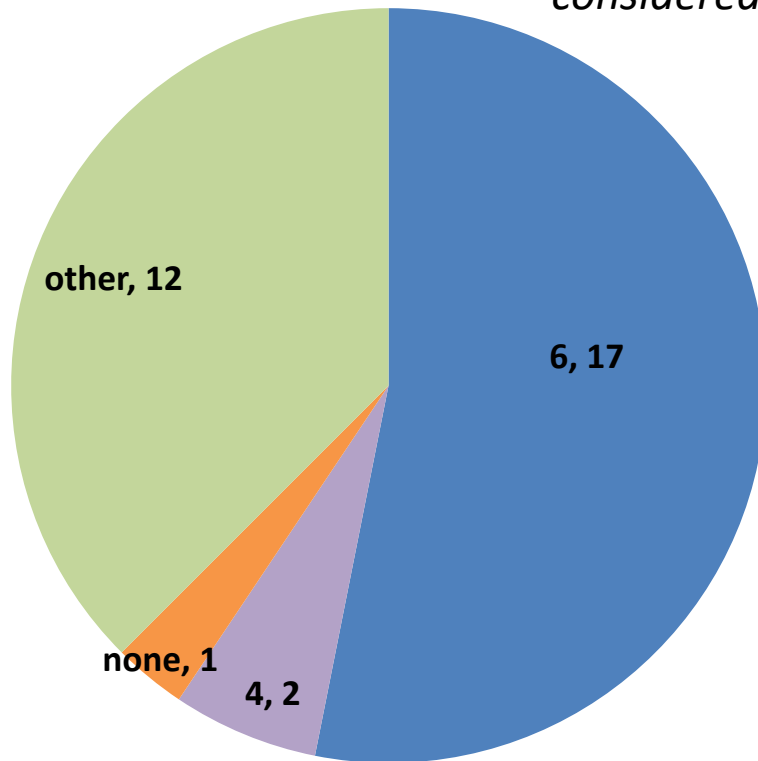




MSIAC How many blast gauges?

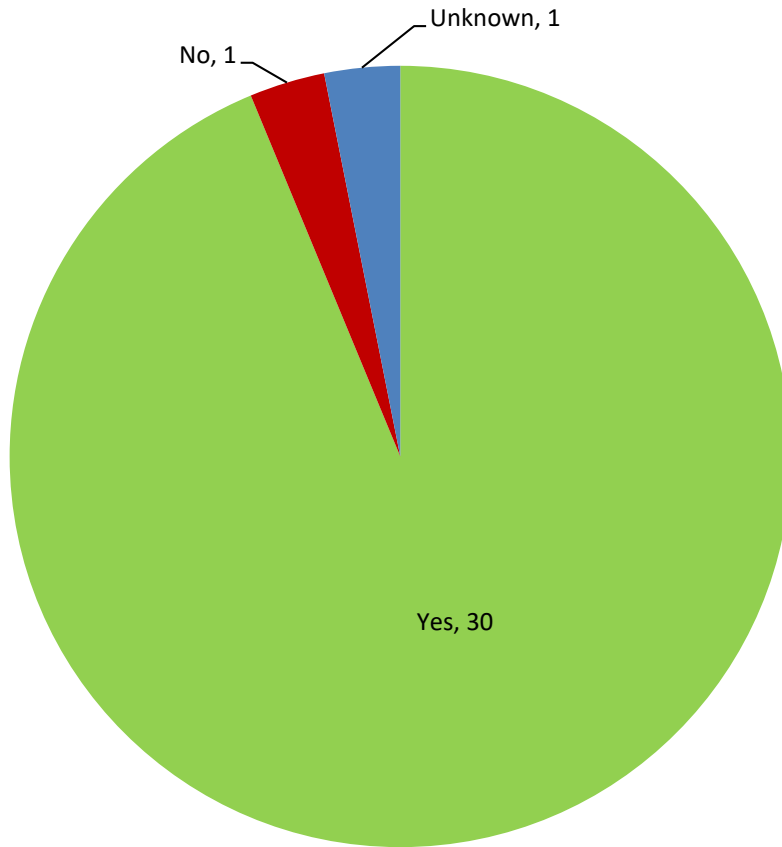
Supporting Munitions Safety

- *Same as current STANAG 4396 requirement: “Pressure gauges may be used to measure the air shock. The transducers should be placed in arrays some distance from the test configuration; they may be in ground or in elevated mounts. The fixtures shall not interfere with the air flow. Precalibration shall be considered if external sensors are used.”*



- *6 (2 lines of 3 distances)*
- *The test center has to place enough gauges to be sure to have enough information to use the response descriptors table*
- *Firstly, donor test evaluation. Gauges (number, position) are chosen to evaluate the response descriptors.*
- *As many as necessary to be able to compare with the pressure history generated by a lone donor charge*
- *We use two lines of five blast gauge each.*
- *Depends on the munition and magnitude of the response.*

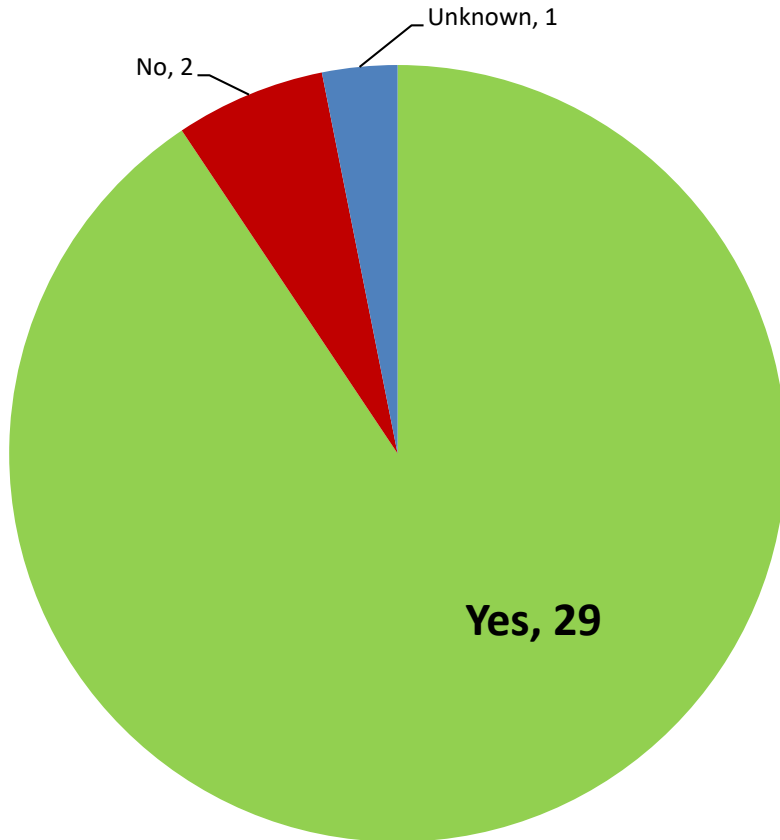
Do you use high speed video?



Reported frame rates (fps)

- 30
- 120
- 1000
- 2000
- 5000
- 7000
- 10000
- 12000
- 20000
- 30000
- 50000
- 75000
- 100000

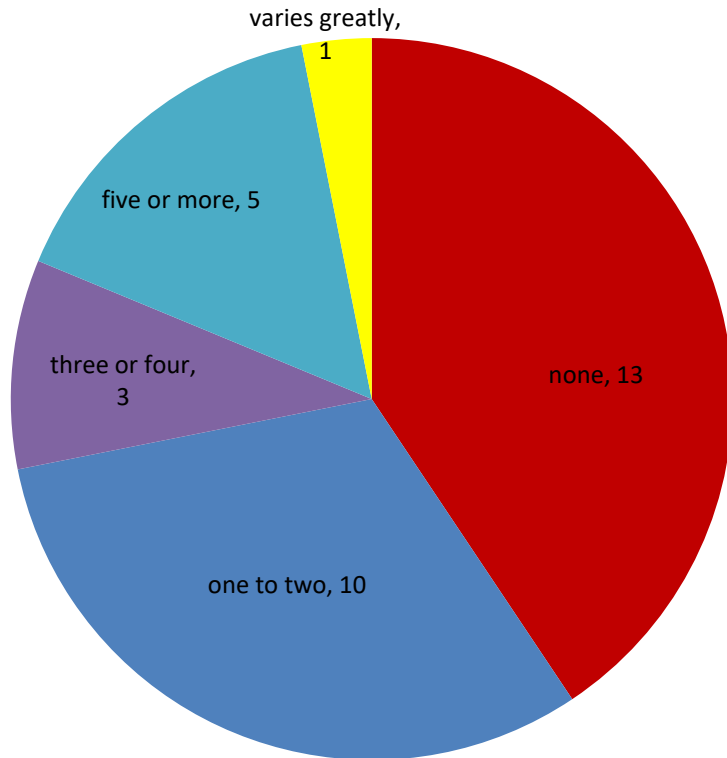
Do you use any witness plates and/or witness screens?



- We use steel or aluminum plate. The thickness depends on the munition characteristics. (5 responses)
- When high explosives charge are involved in the ammunition: 2.5 cm (1 inch thick) mild steel plates of size depending on the item tested. For gun propellant: 2.5 cm (1 inch thick) aluminum plates.

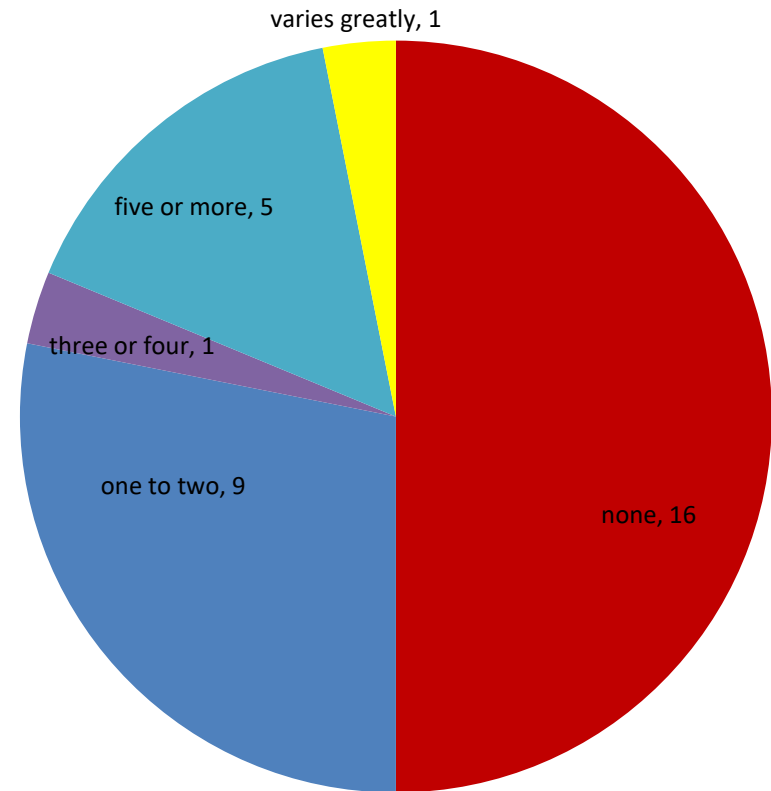
Annual Testing

How many qualification SR tests do you typically perform per year?



None includes no answer

How many developmental engineering SR tests do you typically perform per year?



Much greater number of development engineering tests:
In excess of 15 per year, 8 to 20, few dozens, >100

Baseline Test Data Comment (many similar)

- I think it is a good idea to introduce a calibration test where only the donor is initiated (or ignited) to its most severe reaction. In such test all other acceptors shall be inert. By doing this you will get a very good (and necessary for the assessment of the result) reference of e.g. blast pressure levels, fragmentation of the acceptors and eventual projection distances when you know that only the donor reacted. A calibration test should be mandatory.*

NATO AC/326 SG/B Sympathetic Reaction Custodial Working Group is using this information as part of the process to update STANAG 4382